

# **Establishing a Comprehensive Toolbox for Isotopic Labelling Studies on Terpene Synthases**

Kumulative Dissertation  
zur Erlangung des Doktorgrades (Dr. rer. nat.)  
der  
Mathematisch-Naturwissenschaftlichen Fakultät der  
Rheinischen Friedrich-Wilhelms-Universität Bonn

vorgelegt von

**Jan Rinkel**

aus Braunschweig

Bonn, 2019



Angefertigt mit der Genehmigung der Mathematisch-Naturwissenschaftlichen Fakultät  
der Rheinischen Friedrich-Wilhelms-Universität Bonn.

1. Gutachter: Prof. Dr. Jeroen S. Dickschat  
2. Gutachter: Prof. Dr. Dirk Menche  
Tag der Promotion: 25.10.2019  
Erscheinungsjahr: 2019

Die vorliegende Arbeit wurde in der Zeit vom 01.08.2015 bis zum 21.05.2019 am Kekulé-Institut für Organische Chemie und Biochemie der Rheinischen Friedrich-Wilhelms-Universität Bonn unter der Leitung von Herrn Prof. Dr. Jeroen S. Dickschat angefertigt.

Leitung: Prof. Dr. Jeroen S. Dickschat

Korreferat: Prof. Dr. Dirk Menche

*Meiner Frau Ramona und meinem Sohn Arne.*



## Acknowledgements

Firstly, I wish to thank my supervisor Prof. Dr. Jeroen S. Dickschat for his guidance and his enduring support, which made this thesis possible. For the always open door, the fruitful discussions and his tenacity also in pursuing ambitious ideas I am very grateful. Also, the opportunity to attend conferences and to meet other researchers in the field is acknowledged.

Additionally, I thank Prof. Dr. Dirk Menche for taking the time to referee this work and also Prof. Dr. Rainer Streubel and Prof. Dr. Gabriele M. König for joining the thesis examination committee.

Furthermore, I wish to express my thanks to all current and former members of the Dickschat work group, starting with Dr. Patrick Rabe for his skilful teaching of the work with recombinant terpene synthases and incubation experiments, for all the work he put together with me in our shared projects and for his optimism. I want to thank Lukas Lauterbach for the work conducted together and Dr. Christian A. Citron for introducing me to organic chemistry. For the nice working atmosphere, the productive discussions and the time together I want to thank: Alexander Babczyk, Dr. Lena Barra, Dr. Nelson L. Brock, Dr. Immo Burkhardt, Eike Caldeweyher, Ersin Celik, Erik Daniel, Etilia Dolja, Simone Gaeta, Dr. Anwei Hou, Seocho Kim, Tim A. Klapschinski, Dorota Konvalinkova, Markus Menke, Dr. Khomaizon A. K. Pahirulzaman, Dr. Zhiyang Quan, Neran Reuber, Dr. Ramona Riclea, Dr. Tao Wang and Dr. Zhongfeng Ye. Additionally, I wish to thank former student members of our group, Simon T. Steiner, Laura zur Horst, Britta Nubbemeyer and Thomas Schmitz, for their competent work contributing to this thesis.

I wish to express my thanks to cooperation partners, which contributed to this thesis: Prof. Ikuro Abe and Dr. Takaaki Mitsuhashi, Prof. Dr. Rita Bernhardt and Dr. Martin Litzenburger (also for their hospitality), Prof. Dr. Harro J. Bouwmeester and Dr. Arman Beyraghdar Kashkooli, Prof. Dr. Feng Chen and Dr. Tobias G. Köllner, Prof. Tiangang Liu and Dr. Zhangqian Wang, Prof. Dr. Stefan Schulz and Dr. Lisa Ziesche, Prof. Dr. Konrad Tiefenbacher and Dr. Qi Zhang as well as Prof. Dr. Christoph Wittmann and Dr. Michael Kohlstedt.

Furthermore, the members of the NMR department in Bonn are thanked for their patient processing of numerous samples: Ulrike Weynand, Karin Prochnicki, Hanelore Spitz and Dr. Senada Nozinovic. Additionally, I thank Andreas J. Schneider (HPLC) and Dr. Marianne Engeser, Karin Peters-Pflaumbaum and Christine Sondag (MS).

For financial support, I am very grateful to the Fonds der Chemischen Industrie (FCI), which granted a PhD scholarship to support this work, and also to the DFG (SFB TRR 51, *Roseobacter*).

Finally, I want to thank my wife Ramona Rinkel, who moved with me to Bonn and helped me during the last years with great patience and tolerance. I also wish to thank my parents Aenne and Uwe Rinkel for arousing my interest in science and for their constant support.





## Preamble

This cumulative doctoral thesis “Establishing a Comprehensive Toolbox for Isotopic Labelling Studies on Terpene Synthases” consists of 23 scientific publications including one review article. After a general introduction into the discussed topic (Chapter 1), each chapter represents one publication (Chapters 2–24), which is briefly introduced and summarised to explain the individual work in the context of this thesis, whereas the corresponding publication is attached in the appendix part (Appendices A–K and M–X). Because of the extent of Supporting Information for all publications, printing those was omitted. Most Supporting Information are available free of charge on the publisher’s website and can be accessed using the DOI for each publication included in the appendix part. In cases, where multiple authors contributed to a publication, a statement about my individual work to each project is included on the first page of the chapters. The sequence of chapters was chosen based on their thematic context and, as the second criteria, based on the time of publication. Therefore, the chapters split up into one major part about terpenes and terpene synthases (Chapters 2–20) and two minor parts about fungal volatiles together with biotechnological lignin conversion (Chapters 21 and 22), and selected aspects of the secondary metabolism of marine *Roseobacter* group bacteria (Chapters 23 and 24). All three parts are separately introduced in Chapter 1. A short summary of the complete work focussing on the scientific development is included in Chapter 25.

To fulfil the regulations concerning a cumulative thesis at the Faculty of Mathematics and Natural Sciences at the University of Bonn, one publication with minor contributions by me that arose during the time of the described work is not part of this cumulative thesis as a chapter. Instead, this publication is attached in Appendix L as a chronologically arranged supplement for a comprehensive overview of the work conducted that is based partially on results described in this publication.

Two articles being published within the time of my PhD studies contain minor contributions by me, which are mainly based on work conducted during my master thesis. Therefore, these publications (cited as references [127] and [254] in the main text) are not part of this doctoral thesis.



## Table of contents

1	State of scientific knowledge	1
1.1	Biosynthesis of terpenes	1
1.1.1	Terpenes – a large class of natural products	1
1.1.2	Mevalonate and non-mevalonate pathway	2
1.1.3	Prenyltransferases	5
1.1.4	Terpene synthases	8
1.1.5	Tailoring reactions	14
1.1.6	Isotopically labelled compounds in terpene research	17
1.2	Volatile aromatic compounds from fungi	25
1.3	Biosynthesis and regulation of tropodithietic acid	27
2	Recent highlights in biosynthesis research using stable isotopes	30
3	Lessons from 1,3-Hydride Shifts in Sesquiterpene Cyclizations	33
4	Terpene Cyclases from Social Amoebae	37
5	A detailed view on 1,8-cineol biosynthesis by <i>Streptomyces clavuligerus</i>	40
6	Mechanistic Investigations of Two Bacterial Diterpene Cyclases: Spiroviolene Synthase and Tsukubadiene Synthase	43
7	Mechanisms of the Diterpene Cyclases $\beta$ -Pinacene Synthase from <i>Dictyostelium discoideum</i> and Hydropyrene Synthase from <i>Streptomyces clavuligerus</i>	47
8	Mechanistic Characterization of Two Chimeric Sesterterpene Synthases from <i>Penicillium</i>	50
9	18-Hydroxydolabella-3,7-diene synthase – a diterpene synthase from <i>Chitinophaga pinensis</i>	53
10	Spata-13,17-diene Synthase—An Enzyme with Sesqui-, Di-, and Sesterterpene Synthase Activity from <i>Streptomyces xinghaiensis</i>	56
11	Two Diterpene Synthases for Spiroalbatene and Cembrene A from <i>Allokutzneria albata</i>	60
12	An Isotopic Labelling Strategy to Study Cytochrome P450 Oxidations of Terpenes	63
13	A Clade II-D Fungal Chimeric Diterpene Synthase from <i>Colletotrichum gloeosporioides</i> Produces Dolasta-1(15),8-diene	66
14	A Branched Diterpene Cascade: The Mechanism of Spinodiene Synthase from <i>Saccharopolyspora spinosa</i>	69

15	Addressing the Chemistry of Germacrene A by Isotope Labeling Experiments	72
16	Diterpene Biosynthesis in Actinomycetes: Studies on Cattleylene Synthase and Phomopsene Synthase	75
17	Stereochemical investigations on the biosynthesis of achiral ( <i>Z</i> )- $\gamma$ -bisabolene in <i>Cryptosporangium arvum</i>	78
18	Mechanistic investigations on multiproduct $\beta$ -himachalene synthase from <i>Cryptosporangium arvum</i>	81
19	The EI-MS Fragmentation Mechanisms of Bacterial Sesquiterpenes and Diterpenes	84
20	Sesquiterpene cyclizations catalysed inside the resorcinarene capsule and application in the short synthesis of isolongifolene and isolongifolenone	87
21	Volatiles from the hypoxylaceous fungi <i>Hypoxylon griseobrunneum</i> and <i>Hypoxylon macrocarpum</i>	90
22	From lignin to nylon: Cascaded chemical and biochemical conversion using metabolically engineered <i>Pseudomonas putida</i>	93
23	Characterisation of the L-Cystine $\beta$ -Lyase PatB from <i>Phaeobacter inhibens</i> : An Enzyme Involved in the Biosynthesis of the Marine Antibiotic Tropodithietic Acid	96
24	Acyl-group specificity of AHL synthases involved in quorum-sensing in <i>Roseobacter</i> group bacteria	99
25	Summary and outlook	102
26	References	104
	List of abbreviations	120
	Appendices A – X	121

# Chapter 1

## 1 State of scientific knowledge

### 1.1 Biosynthesis of terpenes

#### 1.1.1 Terpenes – a large class of natural products

Terpenoids constitute the largest class of natural products with more than 50,000 known compounds.<sup>[1]</sup> Even more intriguing than this bare number is the immense structural diversity within this group that fascinated chemists since the beginning of terpene research over a century ago. The most prominent representatives for this group today include the heavily decorated diterpene paclitaxel (**1**, Figure 1), which was originally isolated from the pacific yew *Taxus brevifolia*<sup>[2]</sup> and is now used as an anti-cancer medication,<sup>[3]</sup> the anti-malaria drug artemisinin (**2**) from *Artemisia annua*,<sup>[4]</sup> and ingenol mebutate (**3**) from *Euphorbia peplus*,<sup>[5]</sup> which is used for the treatment of actinic keratosis.<sup>[6]</sup>

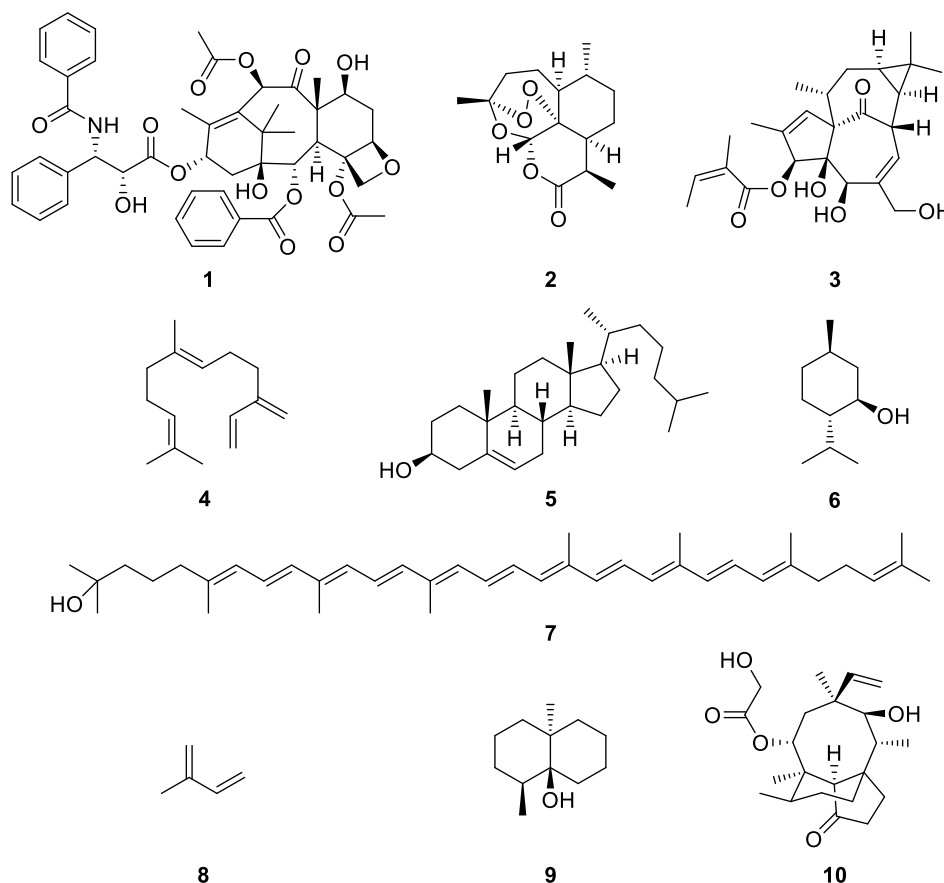


**Figure 1.** Selected compounds from the terpenoid class of natural products.

But also besides these pharmacologically relevant molecules, terpenes have been found to possess various interesting ecological functions, like (*E*)- $\beta$ -farnesene (**4**), which is an alarm pheromone in aphids,<sup>[7]</sup> fulfil essential roles for cellular eukaryotic life as cholesterol (**5**) does by its effect on membrane properties,<sup>[8]</sup> are useful because of their

flavour and olfactory properties like menthol (**6**),<sup>[9]</sup> or serve in light harvesting complexes as the carotenoid rhodopin (**7**).<sup>[10]</sup> A few terpenes are produced globally in high amounts like the volatile plant metabolite isoprene (**8**) with 600 million tons per year,<sup>[11]</sup> which also has effects on atmospheric chemistry. While the occurrence of some terpenoids is limited to only one species, others are found repeatedly from different organisms like **8** from plants, but also geosmin (**9**) from bacteria, especially in soil-dwelling actinomycetes and myxobacteria. This compound is easily recognised by its earthy odour.<sup>[12]</sup> Also antibiotic activities are observed for a few terpenes as for the fungal compound pleuromutilin (**10**), which binds to the peptidyl transferase centre of the bacterial ribosome.<sup>[13]</sup> The often complex, polycyclic structure of terpenes, featuring multiple stereogenic centres also continues to attract the attention of synthetic chemists for the development of new approaches for their preparation.<sup>[14]</sup>

Although these representatives do not share any structural features at first sight, their core structures are all build up from formal isoprene (**8**) units, leading to a characteristic methyl branching pattern. The resulting general sum formula of terpenes as  $(C_5H_8)_n$  was already recognised by Wallach in 1885, who divided the class according to the incorporated units into hemiterpenes ( $C_5H_8$ ), monoterpenes ( $C_{10}H_{16}$ ), sesquiterpenes ( $C_{15}H_{24}$ ), diterpenes ( $C_{20}H_{32}$ ) and polyterpenes like natural rubber based on his investigations on essential oil compounds.<sup>[15]</sup> This directive classification is still in use and was later expanded by sesterterpenes ( $C_{25}H_{40}$ ), triterpenes ( $C_{30}H_{48}$ ) and tetraterpenes ( $C_{40}H_{56}$ ). The extensive work of Ružička represents the next important milestone in terpene chemistry, leading to a structural understanding of this remarkable compound class, commonly referred to as the “isoprene rule”.<sup>[16]</sup> Intriguingly, long before the enzymatic principles of secondary metabolism were established, the classical approach of natural product chemistry with isolation, characterisation and structure elucidation of new natural products led to a remarkable decent prediction of the biosynthetic logic that gives rise to this diverse class.

### 1.1.2 Mevalonate and non-mevalonate pathway

Building up on these structural observations, the biochemists Bloch<sup>[17]</sup> and Lynen both worked on the elucidation of the biosynthetic origin and regulation of medicinally highly important **5**. With the help of isotopic labelling techniques, a fairly new method at that time, they traced back the origin of **5** to acetate. This remarkable masterpiece of biochemical work,<sup>[18]</sup> which also consists of contributions from the laboratories of Cornforth and Popják,<sup>[19]</sup> also yielded the structures of the long sought biological active equivalents of **8**, isopentenyl diphosphate (IPP, **11**, Figure 2)<sup>[20]</sup> and dimethylallyl diphosphate (DMAPP, **12**), together with the identification of two central intermediates in the biosynthesis of **5**, mevalonate (**13**)<sup>[21]</sup> and squalene (**14**).<sup>[22]</sup>

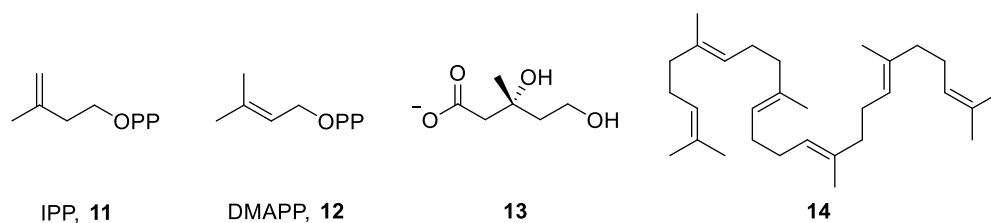
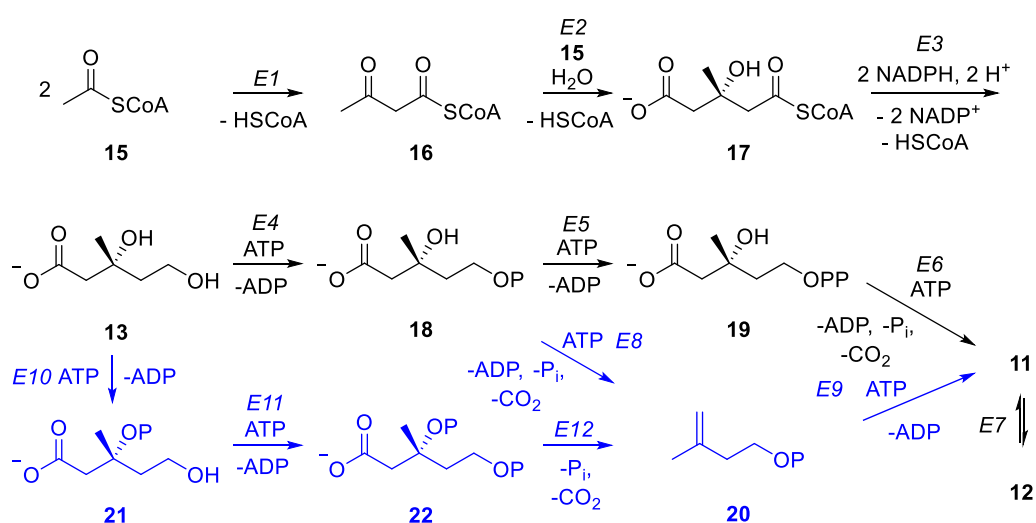


**Figure 2.** Structures of IPP (**11**) and DMAPP (**12**), the biologically active isoprenoid monomers, and of mevalonate (**13**) and squalene (**14**).

The assembly of **11** and **12** constitutes the first step in the biosynthesis of isoprenoids. Currently, there are two distinct pathways known for their formation. The mevalonate pathway (Scheme 1) is named after its intermediate **13** and occurs in fungi, animals and in the cytosol of plants.

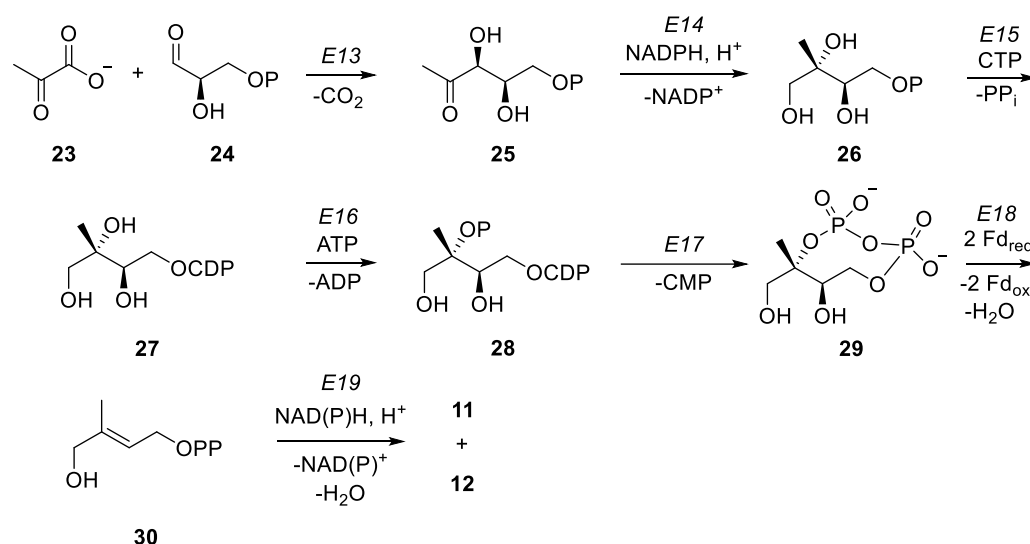


**Scheme 1.** The mevalonate pathway towards **11** and **12** with modifications shown in blue. *E1*: acetoacetyl-CoA thiolase; *E2*: HMG-CoA synthase; *E3*: HMG-CoA reductase; *E4*: mevalonate-5-kinase; *E5*: phosphomevalonate kinase; *E6*: mevalonate-5-diphosphate decarboxylase; *E7*: isopentenyl diphosphate isomerase (IDI); *E8*: mevalonate-5-phosphate decarboxylase; *E9*: isopentenyl phosphate kinase; *E10*: mevalonate-3-kinase; *E11*: mevalonate-3-phosphate-5-kinase; *E12*: putative mevalonate-3,5-bisphosphate decarboxylase.

In the first step, two units of acetyl-CoA (**15**) are fused to yield acetoacetyl-CoA (**16**) by a thiolase in a Claisen-condensation. This reversible reaction also plays a role in other pathways like the  $\beta$ -oxidation of fatty acids.<sup>[23]</sup> With an aldol addition and subsequent hydrolysis of the thioester, a third unit of **15** is used to build up 3-hydroxy-3-methylglutaryl-CoA (HMG-CoA, **17**).<sup>[24]</sup> Then, two equivalents of NADPH are used to reduce the thioester to **13**. This step is rate determining for the mevalonate pathway, therefore heavily regulated and its enzyme, HMG-CoA reductase, is a common drug target to influence cholesterol levels by utilising inhibitors (statins). Two different kinases lead to a sequential phosphorylation of **13** via **18** to mevalonate 5-diphosphate (**19**) with consumption of ATP. Further phosphorylation and decarboxylation yields **11**, which is

equilibrated with its isomer **12** by isopentenyl diphosphate isomerase (IDI). Recently, two archaeal modifications of this pathway were discovered, which involves a different order of phosphorylation steps. In *Haloferax volcanii*,<sup>[25]</sup> **18** is converted to isopentenyl phosphate (**20**), which is then further phosphorylated to **11** by a kinase. Surprisingly, this enzyme is also found in some bacteria and even in eukaryotes suggesting that these modifications are not limited to archaea.<sup>[26]</sup> Yet another branching point from the classical mevalonate pathway was found in *Thermoplasma acidophilum*,<sup>[27]</sup> where **13** is phosphorylated at position 3 to yield **21**, which is then processed to mevalonate-3,5-bisphosphate (**22**). A decarboxylation, which is assumed to proceed without the involvement of ATP, may give **20**, but the corresponding enzyme has not been identified yet. Despite these changes, the overall chemical logic of the mevalonate pathway remains the same.

In contrast, the second known pathway (called non-mevalonate-, DOXP-, or MEP-pathway) towards **11** and **12** is fundamentally different. With isotopic labelling experiments in the late 1980s that led to unexpected incorporations into terpenoids, both observed in bacteria<sup>[28]</sup> by Rohmer and in plants<sup>[29]</sup> by Arigoni, the alternative pathway (Scheme 2) became evident.



**Scheme 2.** The non-mevalonate (MEP, DOXP) pathway towards **11** and **12**. *E13*: DOXP synthase; *E14*: DOXP reductoisomerase (IspC); *E15*: MEP cytidyltransferase (IspD); *E16*: 4-diphosphocytidyl-ME kinase (IspE); *E17*: ME 2,4-cyclodiphosphate synthase (IspF); *E18*: HMB-PP synthase (IspG); *E19*: HMB-PP reductase (IspH).

Starting from pyruvate (**23**) and glyceraldehyde 3-phosphate (**24**), in the first step 1-deoxy-D-xylulose 5-phosphate (DOXP, **25**) is formed under decarboxylation and involvement of thiamine diphosphate (TPP). The DOXP reductoisomerase then catalyses the remarkable transformation of **25** to 2-C-methyl-D-erythritol 4-phosphate (MEP, **26**) via reduction of an aldehyde intermediate by NADPH.<sup>[30]</sup> A cytidyl phosphate moiety is then transferred to **26**, which gives **27** with consumption of cytidine triphosphate (CTP). Further phosphorylation and ring closure via **28** yields the unusual cyclic diphosphate species **29**,<sup>[31]</sup> which is reduced and ring-opened by an enzyme mediated electron

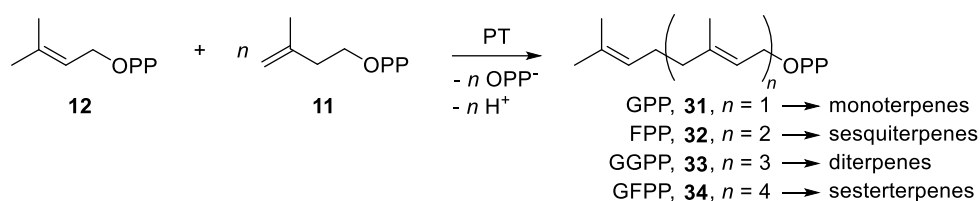


transfer from two ferredoxins (Fd) to give (*E*)-4-hydroxy-3-methylbut-2-enyl diphosphate (HMB-PP, **30**). Consuming NAD(P)H, an iron sulfur cluster dependent reductase converts this intermediate to the isoprenoid precursors **11** and **12** in a 5:1 ratio.<sup>[32]</sup>

The two discussed pathways explain the biosynthetic origin of the terpene monomers including their structural imprint on methyl branching and double bond reactivity that lay the basis for the diversification taking place downstream in terpene biosynthesis.

### 1.1.3 Prenyltransferases

The second step of terpene metabolism involves the chain elongation of **12** by multiple units of **11** towards the oligoprenyl diphosphates. Their different chain lengths determine the classification of the produced terpene as a mono-, sesqui-, or diterpene etc. as stated above (Scheme 3). The chain elongation is catalysed by prenyltransferases (PTs), leading to a first diversification within the terpene class of natural products. Although PTs are also known to transfer prenyl moieties to a large variety of different substrates within primary and secondary metabolism, only the subgroup of the oligoprenyl diphosphate synthases are discussed here.<sup>[33]</sup>



**Scheme 3.** Chain elongation towards the oligoprenyl diphosphates **31-34**.

Fusing both monomeric precursors, geranyl diphosphate (GPP, **31**) is accessible, the starting structure for all monoterpenes. Elongation of **31** with **11** furnishes farnesyl diphosphate (FPP, **32**), leading to the sesquiterpenes. The diterpene precursor geranylgeranyl diphosphate (GGPP, **33**) consists of four isoprene units and is made by elongation of **32**. The biosynthesis of geranylfarnesyl diphosphate (GFPP, **34**) obeys the same chemical logic and gives access to the sesterterpenes. The final chain length is determined by the active site architecture of the PT, which catalyses the elongation in a sequential manner. This results in a flexible substrate scope e. g. a GFPP synthase not only accepts **11** and **12**, but also **11** and any intermediary chain length diphosphate **31-33** to convert them to **34**. Higher terpenes like tri- and tetraterpenes are usually biosynthesised by combining two units of **32** for the first to **14**, a complex reaction catalysed by squalene synthase,<sup>[34]</sup> and two units of **33** for the latter in a similar reaction to phytoene,<sup>[35]</sup> the C<sub>40</sub>-homologue of **14** containing an additional central carbon-carbon double bond.

The first crystal structure of an oligoprenyl diphosphate synthase was that of avian FPP synthase (FPPS).<sup>[36]</sup> Its overall fold (Figure 3) is characterised by 13  $\alpha$ -helices, of which 10 surround the active pocket. Pointing to the interior of this cavity, but located on different sides, two conserved DDxxD motifs are found. Since the catalytic activity of FPPS is metal ion dependent ( $\text{Mg}^{2+}$ ), these negatively charged residues can complex

Mg<sup>2+</sup>-ions, which in turn bind the diphosphate moiety of the substrates activating them for the reaction. Also other divalent metal ions such as Mn<sup>2+</sup> or Co<sup>2+</sup> are known to support PT activity, occasionally also changing the chain length of the product, as observed with a PT from the leaf beetle *Phaedon cochleariae*.<sup>[37]</sup>

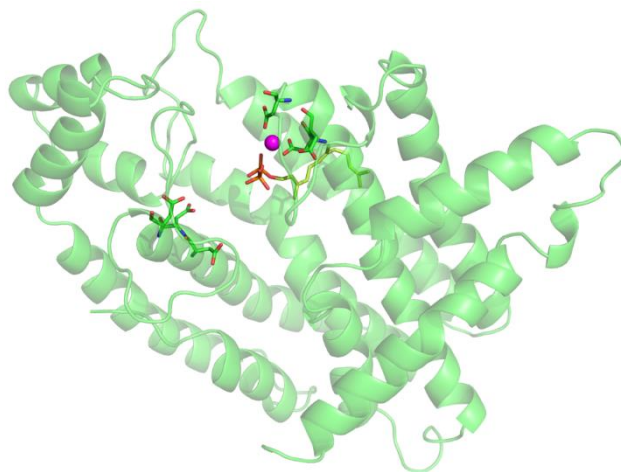
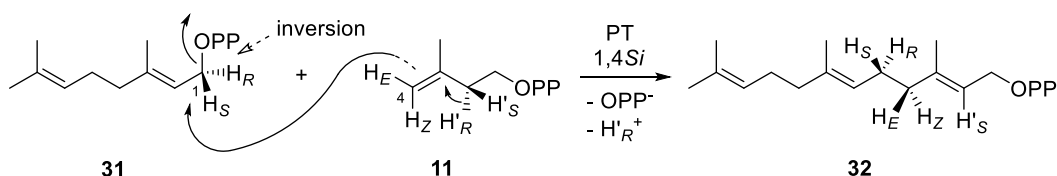


**Figure 3.** Monomeric structure of avian FPPS (PDB 1UBX).<sup>[38]</sup> The aspartate residues of the two DDxD motifs are shown as ball-and-stick model (the assembly on the left side represents the IPP binding site), the bound product FPP is displayed as a wire model, Mg<sup>2+</sup> is coloured in magenta. Figure generated with PyMOL.<sup>[39]</sup>

The chain elongation also features stereochemical aspects that were already experimentally addressed by isotopic labelling studies during Cornforth's and Popják's studies on cholesterol biosynthesis long before any structural insights of PTs were gained. They concluded on a well-defined stereochemical course (Scheme 4), in which a) the attack of IPP leads to an inversion of configuration at the diphosphate bound carbon atom, b) H'<sub>R</sub> is abstracted from C-2 of IPP,<sup>[40]</sup> c) the *Si* face of C-4 of IPP is involved in bond formation<sup>[41]</sup> and d) the newly formed double bond is (*E*)-configured, including the corresponding implications on the conformation of IPP.<sup>[42]</sup> Depending on the location of the abstracted diphosphate moiety, it was also suggested to act as a base taking up H'<sub>R</sub> from IPP.<sup>[43]</sup> Taken together, these stereochemical constraints already gave decent insights into possible active site conformations and positionings.



**Scheme 4.** Stereochemical course of the prenyl transferase reaction exemplified for the formation of **32**.

The discussed features are in line with a crystal structure of FPPS from *Escherichia coli* with bound IPP and the unreactive DMAPP analogon dimethylallyl *S*-thiolodiphosphate (DMSPP),<sup>[44]</sup> which nicely reassembles the reactive conformation of FPPS with its natural substrates (Figure 4). Together with the stereochemical course, the structure also

supports the assumption of  $H_R$  (C-2 of IPP) being abstracted by the leaving diphosphate, because it points towards the correct direction. Since the assembly of oligoprenyl diphosphates is an iterative process, the same orientation and stereochemical course can be assumed for any chain length produced by homologous PTs.

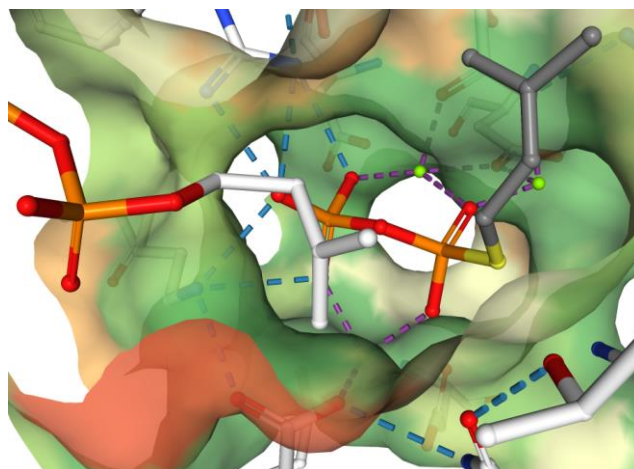
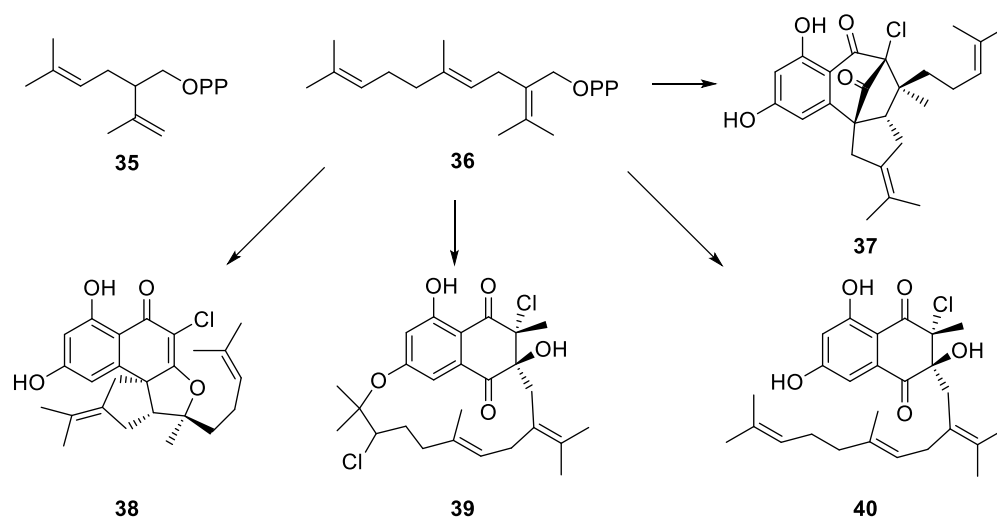


**Figure 4.** Active site view of *E. coli* FPPS in complex with DMSPP (right, carbon atoms shown in grey) and IPP (left, carbon atoms shown in white) rationalises the stereochemical course of the prenyl transferase reaction (PDB 1RQI).<sup>[44]</sup> Hydrogen bridge- (blue) and metal interactions (purple) are indicated by dashed lines.  $Mg^{2+}$  ions are shown in green. Figure generated with NGL viewer.<sup>[45]</sup>

Because of their high relevance for this work, *trans*-isoprenyl diphosphate synthases have been highlighted above, but *cis*-isoprenyl diphosphate synthases are also known, which produce both (*E*)- and (*Z*)-configured double bonds in their products. Exemplified by the well-known undecaprenyl diphosphate synthase (UPPS),<sup>[46]</sup> the overall structure of these enzymes is different from *trans*-PTs, they are able to build longer chains and they do not feature a DDxxD motif, although a  $Mg^{2+}$  dependency is still observed.<sup>[33a]</sup> Members of the *cis*-PT family are also believed to be responsible for the biosynthesis of natural rubber with the incorporation of hundreds to thousands of isoprene units.<sup>[47]</sup> However, observing the enzymatic formation of these polymers *in vitro* still remains challenging.<sup>[48]</sup> Given the more flexible structure of *cis*-PTs, also examples from this group are known, which produce irregular fused isoprenoid chains in their products, for example the recently discovered lavandulyl diphosphate (**35**, Scheme 5) synthase<sup>[49]</sup> or the isosesquilandulyl diphosphate (**36**) synthase.<sup>[50]</sup> These enzymes catalyse a so called “head-to-middle” condensation of two molecules of DMAPP or GPP and DMAPP, respectively, to give **35** and **36**. Although these irregular prenylations are rare, they contribute to the structural variety of terpene natural products, as **36** was proposed as an intermediate in the biosynthesis of merochlorins A-D (**37-40**) from *Streptomyces* sp. CNH-189, which feature antibiotic activities.<sup>[51]</sup>



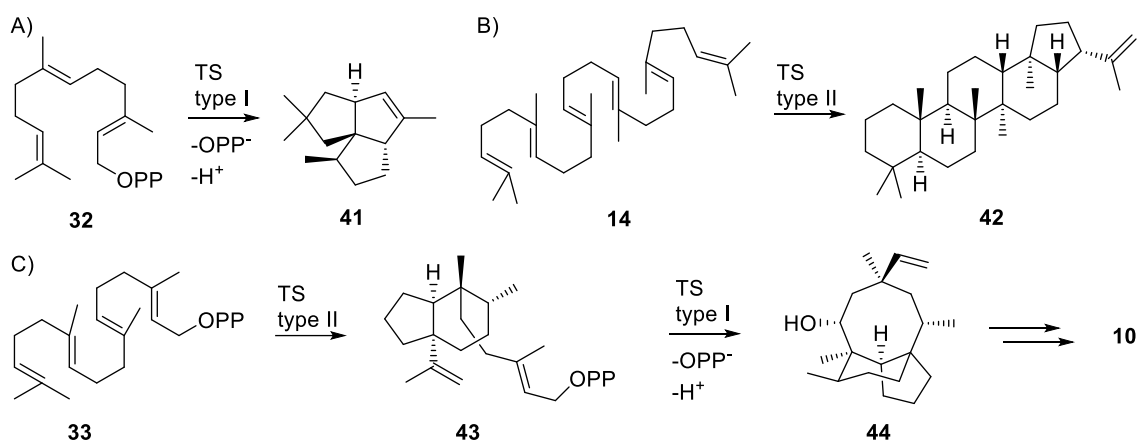
**Scheme 5.** Examples for irregular prenylation products. Structures of lavandulyl- (**35**) and isosesquilandulyl diphosphate (**36**) together with merochlorins A-D (**37-40**), which are thought to be biosynthetically derived from the latter.<sup>[51]</sup>

Taken together, *trans*- and *cis*-PTs represent the second step in terpenoid biosynthesis. By determining the chain length of the oligoprenyl diphosphates, these enzymes play an important role in early diversification and give rise to the sum-formula based classification of terpenes. Conveniently, the stereochemical course of the chain elongation reaction in *trans*-PTs is well defined allowing to use them for isotopic labelling experiments, a feature of central importance in this work.

#### 1.1.4 Terpene synthases

To rationalise the overwhelming structural variety of terpenes from a biosynthetic point of view, understanding both structure and function of terpene synthases (TSs) together with the inherent reactivity of their substrates<sup>[52]</sup> is mandatory. Catalysing cationic transformations, TSs can be classified into two main groups according to their catalytic mechanism.<sup>[53]</sup> Type I enzymes act by abstraction of a diphosphate moiety giving rise to the conversion of the structurally simple linear oligoprenyl diphosphates (e. g. **31-34**) into mostly complex, polycyclic hydrocarbons, alcohols, or ethers. In contrast, type II TSs initiate the reaction by protonation of a double bond or epoxide. Therefore, members of this class can not only accept linear diphosphates, but also hydrocarbons (e. g. **14**) or epoxides. A concept often found in the biosynthesis of terpenes is a combination of both types, namely a type II enzyme acts first to give a precyclised diphosphate, which is then the substrate of a type I TS, leading to diphosphate abstraction and sometimes further cyclisation. Examples for the discussed two types are shown in Scheme 6, including pentalenene synthase, a type-I enzyme from *Streptomyces* UC5319, which converts FPP into the complex tricyclic sesquiterpene pentalenene (**41**).<sup>[54]</sup> Squalene-hopene cyclase is a type-II enzyme involved in the biosynthesis of hopene (**42**) by protonation of **14**.<sup>[55]</sup> Eukaryotic homologues of this enzymes convert epoxidised **14** into lanosterol on the way to **5** in a very similar way.<sup>[56]</sup> At last, in the biosynthesis of **10**, a fusion protein is

involved consisting of a type-II domain, which converts GGPP into mutildienyl diphosphate (**43**), and a type-I domain processing this intermediate by diphosphate abstraction to premutilin (**44**).<sup>[57]</sup>



**Scheme 6.** Exemplified enzymatic reactions for A) a type-I TS (pentalenene synthase), B) a type-II TS (squalene-hopene cyclase) and C) a combined cyclisation using both types (premutilin synthase).

TSs can also be classified according to their domain structures, which also connects to the discussed types. They consist of up to three different  $\alpha$ -helical domains ( $\alpha$ ,  $\beta$ ,  $\gamma$ ), which can occur in different combinations (Figure 5).<sup>[53]</sup> Whereas single domain type-I TCs ( $\alpha$ ) are common in bacteria, multiple domain containing type-I enzymes are usually found in plants like taxadiene synthase from *Taxus brevifolia*,<sup>[58]</sup> which is involved in the biosynthesis of **1**. Interestingly, only the  $\alpha$  domain is catalytically active in this case. The active pocket of a type-II TS, featuring an aspartate rich DxDD motif, is located between domains  $\beta$  and  $\gamma$ , exemplified by bacterial squalene-hopene cyclase.

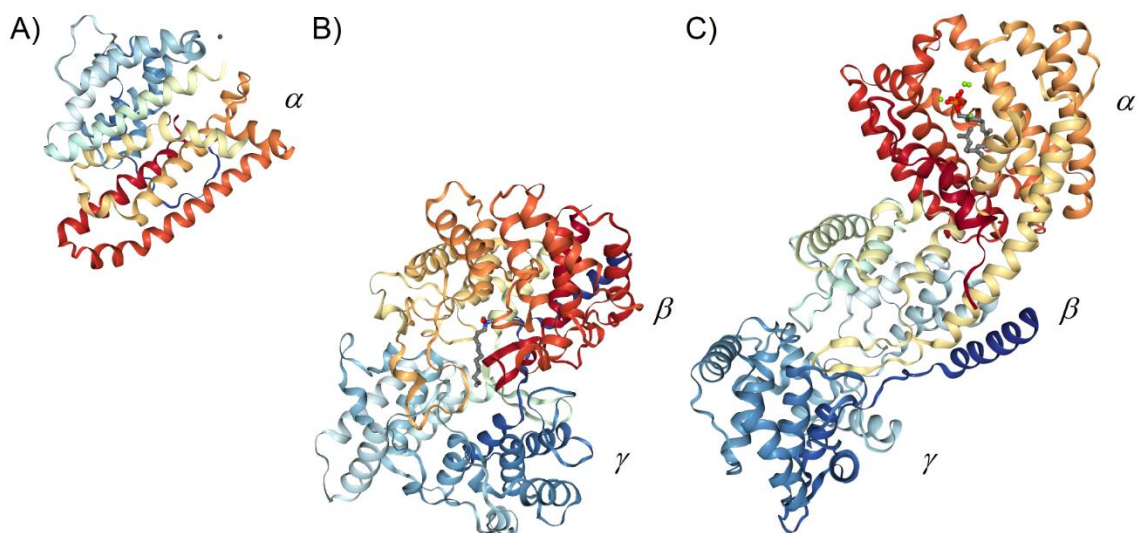


**Figure 5.** Different domain architectures of TSs in A) pentalenene synthase ( $\alpha$ , PDB 1PS1),<sup>[59]</sup> B) squalene-hopene cyclase from *Alicyclobacillus acidocaldarius* ( $\beta\gamma$ , PDB 1SQC),<sup>[55]</sup> and C) taxadiene synthase from *Taxus brevifolia* ( $\alpha\beta\gamma$ , PDB 3P5R).<sup>[58]</sup> Figure created with NGL viewer.<sup>[45]</sup>

Besides these classical TSs, recently also terpene cyclase activity was found with fungal and bacterial enzymes that belong to the UbiA-superfamily.<sup>[60]</sup> UbiA itself is involved in the biosynthesis of ubiquinones, which are part of the respiratory chain, as an aromatic prenyltransferase.<sup>[61]</sup> Although their catalytic function resembles a type-I TS with an abstraction of the diphosphate unit, UbiA-type TSs are integral membrane proteins, contrasting the mostly soluble, sometimes membrane-associated TSs discussed above. Structural analysis of UbiA from the archaeon *Aeropyrum pernix* revealed that these enzymes are surprisingly similar to the  $\alpha$ -fold of a soluble type-I TS, but yet completely integrate into the membrane to also release their product there.<sup>[62]</sup> The diversity of TSs also leaves room for future expansions of this enzyme family, since a few catalytically active members do not possess homology to these known classes and are yet to be structurally characterised.<sup>[63]</sup>

In the presented work, only soluble type-I enzymes were investigated, therefore this group of TSs is introduced in more depth here. Several crystal structures of type-I TSs have been determined<sup>[59,64]</sup> that allow for a detailed discussion of their overall fold, important residues for substrate binding and the architecture of their active sites. Given the overall low amino acid sequence homology of TSs, it is surprising that the overall  $\alpha$ -helical fold is comparable between different enzymes and also feature high similarity to that of *trans*-PTs (Figure 3), which underlines their evolutionary relation.<sup>[53]</sup> The substrate binding site is located between the  $\alpha$ -helices and in many structures, a trinuclear ( $\text{Mg}^{2+}$ )<sub>3</sub>-cluster is found in complex with substrate analogues or inorganic diphosphate. Since organic diphosphates are utilised by all type-I TSs, there are several conserved amino acid residues found to support this assembly, regardless of their final product's structure. To visualise the diphosphate binding, Figure 6 shows the active site of aristolochene synthase from the fungus *Aspergillus terreus*.<sup>[64c]</sup> In this structure, one  $\text{Mg}^{2+}$  is enzymatically bound by N219, S223 and E227, which assembles the so-called NSE triad (N,D)D(L,I,V)x(S,T)xxxE.<sup>[64b]</sup> On a different helix, D90 and D91 are involved in chelating two  $\text{Mg}^{2+}$ -ions. They belong to the aspartate rich motif DDxx(D,E), whereas the third D (or E94 in this case) is usually only found in the second coordination sphere. D91 also forms hydrogen bridges to R314, which is directly involved in diphosphate binding, as is Y315. They represent the RY dimer motif. Another important residue, which binds the diphosphate, is R175. This arginine was described as a "diphosphate sensor" for its different orientation in the open and closed conformation of selina-4(15),7(11)-diene synthase from *S. pristinaespiralis*.<sup>[64f]</sup> Although the diphosphate binding sphere is not described completely by the discussed motifs, they represent the most important features that can be found in this form or in slight variations in almost any type-I TS.

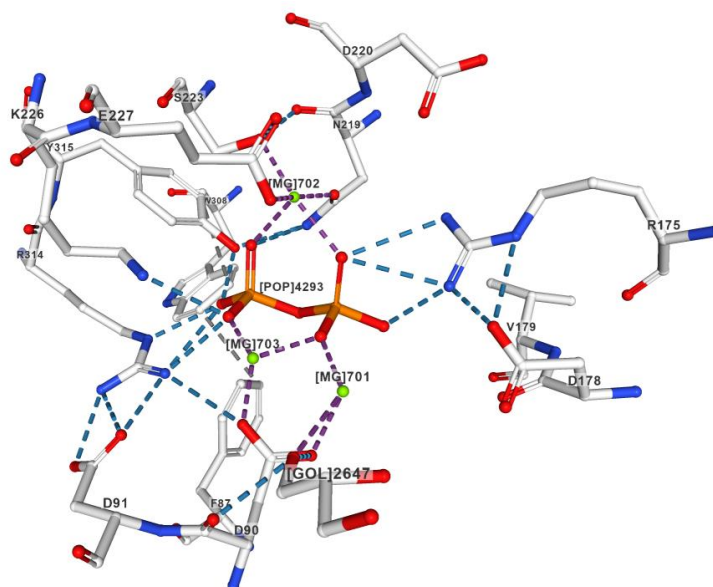


**Figure 6.** Diphosphate binding site view of aristolochene synthase from *Aspergillus terreus* in complex with inorganic diphosphate (PDB 2OA6)<sup>[64c]</sup> showing important conserved motifs in type-I TSs (DDxxD/E motif: bottom; NSE-triad: top; RY dimer: left; R: right). Mg<sup>2+</sup>-ions are coloured in green. Hydrogen bridges (blue) and metal ion bonds (purple) are displayed as dashed lines. Figure created with NGL viewer.<sup>[45]</sup>

Chemically even more important than diphosphate binding is the architecture of the TS's hydrophobic pocket, including its molecular coating. This feature determines, how the substrate is folded, which cationic species and transition states are stabilised and which are destabilised, and finally how the cascade reaction is terminated. Therefore, the active site has direct impact on the TS's product structure and with the versatile chemistry of carbocations including Wagner-Meerwein rearrangements and hydride or proton shifts, the tremendous number of different terpene skeletons is reasoned. However, a detailed systematic investigation of the fragile relationship between active site and product structure is highly challenging and thus the long-term goal of predicting the product of a given, new TS sequence<sup>[65]</sup> is currently out of reach. This situation is quite unique for TSs compared to other enzyme classes of secondary metabolism like polyketide- or non-ribosomal peptide synthases, in which bioinformatic predictions got a lot of attention for their rising accuracy.<sup>[66]</sup> Despite these difficulties, a decent level of understanding for the role of several amino acids in model TSs has been reached, both using computational approaches and site-directed mutagenesis.

Pentalenene synthase, one of the first crystallised TSs, harbours several different aromatic and aliphatic amino acids including L53, F57, F76, F77, V177, V179, T182, V301, and W308 to build up its hydrophobic cavity for the cyclisation.<sup>[59]</sup> Figure 7 shows three of them together with H309, which have been investigated by site-directed mutagenesis.<sup>[67]</sup> Replacing either F76 or F77 by tyrosine led to a 10-fold lower activity combined with a lower yield of recombinant protein, which underlines the importance of these residues both for stabilisation of cationic intermediates (location next to C-1, C-2, and C-3 of FPP) and for maintaining the enzyme's overall folding. The W308F variant

possessed half of the wild type activity, but also germacrene A (**53**) was observed as a side product emphasising that little changes in the cavity's architecture can have significant effect on the observed products. H309 was initially assumed as the active base responsible for the final deprotonation, but this hypothesis was falsified by observing significant activity for **41** in the variants H309A, H309S and H309C. Intriguingly, all of them also produced  $\Delta^6$ -protoilludene (**51**) as an additional side product. While not been involved in any deprotonating events, H309 is therefore still an important residue to conserve the TS's selectivity.

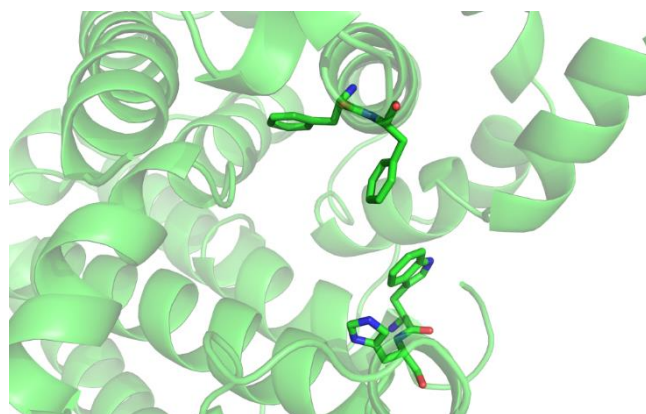
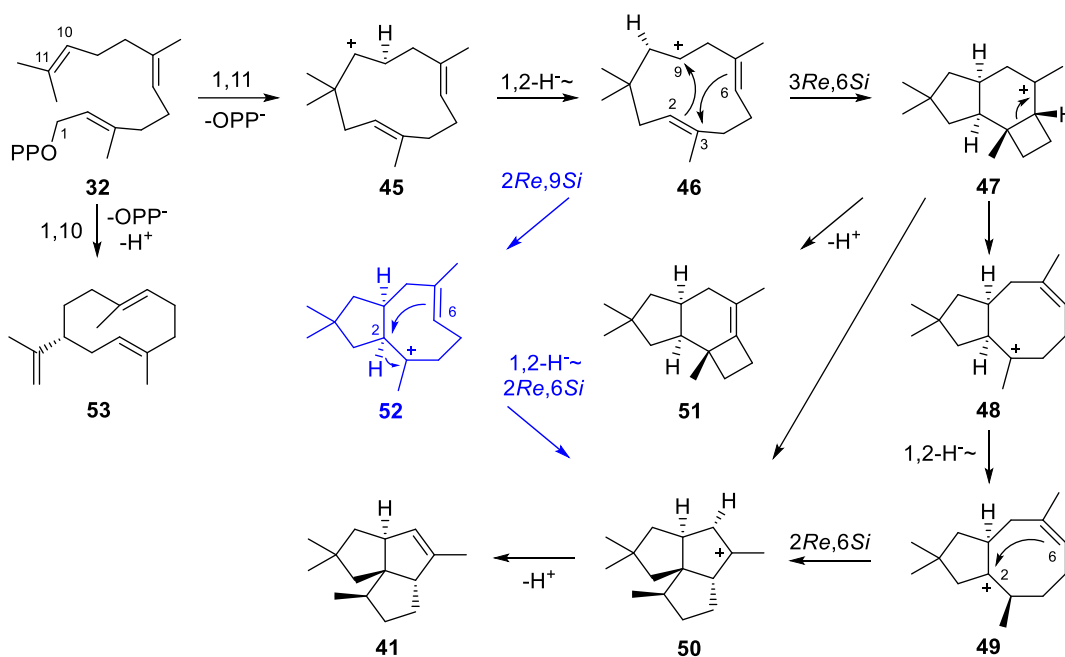


**Figure 7.** Hydrophobic pocket of pentalenene synthase (PDB 1PS1).<sup>[59]</sup> Important residues are shown in a wire model: F76 (top left), F77 (top right), W308 (right), H309 (bottom). Figure generated with PyMOL.<sup>[39]</sup>

The cyclisation mechanism<sup>[52b,68]</sup> towards **41** starts with a 1,11-cyclisation of FPP, which furnishes humulyl cation **45** (Scheme 7). After a 1,2-hydride migration to **46**, a concerted ring closure to the 7-protoilludyl cation **47** is proposed, which either directly reacts to the pentalenyl cation **50** in a dyotropic rearrangement,<sup>[69]</sup> or opens to **48**, which undergoes a 1,2-hydride shift to **49**. With overall lower energetic barriers in gas phase quantum chemical calculations, **49** can cyclise to **50**, which is finally deprotonated to **41**. Contrasting this calculation based mechanism, a classically assumed cyclisation proposed the (*E*)-configured isomer of **48**, **52** as an intermediate on the pathway from **46** to **50**.<sup>[70]</sup> In a well-designed experiment, these two mechanisms were differentiated by observing an isotope effect in the product distribution between **41** and **51** for [6-<sup>2</sup>H]FPP<sup>[71]</sup> in the H309A variant mentioned above.<sup>[68]</sup> If **51** was not a product directly branching from the pathway to **41**, but its formation is considered as a two-step process from **52**, no isotope effect for the deprotonation is expected. Therefore, the observed findings support **47** as an intermediate in the cyclisation mechanism towards **41**. This study represents an outstanding example, how site-directed mutagenesis can even indirectly assist in the investigation of cyclisation mechanisms and how much there is to learn from little changes in the active site of a TS.





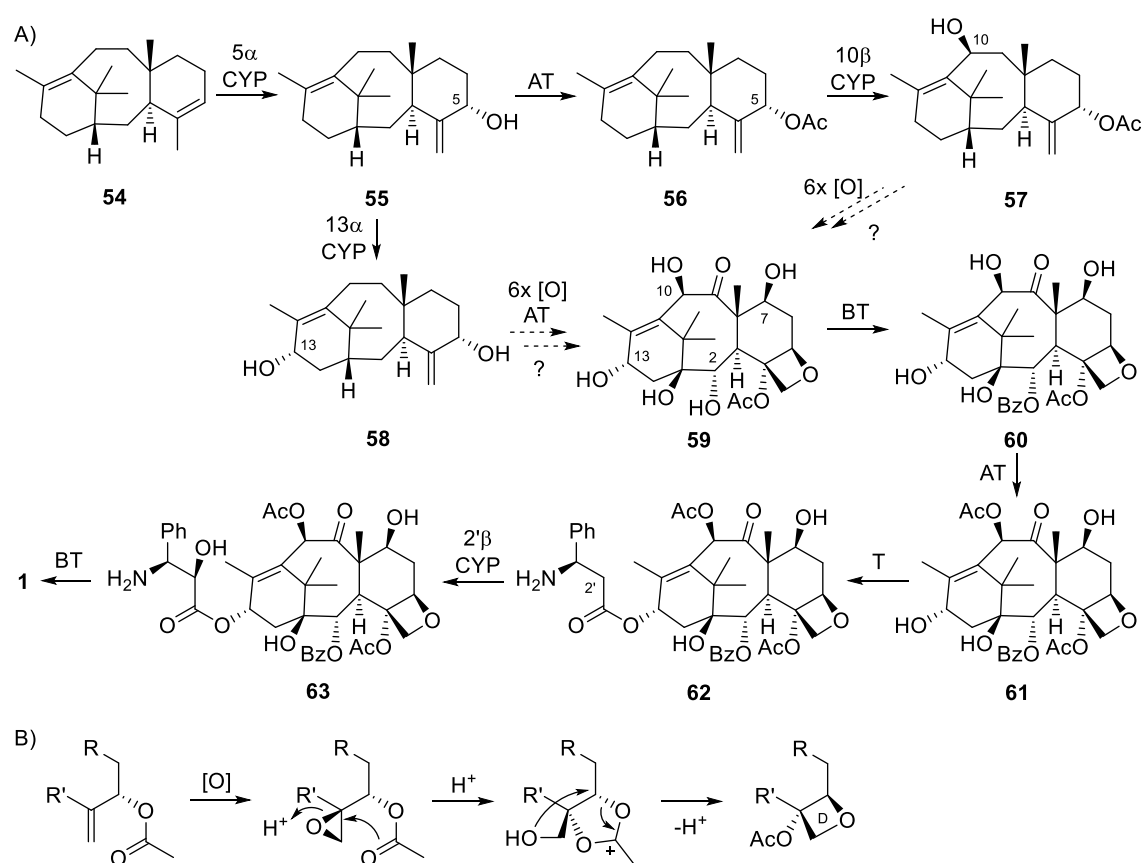
**Scheme 7.** Proposed cyclisation mechanism to pentalenene (**41**) based on quantum chemical calculations (black)<sup>[52a,68,69]</sup> and an initially suggested alternative mechanism (blue).<sup>[59,67,70]</sup>

As exemplified, type-I terpene synthases need to perform two basic functions. Firstly, they coordinate the diphosphate moiety of the substrate with polar amino acids via metal ions. This process involves subtle changes in the overall enzyme fold to archive a closed conformation,<sup>[64f]</sup> is important for capturing the substrate at a defined place and also weakens the C-O bond of the oligoprenyl residue to its diphosphate unit initiating the reaction. Since all TSs share this function, the corresponding amino acids are highly conserved within their sequences and can be used to find and assign TSs. In contrast, the second function, to provide a hydrophobic cavity, is variable on the amino acid level among TSs. Being the heart of diverse terpene biosynthesis, these cavities exclude water from the substrate preventing a premature termination of the cationic cascade, serve in stabilisation of distinct cationic intermediates by cation- $\pi$ <sup>[72]</sup> or hydrophobic interactions and guide the prefolded substrate on the potential energy surface to its product, besides hundreds of theoretically possible reaction pathways.<sup>[52a]</sup> Termination of the cascade can be archived by the bound inorganic diphosphate, by an amino acid residue, or by a water molecule within the active site.

Although the reactions catalysed by these enzymes can be highly complex and therefore stimulating for any chemist, it should be noted that TSs are based on very simple enzymatic concepts and as presented here, can be easily modified to alter the product's structure. Heavy evolutionary<sup>[73]</sup> mutations may also be the reason for the overall low sequence conservation of TSs. This combinatorial approach therefore represents a perfect synergism of life's ability to generate genetically adjustable three dimensional macromolecular structures and the versatile reactivity of carbocations to harvest an almost never-ending source of small-molecule scaffolds that can be modified to fulfil specific biological tasks.

### 1.1.5 Tailoring reactions

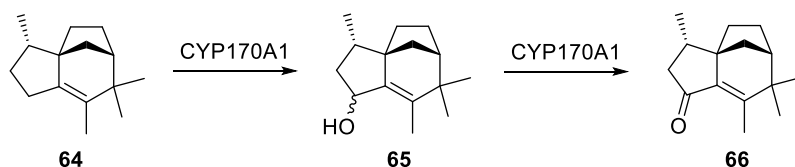
Despite the diverse structures of TS products, bioactivity besides volatile signalling properties is rarely observed among them. This is attributed to the general lack of functional groups in these molecules, especially of oxygen functionalities, resulting in limited water solubility and limited binding options towards pharmacologically relevant targets. One example for a TS product with known bioactivity is the sesquiterpene (*E*)- $\beta$ -caryophyllene, which selectively binds to the CB<sub>2</sub> receptor leading to antiinflammatory properties of the hydrocarbon.<sup>[74]</sup> However, the majority of bioactive terpenoids like **1-3** and **10** have been modified after their cyclisation by oxidation, acylation, or glycosylation. These tailoring steps also add significant diversity to the terpenoid natural products and allow the construction of specific functionalities at the carbon core structure for a biological evaluation. Tailoring pathways can be highly complex, as exemplified by the biosynthesis of **1** (Scheme 8) including 18 steps from the TS product taxa-4,11-diene (**54**).<sup>[75]</sup>



**Scheme 8.** A) Terpene modification steps in the biosynthesis of paclitaxel (**1**)<sup>[75]</sup> and B) proposed mechanism for the formation of oxetane ring D.<sup>[76]</sup> CYP: P450 monooxygenase, AT: acetyltransferase, BT: benzoyltransferase, T: transferase.

Based on the extensive research performed in the laboratories of Croteau, the pathway starts with the introduction of a hydroxy group with an isomerisation of the double bond

to give taxa-4(20),11(12)-dien-5 $\alpha$ -ol (**55**),<sup>[77]</sup> catalysed by a cytochrome P450 monooxygenase (CYP).<sup>[78]</sup> The next steps already suggested a diversification of the pathway, since the 10 $\beta$ -hydroxylase shows higher efficiency with acetylated **56**,<sup>[79]</sup> but also converts **55**. Similar promiscuity is observed with the 13 $\alpha$  hydroxylase<sup>[80]</sup> producing **58** in a reversed order of activity. A determination of a classical “sequence of steps” is therefore difficult and the following hydroxylation and acetylation steps towards the assumed pentaol intermediate **59** have not been characterised in detail up to now, although some CYPs have been found to convert acetylated surrogate substrates to introduce 2 $\alpha$ <sup>[81]</sup> and 7 $\beta$ <sup>[82]</sup> hydroxylations in a random order of steps, suggesting their functions. The reduced selectivity of these reactions may indicate a diversification of the pathway, which later converges to 10-deacetylbaaccatin III (**60**). Contrasting the inefficient isolation of **1** from *Taxus brevifolia*, this compound can be extracted in higher amounts not only from the yew bark, but also from renewable parts of the tree such as needles, and is therefore a starting point for the semisynthetic production of **1** from the faster growing European yew *T. baccata*.<sup>[83]</sup> Also the introduction of the interesting oxetane ring D is cryptic, since no enzymes connected to this moiety have been characterised to date.<sup>[76b]</sup> A currently accepted proposal (Scheme 8B) involves acid catalysed opening of a hypothetic epoxy intermediate by the neighboring acetate unit to give the rearranged product via an 1,3-dioxolan-2-yl cation.<sup>[76a]</sup> Moving forward, a transfer of a benzoyl group from benzoyl-CoA to the taxoid core was shown with a 7,10,13-triacetyl derivative of **59** to give the 2 $\alpha$  benzoylated product,<sup>[84]</sup> a reaction also suitable to produce **60**, which is then acetylated to give baaccatin III (**61**).<sup>[85]</sup> The side chain  $\beta$ -phenylalanine,<sup>[86]</sup> activated as a CoA thioester, is transferred yielding **62**, which is assumed to undergo a final 2' hydroxylation<sup>[87]</sup> with subsequent benzoylation of **63** to produce **1**.<sup>[88]</sup> This complex biosynthesis emphasises the importance of CYPs in the functionalisation of terpenes. However, with their work on albaflavenone biosynthesis in *Streptomyces coelicolor*, Cane and coworkers demonstrated nicely that even the action of one CYP is occasionally enough to promote bioactivity for the final terpenoid. The sesquiterpene *epi*-isozizaene (**64**)<sup>[89]</sup> is oxidised by CYP170A1 in two steps (Scheme 9) via an epimeric mixture of albaflavenols (**65**) to albaflavenone (**66**),<sup>[90]</sup> which possesses antibiotic activity.<sup>[91]</sup>



**Scheme 9.** Oxidation of *epi*-isozizaene (**64**) to albaflavenone (**66**) by CYP170A1 via the albaflavenols (**65**) in *S. coelicolor*.<sup>[90]</sup>

Although there are several other enzyme classes known that catalyse oxidation reactions in secondary metabolism, e. g.  $\alpha$ -ketoglutarate dependent oxygenases,<sup>[92]</sup> CYPs are predominantly found to catalyse the particularly difficult oxidation of a terpene hydrocarbon substrate as a first step of the tailoring reactions. Therefore, this enzyme family is discussed in more depth here.<sup>[93]</sup>

The camphor hydroxylating CYP P450<sub>cam</sub> from *Pseudomonas putida* has long been used as a model system for CYP reactions. From this enzyme, the first crystal structure of a CYP was obtained in 1985.<sup>[94]</sup> With an overall  $\alpha$ -helical fold, a protoporphyrin IX coordinated to a central iron ion (heme, **75**) is found in the active pocket of the enzyme (Figure 8). One axial ligand of Fe is a cysteinato side chain, whereas molecular oxygen can bind on the other side of the heme plane, where also the substrate camphor is captured with C-5 pointing towards the catalytic centre. With its active site architecture, the CYP controls both regio- and stereoselectivity of the reaction, making CYPs a valuable tool for biotechnology<sup>[95]</sup> compared to often unselective chemical oxidation procedures.

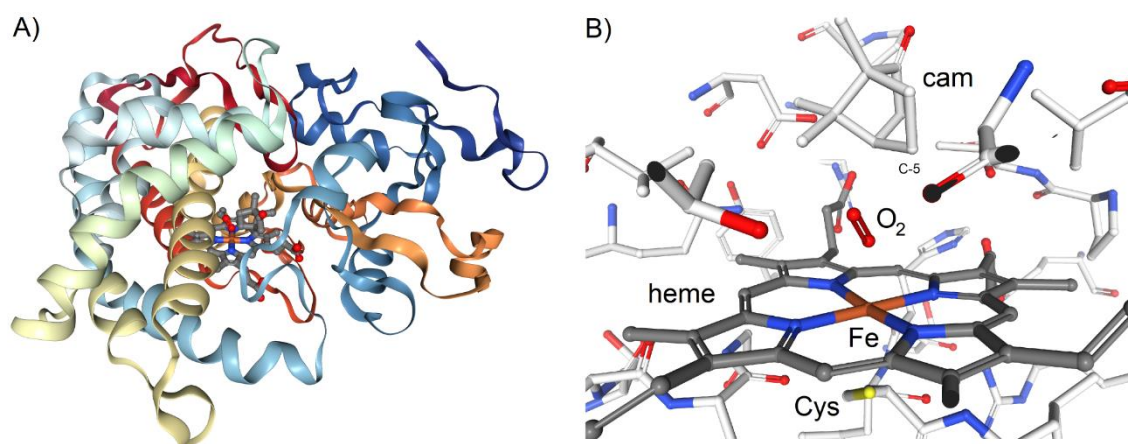
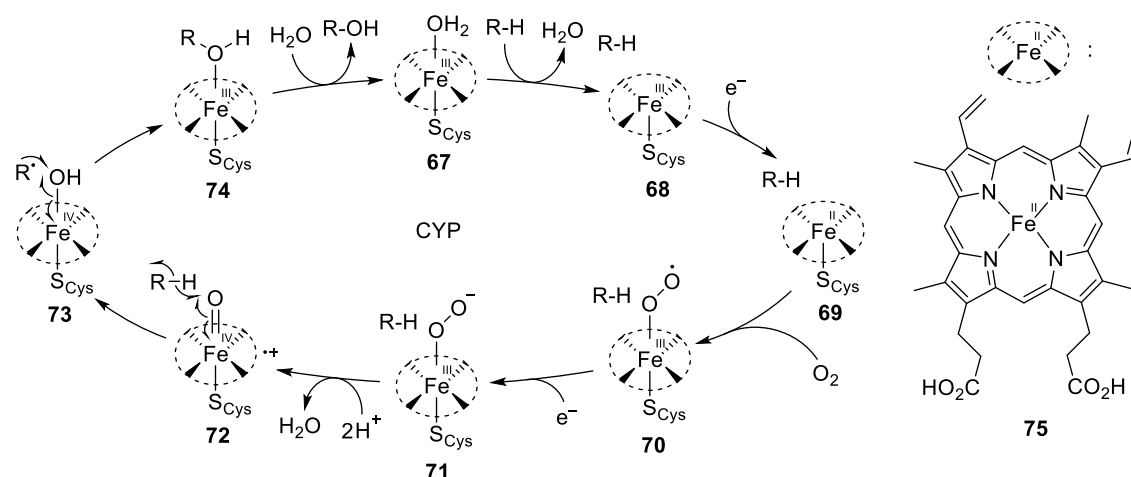


**Figure 8.** Crystal structure of P450<sub>cam</sub> from *P. putida* in complex with heme, molecular oxygen and camphor (PDB 2A1M).<sup>[96]</sup> A) Overall fold with the ligands shown as ball-and-stick model and B) active site view showing the close proximity of the hydroxylation position C-5 of camphor (cam) and the iron centre. Figure created with NGL viewer.<sup>[45]</sup>

The currently accepted catalytic cycle<sup>[97]</sup> for CYP-mediated reactions starts by coordination of the substrate to **68**, replacing the water ligand bound to Fe<sup>III</sup> in the resting state **67** (Scheme 10). This species is reduced to Fe<sup>II</sup> by a one-electron transfer to **69**, which can now coordinate molecular oxygen (**70**). A second electron transfer leads to **71**, which eliminates water by protonation to give **72** (compound I). Since **72** is the active species in the catalytic cycle, reactive enough to abstract hydrogen radicals even at non-stabilised positions, a lot of effort went into the characterisation of its electronic structure.<sup>[98]</sup> In 2010, **72** was prepared by oxidation of CYP119 with *m*CPBA and characterised by Mössbauer-, UV/Vis- and EPR spectroscopy as a Fe<sup>IV</sup>-oxo species exchange coupled to a delocalised, ligand-based radical.<sup>[99]</sup> In a mechanism called oxygen-rebound,<sup>[100]</sup> **72** can first abstract a hydrogen atom from the substrate, leaving a radical on the substrate (**73**), which occasionally lead to rearrangements<sup>[101]</sup> before a hydroxy group is recombined with the radical (rebound) to give the oxidised product in complex with the iron centre (**74**). Exchange with a water ligand to **67** closes the catalytic cycle. Although there is experimental evidence to doubt the universal action of the rebound mechanism,<sup>[102]</sup> its basic concepts are generally accepted. There are multiple systems known to supply the electrons to the reaction site, most of them being coupled

to the oxidation of NAD(P)H.<sup>[103]</sup> In context of terpene oxidising, bacterial CYP systems, small soluble redox proteins, namely iron-sulfur-cluster containing ferredoxins or FMN-dependent flavodoxins are often found to transfer electrons from their NAD(P)H consuming reductases to the CYP. In many cases, the natural redox partners of a CYP remain unknown and are replaced by substitutes as in the example of the *epi*-isozizaene oxidising CYP170A1, whose activity was reconstructed using flavodoxin and flavodoxin reductase from *E. coli*.<sup>[90]</sup> The complex electron supply chain leads to challenges for metabolic engineering in exploiting the synthetic potential of CYPs.<sup>[104]</sup>



**Scheme 10.** Commonly accepted catalytic cycle of a CYP reaction.<sup>[97]</sup>

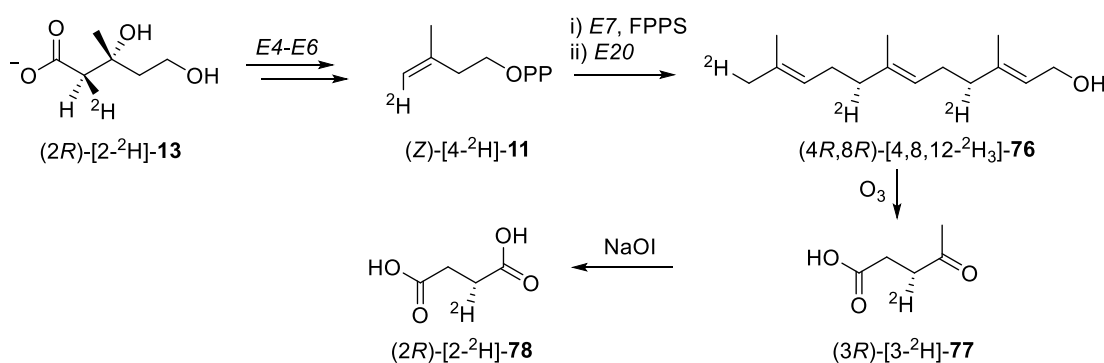
With their remarkable reactivity, CYPs represent an outstanding biosynthetic tool to selectively functionalise TS products paving the way towards highly oxidised, modified terpenoids like **1** with the help of additional O-motif processing enzymes, or preparing bioactive molecules like **66** just by oxidation. Since the bioavailability of highly unpolar molecules, including terpene hydrocarbons, is rather low, enzymes like CYPs not only contribute to the variety of terpenoid natural products, they also activate hydrocarbons making them available again for secondary metabolism, a feature that certainly added a lot of value to the terpene evolutionary success story.

### 1.1.6 Isotopically labelled compounds in terpene research

Organic chemistry nomenclature differentiates between isotopically substituted compounds, which essentially consist only of molecules with the designated nuclides at the specified positions (written in parentheses), and isotopically labelled compounds, which consist of a mixture of isotopically substituted molecules and unlabelled ones (positions and nuclides written in square brackets).<sup>[105]</sup> However, this rule is not generally followed by all publications. Therefore, the designations (parentheses or square brackets) used in the original publications are reproduced here without a re-examination of their correct use. Moreover, the term “isotopically labelled” as utilised in this work includes also the first case of isotopically substituted compounds.

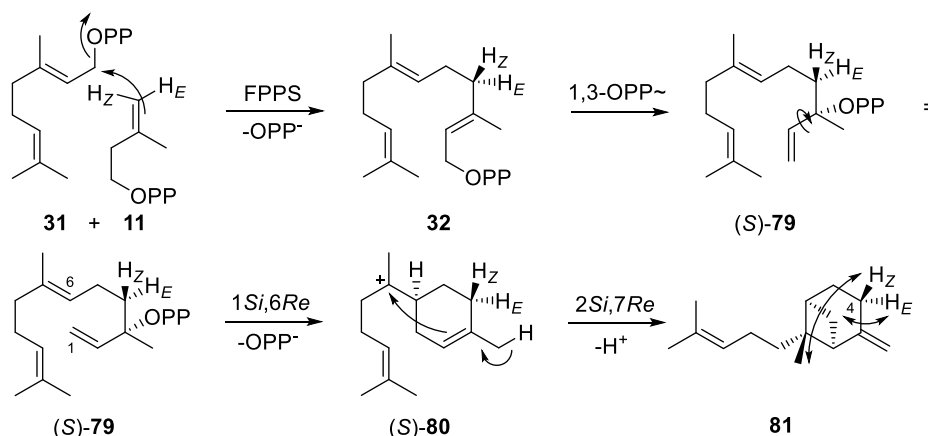
As being hinted already in the discussion of terpene biosynthesis, isotopic labelling experiments have accompanied terpene chemistry since their extensive use during the work on cholesterol (**5**).<sup>[19]</sup> The opportunity to trace back the origin of a single atom in a target structure by changing its isotopic composition to be different from the natural distribution in a precursor molecule represents a great experimental approach to test mechanistic proposals and is therefore also applied in other branches of chemistry.<sup>[106]</sup> Contrasting other labelling approaches, isotopes are mostly indistinguishable by metabolism. An exception are kinetic isotope effects observed predominantly for the different hydrogen isotopes, which may occasionally lead to valuable mechanistic insights as exemplified for pentalenene synthase (Chapter 1.1.4). Particularly for terpene biosynthesis with its high complexity of molecular rearrangement, the use of isotopes is a relatively easy approach to give valuable information in return. This section therefore presents some examples, how the use of isotopes helps elucidating the biosynthesis of terpenes and which important types of experiments have been conducted both in “classical” and in more recent literature.

To investigate the stereochemical course of the prenyltransferase reaction at C-4 of IPP, Cornforth and Popják synthesised selectively deuterated (*2R*)- and (*2S*)-[2-<sup>2</sup>H]mevalonate (**13**) isotopomers, which were converted by a mixture of pig liver enzymes to IPP.<sup>[41]</sup> A chemical degradation strategy revealed a selective incorporation of deuterium from (*2R*)-[2-<sup>2</sup>H]-**13** into the H<sub>Z</sub>-position of **11** (Scheme 11), thereby illuminating the stereochemical course of the mevalonate-5-diphosphate decarboxylase (*E6*). Extending the biosynthetic transformation of the labelled material towards FPP was then used to determine the course of the unknown elongation reaction. To do so, the absolute configuration of the deuterated positions in the enzymatically prepared FPP was determined by a phosphatase reaction to farnesol (**76**) followed by ozonolysis to levulinic acid (**77**) and haloform reaction to succinic acid (**78**), which was compared to a chiral reference compound by optical rotary dispersion measurements to be (*2R*)-[2-<sup>2</sup>H]-**78**. Confirming that no change in the stereochemical information had occurred during the degradation reactions, this finding elegantly demonstrates the reaction of the 4*Si* face of IPP in the prenyltransferase reaction (cf. Scheme 4).



**Scheme 11.** An isotopic labelling experiment inferring the stereochemical course of the PT-reaction using (*2R*)-[2-<sup>2</sup>H]-**13**.<sup>[41]</sup> *E20*: alkaline phosphatase. *E4-E7* refer to the enzymes mentioned in Scheme 1.

Besides the early stages of terpene biosynthesis, most of the terpene labelling experiments reported so far target the centre of terpene scaffold assembly, terpene synthases. Because TSs usually catalyse multiple events in one step, isotopically labelled compounds, especially oligoprenyl diphosphates are a perfect tool to experimentally question their mechanisms.<sup>[107]</sup> A pioneer in the synthesis and the extensive use of these valuable compounds is Cane, who inspired the discussion on TS mechanisms and their stereochemical details by his consequent use of isotopes.<sup>[70]</sup> He also extended the methodology of labelling experiments not only to answer mechanistic questions, but also to investigate structural features of the TS product. In the studies involving *trans*- $\beta$ -bergamotene (**81**) synthase from the fungus *Pseudorotium ovalis*,<sup>[108]</sup> which is involved in the biosynthesis of the antibiotic ovalicin,<sup>[109]</sup> enzymatically prepared enantioselectively labelled FPP isotopomers were used to deduce the absolute configuration of its product **81** (Scheme 12).<sup>[110]</sup>

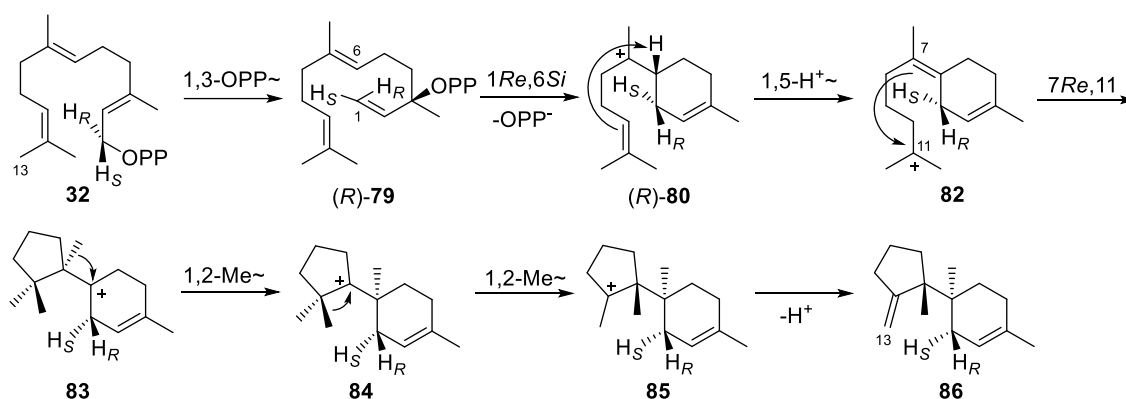


**Scheme 12.** Isotope labelling experiments for determining the absolute configuration of *trans*- $\beta$ -bergamotene (**81**).<sup>[110]</sup> Double headed arrows indicate NOE-correlations.

The isotopomers (*E*)- and (*Z*)-[4-<sup>2</sup>H]IPP were synthesised and used to elongate GPP (**31**) in an FPPS-catalysed reaction to generate two samples of (4*R*)- and (4*S*)-[4-<sup>2</sup>H]FPP. These samples were converted by cell free preparations from *P. ovalis* containing bergamotene synthase to yield labelled **81**. The cyclisation mechanism towards **81** consists of an isomerisation of FPP to (*S*)-nerolidyl diphosphate (NPP, **79**), in which the C-2,C-3 bond can rotate to allow for a 1,6-cyclisation under formation of a (*Z*)-configured double bond. This concept of overall bond isomerisation is frequently discussed in terpene biosynthesis.<sup>[111]</sup> A follow-up ring closure of the bisabolyl cation (**80**) gives **81** after methyl group deprotonation. In this sequence, the labelled position C-4 is not involved in any type of reaction. Therefore, this position can serve as a stereochemical anchor preserving the defined stereochemistry that has been applied to the cyclisation cascade. The incorporation of deuterium into one of the two diastereotopic positions at C-4 was followed elegantly by <sup>2</sup>H-NMR, which reduces the amount of background signals. Together with the relative position of both hydrogen atoms deduced by NOE measurements, the stereochemical outcome of this experiment is conclusive for the absolute configuration of **81** as shown. The efficiency of this method is based on the

difficulties associated with the determination of the absolute configuration by classical approaches, since TS products are usually not easy to crystallise and large amounts for tedious chemical derivatisation are often not obtainable. The described experimental approach was not utilised often in the following two decades of terpene research, but was further developed during the course of this work and applied multiple times on different TS products (see Chapters 4, 6–16 and 18, where more detail is added to the discussion). As an example of determining also structural features of TS products, this experimental design underlines the variety of different questions, isotope labelling experiments can potentially answer.

The mechanism of trichodiene (**86**) synthase, an enzyme which is present in many different fungi including *Fusarium sporotrichioides*,<sup>[64b]</sup> was extensively investigated by labelling experiments and still gives rise to recent discussions in the literature.<sup>[112]</sup> The sesquiterpene **86** is the precursor of many bioactive trichothecene mycotoxins.<sup>[113]</sup> As depicted in Scheme 13, the first steps of the cyclisation mechanism are similar, although enantiomeric, to the discussed mechanism for **81**, namely formation of the bisabolylium cation **80** after isomerisation of FPP to NPP. Then, a 1,5-proton transfer is discussed<sup>[114]</sup> to yield **82**, which is then cyclised to the cuprenyl cation **83** as an alternative to a direct second cyclisation with a following 1,4-hydride shift to **83**. The absolute configuration of this flexible intermediate was recently suggested as (*S*), based on accumulated experimental data including stereochemical analysis of several side products.<sup>[115]</sup> Two suprafacial 1,2-methyl group shifts via **84** and **85** yield the final product **86** after deprotonation.



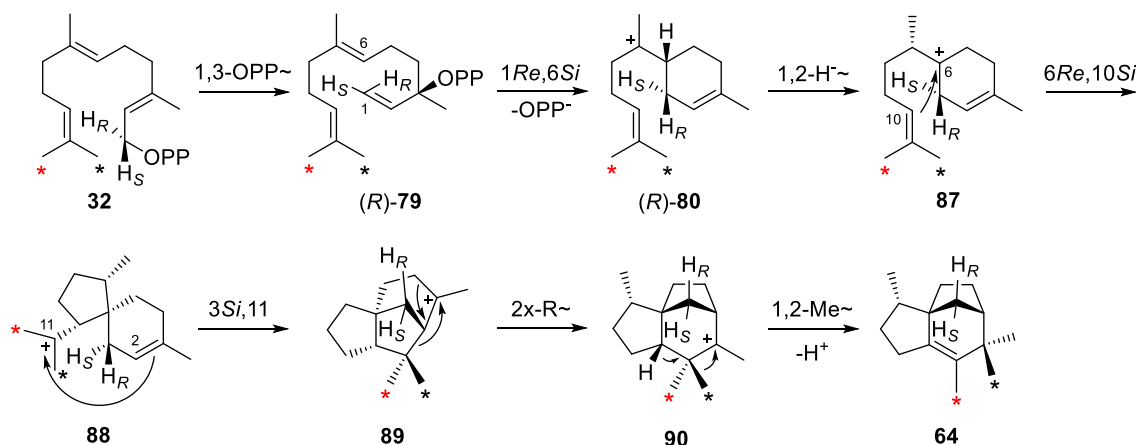
**Scheme 13.** Cyclisation mechanism towards trichodiene (**86**).

The incubation of [1,1-<sup>3</sup>H<sub>2</sub>,12,13-<sup>14</sup>C]FPP showed by retainment of both tritium labels in **86** that the isomerisation of FPP to NPP takes place without deprotonation at C-1. Furthermore, reactions with the stereoselectively tritiated samples (1*R*)- and (1*S*)-[1-<sup>3</sup>H,12,13-<sup>14</sup>C]FPP could demonstrate a net retention of configuration at C-1.<sup>[116]</sup> Together with the determination of (*R*)-NPP (**79**) as the intermediate of trichodiene synthase, which was done by observing the exclusive incorporation of <sup>14</sup>C into **86** from a mixed incubation with (*rac*)-[12,13-<sup>14</sup>C]NPP and (*S*)-(*Z*)-[1-<sup>3</sup>H]NPP,<sup>[117]</sup> these results shed light onto the stereochemical details of the isomerisation. The stereochemical course is explainable by



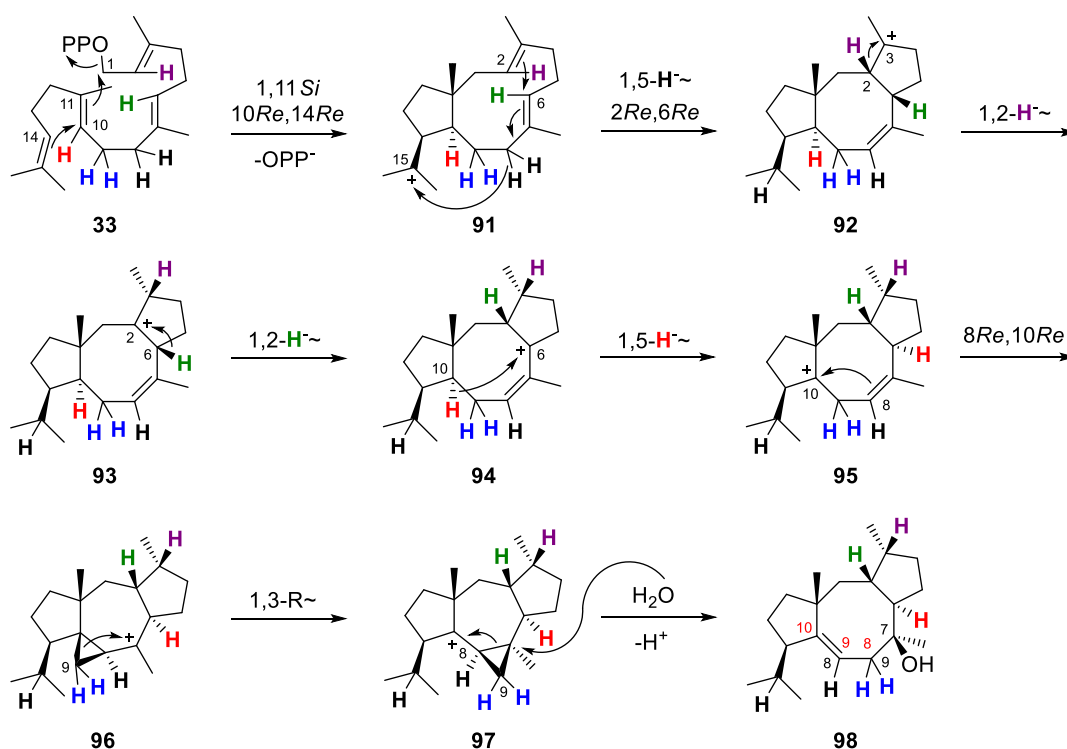
*syn*-allylic rearrangement of OPP to NPP, followed an *anti*-S<sub>N</sub>' attack at the *Re* face of C-1. Also the methyl group migrations in the later steps of the cyclisation mechanism were investigated. Therefore [6,6,6-<sup>2</sup>H<sub>3</sub>]mevalonolactone, the lactonised derivative of **13**, was fed to a trichodiene-producing fungus. Biosynthetically converted to FPP with deuterated internal methyl groups together with C-13, a loss of a single deuterium atom in the produced isotopomer of **86** indicates the origin of the methylene group being C-13 of FPP.<sup>[118]</sup> This selection of labelling experiments performed on the biosynthesis of trichodiene demonstrates, how different approaches and isotope usages can be utilised. However, some questions are not addressable by labelling, e. g. the proton vs. hydride shift discussion leading to the same atom positions in the product. In these cases, quantum chemical calculations are an indispensable approach for the mechanistic discussion.

An example of the synergistic cooperation between labelling experiments and theoretical calculations can also be found in recent work on the mechanism of *epi*-isozizaene (**64**) synthase.<sup>[89]</sup> Starting from (*R*)-**80**, which is built from FPP in the same stereochemical way as in trichodiene biosynthesis, the cyclisation mechanism (Scheme 14) proceeds with a 1,2-hydride shift to **87**, which gives rise to a 6,10-cyclisation. The interesting spirocyclic acorenyl cation **88** further cyclises to the cedryl cation **89**. Avoiding a secondary cation intermediate, a partly concerted, but asynchronous combination of alkyl shifts is discussed based on quantum chemical calculations<sup>[119]</sup> to yield the prezizayl cation **90**. A 1,2-methyl migration followed by deprotonation furnishes the final product **64**. Labelling experiments with (1*R*)- and (1*S*)-[1-<sup>2</sup>H]FPP allowed to follow the stereochemical course at C-1 during the cyclisation, but also the origin of the methyl groups involved in the methyl group migration from **90** to **64** were determined by incubation of [12,12,12-<sup>2</sup>H<sub>3</sub>]FPP and [13,13,13-<sup>2</sup>H<sub>3</sub>]FPP.<sup>[120]</sup> In contrast to the experiments performed with trichodiene synthase, these labelling studies were conducted using the recombinant, purified TS *in vitro*, which gives rise to an elegant NMR-based interpretation of the resulting data.



**Scheme 14.** Cyclisation mechanism towards *epi*-isozizaene (**64**) investigated by isotopic labelling experiments<sup>[120]</sup> and refined by quantum chemical calculations.<sup>[119]</sup> Deuterated methyl groups (-CD<sub>3</sub>) are indicated by asterisks (black: C-12, red: C-13).

How powerful modern labelling experiments can be to uncover mechanistic surprises was recently demonstrated in an outstanding study by Kuzuyama and co-workers on the cyclisation mechanism of cyclooctat-9-en-7-ol (**98**).<sup>[121]</sup> This diterpene is produced by the TS CotB2<sup>[64e]</sup> from GGPP and is further processed by two CYPs (CotB3 and CotB4) to cyclooctatin,<sup>[122]</sup> a potent inhibitor of lysophospholipase from *Streptomyces melanosporofaciens*.<sup>[123]</sup> In a feeding experiment with [U-<sup>13</sup>C<sub>6</sub>]glucose, a strange incorporation pattern at C-8, C-9, and C-10 was observed. While C-9 and C-10 were not connected, instead C-8 and C-10 were simultaneously labelled as observed by a long range decoupled TANGO-HMBC experiment. Therefore, a new mechanistic proposal including an unusual carbon skeleton rearrangement was presented and solidified by labelling experiments with deuterated GGPP isotopomers (Scheme 15).

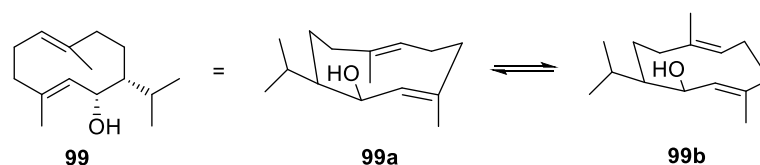


**Scheme 15.** Cyclisation mechanism towards cyclooctat-9-en-7-ol (**98**) catalysed by CotB2. The hydrogen atoms shown in bold and different colours were followed by labelling experiments.<sup>[121,124]</sup> Black carbon numbers refer to their positions in GGPP, red carbon numbers show the original numbering of **98** and cyclooctatin, respectively.

After a concerted 1,11-10,14-ring closure of GGPP using a staircase-like arrangement of the double bonds and the extruded OPP to give cation **91**, a long range 1,5-hydride shift takes place, followed by further cyclisation to fuse the tricyclic cation **92**. This hydride migration was followed by incubation of (8,8-<sup>2</sup>H<sub>2</sub>)GGPP (black) to find one deuterium located at the isopropyl group in **98**. Also the two sequential 1,2-hydride shifts to **94** via **93** were confirmed by incubating (2-<sup>2</sup>H)GGPP (purple) and (6-<sup>2</sup>H)GGPP (green) to find the deuterium atoms at the corresponding positions in **98**<sup>[124]</sup> and thus disprove an alternative 1,3-hydride migration, which is also energetically less favoured according to calculations.<sup>[125]</sup> A 1,5-hydride shift transfers the cationic charge to C-10 in **95**. Also

this migration was followed by (10-<sup>2</sup>H)GGPP (red). After formation of a cyclopropane ring in **96**, the following step of ring movement towards **97** finally leads to a rearranged ordering of carbons in the chain that is released by attack of water to give **98**. Since the hydrogen atoms at C-9 stay at their carbon atom during the cyclopropyl rearrangement, their position allow to follow the new location of C-9 with (9,9-<sup>2</sup>H<sub>2</sub>)GGPP (blue). This beautiful cascade reaction featuring two long range hydrogen migrations still inspires current studies, which also involve quantum chemical calculations on the reaction sequence inside the active site to promote a comprehensive understanding of TS catalysis in general.<sup>[126]</sup>

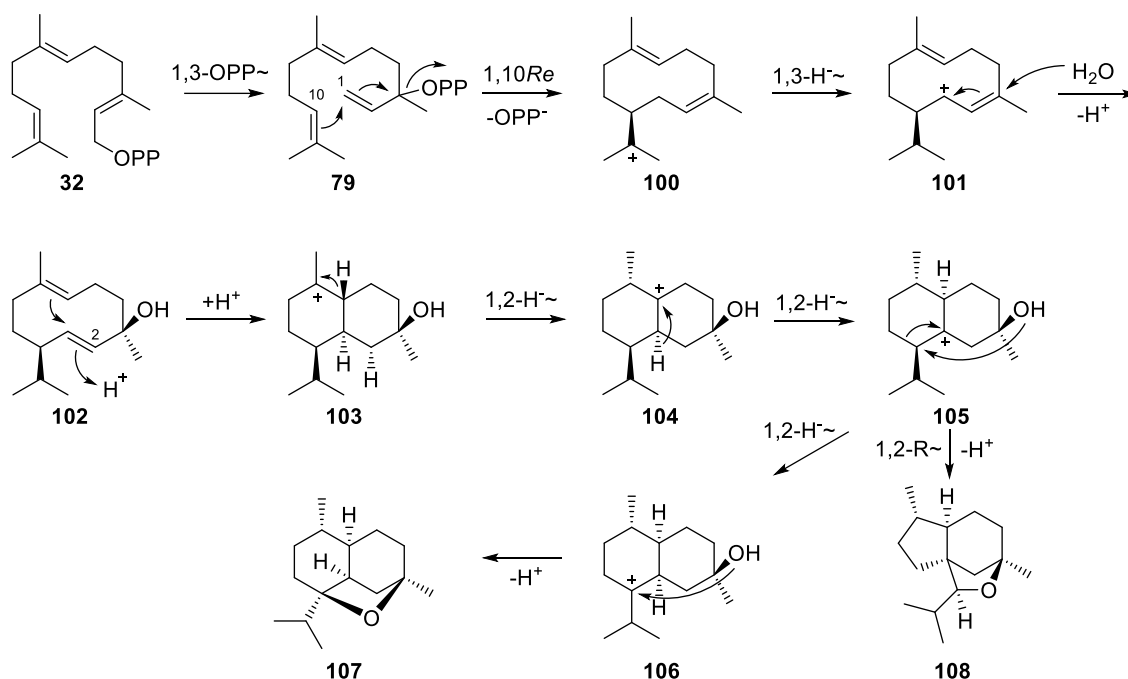
Isotopically labelled compounds can also be utilised to solve analytical problems related to terpene biosynthesis, as has been demonstrated recently in the elucidation of the NMR features of germacra-1(10),4-dien-6-ol (**99**, Scheme 16) by incubation of all fifteen (<sup>13</sup>C<sub>1</sub>)-isotopomers of FPP with the corresponding synthase from *S. pratensis*.<sup>[127]</sup> This extensive work not only cleared up the complicated NMR data of **99** originating from a mixture of its two conformers **99a** and **99b**, a <sup>13</sup>C, <sup>13</sup>C-COSY spectrum<sup>[128]</sup> of fully labelled **99** obtained from (<sup>13</sup>C<sub>15</sub>)FPP also allowed for a detailed assignment of all peaks to **99a** and **99b**. Additionally, the EI-MS fragmentation mechanism and the Cope rearrangement of **99** were studied.



**Scheme 16.** Structure of germacra-1(10),4-dien-6-ol (**99**), which exists as a mixture of conformers **99a** (DD) and **99b** (UD) in solution hampering NMR assignment.

Investigations towards the biosynthesis of corvol ethers A (**107**) and B (**108**) from *Kitasatospora setae*<sup>[129]</sup> also exemplified the use of deuterated water for labelling experiments. During the cyclisation mechanism towards the unusual sesquiterpene ethers catalysed by a single TS, a reprotonation step is observed, opening the opportunity for a deuterium incorporation from the surrounding medium. Starting with an isomerisation of FPP to NPP, a 1,10-cyclisation yields the germacradienyl cation **100** (Scheme 17). A 1,3-hydride migration gives the allylic cation **101**, which is quenched by water to give germacrene-D-4-ol (**102**) as a neutral intermediate. This is reprotonated at C-2 to initiate further cyclisation to **103**. Two sequential 1,2-hydride shifts yield **104** and **105**, which either undergoes an additional 1,2-hydride shift to **106** to furnish corvol ether A (**107**), or stabilises by a Wagner-Meerwein-rearrangement to give corvol ether B (**108**). The critical reprotonation step was followed by an incubation of (2-<sup>13</sup>C)FPP with the recombinant TS in D<sub>2</sub>O, giving rise to a triplet in <sup>13</sup>C-NMR because of direct <sup>13</sup>C-<sup>2</sup>H spin-spin coupling. Also the relative configuration of the introduced hydrogen was evident from HSQC spectroscopy. As a combination of <sup>2</sup>H and <sup>13</sup>C is a suitable tool for a sensitive detection of the deuterium position, the 1,2-hydride shifts were followed by incubation of (6-<sup>13</sup>C,1,1-<sup>2</sup>H<sub>2</sub>)FPP resulting in two triplets in <sup>13</sup>C-NMR for **107** and **108**, which were not observed in case of (7-<sup>13</sup>C,1,1-<sup>2</sup>H<sub>2</sub>)FPP.<sup>[130]</sup> This clearly rules out an alternative 1,3-

hydride shift, which turned out to be less favoured as judged by gas phase quantum chemical calculations.



**Scheme 17.** Cyclisation mechanism towards corvol ethers A (**107**) and B (**108**).<sup>[129–131]</sup>

As shown here in a few cases, although the basic principles remained the same, the style of labelling experiments changed a lot in the past decades together with an evolvement of both analytical methods to detect the labelled position and molecular biology techniques. For example, the development of modern NMR spectroscopy led to a decrease in the use of radioisotopes like  $^{14}\text{C}$  and  $^3\text{H}$  in favour of their corresponding stable isotopes  $^{13}\text{C}$  and  $^2\text{H}$  and superseded the need of chemical degradation reactions to locate the label. Also the recombinant production of enzymes in a heterologous host made the interpretation of results more feasible compared to the work with cell free extracts and tissue based enzyme preparations. However, the improvements made for in vitro techniques did not lead to a reduced value of classical in vivo labelling (feeding-) experiments, which are still widely used and represent an easy and nevertheless powerful method as exemplified with the initial experiment on the mechanism of CotB2. The main disadvantage of labelling experiments is the tedious preparation of labelled compounds and their high costs. This downfall emphasises the need for reliable synthetic methods to implement isotopes at any position needed in a precursor for a good experimental design. Because of the advantageous high diversification in terpene biosynthesis, common labelled precursors such as mevalonate (**13**) or deoxy-D-xylulose for in vivo studies, but also the (oligo-) prenyl diphosphates (**11-12**, **31-34**) for in vitro investigations can be applied repeatedly on different TSs to answer different mechanistic questions, therefore a library of labelled compounds is highly desirable. The synthetic extensions of such an in vitro toolbox and its applications on natural enzymes (Chapters 3–19) and also on an artificial system (Chapter 20) resemble the focus of this thesis to gain deeper insights into the mechanistic riddles provided by terpene biosynthesis.

## 1.2 Volatile aromatic compounds from fungi

Fungi, but also other microorganisms like bacteria,<sup>[132]</sup> emit a large number of small molecules called volatile organic compounds (VOCs), which belong to very different compound classes and include not only terpenes, but also alcohols, esters, hydrocarbons, lactones, acids, ketones, aldehydes, or aromatic compounds.<sup>[133]</sup> While VOCs can be seen as air pollutants<sup>[134]</sup> connected with human health issues,<sup>[135]</sup> they are also specific marker molecules that can be used to detect the presence of a pathogenic strain.<sup>[136]</sup> Naturally, they also contribute to the flavour of edible mushrooms.<sup>[137]</sup> Therefore both structure and source of volatiles are of high interest, but also their biosynthesis as their occurrence might be connected to the production of pathogenicity factors like toxins.<sup>[138]</sup> A special class of VOCs are small aromatic compounds, with some fungal examples being depicted in Figure 9.

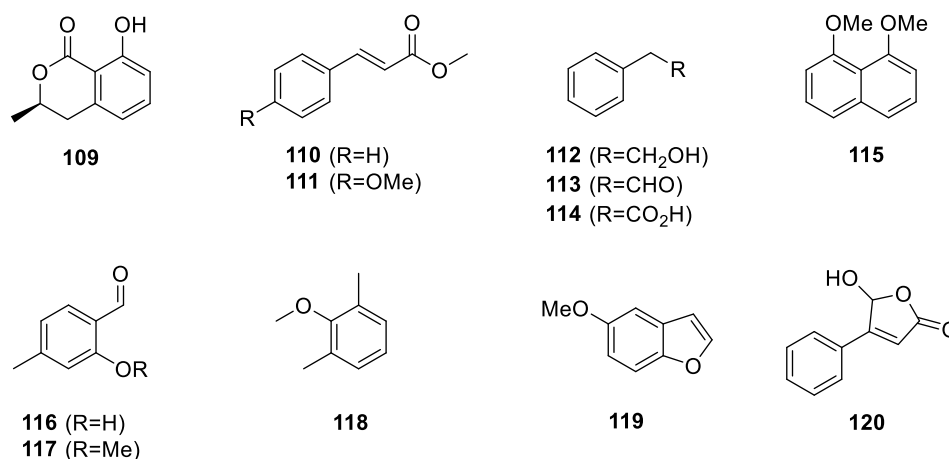
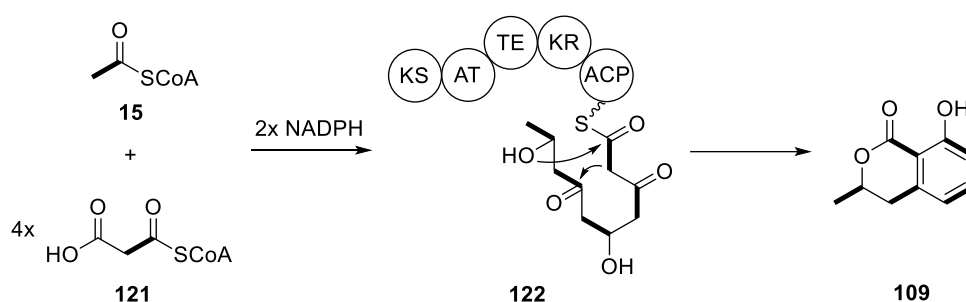


**Figure 9.** Structures of selected aromatic fungal volatiles.

The dihydroisocoumarin mellein (**109**) was found in different *Aspergillus* strains, including *Aspergillus ochraceus*,<sup>[139]</sup> from which the mycotoxin ochratoxin A was first isolated.<sup>[140]</sup> Although **109** resembles the core structure of the toxin, the two molecules do not necessarily co-occur.<sup>[141]</sup> Both methyl cinnamate (**110**) and its methoxylated derivative **111** were isolated from the wood-decaying fungus *Lentinus lepideus*, with **110** mainly contributing to the scent of the fungus.<sup>[142]</sup> A particularly widespread volatile compound is 2-phenylethanol (**112**), which was reported from members of *Trichoderma*, *Fusarium*, *Aspergillus*, *Penicillium*, and *Tuber*, sometimes accompanied by the corresponding aldehyde **113** and the carboxylic acid **114**.<sup>[133]</sup> Also higher aromatic systems like the naphthalene derivative **115**, identified from several *Hypoxyton* strains,<sup>[143]</sup> are occasionally found. The substituted benzaldehydes **116** and **117** were both identified in *H. invadens*,<sup>[143b]</sup> whereas the anisol **118** was found in *Fusarium fujikuroi*.<sup>[144]</sup> The structural variety of aromatic volatiles also includes heterocyclic aromatic systems like the benzofuran **119**, which was isolated from the wood-decaying fungus *Stereum subpileatum*.<sup>[145]</sup> Finally, lactone **120** is a metabolite of the phytopathogenic fungus *Epicloe typhina*, which also shows weak antifungal activities.<sup>[146]</sup>

With this many different structural motifs exemplified by the discussed molecules, a common biosynthetic origin is not evident. Whereas single representatives like **110** and **111** are likely derived from amino acids, most of the aromatic compounds are thought to originate from polyketide synthases, although the responsible biosynthetic gene clusters are only rarely known, e. g. for **109** in *Penicillium nordicum*<sup>[147]</sup> and in *Parastagonospora nodorum*.<sup>[148]</sup>

Polyketides are a large family of natural products produced by polyketide synthases (PKS), which are large multi-domain enzymes or enzyme complexes found in bacteria, fungi, plants and even in few animals. The reactions, these enzymatic machineries catalyse, are similar to those known for fatty acid biosynthesis, but in contrast to fatty acid synthases, polyketides may also only be partially reduced (PR-PKS) or even non-reduced (NR-PKS), leading to different core structures.<sup>[149]</sup> In fungi, mostly iterative PKSs are found, which are reusing their domains multiple times in a cyclic way.<sup>[150]</sup> The production of a small aromatic molecule is exemplified by the biosynthesis of mellein (**109**) shown in Scheme 18.



**Scheme 18.** Biosynthesis of mellein (**109**) by a PR fungal polyketide synthase.<sup>[148]</sup> KS: ketosynthase; AT: acyltransferase; TE: thioesterase; KR: ketoreductase; ACP: acyl carrier protein. The incorporation of acetate units is shown by bold bonds.

Acetyl-CoA (**15**) serves as the starter unit, which is elongated four times by malonyl-CoA (**121**) in an iterative mechanism, in which the bonds are formed by Claisen condensation reactions with a loss of CO<sub>2</sub> in each step. Within two cycles, the ketoreductase (KR) domain additionally acts under consumption of NADPH to yield two alcohol functions in the final product **122**. An intramolecular Knoevenagel condensation fuses the six-membered ring that is aromatised by elimination of water and keto-enol tautomerism. Finally, the lactone is built by an attack of the hydroxy group at the thioester, catalysed by the thioesterase (TE) domain, thereby releasing the product **109** from the machinery. Exemplified by this small PKS, volatile aromatic compounds can be biosynthesised conveniently by polyketide metabolism, either as a target molecule or as a short drop-off (side) product of a larger polyketide.<sup>[151]</sup>

A completely different idea for the source of small aromatic compounds is discussed for fungi that are able to grow on or degrade wood, since its major component, lignin, is a phenolic copolymer. Because of its chemical inertness, lignin-degrading fungi apply reactive enzymatic tools, like laccase, lignin peroxidase or manganese peroxidase.<sup>[152]</sup>

The resulting lignin degradation products are toxic for most fungi, therefore wood-decaying fungi have developed a sophisticated metabolism for small aromatic compounds,<sup>[153]</sup> which might be an additional source for observing those as volatiles.

With lignin being the second-most abundant biopolymer on earth after cellulose, much effort has been put in developing this mostly unused resource towards the production of high value organic chemicals.<sup>[154]</sup> However, the complex, stable structure of lignin and its inhomogeneity from different sources demands for a robust processing, which significantly hampers a sustainable conversion of lignin to petrochemically relevant molecules. A biotechnology-based approach, in which the genes relevant for lignin degradation in nature<sup>[155]</sup> are used for an efficient degradation process by microorganisms may address this problem in a productive way.<sup>[156]</sup>

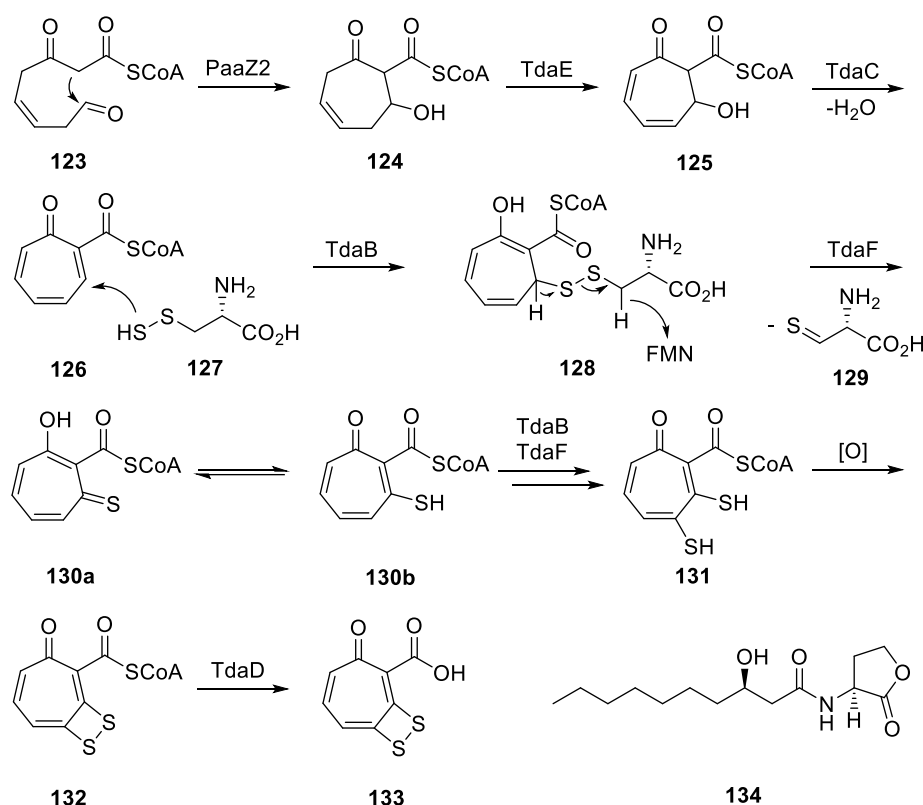
During the course of this work, fungal aromatic volatiles from two *Hypoxylon* strains were identified (Chapter 21) and the sustainable biotechnological conversion of lignin to polyamide 66 (nylon) using genetically engineered bacteria was pursued (Chapter 22).

### 1.3 Biosynthesis and regulation of tropodithietic acid

Tropodithietic acid (TDA, **133**, Scheme 19) is a structurally unique antibiotic produced by different microorganisms including marine  $\alpha$ -proteobacteria, which belong to the *Roseobacter* clade. It features two sulfur atoms arranged in a four-membered ring, a rare motif in natural products. TDA was first isolated in 1984 from *Pseudomonas* sp. CB-104, assigned with the name of its tautomer thiotropocin.<sup>[157]</sup> Although its mechanism of action is still under debate, a recent suggestion involves the role of TDA as a neutral proton antiporter.<sup>[158]</sup> Thereby overcompensating the proton moving force, it takes up extracellular protons, moves through the membrane and exchanges them for cytoplasmic cations. This mechanism is similar to that of polyether antibiotics like salinomycin or monensin.<sup>[159]</sup> TDA plays an important ecological role in controlling algal blooms, which was investigated in the producing model organism *Phaeobacter inhibens* DSM 17395, originally referred to as *P. gallaeciensis* and *Roseobacter gallaeciensis*.<sup>[160]</sup> These  $\alpha$ -proteobacteria live in close relationships to marine eukaryotes like the coccolithophoric microalga *Emiliania huxleyi*,<sup>[161]</sup> for which massive blooms (e. g. covering ocean surfaces of 250,000 km<sup>2</sup>) can be observed occasionally.<sup>[162]</sup> In a symbiosis, the bacteria profit from the rich nutritional sources provided by the alga. In return, *P. inhibens* produces TDA in addition to growth promoting substances, to protect the alga from bacterial phytopathogens. Triggered by the lignin degradation product *p*-coumaric acid, *P. inhibens* changes its metabolism towards a pathogenic phase, in which it attacks its former symbiont *E. huxleyi* by the production of roseobactin, an algicidal class of secondary metabolites, and other metabolites finally leading to cell death.<sup>[163]</sup> This switch may have a crucial role in rationalising the rapid growth and decay of marine algal blooms.

The biosynthesis of TDA is largely unknown, although the gene cluster *tdaA-F* responsible for its production was identified.<sup>[164]</sup> As suggested by early labelling experiments with [U-<sup>13</sup>C<sub>6</sub>]glucose and [1,2-<sup>13</sup>C<sub>2</sub>]phenylacetic acid,<sup>[165]</sup> the metabolic

origin of the tropone backbone is located in the phenylacetic acid catabolic pathway.<sup>[166]</sup> Within the bacterial pathway, aldehyde **123** is usually further oxidised towards the carboxylic acid by the N-terminal dehydrogenase domain of PaaZ to allow for a  $\beta$ -oxidation-like disassembly of the carbon chain. In *P. inhibens*, **123** is proposed to be the branching point towards the biosynthesis of TDA. Interestingly, the dehydrogenase domain of PaaZ can be deactivated by a single point mutation E256Q that leads in turn to ring closure, to give a dehydrated derivative of **124**.<sup>[167]</sup> In *P. inhibens*, a copy of the *paaZ* gene is found, *paaZ2*, in which the dehydrogenase domain is heavily changed compared to the original sequence putatively leading to inactivity. This finding lead to a proposed biosynthetic pathway for TDA starting from **124**, which is shown in Scheme 19.<sup>[168]</sup>



**Scheme 19.** Proposed biosynthesis of tropodithietic acid (TDA, **133**)<sup>[168]</sup> and the structure of its autoinducer (*R*)-3OH-C<sub>10</sub>-HSL (**134**).

In an unknown order of steps, **124** is oxidised by TdaE, an enzyme with high homology to acyl-CoA dehydrogenases. Water may be eliminated from **125** by TdaC, a dehydratase, which furnishes **126**. Their occurrence is also supported by the detection of tropone and its hydrated derivative in headspace extracts from *P. inhibens*,<sup>[169]</sup> which may arise easily by thioester hydrolysis and decarboxylation. The sulfur source in this mechanism, *S*-thiocysteine (**127**), is thought to arise from cystine catalysed by the cystathionine- $\beta$ -lyase-homologue PatB.<sup>[170]</sup> TdaB shows homology to glutathione-*S*-transferases and may therefore catalyse the nucleophilic attack of **127** to **126** to yield the adduct **128**. By an oxidation catalysed by TdaF, this molecule is degraded to **130**. TdaF features a FMN binding site and is similar to phosphopantothenoylecysteine



decarboxylases, which catalyses a similar reaction, completing its cycle by the regeneration of FMN with the reduction of a thioaldehyde.<sup>[171]</sup> A similar mechanism can therefore be assumed for TdaF. To introduce the second sulfur atom, TdaB and TdaF may act a second time on the extended Michael system in **130** to give **131**, which is spontaneously oxidised to **132**. A final cleavage of CoA catalysed by the thioesterase TdaD furnishes TDA (**133**). Since this proposed pathway is mainly based on bioinformatic analysis, an experimental verification of the single steps is desirable, but still pending.

Also the regulation of the TDA biosynthetic gene cluster was investigated revealing that TDA itself acts as an autoinducer for its own production.<sup>[172]</sup> Moreover, it has similar effects at low concentrations compared to known quorum sensing (QS) mediating molecules suggesting that TDA also plays a role in signalling between the bacterial cells.<sup>[173]</sup> QS describes an intracellular communication system that has effects on the regulation of specific genes, which may be involved in the formation of biofilms, production of secondary metabolites or an overall adaptation to environmental influences.<sup>[174]</sup> A model system for studying QS in bacteria is represented by the bioluminescence emission in *Aliivibrio fischeri*.<sup>[175]</sup> In this marine bacterium, the luminescence is heavily influenced by LuxR,<sup>[176]</sup> a transcriptional regulator that is dependent on the presence of *N*-acylhomoserine lactones (AHLs).<sup>[177]</sup> AHLs, which are synthesised from *S*-adenosyl methionine condensed to an acyl donor by AHL synthase LuxI, are therefore signalling molecules that promote the bioluminescence in *A. fischeri* even across the cell border. In this way, the bioluminescence can be restricted to situations of high cell density, e. g. in light organs of marine animals.<sup>[178]</sup> The AHL chain length and functionalisation is thereby specific for the regulation system determined by the LuxR binding pocket and can vary between different species. Since homologous QS systems are widespread in *Roseobacter* clade bacteria,<sup>[179]</sup> also in *P. inhibens* the biosynthesis of TDA is regulated by a similar system, which has been shown to use the AHL (*R*)-3OH-C<sub>10</sub>-homoserine lactone (**134**).<sup>[180]</sup> Although some inducing mechanisms have been disclosed, the details of the symbiotic interactions between TDA producing bacteria and their associated eukaryotes still remain to be discovered to shed more light into the ecological background of this unique natural product.

In this work, the biochemical properties of one enzyme involved in TDA biosynthesis (PatB, Chapter 23) and in vitro substrate selectivities of AHL synthases from *Roseobacter* group bacteria with substrate analogues were studied (Chapter 24).

## Chapter 2

### **Recent highlights in biosynthesis research using stable isotopes**

Jan Rinkel and Prof. Dr. Jeroen S. Dickschat\*

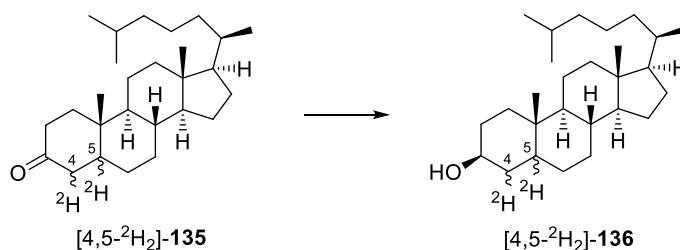
*Beilstein J. Org. Chem.* **2015**, *11*, 2493–2508.

The review “Recent highlights in biosynthesis research using stable isotopes” is attached in Appendix A.

## Introduction

As introduced in Chapter 1.1.6, isotopically labelled compounds have been extensively used in terpene biosynthesis research. To gain a more general overview of this classical method at the beginning of this cumulative doctoral thesis, recent examples for isotopic labelling, including also its applications for other classes of natural products, were condensed to a short review.

The beginning of the successful story of isotope usage to investigate biochemical processes can be dated back to 1935, when Schoenheimer and Rittenberg published an article about their experiments with deuterated fatty acids and their metabolism. They also described a defined feeding experiment with the biochemical conversion of deuterated coprostanone (**135**) to coprostanol (**136**) by humans and dogs (Scheme 20). Already recognising the impact of their method on future investigations, the authors described its numbers of applications as “almost unlimited”.<sup>[181]</sup>



**Scheme 20.** One of the first isotopic labelling experiments in biochemistry: In vivo reduction of deuterated coprostanone (**135**) to deuterated coprostanol (**136**).

The incorporation of <sup>15</sup>N into amino acids<sup>[182]</sup> and the observation of <sup>14</sup>CO<sub>2</sub> fixation in photosynthesis<sup>[183]</sup> represent further ground-breaking results. With isotopes being superior to other chemical labelling methods, because their presence is mostly undetectable for metabolism, during the next decades isotopic labelling experiments quickly turned the focus of biochemistry to dynamic processes rather than static descriptions.<sup>[19]</sup> The rise of NMR spectroscopy shifted the use of isotopes from radioactive to stable, NMR active ones making the position of label accessible without any chemical degradation reactions. However, since the first extensive applications of the isotope tracer technique during the investigations on cholesterol biosynthesis, a lot of different new methods within molecular biology, genetics, biotechnology, structural biology and computational chemistry have evolved and are available to biosynthesis research now. The importance of isotopic labelling approaches is addressable by reviewing recent applications of isotopes in biosynthesis research, structured according to the main classes of natural products namely polyketides, non-ribosomal peptides, hybrids thereof, terpenes, and additionally some aromatic compounds biosynthesised via the shikimate pathway.

## Summary

The short survey through isotopic labelling experiments conducted to elucidate the biosynthesis of various examples from major classes of natural products revealed that this method is still a valuable tool for revealing mechanistic surprises and solidifying biosynthetic proposals.<sup>[184]</sup> This was exemplified on different biosynthetic studies, such as the interesting folding mode in the biosynthesis of the polyketide clostrubin A (**137**, Figure 10),<sup>[185]</sup> the incorporation of acetate and L-isoleucine into trioxacarcin A (**138**)<sup>[186]</sup> and the epoxidation of the polyene intermediate in the assembly of coelimycin P1 (**139**)<sup>[187]</sup> followed by <sup>18</sup>O incorporation.

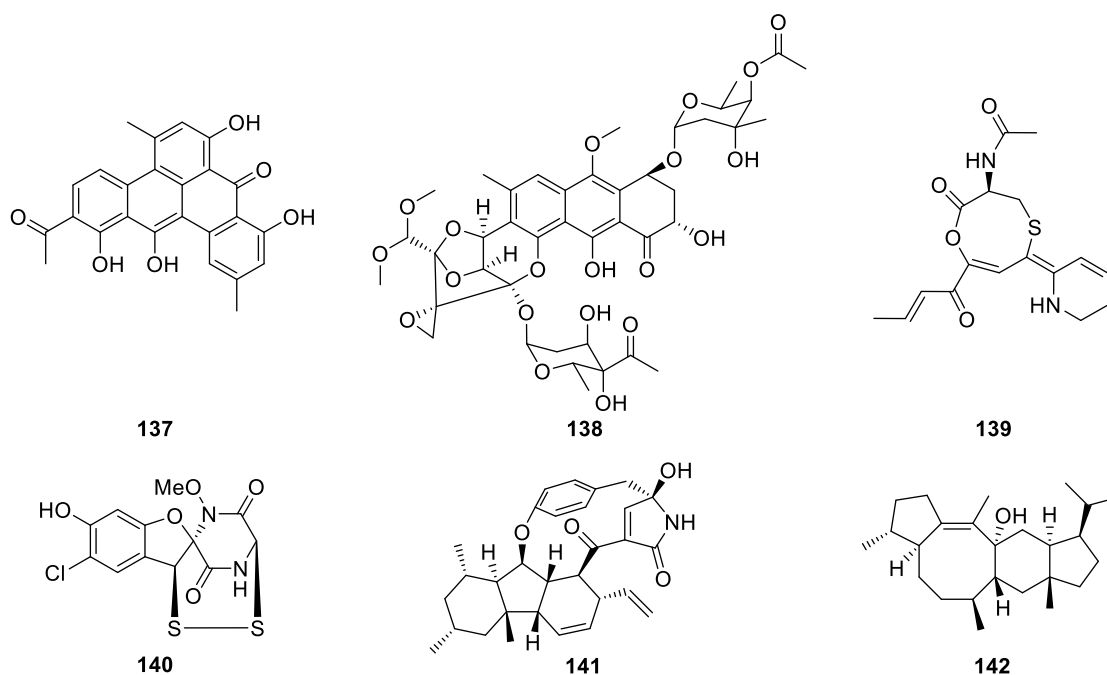


**Figure 10.** Structures of selected reviewed natural products, whose biosyntheses have been investigated using isotopically labelled compounds.

But also besides the polyketide class of natural products, multiple reviewed examples showed the applications of isotopes, such as the biosynthesis of the non-ribosomal peptide synthase (NRPS) product aspirochlorine (**140**),<sup>[188]</sup> which surprisingly turned out to be biosynthesised from two units of phenylalanine instead of glycine and phenylalanine. Additionally the [9]paracyclophane formation in the biosynthesis of the NRPS/PKS hybrid pyrrocidine A (**141**)<sup>[189]</sup> and the cyclisation towards the terpene sesterfisherol (**142**)<sup>[190]</sup> were reviewed in the context of the conducted labelling experiments.

In most of these modern biosynthetic studies, isotopically labelled compounds are not used exclusively, but combined with other methods from molecular biology to give a comprehensive picture of a biosynthetic pathway. From these combined studies, synergistic effects of the applied methods can be concluded that revalue the drawn conclusions. Therefore, even nowadays isotopic labelling experiments remain a highly useful tool sometimes prone to reveal spectacular mechanistic surprises.

## Chapter 3

### Lessons from 1,3-Hydride Shifts in Sesquiterpene Cyclizations

Jan Rinkel, Dr. Patrick Rabe, Dr. Paolina Garbeva and Prof. Dr. Jeroen S. Dickschat\*

*Angew. Chem. Int. Ed.* **2016**, *55*, 13593–13596; *Angew. Chem.* **2016**, *128*, 13791–13794.

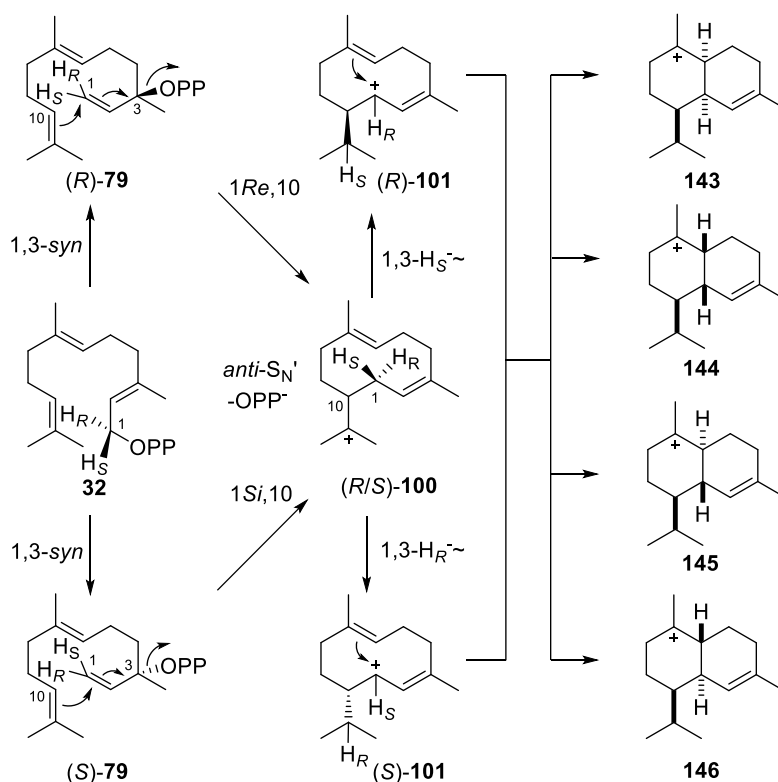
Reprinted from *Angew. Chem. Int. Ed.* **2016**, *55*, 13593–13596 and *Angew. Chem.* **2016**, *128*, 13791–13794 with kind permission from John Wiley and Sons.

The synthesis of the utilised isotopomers of FPP, the incubation experiments with the recombinant TSs and their analyses were performed by me.

The publication “Lessons from 1,3-Hydride Shifts in Sesquiterpene Cyclizations” is attached in Appendix B.

## Introduction

After reviewing recent applications of isotopically labelled compounds in the elucidation of biosynthetic mechanisms, their application for revealing selected aspects in the biosynthesis of cadalanes, a group of sesquiterpenoid natural products, was pursued. All cadalanes share the same initial cyclisation steps starting from FPP to build up a basic skeleton of two fused six-membered rings as shown in Scheme 21. Based on the relative configuration of the tertiary cations **143–146**, they can be subdivided into the amorphanes with their intermediate **143**, the muurolanes originating in **144**, the cadinanes, which are derived from cation **145** and the bulgaranes (from **146**).<sup>[111]</sup> Excluding the latter, rarer group, members associated to the other three classes are abundant sesquiterpenes found frequently in plants, bacteria, and fungi.

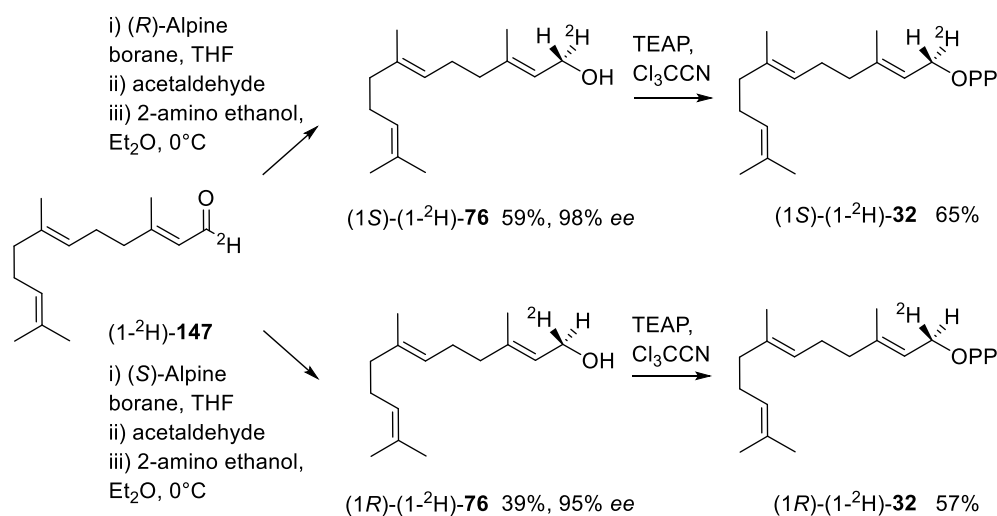


**Scheme 21.** First cyclisation steps towards the cadalane sesquiterpenes.

Studies targeting the stereochemical fate of the C-1 hydrogen atoms, mostly revealed the combination of a 1,3-syn-allylic rearrangement towards NPP (**79**) followed by an anti-S<sub>N</sub>' ring closure.<sup>[191]</sup> These constraints lead to a defined stereochemistry at C-1 in cation **100**, regardless whether (R)-NPP or (S)-NPP is involved in the cyclisation. In turn, this results in either H<sub>R</sub> being in close proximity to the cationic centre in (R)-**100** to undergo a 1,3-hydride shift to (S)-**101** or H<sub>S</sub> is conducting the shift in a reverse situation to give (R)-**101**. This stereochemical link is to be investigated on a broader basis using at C-1 stereoselectively deuterated FPP isotopomers and suitable sesquiterpene synthases made available in previous work<sup>[127,129,192]</sup> for in vitro incubation experiments.

## Summary

Direct evidence for the 1,3-hydride shift in the mechanism of the investigated seven TSs was obtained by incubation of (11-<sup>13</sup>C,1,1-<sup>2</sup>H<sub>2</sub>)FPP resulting in a triplet in <sup>13</sup>C-NMR for all cases. These results also exclude the alternative of two sequential hydride shifts. Although the <sup>13</sup>C-labelling at C-11 dramatically increased the sensitivity of the NMR measurements, the synthesis of a multiple labelled substrate is tedious. Therefore, the stereochemical investigations were carried out without <sup>13</sup>C-label, since the 1,3-hydride shift can also be followed conveniently by GC/MS observing *m/z* of the isopropyl cleavage fragment. Despite multiple approaches towards the target isotopomers (1*R*)- and (1*S*)-(1-<sup>2</sup>H)FPP by enantioselective reduction of farnesal (**147**) or (1-<sup>2</sup>H)farnesal are described in the literature including the use of alcohol dehydrogenase<sup>[116,193]</sup> or BITIP (BINOL derived) catalyst,<sup>[194]</sup> the most practicable way was evaluated by a combination of literature known procedures, namely a Midland reduction<sup>[195]</sup> using (*R*)- and (*S*)-Alpine borane to yield the two enantiomers of (1-<sup>2</sup>H)farnesol (**76**)<sup>[196]</sup> combined with a direct phosphorylation by bis(triethylammonium) phosphate in trichloroacetonitrile<sup>[197]</sup> as shown in Scheme 22. This step is crucial to preserve the stereoinformation at C-1<sup>[194b]</sup> in contrast to the more widely used nucleophilic substitution reaction with tris(tetrabutylammonium) hydrogen diphosphate,<sup>[198]</sup> in which substantial loss of stereoinformation was observed.<sup>[196]</sup>



**Scheme 22.** Synthetic approach towards (1*R*)- and (1*S*)-(1-<sup>2</sup>H)FPP.<sup>[194b,196,197]</sup> TEAP: bis(triethylammonium) phosphate.

Since the absolute configuration of some of the terpene products (corvol ethers **107** and **108**, 4-*epi*-cubebol **150**, Figure 11) were unknown, they were determined by analysis of the common side product germacrene-D-4-ol (**152**) on a chiral GC phase compared to **152** originating as a TS main product from *Collimonas pratensis* with known absolute configuration. With this information and the enantioselectively labelled FPPs in hand, the stereochemical model for the 1,3-hydride shift (Scheme 21) was tested. The results (Figure 11) show the predicted stereochemical course in case of T-muurolol (**148**) synthase from *Roseiflexus castenholzii*,<sup>[192a]</sup> 4-*epi*-cubebol (**150**) synthase from

*Streptosporangium roseum*,<sup>[192c]</sup>  $\gamma$ -cadinene (**151**) synthase from *Chitinophaga pinensis*,<sup>[192a]</sup> corvol ether (**107** and **108**) synthase from *Kitasatospora setae*,<sup>[129]</sup> germacradien-6-ol (**99**) synthase from *Streptomyces pratensis*,<sup>[127]</sup> and germacrene-D-4-ol (**152**) synthase from *Collimonas pratensis*. Intriguingly, the latter TS also forms **151** as a byproduct showing an inverse stereochemical course of the hydride shift connected to the two enantiomers of **151**.

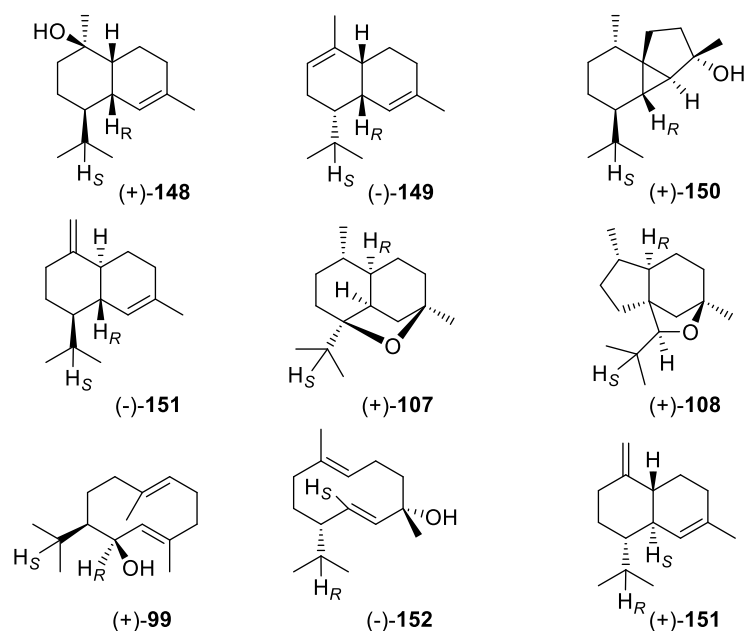


**Figure 11.** Observed stereochemical outcome of the C-1 hydrogen atoms for the investigated TS products.<sup>[131]</sup>

The only example, which does not obey the predicted course, is  $\alpha$ -amorphene (**149**) synthase from *S. viridochromogenes*.<sup>[192a]</sup> This interesting finding could potentially hint to a different cyclisation mechanism for this TS namely an initial 1,6-cyclisation instead of a 1,10-cyclisation as for the other cadalanes. For this different cyclisation mode, which is usually invoked for the related terpene amorpha-4,11-diene and was also connected to other amorphenes in a theoretical study,<sup>[199]</sup> the opposite stereochemical course is expected through a combination of 1,3- and 1,5-hydride shift. Therefore this alternative mechanism can explain the course observed herein.

Although the investigated examples cannot prove the stereochemical model to be valid in all cases (cf. Chapter 18) and therefore strict conclusions on the absolute configuration are difficult, still a lot of insights into TS cyclisation mechanisms are gained from these labelling experiments even hinting to fundamentally different mechanisms as in case of **149**. Also the methods established during the course of this study proved to be a valuable basis for the following work.



# Chapter 4

## Terpene Cyclases from Social Amoebae

Dr. Patrick Rabe, Jan Rinkel, Britta Nubbemeyer, Dr. Tobias G. Köllner, Prof. Dr. Feng Chen and Prof. Dr. Jeroen S. Dickschat\*

*Angew. Chem. Int. Ed.* **2016**, *55*, 15420–15423; *Angew. Chem.* **2016**, *128*, 15646–15649.

Reprinted from *Angew. Chem. Int. Ed.* **2016**, *55*, 15420–15423 and *Angew. Chem.* **2016**, *128*, 15646–15649 with kind permission from John Wiley and Sons.

The incubation experiments of the two investigated TSs with (*R*)- and (*S*)-(1-<sup>2</sup>H)FPP, analysis of the resulting data and kinetic studies of the autoxidation of one TS product were performed by Dr. Patrick Rabe and me.

The publication “Terpene Cyclases from Social Amoebae” is attached in Appendix C.

## Introduction

Whereas TSs are known to be widespread in plants, fungi and bacteria, only quite recently in 2016, TS genes were found in the genome of the social amoeba *Dictyostelium discoideum*.<sup>[200]</sup> This finding represents a new source of TSs from eukaryotes besides plants and fungi. The identified enzymes are phylogenetically more related to fungal than to bacterial ones.

Social amoebae feature a distinctive life cycle, in which the unicellular organisms aggregate to form a multicellular complex finally resulting in the formation of a fruiting body to produce spores.<sup>[201]</sup> While with abundant nutrition single cells are observed, under starvation a multicellular aggregate is formed. Interestingly, the production of terpenes (Figure 12) was also shown to be dependent on the current cellular stage.

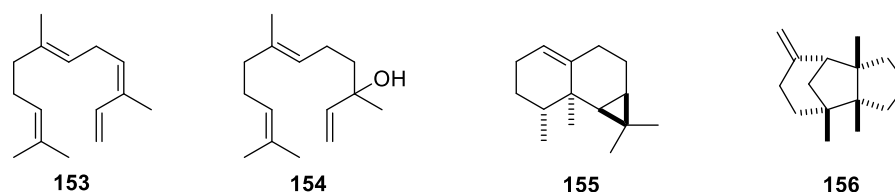
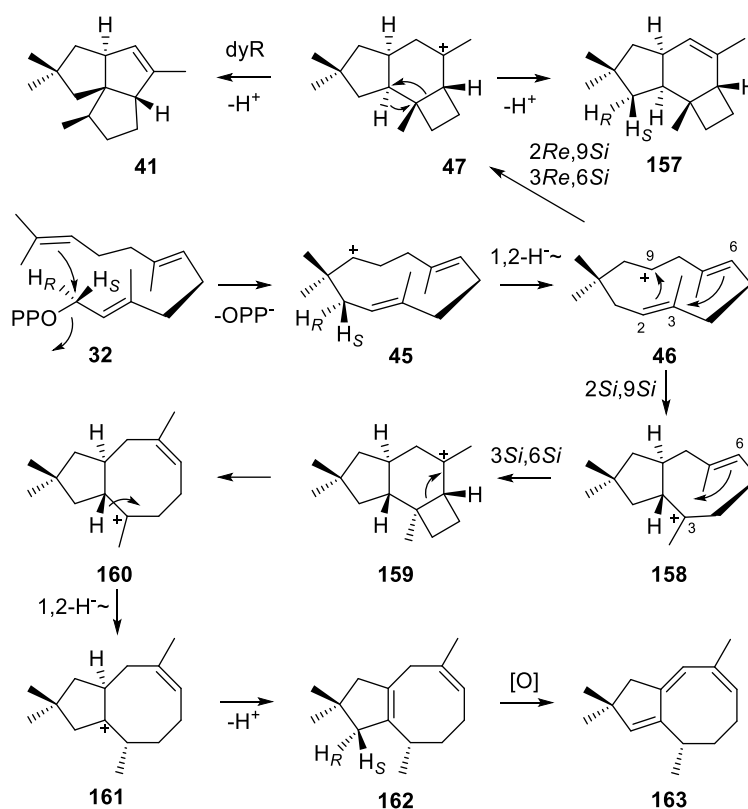


**Figure 12.** Terpenes observed in the headspace of *D. discoideum*.<sup>[200]</sup>

Among the identified sesquiterpenes are besides the acyclic representatives  $\alpha$ -farnesene (**153**) and nerolidol (**154**) also the tricyclic systems calarene (**155**) and  $\beta$ -barbatene (**156**). Since the produced terpenes may also play an ecological role in the cell to cell communication within social amoebae, characterisation of the TSs together with the determination of their development-dependent expression levels are highly interesting. From the eleven putative TS genes in *D. discoideum* (DdTPS 1–11), four were functionally characterised by heterologous expression in *E. coli* and identification of their main products by GC/MS.<sup>[200]</sup> The products of the sesquiterpene synthases DdTPS2 and DdTPS6 remained unknown leaving room for further investigations not only on their product's structures but also on their cyclisation mechanisms. Also the synthesised substrates (*R*)- and (*S*)-(1-<sup>2</sup>H)FPP should be suitable for incubation experiments with these amoebal TSs.

## Summary

The products of the two TSs from *D. discoideum* were identified as the new natural product protoillud-7-ene (**157**, from DdTPS6, Scheme 23) and asterisca-2(9),6-diene (**162**, from DdTPS2). Isotopic labelling experiments additionally shed light on the cyclisation mechanisms and were used to determine the absolute configurations of the products.<sup>[202]</sup> The cyclisation mechanism catalysed by DdTPS6 is similar to the mechanism of pentalenene (**41**) synthase (Scheme 7), while **157** is a simple deprotonation product of the central cation **47**.



**Scheme 23.** Proposed cyclisation mechanisms towards DdTPS6 product **157** and towards DdTPS2 product **162**, and structure of its oxidation product **163**.<sup>[202]</sup>  $H_R$  and  $H_S$  were omitted in the intermediary structures. dyR: dyotropic rearrangement.

In contrast, DdTPS2 branches from **46** to give cation **158** with a different stereochemistry at the bridgeheads. This can cyclise to **159**, which opens to the tertiary cation **160**. One 1,2-hydride migration to **161**, followed by an incubation experiment with (3- $^{13}\text{C}$ ,2- $^2\text{H}$ )FPP, furnishes **162** after deprotonation, which is oxidised after prolonged incubation times to asterisca-1,6,8-triene (**163**). The 1,2-hydride shift from **45** to **46** was addressed by incubation of (2- $^{13}\text{C}$ ,1,1- $^2\text{H}_2$ )DMAPP, which was elongated with IPP by the FPPS from *S. coelicolor* and converted by both TSs. Additionally, all fifteen ( $^{13}\text{C}_1$ )-isotopomers of FPP were used to study selected features of the EI-MS fragmentation mechanism of **157** and **162**, which also revealed a strict stereochemical course regarding the geminal methyl groups by NMR analysis.

Since both product's absolute configurations were not accessible by comparing optical rotary powers, they were assigned by incubation experiments with (*R*)- and (*S*)-(1- $^2\text{H}$ )FPP assuming an inversion of configuration at C-1 during the initial ring closure, which is also observed for pentalenene synthase.<sup>[193]</sup> The incorporation of deuterium into the diastereotopic positions, correlated by NOESY to the stereocentres of the molecules, was thereby followed by  $^1\text{H}$ -NMR and HSQC. Although a lot of labelled material had to be used to obtain suitable spectra, this example represents a successful application of enantioselective labelling for determining the absolute configuration of TS products (cf. Scheme 12).<sup>[110]</sup>

## Chapter 5

### **A detailed view on 1,8-cineol biosynthesis by *Streptomyces clavuligerus***

Jan Rinkel, Dr. Patrick Rabe, Laura zur Horst and Prof. Dr. Jeroen S. Dickschat\*

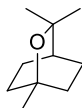
*Beilstein J. Org. Chem.* **2016**, *12*, 2317–2324.

The synthesis of (*R*)- and (*S*)-(1-<sup>2</sup>H)GPP, incubation experiments with these substrates and 1,8-cineol synthase and analyses of the corresponding data were done by me. Moreover, experimental assistance by Laura zur Horst as part of her Bachelor thesis is acknowledged.

The publication “A detailed view on 1,8-cineol biosynthesis by *Streptomyces clavuligerus*” is attached in Appendix D.

## Introduction

The monoterpene ether 1,8-cineol (eucalyptol, **164**, Figure 13) is abundant in several essential oils (e. g. it is the major compound in eucalyptus oil)<sup>[203]</sup> and has long been used in cosmetic and medicinal products for its pleasant smell. The molecule features a mirror plane and is thus achiral, constituting **164** to a member of the rare group of achiral terpenes.



**164**

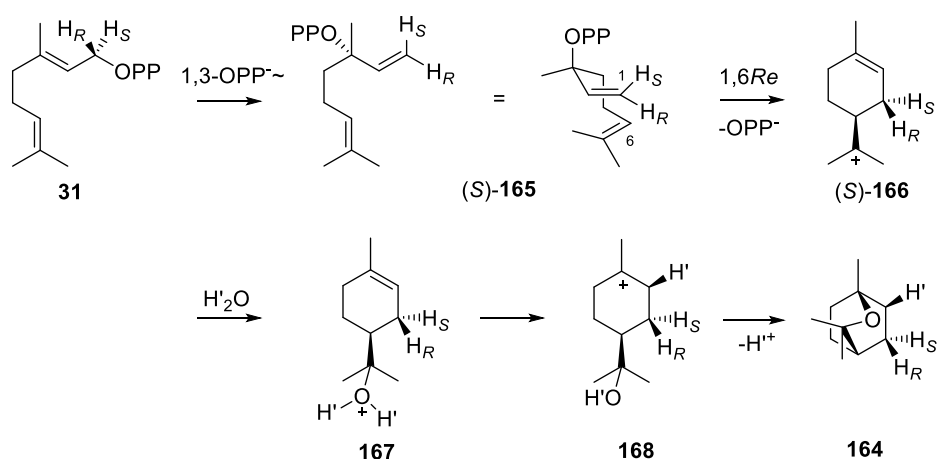
**Figure 13.** Structure of 1,8-cineol (eucalyptol, **164**).

The biosynthesis of **164** was investigated mainly in the plant *Salvia officinalis*, from which a 1,8-cineol synthase was cloned from cDNA and heterologously expressed in *E. coli*.<sup>[204]</sup> Since any intermediary stereochemical information is lost in the final product, the cyclisation mechanism towards **164** may proceed via (*S*)-linalyl diphosphate (LPP, **165**, Scheme 24) and the (*S*)-terpinyl cation (**166**), or in an enantiomeric fashion with (*R*)-linalyl diphosphate and the (*R*)-terpinyl cation. In the plant, this question was addressed both by incubation of the two LPP enantiomers and by isotopic labelling experiments with [1-<sup>3</sup>H]GPP, following the incorporation of label into the two diastereotopic positions in **164** to conclude on a cyclisation mechanism via the (*R*)-terpinyl cation.<sup>[205]</sup> An additional stereochemical feature of the cineol cyclisation is the course of the final ether formation with a formal *syn*- or *anti*-addition of water towards the (*Z*)-double bond. By incubating the recombinant enzyme in D<sub>2</sub>O, an incorporation of deuterium pointing to the same face as the ether-containing bridge was observed (*syn*-addition).<sup>[206]</sup>

In 2011, the first bacterial monoterpene synthase was discovered from the actinomycete *Streptomyces clavuligerus* and shown to produce **164** as well.<sup>[207]</sup> This opens the opportunity to investigate the stereochemical details of the bacterial enzyme and compare them to the outcome observed in *Salvia officinalis*, which for evolutionary reasons do not necessarily have to be the same. Moreover, it is a common observation to find the opposite enantiomer of a terpene from bacteria than the one known from plants.<sup>[1,192c]</sup> This task also include the opportunity to extend the library of enantioselectively deuterated substrates also to the level of monoterpenes by applying the described methodologies.

## Summary

For determining the stereochemical course of the bacterial 1,8-cineol synthase, its coding gene was cloned into the expression vector pYE-Express<sup>[192b]</sup> and the enzyme was purified after heterologous expression in *E. coli*. The recombinant protein was then incubated with (*R*)- and (*S*)-(1-<sup>2</sup>H)GPP, prepared as their FPP analogues, to observe a selective incorporation of deuterium into one methylene group of **164** as followed by HSQC.<sup>[208]</sup> From these experiments and the relative orientation of each proton towards the ether-containing bridge, the opposite stereochemical course of the cyclisation (Scheme 24) compared to the plant TS was concluded, namely the involvement of (*S*)-**166**.



**Scheme 24.** Cyclisation mechanism of 1,8-cineol synthase from *S. clavuligerus*.<sup>[208]</sup>

Additionally, an incubation experiment with (2-<sup>13</sup>C)GPP in D<sub>2</sub>O showed the incorporation of deuterium on the same side as the ether-bridge, which is consistent to the observations in *Salvia officinalis*. However, whether the hydrogen is introduced by the same water molecule attacking the terpinyl cation (**166**) as indicated in Scheme 24, or the double bond is protonated by an additional source such as the diphosphate or an amino acid residue remains elusive.

This study demonstrates that also monoterpenes can be investigated using the same principles introduced earlier and with the special case of achiral 1,8-cineol that even in difficult cases, isotopic labelling experiments can give useful insights to compare TSs with the same product from different source organisms.

## Chapter 6

### **Mechanistic Investigations of Two Bacterial Diterpene Cyclases: Spiroviolene Synthase and Tsukubadiene Synthase**

Dr. Patrick Rabe, Jan Rinkel, Etilia Dolja, Thomas Schmitz, Britta Nubbemeyer, T. Hoang Luu and Prof. Dr. Jeroen S. Dickschat\*

*Angew. Chem. Int. Ed.* **2017**, *56*, 2776–2779; *Angew. Chem.* **2017**, *129*, 2820–2823.

Reprinted from *Angew. Chem. Int. Ed.* **2017**, *56*, 2776–2779 and *Angew. Chem.* **2017**, *129*, 2820–2823 with kind permission from John Wiley and Sons.

My contributions to this work consist in the synthesis of (*R*)- and (*S*)-(1-<sup>13</sup>C,1-<sup>2</sup>H)GPP and (*R*)-(1-<sup>13</sup>C,1-<sup>2</sup>H)FPP. The incubation experiments with the two diterpene synthases with these and other labelled substrates and analyses of the resulting data were performed by Dr. Patrick Rabe and me.

The publication “Mechanistic Investigations of Two Bacterial Diterpene Cyclases: Spiroviolene Synthase and Tsukubadiene Synthase” is attached in Appendix E.

## Introduction

Having targeted both sesquiterpenes and monoterpenes by enantioselectively labelled substrates in the preceding publications, an extension of these principles also for the diterpene group of TS products was desired. This concept is accompanied by several aspects and challenges. Firstly, GGPP (**33**), the universal diterpene precursor, has extended options to cyclise compared to FPP or GPP for its additional isoprene unit(s) giving access to more theoretically possible structures. Although many diterpenes are known from fungi and plants, rather few examples have been characterised from bacteria. Therefore, the investigation of bacterial diterpene synthases (DTs) include an increased probability of discovering new structures compared to sesquiterpenes, where rediscovery of known natural products occurs more often. Secondly, the synthesis of isotopically labelled GGPP isotopomers for the investigation of DTs is far more expensive in terms of working time and material compared to that of FPP. A repetition of the synthetic work leading to the fifteen ( $^{13}\text{C}_1$ )-isotopomers of FPP<sup>[127]</sup> targeting twenty ( $^{13}\text{C}_1$ )GGPPs is therefore undesirable. Instead, an enzymatic extension of the already synthesised FPPs and GPPs to labelled GGPPs with IPP by a prenyltransferase (see Chapter 1.1.3), in this case a GGPP synthase (GGPPS), is a much more feasible possibility and has been used occasionally in the history of terpene research.<sup>[110,194b,202]</sup> To reach the goal of targeting every position by  $^{13}\text{C}$ -labelling, the synthetic work then narrows down to the preparation of five ( $^{13}\text{C}_1$ )-isotopomers of IPP. Also in terms of enantioselectively labelled substrates, a GGPPS is highly useful to transfer the stereochemical information to the inner positions of the GGPP chain in a known stereochemical course.<sup>[40,41]</sup>

In 2015, the group of Ikeda was able to characterise bacterial TSs in an engineered *Streptomyces avermitilis* host,<sup>[209]</sup> which also included five newly identified DTs producing the structures shown in Figure 14.<sup>[210]</sup> Among the new natural products are the tetracyclic diterpenes hydroppyrene (**169**) and hydroppyrenol (**170**), isoelisabethatriene B (**171**) and the clavulatrienes A and B (**172**). Structurally related to the CotB2 product **98**, also cyclooctat-7(8),10(14)-diene (**173**) was identified together with tsukubadiene (**174**) and the odyverdienes A (**175**) and B (**176**).

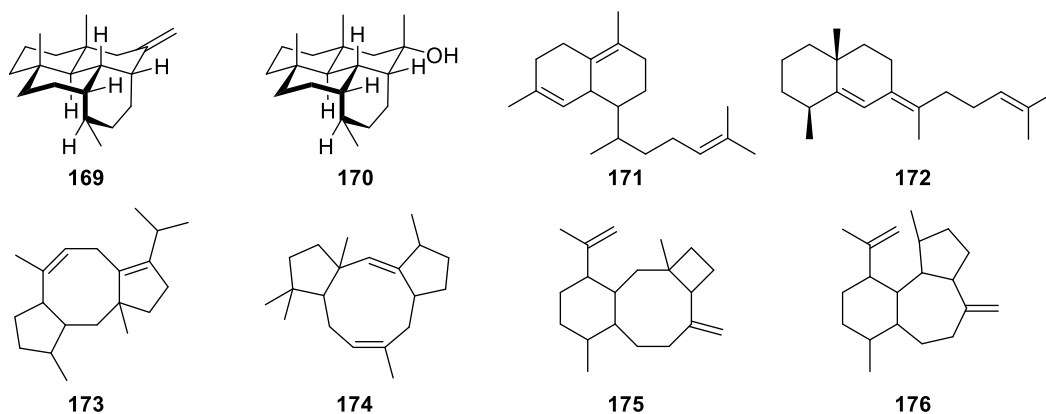


**Figure 14.** Structures of selected newly identified diterpenes by heterologously expressing their DTs in an engineered *S. avermitilis* strain.<sup>[209,210]</sup>

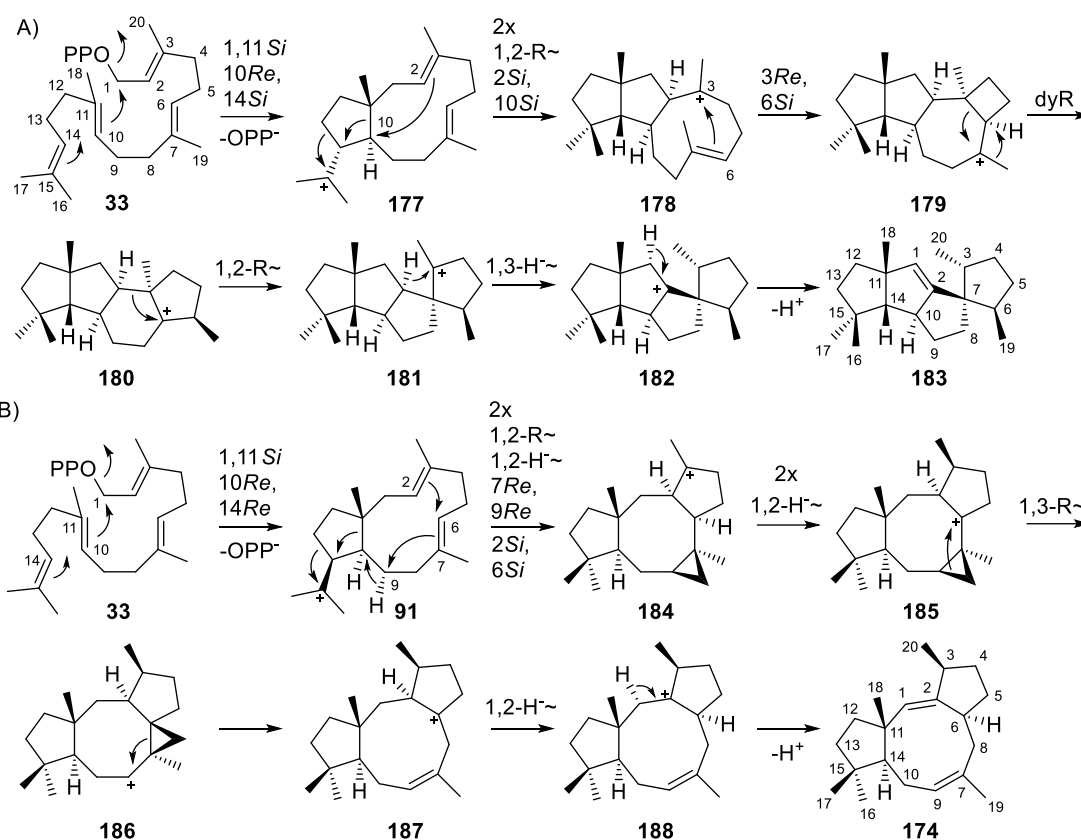


Although this excellent approach provided a rapid access to several new interesting structures, their cyclisation mechanisms remained unknown. Moreover, most of the new natural products were published with their planar structures lacking both relative (**173-176**) and absolute (**171**, **173-176**) configuration. Therefore, one of these DTSs, tsukubadiene (**174**) synthase (TdS) from *S. tsukubaensis* was further studied, combined with the identification of an additional unknown DTS, spiroviolene (**183**, Scheme 25) synthase (SvS) from *S. violens*. With both enzymes, the mentioned principles of isotopic labelling experiments for DTSs were applied.

## Summary

After cloning both DTSs, SvS and TdS, into pYE-Express, the enzymes were expressed, purified and their products were isolated and identified by NMR. The unprecedented spirocyclic diterpene spiroviolene (**183**) features four five-membered rings. The relative configuration of the known natural product tsukubadiene (**174**) was determined by NOESY to be in agreement with the predicted one by comparing calculated NMR data of all stereoisomers to the experimentally measured dataset.<sup>[211]</sup> Extensive labelling experiments were conducted to conclude on both absolute configuration and cyclisation mechanism of **183** and **174**.<sup>[212]</sup> An extension of the existing (<sup>13</sup>C<sub>1</sub>)FPP library<sup>[127]</sup> to the diterpene level was thereby accomplished by cloning and heterologous expression of a GGPPS from *S. cyaneofuscatus* and the synthesis of (1-<sup>13</sup>C)-, (3-<sup>13</sup>C)- and (4-<sup>13</sup>C)IPP, which were complemented with (2-<sup>13</sup>C)- and (20-<sup>13</sup>C)GGPP to target all twenty carbon atoms of **183** and **174** by enzymatic (<sup>13</sup>C<sub>1</sub>)-labelling of their GGPP precursor. This approach proved to be especially useful to challenge the proposed cyclisation mechanisms towards **183** and **174**, which both feature carbon skeleton rearrangements (Scheme 25). Although both enzymes catalyse a similar 1,11-,10,14-cyclisation of GGPP, SvS involves an attack of the 14*Si* face to give **177**, while in TdS' catalysis, cyclisation of 14*Re* takes place to give the diastereomeric cation **91**. Following the mechanism to **183**, one further cyclisation induces a carbon rearrangement to give the tricyclic tertiary cation **178**, which undergoes ring closure to **179**. A dyotropic rearrangement may expand the four-membered ring to give **180**. Then, a Wagner-Meerwein rearrangement assembles the spiro centre in **181**, followed by a 1,3-hydride shift to **182**, which was experimentally addressed by incubation of (3-<sup>13</sup>C,2-<sup>2</sup>H)GGPP. Finally, a deprotonation yields spiroviolene (**183**).

Inspired by the proposed CotB2 catalysed cyclisation mechanism (Scheme 15) towards cyclooctat-9-en-7-ol (**98**),<sup>[121]</sup> the suggested mechanism to build up **174** proceeds via the cyclopropane-containing cation **184**. The two sequential 1,2-hydride migrations to **185** were followed by incubations of (2-<sup>2</sup>H)FPP with (3-<sup>13</sup>C)IPP and GGPPS, which resulted in a shifted singlet excluding a 1,3-hydride shift, and of (3-<sup>13</sup>C,2-<sup>2</sup>H)GGPP showing a triplet. The eight-membered ring is expanded by opening of the cyclopropane moiety to **187**, preceded by a carbon rearrangement to **186**. After a 1,2-hydride shift to yield **188**, tsukubadiene (**174**) is formed after deprotonation. The stereochemical course of both deprotonation steps was investigated by incubations with (*R*)- and (*S*)-(1-<sup>2</sup>H)GGPP.



**Scheme 25.** Proposed cyclisation mechanisms of A) SvS and B) TdS.<sup>[212]</sup>

To address the absolute configurations of both DTS products, the toolbox of enantioselectively deuterated FPPs and GPPs was synthetically extended with a  $^{13}C$ -label at the deuterated C-1 position to give (*R*)- and (*S*)-(1- $^{13}C$ ,1- $^2H$ )GPP and (*R*)- and (*S*)-(1- $^{13}C$ ,1- $^2H$ )FPP, which were elongated to the corresponding labelled GGPPs with known inversion of configuration by GGPPS. Compared to the obtained results in Chapters 4 and 5, which suffered from poor sensitivity leading to the need of purification and the use of high substrate amounts, the additional  $^{13}C$ -label greatly improved the sensitivity in HSQC spectroscopy, resulting in easily interpretable data of the crude incubation extracts. The amount of used labelled material was reduced to 0.5 to 1.0 mg, simplifying and accelerating the whole experimental procedure. By this approach, the absolute configuration of **183** was established based on two stereochemical anchors (C-5 and C-9), whereas one anchor (C-5) was used on **174**. Although C-9 is a methine group in **174**, (*R*)- and (*S*)-(1- $^{13}C$ ,1- $^2H$ )GPP were still useful to determine the stereochemical course of the 1,2-hydride shift connecting **91** and **184**.

All in all, both extending the labelled toolbox to reach the diterpene level with a GGPPS and the introduction of an additional  $^{13}C$ -label to the enantioselectively deuterated substrates described in this study were substantial parts of the following work described below.

## Chapter 7

### **Mechanisms of the Diterpene Cyclases $\beta$ -Pinacene Synthase from *Dictyostelium discoideum* and Hydropyrene Synthase from *Streptomyces clavuligerus***

Jan Rinkel, Dr. Patrick Rabe, Dr. Xinlu Chen, Dr. Tobias G. Köllner, Prof. Dr. Feng Chen and Prof. Dr. Jeroen S. Dickschat\*

*Chem. Eur. J.* **2017**, *23*, 10501–10505.

Reprinted from *Chem. Eur. J.* **2017**, *23*, 10501–10505 with kind permission from John Wiley and Sons.

My contributions to this work include the isolation and characterisation of products from hydropyrene synthase (HpS) by in vitro reactions, the synthesis of (1,1-<sup>2</sup>H<sub>2</sub>)IPP and the conduction and analysis of labelling experiments on HpS. Additionally, the synthesis of both enantiomers of NPP (cf. Chapter 17) performed by me served as a blueprint for the synthesis of the geranylinalyl diphosphate (GLPP) enantiomers by Dr. Patrick Rabe described herein.

The publication “Mechanisms of the Diterpene Cyclases  $\beta$ -Pinacene Synthase from *Dictyostelium discoideum* and Hydropyrene Synthase from *Streptomyces clavuligerus*” is attached in Appendix F.

## Introduction

As discussed for the classic example of trichodiene (**86**) biosynthesis, the tertiary diphosphate intermediate NPP (**79**) represents a convenient way to solve the problem of a C-2,C-3 double bond isomerisation of (*E*) to (*Z*) in sesquiterpene biosynthesis. The same is true for cyclic monoterpenes and the corresponding NPP analogue LPP (**165**) as described in the biosynthesis of 1,8-cineol (**164**, Chapter 5). However, for diterpenes, this concept is rarely discussed, but only requires the intermediary occurrence of geranylinalyl diphosphate (GLPP). During this study, two DTSs were investigated that formed products with a (*Z*)-configured C-2,C-3 double bond. As one of the TSs, hydroxyrene (**169**) synthase (HpS), was already characterised in the engineered *S. avermitilis* host,<sup>[209]</sup> from which the absolute configuration of its products was tentatively assigned based on a crystal structure of epoxidised **169**,<sup>[210]</sup> the second TSs (DdTPS5) originates from the social amoebae *D. discoideum*, for which DTS activity was already observed, but the product could not be identified.<sup>[200]</sup> Therefore, the investigation of the cyclisation mechanisms of both TSs can be seen as an expansion of the work on TSs from social amoebae (Chapter 4) and on known DTSs (TdS, Chapter 6).

## Summary

After *in vitro* incubation of DdTPS5 with GGPP, its product was identified as  $\beta$ -pinacene (**189**, Figure 15), a macrocyclic achiral diterpene which also occurs in the essential oils of *Pinus* trees.<sup>[213]</sup> Also HpS was analysed *in vitro* to re-isolate its main products **169** and **170**, but also isoelisabethatriene (**191**), whereas **171** and biflora-4,10(19),15-triene (**192**) were identified by GC/MS.<sup>[214]</sup>

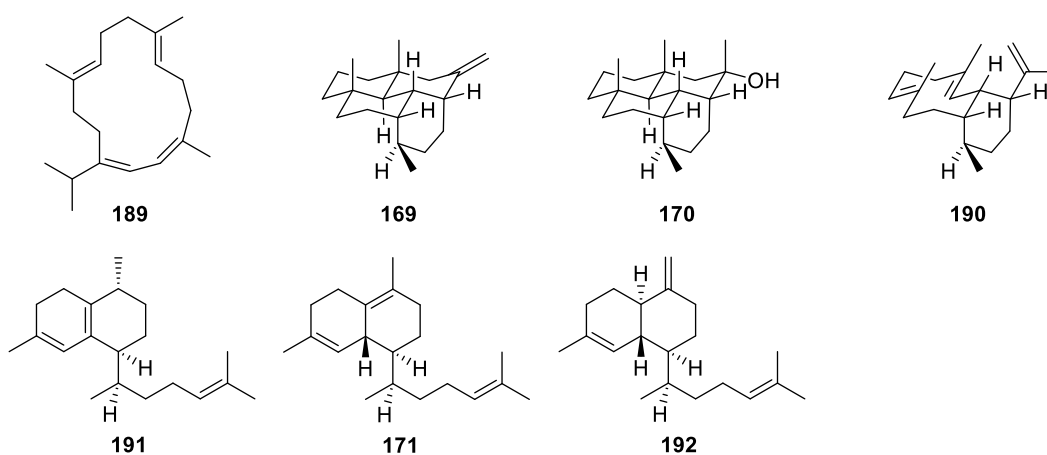


**Figure 15.** Structures of  $\beta$ -pinacene (**189**) and of various HpS products.

Interestingly, the incubation of all twenty enzymatically prepared isotopomers of (<sup>13</sup>C<sub>1</sub>)GGPP with HpS lead to the observation of major peaks not originating from these products. Instead, the unknown dataset was in line with the structure of **190**, which was subsequently isolated, partially purified and named prehydroxyrene. The poor chromatographic behaviour of **190** prevented an earlier GC/MS assignment and further purification, but the discovery of **190** as the neutral intermediate in hydroxyrene

biosynthesis shows the value of ( $^{13}\text{C}_1$ )-labelling in the characterisation of TS products occurring in a mixture.

A 1,2-hydride shift was shown to occur in the cyclisation mechanism towards **189** by the incubation of ( $2\text{-}^2\text{H}$ )DMAPP with IPP, FPPS and GGPPS. Combined with a scrambling of  $^{13}\text{C}$ -label between the geminal methyl groups of **189** observed from enzymatically prepared ( $16\text{-}^{13}\text{C}$ )- and ( $17\text{-}^{13}\text{C}$ )GGPP, this finding supports the stereochemical model shown in Figure 16. Whereas the hydrogen atom conducting a 1,2-hydride migration to the isopropyl group has similar distances to both faces of the cationic centre (indicated by the empty  $p$ -orbital) leading to a loss of stereochemical information on the methyl groups, a 1,3-hydride shift results in a defined situation, because the migrating hydrogen atom cannot reach the opposite face of the cation (cf. Chapter 3). For this principle, also several other examples were encountered during the following chapters.

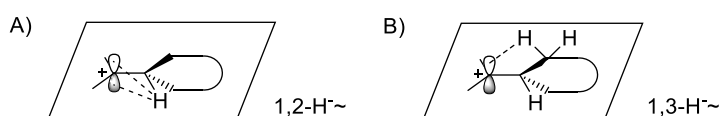


**Figure 16.** The stereochemical course regarding the two geminal methyl groups in TS cyclisations as observed after A) a 1,2-hydride shift (ill-defined) or B) a 1,3-hydride shift (well-defined).

The 1,3-hydride shift during the cyclisation towards **169** was investigated both for the stereochemical course by incubation of synthesised (*R*)- and (*S*)-( $1\text{-}^{13}\text{C}, 1\text{-}^2\text{H}$ )GGPP and the destination of the migrating hydrogen by incubation of ( $7\text{-}^{13}\text{C}$ )FPP and ( $1,1\text{-}^2\text{H}_2$ )IPP with GGPPS resulting in a triplet in  $^{13}\text{C}$ -NMR. Also the absolute configuration of **169**, **170**, **190** and **191** were assigned by  $^{13}\text{C}$ -enhanced enantioselective labelling (cf. Chapter 6) and supported the tentatively assigned absolute configuration of epoxidised **169**. Also, both enantiomers of GLPP were synthesised and incubated with DdTPS5 and HpS, demonstrating that GLPP can serve as a substrate for the production of diterpenes. However, the observed low stereoselectivity of the enzymes with respect to the two applied enantiomers hampered further conclusions on the stereochemical nature of the true intermediates, for the TSs may also catalyse the interconversion of both enantiomers.

Nevertheless, the studies with HpS and its numerous side products underlines the ability of labelling experiments to allow for conclusions even on the composition of complex mixtures. This can be attributed to the high sensitivity of  $^{13}\text{C}$ -labelling in crude extracts, which puts the researcher in the comfortable position to analyse multiple products from one experiment, if suitable reference data are available.

## Chapter 8

### Mechanistic Characterization of Two Chimeric Sesterterpene Synthases from *Penicillium*

Takaaki Mitsuhashi<sup>+</sup>, Jan Rinkel<sup>+</sup>, Dr. Masahiro Okada, Prof. Dr. Ikuro Abe\* and Prof. Dr. Jeroen S. Dickschat\*

*Chem. Eur. J.* **2017**, *23*, 10053–10057.

<sup>+</sup> These authors contributed equally to this work.

Reprinted from *Chem. Eur. J.* **2017**, *23*, 10053–10057 with kind permission from John Wiley and Sons.

With equal contributions to this work, the syntheses of the labelled GFPPs (*R*)- and (*S*)-(1-<sup>13</sup>C,1-<sup>2</sup>H)GFPP, (2-<sup>2</sup>H)GFPP, (2-<sup>13</sup>C)GFPP and (20-<sup>13</sup>C)GFPP together with (4,4-<sup>2</sup>H<sub>2</sub>)IPP were performed by me. The incubation experiments with these and other labelled substrates and the two sesterterpene synthases and their analyses were conducted by Takaaki Mitsuhashi and me during his stay in Bonn.

The publication “Mechanistic Characterization of Two Chimeric Sesterterpene Synthases from *Penicillium*” is attached in Appendix G.

## Introduction

Although the universal precursor of sesterterpenes GFPP (**34**, C<sub>25</sub>) with its five double bonds harbours the inherent reactivity to give rise to numerous terpene skeletons, the number of known sesterterpenes is comparably low.<sup>[215]</sup> Therefore, a genome mining approach focussing on sesterterpene synthases (StTSs) may lead to novel structures that are not found during traditional isolation procedures. While in bacteria, only a StTS producing acyclic sesterterpenes from *Bacillus*,<sup>[216]</sup> a UbiA-type StTS from *Streptomyces*,<sup>[60d]</sup> and a putative type-II StTS from *Amycolatopsis* were characterised so far,<sup>[217]</sup> many fungal StTSs consist of two domains, namely a PT domain and a type-I TS domain.<sup>[218]</sup> This strategy may boost the efficiency of the StTS connected to the poor water solubility of GFPP. In 2013, the first identified example of these chimeric StTSs, ophiobolin F (**193**, Figure 17) synthase from *Aspergillus clavatus*, was reported,<sup>[219]</sup> which was found by its sequence homologies to the chimeric DTS fusicocca-2,10(14)-diene synthase from *Phomopsis amygdali*.<sup>[220]</sup> Based on this successful genome mining approach, also other spectacular chimeric StTSs were identified such the already discussed sesterfisherol (**142**) synthase from *Neosartorya fischeri*,<sup>[190]</sup> but also from other fungi such as *Emericella varicolor*. Examples include stellata-2,6,19-triene (**194**) synthase, which produces the precursor of stellatic acid,<sup>[221]</sup> but also astellifadiene (**195**) synthase,<sup>[222]</sup> whose product structure was determined using the crystalline sponge method.<sup>[223]</sup> Also the highly cyclised sesterterpene quiannulatene (**196**) is produced by a chimeric StTS from *E. varicolor*,<sup>[224]</sup> which catalyses a comparable cyclisation cascade to that leading to **142**.<sup>[225]</sup>

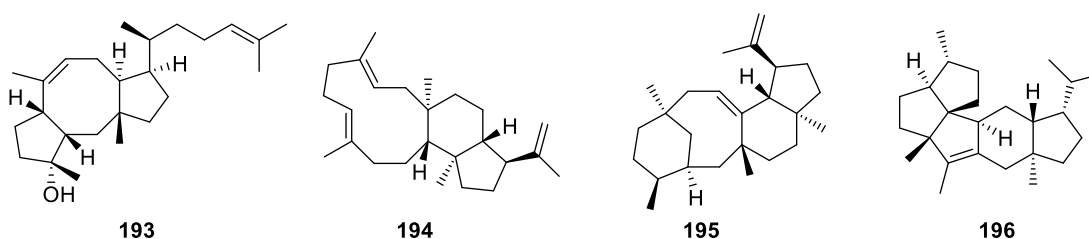


**Figure 17.** Structures of selected products from chimeric fungal sesterterpene synthases.

Because of the bifunctional nature of this enzyme class, the introduced toolbox of isotopically labelled substrates can directly be used to study the cyclisation mechanisms of novel StTSs by elongating them with IPP catalysed by the attached GFPP synthase (GFPPS) domain. For a complete (<sup>13</sup>C<sub>1</sub>)-labelling approach, the substrate library nevertheless has to be extended. This publication therefore focusses on the application of labelled compounds on two newly identified chimeric StTSs from *Penicillium* strains.

## Summary

The first investigated StTS (PbSS) was identified in the genome of *Penicillium brasilianum* and expressed in *Aspergillus oryzae* NSAR1<sup>[226]</sup> to identify its product to be the tricyclic sesterterpene **197** (Figure 18), which was named sesterbrasiliatriene.<sup>[227]</sup> For in vitro characterisation and the application of isotopically labelled substrates, the corresponding gene was cloned from transformed *A. oryzae* cDNA to an *E. coli* expression vector to yield the recombinant protein. While the relative configurations of the eastern and western half of the molecule were assigned separately by NOESY, the enantioselectively labelled substrates (*R*)- and (*S*)-(1-<sup>13</sup>C,1-<sup>2</sup>H)GPP, -FPP, -GGPP, and the newly synthesised -GFPP were used to place four stereochemical anchors to assign both the relative configuration between the separated halves and the absolute configuration as shown. Additionally, the 1,5-hydride shift occurring in the cyclisation towards **197** was followed by an incubation of (7-<sup>13</sup>C)GPP and (4,4-<sup>2</sup>H<sub>2</sub>)IPP resulting in a triplet in <sup>13</sup>C-NMR.

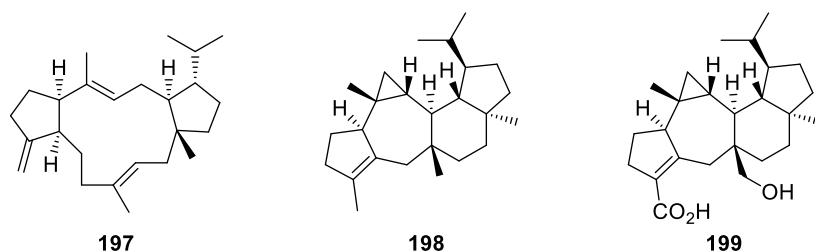


**Figure 18.** Structures of the StTS products sesterbrasiliatriene (**197**) and preasperterpenoid A (**198**) together with the structure of asperterpenoid A (**199**).

Using the same approach, also the second enzyme from *P. verruculosum* was characterised as a preasperterpenoid A (**198**) synthase (PvPS). The structure of **198** is highly reminiscent of asperterpenoid A (**199**), a metabolite isolated from *Aspergillus* sp. 16-5c, which inhibits tyrosine phosphatase B from *Mycobacterium tuberculosis*.<sup>[228]</sup> Also in this case, the deuterium labelled substrates were applied to deduce the absolute configuration of **198**, whereas (*R*)- and (*S*)-(1-<sup>13</sup>C,1-<sup>2</sup>H)FPP could be used to follow the stereochemical course of the 1,5-hydride shift. Incubation with (11-<sup>13</sup>C,1,1-<sup>2</sup>H<sub>2</sub>)FPP determined the isopropyl group of **198** to be the destination of the shifting hydrogen atom and the loss of label from (2-<sup>2</sup>H)GFPP established the deprotonation position.

For both StTSs, all twenty-five carbon atoms in **197** and **198** were (<sup>13</sup>C<sub>1</sub>)-labelled by enzymatic and synthetic preparation of the GFPP isotopomers. To archive this, (2-<sup>13</sup>C)- and (20-<sup>13</sup>C)GFPP were synthesised to complement (1-<sup>13</sup>C)-, (3-<sup>13</sup>C)- and (4-<sup>13</sup>C)IPP for labelling of the first isoprene unit. For single-labelling of the second unit, GGPPS was used, followed by removal of unlabelled FPP by T-muurolool (**148**) synthase, an excess of unlabelled IPP and the StTS to suppress the formation of doubly labelled GFPP.

Taken together, the established labelling techniques were successfully extended and applied on two new fungal StTS. The special case of the large achiral linkers in the macrocyclic structure of **197** also provided the opportunity to solve a problem of relative configuration using selectively labelled oligoprenyl diphosphates.



## Chapter 9

### **18-Hydroxydolabella-3,7-diene synthase – a diterpene synthase from *Chitinophaga pinensis***

Prof. Dr. Jeroen S. Dickschat\*, Jan Rinkel, Dr. Patrick Rabe, Arman Beyraghdar Kashkooli and Prof. Dr. Harro J. Bouwmeester

*Beilstein J. Org. Chem.* **2017**, *13*, 1770–1780.

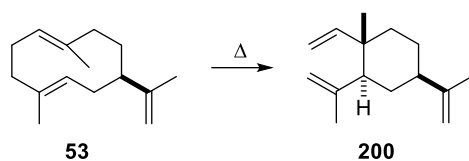
The repeated headspace analysis of *E. coli* BL21 expressing the DTS, the incubation experiments with enantioselectively labelled substrates and their analyses were performed by me.

The publication “18-Hydroxydolabella-3,7-diene synthase – a diterpene synthase from *Chitinophaga pinensis*” is attached in Appendix H.

## Introduction

Characterisation of TSs have been reported from a variety of different heterologous hosts<sup>[229]</sup> including *Streptomyces*,<sup>[209]</sup> *E. coli*,<sup>[192b]</sup> *Aspergillus oryzae*,<sup>[230]</sup> *Saccharomyces cerevisiae*<sup>[231]</sup> or even in plants like *Nicotiana benthamiana*.<sup>[232]</sup> Although these approaches are successful depending on the origin of the corresponding gene, little is known about the restrictions of each host and if the heterologous expression system can influence the reactivity of a TS. Indeed, single reports investigated TSs that produce different terpenes depending on the host, as TPS10 from *Arabidopsis thaliana*, whose product is linalool when expressed in *S. cerevisiae*,<sup>[233]</sup> but  $\beta$ -myrcene and  $\beta$ -ocimene are observed in *E. coli*.<sup>[234]</sup>

With respect to the rapidly growing numbers of genome sequences that were made available through modern sequencing techniques connected to the discussed problems in bioinformatic analysis of TS sequences to predict their products, traditional TS characterisation approaches by far cannot keep track in the chemical identification of TS products. Therefore, a faster approach was reported in 2013 that relies on gene cloning of a TS into an *E. coli* expression vector and follow-up headspace analysis of the *E. coli* expression culture to identify the TS product.<sup>[192a]</sup> One TS from the chitin degrading *Chitinophaga pinensis* was thereby characterised as a germacrene A (**53**, Scheme 26) synthase based on the identification of its Cope rearrangement product  $\beta$ -elemene (**200**) by GC/MS headspace analysis.

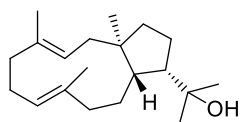


**Scheme 26.** Cope rearrangement of germacrene A (**53**) to  $\beta$ -elemene (**200**).

While this method strongly benefits from the established handling of the fast-growing *E. coli* cells and the quick headspace analysis, there are still some disadvantages for this approach to consider. Firstly, a GC/MS analysis can only identify known TS products by their EI mass spectra and retention indices. Secondly, not every TS product is suitable for headspace analysis, which may lead to false impressions of TS reactivity depending on the volatility of its product(s). Moreover, non-engineered *E. coli* as a host has some limitations regarding precursor availability. For instance, since there is no GGPPS known from *E. coli*, diterpene synthase activity may be overlooked. This case is also true for the discussed TS from *C. pinensis*, which showed DTS activity for in vitro incubations with GGPP being the subject of the introduced publication.

## Summary

Interestingly, sesquiterpene synthase (e. g. **53**) activity was not observed in vitro for the purified, recombinant TS from *C. pinensis*. Instead, a clean conversion of GGPP to the diterpene alcohol 18-hydroxydolabella-3,7-diene (**201**, Figure 19) was found.<sup>[235]</sup> The compound was isolated and characterised by NMR, while its absolute configuration was deduced from incubation experiments with (*R*)- and (*S*)-(1-<sup>13</sup>C,1-<sup>2</sup>H)GGPP complemented with the GGPPS mediated elongation of (*R*)- and (*S*)-(1-<sup>13</sup>C,1-<sup>2</sup>H)GPP with IPP followed by conversion to labelled **201**.



**201**

**Figure 19.** Structure of the DTS product 18-hydroxydolabella-3,7-diene (**202**).

The DTS was also expressed in *N. benthamiana*, which resulted in the production of **201** with a yield of 0.03% of fresh leaf weight underlining the ability of plants to serve as a sustainable production platform for terpenes.<sup>[229]</sup> To exclude experimental errors, the headspace analysis of *E. coli* expressing the TS was repeated to also observe **200** by GC/MS analysis. The detailed reasons for the production of **53** in *E. coli* remain unknown, despite the different conditions of the reaction in this host compared that of the in vitro incubation may lead to a reasonable explanation. Therefore, care should be taken when working with heterologous expression systems for they might not reflect the actual biochemical situation in the TS' native host. Since none of the discussed products have been found in *C. pinensis* cultures, also the in vitro investigations perhaps face the same problems. Overall, this study encourages the continuing work on characterised TSs for interesting aspects of their reactivities may have been overlooked.

## Chapter 10

### **Spata-13,17-diene Synthase—An Enzyme with Sesqui-, Di-, and Sesterterpene Synthase Activity from *Streptomyces xinghaiensis***

Jan Rinkel, Lukas Lauterbach and Prof. Dr. Jeroen S. Dickschat\*

*Angew. Chem. Int. Ed.* **2017**, *56*, 16385–16389; *Angew. Chem.* **2017**, *129*, 16603–16607.

Reprinted from *Angew. Chem. Int. Ed.* **2017**, *56*, 16385–16389 and *Angew. Chem.* **2017**, *129*, 16603–16607 with kind permission from John Wiley and Sons.

My contributions to this work included cloning and heterologous expression of the DTS, isolation and NMR characterisation of its products, incubation experiments with isotopically labelled substrates and analysis of results together with site-directed mutagenesis and metal-ion dependency studies.

The publication “Spata-13,17-diene Synthase—An Enzyme with Sesqui-, Di-, and Sesterterpene Synthase Activity from *Streptomyces xinghaiensis*” is attached in Appendix I.

## Introduction

The majority of TSs only accept one oligoprenyl diphosphate substrate of a defined chain length. This substrate selectivity is explainable by the evolutionary tailoring of the active site architecture, which needs to provide a defined cavity for the cyclisation that usually does not possess the flexibility to cyclise longer or shorter substrates in the same way. However, in plants more promiscuous substrate conversion is occasionally observed, as exemplified by  $\delta$ -selinene synthase and  $\gamma$ -humulene synthase from *Abies grandis* producing both cyclised sesquiterpenes from FPP and cyclised monoterpenes from GPP.<sup>[236]</sup> Several other examples were also reported.<sup>[237]</sup> This promiscuity may also be beneficial for the host organism, because only one enzyme can produce terpenes of different classes depending on the biochemical environment such as precursor availability in different cell compartments. Expanding the substrate scope of terpene synthases also raises the question whether extreme chain lengths are still convertible by a TS. For instance, the biosynthesis of the unusual tetraterpene poduran (**202**, Figure 20), which was isolated from the springtail *Podura aquatica*,<sup>[238]</sup> is completely unknown, still, there might be one TS responsible for the cyclisation of the partially saturated or unsaturated long chain substrate.

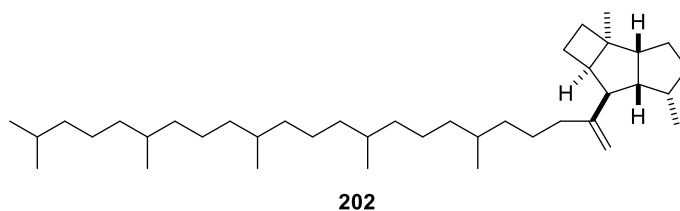


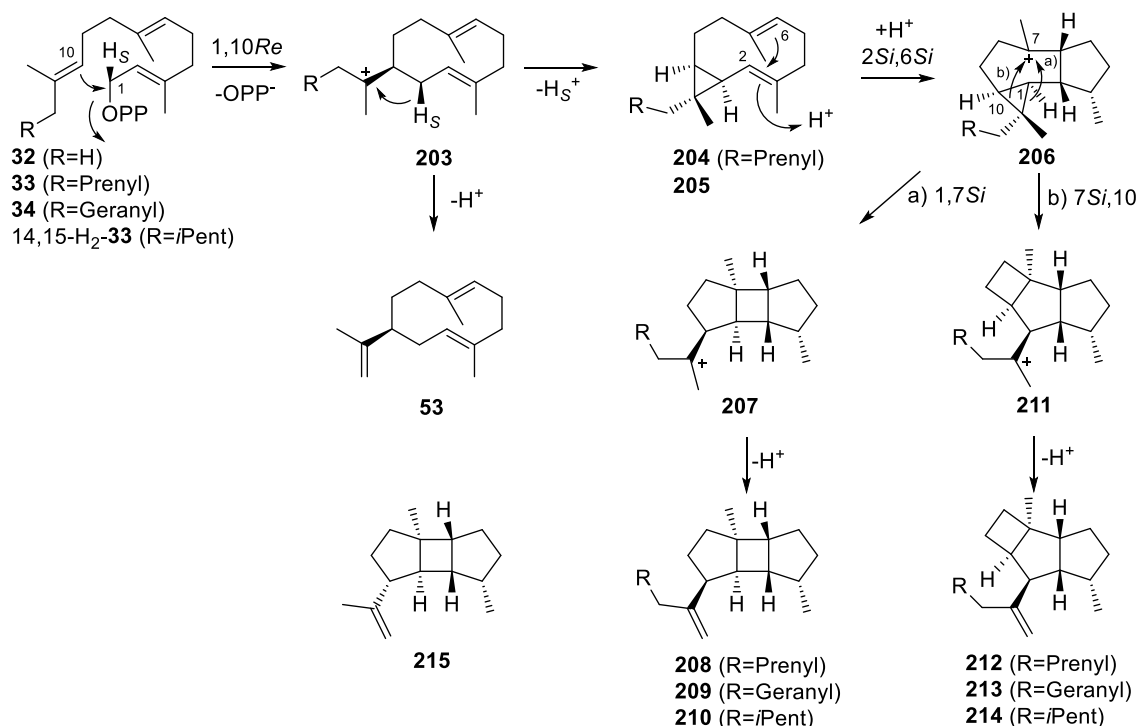
**Figure 20.** Structure of the tetraterpene poduran (**202**) from *Podura aquatica*.<sup>[238]</sup> The relative configurations of the methyl branches are unknown.

Another way to biochemically change the substrate or product scope of a TS are different metal ions. While TSs are usually  $Mg^{2+}$ -dependent, also  $Mn^{2+}$  occasionally works as a good substituent. This was demonstrated with a related PT from the beetle *Phaedon cochleariae*, which produces mainly FPP (82%) in the presence of  $Mg^{2+}$ , whereas the selectivity changes towards GPP (96%), if  $Co^{2+}$  or  $Mn^{2+}$  are present. This mechanism may also be of ecological relevance to switch between mono- and sesquiterpene production.<sup>[37]</sup>

In this publication, a DTS from the marine actinomycete *Streptomyces xinghaiensis* is characterised, which features a surprisingly broad substrate scope by converting FPP, GGPP and GFPP. The cyclisation mechanism was investigated by labelling experiments, the metal ion dependency of the TS was addressed and several structurally important amino acid residues were changed by site-directed mutagenesis.

## Summary

A TS from *S. xinghaiensis* was characterised as a spata-13,17-diene (**208**, Scheme 27) synthase (SpS).<sup>[239]</sup> This diterpene hydrocarbon features a prenyl side chain and a tricyclic core structure with a four-membered ring. As a side product of the conversion with GGPP (**33**), also prenylkelsoene (**212**) could be isolated, which possesses an altered core structure. The conversion of GFPP (**34**) gave the sesterterpene homologues **209** and **213**, from which only **209** was isolated whereas **213** was tentatively assigned based on its similar EI-MS spectrum to **212**. A conversion of FPP did not yield the sesquiterpene core structures. Instead, germacrene A (**53**) was isolated. Combining these results, a cyclisation mechanism was proposed, which is depicted in Scheme 27. After a 1,10*Re*-cyclisation, cations **203** are further converted by deprotonation to build up the cyclopropane ring neutral intermediates **204** and **205**. The known compound cneorubin Y (**204**)<sup>[240]</sup> could also be isolated from the reaction with GGPP. A reprotonation at C-3 induces further 2*Si*,6*Si*-cyclisation to cations **206**, which are the central branching points towards the two different core structures. With an opening of the three-membered ring, either a 1,7*Si*-ring closure leads to **207** (path a) giving rise to the main products **208** and **209** after deprotonation, or a 7*Si*,10-cyclisation yields **211** (path b), which in turn after deprotonation gives the side products **212** and **213**. The sesquiterpene cation **203** may also be deprotonated to yield **53** in case of FPP.



**Scheme 27.** Proposed cyclisation mechanism of SpS<sup>[239]</sup> and the originally reported structure of bourbon-11-ene (prespatane, **215**). For simplicity, multiple structures are occasionally included in one structure number.

This mechanism was supported by conversion of the twenty isotopomers of (<sup>13</sup>C<sub>1</sub>)GGPP to yield labelled diterpenes in the expected positions. The stereochemical course of the deprotonation of **203** was addressed by incubations of (*R*)- and (*S*)-(1-<sup>13</sup>C,1-<sup>2</sup>H)GGPP

and the corresponding GPP and FPP isotopomers were used to assign the absolute configurations. Interestingly, the NMR data of the sesquiterpene core structure of **208** matched very well with the reported chemical shifts of the sesquiterpene bourbon-11-ene (prespatane, **215**),<sup>[241]</sup> suggesting that the reported different relative configuration of this compound needs revision. This would also better explain the biosynthetic relationship of **215** to kelsoene<sup>[241]</sup> (tritomarene) in a similar way as suggested for SpS. Indeed, the same structural revision was also suggested from crystallographic data in a different report, which was published at the same time.<sup>[242]</sup> To investigate the tolerance of SpS towards a saturated side chain as present in a longer version in **202**, 10,11-dihydro-FPP was elongated with IPP by GGPPS to 14,15-dihydro-GGPP, whose incubation with SpS yielded **210**. Also the kelsoene derivative **214** could be observed by GC/MS. Therefore, similar enzymes might also be involved in the biosynthesis of **202**. Besides the well-known conserved motifs of TSs as discussed in Chapter 1.1.4, a sequence alignment of 51 bacterial TSs also revealed several other similarities on the amino acid level. This observation is not surprising, since the overall low sequence conservation compared to the highly similar secondary and tertiary structures of TSs can only be explained by certain structure inducing conserved residues. This was investigated for SpS by site-directed mutagenesis identifying P83, L90, E184 and E217 (which is changed in native SpS to D) to be of structural importance. A comparison of the corresponding positions in the crystal structure of selinadiene synthase<sup>[64f]</sup> lead to their proposed functions as helix turns, part of Mg<sup>2+</sup> binding and part of a salt bridge between different helices. Also different metal ions were tested with Mg<sup>2+</sup> and Mn<sup>2+</sup> promoting activity. Whereas the conversion with Mn<sup>2+</sup> was even higher for the wild type enzyme, the D217E mutant showed no activity with Mn<sup>2+</sup> suggesting a role of the corresponding salt bridge for the size of the metal binding site. Overall, the ability of SpS to catalyse similar reactions on different substrate lengths is remarkable and raises the question, how this reactivity is accomplished by the architecture of the active site, which may contain a hydrophobic flexible tunnel to take up different linear isoprenoid side chains.

# Chapter 11

## Two Diterpene Synthases for Spiroalbatene and Cembrene A from *Allokutzneria albata*

Jan Rinkel, Lukas Lauterbach, Dr. Patrick Rabe and Prof. Dr. Jeroen S. Dickschat\*

*Angew. Chem. Int. Ed.* **2018**, *57*, 3238–3241; *Angew. Chem.* **2018**, *130*, 3292–3296.

Reprinted from *Angew. Chem. Int. Ed.* **2018**, *57*, 3238–3241 and *Angew. Chem.* **2018**, *130*, 3292–3296 with kind permission from John Wiley and Sons.

The isolation of the three diterpene products and their characterisation was contributed by me. I also conducted the labelling experiments and site-directed mutagenesis for both DTSSs and the synthesis of (*E*)- and (*Z*)-(4-<sup>2</sup>H)IPP.

The publication “Two Diterpene Synthases for Spiroalbatene and Cembrene A from *Allokutzneria albata*” is attached in Appendix J.



## Introduction

The structure elucidation of a natural product in general is a challenging task. Apart from crystallographic methods,<sup>[223]</sup> obstacles to face include the complexity of natural products and their availability in only small amounts combined with the insensitivity of NMR spectroscopy. Moreover, the standard set of two-dimensional NMR experiments (<sup>1</sup>H, <sup>1</sup>H-COSY, HSQC, HMBC, NOESY) does not include any direct information of the carbon-carbon connectivities that are exceptionally complex for terpene natural products. Therefore, researchers are often caught in a complicated NMR puzzle while solving the structure, which may occasionally lead to misinterpretation. The direct C,C-bond correlations are provided by the INADEQUATE NMR pulse sequence,<sup>[243]</sup> but this approach suffers from the low natural abundance of <sup>13</sup>C (1.1%) leading to high amounts of required material and extended measuring times. To overcome this problem, fully <sup>13</sup>C-labelled natural products have been prepared and used for a <sup>13</sup>C, <sup>13</sup>C-COSY measurement. This can be accomplished by enzymatic conversions in vitro like for the diterpene miltiradiene (**216**, Figure 21), which was synthesised from [U-<sup>13</sup>C<sub>6</sub>]mevalonate (**13**),<sup>[128a]</sup> but also by in vivo feeding as it has been shown for solwaric acids A (**217**) and B (**218**),<sup>[128b]</sup> for the complex polyketide forazoline A (**219**)<sup>[128c]</sup> and also for the sesquiterpenoid hypodoratoxide (**220**).<sup>[128d]</sup> In the case of **220**, the newly acquired data also led to a revision of a previously suggested structure of this compound.

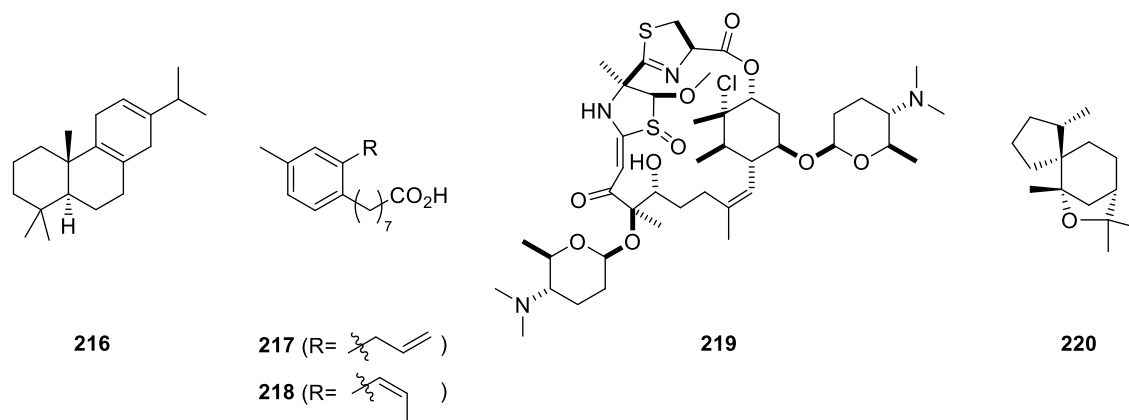
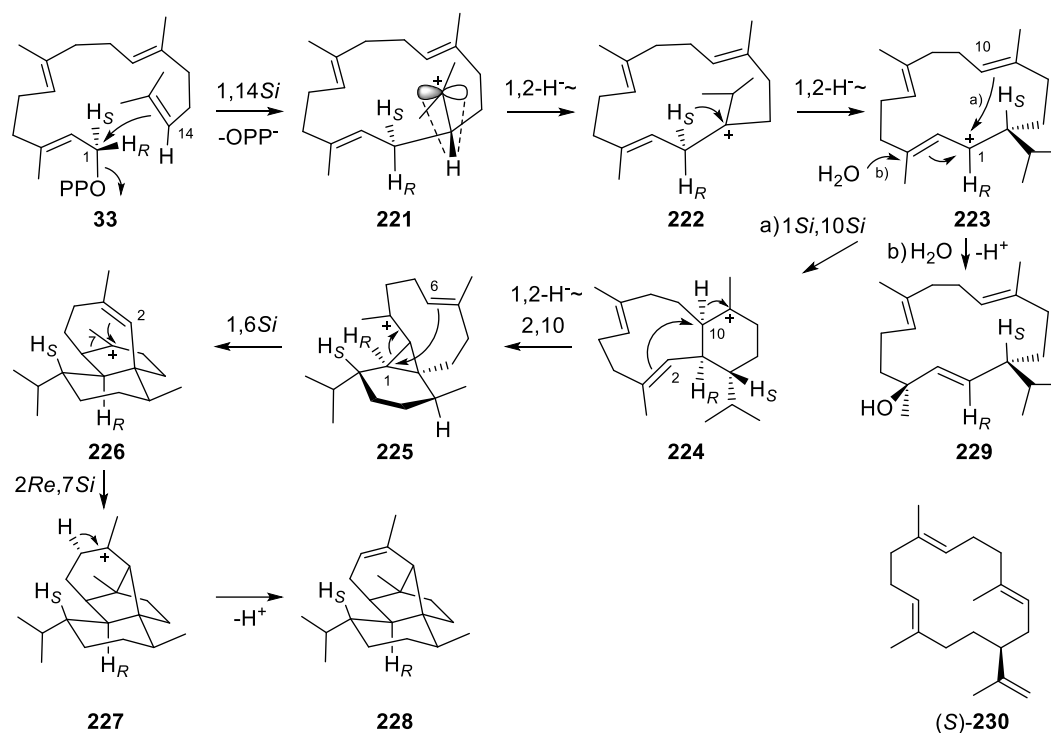


**Figure 21.** Structures of selected natural products investigated by <sup>13</sup>C, <sup>13</sup>C-COSY.

To use this technique also for the in vitro investigation of DTSs circumventing the disadvantages of a partial incorporation of <sup>13</sup>C label from in vivo feeding experiments, the previously described fully labelled (<sup>13</sup>C<sub>15</sub>)FPP, which proved to be helpful in the complex assignment of the NMR data for **99**,<sup>[127]</sup> has to be elongated by GGPPS using (<sup>13</sup>C<sub>5</sub>)IPP to yield (<sup>13</sup>C<sub>20</sub>)GGPP. This publication includes the application of the described approach on the structurally complex product of a newly identified DTS, for which a <sup>13</sup>C, <sup>13</sup>C-COSY spectrum solidified the structure elucidation. Besides that, previously introduced labelling techniques were applied to study the interesting cyclisation mechanism of the TS together with the identification of a second DTS from the same organism, site-directed mutagenesis and metal ion dependency of both enzymes.

## Summary

Two newly identified DTSSs (SaS and CAS) from the actinomycete *Allokutzneria albata* were cloned into an *E. coli* expression vector and the recombinant proteins converted GGPP (**33**) into the diterpene hydrocarbons spiroalbatene (**228**, Scheme 28) and cembrene A (**230**), respectively.<sup>[244]</sup> The structure elucidation for the complex tetracyclic natural product **228** was supported by <sup>13</sup>C,<sup>13</sup>C-COSY, in which all carbon connections except for one (C-6,C-7) were visible. This was accomplished by the synthesis of (<sup>13</sup>C<sub>5</sub>)DMAPP, which was enzymatically isomerised to (<sup>13</sup>C<sub>5</sub>)IPP by isopentenyl diphosphate isomerase (IDI) from *Serratia plymuthica* and follow-up elongation of (<sup>13</sup>C<sub>15</sub>)FPP by this material with GGPPS. Conversion with SaS yielded (<sup>13</sup>C<sub>20</sub>)-**228**. The proposed cyclisation mechanism was investigated by (<sup>13</sup>C<sub>1</sub>)-labelling and is shown in Scheme 28. A 1,14*Si*-cyclisation of GGPP furnishes **221**, which reacts by two sequential 1,2-hydride shifts via **222** to the allylic cation **223**. As discussed in Chapter 7, this process leads to a loss of stereoinformation for the geminal methyl groups, which was observed for **228**. Further cyclisation (path a) gives **224**, which induces a 2,10-cyclisation by a 1,2-hydride shift to yield cation **225**. The tree-membered ring is opened by a 1,6*Si*-cyclisation to give **226**, and further 2*Re*,7*Si*-cyclisation to **227** and deprotonation results in formation of the final product **228**.



**Scheme 28.** Suggested cyclisation mechanism towards spiroalbatene (**228**) and thunbergol (**229**) catalysed by SaS and the structure of cembrene A (**230**).

All hydride migrations and the deprotonation were followed using suitable deuterium labelled substrates, including newly synthesised (3-<sup>13</sup>C,2-<sup>2</sup>H)GPP and (*E*)- and (*Z*)-(4-<sup>2</sup>H)IPP.<sup>[245]</sup> Interestingly, the presence of  $\text{Mn}^{2+}$  in SaS incubations with GGPP led to the formation of thunbergol (**229**), which is a hydrolysis product of **223** (path b).

## Chapter 12

### **An Isotopic Labelling Strategy to Study Cytochrome P450 Oxidations of Terpenes**

Jan Rinkel, Dr. Martin Litzenburger, Prof. Dr. Rita Bernhardt and Prof. Dr. Jeroen S. Dickschat\*

*ChemBioChem* **2018**, *19*, 1498–1501.

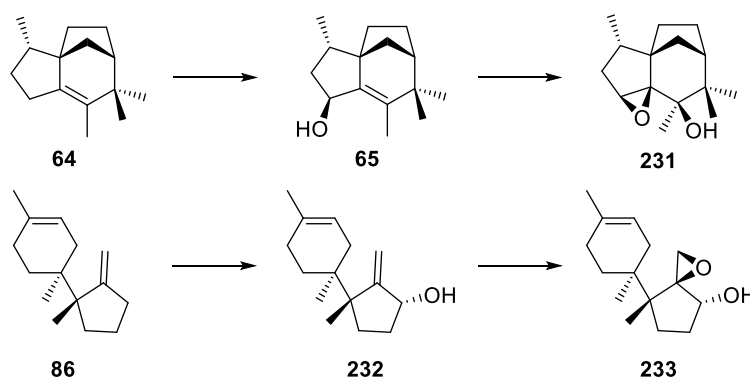
Reprinted from *ChemBioChem* **2018**, *19*, 1498–1501 with kind permission from John Wiley and Sons.

My contributions to this work included the preparation of isotopically labelled terpene substrates, the structure elucidation of terpene oxidation products, the synthetic oxidation of isodaucenol and the synthesis of racemic (1-<sup>2</sup>H)FPP. The incubation experiments using myxobacterial CYPs were performed by Dr. Martin Litzenburger and me.

The publication “An Isotopic Labelling Strategy to Study Cytochrome P450 Oxidations of Terpenes” is attached in Appendix K.

## Introduction

As discussed in Chapter 1.1.5, cytochrome P450 monooxygenases (CYPs) are an important enzyme class responsible for the majority of terpene oxidation reactions. Especially for the first steps on terpene hydrocarbons, their high reactivity is used to introduce oxygen functionalities making the scaffolds synthesised by TSs more accessible for metabolism. The functionalities are thereby not restricted to hydroxy groups, but also acids, aldehydes, ketones and epoxides can be introduced, often with multiple oxidations catalysed by a single CYP. Chemical activation of oxidised positions (e. g. allylic hydrogens) is often discussed in context with the order of oxidation steps, as for example in the largely unknown biosynthesis of PR toxin, a metabolite from *Penicillium roqueforti*.<sup>[246]</sup> Scheme 29 shows two examples of known CYP reaction sequences. Towards the epoxy alcohol **231**, *epi*-isozizaene (**64**) is first oxidised to albaflavenol (**65**) and then the epoxide is introduced by a CYP from *Streptomyces avermitilis*.<sup>[247]</sup> The same sequence, which makes perfect use of chemical activation, is also observed during the oxidation of trichodiene (**86**) towards the trichothecene mycotoxins in *Fusarium graminearum*, building up allyl alcohol **232**, which is further oxidised to **233**.<sup>[248]</sup>

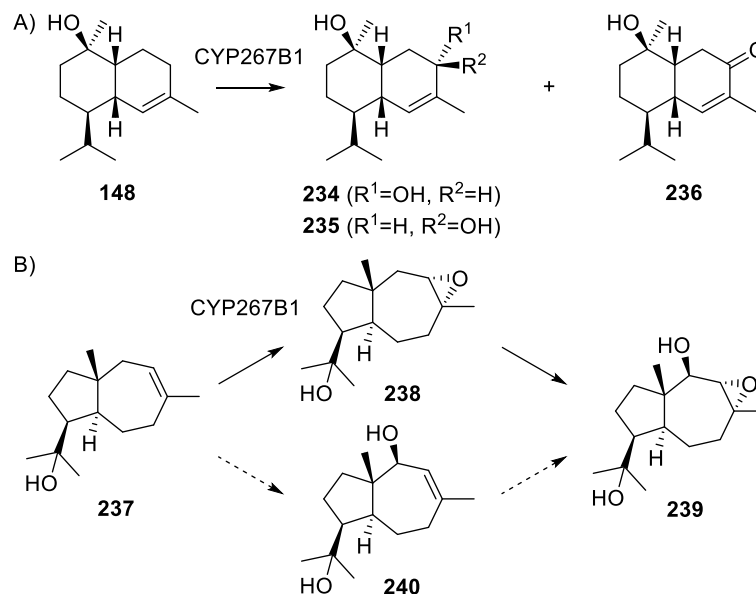


**Scheme 29.** Examples for CYP-mediated terpene oxidations towards  $\alpha,\beta$ -epoxy alcohols.

Building upon the introduced toolbox of isotopically labelled TS substrates, in this publication a combination with the CYP catalysed initial oxidation steps was intended. Although CYP genes are usually genetically clustered with TSs, in vitro investigations on these CYPs are hindered by the need of efficient redox partner proteins. Yet, also artificial combinations of terpenes and CYPs can be used to evaluate the isotopic labelling approach. A well-known model organism for this purpose is the soil-dwelling myxobacterium *Sorangium cellulosum*, in which 21 CYP genes are present.<sup>[249]</sup> Some of them also showed a low substrate specificity,<sup>[250]</sup> making them suitable candidates for terpene oxidations.<sup>[251]</sup>

## Summary

As a suitable terpene substrate, T-muurolol (**148**) was selected, because of the high conversion rates of its corresponding TS,<sup>[192c]</sup> and tested in combination with 9 CYPs from *S. cellulosum*.<sup>[252]</sup> Thereby, CYP267B1 turned out to convert **148** into one main product and two side products with high efficiency. Since the in vitro conversion did not yield enough material for isolation, all fifteen isotopomers of (<sup>13</sup>C<sub>1</sub>)-**148** were enzymatically prepared and converted by CYP267B1. The resulting <sup>13</sup>C-NMR data were used to assign the literature-known structures<sup>[253]</sup> of the allylic alcohols **234** and **235** together with the double oxidation product **236** (Scheme 30). CYP267B1 was also tested with the sesquiterpene alcohol isodauc-8-en-11-ol (**237**),<sup>[254]</sup> and the resulting epoxydiol **239** was isolated. The formation of this double oxidation product is either explainable via epoxide **238**, or as exemplified in Scheme 29, via the allylic alcohol **240**. With the aid of chemical epoxidation of **237** by *m*CPBA, the side product of the reaction was identified as **238**. Surprisingly, also a time resolved experiment and the conversion of **238** to **239** solidified the order of steps to be counterintuitive with **238** as the intermediate. The unknown absolute configurations of **237** and **239** were determined using (*R*)- and (*S*)-(1-<sup>13</sup>C,1-<sup>2</sup>H)GPP and the corresponding FPPs could also infer the stereochemical course of the final hydroxylation step to proceed with retention of configuration. A kinetic isotope effect for this step using racemic (1-<sup>2</sup>H)FPP was not observable.



**Scheme 30.** Terpene oxidations catalysed by CYP267B1 on A) T-muurolol (**148**) and B) isodauc-8-en-11-ol (**237**).

Taken together, the results obtained from the two investigated terpene oxidation systems encourages the combination of the developed labelling toolbox for TSs with CYP catalysed reactions. This was demonstrated by identifying oxidation products in cases of minute available amounts (for **148**), but also by providing insights into the stereochemical course of the oxidation steps (for **237**). Finally, as seen for the unusual order of steps towards **239**, biosynthetic predictions of CYP reactions should be handled with care.

## Chapter 13

### **A Clade II-D Fungal Chimeric Diterpene Synthase from *Colletotrichum gloeosporioides* Produces Dolasta-1(15),8-diene**

Dr. Guangkai Bian<sup>+</sup>, Jan Rinkel<sup>+</sup>, Dr. Zhangqian Wang<sup>+</sup>, Lukas Lauterbach, Dr. Anwei Hou, Yujie Yuan, Prof. Zixin Deng, Prof. Tiangang Liu\* and Prof. Dr. Jeroen S. Dickschat\*

*Angew. Chem. Int. Ed.* **2018**, *57*, 15887–15890; *Angew. Chem.* **2018**, *130*, 16113–16117.

<sup>+</sup> These authors contributed equally to this work.

Reprinted from *Angew. Chem. Int. Ed.* **2018**, *57*, 15887–15890 and *Angew. Chem.* **2018**, *130*, 16113–16117 with kind permission from John Wiley and Sons.

With equal contributions to this work, the isolation and characterisation of the DTS side product from in vitro incubations, all in vitro labelling experiments and their analyses for the elucidation of the product's absolute configuration were performed by me. The investigations on metal ion dependency were contributed by Lukas Lauterbach and me.

The publication "A Clade II-D Fungal Chimeric Diterpene Synthase from *Colletotrichum gloeosporioides* Produces Dolasta-1(15),8-diene" is attached in Appendix M.

## Introduction

In fungi, bifunctional TSs are often encountered, which consists of a PT-domain and a TS-domain. While StTSs of this category have been discussed in Chapter 8, also DTSS contribute to the structural variety of fungal metabolites. Probably the best studied example is fusicocca-2,10(14)-diene (**241**, Figure 22) synthase (PaFS) from *Phomopsis amygdali*,<sup>[220]</sup> which is involved in the biosynthesis of the phytotoxin fusicoccin A (**242**). Also the crystal structure of this hexameric bifunctional TS provided important insights into its function.<sup>[255]</sup> Although the number of known chimeric fungal enzymes is still limited, a phylogenetic analysis already revealed an organisation of the sequences into different clades.<sup>[190,227]</sup> Interestingly, this observation is connected with different initial cyclisation modes. Whereas clade I enzymes catalyse a 1,15-14,18-cyclisation of GFPP (**34**), members of clade II shorten the macrocycle by a 1,11-10,14-cyclisation of GGPP or GFPP. In both modes, a five-membered ring is formed.

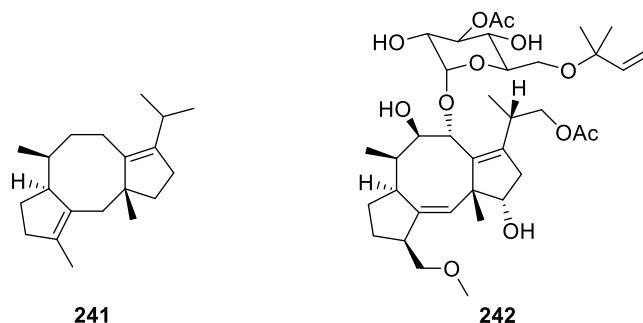
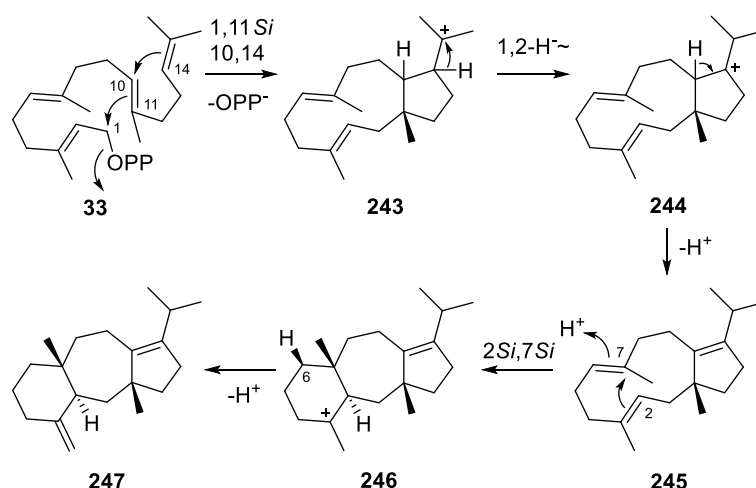


**Figure 22.** Structures of fusicocca-2,10(14)-diene (**241**) and fusicoccin A (**242**).

These enzymes can also be grouped into six subclades (A–F), while there are characterised representatives known from five of these groups.<sup>[218]</sup> This publication deals with the characterisation of one representative bifunctional TS from the uncharacterised branch D, which belongs to the clade II enzymes.

## Summary

The clade II-D enzyme was identified in the genome of the fungus *Colletotrichum gloeosporioides* and overexpressed together with an IDI and *E3* (HMG-CoA reductase, Scheme 1) in its original host to observe the production of a diterpene product. Its structure was determined by cloning the gene from fungal mRNA to construct a terpene overproduction platform in yeast,<sup>[256]</sup> from which the diterpene dolasta-1(15),8-diene (**247**, Scheme 31) was isolated in good yields (7 mg L<sup>-1</sup>). Also an *E. coli* expression vector was constructed to independently isolate **247** accompanied by the side product  $\delta$ -araneosene (**245**) from an in vitro incubation of the purified TS with GGPP.<sup>[257]</sup> The proposed cyclisation mechanism starts with the typical clade II 1,10-11,14-cyclisation to give cation **243**. A 1,2-hydride shift to **244** yields the neutral intermediate **244** after deprotonation. A reprotonation at C-6 induces a further 2,7-ring closure yielding cation **246**, which furnishes **247** after deprotonation.



**Scheme 31.** Proposed cyclisation mechanism towards dolasta-1(15),8-diene (**247**).

The mechanism was supported by labelling experiments with an incubation of (2-<sup>2</sup>H)DMAPP and IPP with the TS to observe deuterium being located at the isopropyl group. The thereby demonstrated 1,2-hydride shift also leads to a scrambling of the geminal methyl group labelling in this case as observed in Chapters 7 and 11. To follow the first deprotonation, the synthesised (2-<sup>2</sup>H)GPP and IPP were incubated with the TS, which yielded unlabelled **247**. The reprotonation was evident from the incubation of (2-<sup>13</sup>C)FPP with IPP and the TS in D<sub>2</sub>O, which also revealed the stereochemical course of the deuterium incorporation. The absolute configuration of the product was investigated by conversion of (*R*)- and (*S*)-(1-<sup>13</sup>C,1-<sup>2</sup>H)GGPP, of the corresponding GPPs and IPP and also by unlabelled DMAPP and (*E*)- and (*Z*)-(4-<sup>13</sup>C,4-<sup>2</sup>H)IPP (synthesised in previous work by combining literature known procedures,<sup>[245,258]</sup> cf. Appendix L),<sup>[259]</sup> with only the latter two experiments giving rise to three stereochemical anchors in **247**. Interestingly, **247** has been described as an acid-catalysed cyclisation product of **245**,<sup>[260]</sup> but not as a natural product. Taken together, the introduction of an (*R*)-configured quaternary stereocentre by the initial cyclisation seems to be common for all clade II enzymes, whereas the tertiary centres could not be addressed during this study.



## Chapter 14

### **A Branched Diterpene Cascade: The Mechanism of Spinodiene Synthase from *Saccharopolyspora spinosa***

Jan Rinkel, Lukas Lauterbach and Prof. Dr. Jeroen S. Dickschat\*

*Angew. Chem. Int. Ed.* **2019**, *58*, 452–455; *Angew. Chem.* **2019**, *131*, 461–465.

Reprinted from *Angew. Chem. Int. Ed.* **2019**, *58*, 452–455 and *Angew. Chem.* **2019**, *131*, 461–465 with kind permission from John Wiley and Sons.

The isolation of products from in vitro incubations with the DTS, their characterisation, labelling experiments and data analyses were performed by me. Additionally, I worked on the synthetic transformations of the main TS product.

The publication “A Branched Diterpene Cascade: The Mechanism of Spinodiene Synthase from *Saccharopolyspora spinosa*” is attached in Appendix N.

## Introduction

As exemplified for 18-hydroxydolabella-3,7-diene synthase (Chapter 9), occasionally the reinvestigation of TSs can lead to surprisingly new results. This is certainly true for a TS from the soil actinomycete *Saccharopolyspora spinosa*,<sup>[261]</sup> which is known for the production of the polyketides spinosyn A (**248**, Figure 23) and D (**249**).<sup>[262]</sup> These compounds are used as potent insecticides. In a previous study, the gene of a TS from this organism was cloned into the *E. coli* expression vector pYE-Express, the recombinant TS was purified and incubated with FPP to yield a mixture of sesquiterpenes with hedycaryol (**250**) as the main product.<sup>[192b]</sup> However, a phylogenetic analysis shows that the closest characterised related TS is CotB2, a diterpene synthase producing **98**.<sup>[122]</sup> Since GGPP as a potential substrate was not tested with the enzyme, the TS was reinvestigated for its DTS activity.

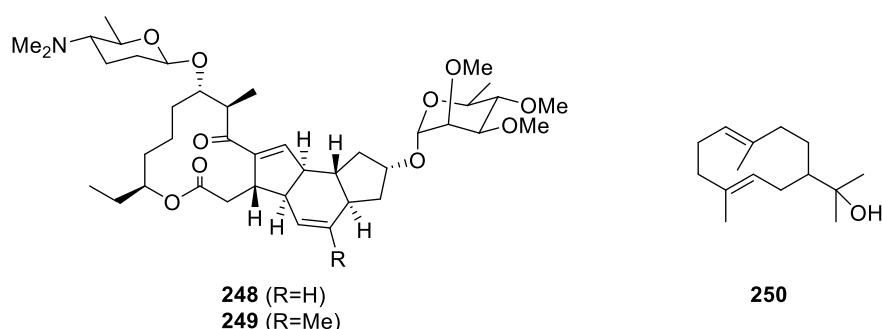


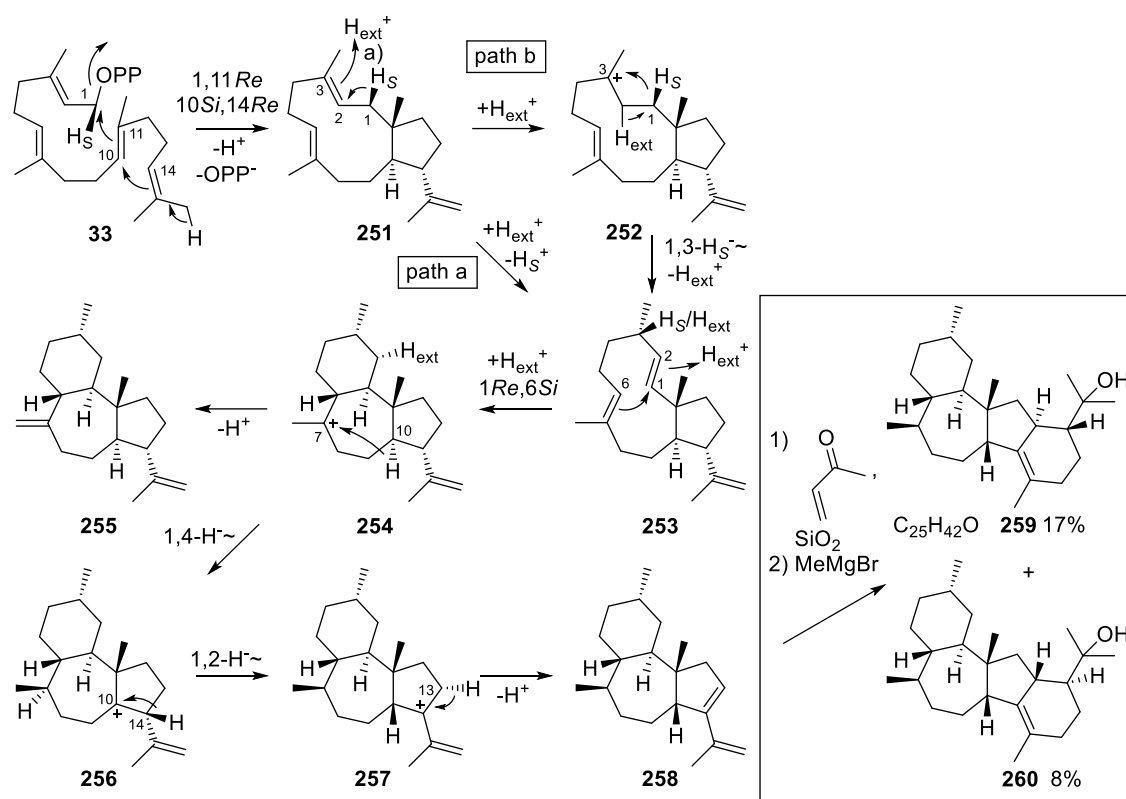
**Figure 23.** Structures of spinosyn A (**248**) and D (**249**) and of hedycaryol (**250**).

An important aspect of the success of in vitro isotopic labelling experiments on TSs, especially compared to in vivo labelling, are the clear incorporation results of labelled atoms. This means that a labelled atom is usually transferred to one defined position in the product with the same isotope ratio as present in the starting material and without any dilution, scrambling or distribution. This is due to TS catalysis, which usually guides the reaction on a clearly defined, stereo-controlled pathway. One deviation from this rule was already discussed in case of the geminal methyl group scrambling for 1,2-hydride shifts to isopropyl groups. Another example for an ill-defined course of a cyclisation mechanism resulting in scrambled atom origins in the product is given in the introduced publication that describes the challenging investigation of a DTS forming its products in a branched mechanism.

## Summary

An incubation of the TS with GGPP resulted in the formation of one main product **258** (Scheme 32), which was named spinodiene A, accompanied by two side products, spinodiene B (**255**) and 2,7,18-dolabellatriene (**253**).<sup>[263]</sup> The structures of **258** and **255** resemble an unprecedented diterpene skeleton. After the absolute configurations were determined by the discussed enantioselective labelling method utilising (*R*)- and (*S*)-(1-<sup>13</sup>C,1-<sup>2</sup>H)GPP, the corresponding FPPs and (*E*)- and (*Z*)-(4-<sup>13</sup>C,4-<sup>2</sup>H)IPP, the cyclisation mechanism was studied in depth by conversion of all twenty (<sup>13</sup>C<sub>1</sub>)-isotopomers of GGPP

and several other labelling experiments. These efforts resulted in a proposed cyclisation mechanism for spinodiene synthase (SoS), which is depicted in Scheme 32.



**Scheme 32.** Proposed cyclisation mechanism catalysed by SoS and the Diels-Alder based synthetic conversion (framed) of spinodiene A (**258**) to sesterterpene alcohols **259** and **260**. Hydrogen atoms from the medium are designated as  $H_{ext}$ .

After an initial 1,11-10,14-cyclisation, the intermediary cation is deprotonated to **251**. This neutral intermediate isomerises to side product **253**, for which two parallel operating pathways are assumed, because a mixed incorporation of label was observed for the hydrogen at C-3. Different experiments showed that one part of H-3 originates from the external medium ( $H_{ext}$ ), suggesting a reprotonation at C-3 and a deprotonation of  $H_S$ -1 (path a), whereas the other part consists of  $H_S$ -1, which fits to a 1,3-hydride shift via cation **252** (path b). These two paths converge to **253**, which is reprotonated at C-2 to induce further 1,6-ring closure to the tertiary cation **254**, whose direct deprotonation product is spinodiene B (**255**). As an alternative, a 1,4-hydride shift of **254** leads to **256**, which stabilises to the allylic cation **257** by a 1,2-hydride shift. The suprafacial hydrogen movements and the final deprotonation to give spinodiene A (**258**), which were followed by labelling experiments without exception (notably the latter by synthesis of (*R*)- and (*S*)-(1-<sup>2</sup>H)IPP being enzymatically isomerised to the labelled DMAPPs), all proceed with an *anti*-stereochemical course with respect to the preceding event.

The unusual conjugated diene moiety in **258** was also exploited to perform Diels-Alder reactions, e. g. with methyl vinyl ketone on  $SiO_2$ <sup>[264]</sup> followed by a Grignard reaction with methylmagnesium bromide to yield the sesterterpene alcohols **259** and **260**, which despite being artificial, obey the isoprene rule.

## Chapter 15

### Addressing the Chemistry of Germacrene A by Isotope Labeling Experiments

Jan Rinkel and Prof. Dr. Jeroen S. Dickschat\*

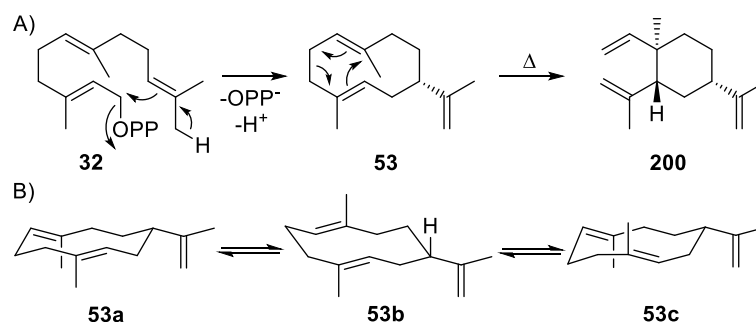
*Org. Lett.* **2019**, *21*, 2426–2429.

Reprinted from *Org. Lett.* **2019**, *21*, 2426–2429 with kind permission from the American Chemical Society. Copyright 2019 American Chemical Society.

The publication “Addressing the Chemistry of Germacrene A by Isotope Labeling Experiments” is attached in Appendix O.

## Introduction

The NMR-based structure elucidation of terpenes is not only challenging by the complex carbon skeletons that are found within this class of natural products, but there are also known examples of conformational isomerism, that severely obscures the signal assignment. For instance, the already discussed sesquiterpene germacradienol **99** consists of two conformers in solution as observed by NMR.<sup>[127]</sup> As it has been demonstrated, isotopically labelled substrates can significantly simplify these complex datasets and allow for an assignment of all signals. A different and even more complex example is constituted by germacrene A (**53**, Scheme 33). This monocyclic sesquiterpene was already isolated in 1970<sup>[265]</sup> and is frequently encountered in mechanistic proposals for sesquiterpene cyclisations. Despite the central role of **53** and its corresponding germacradienyl cations, a complete characterisation of this compound by NMR was never accomplished. Besides of **53** being an unstable molecule that easily undergoes acid catalysed ring closure during purifications and Cope rearrangement to give  $\beta$ -elemene (**200**),<sup>[266]</sup> these difficulties are mainly attributed to the three coexisting conformers of **53** in solution.



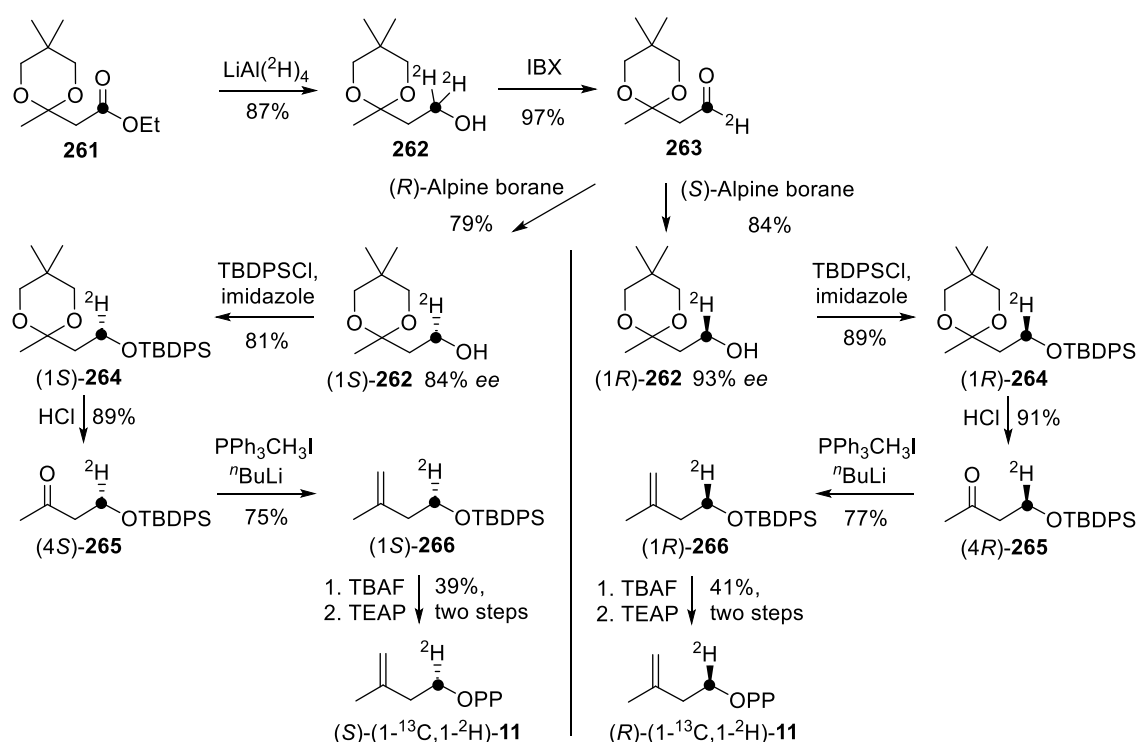
**Scheme 33.** A) Cyclisation of FPP to germacrene A (**53**) and its Cope rearrangement to  $\beta$ -elemene (**200**). B) Structures representing the three conformers of **53** observed in solution.

Their structures **53a–c** were investigated by NOE studies constituting a mixture of 5:3:2.<sup>[267]</sup> Although the  $^{13}\text{C}$ -NMR signals of the main conformer **53a** could be assigned, the signals of **53b** and **53c** were not even found completely, because they are significantly broadened, which lowers the signal intensity. For their similar chemical environment, especially the signals of methylene group hydrogen atoms are heavily overlaying, which makes any assignment of the  $^1\text{H}$ -NMR in the aliphatic region impossible. Therefore, the introduced study targets this problem by an isotopic labelling strategy with the aim to address every diastereotopic hydrogen atom and every carbon position for a complete NMR dataset of this challenging molecule.

## Summary

A germacrene A (**53**) synthase from the marine actinomycete *Micromonospora marina* was cloned and expressed in *E. coli* to prepare all fifteen ( $^{13}\text{C}_1$ )-isotopomers of **53**. The

$^{13}\text{C}$ -NMR data for these samples allowed for an assignment of almost all carbon positions for **53a–c**.<sup>[268]</sup> One position of the minor conformers was obscured by signal overlap. For assigning the  $^1\text{H}$ -NMR data, HSQC experiments with the singly labelled samples were performed to correlate the olefinic- and methyl group signals. Since the available enantioselectively deuterated substrates are insufficient to address every methylene group of **53** (C-9 is missing), (*R*)- and (*S*)-(1- $^{13}\text{C}$ ,1- $^2\text{H}$ )IPP were synthesised according to established synthetic procedures<sup>[212]</sup> (Scheme 34, cf. Chapter 3). Starting from  $^{13}\text{C}$ -labelled ester **261**, a reduction with  $\text{LiAl}(\text{}^2\text{H})_4$  gives doubly deuterated alcohol **262**, which was oxidised to **263**. Enantioselective reduction with Alpine borane yielded the chiral singly deuterated alcohols **262**, which were protected to give the silanes **264**. Acidic deprotection of the ketals furnished the ketones **265**, which were subjected to a Wittig reaction to give the alkenes **266**. These were deprotected and the volatile alcohol was directly phosphorylated to yield the desired labelled substrates. With these molecules in hand, FPPS, the IDI-mediated isomerisation to the labelled DMAPPs and in combination with (*E*)- and (*Z*)-(4- $^{13}\text{C}$ ,4- $^2\text{H}$ )IPP, it was possible to target every methylene group (cf. Chapter 16) in **53a–c** in a stereospecific way to complete the  $^1\text{H}$ -NMR assignment.



**Scheme 34.** Synthesis of (*R*)- and (*S*)-(1- $^{13}\text{C}$ ,1- $^2\text{H}$ )IPP.

The labelled samples of **53** were also subjected to Cope rearrangement to investigate the stereochemical course of this reaction with respect to the incorporation of methylene hydrogen atoms into the olefinic positions of **200** being in line with previous assumptions.<sup>[269]</sup> Using the EI-MS data of the labelled samples, also a putative Cope fragmentation is discussed.

These results emphasise the value of selectively labelled substrates to shed light on complex NMR data by reducing the number of signals. Even with more material, the reached level of assignment would not have been possible using unlabelled **53**.

## Chapter 16

### **Diterpene Biosynthesis in Actinomycetes: Studies on Cattleylene Synthase and Phomopsene Synthase**

Jan Rinkel, Simon T. Steiner and Prof. Dr. Jeroen S. Dickschat\*

*Angew. Chem. Int. Ed.* **2019**, *58*, accepted, DOI: 10.1002/anie.201902950;  
*Angew. Chem.* **2019**, *131*, accepted, DOI: 10.1002/ange.201902950.

Reprinted from *Angew. Chem. Int. Ed.* **2019**, *58* as an accepted article with kind permission from John Wiley and Sons.

The ozonolysis reactions on the two investigated diterpenes, the characterisation and structure elucidation of products and their aldol reactions were performed by me. I also contributed to the characterisation of one diterpene product and to the incubation experiments using the recombinant TSs including their analyses.

The publication “Diterpene Biosynthesis in Actinomycetes: Studies on Cattleylene Synthase and Phomopsene Synthase” is attached in Appendix P.

## Introduction

Building upon the pioneering identification of fusicocca-2,10(14)-diene (**241**) synthase (PaFS),<sup>[220]</sup> also a related homologue of this enzyme was found from the same phytopathogenic fungus, *Phomopsis amygdali*. This bifunctional DTS (PaPS) was shown to produce phomopsene (**267**, Figure 24), and by comparison to its NMR chemical shifts, also a corresponding oxidised metabolite of the fungus could be identified as methyl phomopsenoate (**268**).<sup>[270]</sup> The cyclisation mechanism towards the tetracyclic diterpene **267** was investigated by the enzymatic preparation of deuterated isotopologues starting from labelled IPPs and their analysis by EI-MS.<sup>[258c]</sup>

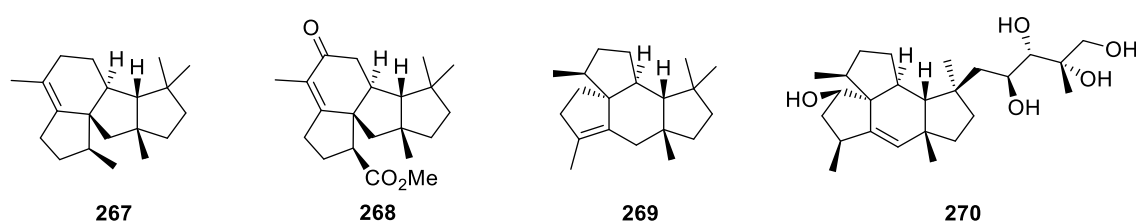


**Figure 24.** Structures of phomopsene (**267**) and related compounds.

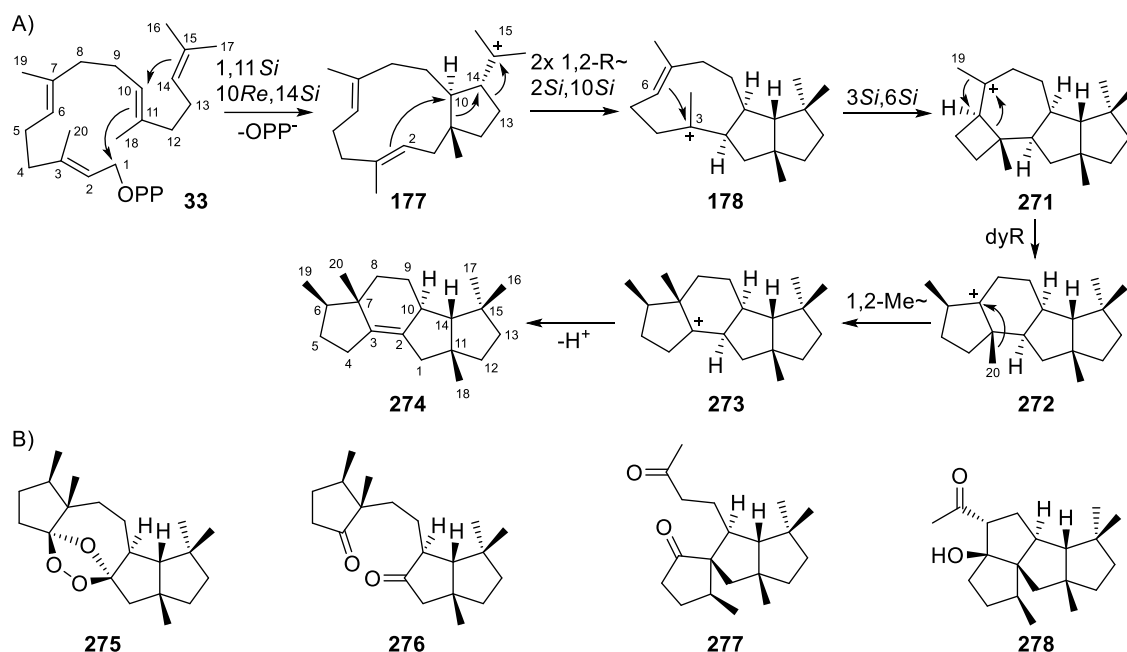
However, the occurrence of **267** seems to be more widespread than initially assumed, since also a bacterial TS from *Allokutzneria albata* producing the same molecule in a mixture with allokutznerene (**269**) was identified (Appendix L).<sup>[259]</sup> Intriguingly, **269** in turn resembles the core structure of mangicdiene,<sup>[271]</sup> the biosynthetic sesterterpene precursor of mangicol A (**270**), which was isolated from a marine *Fusarium* strain and shows anti-inflammatory activities.<sup>[272]</sup> These examples together with other related diterpene structures<sup>[212,271,273]</sup> demonstrate a highly interconnected web of structurally interesting di- and sesterterpenoids from fungi and from bacteria built via similar cyclisation mechanisms. The introduced publication describes the characterisation of three newly identified bacterial DTSs, of which two produce **267** and the product of one was characterised as a new, but still related structure. Therefore, this study expands the enzymatic and structural space of the discussed interesting group of terpenoids.

## Summary

A DTS from *Streptomyces cattleya* was identified as a cattleyene (**274**, Scheme 35) synthase (CyS).<sup>[274]</sup> Its cyclisation mechanism was investigated by conversion of all twenty (<sup>13</sup>C<sub>1</sub>)-isotopomers of GGPP. The results were in line with the proposed mechanism shown in Scheme 35, which starts by cyclisation of GGPP to **177**. Ring expansion, contraction and 2,10-cyclisation yields **178**, which can cyclise to **271**. By a dyotropic rearrangement (dyR) involving 1,2-migration of a methyl group and ring expansion, tertiary cation **272** is furnished. An additional methyl migration gives **273**, which is deprotonated to the final product **274**. Two other DTSs from *Nocardia testacea* und *N. rhamnosiphila* yielded **267**. To expand the chemical space of the two diterpenes, both were subjected to epoxidation and ozonolysis reactions, giving access to the four

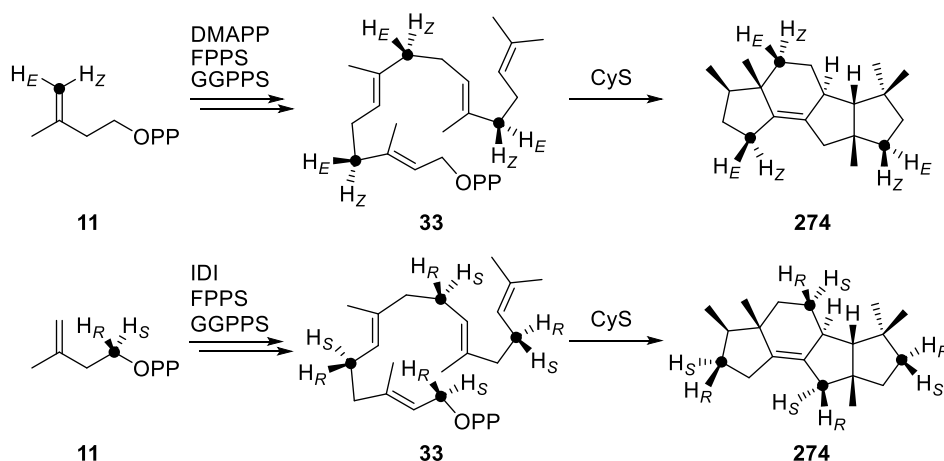


epoxides, but also to the unusual ozonide **275**, the dioxides **276** and **277**, and, by an aldol reaction of **277**, to the alcohol **278**. Although none of these products were found in the organisms, all three DTSSs are clustered with CYPs, indicating oxidation chemistry.



**Scheme 35.** A) Proposed cyclisation mechanism towards cattleyene (**274**). B) Structures of selected synthetically oxidised terpenoids.

Completing the structure elucidation of the new natural product **274**, its absolute configuration was targeted by incubation experiments combining the two previously discussed sets of selectively deuterated and  $^{13}\text{C}$ -labelled IPPs including (*E*)- and (*Z*)-(4- $^{13}\text{C}$ ,4- $^2\text{H}$ )IPP and (*R*)- and (*S*)-(1- $^{13}\text{C}$ ,1- $^2\text{H}$ )IPP. By their enzymatic isomerisation and elongation to labelled GGPPs, all methylene groups of **274** were stereochemically addressed to be in line with the shown absolute configuration (Scheme 36).



**Scheme 36.** Stereochemical assignment of every methylene group in **274** by four incubation experiments using (*E*)- and (*Z*)-(4- $^{13}\text{C}$ ,4- $^2\text{H}$ )IPP and (*R*)- and (*S*)-(1- $^{13}\text{C}$ ,1- $^2\text{H}$ )IPP. Black dots show  $^{13}\text{C}$ -labelled carbon atoms.

## Chapter 17

### **Stereochemical investigations on the biosynthesis of achiral (*Z*)- $\gamma$ -bisabolene in *Cryptosporangium arvum***

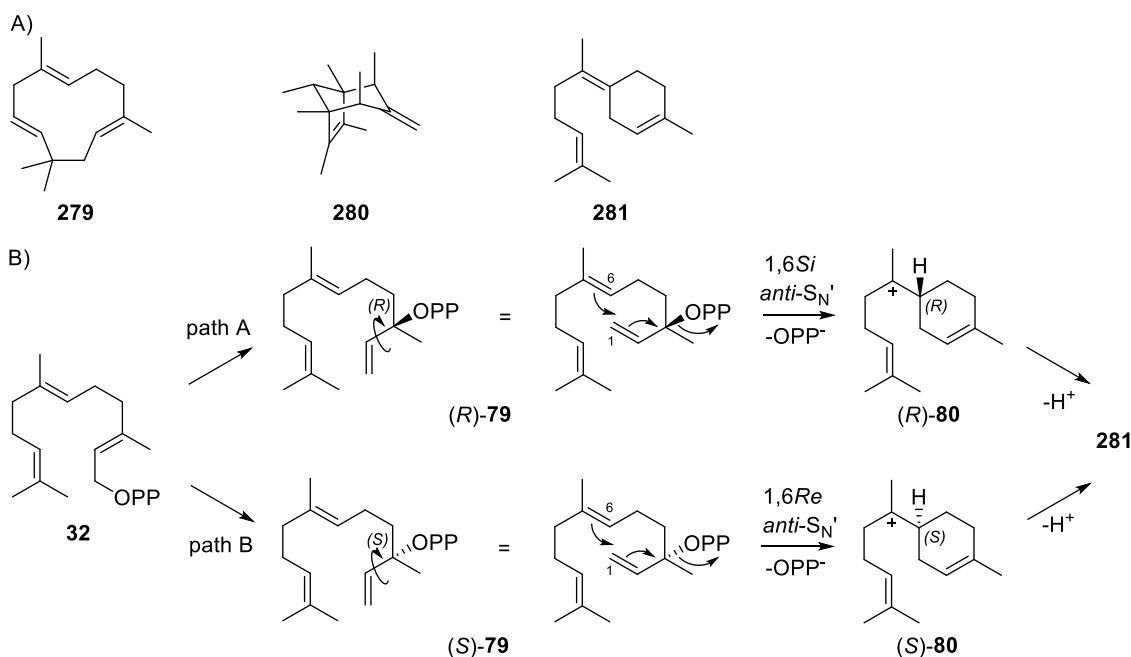
Jan Rinkel and Prof. Dr. Jeroen S. Dickschat\*

*Beilstein J. Org. Chem.* **2019**, *15*, 789–794.

The publication “Stereochemical investigations on the biosynthesis of achiral (*Z*)- $\gamma$ -bisabolene in *Cryptosporangium arvum*” is attached in Appendix Q.

## Introduction

As demonstrated in Chapter 5, the investigation of TSs that produce achiral compounds is a particular challenge. Achiral terpenes are by far the minor case, but there are still important examples known such as the already discussed (*E*)- $\beta$ -farnesene (**4**) and 1,8-cineol (**164**), but also  $\alpha$ -humulene (**279**, Scheme 37), the unusual methylated sesquiterpene sodorifen (**280**)<sup>[275]</sup> and (*Z*)- $\gamma$ -bisabolene (**281**). Contrasting the synthetic efforts towards these molecules, which are certainly free of chiral intermediates, the biosynthesis takes place in a chiral environment. Therefore, the occurrence of chiral intermediates is likely even though this stereochemistry is destroyed towards the final structure. This is exemplified for the cyclisation mechanism towards **281** as depicted in Scheme 37. The 1,6-cyclisation presupposes a (*Z*)-configured C-2,C-3 double bond, which can be archived by the involvement of NPP (**79**), a chiral tertiary diphosphate. NPP is then cyclised to the chiral bisabobyl cation (**80**), which is finally deprotonated to give **281**. Therefore, a TS producing **281** has multiple options for these chiral intermediates. However, inferring the absolute configurations of them is highly challenging, if there are no chiral side products found.

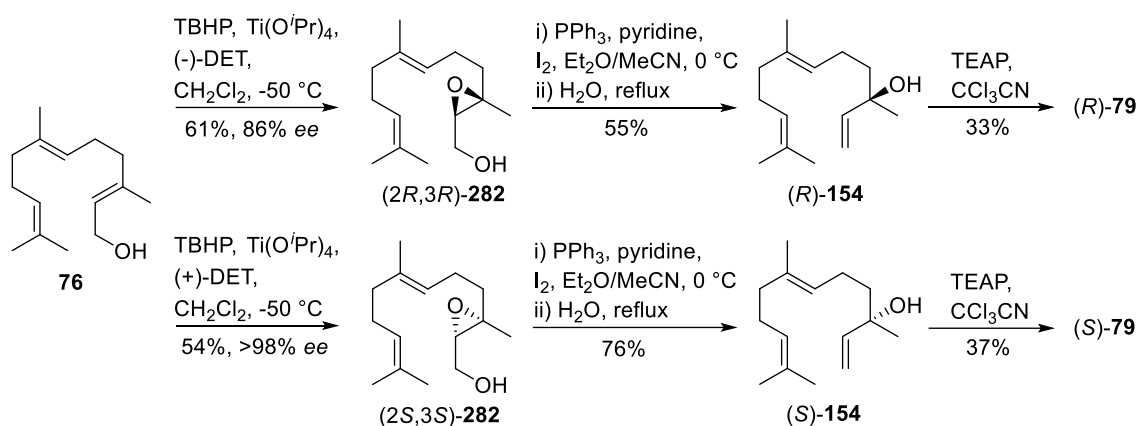


**Scheme 37.** A) Selected structures of achiral TS products. B) Two alternative pathways involving chiral intermediates towards achiral (*Z*)- $\gamma$ -bisabolene (**281**).

This publication describes the investigation of a newly characterised TS for **281** consisting of the approach to test the two enantiomers of NPP for a conclusion of its stereochemical course.

## Summary

A TS from *Cryptosporangium arvum* was cloned, heterologously expressed in *E. coli* and identified as a (*Z*)- $\gamma$ -bisabolene (**281**) synthase (BbS).<sup>[276]</sup> To obtain insights into the stereochemical course of its cyclisation mechanism, (*R*)- and (*S*)-NPP were synthesised (Scheme 38) by Sharpless epoxidation<sup>[277]</sup> of farnesol (**76**) to yield epoxides **282** with good to excellent enantiomeric excesses, followed by iodination and elimination to give the two enantiomers of nerolidol (**154**).<sup>[278]</sup> Their enantiomeric purities were enlarged by preparative HPLC on a chiral stationary phase to result in *ee* >99% for both samples, which were then phosphorylated<sup>[194b,197]</sup> to the chiral NPPs.



**Scheme 38.** Synthesis of (*R*)- and (*S*)-NPP (**79**). TBHP: *tert*-butyl hydroperoxide; DET: diethyl tartrate; TEAP: bis(triethylammonium) phosphate.

Compared to the sluggish conversion of their higher GLPP homologues with hydrophyrene and  $\beta$ -pinacene synthase (Chapter 7),<sup>[214]</sup> the incubations of both NPPs with purified BbS yielded in surprisingly clear results. Whereas (*R*)-NPP gave **281**, the incubation of (*S*)-NPP resulted in the selective formation of **4**, which is explainable by the elimination of diphosphate from an unproductive binding of (*S*)-NPP inside the active site. These findings clearly demonstrate (*R*)-NPP being involved in the BbS catalysed cyclisation mechanism towards **281**. However, the absolute configuration of the bisabolyl cation (**80**) cannot be inferred from these experiments, because it depends upon the diastereotopic face of C-6 involved in cyclisation. Therefore, it remains elusive if **281** is formed from (*R*)-**80** as shown in Scheme 37 and supported by different other sesquiterpene cyclisations involving NPP and **80**,<sup>[110,117,120]</sup> or if the opposite enantiomer (*S*)-**80** is relevant in this case. Nevertheless, the substrates (*R*)- and (*S*)-NPP expand the toolbox to investigate sesquiterpene synthases for the important question towards the stereochemical course of their initial isomerisation reactions.

## Chapter 18

### **Mechanistic investigations on multiproduct $\beta$ -himachalene synthase from *Cryptosporangium arvum***

Jan Rinkel and Prof. Dr. Jeroen S. Dickschat\*

*Beilstein J. Org. Chem.* **2019**, *15*, 1008–1019.

The publication “Mechanistic investigations on multiproduct  $\beta$ -himachalene synthase from *Cryptosporangium arvum*” is attached in Appendix R.

## Introduction

This publication is related to Chapter 10, because it also deals with a TS characterised by high promiscuity with respect to its products but also to its substrates, and simultaneously continues the work on TSs from the soil actinomycete *Cryptosporangium arvum* (Chapter 17). Unlike other classes of enzymes, the selectivity of TSs is easily regulated by evolution with modifying the active site cavity. The reaction of the oligoprenyl diphosphates may then proceed either highly selective to yield only one product, or with a more loose control allowing the unselective nature of the carbon cation chemistry imprinted by the reactive substrates<sup>[52b]</sup> to result in multiple products. Examples begin with 15 different products from *Fusarium sporotrichioides* trichodiene synthase,<sup>[279]</sup> continues with a TS from *Medicago truncatula* with 27 products<sup>[191b]</sup> and probably spikes in  $\gamma$ -humulene synthase from *Abies grandis* from which at least 52 different products have been reported.<sup>[236]</sup> Although being far away from these high numbers, the introduced TS from *C. arvum* also produces quite a few products, which requires a detailed mechanistic model to explain their formations. This aim was approached by isotopic labelling experiments.

## Summary

The TS from *C. arvum* was identified as a multiproduct  $\beta$ -himachalene (**283**) synthase (HcS) possessing additional mono- and diterpene synthase activity.<sup>[280]</sup> Figure 25 shows the observed products from FPP including **283**,  $\alpha$ -himachalene (**284**),  $\gamma$ -himachalene (**285**), longifolene (**286**), longicyclene (**287**),  $\alpha$ -longipinene (**288**), 9-*epi*- $\beta$ -caryophyllene (**289**) and  $\gamma$ -humulene (**290**).

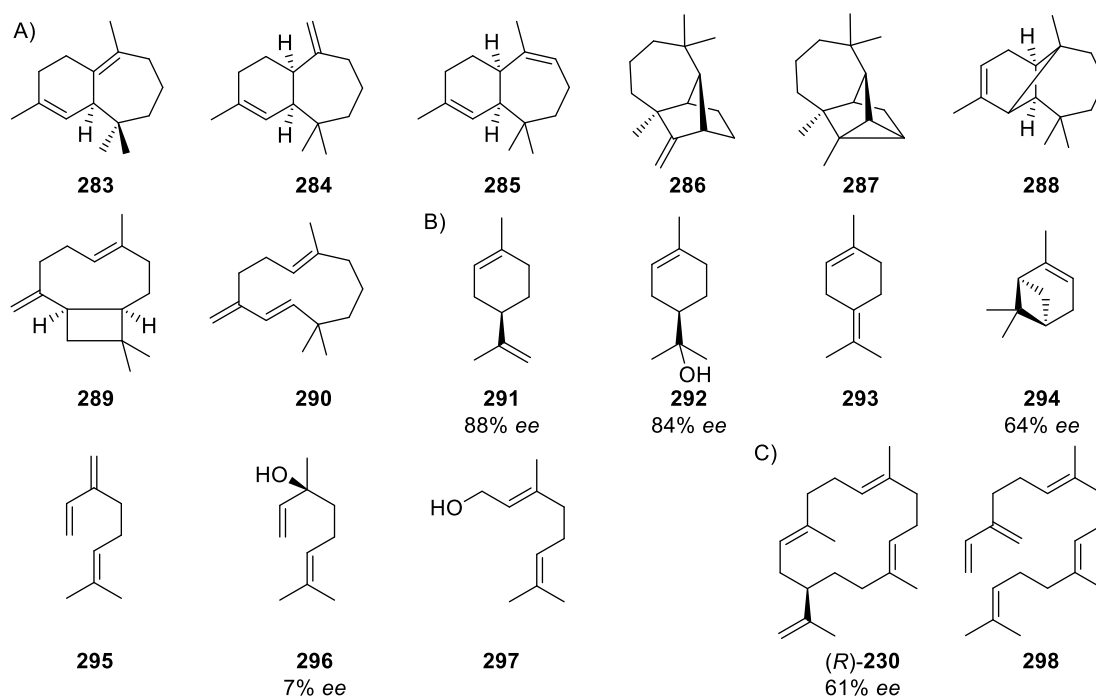
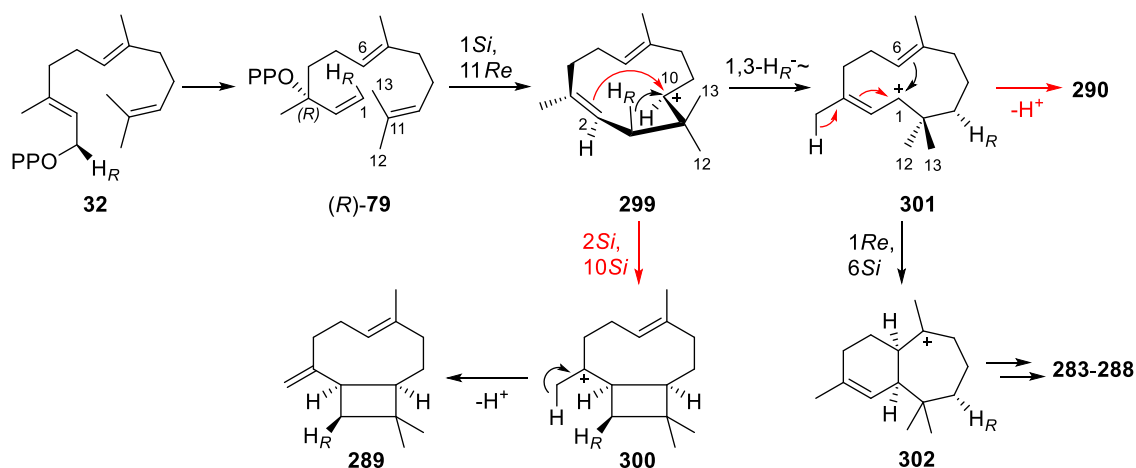


**Figure 25.** Structures of identified products from incubation experiments with HcS and A) FPP, B) GPP and C) GGPP.

Also cyclised monoterpenes from GPP were observed, such as limonene (**291**),  $\alpha$ -terpineol (**292**),  $\alpha$ -terpinolene (**293**) and  $\alpha$ -pinene (**294**), but also acyclic  $\beta$ -myrcene (**295**), linalool (**296**) and geraniol (**297**). Conversion with GGPP yielded cembrene A (**230**) and  $\beta$ -springene (**298**). The absolute configurations of the mono- and diterpene products were investigated by GC on a chiral phase, revealing that enantiomeric mixtures are present. To propose a comprehensive mechanistic picture of the formation of sesquiterpenes by HcS, several labelling experiments were conducted. The cyclisation (Scheme 39) starts by isomerisation of FPP to (*R*)-NPP, which was solidified by incubation of both enantiomeric NPPs. A 1*Si*,11*Re*-ring closure yields cation **299**, which either undergoes a 2*Si*,10*Si*-cyclisation to form the caryophyllenyl cation **300** giving rise to the side product **289**, or stabilises by a 1,3-hydride shift to the allylic cation **301**. After 1*Re*,6*Si*-ring closure, himachalyl cation **302** is furnished, which is discussed to be the precursor of **283–288**.<sup>[281]</sup>



**Scheme 39.** Proposed initial cyclisation mechanism of FPP catalysed by HcS. Alternative mechanistic and reaction arrows at branching points are shown in red.

Intriguingly, the initial cyclisation of (*R*)-NPP as deduced by following the stereochemical course of the C-1 hydrogen atoms towards **289** proceeds by a formal *syn*- $S_N'$  reaction contrasting the usual *anti*-case (cf. Chapter 3).<sup>[191]</sup> This result emphasises that predictions of this stereochemical link should be made with care, especially for flexible situations like the 1,11-cyclisation towards **299**. The reactive conformation of NPP to allow for this cyclisation is also characterised by the diphosphate moiety being bound near the “backside” of the formed cation (with respect to the presentation shown in Scheme 39). This positioning is also suitable for the diphosphate to be involved in deprotonation of the cyclising cation at multiple positions, giving rise to the observed low selectivity of HcS. In fact, the stereochemical courses of the deprotonation events for **285**, **287** and **288** as followed by labelling experiments all showed the abstraction of the “backwards” pointing hydrogen.

Taken together, the experiments performed with HcS represent a nice example how detailed stereochemical investigations can lead to an idea about the backgrounds of an observed TS reactivity at the molecular level.

## Chapter 19

### The EI-MS Fragmentation Mechanisms of Bacterial Sesquiterpenes and Diterpenes

Jan Rinkel, Dr. Patrick Rabe and Prof. Dr. Jeroen S. Dickschat\*

*Eur. J. Org. Chem.* **2019**, 351–359.

Reprinted from *Eur. J. Org. Chem.* **2019**, 351–359 with kind permission from John Wiley and Sons.

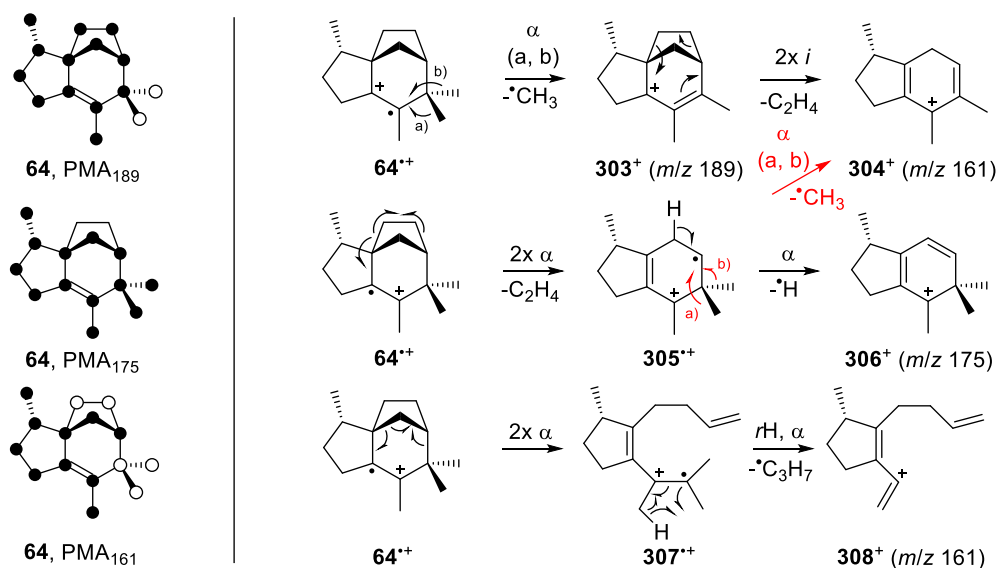
The preparation and analysis of singly labelled isotopomers of T-muurolol (**148**), the GC/MS analysis of labelled SpS and SaS products and HR-MS/MS experiments were performed by me.

The publication “The EI-MS Fragmentation Mechanisms of Bacterial Sesquiterpenes and Diterpenes” is attached in Appendix S.



## Introduction

This chapter concludes the presented work on natural TSs with the investigation of EI-MS fragmentation mechanisms. This beneficial aspect of singly ( $^{13}\text{C}_1$ )-labelling has been already included in some publications discussed in Chapters 4, 15, 16 and 18, but will be presented in more detail here. The conversion of all ( $^{13}\text{C}_1$ )-isotopomers with a purified TS results in the formation of specifically labelled terpenes. Besides the NMR investigation providing valuable insights into the cyclisation mechanism of a TS, these samples can also be used for a position-specific mass shift analysis (PMA)<sup>[127,282]</sup> by GC/MS. With this method, all obtained mass spectra are compared to that of the unlabelled compound to identify, which carbon position contributes to a selected fragment ion by a mass shift of +1 Da. Combining these information, the carbons included in the fragment can be determined precisely to suggest fragmentation mechanisms. Since EI-MS spectra are hard to predict,<sup>[283]</sup> especially for complex molecules such as terpenes, a better understanding of these mechanisms may lead to more precise predictions of unknown trace metabolites. Previous studies to investigate terpene fragmentations heavily relied on the synthetic preparation of labelled terpenes<sup>[284]</sup> or in vivo feeding experiments, which may result in the dilution of label.<sup>[12a,285]</sup> Thus, the opportunity provided by the enzymatic synthesis of all ( $^{13}\text{C}_1$ )-isotopomers can be considered as unique. Scheme 40 shows three PMAs for *epi*-isozizaene (**64**) as an example together with proposed fragmentation mechanisms explaining them.<sup>[282]</sup> PMA<sub>189</sub> can be rationalised by ionisation of the double bond to **64<sup>++</sup>** followed by a cleavage of either of the two methyl groups to **303<sup>+</sup>**. Two inductive cleavages (*i*) of this cation gives rise to **304<sup>+</sup>**, which contributes to PMA<sub>161</sub>. Also the ethylene bridge of **64<sup>++</sup>** may lose ethene by two  $\alpha$  fragmentations to yield **305<sup>++</sup>**, which can lose a hydrogen atom to explain PMA<sub>175</sub> by **306<sup>+</sup>**, or also contribute to PMA<sub>161</sub> by the loss of a methyl group to **304<sup>+</sup>**. Finally, PMA<sub>161</sub> missing the quaternary carbon can be explained by two  $\alpha$  cleavages to **307<sup>++</sup>** followed by a hydrogen rearrangement (*rH*) and the loss of a propyl radical to yield **308<sup>+</sup>**.



**Scheme 40.** Selected PMAs ( $m/z = 189, 175, 161$ ) for *epi*-isozizaene (**64**). Full or partial incorporation of  $^{13}\text{C}$  into fragments is represented by black or white dots, respectively.<sup>[282]</sup>

These examples already demonstrate the complexity of multiple reaction pathways contributing to an observed mass signal. However, even in these situations, PMA provides important insights into the structural features of contributing ions.

The introduced publication presents the application of this technique to study the EI-MS fragmentation mechanisms of one sesquiterpene and several diterpenes from TSs that have been discussed in previous chapters of this work.

## Summary

The PMA methodology was applied on T-muurolool (**148**)<sup>[192c]</sup> and the diterpene products tsukubadiene (**174**, Chapter 6),<sup>[212]</sup> spata-13,17-diene and prenylkelsoene (**208** and **212**, Chapter 10),<sup>[239]</sup> and spiroalbatene (**228**, Chapter 11).<sup>[244]</sup> Figure 26 shows selected PMAs observed for these terpenes.<sup>[286]</sup>

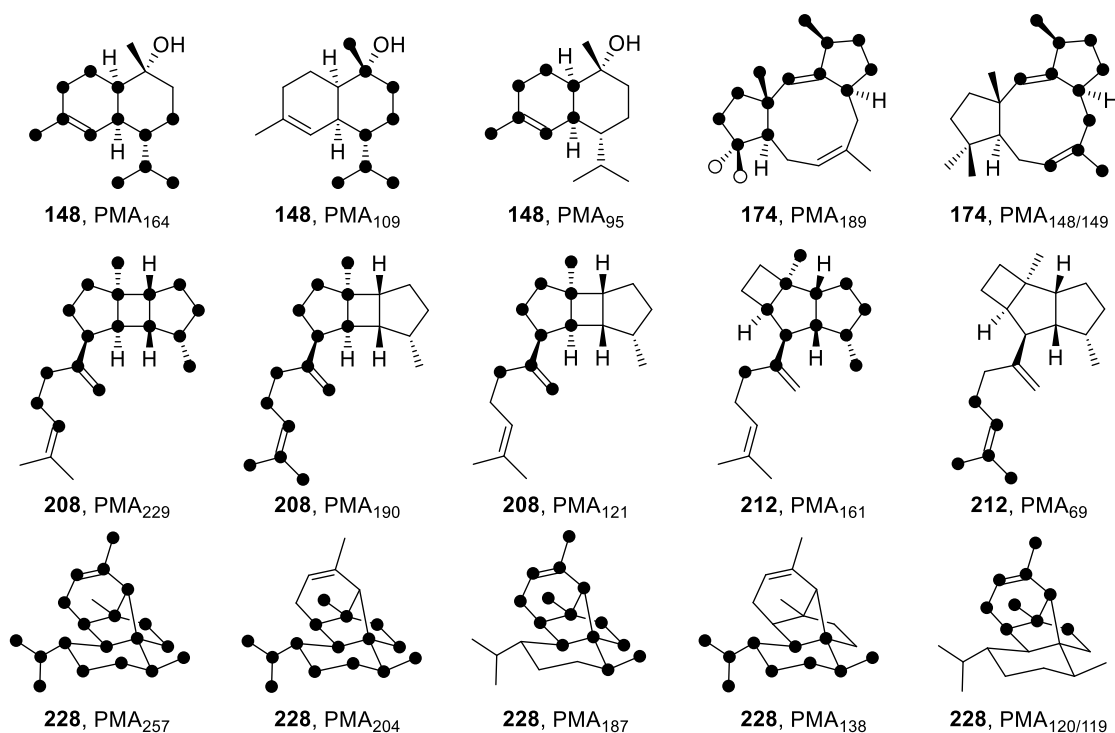


**Figure 26.** Selected PMAs of the investigated terpenes.<sup>[286]</sup>

Based on this information, suitable EI-MS fragmentation mechanisms were proposed and discussed. Some mother/daughter ion relationships, for instance PMAs 190 and 121 of **208**, were also investigated by HR-MS/MS experiments by fragmenting ions of selected masses for the second time.

In conclusion, the detailed investigation of EI mass spectra obtained from labelled compounds, which have been conveniently made available through enzymatic synthesis provides interesting insights into the fragmentation mechanisms of complex carbon scaffolds. These insights may be used for developing better prediction models for EI-MS, which has become a standard analytical method for the detection of trace compounds especially important in the field of natural product chemistry.

## Chapter 20

### **Sesquiterpene cyclizations catalysed inside the resorcinarene capsule and application in the short synthesis of isolongifolene and isolongifolenone**

Dr. Qi Zhang, Jan Rinkel, Prof. Dr. Bernd Goldfuss, Prof. Dr. Jeroen S. Dickschat and Prof. Dr. Konrad Tiefenbacher\*

*Nat. Catal.* **2018**, *1*, 609–615.

Reprinted from *Nat. Catal.* **2018**, *1*, 609–615 with kind permission from Springer Nature.

The synthesis of (2Z)-(1-<sup>13</sup>C)cyclofarnesyl acetate and the analysis of the corresponding labelling experiment were performed by me.

The publication “Sesquiterpene cyclizations catalysed inside the resorcinarene capsule and application in the short synthesis of isolongifolene and isolongifolenone” is attached in Appendix T.

## Introduction

The elegant cyclisation reactions catalysed by TSs have also gained a lot of attention from synthetic chemists. Since the total synthesis of terpenes represents a general challenge for their complex carbon frameworks, which require multiple step transformations with functional groups that need to be removed afterwards, nature's strategy to assemble these molecules in just one step is appealing. However, a biomimetic approach is still a huge challenge, because artificial catalysts that mimic the complex architecture of TSs are not available. Instead, some reports focus on cationic transformations in solution with the aid of strong Brønsted or Lewis acids.<sup>[287]</sup> While the reactions described are also taking place inside of a TS, important features for their catalysis are missing, which lowers the selectivity and occasionally limits the application of these reactions in total synthesis. Another approach are supramolecular capsules or cages, which provide a confined space shielding the reactive cationic intermediates from their surroundings. One example consists of resorcinarene **309** (Figure 27) and its derivatives with varied R groups building up a hexameric capsule with eight molecules of water in apolar solvents.<sup>[288]</sup> Defining an internal volume of 1.4 nm<sup>3</sup>, these capsules allow guest molecules to enter the cavity. For this "enzyme-like" behaviour, they have been applied in the catalysis of different other chemical reactions<sup>[289]</sup> and, more recently, also to mimic monoterpene cyclisations.<sup>[290]</sup> An important benefit are cation- $\pi$  interactions provided by the aromatic cavity and the possibility to vary the cation-creating leaving group.

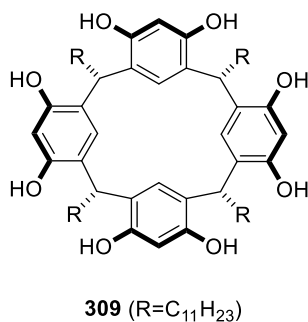
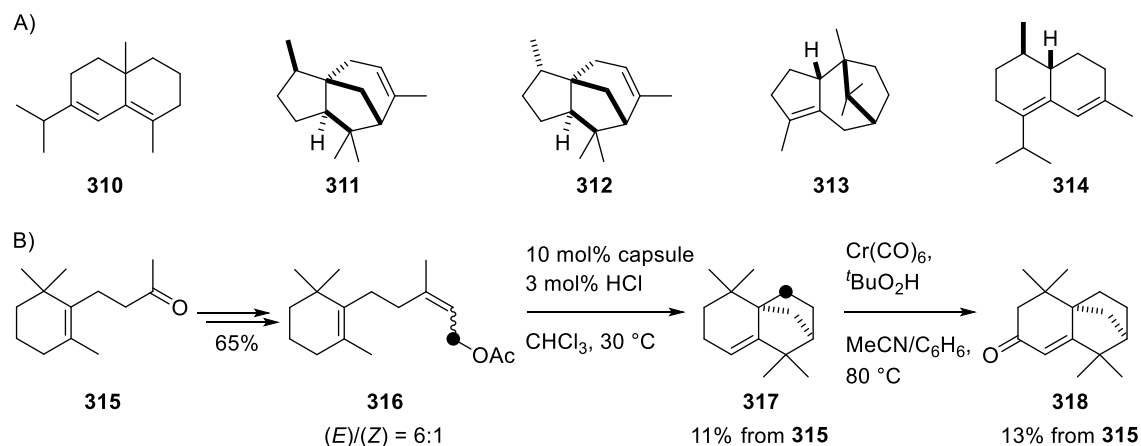


**Figure 27.** Structure of resorcinarene **309**, which assembles to cage-like structures in apolar solvents.

Although the synthesis of monoterpenes by this artificial, TS-like catalyst is an important step demonstrating the capability of the capsule, the chemical space of monoterpenes and the applications of them in total synthesis are limited. Therefore, the introduced study focusses on the synthesis of sesquiterpenes by the supramolecular assembly. Since also the cyclisation mechanisms taking place inside the catalyst are of interest, an isotopic labelling strategy is used to highlight mechanistic aspects.

## Summary

The resorcinarene capsule was applied on the synthesis of sesquiterpenes.<sup>[291]</sup> With the reaction being supplemented by 3 mol% HCl and performed in chloroform, the catalyst was able to convert different geometrical isomers of farnesol (**76**) and farnesyl acetate into a mixture of sesquiterpenes, while  $\delta$ -selinene (**310**, Scheme 41), 2-*epi*- $\alpha$ -cedrene (**311**),  $\alpha$ -cedrene (**312**),  $\epsilon$ -patchoulene (**313**) and 10-*epi*-zonarene (**314**) were identified as the main products. Although the complexity of these structures is remarkable, the overwhelming cyclisation possibilities of the linear substrates leads to a rather unselective outcome of these reactions decreasing the yield and hampering product isolation. Therefore, precyclised sesquiterpene substrates were also tested. It turned out that the reaction of cyclofarnesyl acetate (**316**) with the capsule gives isolongifolene (**317**) in good yields. Employing this strategy in a sequential synthesis, the conversion of inexpensive dihydro- $\beta$ -ionone (**315**) to **317** (11% yield) and further to isolongifolenone (**318**, 13% yield) was demonstrated.



**Scheme 41.** A) Main sesquiterpene products obtained by conversion of geometrical isomers of farnesol (**76**) and farnesyl acetate with the capsule. B) Synthesis of isolongifolene (**317**) and isolongifolenone (**318**) from **315** using an artificial terpene cyclisation as a key step. The black dots represent  $^{13}\text{C}$ -labelled carbon atoms in a labelling experiment with (2*Z*)-(1- $^{13}\text{C}$ )-**316**. The labelled atoms are not part of the synthesis.

Also the cyclisation mechanism towards **317** in this reaction was investigated by the conversion of synthesised (2*Z*)-(1- $^{13}\text{C}$ )-**316** with the capsule. Localisation of the labelled carbon atom in the ethylene- rather than the methylene bridge of **317** suggests a skeletal rearrangement contrasting a shorter sequence with a simple methyl migration. Both reaction pathways were analysed by quantum chemical calculations being in favour for the rearrangement option.

With the short and efficient synthesis of the complex sesquiterpene **315** being most impressive, the conversions of the linear substrates demonstrated that there are still many issues to solve until the long-term goal of an artificial TS-like catalyst tuneable to produce selected structures of defined absolute configurations is in reach.<sup>[292]</sup> In turn, these efforts also emphasise the synthetic value of natural TSs.

## Chapter 21

### **Volatiles from the hypoxylaceous fungi *Hypoxyton griseobrunneum* and *Hypoxyton macrocarpum***

Jan Rinkel, Alexander Babczyk, Dr. Tao Wang, Prof. Dr. Marc Stadler and Prof. Dr. Jeroen S. Dickschat\*

*Beilstein J. Org. Chem.* **2018**, *14*, 2974–2990.

The synthesis of reference compounds for the identification of volatiles and the conduction and analysis of a feeding experiment with *H. griseobrunneum* was contributed by me.

The publication “Volatiles from the hypoxylaceous fungi *Hypoxyton griseobrunneum* and *Hypoxyton macrocarpum*” is attached in Appendix U.

## Introduction

As discussed in Chapter 1.2, volatiles are important contributors to the natural taste and smell of fungi,<sup>[133,137,293]</sup> but also can be used as sensors to detect the production of harmful metabolites, like the sesquiterpene aristolochene (**319**, Figure 28) indicating the production of PR toxin in *Penicillium roqueforti*,<sup>[138]</sup> or determine the presence of a certain bacterial or fungal strain, which can be used for medicinal reasons.<sup>[294]</sup> The ecological roles of fungal volatiles are not known in most cases, although some molecules have been shown to participate in the communication between different strains and species.<sup>[295]</sup> Also, bioactivity is sometimes observed, as for lactone **320**, which inhibits the germination of ash seeds and was identified from the pathogenic fungus *Hymenoscyphus pseudoalbidus*.<sup>[296]</sup> Therefore, the identification of fungal volatiles is of interest to address ecological and applicational questions.

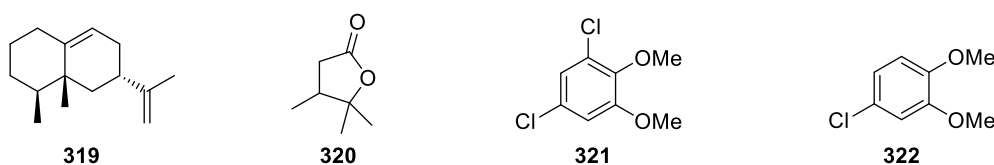


**Figure 28.** Structures of selected fungal volatiles.

Because of the small amounts to be dealt with, the analysis of volatiles is usually based on GC/MS.<sup>[297]</sup> For sample collection, methods like the solid phase microextraction (SPME),<sup>[298]</sup> which uses fused silica fibres, or the closed-loop stripping apparatus (CLSA),<sup>[299]</sup> in which air is constantly pumped through a charcoal filter to trap the volatiles, are frequently used. The identification is based on EI-MS compound libraries and retention indices, which are standardised by comparison with alkanes.<sup>[300]</sup> Besides being unable to identify unknown compounds without reference material, the unambiguous compound identification also struggles with isomers of known compounds, which have similar mass spectra and retention indices. For instance, the chlorinated dimethoxybenzene derivatives **321** and **322** identified in the headspace of an endophytic *Geniculosporium* sp. had to be synthesised along with all other possible regioisomers to delineate the substitution pattern of the natural products.<sup>[301]</sup>

Following these principles, the introduced publication deals with the identification of mostly aromatic volatiles from the fungi *Hypoxyton griseobrunneum* and *H. macrocarpum*, which are interesting targets for headspace analyses because of their strong odour<sup>[302]</sup> and not much is known about their volatiles, although *Hypoxyton* in general is a rich source of secondary metabolites.<sup>[303]</sup> As a connecting tie to the work on TSs presented above, also biosynthetic investigations using isotopically labelled compounds in a feeding experiment are included.

## Summary

The volatiles released from the two fungal strains *H. griseobrunneum* and *H. macrocarpum* were collected by CLSA and analysed by GC/MS.<sup>[304]</sup> The majority of compounds belonged to the class of aromatic volatiles, but also other natural products were present, such as terpenes (e. g. 1,8-cineol, **164**, is produced by *H. griseobrunneum*), pyrazines, alcohols, ketones and esters. Although the identification of most compounds was directly evident from their mass spectra and retention indices, especially the highly substituted aromatic volatiles, which dominated the bouquets of both species, were identified by comparison with standards and synthesised compounds. Some of the more challenging cases are shown in Figure 29, including the trimethoxybenzene **323**, for which all isomers were commercially available.

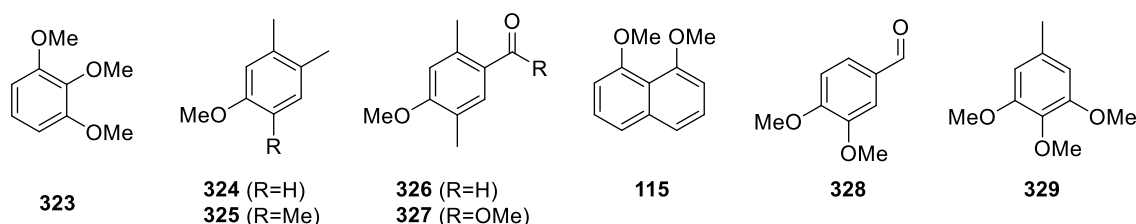


**Figure 29.** Structures of selected identified aromatic volatiles from *H. griseobrunneum* (**323–327** and **115**) and *H. macrocarpum* (**328** and **329**).

This strategy was also applicable to the assignment of the dimethylanisol **324** in comparison with its other five isomers and the six isomers of trimethylphenol with similar mass spectra, partially obtained by synthesis. The trimethylanisol **325** was identified as the main compound in the headspace extract of *H. griseobrunneum* by comparison of all synthesised six isomers. Its biosynthesis by a putative small PKS machinery was also investigated by a feeding experiment with (*methyl*-<sup>2</sup>H<sub>3</sub>)methionine to the fungus, which allowed to observe an incorporation of up to three labelled methyl groups into **325** in line with two C-methylations by S-adenosyl methionine (SAM) during PKS assembly and one O-methylation. The same enzyme might also be responsible for the formation of **324** as a side product. Similarly, also benzaldehyde **326** and the methyl ester **327** are possible PKS-derived products. The corresponding dihydroxynaphthalene derivative of the identified naphthalene **115**, which is also found in other fungi,<sup>[143]</sup> is a known precursor of the melanin pigments.<sup>[305]</sup> From *H. macrocarpum*, the dimethoxybenzaldehyde **328** was identified by comparison of the six commercially available isomers. Additionally, the widespread trimethoxytoluene **329** was identified with partially synthetic standards.

Taken together, the complex mixtures of differently substituted aromatic volatiles obtained from the two *Hypoxylon* strains required the comparison of the natural products to synthetic or commercially available standards to establish their substitution patterns. Also the PKS origin of some identified benzene derivatives is discussed. As *Hypoxylon* strains are usually found on dead wood, they are expected to have a rich metabolism for small aromatic compounds, and as shown here, they do not only originate from the natural lignin degradation, but also from de-novo biosynthesis.



## Chapter 22

### **From lignin to nylon: Cascaded chemical and biochemical conversion using metabolically engineered *Pseudomonas putida***

Dr. Michael Kohlstedt, Sören Starck, Nadja Barton, Dr. Jessica Stolzenberger, Dr. Mirjam Selzer, Kerstin Mehlmann, Roland Schneider, Prof. Dr. Daniel Pleissner, Jan Rinkel, Prof. Dr. Jeroen S. Dickschat, Dr. Joachim Venus, Dr. Jozef B. J. H. van Duuren and Prof. Dr. Christoph Wittmann\*

*Metab. Eng.* **2018**, *47*, 279–293.

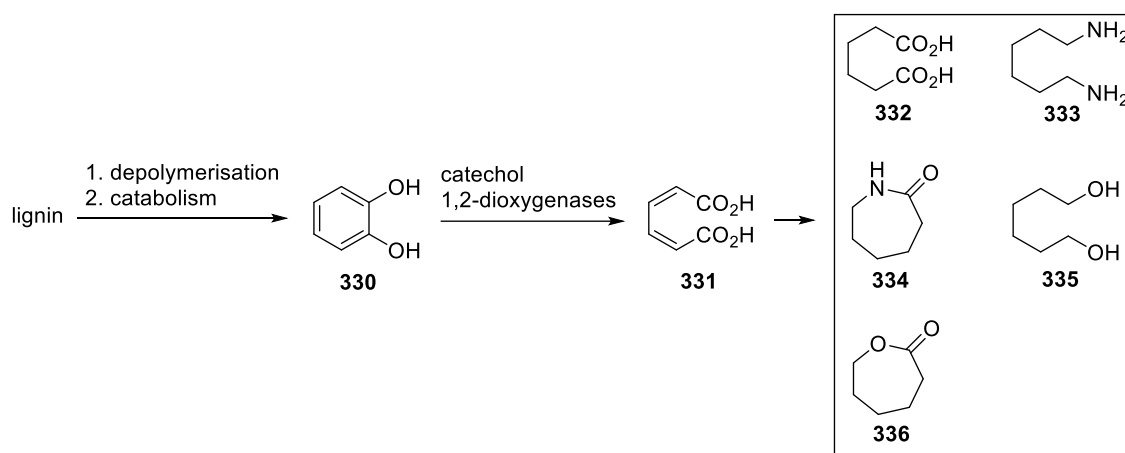
Reprinted from *Metab. Eng.* **2018**, *47*, 279–293 with kind permission from Elsevier.

The hydrogenation reactions of the isolated muconic acid to adipic acid, the purity determination of both products and the conversion of the latter to nylon 6,6 for test purposes was performed by me.

The publication “From lignin to nylon: Cascaded chemical and biochemical conversion using metabolically engineered *Pseudomonas putida*” is attached in Appendix V.

## Introduction

As discussed in Chapter 1.2, fungi play a central role in the degradation of lignin, which is the second most abundant biopolymer on earth after cellulose. However, the polyaromatic structure of lignin<sup>[306]</sup> makes any utilisation of this material impossible for most organisms, but also leads to technical difficulties in the economic use. Therefore, lignin mostly serves as an energy source, but not for the production of chemicals. As lignin represents a renewable material, a better application within green chemistry is strongly desirable.<sup>[307]</sup> Since the natural depolymerisation of lignin is usually slow, the polymer can be broken down to its small aromatic monomers by basic or thermal treatment, that are then susceptible to the catabolic pathways of microorganisms such as *Pseudomonas putida*.<sup>[308]</sup> In this organism, several enzymes convert one of the monomers, benzoate, to catechol (**330**, Scheme 42), which is oxidised to (*Z,Z*)-muconic acid (**331**). This open chain diacid is further converted via the  $\beta$ -keto adipate pathway to acetyl-CoA (**15**) and succinyl-CoA and is thus funnelled to central metabolism.<sup>[309]</sup> For biotechnological applications, **331** represents an interesting target,<sup>[310]</sup> because the C<sub>6</sub>-building block gives access to important bulk chemicals used for the production of polymers, such as adipic acid (**332**), hexamethylenediamine (**333**),  $\epsilon$ -caprolactam (**334**), 1,6-hexanediol (**335**) or  $\epsilon$ -caprolactone (**336**). Therefore, a more sustainable production of these petrochemicals from the underutilised renewable lignin represents the long-term goal.

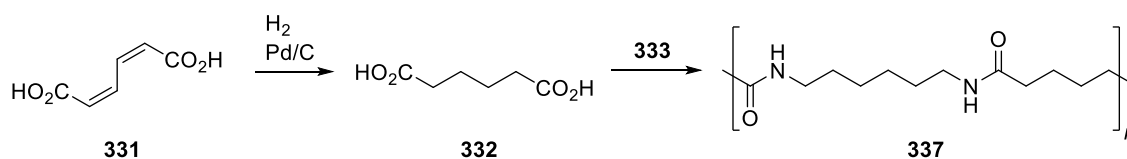


**Scheme 42.** Sustainable synthesis of (*Z,Z*)-muconic acid (**331**) from lignin. Accessible industrial polymer building blocks are shown in a box.

However, most of the lignin monomers are converted to protocatechuate in *P. putida*, which is processed to  $\beta$ -keto adipate via a pathway independent of **331**. Using a metabolic engineering approach, this problem was addressed recently by the expression of a protocatechuate decarboxylase, converting protocatechuate to **330**.<sup>[311]</sup> Together with a gene deletion targeting the enzyme downstream to **331**,<sup>[312]</sup> these modifications significantly increased the yield of **331** from *P. putida*. In the introduced publication, these principles were combined to generate a high-yield *P. putida* producing strain for **331**, which was converted chemically to nylon 6,6 demonstrating the complete value chain.

## Summary

Because of the introduced metabolic funnel for protocatechuate and phenol converging to catechol (**330**), the high levels of this toxic compound<sup>[313]</sup> represented the bottleneck for the production of **331**. Therefore, also the second native catechol 1,2-dioxygenase was put under the control of the native  $P_{\text{cat}}$  promoter, which is induced by **331**. This led to a significantly higher catechol tolerance and higher conversion rates with a titre of  $64.2 \text{ g L}^{-1}$  from **330**.<sup>[314]</sup> Also a pilot-scale 50 L fermentation with catechol was carried out, demonstrating that regeneration phases enhance the long-term production performance of the fed-batch process. However, the purity of the material obtained from this conversion (as a mixture of stereoisomers) was not reached by that resulting from feeding of softwood lignin hydrolysate to the engineered strain. With a titre of  $13 \text{ g L}^{-1}$  starting from the complex mixture of aromatic compounds, major contaminants of the obtained material were 3-methylmuconic acid and 2-methylmuconic acid, originating from the low selectivity of phenol hydroxylase<sup>[315]</sup> not only accepting phenol, but also cresols. Nevertheless, the obtained material was successfully hydrogenated to obtain **332**, which was treated with thionyl chloride and converted with **333** to nylon 6,6 (**337**, Scheme 43). Although only performed on a small scale, this conversion represents the first demonstration of the whole value chain from lignin to nylon.



**Scheme 43.** Synthesis of polyamide 66 (**337**) from lignin-originating **331**.

Despite of the persisting challenges connected to the inhomogeneous nature of lignin, the engineered microbial strains described in this study and also in others, which for example addressed the issue of a glucose-free production of **331**,<sup>[316]</sup> raise the hopes towards a sustainable and yet economical production of bulk chemicals from renewable sources such as lignin.

## Chapter 23

### **Characterisation of the L-Cystine $\beta$ -Lyase PatB from *Phaeobacter inhibens*: An Enzyme Involved in the Biosynthesis of the Marine Antibiotic Tropodithietic Acid**

Prof. Dr. Jeroen S. Dickschat\*, Jan Rinkel, Tim Klapschinski and Dr. Jörn Petersen

*ChemBioChem* **2017**, *18*, 2260–2267.

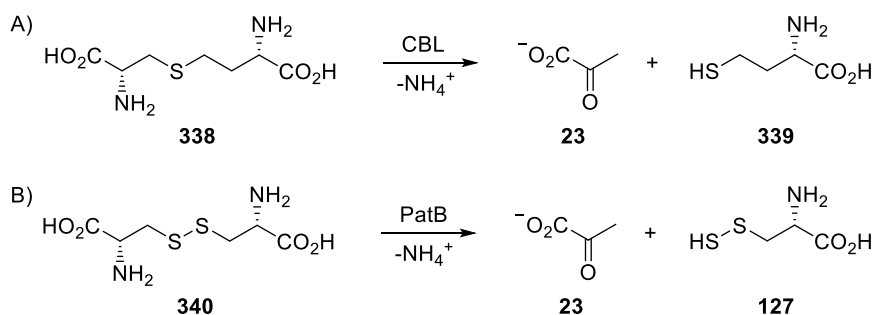
Reprinted from *ChemBioChem* **2017**, *18*, 2260–2267 with kind permission from John Wiley and Sons.

The analysis of kinetic data for different PatB substrates and the UV/Vis characterisation of PatB and its variants were contributed by me. Additionally, I prepared apo- and holo-PatB for MALDI-MS measurements.

The publication “Characterisation of the L-Cystine  $\beta$ -Lyase PatB from *Phaeobacter inhibens*: An Enzyme Involved in the Biosynthesis of the Marine Antibiotic Tropodithietic Acid” is attached in Appendix W.

## Introduction

As discussed in Chapter 1.3, the dithiet ring system containing two sulfur atoms is a characteristic structural feature of the marine antibiotic tropodithietic acid (TDA, **133**). Surprisingly, it is not directly involved in the currently discussed mode of action for **133** as a neutral H<sup>+</sup>/M<sup>+</sup> antiporter,<sup>[158]</sup> although this motif has an impact on the electron density within the tropone ring, which can modulate the proton binding affinity. The sulfur source of **133** was investigated by feeding experiments with *Phaeobacter inhibens* using the labelled substrates NaH<sup>34</sup>SO<sub>4</sub>, (<sup>34</sup>S)cysteine and its dimer (<sup>34</sup>S<sub>2</sub>)cystine (**340**, Scheme 44), all resulting in labelled **133**, which suggests that sulfur amino acid metabolism is involved in the incorporation.<sup>[168]</sup> Bioinformatic analysis resulted in a proposed model for TDA biosynthesis as depicted in Scheme 19, suggesting S-thiocysteine (**127**) as the direct sulfur source, built up from **340** by a β-lyase reaction. A deletion of a gene encoding for PatB, a protein closely related to a cystathionine (**338**) β-lyase (CBL), completely abolished TDA production, which supports the suggested model. CBLs are usually involved in the biosynthesis of methionine by plants, bacteria and yeast,<sup>[317]</sup> for their product, homocysteine (**339**) can directly be methylated by methionine synthase. Intriguingly, a strong cytotoxic effect of the CBL from *Bordetella avium* towards eukaryotic cells was attributed to its ability to not only convert **338**, but also cystine (**340**), leading to instable **127**,<sup>[170a]</sup> which is consequently the same reaction discussed for PatB during the biosynthesis of TDA as shown in Scheme 44. Also the CBL from *E. coli* shows a broadened substrate tolerance including the conversion of **340**.<sup>[318]</sup>



**Scheme 44.** A) Catalysed reaction of a cystathionine (**338**) β-lyase (CBL) and B) reaction catalysed by its homologue PatB for the formation of S-thiocysteine (**127**), the putative sulfur source in the biosynthesis of TDA (**133**).

Indeed, a heterologously expressed recombinant PatB from *P. inhibens* fused to the solubility enhancing NusA-tag, was shown to convert **340** to **127**, but did not accept **338**,<sup>[170b]</sup> thereby contradicting an earlier suggestion for the PatB substrate.<sup>[319]</sup> Additionally, a gene deletion abolished the production of roseobacticides, a class of algicidal metabolites, which are structurally and likely also biosynthetically related to TDA.

In this publication, a more detailed biochemical characterisation of recombinant PatB is presented, including kinetic parameters, site-directed mutagenesis, substrate tolerance and product identification by different methods.

## Summary

The gene encoding for PatB was cloned into an *E. coli* expression vector to yield the recombinant protein for in vitro tests.<sup>[320]</sup> UV/Vis analysis and MALDI-ToF MS measurements of apo- and holo-PatB demonstrated the binding of pyridoxal 5'-phosphate (PLP) to the enzyme, which is a known feature for CBLs because this cofactor is needed for catalytic activity.<sup>[317]</sup> The instability of **127**<sup>[321]</sup> hampered its direct detection as the product of the enzymatic reaction with **340**. However, besides the positive test for free thiol groups by 5,5'-dithiobis(2-nitrobenzoic acid) (Ellman's reagent),<sup>[322]</sup> **127** could be trapped by methylation with dimethyl sulfate and the corresponding product was identified by HPLC-MS to be identical to a synthetic standard. The second product pyruvate (**23**) was detected by its reaction with 4-fluorophenylhydrazine to two stereoisomeric products containing a hydrazone moiety. Also, Nessler's reagent was used to detect ammonium, thereby establishing the function of PatB as a cystine  $\beta$ -lyase. In contrast to previous in vitro results, PatB accepted **338**, but also selenocystine, (*S*-methylthio)cysteine and methionine, the latter two producing volatile sulfur compounds that were detected by headspace analysis. The pH and temperature optimum, determined to pH 8.75 at 30 °C and kinetic data were obtained by enzymatic reactions in the presence of Ellman's reagent, which allowed for a UV/Vis spectroscopic monitoring of the reaction progress. By this approach, the preference of PatB for **340** compared to the lower efficiency of the reaction with **338** was evident. Similar observation have been made for an enzyme characterised also as a cystine  $\beta$ -lyase from *Synechocystis*, which is assumed to be involved in the biosynthesis of FeS clusters via its product **127**.<sup>[323]</sup> A lysine residue, which is highly conserved among CBLs for binding of the PLP cofactor,<sup>[317]</sup> was targeted by site directed mutagenesis for PatB, which resulted in an inactive protein yet still harbouring PLP by putative non-covalent binding.

Taken together, the detailed in vitro investigation of PatB confirms its role to produce *S*-thiocysteine (**127**), which likely acts as the sulfur source for TDA. However, similar studies on the other active enzymes from the TDA biosynthetic gene cluster are necessary to elucidate the exact mechanism, how the incorporation of sulfur is accomplished on an enzymatic level, although reasonable suggestions have been made.

## Chapter 24

### **Acyl-group specificity of AHL synthases involved in quorum-sensing in *Roseobacter* group bacteria**

Lisa Ziesche, Jan Rinkel, Prof. Dr. Jeroen S. Dickschat and Prof. Dr. Stefan Schulz\*

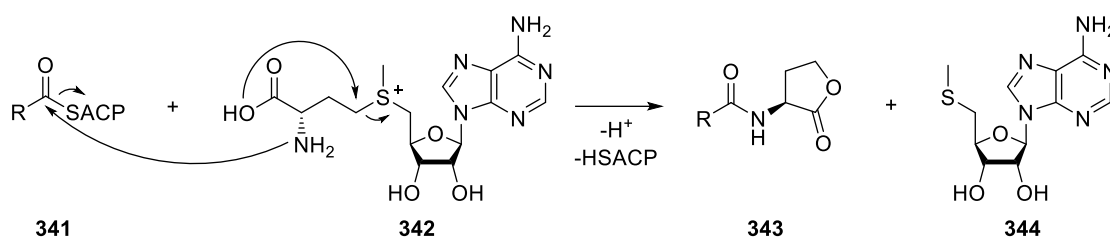
*Beilstein J. Org. Chem.* **2018**, *14*, 1309–1316.

The in vitro experiments with the recombinant AHL synthases using the substrate analogues, which were synthesised by Lisa Ziesche, and their analyses were performed by me.

The publication “Acyl-group specificity of AHL synthases involved in quorum-sensing in *Roseobacter* group bacteria” is attached in Appendix X.

## Introduction

As introduced in Chapter 1.3, quorum sensing (QS) is an important process for bacterial inter cell communication. Because it also controls the formation of biofilms,<sup>[324]</sup> which are of clinical relevance, understanding the molecular mechanisms of QS is crucial not only for medicinal reasons, but also to investigate the chemical ecology of different strains. An important compound class, which mediate these interactions, consists of *N*-acylhomoserine lactones (AHLs, **343**, Scheme 45). With the first compound from this class, 3-oxohexanoylhomoserine lactone (3-oxo-C6:0-HSL), being identified in the model organism *Aliivibrio fischeri* as an autoinducer for its bioluminescence,<sup>[177]</sup> AHLs were also detected in various other organisms as exemplified by the identification of (*R*)-3-OH-C10:0-HSL (**134**) as an inducer of TDA (**133**) biosynthesis in *P. inhibens*.<sup>[180]</sup> The importance of these signalling molecules in *Roseobacter* group bacteria is also reflected in their common occurrence, as AHLs were detected in 19 out of 24 isolated strains from macroalgal surfaces with single strains producing up to eight different AHLs.<sup>[179b]</sup> The structural variety of AHLs is thereby limited to different chain lengths, the positions of unsaturations and oxygen functionalities like alcohols or ketones. However, since AHLs bind to transcriptional regulator proteins (named LuxR homologues in reminiscence to the studies with *A. fischeri*), the structural composition of the chain may have severe impact on the binding affinities, making the chemical signals strain-specific or allowing multiple different signals.<sup>[325]</sup> The biosynthesis of these autoinducers is catalysed by AHL synthases (LuxI homologues) connecting *S*-adenosyl methionine (SAM, **342**) to a fatty-acid derived acyl residue, which is bound to an acyl carrier protein (ACP, **341**) or to CoA,<sup>[326]</sup> and cyclising the product to yield the AHL (**343**) and 5'-deoxy-5'-thiomethyladenosine (**344**) as a good leaving group.



**Scheme 45.** Biosynthesis of *N*-acylhomoserine lactones (AHLs, **343**) by an AHL synthase.

Recently, a few crystal structure analyses of AHL synthases laid the molecular basis for their selectivity and also gave insights, how their catalysis can be inhibited by small molecules.<sup>[327]</sup>

Because of the unclear relationship between the observed AHLs and their corresponding synthases of unknown selectivity in *Roseobacter* group bacteria, the introduced publication deals with the characterisation of AHL synthases from the two model organisms *P. inhibens* and *Dinoroseobacter shibae* by *in vitro* incubations with synthetically prepared substrate analogues.



## Summary

The AHL production by four different *Roseobacter* strains was analysed, confirming the established presence of **134** together with C16:0-HSL, C16:1-HSL and C18:1-HSL in *P. inhibens*, whereas *D. shibae* contained significant amounts of C18:2-HSL, accompanied by 3-oxo-C14:0-HSL, C14:1-HSL and C18:1-HSL.<sup>[328]</sup> An analysis of the fatty acid content demonstrated no correlation between their occurrence and the observed AHLs, as all strains showed a comparable distribution of fatty acids with 11Z-C18:1 being most abundant. As with the selectivity of the AHL synthases and the activation and distribution of fatty acids as ACP- or CoA-bound adducts at least two important factors are hampering a direct coupling of fatty acid- to AHL occurrence, this result is reasonable. To gain more insights into the selectivity of the involved AHL synthases, three enzymes, LuxI<sub>1</sub> and LuxI<sub>2</sub> from *D. shibae* and Pgal<sub>2</sub> from *P. inhibens*, were cloned from genomic DNA into an *E. coli* expression vector for in vitro tests with the recombinant proteins. As AHL synthases possess specific binding sites for the phosphopantetheinyl linker present in both CoA and ACP, abbreviated versions of the substrates, *N*-pantothenoyl-cysteamine thioesters, were synthesised reflecting different chain lengths and unsaturations as well as the 3-OH-C10:0-version. Taking these substrate analogues in incubation experiments employing the AHL synthases and SAM, the successful formation of AHLs was observed by GC/MS. It turned out that Pgal<sub>2</sub> accepted all substrates except for the very short C4:0 and the very long C20:0 version. In contrast, LuxI<sub>1</sub> showed a strong preference for 2*E*,11*Z*-C18:2, which is in line with the previous observation of the corresponding AHL as a product of this enzyme.<sup>[329]</sup> LuxI<sub>2</sub> showed only small activities with the C14:0 and the 3-OH-C10:0 substrate and is therefore probably responsible for the production of C14:0-HSL and 3-oxo-C14:0-HSL in its host. For the promiscuous AHL synthase Pgal<sub>2</sub>, also competition experiments employing the same amounts of substrates and a limited amount of SAM were performed to determine its preferred substrate. Distributed evenly to both sides of the chain-length spectrum, the highest conversion was observed for C10:0 and C12:0 substrates.

Taken together, the substrate tolerance of the three investigated enzymes were very different including the selective LuxI<sub>1</sub> but also the promiscuous Pgal<sub>2</sub>. Since the product of the other AHL synthase in *P. inhibens* is known to be **134**,<sup>[180]</sup> its promiscuity may result in the production of long chain AHLs that were observed in this organism. Therefore, the in vitro tests with the substrate analogues allowed for a detailed characterisation of the enzymes with implications on the biologically relevant AHLs. However, to fully account for the QS signalling system, all three components, AHL synthases including their precursor availability, the signalling molecule itself and the corresponding transcriptional regulator protein with their selectivities have to be taken into consideration.

# Chapter 25

## Summary and outlook

The major part of this work focusses on mechanistic investigations on terpene synthases (TSs) and on the structure elucidation of their products by extensive isotopic labelling experiments. It is therefore placed in the long and yet exciting history of isotope usage in terpene chemistry, starting from the elucidation of cholesterol biosynthesis<sup>[19]</sup> and continued by pioneering experiments by Cane on the mechanisms of sesquiterpene synthases.<sup>[70]</sup> Although the principles of the tracer technique remained the same during more than half of a century of research, modern methods like the routine expression of recombinant proteins for in vitro experiments combined with more sensitive NMR spectroscopy certainly left their imprint on experimental design, practical work and robustness of the obtained results. For instance, a mixed incorporation of labelled atoms by in vitro experiments can result in a difficult interpretation, but still harbours insights into the investigated cyclisation mechanism as shown with spinodiene synthase (Chapter 14). The same result obtained by in vivo feeding experiments may lead to no conclusion at all, given the high number of metabolic reactions, the uncontrollable dilution of label and other effects that have to be taken into consideration for the observed result.

Following these principles, the conducted experiments built upon the established expression of terpene synthases and the systematic (<sup>13</sup>C<sub>1</sub>)-labelling of FPP as included in a previous doctoral thesis from this workgroup.<sup>[330]</sup> The major aspect added to the toolbox of isotopically labelled compounds are the discussed stereoselectively deuterated and <sup>13</sup>C labelled substrates allowing for a rapid and reliable assignment of the absolute configurations of TS products. As to be seen in the mostly chronological structure of this thesis, the principle of stereoselective labelling underwent a development during the course of this work, starting from enantioselectively deuterated FPPs at C-1, which were used for GC/MS based analysis of hydride shifts (Chapter 3), but proved to be impracticable for a sensitive methylene group assignment (Chapter 4). The analogously deuterated GPPs allowed to include monoterpenes into the investigations (Chapter 5), but significant progress was archived by the introduction of a <sup>13</sup>C-labelled atom at the same position (Chapter 6), which did not change the principle, but allowed for a highly sensitive detection. Also the utilisation of prenyltransferases gave rise to a flexible combination of labelled substrates in a stereochemically defined way and thus reduced the synthetic workload to address certain positions. The synthesis of (*E*)- and (*Z*)-(4-<sup>13</sup>C,4-<sup>2</sup>H)IPP (Appendix L) and (*R*)- and (*S*)-(1-<sup>13</sup>C,1-<sup>2</sup>H)IPP (Chapter 15) finally merged these efforts to target every methylene group in oligoprenyl diphosphates as exemplified in Chapter 16.

However, the driving force behind this development has always been the individual TSs with their interesting cyclisation mechanisms and the breath-taking structures of their products. Although 29 different TSs are discussed during the course of this work, most of them added new aspects and unexpected results, which were certainly worth investigating. Also the site-directed mutagenesis and the synthetic efforts on terpene

products to expand and explore their chemical space emphasise that the characterisation of a new TS is far from a routine operation, but individual experiments have to be designed to account for all the different features being included in their complex catalysis.

As demonstrated here, mechanistic patterns or predictions associated with TSs should be taken with care, as for example the discussed *anti*-S<sub>N</sub>' reaction for the initial cyclisation step of tertiary diphosphates, which is followed in most, but not in every cases (Chapter 18). Therefore, there is still a lot to learn about the mechanistic secrets of TSs, which leaves room for future investigations. Given the growing number of sequenced genomes harbouring new TSs, a continuous research on this field is required for the detection of new natural products and new mechanistic insights. Although the long-term goal of predicting TS products from the sequence seems to be out of range considering today's point of view, only an ongoing effort in TS characterisation including their structures and the experimental and computational comprehending of their mechanisms will allow for a solid database, that theoretical predictions and helpful phylogenetic analyses can build upon. As shown here, isotopically labelled compounds can contribute to the experimental part of this journey. However, scientific virtues like curiosity and questioning of earlier results should always be of central importance, as the complex nature of TSs might not have been fully addressed by previous methods (Chapters 9 and 14).

Besides the characterisation of TSs, also other interesting aspects of natural product chemistry are included in this thesis, either connected to terpenes as shown by the application of labelling to CYP-mediated terpene oxidations and the investigations of artificial TS-like catalysts (Chapters 12 and 20), or the identification of fungal volatiles and the sustainable conversion of the biopolymer lignin to the artificial polymer nylon 6,6 with the help of engineered microbes (Chapters 21 and 22). With the characterisation of PatB being involved in the biosynthesis of tropodithietic acid and the substrate selectivity of quorum sensing related AHL synthases from marine bacteria, selected aspects related to the secondary metabolism of *Roseobacter* group bacteria were also investigated (Chapters 23 and 24).

In summary, this doctoral thesis includes the synthesis and application of isotopically labelled compounds for in vitro experiments with several mono-, sesqui-, di- and sesterterpene synthases. On the one hand, the advantages of the tracer technique are shown by determining the absolute configurations of the products and stereochemical aspects of hydride migrations by converting stereoselectively deuterated, <sup>13</sup>C labelled probes, but also by testing mechanistic hypotheses and systematically investigating EI-MS fragmentation mechanisms with (<sup>13</sup>C<sub>1</sub>)-labelling. On the other hand, these methodical improvements are interwoven with the characterisation of new TSs including the discovery of unprecedented natural products, their chemical derivatisation and surprising mechanistic aspects. Therefore, this thesis contributes to a more comprehensive and growing picture of these astonishing enzymes, by which nature exploits the versatile chemistry of carbocations with an evolutionary playground to create the largest group of natural products.

## Chapter 26

### References

- [1] J. S. Dickschat, *Nat. Prod. Rep.* **2016**, 33, 87–110.
- [2] M. C. Wani, H. L. Taylor, M. E. Wall, P. Coggon, A. T. McPhail, *J. Am. Chem. Soc.* **1971**, 93, 2325–2327.
- [3] V. D. Nikolic, I. M. Savic, I. M. Savic, L. B. Nikolic, M. Z. Stankovic, V. D. Marinkovic, *Cent. Eur. J. Med.* **2011**, 6, 527–536.
- [4] Y. Tu, *Nat. Med.* **2011**, 17, 1217–1220.
- [5] R. S. Fallen, M. Gooderham, *Skin Therapy Lett.* **2012**, 17, 1–3.
- [6] M. Lebwohl, N. Swanson, L. L. Anderson, A. Melgaard, Z. Xu, B. Berman, *N. Engl. J. Med.* **2012**, 366, 1010–1019.
- [7] W. S. Bowers, L. R. Nault, R. E. Webb, S. R. Dutky, *Science* **1972**, 177, 1121–1122.
- [8] P. L. Yeagle, *Biochim. Biophys. Acta* **1985**, 822, 267–287.
- [9] R. Eccles, *J. Pharm. Pharmacol.* **1994**, 46, 618–630.
- [10] N. J. Fraser, H. Hashimoto, R. J. Cogdell, *Photosynth. Res.* **2001**, 70, 249–256.
- [11] A. Guenther, T. Karl, P. Harley, C. Wiedinmyer, P. I. Palmer, C. Geron, *Atmos. Chem. Phys.* **2006**, 6, 3181–3210.
- [12] a) J. S. Dickschat, H. B. Bode, T. Mahmud, R. Müller, S. Schulz, *J. Org. Chem.* **2005**, 70, 5174–5182; b) D. E. Cane, X. He, S. Kobayashi, S. Omura, H. Ikeda, *J. Antibiot.* **2006**, 59, 471–479; c) J. Jiang, X. He, D. E. Cane, *Nat. Chem. Biol.* **2007**, 3, 711–715.
- [13] C. Davidovich, A. Bashan, T. Auerbach-Nevo, R. D. Yaggie, R. R. Gontarek, A. Yonath, *Proc. Natl. Acad. Sci. USA* **2007**, 104, 4291–4296.
- [14] a) T. J. Maimone, P. S. Baran, *Nat. Chem. Biol.* **2007**, 3, 396–407; b) D. Urabe, T. Asaba, M. Inoue, *Chem. Rev.* **2015**, 115, 9207–9231; c) K. Hung, X. Hu, T. J. Maimone, *Nat. Prod. Rep.* **2018**, 35, 174–202; d) J. Chen, B. Liu, *Synlett* **2018**, 29, 863–873.
- [15] O. Wallach, *Justus Liebigs Ann. Chem.* **1885**, 227, 277–302.
- [16] L. Ruzicka, *Experientia* **1953**, 9, 357–367.
- [17] D. E. Vance, H. Goldfine, *Biochem. Biophys. Res. Commun.* **2002**, 292, 1117–1127.
- [18] K. Bloch, *Science* **1965**, 150, 19–28.
- [19] E. P. Kennedy, *J. Biol. Chem.* **2001**, 276, 42619–42631.
- [20] S. Chaykin, J. Law, A. H. Phillips, T. T. Tchen, K. Bloch, *Proc. Natl. Acad. Sci. USA* **1958**, 44, 998–1004.
- [21] a) P. A. Tavormina, M. H. Gibbs, J. W. Huff, *J. Am. Chem. Soc.* **1956**, 78, 4498–4499; b) D. E. Wolf, C. H. Hoffman, P. E. Aldrich, H. R. Skeggs, L. D. Wright, K. Folkers, *J. Am. Chem. Soc.* **1956**, 78, 4499.
- [22] R. G. Langdon, K. Bloch, *J. Biol. Chem.* **1953**, 200, 129–134.

- [23] S. Thompson, F. Mayerl, O. P. Peoples, S. Masamune, A. J. Sinskey, C. T. Walsh, *Biochemistry* **1989**, *28*, 5735–5742.
- [24] H. Rudney, *J. Biol. Chem.* **1957**, *227*, 363–377.
- [25] J. C. Vannice, D. A. Skaff, A. Keightley, J. K. Addo, G. J. Wyckoff, H. M. Miziorko, *J. Bacteriol.* **2014**, *196*, 1055–1063.
- [26] N. Dellas, S. T. Thomas, G. Manning, J. P. Noel, *eLife* **2013**, *2*, e00672.
- [27] J. M. Vinokur, T. P. Korman, Z. Cao, J. U. Bowie, *Biochemistry* **2014**, *53*, 4161–4168.
- [28] a) G. Flesch, M. Rohmer, *Eur. J. Biochem.* **1988**, *175*, 405–411; b) M. Rohmer, B. Sutter, H. Sahm, *J. Chem. Soc., Chem. Commun.* **1989**, 1471–1472; c) D. Zhou, R. H. White, *Biochem. J.* **1991**, *273*, 627–634; d) M. Rohmer, M. Knani, P. Simonin, B. Sutter, H. Sahm, *Biochem. J.* **1993**, *295*, 517–524.
- [29] W. Eisenreich, M. Schwarz, A. Cartayrade, D. Arigoni, M. H. Zenk, A. Bacher, *Chem. Biol.* **1998**, *5*, R221-R233.
- [30] S. Steinbacher, J. Kaiser, W. Eisenreich, R. Huber, A. Bacher, F. Rohdich, *J. Biol. Chem.* **2003**, *278*, 18401–18407.
- [31] D. L. Turner, H. Santos, P. Fareleira, I. Pacheco, J. LeGall, A. V. Xavier, *Biochem. J.* **1992**, *285*, 387–390.
- [32] a) R. Laupitz, T. Gräwert, C. Rieder, F. Zepeck, A. Bacher, D. Arigoni, F. Rohdich, W. Eisenreich, *Chem. Biodivers.* **2004**, *1*, 1367–1376; b) C. A. Citron, N. L. Brock, P. Rabe, J. S. Dickschat, *Angew. Chem. Int. Ed.* **2012**, *51*, 4053–4057.
- [33] a) P.-H. Liang, T.-P. Ko, A. H.-J. Wang, *Eur. J. Biochem.* **2002**, *269*, 3339–3354; b) C. D. Poulter, *Phytochem. Rev.* **2006**, *5*, 17–26; c) J. Winkelblech, A. Fan, S.-M. Li, *Appl. Microbiol. Biotechnol.* **2015**, *99*, 7379–7397; d) R. Nagel, A. Schmidt, R. J. Peters, *Planta* **2019**, *249*, 9–20.
- [34] B. S. J. Blagg, M. B. Jarstfer, D. H. Rogers, C. D. Poulter, *J. Am. Chem. Soc.* **2002**, *124*, 8846–8853.
- [35] D. Iwata-Reuyl, S. K. Math, S. B. Desai, C. D. Poulter, *Biochemistry* **2003**, *42*, 3359–3365.
- [36] L. C. Tarshis, M. Yan, C. D. Poulter, J. C. Sacchettini, *Biochemistry* **1994**, *33*, 10871–10877.
- [37] S. Frick, R. Nagel, A. Schmidt, R. R. Bodemann, P. Rahfeld, G. Pauls, W. Brandt, J. Gershenzon, W. Boland, A. Burse, *Proc. Natl. Acad. Sci. USA* **2013**, *110*, 4194–4199.
- [38] L. C. Tarshis, P. J. Proteau, B. A. Kellogg, J. C. Sacchettini, C. D. Poulter, *Proc. Natl. Acad. Sci. USA* **1996**, *93*, 15018–15023.
- [39] L. L. C. Schrödinger, *The PyMOL Molecular Graphics System, Version 2.0*, **2015**.
- [40] J. W. Cornforth, R. H. Cornforth, C. Donninger, G. Popják, *Proc. Roy. Soc., Ser. B* **1966**, *163*, 492–514.
- [41] J. W. Cornforth, R. H. Cornforth, G. Popják, L. Yengoyan, *J. Biol. Chem.* **1966**, *241*, 3970–3987.
- [42] a) G. Popják, J. W. Cornforth, *Biochem. J.* **1966**, *101*, 553–568; b) J. W. Cornforth, *Angew. Chem. Int. Ed.* **1968**, *7*, 903–911.

- [43] C. D. Poulter, H. C. Rilling, *Biochemistry* **1976**, *15*, 1079–1083.
- [44] D. J. Hosfield, Y. Zhang, D. R. Dougan, A. Broun, L. W. Tari, R. V. Swanson, J. Finn, *J. Biol. Chem.* **2004**, *279*, 8526–8529.
- [45] A. S. Rose, A. R. Bradley, Y. Valasatava, J. M. Duarte, A. Prlic, P. W. Rose, *Bioinformatics* **2018**, *34*, 3755–3758.
- [46] K.-H. Teng, P.-H. Liang, *Bioorg. Chem.* **2012**, *43*, 51–57.
- [47] K. Cornish, *Nat. Prod. Rep.* **2001**, *18*, 182–189.
- [48] S. Yamashita, H. Yamaguchi, T. Waki, Y. Aoki, M. Mizuno, F. Yanbe, T. Ishii, A. Funaki, Y. Tozawa, Y. Miyagi-Inoue, K. Fushihara, T. Nakayama, S. Takahashi, *eLife* **2016**, *5*, e19022.
- [49] M. Liu, C.-C. Chen, L. Chen, X. Xiao, Y. Zheng, J.-W. Huang, W. Liu, T.-P. Ko, Y.-S. Cheng, X. Feng, E. Oldfield, R.-T. Guo, Y. Ma, *Angew. Chem. Int. Ed.* **2016**, *55*, 4721–4724.
- [50] J. Gao, T.-P. Ko, L. Chen, S. R. Malwal, J. Zhang, X. Hu, F. Qu, W. Liu, J.-W. Huang, Y.-S. Cheng, C.-C. Chen, Y. Yang, Y. Zhang, E. Oldfield, R.-T. Guo, *Angew. Chem. Int. Ed.* **2018**, *57*, 683–687.
- [51] L. Kaysser, P. Bernhardt, S.-J. Nam, S. Loesgen, J. G. Ruby, P. Skewes-Cox, P. R. Jensen, W. Fenical, B. S. Moore, *J. Am. Chem. Soc.* **2012**, *134*, 11988–11991.
- [52] a) D. J. Tantillo, *Nat. Prod. Rep.* **2011**, *28*, 1035–1053; b) D. J. Tantillo, *Angew. Chem. Int. Ed.* **2017**, *56*, 10040–10045.
- [53] D. W. Christianson, *Chem. Rev.* **2017**, *117*, 11570–11648.
- [54] D. E. Cane, A. M. Tillman, *J. Am. Chem. Soc.* **1983**, *105*, 122–124.
- [55] K. U. Wendt, K. Poralla, G. E. Schulz, *Science* **1997**, *277*, 1811–1815.
- [56] E. J. Corey, H. Cheng, C. H. Baker, S. P. T. Matsuda, D. Li, X. Song, *J. Am. Chem. Soc.* **1997**, *119*, 1277–1288.
- [57] M. Xu, M. Jia, Y. J. Hong, X. Yin, D. J. Tantillo, P. J. Proteau, R. J. Peters, *Org. Lett.* **2018**, *20*, 1200–1202.
- [58] M. Köksal, Y. Jin, R. M. Coates, R. Croteau, D. W. Christianson, *Nature* **2011**, *469*, 116–120.
- [59] C. A. Lesburg, G. Zhai, D. E. Cane, D. W. Christianson, *Science* **1997**, *277*, 1820–1824.
- [60] a) H.-C. Lin, Y.-H. Chooi, S. Dhingra, W. Xu, A. M. Calvo, Y. Tang, *J. Am. Chem. Soc.* **2013**, *135*, 4616–4619; b) C. Schmidt-Dannert, *Biosynthesis of Terpenoid Natural Products in Fungi in Biotechnology of isoprenoids*, Vol. 148 (Eds.: J. Schrader, J. Bohlmann, J. Alonso-Gutierrez), Springer, Cham, **2015**, pp. 19–61; c) Y.-L. Yang, S. Zhang, K. Ma, Y. Xu, Q. Tao, Y. Chen, J. Chen, S. Guo, J. Ren, W. Wang, Y. Tao, W.-B. Yin, H. Liu, *Angew. Chem. Int. Ed.* **2017**, *56*, 4749–4752; d) Y. Yang, Y. Zhang, S. Zhang, Q. Chen, K. Ma, L. Bao, Y. Tao, W. Yin, G. Wang, H. Liu, *J. Nat. Prod.* **2018**, *81*, 1089–1092.
- [61] a) I. G. Young, R. A. Leppik, J. A. Hamilton, F. Gibson, *J. Bacteriol.* **1972**, *110*, 18–25; b) W. Li, *Trends Biochem. Sci.* **2016**, *41*, 356–370.
- [62] W. Cheng, W. Li, *Science* **2014**, *343*, 878–881.
- [63] R. Schor, C. Schotte, D. Wibberg, J. Kalinowski, R. J. Cox, *Nat. Commun.*, *9*, 1963.

- [64] a) C. M. Starks, K. Back, J. Chappell, J. P. Noel, *Science* **1997**, *277*, 1815–1820; b) M. J. Rynkiewicz, D. E. Cane, D. W. Christianson, *Proc. Natl. Acad. Sci. USA* **2001**, *98*, 13543–13548; c) E. Y. Shishova, L. Di Costanzo, D. E. Cane, D. W. Christianson, *Biochemistry* **2007**, *46*, 1941–1951; d) J. A. Aaron, X. Lin, D. E. Cane, D. W. Christianson, *Biochemistry* **2010**, *49*, 1787–1797; e) R. Janke, C. Görner, M. Hirte, T. Brück, B. Loll, *Acta Cryst. D* **2014**, *70*, 1528–1537; f) P. Baer, P. Rabe, K. Fischer, C. A. Citron, T. A. Klapschinski, M. Groll, J. S. Dickschat, *Angew. Chem. Int. Ed.* **2014**, *53*, 7652–7656; g) P. Baer, P. Rabe, C. A. Citron, C. C. de Oliveira Mann, N. Kaufmann, M. Groll, J. S. Dickschat, *ChemBioChem* **2014**, *15*, 213–216.
- [65] a) B.-X. Tian, F. H. Wallrapp, G. L. Holiday, J.-Y. Chow, P. C. Babbitt, C. D. Poulter, M. P. Jacobson, *PLOS Comp. Biol.* **2014**, *10*, e1003874; b) J.-Y. Chow, B.-X. Tian, G. Ramamoorthy, B. S. Hillerich, R. D. Seidel, S. C. Almo, M. P. Jacobson, C. D. Poulter, *Proc. Natl. Acad. Sci. USA* **2015**, *112*, 5661–5666.
- [66] a) H. Jenke-Kodama, E. Dittmann, *Nat. Prod. Rep.* **2009**, *26*, 874–883; b) K. Blin, T. Wolf, M. G. Chevrette, X. Lu, C. J. Schwalen, S. A. Kautsar, H. G. Suarez Duran, de los Santos, Emmanuel L. C., H. U. Kim, M. Nave, J. S. Dickschat, D. A. Mitchell, E. Shelest, R. Breitling, E. Takano, S. Y. Lee, T. Weber, M. H. Medema, *Nucleic Acids Res.* **2017**, *45*, W36-41.
- [67] M. Seemann, G. Zhai, J.-W. de Kraker, C. M. Paschall, D. W. Christianson, D. E. Cane, *J. Am. Chem. Soc.* **2002**, *124*, 7681–7689.
- [68] L. Zu, M. Xu, M. W. Lodewyk, D. E. Cane, R. J. Peters, D. J. Tantillo, *J. Am. Chem. Soc.* **2012**, *134*, 11369–11371.
- [69] P. Gutta, D. J. Tantillo, *J. Am. Chem. Soc.* **2006**, *128*, 6172–6179.
- [70] D. E. Cane, *Chem. Rev.* **1990**, *90*, 1089–1103.
- [71] D. E. Cane, M. Tandon, *Tetrahedron Lett.* **1994**, *35*, 5355–5358.
- [72] a) H. Sato, K. Narita, A. Minami, M. Yamazaki, C. Wang, H. Suemune, S. Nagano, T. Tomita, H. Oikawa, M. Uchiyama, *Sci. Rep.*, *8*, 2473; b) D. A. Dougherty, *Acc. Chem. Res.* **2013**, *46*, 885–893.
- [73] X. Chen, T. G. Köllner, G. Shaulsky, Q. Jia, J. S. Dickschat, J. Gershenzon, F. Chen, *Sci. Rep.* **2018**, *8*, 14361.
- [74] J. Gertsch, M. Leonti, S. Raduner, I. Racz, J.-Z. Chen, X.-Q. Xie, K.-H. Altmann, M. Karsak, A. Zimmer, *Proc. Natl. Acad. Sci. USA* **2008**, *105*, 9099–9104.
- [75] R. Croteau, R. E. B. Ketchum, R. M. Long, R. Kaspera, M. R. Wildung, *Phytochem. Rev.* **2006**, *5*, 75–97.
- [76] a) F. Gueritte-Voegelein, D. Guenard, P. Potier, *J. Nat. Prod.* **1987**, *50*, 9–18; b) R. Kaspera, J. L. Cape, J. A. Faraldos, R. E. B. Ketchum, R. B. Croteau, *Tetrahedron Lett.* **2010**, *51*, 2017–2019.
- [77] S. Jennewein, R. M. Long, R. M. Williams, R. Croteau, *Chem. Biol.* **2004**, *11*, 379–387.
- [78] R. Kaspera, R. Croteau, *Phytochem. Rev.* **2006**, *5*, 433–444.
- [79] A. Schoendorf, C. D. Rithner, R. M. Williams, R. B. Croteau, *Proc. Natl. Acad. Sci. USA* **2001**, *98*, 1501–1506.

- [80] S. Jennewein, C. D. Rithner, R. M. Williams, R. B. Croteau, *Proc. Natl. Acad. Sci. USA* **2001**, *98*, 13595–13600.
- [81] M. Chau, R. Croteau, *Arch. Biochem. Biophys.* **2004**, *427*, 48–57.
- [82] M. Chau, S. Jennewein, K. Walker, R. Croteau, *Chem. Biol.* **2004**, *11*, 663–672.
- [83] P. M. Dewick, *Medicinal natural products. A biosynthetic approach*, John Wiley and Sons Ltd, Chichester, **2009**.
- [84] K. Walker, R. Croteau, *Proc. Natl. Acad. Sci. USA* **2000**, *97*, 13591–13596.
- [85] S.-L. Lin, T. Wei, J.-F. Lin, L.-Q. Guo, G.-P. Wu, J.-B. Wei, J.-J. Huang, P.-L. Ouyang, *Mol. Biotechnol.* **2018**, *60*, 492–505.
- [86] K. D. Walker, K. Klettke, T. Akiyama, R. Croteau, *J. Biol. Chem.* **2004**, *279*, 53947–53954.
- [87] R. M. Long, R. Croteau, *Biochem. Biophys. Res. Commun.* **2005**, *338*, 410–417.
- [88] K. Walker, R. Long, R. Croteau, *Proc. Natl. Acad. Sci. USA* **2002**, *99*, 9166–9171.
- [89] X. Lin, R. Hopson, D. E. Cane, *J. Am. Chem. Soc.* **2006**, *128*, 6022–6023.
- [90] B. Zhao, X. Lin, L. Lei, D. C. Lamb, S. L. Kelly, M. R. Waterman, D. E. Cane, *J. Biol. Chem.* **2008**, *283*, 8183–8189.
- [91] H. Gürtler, R. Pedersen, U. Anthoni, C. Christophersen, P. H. Nielsen, E. M. H. Wellington, C. Pedersen, K. Bock, *J. Antibiot.* **1994**, *47*, 434–439.
- [92] S.-S. Gao, N. Naowarajna, R. Cheng, X. Liu, P. Liu, *Nat. Prod. Rep.* **2018**, *35*, 792–837.
- [93] a) B. Meunier, S. P. de Visser, S. Shaik, *Chem. Rev.* **2004**, *104*, 3947–3980; b) P. R. Ortiz de Montellano, *Chem. Rev.* **2010**, *110*, 932–948.
- [94] T. L. Poulos, B. C. Finzel, I. C. Gunsalus, G. C. Wagner, J. Kraut, *J. Biol. Chem.* **1985**, *260*, 16122–16130.
- [95] H. M. Girvan, A. W. Munro, *Curr. Opin. Chem. Biol.* **2016**, *31*, 136–145.
- [96] S. Nagano, T. L. Poulos, *J. Biol. Chem.* **2005**, *280*, 31659–31663.
- [97] H. L. R. Cooper, J. T. Groves, *Arch. Biochem. Biophys.* **2011**, *507*, 111–118.
- [98] a) J. T. Groves, *Proc. Natl. Acad. Sci. USA* **2003**, *100*, 3569–3574; b) M. Newcomb, R. Zhang, R. E. P. Chandrasena, J. A. Halgrimson, J. H. Horner, T. M. Makris, S. G. Sligar, *J. Am. Chem. Soc.* **2006**, *128*, 4580–4581; c) C. Jung, *Biochim. Biophys. Acta* **2011**, *1814*, 46–57.
- [99] J. Rittle, M. T. Green, *Science* **2010**, *330*, 933–937.
- [100] a) J. T. Groves, G. A. McClusky, *J. Am. Chem. Soc.* **1976**, *98*, 859–861; b) X. Huang, J. T. Groves, *J. Biol. Inorg. Chem.* **2017**, *22*, 185–207.
- [101] P. R. Ortiz de Montellano, S. D. Nelson, *Arch. Biochem. Biophys.* **2011**, *507*, 95–110.
- [102] K.-B. Cho, X. Wu, Y.-M. Lee, Y. H. Kwon, S. Shaik, W. Nam, *J. Am. Chem. Soc.* **2012**, *134*, 20222–20225.
- [103] a) F. Hannemann, A. Bichet, K. M. Ewen, R. Bernhardt, *Biochim. Biophys. Acta* **2007**, *1770*, 330–344; b) K. J. McLean, D. Luciakova, J. Belcher, K. L. Tee, A. W. Munro, *Adv. Exp. Med. Biol.* **2015**, *851*, 299–317.
- [104] H. Renault, J.-E. Bassard, B. Hamberger, D. Werck-Reichhart, *Curr. Opin. Plant Biol.* **2014**, *19*, 27–34.



- [105] IUPAC, *Pure Appl. Chem.* **1979**, *51*, 353–380.
- [106] J. Atzrodt, V. Derdau, W. J. Kerr, M. Reid, *Angew. Chem. Int. Ed.* **2018**, *57*, 1758–1784.
- [107] J. S. Dickschat, *Eur. J. Org. Chem.* **2017**, 4872–4882.
- [108] D. E. Cane, G. G. S. King, *Tetrahedron Lett.* **1976**, *51*, 4737–4740.
- [109] H. P. Sigg, H. P. Weber, *Helv. Chim. Acta* **1968**, *51*, 1395–1408.
- [110] D. E. Cane, D. B. McIlwaine, J. S. Oliver, *J. Am. Chem. Soc.* **1990**, *112*, 1285–1286.
- [111] D. Arigoni, *Pure Appl. Chem.* **1975**, *41*, 219–245.
- [112] a) M. Dixit, M. Weitman, J. Gao, D. T. Major, *ACS Catal.* **2017**, *7*, 812–818; b) Y.-H. Wang, H. Xie, J. Zhou, F. Zhang, R. Wu, *ACS Catal.* **2017**, *7*, 5841–5846; c) M. Dixit, M. Weitman, J. Gao, D. T. Major, *ACS Catal.* **2018**, *8*, 1371–1375; d) Y.-H. Wang, F. Zhang, J. Zhou, H. Xie, R. Wu, *ACS Catal.* **2018**, *8*, 1363–1370.
- [113] Y. Li, Z. Wang, R. C. Beier, J. Shen, D. de Smet, S. de Saeger, S. Zhang, *J. Agric. Food Chem.* **2011**, *59*, 3441–3453.
- [114] Y. J. Hong, D. J. Tantillo, *Org. Lett.* **2006**, *8*, 4601–4604.
- [115] I. Burkhardt, J. S. Dickschat, *Chem. Commun.* **2018**, *54*, 3540–3542.
- [116] D. E. Cane, H.-J. Ha, C. Pargellis, F. Waldmeier, S. Swanson, P. P. N. Murthy, *Bioorg. Chem.* **1985**, *13*, 246–265.
- [117] D. E. Cane, H. J. Ha, *J. Am. Chem. Soc.* **1988**, *110*, 6865–6870.
- [118] J. S. Dickschat, N. L. Brock, C. A. Citron, B. Tudzynski, *ChemBioChem* **2011**, *12*, 2088–2095.
- [119] a) Y. J. Hong, D. J. Tantillo, *J. Am. Chem. Soc.* **2009**, *131*, 7999–8015; b) R. P. Pemberton, K. C. Ho, D. J. Tantillo, *Chem. Sci.* **2015**, *6*, 2347–2353.
- [120] X. Lin, D. E. Cane, *J. Am. Chem. Soc.* **2009**, *131*, 6332–6333.
- [121] A. Meguro, Y. Motoyoshi, K. Teramoto, S. Ueda, Y. Totsuka, Y. Ando, T. Tomita, S.-Y. Kim, T. Kimura, M. Igarashi, R. Sawa, T. Shinada, M. Nishiyama, T. Kuzuyama, *Angew. Chem. Int. Ed.* **2015**, *54*, 4353–4356.
- [122] S.-Y. Kim, P. Zhao, M. Igarashi, R. Sawa, T. Tomita, M. Nishiyama, T. Kuzuyama, *Chem. Biol.* **2009**, *16*, 736–743.
- [123] a) T. Aoyama, H. Naganawa, Y. Muraoka, T. Aoyagi, T. Takeuchi, *J. Antibiot.* **1992**, *45*, 1703–1704; b) T. Aoyagi, T. Aoyama, F. Kojima, S. Hattori, Y. Honma, M. Hamada, T. Takeuchi, *J. Antibiot.* **1992**, *45*, 1587–1591.
- [124] H. Sato, K. Teramoto, Y. Masumoto, N. Tezuka, K. Sakai, S. Ueda, Y. Totsuka, T. Shinada, M. Nishiyama, C. Wang, T. Kuzuyama, M. Uchiyama, *Sci. Rep.* **2015**, *5*, 18471.
- [125] Y. J. Hong, D. J. Tantillo, *Org. Biomol. Chem.* **2015**, *13*, 10273–10278.
- [126] R. Driller, S. Janke, M. Fuchs, E. Warner, A. R. Mhashal, D. T. Major, M. Christmann, T. Brück, B. Loll, *Nat. Commun.* **2018**, *9*, 3971.
- [127] P. Rabe, L. Barra, J. Rinkel, R. Riclea, C. A. Citron, T. A. Klapschinski, A. Janusko, J. S. Dickschat, *Angew. Chem. Int. Ed.* **2015**, *54*, 13448–13451.
- [128] a) Y. Sugai, Y. Ueno, K.-i. Hayashi, S. Oogami, T. Toyomasu, S. Matsumoto, M. Natsume, H. Nozaki, H. Kawaide, *J. Biol. Chem.* **2011**, *286*, 42840–42847; b) G.

- A. Ellis, T. P. Wyche, C. G. Fry, D. R. Braun, T. S. Bugni, *Mar. Drugs* **2014**, *12*, 1013–1022; c) T. P. Wyche, J. S. Piotrowski, Y. Hou, D. Braun, R. Deshpande, S. McIlwain, I. M. Ong, C. L. Myers, I. A. Guzei, W. M. Westler, D. R. Andes, T. S. Bugni, *Angew. Chem. Int. Ed.* **2014**, *53*, 11583–11586; d) L. Barra, K. Ibrom, J. S. Dickschat, *Angew. Chem. Int. Ed.* **2015**, *54*, 6637–6640.
- [129] P. Rabe, K. A. K. Pahirulzaman, J. S. Dickschat, *Angew. Chem. Int. Ed.* **2015**, *54*, 6041–6045.
- [130] P. Rabe, A. Janusko, B. Goldfuss, J. S. Dickschat, *ChemBioChem* **2016**, *17*, 146–149.
- [131] J. Rinkel, P. Rabe, P. Garbeva, J. S. Dickschat, *Angew. Chem. Int. Ed.* **2016**, *55*, 13593–13596.
- [132] S. Schulz, J. S. Dickschat, *Nat. Prod. Rep.* **2007**, *24*, 814–842.
- [133] J. S. Dickschat, *Nat. Prod. Rep.* **2017**, *34*, 310–328.
- [134] L. Molhave, *Indoor Air* **1991**, *1*, 357–376.
- [135] U. B. Nurmatov, N. Tagieva, S. Semple, G. Devereux, A. Sheikh, *Prim. Care Resp. J.* **2013**, *22*, PS9.
- [136] A. H. Jalal, F. Alam, S. Roychoudhury, Y. Umasankar, N. Pala, S. Bhansali, *ACS Sens.* **2018**, *3*, 1246–1263.
- [137] R. Zawirska-Wojtasiak, *Food Chem.* **2004**, *86*, 113–118.
- [138] H. H. Jeleń, *J. Agric. Food Chem.* **2002**, *50*, 6569–6574.
- [139] J. H. Moore, N. D. Davis, U. L. Diener, *Appl. Microbiol.* **1972**, *23*, 1067–1072.
- [140] K. J. van der Merwe, P. S. Steyn, L. Fourie, D. E. B. Scott, J. J. Theron, *Nature* **1965**, *205*, 1112–1113.
- [141] H. H. Jeleń, J. Grabarkiewicz-Szczęśna, *J. Agric. Food Chem.* **2005**, *53*, 1678–1683.
- [142] J. H. Birkinshaw, W. P. K. Findlay, *Biochem. J.* **1940**, *34*, 82–88.
- [143] a) C.-W. Chang, H.-S. Chang, M.-J. Cheng, T.-W. Liu, S.-Y. Hsieh, G.-F. Yuan, I.-S. Chen, *Chem. Biodivers.* **2014**, *11*, 949–961; b) J. S. Dickschat, T. Wang, M. Stadler, *Beilstein J. Org. Chem.* **2018**, *14*, 734–746.
- [144] N. L. Brock, B. Tudzynski, J. S. Dickschat, *ChemBioChem* **2011**, *12*, 2667–2676.
- [145] J. H. Birkinshaw, P. Chaplen, W. P. K. Findlay, *Biochem. J.* **1957**, *66*, 188–192.
- [146] H. Koshino, T. Yoshihara, M. Okuno, S. Sakamura, A. Tajimi, T. Shimanuki, *Biosci. Biotechnol. Biochem.* **1992**, *56*, 1096–1099.
- [147] R. Geisen, M. Schmidt-Heydt, A. Karolewicz, *Mycotoxin Res.* **2006**, *22*, 134–141.
- [148] Y.-H. Chooi, C. Krill, R. A. Barrow, S. Chen, R. Trengove, R. P. Oliver, P. S. Solomon, *Appl. Environ. Microbiol.* **2015**, *81*, 177–186.
- [149] a) J. Staunton, K. J. Weissman, *Nat. Prod. Rep.* **2001**, *18*, 380–416; b) C. Hertweck, *Angew. Chem. Int. Ed.* **2009**, *48*, 4688–4716; c) C. Khosla, *J. Org. Chem.* **2009**, *74*, 6416–6420.
- [150] L. Hang, N. Liu, Y. Tang, *ACS Catal.* **2016**, *6*, 5935–5945.
- [151] J. A. Kalaitzis, B. S. Moore, *J. Nat. Prod.* **2004**, *67*, 1419–1422.
- [152] a) M. Dashtban, H. Schraft, T. A. Syed, W. Qin, *Int. J. Biochem. Mol. Biol.* **2010**, *1*, 36–50; b) Y. Su, X. Yu, Y. Sun, G. Wang, H. Chen, G. Chen, *Sci. Rep.* **2018**, *8*,

- 5385; c) L. F. Longe, J. Couvreur, M. Leriche Grandchamp, G. Garnier, F. Allais, K. Saito, *ACS Sustainable Chem. Eng.* **2018**, *6*, 10097–10107.
- [153] M. R. Mäkelä, M. Marinović, P. Nousiainen, A. J. M. Liwanag, I. Benoit, J. Sipilä, A. Hatakka, R. P. de Vries, K. S. Hildén, *Adv. Appl. Microbiol.* **2015**, *91*, 63–137.
- [154] S. Gillet, M. Aguedo, L. Petitjean, A. R. C. Morais, Lopes, A. M. da Costa, R. M. Łukasik, P. T. Anastas, *Green Chem.* **2017**, *19*, 4200–4233.
- [155] G. Janusz, A. Pawlik, J. Sulej, U. Świdorska-Burek, A. Jarosz-Wilkolazka, A. Paszczyński, *FEMS Microbiol. Rev.* **2017**, *41*, 941–962.
- [156] A. B. Orth, M. Tien, *Biotechnology of Lignin Degradation in Genetics and Biotechnology, Vol. 2* (Ed.: U. Kück), Springer, Berlin, Heidelberg, **1995**, pp. 287–302.
- [157] a) K. Kintaka, H. Ono, S. Tsubotani, S. Harada, O. Hisayoshi, *J. Antibiot.* **1984**, *37*, 1294–1300; b) S. Tsubotani, Y. Wada, K. Kamiya, H. Okazaki, S. Harada, *Tetrahedron Lett.* **1984**, *25*, 419–422.
- [158] M. Z. Wilson, R. Wang, Z. Gitai, M. R. Seyedsayamdost, *Proc. Natl. Acad. Sci. USA* **2016**, *113*, 1630–1635.
- [159] J. Rutkowski, B. Brzezinski, *BioMed Res. Int.* **2013**, 162513.
- [160] a) C. Ruiz-Ponte, V. Cilia, C. Lambert, J. L. Nicolas, *Int. J. Syst. Bacteriol.* **1998**, *48*, 537–542; b) N. Buddruhs, S. Pradella, M. Göker, O. Päuker, R. Pukall, C. Spröer, P. Schumann, J. Petersen, T. Brinkhoff, *Int. J. Syst. Evol. Microbiol.* **2013**, *63*, 4340–4349.
- [161] M. R. Seyedsayamdost, R. J. Case, R. Kolter, J. Clardy, *Nat. Chem.* **2011**, *3*, 331–335.
- [162] P. M. Holligan, E. Fernández, J. Aiken, W. M. Balch, P. Boyd, P. H. Burkill, M. Finch, S. B. Groom, G. Malin, K. Muller, D. A. Purdie, C. Robinson, C. C. Trees, S. M. Turner, P. van der Wal, *Global Biogeochem. Cycles* **1993**, *7*, 879–900.
- [163] A. R. Bramucci, R. J. Case, *Sci. Rep.* **2019**, *9*, 5215.
- [164] H. Geng, J. B. Bruhn, K. F. Nielsen, L. Gram, R. Belas, *Appl. Environ. Microbiol.* **2008**, *74*, 1535–1545.
- [165] D. E. Cane, Z. Wu, J. E. van Epp, *J. Am. Chem. Soc.* **1992**, *114*, 8479–8483.
- [166] a) R. Teufel, V. Mascaraque, W. Ismail, M. Voss, J. Perera, W. Eisenreich, W. Haehnel, G. Fuchs, *Proc. Natl. Acad. Sci. USA* **2010**, *107*, 14390–14395; b) Y. Li, M. Wang, Q. Zhao, X. Shen, J. Wang, Y. Yan, X. Sun, Q. Yuan, *ACS Synth. Biol.* **2019**, *8*, 876–883.
- [167] R. Teufel, C. Gantert, M. Voss, W. Eisenreich, W. Haehnel, G. Fuchs, *J. Biol. Chem.* **2011**, *286*, 11021–11034.
- [168] N. L. Brock, A. Nikolay, J. S. Dickschat, *Chem. Commun.* **2014**, *50*, 5487–5489.
- [169] V. Thiel, T. Brinkhoff, J. S. Dickschat, S. Wickel, J. Grunenberg, I. Wagner-Döbler, M. Simon, S. Schulz, *Org. Biomol. Chem.* **2010**, *8*, 234–246.
- [170] a) C. R. Gentry-Weeks, J. Spokes, J. Thompson, *J. Biol. Chem.* **1995**, *270*, 7695–7702; b) R. Wang, É. Gallant, M. R. Seyedsayamdost, *mBio* **2016**, *7*, e02118-15.
- [171] E. Strauss, T. P. Begley, *J. Am. Chem. Soc.* **2001**, *123*, 6449–6450.
- [172] H. Geng, R. Belas, *J. Bacteriol.* **2010**, *192*, 4377–4387.

- [173] P. G. Beyersmann, J. Tomasch, K. Son, R. Stocker, M. Göker, I. Wagner-Döbler, M. Simon, T. Brinkhoff, *Sci. Rep.* **2017**, *7*, 730.
- [174] a) A. Camilli, B. L. Bassler, *Science* **2006**, *311*, 1113–1116; b) D. Patzelt, H. Wang, I. Buchholz, M. Rohde, L. Gröbe, S. Pradella, A. Neumann, S. Schulz, S. Heyber, K. Münch, R. Münch, D. Jahn, I. Wagner-Döbler, J. Tomasch, *ISME J.* **2013**, *7*, 2274–2286.
- [175] a) K. H. Nealson, T. Platt, J. W. Hastings, *J. Bacteriol.* **1970**, *104*, 313–322; b) A. Eberhard, *J. Bacteriol.* **1972**, *109*, 1101–1105; c) T. Miyashiro, E. G. Ruby, *Mol. Microbiol.* **2012**, *84*, 795–806.
- [176] J. Engebrecht, K. Nealson, M. Silverman, *Cell* **1983**, *32*, 773–781.
- [177] A. Eberhard, A. L. Burlingame, C. Eberhard, G. L. Kenyon, K. H. Nealson, N. J. Oppenheimer, *Biochemistry* **1981**, *20*, 2444–2449.
- [178] M. J. McFall-Ngai, *Annu. Rev. Microbiol.* **2014**, *68*, 177–194.
- [179] a) J. Zan, Y. Liu, C. Fuqua, R. T. Hill, *Int. J. Mol. Sci.* **2014**, *15*, 654–669; b) L. Ziesche, H. Bruns, M. Dogs, L. Wolter, F. Mann, I. Wagner-Döbler, T. Brinkhoff, S. Schulz, *ChemBioChem* **2015**, *16*, 2094–2107.
- [180] M. Berger, A. Neumann, S. Schulz, M. Simon, T. Brinkhoff, *J. Bacteriol.* **2011**, *193*, 6576–6585.
- [181] R. Schoenheimer, D. Rittenberg, *Science* **1935**, *82*, 156–157.
- [182] G. L. Foster, R. Schoenheimer, D. Rittenberg, *J. Biol. Chem.* **1939**, *127*, 319–327.
- [183] J. A. Bassham, A. A. Benson, M. Calvin, *J. Biol. Chem.* **1950**, *185*, 781–787.
- [184] J. Rinkel, J. S. Dickschat, *Beilstein J. Org. Chem.* **2015**, *11*, 2493–2508.
- [185] S. Pidot, K. Ishida, M. Cyrulies, C. Hertweck, *Angew. Chem. Int. Ed.* **2014**, *53*, 7856–7859.
- [186] M. Zhang, X.-F. Hou, L.-H. Qi, Y. Yin, Q. Li, H.-X. Pan, X.-Y. Chen, G.-L. Tang, *Chem. Sci.* **2015**, *6*, 3440–3447.
- [187] J. P. Gomez-Escribano, L. Song, D. J. Fox, V. Yeo, M. J. Bibb, G. L. Challis, *Chem. Sci.* **2012**, *3*, 2716–2720.
- [188] P. Chankhamjon, D. Boettger-Schmidt, K. Scherlach, B. Urbansky, G. Lackner, D. Kalb, H.-M. Dahse, D. Hoffmeister, C. Hertweck, *Angew. Chem. Int. Ed.* **2014**, *53*, 13409–13413.
- [189] A. Ear, S. Amand, F. Blanchard, A. Blond, L. Dubost, D. Buisson, B. Nay, *Org. Biomol. Chem.* **2015**, *13*, 3662–3666.
- [190] Y. Ye, A. Minami, A. Mandi, C. Liu, T. Taniguchi, T. Kuzuyama, K. Monde, K. Gomi, H. Oikawa, *J. Am. Chem. Soc.* **2015**, *137*, 11846–11853.
- [191] a) D. E. Cane, M. Tandon, *J. Am. Chem. Soc.* **1995**, *117*, 5602–5603; b) S. Garms, T. G. Köllner, W. Boland, *J. Org. Chem.* **2010**, *75*, 5590–5600; c) Y. Hu, W. K.W. Chou, R. Hopson, D. E. Cane, *Chem. Biol.* **2011**, *18*, 32–37.
- [192] a) P. Rabe, J. S. Dickschat, *Angew. Chem. Int. Ed.* **2013**, *52*, 1810–1812; b) J. S. Dickschat, K. A. K. Pahirulzaman, P. Rabe, T. A. Klapschinski, *ChemBioChem* **2014**, *15*, 810–814; c) P. Rabe, T. Schmitz, J. S. Dickschat, *Beilstein J. Org. Chem.* **2016**, *12*, 1839–1850.

- [193] D. E. Cane, J. S. Oliver, P. H. M. Harrison, C. Abell, B. R. Hubbard, C. T. Kane, R. Lattman, *J. Am. Chem. Soc.* **1990**, *112*, 4513–4524.
- [194] a) G. E. Keck, D. Krishnamurthy, *J. Org. Chem.* **1996**, *61*, 7638–7639; b) H. V. Thulasiram, R. M. Phan, S. B. Rivera, C. D. Poulter, *J. Org. Chem.* **2006**, *71*, 1739–1741.
- [195] M. M. Midland, S. Greer, A. Tramontano, S. A. Zderic, *J. Am. Chem. Soc.* **1979**, *101*, 2352–2355.
- [196] R. L. Edelstein, V. A. Weller, M. D. Distefano, J. S. Tung, *J. Org. Chem.* **1998**, *63*, 5298–5299.
- [197] R. K. Keller, R. Thompson, *J. Chromatogr. A* **1993**, *645*, 161–167.
- [198] a) V. J. Davisson, A. B. Woodside, T. R. Neal, K. E. Stremmer, M. Muehlbacher, C. D. Poulter, *J. Org. Chem.* **1986**, *51*, 4768–4779; b) A. B. Woodside, Z. Huang, C. D. Poulter, *Org. Synth.* **1988**, *66*, 211.
- [199] Y. J. Hong, D. J. Tantillo, *Chem. Sci.* **2010**, *1*, 609–614.
- [200] X. Chen, T. G. Köllner, Q. Jia, A. Norris, B. Santhanam, P. Rabe, J. S. Dickschat, G. Shaulsky, J. Gershenzon, F. Chen, *Proc. Natl. Acad. Sci. USA* **2016**, *113*, 12132–12137.
- [201] R. H. Kessin, *Dictyostelium. Evolution, cell biology, and the development of multicellularity*, Cambridge University Press, Cambridge, **2001**.
- [202] P. Rabe, J. Rinkel, B. Nubbemeyer, T. G. Köllner, F. Chen, J. S. Dickschat, *Angew. Chem. Int. Ed.* **2016**, *55*, 15420–15423.
- [203] D. J. Boland (Ed.), *Eucalyptus leaf oils. Use, chemistry, distillation, and marketing*, Inkata Press, Melbourne, **1991**.
- [204] M. L. Wise, T. J. Savage, E. Katahira, R. Croteau, *J. Biol. Chem.* **1998**, *273*, 14891–14899.
- [205] R. Croteau, W. R. Alonso, A. E. Koepp, M. A. Johnson, *Arch. Biochem. Biophys.* **1994**, *309*, 184–192.
- [206] M. L. Wise, M. Urbansky, G. L. Helms, R. M. Coates, R. Croteau, *J. Am. Chem. Soc.* **2002**, *124*, 8546–8547.
- [207] C. Nakano, H.-K. Kim, Y. Ohnishi, *ChemBioChem* **2011**, *12*, 1988–1991.
- [208] J. Rinkel, P. Rabe, L. zur Horst, J. S. Dickschat, *Beilstein J. Org. Chem.* **2016**, *12*, 2317–2324.
- [209] Y. Yamada, T. Kuzuyama, M. Komatsu, K. Shin-ya, S. Omura, D. E. Cane, H. Ikeda, *Proc. Natl. Acad. Sci. USA* **2015**, *112*, 857–862.
- [210] Y. Yamada, S. Arima, T. Nagamitsu, K. Johmoto, H. Uekusa, T. Eguchi, K. Shin-ya, D. E. Cane, H. Ikeda, *J. Antibiot.* **2015**, *68*, 385–394.
- [211] Q. N. N. Nguyen, D. J. Tantillo, *J. Antibiot.* **2016**, *69*, 534–540.
- [212] P. Rabe, J. Rinkel, E. Dolja, T. Schmitz, B. Nubbemeyer, T. H. Luu, J. S. Dickschat, *Angew. Chem. Int. Ed.* **2017**, *56*, 2776–2779.
- [213] V. A. Raldugin, N. K. Kashtanova, V. A. Pentegova, *Chem. Nat. Compd.* **1971**, *7*, 582–585.
- [214] J. Rinkel, P. Rabe, X. Chen, T. G. Köllner, F. Chen, J. S. Dickschat, *Chem. Eur. J.* **2017**, *23*, 10501–10505.

- [215] L. Wang, B. Yang, X.-P. Lin, X.-F. Zhou, Y. Liu, *Nat. Prod. Rep.* **2013**, *30*, 455–473.
- [216] T. Sato, H. Yamaga, S. Kashima, Y. Murata, T. Shinada, C. Nakano, T. Hoshino, *ChemBioChem* **2013**, *14*, 822–825.
- [217] S.-H. Kim, W. Lu, M. K. Ahmadi, D. Montiel, M. A. Ternei, S. F. Brady, *ACS Synth. Biol.* **2019**, *8*, 109–118.
- [218] a) T. Mitsushashi, I. Abe, *ChemBioChem* **2018**, *19*, 1106–1114; b) A. Minami, T. Ozaki, C. Liu, H. Oikawa, *Nat. Prod. Rep.* **2018**, *35*, 1330–1346.
- [219] R. Chiba, A. Minami, K. Gomi, H. Oikawa, *Org. Lett.* **2013**, *15*, 594–597.
- [220] T. Toyomasu, M. Tsukahara, A. Kaneko, R. Niida, W. Mitsushashi, T. Dairi, N. Kato, T. Sassa, *Proc. Natl. Acad. Sci. USA* **2007**, *104*, 3084–3088.
- [221] Y. Matsuda, T. Mitsushashi, Z. Quan, I. Abe, *Org. Lett.* **2015**, *17*, 4644–4647.
- [222] Y. Matsuda, T. Mitsushashi, S. Lee, M. Hoshino, T. Mori, M. Okada, H. Zhang, F. Hayashi, M. Fujita, I. Abe, *Angew. Chem. Int. Ed.* **2016**, *55*, 5785–5788.
- [223] Y. Inokuma, S. Yoshioka, J. Ariyoshi, T. Arai, Y. Hitora, K. Takada, S. Matsunaga, K. Rissanen, M. Fujita, *Nature* **2013**, *495*, 461–466.
- [224] M. Okada, Y. Matsuda, T. Mitsushashi, S. Hoshino, T. Mori, K. Nakagawa, Z. Quan, B. Qin, H. Zhang, F. Hayashi, H. Kawaide, I. Abe, *J. Am. Chem. Soc.* **2016**, *138*, 10011–10018.
- [225] H. Sato, T. Mitsushashi, M. Yamazaki, I. Abe, M. Uchiyama, *Angew. Chem. Int. Ed.* **2018**, *57*, 14752–14757.
- [226] F. J. Jin, J.-i. Maruyama, P. R. Juvvadi, M. Arioka, K. Kitamoto, *FEMS Microbiol. Lett.* **2004**, *239*, 79–85.
- [227] T. Mitsushashi, J. Rinkel, M. Okada, I. Abe, J. S. Dickschat, *Chem. Eur. J.* **2017**, *23*, 10053–10057.
- [228] X. Huang, H. Huang, H. Li, X. Sun, H. Huang, Y. Lu, Y. Lin, Y. Long, Z. She, *Org. Lett.* **2013**, *15*, 721–723.
- [229] K. Kemper, M. Hirte, M. Reinbold, M. Fuchs, T. Brück, *Beilstein J. Org. Chem.* **2017**, *13*, 845–854.
- [230] K. Sakai, H. Kinoshita, T. Nihira, *Appl. Microbiol. Biotechnol.* **2012**, *93*, 2011–2022.
- [231] S. C. Kampranis, A. M. Makris, *Comput. Struct. Biotechnol. J.* **2012**, *3*, e201210006.
- [232] Q. Liu, M. Majdi, K. Cankar, M. Goedbloed, T. Charnikhova, F. W. A. Verstappen, R. C. H. de Vos, J. Beekwilder, S. van der Krol, H. J. Bouwmeester, *PloS one* **2011**, *6*, e23255.
- [233] J.-F. Ginglinger, B. Boachon, R. Höfer, C. Paetz, T. G. Köllner, L. Miesch, R. Lugan, R. Baltenweck, J. Mutterer, P. Ullmann, F. Beran, P. Claudel, F. Verstappen, M. J. C. Fischer, F. Karst, H. Bouwmeester, M. Miesch, B. Schneider, J. Gershenzon, J. Ehltling, D. Werck-Reichhart, *Plant Cell* **2013**, *25*, 4640–4657.
- [234] J. Bohlmann, D. Martin, N. J. Oldham, J. Gershenzon, *Arch. Biochem. Biophys.* **2000**, *375*, 261–269.
- [235] J. S. Dickschat, J. Rinkel, P. Rabe, A. B. Kashkooli, H. J. Bouwmeester, *Beilstein J. Org. Chem.* **2017**, *13*, 1770–1780.

- [236] C. L. Steele, J. Crock, J. Bohlmann, R. Croteau, *J. Biol. Chem.* **1998**, 273, 2078–2089.
- [237] L. Pazouki, Ü. Niinemets, *Front. Plant Sci.* **2016**, 7, 1019.
- [238] S. Schulz, C. Messer, K. Dettner, *Tetrahedron Lett.* **1997**, 38, 2077–2080.
- [239] J. Rinkel, L. Lauterbach, J. S. Dickschat, *Angew. Chem. Int. Ed.* **2017**, 56, 16385–16389.
- [240] D. Trautmann, B. Epe, U. Oelbermann, A. Mondon, *Chem. Ber.* **1980**, 113, 3848–3865.
- [241] G. M. König, A. D. Wright, *J. Org. Chem.* **1997**, 62, 3837–3840.
- [242] R. D. Kersten, S. Lee, D. Fujita, T. Pluskal, S. Kram, J. E. Smith, T. Iwai, J. P. Noel, M. Fujita, J.-K. Weng, *J. Am. Chem. Soc.* **2017**, 139, 16838–16844.
- [243] J. Buddrus, H. Bauer, *Angew. Chem. Int. Ed.* **1987**, 26, 625–642.
- [244] J. Rinkel, L. Lauterbach, P. Rabe, J. S. Dickschat, *Angew. Chem. Int. Ed.* **2018**, 57, 3238–3241.
- [245] D. C. Braddock, K. K. Hii, J. M. Brown, *Angew. Chem. Int. Ed.* **1998**, 37, 1720–1723.
- [246] R. Riclea, J. S. Dickschat, *Angew. Chem. Int. Ed.* **2015**, 54, 12167–12170.
- [247] S. Takamatsu, X. Lin, A. Nara, M. Komatsu, D. E. Cane, H. Ikeda, *Microb. Biotechnol.* **2011**, 4, 184–191.
- [248] T. Tokai, H. Koshino, N. Takahashi-Ando, M. Sato, M. Fujimura, M. Kimura, *Biochem. Biophys. Res. Commun.* **2007**, 353, 412–417.
- [249] Y. Khatri, F. Hannemann, K. M. Ewen, D. Pistorius, O. Perlova, N. Kagawa, A. O. Brachmann, R. Müller, R. Bernhardt, *Chem. Biol.* **2010**, 17, 1295–1305.
- [250] a) M. Litzenburger, F. Kern, Y. Khatri, R. Bernhardt, *Drug Metab. Dispos.* **2015**, 43, 392–399; b) F. Kern, Y. Khatri, M. Litzenburger, R. Bernhardt, *Drug Metab. Dispos.* **2016**, 44, 495–504.
- [251] Y. Yuan, M. Litzenburger, S. Cheng, G. Bian, B. Hu, P. Yan, Y. Cai, Z. Deng, R. Bernhardt, T. Liu, *ChemBioChem* **2019**, 20, 677–682.
- [252] J. Rinkel, M. Litzenburger, R. Bernhardt, J. S. Dickschat, *ChemBioChem* **2018**, 19, 1498–1501.
- [253] a) C.-L. Wu, S.-C. Chien, S.-Y. Wang, Y.-H. Kuo, S.-T. Chang, *Holzforschung* **2005**, 59, 620–627; b) L. Ding, R. Pfoh, S. Rühl, S. Qin, H. Laatsch, *J. Nat. Prod.* **2009**, 72, 99–101.
- [254] P. Rabe, J. Rinkel, T. A. Klapschinski, L. Barra, J. S. Dickschat, *Org. Biomol. Chem.* **2016**, 14, 158–164.
- [255] M. Chen, W. K. W. Chou, T. Toyomasu, D. E. Cane, D. W. Christianson, *ACS Chem. Biol.* **2016**, 11, 889–899.
- [256] G. Bian, A. Hou, Y. Yuan, B. Hu, S. Cheng, Z. Ye, Y. Di, Z. Deng, T. Liu, *Org. Lett.* **2018**, 20, 1626–1629.
- [257] G. Bian, J. Rinkel, Z. Wang, L. Lauterbach, A. Hou, Y. Yuan, Z. Deng, T. Liu, J. S. Dickschat, *Angew. Chem. Int. Ed.* **2018**, 57, 15887–15890.
- [258] a) H. Siegel, D. Seebach, *J. Label. Compd. Radiopharm.* **1980**, 17, 279–287; b) C. Rink, V. Navickas, M. E. Maier, *Org. Lett.* **2011**, 13, 2334–2337; c) S. S. Shinde,

- A. Minami, Z. Chen, T. Tokiwano, T. Toyomasu, N. Kato, T. Sassa, H. Oikawa, *J. Antibiot.* **2017**, *70*, 632–638.
- [259] L. Lauterbach, J. Rinkel, J. S. Dickschat, *Angew. Chem. Int. Ed.* **2018**, *57*, 8280–8283.
- [260] L. Jenny, H.-J. Borschberg, P. Acklin, *Tetrahedron* **1996**, *52*, 1549–1556.
- [261] F. P. Mertz, R. C. Yao, *Int. J. Syst. Bacteriol.* **1990**, *40*, 34–39.
- [262] H. J. Kim, M. W. Ruszczycky, S.-h. Choi, Y.-n. Liu, H.-w. Liu, *Nature* **2011**, *473*, 109–112.
- [263] J. Rinkel, L. Lauterbach, J. S. Dickschat, *Angew. Chem. Int. Ed.* **2019**, *58*, 452–455.
- [264] V. V. Veselovsky, A. S. Gybin, A. V. Lozanova, A. M. Moiseenkov, W. A. Smit, R. Caple, *Tetrahedron Lett.* **1988**, *29*, 175–178.
- [265] A. J. Weinheimer, W. W. Youngblood, P. H. Washecheck, T. K.B. Karns, L. S. Ciereszko, *Tetrahedron Lett.* **1970**, *11*, 497–500.
- [266] A. M. Adio, *Tetrahedron* **2009**, *65*, 1533–1552.
- [267] J. A. Faraldos, S. Wu, J. Chappell, R. M. Coates, *Tetrahedron* **2007**, *63*, 7733–7742.
- [268] J. Rinkel, J. S. Dickschat, *Org. Lett.* **2019**, *21*, 2426–2429.
- [269] J.-W. de Kraker, M. C. R. Franssen, A. de Groot, T. Shibata, H. J. Bouwmeester, *Phytochemistry* **2001**, *58*, 481–487.
- [270] T. Toyomasu, A. Kaneko, T. Tokiwano, Y. Kanno, Y. Kanno, R. Niida, S. Miura, T. Nishioka, C. Ikeda, W. Mitsuhashi, T. Dairi, T. Kawano, H. Oikawa, N. Kato, T. Sassa, *J. Org. Chem.* **2009**, *74*, 1541–1548.
- [271] G. Bian, Y. Han, A. Hou, Y. Yuan, X. Liu, Z. Deng, T. Liu, *Metab. Eng.* **2017**, *42*, 1–8.
- [272] M. K. Renner, P. R. Jensen, W. Fenical, *J. Org. Chem.* **2000**, *65*, 4843–4852.
- [273] B. Qin, Y. Matsuda, T. Mori, M. Okada, Z. Quan, T. Mitsuhashi, T. Wakimoto, I. Abe, *Angew. Chem. Int. Ed.* **2016**, *55*, 1658–1661.
- [274] J. Rinkel, S. T. Steiner, J. S. Dickschat, *Angew. Chem. Int. Ed.* **2019**, *58*, accepted, DOI: 10.1002/anie.201902950.
- [275] a) S. H. von Reuß, M. Kai, B. Piechulla, W. Francke, *Angew. Chem. Int. Ed.* **2010**, *49*, 2009–2010; b) S. von Reuss, D. Domik, M. C. Lemfack, N. Magnus, M. Kai, T. Weise, B. Piechulla, *J. Am. Chem. Soc.* **2018**, *140*, 11855–11862.
- [276] J. Rinkel, J. S. Dickschat, *Beilstein J. Org. Chem.* **2019**, *15*, 789–794.
- [277] T. Katsuki, K. B. Sharpless, *J. Am. Chem. Soc.* **1980**, *102*, 5974–5976.
- [278] C. Le Thanh, K. R. Chauhan, *Nat. Prod. Commun.* **2014**, *9*, 297–298.
- [279] L. S. Vedula, J. Jiang, T. Zakharian, D. E. Cane, D. W. Christianson, *Arch. Biochem. Biophys.* **2008**, *469*, 184–194.
- [280] J. Rinkel, J. S. Dickschat, *Beilstein J. Org. Chem.* **2019**, *15*, 1008–1019.
- [281] M. Isegawa, S. Maeda, D. J. Tantillo, K. Morokuma, *Chem. Sci.* **2014**, *5*, 1555–1560.
- [282] P. Rabe, T. A. Klapschinski, J. S. Dickschat, *ChemBioChem* **2016**, *17*, 1333–1337.
- [283] C. A. Bauer, S. Grimme, *J. Phys. Chem. A* **2016**, *120*, 3755–3766.



- [284] a) J. Karliner, C. Djerassi, *J. Org. Chem.* **1966**, *31*, 1945–1956; b) D. S. Weinberg, C. Djerassi, *J. Org. Chem.* **1966**, *31*, 115–119; c) R. R. Muccino, C. Djerassi, *J. Am. Chem. Soc.* **1973**, *95*, 8726–8733.
- [285] D. Spiteller, A. Jux, J. Piel, W. Boland, *Phytochemistry* **2002**, *61*, 827–834.
- [286] J. Rinkel, P. Rabe, J. S. Dickschat, *Eur. J. Org. Chem.* **2019**, 351–359.
- [287] a) C. D. Gutsche, J. R. Maycock, C. T. Chang, *Tetrahedron* **1968**, *24*, 859–876; b) N. H. Andersen, D. D. Syrdal, *Tetrahedron Lett.* **1972**, *13*, 2455–2458; c) Y. Ohta, Y. Hirose, *Chem. Lett.* **1972**, *1*, 263–266; d) M. P. Polovinka, D. V. Korchagina, Y. V. Gatilov, I. Y. Bagrianskaya, V. A. Barkhash, V. B. Perutskii, N. D. Ungur, P. F. Vlad, V. V. Shcherbukhin, N. S. Zefirov, *J. Org. Chem.* **1994**, *59*, 1509–1517.
- [288] L. R. MacGillivray, J. L. Atwood, *Nature* **1997**, *389*, 469–472.
- [289] a) G. Bianchini, G. La Sorella, N. Canever, A. Scarso, G. Strukul, *Chem. Commun.* **2013**, *49*, 5322–5324; b) Q. Zhang, K. Tiefenbacher, *J. Am. Chem. Soc.* **2013**, *135*, 16213–16219.
- [290] a) Q. Zhang, K. Tiefenbacher, *Nat. Chem.* **2015**, *7*, 197–202; b) Q. Zhang, L. Catti, J. Pleiss, K. Tiefenbacher, *J. Am. Chem. Soc.* **2017**, *139*, 11482–11492.
- [291] Q. Zhang, J. Rinkel, B. Goldfuss, J. S. Dickschat, K. Tiefenbacher, *Nat. Catal.* **2018**, *1*, 609–615.
- [292] D. T. Major, *Nat. Catal.* **2018**, *1*, 567–568.
- [293] a) E. Kaminski, S. Stawicki, E. Wasowicz, *Appl. Microbiol.* **1974**, *27*, 1001–1004; b) J. L. Kinderlerer, *J. Appl. Bacteriol.* **1989**, *67*, 133–144.
- [294] S. Sethi, R. Nanda, T. Chakraborty, *Clin. Microbiol. Rev.* **2013**, *26*, 462–475.
- [295] D. Kandasamy, J. Gershenzon, A. Hammerbacher, *J. Chem. Ecol.* **2016**, *42*, 952–969.
- [296] C. A. Citron, C. Junker, B. Schulz, J. S. Dickschat, *Angew. Chem. Int. Ed.* **2014**, *53*, 4346–4349.
- [297] J. S. Dickschat, *Nat. Prod. Rep.* **2014**, *31*, 838–861.
- [298] C. L. Arthur, J. Pawliszyn, *Anal. Chem.* **1990**, *62*, 2145–2148.
- [299] K. Grob, F. Zürcher, *J. Chromatogr. A* **1976**, *117*, 285–294.
- [300] E. Kováts, *Helv. Chim. Acta* **1958**, *41*, 1915–1932.
- [301] T. Wang, P. Rabe, C. A. Citron, J. S. Dickschat, *Beilstein J. Org. Chem.* **2013**, *9*, 2767–2777.
- [302] a) Z. Pouzar, *Czech Mycol.* **1978**, *32*, 19–21; b) A. Mühlbauer, D. Triebel, D. Persoh, H. Wollweber, S. Seip, M. Stadler, *Mycol. Progress* **2002**, *1*, 235–248.
- [303] S. E. Helaly, B. Thongbai, M. Stadler, *Nat. Prod. Rep.* **2018**, *35*, 992–1014.
- [304] J. Rinkel, A. Babczyk, T. Wang, M. Stadler, J. S. Dickschat, *Beilstein J. Org. Chem.* **2018**, *14*, 2974–2990.
- [305] A. A. Bell, M. H. Wheeler, *Annu. Rev. Phytopathol.* **1986**, *24*, 411–451.
- [306] R. Vanholme, B. Demedts, K. Morreel, J. Ralph, W. Boerjan, *Plant Physiol.* **2010**, *153*, 895–905.
- [307] R. Rinaldi, R. Jastrzebski, M. T. Clough, J. Ralph, M. Kennema, P. C. A. Bruijninx, B. M. Weckhuysen, *Angew. Chem. Int. Ed.* **2016**, *55*, 8164–8215.

- [308] J. G. Linger, D. R. Vardon, M. T. Guarnieri, E. M. Karp, G. B. Hunsinger, M. A. Franden, C. W. Johnson, G. Chupka, T. J. Strathmann, P. T. Pienkos, G. T. Beckham, *Proc. Natl. Acad. Sci. USA* **2014**, *111*, 12013–12018.
- [309] C. S. Harwood, R. E. Parales, *Annu. Rev. Microbiol.* **1996**, *50*, 553–590.
- [310] N.-Z. Xie, H. Liang, R.-B. Huang, P. Xu, *Biotechnol. Adv.* **2014**, *32*, 615–622.
- [311] C. W. Johnson, D. Salvachúa, P. Khanna, H. Smith, D. J. Peterson, G. T. Beckham, *Metab. Eng. Commun.* **2016**, *3*, 111–119.
- [312] J. B. J. H. van Duuren, D. Wijte, A. Leprince, B. Karge, J. Puchalka, J. Wery, V. A. P. Martins dos Santos, G. Eggink, A. E. Mars, *J. Biotechnol.* **2011**, *156*, 163–172.
- [313] W. Park, C. O. Jeon, H. Cadillo, C. DeRito, E. L. Madsen, *Appl. Microbiol. Biotechnol.* **2004**, *64*, 429–435.
- [314] M. Kohlstedt, S. Starck, N. Barton, J. Stolzenberger, M. Selzer, K. Mehlmann, R. Schneider, D. Pleissner, J. Rinkel, J. S. Dickschat, J. Venus, J. B. J. H. van Duuren, C. Wittmann, *Metab. Eng.* **2018**, *47*, 279–293.
- [315] I. Nordlund, J. Powlowski, V. Shingler, *J. Bacteriol.* **1990**, *172*, 6826–6833.
- [316] T. Sonoki, K. Takahashi, H. Sugita, M. Hatamura, Y. Azuma, T. Sato, S. Suzuki, N. Kamimura, E. Masai, *ACS Sustainable Chem. Eng.* **2018**, *6*, 1256–1264.
- [317] U. Breiting, T. Clausen, S. Ehlert, R. Huber, B. Laber, F. Schmidt, E. Pohl, A. Messerschmidt, *Plant Physiol.* **2001**, *126*, 631–642.
- [318] J. R. Uren, *Cystathionine  $\beta$ -lyase from Escherichia coli* in *Methods in Enzymology: Sulfur and Sulfur Amino Acids*, Vol. 143 (Eds.: W. B. Jakoby, O. W. Griffith), Elsevier, Amsterdam, **1987**, pp. 483–486.
- [319] S. Thole, D. Kalhoefer, S. Voget, M. Berger, T. Engelhardt, H. Liesegang, A. Wollherr, S. Kjelleberg, R. Daniel, M. Simon, T. Thomas, T. Brinkhoff, *ISME J.* **2012**, *6*, 2229–2244.
- [320] J. S. Dickschat, J. Rinkel, T. Klapschinski, J. Petersen, *ChemBioChem* **2017**, *18*, 2260–2267.
- [321] D. J. Smith, V. Venkatraghavan, *Synth. Commun.* **1985**, *15*, 945–950.
- [322] G. L. Ellman, *Arch. Biochem. Biophys.* **1959**, *82*, 70–77.
- [323] a) T. Lang, D. Kessler, *J. Biol. Chem.* **1999**, *274*, 189–195; b) T. Clausen, J. T. Kaiser, C. Steegborn, R. Huber, D. Kessler, *Proc. Natl. Acad. Sci. USA* **2000**, *97*, 3856–3861.
- [324] Y.-H. Li, X. Tian, *Sensors* **2012**, *12*, 2519–2538.
- [325] a) Y. Tashiro, Y. Kimura, M. Furubayashi, A. Tanaka, K. Terakubo, K. Saito, S. Kawai-Noma, D. Umeno, *J. Gen. Appl. Microbiol.* **2016**, *62*, 240–247; b) J. P. Gerdt, D. M. Wittenwyler, J. B. Combs, M. E. Boursier, J. W. Brummond, H. Xu, H. E. Blackwell, *ACS Chem. Biol.* **2017**, *12*, 2457–2464.
- [326] A. Lindemann, G. Pessi, A. L. Schaefer, M. E. Mattmann, Q. H. Christensen, A. Kessler, H. Hennecke, H. E. Blackwell, E. P. Greenberg, C. S. Harwood, *Proc. Natl. Acad. Sci. USA* **2011**, *108*, 16765–16770.
- [327] a) W. T. Watson, T. D. Minogue, D. L. Val, S. B. von Bodman, M. E.A. Churchill, *Mol. Cell* **2002**, *9*, 685–694; b) T. A. Gould, H. P. Schweizer, M. E. A. Churchill, *Mol. Microbiol.* **2004**, *53*, 1135–1146; c) J. Chung, E. Goo, S. Yu, O. Choi, J. Lee,

- J. Kim, H. Kim, J. Igarashi, H. Suga, J. S. Moon, I. Hwang, S. Rhee, *Proc. Natl. Acad. Sci. USA* **2011**, *108*, 12089–12094; d) S.-H. Dong, N. D. Frane, Q. H. Christensen, E. P. Greenberg, R. Nagarajan, S. K. Nair, *Proc. Natl. Acad. Sci. USA* **2017**, *114*, 9092–9097.
- [328] L. Ziesche, J. Rinkel, J. S. Dickschat, S. Schulz, *Beilstein J. Org. Chem.* **2018**, *14*, 1309–1316.
- [329] A. Neumann, D. Patzelt, I. Wagner-Döbler, S. Schulz, *ChemBioChem* **2013**, *14*, 2355–2361.
- [330] P. Rabe, *Mechanistic studies on bacterial terpene synthases*. PhD thesis, University of Bonn, Bonn, **2015**.

## List of abbreviations

A(T/D)P	adenosine (tri/di)phosphate
AT	acetyltransferase
BT	benzoyltransferase
CLSA	closed-loop stripping apparatus
C(T/D/M)P	cytidine (tri/di/mono)phosphate
CoA	coenzyme A
CYP	cytochrome P450 monooxygenase
DOXP	1-deoxy-D-xylulose 5-phosphate
DTS	diterpene synthase
<i>E</i>	enzyme
EI	electron ionisation
Fd	ferredoxin
GC	gas chromatography
GC/MS	gas chromatography coupled to electron ionisation mass spectrometry
HMB-PP	( <i>E</i> )-4-hydroxy-3-methylbut-2-enyl diphosphate
HMG	3-hydroxy-3-methylglutaryl
IBX	2-iodoxybenzoic acid
MALDI-ToF	matrix-assisted laser desorption/ionisation coupled with time of flight mass spectrometry
ME	2- <i>C</i> -methyl-D-erythritol
MEP	2- <i>C</i> -methyl-D-erythritol 4-phosphate
MS	mass spectrometry
NADP <sup>+</sup>	nicotinamide adenine dinucleotide phosphate
NADPH	nicotinamide adenine dinucleotide phosphate hydride
NMR	nuclear magnetic resonance
OP	monophosphate (PO <sub>4</sub> <sup>2-</sup> )
OPP	diphosphate (P <sub>2</sub> O <sub>7</sub> <sup>3-</sup> )
PDB	Protein Data Bank
P <sub>i</sub>	inorganic phosphate
PP <sub>i</sub>	inorganic diphosphate
PT	prenyltransferase
StTS	sesterterpene synthase
T	transferase
TBDPS	<i>tert</i> -butyldiphenylsilyl
TEAP	bis(triethylammonium) phosphate
TLC	thin-layer chromatography
TS	terpene synthase

## Appendices A – X



# Appendix A

## Recent highlights in biosynthesis research using stable isotopes

*Beilstein J. Org. Chem.* **2015**, *11*, 2493–2508.

DOI:10.3762/bjoc.11.271







## Recent highlights in biosynthesis research using stable isotopes

Jan Rinkel and Jeroen S. Dickschat\*

### Review

Open Access

Address:

Kekulé-Institute of Organic Chemistry and Biochemistry,  
Gerhard-Domagk-Str. 1, 53121 Bonn, Germany

Email:

Jeroen S. Dickschat\* - dickschat@uni-bonn.de

\* Corresponding author

Keywords:

biosynthesis; enzyme mechanisms; isotopes; labeling experiments;  
natural products

*Beilstein J. Org. Chem.* **2015**, *11*, 2493–2508.

doi:10.3762/bjoc.11.271

Received: 24 September 2015

Accepted: 23 November 2015

Published: 09 December 2015

This article is part of the Thematic Series "Natural products in synthesis and biosynthesis II".

Associate Editor: A. Kirschning

© 2015 Rinkel and Dickschat; licensee Beilstein-Institut.

License and terms: see end of document.

### Abstract

The long and successful history of isotopic labeling experiments within natural products research has both changed and deepened our understanding of biosynthesis. As demonstrated in this article, the usage of isotopes is not at all old-fashioned, but continues to give important insights into biosynthetic pathways of secondary metabolites. This review with 85 cited references is structured by separate discussions of compounds from different classes including polyketides, non-ribosomal peptides, their hybrids, terpenoids, and aromatic compounds formed via the shikimate pathway. The text does not aim at a comprehensive overview, but instead a selection of recent important examples of isotope usage within biosynthetic studies is presented, with a special emphasis on mechanistic surprises.

### Introduction

This year may be seen as the 80th anniversary of using isotopes in biosynthetic and biochemical research. Since the first experiments performed by Schoenheimer and Rittenberg in 1935 using deuterated fatty acids and sterols to follow their fate in a living organism [1], a lot of new synthetic and analytical methods for the detection of isotopes have been developed that today allow for nearly unlimited applications in biosynthesis research. The basic principle of labeling an organic molecule in a way that is incognito for metabolism, but easy to follow for

the researcher still remains the same. The first application of this idea probably was the investigation on fatty acid degradation by Knoop in 1904, even long before isotopes were discovered. He used "chemically labeled" fatty acids with a phenyl residue in  $\omega$ -position bearing an odd or an even number of carbon atoms in the chain and fed it to dogs [2] to draw important conclusions on the  $\beta$ -oxidation of fatty acids [3] from the reisolated material. However, changing the chemical nature of the metabolite did not prove to be suitable for broader applica-

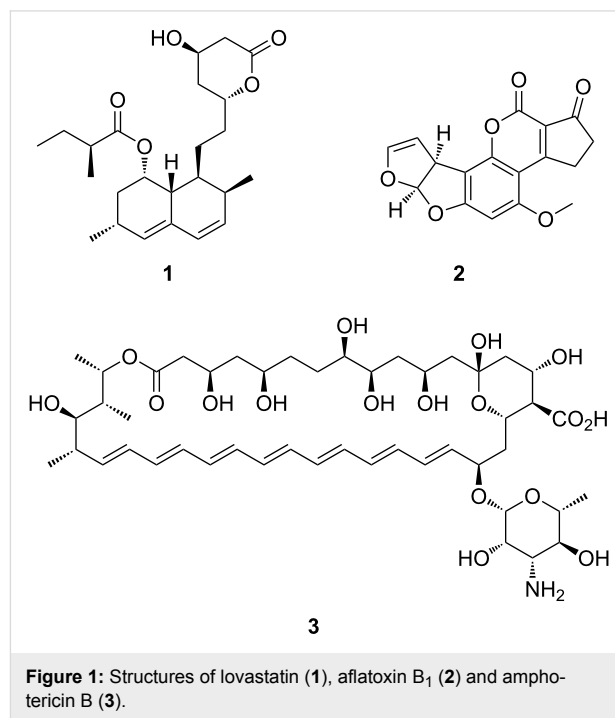
tions, and therefore, after the discovery of the isotopes by Frederick Soddy, for which he was awarded the Nobel prize in 1921, the first labeling experiments using isotopes quickly changed the way of investigating metabolic pathways and promoted a new dynamic view on biosynthesis research [4], leading to numerous breakthroughs such as the discovery of cholesterol biosynthesis [5]. With the rise of NMR and MS methods the usage of radioactive nuclei such as  $^{14}\text{C}$  and  $^3\text{H}$  shifted towards stable isotopes such as  $^{13}\text{C}$  and  $^2\text{H}$  [6], with the consequence that chemical degradation methods in natural products chemistry are almost vanished today. The usage of isotopically labeled precursors depends on careful interpretations of the incorporation pattern, which sometimes may lead to errors if unknown metabolic pathways are involved, as in the prominent example of the deoxyxylulose phosphate way in terpene biosynthesis [7,8]. Thus, a critical analysis of labeling experiments is required and may hint towards undiscovered metabolic pathways or enzyme functions [9]. As demonstrated in this article, the isotopic labeling technique continues to be an inspiring source of useful information in biosynthesis research. Isotopes have also found their way to many other applications, e.g., in systems biology including proteomics [10], lipidomics [11] and metabolomics [12], or for mapping isotopic fingerprints of whole organisms in metabolic flux studies [13], but these aspects will not be discussed here. Instead, this review highlights recent biosynthetic studies using isotopes from major classes of natural products including polyketides, non-ribosomal peptides, hybrids thereof, isoprenoids and a few aromatic compounds that arise via the shikimate pathway. It does not provide a comprehensive overview of all the work conducted, but tries to create a diversified picture of isotope usage in the study of selected interesting natural products. IUPAC nomenclature allows to distinguish isotopically substituted (every molecule in a sample is labeled at the designated position) and isotopically labeled compounds (a fraction of the molecules in a sample is labeled) by use of round or square brackets, respectively [14]. The assignments used in this article are based on the presentations in the original publications, even if the nomenclature in the original work may not precisely follow the IUPAC rules.

## Review

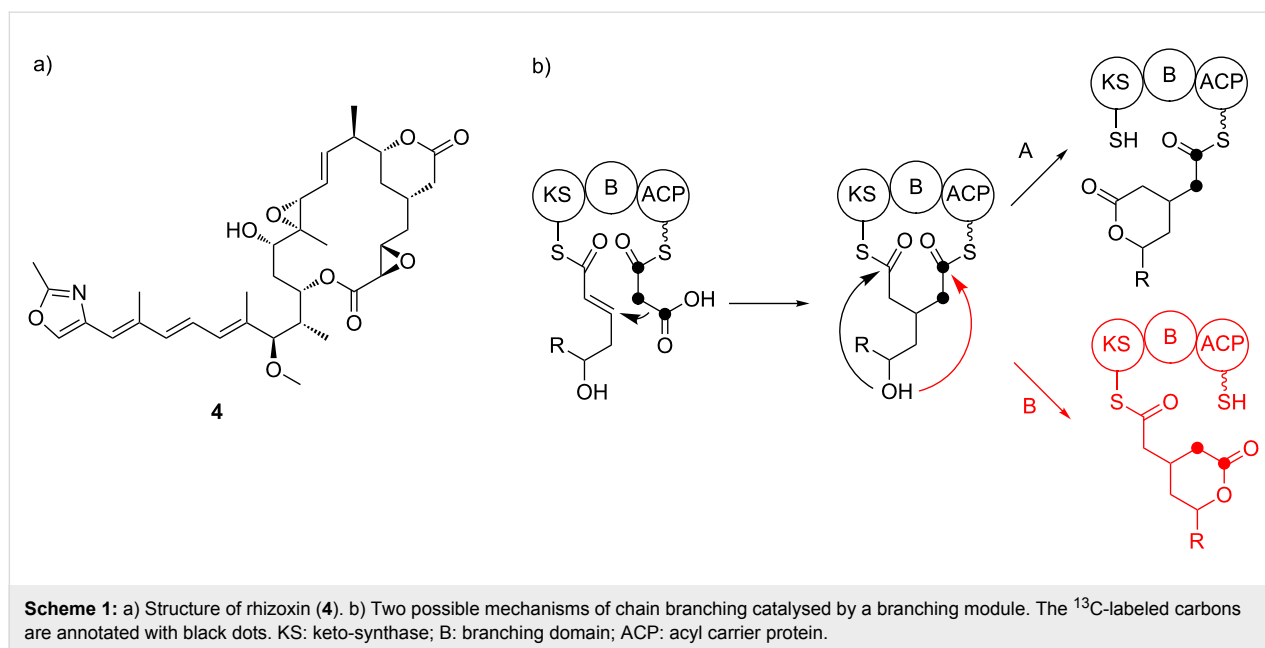
### Polyketides

Polyketide synthases (PKS) are multidomain enzymes that catalyze the formation of natural products via reaction steps similar to fatty acid biosynthesis, in which  $\text{C}_2$ -units are fused in Claisen condensations and modified in an iterative or modular fashion [15]. In contrast to fatty acid synthases (FAS), PKSs do not necessarily process the initially formed 3-keto functions through a complete reductive cycle, which leads to structurally diverse products as shown in Figure 1 for lovastatin (**1**), an

inhibitor of 3-hydroxy-3-methylglutaryl CoA reductase [16], aflatoxin B<sub>1</sub> (**2**) [17] and the potent antifungal agent amphoterin B (**3**) [18], which affects membrane integrity.



The products of polyketide synthases (PKS) belong to the first secondary metabolites that were investigated using isotopically labeled compounds [19]. Feeding experiments using (1,2- $^{13}\text{C}_2$ )acetate and (1- $^{13}\text{C}$ ) or (2- $^{13}\text{C}$ )acetate are a convenient and simple source of information on intact acetate units, chain direction and modifications of PKS derived natural products. *Sensu stricto*, polyketides (i.e., polymers of the “ketide” group  $-\text{CH}_2-\text{CO}-$ ) are structurally made of malonyl-CoA building blocks leading to a linear chain assembly. However, many examples deviate from this rule, and the biological activities shown by these polyketides may in many cases especially depend on their branched side chains silhouetting them against the bulk of other PKS products [20]. Known reasons for branched polyketides at the  $\alpha$ -position of the growing chain include the usage of different elongation units such as methylmalonyl-CoA, or methylation of the nucleophilic  $\alpha$ -position by *S*-adenosyl methionine (SAM) [21]. Branching in the  $\beta$ -position is less common and proceeds through a  $\beta$ -aldol attack of an acetyl nucleophile at the growing chain. This mechanism is similar to the formation of hydroxymethylglutaryl-CoA along the mevalonate pathway in isoprenoid biosynthesis [22]. Recently, a different additional mechanism of  $\beta$ -branching was reported, in which a special PKS module is catalyzing the reaction [20]. It was investigated in the biosynthesis of the phytoxin rhizoxin (**4**, Scheme 1), a potent antimetabolic agent binding

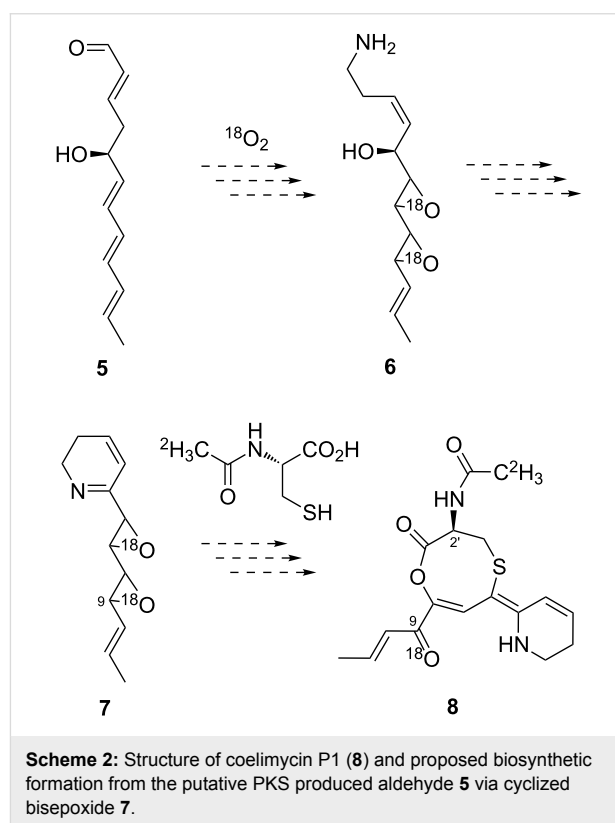


to  $\beta$ -tubulin from the bacterium *Burkholderia rhizoxinica*, which lives in symbiosis with the fungus *Rhizopus microsporus* [23]. The mechanism includes a Michael addition of a malonyl moiety to the  $\alpha,\beta$ -unsaturated thioester bound to the keto-synthase domain (KS).

After this reaction, the polyketide chain is bound to the KS and the acyl carrier protein (ACP). The following lactonization to generate the  $\delta$ -lactone structure in **4** can either proceed via nucleophilic attack of the  $\delta$ -hydroxy function at the KS-bound (A) or at the ACP-bound thioester (B) with subsequent loading of the polyketide onto the ACP. To distinguish both mechanisms,  $^{13}\text{C}$ -labeled malonyl-CoA and an *N*-acetylcysteamine (SNAC) thioester as synthetic analogon were used as substrates for an in vitro construct of the branching module. NMR experiments on the ACP-bound product unambiguously showed the labeled  $^{13}\text{C}$  signals in the linear polyketide chain and not in the lactone ring, thus supporting mechanism A. Therefore, this labeling experiment took an important role on the road to a better understanding of this unusual mechanism.

An interesting feeding experiment was performed for the elucidation of both absolute configuration and biosynthesis of the polyketid alkaloid coelimycin P1 (**8**, Scheme 2). The compound was isolated from *Streptomyces coelicolor* M145 after genetically engineered increase of the metabolic flux and is the product of a polyketide biosynthetic gene cluster [24].

To test whether *N*-acetylcysteine could be a biosynthetic precursor of the unusual 1,5-oxathioecane structure, feeding experiments using both (2*S*)- and (2*R*)-*N*-(( $^2\text{H}_3$ )acetyl)cysteine

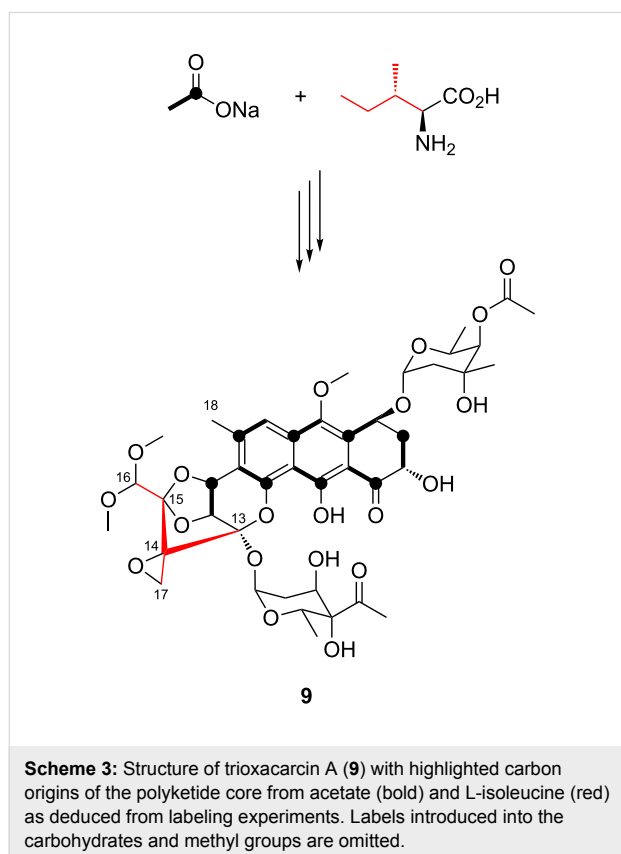


were performed. The deuterium atoms of both precursors were incorporated into **8**, showing the direct biosynthetic relationship of the amino acid derivative and indicating that the addition of *N*-acetylcysteine might not be catalyzed by an enzyme. Exploiting the only stereocenter of **8** being located in the incorporated residue, also the absolute configuration of **8** could be

deduced from these labeling experiments as (2'R) via comparison of the retention times of both compounds to naturally occurring **8** on a homochiral stationary LC phase.

To investigate the proposed structure of **7**, which likely exhibits the antibiotic properties connected to the bacterial strain as a highly reactive bisepoxide, *S. coelicolor* M1157 was grown in an  $^{18}\text{O}_2$  atmosphere. MS/MS measurements indicated a direct incorporation of  $^{18}\text{O}$  at the C-9 carbonyl group. This result supports the activity of putative epoxidases processing the linear unsaturated PKS precursor **5** to amine **6**. Oxidation of the hydroxy function and subsequent ring closure would then lead to the proposed antibiotic **7**. The other oxygen atom is lost during biosynthesis and is therefore undetectable. This example shows how well-designed labeling experiments can support biosynthetic investigations especially on highly derivatized and altered polyketide products.

Emphasizing the same principle, the biosynthesis of trioxacarcin A (**9**, Scheme 3), a complex aromatic natural product originally isolated from *Streptomyces bottropensis* DO-45 and showing remarkable antibacterial and antitumor properties [25], was investigated using isotopically labeled precursors to gain insight into the used building blocks for the unusual polyketide core [26]. Compound **9** features a trisketal structure in addition

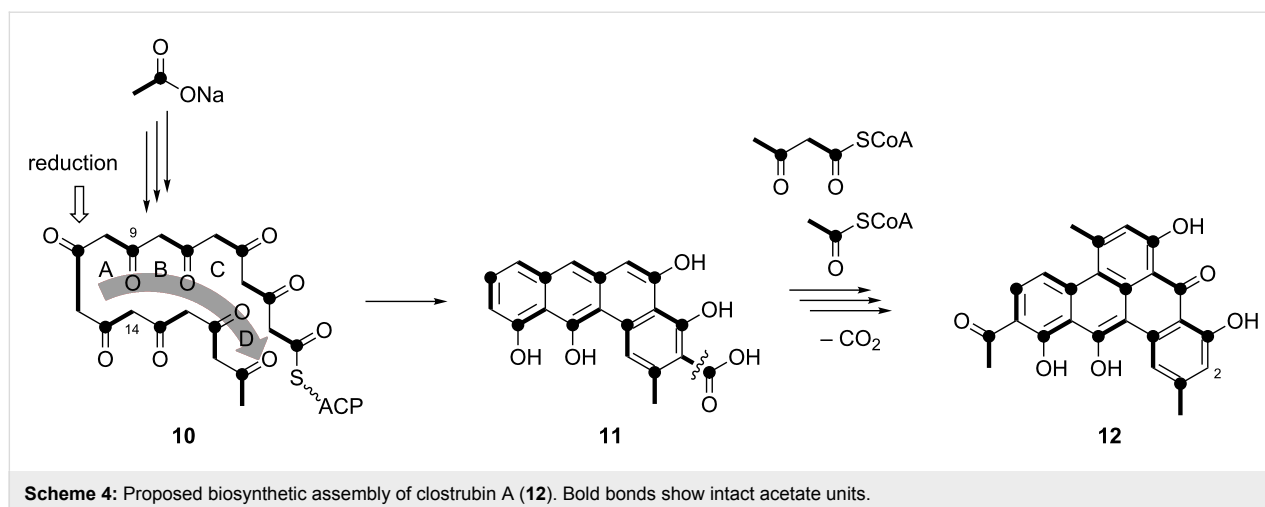


to the spiro-epoxide at C-14, which is believed to be the active part of the molecule for interaction with DNA. This was supported by the isolation of gutingimycin, a guanine-adduct of **9** [27]. However, very little was known about the biosynthetic assembly of the complex antibiotic. Feeding of  $[1-^{13}\text{C}]$ -,  $[2-^{13}\text{C}]$ - and  $[1,2-^{13}\text{C}_2]$ acetate to *S. bottropensis* and analysis of the produced **9** via  $^{13}\text{C}$  NMR yielded the carbon origins of the polyketide core. The regular incorporation pattern in the tricyclic aromatic moiety suggests a normal PKS assembly line. Moreover, a decarboxylation step is indicated by incorporation of the acetate methyl carbon atom into C-18. In contrast, the origins of C-13 to C-17 remained unclear because of low incorporation of acetate into this part of the molecule.

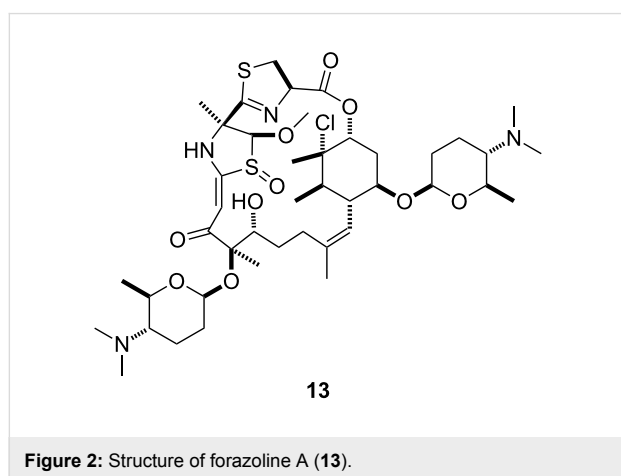
The location of these five carbons at the end of the proposed linear PKS chain indicated the use of an unusual starter unit, most likely isoleucine-derived 2-methylbutyryl-CoA. Indeed, feeding of  $[\text{U}-^{13}\text{C}_6]$ -L-isoleucine resulted in a mass shift of +5  $m/z$  compared to the unlabeled compound. In conclusion, these feeding experiments using isotopically labeled precursors supported the biosynthetic assembly from an unusual PKS starter unit which results in the remarkable scaffold for the bioactivity-generating functionalities.

A similar study showing the enduring significance of labeled acetate in PKS research deals with the fusion of the polycyclic aromatic pigment clostrubin A (**12**) from *Clostridium beijerinckii*, a strictly anaerobic bacterium [28]. The purple colored compound features a benzo[*a*]tetraphene skeleton, which is unique in known polyphenolic natural products. Moreover, feeding experiments using  $[1-^{13}\text{C}]$ - or  $[1,2-^{13}\text{C}_2]$ acetate revealed the PKS chain to build up an angucyclic scaffold (in **11**) first, which then probably fuses the fifth ring via reaction with acetoacetyl-CoA (Scheme 4), with folding of the linear PKS chain **10** downwards with respect to the D ring. For the A ring, C-9 and C-14 are connected. This folding differs from the biosynthesis of all known angucyclic cores, which are fused in an upwards folding connecting C-7 and C-12 for the formation of the A ring [29].

Despite the fact that the biosynthesis of this polyphenol cannot be deduced completely from labeled acetate feeding experiments, the results laid the ground for the discovery of the unusual chain folding and the loss of one carbon atom through the singly labeled C-2 position. These recent findings of Hertweck and co-workers are an interesting extension of the pioneering work by Bringmann et al. on the anthraquinone crysophanol, for which different folding modes in fungi (F type folding) and in bacteria (S type, “*Streptomyces*” type) were found by isotopic labeling experiments for one and the same compound [30].



As an additional concluding remark of this chapter, the role of isotopic labeling in the structure elucidation of complex polyketide natural products will be discussed. Especially in combination with two-dimensional NMR spectroscopic techniques, several powerful tools are becoming more interesting to natural products research. Production of new compounds in a labeled medium and analyzing the  $^{13}\text{C}$ ,  $^{13}\text{C}$ -COSY spectrum of the resulting fully  $^{13}\text{C}$ -labeled natural product as in case of forazoline A (**13**) can easily determine the carbon skeleton (Figure 2). This technique was also used for the elucidation of marine aromatic acids [31]. Even the nitrogen–carbon connectivities can be investigated by fermentation in a  $^{15}\text{N}$ -labeled medium and analysis of the resulting product with  $^{13}\text{C}$ ,  $^{15}\text{N}$ -HMQC [32]. These applications represent helpful additions to the repertoire for structure elucidation of complex natural products, which can be produced under laboratory conditions in sufficient amounts.



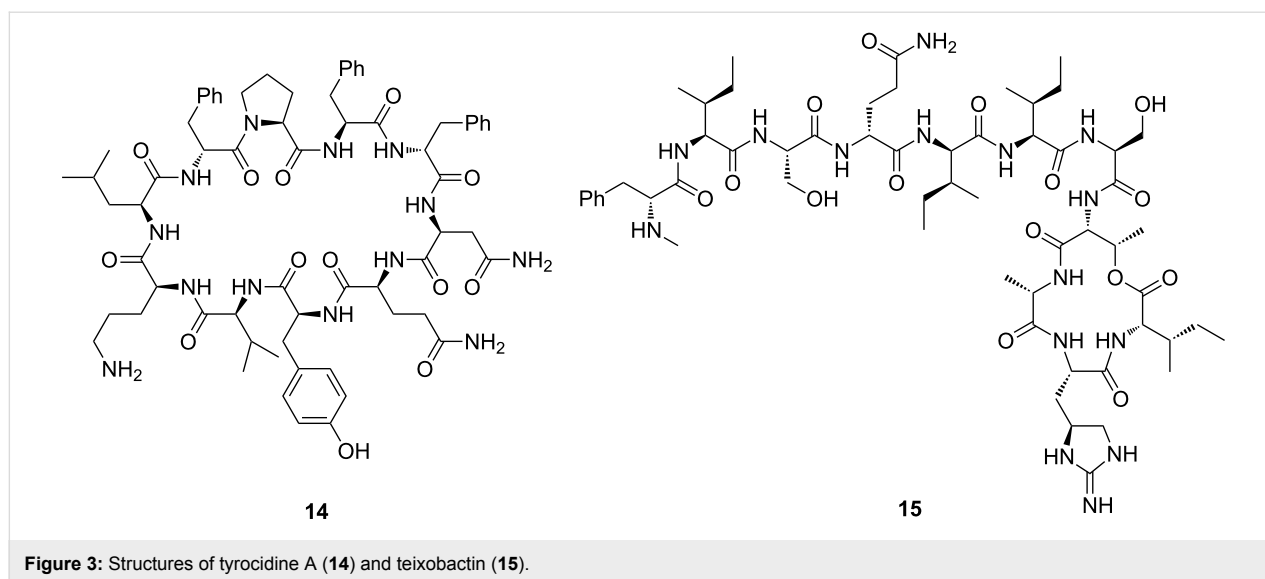
## Non-ribosomal peptides

Non-ribosomal peptides often exhibit a high bioactivity and are biosynthesized by non-ribosomal peptide synthetases (NRPS)

[33], which work RNA-independent and catalyze the assembly of both proteinogenic and non-proteinogenic amino acids in a modular fashion. Moreover, NRPSs can contain additional modifying modules, e.g., epimerization domains, resulting in a greater structural variety than ribosomal peptides usually have. Two examples are the membrane disrupting decapeptide antibiotic tyrocidine A (**14**) [34] and teixobactin (**15**) [35], a recently discovered multi-target antibiotic rising high hopes in the treatment of resistant pathogens (Figure 3).

Producing an isotopologue of the desired compound by feeding of labeled precursors or growing the producing organism in labeled medium can simplify structure elucidation by giving access to the sum formula by mass spectrometry, which is not in all cases easily accessible for the unlabeled compound. In particular, advanced mass spectrometry techniques in combination with labeled amino acids catch a growing attention for the often challenging structure elucidation of NRPS products. To give insights into the assembled building blocks and the sum formula of the desired compound, either the traditional way of providing isotopically labeled amino acids to the NRPS can be used, or completely labeled media can be supplemented with non-labeled building blocks in an inverse feeding experiment [36]. The latter method is particularly advantageous, if the compound contains precursors that are not commercially available in a labeled way. Incorporation into the NRPS product [37–41] can be followed by  $\text{MS}^n$  that may even give information about the position of incorporation.

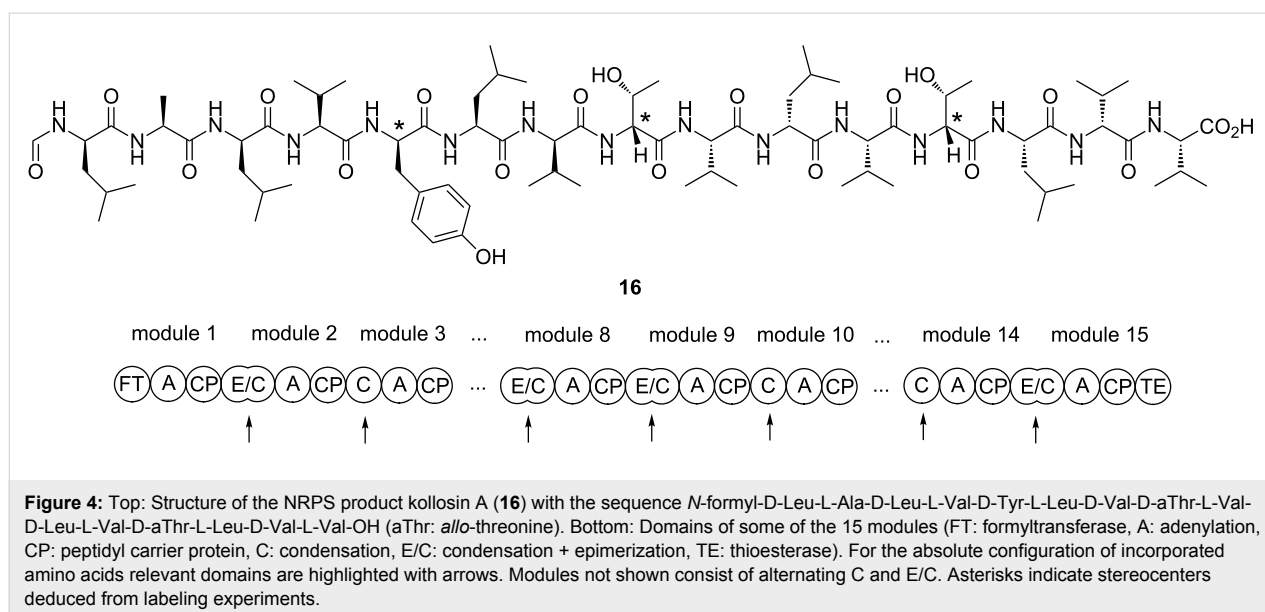
Another very interesting method for structure elucidation of NRPS products using isotopic labelings was recently developed by Bode and co-workers [36]. The method is designed to investigate the absolute configuration of the amino acid building blocks without hydrolysing the NRPS product, can be performed on minute amounts of material, and was first



applied to different cyclic peptides from *Photorhabdus* and *Xenorhabdus* species [42] and for activity testing of heterologously expressed SAM-epimerases from various bacteria [43]. In a follow-up study the recently discovered NRPS product kollosin A (**16**, Figure 4) was investigated. This pentadecapeptide is made by the largest known NRPS that consists of 15 modules and is encoded by a single 49.1 kbp gene found in the entomopathogenic bacterium *Photorhabdus luminescens* [44]. Despite the non-detectable expression under various fermentation conditions, it was possible to express the machinery using a promoter exchange [45] in the native host.

Bioinformatics allowed for the annotation of several epimerization domains in the kollosin A NRPS, but it is hard to

determine the actual activity of each of these functions. To overcome this problem, L-[<sup>2</sup>H<sub>8</sub>]valine, L-[<sup>2</sup>H<sub>10</sub>]leucine, L-[<sup>2</sup>H<sub>7</sub>,<sup>15</sup>N]tyrosine and L-[<sup>2</sup>H<sub>5</sub>,<sup>15</sup>N]threonine were fed to *P. luminescens*. The loss of one deuterium atom for an incorporated labeled amino acid (from C<sub>α</sub>) directly supports an epimerase function within the corresponding NRPS module, and the incorporated building block can be assigned as D-configured. In this example, epimerization activity was shown for tyrosine and both threonine building blocks, marked by asterisks in Figure 4. Moreover, one leucine could be determined as D-configured according to incorporation in truncated fragments of **16**. For the elucidation of the second stereocenter in both threonines, solid phase synthesis of the peptide was performed, which confirmed the structure of **16** with two



*allo*-threonines. In conclusion, all bioinformatically assigned epimerization functions of the kollosin A NRPS were shown to be active, resulting in an alternating incorporation of L- and D-configured amino acids into kollosin A except for modules 8 and 9.

This example proves that the use of isotopically labeled compounds can be a valuable addition to the common repertoire of structure elucidation for minimal amounts of material and provides an interesting combination of bioinformatic, synthetic and labeling techniques.

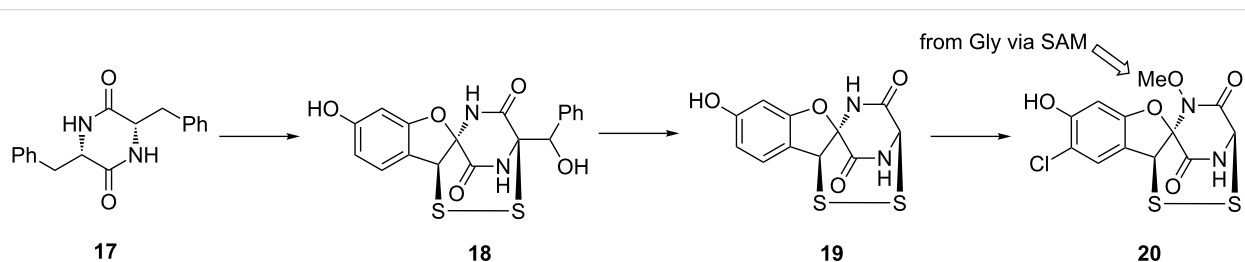
NRPS products are frequently modified by tailoring enzymes. This can extend to a complexity, which obscures the initial building blocks to the eye of the observer. Labeling experiments can in these cases clarify the origins even if they seem to be obvious in the beginning. The structure of aspirochlorine (**20**, Scheme 5), a toxin from *Aspergillus oryzae*, provides an interesting example. Its importance arises from the use of the producing organism in Asian food industry [46]. The biosynthesis of **20** can be hypothesized from phenylalanine and glycine. To investigate this, (*ring*-<sup>2</sup>H<sub>5</sub>)Phe and (2-<sup>13</sup>C)Gly were fed and incorporation of two <sup>2</sup>H and one <sup>13</sup>C atom was confirmed by MS analysis [47]. However, structure elucidation of the biosynthetic intermediates **18** and **19** that were isolated from deletion mutants suggested a different assembly from two Phe via the dimeric structure **17**, which was further supported by the incorporation of two <sup>13</sup>C atoms after feeding of (1-<sup>13</sup>C)Phe. Therefore, (<sup>13</sup>C<sub>2</sub>, <sup>15</sup>N)Gly was fed to *A. oryzae*, pointing to incorporation of one <sup>13</sup>C by MS analysis. To finally solve this riddle, feeding experiments with (<sup>13</sup>C<sub>2</sub>)Gly were performed on a preparative scale to unambiguously assign the <sup>13</sup>C-labeled positions via NMR. It turned out that the label was incorporated into the *N*-methoxy group, and not into the presumptive glycine unit of the diketopiperazine structure. In summary, these results support an unusual conversion of one phenylalanine-derived side chain to a glycin-like moiety.

The observed incorporation of labeled Gly into the methyl group was rationalized by glycine degradation, directing the

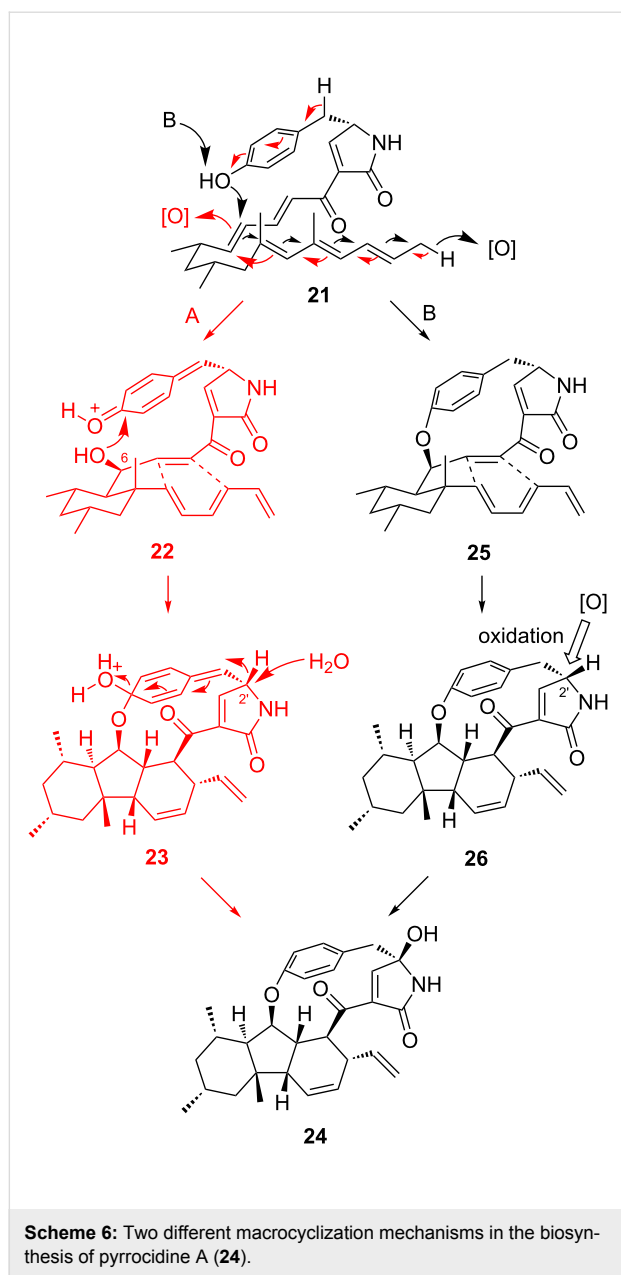
labeling via tetrahydrofolate and SAM into aspirochlorine biosynthesis. The conversion of the Phe residue to Gly may proceed through either oxidative C–C bond cleavage or a retro-aldol reaction in **18**, in agreement with the detection of (*ring*-<sup>2</sup>H<sub>5</sub>)benzoic acid in culture extracts from labeling experiments with (*ring*-<sup>2</sup>H<sub>5</sub>)Phe. This interconversion of two proteinogenic amino acids in the biosynthesis of an NRPS compound from secondary metabolism is unprecedented and its discovery was strongly supported by the careful evaluation of feeding experiments with labeled precursors.

### PKS/NRPS-Hybrids

The formation of interesting structural motifs in natural products is an exciting aspect in the field of biosynthetic research and gives insights to the synthetic abilities of nature fusing structures, whose formation usually requires sophisticated chemistry in organic laboratories. Prominent examples are [*n*]paracyclophane moieties in natural products such as haouamines [48] or fijiolides [49,50]. As for the [7]paracyclophane in haouamine A and B, a reasonable suggestion for compensating the high barrier of a bended benzene ring includes intermediate loss of aromaticity followed by rearomatization during the formation of the cyclophane ring [51]. However, a recently investigated example shows, that breaking the aromatic character of a phenyl ring is not necessary for building up a bended aryl ether in a biological scaffold. In this study, <sup>13</sup>C- and <sup>18</sup>O-labeled L-tyrosine was used to elucidate the biosynthesis of pyrrocidines such as pyrrocidine A (**24**, Scheme 6) bearing a [9]paracyclophane moiety in the fungus *Acremonium zeae* [52]. Compound **24** is the product of a mixed PKS and NRPS machinery containing nine acetate units, five methyl groups from SAM and one L-tyrosine [53]. Two possible mechanisms for the cyclization of the linear precursor **21** were hypothesized. In route A, an oxidation of the aromatic ring would lead to an electrophilic center at the quinone moiety in **22**, which can be attacked by the C-6 hydroxy group. The energy barrier of a distorted benzene ring would then be compensated by rearomatization in **23** after intramolecular Diels–Alder reaction. This mechanism would involve a 1,2-hydride shift and a nucleophilic attack of water at C-2'.

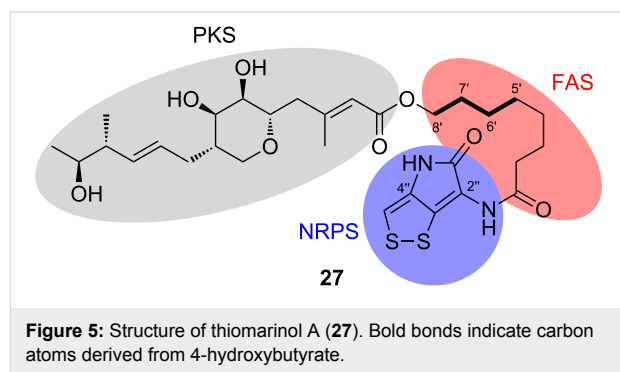


**Scheme 5:** Proposed biosynthesis of aspirochlorine (**20**) via **18** and **19**.



The second discussed route starts with a nucleophilic attack of the phenolic oxygen at C-6 to close the macrocycle in **25**. In this mechanism, the aromaticity of the phenol ring remains untouched. Intramolecular Diels–Alder reaction gives rise to the hexacyclic system **26**, which would then be oxidized to pyrrocidine A (**24**) at C-2'. In contrast to route A, the phenolic oxygen is conserved here. To distinguish between these mechanisms, (4'-hydroxy- $^{18}\text{O}$ ,1- $^{13}\text{C}$ )-L-tyrosine was enantioselectively synthesized and fed to *A. zea*. Both labels were incorporated into **24**, thus providing evidence for mechanism B and a paracyclophane formation without intermediate loss of aromaticity. This kind of tyrosine reporter might also prove useful in other biosynthetic studies.

Sometimes the biosynthesis of mixed PKS/NRPS/FAS natural products involves the discovery of surprising building blocks as recently shown for thiomarinol A (**27**, Figure 5) from the marine bacterium *Pseudoalteromonas* sp. SANK 73390 [54], which exhibits antibiotic activity against methicillin-resistant *Staphylococcus aureus* (MRSA) [55].



Particularly interesting results of feeding experiments with [1,2- $^{13}\text{C}_2$ ]-, [2- $^{13}\text{C}$ ]- and [1- $^{13}\text{C}$ , $^{18}\text{O}_2$ ]acetate were the unexpectedly low incorporation into C-5' to C-8' of the octanoate side chain, whereas approximately the double incorporation rates were observed in the PKS part of the molecule. To test a hypothetical  $\text{C}_4$ -starter unit for the fatty acid synthase, [2,3- $^{13}\text{C}_2$ ]succinate was fed to *Pseudoalteromonas* SANK 73390, which showed an intact incorporation of labeling into C-6' and C-7' of **27**. Moreover, also [2,3- $^{13}\text{C}_2$ ]-4-hydroxybutyrate was incorporated with appearance of labeling in the same positions. The proposed origin of the pyrrothine unit from two cysteines was confirmed by feeding of [2,2'- $^{13}\text{C}_2$ ]cystine and detection of the label at C-2'' and C-4''. As deduced from these experiments in combination with genetic studies, the biosynthesis of thiomarinol A (**27**) proceeds via coupling of 4-hydroxybutyrate to the PKS product, two cycles of chain elongation and finally coupling with the NRPS product pyrrothine.

## Terpenes

Terpenoids constitute the largest group of natural products and are remarkably diverse in structure, bioactivity, and use. Prominent examples such as the antimalaria drug artemisinin (**28**) from *Artemisia annua*, ingenol (**29**) and its derivatives from *Euphorbia ingens* [56], or the anticancer drug paclitaxel (**30**) feature highly functionalized polycyclic carbon skeletons (Figure 6).

The fascination of terpene biosynthesis arises from the complexity and variety of carbon scaffolds, terpene cyclases are able to build up using few linear oligoprenyl diphosphate precursors. This promotes investigations using isotopically



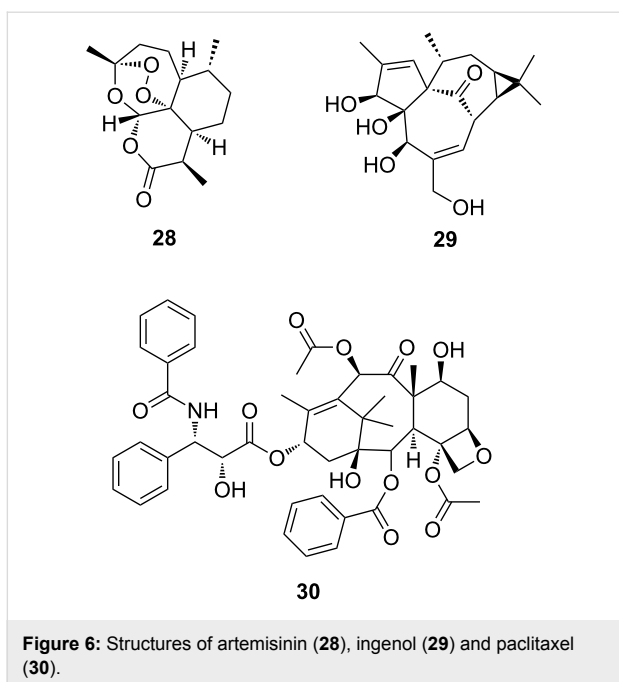


**Figure 6:** Structures of artemisinin (28), ingenol (29) and paclitaxel (30).

labeled compounds both on acetate- and mevalonate/deoxyxylulose-level for in vivo feeding experiments or oligoprenyl diphosphates for in vitro studies to understand the often complex cyclization cascades catalyzed by a single enzyme. In many cases, isotopes represent the only way of elucidating proposed hydride shifts, carbon–carbon rearrangements and cyclizations experimentally.

The structure elucidation of terpenoids can be challenging because of the multicyclic carbon skeletons with several contiguous stereocenters. The assistance of  $^{13}\text{C}$  labels can in such cases be especially helpful, and if completely  $^{13}\text{C}$ -labeled carbon backbones can be made accessible,  $^{13}\text{C}$ ,  $^{13}\text{C}$ -COSY experiments are possible that allow for a comparably easy structure elucidation even for minimal amounts of material. As recently demonstrated for hypodoratoxide (31) from *Hypomyces odoratus* DSM 11934, such labeled products can be obtained by feeding of terpene precursors to an actively growing culture [57]. The application of  $^{13}\text{C}$ ,  $^{13}\text{C}$ -COSY for hypodoratoxide led to a revision of the previously proposed structure 32 [58], showing the significance of this technique in comparison to unlabeled standard 2D NMR methods. Alternatively, a completely  $^{13}\text{C}$ -labeled terpene can be made in vitro by usage of enzymes. This approach was used for investigating the structure of miltiradiene (33, Figure 7), a diterpene from *Selaginella moellendorffii*, starting from uniformly labeled mevalonate [59].

Despite the tools for structure elucidation, labeled compounds continue to offer interesting insights into terpene synthase catalyzed cyclizations. Labeled oligoprenyl diphosphates, the

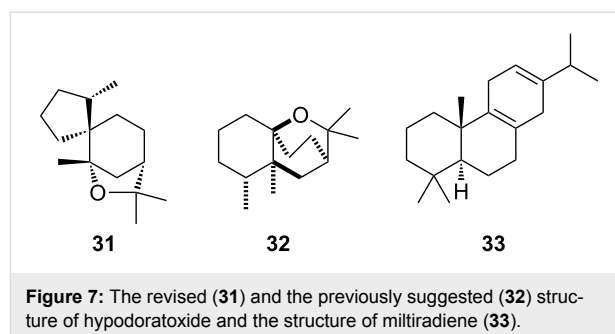


**Figure 7:** The revised (31) and the previously suggested (32) structure of hypodoratoxide and the structure of miltiradiene (33).

substrates for these enzymes, can be made available by synthesis and provide an excellent tool for such investigations, as recently demonstrated for sesquiterpenes by the synthesis of all 15 singly  $^{13}\text{C}$ -labeled isotopomers of farnesyl diphosphate (FPP) [60]. These precursors were used to unambiguously assign both  $^{13}\text{C}$  NMR and (via HSQC)  $^1\text{H}$  NMR data of (1(10)*E*,4*E*)-germacradien-6-ol (34) from *Streptomyces pratensis*. The NMR spectra of this compound are complicated because of a mixture of conformers (Figure 8) that prevented a full assignment of NMR data by conventional methods.

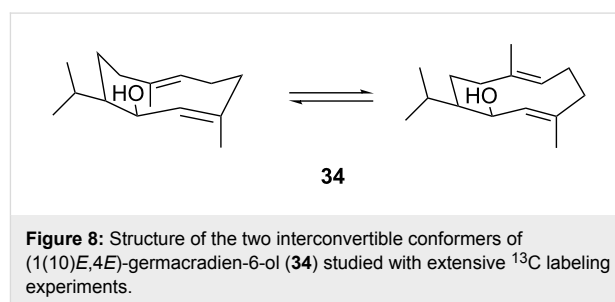
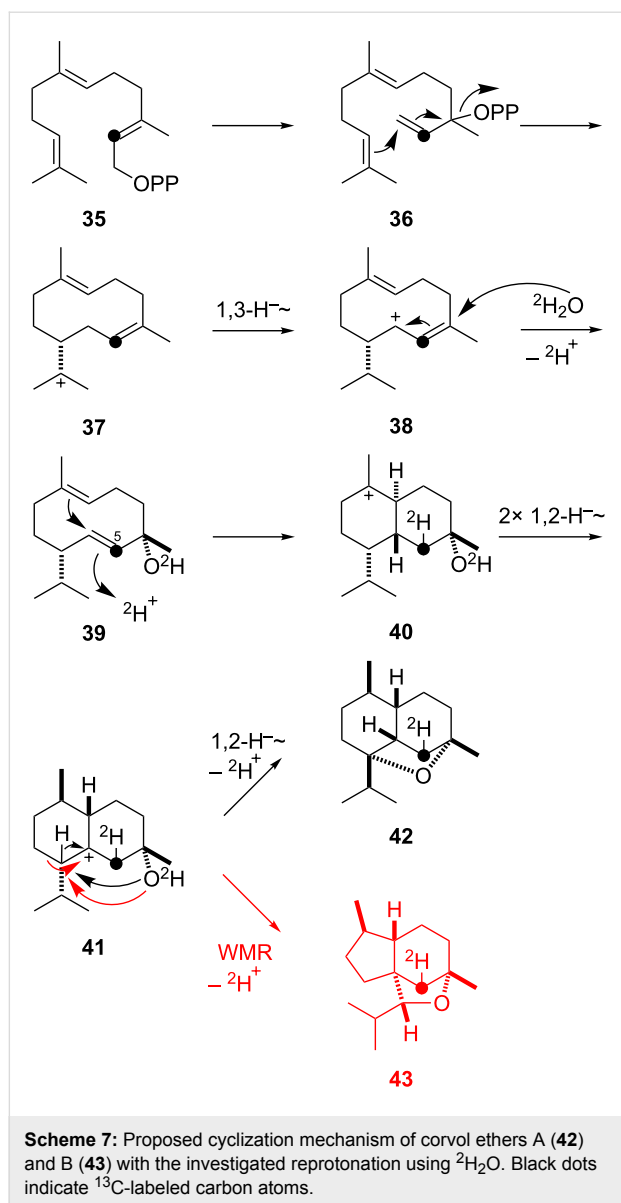


**Figure 8:** Structure of the two interconvertible conformers of (1(10)*E*,4*E*)-germacradien-6-ol (34) studied with extensive  $^{13}\text{C}$  labeling experiments.

To correlate a conformational signal set, ( $\text{U-}^{13}\text{C}_{15}$ )FPP was synthesized and  $^{13}\text{C}$ ,  $^{13}\text{C}$ -COSY showed the connected carbon skeleton for each conformer. The 15 obtained labeled natural products also allowed a detailed analysis of the EIMS-fragmentation reactions of 34 by comparison of the  $^{13}\text{C}$ -including fragments.

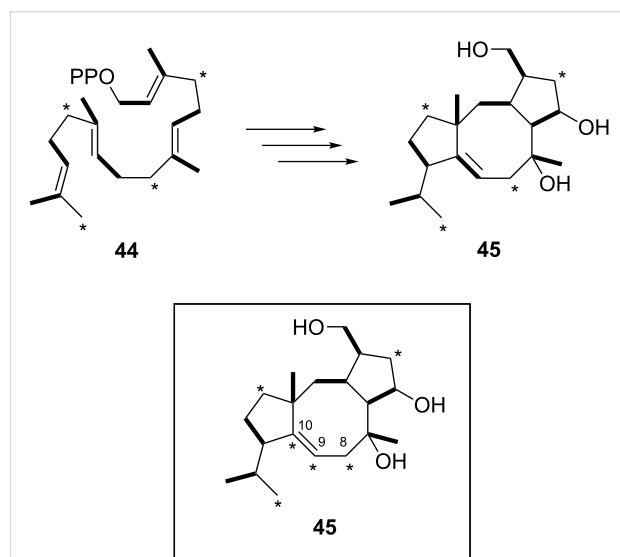
Singly labeled FPP isotopomers also proved valuable to investigate reprotonation steps in sesquiterpene cyclization mechanisms by incubation in deuterium oxide. The biosynthesis of the recently discovered corvol ethers A (42) and B (43) provides an interesting example (Scheme 7) [61].

The proposed mechanism starts with isomerization of farnesyl diphosphate (FPP, 35) to nerolidyl diphosphate (36) followed by 1,10-ring closure to the helminthogermacradienyl cation (37). A 1,3-hydride shift to the allylic cation 38 and attack of water gives the neutral intermediate germacrene D-4-ol (39). Reprotonation induces the formation of the bicyclic system 40, which



can rearrange via two sequential 1,2-hydride shifts to the cation **41**. The attack of the hydroxy function and either a 1,2-hydride shift or a Wagner–Meerwein rearrangement in a concerted process leads to **42** and **43**. The protonation of C-5 was shown by using ( $2\text{-}^{13}\text{C}$ )FPP as a substrate for an in vitro incubation of the terpene synthase in  $\text{D}_2\text{O}$  leading to characteristic strongly enhanced triplets for the labeled carbons of **42** and **43** in the  $^{13}\text{C}$  NMR spectrum. As an extension to these experiments, the stereochemical course of reprotonation of a neutral intermediate can be followed by comparing the HSQC spectra of the labeled and the unlabeled compounds, if combined with a NOESY based assignment of the signals for the relevant diastereotopic protons, as recently performed to investigate the mechanisms for intermedeol and neomeranol B biosynthesis [62].

Cyclooctat-9-en-7-ol (**52**), a member of the fusicoccane family of diterpenoids, is the biosynthetic precursor of cyclooctatin (**45**) [63], a potent inhibitor of lysophospholipase, which was isolated from *Streptomyces melanosporofaciens* [64]. The cyclization of geranylgeranyl diphosphate (GGPP, **44**) to **52** features an unexpected carbon backbone rearrangement, which was shown recently by Kuzuyama and co-workers using isotopically labeled glucose in vivo and labeled GGPP in vitro [65]. The reaction is catalysed by the enzyme CotB2, the first structurally characterized bacterial diterpene cyclase [66]. After identification of the biosynthetic gene cluster, a mechanism involving a deprotonation–reprotonation sequence and two 1,2-hydride shifts was proposed [67]. However, a simple feeding experiment performed with a *S. albus* transformant and [ $\text{U-}^{13}\text{C}_6$ ]glucose revealed an unexpected labeling pattern in **45**, which could not be explained by the anticipated GGPP labeling following the deoxyxylulosephosphate pathway [68] and the initially suggested mechanism for GGPP cyclization (Scheme 8).



The missing  $^{13}\text{C}$ ,  $^{13}\text{C}$ -coupling between C-9 and C-10 excluded a simple mechanistic assembly of the tricyclic system. Instead, advanced NMR experiments focusing on  $^2J_{\text{C,C}}$ -couplings revealed that C-8 and C-10 originate from the same glucose molecule. To account for this surprising observation, a new mechanistic proposal was suggested involving a carbon–carbon-bond rearrangement and several hydride shifts, which were confirmed with elegant labeling experiments using

(9,9- $^2\text{H}_2$ )GGPP (a), (10- $^2\text{H}$ )GGPP (b), and (8,8- $^2\text{H}_2$ )GGPP (c) in incubation experiments with recombinant CotB2 (Scheme 9).

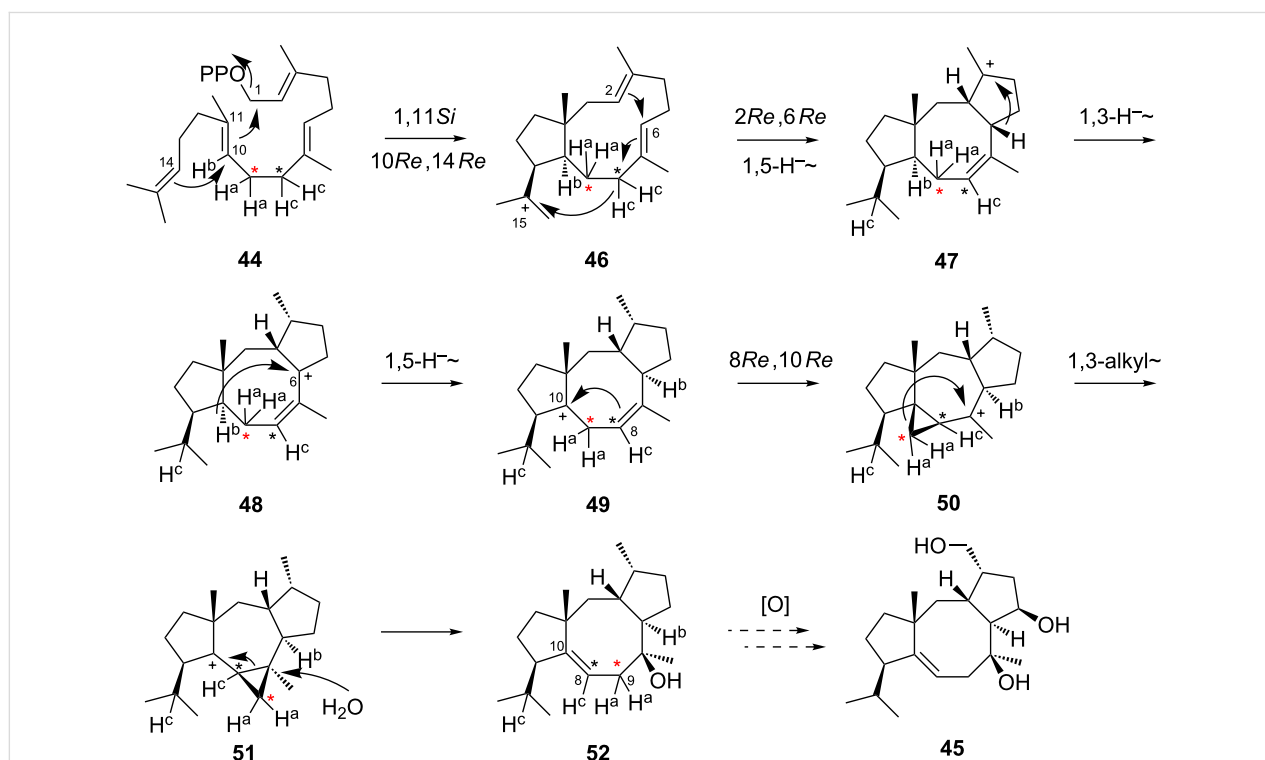
A mechanism that is in line with all labeling experiments proceeds via GGPP cyclization to form the bicyclic cation **46**, followed by a second cyclization and a 1,5-hydride shift to yield **47**. This unusual hydride migration was experimentally supported by location of  $\text{H}^c$  at C-15 of **52**. A 1,3-hydride shift generates the allylic cation **48**, which can undergo another 1,5-hydride shift to the tertiary cation **49**. This step was elucidated using (10- $^2\text{H}$ )GGPP to follow the transannular movement of  $\text{H}^b$ . Ring contraction leads to the tetracyclic cation **50**, which rearranges to **51** explaining the observed lost linkage between C-9 and C-10. Quenching of this cation with water leads to the diterpenoid product cyclooctat-9-en-7-ol (**52**). Further oxidation by the cytochrome P450-hydroxylases CotB3 and CotB4 yields the biologically active compound cyclooctatin (**45**) [67].

This outstanding study exemplifies the scope of isotopic labeling experiments in the elucidation of terpene biosynthesis by combined in vivo and in vitro labeling techniques to achieve a better understanding of nature's astonishing mechanistic toolbox utilized by terpene synthases. Additionally, the unexpected outcome of the initial feeding experiment gives an ideal example as to why isotopic labeling experiments are not at all

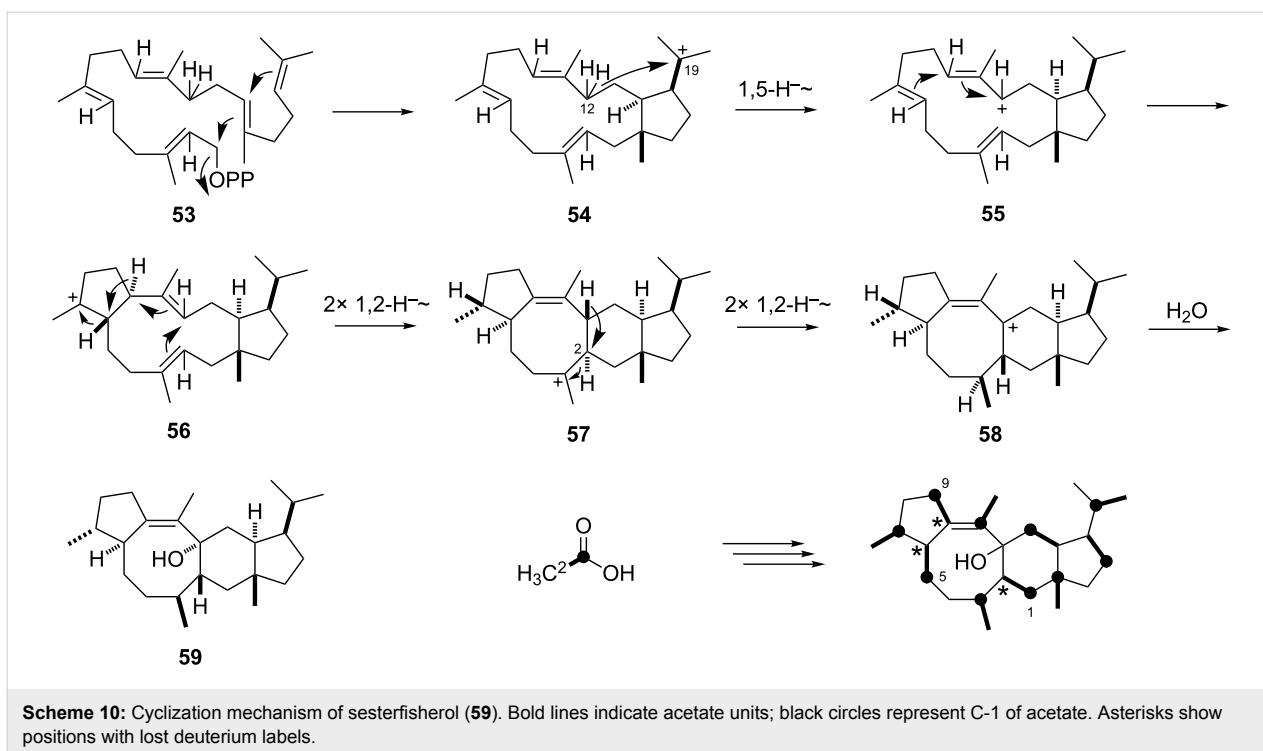
old-fashioned, but rather still yield important mechanistic insights in biosynthetic pathways that would otherwise never be obtained.

Emphasizing the same principle, feeding of even simpler precursors such as labeled acetate can give useful hints to carbon and hydrogen rearrangement, as shown for sesterfisherol (**59**, Scheme 10), the product of a bifunctional sesterterpene cyclase ( $C_{25}$ ) from *Neosartorya fischeri* [69]. In this case, [ $1\text{-}^{13}\text{C}, 2\text{-}^3\text{H}$ ]acetate was fed and the resulting labeling pattern of an epoxidation product was analyzed by  $^{13}\text{C}$  NMR, revealing a loss of deuterium from carbons C-2, C-6 and C-10 by hydride shifts during terpene cyclization that was concluded from missing upfield-shifted  $^{13}\text{C}$  NMR signals of the neighboring  $^{13}\text{C}$ -labeled carbons C-1, C-5 and C-9, while corresponding upfield-shifted signals were observed for all other expected cases (C-3, C-7, C-11, C-13, C-15, C-17, C-19).

These results are in line with the proposed cyclization mechanism starting from geranylarnesyl diphosphate (GFPP, **53**), which undergoes two cyclizations yielding cation **54**. A 1,5-hydride shift at C-12 to C-19 leads to the allylic cation **55**. Additional ring closure fuses the tricyclic system **56**, which rearranges to the tertiary cation **57** by two sequential 1,2-hydride shifts and another cyclization. Two 1,2-hydride



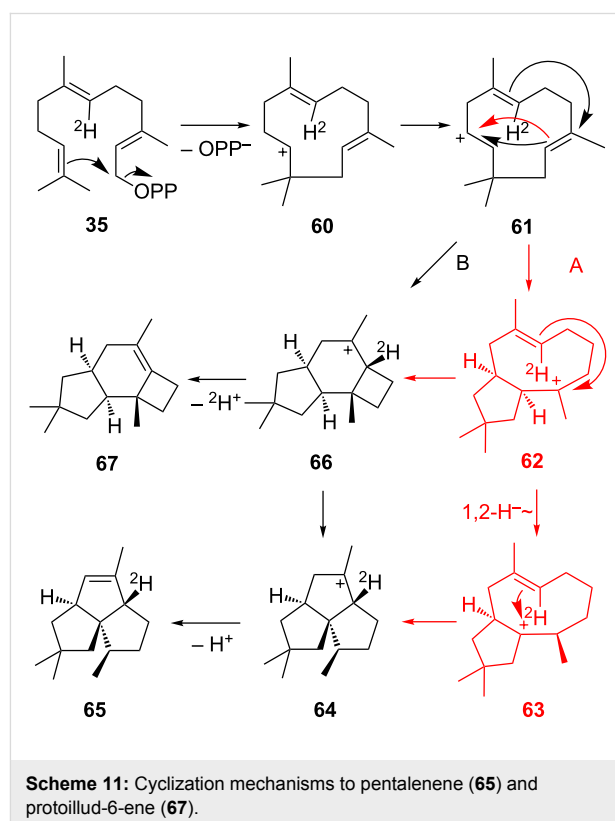
**Scheme 9:** Proposed mechanism of the cyclooctat-9-en-7-ol (**52**) biosynthesis catalysed by CotB2. Annotated hydrogen atoms (a–c) were investigated by deuterium labeling. Asterisks are used to follow the rearrangement of C-8 and C-9 (carbon numbers as for GGPP).



shifts yield the allylic cation **58**, which is finally quenched by water to the sesterterpene product **59**. The involved 1,2-hydride shifts along this pathway explain the missing upfield-shifted  $^{13}\text{C}$  signals mentioned above. To investigate the 1,5-hydride shift,  $(8,8\text{-}^2\text{H}_2)\text{GGPP}$  and IPP were used for an *in vitro* reaction with the recombinant terpene synthase, utilizing the bifunctional character of the enzyme to form  $(12,12\text{-}^2\text{H}_2)\text{GFPP}$  and its subsequent cyclization to  $(^2\text{H}_2)\text{-59}$ . NMR data of the obtained labeled product indicated a migration of the C-12 deuterium atoms to C-19 and to C-2, thus proving evidence for the proposed hydride migrations from **54** to **55** and from **57** to **58**.

The application of isotopes in mechanistic investigations is by far not limited to following atoms through the biosynthetic assembly of natural product. Also the kinetic isotope effect can be used to probe mechanistic proposals, as elegantly shown for the pentalenene (**65**) cyclization mechanism. Pentalenene synthase is one of the first and best investigated bacterial terpene cyclases both structurally [70] and functionally [71]. The initially suggested mechanism of building up its tricyclic structure is shown in Scheme 11 as pathway A and involves a 1,11-cyclization of FPP to the humulyl cation **60**. A deprotonation–reprotonation sequence leads to cation **61**, which is converted to a bicyclic secoillud-6-en-3-yl cation (**62**). A subsequent 1,2-hydride migration to **63** followed by ring closure gives **64**, which is deprotonated to give pentalenene (**65**). Quantum chemical calculations led to the suggestion of the protoilludyl cation **66** as central intermediate between **61** and **64**

(pathway B), which is directly formed from **61** [72]. Interestingly, this proposal is also in line with all previously conducted labeling experiments.

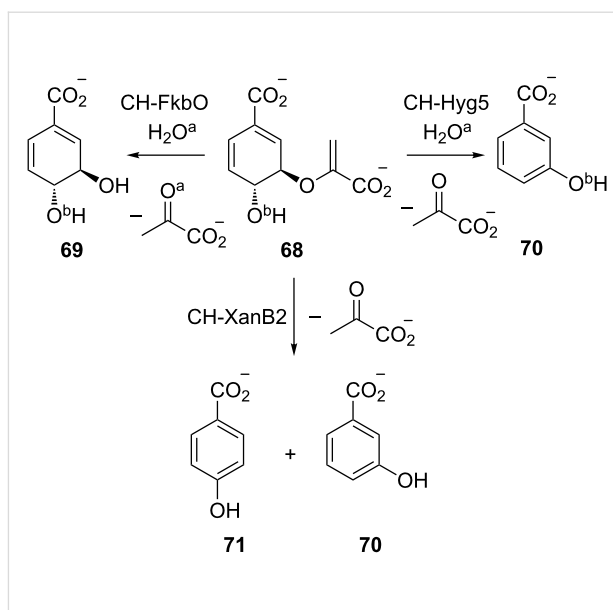


To address this mechanistic question experimentally, an elegant approach was recently presented in a collaborative work by the groups of Tantillo, Peters and Cane [73]. A H309A mutant of pentalenene synthase produces both **65** and the side product protoillud-6-ene (**67**). Using this mutant, experiments with (6-<sup>2</sup>H)FPP were performed to exploit the different branching points of both mechanisms towards **65** and **67**. Assuming there is no fast equilibrium between cations **62** and **66**, cyclization via pathway B should influence the product ratio of **65** and **67** due to the easier loss of protium in comparison to deuterium in the deprotonation to **67**, whereas for pathway A no such influence would be expected. Indeed, the observed product ratio shifted towards pentalenene in the experiment with the labeled precursor, supporting the mechanism via cation **66**. This isotopically sensitive branching experiment shows the usefulness of labeling studies even in cases where two possible mechanisms lead to the same atom arrangement in the natural product.

### Aromatic compounds via the shikimate pathway

Recently, a series of H<sub>2</sub><sup>18</sup>O-based labeling experiments were used by Andexer et al. to elucidate the mechanism of chorismatases [74]. Biochemically, chorismate (**68**) plays an important role at the border of primary and secondary metabolism for many natural products made from aromatic building blocks [75]. Chorismatases were, e.g., found to be involved in the formation of the starter unit 3,4-*trans*-dihydroxycyclohexa-1,5-dienecarboxylate (**69**) for biosynthesis of the important immunosuppressants FK506, FK520 and rapamycin [76]. This family of enzymes catalyzes the conversion of chorismate (**68**) to different hydroxybenzoates and dihydroxybenzoates (Scheme 12).

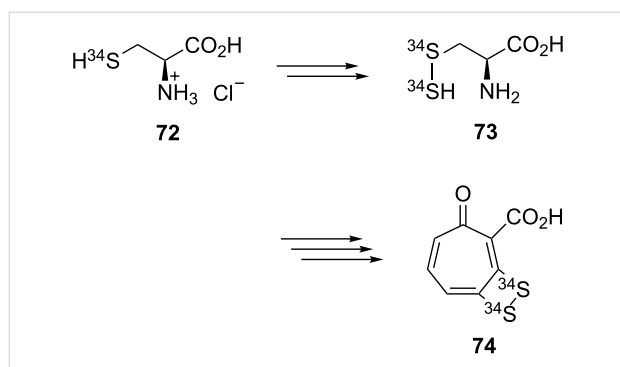
The FkbO-subfamily catalyses the formation of 3,4-*trans*-dihydroxycyclohexa-1,5-dienecarboxylate (**69**). This reaction is thought to occur via a protonation of the terminal double bond in the enol pyruvate moiety and subsequent attack of water at the cationic position to induce the cleavage of pyruvate. To support this mechanism, the enzymatic reaction was performed in <sup>18</sup>O-labeled water to yield labeled pyruvate as expected. However, conducting the same experiment for the Hyg5-subfamily of chorismatases, which produce 3-hydroxybenzoate (**70**), did not yield in any labeled pyruvate. This surprising result contradicts an elimination mechanism in the formation of **70** and demands for a new mechanistic proposal. Alternatively, an intramolecular attack at C-3 by the neighbouring hydroxy group at C-4 to cleave the activated pyruvate via an oxirane intermediate can be thought of. To test this hypothesis, chorismate with an <sup>18</sup>O label in its hydroxy function was prepared enzymatically starting from isochorismate. This label was



**Scheme 12:** Reactions of chorismate catalyzed by three different enzyme subfamilies. Oxygen atoms originating from water are labeled as O<sup>a</sup>, whereas <sup>18</sup>O labels in the hydroxy group of chorismate are annotated as O<sup>b</sup>. The XanB2-reaction was not investigated (missing label).

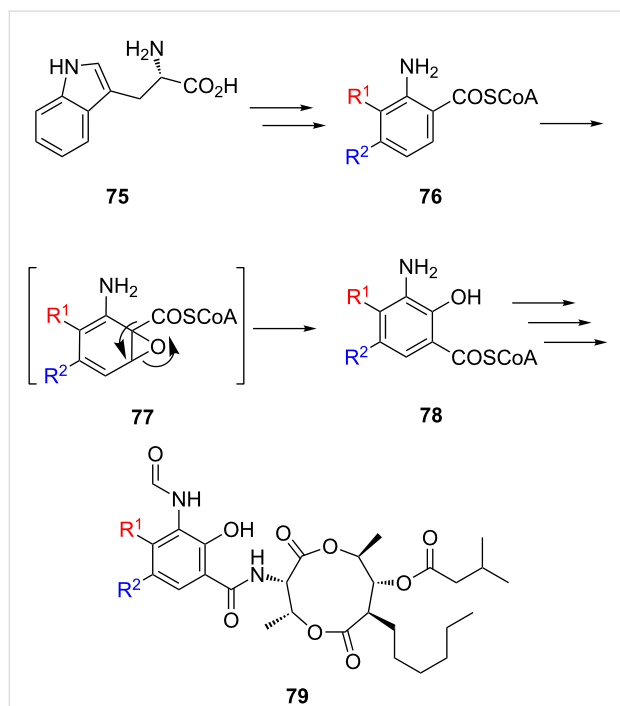
retained during the reaction supporting the oxirane intermediate. The mechanism was also proposed for the XanB2-subfamily, which shows an unselective opening of the oxirane ring to produce both **70** and 4-hydroxybenzoate (**71**). This study created an interesting example of <sup>18</sup>O usage to distinguish two different mechanisms of action within the same family of enzymes.

Due to the poor availability of isotopically labeled sulfur compounds, corresponding labeling experiments are rare, but can provide interesting insights into the biosynthesis of sulfur containing natural products. Besides the recently presented synthetic developments towards <sup>36</sup>S-labeled SAM and methionine [77], also [<sup>34</sup>S]cysteine has been made accessible by synthesis from elemental <sup>34</sup>S<sub>8</sub> and used to study the sulfur source in tropodithietic acid (TDA, **74**, Scheme 13) biosynthesis [78]. TDA is a marine antibiotic which was originally isolated from *Pseudomonas* species [79] showing no observable resistance in important pathogens up to now [80]. The biosynthesis of the tropone core proceeds via the phenylalanine degradation pathway, as was shown by labeling experiments with (<sup>13</sup>C)Phe and [<sup>13</sup>C<sub>6</sub>]glucose, and incorporation into phenylacetate [81] and TDA [82]. To resolve the sulfur precursor of TDA, (<sup>34</sup>S)Cys (**72**) was synthesized and fed to *Phaeobacter inhibens* to observe an incorporation rate of 87% into both sulfur atoms of TDA. This result together with mutations of relevant genes of the primary sulfur metabolism pointed towards an introduction of sulfur from Cys via (*S*)-thiocysteine (**73**) into TDA.



**Scheme 13:** Incorporation of sulfur into tropodithietic acid (**72**) via cysteine.

Antimycins such as antimycin A1 (**79**) are known for their inhibitory effect on the respiratory chain [83] and are widely used as antibiotics in fish farming industry. All compounds from this class feature a nine-membered dilactone core and a 3-formamidosalicylic acid moiety [84]. The latter provides an interesting biosynthetic rearrangement starting from tryptophan, which was investigated both by isotopic labeling experiments and by using fluorine as a positional label of the aromatic structure [85]. The formamido-residue in antimycine A1 (**79**,  $R^1 = R^2 = H$ , Scheme 14) is located in the *meta*-position with respect to the carboxylic acid moiety, whereas in the precursor molecule **76**, derived from tryptophan (**75**) via the well-known



**Scheme 14:** Biosynthetic proposal for the starter unit of antimycin biosynthesis. The hydrogens at positions  $R^1$  and  $R^2$  were replaced by fluorine in the feeding experiments with fluoroanthranilic acids.

Trp degradation pathway, the corresponding amino group is found in the *ortho*-position. An unusual 1,2-shift via the oxirane intermediate **77** was proposed for the formation of the starter unit **78**.

Using fluorine as a non-reactive anchor on the benzene ring in feeding experiments with different isomers of fluoroanthranilic acid, the fate of the amino and the carboxylic acid group in the biosynthesis of antimycins could be followed [85]. Incorporation of 3-fluoro ( $R^1 = F$ ) and 4-fluoroanthranilic acid ( $R^2 = F$ ) into antimycins was observed with retention of the position for the amino group, but migration of the carboxylic acid group relative to the fluorine label. This example shows that chemical labelings that are usually much cheaper than isotopic labelings can in special cases be useful to address biosynthetic problems, as was impressively demonstrated in the cutting-edge experiments by Knoop more than one century ago.

## Conclusion

The examples of isotope usage presented in this review article emphasize the important role of labeling methods on the road to a better understanding of nature's ways to assemble complex molecular structures. Although the principle of isotopic labeling itself did not change throughout 80 years of biochemical applications, isotopes are continuing to inspire biosynthetic studies to generate tailored methods for the specific problems evolved by natural products. As delineated here, labeling techniques are especially powerful in combination with other chemical and biological methods to give rise to a complete picture of biosynthetic conversions, both on enzymatic and molecular level. Some surprising results would probably still remain uncovered without the carefully designed usage of isotopes. Despite the exclusivity isotopic labeling techniques have lost to a lot of new bioinformatical, biotechnological and biological methods in the study of biosynthetic pathways, they still represent an indispensable tool in natural product research.

## References

- Schoenheimer, R.; Rittenberg, D. *Science* **1935**, *82*, 156–157. doi:10.1126/science.82.2120.156
- Knoop, F. *Beitr. Chem. Physiol. Pathol.* **1904**, *6*, 150–162.
- Ghisla, S. *Eur. J. Biochem.* **2004**, *271*, 459–461. doi:10.1046/j.1432-1033.2003.03952.x
- Kennedy, E. P. *J. Biol. Chem.* **2001**, *276*, 42619–42631. doi:10.1074/jbc.R100051200
- Liscum, L. Cholesterol biosynthesis. In *Biochemistry of Lipids, Lipoproteins and Membranes*; Vance, J. E.; Vance, D. E., Eds.; Elsevier: Amsterdam, 2008; pp 399–421. doi:10.1016/B978-044453219-0.50016-7
- Simpson, T. J. *Nat. Prod. Rep.* **2014**, *31*, 1247–1252. doi:10.1039/C4NP00065J
- Rohmer, M. *Nat. Prod. Rep.* **1999**, *16*, 565–574. doi:10.1039/a709175c

8. Eisenreich, W.; Schwarz, M.; Cartayrade, A.; Arigoni, D.; Zenk, M. H.; Bacher, A. *Chem. Biol.* **1998**, *5*, R221–R233. doi:10.1016/S1074-5521(98)90002-3
9. Mahmud, T. *J. Labelled Compd. Radiopharm.* **2007**, *50*, 1039–1051. doi:10.1002/jlcr.1391
10. Julka, S.; Regnier, F. *J. Proteome Res.* **2004**, *3*, 350–363. doi:10.1021/pr0340734
11. Postle, A. D.; Hunt, A. N. *J. Chromatogr., B* **2009**, *877*, 2716–2721. doi:10.1016/j.jchromb.2009.03.046
12. Chokkathukalam, A.; Kim, D.-H.; Barrett, M. P.; Breitling, R.; Creek, D. J. *Bioanalysis* **2014**, *6*, 511–524. doi:10.4155/bio.13.348
13. Tang, J. K.-H.; You, L.; Blankenship, R. E.; Tang, Y. J. *J. R. Soc., Interface* **2012**, *9*, 2767–2780. doi:10.1098/rsif.2012.0396
14. IUPAC. *Pure Appl. Chem.* **1979**, *51*, 353–380. doi:10.1351/pac197951020353
15. Hertweck, C. *Angew. Chem., Int. Ed.* **2009**, *48*, 4688–4716. doi:10.1002/anie.200806121
16. Witter, D. J.; Vederas, J. C. *J. Org. Chem.* **1996**, *61*, 2613–2623. doi:10.1021/jo952117p
17. Do, J. H.; Choi, D.-K. *Biotechnol. Bioprocess Eng.* **2007**, *12*, 585–593. doi:10.1007/BF02931073
18. McNamara, C. M.; Box, S.; Crowthorpe, J. M.; Hickman, B. S.; Norwood, T. J.; Rawlings, B. J. *J. Chem. Soc., Perkin Trans. 1* **1998**, 83–88. doi:10.1039/a704545j
19. Bentley, R. *Crit. Rev. Biotechnol.* **1999**, *19*, 1–40. doi:10.1080/0738-859991229189
20. Bretschneider, T.; Heim, J. B.; Heine, D.; Winkler, R.; Busch, B.; Kusebauch, B.; Stehle, T.; Zocher, G.; Hertweck, C. *Nature* **2013**, *502*, 124–128. doi:10.1038/nature12588
21. Wilson, M. C.; Moore, B. S. *Nat. Prod. Rep.* **2012**, *29*, 72–86. doi:10.1039/C1NP00082A
22. Calderone, C. T. *Nat. Prod. Rep.* **2008**, *25*, 845–853. doi:10.1039/b807243d
23. Scherlach, K.; Partida-Martinez, L. P.; Dahse, H.-M.; Hertweck, C. *J. Am. Chem. Soc.* **2006**, *128*, 11529–11536. doi:10.1021/ja062953o
24. Gomez-Escribano, J. P.; Song, L.; Fox, D. J.; Yeo, V.; Bibb, M. J.; Challis, G. L. *Chem. Sci.* **2012**, *3*, 2716–2720. doi:10.1039/c2sc20410j
25. Tamaoki, T.; Shirahata, K.; Iida, T.; Tomita, F. *J. Antibiot.* **1981**, *34*, 1525–1530. doi:10.7164/antibiotics.34.1525
26. Zhang, M.; Hou, X.-F.; Qi, L.-H.; Yin, Y.; Li, Q.; Pan, H.-X.; Chen, X.-Y.; Tang, G.-L. *Chem. Sci.* **2015**, *6*, 3440–3447. doi:10.1039/C5SC00116A
27. Maskey, R. P.; Sevvana, M.; Usón, I.; Helmke, E.; Laatsch, H. *Angew. Chem., Int. Ed.* **2004**, *43*, 1281–1283. doi:10.1002/anie.200352312
28. Pidot, S.; Ishida, K.; Cyrulies, M.; Hertweck, C. *Angew. Chem., Int. Ed.* **2014**, *53*, 7856–7859. doi:10.1002/anie.201402632
29. Fritzsche, K.; Ishida, K.; Hertweck, C. *J. Am. Chem. Soc.* **2008**, *130*, 8307–8316. doi:10.1021/ja800251m
30. Bringmann, G.; Noll, T. F.; Gulder, T. A. M.; Grüne, M.; Dreyer, M.; Wilde, C.; Pankewitz, F.; Hilker, M.; Payne, G. D.; Jones, A. L.; Goodfellow, M.; Fiedler, H.-P. *Nat. Chem. Biol.* **2006**, *2*, 429–433. doi:10.1038/nchembio805
31. Ellis, G. A.; Wyche, T. P.; Fry, C. G.; Braun, D. R.; Bugni, T. S. *Mar. Drugs* **2014**, *12*, 1013–1022. doi:10.3390/md12021013
32. Wyche, T. P.; Piotrowski, J. S.; Hou, Y.; Braun, D.; Deshpande, R.; McIlwain, S.; Ong, I. M.; Myers, C. L.; Guzei, I. A.; Westler, W. M.; Andes, D. R.; Bugni, T. S. *Angew. Chem., Int. Ed.* **2014**, *53*, 11583–11586. doi:10.1002/anie.201405990
33. Finking, R.; Marahiel, M. A. *Annu. Rev. Microbiol.* **2004**, *58*, 453–488. doi:10.1146/annurev.micro.58.030603.123615
34. Mootz, H. D.; Marahiel, M. A. *J. Bacteriol.* **1997**, *179*, 6843–6850.
35. Ling, L. L.; Schneider, T.; Peoples, A. J.; Spoering, A. L.; Engels, I.; Conlon, B. P.; Mueller, A.; Schäberle, T. F.; Hughes, D. E.; Epstein, S.; Jones, M.; Lazarides, L.; Steadman, V. A.; Cohen, D. R.; Felix, C. R.; Fetterman, K. A.; Millett, W. P.; Nitti, A. G.; Zullo, A. M.; Chen, C.; Lewis, K. *Nature* **2015**, *517*, 455–459. doi:10.1038/nature14098
36. Bode, H. B.; Reimer, D.; Fuchs, S. W.; Kirchner, F.; Dauth, C.; Kegler, C.; Lorenzen, W.; Brachmann, A. O.; Grün, P. *Chem. – Eur. J.* **2012**, *18*, 2342–2348. doi:10.1002/chem.201103479
37. Fuchs, S. W.; Proschak, A.; Jaskolla, T. W.; Karas, M.; Bode, H. B. *Org. Biomol. Chem.* **2011**, *9*, 3130–3132. doi:10.1039/c1ob05097d
38. Zhou, Q.; Dowling, A.; Heide, H.; Wöhrner, J.; Brandt, U.; Baum, J.; French-Constant, R.; Bode, H. B. *J. Nat. Prod.* **2012**, *75*, 1717–1722. doi:10.1021/np300279g
39. Zhou, Q.; Grundmann, F.; Kaiser, M.; Schiell, M.; Gaudriault, S.; Batzer, A.; Kurz, M.; Bode, H. B. *Chem. – Eur. J.* **2013**, *19*, 16772–16779. doi:10.1002/chem.201302481
40. Kronenwerth, M.; Bozhüyük, K. A. J.; Kahnt, A. S.; Steinhilber, D.; Gaudriault, S.; Kaiser, M.; Bode, H. B. *Chem. – Eur. J.* **2014**, *20*, 17478–17487. doi:10.1002/chem.201403979
41. Reimer, D.; Nollmann, F. I.; Schultz, K.; Kaiser, M.; Bode, H. B. *J. Nat. Prod.* **2014**, *77*, 1976–1980. doi:10.1021/np500390b
42. Kegler, C.; Nollmann, F. I.; Ahrendt, T.; Fleischhacker, F.; Bode, H. B. *ChemBioChem* **2014**, *15*, 826–828. doi:10.1002/cbic.201300602
43. Morinaka, B. I.; Vagstad, A. L.; Helf, M. J.; Gugger, M.; Kegler, C.; Freeman, M. F.; Bode, H. B.; Piel, J. *Angew. Chem., Int. Ed.* **2014**, *53*, 8503–8507. doi:10.1002/anie.201400478
44. Bode, H. B.; Brachmann, A. O.; Jadhav, K. B.; Seyfarth, L.; Dauth, C.; Fuchs, S. W.; Kaiser, M.; Waterfield, N. R.; Sack, H.; Heinemann, S. H.; Arndt, H.-D. *Angew. Chem., Int. Ed.* **2015**, *54*, 10352–10355. doi:10.1002/anie.201502835
45. Bode, H. B.; Brachmann, A. O.; Kegler, C.; Simsek, R.; Dauth, C.; Zhou, Q.; Kaiser, M.; Klemmt, P.; Bode, H. B. *ChemBioChem* **2015**, *16*, 1115–1119. doi:10.1002/cbic.201500094
46. Bourdichon, F.; Casaregola, S.; Farrokhi, C.; Frisvad, J. C.; Gerds, M. L.; Hammes, W. P.; Harnett, J.; Huys, G.; Laulund, S.; Ouweland, A.; Powell, I. B.; Prajapati, J. B.; Seto, Y.; Ter Schure, E.; van Boven, A.; Vankerckhoven, V.; Zgoda, A.; Tuijelaars, S.; Hansen, E. B. *Int. J. Food Microbiol.* **2012**, *154*, 87–97. doi:10.1016/j.ijfoodmicro.2011.12.030
47. Chankhamjon, P.; Boettger-Schmidt, D.; Scherlach, K.; Urbansky, B.; Lackner, G.; Kalb, D.; Dahse, H.-M.; Hoffmeister, D.; Hertweck, C. *Angew. Chem., Int. Ed.* **2014**, *53*, 13409–13413. doi:10.1002/anie.201407624
48. Garrido, L.; Zubía, E.; Ortega, M. J.; Salvá, J. *J. Org. Chem.* **2003**, *68*, 293–299. doi:10.1021/jo020487p
49. Nam, S.-J.; Gaudêncio, S. P.; Kauffman, C. A.; Jensen, P. R.; Kondratyuk, T. P.; Marler, L. E.; Pezzuto, J. M.; Fenical, W. *J. Nat. Prod.* **2010**, *73*, 1080–1086. doi:10.1021/np100087c
50. Heinz, C.; Cramer, N. *J. Am. Chem. Soc.* **2015**, *137*, 11278–11281. doi:10.1021/jacs.5b07964
51. Matveenko, M.; Liang, G.; Lauterwasser, E. M. W.; Zubía, E.; Trauner, D. *J. Am. Chem. Soc.* **2012**, *134*, 9291–9295. doi:10.1021/ja301326k
52. Ear, A.; Amand, S.; Blanchard, F.; Blond, A.; Dubost, L.; Buisson, D.; Nay, B. *Org. Biomol. Chem.* **2015**, *13*, 3662–3666. doi:10.1039/C5OB00114E
53. Oikawa, H. *J. Org. Chem.* **2003**, *68*, 3552–3557. doi:10.1021/jo0267596

54. Murphy, A. C.; Gao, S.-S.; Han, L.-C.; Carobene, S.; Fukuda, D.; Song, Z.; Hothersall, J.; Cox, R. J.; Crosby, J.; Crump, M. P.; Thomas, C. M.; Willis, C. L.; Simpson, T. *J. Chem. Sci.* **2014**, *5*, 397–402. doi:10.1039/C3SC52281D
55. Shiozawa, H.; Kagasaki, T.; Kinoshita, T.; Haruyama, H.; Domon, H.; Utsui, Y.; Kodama, K.; Takahashi, S. *J. Antibiot.* **1993**, *46*, 1834–1842. doi:10.7164/antibiotics.46.1834
56. Kuwajima, I.; Tanino, K. *Chem. Rev.* **2005**, *105*, 4661–4670. doi:10.1021/cr040636z
57. Barra, L.; Ibrom, K.; Dickschat, J. S. *Angew. Chem., Int. Ed.* **2015**, *54*, 6637–6640. doi:10.1002/anie.201501765
58. Kühne, B.; Hanssen, H.-P.; Abraham, W.-R.; Wray, V. *Phytochemistry* **1991**, *30*, 1463–1465. doi:10.1016/0031-9422(91)84187-W
59. Sugai, Y.; Ueno, Y.; Hayashi, K.-i.; Oogami, S.; Toyomasu, T.; Matsumoto, S.; Natsume, M.; Nozaki, H.; Kawaide, H. *J. Biol. Chem.* **2011**, *286*, 42840–42847. doi:10.1074/jbc.M111.302703
60. Rabe, P.; Barra, L.; Rinkel, J.; Riclea, R.; Citron, C. A.; Klapschinski, T. A.; Janusko, A.; Dickschat, J. S. *Angew. Chem., Int. Ed.* **2015**, *54*, 13448–13451. doi:10.1002/anie.201507615
61. Rabe, P.; Pahirulzaman, K. A. K.; Dickschat, J. S. *Angew. Chem., Int. Ed.* **2015**, *54*, 6041–6045. doi:10.1002/anie.201501119
62. Rabe, P.; Rinkel, J.; Klapschinski, T. A.; Barra, L.; Dickschat, J. S. *Org. Biomol. Chem.* **2015**, in press. doi:10.1039/C5OB01998B
63. Aoyama, T.; Naganawa, H.; Muraoka, Y.; Aoyagi, T.; Takeuchi, T. *J. Antibiot.* **1992**, *45*, 1703–1704. doi:10.7164/antibiotics.45.1703
64. Aoyagi, T.; Aoyama, T.; Kojima, F.; Hattori, S.; Honma, Y.; Hamada, M.; Takeuchi, T. *J. Antibiot.* **1992**, *45*, 1587–1591. doi:10.7164/antibiotics.45.1587
65. Meguro, A.; Motoyoshi, Y.; Teramoto, K.; Ueda, S.; Totsuka, Y.; Ando, Y.; Tomita, T.; Kim, S.-Y.; Kimura, T.; Igarashi, M.; Sawa, R.; Shinada, T.; Nishiyama, M.; Kuzuyama, T. *Angew. Chem., Int. Ed.* **2015**, *54*, 4353–4356. doi:10.1002/anie.201411923
66. Janke, R.; Görner, C.; Hirte, M.; Brück, T.; Loll, B. *Acta Crystallogr., Sect. D* **2014**, *70*, 1528–1537. doi:10.1107/S1399004714005513
67. Kim, S.-Y.; Zhao, P.; Igarashi, M.; Sawa, R.; Tomita, T.; Nishiyama, M.; Kuzuyama, T. *Chem. Biol.* **2009**, *16*, 736–743. doi:10.1016/j.chembiol.2009.06.007
68. Rohmer, M.; Knani, M.; Simonin, P.; Sutter, B.; Sahm, H. *Biochem. J.* **1993**, *295*, 517–524. doi:10.1042/bj2950517
69. Ye, Y.; Minami, A.; Mandi, A.; Liu, C.; Taniguchi, T.; Kuzuyama, T.; Monde, K.; Gomi, K.; Oikawa, H. *J. Am. Chem. Soc.* **2015**, *137*, 11846–11853. doi:10.1021/jacs.5b08319
70. Lesburg, C. A.; Zhai, G.; Cane, D. E.; Christianson, D. W. *Science* **1997**, *277*, 1820–1824. doi:10.1126/science.277.5333.1820
71. Cane, D. E.; Sohng, J.-K.; Lamberson, C. R.; Rudnicki, S. M.; Wu, Z.; Lloyd, M. D.; Oliver, J. S.; Hubbard, B. R. *Biochemistry* **1994**, *33*, 5846–5857. doi:10.1021/bi00185a024
72. Gutta, P.; Tantillo, D. J. *J. Am. Chem. Soc.* **2006**, *128*, 6172–6179. doi:10.1021/ja058031n
73. Zu, L.; Xu, M.; Lodewyk, M. W.; Cane, D. E.; Peters, R. J.; Tantillo, D. J. *J. Am. Chem. Soc.* **2012**, *134*, 11369–11371. doi:10.1021/ja3043245
74. Hubrich, F.; Juneja, P.; Müller, M.; Diederichs, K.; Welte, W.; Andexer, J. N. *J. Am. Chem. Soc.* **2015**, *137*, 11032–11037. doi:10.1021/jacs.5b05559
75. Floss, H. G. *Nat. Prod. Rep.* **1997**, *14*, 433–452. doi:10.1039/np9971400433
76. Andexer, J. N.; Kendrew, S. G.; Nur-e-Alam, M.; Lazos, O.; Foster, T. A.; Zimmermann, A.-S.; Warneck, T. D.; Suthar, D.; Coates, N. J.; Koehn, F. E.; Skotnicki, J. S.; Carter, G. T.; Gregory, M. A.; Martin, C. J.; Moss, S. J.; Leadlay, P. F.; Wilkinson, B. *Proc. Natl. Acad. Sci. U. S. A.* **2011**, *108*, 4776–4781. doi:10.1073/pnas.1015773108
77. Poulin, M. B.; Du, Q.; Schramm, V. L. *J. Org. Chem.* **2015**, *80*, 5344–5347. doi:10.1021/acs.joc.5b00608
78. Brock, N. L.; Nikolay, A.; Dickschat, J. S. *Chem. Commun.* **2014**, *50*, 5487–5489. doi:10.1039/c4cc01924e
79. Kintaka, K.; Ono, H.; Tsubotani, S.; Harada, S.; Okazaki, H. *J. Antibiot.* **1984**, *37*, 1294–1300. doi:10.7164/antibiotics.37.1294
80. Harrington, C.; Reen, F. J.; Mooij, M. J.; Stewart, F. A.; Chabot, J.-B.; Guerra, A. F.; Glöckner, F. O.; Nielsen, K. F.; Gram, L.; Dobson, A. D. W.; Adams, C.; O'Gara, F. *Mar. Drugs* **2014**, *12*, 5960–5978. doi:10.3390/md12125960
81. Berger, M.; Brock, N. L.; Liesegang, H.; Dogs, M.; Preuth, I.; Simon, M.; Dickschat, J. S.; Brinkhoff, T. *Appl. Environ. Microbiol.* **2012**, *78*, 3539–3551. doi:10.1128/AEM.07657-11
82. Cane, D. E.; Wu, Z.; van Epp, J. E. *J. Am. Chem. Soc.* **1992**, *114*, 8479–8483. doi:10.1021/ja00048a019
83. Tappel, A. L. *Biochem. Pharmacol.* **1960**, *3*, 289–296. doi:10.1016/0006-2952(60)90094-0
84. Seipke, R. F.; Hutchings, M. I. *Beilstein J. Org. Chem.* **2013**, *9*, 2556–2563. doi:10.3762/bjoc.9.290
85. Schoenian, I.; Paetz, C.; Dickschat, J. S.; Aigle, B.; Leblond, P.; Spitteller, D. *ChemBioChem* **2012**, *13*, 769–773. doi:10.1002/cbic.201200033

## License and Terms

This is an Open Access article under the terms of the Creative Commons Attribution License (<http://creativecommons.org/licenses/by/2.0>), which permits unrestricted use, distribution, and reproduction in any medium, provided the original work is properly cited.

The license is subject to the *Beilstein Journal of Organic Chemistry* terms and conditions: (<http://www.beilstein-journals.org/bjoc>)

The definitive version of this article is the electronic one which can be found at: [doi:10.3762/bjoc.11.271](https://doi.org/10.3762/bjoc.11.271)



## Appendix B

### Lessons from 1,3-Hydride Shifts in Sesquiterpene Cyclizations

*Angew. Chem. Int. Ed.* **2016**, *55*, 13593–13596.

DOI:10.1002/anie.201608042

&

*Angew. Chem.* **2016**, *128*, 13791–13794.

DOI:10.1002/ange.201608042



## Terpene Biosynthesis

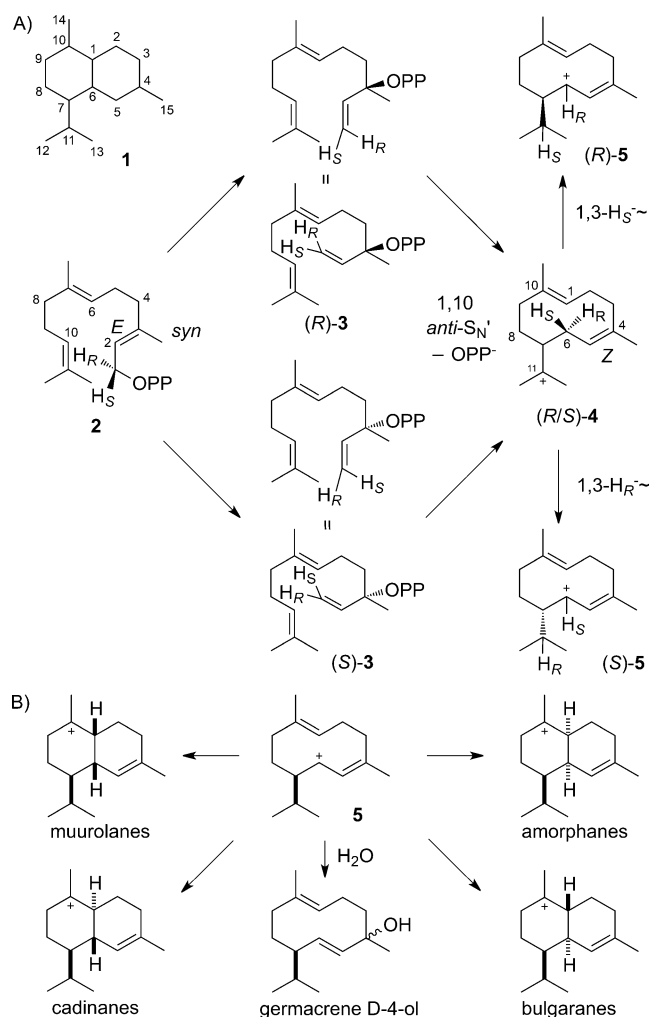
International Edition: DOI: 10.1002/anie.201608042  
German Edition: DOI: 10.1002/ange.201608042

## Lessons from 1,3-Hydride Shifts in Sesquiterpene Cyclizations

Jan Rinkel, Patrick Rabe, Paolina Garbeva, and Jeroen S. Dickschat\*

**Abstract:** Stereospecifically labelled precursors were subjected to conversion by seven bacterial sesquiterpene cyclases to investigate the stereochemistry of their initial 1,10-cyclisation-1,3-hydride shift cascades. Enzymes with products of known absolute configuration showed a coherent stereochemical course, except for (–)- $\alpha$ -amorphene synthase, for which the obtained results are better explained by an initial 1,6-cyclisation. The link between the absolute configuration of the product and the stereochemical course of the 1,3-hydride shifts enabled assignment of the absolute configurations of three enzyme products, which were confirmed independently through the absolute configuration of the common byproduct germacrene D-4-ol.

Arguably, the most complex carbon skeletons in nature are synthesised by terpene cyclases. The mechanistic details of reactions catalysed by this fascinating class of enzymes that convert simple oligoprenyl diphosphates into (poly)cyclic hydrocarbons or alcohols have promoted scientific discussion for several decades.<sup>[1]</sup> With the rise of computational methods, even long-accepted mechanisms have come under debate, thereby widening our understanding of carbocation chemistry.<sup>[2]</sup> Classical isotope labelling experiments are currently undergoing a revival and offer a complementary approach to unravel biosynthetic surprises.<sup>[3]</sup> One of the first examples of a detailed view on terpene cyclisation mechanisms is presented by the work on the cadalane sesquiterpenes. This frequently occurring group of natural products is defined by the carbon skeleton **1**, which bears two six-membered rings, and members of the group share a biosynthesis through an initial isomerisation of farnesyl diphosphate (FPP, **2**) to nerolidyl diphosphate (NPP, **3**), followed by a 1,10-cyclisation to the helminthogermacrene cation **4** (Scheme 1 A). Through this process, the (2*E*) double bond in FPP ends up as a (4*Z*) double bond in **4**. After Arigoni's fundamental thoughts on the fate of the C-1 hydrogen atoms,<sup>[4]</sup> several well-designed studies have been carried out to investigate the stereochemical course to various terpenoid products, including (+)-1-*epi*-cubenol from *Streptomyces* sp. LL-B7,<sup>[5]</sup> cadalanes from *Medicago truncatula*,<sup>[6]</sup> and (–)- $\delta$ -cadinene and (+)-T-muur-



**Scheme 1.** A) Initial 1,10-cyclisation of FPP via (S)- or (R)-NPP to cation **5**. Its absolute configuration is linked to the enantiotopic hydrogens (in **2**), only one of which stereospecifically undergoes the 1,3-shift. Note that H<sub>S</sub> migrates in the formation of (R)-**5**, while H<sub>R</sub> migration occurs to give (S)-**5**. B) Reactions of **5** to give cadalanes and germacrene D-4-ol.

[\*] J. Rinkel, Dr. P. Rabe, Prof. Dr. J. S. Dickschat  
Kekulé-Institut für Organische Chemie und Biochemie  
Rheinische Friedrich-Wilhelms-Universität Bonn  
Gerhard-Domagk-Straße 1, 53121 Bonn (Germany)  
E-mail: dickschat@uni-bonn.de

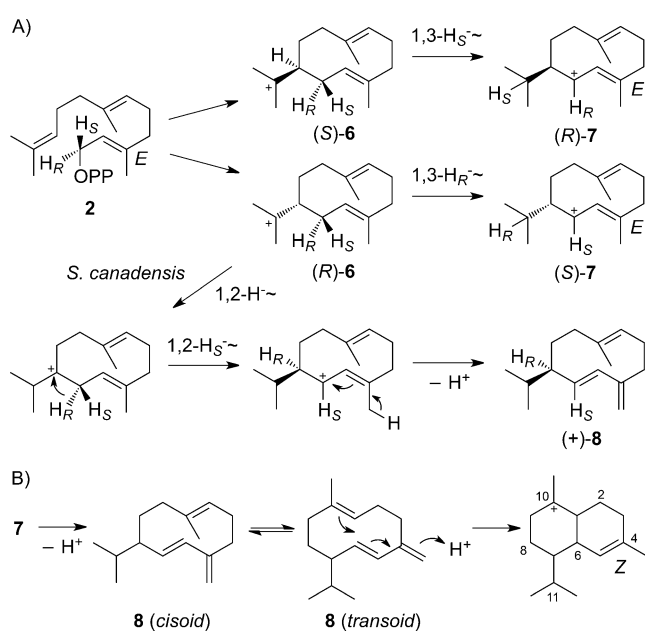
Dr. P. Garbeva, Prof. Dr. J. S. Dickschat  
Nederlands Instituut voor Ecologie  
Koninklijke Nederlandse Akademie van Wetenschappen  
Droevendaalsesteeg 10, 6708 PB Wageningen (The Netherlands)

Supporting information and the ORCID identification number(s) for the author(s) of this article can be found under <http://dx.doi.org/10.1002/anie.201608042>.

olol from *S. clavuligerus*.<sup>[7]</sup> In these examples, incubation with stereospecifically deuterated FPPs showed a combination of *syn* allylic rearrangement to NPP and *anti*-S<sub>N</sub>' ring closure to give cation **4**. These stereochemical constraints result in a defined absolute stereochemistry at C-6, regardless of the intermediacy of (R)- or (S)-NPP, the identity of which cannot be concluded solely from these experiments. Considering the close proximity of the moving hydrogen atom to its destination, the subsequent 1,3-hydride shift of one of the two stereochemically distinct hydrogens (H<sub>S</sub> and H<sub>R</sub>) at C-6 can be used to infer the configuration at C-7. The importance of

cation **5** as a precursor for a great variety of sesquiterpenes (Scheme 1B) encourages a detailed investigation of the stereochemical course of its formation, not only for mechanistic reasons, but also for delineating the absolute configuration of the terpenoid product. This information is otherwise hard to access, especially for hydrocarbons that usually do not readily crystallize.

Besides cadalanes, the model also applies to germacrane, with the important difference of a (4*E*)- instead of a (4*Z*)-configured double bond (Scheme 2A). Therefore, NPP is formally not needed for cyclisation. After S<sub>N</sub>2-like direct ring closure to cation **6**, a 1,3-hydride shift leads to allylic cation **7**



**Scheme 2.** A) A stereochemical model for the biosynthesis of germacrane. B) An alternative cyclisation to cadalanes via germacrene D (**8**).

with specific migration of H<sub>S</sub> in case of (*R*)-**7** and H<sub>R</sub> in the formation of (*S*)-**7**. Germacrene D (**8**) is discussed as a neutral intermediate, which bypasses the need for NPP in creating a (4*Z*) double bond through an equilibrium between a *cisoid* and a *transoid* conformer, the latter of which gives access to cadalanes through a protonation-induced cyclisation (Scheme 2B).<sup>[4]</sup> Interestingly, (–)-germacrene D synthase from *Solidago canadensis* follows the usual mechanism through a 1,3-hydride shift from (*R*)-**6** to (*S*)-**7** with migration of H<sub>R</sub>, but the synthase producing the enantiomer (+)-germacrene D (**8**) in the same plant also catalyzes the transformation starting from (*R*)-**6** through two consecutive 1,2-hydride shifts.<sup>[8]</sup> Furthermore, the geosmin synthase from *Streptomyces coelicolor* A3(2) provides a reversed stereochemical course of the 1,3-hydride shift, with migration of H<sub>S</sub> through

**Table 1:** Investigated sesquiterpene cyclases.

Entry	Main product(s)	Source organism	Accession no.
cadalanes			
1	(+)-T-muurolool ( <b>9</b> )	<i>Roseiflexus castenholzii</i>	WP_012119179
2	(–)-α-amorphene ( <b>10</b> )	<i>Streptomyces viridochromogenes</i>	WP_039931950
3	(+)-4- <i>epi</i> -cubebol ( <b>11</b> )	<i>Streptosporangium roseum</i>	WP_012893303
4	(–)-γ-cadinene ( <b>12</b> )	<i>Chitinophaga pinensis</i>	WP_012792334
5	(+)-corvol ethers A ( <b>13</b> ) and B ( <b>14</b> )	<i>Kitasatospora setae</i>	BAJ27126
germacranes			
6	(+)-germacradien-6-ol ( <b>15</b> )	<i>Streptomyces pratensis</i>	ADW03055
7	(–)-germacrene D-4-ol ( <b>16</b> )	<i>Collimonas pratensis</i>	AMP04969

the reaction of (*R*)-**6** from a different conformation to yield intermediate (*S*)-**7** on the way to the side product (–)-**8**.<sup>[9]</sup> These diverse results prompted us to investigate the discussed principles on a broader basis for terpene cyclases.

For this purpose, the enzymes summarized in Table 1 were used. The terpene synthases 1–6 were functionally expressed. The structures of their products (**9**–**15**; Figure 1), along with full NMR data, were published previously,<sup>[10–12]</sup> and only the absolute configurations of (+)-4-*epi*-cubebol and the corvol ethers remained unknown. In addition, the gene for a terpene

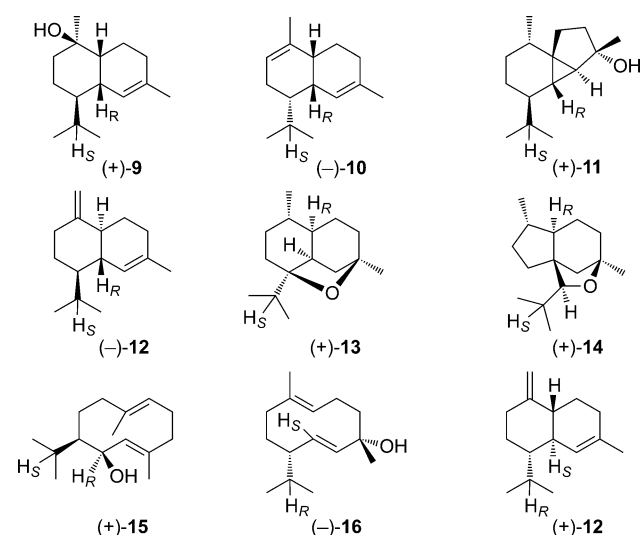


**Figure 1.** Structures of the main products obtained with terpene cyclases 1–7 (Table 1) and results of incubation experiments with (1*R*)- and (1*S*)-(1-<sup>2</sup>H)FPP.

cyclase from *Collimonas pratensis*, which was cloned into the expression vector pACYCDuet-1, was expressed.<sup>[13]</sup> The protein did not accept geranyl diphosphate (GPP) and geranylgeranyl diphosphate (GGPP), but efficiently converted FPP into the main product germacrene D-4-ol (**16**), which was isolated and showed identical NMR spectra to a synthetic standard<sup>[14]</sup> and the compound isolated from *Pinus sylvestris*.<sup>[15]</sup> The optical rotation also had the same sign as the compound from *Pinus sylvestris* ( $[\alpha]_{\text{D}}^{20} = -93$ ,  $c = 0.20$ , (2H<sub>6</sub>)benzene; lit.:  $[\alpha]_{\text{D}}^{25} = -181$ ,  $c = 0.61$ , CHCl<sub>3</sub>),<sup>[15]</sup> thus establishing the natural product from *C. pratensis* as (–)-(4*S*,7*S*)-germacrene D-4-ol. A few side products of the

germacrene D-4-ol synthase were identified by GC/MS (Figure S1 in the Supporting Information), one of which ( $\gamma$ -cadinene, **12**) is important for the further discussion. To elucidate a possible role of the neutral intermediate germacrene D (Scheme 2B) in the reactions of the seven cyclases, incubations with FPP were carried out in  $^2\text{H}_2\text{O}$  buffer.<sup>[6]</sup> However, except for the corvol ethers, which are formed through reprotonation of the neutral intermediate **16**,<sup>[11]</sup> no deuterium incorporation was observed by GC/MS, thus indicating a negligible role of germacrene D in the cyclisation mechanisms of these seven enzymes.

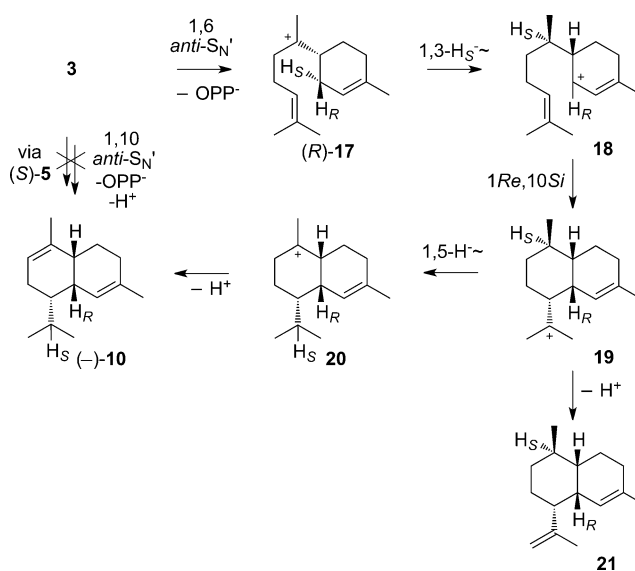
For a rapid and sensitive  $^{13}\text{C}$ -NMR based test of the 1,3-hydride shift,  $(11\text{-}^{13}\text{C}, 1,1\text{-}^2\text{H}_2)\text{FPP}$  was synthesized in four steps from  $(10\text{-}^{13}\text{C})\text{geranylacetone}$ , which is itself accessible through a previously reported route from geraniol<sup>[16]</sup> (Scheme S1 in the Supporting Information). Incubation of this compound with each of the seven enzymes, followed by extraction with  $(^2\text{H}_6)\text{benzene}$  and direct  $^{13}\text{C}$ -NMR analysis resulted in the observation of strongly enhanced triplets for C-11 of the main product(s) due to  $^{13}\text{C}$ - $^2\text{H}$  spin-spin coupling, which is indicative of 1,3-hydride migration (Figure S2). For the synthases for 4-*epi*-cubebol, corvol ethers,  $\gamma$ -cadinene, and germacradien-6-ol, one additional triplet appeared in the spectra with a chemical shift that matches C-11 of **16**, which can be formed from cation **5** through attack by water.

To elucidate the stereochemical courses of the observed hydride shifts,  $(1R)$ - and  $(1S)$ - $(1\text{-}^2\text{H})\text{FPP}$  were synthesized through Alpine borane reduction of  $(1\text{-}^2\text{H})\text{farnesal}$ <sup>[17]</sup> as a key step (Scheme S2). The two enantiomers,  $(1R)$ - and  $(1S)$ - $(1\text{-}^2\text{H})\text{farnesol}$ , were obtained with more than 95% *ee* according to Mosher ester analysis (Figure S3). The EI mass spectra of the enzyme products **9–16** show strong cleavage of the isopropyl group. This allows deuterium within this isopropyl group ( $m/z = 161$ ) or within the other portion of the analyte ( $m/z = 162$ ) to be localized for each compound obtained from  $(1R)$ - or  $(1S)$ - $(1\text{-}^2\text{H})\text{FPP}$  (Figure S4). For the main products **9** and **12** of enzymes 1 and 4, for which the absolute configurations are known, the expected stereochemical course was observed, that is, migration of  $\text{H}_\text{S}$  in the formation of  $(R)$ -**5** from  $(S)$ -**4**. Notably, a reversed stereochemical outcome was observed for **12**, depending on its enzymatic source. While for  $\gamma$ -cadinene synthase from *Chitinophaga pinensis*  $\text{H}_\text{S}$  migrates, the opposite outcome (migration of  $\text{H}_\text{R}$ ) is observed for the side product **12** with germacrene D-4-ol synthase from *C. pratensis*. According to the model, this observation leads to the assignment of a different absolute configuration for **12**, which was confirmed by separation of the products by GC on a homochiral stationary phase (Figure S5). The delineated absolute configuration of  $(+)\text{-12}$  for the side product of the *Collimonas* terpene synthase is in line with the absolute configuration of the main product  $(4S,7S)\text{-16}$ . The formation of **12** by the germacrene D-4-ol synthase from *C. pratensis* also suggests that **16** is produced via NPP and cation **4**, and not through direct cyclisation of FPP to **6**. However, the formation of **15**, a compound with known absolute configuration, by the germacradien-6-ol synthase from *Streptomyces pratensis* must follow the direct FPP-cyclisation mechanism. Incubations of  $(1R)$ - and  $(1S)$ - $(1\text{-}^2\text{H})\text{FPP}$  with enzyme 6 indicated the expected stereochemical course with migration

of  $\text{H}_\text{S}$ . The absolute configurations of  $(+)\text{-4-epi-cubebol}$ ,  $(+)\text{-corvol ether A}$ , and  $(+)\text{-corvol ether B}$  are unknown, but could be inferred from the observed shift of  $\text{H}_\text{S}$ , which points to their biosynthesis via  $(R)$ -**5** (cyclisation mechanisms for **11**, **13**, and **14** are shown in Scheme S3). The absolute configurations of all three compounds were independently deduced from that of their byproduct  $(4R,7R)\text{-16}$ , which could be clearly separated from its enantiomer, obtained with the *Collimonas* terpene cyclase, by GC on a homochiral stationary phase, as could the byproduct  $(4R,7R)\text{-16}$  of enzymes 1, 4 and 6 (Figure S6).

The case of  $(-)\text{-}\alpha\text{-amorphene}$  synthase gave puzzling results at first sight. Despite the known absolute configuration of **10** as shown in Figure 1,  $\text{H}_\text{S}$  was found to migrate. Furthermore, no traces of germacrene D-4-ol could be detected in the extracts, in contrast to all other investigated systems [for T-muurolool synthase, the amounts of germacrene D-4-ol were below the limits of detection by NMR, (Figure S2), but traces could be detected by GC/MS (Figure S6)]. Cyclisation mechanisms through an initial 1,10-cyclisation have been proposed for amorpha-4,11-diene and amorphenes,<sup>[18]</sup> but for amorpha-4,11-diene, a pathway through initial 1,6-cyclisation is also frequently invoked.<sup>[18a,19]</sup> This pathway starts from NPP (**3**), with an *anti*- $\text{S}_\text{N}'$  cyclisation to the  $(R)$ -bisabolyl cation (**17**; Scheme 3). Induced by the neighboring stereocenter, it is specifically  $\text{H}_\text{S}$  that undergoes a 1,3-hydride shift to form cation **18**. A subsequent  $1\text{Re}, 10\text{Si}$  cyclisation leads to cation **19**, which gives amorpha-4,11-diene (**21**) upon deprotonation. The original  $\text{H}_\text{S}$  can now undergo a 1,5-hydride shift to the amorphenyl cation **20**, which is deprotonated to  $(-)\text{-}\alpha\text{-amorphene}$  (**10**).

Recently, Hong and Tantillo have shown by quantum chemical calculations that 1) specifically  $\text{H}_\text{S}$  should migrate in the initial 1,3-hydride shift, 2) the 1,5-hydride shift from **19** to **20** has a low barrier, thus linking the pathway to amorpha-4,11-diene and also to the amorphenes, and 3) the pathway



**Scheme 3.** A stereochemical model for proposed 1,6-cyclisation in  $(-)\text{-}\alpha\text{-amorphene}$  biosynthesis versus the expected outcome for 1,10-cyclisation.

through initial 1,6-cyclisation is energetically favored over the 1,10-cyclisation pathway.<sup>[20]</sup> The pathway in Scheme 3 explains our experimental finding of H<sub>5</sub> migration to C-11 of **10** and provides first experimental evidence for the biosynthetic model proposed by Hong and Tantillo. Moreover, the usage of a different pathway to **10** compared to the other cadalane sesquiterpenes, as discussed in this study, explains the absence of germacrene D-4-ol from enzyme reactions with  $\alpha$ -amorphene synthase.

In summary, we have characterized a new bacterial terpene cyclase from *Collimonas pratensis* as a (–)-germacrene D-4-ol synthase. Incubation experiments with (11-<sup>13</sup>C,1,1-<sup>2</sup>H<sub>2</sub>)FPP revealed deuterium transfer from C-1 to C-11 for seven bacterial terpene cyclases, while the use of stereospecifically labelled (1R)- and (1S)-(1-<sup>2</sup>H)FPP showed that the fate of the enantiotopic hydrogen atoms at C-1 is linked to the absolute configuration of the product. This knowledge was used to delineate the previously unknown absolute configurations of three terpenes. The assignments were independently confirmed through analysis of the common side product germacrene D-4-ol by GC on a homochiral stationary phase. Only for  $\alpha$ -amorphene synthase did the outcome of incubation experiments with (1R)- and (1S)-(1-<sup>2</sup>H)FPP not match the model, but this can be explained by a recently proposed theory-based cyclisation mechanism through initial 1,6-cyclisation,<sup>[20]</sup> thus giving first experimental evidence for its correctness.

## Acknowledgments

This work was funded by the DFG (DI1536/7-1) and by the Fonds der Chemischen Industrie with a PhD scholarship to JR. This publication is no. 6159 of the Netherlands Institute of Ecology (NIOO-KNAW).

**Keywords:** biosynthesis · hydride shifts · isotopes · stereochemistry · terpenes

**How to cite:** *Angew. Chem. Int. Ed.* **2016**, *55*, 13593–13596  
*Angew. Chem.* **2016**, *128*, 13791–13794

- [1] a) J. S. Dickschat, *Nat. Prod. Rep.* **2016**, *33*, 87; b) D. W. Christianson, *Chem. Rev.* **2006**, *106*, 3412; c) D. E. Cane, *Chem. Rev.* **1990**, *90*, 1089.  
[2] D. J. Tantillo, *Nat. Prod. Rep.* **2011**, *28*, 1035.  
[3] a) J. Rinkel, J. S. Dickschat, *Beilstein J. Org. Chem.* **2015**, *11*, 2493; b) A. Meguro, Y. Motoyoshi, K. Teramoto, S. Ueda, Y. Totsuka, Y. Ando, T. Tomita, S.-Y. Kim, T. Kimura, M. Igarashi,

- R. Sawa, T. Shinada, M. Nishiyama, T. Kuzuyama, *Angew. Chem. Int. Ed.* **2015**, *54*, 4353; *Angew. Chem.* **2015**, *127*, 4427; c) Y. Matsuda, T. Mitsuhashi, S. Lee, N. Hoshino, T. Mori, M. Okada, H. Zhang, F. Hayashi, M. Fujita, I. Abe, *Angew. Chem. Int. Ed.* **2016**, *55*, 5785; *Angew. Chem.* **2016**, *128*, 5879; d) Y. Ye, A. Minami, A. Mandi, C. Liu, T. Taniguchi, T. Kuzuyama, K. Monde, K. Gomi, H. Oikawa, *J. Am. Chem. Soc.* **2015**, *137*, 11846; e) I. Burkhardt, T. Siemon, M. Henrot, L. Studt, S. Rösler, B. Tudzynski, M. Christmann, J. S. Dickschat, *Angew. Chem. Int. Ed.* **2016**, *55*, 8748; *Angew. Chem.* **2016**, *128*, 8890; f) P. Rabe, A. Janusko, B. Goldfuss, J. S. Dickschat, *ChemBioChem* **2016**, *17*, 146; g) P. Rabe, J. Rinkel, T. A. Klapschinski, L. Barra, J. S. Dickschat, *Org. Biomol. Chem.* **2016**, *14*, 158.  
[4] D. Arigoni, *Pure Appl. Chem.* **1975**, *41*, 219.  
[5] D. E. Cane, M. Tandon, *J. Am. Chem. Soc.* **1995**, *117*, 5602.  
[6] S. Garms, T. G. Köllner, W. Boland, *J. Org. Chem.* **2010**, *75*, 5590.  
[7] Y. Hu, W. K. Chou, R. Hopson, D. E. Cane, *Chem. Biol.* **2011**, *18*, 32.  
[8] a) C. O. Schmidt, H. J. Bouwmeester, S. Franke, W. A. König, *Chirality* **1999**, *11*, 353; b) M. Niwa, M. Iguchi, S. Yamamura, *Chem. Pharm. Bull.* **1980**, *28*, 997.  
[9] X. He, D. E. Cane, *J. Am. Chem. Soc.* **2004**, *126*, 2678.  
[10] a) P. Rabe, J. S. Dickschat, *Angew. Chem. Int. Ed.* **2013**, *52*, 1810; *Angew. Chem.* **2013**, *125*, 1855; b) J. S. Dickschat, K. A. K. Pahirulzaman, P. Rabe, T. A. Klapschinski, *ChemBioChem* **2014**, *15*, 810; c) P. Rabe, T. Schmitz, J. S. Dickschat, *Beilstein J. Org. Chem.* **2016**, *12*, 1839.  
[11] P. Rabe, K. A. K. Pahirulzaman, J. S. Dickschat, *Angew. Chem. Int. Ed.* **2015**, *54*, 6041; *Angew. Chem.* **2015**, *127*, 6139.  
[12] P. Rabe, L. Barra, J. Rinkel, R. Riclea, C. A. Citron, T. A. Klapschinski, A. Janusko, J. S. Dickschat, *Angew. Chem. Int. Ed.* **2015**, *54*, 13448; *Angew. Chem.* **2015**, *127*, 13649.  
[13] C. Song, R. Schmidt, V. de Jager, D. Krzyzanowska, E. Jongedijk, K. Cankar, J. Beekwilder, A. van Veen, W. de Boer, J. A. van Veen, P. Garbeva, *BMC Genomics* **2015**, *16*, 1103.  
[14] O. Smitt, H.-E. Högberg, *Synlett* **2002**, 1273.  
[15] O. Nordin, E. Hedenström, H. E. Högberg, *Acta Chem. Scand.* **1999**, *53*, 124.  
[16] a) N. S. George, K. E. Anderson, A. G. M. Barrett, *Eur. J. Org. Chem.* **2013**, 7604; b) C. A. Citron, P. Rabe, L. Barra, C. Nakano, T. Hoshino, J. S. Dickschat, *Eur. J. Org. Chem.* **2014**, 7684.  
[17] R. L. Edelstein, V. A. Weller, M. D. Distefano, J. S. Tung, *J. Org. Chem.* **1998**, *63*, 5298.  
[18] a) S.-H. Kim, K. Heo, Y.-J. Chang, S.-H. Park, S.-K. Rhee, S.-U. Kim, *J. Nat. Prod.* **2006**, *69*, 758; b) C. L. Steele, J. Crock, J. Bohlmann, R. Croteau, *J. Biol. Chem.* **1998**, *273*, 2078.  
[19] a) F. Lopez-Gallego, S. A. Agger, D. Abate-Pella, M. D. Distefano, C. Schmidt-Dannert, *ChemBioChem* **2010**, *11*, 1093; b) S. Picaud, P. Mercke, X. He, O. Sterner, M. Brodelius, D. E. Cane, P. E. Brodelius, *Arch. Biochem. Biophys.* **2006**, *448*, 150.  
[20] Y. J. Hong, D. J. Tantillo, *Chem. Sci.* **2010**, *1*, 609.

Received: August 17, 2016

Published online: September 26, 2016

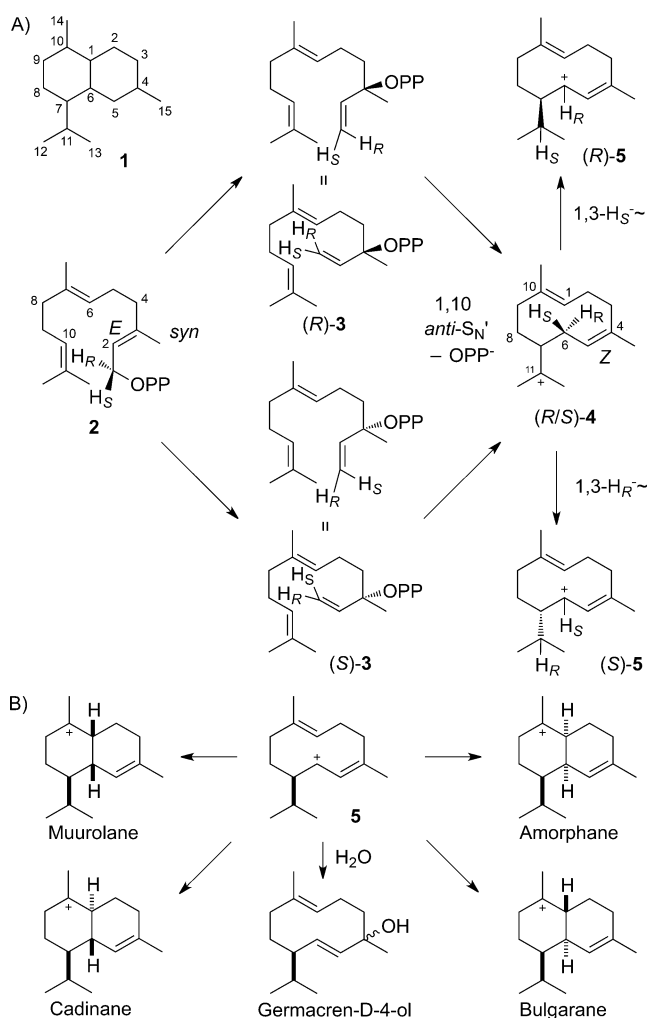
## Über 1,3-Hydridverschiebungen in Sesquiterpen-Cyclisierungen

Jan Rinkel, Patrick Rabe, Paolina Garbeva und Jeroen S. Dickschat\*

**Abstract:** Stereospezifisch markierte Vorstufen wurden mit sieben bakteriellen Sesquiterpencyclasen konvertiert, um den stereochemischen Verlauf ihrer initialen Kaskaden aus 1,10-Cyclisierung und 1,3-Hydridverschiebung zu untersuchen. Enzyme mit Produkten bekannter absoluter Konfiguration zeigten einen kohärenten stereochemischen Kurs, mit Ausnahme der (–)- $\alpha$ -Amorphen-Synthase, für die die erhaltenen Ergebnisse besser durch initiale 1,6-Cyclisierung erklärbar sind. Der Zusammenhang zwischen der absoluten Konfiguration des Produktes und dem stereochemischen Verlauf der 1,3-Hydridverschiebung ermöglichte die Zuordnung der absoluten Konfigurationen für drei Enzymprodukte, die unabhängig über die absolute Konfiguration des gemeinsamen Nebenproduktes Germacren-D-4-ol bestimmt wurden.

Die wohl komplexesten Kohlenstoffgerüste werden in der Natur von Terpencyclasen synthetisiert. Die mechanistischen Details der Reaktionen, die von dieser faszinierenden Klasse von Enzymen katalysiert werden, die simple Oligoprenyldiphosphate in (poly)cyclische Kohlenwasserstoffe oder Alkohole konvertieren, haben seit mehreren Jahrzehnten die wissenschaftliche Diskussion beflügelt.<sup>[1]</sup> Mit dem Aufkommen quantenchemischer Rechnungen werden sogar lange akzeptierte Mechanismen neu debattiert, wodurch unser Verständnis der Carbokationenchemie erweitert wird.<sup>[2]</sup> Klassische Isotopenmarkierungsexperimente erfahren zugleich einen neuerlichen Aufschwung und bieten einen komplementären Zugang zur Entdeckung überraschender Biosyntheseprozesse.<sup>[3]</sup> Eines der ersten Beispiele für detaillierte Einblicke in Terpencyclisierungsmechanismen ist mit den Arbeiten an Cadalan-Sesquiterpenen gegeben. Diese verbreitet auftretende Gruppe von Naturstoffen wird durch das Kohlenstoffgerüst **1** aus zwei sechsgliedrigen Ringen definiert, die eine Biosynthese über eine initiale Isomerisierung von Farnesyldiphosphat (FPP, **2**) zu Nerolidyldiphosphat (NPP, **3**) gefolgt von einer 1,10-Cyclisierung zum Helminthogermacrenyl-Kation **4** gemein haben (Schema 1 A). Durch diesen Prozess geht die (2E)-Doppelbindung in FPP in eine (4Z)-Doppelbindung in **4** über. Nach Arigonis Überlegungen über den Verbleib der C1-gebundenen Wasserstoffatome<sup>[4]</sup>

wurde der stereochemische Verlauf zu diversen Terpenoiden einschließlich (+)-1-*epi*-Cubenol aus *Streptomyces* sp. LL-B7,<sup>[5]</sup> den Cadalanen aus *Medicago truncatula*<sup>[6]</sup> sowie (–)- $\delta$ -Cadinen und (+)-T-Muurolool aus *S. clavuligerus*<sup>[7]</sup> in einer Reihe gut geplanter Experimente untersucht. In diesen Beispielen deuteten Inkubationsexperimente mit stereospezifisch deuterierten FPPs auf eine Kombination aus *syn*-allylischer Umlagerung zu NPP und *anti*-S<sub>N</sub>'-Ringschluss zum Kation **4**. Diese stereochemischen Erfordernisse resultieren in einer definierten absoluten Konfiguration an C6, unabhängig von der Natur des Intermediates (*R*)- oder (*S*)-NPP, dessen Identität alleine auf Basis dieser Experimente nicht



**Scheme 1.** A) Initiale 1,10-Cyclisierung von FPP über (*S*)- oder (*R*)-NPP zu Kation **5**. Dessen absolute Konfiguration ist mit den (in **2**) enantiotopen Wasserstoffen verknüpft, von denen nur eines stereospezifisch eine 1,3-Verschiebung eingeht. Dabei wandert H<sub>S</sub> im Fall von (*R*)-**5** wohingegen H<sub>R</sub> für die Reaktion zu (*S*)-**5** springt. B) Reaktionen von **5** zu Cadalanen und zu Germacren-D-4-ol.

[\*] J. Rinkel, Dr. P. Rabe, Prof. Dr. J. S. Dickschat  
Kekulé-Institut für Organische Chemie und Biochemie  
Rheinische Friedrich-Wilhelms-Universität Bonn  
Gerhard-Domagk-Straße 1, 53121 Bonn (Deutschland)  
E-Mail: dickschat@uni-bonn.de

Dr. P. Garbeva, Prof. Dr. J. S. Dickschat  
Nederlands Instituut voor Ecologie  
Koninklijke Nederlandse Akademie van Wetenschappen  
Droevendaalsesteeg 10, 6708 PB Wageningen (Niederlande)

Hintergrundinformationen und die Identifikationsnummer (ORCID) eines Autors sind unter <http://dx.doi.org/10.1002/ange.201608042> zu finden.

geklärt werden kann. Berücksichtigt man die räumliche Nähe des wandernden Wasserstoffatoms zu seinem Zielatom, so kann die folgende 1,3-Hydridverschiebung eines der beiden stereochemisch unterschiedlichen Wasserstoffatome  $H_S$  und  $H_R$  an C6 genutzt werden, um die Konfiguration an C7 abzuleiten. Die Bedeutung von Kation **5** als Vorstufe einer großen Diversität von Sesquiterpenen (Schema 1B) motiviert zu einer gründlichen Untersuchung des stereochemischen Verlaufes seiner Bildung – nicht nur aus mechanistischem Interesse, sondern auch, um die absoluten Konfigurationen von Terpenen ableiten zu können. Diese Information ist ansonsten insbesondere für im allgemeinen nicht gut kristallisierbare Kohlenwasserstoffe schlecht zugänglich.

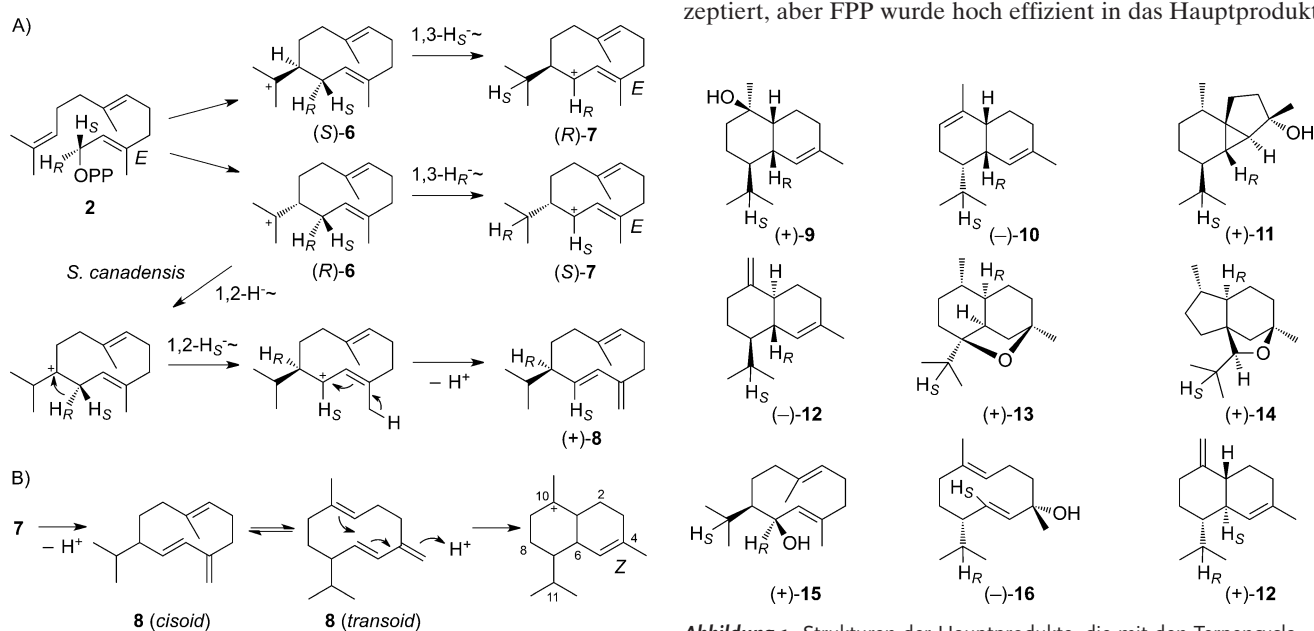
Neben den Cadalanen ist das Modell auch auf Germacrane anwendbar, mit dem wichtigen Unterschied einer (4*E*)- anstelle einer (4*Z*)-konfigurierten Doppelbindung (Schema 2A). Daher muss NPP formal für die Cyclisierung nicht berücksichtigt werden. Nach  $S_N2$ -artigem direktem Ringschluss zu Kation **6** führt eine 1,3-Hydridverschiebung zum Allylkation **7**, wobei  $H_S$  spezifisch in der Reaktion zu (*R*)-**7** wandert und eine Verschiebung von  $H_R$  zu (*S*)-**7** führt. Germacren D (**8**) wird als neutrales Intermediat diskutiert, das die Notwendigkeit von NPP zur Bildung einer (4*Z*)-Doppelbindung durch ein Gleichgewicht zwischen seinem cisoiden und transoiden Konformer und nachfolgende durch Protonierung induzierte Cyclisierung obsolet macht (Schema 2B).<sup>[4]</sup> Interessanterweise folgt die (–)-Germacren-D-Synthese aus *Solidago canadensis* dem üblichen Mechanismus über eine 1,3-Hydridverschiebung von (*R*)-**6** zu (*S*)-**7** mit

**Tabelle 1:** Untersuchte Sesquiterpencyclasen.

Nr.	Hauptprodukt(e)	Quellorganismus	Zugangscode
<i>Cadalane</i>			
1	(+)-T-Muurolol ( <b>9</b> )	<i>Roseiflexus castenholzii</i>	WP_012119179
2	(–)- $\alpha$ -Amorphen ( <b>10</b> )	<i>Streptomyces viridochromogenes</i>	WP_039931950
3	(+)-4- <i>epi</i> -Cubebol ( <b>11</b> )	<i>Streptosporangium roseum</i>	WP_012893303
4	(–)- $\gamma$ -Cadinen ( <b>12</b> )	<i>Chitinophaga pinensis</i>	WP_012792334
5	(+)-Corvolether A ( <b>13</b> ) und B ( <b>14</b> )	<i>Kitasatospora setae</i>	BAJ27126
<i>Germacrane</i>			
6	(+)-Germacradien-6-ol ( <b>15</b> )	<i>Streptomyces pratensis</i>	ADW03055
7	(–)-Germacren-D-4-ol ( <b>16</b> )	<i>Collimonas pratensis</i>	AMP04969

einer Verschiebung von  $H_R$ , während die Synthese für das Enantiomer (+)-Germacren D (**8**) aus derselben Pflanze die Transformation ebenfalls ausgehend von (*R*)-**6** über zwei konsekutive 1,2-Hydridverschiebungen katalysiert.<sup>[8]</sup> Weiterhin zeigt die Geosmin-Synthese aus *Streptomyces coelicolor* A3(2) einen umgekehrten stereochemischen Kurs für die 1,3-Hydridverschiebung unter Wanderung von  $H_S$  durch Reaktion von (*R*)-**6** aus einer unterschiedlichen Konformation zum Intermediat (*S*)-**7** auf dem Weg zum Nebenprodukt (–)-**8**.<sup>[9]</sup> Diese unterschiedlichen Ergebnisse veranlassten uns, die diskutierten Prinzipien auf einer breiteren Basis von Terpencyclasen zu studieren.

Zu diesem Zweck wurden die in Tabelle 1 gelisteten Enzyme verwendet. Die Terpensynthasen 1–6 wurden funktional exprimiert, und die Strukturen ihrer Produkte **9–15** (Abbildung 1) wurden mit ihren jeweiligen vollständigen NMR-Datensätzen in vorherigen Arbeiten publiziert,<sup>[10–12]</sup> lediglich die absoluten Konfigurationen von (+)-4-*epi*-Cubebol und der Corvolether blieben unbekannt. Darüber hinaus wurde das Gen einer Terpencyclase aus *Collimonas pratensis*, das in den Expressionsvektor pACYCDuet-1 kloniert wurde, exprimiert.<sup>[13]</sup> Weder Geranyldiphosphat (GPP) noch Geranylgeranyldiphosphat (GGPP) wurden vom Enzym akzeptiert, aber FPP wurde hoch effizient in das Hauptprodukt



**Schema 2.** A) Stereochemisches Modell für Germacrane. B) Alternative Cyclisierung zu Cadalanen über Germacren D (**8**).

**Abbildung 1.** Strukturen der Hauptprodukte, die mit den Terpencyclasen 1–7 (Tabelle 1) erhalten wurden, und Ergebnisse der Inkubationsexperimente mit (1*R*)- und (1*S*)-(1-<sup>2</sup>H)FPP.



Germacren-D-4-ol (**16**) überführt, das isoliert wurde und zu einem synthetischen Standard<sup>[14]</sup> und der aus *Pinus sylvestris* isolierten Verbindung identische NMR-Spektren zeigte.<sup>[15]</sup> Der Drehwert wies weiterhin dasselbe Vorzeichen wie die Verbindung aus *Pinus sylvestris* auf ( $[\alpha]_D^{20} = -93$ ,  $c = 0.20$ , (<sup>2</sup>H<sub>6</sub>)Benzol; Lit.:  $[\alpha]_D^{25} = -181$ ,  $c = 0.61$ , CHCl<sub>3</sub>),<sup>[15]</sup> wodurch der Naturstoff aus *C. pratensis* als (–)-(4*S*,7*S*)-Germacren-D-4-ol etabliert wurde. Einige Nebenprodukte der Germacren-D-4-ol-Synthase wurden per GC/MS identifiziert (siehe Abbildung S1 in den Hintergrundinformationen), von denen eines ( $\gamma$ -Cadinen, **12**) für die weitere Diskussion von Belang ist. Um eine mögliche Rolle des neutralen Intermediates Germacren D (Schema 2B) für die sieben Cyclasen zu erkennen, wurden Inkubationsexperimente mit FPP in <sup>2</sup>H<sub>2</sub>O-Puffer durchgeführt.<sup>[6]</sup> Abgesehen vom Fall der Corvolether, die bekanntlich durch Reprotonierung des neutralen Intermediates **16** gebildet werden,<sup>[11]</sup> konnte kein Einbau von Deuterium per GC/MS beobachtet werden, was eine vernachlässigbare Rolle von Germacren D für die Cyclisierungsmechanismen aller sieben Enzyme anzeigt.

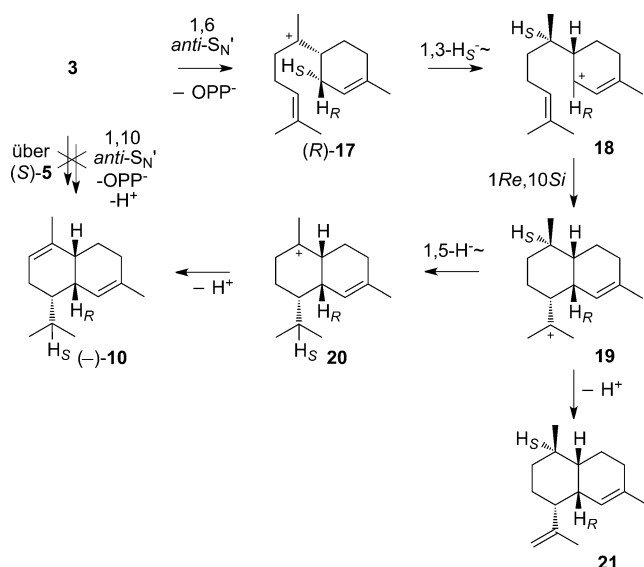
Für einen schnellen und empfindlichen <sup>13</sup>C-NMR-basierenden Test der auftretenden 1,3-Hydridverschiebungen wurde (11-<sup>13</sup>C,1,1-<sup>2</sup>H<sub>2</sub>)FPP in vier Schritten aus (10-<sup>13</sup>C)Geranylaceton synthetisiert, das selbst über eine zuvor berichtete Route aus Geraniol zugänglich ist<sup>[16]</sup> (Schema S1). Dessen Inkubation mit allen sieben Enzymen gefolgt von Extraktion mit (<sup>2</sup>H<sub>6</sub>)Benzol und direkter <sup>13</sup>C-NMR-Analyse resultierte in der Beobachtung stark erhöhter Triplets für C11 der Hauptprodukte, die sich aufgrund einer <sup>13</sup>C-<sup>2</sup>H-Spin-Spin-Kopplung ergeben und für die 1,3-Hydridwanderung indikativ sind (Abbildung S2). In den Fällen der Synthesen für 4-*epi*-Cubebol, die Corvolether,  $\gamma$ -Cadinen und Germacradien-6-ol erschien ein zusätzliches Triplett in den Spektren, dessen chemische Verschiebung auf C11 von **16** passte, das aus Kation **5** durch den Angriff von Wasser hervorgehen kann.

Um die stereochemischen Verläufe der beobachteten Hydridverschiebungen zu studieren, wurden (1*R*)- und (1*S*)-(1-<sup>2</sup>H)FPP unter Verwendung einer Reduktion von (1-<sup>2</sup>H)Farnesal mit Alpine-Boran<sup>[17]</sup> als Schlüsselschritt synthetisiert (Schema S2). Die beiden Enantiomere (1*R*)- und (1*S*)-(1-<sup>2</sup>H)Farnesol wurden mit > 95 % *ee* erhalten, wie durch eine Analyse von Mosher-Estern nachgewiesen wurde (Abbildung S3). Die EI-Massenspektren aller Enzymprodukte **9–16** zeigen eine starke Abspaltung der Isopropylgruppe. Somit kann Deuterium innerhalb dieser Isopropylgruppe (*m/z* 161) oder im anderen Teil des Analyten (*m/z* 162) für jede Verbindung lokalisiert werden, die aus (1*R*)- oder (1*S*)-(1-<sup>2</sup>H)FPP erhalten wurde (Abbildung S4). Für die Hauptprodukte **9** und **12** der Enzyme 1 und 4, für die die absoluten Konfigurationen bekannt sind, wurde der erwartete stereochemische Kurs beobachtet, d. h. Wanderung von H<sub>5</sub> in der Bildung von (*R*)-**5** aus (*S*)-**4**. Bemerkenswerterweise wurde ein gegensätzlicher stereochemischer Verlauf für **12** in Abhängigkeit von seiner enzymatischen Quelle beobachtet. Während für die  $\gamma$ -Cadinen-Synthase aus *Chitinophaga pinensis* H<sub>5</sub> wandert, wird Gegenteiliges (Wanderung von H<sub>R</sub>) für das Nebenprodukt **12** der Germacren-D-4-ol-Synthase aus *C. pratensis* gefunden. Auf Basis des Modells führt diese Beobachtung auf die Zuordnung unterschiedlicher absoluter

Konfigurationen für **12**, was durch eine Trennung der Produkte durch GC an einer homochiralen stationären Phase bestätigt wurde (Abbildung S5). Die abgeleitete absolute Konfiguration von (+)-**12** für das Nebenprodukt der Terpensynthase aus *Collimonas* ist in Übereinstimmung mit der absoluten Konfiguration des Hauptproduktes (4*S*,7*S*)-**16**. Die Bildung von **12** durch die Germacren-D-4-ol-Synthase aus *C. pratensis* weist ebenfalls darauf hin, dass **16** über NPP und Kation **4**, aber nicht über direkte Cyclisierung von FPP zu **6** gebildet wird. Die Bildung von **15**, einer Verbindung mit bekannter absoluter Konfiguration, durch die Germacradien-6-ol-Synthase aus *Streptomyces pratensis* muss hingegen einem direkten Cyclisierungsmechanismus von FPP folgen. Inkubationen von (1*R*)- und (1*S*)-(1-<sup>2</sup>H)FPP mit Enzym 6 zeigten den erwarteten stereochemischen Verlauf mit Wanderung von H<sub>5</sub> an. Die absoluten Konfigurationen von (+)-4-*epi*-Cubebol, (+)-Corvolether A und (+)-Corvolether B sind unbekannt, konnten aber aus der beobachteten Verschiebung von H<sub>5</sub> abgeleitet werden, die auf eine Biosynthese über (*R*)-**5** hinweist (Cyclisierungsmechanismen für **11**, **13** und **14** sind in Schema S3 gezeigt). Die absoluten Konfigurationen aller drei Verbindungen wurden unabhängig auf Grundlage des Nebenproduktes (4*R*,7*R*)-**16** bestätigt, das per GC an homochiraler stationärer Phase klar von seinem Enantiomer getrennt werden konnte, das mithilfe der Terpenyclase aus *Collimonas* erhalten wurde. Entsprechendes galt für das Nebenprodukt (4*R*,7*R*)-**16** der Enzyme 1, 4 und 6 (Abbildung S6).

Die (–)- $\alpha$ -Amorphen-Synthase lieferte auf den ersten Blick schlecht erklärbare Ergebnisse. Trotz der bekannten absoluten Konfiguration von **10** wie in Abbildung 1 gezeigt wurde die Wanderung von H<sub>5</sub> beobachtet. Darüber hinaus konnten im Unterschied zu den anderen untersuchten Systemen keine Spuren von Germacren-D-4-ol in den Extrakten gefunden werden (für die T-Muurolol-Synthase war die Menge an Germacren-D-4-ol per NMR nicht detektierbar, Abbildung S2, aber per GC/MS konnten Spuren detektiert werden, Abbildung S6). Für Amorpha-4,11-dien und die Amorphene wurden Cyclisierungsmechanismen über eine initiale 1,10-Cyclisierung vorgeschlagen,<sup>[18]</sup> aber für Amorpha-4,11-dien wurde auch ein Mechanismus über initiale 1,6-Cyclisierung ins Spiel gebracht.<sup>[18a,19]</sup> Dieser Mechanismus startet von NPP (**3**) über eine *anti*-S<sub>N</sub>'-Cyclisierung zum (*R*)-Bisabolyll-Kation (**17**) (Schema 3). Induziert durch das benachbarte Stereozentrum wandert spezifisch H<sub>5</sub> in einer 1,3-Hydridverschiebung zur Bildung von Kation **18**. Eine folgende 1*Re*,10*Si*-Cyclisierung führt zu Kation **19**, der Vorstufe von Amorpha-4,11-dien (**21**) per Deprotonierung. Das ursprüngliche H<sub>5</sub> kann nun in einer 1,5-Wasserstoffverschiebung zum Amorphenyl-Kation **20** reagieren, das zu (–)- $\alpha$ -Amorphen (**10**) deprotoniert wird.

Jüngst haben Hong und Tantillo durch quantenchemische Rechnungen gezeigt, dass 1) in der initialen 1,3-Hydridverschiebung spezifisch H<sub>5</sub> wandern sollte, 2) die 1,5-Hydridverschiebung von **19** zu **20** eine niedrige Barriere aufweist, wodurch die Pfade zu Amorpha-4,11-dien und zu den Amorphenen verbunden sind, und 3) der Weg über eine initiale 1,6-Cyclisierung energetisch gegenüber dem mit initialer 1,10-Cyclisierung bevorzugt ist.<sup>[20]</sup> Der Weg in Schema 3 erklärt unsere experimentelle Beobachtung der Wanderung



**Schema 3.** Stereochemisches Modell der vorgeschlagenen 1,6-Cyclisierung in der (–)- $\alpha$ -Amorphen-Biosynthese, verglichen mit dem erwarteten Verlauf in der 1,10-Cyclisierung.

von  $H_S$  nach C11 von **10**, wodurch ein erster experimenteller Nachweis für das Modell von Hong und Tantillo gegeben ist. Weiterhin erklärt die Verwendung eines anderen Weges zu **10** als zu den übrigen Cadalan-Sesquiterpenen, die in dieser Studie diskutiert werden, die Abwesenheit von Germacren-D-4-ol in den Enzymreaktionen mit der  $\alpha$ -Amorphen-Synthese.

In Summe haben wir eine neue bakterielle Terpen cyclase aus *Collimonas pratensis* als (–)-Germacren-D-4-ol-Synthase charakterisiert. Inkubationsexperimente mit (11- $^{13}C$ ,1,1- $^2H$ )FPP offenbarten einen Deuteriumtransfer von C1 nach C11 für sieben bakterielle Terpen cyclasen, während die Verwendung von stereospezifisch markiertem (1*R*)- und (1*S*)-(1- $^2H$ )FPP zeigte, dass das Schicksal der enantiotopen Wasserstoffatome an C1 mit der absoluten Konfiguration des Produktes verknüpft ist. Dieses Wissen konnte genutzt werden, um die zuvor unbekannt absoluten Konfigurationen von drei Terpenen abzuleiten. Die Zuordnungen wurden unabhängig durch Analyse des gemeinsamen Nebenproduktes Germacren-D-4-ol per GC an homochiraler stationärer Phase bestätigt. Nur für die  $\alpha$ -Amorphen-Synthese ergaben die Experimente mit (1*R*)- und (1*S*)-(1- $^2H$ )FPP Unstimmigkeiten gegenüber dem Modell, die Ergebnisse sind jedoch mithilfe eines jüngst auf Basis von quantenchemischen Rechnungen entwickelten Mechanismus über initiale 1,6-Cyclisierung erklärbar,<sup>[20]</sup> sodass hier ein erster experimenteller Nachweis erfolgt.

### Danksagung

Diese Arbeiten wurden durch die DFG (DI1536/7-1) und durch den Fonds der Chemischen Industrie mit einem Doktorandenstipendium an J.R. unterstützt. Dies ist Publikation Nr. 6159 des Niederländischen Institutes für Ökologie (NIOO-KNAW).

**Stichwörter:** Biosynthese · Hydridverschiebungen · Isotope · Stereochemie · Terpene

**Zitierweise:** *Angew. Chem. Int. Ed.* **2016**, *55*, 13593–13596  
*Angew. Chem.* **2016**, *128*, 13791–13794

- [1] a) J. S. Dickschat, *Nat. Prod. Rep.* **2016**, *33*, 87; b) D. W. Christianson, *Chem. Rev.* **2006**, *106*, 3412; c) D. E. Cane, *Chem. Rev.* **1990**, *90*, 1089.
- [2] D. J. Tantillo, *Nat. Prod. Rep.* **2011**, *28*, 1035.
- [3] a) J. Rinkel, J. S. Dickschat, *Beilstein J. Org. Chem.* **2015**, *11*, 2493; b) A. Meguro, Y. Motoyoshi, K. Teramoto, S. Ueda, Y. Totsuka, Y. Ando, T. Tomita, S.-Y. Kim, T. Kimura, M. Igarashi, R. Sawa, T. Shinada, M. Nishiyama, T. Kuzuyama, *Angew. Chem. Int. Ed.* **2015**, *54*, 4353; *Angew. Chem.* **2015**, *127*, 4427; c) Y. Matsuda, T. Mitsuhashi, S. Lee, N. Hoshino, T. Mori, M. Okada, H. Zhang, F. Hayashi, M. Fujita, I. Abe, *Angew. Chem. Int. Ed.* **2016**, *55*, 5785; *Angew. Chem.* **2016**, *128*, 5879; d) Y. Ye, A. Minami, A. Mandi, C. Liu, T. Taniguchi, T. Kuzuyama, K. Monde, K. Gomi, H. Oikawa, *J. Am. Chem. Soc.* **2015**, *137*, 11846; e) I. Burkhardt, T. Siemon, M. Henrot, L. Studt, S. Rösler, B. Tudzynski, M. Christmann, J. S. Dickschat, *Angew. Chem. Int. Ed.* **2016**, *55*, 8748; *Angew. Chem.* **2016**, *128*, 8890; f) P. Rabe, A. Janusko, B. Goldfuss, J. S. Dickschat, *ChemBioChem* **2016**, *17*, 146; g) P. Rabe, J. Rinkel, T. A. Klapschinski, L. Barra, J. S. Dickschat, *Org. Biomol. Chem.* **2016**, *14*, 158.
- [4] D. Arigoni, *Pure Appl. Chem.* **1975**, *41*, 219.
- [5] D. E. Cane, M. Tandon, *J. Am. Chem. Soc.* **1995**, *117*, 5602.
- [6] S. Garms, T. G. Köllner, W. Boland, *J. Org. Chem.* **2010**, *75*, 5590.
- [7] Y. Hu, W. K. Chou, R. Hopson, D. E. Cane, *Chem. Biol.* **2011**, *18*, 32.
- [8] a) C. O. Schmidt, H. J. Bouwmeester, S. Franke, W. A. König, *Chirality* **1999**, *11*, 353; b) M. Niwa, M. Iguchi, S. Yamamura, *Chem. Pharm. Bull.* **1980**, *28*, 997.
- [9] X. He, D. E. Cane, *J. Am. Chem. Soc.* **2004**, *126*, 2678.
- [10] a) P. Rabe, J. S. Dickschat, *Angew. Chem. Int. Ed.* **2013**, *52*, 1810; *Angew. Chem.* **2013**, *125*, 1855; b) J. S. Dickschat, K. A. K. Pahirulzaman, P. Rabe, T. A. Klapschinski, *ChemBioChem* **2014**, *15*, 810; c) P. Rabe, T. Schmitz, J. S. Dickschat, *Beilstein J. Org. Chem.* **2016**, *12*, 1839.
- [11] P. Rabe, K. A. K. Pahirulzaman, J. S. Dickschat, *Angew. Chem. Int. Ed.* **2015**, *54*, 6041; *Angew. Chem.* **2015**, *127*, 6139.
- [12] P. Rabe, L. Barra, J. Rinkel, R. Riclea, C. A. Citron, T. A. Klapschinski, A. Janusko, J. S. Dickschat, *Angew. Chem. Int. Ed.* **2015**, *54*, 13448; *Angew. Chem.* **2015**, *127*, 13649.
- [13] C. Song, R. Schmidt, V. de Jager, D. Krzyzanowska, E. Jongedijk, K. Cankar, J. Beekwilder, A. van Veen, W. de Boer, J. A. van Veen, P. Garbeva, *BMC Genomics* **2015**, *16*, 1103.
- [14] O. Smitt, H.-E. Högberg, *Synlett* **2002**, 1273.
- [15] O. Nordin, E. Hedenström, H. E. Högberg, *Acta Chem. Scand.* **1999**, *53*, 124.
- [16] a) N. S. George, K. E. Anderson, A. G. M. Barrett, *Eur. J. Org. Chem.* **2013**, 7604; b) C. A. Citron, P. Rabe, L. Barra, C. Nakano, T. Hoshino, J. S. Dickschat, *Eur. J. Org. Chem.* **2014**, 7684.
- [17] R. L. Edelstein, V. A. Weller, M. D. Distefano, J. S. Tung, *J. Org. Chem.* **1998**, *63*, 5298.
- [18] a) S.-H. Kim, K. Heo, Y.-J. Chang, S.-H. Park, S.-K. Rhee, S.-U. Kim, *J. Nat. Prod.* **2006**, *69*, 758; b) C. L. Steele, J. Crock, J. Bohlmann, R. Croteau, *J. Biol. Chem.* **1998**, *273*, 2078.
- [19] a) F. Lopez-Gallego, S. A. Agger, D. Abate-Pella, M. D. Distefano, C. Schmidt-Dannert, *ChemBioChem* **2010**, *11*, 1093; b) S. Picaud, P. Mercke, X. He, O. Sterner, M. Brodelius, D. E. Cane, P. E. Brodelius, *Arch. Biochem. Biophys.* **2006**, *448*, 150.
- [20] Y. J. Hong, D. J. Tantillo, *Chem. Sci.* **2010**, *1*, 609.

Eingegangen am 17. August 2016

Online veröffentlicht am 26. September 2016

# Appendix C

## Terpene Cyclases from Social Amoebae

*Angew. Chem. Int. Ed.* **2016**, *55*, 15420–15423.

DOI:10.1002/anie.201608971

&

*Angew. Chem.* **2016**, *128*, 15646–15649.

DOI:10.1002/ange.201608971



## Terpenes

International Edition: DOI: 10.1002/anie.201608971  
German Edition: DOI: 10.1002/ange.201608971

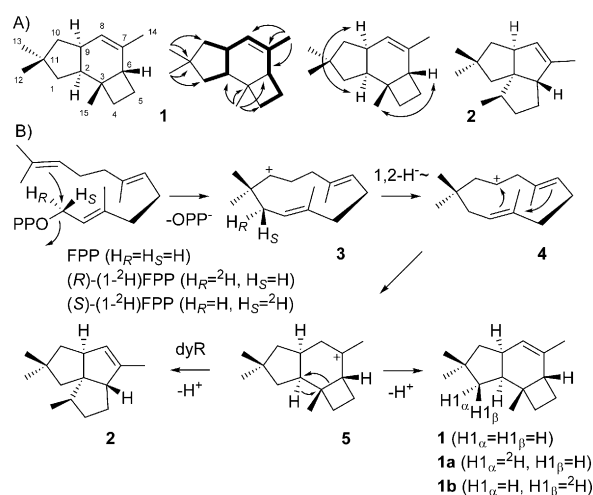
## Terpene Cyclases from Social Amoebae

Patrick Rabe, Jan Rinkel, Britta Nubbemeyer, Tobias G. Köllner, Feng Chen, and Jeroen S. Dickschat\*

**Abstract:** Genome sequences of social amoebae reveal the presence of terpene cyclases (TCs) in these organisms. Two TCs from *Dictyostelium discoideum* converted farnesyl diphosphate into (2*S*,3*R*,6*S*,9*S*)-(–)-protoillud-7-ene and (3*S*)-(+)-asterisca-2(9),6-diene. The enzyme mechanisms and EI-MS fragmentations of the products were studied by labeling experiments.

**T**ype I terpene cyclases (TCs) convert oligoprenyl diphosphates (OPPs) into terpenes by diphosphate (PP) abstraction and multistep cyclizations via cationic intermediates.<sup>[1]</sup> Their crystal structures display a (Mg<sup>2+</sup>)<sub>3</sub> cluster in the active site that binds to the substrate's PP, an aspartate-rich motif (DDXXD), an NSE/DTE triad (NSE in bacteria/fungi, DTE in plants), and a RY dimer.<sup>[2]</sup> Bacterial selinadiene synthase shows an induced fit mechanism in which a conserved arginine (PP sensor, Arg178) located on helix G moves upon substrate binding to install hydrogen bonds to its PP.<sup>[2c]</sup> The carbonyl group of Gly182 (effector) shifts towards C3 of the substrate and assists in ionization by donating electron density into the π\* orbital of the C2=C3 bond. While the same structural situation is found in fungal TCs, plant enzymes also show a PP sensor, but that is located on helix H. Microbial TCs and microbial type TCs from plants<sup>[3]</sup> are composed of a single α domain, while typical plant enzymes consist of αβ or αβγ domains, but only the α domain plays a role in catalysis.<sup>[4]</sup> Recently the genomes of several social amoebae were sequenced.<sup>[5]</sup> These soil organisms have uni- and multicellular life stages and encode a large number of secondary metabolite genes, but knowledge about the metabolites is lacking. While terpene production by bacteria, fungi, and plants is well established,<sup>[6]</sup> only recent work showed that the social amoeba *Dictyostelium discoideum* produces terpenes depending on its developmental stage.<sup>[7]</sup> Herein we describe the first characterization of TCs from *D. discoideum* and isotopic labeling experiments<sup>[8]</sup> to investigate the enzyme mechanisms and EI-MS fragmentations of their products.

A phylogenetic analysis<sup>[7]</sup> showed that TCs from social amoebae are most closely related to fungal enzymes (Figure S1 in the Supporting Information). Two of the eleven TC genes from *D. discoideum* AX4 (*DdTPS1-11*) were expressed in *Escherichia coli* (Figure S2). Both proteins DdTPS6 and DdTPS2 exhibit all highly conserved motifs as in bacterial and fungal enzymes (Figure S3). Incubation of DdTPS6 with farnesyl diphosphate (FPP) resulted in a major sesquiterpene (**1**) and traces of pentalenene (**2**, Scheme 1 A, Figure S4),



**Scheme 1.** A) Protoillud-7-ene (**1**), continuous spin system (bold), key HMBC and NOESY correlations (single and double headed arrows), and pentalenene (**2**). B) Cyclization of FPP to **1** and **2**.

while no products were obtained from geranyl (GPP) and geranylgeranyl diphosphate (GGPP). Compound **1** was purified and analyzed by NMR spectroscopy, resulting in the structure of protoillud-7-ene (**1**; Table S1 and Figures S5–S12). The relative configuration was determined by NOESY revealing two *cis*-fused ring systems (Scheme 1 A and Figure S13). The skeleton was confirmed by <sup>13</sup>C,<sup>13</sup>C-COSY analysis<sup>[9]</sup> of (<sup>13</sup>C<sub>15</sub>)-**1** obtained enzymatically from (<sup>13</sup>C<sub>15</sub>)FPP.<sup>[9a]</sup> The <sup>13</sup>C NMR data were identical to those for synthetic *rac*-**1** (two reported shifts need correction, Table S1),<sup>[10]</sup> but the optical rotation of **1** ( $[\alpha]_D^{21} = -54.3$ , *c* 0.05, C<sub>6</sub>D<sub>6</sub>) did not allow conclusions to be drawn on the absolute configuration.

The biosynthesis of **1** (Scheme 1 B) starts by 1,11-cyclization of FPP to the humulyl cation (**3**). A 1,2-hydride shift to **4** and cyclization furnishes the protoilludyl cation (**5**) that yields **1** upon deprotonation, while **2** is formed from **5** by dyotropic rearrangement and deprotonation.<sup>[11]</sup> Notably, pentalenene synthase (PS) from *Streptomyces exfoliatus* UC5319 converts

[\*] Dr. P. Rabe, J. Rinkel, B. Nubbemeyer, Prof. Dr. J. S. Dickschat  
 Kekulé-Institut für Organische Chemie und Biochemie  
 Rheinische Friedrich-Wilhelms-Universität Bonn  
 Gerhard-Domagk-Strasse 1, 53121 Bonn (Germany)  
 E-mail: dickschat@uni-bonn.de

Dr. T. G. Köllner  
 Max Planck Institute for Chemical Ecology  
 Hans-Knöll-Strasse 8, 07745 Jena (Germany)

Prof. Dr. F. Chen  
 Department of Plant Sciences, University of Tennessee  
 2431 Joe Johnson Drive, Knoxville, TN 37996-4561 (USA)

Supporting information and the ORCID identification number(s) for the author(s) of this article can be found under <http://dx.doi.org/10.1002/anie.201608971>.

FPP into **2** as a single product, but the H309A mutant also makes minor amounts of protoillud-6-ene, a double bond isomer of **1**.<sup>[12]</sup> Enzymatic conversion of (*R*)- and (*S*)-(1-<sup>2</sup>H)FPP with PS and presilphiperfolan-8 $\beta$ -ol synthase from *Botrytis cinerea* revealed inversion of configuration at C1 in the 1,11-cyclization to **3**.<sup>[13]</sup> Assuming the same mechanism for DdTPS6, the absolute configuration of **1** was determined by conversion of (*R*)-(1-<sup>2</sup>H)FPP that was synthesized with 95% *ee* (Figure S14).<sup>[14]</sup> <sup>1</sup>H NMR spectroscopic analysis of the product **1a** showed introduction of labeling into H1 $_{\alpha}$  by a simplified multiplicity of the signal for H2 (Figure 1A) and a strongly reduced cross peak for the H1 $_{\alpha}$ -C1 correlation in the HSQC spectrum (Figure 1B). Consistent results were obtained for **1b** from (*S*)-(1-<sup>2</sup>H)FPP (98% *ee*, Figure S14). Together, these data revealed the absolute configuration of (2*S*,3*R*,6*S*,9*S*)-**1**. GC analysis on a chiral stationary phase showed identical retention times for **2** from DdTPS6 and from *Streptomyces arenae* Tü469<sup>[15]</sup> encoding a PS with high homology to the *S. exfoliatus* enzyme (Figure S15), which

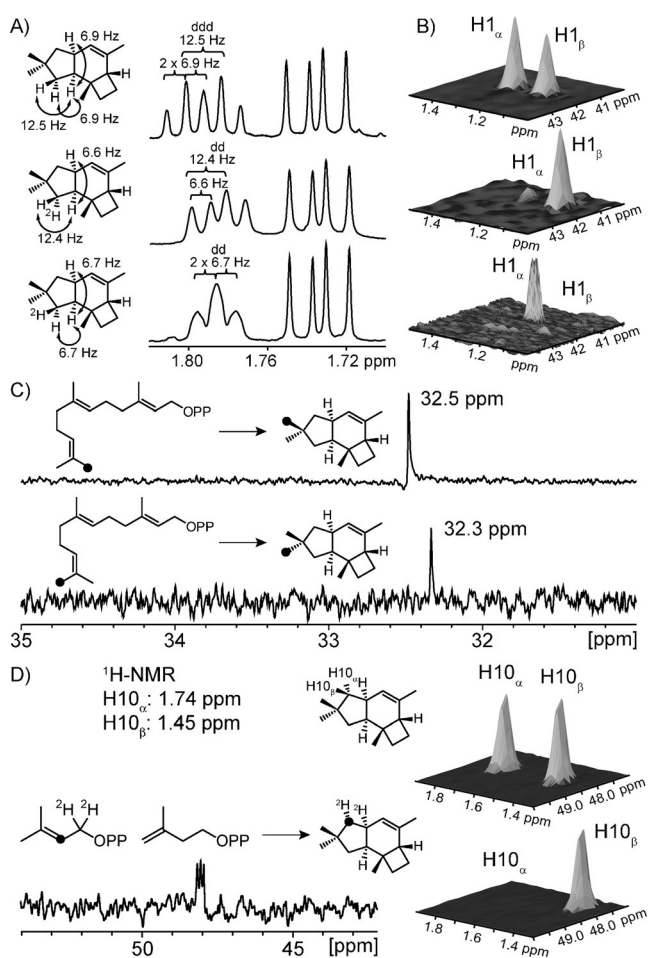
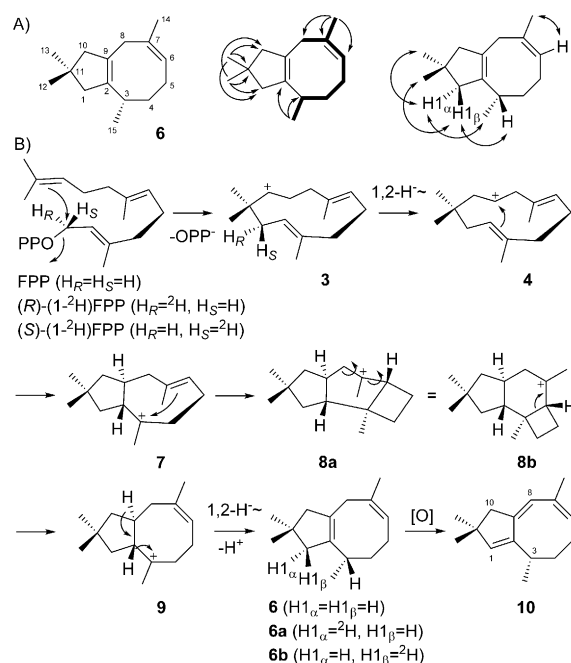


**Figure 1.** Analysis of **1**, **1a**, and **1b** by A) <sup>1</sup>H NMR and B) HSQC spectroscopy. C) <sup>13</sup>C NMR spectra of labeled **1** obtained enzymatically from (12-<sup>13</sup>C)- and (13-<sup>13</sup>C)FPP. D) Partial HSQC spectrum for C10 of unlabeled **1** showing cross peaks for H10 $_{\alpha}$  and H10 $_{\beta}$ , <sup>13</sup>C NMR and HSQC spectrum for C10 of (10-<sup>13</sup>C,9,10-<sup>2</sup>H<sub>2</sub>)-**1** obtained enzymatically from (2-<sup>13</sup>C,1,1-<sup>2</sup>H<sub>2</sub>)DMAPP and IPP. Black dots indicate <sup>13</sup>C-labeled carbon atoms.

points to identical enantiomers of **2** and confirms the absolute configuration of **1** that is a new natural product.

Incubation of OPPs in D<sub>2</sub>O buffer can reveal reprotonation steps in terpene cyclizations by deuterium uptake.<sup>[16]</sup> However, such an experiment with DdTPS6 did not result in deuterium incorporation into **1** (Figure S16A), showing that  $\alpha$ -humulene or a similar compound is not an intermediate. The stereochemical course of the 1,11-cyclization to **1** in terms of the fate of the terminal *E*- and *Z*-methyl groups of FPP was shown by enzymatic conversion of (12-<sup>13</sup>C)- and (13-<sup>13</sup>C)FPP.<sup>[9a]</sup> Product analysis by <sup>13</sup>C NMR spectroscopy showed a tightly controlled 1,11-cyclization as reported for other TCs including PS (Figure 1C).<sup>[13b,17]</sup> A possibility to follow the proposed 1,2-hydride shift from **3** to **4** is by using (10-<sup>13</sup>C,9,9-<sup>2</sup>H<sub>2</sub>)FPP. However, its synthesis would require a multi-step manipulation.<sup>[18]</sup> Inspired by recent reports on bifunctional enzymes with OPP synthase and TC activity,<sup>[16g,19]</sup> (2-<sup>13</sup>C,1,1-<sup>2</sup>H<sub>2</sub>)dimethylallyl diphosphate (DMAPP) was synthesized in three steps (Scheme S1) and used with isopentenyl diphosphate (IPP) and the FPP synthase from *Streptomyces coelicolor* (WP\_011031165). Its gene was cloned by homologous recombination in yeast,<sup>[20]</sup> for the enzymatic synthesis of (10-<sup>13</sup>C,9,9-<sup>2</sup>H<sub>2</sub>)FPP (Scheme S2). Further conversion with DdTPS6 gave labeled **1** with a triplet for C-10 in the <sup>13</sup>C NMR spectrum (Figure 1D), indicating that deuterium was directly bound to the <sup>13</sup>C atom. The HSQC spectrum of labeled **1** revealed deuterium incorporation into H10 $_{\alpha}$ .

Incubation of DdTPS2 with FPP yielded a sesquiterpene hydrocarbon (**6**, Scheme 2, Figure S17), while no products were formed from GPP and GGPP. Structure elucidation by NMR spectroscopy including <sup>13</sup>C, <sup>13</sup>C-COSY of enzymatically prepared (<sup>13</sup>C<sub>15</sub>)-**6** resulted in the structure of asterisca-2(9),6-diene (Table S2 and Figures S18–S25) that was isolated before



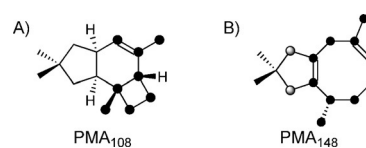
**Scheme 2.** A) Asterisca-2(9),6-diene (**6**), continuous spin system shown in bold, key HMBC and NOESY correlations (single and double headed arrows). B) Cyclization of FPP to **6** and autoxidation to **10**.

from the aeolid nudibranch *Phylloidesmium magnum*,<sup>[21]</sup> but the assigned absolute configuration was based on NMR methods that only allow for determination of the relative configuration (ROESY) and is thus doubtful. A peculiar problem of its biosynthesis is the required isomerization of the 6*E* double bond in FPP to the 6*Z* double bond in **6**. A plausible mechanism starts with 1,11-cyclization of FPP to **3** followed by a 1,2-hydride shift to **4** and cyclization to the (*E*)-cyclooctene **7**. Its strained nature induces cyclization to **8a**. A conformational rearrangement to **8b** allows for ring opening to **9** with a 6*Z* configuration, and final 1,2-hydride migration and deprotonation result in **6**. The enzymatic conversion of (*R*)- and (*S*)-(1-<sup>2</sup>H)FPP proceeded with incorporation of labeling into H1<sub>α</sub> of **6a** and H1<sub>β</sub> of **6b**, as determined by HSQC spectroscopy (Figure S26). Together with the observed NOESY correlation between H1<sub>α</sub> and H15, but not between H1<sub>β</sub> and H15, and an assumed inversion at C-1 in the 1,11-cyclization of FPP,<sup>[13]</sup> this allowed to conclude the absolute configuration of (3*S*)-**6**. The optical rotation ( $[\alpha]_{\text{D}}^{25} = -88.0$ ,  $c$  0.216, CDCl<sub>3</sub>) pointed to the same enantiomer in *P. magnum* ( $[\alpha]_{\text{D}}^{24} = -84.6$ ,  $c$  0.40, CHCl<sub>3</sub>).<sup>[21]</sup>

The cyclization mechanism of DdTPS2 was investigated by incubation of FPP in D<sub>2</sub>O that did not result in deuterium uptake (Figure S16B), suggesting that  $\alpha$ -humulene or a similar compound is not an intermediate towards **6**. The pathway to **6** was confirmed by enzymatic conversion of all 15 isotopomers of (<sup>13</sup>C<sub>1</sub>)FPP yielding labeled **6** with the <sup>13</sup>C marker in the expected positions (Figure S27). Specifically, <sup>13</sup>C NMR spectroscopic analysis of the products obtained from (12-<sup>13</sup>C)- and (13-<sup>13</sup>C)FPP revealed the corresponding stereochemical course for the geminal methyl groups of FPP as with DdTPS6 (Figure S28A). The second 1,2-hydride shift from **9** to **6** was evident from enzymatic conversion of (3-<sup>13</sup>C,2-<sup>2</sup>H)FPP, synthesized with a deuteration grade of 70% as reported,<sup>[17b]</sup> and product analysis by <sup>13</sup>C NMR spectroscopy that gave a triplet because of <sup>13</sup>C-<sup>2</sup>H spin coupling (Figure S28B). Similarly, incubation of (2-<sup>13</sup>C,1,1-<sup>2</sup>H<sub>2</sub>)DMAPP, IPP, *S. coelicolor* FPP synthase and DdTPS2 allowed to follow the 1,2-hydride migration from **3** to **4** (Figure S28C). Product analysis by GC/MS indicated the loss of deuterium in the final deprotonation (Figure S29). In this case the stereochemical course of the deuterium migration could not be followed, because both hydrogens H10<sub>α</sub> and H10<sub>β</sub> have the same chemical shifts ( $\delta = 2.16$  ppm). Overall, the initial cyclization steps from FPP to **4** including the stereochemical course with respect to the fate of C12 and C13 proved to be the same for both investigated TCs.

Prolonged reaction times of FPP incubation with DdTPS2 yielded a product with a mass of 202.1712 Da corresponding to C<sub>15</sub>H<sub>22</sub> (calculated: 202.1716 Da), likely formed by autoxidation in the presence of air. Its structure was elucidated by NMR spectroscopy (Table S3 and Figures S30–S35) as asterisca-1,6,8-triene (**10**, Scheme 2), a new natural product, while its absolute configuration (3*S*) was inferred from that of **6**. Furthermore, an unstable oxidation product C<sub>15</sub>H<sub>24</sub>O<sub>2</sub> was observed by GC/MS-QTOF. Incubation of isolated **6** in an enzyme-free buffer resulted in the formation of the same autoxidation products (kinetics of the formation and degradation of **6** are shown in Figure S36).

Following our previous studies on the EI-MS fragmentation mechanisms of terpenes,<sup>[9a,17b,22]</sup> **1** and **6** were investigated by enzymatic conversion of all 15 (<sup>13</sup>C<sub>1</sub>)FPP isotopomers. A position-specific mass shift analysis (PMA<sub>*m/z*</sub>) indicates which carbon atom, if <sup>13</sup>C-labeled, increases a fragment ion *m/z* by +1 and contributes to its formation (black in Scheme 3; mass spectra in Figures S37 and S38, further PMAs in Schemes S3–S5). If multiple mechanisms lead to fragment ions of the same mass that represent different parts of the skeleton, labeled carbon atoms that partially contribute to the ions of the respective mass only lead to a partial mass shift (gray in Scheme 3). Notably, the base peak ion of **1** is formed by loss of C1-2-9-10-11-12-13, while the base peak ion of **6** arises by cleavage of C11-12-13 plus C1 or C10. High-resolution MS<sup>2</sup> analyses (Figures S39–S45 and Tables S4–S10) further corroborated the fragmentation mechanisms.



**Scheme 3.** PMAs for EI-MS base peak ions of A) **1** and B) **6**. Black carbon atoms contribute fully and gray carbon atoms contribute partially to a fragment ion.

In summary, we have characterized the first two TCs from social amoebae that are by sequence most similar to fungal enzymes,<sup>[7]</sup> which is also reflected by the same localization of the PP sensor on helix G. Their products were identified as (2*S*,3*R*,6*S*,9*S*)-(–)-protoillud-7-ene, a new natural product, and (3*S*)-(+)-asterisca-2(9),6-diene that was previously reported from the mollusk *Phylloidesmium magnum*.<sup>[21]</sup> Both compounds are also present in *D. discoideum* headspace extracts.<sup>[7]</sup> While many TCs from plants, bacteria, and fungi have been characterized to date, it is intriguing to see that tapping social amoebae as an unexplored source of natural products gives access to a new chemical space. The cyclization mechanisms of DdTPS2 and DdTPS6 were investigated via isotopic labeling experiments, revealing the same initial 1,11-cyclization, while the terminal steps towards their unique products differed. These findings are in line with a fairly high sequence identity (46%). Because of the lack of specifically labeled material the complex EI-MS fragmentations of terpenes are difficult to investigate. Herein we have made the complete sets of (<sup>13</sup>C<sub>1</sub>)-labeled sesquiterpenes accessible, which allowed this problem to be addressed.

### Acknowledgements

This work was funded by the DFG (DI1536/7-1) and by the Fonds der Chemischen Industrie with a PhD scholarship to J.R.

**Keywords:** biosynthesis · isotopes · mass spectrometry · social amoebae · terpenes

How to cite: *Angew. Chem. Int. Ed.* **2016**, *55*, 15420–15423  
*Angew. Chem.* **2016**, *128*, 15646–15649

- [1] J. S. Dickschat, *Nat. Prod. Rep.* **2016**, *33*, 87.
- [2] a) C. M. Starks, K. Back, J. Chappell, J. P. Noel, *Science* **1997**, *277*, 1815; b) M. Köksal, Y. Jin, R. M. Coates, R. Croteau, D. W. Christianson, *Nature* **2011**, *469*, 116; c) P. Baer, P. Rabe, K. Fischer, C. A. Citron, T. A. Klapschinski, M. Groll, J. S. Dickschat, *Angew. Chem. Int. Ed.* **2014**, *53*, 7652; *Angew. Chem.* **2014**, *126*, 7783.
- [3] G.-L. Li, T. G. Köllner, Y. Yin, Y.-F. Jiang, H. Chen, Y. Xu, J. Gershenzon, E. Pichersky, F. Chen, *Proc. Natl. Acad. Sci. USA* **2012**, *109*, 14711.
- [4] E. Oldfield, F.-Y. Lin, *Angew. Chem. Int. Ed.* **2012**, *51*, 1124; *Angew. Chem.* **2012**, *124*, 1150.
- [5] a) L. Eichinger, J. A. Pachebat, G. Glöckner, M.-A. Rajandream, R. Sugang, M. Berriman, et al., *Nature* **2005**, *435*, 43; b) A. J. Heide, H. M. Lawal, M. Felder, C. Schilde, N. R. Helps, B. Tunggal, et al., *Genome Res.* **2011**, *21*, 1882–1891.
- [6] a) C. A. Citron, J. Gleitzmann, G. Laurenzano, R. Pukall, J. S. Dickschat, *ChemBioChem* **2012**, *13*, 202; b) Y. Yamada, T. Kuzuyama, M. Komatsu, K. Shin-ya, S. Omura, D. E. Cane, H. Ikeda, *Proc. Natl. Acad. Sci. USA* **2015**, *112*, 857; c) M. B. Quinn, C. M. Flynn, C. Schmidt-Dannert, *Nat. Prod. Rep.* **2014**, *31*, 1449; d) J. Degenhardt, T. G. Köllner, J. Gershenzon, *Phytochemistry* **2009**, *70*, 1621.
- [7] X. Chen, T. G. Köllner, Q. Jia, A. Norris, B. Santhanam, P. Rabe, J. S. Dickschat, G. Shaulsky, J. Gershenzon, F. Chen, *Proc. Natl. Acad. Sci. USA* **2016**, *113*, 12132.
- [8] J. Rinkel, J. S. Dickschat, *Beilstein J. Org. Chem.* **2015**, *11*, 2493.
- [9] a) P. Rabe, L. Barra, J. Rinkel, R. Riclea, C. A. Citron, T. A. Klapschinski, A. Janusko, J. S. Dickschat, *Angew. Chem. Int. Ed.* **2015**, *54*, 13448; *Angew. Chem.* **2015**, *127*, 13649; b) Y. Sugai, Y. Ueno, K. Hayashi, S. Oogami, T. Toyomasu, S. Matsumoto, M. Natsume, H. Nozaki, H. Kawaide, *J. Biol. Chem.* **2011**, *286*, 42840; c) G. A. Ellis, T. P. Wyche, C. G. Fry, D. R. Braun, T. S. Bugni, *Mar. Drugs* **2014**, *12*, 1013; d) T. P. Wyche, J. S. Piotrowski, Y. Hou, D. Braun, R. Deshpande, S. McIlwain, I. M. Ong, C. L. Myers, I. A. Guzei, W. M. Westler, D. R. Andes, T. S. Bugni, *Angew. Chem. Int. Ed.* **2014**, *53*, 11583; *Angew. Chem.* **2014**, *126*, 11767; e) L. Barra, K. Ibrom, J. S. Dickschat, *Angew. Chem. Int. Ed.* **2015**, *54*, 6637; *Angew. Chem.* **2015**, *127*, 6737.
- [10] H. Takeshita, I. Kouno, M. Iino, H. Iwabuchi, D. Nomura, *Bull. Chem. Soc. Jpn.* **1980**, *53*, 3641.
- [11] a) P. Gutta, D. J. Tantillo, *J. Am. Chem. Soc.* **2006**, *128*, 6172; b) L. Zu, M. Xu, M. W. Lodewyk, D. E. Cane, R. J. Peters, D. J. Tantillo, *J. Am. Chem. Soc.* **2012**, *134*, 11369.
- [12] M. Seemann, G. Zhai, K. Umezawa, D. E. Cane, *J. Am. Chem. Soc.* **1999**, *121*, 591.
- [13] a) D. E. Cane, J. S. Oliver, P. H. M. Harrison, C. Abell, B. R. Hubbard, C. T. Kane, R. Lattman, *J. Am. Chem. Soc.* **1990**, *112*, 4513; b) C.-M. Wang, R. Hopson, X. Lin, D. E. Cane, *J. Am. Chem. Soc.* **2009**, *131*, 8360.
- [14] J. Rinkel, P. Rabe, P. Garbeva, J. S. Dickschat, *Angew. Chem. Int. Ed.* **2016**, *55*, 13593; *Angew. Chem.* **2016**, *128*, 13791.
- [15] P. Rabe, C. A. Citron, J. S. Dickschat, *ChemBioChem* **2013**, *14*, 2345.
- [16] a) J. Jiang, X. He, D. E. Cane, *J. Am. Chem. Soc.* **2006**, *128*, 8128; b) D. J. Miller, J. Gao, D. G. Truhlar, N. J. Young, V. Gonzalez, R. K. Allemann, *Org. Biomol. Chem.* **2008**, *6*, 2346; c) P. Rabe, K. A. K. Pahirulzaman, J. S. Dickschat, *Angew. Chem. Int. Ed.* **2015**, *54*, 6041; *Angew. Chem.* **2015**, *127*, 6139; d) P. Rabe, J. Rinkel, T. A. Klapschinski, L. Barra, J. S. Dickschat, *Org. Biomol. Chem.* **2016**, *14*, 158; e) P. Rabe, A. Janusko, B. Goldfuss, J. S. Dickschat, *ChemBioChem* **2016**, *17*, 146; f) I. Burkhardt, T. Siemon, M. Henrot, L. Studt, S. Rösler, B. Tudzynski, M. Christmann, J. S. Dickschat, *Angew. Chem. Int. Ed.* **2016**, *55*, 8748; *Angew. Chem.* **2016**, *128*, 8890; g) Y. Matsuda, T. Mitsuhashi, S. Lee, M. Hoshino, T. Mori, M. Okada, H. Zhang, F. Hayashi, M. Fujita, I. Abe, *Angew. Chem. Int. Ed.* **2016**, *55*, 5785; *Angew. Chem.* **2016**, *128*, 5879.
- [17] a) D. E. Cane, T. Rossi, A. M. Tillman, J. P. Pachlatko, *J. Am. Chem. Soc.* **1981**, *103*, 1838; b) T. A. Klapschinski, P. Rabe, J. S. Dickschat, *Angew. Chem. Int. Ed.* **2016**, *55*, 10141; c) P. Rabe, T. Schmitz, J. S. Dickschat, *Beilstein J. Org. Chem.* **2016**, *12*, 1839; d) J. S. Dickschat, *Nat. Prod. Rep.* **2011**, *28*, 1917.
- [18] C. A. Citron, P. Rabe, L. Barra, C. Nakano, T. Hoshino, J. S. Dickschat, *Eur. J. Org. Chem.* **2014**, 7684.
- [19] a) T. Toyomasu, M. Tsukahara, A. Kaneko, R. Niida, W. Mitsuhashi, T. Dairi, N. Kato, T. Sassa, *Proc. Natl. Acad. Sci. USA* **2007**, *104*, 3084; b) R. Chiba, A. Minami, K. Gomi, H. Oikawa, *Org. Lett.* **2013**, *15*, 594; c) Y. Ye, A. Minami, A. Mandi, C. Liu, T. Taniguchi, T. Kuzuyama, K. Monde, K. Gomi, H. Oikawa, *J. Am. Chem. Soc.* **2015**, *137*, 11846; d) B. Qin, Y. Matsuda, T. Mori, M. Okada, Z. Quan, T. Mitsuhashi, T. Wakimoto, I. Abe, *Angew. Chem. Int. Ed.* **2016**, *55*, 1658; *Angew. Chem.* **2016**, *128*, 1690.
- [20] J. S. Dickschat, K. A. K. Pahirulzaman, P. Rabe, T. A. Klapschinski, *ChemBioChem* **2014**, *15*, 810.
- [21] S.-C. Mao, M. Gavagnin, E. Mollo, Y.-W. Guo, *Biochem. Syst. Ecol.* **2011**, *39*, 408.
- [22] a) P. Rabe, T. A. Klapschinski, J. S. Dickschat, *ChemBioChem* **2016**, *17*, 1333; b) P. Rabe, J. S. Dickschat, *Beilstein J. Org. Chem.* **2016**, *12*, 1380.

Received: September 13, 2016

Revised: October 26, 2016

Published online: November 10, 2016



## Terpene

Deutsche Ausgabe: DOI: 10.1002/ange.201608971  
Internationale Ausgabe: DOI: 10.1002/anie.201608971

## Terpencyclasen aus sozialen Amöben

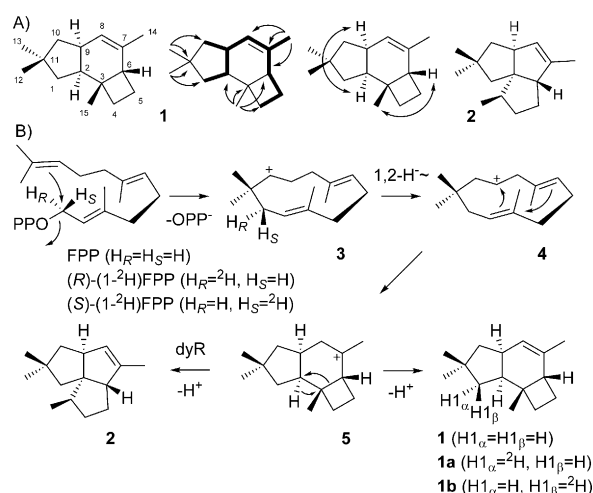
Patrick Rabe, Jan Rinkel, Britta Nubbemeyer, Tobias G. Köllner, Feng Chen und Jeroen S. Dickschat\*

**Abstract:** Genomsequenzierung von sozialen Amöben zeigte die Präsenz von Terpencyclasen (TCs) in diesen Organismen. Zwei TCs aus *Dictyostelium discoideum* konvertierten Farnesyldiphosphat in (2*S*,3*R*,6*S*,9*S*)-(–)-Protoillud-7-en und (3*S*)-(+)-Asterisca-2(9),6-dien. Die Enzymmechanismen und EI-MS-Fragmentierungen der Produkte wurden durch Markierungsexperimente studiert.

Typ-I-Terpencyclasen (TCs) konvertieren Oligoprenyldiphosphate (OPPs) in Terpene durch Abstraktion des Diphosphates (PP) und mehrstufige Cyclisierungen über kationische Intermediate.<sup>[1]</sup> Ihre Kristallstrukturen zeigen einen (Mg<sup>2+</sup>)<sub>3</sub>-Cluster im aktiven Zentrum, das an das PP des Substrates, ein Aspartat-reiches Motiv (DDXXD), eine NSE/DTE-Triade (NSE in Bakterien/Pilzen, DTE in Pflanzen) und ein RY-Dimer bindet.<sup>[2]</sup> Die bakterielle Selinadien-Synthase zeichnet sich durch einen Induced-Fit-Mechanismus aus, in dem ein in Helix G lokalisiertes, konserviertes Arginin (PP-Sensor, Arg 178) bei Substratbindung Wasserstoffbrücken zu dessen PP bildet.<sup>[2c]</sup> Die Carbonylgruppe von Gly 182 (Effektor) bewegt sich in Richtung auf C3 des Substrates und assistiert in der Ionisierung, indem Elektronendichte in das π\*-Orbital der C2=C3-Bindung doniert wird. Während für pilzliche TCs dieselbe Struktursituation gefunden wird, haben pflanzliche Enzyme ebenfalls einen PP-Sensor, der sich aber in Helix H befindet. Mikrobielle TCs und solche des mikrobiellen Typs aus Pflanzen<sup>[3]</sup> bestehen aus einer einzigen α-Domäne, während typische pflanzliche Enzyme eine αβ- oder αβγ-Domänenstruktur zeigen, wobei aber nur die α-Domäne in der Katalyse eine Rolle spielt.<sup>[4]</sup> Jüngst wurden die Genome einer Reihe sozialer Amöben sequenziert.<sup>[5]</sup> Diese Bodenorganismen haben ein- und vielzellige Lebensabschnitte und kodieren eine große Zahl von Genen für Sekundärmetaboliten, es fehlt aber die Kenntnis über die zugehörigen Naturstoffe. Die Terpenproduktion durch Bakterien, Pilze und Pflanzen ist gut etabliert,<sup>[6]</sup> aber erst jüngste Arbeiten ergaben, dass die soziale Amöbe *Dictyostelium*

*discoideum* Terpene in Abhängigkeit von der Entwicklungsstufe produziert.<sup>[7]</sup> Hier beschreiben wir die erste Charakterisierung von TCs aus *D. discoideum* und Isotopenmarkierungsexperimente<sup>[8]</sup> zur Untersuchung der Enzymmechanismen und EI-MS-Fragmentierung ihrer Produkte.

Eine phylogenetische Analyse<sup>[7]</sup> zeigte, dass TCs aus sozialen Amöben am nächsten mit pilzlichen Enzymen verwandt sind (Abbildung S1 der Hintergrundinformationen). Zwei der elf TC-Gene aus *D. discoideum* AX4 (*DdTPS1-11*) wurden in *Escherichia coli* exprimiert (Abbildung S2). Beide Proteine DdTPS6 und DdTPS2 weisen alle hochkonservierten Motive wie in bakteriellen und pilzlichen Enzymen auf (Abbildung S3). Inkubation von DdTPS6 mit Farnesyldiphosphat (FPP) resultierte in einem Hauptprodukt-Sesquiterpen (**1**) und Spuren von Pentalenen (**2**; Schema 1 A, Ab-



**Scheme 1.** A) Protoillud-7-en (**1**), kontinuierliches Spinsystem (fett), diagnostische HMBC- und NOESY-Korrelationen (einfache und Doppelpfeile) sowie Pentalenen (**2**). B) Cyclisierung von FPP zu **1** und **2**.

[\*] Dr. P. Rabe, J. Rinkel, B. Nubbemeyer, Prof. Dr. J. S. Dickschat  
Kekulé-Institut für Organische Chemie und Biochemie  
Rheinische Friedrich-Wilhelms-Universität Bonn  
Gerhard-Domagk-Straße 1, 53121 Bonn (Deutschland)  
E-Mail: dickschat@uni-bonn.de

Dr. T. G. Köllner  
Max-Planck-Institut für chemische Ökologie  
Hans-Knöll-Straße 8, 07745 Jena (Deutschland)

Prof. Dr. F. Chen  
Department of Plant Sciences, University of Tennessee  
2431 Joe Johnson Drive, Knoxville, TN 37996-4561 (USA)

Hintergrundinformationen und die Identifikationsnummer (ORCID) eines Autors sind unter <http://dx.doi.org/10.1002/ange.201608971> zu finden.

bildung S4), während aus Geranyl- (GPP) und Geranylgeranyldiphosphat (GGPP) keine Produkte erhalten wurden. Verbindung **1** wurde gereinigt und NMR-spektroskopisch als Protoillud-7-en (**1**) identifiziert (Tabelle S1 und Abbildungen S5–S12). Die relative Konfiguration wurde per NOESY bestimmt, was zwei *cis*-anellierte Ringsysteme aufzeigte (Schema 1 A und Abbildung S13). Das Gerüst wurde durch <sup>13</sup>C, <sup>13</sup>C-COSY-Analyse<sup>[9]</sup> von enzymatisch aus (<sup>13</sup>C<sub>15</sub>)FPP<sup>[9a]</sup> gewonnenem (<sup>13</sup>C<sub>15</sub>)-**1** bestätigt. Die <sup>13</sup>C-NMR-Daten waren identisch zu den für *rac*-**1** publizierten (zwei der berichteten chemischen Verschiebungen müssen korrigiert werden; Tabelle S1),<sup>[10]</sup> aber der Drehwert von **1** ([α]<sub>D</sub><sup>21</sup> = –54.3, *c* = 0.05,

$C_6D_6$ ) erlaubte keine Rückschlüsse auf die absolute Konfiguration.

Die Biosynthese von **1** (Schema 1B) startet mit einer 1,11-Cyclisierung von FPP zum Humulylkation (**3**). Eine 1,2-Hydridverschiebung zu **4** und Cyclisierung ergibt das Protoilludylkation (**5**), aus dem **1** durch Deprotonierung hervorgeht, während **2** durch dyotrope Umlagerung und Deprotonierung aus **5** gebildet wird.<sup>[11]</sup> Bemerkenswerterweise konvertiert die Pentalenen-Synthase (PS) aus *Streptomyces exfoliatus* UC5319 Farnesyldiphosphat in das einzige Produkt **2**, die H309A-Mutante erzeugt aber auch kleine Mengen an Protoillud-6-en, einem Doppelbindungsisomer von **1**.<sup>[12]</sup> Enzymatische Umwandlung von (*R*)- und (*S*)-(1-<sup>2</sup>H)FPP mit PS und Presilphiperfolan-8 $\beta$ -ol-Synthase aus *Botrytis cinerea* verlaufen mit Inversion der Konfiguration an C1 in der 1,11-Cyclisierung zu **3**.<sup>[13]</sup> Nimmt man für DdTPS6 denselben Mechanismus an, kann die absolute Konfiguration von **1** durch Umsetzung von (*R*)-(1-<sup>2</sup>H)FPP ermittelt werden, das mit 95% *ee* synthetisiert wurde (Abbildung S14).<sup>[14]</sup> Die <sup>1</sup>H-NMR-Analyse des Produktes **1a** ergab einen Einbau der Markierung in H1 $_{\alpha}$  aus der vereinfachten Multiplizität des Signals für H2 (Abbildung 1A) und dem stark reduzierten Kreuzpeak für die H1 $_{\alpha}$ -C1-Korrelation im HSQC-Spektrum (Abbildung 1B). Übereinstimmende Ergebnisse wurden für **1b** aus (*S*)-(1-<sup>2</sup>H)FPP gefunden (98% *ee*; Abbildung S14). Zusammen verweisen diese Daten auf die absolute Konfiguration von (2*S*,3*R*,6*S*,9*S*)-**1**. Die GC-Analyse an chiraler stationärer Phase ergab identische Retentionszeiten für **2** von DdTPS6 und aus *Streptomyces arenae* Tü469,<sup>[15]</sup> der eine PS mit hoher Homologie zum Enzym aus *S. exfoliatus* kodiert (Abbildung S15), was für identische Enantiomere von **2** spricht und die absolute Konfiguration des neuen Naturstoffes **1** bestätigt.

Die Inkubation von OPPs in D<sub>2</sub>O-Puffer kann Reprotonierungsschritte in Terpencyclisierungen durch Deuteriumaufnahme aufdecken.<sup>[16]</sup> Ein solches Experiment mit DdTPS6 ergab keinen Deuteriumeinbau in **1** (Abbildung S16A), sodass  $\alpha$ -Humulen oder eine ähnliche Verbindung nicht als Intermediat in Betracht kommen. Der stereochemische Verlauf der 1,11-Cyclisierung zu **1** hinsichtlich des Schicksals der terminalen *E*- und *Z*-Methylgruppen von FPP wurde durch enzymatische Konversion von (12-<sup>13</sup>C)- und (13-<sup>13</sup>C)FPP gezeigt.<sup>[9a]</sup> Produktanalyse per <sup>13</sup>C-NMR-Spektroskopie zeigte eine strikt kontrollierte 1,11-Cyclisierung, wie zuvor für andere TCs inklusive PS berichtet (Abbildung 1C).<sup>[13b,17]</sup> Es ist möglich, die vorgeschlagene 1,2-Hydridverschiebung von **3** nach **4** mithilfe von (10-<sup>13</sup>C,9,9-<sup>2</sup>H<sub>2</sub>)FPP nachzuvollziehen. Allerdings erfordert dessen Gewinnung eine vielstufige Synthese.<sup>[18]</sup> Inspiriert durch die jüngsten Berichte über bifunktionale Enzyme mit einer OPP-Synthase- und TC-Aktivität<sup>[16g,19]</sup> wurde stattdessen (2-<sup>13</sup>C,1,1-<sup>2</sup>H<sub>2</sub>)Dimethylallyldiphosphat (DMAPP) in drei Stufen synthetisiert (Schema S1) und mit Isopentenylidiphosphat (IPP) und der FPP-Synthase aus *Streptomyces coelicolor* (WP\_011031165) verwendet. Dessen Gen wurde durch homologe Rekombination in Hefe<sup>[20]</sup> zum Zweck der enzymatischen Synthese von (10-<sup>13</sup>C,9,9-<sup>2</sup>H<sub>2</sub>)FPP kloniert (Schema S2). Weitere Umsetzung mit DdTPS6 ergab markiertes **1** mit einem Triplet für C-10 im <sup>13</sup>C-NMR-Spektrum (Abbildung 1D), das die direkte

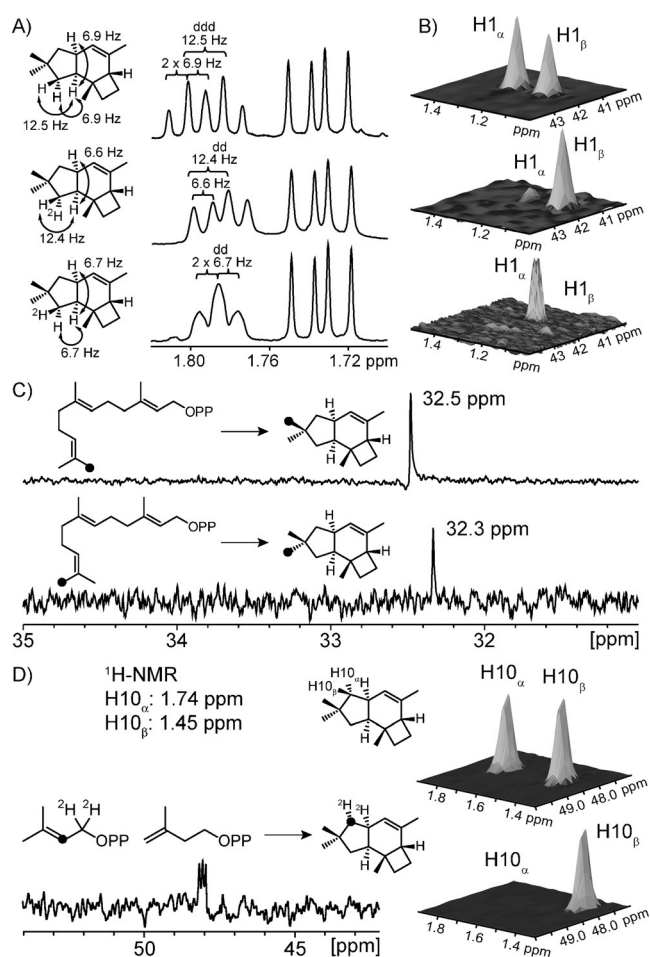
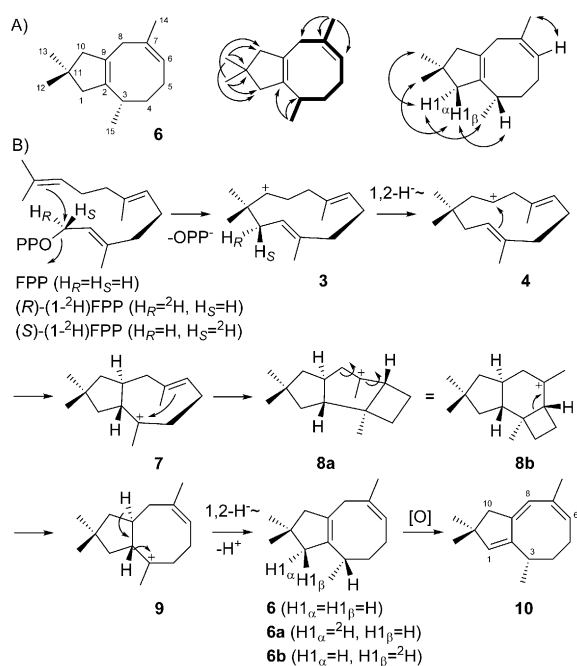


**Abbildung 1.** Analyse von **1**, **1a** und **1b** per A) <sup>1</sup>H-NMR und B) HSQC-Spektroskopie. C) <sup>13</sup>C-NMR-Spektren von markiertem **1**, das enzymatisch aus (12-<sup>13</sup>C)- und (13-<sup>13</sup>C)FPP erhalten wurde. D) Partielles HSQC-Spektrum für C10 von unmarkiertem **1** mit Kreuzpeaks für H10 $_{\alpha}$  und H10 $_{\beta}$ , <sup>13</sup>C-NMR und HSQC-Spektrum für C10 von (10-<sup>13</sup>C,9,10-<sup>2</sup>H<sub>2</sub>)-**1**, das enzymatisch aus (2-<sup>13</sup>C,1,1-<sup>2</sup>H<sub>2</sub>)DMAPP und IPP erhalten wurde. Schwarze Punkte verweisen auf <sup>13</sup>C-markierte Kohlenstoffe.

Anbindung von Deuterium an <sup>13</sup>C nachwies. Das HSQC-Spektrum von markiertem **1** deutete auf den Einbau von Deuterium in H10 $_{\alpha}$  hin.

Inkubation von DdTPS2 mit FPP lieferte einen Sesquiterpenkohlenwasserstoff (**6**; Schema 2, Abbildung S17), aber keine Produkte aus GPP und GGPP. Strukturaufklärung per NMR-Spektroskopie inklusive <sup>13</sup>C,<sup>13</sup>C-COSY an enzymatisch generiertem (1<sup>3</sup>C<sub>15</sub>)-**6** ergab die Struktur von Asterisca-2(9),6-dien (Tabelle S2 und Abbildungen S18–S25), das zuvor aus dem Nacktkiemer *Phylloidesmium magnum* isoliert worden war,<sup>[21]</sup> aber die absolute Konfiguration war auf Basis NMR-spektroskopischer Methoden zugeordnet worden, mit denen nur die relative Konfiguration zugänglich ist (ROESY) und die daher zweifelhaft ist. Ein besonderes Problem der Biosynthese ist die erforderliche Isomerisierung der 6*E*-Doppelbindung in FPP zur 6*Z*-Doppelbindung in **6**. Ein plausibler Mechanismus startet mit der 1,11-Cyclisierung von FPP zu **3**, gefolgt von einer 1,2-Hydridverschiebung zu **4** und Cyclisierung zum (*E*)-Cycloocten **7**. Dessen gespannte Natur indu-



**Schema 2.** A) Asterisca-2(9),6-dien (**6**), kontinuierliches Spinsystem (fett), diagnostische HMBC- und NOESY-Korrelationen (einfache und Doppelpfeile). B) Cyclisierung von FPP zu **6** und Autoxidation zu **10**.

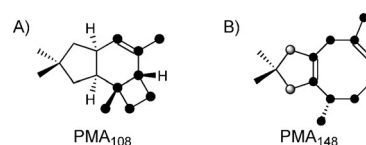
ziert eine Cyclisierung zu **8a**. Eine Konformationsänderung zu **8b** ermöglicht die Ringöffnung zu **9** mit einer 6Z-Konfiguration, gefolgt von einer finalen 1,2-Hydridverschiebung zu **6**. Die enzymatische Konversion von (R)- und (S)-(1- $^2H$ )FPP verläuft mit Einbau der Markierung in  $H_{1\alpha}$  von **6a** und  $H_{1\beta}$  von **6b**, wie durch HSQC-Spektroskopie bestimmt wurde (Abbildung S26). Zusammen mit der beobachteten NOESY-Korrelation zwischen  $H_{1\alpha}$  und  $H_{15}$ , aber nicht zwischen  $H_{1\beta}$  und  $H_{15}$ , und der anzunehmenden Inversion an C-1 in der 1,11-Cyclisierung von FPP<sup>[13]</sup> erlaubten diese Experimente, auf die absolute Konfiguration von (3S)-**6** zu schließen. Der Drehwert ( $[\alpha]_D^{25} = -88.0$ ,  $c = 0.216$ ,  $CDCl_3$ ) verwies auf dasselbe Enantiomer in *P. magnum* ( $[\alpha]_D^{24} = -84.6$ ,  $c = 0.40$ ,  $CHCl_3$ ).<sup>[21]</sup>

Der Cyclisierungsmechanismus von DdTPS2 wurde durch Inkubation von FPP in  $D_2O$  untersucht, die keine Deuteriumaufnahme ergab (Abbildung S16B), sodass  $\alpha$ -Humulen oder eine ähnliche Verbindung nicht als Intermediat zu **6** anzunehmen ist. Der Reaktionsweg zu **6** wurde zunächst durch enzymatische Umsetzung aller 15 Isotopomere von ( $^{13}C_1$ )FPP bestätigt, was in allen Fällen markiertes **6** mit einem Einbau von  $^{13}C$  in den erwarteten Positionen lieferte (Abbildung S27). Insbesondere zeigte die  $^{13}C$ -NMR-Analyse der aus (12- $^{13}C$ )- und (13- $^{13}C$ )FPP erhaltenen Produkte einen mit DdTPS6 übereinstimmenden stereochemischen Verlauf für die geminalen Methylgruppen von FPP (Abbildung S28A). Die zweite 1,2-Hydridverschiebung von **9** zu **6** wurde durch enzymatische Konversion von (3- $^{13}C,2$ - $^2H$ )FPP, synthetisiert mit einem Deuterierungsgrad von 70% wie berichtet,<sup>[17b]</sup> und Produktanalyse per  $^{13}C$ -NMR-Spektroskopie bewiesen, was ein Triplett wegen der  $^{13}C$ - $^2H$ -Spinkopplung lieferte (Abbildung S28B). Auf ähnliche Weise ermöglichte

die Inkubation von (2- $^{13}C,1,1$ - $^2H_2$ )DMAPP, IPP, *S. coelicolor* FPP-Synthase und DdTPS2 den Nachweis der 1,2-Hydridwanderung von **3** nach **4** (Abbildung S28C). Die Analyse des Produktes per GC/MS zeigte den Verlust von Deuterium im finalen Deprotonierungsschritt an (Abbildung S29). In diesem Fall konnte der stereochemische Verlauf der Deuteriumwanderung nicht verfolgt werden, da beide Wasserstoffatome  $H_{10\alpha}$  und  $H_{10\beta}$  dieselbe chemische Verschiebung zeigen ( $\delta = 2.16$  ppm). Insgesamt stimmen die initialen Cyclisierungsschritte von FPP zu **4** inklusive des stereochemischen Verlaufs hinsichtlich des Schicksals von C12 und C13 für die beiden untersuchten TCs überein.

Verlängerte Reaktionszeiten für die FPP-Inkubation mit DdTPS2 ergaben ein Produkt der Masse 202.1712 Da entsprechend der Formel  $C_{15}H_{22}$  (ber.: 202.1716 Da), das wahrscheinlich durch Autoxidation an Luft gebildet wird. Dessen Struktur wurde per NMR-Spektroskopie (Tabelle S3 und Abbildungen S30–S35) als Asterisca-1,6,8-trien (**10**; Schema 2), ein neuer Naturstoff, aufgeklärt, während die absolute Konfiguration (3S) aus derjenigen von **6** abgeleitet wurde. Weiterhin wurde ein instabiles Oxidationsprodukt  $C_{15}H_{24}O_2$  durch GC/MS-QTOF beobachtet. Die Inkubation von isoliertem **6** in enzymfreiem Puffer resultierte in der Bildung desselben Autoxidationsproduktes (die Kinetik der Bildung und des Abbaus von **6** sind in Abbildung S36 dargestellt).

Aufbauend auf unseren früheren Studien zu den EI-MS-Fragmentierungsmechanismen von Terpenen<sup>[9a,17b,22]</sup> wurden **1** und **6** durch enzymatische Umsetzung aller 15 ( $^{13}C_1$ )FPP-Isotopomere untersucht. Eine positionsspezifische Massenverschiebungsanalyse (PMA<sub>*m/z*</sub>) zeigt an, welches C-Atom, wenn es  $^{13}C$ -markiert ist, ein Fragment-Ion *m/z* um +1 erhöht und zu seiner Bildung beiträgt (schwarz in Schema 3; Mas-



**Schema 3.** PMAs für die EI-MS-Basionen von A) **1** und B) **6**. Schwarze Kohlenstoffatome tragen vollständig, graue partiell zur Bildung eines Fragment-Ions bei.

senspektren in Abbildungen S37 und S38, weitere PMAs in Schemata S3–S5). Wenn multiple Mechanismen zu Fragment-Ionen derselben Masse führen, die aber unterschiedliche Teile des Gerüsts repräsentiert, ergeben markierte Kohlenstoffatome, die nur partiell zur Bildung der Fragment-Ionen der jeweiligen Masse beitragen, auch nur eine partielle Massenverschiebung (grau in Schema 3). Insbesondere wird das Basision von **1** durch den Verlust von C1-2-9-10-11-12-13 gebildet, während das Basision von **6** aus der Abspaltung von C11-12-13 plus C1 oder C10 hervorgeht. Hochoflösende MS<sup>2</sup>-Analysen (Abbildungen S39–S45 und Tabellen S4–S10) bestätigten die Fragmentierungsmechanismen.

Zusammenfassend haben wir die ersten beiden TCs aus sozialen Amöben charakterisiert, die hinsichtlich Sequenz den pilzlichen Enzymen am ähnlichsten sind,<sup>[7]</sup> was durch die

Lokalisation des PP-Sensors in Helix G reflektiert wird. Ihre Produkte wurden als (2*S*,3*R*,6*S*,9*S*)-(-)-Protoillud-7-en, ein neuer Naturstoff, und (3*S*)-(+)-Asterisca-2(9),6-dien, über das zuvor aus dem Weichtier *Phyllodesmium magnum* berichtet wurde,<sup>[21]</sup> identifiziert. Beide Verbindungen treten auch im Duftstoffprofil von *D. discoideum* auf.<sup>[7]</sup> In Anbetracht der Tatsache, dass bis heute viele TCs aus Pflanzen, Bakterien und Pilzen charakterisiert wurden, ist es faszinierend zu erkennen, dass das Anzapfen sozialer Amöben als eine unerkundete Quelle von Naturstoffen die Tür zu einem neuen chemischen Strukturraum öffnet. Die Cyclisierungsmechanismen von DdTPS2 und DdTPS6 wurden durch Isotopenmarkierungsexperimente untersucht, die dieselbe initiale 1,11-Cyclisierung aufzeigten, wohingegen sich die letzten Schritte zu den einzigartigen Produkten unterschieden. Diese Erkenntnisse stimmen mit der recht hohen Sequenzidentität (46%) überein. Wegen der schlechten Zugänglichkeit spezifisch markierten Materials sind die komplexen EI-MS-Fragmentierungen von Terpenen schwierig zu studieren. Hier haben wir die kompletten Sätze der (<sup>13</sup>C<sub>n</sub>)-markierten Sesquiterpene zugänglich gemacht, sodass das Problem adressiert werden konnte.

### Danksagung

Diese Arbeit wurde von der DFG (DI1536/7-1) und dem FCI mit einem Doktorandenstipendium an JR gefördert.

**Stichwörter:** Biosynthese · Isotopen · Massenspektrometrie · Soziale Amöben · Terpene

**Zitierweise:** *Angew. Chem. Int. Ed.* **2016**, *55*, 15420–15423  
*Angew. Chem.* **2016**, *128*, 15646–15649

- [1] J. S. Dickschat, *Nat. Prod. Rep.* **2016**, *33*, 87.  
[2] a) C. M. Starks, K. Back, J. Chappell, J. P. Noel, *Science* **1997**, *277*, 1815; b) M. Köksal, Y. Jin, R. M. Coates, R. Croteau, D. W. Christianson, *Nature* **2011**, *469*, 116; c) P. Baer, P. Rabe, K. Fischer, C. A. Citron, T. A. Klapschinski, M. Groll, J. S. Dickschat, *Angew. Chem. Int. Ed.* **2014**, *53*, 7652; *Angew. Chem.* **2014**, *126*, 7783.  
[3] G.-L. Li, T. G. Köllner, Y. Yin, Y.-F. Jiang, H. Chen, Y. Xu, J. Gershenzon, E. Pichersky, F. Chen, *Proc. Natl. Acad. Sci. USA* **2012**, *109*, 14711.  
[4] E. Oldfield, F.-Y. Lin, *Angew. Chem. Int. Ed.* **2012**, *51*, 1124; *Angew. Chem.* **2012**, *124*, 1150.  
[5] a) L. Eichinger et al., *Nature* **2005**, *435*, 43; b) A. J. Heide et al., *Genome Res.* **2011**, *21*, 1882–1891.  
[6] a) C. A. Citron, J. Gleitzmann, G. Laurenzano, R. Pukall, J. S. Dickschat, *ChemBioChem* **2012**, *13*, 202; b) Y. Yamada, T. Kuzuyama, M. Komatsu, K. Shin-ya, S. Omura, D. E. Cane, H. Ikeda, *Proc. Natl. Acad. Sci. USA* **2015**, *112*, 857; c) M. B. Quinn, C. M. Flynn, C. Schmidt-Dannert, *Nat. Prod. Rep.* **2014**, *31*, 1449; d) J. Degenhardt, T. G. Köllner, J. Gershenzon, *Phytochemistry* **2009**, *70*, 1621.  
[7] X. Chen, T. G. Köllner, Q. Jia, A. Norris, B. Santhanam, P. Rabe, J. S. Dickschat, G. Shaulsky, J. Gershenzon, F. Chen, *Proc. Natl. Acad. Sci. USA* **2016**, *113*, 12132.  
[8] J. Rinkel, J. S. Dickschat, *Beilstein J. Org. Chem.* **2015**, *11*, 2493.  
[9] a) P. Rabe, L. Barra, J. Rinkel, R. Riclea, C. A. Citron, T. A. Klapschinski, A. Janusko, J. S. Dickschat, *Angew. Chem. Int. Ed.* **2015**, *54*, 13448; *Angew. Chem.* **2015**, *127*, 13649; b) Y. Sugai, Y. Ueno, K. Hayashi, S. Oogami, T. Toyomasu, S. Matsumoto, M. Natsume, H. Nozaki, H. Kawaide, *J. Biol. Chem.* **2011**, *286*, 42840; c) G. A. Ellis, T. P. Wyche, C. G. Fry, D. R. Braun, T. S. Bugni, *Mar. Drugs* **2014**, *12*, 1013; d) T. P. Wyche, J. S. Piotrowski, Y. Hou, D. Braun, R. Deshpande, S. McIlwain, I. M. Ong, C. L. Myers, I. A. Guzei, W. M. Westler, D. R. Andes, T. S. Bugni, *Angew. Chem. Int. Ed.* **2014**, *53*, 11583; *Angew. Chem.* **2014**, *126*, 11767; e) L. Barra, K. Ibrom, J. S. Dickschat, *Angew. Chem. Int. Ed.* **2015**, *54*, 6637; *Angew. Chem.* **2015**, *127*, 6737.  
[10] H. Takeshita, I. Kouno, M. Iino, H. Iwabuchi, D. Nomura, *Bull. Chem. Soc. Jpn.* **1980**, *53*, 3641.  
[11] a) P. Gutta, D. J. Tantillo, *J. Am. Chem. Soc.* **2006**, *128*, 6172; b) L. Zu, M. Xu, M. W. Lodewyk, D. E. Cane, R. J. Peters, D. J. Tantillo, *J. Am. Chem. Soc.* **2012**, *134*, 11369.  
[12] M. Seemann, G. Zhai, K. Umezawa, D. E. Cane, *J. Am. Chem. Soc.* **1999**, *121*, 591.  
[13] a) D. E. Cane, J. S. Oliver, P. H. M. Harrison, C. Abell, B. R. Hubbard, C. T. Kane, R. Lattman, *J. Am. Chem. Soc.* **1990**, *112*, 4513; b) C.-M. Wang, R. Hopson, X. Lin, D. E. Cane, *J. Am. Chem. Soc.* **2009**, *131*, 8360.  
[14] J. Rinkel, P. Rabe, P. Garbeva, J. S. Dickschat, *Angew. Chem. Int. Ed.* **2016**, *55*, 13593; *Angew. Chem.* **2016**, *128*, 13791.  
[15] P. Rabe, C. A. Citron, J. S. Dickschat, *ChemBioChem* **2013**, *14*, 2345.  
[16] a) J. Jiang, X. He, D. E. Cane, *J. Am. Chem. Soc.* **2006**, *128*, 8128; b) D. J. Miller, J. Gao, D. G. Truhlar, N. J. Young, V. Gonzalez, R. K. Allemann, *Org. Biomol. Chem.* **2008**, *6*, 2346; c) P. Rabe, K. A. K. Pahirulzaman, J. S. Dickschat, *Angew. Chem. Int. Ed.* **2015**, *54*, 6041; *Angew. Chem.* **2015**, *127*, 6139; d) P. Rabe, J. Rinkel, T. A. Klapschinski, L. Barra, J. S. Dickschat, *Org. Biomol. Chem.* **2016**, *14*, 158; e) P. Rabe, A. Janusko, B. Goldfuss, J. S. Dickschat, *ChemBioChem* **2016**, *17*, 146; f) I. Burkhardt, T. Siemon, M. Henrot, L. Studt, S. Rösler, B. Tudzynski, M. Christmann, J. S. Dickschat, *Angew. Chem. Int. Ed.* **2016**, *55*, 8748; *Angew. Chem.* **2016**, *128*, 8890; g) Y. Matsuda, T. Mitsuhashi, S. Lee, M. Hoshino, T. Mori, M. Okada, H. Zhang, F. Hayashi, M. Fujita, I. Abe, *Angew. Chem. Int. Ed.* **2016**, *55*, 5785; *Angew. Chem.* **2016**, *128*, 5879.  
[17] a) D. E. Cane, T. Rossi, A. M. Tillman, J. P. Pachlatko, *J. Am. Chem. Soc.* **1981**, *103*, 1838; b) T. A. Klapschinski, P. Rabe, J. S. Dickschat, *Angew. Chem. Int. Ed.* **2016**, *55*, 10141; c) P. Rabe, T. Schmitz, J. S. Dickschat, *Beilstein J. Org. Chem.* **2016**, *12*, 1839; d) J. S. Dickschat, *Nat. Prod. Rep.* **2011**, *28*, 1917.  
[18] C. A. Citron, P. Rabe, L. Barra, C. Nakano, T. Hoshino, J. S. Dickschat, *Eur. J. Org. Chem.* **2014**, 7684.  
[19] a) T. Toyomasu, M. Tsukahara, A. Kaneko, R. Niida, W. Mitsuhashi, T. Dairi, N. Kato, T. Sassa, *Proc. Natl. Acad. Sci. USA* **2007**, *104*, 3084; b) R. Chiba, A. Minami, K. Gomi, H. Oikawa, *Org. Lett.* **2013**, *15*, 594; c) Y. Ye, A. Minami, A. Mandi, C. Liu, T. Taniguchi, T. Kuzuyama, K. Monde, K. Gomi, H. Oikawa, *J. Am. Chem. Soc.* **2015**, *137*, 11846; d) B. Qin, Y. Matsuda, T. Mori, M. Okada, Z. Quan, T. Mitsuhashi, T. Wakimoto, I. Abe, *Angew. Chem. Int. Ed.* **2016**, *55*, 1658; *Angew. Chem.* **2016**, *128*, 1690.  
[20] J. S. Dickschat, K. A. K. Pahirulzaman, P. Rabe, T. A. Klapschinski, *ChemBioChem* **2014**, *15*, 810.  
[21] S.-C. Mao, M. Gavagnin, E. Mollo, Y.-W. Guo, *Biochem. Syst. Ecol.* **2011**, *39*, 408.  
[22] a) P. Rabe, T. A. Klapschinski, J. S. Dickschat, *ChemBioChem* **2016**, *17*, 1333; b) P. Rabe, J. S. Dickschat, *Beilstein J. Org. Chem.* **2016**, *12*, 1380.

Eingegangen am 13. September 2016,  
veränderte Fassung am 26. Oktober 2016  
Online veröffentlicht am 10. November 2016

## Appendix D

### **A detailed view on 1,8-cineol biosynthesis by *Streptomyces clavuligerus***

*Beilstein J. Org. Chem.* **2016**, *12*, 2317–2324.

DOI:10.3762/bjoc.12.225





# A detailed view on 1,8-cineol biosynthesis by *Streptomyces clavuligerus*

Jan Rinkel, Patrick Rabe, Laura zur Horst and Jeroen S. Dickschat\*

## Full Research Paper

Open Access

### Address:

Kekulé-Institute of Organic Chemistry and Biochemistry, University of Bonn, Gerhard-Domagk-Straße 1, 53121 Bonn, Germany

### Email:

Jeroen S. Dickschat\* - dickschat@uni-bonn.de

\* Corresponding author

### Keywords:

biosynthesis; enzyme mechanisms; isotopic labelling; stereochemistry; terpenes

*Beilstein J. Org. Chem.* **2016**, *12*, 2317–2324.

doi:10.3762/bjoc.12.225

Received: 18 August 2016

Accepted: 28 October 2016

Published: 04 November 2016

This article is part of the Thematic Series "Chemical biology".

Guest Editor: H. B. Bode

© 2016 Rinkel et al.; licensee Beilstein-Institut.

License and terms: see end of document.

## Abstract

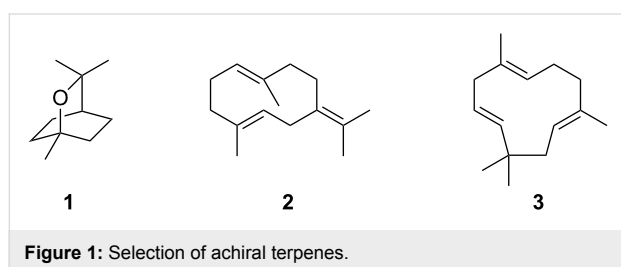
The stereochemical course of the cyclisation reaction catalysed by the bacterial 1,8-cineol synthase from *Streptomyces clavuligerus* was investigated using stereospecifically deuterated substrates. In contrast to the well investigated plant enzyme from *Salvia officinalis*, the reaction proceeds via (*S*)-linalyl diphosphate and the (*S*)-terpinyl cation, while the final cyclisation reaction is in both cases a *syn* addition, as could be shown by incubation of (2-<sup>13</sup>C)geranyl diphosphate in deuterium oxide.

## Introduction

Among all classes of natural products the climax of structural diversity and complexity is reached within the largest, the terpenoids. An estimated number of 75,000 different compounds are known from all kinds of organisms including plants [1], bacteria [2-5], fungi [6] and, as recently shown, even social amoebae [7]. These molecules are all made from only a handful of linear and achiral precursors such as geranyl diphosphate (GPP, monoterpenes), farnesyl diphosphate (FPP, sesquiterpenes) and geranylgeranyl diphosphate (GGPP, diterpenes). Terpene cyclases (type I) contain a trinuclear (Mg<sup>2+</sup>)<sub>3</sub> cluster in their active site that is stabilised by binding to several highly conserved motifs including the aspartate-rich motif (DDXXD) and the NSE triad (ND(L,I,V)XSXXXE, modified in plants to a DTE triad: DD(L,I,V)XTXXXE) [8]. Their substrates bind with

the diphosphate portion to the (Mg<sup>2+</sup>)<sub>3</sub> cluster and via hydrogen bridges to a highly conserved arginine (diphosphate sensor) and a RY dimer [9]. The substrate is ionised by diphosphate abstraction and the resulting allyl cation undergoes a domino reaction via a series of cationic intermediates and a final deprotonation or attack of water to yield a terpene hydrocarbon or alcohol. This reaction cascade proceeds in a hydrophobic cavity from which water is excluded to enable carbocation chemistry in an aqueous environment. Furthermore, the hydrophobic cavity provides a template that arranges the substrate in a certain conformation to determine the formation of a specific product. Single residues such as phenylalanines are involved in the stabilisation of cationic intermediates, e.g., by cation- $\pi$  interactions [8-10]. The overall process usually generates an en-

antiomerically pure (poly)cyclic terpene with several stereogenic centres. A large variety of carbon skeletons is accessible, e.g., more than 120 skeletons each representing various stereoisomers and constitutional isomers with different positioning of olefinic double bonds or alcohol functions are known just for sesquiterpenes [11]. The structural diversity of terpenoids can be further increased by the action of tailoring enzymes such as cytochrome P450 monooxygenases and acyl transferases [12,13]. Very few cases are known in which terpene cyclases generate an achiral product as exemplified by the monoterpene 1,8-cineol (eucalyptol, **1**) and the sesquiterpenes germacrene B (**2**) and  $\alpha$ -humulene (**3**) (Figure 1).



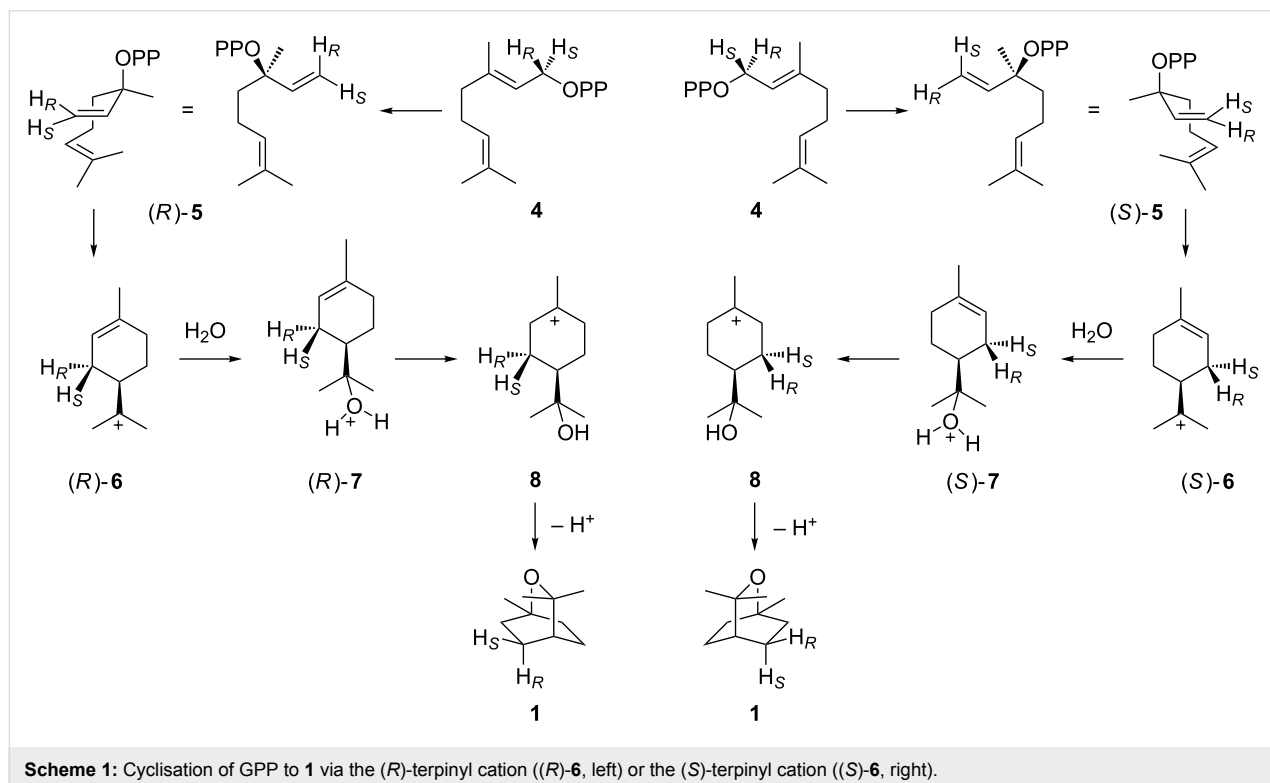
A direct 1,6-cyclisation of the monoterpene precursor GPP to **1** is prevented by the topological constraints associated with the (*2E*) geometry which necessitates the isomerisation of GPP (**4**) to linalyl diphosphate (LPP, **5**) followed by an *anti,endo*-S<sub>N</sub>'-cyclisation [14], but the stereochemical course of this reaction is

not readily clear and may proceed via either enantiomer of the  $\alpha$ -terpinyl cation (**6**, Scheme 1). Isotopic labelling experiments currently experience a revival [15] and are a very powerful method to follow the enzyme mechanisms of terpene cyclases [16–24] including the stereochemical courses of the cyclisation reactions (reviewed in [25]). While the stereochemical course of the GPP cyclisation to **1** has been investigated for the 1,8-cineol synthase from *Salvia officinalis* [26,27], it is unknown for the bacterial enzyme that was recently reported from *Streptomyces clavuligerus* [28]. Here we describe isotopic labelling experiments that gave insights into the cyclisation mechanism of the bacterial 1,8-cineol synthase.

## Results

### The absolute configuration of the intermediate terpinyl cation

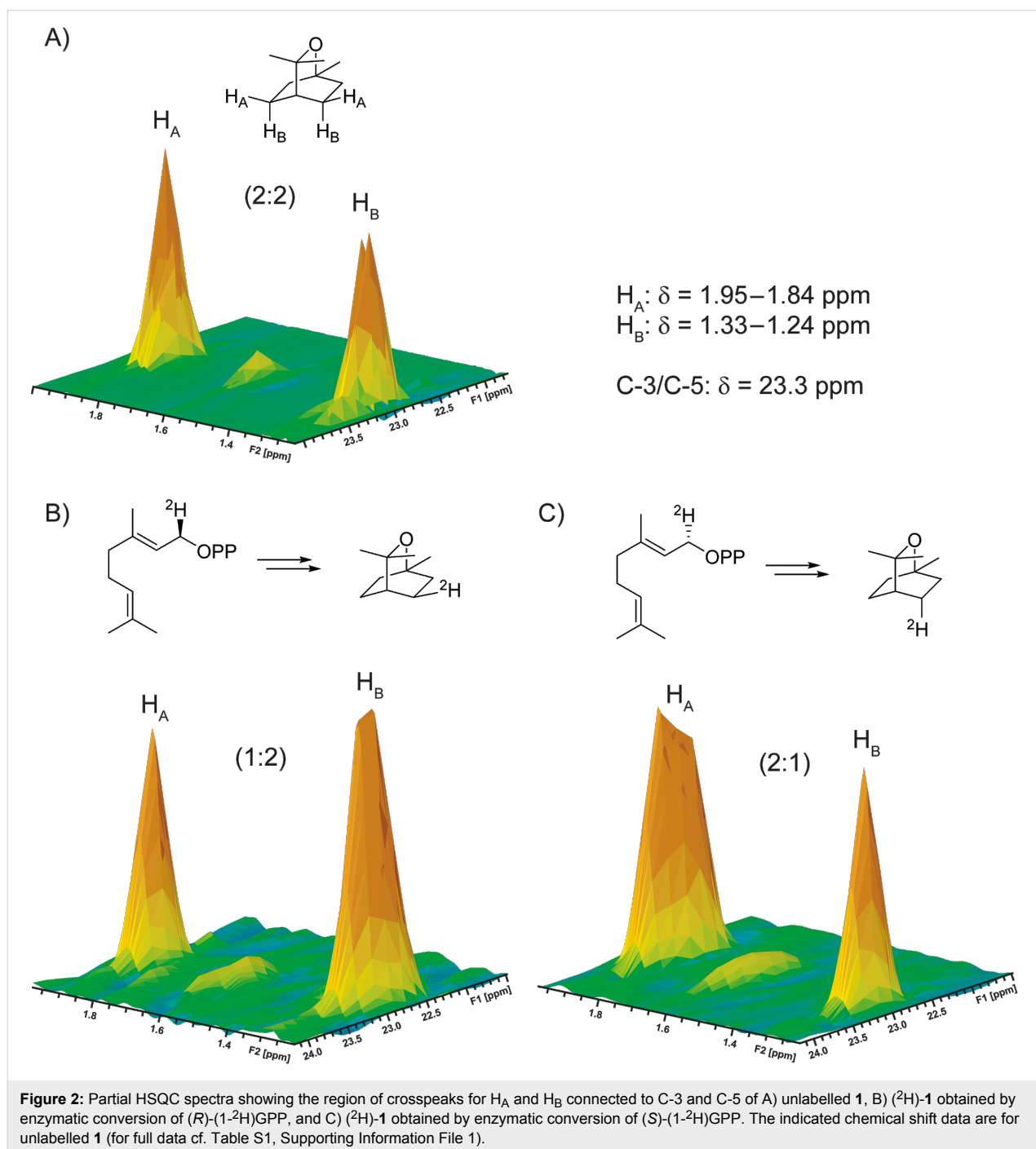
While the two possible cyclisation pathways via (*R*)- and (*S*)-**6** to **1** cannot be distinguished with unlabelled GPP, its two enantiotopic protons at C-1 (indicated by H<sub>R</sub> for the *pro-R* hydrogen and H<sub>S</sub> for the *pro-S* hydrogen) end up in diastereotopic positions of **1**. Thus, a labelling experiment using the deuterated substrates (*R*)-(1-<sup>2</sup>H)GPP (H<sub>R</sub> = <sup>2</sup>H, H<sub>S</sub> = H) and (*S*)-(1-<sup>2</sup>H)GPP (H<sub>R</sub> = H, H<sub>S</sub> = <sup>2</sup>H) can give insights whether the cyclisation proceeds via (*R*)- or (*S*)-**6**, by determination in which of the distinguishable diastereotopic positions the label ends up. The synthesis of the two enantiomers of (1-<sup>2</sup>H)GPP (Scheme S1, Supporting Information File 1) was performed by





Alpine borane reduction [29] (both enantiomers of this reagent are commercially available) of (1-<sup>2</sup>H)geraniol to (*R*)- and (*S*)-(1-<sup>2</sup>H)geraniol that were obtained with high enantiomeric excess (>95% ee) as determined by Mosher ester analysis (Figure S1, Supporting Information File 1). The alcohols were subsequently converted into the corresponding diphosphates using triethylammonium phosphate in trichloroacetonitrile [30,31]. The gene encoding the 1,8-cineol synthase [28] was cloned into the yeast-to-*Escherichia coli* shuttle vector pYE-

Express by homologous recombination in yeast [32], followed by expression in *E. coli* BL21. The protein was purified by Ni<sup>2+</sup>-NTA affinity chromatography and used to convert both (*R*)- and (*S*)-(1-<sup>2</sup>H)GPP into (<sup>2</sup>H)-**1** (in agreement with the findings described in reference [28], **1** is the only product from unlabelled GPP as was shown by GC-MS, Figure S2, Supporting Information File 1). The obtained products were analysed by HSQC spectroscopy (Figure 2). While for unlabelled **1** a 2:2 signal intensity is observed for the crosspeaks representing the



two pairs of enantiotopic hydrogens  $H_A$  and  $H_B$  connected to carbons C-3 and C-5, the sample obtained from (*R*)-(1- $^2\text{H}$ )GPP gave a 1:2 ratio of signal intensities (i.e.,  $H_A = 2H$ ), while the sample from (*S*)-(1- $^2\text{H}$ )GPP resulted in ratio of 2:1 by peak integration (i.e.,  $H_B = 2H$ ), indicating the cyclisation via (*S*)-LPP ((*S*)-5) and the (*S*)-terpinyl cation ((*S*)-6) (Scheme 1, right).

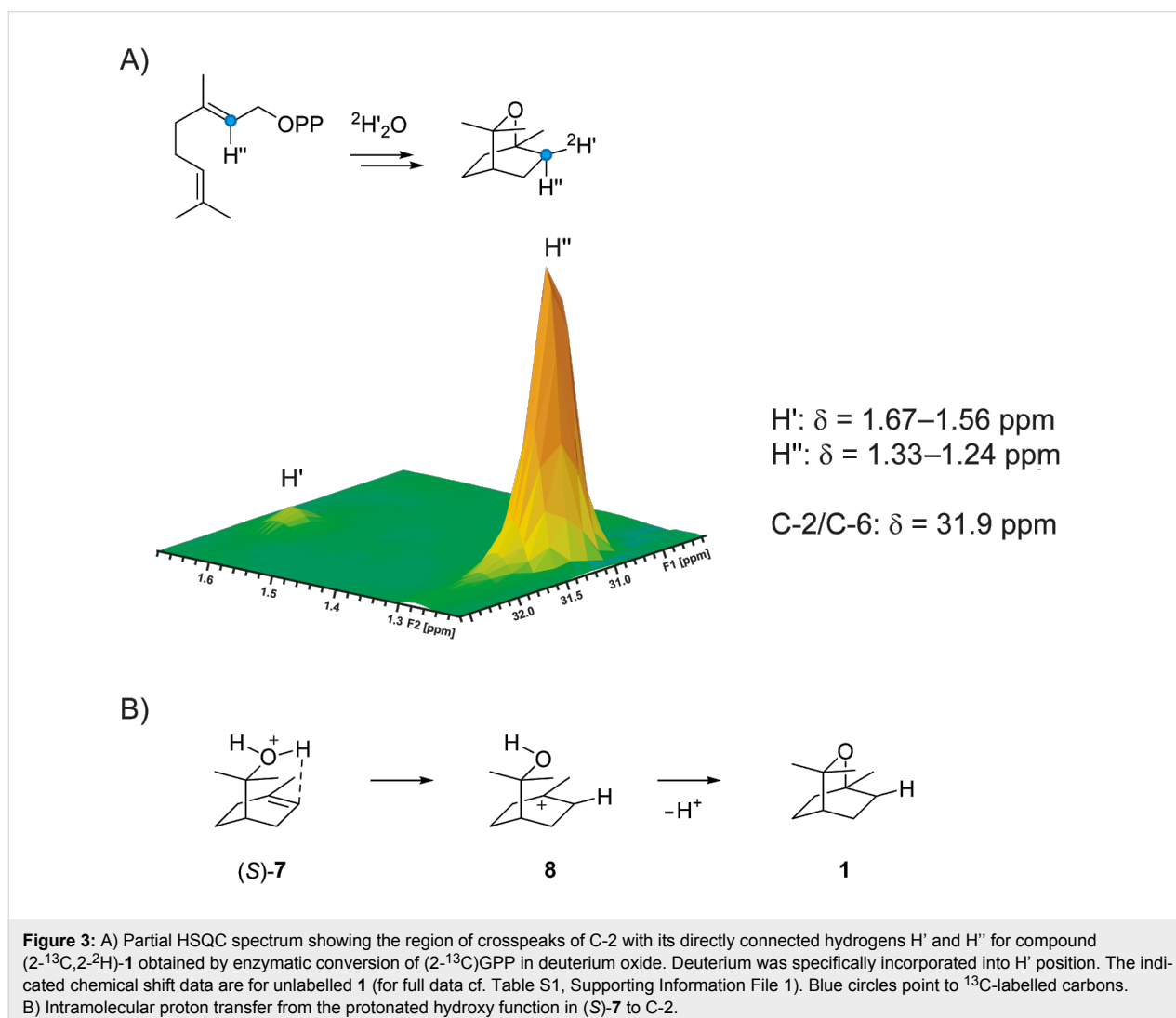
### Syn versus anti addition in the final ring closure

The final cyclisation step from (*S*)-7 via 8 to 1 can in principle proceed either via a *syn* or an *anti* addition to the olefinic double bond, requiring a protonation of the original C-2 of GPP. To distinguish between these alternatives ( $2\text{-}^{13}\text{C}$ )GPP was synthesised from sulcatone (Scheme S2, Supporting Information File 1) and converted by the 1,8-cineol synthase in deuterium oxide. The obtained product was analysed by HSQC spectroscopy (Figure 3A), showing that deuterium is taken up into the *exo* position at the  $^{13}\text{C}$ -labelled C-2 of 1 (indicated by  $H'$ ),

while the *endo* position ( $H''$ ) is occupied by the proton from the substrate, resulting in a strong crosspeak [22]. Furthermore, deuterium incorporation at C-2 was indicated by a strongly enhanced triplet in the  $^{13}\text{C}$  NMR spectrum due to  $^{13}\text{C}$ - $^2\text{H}$ -spin coupling (Figure S4, Supporting Information File 1) [11,20,23]. This finding is in agreement with a *syn* addition to the olefinic double bond of (*S*)-7 in the final cyclisation step. It is possible that the proton is directly transferred from the protonated hydroxy function in (*S*)-7 to C-2 (Figure 3B). Alternatively, a deprotonation of (*S*)-7 to the hypothetical neutral intermediate  $\alpha$ -terpineol followed by reprotonation at C-2 from the *Si* face can be assumed, but these two alternatives cannot be distinguished based on the labelling experiments described here.

### Discussion

Plant and bacterial terpene cyclases show important structural differences [33]. While plant monoterpene synthases are





*romyces cerevisiae* FY834 together with linearised vector pYE-Express [32] (EcoRI and HindIII digestion) using the LiOAc/SS carrier DNA protocol [39]. Transformed cells were plated on SM-URA medium (20 g glucose, 1.7 g yeast nitrogen base, 5 g ammonium sulphate, 0.77 g nutritional supplement minus uracil, 24 g agar, 1 L water) and grown for 3 days at 28 °C. Plasmids were isolated using the kit Zymoprep Yeast Plasmid Miniprep II (Zymo Research, Irvine, USA), shuttled in *E. coli* BL21 by electroporation and confirmed by sequencing.

### Incubation experiments with (1*R*)- and (1*S*)-(1-<sup>2</sup>H)GPP

A preculture of *E. coli* BL21 cells carrying the plasmid pYE\_WP003952918 in 2YT medium (16 g trypton, 10 g yeast extract, 5 g NaCl, 1 L water, pH 7.2) was grown overnight to inoculate a 2YT main culture (2 L). The cultures were shaken at 160 rpm, 37 °C until OD<sub>600</sub> = 0.4 was reached. Prior to induction with IPTG (0.4 mM), the cultures were cooled down to 18 °C. After incubation overnight (160 rpm, 18 °C), cells were harvested by centrifugation (5000g, 4 °C, 45 min) and resuspended in binding buffer (20 mL; 20 mM Na<sub>2</sub>HPO<sub>4</sub>, 0.5 mM NaCl, 20 mM imidazole, 1 mM MgCl<sub>2</sub>, pH 7.0). The cells were crushed by ultra-sonification (6 × 1 min, 4 °C) and the cell debris pellet was separated by centrifugation (10 min, 15500g, 4 °C). The soluble fraction was loaded onto a Ni<sup>2+</sup>-NTA affinity column (Novagen) and treated with binding buffer (2 × 10 mL). The target protein was then eluted with elution buffer (2 × 10 mL; 20 mM Na<sub>2</sub>HPO<sub>4</sub>, 0.5 M NaCl, 0.5 M imidazole, 1 mM MgCl<sub>2</sub>, pH 7.0) and used directly for incubations with 5 mg of (1*R*)- and (1*S*)-(1-<sup>2</sup>H)GPP, solved in incubation buffer (50 mM Tris/HCl, 10 mM MgCl<sub>2</sub>, 20% v/v glycerol, pH 8.2) to reach a final substrate concentration of 0.2 mg/mL. The enzyme reaction was incubated for 2 h at 28 °C, overlaid with 400 μL (<sup>2</sup>H<sub>6</sub>)benzene and further incubated overnight. The organic phase was separated, dried over MgSO<sub>4</sub> and directly analysed by GC–MS and NMR.

### Incubation experiment with (2-<sup>13</sup>C)GPP

Enzyme purification starting from an *E. coli* expression culture (0.5 L) was performed as described above. The last washing fraction was substituted with <sup>2</sup>H<sub>2</sub>O-based binding buffer and elution was done with <sup>2</sup>H<sub>2</sub>O-based elution buffer. The first elution fraction was incubated with (2-<sup>13</sup>C)GPP (0.8 mg) for 16 h at 28 °C. The enzyme reaction was extracted with (<sup>2</sup>H<sub>6</sub>)benzene (0.6 mL), dried with MgSO<sub>4</sub> and the extract was analysed directly by GC–MS and NMR.

### NMR spectroscopy

To record NMR spectra, instruments AV Avance DMX-500 (500 MHz), DPX-400 (400 MHz) and AV III HD Cryo (700 MHz) from Bruker were used. Solvent signals were used

to reference the spectra (<sup>1</sup>H NMR, residual proton signals: (<sup>2</sup>H<sub>6</sub>)benzene δ = 7.16; <sup>13</sup>C NMR: (<sup>2</sup>H<sub>6</sub>)benzene δ = 128.06) [40].

### GC–MS analysis

An Agilent 7890B gas chromatograph equipped with a HP5-MS silica column (30 m, 0.25 mm inner diameter, 0.50 μm film) connected to an Agilent 5977A inert mass selective detector was used to acquire GC–MS data. Instrumental settings were: (1) inlet pressure: 77.1 kPa, He: 23.3 mL/min, (2) transfer line: 250 °C, (3) electron energy: 70 eV. The GC was set to 50 °C starting temperature for 5 min, then increasing with 5 °C per minute to 320 °C and holding this temperature for another 5 min. The injection volume was 2 μL and the inlet was operating in split mode (10:1, 60 s valve time). Helium was used as the carrier gas at 1 mL/min. Retention indices were determined against a homologous series of *n*-alkanes (C<sub>8</sub>–C<sub>40</sub>).

### Synthesis of (2-<sup>13</sup>C)geranyl diphosphate

(2-<sup>13</sup>C)Geraniol was synthesised as reported previously [41]. The synthetic (2-<sup>13</sup>C)geraniol (16 mg, 0.072 mmol, 1.0 equiv) was dissolved in dry THF (0.3 mL) and PBr<sub>3</sub> (8.1 mg, 0.029 mmol, 0.4 equiv) was added at 0 °C. The solution was stirred for 45 min at room temperature. The reaction mixture was hydrolyzed by addition of ice cold water and extracted three times with pentane. The combined organic layers were dried over MgSO<sub>4</sub> and the solvent was removed under reduced pressure. The crude product was used for phosphorylation.

In a second flask, to a solution of (*n*-Bu<sub>4</sub>)<sub>3</sub>HP<sub>2</sub>O<sub>7</sub> (97 mg, 0.11 mmol, 1.5 equiv) in dry CH<sub>3</sub>CN (1.0 mL) the crude product of the allyl bromide (1.0 equiv) was added and the reaction mixture was stirred for 2 h at room temperature and then concentrated under reduced pressure. The colorless oil was loaded onto an ion exchange column (DOWEX 50W-X8, NH<sub>4</sub><sup>+</sup> form). Elution of the product was performed by addition of two column volumes of ion exchange buffer (0.03 M NH<sub>4</sub>HCO<sub>3</sub> in 2% iPrOH/H<sub>2</sub>O). Freeze drying yielded the product as a white solid (14.1 mg, 0.04 mmol, 55%).

<sup>1</sup>H NMR (500 MHz, H<sub>2</sub>O) δ 5.37 (dt, <sup>1</sup>J<sub>(C,H)</sub> = 156.7 Hz, <sup>3</sup>J<sub>(H,H)</sub> = 6.9 Hz, 1H, CH), 5.16–5.11 (m, 1H, 1 × CH), 4.44–4.38 (m, 2H, 1 × CH<sub>2</sub>), 2.12–2.06 (m, 2H, 1 × CH<sub>2</sub>), 2.06–2.00 (m, 2H, 1 × CH<sub>2</sub>), 1.65 (d, <sup>3</sup>J<sub>(C,H)</sub> = 5.2 Hz, 3H, 1 × CH<sub>3</sub>), 1.62 (s, 3H, 1 × CH<sub>3</sub>), 1.56 (s, 3H, 1 × CH<sub>3</sub>) ppm; <sup>13</sup>C NMR (125 MHz, H<sub>2</sub>O) δ 141.9 (d, <sup>1</sup>J<sub>(C,C)</sub> = 72.7 Hz, 1 × C<sub>q</sub>), 133.7 (1 × C<sub>q</sub>), 124.1 (1 × CH), 119.6 (d, <sup>3</sup>J<sub>(P,C)</sub> = 8.2 Hz, 1 × <sup>13</sup>CH), 38.8 (d, <sup>2</sup>J<sub>(C,C)</sub> = 2.7 Hz, 1 × CH<sub>2</sub>), 25.6 (d, <sup>3</sup>J<sub>(C,C)</sub> = 2.9 Hz, 1 × CH<sub>2</sub>), 24.8 (1 × CH<sub>3</sub>), 16.9 (1 × CH<sub>3</sub>), 15.6 (d, <sup>2</sup>J<sub>(C,C)</sub> = 1.2 Hz, 1 × CH<sub>3</sub>) ppm; <sup>31</sup>P NMR (202 MHz, H<sub>2</sub>O) δ –10.0 (m, 1 × P), –10.6 (m, 1 × P) ppm.

## Supporting Information

Synthesis schemes, Mosher ester analysis of (*R*)- and (*S*)-(1-<sup>2</sup>H)GPP, gas chromatogram of the enzyme product of 1,8-cineol synthase, <sup>13</sup>C NMR of the enzyme product from (2-<sup>13</sup>C)GPP in deuterium oxide buffer, and full NMR data of **1**.

### Supporting Information File 1

Additional material.

[<http://www.beilstein-journals.org/bjoc/content/supplementary/1860-5397-12-225-S1.pdf>]

## Acknowledgements

This work was funded by the DFG (DI1536/7-1) and by a Ph.D. scholarship of the Fonds der Chemischen Industrie to JR.

## References

- Degenhardt, J.; Köllner, T. G.; Gershenzon, J. *Phytochemistry* **2009**, *70*, 1621–1637. doi:10.1016/j.phytochem.2009.07.030
- Citron, C. A.; Gleitzmann, J.; Laurenzano, G.; Pukall, R.; Dickschat, J. S. *ChemBioChem* **2012**, *13*, 202–214. doi:10.1002/cbic.201100641
- Rabe, P.; Citron, C. A.; Dickschat, J. S. *ChemBioChem* **2013**, *14*, 2345–2354. doi:10.1002/cbic.201300329
- Citron, C. A.; Barra, L.; Wink, J.; Dickschat, J. S. *Org. Biomol. Chem.* **2015**, *13*, 2673–2683. doi:10.1039/C4OB02609H
- Yamada, Y.; Kuzuyama, T.; Komatsu, M.; Shin-ya, K.; Omura, S.; Cane, D. E.; Ikeda, H. *Proc. Natl. Acad. Sci. U. S. A.* **2015**, *112*, 857–862. doi:10.1073/pnas.1422108112
- Quin, M. B.; Flynn, C. M.; Schmidt-Dannert, C. *Nat. Prod. Rep.* **2014**, *31*, 1449–1473. doi:10.1039/C4NP00075G
- Chen, X.; Köllner, T. G.; Jia, Q.; Norris, A.; Santhanam, B.; Rabe, P.; Dickschat, J. S.; Shaulsky, G.; Gershenzon, J.; Chen, F. *Proc. Natl. Acad. Sci. U. S. A.* **2016**, *113*, 12132–12137. doi:10.1073/pnas.1610379113
- Starks, C. M.; Back, K.; Chappell, J.; Noel, J. P. *Science* **1997**, *277*, 1815–1820. doi:10.1126/science.277.5333.1815
- Baer, P.; Rabe, P.; Fischer, K.; Citron, C. A.; Klapschinski, T. A.; Groll, M.; Dickschat, J. S. *Angew. Chem., Int. Ed.* **2014**, *53*, 7652–7656. doi:10.1002/anie.201403648
- Lesburg, C. A.; Zhai, G.; Cane, D. E.; Christianson, D. W. *Science* **1997**, *277*, 1820–1824. doi:10.1126/science.277.5333.1820
- Klapschinski, T. A.; Rabe, P.; Dickschat, J. S. *Angew. Chem., Int. Ed.* **2016**, *55*, 10141–10144. doi:10.1002/anie.201605425
- Bogazkaya, A. M.; von Bühler, C. J.; Kriening, S.; Busch, A.; Seifert, A.; Pleiss, J.; Laschat, S.; Urlacher, V. B. *Beilstein J. Org. Chem.* **2014**, *10*, 1347–1353. doi:10.3762/bjoc.10.137
- Huber, T.; Weisheit, L.; Magauer, T. *Beilstein J. Org. Chem.* **2015**, *11*, 2521–2539. doi:10.3762/bjoc.11.273
- Croteau, R.; Alonso, W. R.; Koepf, A. E.; Johnson, M. A. *Arch. Biochem. Biophys.* **1994**, *309*, 184–192. doi:10.1006/abbi.1994.1101
- Rinkel, J.; Dickschat, J. S. *Beilstein J. Org. Chem.* **2015**, *11*, 2493–2508. doi:10.3762/bjoc.11.271
- Meguro, A.; Motoyoshi, Y.; Teramoto, K.; Ueda, S.; Totsuka, Y.; Ando, Y.; Tomita, T.; Kim, S.-Y.; Kimura, T.; Igarashi, M.; Sawa, R.; Shinada, T.; Nishiyama, M.; Kuzuyama, T. *Angew. Chem., Int. Ed.* **2015**, *54*, 4353–4356. doi:10.1002/anie.201411923
- Matsuda, Y.; Mitsuhashi, T.; Lee, S.; Hoshino, N.; Mori, T.; Okada, M.; Zhang, H.; Hayashi, F.; Fujita, M.; Abe, I. *Angew. Chem., Int. Ed.* **2016**, *55*, 5785–5788. doi:10.1002/anie.201601448
- Okada, M.; Matsuda, Y.; Mitsuhashi, T.; Hoshino, S.; Mori, T.; Nakagawa, K.; Quan, Z.; Qin, B.; Zhang, H.; Hayashi, F.; Kawaide, H.; Abe, I. *J. Am. Chem. Soc.* **2016**, *138*, 10011–10018. doi:10.1021/jacs.6b05799
- Ye, Y.; Minami, A.; Mandi, A.; Liu, C.; Taniguchi, T.; Kuzuyama, T.; Monde, K.; Gomi, K.; Oikawa, H. *J. Am. Chem. Soc.* **2015**, *137*, 11846–11853. doi:10.1021/jacs.5b08319
- Burkhardt, I.; Siemon, T.; Henrot, M.; Studt, L.; Rösler, S.; Tudzynski, B.; Christmann, M.; Dickschat, J. S. *Angew. Chem., Int. Ed.* **2016**, *55*, 8748–8751. doi:10.1002/anie.201603782
- Rabe, P.; Janusko, A.; Goldfuss, B.; Dickschat, J. S. *ChemBioChem* **2016**, *17*, 146–149. doi:10.1002/cbic.201500543
- Rabe, P.; Rinkel, J.; Klapschinski, T. A.; Barra, L.; Dickschat, J. S. *Org. Biomol. Chem.* **2016**, *14*, 158–164. doi:10.1039/C5OB01998B
- Rabe, P.; Pahirulzaman, K. A. K.; Dickschat, J. S. *Angew. Chem., Int. Ed.* **2015**, *54*, 6041–6045. doi:10.1002/anie.201501119
- Rabe, P.; Schmitz, T.; Dickschat, J. S. *Beilstein J. Org. Chem.* **2016**, *12*, 1839–1850. doi:10.3762/bjoc.12.173
- Dickschat, J. S. *Nat. Prod. Rep.* **2011**, *28*, 1917–1936. doi:10.1039/c1np00063b
- Wise, M. L.; Savage, T. J.; Katahira, E.; Croteau, R. *J. Biol. Chem.* **1998**, *273*, 14891–14899. doi:10.1074/jbc.273.24.14891
- Wise, M. L.; Urbansky, M.; Helms, G. L.; Coates, R. M.; Croteau, R. *J. Am. Chem. Soc.* **2002**, *124*, 8546–8547. doi:10.1021/ja0265714
- Nakano, C.; Kim, H.-K.; Ohnishi, Y. *ChemBioChem* **2011**, *12*, 1988–1991. doi:10.1002/cbic.201100330
- Edelstein, R. L.; Weller, V. A.; Distefano, M. D.; Tung, J. S. *J. Org. Chem.* **1998**, *63*, 5298–5299. doi:10.1021/jo980304s
- Thulasiram, H. V.; Phan, R. M.; Rivera, S. B.; Poulter, C. D. *J. Org. Chem.* **2006**, *71*, 1739–1741. doi:10.1021/jo052384n
- Keller, R. K.; Thompson, R. *J. Chromatogr. A* **1993**, *645*, 161–167. doi:10.1016/0021-9673(93)80630-Q
- Dickschat, J. S.; Pahirulzaman, K. A. K.; Rabe, P.; Klapschinski, T. A. *ChemBioChem* **2014**, *15*, 810–814. doi:10.1002/cbic.201300763
- Oldfield, E.; Lin, F.-Y. *Angew. Chem., Int. Ed.* **2012**, *51*, 1124–1137. doi:10.1002/anie.201103110
- Whittington, D. A.; Wise, M. L.; Urbansky, M.; Coates, R. M.; Croteau, R. B.; Christianson, D. W. *Proc. Natl. Acad. Sci. U. S. A.* **2002**, *99*, 15375–15380. doi:10.1073/pnas.232591099
- Hyatt, D. C.; Youn, B.; Zhao, Y.; Santhamma, B.; Coates, R. M.; Croteau, R. B.; Kang, C. *Proc. Natl. Acad. Sci. U. S. A.* **2007**, *104*, 5360–5365. doi:10.1073/pnas.0700915104
- Baer, P.; Rabe, P.; Citron, C. A.; de Oliveira Mann, C. C.; Kaufmann, N.; Groll, M.; Dickschat, J. S. *ChemBioChem* **2014**, *15*, 213–216. doi:10.1002/cbic.201300708
- Ding, L.; Goerls, H.; Dornblut, K.; Lin, W.; Maier, A.; Fiebig, H.-H.; Hertweck, C. *J. Nat. Prod.* **2015**, *78*, 2963–2967. doi:10.1021/acs.jnatprod.5b00674
- Dickschat, J. S. *Nat. Prod. Rep.* **2016**, *33*, 87–110. doi:10.1039/C5NP00102A
- Gietz, R. D.; Schiestl, R. H. *Nat. Protoc.* **2007**, *2*, 31–34. doi:10.1038/nprot.2007.13

40. Fulmer, G. R.; Miller, A. J. M.; Sherden, N. H.; Gottlieb, H. E.; Nudelman, A.; Stoltz, B. M.; Bercaw, J. E.; Goldberg, K. I. *Organometallics* **2010**, *29*, 2176–2179. doi:10.1021/om100106e
41. Rabe, P.; Barra, L.; Rinkel, J.; Riclea, R.; Citron, C. A.; Klapschinski, T. A.; Janusko, A.; Dickschat, J. S. *Angew. Chem., Int. Ed.* **2015**, *54*, 13448–13451. doi:10.1002/anie.201507615

## License and Terms

This is an Open Access article under the terms of the Creative Commons Attribution License (<http://creativecommons.org/licenses/by/4.0>), which permits unrestricted use, distribution, and reproduction in any medium, provided the original work is properly cited.

The license is subject to the *Beilstein Journal of Organic Chemistry* terms and conditions: (<http://www.beilstein-journals.org/bjoc>)

The definitive version of this article is the electronic one which can be found at:  
[doi:10.3762/bjoc.12.225](https://doi.org/10.3762/bjoc.12.225)

## Appendix E

### **Mechanistic Investigations of Two Bacterial Diterpene Cyclases: Spiroviolene Synthase and Tsukubadiene Synthase**

*Angew. Chem. Int. Ed.* **2017**, *56*, 2776–2779.

DOI:10.1002/anie.201612439

&

*Angew. Chem.* **2017**, *129*, 2820–2823.

DOI:10.1002/ange.201612439





## Biosynthesis

International Edition: DOI: 10.1002/anie.201612439  
German Edition: DOI: 10.1002/ange.201612439Mechanistic Investigations of Two Bacterial Diterpene Cyclases:  
Spiroviolene Synthase and Tsukubadiene Synthase

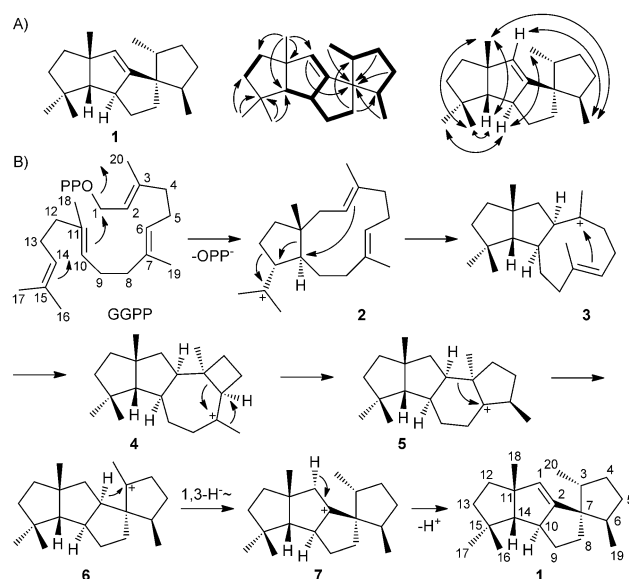
Patrick Rabe, Jan Rinkel, Etilia Dolja, Thomas Schmitz, Britta Nubbemeyer, T. Hoang Luu, and Jeroen S. Dickschat\*

**Abstract:** The mechanisms of two diterpene cyclases from streptomycetes—one with an unknown product that was identified as the spirocyclic hydrocarbon spiroviolene and one with the known product tsukubadiene—were investigated in detail by isotope labeling experiments. Although the structures of the products were very different, the cyclization mechanisms of both enzymes proceed through the same initial cyclization reactions, before they diverge towards the individual products, which is reflected in the close phylogenetic relationship of the enzymes.

The pioneering work by Otto Wallach in the 19th Century culminated in the identification of numerous terpenes from plants.<sup>[1]</sup> Much later it became evident that fungi,<sup>[2]</sup> bacteria,<sup>[3]</sup> and even eukaryotic microorganisms such as social amoebae<sup>[4]</sup> also produce a large variety of terpenes. The impressive conversions of linear precursors (oligoprenyl diphosphates, OPPs) into structurally complex, usually polycyclic, and chiral terpenes with several stereocenters proceed via cationic intermediates and are catalyzed by terpene cyclases (TCs). Many enzymes from bacteria have been investigated during the last two decades,<sup>[5]</sup> but the number of fully characterized diterpene cyclases (DTCs) is still limited.<sup>[6]</sup> Herein we report on the remarkable mechanisms of two bacterial DTCs that were uncovered by isotope labeling experiments.<sup>[7]</sup>

A gene for a TC homologue from *Streptomyces violens* NRRL ISP-5597, which exhibits all the highly conserved motifs of type I enzymes including the aspartate-rich motif (<sup>85</sup>DDHRC D), the NSE triad (<sup>226</sup>NDRHSLRKE),<sup>[8]</sup> the pyrophosphate sensor (Arg180),<sup>[9]</sup> and the <sup>312</sup>RY dimer (Figure S1), was cloned into the expression vector pYE-Express.<sup>[10]</sup> The recombinant purified protein (Figure S2) converted geranylgeranyl diphosphate (GGPP) into a diterpene hydrocarbon (Figure S3), while geranyl (GPP) and farnesyl diphosphate (FPP) were not accepted. The structure of the diterpene was elucidated by NMR spectroscopy (Table S3, Figures S4–S10), with three contiguous spin systems identified in the <sup>1</sup>H,<sup>1</sup>H-COSY spectrum. Their interconnection was delineated from key HMBC correlations,

while the relative configuration was established by NOESY correlations (Scheme 1 A), thereby resulting in the structure of (–)-spiroviolene (**1**) ( $[\alpha]_{\text{D}}^{21} = -5.6$  ( $c = 0.2$ , C<sub>6</sub>D<sub>6</sub>)).



**Scheme 1.** A) Structure of spiroviolene (**1**), continuous spin systems in <sup>1</sup>H,<sup>1</sup>H-COSY (bold), key HMBC and NOESY correlations (single- and double-headed arrows, respectively). B) Cyclization of GGPP to form **1**. The numbering of the carbon atoms of **1** indicates the origin of each carbon atom from GGPP.

The proposed biosynthesis of **1** by the spiroviolene synthase (SvS) starts with the cyclization of GGPP to form the bicyclic cation **2**, followed by a double Wagner–Meerwein rearrangement (WMR) and cyclization to form **3**. If the transformation of GGPP to **2** and of **2** to **3** are formulated as concerted processes, with the electron density migrating along the C14–C15 and C10–C14 bonds, secondary cation intermediates can be avoided and retention of configuration at C10 and C14 can be assumed. A third cyclization to generate **4** and dyotropic rearrangement<sup>[11]</sup> yield **5**, which can undergo a ring contraction to produce the spirocyclic cation **6**. A 1,3-hydride migration to form **7** followed by deprotonation result in **1**. This hypothetical pathway was tested by conversion of all 20 isotopomers of (<sup>13</sup>C<sub>1</sub>)GGPP with SvS. Although a route for their chemical synthesis was established,<sup>[12]</sup> an easier approach to the labeled probes is by enzymatic reactions of the 15 isotopomers of (<sup>13</sup>C<sub>1</sub>)FPP that we have previously synthesized<sup>[13]</sup> and isopentenyl diphosphate (IPP), or of FPP and synthetic (1-<sup>13</sup>C)IPP, (3-<sup>13</sup>C)IPP, or (4-<sup>13</sup>C)IPP

[\*] Dr. P. Rabe, J. Rinkel, E. Dolja, T. Schmitz, B. Nubbemeyer, T. H. Luu, Prof. Dr. J. S. Dickschat  
Kekulé-Institut für Organische Chemie und Biochemie, Rheinische Friedrich-Wilhelms-Universität Bonn  
Gerhard-Domagk-Strasse 1, 53121 Bonn (Germany)  
E-mail: dickschat@uni-bonn.de

Supporting information and the ORCID identification number(s) for the author(s) of this article can be found under:  
<http://dx.doi.org/10.1002/anie.201612439>.

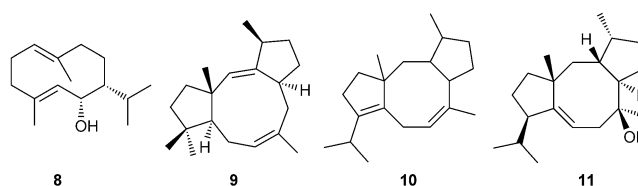
(Scheme S1). The elongations were performed using the GGPP synthase (GGPPS) from *Streptomyces cyaneofuscatus*. Only (2-<sup>13</sup>C)GGPP and (20-<sup>13</sup>C)GGPP were directly synthesized (Scheme S2). Small-scale reactions (1 mg) of the 20 isotopomers of (<sup>13</sup>C<sub>1</sub>)GGPP with SvS followed by extraction with C<sub>6</sub>D<sub>6</sub> and direct <sup>13</sup>C NMR analysis without product purification showed the <sup>13</sup>C label in the expected positions in all cases (Figure S11). For the geminal methyl groups C16 and C17 of GGPP SvS showed a strictly controlled stereochemical course (Figures S11R + S), as observed for most terpene cyclases.<sup>[5d,e,14]</sup> One of the few exceptions is (–)-guaia-6,10-(14)-diene synthase from *Fusarium fujikuroi*, which reveals a distribution of the label between C12 and C13 of FPP.<sup>[15]</sup>

Stereoselectively deuterated OPPs can be used for the determination of the absolute configurations of terpenes and of the intermediate  $\alpha$ -terpinyl cation en route to the achiral monoterpene 1,8-cineol.<sup>[5f,13d,16,17]</sup> The enzymatic conversion of these probes results in products with the deuterium label in diastereotopic positions, which can be distinguished by NMR spectroscopy. To increase the sensitivity of the probes in HSQC spectroscopy both enantiomers of (1-<sup>13</sup>C,1-<sup>2</sup>H)GPP and (1-<sup>13</sup>C,1-<sup>2</sup>H)FPP were synthesized with an additional <sup>13</sup>C label (Scheme S3) and with high enantiomeric purity (Figure S12). Incubation of SvS and GGPPS with (*R*)- and (*S*)-(1-<sup>13</sup>C,1-<sup>2</sup>H)FPP and IPP followed by product analysis by HSQC and comparison to the unlabeled compound allowed assignment of one of the two stereochemically different hydrogen atoms at the <sup>13</sup>C-labeled carbon atom to the site of deuterium incorporation and the other one to the site of protium incorporation, with a known absolute configuration of the stereocenter at this carbon atom (Figure S13). The absolute configuration of the other stereocenters in **1** was deduced by assignment of their relative configuration with respect to the stereocenter at the labeled carbon atom, thus resulting in the structure of (3*R*,6*R*,10*S*,11*R*,14*R*)-**1**. Consistent findings were obtained using the same strategy for the conversion of (*R*)- and (*S*)-(1-<sup>13</sup>C,1-<sup>2</sup>H)GPP (Figure S14). These experiments make use of the known inversion of configuration in chain elongations of OPPs with IPP by OPP synthases.<sup>[18]</sup>

The 1,3-hydride shift from **6** to **7** was investigated by conversion of (3-<sup>13</sup>C,2-<sup>2</sup>H)GGPP, which was prepared by using a reported method for deuterium introduction at C2 (Scheme S4).<sup>[19]</sup> With this probe, the hydride migration resulted in a direct bond between deuterium and the <sup>13</sup>C-labeled carbon atom in **1**, as indicated by a triplet in the <sup>13</sup>C NMR spectrum of the obtained product as a result of <sup>13</sup>C-<sup>2</sup>H spin coupling (Figure S15). The stereochemical course of the final deprotonation step was addressed using (*R*)- and (*S*)-(1-<sup>2</sup>H)GGPP (Scheme S3). GC/MS analysis of the enzyme products revealed the specific loss of deuterium from (*S*)-(1-<sup>2</sup>H)GGPP but not from the *R* enantiomer (Figure S16). These experiments demonstrate that the proton *syn* to the migrating hydride in the reaction from **6** to **7** is abstracted, if inversion of configuration at C1 is assumed for the initial 1,1-cyclization, as described for several terpene cyclases.<sup>[13b,20]</sup> A candidate base for the deprotonation of **7** is the diphosphate anion that leaves C1 of GGPP towards the

backside of the projection plane (Scheme 1) and is thus perfectly oriented to take up the proton in the final step.

A BLAST search using the SvS sequence as a probe was performed to identify closely related enzymes in other bacteria. A phylogenetic tree constructed from SvS and the 65 closest hits is shown in Figure S17. Organisms that were available from the DSMZ strain collection and that encode the most closely related enzymes to the SvS from *S. violens* were investigated for their production of **1**, which could be shown for the streptomycetes *S. ochraceiscleroticus*, *S. sclerotialis*, and *S. ambofaciens* as well as the actinomycete *Allokutzneria albata* (Figure S18). Closely related enzymes include the cyclases for (+)-(1(10)*E*,4*E*,6*S*,7*R*)-germacradien-6-ol (**8**, Scheme 2),<sup>[13]</sup> tsukubadiene (**9**), and cyclooctat-

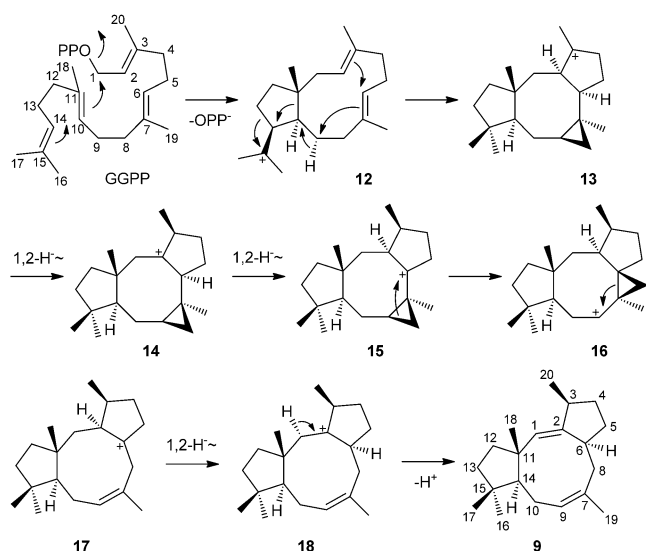


**Scheme 2.** Terpenes produced by enzymes with a close relationship to SvS (**8**–**10**) and structure of cyclooctat-9-en-7-ol (**11**).

7(8),10(14)-diene (**10**).<sup>[6b]</sup> Although their enzymes are phylogenetically distant, the structural similarity of the products **10** and cyclooctat-9-en-7-ol (**11**) suggests that the cyclization mechanism for **10** may be similar to the mechanism for **11**, which proceeds through a surprising rearrangement of a cyclopropane intermediate.<sup>[6a]</sup> This prompted us to investigate whether **9** is also formed by a related mechanism.

For this purpose, the gene for the tsukubadiene synthase (TdS) from *Streptomyces tsukubaensis* NRRL 18488 was cloned and expressed in *E. coli* (Figure S2). Consistent with the reported findings by heterologous expression in *Streptomyces avermitilis*,<sup>[6b]</sup> the purified protein converted GGPP into a single product (Figure S19), while GPP and FPP were not accepted. Since only the planar structure of **9** had been reported, the diterpene product was isolated and its structure fully elucidated by extensive NMR spectroscopy (Table S4, Figures S20–S26). The relative configuration determined by NOESY experiments, as shown in Scheme 2, was in line with the suggested structure based on a comparison of the recorded and calculated NMR data for all stereoisomers of **9**.<sup>[21]</sup>

The proposed cyclization mechanism of TdS starts with the cyclization of GGPP to **12** (Scheme 3). The further reactions, including a ring expansion and ring contraction by WMR, a 1,2-hydride migration, as well as a 7,9- and a 2,6-cyclization to form **13**, may be a concerted process with retention of configuration at C14 to avoid secondary cation intermediates. Two subsequent 1,2-hydride migrations via **14** to generate **15** may be followed by a rearrangement of the cyclopropane ring, similar to a key step in the biosynthesis of **11**.<sup>[6a]</sup> A ring opening to produce **17**, 1,2-hydride migration to form **18**, and deprotonation yield **9**. This suggested mechanism was tested by conversion of all 20 isotopomers of



**Scheme 3.** Cyclization of GGPP to generate **9**. The numbering of the carbon atoms of **9** indicates the origin for each carbon atom from GGPP.

( $^{13}\text{C}_1$ )GGPP with TdS, which resulted in the appearance of label in each of the expected positions and, thus, confirmed the model (Figures S27 and S28).

The absolute configuration of **9** was determined by the same strategy as described above for **1**. The conversion of both enantiomers of (1- $^{13}\text{C}$ ,1- $^2\text{H}$ )FPP yielded products with specific incorporation of deuterium into one of two stereochemically distinct hydrogen atoms, as determined by HSQC (Figure S29). The experiments with both labeled probes consistently established the absolute configuration of (3*S*,6*S*,11*R*,14*S*)-**9**.

The stereochemical course of the 1,2-hydride shift from C9 to C10 in the reaction from **12** to **13** was investigated by enzymatic conversion of (*R*)- and (*S*)-(1- $^{13}\text{C}$ ,1- $^2\text{H}$ )GPP and IPP with GGPPs and TdS. The  $^{13}\text{C}$  NMR spectrum of the product obtained from (*R*)-(1- $^{13}\text{C}$ ,1- $^2\text{H}$ )GPP showed a strong triplet for C9, while the product formed from the *S* enantiomer exhibited an upfield-shifted singlet that indicated the presence of a deuterium at a neighboring carbon atom (Figure S30).  $^1\text{H}$  NMR analysis of the product obtained from (*S*)-(1- $^2\text{H}$ )GPP<sup>[17]</sup> revealed simplified multiplicities for H9 and H14, and demonstrated the specific incorporation of deuterium into H10<sub>β</sub>, which was confirmed by NOESY experiments (Figures S30 and S31). Overall, these data established the stereospecific migration of H9<sub>α</sub> with inversion of configuration at C10 in the step from **12** to **13**.

The two sequential 1,2-hydride shifts from intermediate **13** to **14** and from **14** to **15** were addressed with deuterated and  $^{13}\text{C}$ -labeled substrates. The possibility of a single 1,3-hydride migration with direct formation of **15** from **13** was also taken into consideration.  $^{13}\text{C}$  NMR analysis of the product obtained from (3- $^{13}\text{C}$ )IPP and (2- $^2\text{H}$ )FPP (Schemes S1 and S4) with GGPPs and TdS showed a singlet for the C3 atom of **9**, which is not consistent with a possible 1,3-hydride transfer (Figure S32B). Comparison of the chemical shift for C3 to the  $^{13}\text{C}$  NMR data of unlabeled **9** (Figure S32A)

indicated a slight upfield shift ( $\delta\Delta = 0.04$  ppm), in agreement with deuterium being attached to a neighboring carbon atom (C6). In contrast, incubation of (3- $^{13}\text{C}$ ,2- $^2\text{H}$ )GGPP (Scheme S4) with TdS gave a product showing a strong triplet in the  $^{13}\text{C}$  NMR spectrum (Figure S32C,  $^1J_{\text{C,D}} = 19.6$  Hz,  $\delta\Delta = 0.44$  ppm). These data established the direct  $^{13}\text{C}$ - $^2\text{H}$  connection, which is in agreement with two sequential 1,2-hydride shifts. Similar findings were reported for the cyclization mechanisms of cyclooctat-9-en-7-ol synthase<sup>[22]</sup> and corvul ether synthase.<sup>[23]</sup> The tentatively assigned relative orientation of the cyclopropane ring in the intermediates **13**–**16** cannot be deduced with certainty from the structure of the final product **9**, but the orientation as shown in Scheme 3 requires an inversion of configuration at C6 in the conversion of **14** into **16**, which seems more likely than retention of configuration.

As demonstrated by enzymatic cyclization of stereospecifically deuterated (*R*)- and (*S*)-(1- $^2\text{H}$ )GGPP, the final deprotonation step towards **9** proceeds with loss of deuterium from the *S* enantiomer, while the deuterium from the *R* enantiomer is retained (Figure S33). Assuming inversion of configuration in the initial 1,11-cyclization,<sup>[14b,20]</sup> these experiments reveal a deprotonation from C1 *syn* to the migrating hydride in the reaction from **17** to **18**. The diphosphate anion leaves C1 towards the backside of the projection plane (Scheme 3) and is perfectly located to act as the base in the terminal deprotonation to **9**.

Isotope labeling experiments continue to be an important method to obtain mechanistic insights into the remarkable reactions of terpene cyclases.<sup>[5b,6a,13,14d,15,24]</sup> We have shown here that not only many details of the cyclization mechanism, including stereochemical aspects, but also the absolute configurations of terpenes can be elucidated using stereospecifically deuterated precursors. The knowledge of the absolute configurations of **1** and **9** allows for a comparison of the cyclization mechanisms of SvS and TdS. The first elementary reaction for both enzymes proceeds by 1,11*Si*-cyclization of GGPP. In this step, the same absolute configuration at C11 is installed and is not changed during the further process. Simultaneously, SvS catalyzes a 10*Re*,14*Si*-cyclization, while for TdS a 10*Re*,14*Re* process is observed, which requires a different relative orientation of C10 and C15 of the folded GGPP in the active site. The methyl group C16 and H14, which are *cis*-oriented in GGPP, end up in both cases on the same faces of **1** and **9**, thus showing the strict stereochemical course in the 10,14-cyclization by both enzymes. The initially formed bicyclic cations **2** and **12** are diastereomers, and the downstream reactions to the individual products deviate to yield the structurally very different products **1** and **9**. However, the final deprotonation step proceeds in both cases from the side to which the diphosphate is expelled in the ionization step, thereby suggesting that diphosphate may act as the base in the terminal step. It is interesting to note that SvS and TdS are closely related, as shown by a phylogenetic analysis of more than 1000 bacterial terpene cyclases (Figure S34), which suggests that a few critical substitutions in the amino acid sequence of a terpene cyclase can cause a minor change of the substrate's conformational fold in the active site, but with a dramatic effect on the structure of the product.

## Acknowledgements

This work was funded by the DFG (DI1536/7-1) and by the Fonds der Chemischen Industrie.

**Keywords:** biosynthesis · isotopes · NMR spectroscopy · reaction mechanisms · terpenes

**How to cite:** *Angew. Chem. Int. Ed.* **2017**, *56*, 2776–2779  
*Angew. Chem.* **2017**, *129*, 2820–2823

- [1] O. Wallach, *Justus Liebig's Ann. Chem.* **1885**, *227*, 277.
- [2] M. B. Quin, C. M. Flynn, C. Schmidt-Dannert, *Nat. Prod. Rep.* **2014**, *31*, 1449.
- [3] a) N. N. Gerber, H. A. Lechevalier, *Appl. Microbiol.* **1965**, *13*, 935; b) K. Wilkins, C. Schöller, *Actinomycetologica* **2009**, *23*, 27; c) C. A. Citron, J. Gleitzmann, G. Laurenzano, R. Pukall, J. S. Dickschat, *ChemBioChem* **2012**, *13*, 202.
- [4] X. Chen, T. G. Köllner, Q. Jia, A. Norris, B. Santhanam, P. Rabe, J. S. Dickschat, G. Shaulsky, J. Gershenzon, F. Chen, *Proc. Natl. Acad. Sci. USA* **2016**, *113*, 12132.
- [5] Reviewed in: a) J. S. Dickschat, *Nat. Prod. Rep.* **2016**, *33*, 87; following reports: b) P. Rabe, J. Rinkel, T. A. Klapschinski, L. Barra, J. S. Dickschat, *Org. Biomol. Chem.* **2016**, *14*, 158; c) A. Schiffrin, Y. Khatri, P. Kirsch, V. Thiel, S. Schulz, R. Bernhardt, *Org. Biomol. Chem.* **2016**, *14*, 3385; d) T. A. Klapschinski, P. Rabe, J. S. Dickschat, *Angew. Chem. Int. Ed.* **2016**, *55*, 10141; *Angew. Chem.* **2016**, *128*, 10296; e) P. Rabe, T. Schmitz, J. S. Dickschat, *Beilstein J. Org. Chem.* **2016**, *12*, 1839; f) J. Rinkel, P. Rabe, P. Garbeva, J. S. Dickschat, *Angew. Chem. Int. Ed.* **2016**, *55*, 13593; *Angew. Chem.* **2016**, *128*, 13791.
- [6] a) A. Meguro, Y. Motoyoshi, K. Teramoto, S. Ueda, Y. Totsuka, Y. Ando, T. Tomita, S.-Y. Kim, T. Kimura, M. Igarashi, R. Sawa, T. Shinada, M. Nishiyama, T. Kuzuyama, *Angew. Chem. Int. Ed.* **2015**, *54*, 4353; *Angew. Chem.* **2015**, *127*, 4427; b) Y. Yamada, T. Kuzuyama, M. Komatsu, K. Shin-ya, S. Omura, D. E. Cane, H. Ikeda, *Proc. Natl. Acad. Sci. USA* **2015**, *112*, 857; c) A. Meguro, T. Tomita, M. Nishiyama, T. Kuzuyama, *ChemBioChem* **2013**, *14*, 316; d) M. J. Smanski, R. M. Peterson, S.-X. Huang, B. Shen, *Curr. Opin. Chem. Biol.* **2012**, *16*, 132.
- [7] J. Rinkel, J. S. Dickschat, *Beilstein J. Org. Chem.* **2015**, *11*, 2493.
- [8] a) C. M. Starks, K. Back, J. Chappell, J. P. Noel, *Science* **1997**, *277*, 1815; b) M. Köksal, Y. Jin, R. M. Coates, R. Croteau, D. W. Christianson, *Nature* **2011**, *469*, 116.
- [9] P. Baer, P. Rabe, K. Fischer, C. A. Citron, T. A. Klapschinski, M. Groll, J. S. Dickschat, *Angew. Chem. Int. Ed.* **2014**, *53*, 7652; *Angew. Chem.* **2014**, *126*, 7783.
- [10] J. S. Dickschat, K. A. K. Pahirulzaman, P. Rabe, T. A. Klapschinski, *ChemBioChem* **2014**, *15*, 810.
- [11] P. Gutta, D. J. Tantillo, *J. Am. Chem. Soc.* **2006**, *128*, 6172.
- [12] C. A. Citron, P. Rabe, L. Barra, C. Nakano, T. Hoshino, J. S. Dickschat, *Eur. J. Org. Chem.* **2014**, 7684.
- [13] P. Rabe, L. Barra, J. Rinkel, R. Riclea, C. A. Citron, T. A. Klapschinski, A. Janusko, J. S. Dickschat, *Angew. Chem. Int. Ed.* **2015**, *54*, 13448; *Angew. Chem.* **2015**, *127*, 13649.
- [14] a) D. E. Cane, T. Rossi, A. M. Tillman, J. P. Pachlatko, *J. Am. Chem. Soc.* **1981**, *103*, 1838; b) C.-M. Wang, R. Hopson, X. Lin, D. E. Cane, *J. Am. Chem. Soc.* **2009**, *131*, 8360; c) N. L. Brock, S. R. Ravella, S. Schulz, J. S. Dickschat, *Angew. Chem. Int. Ed.* **2013**, *52*, 2100; *Angew. Chem.* **2013**, *125*, 2154; d) P. Rabe, J. Rinkel, B. Nubbemeyer, T. G. Köllner, F. Chen, J. S. Dickschat, *Angew. Chem. Int. Ed.* **2016**, *55*, 15420; *Angew. Chem.* **2016**, *128*, 15646.
- [15] I. Burkhardt, T. Siemon, M. Henrot, L. Studt, S. Rösler, B. Tudzynski, M. Christmann, J. S. Dickschat, *Angew. Chem. Int. Ed.* **2016**, *55*, 8748; *Angew. Chem.* **2016**, *128*, 8890.
- [16] D. E. Cane, D. B. McIlwaine, J. S. Oliver, *J. Am. Chem. Soc.* **1990**, *112*, 1285.
- [17] J. Rinkel, P. Rabe, L. zur Horst, J. S. Dickschat, *Beilstein J. Org. Chem.* **2016**, *12*, 2317.
- [18] H. V. Thulasiram, C. D. Poulter, *J. Am. Chem. Soc.* **2006**, *128*, 15819.
- [19] J. A. Faraldos, S. Wu, J. Chappell, R. M. Coates, *J. Am. Chem. Soc.* **2010**, *132*, 2998.
- [20] D. E. Cane, J. S. Oliver, P. H. M. Harrison, C. Abell, B. R. Hubbard, C. T. Kane, R. Lattman, *J. Am. Chem. Soc.* **1990**, *112*, 4513.
- [21] Q. N. N. Nguyen, D. J. Tantillo, *J. Antibiot.* **2016**, *69*, 534.
- [22] H. Sato, K. Teramoto, Y. Masumoto, N. Tezuka, K. Sakai, S. Ueda, Y. Totsuka, T. Shinada, M. Nishiyama, C. Wang, T. Kuzuyama, M. Uchiyama, *Sci. Rep.* **2015**, *5*, 18471.
- [23] a) P. Rabe, A. Janusko, B. Goldfuss, J. S. Dickschat, *ChemBioChem* **2016**, *17*, 146; b) P. Rabe, K. A. K. Pahirulzaman, J. S. Dickschat, *Angew. Chem. Int. Ed.* **2015**, *54*, 6041; *Angew. Chem.* **2015**, *127*, 6139.
- [24] a) Y. Matsuda, T. Mitsuhashi, S. Lee, M. Hoshino, T. Mori, M. Okada, H. Zhang, F. Hayashi, M. Fujita, I. Abe, *Angew. Chem. Int. Ed.* **2016**, *55*, 5785; *Angew. Chem.* **2016**, *128*, 5879; b) B. Qin, Y. Matsuda, T. Mori, M. Okada, Z. Quan, T. Mitsuhashi, T. Wakimoto, I. Abe, *Angew. Chem. Int. Ed.* **2016**, *55*, 1658; *Angew. Chem.* **2016**, *128*, 1690; c) M. Matsuda, T. Mitsuhashi, Z. Quan, I. Abe, *Org. Lett.* **2015**, *17*, 4644; d) R. Chiba, A. Minami, K. Gomi, H. Oikawa, *Org. Lett.* **2013**, *15*, 594; e) R. Riclea, J. S. Dickschat, *Angew. Chem. Int. Ed.* **2015**, *54*, 12167; *Angew. Chem.* **2015**, *127*, 12335; f) M. Okada, Y. Matsuda, T. Mitsuhashi, S. Hoshino, T. Mori, K. Nakagawa, Z. Quan, B. Qin, H. Zhang, F. Hayashi, H. Kawaide, I. Abe, *J. Am. Chem. Soc.* **2016**, *138*, 10011.

Manuscript received: December 22, 2016

Final Article published: January 31, 2017

## Biosynthesen

Deutsche Ausgabe: DOI: 10.1002/ange.201612439  
Internationale Ausgabe: DOI: 10.1002/anie.201612439Mechanistische Studien an zwei bakteriellen Diterpencyclasen:  
Spiroviolen-Synthase und Tsukubadien-Synthase

Patrick Rabe, Jan Rinkel, Etilia Dolja, Thomas Schmitz, Britta Nubbemeyer, T. Hoang Luu und Jeroen S. Dickschat\*

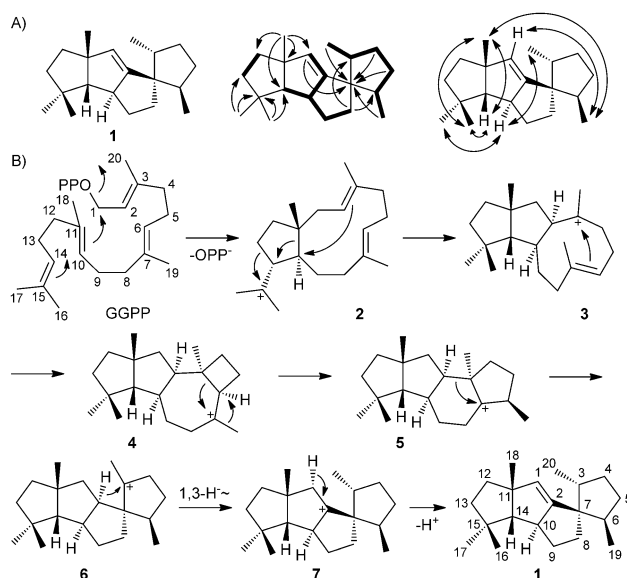
**Abstract:** Die Mechanismen von zwei Diterpencyclasen aus *Streptomyces* – eine mit unbekanntem Produkt, das als der spirocyclische Kohlenwasserstoff Spiroviolen identifiziert wurde, und eine mit dem bekannten Produkt Tsukubadien – wurden detailliert durch Isotopenmarkierungsexperimente untersucht. Obwohl die Strukturen der Produkte sehr unterschiedlich sind, beginnen die Cyclisierungsmechanismen beider Enzyme mit derselben Cyclisierungsreaktion, bevor sie auf dem Weg zu ihren individuellen Produkten divergieren. Dies spiegelt die nahe phylogenetische Verwandtschaft der Enzyme wider.

Die bahnbrechenden Arbeiten von Otto Wallach im 19. Jahrhundert kulminierten in der Identifizierung einer Vielzahl von Terpenen aus Pflanzen.<sup>[1]</sup> Viel später wurde erkannt, dass auch Pilze,<sup>[2]</sup> Bakterien<sup>[3]</sup> und sogar eukaryotische Mikroorganismen wie soziale Amöben<sup>[4]</sup> vielfältige Terpene produzieren. Die beeindruckenden Umsetzungen linearer Vorstufen (Oligoprenyldiphosphate, OPPs) in strukturell komplexe, im allgemeinen polycyclische und chirale Terpene mit mehreren Stereozentren verlaufen über kationische Intermediate und werden durch Terpencyclasen (TCs) katalysiert. Im Hinblick auf Bakterien wurden in den vergangenen zwei Jahrzehnten viele Enzyme dieser Familie studiert,<sup>[5]</sup> aber die Anzahl charakterisierter Diterpencyclasen (DTCs) ist noch immer gering.<sup>[6]</sup> Hier berichten wir über die ungewöhnlichen Mechanismen von zwei bakteriellen DTCs, die durch Isotopenmarkierungsexperimente aufgedeckt wurden.<sup>[7]</sup>

Ein Gen für eine TC aus *Streptomyces violens* NRRL ISP-5597, die alle hochkonservierten Motive von Enzymen des Typs I einschließlich des Aspartat-reichen Motivs (<sup>85</sup>DDHRCDD), der NSE-Triade (<sup>226</sup>NDRHSLRKE),<sup>[8]</sup> des Pyrophosphatsensors (Arg 180)<sup>[9]</sup> und des <sup>312</sup>RY-Dimers aufweist (Abbildung S1), wurde in den Expressionsvektor pYE-Express kloniert.<sup>[10]</sup> Das rekombinante gereinigte Protein (Abbildung S2) konvertierte Geranylgeranyldiphosphat (GGPP) in einen Diterpen-Kohlenwasserstoff (Abbildung S3), während Geranyl- (GPP) und Farnesyldiphosphat

(FPP) nicht akzeptiert wurden. Die Struktur des Diterpens wurde per NMR-Spektroskopie aufgeklärt (Tabelle S3, Abbildungen S4–S10), was drei geschlossene Spinsysteme im <sup>1</sup>H,<sup>1</sup>H-COSY-Spektrum aufzeigte. Ihre Verknüpfung wurde aus diagnostischen HMBC-Korrelationen abgeleitet, und die relative Konfiguration wurde auf Basis von NOESY-Korrelationen etabliert (Schema 1 A), sodass sich die Struktur von (–)-Spiroviolen (**1**) ergab ( $[\alpha]_{\text{D}}^{21} = -5.6$  (c 0.2, C<sub>6</sub>D<sub>6</sub>)).

Ein Vorschlag zur Biosynthese von **1** durch die Spiroviolen-Synthase (SvS) startet mit der Cyclisierung von GGPP zum bicyclischen Kation **2**, gefolgt von einer doppelten Wagner-Meerwein-Umlagerung (WMU) und Cyclisierung zu **3**. Wenn die Reaktionen von GGPP zu **2** und von **2** zu **3** als konzertierter Prozess mit entlang der C14-C15- und C10-C14-Bindungen wandernder Elektronendichte formuliert werden, können sekundäre Kationen als Intermediate vermieden werden, und es folgt Retention der Konfiguration an C10 und C14. Eine dritte Cyclisierung zu **4** und dyotrope Umlagerung<sup>[11]</sup> führen zu **5**, das durch Ringkontraktion zum spirocyclischen Kation **6** reagiert. Eine 1,3-Hydridwanderung zu **7** und Deprotonierung liefern **1**. Dieser hypothetische Weg wurde durch Umsetzung aller 20 Isotopomere von (<sup>13</sup>C<sub>1</sub>)GGPP mit SvS geprüft. Obwohl eine Route für deren



**Scheme 1.** A) Struktur von Spiroviolen (**1**), kontinuierliche Spinsysteme im <sup>1</sup>H,<sup>1</sup>H-COSY (fett), diagnostische HMBC- und NOESY-Korrelationen (einfache und Doppelpfeile). B) Cyclisierung von GGPP zu **1**. Die Nummerierung der Kohlenstoffatome von **1** verweist auf den Ursprung dieser Atome aus GGPP.

[\*] Dr. P. Rabe, J. Rinkel, E. Dolja, T. Schmitz, B. Nubbemeyer, T. H. Luu, Prof. Dr. J. S. Dickschat  
Kekulé-Institut für Organische Chemie und Biochemie  
Rheinische Friedrich-Wilhelms-Universität Bonn  
Gerhard-Domagk-Straße 1, 53121 Bonn (Deutschland)  
E-Mail: dickschat@uni-bonn.de

Hintergrundinformationen und die Identifikationsnummer (ORCID) eines Autors sind unter:  
<http://dx.doi.org/10.1002/ange.201612439> zu finden.

chemische Synthese etabliert worden ist,<sup>[12]</sup> ist ein einfacherer Zugang zu den markierten Proben durch enzymatische Reaktion der 15 Isotomere von (<sup>13</sup>C<sub>1</sub>)FPP, die wir zuvor synthetisiert hatten,<sup>[13]</sup> und Isopentenylidiphosphat (IPP) oder von FPP und synthetischem (1-<sup>13</sup>C)IPP, (3-<sup>13</sup>C)IPP oder (4-<sup>13</sup>C)IPP möglich (Schema S1). Die Verlängerungen wurden mit der GGPP-Synthase (GGPPS) aus *Streptomyces cyaneofuscatus* durchgeführt. Lediglich (2-<sup>13</sup>C)GGPP und (20-<sup>13</sup>C)GGPP wurden direkt synthetisiert (Schema S2). Reaktionen im kleinen Maßstab (1 mg) der 20 Isotomere von (<sup>13</sup>C<sub>1</sub>)GGPP mit SvS, gefolgt von Extraktion mit C<sub>6</sub>D<sub>6</sub> und direkter <sup>13</sup>C-NMR-Analyse ohne Produktreinigung, ergaben für alle Fälle eine <sup>13</sup>C-Markierung in den zu erwartenden Positionen (Abbildung S11). Im Hinblick auf das Schicksal der geminalen Methylgruppen C16 und C17 von GGPP zeigte die SvS eine strenge Kontrolle des stereochemischen Verlaufs (Abbildungen S11R + S), wie es für die meisten Terpenocyclasen beobachtet wurde.<sup>[5d,e,14]</sup> Eine der wenigen Ausnahmen ist die (–)-Guaia-6,10(14)-dien-Synthase aus *Fusarium fujikuroi*, die zu einer Verteilung der Markierungen aus C12 und C13 von FPP führt.<sup>[15]</sup>

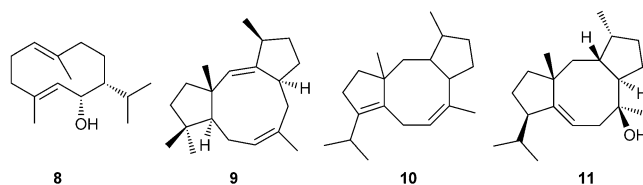
Stereoselektiv deuterierte OPPs können für die Bestimmung der absoluten Konfigurationen von Terpenen und des intermediären  $\alpha$ -Terpinyl-Kations auf dem Weg zum achiralen Monoterpen 1,8-Cineol genutzt werden.<sup>[5f,13d,16,17]</sup> Die enzymatische Umsetzung dieser Proben liefert Produkte mit Deuteriummarkierung in diastereotopen Positionen, die NMR-spektroskopisch unterschieden werden können. Um die Empfindlichkeit dieser Proben in der HSQC-Spektroskopie zu erhöhen, wurden beide Enantiomere von (1-<sup>13</sup>C,1-<sup>2</sup>H)GPP und (1-<sup>13</sup>C,1-<sup>2</sup>H)FPP mit einer zusätzlichen <sup>13</sup>C-Markierung (Schema S3) und mit hoher Enantiomerenreinheit synthetisiert (Abbildung S12). Die Inkubation von SvS und GGPPS mit (*R*)- und (*S*)-(1-<sup>13</sup>C,1-<sup>2</sup>H)FPP und IPP, gefolgt von Produktanalyse per HSQC im Vergleich mit der unmarkierten Verbindung, ermöglichte die Zuordnung von einem der zwei stereochemisch unterschiedlichen Wasserstoffatomen am <sup>13</sup>C-markierten Kohlenstoffatom als Position des Deuteriumeinbaus und die andere Position als diejenige des Protiumeinbaus mit bekannter absoluter Konfiguration des Stereozentrums an diesem Kohlenstoffatom (Abbildung S13). Die absoluten Konfigurationen der anderen Stereozentren in **1** wurden durch Zuweisung der relativen Konfigurationen in Bezug auf das bekannte Stereozentrum am markierten Kohlenstoffatom abgeleitet, woraus sich die Struktur von (3*R*,6*R*,10*S*,11*R*,14*R*)-**1** ergab. Konsistente Ergebnisse wurden mittels derselben Strategie durch Umsetzung von (*R*)- und (*S*)-(1-<sup>13</sup>C,1-<sup>2</sup>H)GPP erhalten (Abbildung S14). Diese Experimente stützen sich auf die bekannte Inversion der Konfiguration in Kettenverlängerungen von OPPs mit IPP durch OPP-Synthasen.<sup>[18]</sup>

Die 1,3-Hydridverschiebung von **6** zu **7** wurde durch Umsetzung von (3-<sup>13</sup>C,2-<sup>2</sup>H)GGPP, das über eine bekannte Methode zur Einführung von Deuterium an C2 präpariert wurde (Schema S4), untersucht.<sup>[19]</sup> Mit dieser Probe ergab die Hydridwanderung eine direkte Bindung von Deuterium zum <sup>13</sup>C-markierten Kohlenstoffatom in **1**, was durch ein Triplett im <sup>13</sup>C-NMR-Spektrum des erhaltenen Produktes aufgrund einer <sup>13</sup>C-<sup>2</sup>H-Spinnkopplung nachgewiesen wurde (Abbil-

dung S15). Der stereochemische Verlauf des finalen Deprotonierungsschrittes wurde mit (*R*)- und (*S*)-(1-<sup>2</sup>H)GGPP adressiert (Schema S3). GC/MS-Analyse des Enzymproduktes zeigte den spezifischen Verlust von Deuterium aus (*S*)-(1-<sup>2</sup>H)GGPP und dessen Verbleib in **1** aus dem (*R*)-Enantiomer (Abbildung S16). Diese Experimente demonstrieren, dass das zum in der Reaktion von **6** nach **7** wandernden Hydrids synständige Proton abstrahiert wird, sofern Inversion der Konfiguration an C1 für die initiale 1,11-Cyclisierung angenommen wird, wie es für diverse Terpenocyclasen beschrieben ist.<sup>[13b,20]</sup> Eine mögliche Base für die Deprotonierung von **7** ist das Diphosphat-Anion, das C1 von GGPP in Richtung auf den rückwärtigen Raum der Projektionsebene verlässt (Schema 1) und daher für die Aufnahme des Protons perfekt positioniert ist.

Eine BLAST-Suche mit der SvS-Sequenz als Sonde wurde durchgeführt, um nahe verwandte Enzyme aus Bakterien zu identifizieren. Ein phylogenetischer Baum, der aus SvS und den 65 nächsten Verwandten erstellt wurde, ist in Abbildung S17 gezeigt. Organismen, die aus der Stammsammlung des DSMZ verfügbar waren und die die nächsten verwandten Enzyme zu SvS aus *S. violens* kodieren, wurden auf die Produktion von **1** untersucht, die für die Streptomyceten *S. ochraceiscleroticus*, *S. sclerotialis* und *S. ambofaciens* sowie den Actinomyceten *Allokutzneria albata* gezeigt werden konnte (Abbildung S18). Nahe verwandte Enzyme sind auch die Cyclasen für (+)-(1(10)*E*,4*E*,6*S*,7*R*)-Germacradien-6-ol (**8**, Schema 2),<sup>[13]</sup> Tsukubadien (**9**) und Cyclooctat-7(8),10(14)-dien (**10**).<sup>[6b]</sup> Obwohl ihre Enzyme phylogenetisch distal sind, lässt die strukturelle Ähnlichkeit der Produkte **10** und Cyclooctat-9-en-7-ol (**11**) vermuten, dass der Cyclisierungsmechanismus für **10** ähnlich zu demjenigen für **11** ist, der über eine überraschende Umlagerung eines Cyclopropan-Intermediates abläuft.<sup>[6a]</sup> Diese Überlegung veranlasste uns zu untersuchen, ob auch **9** über einen analogen Mechanismus gebildet wird.

Zu diesem Zweck wurde das Gen der Tsukubadien-Synthase (TdS) aus *Streptomyces tsukubaensis* NRRL 18488 kloniert und in *E. coli* exprimiert (Abbildung S2). In Übereinstimmung mit den Ergebnissen aus der heterologen Expression in *Streptomyces avermitilis*<sup>[6b]</sup> wandelte das gereinigte Protein GGPP in ein einziges Produkt um (Abbildung S19), während GPP und FPP nicht akzeptiert wurden. Da bisher nur über die Planarstruktur von **9** berichtet worden war, wurde das Diterpen isoliert und dessen Struktur durch NMR-Spektroskopie vollständig aufgeklärt (Tabelle S4, Abbildungen S20–S26). Die aus dem NOESY abgeleitete relative Konfiguration, wie in Schema 2 gezeigt, stimmte mit der



**Schema 2.** Terpene, die durch Enzyme mit naher Verwandtschaft zur SvS gebildet werden (**8–10**) und die Struktur von Cyclooctat-9-en-7-ol (**11**).

auf Basis eines Vergleichs von gemessenen mit berechneten NMR-Daten für alle Stereoisomere von **9** vorgeschlagenen Struktur überein.<sup>[21]</sup>

Der mögliche Cyclisierungsmechanismus von TdS beginnt mit der Cyclisierung von GGPP zu **12** (Schema 3). Die weiteren Reaktionen beinhalten eine Ringerweiterung und Ringverengung durch WMU, eine 1,2-Hydridwanderung, eine 7,9- und eine 2,6-Cyclisierung zu **13** und verlaufen wahrscheinlich konzertiert mit Retention der Konfiguration an C14, um sekundäre Kationen als Intermediate zu vermeiden. Auf zwei anschließende 1,2-Hydridwanderungen über **14** zu **15** folgt möglicherweise eine Umlagerung eines Cyclopropanringes, wie sie auch in einem Schlüsselschritt der Biosynthese von **11** stattfindet.<sup>[6a]</sup> Eine Ringöffnung zu **17**, 1,2-Hydridverschiebung zu **18** und Deprotonierung liefern **9**. Dieser vorgeschlagene Mechanismus wurde durch Umsetzung aller 20 Isotomere von (<sup>13</sup>C<sub>1</sub>)GGPP mit TdS getestet, was in dem Auftreten der Markierung in der jeweils erwarteten Position resultierte und somit das Modell bestätigte (Abbildungen S27 und S28).

Die absolute Konfiguration von **9** wurde über dieselbe Strategie wie für **1** beschrieben bestimmt. Die Umsetzung beider Enantiomere von (1-<sup>13</sup>C,1-<sup>2</sup>H)FPP ergab Produkte mit spezifischem Deuteriumeinbau in eine von zwei stereochemisch unterschiedlichen Wasserstoff-Positionen, was per HSQC nachgewiesen wurde (Abbildung S29). Die Experimente mit beiden markierten Proben etablierten übereinstimmend die absolute Konfiguration von (3*S*,6*S*,11*R*,14*S*)-**9**.

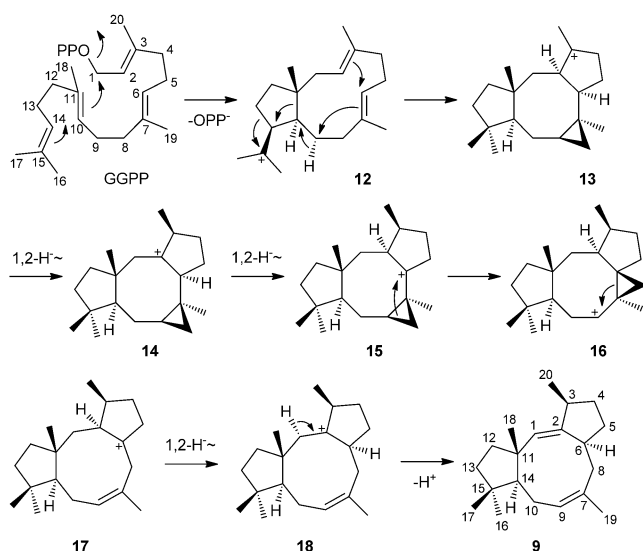
Der stereochemische Verlauf der 1,2-Hydridverschiebung von C9 nach C10 in der Reaktion von **12** zu **13** wurde durch enzymatische Umsetzung von (*R*)- und (*S*)-(1-<sup>13</sup>C,1-<sup>2</sup>H)GPP mit IPP, GGPPS und TdS untersucht. Das <sup>13</sup>C-NMR-Spektrum des aus (*R*)-(1-<sup>13</sup>C,1-<sup>2</sup>H)GPP erhaltenen Produktes zeigte ein intensives Triplett für C9, wohingegen das aus dem (*S*)-Enantiomer gebildete Produkt ein hochfeldverschobenes Singulett aufwies, das die Präsenz eines Deuteriumatoms an

einem benachbarten Kohlenstoffatom anzeigte (Abbildung S30). <sup>1</sup>H-NMR-Analyse des aus (*S*)-(1-<sup>2</sup>H)GPP<sup>[17]</sup> erhaltenen Produktes ergab vereinfachte Multiplizitäten für H9 und H14 und demonstrierte den spezifischen Einbau des Deuteriums in H10<sub>β</sub>, was durch NOESY bestätigt wurde (Abbildungen S30 und S31). In Summe zeigen diese Daten die stereospezifische Wanderung von H9<sub>α</sub> mit Inversion der Konfiguration an C10 in dem Schritt von **12** nach **13**.

Die zwei sequenziellen 1,2-Hydridverschiebungen von Intermediat **13** nach **14** und von **14** nach **15** wurden mit deuterierten und <sup>13</sup>C-markierten Substraten adressiert. Die Möglichkeit einer einzelnen 1,3-Hydridwanderung mit direkter Bildung von **15** aus **13** wurde ebenfalls in Betracht gezogen. <sup>13</sup>C-NMR-Analyse des aus (3-<sup>13</sup>C)IPP und (2-<sup>2</sup>H)FPP erhaltenen Produktes (Schemata S1 und S4) mit GGPPS und TdS zeigte ein Singulett für C3 von **9**, was einem möglichen 1,3-Hydridtransfer widerspricht (Abbildung S32B). Vergleich der chemischen Verschiebung für C3 mit den <sup>13</sup>C-NMR-Daten von unmarkiertem **9** (Abbildung S32A) zeigte eine leichte Hochfeldverschiebung ( $\delta\Delta = 0.04$  ppm), was in Übereinstimmung mit der Anbindung von Deuterium an einem benachbarten Kohlenstoffatom ist (C6). Stattdessen ergab die Inkubation von (3-<sup>13</sup>C,2-<sup>2</sup>H)GGPP (Schema S4) mit TdS ein Produkt, für das ein intensives Triplett im <sup>13</sup>C-NMR-Spektrum zu sehen war (Abbildung S32C,  $J_{C,D} = 19.6$  Hz,  $\delta\Delta = 0.44$  ppm). Diese Beobachtung verwies auf eine direkte <sup>13</sup>C-<sup>2</sup>H-Bindung, die in Übereinstimmung mit zwei sequenziellen 1,2-Hydridverschiebungen ist. Ähnliche Ergebnisse wurden für die Cyclisierungsmechanismen der Synthesen für Cyclooctat-9-en-7-ol<sup>[22]</sup> und die Corvolether berichtet.<sup>[23]</sup> Die vorläufig zugewiesene relative Orientierung des Cyclopropanringes in den Intermediaten **13–16** kann nicht mit Sicherheit aus der Struktur des finalen Produktes **9** abgeleitet werden, aber die Orientierung wie sie in Schema 3 gezeigt ist verlangt Inversion der Konfiguration an C6 in dem Schritt von **14** nach **16**, was wahrscheinlicher als Retention der Konfiguration erscheint.

Wie durch enzymatische Cyclisierung von stereospezifisch deuteriertem (*R*)- und (*S*)-(1-<sup>2</sup>H)GGPP gezeigt verläuft die letzte Deprotonierung zu **9** mit Verlust von Deuterium aus dem *S*-Enantiomer, während Deuterium aus dem *R*-Enantiomer im Molekül verbleibt (Abbildung S33). Nimmt man für die initiale 1,11-Cyclisierung Inversion der Konfiguration an,<sup>[14b,20]</sup> so decken diese Experimente eine Deprotonierung des zu dem wandernden Hydrid in der Reaktion von **17** nach **18** *syn*-ständigen Wasserstoffatoms an C1 auf. Das Diphosphat-Anion verlässt C1 in den rückwärtigen Halbraum der Projektionsebene (Schema 3) und ist perfekt positioniert um als Base in der abschließenden Deprotonierung zu **9** zu agieren.

Isotopenmarkierungsexperimente bleiben eine wichtige Methode um mechanistische Einblicke in die bemerkenswerten Reaktionen von Terpencyclasen zu erhalten.<sup>[5b,6a,13,14d,15,24]</sup> Wir haben hier gezeigt, dass nicht nur viele Details inklusive stereochemischer Aspekte, sondern auch die absoluten Konfigurationen von Terpenen mit stereospezifisch deuterierten Vorläufern aufgeklärt werden können. Die Kenntnis der absoluten Konfigurationen von **1** und **9** erlaubt einen Vergleich der Cyclisierungsmechanismen von



**Schema 3.** Cyclisierung von GGPP zu **9**. Die Nummerierung der Kohlenstoffatome von **9** verweist auf den Ursprung für jedes Atom aus GGPP.

SvS und TdS. Die ersten Elementarschritte beider Enzyme umfassen eine 1,11*Si*-Cyclisierung von GGPP. In diesem Schritt wird dieselbe absolute Konfiguration an C11 installiert, die während des weiteren Prozesses nicht mehr verändert wird. SvS katalysiert simultan eine 10*Re*,14*Si*-Cyclisierung, während für TdS ein 10*Re*,14*Re*-Prozess beobachtet wird, was eine unterschiedliche relative Orientierung von C10 und C15 des im aktiven Zentrum gefalteten GGPPs verlangt. Die Methylgruppe C16 und H14, die in GGPP *cis*-orientiert sind, enden in beiden Fällen auf derselben Seite von **1** und **9**, was den strikten stereochemischen Verlauf der 10,14-Cyclisierung für beide Enzyme belegt. Die initial gebildeten bicyclischen Kationen **2** und **12** sind Diastereomere und die weiterführenden Reaktionen weichen voneinander ab um zu den individuellen Produkten **1** und **9** zu gelangen, aber die finalen Deprotonierungsschritte verlaufen in beiden Fällen mit Abstraktion des Protons von der Seite, zu der das Diphosphat im Ionisierungsschritt austritt. Dies lässt vermuten, dass das Diphosphat im letzten Schritt als Base agiert. Es ist interessant festzustellen, dass SvS und TdS, wie die phylogenetische Analyse von mehr als 1000 bakteriellen Terpenocyclasen zeigt, nahe verwandt sind (Abbildung S34), so dass möglicherweise wenige kritische Substitutionen in der Aminosäuresequenz einer Terpenocyclase genügen, eine geringfügige Konformationsänderung des Substrates im aktiven Zentrum zu bewirken, die aber einen drastischen Effekt auf die Struktur des Produktes haben kann.

## Danksagung

Diese Arbeit wurde durch die DFG (DI1536/7-1) und den Fonds der Chemischen Industrie gefördert.

**Stichwörter:** Biosynthesen · Isotope · NMR-Spektroskopie · Reaktionsmechanismen · Terpene

**Zitierweise:** *Angew. Chem. Int. Ed.* **2017**, *56*, 2776–2779  
*Angew. Chem.* **2017**, *129*, 2820–2823

- [1] O. Wallach, *Justus Liebigs Ann. Chem.* **1885**, 227, 277.
- [2] M. B. Quin, C. M. Flynn, C. Schmidt-Dannert, *Nat. Prod. Rep.* **2014**, *31*, 1449.
- [3] a) N. N. Gerber, H. A. Lechevalier, *Appl. Microbiol.* **1965**, *13*, 935; b) K. Wilkins, C. Schöller, *Actinomycetologica* **2009**, *23*, 27; c) C. A. Citron, J. Gleitzmann, G. Laurenzano, R. Pukall, J. S. Dickschat, *ChemBioChem* **2012**, *13*, 202.
- [4] X. Chen, T. G. Köllner, Q. Jia, A. Norris, B. Santhanam, P. Rabe, J. S. Dickschat, G. Shaulsky, J. Gershenzon, F. Chen, *Proc. Natl. Acad. Sci. USA* **2016**, *113*, 12132.
- [5] Reviewed in: a) J. S. Dickschat, *Nat. Prod. Rep.* **2016**, *33*, 87; following reports: b) P. Rabe, J. Rinkel, T. A. Klapschinski, L. Barra, J. S. Dickschat, *Org. Biomol. Chem.* **2016**, *14*, 158; c) A. Schiffrin, Y. Khatri, P. Kirsch, V. Thiel, S. Schulz, R. Bernhardt, *Org. Biomol. Chem.* **2016**, *14*, 3385; d) T. A. Klapschinski, P. Rabe, J. S. Dickschat, *Angew. Chem. Int. Ed.* **2016**, *55*, 10141; *Angew. Chem.* **2016**, *128*, 10296; e) P. Rabe, T. Schmitz, J. S. Dickschat, *Beilstein J. Org. Chem.* **2016**, *12*, 1839; f) J. Rinkel, P. Rabe, P. Garbeva, J. S. Dickschat, *Angew. Chem. Int. Ed.* **2016**, *55*, 13593; *Angew. Chem.* **2016**, *128*, 13791.
- [6] a) A. Meguro, Y. Motoyoshi, K. Teramoto, S. Ueda, Y. Totsuka, Y. Ando, T. Tomita, S.-Y. Kim, T. Kimura, M. Igarashi, R. Sawa, T. Shinada, M. Nishiyama, T. Kuzuyama, *Angew. Chem. Int. Ed.* **2015**, *54*, 4353; *Angew. Chem.* **2015**, *127*, 4427; b) Y. Yamada, T. Kuzuyama, M. Komatsu, K. Shin-ya, S. Omura, D. E. Cane, H. Ikeda, *Proc. Natl. Acad. Sci. USA* **2015**, *112*, 857; c) A. Meguro, T. Tomita, M. Nishiyama, T. Kuzuyama, *ChemBioChem* **2013**, *14*, 316; d) M. J. Smanski, R. M. Peterson, S.-X. Huang, B. Shen, *Curr. Opin. Chem. Biol.* **2012**, *16*, 132.
- [7] J. Rinkel, J. S. Dickschat, *Beilstein J. Org. Chem.* **2015**, *11*, 2493.
- [8] a) C. M. Starks, K. Back, J. Chappell, J. P. Noel, *Science* **1997**, *277*, 1815; b) M. Köksal, Y. Jin, R. M. Coates, R. Croteau, D. W. Christianson, *Nature* **2011**, *469*, 116.
- [9] P. Baer, P. Rabe, K. Fischer, C. A. Citron, T. A. Klapschinski, M. Groll, J. S. Dickschat, *Angew. Chem. Int. Ed.* **2014**, *53*, 7652; *Angew. Chem.* **2014**, *126*, 7783.
- [10] J. S. Dickschat, K. A. K. Pahirulzaman, P. Rabe, T. A. Klapschinski, *ChemBioChem* **2014**, *15*, 810.
- [11] P. Gutta, D. J. Tantillo, *J. Am. Chem. Soc.* **2006**, *128*, 6172.
- [12] C. A. Citron, P. Rabe, L. Barra, C. Nakano, T. Hoshino, J. S. Dickschat, *Eur. J. Org. Chem.* **2014**, 7684.
- [13] P. Rabe, L. Barra, J. Rinkel, R. Riclea, C. A. Citron, T. A. Klapschinski, A. Janusko, J. S. Dickschat, *Angew. Chem. Int. Ed.* **2015**, *54*, 13448; *Angew. Chem.* **2015**, *127*, 13649.
- [14] a) D. E. Cane, T. Rossi, A. M. Tillman, J. P. Pachlatko, *J. Am. Chem. Soc.* **1981**, *103*, 1838; b) C.-M. Wang, R. Hopson, X. Lin, D. E. Cane, *J. Am. Chem. Soc.* **2009**, *131*, 8360; c) N. L. Brock, S. R. Ravella, S. Schulz, J. S. Dickschat, *Angew. Chem. Int. Ed.* **2013**, *52*, 2100; *Angew. Chem.* **2013**, *125*, 2154; d) P. Rabe, J. Rinkel, B. Nubbemeyer, T. G. Köllner, F. Chen, J. S. Dickschat, *Angew. Chem. Int. Ed.* **2016**, *55*, 15420; *Angew. Chem.* **2016**, *128*, 15646.
- [15] I. Burkhardt, T. Siemon, M. Henrot, L. Studt, S. Rösler, B. Tudzynski, M. Christmann, J. S. Dickschat, *Angew. Chem. Int. Ed.* **2016**, *55*, 8748; *Angew. Chem.* **2016**, *128*, 8890.
- [16] D. E. Cane, D. B. McIlwaine, J. S. Oliver, *J. Am. Chem. Soc.* **1990**, *112*, 1285.
- [17] J. Rinkel, P. Rabe, L. zur Horst, J. S. Dickschat, *Beilstein J. Org. Chem.* **2016**, *12*, 2317.
- [18] H. V. Thulasiram, C. D. Poulter, *J. Am. Chem. Soc.* **2006**, *128*, 15819.
- [19] J. A. Faraldos, S. Wu, J. Chappell, R. M. Coates, *J. Am. Chem. Soc.* **2010**, *132*, 2998.
- [20] D. E. Cane, J. S. Oliver, P. H. M. Harrison, C. Abell, B. R. Hubbard, C. T. Kane, R. Lattman, *J. Am. Chem. Soc.* **1990**, *112*, 4513.
- [21] Q. N. N. Nguyen, D. J. Tantillo, *J. Antibiot.* **2016**, *69*, 534.
- [22] H. Sato, K. Teramoto, Y. Masumoto, N. Tezuka, K. Sakai, S. Ueda, Y. Totsuka, T. Shinada, M. Nishiyama, C. Wang, T. Kuzuyama, M. Uchiyama, *Sci. Rep.* **2015**, *5*, 18471.
- [23] a) P. Rabe, A. Janusko, B. Goldfuss, J. S. Dickschat, *ChemBioChem* **2016**, *17*, 146; b) P. Rabe, K. A. K. Pahirulzaman, J. S. Dickschat, *Angew. Chem. Int. Ed.* **2015**, *54*, 6041; *Angew. Chem.* **2015**, *127*, 6139.
- [24] a) Y. Matsuda, T. Mitsuhashi, S. Lee, M. Hoshino, T. Mori, M. Okada, H. Zhang, F. Hayashi, M. Fujita, I. Abe, *Angew. Chem. Int. Ed.* **2016**, *55*, 5785; *Angew. Chem.* **2016**, *128*, 5879; b) B. Qin, Y. Matsuda, T. Mori, M. Okada, Z. Quan, T. Mitsuhashi, T. Wakimoto, I. Abe, *Angew. Chem. Int. Ed.* **2016**, *55*, 1658; *Angew. Chem.* **2016**, *128*, 1690; c) M. Matsuda, T. Mitsuhashi, Z. Quan, I. Abe, *Org. Lett.* **2015**, *17*, 4644; d) R. Chiba, A. Minami, K. Gomi, H. Oikawa, *Org. Lett.* **2013**, *15*, 594; e) R. Riclea, J. S. Dickschat, *Angew. Chem. Int. Ed.* **2015**, *54*, 12167; *Angew. Chem.* **2015**, *127*, 12335; f) M. Okada, Y. Matsuda, T. Mitsuhashi, S. Hoshino, T. Mori, K. Nakagawa, Z. Quan, B. Qin, H. Zhang, F. Hayashi, H. Kawaide, I. Abe, *J. Am. Chem. Soc.* **2016**, *138*, 10011.

Eingegangen am 22. Dezember 2016  
endgültige Fassung veröffentlicht am 1. Februar 2017



## Appendix F

### **Mechanisms of the Diterpene Cyclases $\beta$ -Pinacene Synthase from *Dictyostelium discoideum* and Hydropyrene Synthase from *Streptomyces clavuligerus***

*Chem. Eur. J.* **2017**, *23*, 10501–10505.

DOI:10.1002/chem.201702704



## Enzymes

Mechanisms of the Diterpene Cyclases  $\beta$ -Pinacene Synthase from *Dictyostelium discoideum* and Hydropyrene Synthase from *Streptomyces clavuligerus*Jan Rinkel,<sup>[a]</sup> Patrick Rabe,<sup>[a]</sup> Xinlu Chen,<sup>[b]</sup> Tobias G. Köllner,<sup>[c]</sup> Feng Chen,<sup>[b]</sup> and Jeroen S. Dickschat\*<sup>[a]</sup>

**Abstract:** Two diterpene cyclases, one from the social amoeba *Dictyostelium discoideum* and the other from the bacterium *Streptomyces clavuligerus*, with products containing a *Z*-configured double bond between the original C2 and C3 of geranylgeranyl diphosphate, were extensively investigated for their mechanisms through isotopic labelling experiments. The participation of geranylgeranyl diphosphate, in analogy to the role of linalyl and nerolidyl diphosphate for mono- and sesquiterpene biosynthesis, as an intermediate towards diterpenes with a *Z*-configured C2=C3 double bond is discussed.

During the past decades, soil bacteria have been recognised as producers of a large variety of terpenes.<sup>[1]</sup> Starting from the identification of the pentalene synthase,<sup>[2]</sup> this work was extended by the characterisation of several bacterial terpene cyclases (TCs).<sup>[3]</sup> Recently, also social amoebae were shown to contribute to the terpene production in soil and first TCs from these organisms have been reported.<sup>[4]</sup> The type I of these remarkable enzymes contains an (Mg<sup>2+</sup>)<sub>3</sub> cluster for binding of the oligoprenyl diphosphate (OPP) substrate that is itself bound to the highly conserved aspartate-rich motif DDXX(X)(D,E), the NSE triad NDXSXX(R,K)(E,D) and the RY dimer.<sup>[5]</sup> OPP binding causes closure of the active site under movement of a catalytically active arginine,<sup>[6]</sup> followed by substrate ionisation via diphosphate (PP) abstraction to initiate the cyclisation via cationic intermediates. The dynamics of the cyclisation may be followed by modelling the reactions in the

active centre of a TC<sup>[7]</sup> or by isotopic labelling experiments.<sup>[8]</sup> While the reactions of monoterpene cyclases always proceed via isomerisation of geranyl PP (GPP) to linalyl PP (LPP), for sesquiterpene cyclases the corresponding isomerisation of farnesyl PP (FPP) to nerolidyl PP (NPP) is only strictly required for products with a *Z*-configured double bond between the original C2 and C3 of FPP.<sup>[9]</sup> Here, we present the elucidation of the cyclisation mechanisms of two diterpene cyclases, one new enzyme from the social amoeba *Dictyostelium discoideum* that was demonstrated to be a  $\beta$ -pinacene synthase in this study, and the hydropyrene synthase from *Streptomyces clavuligerus*,<sup>[10]</sup> by isotopic labelling strategies. Both enzymes form products with *Z*-configured double bonds.

One of the TCs from *D. discoideum*, DdTPS5, exhibits all highly conserved motifs of a TC (Figure S1 in the Supporting Information), and was recently shown to have diterpene synthase activity, but the chemical identity of the diterpene product was not known.<sup>[4a]</sup> For a detailed investigation, DdTPS5 was expressed in *Escherichia coli* with an N-terminal His-tag. The purified enzyme did not convert GPP and FPP, but yielded a diterpene hydrocarbon from GGPP (geranylgeranyl pyrophosphate, Figure S3), which was isolated and identified by one- and two-dimensional NMR spectroscopy (Table S3 and Figures S4–S10 in the Supporting Information) as  $\beta$ -pinacene (**1**), a monocyclic diterpene with 1(14)*E*,2*Z*,6*E*,10*E* configuration and a known constituent of the essential oils from *Pinus koraiensis* and *Pinus sibirica*.<sup>[11]</sup> These experiments established the enzyme as  $\beta$ -pinacene synthase (PcS). The reaction mechanism from GGPP to **1** requires the isomerisation of GGPP to geranylgeranyl linalyl PP (GLPP) that can cyclise to cation **A** with a 2*Z* double bond, followed by a 1,2-hydride shift to **B** and deprotonation to **1** (Scheme 1). An alternative from **A** to **1** is a 1,3-hydride migration of H<sub>1R</sub> or H<sub>1S</sub> and deprotonation from C14 (not shown). The isomerisation of GGPP may proceed via either (*S*- or (*R*)-GLPP, and—in analogy to LPP (linalyl PP) and NPP (nerolidyl PP) cyclisations—through *syn*-allylic transposition of PP, with opposite consequences on the fate of H<sub>1R</sub> and H<sub>1S</sub> of GGPP. For the ring closure, an *anti*-S<sub>N</sub>2' attack of C14 at C1 can be assumed, resulting in **A** with the same absolute orientation for H<sub>1R</sub> and H<sub>1S</sub> via both enantiomers of GLPP.

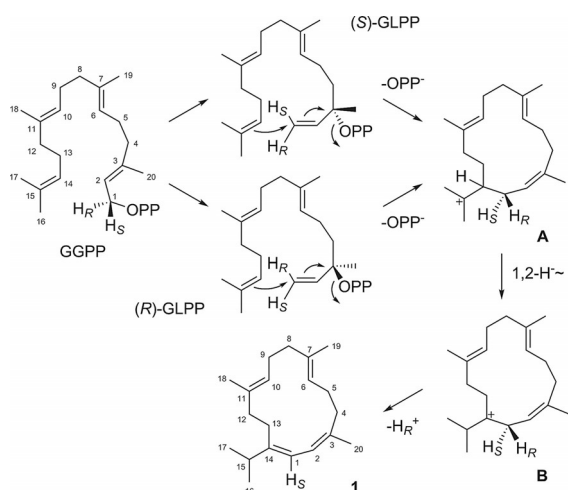
This mechanism can be tested by enzymatic conversion of (14-<sup>2</sup>H)GGPP to validate the 1,2-hydride shift from **A** to **B**. However, the labelled monomer (2-<sup>2</sup>H)dimethylallyl PP (DMAPP) is easier accessible by synthesis (Scheme S1 in the Supporting Information) and was used for the elongation to (14-<sup>2</sup>H)GGPP

[a] J. Rinkel, Dr. P. Rabe, Prof. Dr. J. S. Dickschat  
Kekulé-Institute of Organic Chemistry and Biochemistry  
University of Bonn  
Gerhard-Domagk-Straße 1, 53121 Bonn (Germany)  
E-mail: dickschat@uni-bonn.de

[b] Dr. X. Chen, Prof. Dr. F. Chen  
Department of Plant Sciences  
University of Tennessee  
2431 Joe Johnson Drive, Knoxville, TN 37996-4561 (USA)

[c] Dr. T. G. Köllner  
Max Planck Institute for Chemical Ecology  
Hans-Knöll-Straße 8, 07745 Jena (Germany)

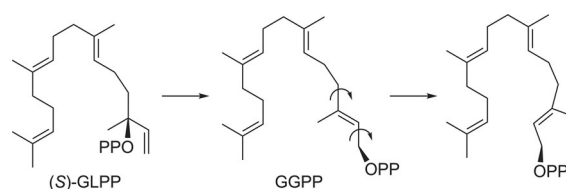
Supporting information and the ORCID identification number(s) for the author(s) of this article can be found under <https://doi.org/10.1002/chem.201702704>.



**Scheme 1.** Cyclisation mechanism from GGPP (geranylgeranyl pyrophosphate) to  $\beta$ -pinacene (**1**).

with isopentenyl PP (IPP) through the FPP synthase (FPPS) from *Streptomyces coelicolor*<sup>[4b]</sup> and the GGPP synthase (GGPPS) from *S. cyaneofuscatus* (note that the combination of FPPS and GGPPS is more effective than GGPPS alone).<sup>[12]</sup> The subsequent cyclisation by PcS yielded a product with retained deuterium that could be located in the *iPr* group by inspection of the EI-MS (electron impact) fragmentation pattern (Figure S11), in agreement with the 1,2-hydride shift from **A** to **B**.<sup>[13]</sup> The conversion of both (*R*)- and (*S*)-(1-<sup>2</sup>H)GGPP revealed the specific loss of H<sub>1<sub>R</sub></sub> and retainment of H<sub>1<sub>S</sub></sub> in the final deprotonation step (Figure S11). This result may point to (*R*)-GLPP as intermediate, because PP will leave towards the front side of the projection plane of Scheme 1 in the cyclisation to **A** and is thus perfectly located for the terminating abstraction of H<sub>1<sub>R</sub></sub>, similar to the observations made with spiroviolene synthase and tsukubadiene synthase, in which PP likely acts as base.<sup>[12]</sup> On the other hand, for tobacco *epi*-aristolochene synthase, a specific amino acid residue (Tyr520) and not the PP anion was suggested to participate in the deprotonation step,<sup>[7c]</sup> which challenges the argumentation above. The conversion of the pure GLPP enantiomers (Scheme S2 and Figure S12 in the Supporting Information) by PcS yielded small amounts of **1** in both cases (Figure S13; the lower efficiency than for the conversion of GGPP is at least in part due to rapid decomposition of GLPP, as revealed by controls without enzyme). This finding is explainable by uptake of both GLPP enantiomers into the active site. Coordination of the PP moiety of the wrong enantiomer to the (Mg<sup>2+</sup>)<sub>3</sub> cluster results in an exchanged positioning of the Me group C20 and the C1–C2 vinyl group, preventing the 1,14-cyclisation, but the docked non-native GLPP enantiomer may react to GGPP by allylic transposition of PP, followed by a conformational change that opens the way to a cyclisation via the native GLPP stereoisomer (Scheme 2).

The conversion of (16-<sup>13</sup>C)- and (17-<sup>13</sup>C)GGPP with PcS, obtained from (12-<sup>13</sup>C)- and (13-<sup>13</sup>C)FPP and IPP through GGPPS, yielded **1** with a shared labelling in both Me groups of the *iPr* moiety (Figure S14). The stereochemical course for the terminal geminal Me groups of OPP substrates is tightly controlled for



**Scheme 2.** Conversion of the non-native GLPP (geranyllyllyl PP) enantiomer (hypothetically (*S*)-GLPP) by PcS ( $\beta$ -pinacene synthase). Analogous reactions are possible from (*R*)-GLPP.

most investigated TCs.<sup>[4b,12,14]</sup> One of the few enzymes causing a similar distribution of labelling is (1*R*,4*R*,5*S*)-guaia-6,10(14)-diene synthase (GdS) from *Fusarium fujikuroi*.<sup>[15]</sup> Notably, the cyclisation reactions of GdS and PcS both proceed with a 1,2-hydride shift into an *iPr* group, while for systems with 1,3-hydride shifts such as the TCs for T-muurolool, 4-*epi*-cubebol and  $\gamma$ -cadinene always a strict stereochemical course is found.<sup>[14e]</sup> These findings reflect the different topological constraints of the two possible reactions: For the 1,2-hydride shift, the equal distances of the moving hydride to the two planes of the cation cause a scrambling of labelling in the *iPr* group, while the well-defined target plane for the 1,3-hydride migration does not (Figure 1). In contrast to the observations made here and with GdS, a conformational pre-organisation could enforce a defined stereochemical course for the 1,2-hydride shifts in other systems.

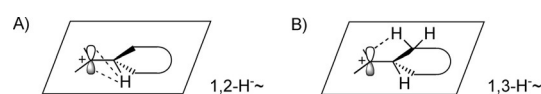
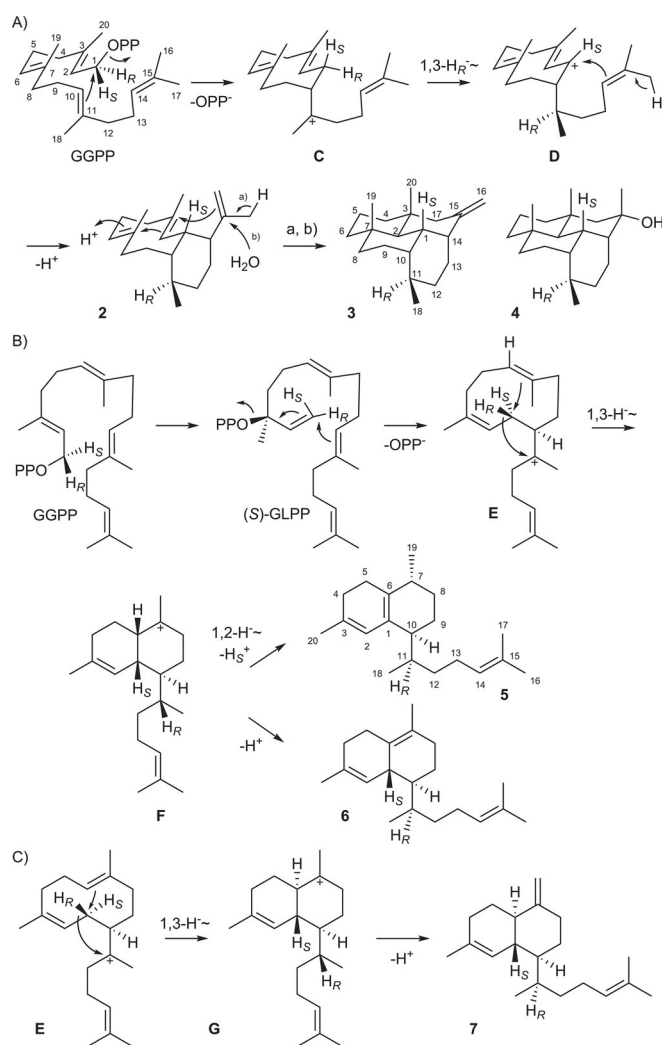


**Figure 1.** Topological constraints for A) 1,2- and B) 1,3-hydride transfers into *iPr* groups during terpene cyclisations.

For mechanistic investigations on the hydrophyrene synthase (HpS, Figure S1) from *S. clavuligerus*, the corresponding gene was cloned into the *E. coli* expression vector pYE-Express.<sup>[16]</sup> The purified protein gave no products from GPP and FPP, but produced a mixture of diterpenes, including hydrophyrene (**3**), hydrophyrenol (**4**), isoelisabethatriene (**5**) and traces of isoelisabethatriene B (**6**) from GGPP (Figure S15), in agreement with the results from the heterologous expression in *Streptomyces avermitilis*.<sup>[10]</sup> In addition to the identification through comparison of recorded to published mass spectra,<sup>[10]</sup> the known products **3–5** of HpS were re-isolated and unambiguously characterised by NMR (Tables S4–S6), only the production of **6** was too low for its isolation. A further compound that was so far not reported from HpS was tentatively identified by GC-MS as biflora-4,10(19),15-triene (**7**), based on an identical mass spectrum to a library spectrum and on a retention index that matched published data (Figure S15). A possible cyclisation mechanism to **3** and **4** starts with 1,10-cyclisation of GGPP to **C**, followed by a 1,3-hydride shift to **D** and a second ring closure with deprotonation to **2** (Scheme 3). Reprotonation at C6 induces two more ring closures to set the unique carbon skeleton of **3** and **4** that arise by final deprotonation or attack of



**Scheme 3.** Cyclisation mechanism of HpS (hydropyrene synthase). A) Cyclisation of GGPP via **2** to **3** and **4**, B) cyclisation of GGPP to **5** and **6** and C) cyclisation of GGPP to **7**.

water. The formation of **5** and **6** with a *Z* double bond in their bicyclic system requires GGPP isomerisation to GLPP, a 1,10-cyclisation to **E** and a 1,3-hydride migration and second ring closure to **F**. Another 1,2-hydride shift and deprotonation results in **5**, while **6** requires simple deprotonation. The reactions to **7** start from **E** in a different conformation and proceed via a 1,3-hydride shift and cyclisation to **G** and deprotonation.

These mechanisms were tested by conversion of all 20 isotopomers of (<sup>13</sup>C<sub>1</sub>)GGPP, prepared with GGPPS from the 15 isotopomers of (<sup>13</sup>C<sub>1</sub>)FPP and IPP, from FPP and (1-<sup>13</sup>C)IPP, (3-<sup>13</sup>C)IPP and (4-<sup>13</sup>C)IPP, and by direct synthesis of (2-<sup>13</sup>C)GGPP and (20-<sup>13</sup>C)GGPP.<sup>[12,17]</sup> All 20 GGPP isotopomers were converted by HpS in small scale reactions (1 mg), followed by extraction with C<sub>6</sub>D<sub>6</sub> and direct <sup>13</sup>C-NMR analysis without product purification. In each sample, strong <sup>13</sup>C-NMR signals for the labelled carbons of **3**, **4** and **5** were observed, with the labelling in the expected positions and without a distribution of labelling from C16 and C17 (Figures S16–S18). In all 20 experiments, major signals appeared that could not be assigned to a known product, but were in line with intermediate **2** (Figure S19). The

isolation of this compound turned out to be difficult, because of its instability under the conditions of column chromatography, but swift work yielded an almost pure sample of sufficient quality for unambiguous structure elucidation by NMR (Table S7 and Figures S20–S26). The neutral biosynthesis intermediate **2** was named prehydropyrene.

The mechanism of HpS was further tested using doubly labelled probes. The 1,3-hydride shift from **C** to **D** and from **E** to **F** was addressed by conversion of (*S*)- and (*R*)-(1-<sup>13</sup>C,1-<sup>2</sup>H)GGPP, synthesised with high enantiomeric purity (Scheme S3 and Figure S27), and product analysis by <sup>13</sup>C-NMR, which yielded enhanced triplets for C1 of **2**, **3** and **4** from (*S*)-(1-<sup>13</sup>C,1-<sup>2</sup>H)GGPP, but a singlet for **5** (Figure S28A). These data indicated the stereospecific migration of H1<sub>R</sub> from C1 and are in line with the loss of H1<sub>S</sub> in the final step to **5**, as confirmed by GC-MS (Figure S29). Using the *R* enantiomer, a singlet was observed for all four compounds, again consistent with migration of H1<sub>R</sub> (Figure S28B). The final destination of this hydrogen at C11 was proven using (7-<sup>13</sup>C)FPP and (2,2-<sup>2</sup>H<sub>2</sub>)IPP, synthesised as shown in Scheme S4, with an enzyme mix of GGPPS and HpS, which produced triplets for C11 of **3** and **4** and pointed to attachment of deuterium to this carbon (Figure S28C). Notably, the stereochemical course of the hydride movement is the same in both cases, regardless of the double bond configuration at C2 for both **C** and **E**. The reprotonation of **2** towards **3** and **4** was investigated by incubation of (2-<sup>13</sup>C)FPP and IPP with GGPPS and HpS in a deuterium oxide buffer, resulting in upfield shifted triplets for C6 in the <sup>13</sup>C-NMR, besides singlets for the non-deuterated compounds due to residual water in the enzyme preparation (Figure S30). HSQC analysis of the products allowed to follow the stereochemical course of the reprotonation with specific incorporation of deuterium into H6<sub>β</sub> (Figure S31).

The absolute configuration of a terpene can be deduced from enantioselectively deuterated precursors by incorporation of labelling into one of two diastereotopic positions, if the stereocentre at the deuterated carbon remains unchanged (or is changed with a known course) during terpene biosynthesis, because the configurations of all other stereogenic centres in the product can be inferred from their relative orientation to this stereogenic centre.<sup>[4b,12,13,18]</sup> Using this approach, the absolute configurations of **3**, **4** and **5** were delineated from incubations of (*R*)- and (*S*)-(1-<sup>13</sup>C,1-<sup>2</sup>H)FPP with IPP, GGPPS and HpS (Figure S32–S34), which resulted in the absolute configurations for **2**, **3**, **4** and **5** as in Scheme 3. Consistent findings were obtained using both enantiomers of (1-<sup>13</sup>C,1-<sup>2</sup>H)GPP (Figure S35–S37). These experiments were built on the known inversion of configuration at C1 in the OPP elongations with IPP<sup>[19]</sup> and confirmed the tentatively assigned absolute configuration for **3** from crystallographic data of its epoxide.<sup>[10b]</sup> The HpS product (–)-**5** ([α]<sub>D</sub><sup>20</sup> = –5.5°, *c* 0.1, C<sub>6</sub>D<sub>6</sub>) is likely the enantiomer of isoelisabethatriene isolated from the coral *Pseudopterogorgia elisabethae*.<sup>[20]</sup> While no optical rotary power was reported, its absolute configuration can be tentatively assigned based on the fact that **5** is biosynthetically linked to the pseudopterogens that were isolated from the same organism and for which the absolute configurations are well established.<sup>[21]</sup>

A model for the stereochemical course of the reactions towards **5** and the installation of its absolute configuration involves an *anti*- $S_N2'$  reaction in the 1,10-cyclisation of (*S*)-GLPP to **E** that establishes a *syn* orientation of H<sub>1R</sub> and C11, as required for the next 1,3-hydride shift to **F** and the correct absolute configuration at C10 (a hypothetical pathway via (*R*)-GLPP would produce **E** with *syn*-oriented H<sub>1S</sub> and C11). The second ring closure to **F** likely proceeds with inversion at C1, which defines the absolute configuration at this carbon. The *cis*-decalin system of **F** can be inferred from the configuration at C7 of **5**, because the 1,2-hydride shift from **F** to **5** must be suprafacial. Conclusively, the configurations of all stereocentres in **F** can be deduced either from those in the product **5** or from the observed H<sub>1R</sub> shift from **E** to **F**. This information can finally be used to deduce the tentative structure of **6**, a compound that is produced in too low amounts for isolation and structure elucidation, because it likely arises directly from **F**. In this context it is interesting to note that both deprotonations from **F** to **5** and **6** happen from the same hemisphere above the projection plane of Scheme 3, which is identical to the hemisphere into which the PP anion is expelled from (*S*)-GLPP, consistent with PP acting as the terminating base. The cyclisation of **E** to the *trans*-decalin system of **G** results in the deprotonation of the Me group C19, which also points into this hemisphere, to yield **7**. However, similar to the observations made with PcS, both (*S*)- and (*R*)-GLPP were converted by HpS, albeit with lower efficiency as for GGPP, but clearly yielding **3**, **4** and **5** (Figure S38). The same mechanism as discussed above for PcS can explain the product formation from both GLPP enantiomers (Scheme 2).

In summary, we have investigated the mechanistic details of each single elementary reaction along the cyclisation cascades of two diterpene cyclases by extensive labelling experiments. PcS from *D. discoideum*, previously shown to have diterpene cyclase activity,<sup>[4a]</sup> is a newly characterised enzyme producing  $\beta$ -pinacene. For several products of HpS from *S. clavuligerus*, the absolute configurations were elucidated and a mechanistically predicted neutral intermediate was discovered by <sup>13</sup>C-labelling experiments that was previously overlooked, likely because of its instability. Notably, both enzymes PcS and HpS form products with a *Z*-configured double bond that are explainable by GGPP isomerisation to GLPP. Both of its enantiomers were accepted by PcS and HpS, albeit with lower efficiency than for GGPP, which reflects the adaptation of the enzymes to their natural substrates. It is interesting to see that diterpene cyclases use the same strategy of substrate isomerisation by allylic PP transposition for the installation of *Z* double bonds as is well established for mono- and sesquiterpene cyclases.

## Acknowledgements

This work was funded by the DFG (DI1536/7-1) and by the Fonds der Chemischen Industrie. We thank Britta Nubbemeyer and Thomas Schmitz for assistance in the experimental work and for careful checking of the manuscript.

## Conflict of interest

The authors declare no conflict of interest.

**Keywords:** biosynthesis • enzyme mechanisms • isotopes • soil microorganisms • terpenes

- [1] a) N. N. Gerber, H. A. Lechevalier, *Appl. Microbiol.* **1965**, *13*, 935; b) L. L. Medsker, D. Jenkins, J. F. Thomas, C. Koch, *Environ. Sci. Technol.* **1969**, *3*, 476; c) C. E. G. Schöller, H. Gürtler, R. Pedersen, S. Molin, K. Wilkins, *J. Agric. Food Chem.* **2002**, *50*, 2615; d) C. A. Citron, J. Gleitzmann, G. Laurenzano, R. Pukall, J. S. Dickschat, *ChemBioChem* **2012**, *13*, 202.
- [2] D. E. Cane, J.-K. Sohng, C. R. Lamberson, S. M. Rudnicki, Z. Wu, M. D. Lloyd, J. S. Oliver, B. R. Hubbard, *Biochemistry* **1994**, *33*, 5846.
- [3] Reviewed in: J. S. Dickschat, *Nat. Prod. Rep.* **2016**, *33*, 87.
- [4] a) X. Chen, T. G. Köllner, Q. Jia, A. Norris, B. Santhanam, P. Rabe, J. S. Dickschat, G. Shaulsky, J. Gershenzon, F. Chen, *Proc. Natl. Acad. Sci. USA* **2016**, *113*, 12132; b) P. Rabe, J. Rinkel, B. Nubbemeyer, T. G. Köllner, F. Chen, J. S. Dickschat, *Angew. Chem. Int. Ed.* **2016**, *55*, 15420; *Angew. Chem.* **2016**, *128*, 15646.
- [5] a) C. M. Starks, K. Back, J. Chappell, J. P. Noel, *Science* **1997**, *277*, 1815; b) C. A. Lesburg, G. Zhai, D. E. Cane, D. W. Christianson, *Science* **1997**, *277*, 1820.
- [6] P. Baer, P. Rabe, K. Fischer, C. A. Citron, T. A. Klapschinski, M. Groll, J. S. Dickschat, *Angew. Chem. Int. Ed.* **2014**, *53*, 7652; *Angew. Chem.* **2014**, *126*, 7783.
- [7] a) J.-Y. Chow, B.-X. Tian, G. Ramamoorthy, B. S. Hillerich, R. D. Seidel, S. C. Almo, M. P. Jacobson, C. D. Poulter, *Proc. Natl. Acad. Sci. USA* **2015**, *112*, 5661; b) P. Schrepfer, A. Büttner, C. Goerner, M. Hertel, J. van Rijn, F. Wallrapp, W. Eisenreich, V. Sieber, R. Kourist, T. Brück, *Proc. Natl. Acad. Sci. USA* **2016**, *113*, E958; c) T. E. O'Brien, S. J. Bertolani, D. J. Tantillo, J. B. Siegel, *Chem. Sci.* **2016**, *7*, 4009.
- [8] a) J. Rinkel, J. S. Dickschat, *Beilstein J. Org. Chem.* **2015**, *11*, 2493; b) A. Meguro, Y. Motoyoshi, K. Teramoto, S. Ueda, Y. Totsuka, Y. Ando, T. Tomita, S.-Y. Kim, T. Kimura, M. Igarashi, R. Sawa, T. Shinada, M. Nishiyama, T. Kuzuyama, *Angew. Chem. Int. Ed.* **2015**, *54*, 4353; *Angew. Chem.* **2015**, *127*, 4427; c) Y. Matsuda, T. Mitsuhashi, S. Lee, M. Hoshino, T. Mori, M. Okada, H. Zhang, F. Hayashi, M. Fujita, I. Abe, *Angew. Chem. Int. Ed.* **2016**, *55*, 5785; *Angew. Chem.* **2016**, *128*, 5879; d) B. Qin, Y. Matsuda, T. Mori, M. Okada, Z. Quan, T. Mitsuhashi, T. Wakimoto, I. Abe, *Angew. Chem. Int. Ed.* **2016**, *55*, 1658; *Angew. Chem.* **2016**, *128*, 1690; e) X. Lin, R. Hopson, D. E. Cane, *J. Am. Chem. Soc.* **2006**, *128*, 6022.
- [9] D. E. Cane, *Acc. Chem. Res.* **1985**, *18*, 220.
- [10] a) Y. Yamada, T. Kuzuyama, M. Komatsu, K. Shin-ya, S. Omura, D. E. Cane, H. Ikeda, *Proc. Natl. Acad. Sci. USA* **2015**, *112*, 857; b) Y. Yamada, S. Arima, T. Nagamitsu, K. Johmotsu, H. Uekusa, T. Eguchi, K. Shin-ya, D. E. Cane, H. Ikeda, *J. Antibiot.* **2015**, *68*, 385.
- [11] V. A. Raldugin, N. K. Kashtanova, V. A. Pentegova, *Chem. Nat. Compd.* **1971**, *7*, 582.
- [12] P. Rabe, J. Rinkel, E. Dolja, T. Schmitz, B. Nubbemeyer, T. H. Luu, J. S. Dickschat, *Angew. Chem. Int. Ed.* **2017**, *56*, 2776; *Angew. Chem.* **2017**, *129*, 2820.
- [13] J. Rinkel, P. Rabe, P. Garbeva, J. S. Dickschat, *Angew. Chem. Int. Ed.* **2016**, *55*, 13593; *Angew. Chem.* **2016**, *128*, 13791.
- [14] a) D. E. Cane, T. Rossi, A. M. Tillman, J. P. Pachlatko, *J. Am. Chem. Soc.* **1981**, *103*, 1838; b) C.-M. Wang, R. Hopson, X. Lin, D. E. Cane, *J. Am. Chem. Soc.* **2009**, *131*, 8360; c) N. L. Brock, S. R. Ravella, S. Schulz, J. S. Dickschat, *Angew. Chem. Int. Ed.* **2013**, *52*, 2100; *Angew. Chem.* **2013**, *125*, 2154; d) T. A. Klapschinski, P. Rabe, J. S. Dickschat, *Angew. Chem. Int. Ed.* **2016**, *55*, 10141; *Angew. Chem.* **2016**, *128*, 10296; e) P. Rabe, T. Schmitz, J. S. Dickschat, *Beilstein J. Org. Chem.* **2016**, *12*, 1839.
- [15] I. Burkhardt, T. Siemon, M. Henrot, L. Studt, S. Rösler, B. Tudzynski, M. Christmann, J. S. Dickschat, *Angew. Chem. Int. Ed.* **2016**, *55*, 8748; *Angew. Chem.* **2016**, *128*, 8890.
- [16] J. S. Dickschat, K. A. K. Pahirulzaman, P. Rabe, T. A. Klapschinski, *ChemBioChem* **2014**, *15*, 810.

- [17] P. Rabe, L. Barra, J. Rinkel, R. Riclea, C. A. Citron, T. A. Klapschinski, A. Janusko, J. S. Dickschat, *Angew. Chem. Int. Ed.* **2015**, *54*, 13448; *Angew. Chem.* **2015**, *127*, 13649.
- [18] a) D. E. Cane, D. B. McIlwaine, J. S. Oliver, *J. Am. Chem. Soc.* **1990**, *112*, 1285; b) J. Rinkel, P. Rabe, L. zur Horst, J. S. Dickschat, *Beilstein J. Org. Chem.* **2016**, *12*, 2317.
- [19] H. V. Thulasiram, C. D. Poulter, *J. Am. Chem. Soc.* **2006**, *128*, 15819.
- [20] A. C. Kohl, R. G. Kerr, *Mar. Drugs* **2003**, *1*, 54.
- [21] a) S. A. Look, W. Fenical, G. K. Matsumoto, J. Clardy, *J. Org. Chem.* **1986**, *51*, 5140; b) A. C. Coleman, R. G. Kerr, *Tetrahedron* **2000**, *56*, 9569.

---

Manuscript received: June 12, 2017

Version of record online: July 11, 2017





## Appendix G

### **Mechanistic Characterization of Two Chimeric Sesterterpene Synthases from *Penicillium***

*Chem. Eur. J.* **2017**, *23*, 10053–10057.

DOI:10.1002/chem.201702766



Enzymes

# Mechanistic Characterization of Two Chimeric Sesterterpene Synthases from *Penicillium*

Takaaki Mitsuhashi<sup>+, [a]</sup>, Jan Rinkel<sup>+, [b]</sup>, Masahiro Okada,<sup>[a]</sup> Ikuro Abe,<sup>\*, [a]</sup> and Jeroen S. Dickschat<sup>\*, [b]</sup>

**Abstract:** The products of two bifunctional fungal sesterterpene synthases (StTPS), with prenyl transferase (PT) and terpene synthase (TPS) domains from *Penicillium*, were structurally characterized and their mechanisms studied in detail by labeling experiments. A phylogenetic analysis of the TPS domains of the new and previously characterized enzymes revealed six distinct clades. Enzymes from the same clade catalyze a common initial cyclization step, which suggests the potential for structural predictions from amino acid sequences.

One of the most fascinating aspects of natural products is their strictly controlled enantioselective biosynthesis by enzymes. For most classes, each stereocenter is set in an individual reaction during backbone assembly, as in polyketides for which a high level of understanding for the chirality transfer from the biocatalyst to the substrate has been reached.<sup>[1]</sup> Contrary to that, terpene biosynthesis proceeds first by assembly of an achiral linear precursor that is subsequently converted through a terpene synthase (TPS) into a chiral product with multiple stereocenters that are all defined in one step. The overall process is a cascade via cationic intermediates that makes use of the substrate's inherent reactivity,<sup>[2]</sup> while the role of the TPS seems to be limited to initiate the reaction by substrate ionization, guide it by controlling its conformation and stabilizing the reactive intermediates, and safeguard it by providing an essentially water-free cavity. Many of these fascinating enzymes have been investigated from plants,<sup>[3]</sup> bacteria,<sup>[4]</sup> fungi,<sup>[5]</sup> and social amoebae,<sup>[4h,6]</sup> but almost all known TPSs produce mono-, sesqui-, or diterpenes. One of the most intriguing aspects of fungal terpene biosynthesis is the recent discovery of a series of bifunctional enzymes with PT and TPS domains, including those with GFPP (geranylarnesyl pyrophosphate) syn-

thase (GFPPS) and sesterterpene synthase (StTPS) activities for astellifadiene,<sup>[7]</sup> ophiobolin,<sup>[8]</sup> sesterfisherol,<sup>[9]</sup> stellatriene,<sup>[10]</sup> and quiannulatene.<sup>[11]</sup> Here, we describe two new members of this astonishing enzyme family from *Penicillium*.

Genome analysis of *Penicillium brasilianum* NBRC 6234 revealed the presence of a new bifunctional StTPS gene (DDBJ accession no. LC228601) with a TPS domain that is phylogenetically distant from any characterized homolog (Figure S1 in the Supporting Information), suggesting a potentially new cyclization mode and product for this enzyme.<sup>[9]</sup> To determine its function, the gene was heterologously expressed in the efficient host *Aspergillus oryzae* NSAR1.<sup>[12,13]</sup> GC-MS analysis of mycelial extracts of the *A. oryzae* transformant revealed the presence of a sesterterpene hydrocarbon **1** (Figure S2), which was produced in high amounts (19.3 mg L<sup>-1</sup> isolated yield) featuring the formula C<sub>25</sub>H<sub>40</sub>, as determined by HREI-MS. The <sup>13</sup>C-NMR spectrum showed 25 signals, including six for olefinic carbons (Table S3), which suggested a tricyclic skeleton. Extensive one- and two-dimensional NMR spectroscopy, including a <sup>13</sup>C, <sup>13</sup>C incredible natural abundance double quantum transfer experiment (INADEQUATE), established the planar structure of a 5-12-5 tricyclic system (Figure 1A and Figures S3–S10 in the Supporting Information).

The relative configuration of **1** was determined by nuclear Overhauser effect spectroscopy (NOESY, Figure 1B). A strong correlation between H6 and H10 revealed *cis* configuration for the western half of **1**, while correlations between H10 and H9 $\alpha$  and between H5 $\beta$  and H24 $\alpha$  allowed assigning the C9 and C5

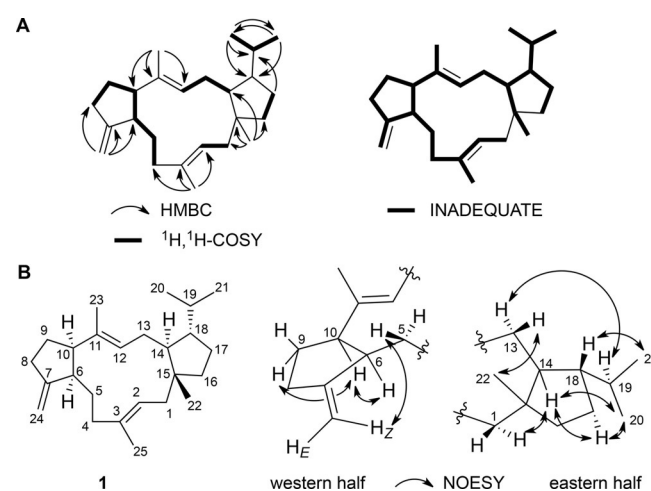


Figure 1. Structure elucidation of **1** by NMR spectroscopy.

[a] T. Mitsuhashi,<sup>†</sup> Dr. M. Okada, Prof. Dr. I. Abe  
Graduate School of Pharmaceutical Science  
University of Tokyo, 7-3-1 Hongo, Bunkyo-ku, Tokyo 113-0033 (Japan)  
E-mail: abei@mol.f.u-tokyo.ac.jp

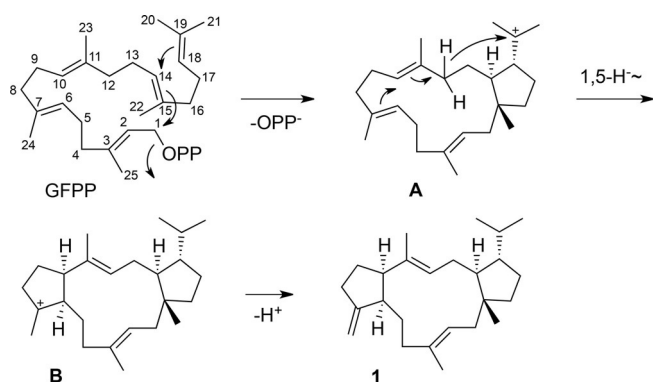
[b] J. Rinkel,<sup>†</sup> Prof. Dr. J. S. Dickschat  
Kekulé-Institute of Organic Chemistry and Biochemistry  
University of Bonn, Gerhard-Domagk-Straße 1, 53121 Bonn (Germany)  
E-mail: dickschat@uni-bonn.de

[†] These authors contributed equally to this work.

Supporting information and the ORCID identification number(s) for the author(s) of this article can be found under <https://doi.org/10.1002/chem.201702766>.

hydrogens. The *trans* orientation of H14 and Me22 and distinctions for H $\alpha$  and H $\beta$  at C1 and C13 for the eastern half were established by correlations of H1 $\alpha$  and H14 and of H13 $\beta$  and H22, respectively. The relative orientation of the *i*Pr group was determined from H18 to H21 and H13 $\alpha$  to H19 correlations, while a H18–H20 correlation was not found. The missing COSY crosspeak for H18–H19 supported a dihedral H18–C18–C19–H19 angle of ca. 90°, which together with NOESY correlations of H20 and H14/H17 $\alpha$  revealed the *cis* relation between H14 and the *i*Pr. The long linkers in the 12-membered ring did not allow defining the relative configurations between the western and eastern halves of **1**.

The sesterterpene **1** was named sesterbrasiliatriene and its producing enzyme *Penicillium brasilianum* sesterbrasiliatriene synthase (PbSS). For in vitro characterization of PbSS, its coding DNA was obtained from RNA of the *A. oryzae* pbSS transformant and expressed in *Escherichia coli* (Figure S11). The biosynthesis of **1** (Scheme 1) can be rationalized by a 1,15- and



**Scheme 1.** Cyclization of GFPP to sesterbrasiliatriene (**1**) by PbSS (*Penicillium brasilianum* sesterbrasiliatriene synthase).

simultaneous 14,18-cyclization of GFPP to cation **A**. A 1,5-hydride shift with 6,10-cyclization results in **B**, which is the precursor of **1** by deprotonation. This proposal was challenged by PbSS conversion of all 25 isotopomers of (<sup>13</sup>C<sub>1</sub>)GFPP that were obtained from previously synthesized (<sup>13</sup>C<sub>1</sub>)FPPs<sup>[14]</sup> (FPP farnesyl pyrophosphate), (<sup>13</sup>C<sub>1</sub>)GGPPs<sup>[49]</sup> (GGPP geranylgeranyl pyrophosphate), and (<sup>13</sup>C<sub>1</sub>)IPP<sup>[49]</sup> (IPP isopentenyl pyrophosphate) by using the enzyme's GFPPs (Scheme S1, Table S4). The precursors (2-<sup>13</sup>C)GFPP, (25-<sup>13</sup>C)GFPP, and (10-<sup>13</sup>C)GPP (GPP geranyl pyrophosphate) used in these experiments were synthesized in this work (Scheme S2). The resulting (<sup>13</sup>C<sub>1</sub>)GFPPs were directly converted by the TPS domain of PbSS, resulting in the <sup>13</sup>C-NMR detection of labeling in the expected positions in all 25 cases, which strongly supported the model (Figure S12). In three experiments, FPP was elongated with (1-<sup>13</sup>C)IPP, (3-<sup>13</sup>C)IPP, or (4-<sup>13</sup>C)IPP, resulting in doubly labeled GFPPs and, consequently, **1**. The introduction of labeling only in the first FPP elongation was achieved using the GGPP synthase (GGPPS) from *Streptomyces cyaneofuscatus*,<sup>[49]</sup> followed by extension with unlabeled IPP using PbSS. Since the (<sup>13</sup>C<sub>1</sub>)GGPP intermediates were not isolated and minor quantities of labeled IPP remained after the first step, small but strongly suppressed

peaks for the second label were also observed. The experiments with (20-<sup>13</sup>C)GFPP and (21-<sup>13</sup>C)GFPP revealed a strictly controlled stereochemical course with respect to the fate of the geminal Me groups, which closely resembles the observations for several other TPSs.<sup>[4deg,6,15]</sup> One of the few enzymes showing a distribution of labeling is the (1*R*,4*R*,5*S*)-guaia-6,10(14)-diene TPS from *Fusarium fujikuroi*.<sup>[5c]</sup>

Stereoselectively deuterated oligoprenyl diphosphates (OPPs) can be used to determine the absolute configurations of terpenes,<sup>[4f,6]</sup> because the problem is simplified to identifying the relative orientations of the stereocenters in a terpene to the stereocenter carrying the deuterium labeling. For this purpose, the previously synthesized pure enantiomers of (1-<sup>13</sup>C,1-<sup>2</sup>H)GPP, (1-<sup>13</sup>C,1-<sup>2</sup>H)FPP, and (1-<sup>13</sup>C,1-<sup>2</sup>H)GGPP<sup>[4f-h]</sup> were converted by PbSS, while (*R*)- and (*S*)-(1-<sup>13</sup>C,1-<sup>2</sup>H)GFP were synthesized here analogously (Scheme S3, Figure S13) and used for the same purpose. The additional <sup>13</sup>C label in these probes increased sensitivity in HSQC analyzes, which gave one strong crosspeak for a C–H correlation in each experiment (Figures S14–S17), while the missing crosspeak in comparison to unlabeled **1** indicated occupation of the respective position by deuterium. All eight experiments consistently pointed to the absolute configuration of (6*R*,10*R*,14*S*,15*R*,18*S*)-**1**, which also completed the relative orientation of the distant western and eastern halves. The interpretation of the experiments with GPP, FPP, and GGPP was based on the known inversion of configuration at C1 in chain elongations of OPPs with IPP.<sup>[16]</sup> Also for the initial GFPP cyclization to **A**, inversion of configuration at C1 was assumed, as reported for several other TPSs.<sup>[15b,17]</sup> The 5-12-5 tricyclic system of **1** is also known from the sesterterpenoid variculanol,<sup>[18]</sup> but with different relative configuration at C18.

The proposed 1,5-hydride shift from **A** to **B** was investigated by incubation of PbSS with (7-<sup>13</sup>C)GPP and (4,4-<sup>2</sup>H<sub>2</sub>)IPP, which was synthesized from ethyl acetoacetate (Scheme S4). The PbSS-PT domain generated (19-<sup>13</sup>C,4,4,8,8,12,12-<sup>2</sup>H<sub>6</sub>)GFPP that was cyclized by the TC domain to a product exhibiting an enhanced triplet for C19 in the <sup>13</sup>C-NMR spectrum (Figure S18,  $\Delta\delta = 0.61$  ppm,  $^1J_{CD} = 19.0$  Hz), which supported the 1,5-hydride shift. Feeding of sodium (1-<sup>13</sup>C,2H<sub>3</sub>)acetate or (2-<sup>13</sup>C,2H<sub>3</sub>)acetate to the *A. oryzae* transformant harboring PbSS also resulted in labeling patterns consistent with the proposed cyclization mechanism for **1** (Tables S5 and S6, Figures S19 and S20).

Heterologous expression of a second putative StTPS gene from *Penicillium verruculosum* TPU1311<sup>[19]</sup> (DDBJ accession no. LC228602) in *A. oryzae* NSAR1 resulted in the production of a sesterterpene hydrocarbon (19.8 mgL<sup>-1</sup> isolated yield, Figure S2), for which the formula of C<sub>25</sub>H<sub>40</sub> was confirmed by HREI-MS. The <sup>13</sup>C-NMR displayed 25 signals including two for olefinic carbons (Table S7), suggesting a pentacyclic skeleton. One- and two-dimensional NMR (Figures S21–S28) established the planar structure with a 5-7-3-6-5-membered ring system (Figure 2A). The relative configuration and assignments for H $\alpha$  and H $\beta$  at C1, C5, and C13 were determined by NOESY (Figure 2B), resulting in the structure of **2**, the likely biosynthetic precursor of asperterpenoid **A** (**3**) from *Aspergillus*.<sup>[20]</sup> The com-

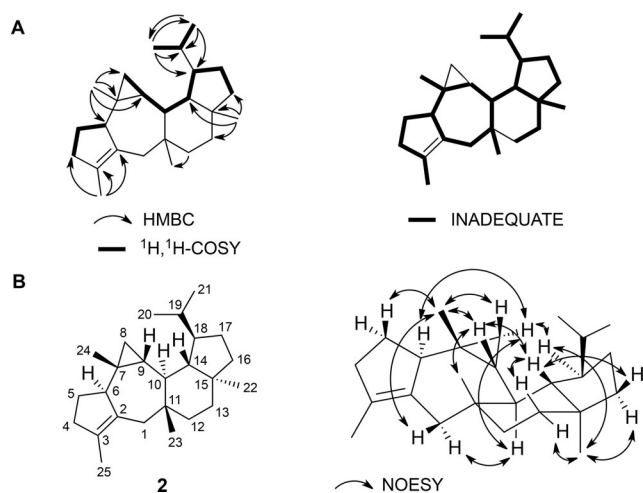
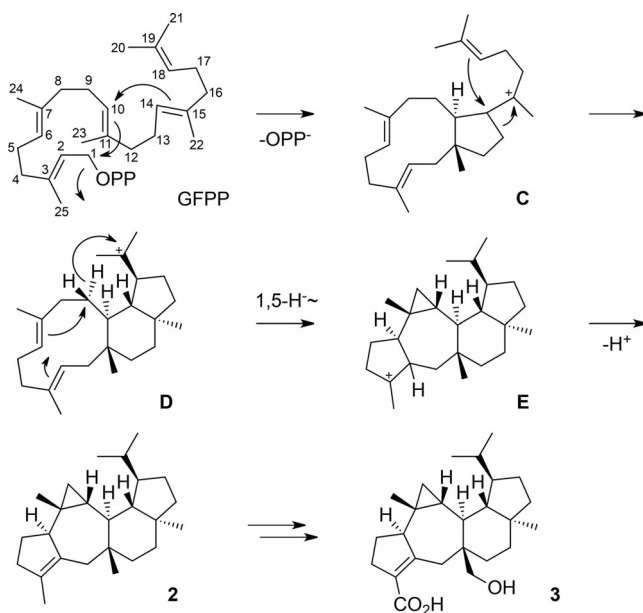


**Figure 2.** Structure elucidation of **2** by NMR spectroscopy.

pound was named preasperterpenoid A and the enzyme *Penicillium verruculosum* preasperterpenoid A synthase (PvPS).

PvPS was also expressed in *E. coli* and purified for in vitro studies. The proposed biosynthesis of **2** (Scheme 2) starts from GFPP by 1,11- and 10,14-cyclization to **C**, followed by ring ex-



**Scheme 2.** Cyclization of GFPP to preasperterpenoid A (**2**) by PvPS (*Penicillium verruculosum* preasperterpenoid A synthase) and its hypothetical conversion into asperterpenoid A (**3**) by *Aspergillus*.

pansion with a third cyclization to **D**. A 1,5-hydride migration with two more cyclization events results in **E**, which yields **2** by deprotonation. Each transformation from GFPP to **E** is composed of at least two elementary reactions to avoid intermediate secondary cations.<sup>[21]</sup> This mechanism for PvPS was strongly supported by conversion of all 25 (<sup>13</sup>C<sub>1</sub>)GFPP isotopomers obtained from shorter labeled precursors using the PT domain of PvPS and the GGPPs from *S. cyaneofuscatum* as explained

above (Table S4).<sup>[49]</sup> Their cyclization by the TPS domain of PvPS resulted in the incorporation of labeling in the expected positions in all cases (Figure S29). The labeling experiments in the geminal Me groups showed again no distribution of labeling.

The absolute configuration of **2** was determined using (*R*- and (*S*)-(1-<sup>13</sup>C,1-<sup>2</sup>H)GPP and the corresponding GGPP and GFPP analogs. Product analysis by HSQC pointed in all six cases to the absolute configuration of (6*S*,7*R*,9*R*,10*S*,11*R*,14*S*,15*S*,18*R*)-**2** (Figures S30–S32), which matches the absolute configuration of **3**<sup>[20]</sup> and further supports **2** as its precursor. The 1,5-hydride migration from **D** to **E** was investigated by incubation of both enantiomers of (1-<sup>13</sup>C,1-<sup>2</sup>H)FPP with IPP and PvPS. Product analysis through <sup>13</sup>C-NMR yielded a triplet for C9 from (*R*- and a singlet from (*S*)-(1-<sup>13</sup>C,1-<sup>2</sup>H)FPP, indicating the stereospecific migration of the 1-*pro-S* hydrogen of FPP that is equal to the 9-*pro-S* hydrogen of GFPP (Figure S33). The destination of the migrating hydrogen was evident from a PvPS incubation of IPP and (11-<sup>13</sup>C,1,1-<sup>2</sup>H<sub>2</sub>)FPP, which resulted in a triplet for C19, showing attachment of deuterium at this carbon (Figure S34). The final deprotonation from C2 of GFPP was shown using (2-<sup>2</sup>H)GFPP, which was synthesized according to a reported method (Scheme S5).<sup>[22]</sup> Product analysis by GC-MS indicated the loss of deuterium by an unchanged mass spectrum in comparison to unlabeled **2** (Figure S35). Feeding experiments with sodium (1-<sup>13</sup>C,2-<sup>3</sup>H<sub>3</sub>)- and (2-<sup>13</sup>C,2-<sup>3</sup>H<sub>3</sub>)acetate supported the proposed GFPP cyclization to **2** in all aspects (Tables S8 and S9, Figures S36 and S37).

In summary, we have characterized the products of two bifunctional fungal StTPSs, PbSS and PvPS, from *Penicillium* and investigated their cyclization mechanisms by isotopic labeling experiments. Notably, a phylogenetic analysis of their TPS domains together with those of previously studied homologs revealed grouping in six clades A–F (Figure 3, for an enlarged version see Figure S1 in the Supporting Information). PvPS and all known StTPSs of clade B uniformly generate an 11–5-membered ring system in the initial cyclization step, while PbSS forms an own clade E with an uncharacterized enzyme from *Aspergillus clavatus*, which reflects the unique cyclization mode of this enzyme. The closest characterized PbSS homologs are the StTPSs for sesterfisherol and quiannulatene that exhibit similar initial cyclization modes, but with different stereochemical courses. Further research on this interesting class of enzymes will show whether the correlation between the cyclization mechanism and phylogenetic relationship, which seems to be supported by the accumulated data, may lead to a better predictability of the product structure, including its stereochemistry from the amino acid sequence of a TPS.

## Acknowledgements

This work was funded by the DFG (DI1536/9-1), the Fonds der Chemischen Industrie, and JSPS KAKENHI (grant numbers 15H01836, 16H06443, and 17H05429). We thank Prof. K. Gomi (Tohoku University) and Prof. K. Kitamoto (The University of Tokyo) for the *Aspergillus* expression vectors and strain, and

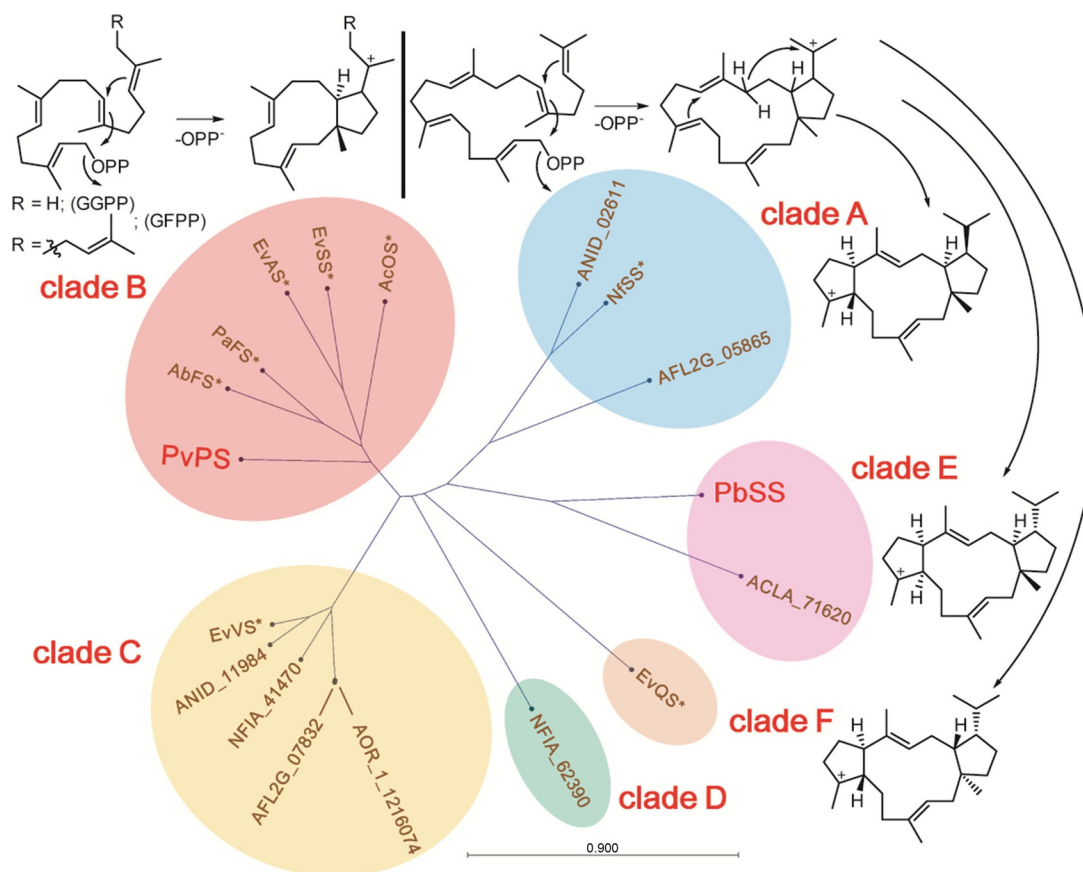


**Figure 3.** Phylogenetic analysis of related TPSs (terpene synthases) correlated to their initial cyclisation steps. Characterized StTPSs (sesterterpene synthases) are marked with asterisks and listed with their corresponding products in Table S1 (Supporting Information).

Prof. H. Yamazaki (Tohoku Pharmaceutical University) for the *P. verruculosum* strain.

**Keywords:** biosynthesis · carbocations · enzyme mechanisms · isotopes · terpenes

- [1] a) A. Baerga-Ortiz, B. Popovic, A. P. Siskos, H. M. O'Hare, D. Spiteller, M. G. Williams, N. Campillo, J. B. Spencer, P. F. Leadlay, *Chem. Biol.* **2006**, *13*, 277; b) D. H. Kwan, Y. Sun, F. Schulz, H. Hong, B. Popovic, J. C. C. Sim-Stark, S. F. Haydock, P. F. Leadlay, *Chem. Biol.* **2008**, *15*, 1231.
- [2] D. J. Tantillo, *Angew. Chem. Int. Ed.* **2017**, *56*, <https://doi.org/10.1002/anie.201702363>.
- [3] a) Q. Jia, G. Li, T. G. Köllner, J. Fu, X. Chen, W. Xiong, B. J. Crandall-Stotler, J. L. Bowman, D. J. Weston, Y. Zhang, L. Chen, Y. Xie, F.-W. Li, C. J. Rothfels, A. Larsson, S. W. Graham, D. W. Stevenson, G. K. Wong, J. Gershenzon, F. Chen, *Proc. Natl. Acad. Sci. USA* **2016**, *113*, 12328; b) W. Schwab, M. Wüst, *J. Agric. Food Chem.* **2015**, *63*, 10591; c) F. Chen, D. Tholl, J. Bohlmann, E. Pichersky, *Plant J.* **2011**, *66*, 212.
- [4] a) J. S. Dickschat, *Nat. Prod. Rep.* **2016**, *33*, 87; b) P. Rabe, J. Rinkel, T. A. Klapschinski, L. Barra, J. S. Dickschat, *Org. Biomol. Chem.* **2016**, *14*, 158; c) A. Schiffrin, Y. Khatri, P. Kirsch, V. Thiel, S. Schulz, R. Bernhardt, *Org. Biomol. Chem.* **2016**, *14*, 3385; d) T. A. Klapschinski, P. Rabe, J. S. Dickschat, *Angew. Chem. Int. Ed.* **2016**, *55*, 10141; *Angew. Chem.* **2016**, *128*, 10296; e) P. Rabe, T. Schmitz, J. S. Dickschat, *Beilstein J. Org. Chem.* **2016**, *12*, 1839; f) J. Rinkel, P. Rabe, P. Garbeva, J. S. Dickschat, *Angew. Chem. Int. Ed.* **2016**, *55*, 13593; *Angew. Chem.* **2016**, *128*, 13791; g) P. Rabe, J. Rinkel, E. Dolja, T. Schmitz, B. Nubbemeyer, T. H. Luu, J. S. Dickschat, *Angew. Chem. Int. Ed.* **2017**, *56*, 2776; *Angew. Chem.* **2017**, *129*, 2820; h) J. Rinkel, P. Rabe, X. Chen, T. Köllner, F. Chen, J. S. Dickschat, *Eur. J. Org. Chem.* **2017**, <https://doi.org/10.1002/ejoc.201700482>.
- [5] a) M. B. Quinn, C. M. Flynn, C. Schmidt-Dannert, *Nat. Prod. Rep.* **2014**, *31*, 1449; b) J. J. Shaw, T. Berbasova, T. Sasaki, K. Jefferson-George, D. J. Spakowicz, B. F. Dunican, C. E. Portero, A. Narvaez-Trujillo, S. A. Strobel, *J. Biol. Chem.* **2015**, *290*, 8511; c) I. Burkhardt, T. Simon, M. Henrot, L. Studt, S. Rösler, B. Tudzynski, M. Christmann, J. S. Dickschat, *Angew. Chem. Int. Ed.* **2016**, *55*, 8748; *Angew. Chem.* **2016**, *128*, 8890; d) N. L. Brock, K. Huss, B. Tudzynski, J. S. Dickschat, *ChemBioChem* **2013**, *14*, 311; e) S. P. McCormick, N. J. Alexander, L. J. Harris, *Appl. Environ. Microbiol.* **2010**, *76*, 136; f) H.-C. Lin, Y.-H. Chooi, S. Dhingra, W. Xu, A. M. Calvo, Y. Tang, *J. Am. Chem. Soc.* **2013**, *135*, 4616; g) C. Pinedo, C.-M. Wang, J.-M. Pradier, B. Dalmais, M. Choquer, P. Le Pecheur, G. Morgant, I. G. Collado, D. E. Cane, M. Viaud, *ACS Chem. Biol.* **2008**, *3*, 791; h) T. Toyomasu, M. Tsukahara, A. Kaneko, R. Niida, W. Mitsuhashi, T. Dairi, N. Kato, T. Sassa, *Proc. Natl. Acad. Sci. USA* **2007**, *104*, 3084; i) T. Toyomasu, A. Kaneko, T. Tokiwano, Y. Kanno, Y. Kanno, R. Niida, S. Miura, T. Nishioka, C. Ikeda, W. Mitsuhashi, T. Dairi, T. Kawano, H. Oikawa, N. Kato, T. Sassa, *J. Org. Chem.* **2009**, *74*, 1541; j) B. Qin, Y. Matsuda, T. Mori, M. Okada, Z. Quan, T. Mitsuhashi, T. Wakimoto, I. Abe, *Angew. Chem. Int. Ed.* **2016**, *55*, 1658; *Angew. Chem.* **2016**, *128*, 1690.
- [6] P. Rabe, J. Rinkel, B. Nubbemeyer, T. G. Köllner, F. Chen, J. S. Dickschat, *Angew. Chem. Int. Ed.* **2016**, *55*, 15420; *Angew. Chem.* **2016**, *128*, 15646.
- [7] Y. Matsuda, T. Mitsuhashi, S. Lee, M. Hoshino, T. Mori, M. Okada, H. Zhang, F. Hayashi, M. Fujita, I. Abe, *Angew. Chem. Int. Ed.* **2016**, *55*, 5785; *Angew. Chem.* **2016**, *128*, 5879.
- [8] R. Chiba, A. Minami, K. Gomi, H. Oikawa, *Org. Lett.* **2013**, *15*, 594.
- [9] Y. Ye, A. Minami, A. Mandi, C. Liu, T. Taniguchi, T. Kuzuyama, K. Monde, K. Gomi, H. Oikawa, *J. Am. Chem. Soc.* **2015**, *137*, 11846.
- [10] Y. Matsuda, T. Mitsuhashi, Z. Quan, I. Abe, *Org. Lett.* **2015**, *17*, 4644.
- [11] M. Okada, Y. Matsuda, T. Mitsuhashi, S. Hoshino, T. Mori, K. Nakagawa, Z. Quan, B. Qin, H. Zhang, F. Hayashi, H. Kawaide, I. Abe, *J. Am. Chem. Soc.* **2016**, *138*, 10011.

- [12] F. J. Jin, J. Maruyama, P. R. Juvvadi, M. Arioka, K. Kitamoto, *FEMS Microbiol. Lett.* **2004**, *239*, 79.
- [13] a) Y. Matsuda, T. Wakimoto, T. Mori, T. Awakawa, I. Abe, *J. Am. Chem. Soc.* **2014**, *136*, 15326; b) Y. Matsuda, T. Iwabuchi, T. Wakimoto, T. Awakawa, I. Abe, *J. Am. Chem. Soc.* **2015**, *137*, 3393.
- [14] P. Rabe, L. Barra, J. Rinkel, R. Riclea, C. A. Citron, T. A. Klapschinski, A. Janusko, J. S. Dickschat, *Angew. Chem. Int. Ed.* **2015**, *54*, 13448; *Angew. Chem.* **2015**, *127*, 13649.
- [15] a) D. E. Cane, T. Rossi, A. M. Tillman, J. P. Pachlatko, *J. Am. Chem. Soc.* **1981**, *103*, 1838; b) C.-M. Wang, R. Hopson, X. Lin, D. E. Cane, *J. Am. Chem. Soc.* **2009**, *131*, 8360; c) N. L. Brock, S. R. Ravella, S. Schulz, J. S. Dickschat, *Angew. Chem. Int. Ed.* **2013**, *52*, 2100; *Angew. Chem.* **2013**, *125*, 2154; d) X. Lin, D. E. Cane, *J. Am. Chem. Soc.* **2009**, *131*, 6332.
- [16] a) J. W. Cornforth, R. H. Cornforth, C. Donninger, G. Popjak, *Proc. R. Soc. London Ser. B* **1966**, *163*, 492; b) H. V. Thulasiram, C. D. Poulter, *J. Am. Chem. Soc.* **2006**, *128*, 15819.
- [17] a) D. E. Cane, J. S. Oliver, P. H. M. Harrison, C. Abell, B. R. Hubbard, C. T. Kane, R. Lattman, *J. Am. Chem. Soc.* **1990**, *112*, 4513; b) D. E. Cane, P. C. Prabhakaran, E. J. Salaski, P. H. M. Harrison, H. Noguchi, B. J. Rawlings, *J. Am. Chem. Soc.* **1989**, *111*, 8914; c) P. Rabe, M. Samborsky, P. F. Leadlay, J. S. Dickschat, *Org. Biomol. Chem.* **2017**, *15*, 2353.
- [18] S. Bux, R. Reamer, D. Zink, D. Schmatz, A. Dombrowski, M. Goetz, *J. Org. Chem.* **1991**, *56*, 5618.
- [19] H. Yamazaki, W. Nakayama, O. Takahashi, R. Kirikoshi, Y. Izumikawa, K. Iwasaki, K. Toraiwa, K. Ukai, H. Rotinsulu, D. S. Wewengkang, *Bioorg. Med. Chem. Lett.* **2015**, *25*, 3087.
- [20] X. Huang, H. Huang, H. Li, X. Sun, H. Huang, Y. Lu, Y. Lin, Y. Long, Z. She, *Org. Lett.* **2013**, *15*, 721.
- [21] a) D. J. Tantillo, *Chem. Soc. Rev.* **2010**, *39*, 2847; b) B. A. Hess, L. Smentek, *Angew. Chem. Int. Ed.* **2013**, *52*, 11029.
- [22] J. A. Faraldos, S. Wu, J. Chappell, R. M. Coates, *J. Am. Chem. Soc.* **2010**, *132*, 2998.

---

Manuscript received: June 13, 2017

Accepted manuscript online: June 16, 2017

Version of record online: July 3, 2017





## Appendix H

### **18-Hydroxydolabella-3,7-diene synthase – a diterpene synthase from *Chitinophaga pinensis***

*Beilstein J. Org. Chem.* **2017**, *13*, 1770–1780.

DOI:10.3762/bjoc.13.171





## 18-Hydroxydolabella-3,7-diene synthase – a diterpene synthase from *Chitinophaga pinensis*

Jeroen S. Dickschat<sup>\*1</sup>, Jan Rinkel<sup>1</sup>, Patrick Rabe<sup>1</sup>, Arman Beyraghdar Kashkooli<sup>2</sup> and Harro J. Bouwmeester<sup>3</sup>

### Full Research Paper

[Open Access](#)**Address:**

<sup>1</sup>Kekulé-Institute of Organic Chemistry and Biochemistry, University of Bonn, Gerhard-Domagk-Straße 1, 53121 Bonn, Germany,

<sup>2</sup>Laboratory of Plant Physiology, Wageningen University, Droevendaalsesteeg 1, 6708 PB Wageningen, The Netherlands, and

<sup>3</sup>Swammerdam Institute for Life Sciences, University of Amsterdam, Sciencepark 904, 1098 XH Amsterdam, The Netherlands

**Email:**

Jeroen S. Dickschat<sup>\*</sup> - dickschat@uni-bonn.de

<sup>\*</sup> Corresponding author

**Keywords:**

biosynthesis; *Chitinophaga pinensis*; *Nicotiana benthamiana*; structure elucidation; terpenes

*Beilstein J. Org. Chem.* **2017**, *13*, 1770–1780.

doi:10.3762/bjoc.13.171

Received: 21 June 2017

Accepted: 09 August 2017

Published: 23 August 2017

This article is part of the Thematic Series "Lipids: fatty acids and derivatives, polyketides and isoprenoids".

Associate Editor: A. Kirschning

© 2017 Dickschat et al.; licensee Beilstein-Institut.

License and terms: see end of document.

## Abstract

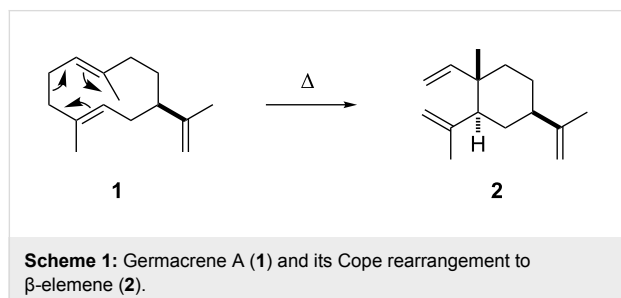
The product obtained in vitro from a diterpene synthase encoded in the genome of the bacterium *Chitinophaga pinensis*, an enzyme previously reported to have germacrene A synthase activity during heterologous expression in *Escherichia coli*, was identified by extensive NMR-spectroscopic methods as 18-hydroxydolabella-3,7-diene. The absolute configuration of this diterpene alcohol and the stereochemical course of the terpene synthase reaction were addressed by isotopic labelling experiments. Heterologous expression of the diterpene synthase in *Nicotiana benthamiana* resulted in the production of 18-hydroxydolabella-3,7-diene also in planta, while the results from the heterologous expression in *E. coli* were shown to be reproducible, revealing that the expression of one and the same terpene synthase in different heterologous hosts may yield different terpene products.

## Introduction

Terpene synthases convert a handful of simple linear and achiral oligoprenyl diphosphates in just one enzymatic step into a remarkable diversity of usually polycyclic structurally complex lipophilic terpenes with multiple stereogenic centres. In their active sites type I terpene synthases contain the highly conserved aspartate-rich motif DDXX(X)(D,E) and the NSE

triad NDXXSXX(R,K)(E,D), modified to a DTE triad in plants, for binding of the Mg<sup>2+</sup> cofactor that forms a trinuclear (Mg<sup>2+</sup>)<sub>3</sub> cluster to which the diphosphate portion of the substrate binds. Upon substrate binding the active site closes, resulting in hydrogen bonds between the substrate's diphosphate and the pyrophosphate sensor, a highly conserved arginine located

43 amino acids upstream of the NSE triad, and the RY dimer, a highly conserved motif at the C-terminus. The substrate is ionised by extrusion of diphosphate, yielding a highly reactive allyl cation that can react in a cyclisation cascade by attack of olefinic double bonds to the cationic centre, hydride shifts and Wagner–Meerwein rearrangements. The process is usually terminated by deprotonation or attack of water to yield a lipophilic terpene hydrocarbon or alcohol. Among the first investigated terpene synthases were the (+)- and (–)-bornyl diphosphate synthases from the plants *Salvia officinalis* and *Tanacetum vulgare* forming a more polar product by the unusual termination via reattack of diphosphate [1], the trichodiene synthase from the fungus *Trichothecium roseum* [2], and pentalenene synthase from *Streptomyces exfoliatus* [3]. Recently, the first terpene synthases were reported from a eukaryotic soil microorganism, the social amoeba *Dictyostelium discoideum* [4,5]. With respect to bacterial enzymes, many terpene synthases have been identified and their products have been structurally characterised (reviewed in [6], following reports: [7–14]). One possible method to investigate the products of terpene synthases is the expression of terpene synthase genes in a heterologous host, as was recently performed for a large number of bacterial enzymes in an engineered *Streptomyces avermitilis* strain from which the biosynthesis genes for all other natural products were deleted, allowing a relatively easy purification of the terpene synthase products from culture extracts [15,16]. The heterologous expression of terpene synthase genes in *Escherichia coli* is also frequently successful, resulting in the production of volatile terpenes by this bacterium that can be detected in headspace extracts [17,18]. In one of these previous reports [17] we have described a terpene synthase from *Chitinophaga pinensis* DSM 2588 (accession number WP\_012789469) as a sesquiterpene synthase for germacrene A (**1**), which was based on the identification of this compound and its Cope rearrangement product  $\beta$ -elemene (**2**) formed by the thermal impact during GC–MS analysis [19] in *E. coli* headspace extracts under heterologous expression of the terpene synthase gene (Scheme 1). Here we present the diterpene synthase activity of this enzyme in in vitro experiments and the first heterologous expression of a bacterial terpene synthase gene in a plant, *Nicotiana benthamiana*.



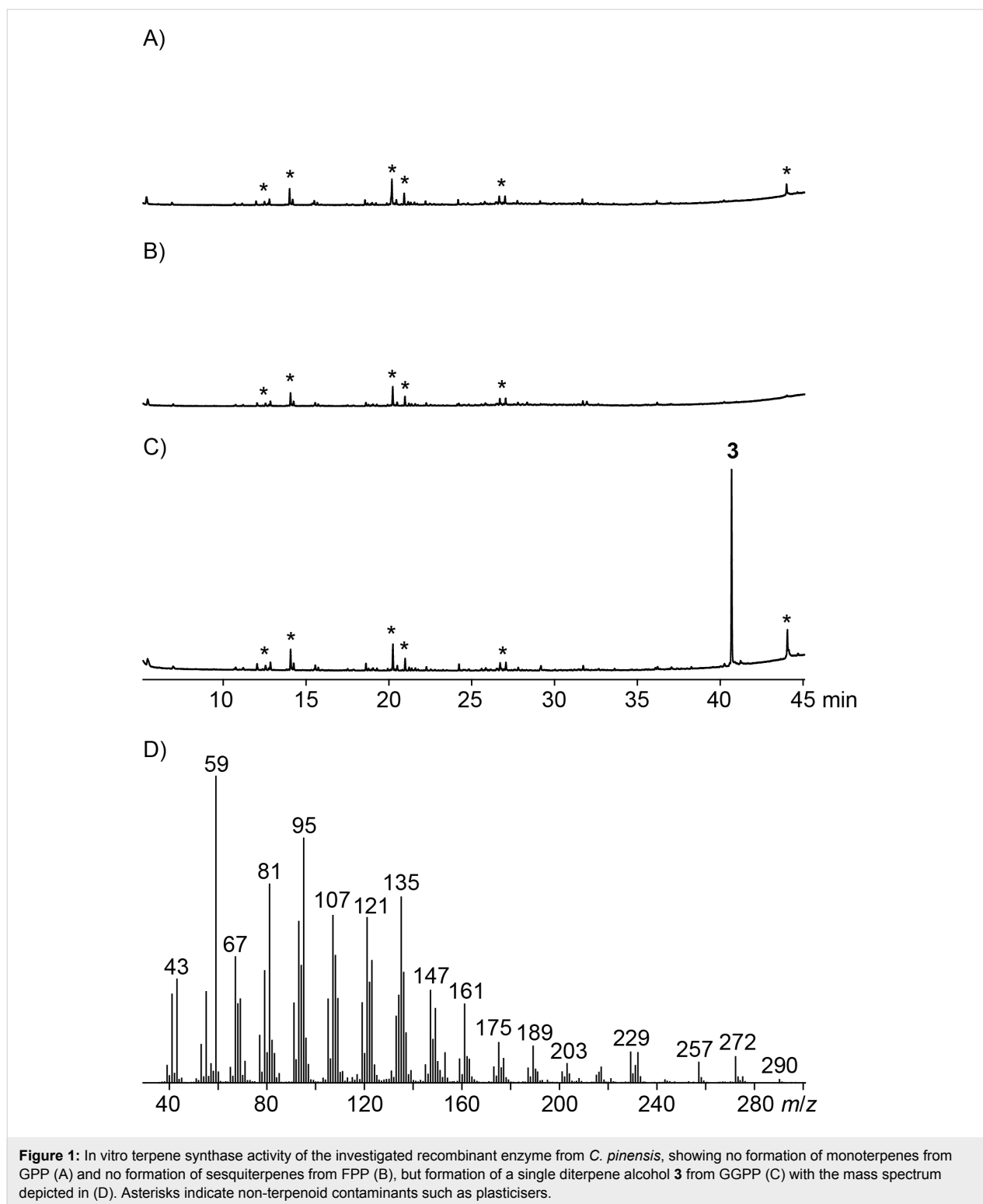
## Results and Discussion

### Characterisation of a diterpene synthase from *Chitinophaga pinensis* in vitro

The terpene synthase from *C. pinensis* was heterologously expressed in *E. coli* as a recombinant protein with a C-terminal polyhistidine tag using a previously reported pET28c-based expression construct [17] and purified by Ni-NTA affinity chromatography (Figure S1, Supporting Information File 1). The purified enzyme was tested in in vitro experiments for mono-, sesqui- and diterpene activity by incubation with geranyl (GPP), farnesyl (FPP) and geranylgeranyl diphosphate (GGPP) as substrates, which yielded a single product **3** only from GGPP, but no products from FPP and GPP as demonstrated by GC–MS analysis (Figure 1). The mass spectrum of **3** showed a molecular ion at  $m/z = 290$  pointing to a diterpene alcohol and a base peak ion at  $m/z = 59$  indicative of a 2-hydroxyisopropyl group that frequently occurs in terpene alcohols. Both findings, i.e., no production of sesquiterpenes from FPP in in vitro experiments with recombinant purified enzyme as well as the emission of sesquiterpenes by *E. coli* during heterologous expression, were fully reproducible (Figure S2, Supporting Information File 1).

The compound **3** obtained from the in vitro incubation of GGPP was purified and its structure was elucidated by extensive one- and two-dimensional NMR spectroscopic methods (Table 1, Figures S3–S9, Supporting Information File 1). The  $^{13}\text{C}$  NMR spectrum showed five signals for methyl groups, seven aliphatic  $\text{CH}_2$  groups, two aliphatic and two olefinic CH groups, and four signals for quaternary carbons including one connected to oxygen and two olefinic carbons, suggesting the structure of a bicyclic diterpene alcohol. The  $^1\text{H}, ^1\text{H}$ -COSY spectrum revealed three contiguous spin systems for C2–C3, C5–C6–C7, and C9–C10–C11–C12–C13–C14 (Scheme 2). Key HMBC correlations from H19 and H20 to C12 and C18 placed the 2-hydroxyisopropyl group at C12, while HMBC correlations from H17 to C6, C7, C8 and C9 located the C8–C17 fragment between C7 and C9. HMBC crosspeaks between H16 and C3, C4 and C5 indicated the C3–C4–C5 connection, and HMBC correlations between H15 and C1, C2 and C14, and between H11, C1 and C2 established the bonds between the quaternary carbon C1 and its four neighbours. Diagnostic NOESY correlations between H11 and H2 $\beta$ , H3 and H7, between H12 and H2 $\beta$ , and between H10 $\alpha$  and H15 established the relative configuration of **3**, resulting in the structure of (1*R*\*,3*E*,7*E*,11*S*\*,12*S*\*)-18-hydroxydolabella-3,7-diene and identifying the terpene synthase from *C. pinensis* as 18-hydroxydolabella-3,7-diene synthase (HdS).

The proposed cyclisation mechanism from GGPP to **3** is likely a concerted one-step process with 1,11- and 10,14-cyclisation and concomitant attack of water at C15 (Scheme 2). We have



recently shown that the absolute configurations of terpenes can be determined by enzymatic conversion of stereoselectively deuterated terpene precursors, because the problem of determining the absolute configuration of the terpene under investigation is simplified to a problem of delineating the relative ori-

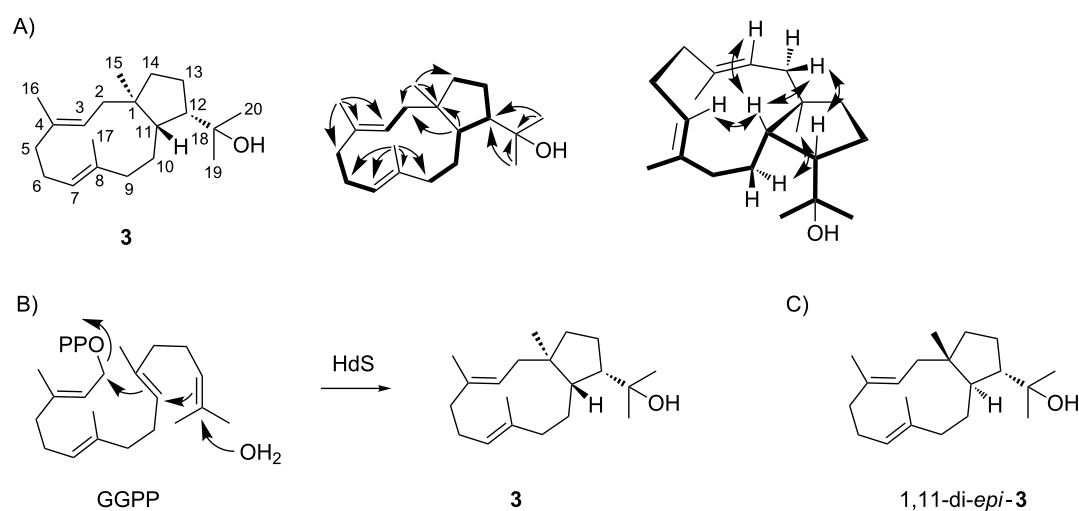
entation of its stereocentres to the known absolute configuration at the deuterated carbon [12,13]. This approach was used to determine the absolute configuration of **3** using both enantiomers of (*R*)- and (*S*)-(1-<sup>13</sup>C,1-<sup>2</sup>H)GGPP [14], (*R*)- and (*S*)-(1-<sup>13</sup>C,1-<sup>2</sup>H)FPP, and (*R*)- and (*S*)-(1-<sup>13</sup>C,1-<sup>2</sup>H)GPP [12] in which

**Table 1:** NMR data of **3** recorded in C<sub>6</sub>D<sub>6</sub>.

C <sup>a</sup>	<sup>13</sup> C (δ) <sup>b</sup>	<sup>1</sup> H (δ, m, J, int) <sup>c</sup>
1	47.5 (C <sub>q</sub> )	–
2	42.6 (CH <sub>2</sub> )	2.19 (m, 1H, Hβ) 1.71 (dd, J = 6.2, J = 13.8, 1H, Hα)
3	126.5 (CH)	5.16 (dd, J = 9.7, J = 5.8, 1H)
4	134.0 (C <sub>q</sub> )	–
5	40.2 (CH <sub>2</sub> )	2.12 (m, 1H) 2.06 (m, 1H)
6	25.0 (CH <sub>2</sub> )	2.22 (m, 1H, Hβ) 2.05 (m, 1H, Hα)
7	128.2 (CH)	4.87 (dd, J = 10.0, J = 4.3, 1H)
8	134.0 (C <sub>q</sub> )	–
9	39.2 (CH <sub>2</sub> )	2.27 (m, 1H, Hα) 2.14 (m, 1H, Hβ)
10	23.7 (CH <sub>2</sub> )	2.13 (m, 1H, Hβ) 1.23 (m, 1H, Hα)
11	42.1 (CH)	1.84 (m, 1H)
12	53.7 (CH)	1.84 (ddd, J = 10.4, J = 7.4, J = 7.4, 1H)
13	26.0 (CH <sub>2</sub> )	1.53 (m, 1H) 1.53 (m, 1H)
14	41.3 (CH <sub>2</sub> )	1.47 (m, 1H, Hα) 1.39 (m, 1H, Hβ)
15	24.9 (CH <sub>3</sub> )	1.08 (s, 3H)
16	16.6 (CH <sub>3</sub> )	1.59 (s, 3H)
17	16.0 (CH <sub>3</sub> )	1.47 (s, 3H)
18	72.1 (C <sub>q</sub> )	–
19	30.8 (CH <sub>3</sub> )	1.11 (s, 3H)
20	30.7 (CH <sub>3</sub> )	1.18 (s, 3H)

<sup>a</sup>Carbon numbering as shown in Scheme 2. <sup>b</sup>Chemical shifts δ in ppm and assignment of carbons by <sup>13</sup>C-DEPT135 spectroscopy.

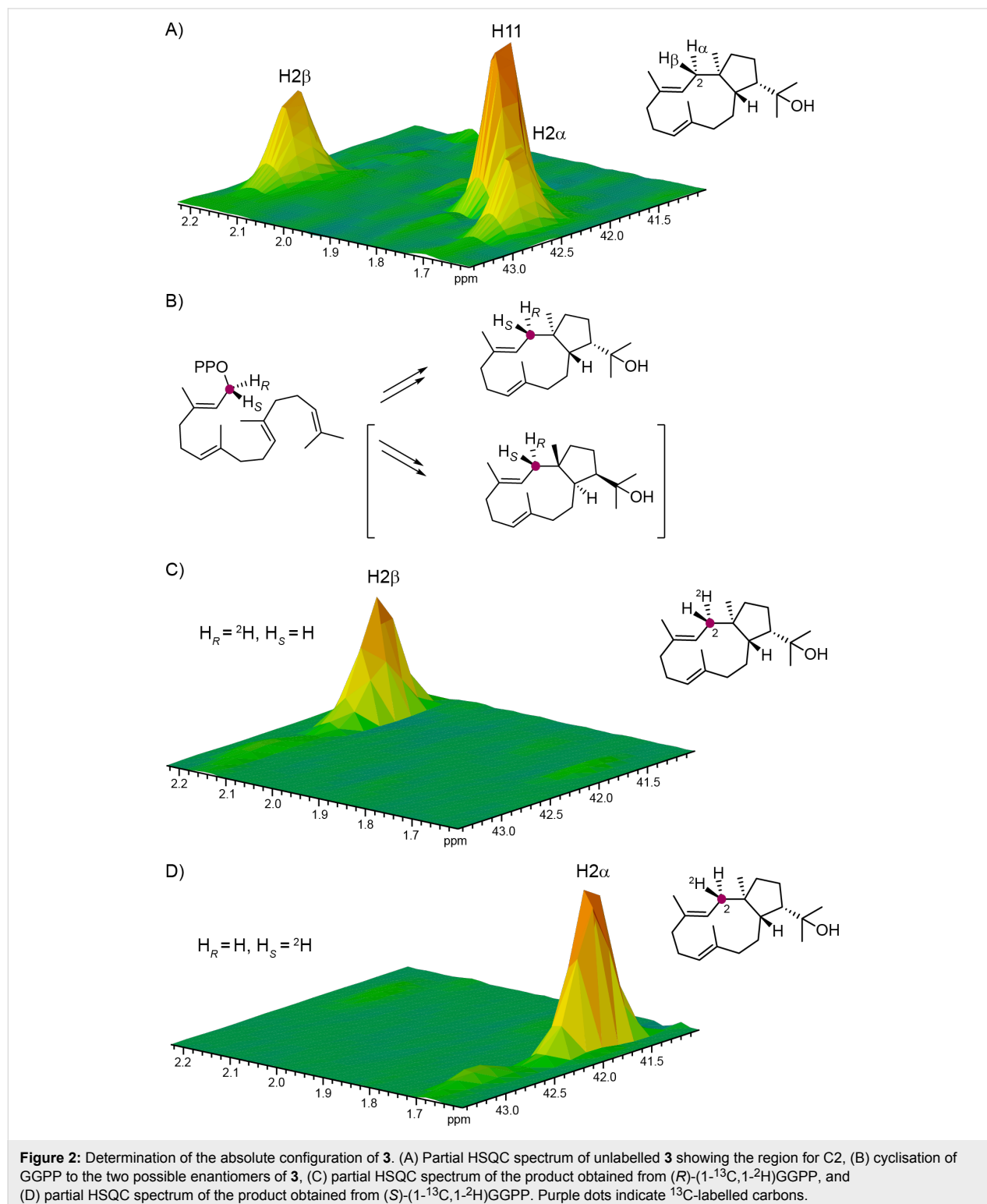
<sup>c</sup>Chemical shifts δ in ppm, multiplicity m (s = singlet, d = doublet, t = triplet, m = multiplet), coupling constants J are given in Hertz.



**Scheme 2:** Product obtained from the diterpene synthase from *C. pinensis*. (A) Structure of (1*R*,3*E*,7*E*,11*S*,12*S*)-18-hydroxydolabella-3,7-diene (**3**), contiguous <sup>1</sup>H, <sup>1</sup>H-COSY spin systems (bold), and diagnostic HMBC and NOESY correlations (single and double headed arrows). (B) Cyclisation mechanism for the conversion of GGPP into **3** by HdS. (C) Structure of the known stereoisomer 1,11-di-*epi*-**3**.

the additional  $^{13}\text{C}$  labels were introduced to increase sensitivity in the HSQC analysis of the obtained terpene products. Incubation of (*R*)-(1- $^{13}\text{C}$ ,1- $^2\text{H}$ )GGPP with HdS resulted in the specific incorporation of the deuterium labelling into the  $2\alpha$  position as indicated by a diminished crosspeak in the HSQC spectrum,

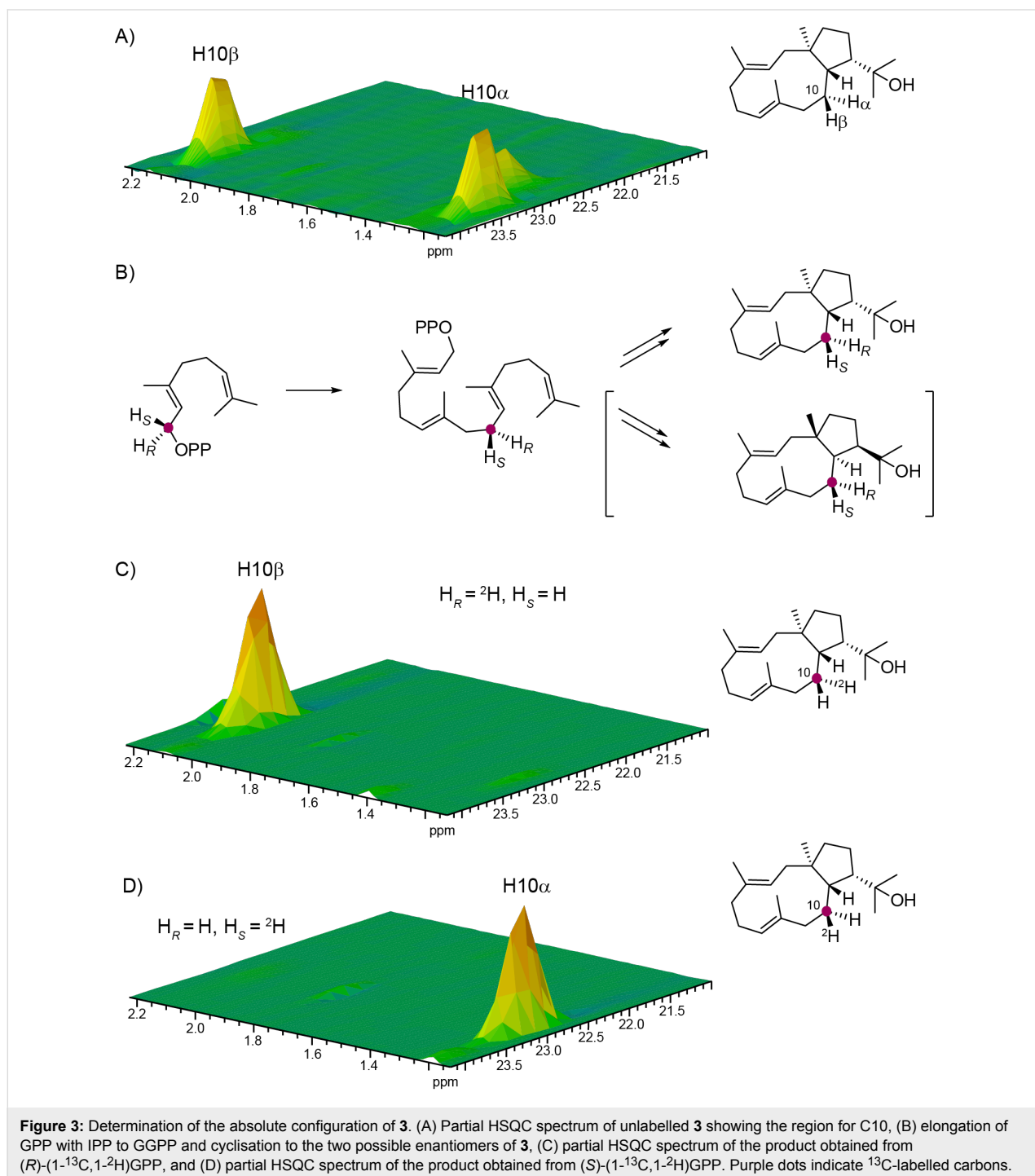
while the crosspeak for  $\text{H}2\beta$  was strongly enhanced because of the  $^{13}\text{C}$  labelling of  $\text{C}2$  (Figure 2). Consistently, the substrate (*S*)-(1- $^{13}\text{C}$ ,1- $^2\text{H}$ )GGPP gave a product with specific incorporation of the deuterium label into the  $2\beta$  position. Assuming inversion of configuration at  $\text{C}1$  for the cyclisation of GGPP to



**3** as reported for several other terpene synthases [13,20–22], these findings point to the absolute configuration of (1*R*,3*E*,7*E*,11*S*,12*S*)-18-hydroxydolabella-3,7-diene.

For the incubation experiments with (*R*)- and (*S*)-(1-<sup>13</sup>C,1-<sup>2</sup>H)GPP, the terpene monomer IPP, HdS and the GGPP synthase (GGPPS) from *S. cyaneofuscatus* [12] were added to the reaction mixtures for an enzymatic elongation of the GPP

isotopomers to the corresponding GGPPs. It is well established that the elongations of oligoprenyl diphosphates with IPP by type I oligoprenyl diphosphate synthases proceeds with inversion of configuration at C1 [23,24]. The conversion of the obtained labelled GGPPs by HdS gave a stereospecific incorporation of the deuterium labelling into H10α from (*R*)-(1-<sup>13</sup>C,1-<sup>2</sup>H)GPP and into H10β from (*S*)-(1-<sup>13</sup>C,1-<sup>2</sup>H)GPP (Figure 3), which pointed to the same absolute configuration for **3** as

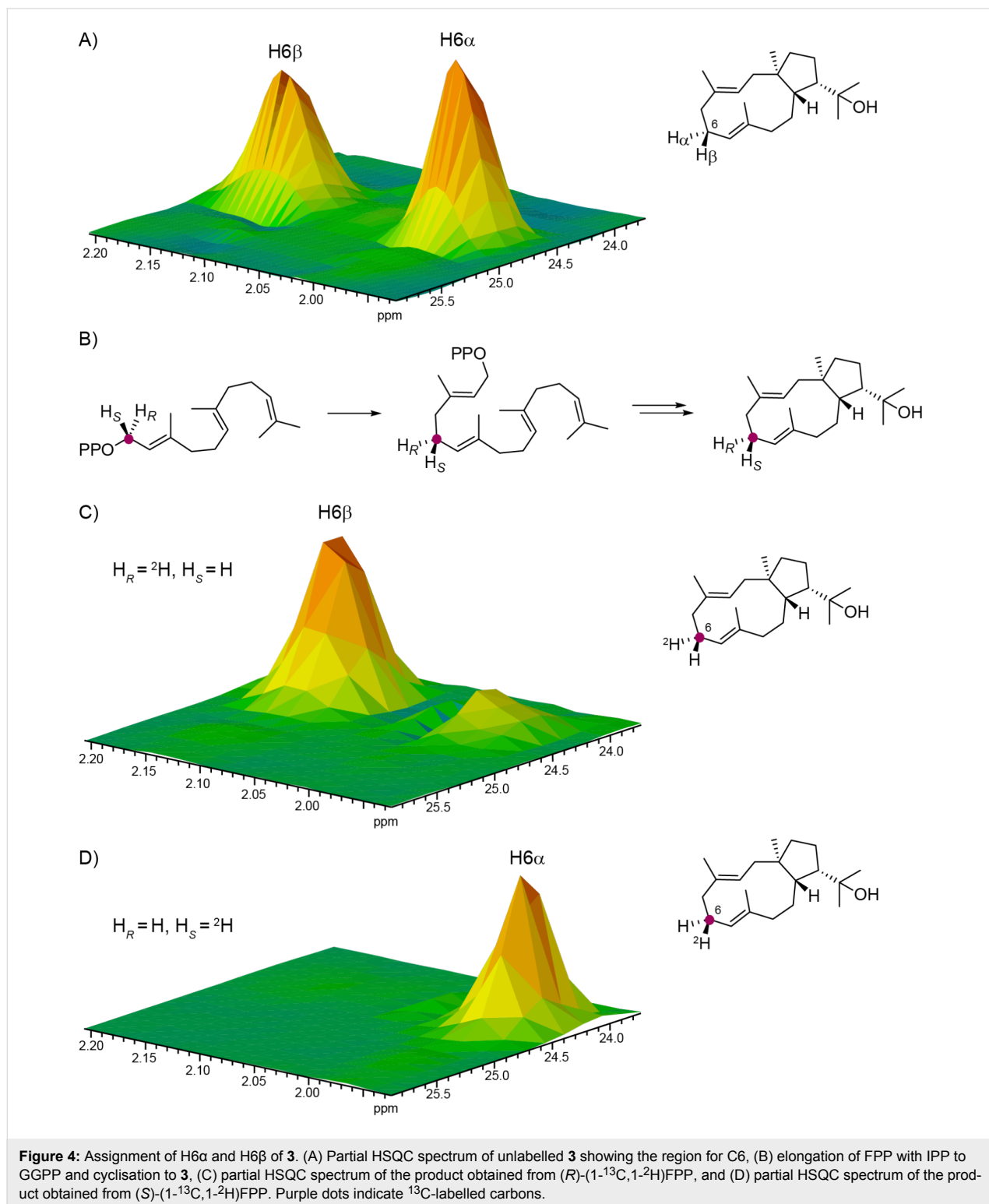




deduced from the experiments with the two enantiomers of  $(1-^{13}\text{C},1-^2\text{H})\text{GGPP}$ .

Similar incubation experiments were performed with  $(R)$ - and  $(S)$ - $(1-^{13}\text{C},1-^2\text{H})\text{FPP}$ , IPP, GGPPS and HdS, resulting in the

stereospecific incorporation of deuterium labelling into the hydrogens at C6 of **3** (Figure 4). These experiments could not be used to confirm the absolute configuration of the diterpene, because the signals for H6 $\alpha$  and H6 $\beta$  could not be unambiguously assigned from the NMR spectra of the unlabelled com-



pound. Instead, the results from these incubation experiments were used for this assignment.

HdS exhibited a defined stereochemical course with respect to the methyl groups in the hydroxyisopropyl group of **3**, as was indicated by conversion of (12-<sup>13</sup>C)FPP and (13-<sup>13</sup>C)FPP [25] with IPP by GGPPS and HdS that resulted in the specific incorporation of labelling into the carbon atoms absorbing at 30.8 ppm and 30.7 ppm, respectively (Figure 5).

### Functional characterisation of bacterial diterpene synthase in planta

To test the catalytic activity of HdS in planta, its corresponding gene was transiently expressed in *N. benthamiana*. Since we have shown before that the mitochondria are a suitable subcellular compartment for the heterologous production of terpenes [26], and it is known that one of the multiple GGPP synthases in plants are targeted to the mitochondria [27], we decided to attempt the expression of HdS with mitochondrial targeting (HdS-mit). A construct without targeting signal (HdS; resulting in cytoplasmic localisation) and an empty vector were used as controls. A *p19* construct [28] was co-infiltrated in all treatments to suppress endogenous silencing of *N. benthamiana*

upon agroinfiltration. No difference was found by GC–MS in EtOAc extracts of *N. benthamiana* leaves expressing an empty vector or HdS, while the chromatogram of an extract obtained from HdS-mit expressing leaves revealed an additional major compound (Figure 6). This compound (retention time of 21.08 min) was identified as 18-hydroxydolabella-3,7-diene by GC–MS, using the diterpene alcohol obtained by the in vitro incubations of GGPP with HdS as an authentic standard. A preparative scale isolation of **3** from plant leaves expressing HdS-mit yielded 26.2 mg of the pure diterpene alcohol from 100 g of fresh leaves (0.03% of fresh leaf weight). The obtained material was identical to **3** obtained by in vitro incubation of GGPP with recombinant HdS by <sup>1</sup>H and <sup>13</sup>C NMR spectroscopy.

A compound with the same structure as determined from our experiments for (1*R*,3*E*,7*E*,11*S*,12*S*)-18-hydroxydolabella-3,7-diene (**3**), but with different NMR data, was recently reported from the brown alga *Dilophus spiralis* [29]. In this study, a revision for the previously reported structure of (1*S*,3*E*,7*E*,11*R*,12*S*)-18-hydroxydolabella-3,7-diene (1,11-di-*epi*-**3**) for a compound isolated from the brown alga *Dictyota dichotoma* [30] was suggested (Scheme 2C). The same natural

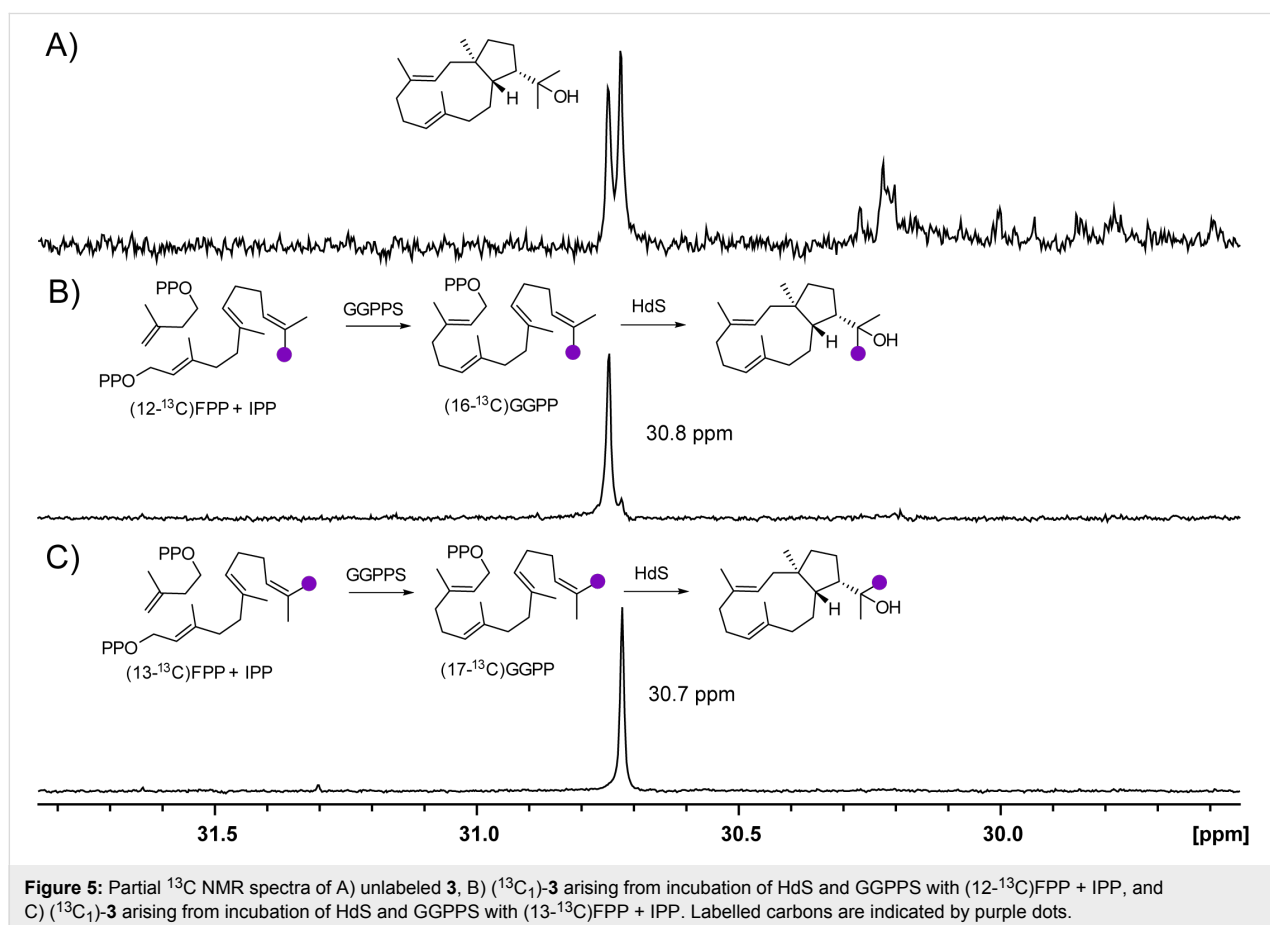
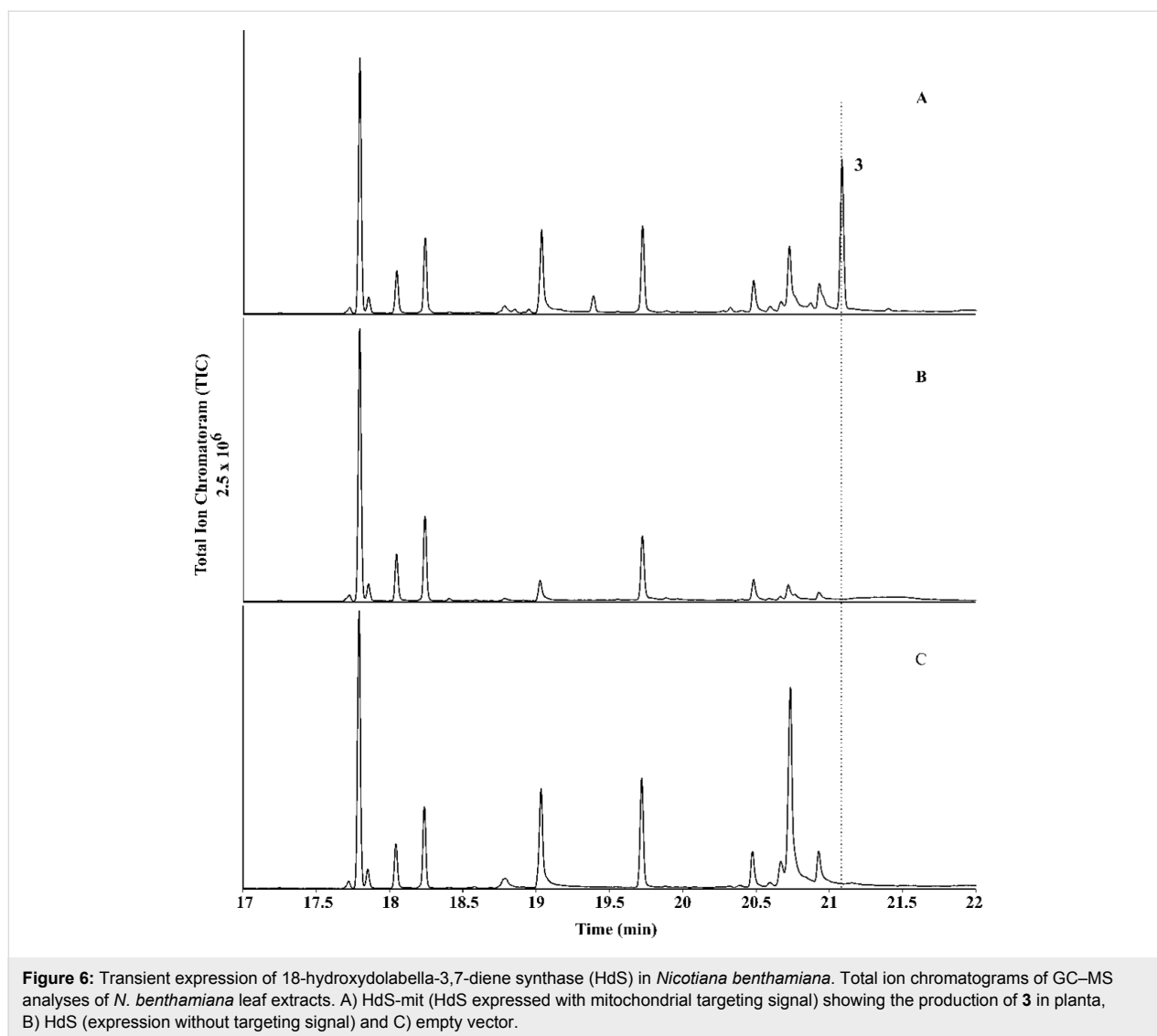


**Figure 5:** Partial <sup>13</sup>C NMR spectra of A) unlabeled **3**, B) (13C<sub>1</sub>)-**3** arising from incubation of HdS and GGPPS with (12-<sup>13</sup>C)FPP + IPP, and C) (13C<sub>1</sub>)-**3** arising from incubation of HdS and GGPPS with (13-<sup>13</sup>C)FPP + IPP. Labeled carbons are indicated by purple dots.



product is known from the higher plant *Aglaia odorata* [31], but in this case the reason for the assignment of the reported absolute configuration is unclear, because no optical rotation has been included in this study. It is difficult to judge what the correct structure for the compounds isolated from the brown algae and from *A. odorata* is, but the NMR data and isotopic labelling experiments presented here clearly point to the structure of **3** for the material obtained by us from the diterpene synthase from *C. pinensis*.

## Conclusion

In this study we have reinvestigated a terpene synthase from *Chitinophaga pinensis* that was previously characterised as germacrene A synthase by heterologous expression in *E. coli*. While this result could be reproduced during the course of the present study, the recombinant purified enzyme surprisingly only showed diterpene synthase activity (it did not produce any

product from GPP nor FPP) and the obtained product was identified as (1*R*,3*E*,7*E*,11*S*,12*S*)-18-hydroxydolabella-3,7-diene. Notably, heterologous expression in the plant *Nicotiana benthamiana* and targeting to the mitochondria resulted in the production of the same diterpene alcohol. Although the mitochondria of *N. benthamiana* also produce FPP [32], again no germacrene D was detected. Taken together, these experiments demonstrate that the expression of one and the same terpene synthase in different organisms may lead to the formation of different products and even an altered substrate specificity. Indeed, it has been shown before that small alterations in the conditions such as a change of the metal cofactor can result in a switch from FPP to GPP synthase activity for an oligoprenyl diphosphate synthase from the beetle *Phaedon cochleariae* [33]. Similar small changes of the conditions, e.g., of the pH or the presence of different metal cofactors, may also change the product profile of a terpene synthase in different heterologous hosts.

Changes in the product profile of terpene synthases depending on the host that was used to express the gene have been reported by Ginglinger et al., who have shown that *Arabidopsis* TPS10 produced mainly linalool when expressed in yeast and *N. benthamiana*, while the *E. coli* expressed protein catalysed the formation of mainly  $\beta$ -myrcene and  $\beta$ -ocimene [34]. The authors suggested different cofactor availabilities and biochemical conditions in the different hosts as the reason for their findings. Also Fischer et al. pointed out the effect that the host can have on the product specificity of terpene synthases [35]. In this context substrate availability is another issue to be considered: While no GGPP synthase is known in *E. coli*, this diterpene precursor is produced in the mitochondria of *N. benthamiana*. The yield of 18-hydroxydolabella-3,7-diene in planta of 26.2 mg per 100 g of fresh leaves is useful for the preparative scale production of the diterpene alcohol that can easily be isolated by extraction and column chromatography, which underpins the potential of plants, besides the recently reviewed microbial hosts for the sustainable production of diterpenes [36], as expression systems for secondary metabolite genes. The function of the investigated terpene synthase from *C. pinensis* in its natural context remains elusive, since neither (1*R*,3*E*,7*E*,11*S*,12*S*)-18-hydroxydolabella-3,7-diene nor germacrene A or its Cope rearrangement product  $\beta$ -elemene could be detected in laboratory cultures [37].

## Supporting Information

### Supporting Information File 1

Experimental details for gene expression and enzyme incubation experiments, NMR spectra of (1*R*,3*E*,7*E*,11*S*,12*S*)-18-hydroxydolabella-3,7-diene, and heterologous expression in *Nicotiana benthamiana*. [<http://www.beilstein-journals.org/bjoc/content/supplementary/1860-5397-13-171-S1.pdf>]

## Acknowledgements

This work was funded by the DFG (DI1536/7-1) and by the Fonds der Chemischen Industrie.

## References

- Croteau, R.; Felton, N. M.; Wheeler, C. J. *J. Biol. Chem.* **1985**, *260*, 5956–5962.
- Cane, D. E.; Swanson, S.; Murthy, P. P. N. *J. Am. Chem. Soc.* **1981**, *103*, 2136–2138. doi:10.1021/ja00398a063
- Cane, D. E.; Pargellis, C. *Arch. Biochem. Biophys.* **1987**, *254*, 421–429. doi:10.1016/0003-9861(87)90120-2
- Rabe, P.; Rinkel, J.; Nubbemeyer, B.; Köllner, T. G.; Chen, F.; Dickschat, J. S. *Angew. Chem., Int. Ed.* **2016**, *55*, 15420–15423. doi:10.1002/anie.201608971
- Chen, X.; Köllner, T. G.; Jia, Q.; Norris, A.; Santhanam, B.; Rabe, P.; Dickschat, J. S.; Shaulsky, G.; Gershenzon, J.; Chen, F. *Proc. Natl. Acad. Sci. U. S. A.* **2016**, *113*, 12132–12137. doi:10.1073/pnas.1610379113
- Dickschat, J. S. *Nat. Prod. Rep.* **2016**, *33*, 87–110. doi:10.1039/C5NP00102A
- Rabe, P.; Rinkel, J.; Klapschinski, T. A.; Barra, L.; Dickschat, J. S. *Org. Biomol. Chem.* **2016**, *14*, 158–164. doi:10.1039/C5OB01998B
- Schiffrin, A.; Khatri, Y.; Kirsch, P.; Thiel, V.; Schulz, S.; Bernhardt, R. *Org. Biomol. Chem.* **2016**, *14*, 3385–3393. doi:10.1039/C6OB00130K
- Klapschinski, T. A.; Rabe, P.; Dickschat, J. S. *Angew. Chem., Int. Ed.* **2016**, *55*, 10141–10144. doi:10.1002/anie.201605425
- Rabe, P.; Schmitz, T.; Dickschat, J. S. *Beilstein J. Org. Chem.* **2016**, *12*, 1839–1850. doi:10.3762/bjoc.12.173
- Rinkel, J.; Rabe, P.; Garbeva, P.; Dickschat, J. S. *Angew. Chem., Int. Ed.* **2016**, *55*, 13593–13596. doi:10.1002/anie.201608042
- Rabe, P.; Rinkel, J.; Dolja, E.; Schmitz, T.; Nubbemeyer, B.; Luu, T. H.; Dickschat, J. S. *Angew. Chem., Int. Ed.* **2017**, *56*, 2776–2779. doi:10.1002/anie.201612439
- Rabe, P.; Samborsky, M.; Leadlay, P. F.; Dickschat, J. S. *Org. Biomol. Chem.* **2017**, *15*, 2353–2358. doi:10.1039/C7OB00234C
- Rinkel, J.; Rabe, P.; Chen, X.; Köllner, T. G.; Chen, F.; Dickschat, J. S. *Chem. – Eur. J.* **2017**, *23*, 10501–10505. doi:10.1002/chem.201702704
- Yamada, Y.; Kuzuyama, T.; Komatsu, M.; Shin-ya, K.; Omura, S.; Cane, D. E.; Ikeda, H. *Proc. Natl. Acad. Sci. U. S. A.* **2015**, *112*, 857–862. doi:10.1073/pnas.1422108112
- Yamada, Y.; Arima, S.; Nagamitsu, T.; Johmoto, K.; Uekusa, H.; Eguchi, T.; Shin-ya, K.; Cane, D. E.; Ikeda, H. *J. Antibiot.* **2015**, *68*, 385–394. doi:10.1038/ja.2014.171
- Rabe, P.; Dickschat, J. S. *Angew. Chem., Int. Ed.* **2013**, *52*, 1810–1812. doi:10.1002/anie.201209103
- Dickschat, J. S.; Pahirulzaman, K. A. K.; Rabe, P.; Klapschinski, T. A. *ChemBioChem* **2014**, *15*, 810–814. doi:10.1002/cbic.201300763
- de Kraker, J.-W.; Franssen, M. C. R.; de Groot, A.; König, W. A.; Bouwmeester, H. *J. Plant Physiol.* **1998**, *117*, 1381–1392. doi:10.1104/pp.117.4.1381
- Cane, D. E.; Oliver, J. S.; Harrison, P. H. M.; Abell, C.; Hubbard, B. R.; Kane, C. T.; Lattman, R. *J. Am. Chem. Soc.* **1990**, *112*, 4513–4524. doi:10.1021/ja00167a059
- Cane, D. E.; Prabhakaran, P. C.; Salaski, E. J.; Harrison, P. H. M.; Noguchi, H.; Rawlings, B. J. *J. Am. Chem. Soc.* **1989**, *111*, 8914–8916. doi:10.1021/ja00206a022
- Wang, C.-M.; Hopson, R.; Lin, X.; Cane, D. E. *J. Am. Chem. Soc.* **2009**, *131*, 8360–8361. doi:10.1021/ja9021649
- Cornforth, J. W.; Cornforth, R. H.; Donninger, C.; Popjak, G. *Proc. R. Soc. London, Ser. B* **1966**, *163*, 492–514. doi:10.1098/rspb.1966.0004
- Thulasiram, H. V.; Poulter, C. D. *J. Am. Chem. Soc.* **2006**, *128*, 15819–15823. doi:10.1021/ja065573b
- Rabe, P.; Barra, L.; Rinkel, J.; Riclea, R.; Citron, C. A.; Klapschinski, T. A.; Janusko, A.; Dickschat, J. S. *Angew. Chem., Int. Ed.* **2015**, *54*, 13448–13451. doi:10.1002/anie.201507615
- Liu, Q.; Majdi, M.; Cankar, K.; Goedbloed, M.; Charnikhova, T.; Verstappen, F. W. A.; de Vos, R. C. H.; Beekwilder, J.; van der Krol, S.; Bouwmeester, H. *J. PLoS One* **2011**, *6*, e23255. doi:10.1371/journal.pone.0023255
- Okada, K.; Saito, T.; Nakagawa, T.; Kawamukai, M.; Kamiya, Y. *Plant Physiol.* **2000**, *122*, 1045–1056. doi:10.1104/pp.122.4.1045

28. Voinnet, O.; Rivas, S.; Mestre, P.; Baulcombe, D. *Plant J.* **2003**, *33*, 949–956. doi:10.1046/j.1365-313X.2003.01676.x
29. Ioannou, E.; Quesada, A.; Rahman, M. M.; Gibbons, S.; Vagias, C.; Roussis, V. *J. Nat. Prod.* **2011**, *74*, 213–222. doi:10.1021/np1006586
30. Amico, V.; Currenti, R.; Oriente, G.; Piattelli, M.; Tringali, C. *Phytochemistry* **1981**, *20*, 848–849. doi:10.1016/0031-9422(81)85196-5
31. Cai, X.-H.; Luo, X.-D.; Zhou, J.; Hao, X.-J. *Helv. Chim. Acta* **2005**, *88*, 2938–2943. doi:10.1002/hlca.200590236
32. Kappers, I. F.; Aharoni, A.; van Herpen, T. W. J. M.; Luckerhoff, L. L. P.; Dicke, M.; Bouwmeester, H. J. *Science* **2005**, *309*, 2070–2072. doi:10.1126/science.1116232
33. Frick, S.; Nagel, R.; Schmidt, A.; Bodemann, R. R.; Rahfeld, P.; Pauls, G.; Brandt, W.; Gershenzon, J.; Boland, W.; Burse, A. *Proc. Natl. Acad. Sci. U. S. A.* **2013**, *110*, 4194–4199. doi:10.1073/pnas.1221489110
34. Ginglinger, J. F.; Boachon, B.; Höfer, R.; Paetz, C.; Köllner, T. G.; Miesch, L.; Lugan, R.; Baltenweck, R.; Mutterer, J.; Ullmann, P.; Beran, F.; Claudel, P.; Verstappen, F.; Fischer, M. J. C.; Karst, F.; Bouwmeester, H.; Miesch, M.; Schneider, B.; Gershenzon, J.; Ehling, J.; Werck-Reichhart, D. *Plant Cell* **2013**, *25*, 4640–4657. doi:10.1105/tpc.113.117382
35. Fischer, M. J. C.; Meyer, S.; Claudel, P.; Perrin, M.; Ginglinger, J. F.; Gertz, C.; Masson, J. E.; Werck-Reinhardt, D.; Huguency, P.; Karst, F. *J. Biotechnol.* **2013**, *163*, 24–29. doi:10.1016/j.jbiotec.2012.10.012
36. Kemper, K.; Hirte, M.; Reinbold, M.; Fuchs, M.; Brück, T. *Beilstein J. Org. Chem.* **2017**, *13*, 845–854. doi:10.3762/bjoc.13.85
37. Citron, C. A.; Gleitzmann, J.; Laurenzano, G.; Pukall, R.; Dickschat, J. S. *ChemBioChem* **2012**, *13*, 202–214. doi:10.1002/cbic.201100641

## License and Terms

This is an Open Access article under the terms of the Creative Commons Attribution License (<http://creativecommons.org/licenses/by/4.0>), which permits unrestricted use, distribution, and reproduction in any medium, provided the original work is properly cited.

The license is subject to the *Beilstein Journal of Organic Chemistry* terms and conditions: (<http://www.beilstein-journals.org/bjoc>)

The definitive version of this article is the electronic one which can be found at:  
[doi:10.3762/bjoc.13.171](https://doi.org/10.3762/bjoc.13.171)



# Appendix I

## **Spata-13,17-diene Synthase—An Enzyme with Sesqui-, Di-, and Sesterterpene Synthase Activity from *Streptomyces xinghaiensis***

*Angew. Chem. Int. Ed.* **2017**, *56*, 16385–16389.

DOI:10.1002/anie.201711142

&

*Angew. Chem.* **2017**, *129*, 16603–16607.

DOI:10.1002/ange.201711142





## Enzyme Mechanisms

International Edition: DOI: 10.1002/anie.201711142

German Edition: DOI: 10.1002/ange.201711142

Spata-13,17-diene Synthase—An Enzyme with Sesqui-, Di-, and Sesterterpene Synthase Activity from *Streptomyces xinghaiensis*

Jan Rinkel, Lukas Lauterbach, and Jeroen S. Dickschat\*

Dedicated to Professor Stefan Schulz on the occasion of his 60th birthday

**Abstract:** A terpene synthase from the marine bacterium *Streptomyces xinghaiensis* has been characterised, including a full structure elucidation of its products from various substrates and an in-depth investigation of the enzyme mechanism by isotope labelling experiments, metal cofactor variations, and mutation experiments. The results revealed an interesting dependency of  $Mn^{2+}$  catalysis on the presence of Asp-217, a residue that is occupied by a highly conserved Glu in most other bacterial terpene synthases.

In terms of their structural variability, complexity, and distribution, terpenes constitute one of the most successful classes of natural products. They are synthesised from geranyl (GPP), farnesyl (FPP), geranylgeranyl (GGPP), and geranyl-farnesyl diphosphate (GFPP), as well as even larger isoprenoid oligomers by terpene synthases (TSs) that usually generate a polycyclic carbon framework with multiple stereogenic centres in just one enzymatic step. Although multiproduct TSs such as MtTPS5 from *Medicago truncatula* are known,<sup>[1]</sup> many enzymes selectively produce a single compound with astonishing accuracy. This precision is particularly remarkable because the action of a TS on a substrate seems to be limited to its ionisation, either by abstraction of diphosphate (type I enzymes) or by protonation (type II). Moreover, the TS provides a shaped and essentially water-free cavity to arrange the substrate in a reactive conformation. The reaction cascade that proceeds via cationic intermediates thus makes use of the inherent substrate reactivity.<sup>[2]</sup> Although several type I mono- and sesquiterpene synthases (STSs) have been reported from bacteria,<sup>[3]</sup> the only characterised diterpene synthases (DTSs) of this class for which the intriguing product structures and enzyme mechanisms have been thoroughly studied are the enzymes for cyclooctat-9-en-7-ol, spiroviolene, tsukubadiene, and 18-hydroxydolabella-3,7-diene, as well as the multiproduct DTS for hydrophyrene.<sup>[4]</sup> Here we present the characterisation of a TS from *Streptomyces xinghaiensis*, a marine actinomycete that has been isolated from sediments near Dalian, China.<sup>[5]</sup> This TS shows

a broad substrate spectrum and an interesting metal cofactor dependency.

The gene for an unknown TS from *S. xinghaiensis* S187 (accession no. WP\_095757924) was cloned into the expression vector pYE-Express<sup>[6]</sup> by homologous recombination in yeast and expressed in *Escherichia coli*. The predicted gene product exhibited all the highly conserved motifs for a functional type I TS,<sup>[7]</sup> including the aspartate-rich motif (<sup>74</sup>DDQLD), the pyrophosphate (PP) sensor Arg-173, the NSE triad (<sup>119</sup>NDWYSLGKE), and the <sup>307</sup>RY dimer (Figure S1 in the Supporting Information). The closest characterised homologue of this enzyme is the (+)-*epi*-cubenol synthase from *Streptomyces griseus* NBRC 13350 which has 51 % identical amino acid residues.<sup>[8]</sup> The protein was purified (Figure S2) and incubated with GPP, FPP, GGPP, and GFPP. Of these substrates, GPP was not accepted, whereas GGPP and GFPP were converted efficiently into a di- or sesterterpene hydrocarbon, respectively, accompanied by a few side products (Figure 1). The diterpene hydrocarbons **1** and **2** were also detected in headspace extracts from *S. xinghaiensis* (Figure S3).

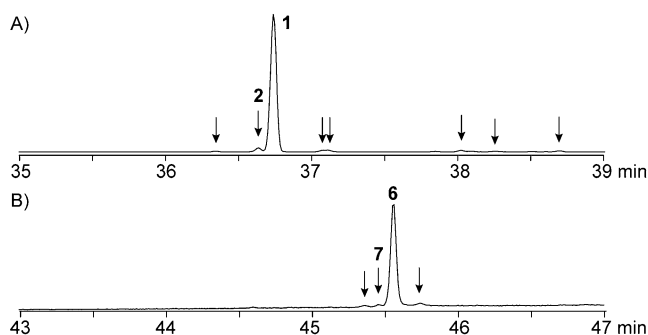
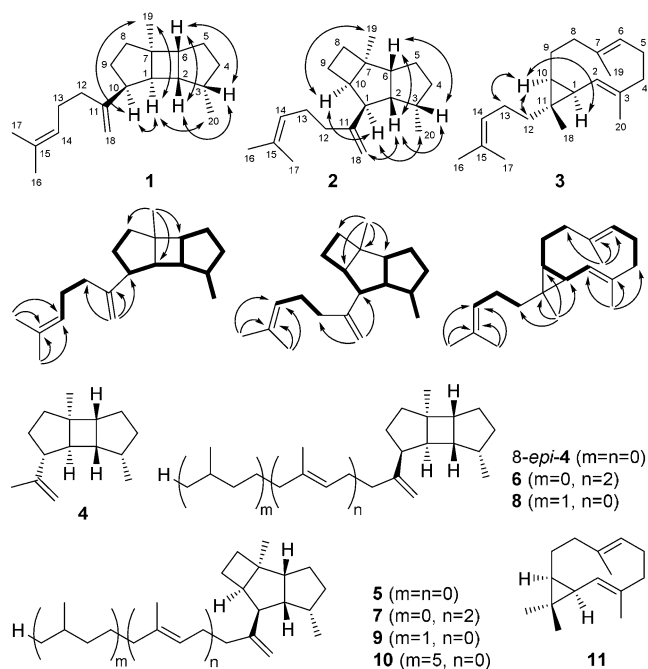


**Figure 1.** Total ion chromatograms of products obtained from an incubation of A) GGPP and B) GFPP with SpS. Arrows point to minor enzyme products, the numbers at peaks refer to the compound numbers in Scheme 1.

The main diterpene **1** was isolated by column chromatography (6 mg of pure product, 14 %) and its structure was elucidated by NMR spectroscopy to be spata-13,17-diene (Table S2, Figures S4–S10; the most relevant 2D NMR correlations are highlighted in Scheme 1), thus establishing the TS from *S. xinghaiensis* as spata-13,17-diene synthase (SpS). Two minor products could also be isolated and were identified by NMR spectroscopy as prenylkelsoene (**2**; 0.6 mg, 1 %) and the known compound cneorubin Y<sup>[9]</sup> (**3**;

[\*] J. Rinkel, L. Lauterbach, Prof. Dr. J. S. Dickschat  
Kekulé-Institute of Organic Chemistry and Biochemistry  
University of Bonn  
Gerhard-Domagk-Strasse 1, 53121 Bonn (Germany)  
E-mail: dickschat@uni-bonn.de

Supporting information and the ORCID identification number(s) for the author(s) of this article can be found under:  
<https://doi.org/10.1002/anie.201711142>.



**Scheme 1.** Products of SpS and structures of related natural products. Single-headed arrows indicate HMBC, double-headed arrows indicate NOESY correlations, and bold lines show contiguous spin systems in the  $^1\text{H}, ^1\text{H}$ -COSY spectrum. The carbon atom numbering for 1–3 follows the GGPP numbering to indicate the biosynthetic origin of each carbon atom. This numbering is different to previously introduced numbering systems (see comment on page 1 of the Supporting Information).

0.8 mg, 2%; Tables S3 and S4, Figures S11–S23). The latter compound is not detectable by GC/MS, likely because it contains a Cope system that results in thermal instability, as described for germacrene.<sup>[10]</sup> The diterpenes **1** and **2** are new natural products.

GFPP was also accepted by SpS and resulted in the formation of a main product and a few side products. The main product (0.9 mg, 1%) was identified by NMR spectroscopy (Table S5, Figures S25–S31) and GC/MS (Figure S32) as the higher homologue of **1**, namely prenylspata-13,17-diene (**6**). The homologue of **2**, geranylkelsoene (**7**), was also tentatively identified by GC/MS on the basis of the characteristic loss of ethylene from the cyclobutane portion (Figure S33). The sesterterpenes **6** and **7** are new natural products, and SpS is the first bacterial TS reported to have sesterterpene synthase activity.

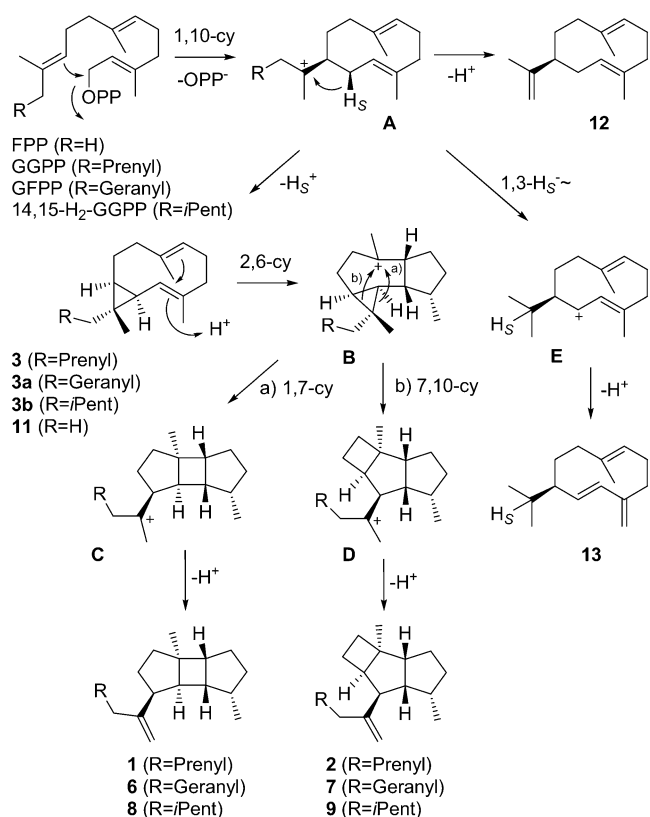
The corresponding sesquiterpene to **3** is the widespread compound bicyclogermacrene (**11**). Notably, FPP was also accepted by SpS and converted into a mixture of **11**, germacrene A (**12**), and germacrene D (**13**), which were partially detected as their Cope rearrangement products by GC/MS (Figure S34, Table S6). Compound **12** was also isolated and characterised by NMR spectroscopy, with data identical to those previously reported.<sup>[11]</sup>

Poduran (**10**) is a tetraterpenoid with the same tricyclic core as in **2** as well as a saturated side chain that was reported in the springtail *Podura aquatica*.<sup>[12]</sup> The broad substrate specificity of SpS suggested that a similar enzyme may be

responsible for the biosynthesis of **10**. This prompted us to investigate whether 14,15-dihydro-GGPP can also be converted. For this purpose, 10,11-dihydro-FPP was synthesised (Scheme S1), elongated with IPP by the GGPP synthase (GGPPS) from *Streptomyces cyaneofuscatus*,<sup>[4b]</sup> and converted by SpS. This yielded 1.8 mg (5%) of spat-13-ene (**8**; Table S7, Figures S32 and S35–S41). A minor product was tentatively identified from its mass spectrum as isopentylkelsoene (**9**), which showed a loss of 28 Da from the molecular ion (Figure S33), as reported for **10**.<sup>[12]</sup>

The biosynthesis of **1** and **2** can be rationalised by 1,10-cyclisation of **1**, followed by deprotonation with formation of a cyclopropane ring to give **3** (Scheme 2). This neutral intermediate can be reprotonated at C-3 for a second cyclisation to **B**. This cation can react by two alternative ring openings of the cyclopropane, either by pathway a to give **C**, which is the precursor of **1**, or by pathway b to give **D**, the direct precursor of **2**. Starting from GFPP or 14,15-dihydro-GGPP, essentially the same reactions can explain the formation of **6/7** and **8/9**, respectively, via the hypothetical intermediates **3a** and **3b**. In contrast, the enzymatic conversion of FPP stopped at **11** and did not proceed to tricyclic analogues of **1** and **2**, but produced major amounts of **12** by an alternative deprotonation of **A**, and **13** by a 1,3-hydride migration and deprotonation.

The proposed biosynthetic pathway of Scheme 2 was investigated by incubation of all 20 isotopomers of ( $^{13}\text{C}_1$ )GGPP, obtained by chemical synthesis or enzymatically from the corresponding labelled FPP or IPP isotopomers



**Scheme 2.** Biosynthetic mechanism for SpS. Cy=cyclisation.

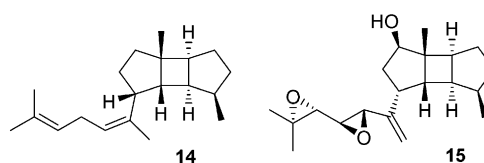
using *S. cyaneofuscatu*s GGPPS,<sup>[4b,13]</sup> which resulted in incorporation of the label at the expected positions of **1–3** in all cases (Figures S42–S44). In particular, these results demonstrate the formation of **1** by ring closure to form the cyclopropane in **3** and reverse ring opening with rearrangement of the carbon backbone.

The sesquiterpene prespatane (bourbon-11-ene, **4**) has been reported from the sponge *Cymbastella hooperi*<sup>[14]</sup> as well as from several liverworts<sup>[15]</sup> and actinobacteria.<sup>[16]</sup> In all these organisms, **4** co-occurs with kelsoene (tritomenene, **5**), but the different relative orientation of the isopropenyl group seems to exclude a simple biosynthetic mechanism via the common intermediate **11**, as we found for the pairs **1 + 2** and **6 + 7**. A comparison of the <sup>13</sup>C NMR data of **1** and **2** with those reported for **4** and **5**<sup>[14]</sup> suggests that the structure of **4** needs correction to 8-*epi*-**4**, which also better fits into the biosynthesis scheme (Figure S45). The structural revision of prespatane was recently also independently described by Weng and co-workers.<sup>[17]</sup> In this report a biosynthesis of 8-*epi*-**4** via germacrene A, B, or C was suggested, but the intermediacy of the larger homologue **3** of bicyclogermacrene (**11**) can better explain the common formation of the two products **1** and **2**.

The reprotonation of **3** at C-3 for the second cyclisation to **B** (Scheme 2) was investigated by incubation of (3-<sup>13</sup>C)IPP<sup>[4b]</sup> and FPP with GGPPS and SpS in D<sub>2</sub>O. The obtained product (3-<sup>13</sup>C,3-<sup>2</sup>H)-**1** showed a triplet in the <sup>13</sup>C NMR spectrum, in agreement with reprotonation at C-3 (Figure S46). The stereochemical course of the deprotonation from **A** to **3** was investigated by enzymatic conversion of (*S*)- and (*R*)-(1-<sup>13</sup>C,1-<sup>2</sup>H)GGPP<sup>[18]</sup> with SpS. Labelled **1** obtained from (*S*)-(1-<sup>13</sup>C,1-<sup>2</sup>H)GGPP showed a singlet in the <sup>13</sup>C NMR spectrum, while (*R*)-(1-<sup>13</sup>C,1-<sup>2</sup>H)GGPP gave a product exhibiting a triplet as a consequence of <sup>13</sup>C-<sup>2</sup>H spin coupling, thus establishing the loss of the *pro-S* and retention of the *pro-R* hydrogen atoms from C-1 in the cyclisation to form **3**. This was also supported by GC/MS analysis (Figure S47). Analogous results were obtained for **6** with (*S*)- and (*R*)-(1-<sup>13</sup>C,1-<sup>2</sup>H)GFPP<sup>[13b]</sup> (Figure S48) and for **11** with (*S*)- and (*R*)-(1-<sup>2</sup>H)FPP (Figure S49). In the case of **13**, a stereospecific shift of the *pro-S* hydrogen atom into the isopropyl group was observed by GC/MS (Figure S50). Assuming inversion of the configuration at C-1 for the initial 1,10-cyclisation step to **A**, as reported for other terpene cyclisations,<sup>[19]</sup> these data are in favour of the absolute configurations of the products of SpS as shown in Scheme 2. In particular, the stereochemical course of the 1,3-hydride shift from C-1 of FPP into the isopropyl group, as for **13**, was shown to be indicative of the absolute configuration of sesquiterpenes.<sup>[20]</sup>

The absolute configuration of **12** was independently established from the optical rotation of the isolated compound ( $[\alpha]_{\text{D}}^{20} = -7.2$ ,  $c = 0.5$ , CCl<sub>4</sub>) through comparison with different literature data for **12** ( $[\alpha]_{\text{D}}^{25} = -3.2$ ,  $c = 14.4$ , CCl<sub>4</sub>;  $[\alpha]_{\text{D}}^{25} = -26.8$ ,  $c = 1.0$ , CCl<sub>4</sub>) and its enantiomer ( $[\alpha]_{\text{D}}^{25} = +42.1$ ,  $c = 1.0$ , CCl<sub>4</sub>).<sup>[10b,21]</sup> Compound **12** was also converted into its Cope rearrangement product  $\beta$ -elemene in refluxing toluene to yield a material with  $[\alpha]_{\text{D}}^{20} = +17.9$  ( $c = 0.06$ , CHCl<sub>3</sub>), consistent with the earlier reported conversion of (+)-**12** into (–)- $\beta$ -elemene ( $[\alpha]_{\text{D}}^{25} = -15.8$  ( $c = 0.50$ , CHCl<sub>3</sub>)).<sup>[10b]</sup> The absolute configurations of **1–3** were investigated by elonga-

tion of the stereoselectively deuterated (*R*)- and (*S*)-(1-<sup>13</sup>C,1-<sup>2</sup>H)GPP and (*R*)- and (*S*)-(1-<sup>13</sup>C,1-<sup>2</sup>H)FPP<sup>[4b]</sup> to the corresponding GGPPs using *S. cyaneofuscatu*s GGPPS (Figures S51–S56). This reaction is known to proceed with inversion of the configuration at C-1 of GPP and FPP.<sup>[22]</sup> The obtained stereoselectively deuterated GGPP isotopologues were converted into **1–3** by SpS. The installed stereochemical anchors with known absolute configurations allowed the absolute configurations at the other stereocentres to be deduced simply by solving the relative configurations of the obtained stereoselectively deuterated products. The additional <sup>13</sup>C label was introduced to allow efficient and sensitive product analysis by HSQC. The deduced absolute configurations of **1–3** are in line with their biosynthetic relationship. The absolute configuration of **1** corresponds to that of prespatane (8-*epi*-**4**) from the alga *Laurencia pacifica*.<sup>[17]</sup> The same absolute configuration as found here for **3** can be assigned to **3** from *Cneorum tricoccon* on the basis of the same sign of their optical rotations (found here:  $[\alpha]_{\text{D}}^{20} = -31$ ,  $c = 0.05$ , acetone, reported:  $[\alpha]_{\text{D}}^{20} = -49.1$ , 0.3%, acetone).<sup>[9]</sup> The absolute configuration of **2** ( $[\alpha]_{\text{D}}^{20} = +20$  ( $c = 0.05$ , C<sub>6</sub>D<sub>6</sub>)) is the same as that reported for natural (+)-kelsoene, which was established by synthesis of its enantiomer.<sup>[23]</sup> The main product **1** of SpS is structurally related to a series of spatanes, including (13*Z*)-spata-13(15),17-diene (**14**) and spatol (**15**, Scheme 3), known from different brown algae.<sup>[24]</sup> These compounds exhibit the opposite absolute configuration as determined for **1**.



Scheme 3. Known spatanes from brown algae.

Several TSs have been investigated by site-directed mutagenesis, including the fungal trichodiene synthase and the bacterial TSs for pentalenene, *epi*-isozizaene, (2*Z*,6*E*)-hedycaryol, and selina-4(15),7(11)-diene (Tables S8–S12).<sup>[7a,25]</sup> This work underpinned the importance of highly conserved motifs such as the Asp-rich motif,<sup>[7,25c,f]</sup> the NSE triad,<sup>[7a]</sup> the RY dimer,<sup>[7b,25a,b]</sup> and the PP sensor<sup>[7b]</sup> for catalysis. A detailed analysis of 51 characterised bacterial type I TSs,<sup>[3]</sup> their close relatives with presumably the same function from sequenced bacteria, and SpS by sequence alignment resulted in the identification of four highly conserved amino acid residues, whose importance for catalysis have not been shown so far. These include P83 and L90, located 21 and 14 positions upstream, respectively, of the Asp-rich motif, and E184 and E217 that are placed 19 positions upstream and 14 positions downstream, respectively, of the PP sensor (Table S13, SpS numbering, the usually found E217 is altered to D217 in native SpS). P83A exchange resulted in a poor yield of a soluble enzyme and a complete loss of activity (Figures S57 and S58). The L90A variant also showed a lower expression level and significantly reduced activity (3%) compared to native SpS. The crystal structure of

selinadiene synthase from *Streptomyces pristinaespiralis*<sup>[7b]</sup> shows that its corresponding residues (P61 and V68) have an important structural role at the link between two  $\alpha$ -helices (Figure S59). Their exchange in SpS may result in an incorrect enzyme folding, thereby causing poor activity and a low yield of the enzyme. The efficiently expressed E184Q variant of SpS was nearly inactive (0.5%). The structure of selinadiene synthase shows that the corresponding E159 is involved in Mg<sup>2+</sup> binding (Figure S60), which may be critical for activity. Exchange of D217 to the usual Glu (D217E) resulted in an increased expression and catalytic efficiency (170%). A comparison with the structure of selinadiene synthase reveals that the corresponding E192 in helix G is part of a salt bridge to R144 in helix F (Figures S60 and S61). In SpS, D217 can substitute for this function, but the D217E variation seems to fit better to the structural requirements of a type I TS.

Catalysis by type I TSs requires a trinuclear cluster of divalent cations (usually Mg<sup>2+</sup> or Mn<sup>2+</sup>) that binds to the Asp-rich motif, the NSE/DTE triad, and the PP of the substrate to initiate its ionisation.<sup>[26]</sup> Other divalent cations have sometimes been reported to be ineffective for catalysis,<sup>[27]</sup> but most of the recently described enzymes have not been systematically investigated for their metal-ion dependency. Incubation experiments with SpS and various cations (Mg<sup>2+</sup>, Ca<sup>2+</sup>, Mn<sup>2+</sup>, Fe<sup>2+</sup>, Co<sup>2+</sup>, Ni<sup>2+</sup>, Cu<sup>2+</sup>, Zn<sup>2+</sup>) resulted in efficient catalysis by Mg<sup>2+</sup> and—with rates about threefold higher—by Mn<sup>2+</sup> (Figure S62), while no product was obtained with all other cations. Interestingly, incubation of the highly productive D217E variant with Mn<sup>2+</sup> gave no diterpene product from GGPP, possibly because this mutation causes a conformational rearrangement in helices F and G that disturbs the active-site residues involved in the binding of metal cofactors. A BLAST search and phylogenetic analysis (Figure S63) revealed the presence of two closely related homologues of SpS in *Streptomyces albus* NRRL F-4971 (WP\_030543144, 89% identity) and in *Streptomyces fradiae* ATCC 19609 (WP\_050363727, 96%). Both enzymes also exhibit an aspartate residue in the position corresponding to Asp-217 of SpS. Future experiments will address whether the requirement of a metal cofactor also for other bacterial TSs can be tuned by mutation of this highly conserved Asp.

## Acknowledgements

This work was funded by the DFG (DI1536/7-1) and by the Fonds der Chemischen Industrie. We thank Seocho Kim for skillful assistance in the synthesis of 10,11-dihydro-FPP.

## Conflict of interest

The authors declare no conflict of interest.

**Keywords:** biosynthesis · enzyme mechanisms · isotopes · metal cofactors · terpenes

**How to cite:** *Angew. Chem. Int. Ed.* **2017**, *56*, 16385–16389  
*Angew. Chem.* **2017**, *129*, 16603–16607

- [1] S. Garms, T. G. Köllner, W. Boland, *J. Org. Chem.* **2010**, *75*, 5590.
- [2] D. J. Tantillo, *Angew. Chem. Int. Ed.* **2017**, *56*, 10040; *Angew. Chem.* **2017**, *129*, 10172.
- [3] J. S. Dickschat, *Nat. Prod. Rep.* **2016**, *33*, 87.
- [4] a) A. Meguro, Y. Motoyoshi, K. Teramoto, S. Ueda, Y. Totsuka, Y. Ando, T. Tomita, S.-Y. Kim, T. Kimura, M. Igarashi, R. Sawa, T. Shinada, M. Nishiyama, T. Kuzuyama, *Angew. Chem. Int. Ed.* **2015**, *54*, 4353; *Angew. Chem.* **2015**, *127*, 4427; b) P. Rabe, J. Rinkel, E. Dolja, T. Schmitz, B. Nubbemeyer, T. H. Luu, J. S. Dickschat, *Angew. Chem. Int. Ed.* **2017**, *56*, 2776; *Angew. Chem.* **2017**, *129*, 2820; c) J. S. Dickschat, J. Rinkel, P. Rabe, A. Beyraghdar Kashkooli, H. J. Bouwmeester, *Beilstein J. Org. Chem.* **2017**, *13*, 1770; d) Y. Yamada, T. Kuzuyama, M. Komatsu, K. Shin-ya, S. Omura, D. E. Cane, H. Ikeda, *Proc. Natl. Acad. Sci. USA* **2015**, *112*, 857.
- [5] X. Q. Zhao, W. J. Li, W. C. Jiao, Y. Li, W. J. Yuan, Y. Q. Zhang, H. P. Klenk, J. W. Suh, F. W. Bai, *Int. J. Syst. Evol. Microbiol.* **2009**, *59*, 2870.
- [6] J. S. Dickschat, K. A. K. Pahirulzaman, P. Rabe, T. A. Klapschinski, *ChemBioChem* **2014**, *15*, 810.
- [7] a) M. Seemann, G. Zhai, J.-W. de Kraker, C. M. Paschall, D. W. Christianson, D. E. Cane, *J. Am. Chem. Soc.* **2002**, *124*, 7681; b) P. Baer, P. Rabe, K. Fischer, C. A. Citron, T. A. Klapschinski, M. Groll, J. S. Dickschat, *Angew. Chem. Int. Ed.* **2014**, *53*, 7652; *Angew. Chem.* **2014**, *126*, 7783.
- [8] C. Nakano, T. Tezuka, S. Horinouchi, Y. Ohnishi, *J. Antibiot.* **2012**, *65*, 551.
- [9] D. Trautmann, B. Epe, U. Oelbermann, A. Mondon, *Chem. Ber.* **1980**, *113*, 3848.
- [10] a) J. de Kraker, M. C. R. Franssen, A. de Groot, T. Shibata, H. J. Bouwmeester, *Phytochemistry* **2001**, *58*, 481; b) J. A. Faraldos, S. Wu, J. Chappell, R. M. Coates, *Tetrahedron* **2007**, *63*, 7733; c) P. Rabe, L. Barra, J. Rinkel, R. Riclea, C. A. Citron, T. A. Klapschinski, A. Janusko, J. S. Dickschat, *Angew. Chem. Int. Ed.* **2015**, *54*, 13448; *Angew. Chem.* **2015**, *127*, 13649.
- [11] A. M. Adio, C. Paul, H. Tesso, P. Kloth, W. A. König, *Tetrahedron: Asymmetry* **2004**, *15*, 1631.
- [12] S. Schulz, C. Messer, K. Dettner, *Tetrahedron Lett.* **1997**, *38*, 2077.
- [13] T. Mitsuhashi, J. Rinkel, M. Okada, I. Abe, J. S. Dickschat, *Chem. Eur. J.* **2017**, *23*, 10053.
- [14] G. M. König, A. D. Wright, *J. Org. Chem.* **1997**, *62*, 3837.
- [15] a) K. Nabeta, K. Yamamoto, M. Hashimoto, H. Koshino, K. Funatsuki, K. Katoh, *Chem. Commun.* **1998**, 1485; b) U. Warmers, K. Wihstutz, N. Bülow, C. Fricke, W. A. König, *Phytochemistry* **1998**, *49*, 1723; c) U. Warmers, W. A. König, *Phytochemistry* **1999**, *52*, 1519; d) S. H. von Reuß, C.-L. Wu, H. Muhle, W. A. König, *Phytochemistry* **2004**, *65*, 2277.
- [16] C. A. Citron, J. Gleitzmann, G. Laurenzano, R. Pukall, J. S. Dickschat, *ChemBioChem* **2012**, *13*, 202.
- [17] R. D. Kersten, S. Lee, D. Fujita, T. Pluskal, S. Kram, J. E. Smith, T. Iwai, J. P. Noel, M. Fujita, J.-K. Weng, *J. Am. Chem. Soc.* **2017**, DOI: <https://doi.org/10.1021/jacs.7b09452>.
- [18] J. Rinkel, P. Rabe, X. Chen, T. G. Köllner, F. Chen, J. S. Dickschat, *Chem. Eur. J.* **2017**, *23*, 10501.
- [19] a) C.-M. Wang, R. Hopson, X. Lin, D. E. Cane, *J. Am. Chem. Soc.* **2009**, *131*, 8360; b) D. E. Cane, J. S. Oliver, P. H. M. Harrison, C. Abell, B. R. Hubbard, C. T. Kane, R. Lattman, *J. Am. Chem. Soc.* **1990**, *112*, 4513; c) D. E. Cane, P. C. Prabhakaran, E. J. Salaski, P. H. M. Harrison, H. Noguchi, B. J. Rawlings, *J. Am. Chem. Soc.* **1989**, *111*, 8914; d) P. Rabe, M. Samborsky, P. F. Leadlay, J. S. Dickschat, *Org. Biomol. Chem.* **2017**, *15*, 2353.
- [20] J. Rinkel, P. Rabe, P. Garbeva, J. S. Dickschat, *Angew. Chem. Int. Ed.* **2016**, *55*, 13593; *Angew. Chem.* **2016**, *128*, 13791.

- [21] a) A. J. Weinheimer, W. W. Youngblood, P. H. Washecheck, T. K. B. Karns, L. S. Ciereszko, *Tetrahedron Lett.* **1970**, *11*, 497; b) C. Nishino, W. S. Bowers, M. E. Montgomery, L. R. Nault, M. W. Nielson, *J. Chem. Ecol.* **1977**, *3*, 349.
- [22] H. V. Thulasiram, C. D. Poulter, *J. Am. Chem. Soc.* **2006**, *128*, 15819.
- [23] S. Fietz-Razavian, S. Schulz, I. Dix, P. G. Jones, *Chem. Commun.* **2001**, 2154.
- [24] a) B. N. Ravi, R. J. Wells, *Aust. J. Chem.* **1982**, *35*, 129; b) W. H. Gerwick, W. Fenical, D. van Engen, J. Clardy, *J. Am. Chem. Soc.* **1980**, *102*, 7993.
- [25] a) D. E. Cane, J. H. Shim, Q. Xue, B. C. Fitzsimons, T. M. Hohn, *Biochemistry* **1995**, *34*, 2480; b) D. E. Cane, Q. Xue, *J. Am. Chem. Soc.* **1996**, *118*, 1563; c) D. Cane, Q. Xue, B. Fitzsimons, *Biochemistry* **1996**, *35*, 12369; d) M. Seemann, G. Zhai, K. Umezawa, D. Cane, *J. Am. Chem. Soc.* **1999**, *121*, 591; e) J. A. Aaron, X. Lin, D. E. Cane, D. W. Christianson, *Biochemistry* **2010**, *49*, 1787; f) P. Baer, P. Rabe, C. A. Citron, C. C. de Oliveira Mann, N. Kaufmann, M. Groll, J. S. Dickschat, *ChemBioChem* **2014**, *15*, 213.
- [26] D. W. Christianson, *Chem. Rev.* **2017**, *117*, 11570.
- [27] a) A. J. Poulse, R. Croteau, *Arch. Biochem. Biophys.* **1978**, *191*, 400; b) R. Croteau, F. Karp, *Arch. Biochem. Biophys.* **1979**, *198*, 512; c) J. I. M. Rajaonarivony, J. Gershenzon, R. Croteau, *Arch. Biochem. Biophys.* **1992**, *296*, 49; d) D. E. Cane, J.-K. Sohng, C. R. Lamberson, S. M. Rudnicki, Z. Wu, M. D. Lloyd, J. S. Oliver, B. R. Hubbard, *Biochemistry* **1994**, *33*, 5846.

Manuscript received: October 30, 2017

Accepted manuscript online: November 10, 2017

Version of record online: November 23, 2017



## Enzymmechanismen

Deutsche Ausgabe: DOI: 10.1002/ange.201711142  
Internationale Ausgabe: DOI: 10.1002/anie.201711142Spata-13,17-dien-Synthase – ein Enzym mit Sesqui-, Di- und Sesterterpen-Synthase-Aktivität aus *Streptomyces xinghaiensis*

Jan Rinkel, Lukas Lauterbach und Jeroen S. Dickschat\*

Professor Stefan Schulz zum 60. Geburtstag gewidmet

**Abstract:** Eine Terpensynthase aus dem marinen Bakterium *Streptomyces xinghaiensis* wurde charakterisiert, einschließlich einer vollen Strukturaufklärung ihrer Produkte aus verschiedenen Substraten. Weiterhin wurden detaillierte Untersuchungen des Enzymmechanismus durch Isotopenmarkierungsexperimente, Variationen des Metallcofaktors und Mutageneseexperimente durchgeführt. Die Daten zeigten eine Abhängigkeit der  $Mn^{2+}$ -katalysierten Reaktion von der Gegenwart von Asp-217, einem Rest, der in anderen bakteriellen Terpensynthasen von einem hochkonservierten Glu eingenommen wird.

Terpene sind in Bezug auf ihre Strukturvariabilität, Komplexität und Verbreitung eine der erfolgreichsten Naturstoffklassen. Sie werden aus den Vorstufen Geranyl- (GPP), Farnesyl- (FPP), Geranylgeranyl- (GGPP) und Geranylgeranylgeranyl- (GGPP) sowie noch längeren isoprenoiden Oligomeren durch Terpensynthasen (TSs) synthetisiert, die meist ein polycyclisches Kohlenstoffgerüst mit vielen Stereozentren in einem einzigen enzymatischen Schritt aufbauen. Während manche TSs wie MtTPS5 aus *Medicago truncatula* mehrere Produkte bilden,<sup>[1]</sup> produzieren viele Enzyme selektiv und mit erstaunlicher Genauigkeit nur eine einzige Verbindung. Diese Präzision ist besonders bemerkenswert, weil die Aktivität einer TS für ein Substrat auf dessen Ionisierung entweder durch Abstraktion des Diphosphats (Enzyme des Typs I) oder durch Protonierung (Typ II) beschränkt zu sein scheint. Darüber hinaus bieten sie eine vorgeformte und im wesentlichen wasserfreie Kavität, in der das Substrat eine reaktive Konformation einnimmt. Die Reaktionskaskade über kationische Intermediate macht dann von der inhärenten Reaktivität des Substrates Gebrauch.<sup>[2]</sup> Während viele Mono- und Sesquiterpensynthasen (STs) des Typs I (STs) aus Bakterien beschrieben worden sind,<sup>[3]</sup> sind die einzigen charakterisierten Diterpensynthasen (DTs) dieser Klasse, für die die faszinierenden Strukturen der Produkte sowie die Enzymmechanismen umfangreich untersucht wurden, die Enzyme für Cyclooctat-9-en-7-ol, Spiroviolen, Tsukubadien und 18-Hydroxydolabella-3,7-dien sowie die Hydropyren-Synthase, die mehrere Produkte generiert.<sup>[4]</sup>

Hier berichten wir über die Charakterisierung einer TS aus *Streptomyces xinghaiensis*, einem marinen Actinomyceten, der aus Sedimenten in der Nähe von Dalian (China) isoliert worden ist.<sup>[5]</sup> Die TS zeigt ein breites Substratspektrum und eine Abhängigkeit vom Metallcofaktor.

Das Gen für eine unbekannte TS aus *S. xinghaiensis* S187 (Zugangscode WP\_095757924) wurde durch homologe Rekombination in Hefe in den Expressionsvektor pYE-Express<sup>[6]</sup> kloniert und in *Escherichia coli* exprimiert. Das vorhergesagte Translationsprodukt wies alle hochkonservierten Motive für eine funktionale TS des Typs I auf,<sup>[7]</sup> inklusive des Aspartat-reichen Motivs (<sup>74</sup>DDQLD), des Pyrophosphat-(PP)-Sensors Arg-173, der NSE-Triade (<sup>119</sup>NDWYSLGKE) und des <sup>307</sup>RY-Dimers (Abbildung S1 der Hintergrundinformationen). Das am nächsten verwandte, charakterisierte Homologe dieses Enzyms ist die (+)-*epi*-Cubebol-Synthase aus *Streptomyces griseus* NBRC 13350 mit 51 % identischen Aminosäureresten.<sup>[8]</sup> Das Protein wurde gereinigt (Abbildung S2) und mit GPP, FPP, GGPP sowie GFPP inkubiert. Von diesen Substraten wurde GPP nicht akzeptiert, während GGPP und GFPP effizient in einen Di- bzw. Sesterterpen-Kohlenwasserstoff umgesetzt wurden, der jeweils durch wenige Nebenprodukte begleitet wurde (Abbildung 1). Die Diterpen-Kohlenwasserstoffe **1** und **2** wurden außerdem in Duftstoffextrakten von *S. xinghaiensis* detektiert (Abbildung S3).

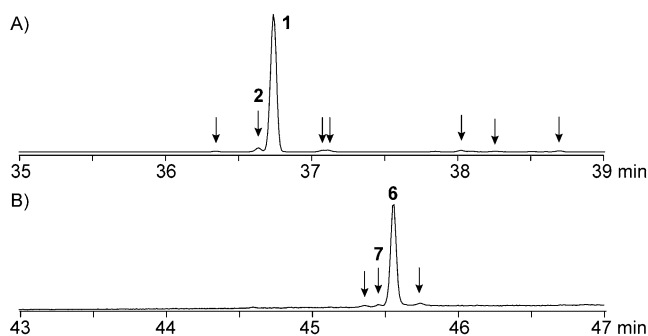
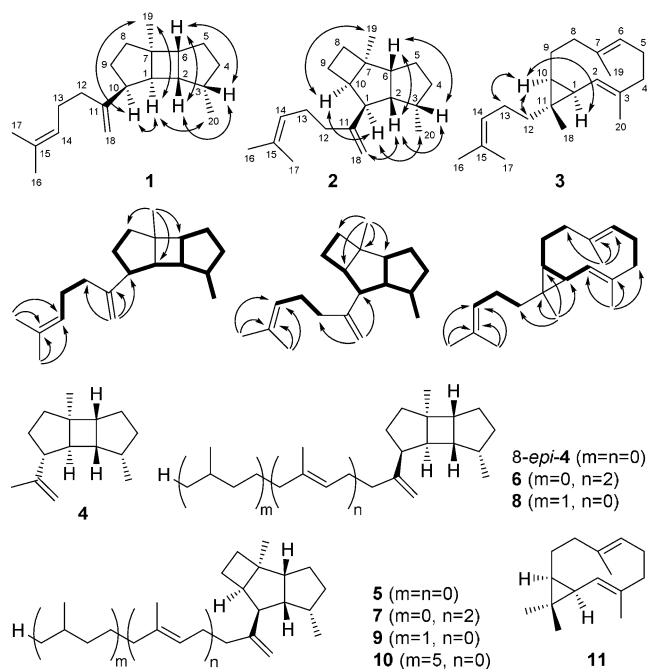


**Abbildung 1.** Totalionenstromchromatogramm der Produkte aus einer Inkubation von A) GGPP und B) GFPP mit SpS. Pfeile weisen auf Nebenprodukte der Enzymreaktion, Zahlen an Peaks auf Verbindungsnummern wie in Schema 1.

Das Diterpen **1** wurde durch Säulenchromatographie isoliert (6 mg erhaltenes Produkt, 14 %), und seine Struktur wurde durch NMR-Spektroskopie als Spata-13,17-dien bestimmt (Tabelle S2, Abbildungen S4–S10; die wichtigsten 2D-NMR-Korrelationen sind in Schema 1 gezeigt), wodurch die

[\*] J. Rinkel, L. Lauterbach, Prof. Dr. J. S. Dickschat  
Kekulé-Institut für Organische Chemie und Biochemie  
Universität Bonn  
Gerhard-Domagk-Straße 1, 53121 Bonn (Deutschland)  
E-Mail: dickschat@uni-bonn.de

Hintergrundinformationen und die Identifikationsnummer (ORCID) eines Autors sind unter:  
<https://doi.org/10.1002/ange.201711142> zu finden.



**Scheme 1.** Produkte von SpS und Strukturen verwandter Naturstoffe. Einfache Pfeile verweisen auf HMBC-, Doppelpfeile auf NOESY-Korrelationen, fette Linien zeigen zusammenhängende Spinsysteme im  $^1\text{H}$ ,  $^1\text{H}$ -COSY-Spektrum an. Die Kohlenstoff-Nummerierungen für **1–3** folgen der GGPP-Nummerierung, um den biosynthetischen Ursprung für jedes Kohlenstoffatom aufzuzeigen. Diese Nummerierung unterscheidet sich von früher eingeführten Systemen (siehe Kommentar auf Seite 1 der Hintergrundinformationen).

TS aus *S. xinghaiensis* als Spata-13,17-dien-Synthase (SpS) identifiziert wurde. Auch zwei Nebenprodukte konnten isoliert und per NMR-Spektroskopie als Prenylkelsoen (**2**; 0.6 mg, 1%) und die bekannte Verbindung Cneorubin Y<sup>[9]</sup> (**3**; 0.8 mg, 2%) identifiziert werden (Tabellen S3 und S4, Abbildungen S11–S23). Letztgenannte Verbindung konnte nicht per GC/MS detektiert werden, vermutlich weil sie ein Cope-System enthält, aus dem eine thermische Instabilität resultiert, wie sie für Germacrene beschrieben wurde.<sup>[10]</sup> Die Diterpene **1** und **2** sind neue Naturstoffe.

GFPP wurde ebenfalls von der SpS akzeptiert und in ein Haupt- und mehrere Nebenprodukte umgesetzt. Das Hauptprodukt (0.9 mg, 1%) wurde per NMR-Spektroskopie (Tabelle S5, Abbildungen S25–S31) und GC/MS (Abbildung S32) als das höhere Homologe von **1**, Prenylspata-13,17-dien (**6**), identifiziert. Das Homologe von **2**, Geranylkelsoen (**7**), konnte ebenfalls vorläufig per GC/MS auf Basis des charakteristischen Verlustes von Ethylen aus der Cyclobutaneinheit identifiziert werden (Abbildung S33). Die Sesterterpene **6** und **7** sind neue Naturstoffe, und SpS ist die erste bakterielle TS, für die Sesterterpensynthase-Aktivität berichtet wurde.

Das entsprechende Sesquiterpen zu **3** ist die weit verbreitete Verbindung Bicyclogermacren (**11**). Bemerkenswerterweise wurde auch FPP von der SpS akzeptiert und in eine Mischung von **11**, Germacren A (**12**) und Germacren D (**13**) umgesetzt, die zum Teil in Form ihrer Cope-Umlagerungsprodukte per GC/MS detektiert wurden (Abbildung S34,

Tabelle S6). Verbindung **12** wurde isoliert und NMR-spektroskopisch charakterisiert, was übereinstimmende Daten mit früher berichteten ergab.<sup>[11]</sup>

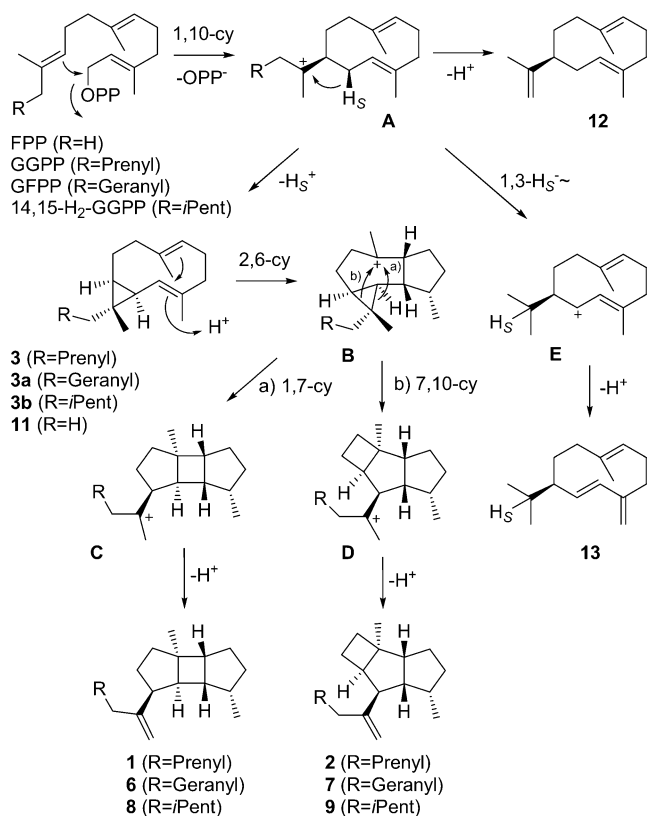
Poduran (**10**) ist ein Tetraterpenoid mit derselben tricyclischen Kernstruktur wie in **2** und einer gesättigten Seitenkette, das aus dem Springschwanz *Podura aquatica* bekannt ist.<sup>[12]</sup> Die breite Substratspezifität von SpS ließ vermuten, dass ein ähnliches Enzym für die Biosynthese von **10** verantwortlich sein könnte. Dies veranlasste uns zu untersuchen, ob 14,15-Dihydro-GGPP umgesetzt werden kann. Zu diesem Zweck wurde 10,11-Dihydro-FPP synthetisiert (Schema S1), mit IPP durch die GGPP-Synthase (GGPPS) aus *Streptomyces cyaneofuscatus* verlängert<sup>[4b]</sup> und durch die SpS umgesetzt, wodurch 1.8 mg (5%) von Spat-13-en (**8**) erhalten wurden (Tabelle S7, Abbildungen S32 und S35–S41). Ein Nebenprodukt wurde vorläufig als Isopentylkelsoen (**9**) identifiziert; Grundlage hierfür war das Massenspektrum, das eine Abspaltung von 28 Da vom Molecularion zeigte (Abbildung S33), wie sie auch für **10** berichtet wurde.<sup>[12]</sup>

Die Biosynthese von **1** und **2** startet mit einer 1,10-Cyclisierung zu **A**, gefolgt von einer Deprotonierung unter Bildung des Cyclopropanrings in **3**. Dieses neutrale Intermediat kann an C-3 für eine zweite Cyclisierung zu **B** reprotoniert werden. Dieses Kation kann in zwei alternativen Ringöffnungen des Cyclopropanrings weiterreagieren, entweder über Weg a zu **C** als Vorstufe für **1** oder über Weg b zu **D**, der direkten Vorstufe von **2**. Ausgehend von GFPP oder 14,15-Dihydro-GGPP können entsprechende Reaktionen die Bildung von **6/7** und **8/9** über die hypothetischen Intermediate **3a** und **3b** erklären. Im Unterschied dazu stoppt die enzymatische Umsetzung von FPP bei **11** und läuft nicht weiter zu den tricyclischen Analoga von **1** und **2**, es werden aber größere Mengen an **12** durch alternative Deprotonierung von **A** und **13** durch 1,3-Hydridwanderung und Deprotonierung gebildet.

Die in Schema 2 vorgeschlagene Biosynthese wurde durch Inkubation aller zwanzig Isotomere von ( $^{13}\text{C}_1$ )GGPP getestet, die durch chemische Synthese oder enzymatisch aus den entsprechenden markierten Isotomeren von FPP oder IPP mit der GGPPS aus *S. cyaneofuscatus* hergestellt wurden.<sup>[4b,10,13]</sup> Diese Experimente resultierten in allen Fällen im Einbau der Markierung in den erwarteten Positionen von **1–3** (Abbildungen S42–S44). Insbesondere demonstrieren diese Ergebnisse die Bildung von **1** durch Schließen des Cyclopropanrings zu **3** und reverse Ringöffnung mit Umlagerung des Kohlenstoffgerüsts.

Das Sesquiterpen Prespatan (Bourbon-11-en, **4**) wurde aus dem Schwamm *Cymbastella hooperi*<sup>[14]</sup> und aus diversen Lebermoosen<sup>[15]</sup> und Actinobakterien berichtet.<sup>[16]</sup> In all diesen Organismen wird **4** von Kelsoen (Tritomaren, **5**) begleitet, aber die unterschiedliche relative Orientierung der Isopropenylgruppe scheint einen einfachen Biosynthesemechanismus über das gemeinsame Intermediat **11**, den wir für die Paare **1+2** und **6+7** gefunden haben, auszuschließen. Ein Vergleich der  $^{13}\text{C}$ -NMR-Daten von **1** und **2** zu den für **4** und **5** berichteten<sup>[14]</sup> spricht dafür, dass die Struktur von **4** zu der von 8-*epi*-**4** korrigiert werden muss, die überdies besser in das Biosyntheschema passt (Abbildung S45). Die Strukturrevision für Prespatan wurde jüngst auch unabhängig von Weng und Mitarbeitern beschrieben.<sup>[17]</sup> In diesem Bericht





**Schema 2.** Biosynthetischer Mechanismus für SpS. cy = Cyclisierung.

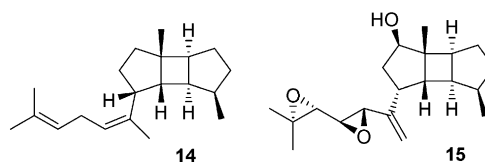
wird eine Biosynthese für 8-*epi*-4 über Germacren A, B oder C diskutiert, aber das größere Homologe **3** von Bicyclogermacren (**11**) kann als Intermediat die gleichzeitige Bildung der Produkte **1** und **2** besser erklären.

Die Reprotonierung von **3** an C-3 für die zweite Cyclisierung zu **B** (Schema 2) wurde durch Inkubation von (3-<sup>13</sup>C)IPP<sup>[4b]</sup> und FPP mit GGPPS und SpS in D<sub>2</sub>O studiert. Das erhaltene Produkt (3-<sup>13</sup>C,3-<sup>2</sup>H)-**1** zeigt ein Triplett im <sup>13</sup>C-NMR-Spektrum, wie es für die Reprotonierung an C-3 erwartet wird (Abbildung S46). Der stereochemische Verlauf der Deprotonierung von **A** zu **3** wurde durch enzymatische Umsetzung von (*S*)- und (*R*)-(1-<sup>13</sup>C,1-<sup>2</sup>H)GGPP<sup>[18]</sup> mit SpS untersucht. Markiertes **1**, das aus (*S*)-(1-<sup>13</sup>C,1-<sup>2</sup>H)GGPP erhalten wurde, zeigte ein Singulett im <sup>13</sup>C-NMR-Spektrum, während (*R*)-(1-<sup>13</sup>C,1-<sup>2</sup>H)GGPP ein Produkt ergab, das wegen der <sup>13</sup>C-<sup>2</sup>H-Spinnkopplung ein Triplett aufwies, wodurch der Verlust des *pro-S*- und die Erhaltung des *pro-R*-Wasserstoffatoms an C-1 in der Cyclisierung zu **3** aufgezeigt wurden. Dieser Befund wurde auch durch GC/MS-Analyse gestützt (Abbildung S47). Analoge Ergebnisse wurden für **6** mit (*S*)- und (*R*)-(1-<sup>13</sup>C,1-<sup>2</sup>H)GFPP<sup>[13]</sup> (Abbildung S48) und für **11** mit (*S*)- und (*R*)-(1-<sup>2</sup>H)FPP erhalten (Abbildung S49). Für **13** wurde per GC/MS eine stereospezifische Verschiebung des *pro-S*-Wasserstoffatoms in die Isopropylgruppe beobachtet (Abbildung S50). Nimmt man Inversion der Konfiguration an C-1 für die initiale 1,10-Cyclisierung zu **A** an, die für andere Terpencyclisierungen gefunden wurde,<sup>[19]</sup> sprechen diese Daten für eine absolute Konfiguration der Produkte von SpS, wie in Schema 2 gezeigt. Für Sesquiterpene konnte gezeigt

werden, dass der stereochemische Verlauf der 1,3-Hydridverschiebung von C-1 des FPP in die Isopropylgruppe (wie hier für **13** nachvollzogen) für ihre absoluten Konfigurationen diagnostisch ist.<sup>[20]</sup>

Die absolute Konfiguration von **12** wurde unabhängig durch Isolierung der Verbindung, Bestimmung des Drehwertes ( $[\alpha]_D^{20} = -7.2$ ,  $c = 0.5$ , CCl<sub>4</sub>) und Vergleich mit verschiedenen Literaturwerten für **12** ( $[\alpha]_D^{25} = -3.2$ ,  $c = 14.4$ , CCl<sub>4</sub>;  $[\alpha]_D^{25} = -26.8$ ,  $c = 1.0$ , CCl<sub>4</sub>) und sein Enantiomer ( $[\alpha]_D^{25} = +42.1$ ,  $c = 1.0$ , CCl<sub>4</sub>) ermittelt.<sup>[10b,21]</sup> Verbindung **12** wurde in siedendem Toluol auch in das Cope-Umlagerungsprodukt β-Element umgewandelt, was ein Material mit  $[\alpha]_D^{20} = +17.9$  ( $c = 0.06$ , CHCl<sub>3</sub>) ergab. Dies ist in Einklang mit der früher berichteten Umwandlung von (+)-**12** zu (–)-β-Element ( $[\alpha]_D^{25} = -15.8$  ( $c = 0.50$ , CHCl<sub>3</sub>)).<sup>[10b]</sup> Die absoluten Konfigurationen von **1–3** wurden durch Umsetzung von stereoselektiv deuteriertem (*R*)- und (*S*)-(1-<sup>13</sup>C,1-<sup>2</sup>H)GPP und (*R*)- und (*S*)-(1-<sup>13</sup>C,1-<sup>2</sup>H)FPP<sup>[4b]</sup> die mit der GGPPS aus *S. cyaneofuscatus* zu den entsprechenden GGPPs verlängert wurden, ermittelt (Abbildungen S51–S56). Diese Verlängerung läuft bekanntermaßen unter Inversion der Konfiguration an C-1 von GPP und FPP ab.<sup>[22]</sup> Die erhaltenen, stereoselektiv deuterierten Isotopologe von GGPP wurden mit SpS zu **1–3** umgesetzt. Die installierten stereochemischen Anker mit bekannten absoluten Konfigurationen ermöglichten es, die absoluten Konfigurationen der übrigen Stereozentren in den deuterierten Produkten durch Klärung der relativen Konfigurationen zu bestimmen. Die zusätzliche <sup>13</sup>C-Markierung wurde für eine effiziente und empfindliche Produktanalyse per HSQC eingeführt. Die abgeleiteten absoluten Konfigurationen für **1–3** sind im Einklang mit ihrer biosynthetischen Verwandtschaft. Die absolute Konfiguration von **1** entspricht außerdem derjenigen von Prespatan (8-*epi*-4) aus der Alge *Laurencia pacifica*.<sup>[17]</sup> Dieselbe absolute Konfiguration, wie hier für **3** gefunden, kann auch für **3** aus *Cneorum tricoccon* angenommen werden, da ihre Drehwerte dasselbe Vorzeichen aufweisen (hier:  $[\alpha]_D^{20} = -31$ ,  $c = 0.05$ , Aceton, berichtet:  $[\alpha]_D^{20} = -49.1$ , 0.3%, Aceton).<sup>[9]</sup> Die absolute Konfiguration von **2** ( $[\alpha]_D^{20} = +20$  ( $c = 0.05$ , C<sub>6</sub>D<sub>6</sub>)) ist dieselbe wie für natürliches (+)-Kelsoen, die durch Synthese des Enantiomers zugeordnet wurde.<sup>[23]</sup> Das Hauptprodukt **1** von SpS ist strukturell mit einer Reihe von Spatanen verwandt, die aus Braunalgen bekannt sind, z. B. (13*Z*)-Spata-13(15),17-dien (**14**) und Spatol (**15**; Schema 3).<sup>[24]</sup> Diese Verbindungen weisen die entgegengesetzte absolute Konfiguration zu der für **1** bestimmten auf.

Diverse TSs sind durch ortsgerechte Mutagenese studiert worden, unter anderem die pilzliche Trichodien-Synthase und die bakteriellen TSs für Pentalenen, *epi*-Isozaen, (2*Z*,6*E*)-Hedycaryol und Selina-4(15),7(11)-dien (Tabelle S8–S12).<sup>[7a,25]</sup> Diese Arbeit unterstrich die Bedeutung der



**Schema 3.** Bekannte Spatane aus Braunalgen.

hochkonservierten Motive wie des Asp-reichen Motivs,<sup>[7,25c,f]</sup> der NSE-Triade,<sup>[7a]</sup> des RY-Dimers<sup>[7b,25a,b]</sup> und des PP-Sensors<sup>[7b]</sup> für katalytische Aktivität. Eine detaillierte Analyse von 51 charakterisierten bakteriellen TSs des Typs I,<sup>[3]</sup> ihrer nächsten Verwandten mit angenommener gleicher Funktion aus sequenzierten Bakterien und SpS durch Sequenzalignment führte zur Identifizierung von vier hochkonservierten Aminosäureresten, deren Rolle für die katalytische Aktivität bisher nicht aufgeklärt wurde. Dazu gehören P83 und L90, die 21 bzw. 14 Positionen vor dem Asp-reichen Motiv lokalisiert sind, sowie E184 und E217, die 19 Positionen vor bzw. 14 nach dem PP-Sensor lokalisiert sind (Tabelle S13, SpS-Nummerierung; der üblicherweise gefundene Rest E217 ist in natürlicher SpS zu D217 verändert). Der Austausch P83A ergab schlechte Ausbeuten an löslichem Enzym und einen kompletten Verlust der katalytischen Aktivität (Abbildungen S57 und S58). Auch die L90A-Variante zeigte eine geringere Expression und signifikant reduzierte Aktivität (3%) gegenüber natürlicher SpS. Die Kristallstruktur der Selinadien-Synthese aus *Streptomyces pristinaespiralis*<sup>[7b]</sup> offenbart, dass die entsprechenden Reste (P61 und V68) eine wichtige strukturgebende Rolle an der Verbindungsstelle zweier  $\alpha$ -Helices spielen (Abbildung S59). Ihr Austausch in SpS resultiert möglicherweise in einer inkorrekten Enzymfaltung, die eine geringe Aktivität und Ausbeute an Enzym bedingt. Die effizient exprimierte E184Q-Variante von SpS war nahezu inaktiv (0.5%). Die Struktur der Selinadien-Synthese zeigt, dass das entsprechende E159 an der Bindung von  $Mg^{2+}$  beteiligt ist (Abbildung S60), was für die Aktivität entscheidend sein mag. Austausch von D217 zu dem üblichen Glu (D217E) ergab eine erhöhte Expression und katalytische Aktivität (170%). Ein Vergleich mit der Struktur der Selinadien-Synthese zeigt, dass der entsprechende Rest E192 in Helix G eine Salzbrücke zu R144 in Helix F bildet (Abbildungen S60 und S61). In SpS kann D217 diese Funktion übernehmen, aber die D217E-Variante scheint die strukturellen Erfordernisse einer TS des Typs I besser zu erfüllen.

Katalyse durch TSs des Typs I erfordert einen dreikernigen Cluster zweiwertiger Kationen (meist  $Mg^{2+}$  oder  $Mn^{2+}$ ), der an das Asp-reiche Motiv, die NSE/DTE-Triade und das PP des Substrates zum Zwecke seiner Ionisierung bindet.<sup>[26]</sup> Andere zweiwertige Kationen erwiesen sich oft als ineffizient,<sup>[27]</sup> aber die meisten jüngst beschriebenen Enzyme wurden in dieser Hinsicht nicht systematisch untersucht. Inkubationsexperimente mit SpS und verschiedenen Kationen ( $Mg^{2+}$ ,  $Ca^{2+}$ ,  $Mn^{2+}$ ,  $Fe^{2+}$ ,  $Co^{2+}$ ,  $Ni^{2+}$ ,  $Cu^{2+}$ ,  $Zn^{2+}$ ) ergaben effiziente Katalyse durch  $Mg^{2+}$  und – mit ca. dreifach erhöhter Rate – durch  $Mn^{2+}$  (Abbildung S62), während alle anderen Kationen kein Produkt lieferten. Interessanterweise ergab die Inkubation der hochproduktiven D217E-Variante mit  $Mn^{2+}$  kein Diterpen aus GGPP, möglicherweise weil diese Mutation eine Konformationsänderung in den Helices F und G hervorruft, welche die an der Bindung des Metallcofaktors beteiligten Reste stört. Eine BLAST-Suche und phylogenetische Analyse (Abbildung S63) verwies auf die Präsenz von zwei nahe verwandten Homologen der SpS in *Streptomyces albus* NRRL F-4971 (WP\_030543144, 89% Identität) und in *Streptomyces fradiae* ATCC 19609 (WP\_050363727, 96%). Beide Enzyme haben ebenfalls einen Asp-Rest in der Asp-

217 von SpS entsprechenden Position. Zukünftige Experimente werden sich der Frage widmen, ob die Erfordernisse an den Metallcofaktor auch für andere bakterielle TSs durch Mutation dieses hochkonservierten Asp moduliert werden können.

### Danksagung

Diese Arbeit wurde von der DFG (DI1536/7-1) und dem FCI gefördert. Wir danken Seocho Kim für kundige Assistenz bei der Synthese von 10,11-Dihydro-FPP.

### Interessenkonflikt

Die Autoren erklären, dass keine Interessenkonflikte vorliegen.

**Stichwörter:** Biosynthese · Enzymmechanismen · Isotope · Metallcofaktoren · Terpene

**Zitierweise:** *Angew. Chem. Int. Ed.* **2017**, *56*, 16385–16389  
*Angew. Chem.* **2017**, *129*, 16603–16607

- [1] S. Garms, T. G. Köllner, W. Boland, *J. Org. Chem.* **2010**, *75*, 5590.
- [2] D. J. Tantillo, *Angew. Chem. Int. Ed.* **2017**, *56*, 10040; *Angew. Chem.* **2017**, *129*, 10172.
- [3] J. S. Dickschat, *Nat. Prod. Rep.* **2016**, *33*, 87.
- [4] a) A. Meguro, Y. Motoyoshi, K. Teramoto, S. Ueda, Y. Totsuka, Y. Ando, T. Tomita, S.-Y. Kim, T. Kimura, M. Igarashi, R. Sawa, T. Shinada, M. Nishiyama, T. Kuzuyama, *Angew. Chem. Int. Ed.* **2015**, *54*, 4353; *Angew. Chem.* **2015**, *127*, 4427; b) P. Rabe, J. Rinkel, E. Dolja, T. Schmitz, B. Nubbemeyer, T. H. Luu, J. S. Dickschat, *Angew. Chem. Int. Ed.* **2017**, *56*, 2776; *Angew. Chem.* **2017**, *129*, 2820; c) J. S. Dickschat, J. Rinkel, P. Rabe, A. Beyraghdar Kashkooli, H. J. Bouwmeester, *Beilstein J. Org. Chem.* **2017**, *13*, 1770; d) Y. Yamada, T. Kuzuyama, M. Komatsu, K. Shin-ya, S. Omura, D. E. Cane, H. Ikeda, *Proc. Natl. Acad. Sci. USA* **2015**, *112*, 857.
- [5] X. Q. Zhao, W. J. Li, W. C. Jiao, Y. Li, W. J. Yuan, Y. Q. Zhang, H. P. Klenk, J. W. Suh, F. W. Bai, *Int. J. Syst. Evol. Microbiol.* **2009**, *59*, 2870.
- [6] J. S. Dickschat, K. A. K. Pahirulzaman, P. Rabe, T. A. Klapschinski, *ChemBioChem* **2014**, *15*, 810.
- [7] a) M. Seemann, G. Zhai, J.-W. de Kraker, C. M. Paschall, D. W. Christianson, D. E. Cane, *J. Am. Chem. Soc.* **2002**, *124*, 7681; b) P. Baer, P. Rabe, K. Fischer, C. A. Citron, T. A. Klapschinski, M. Groll, J. S. Dickschat, *Angew. Chem. Int. Ed.* **2014**, *53*, 7652; *Angew. Chem.* **2014**, *126*, 7783.
- [8] C. Nakano, T. Tezuka, S. Horinouchi, Y. Ohnishi, *J. Antibiot.* **2012**, *65*, 551.
- [9] D. Trautmann, B. Epe, U. Oelbermann, A. Mondon, *Chem. Ber.* **1980**, *113*, 3848.
- [10] a) J. de Kraker, M. C. R. Franssen, A. de Groot, T. Shibata, H. J. Bouwmeester, *Phytochemistry* **2001**, *58*, 481; b) J. A. Faraldos, S. Wu, J. Chappell, R. M. Coates, *Tetrahedron* **2007**, *63*, 7733; c) P. Rabe, L. Barra, J. Rinkel, R. Riclea, C. A. Citron, T. A. Klapschinski, A. Janusko, J. S. Dickschat, *Angew. Chem. Int. Ed.* **2015**, *54*, 13448; *Angew. Chem.* **2015**, *127*, 13649.
- [11] A. M. Adio, C. Paul, H. Tesso, P. Kloth, W. A. König, *Tetrahedron: Asymmetry* **2004**, *15*, 1631.
- [12] S. Schulz, C. Messer, K. Dettner, *Tetrahedron Lett.* **1997**, *38*, 2077.

- [13] T. Mitsuhashi, J. Rinkel, M. Okada, I. Abe, J. S. Dickschat, *Chem. Eur. J.* **2017**, *23*, 10053.
- [14] G. M. König, A. D. Wright, *J. Org. Chem.* **1997**, *62*, 3837.
- [15] a) K. Nabeta, K. Yamamoto, M. Hashimoto, H. Koshino, K. Funatsuki, K. Katoh, *Chem. Commun.* **1998**, 1485; b) U. Warmers, K. Wihstutz, N. Bülow, C. Fricke, W. A. König, *Phytochemistry* **1998**, *49*, 1723; c) U. Warmers, W. A. König, *Phytochemistry* **1999**, *52*, 1519; d) S. H. von Reuß, C.-L. Wu, H. Muhle, W. A. König, *Phytochemistry* **2004**, *65*, 2277.
- [16] C. A. Citron, J. Gleitzmann, G. Laurenzano, R. Pukall, J. S. Dickschat, *ChemBioChem* **2012**, *13*, 202.
- [17] R. D. Kersten, S. Lee, D. Fujita, T. Pluskal, S. Kram, J. E. Smith, T. Iwai, J. P. Noel, M. Fujita, J.-K. Weng, *J. Am. Chem. Soc.* **2017**, DOI: <https://doi.org/10.1021/jacs.7b09452>.
- [18] J. Rinkel, P. Rabe, X. Chen, T. G. Köllner, F. Chen, J. S. Dickschat, *Chem. Eur. J.* **2017**, *23*, 10501.
- [19] a) C.-M. Wang, R. Hopson, X. Lin, D. E. Cane, *J. Am. Chem. Soc.* **2009**, *131*, 8360; b) D. E. Cane, J. S. Oliver, P. H. M. Harrison, C. Abell, B. R. Hubbard, C. T. Kane, R. Lattman, *J. Am. Chem. Soc.* **1990**, *112*, 4513; c) D. E. Cane, P. C. Prabhakaran, E. J. Salaski, P. H. M. Harrison, H. Noguchi, B. J. Rawlings, *J. Am. Chem. Soc.* **1989**, *111*, 8914; d) P. Rabe, M. Samborsky, P. F. Leadlay, J. S. Dickschat, *Org. Biomol. Chem.* **2017**, *15*, 2353.
- [20] J. Rinkel, P. Rabe, P. Garbeva, J. S. Dickschat, *Angew. Chem. Int. Ed.* **2016**, *55*, 13593; *Angew. Chem.* **2016**, *128*, 13791.
- [21] a) A. J. Weinheimer, W. W. Youngblood, P. H. Washecheck, T. K. B. Karns, L. S. Ciereszko, *Tetrahedron Lett.* **1970**, *11*, 497; b) C. Nishino, W. S. Bowers, M. E. Montgomery, L. R. Nault, M. W. Nielson, *J. Chem. Ecol.* **1977**, *3*, 349.
- [22] H. V. Thulasiram, C. D. Poulter, *J. Am. Chem. Soc.* **2006**, *128*, 15819.
- [23] S. Fietz-Razavian, S. Schulz, I. Dix, P. G. Jones, *Chem. Commun.* **2001**, *50*, 2154.
- [24] a) B. N. Ravi, R. J. Wells, *Aust. J. Chem.* **1982**, *35*, 129; b) W. H. Gerwick, W. Fenical, D. van Engen, J. Clardy, *J. Am. Chem. Soc.* **1980**, *102*, 7993.
- [25] a) D. E. Cane, J. H. Shim, Q. Xue, B. C. Fitzsimons, T. M. Hohn, *Biochemistry* **1995**, *34*, 2480; b) D. E. Cane, Q. Xue, *J. Am. Chem. Soc.* **1996**, *118*, 1563; c) D. Cane, Q. Xue, B. Fitzsimons, *Biochemistry* **1996**, *35*, 12369; d) M. Seemann, G. Zhai, K. Umegawa, D. Cane, *J. Am. Chem. Soc.* **1999**, *121*, 591; e) J. A. Aaron, X. Lin, D. E. Cane, D. W. Christianson, *Biochemistry* **2010**, *49*, 1787; f) P. Baer, P. Rabe, C. A. Citron, C. C. de Oliveira Mann, N. Kaufmann, M. Groll, J. S. Dickschat, *ChemBioChem* **2014**, *15*, 213.
- [26] D. W. Christianson, *Chem. Rev.* **2017**, *117*, 11570.
- [27] a) A. J. Poulou, R. Croteau, *Arch. Biochem. Biophys.* **1978**, *191*, 400; b) R. Croteau, F. Karp, *Arch. Biochem. Biophys.* **1979**, *198*, 512; c) J. I. M. Rajaonarivony, J. Gershenson, R. Croteau, *Arch. Biochem. Biophys.* **1992**, *296*, 49; d) D. E. Cane, J.-K. Sohng, C. R. Lamberson, S. M. Rudnicki, Z. Wu, M. D. Lloyd, J. S. Oliver, B. R. Hubbard, *Biochemistry* **1994**, *33*, 5846.

Manuskript erhalten: 30. Oktober 2017

Akzeptierte Fassung online: 10. November 2017

Endgültige Fassung online: 23. November 2017



## Appendix J

### Two Diterpene Synthases for Spiroalbatene and Cembrene A from *Allokutzneria albata*

*Angew. Chem. Int. Ed.* **2018**, *57*, 3238–3241.

DOI:10.1002/anie.201800385

&

*Angew. Chem.* **2018**, *130*, 3292–3296.

DOI:10.1002/ange.201800385



## Enzyme Mechanisms

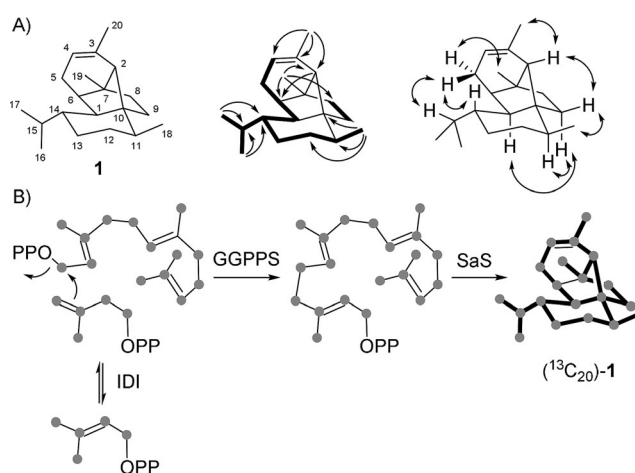
International Edition: DOI: 10.1002/anie.201800385  
German Edition: DOI: 10.1002/ange.201800385Two Diterpene Synthases for Spiroalbatene and Cembrene A from *Allokutzneria albata*

Jan Rinkel, Lukas Lauterbach, Patrick Rabe, and Jeroen S. Dickschat\*

**Abstract:** Two bacterial diterpene synthases from the actinomycete *Allokutzneria albata* were investigated, resulting in the identification of the structurally unprecedented compound spiroalbatene from the first and cembrene A from the second enzyme. Both enzymes were thoroughly investigated in terms of their mechanisms by isotope labeling experiments, site-directed mutagenesis, and variation of the metal cofactors and pH value. For spiroalbatene synthase, the pH- and Mn<sup>2+</sup>-dependent formation of the side product thunbergol was observed, which is biosynthetically linked to spiroalbatene.

The astonishing structural complexity of terpenes is reflected by hundreds of known polycyclic carbon skeletons. These are all formed by terpene synthases (TS) in a single enzymatic step from a few linear oligoprenyl diphosphate (OPP) precursors, including geranyl diphosphate (GPP) for monoterpenes (C<sub>10</sub>), farnesyl PP (FPP) for sesquiterpenes (C<sub>15</sub>), geranylgeranyl PP (GGPP) for diterpenes (C<sub>20</sub>), and geranylgeranylgeranyl PP (GGGPP) for sesterterpenes (C<sub>25</sub>).<sup>[1]</sup> Starting from the pentalene synthase from *Streptomyces exfoliatus*,<sup>[2]</sup> previous research has resulted in the discovery of several bacterial mono- (MTSs) and sesquiterpene synthases (STSs).<sup>[1]</sup> In contrast, only a few type I diterpene synthases (DTSs), including those for cyclooctat-9-en-7-ol (CotB2), spiroviolene, tsukubadiene, hydropyrene, 18-hydroxydolabella-3,7-diene, and spata-13,17-diene, have been characterized,<sup>[3]</sup> with spata-13,17-diene synthase as the first bacterial enzyme also making sesterterpenes.<sup>[3f]</sup> As GGPP has more options to react than GPP and FPP, the chance to discover new compounds is higher for diterpenes than for mono- and sesquiterpenes. It is not possible to predict directly from the amino acid sequence of a TS which substrate preference it has, but a phylogeny of TSs can unravel candidates with a relationship close enough to a characterized DTS to suspect DTS activity, and distant enough to ensure that the TS does not make the same product as the known enzyme. Using this approach, we have identified two TSs from the tropical soil isolate *Allokutzneria albata* DSM 44149<sup>[4]</sup> with close relationships to other bacterial DTSs, as can be seen from a phylogenetic tree constructed from 2728 bacterial TSs (see the Supporting Information, Figure S1).

The genes for both enzymes were cloned into the expression vector pYE-Express<sup>[5]</sup> by homologous recombination in yeast, followed by gene expression in *Escherichia coli* and protein purification (Figure S2; accession numbers are given in the Supporting Information). The first enzyme did not accept GPP, FPP, and GGPP, but GGPP was efficiently converted into a diterpene hydrocarbon (Figure S3). This compound was purified, and its structure was elucidated by NMR spectroscopy (Table S2 and Figures S4–S10). The most relevant <sup>1</sup>H,<sup>1</sup>H COSY, HMBC, and NOESY correlations are shown in Scheme 1 A, and correspond to the structure of a spiro-tetracyclic diterpene with a novel skeleton, for which we propose the name spiroalbatene (**1**). Thus the DTS was identified as spiroalbatene synthase (SaS).

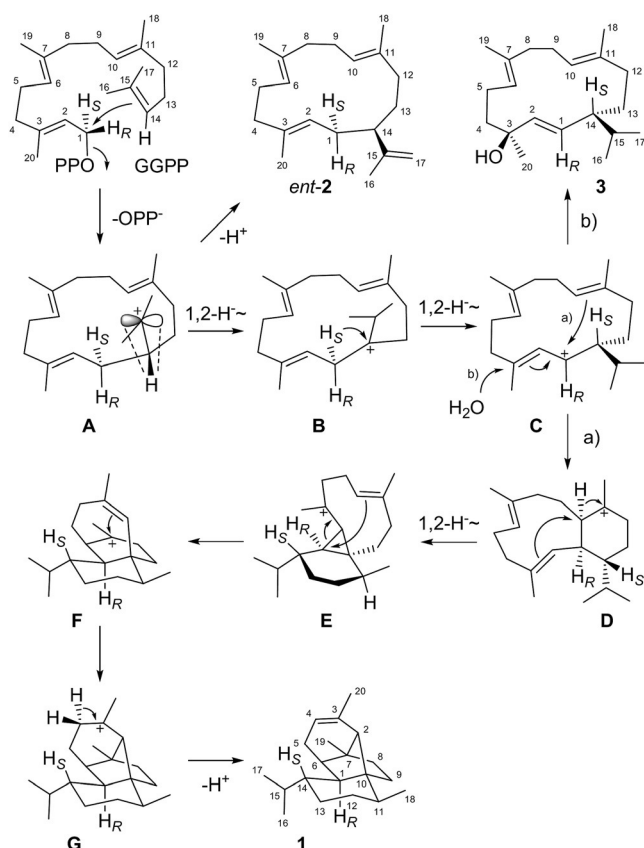


**Scheme 1.** Spiroalbatene (**1**). A) The carbon numbering for **1** indicates which carbon atom is derived from which carbon atom of GGPP by the same number. Bold lines: <sup>1</sup>H,<sup>1</sup>H COSY correlations, single-headed arrows: HMBC correlations, double-headed arrows: NOESY correlations. B) Enzymatic synthesis of (<sup>13</sup>C<sub>20</sub>)-**1**. Gray dots represent <sup>13</sup>C atoms, and bold lines indicate <sup>13</sup>C,<sup>13</sup>C COSY correlations.

Further support for the structure of **1** was obtained by <sup>13</sup>C,<sup>13</sup>C COSY NMR spectroscopy. For this purpose, we prepared completely isotopically substituted (<sup>13</sup>C<sub>20</sub>)GGPP from (<sup>13</sup>C<sub>15</sub>)FPP.<sup>[6]</sup> During our previous synthesis of this compound, (<sup>13</sup>C<sub>5</sub>)-3,3-dimethylallyl alcohol was also made available, which was converted into (<sup>13</sup>C<sub>5</sub>)DMAPP. Incubation of both compounds with the isopentenyl diphosphate isomerase (IDI) from *Serratia plymuthica*, the GGPP synthase (GGPPS) from *Streptomyces cyaneofuscatus*,<sup>[3c]</sup> and SaS resulted in the efficient production of (<sup>13</sup>C<sub>20</sub>)-**1** (Scheme 1 B). In the <sup>13</sup>C,<sup>13</sup>C COSY NMR spectrum of this compound (Figure S11), cross-peaks were observed for all C–C connectivities, apart from one.

[\*] J. Rinkel, L. Lauterbach, Dr. P. Rabe, Prof. Dr. J. S. Dickschat  
Kekulé-Institute of Organic Chemistry and Biochemistry  
University of Bonn  
Gerhard-Domagk-Straße 1, 53121 Bonn (Germany)  
E-mail: dickschat@uni-bonn.de

Supporting information and the ORCID identification number(s) for the author(s) of this article can be found under:  
<https://doi.org/10.1002/anie.201800385>.



**Scheme 2.** Cyclization mechanism from GGPP to **1** by SaS, hypothetical formation of *ent*-**2** from **A**, and formation of **3** from **C**.

A biosynthetic model for **1** is shown in Scheme 2. Starting from GGPP, a 1,14-cyclization to cation **A** is followed by a 1,2-hydride migration to give **B**. Another 1,2-hydride shift to **C** and ring closure result in **D**, which, upon a third 1,2-hydride shift and cyclization, yields the cyclopropane intermediate **E**. Opening of the three-membered ring with concomitant ring closure produces **F**. If the conversion of **E** into **F** proceeds in a concerted fashion, a secondary cation intermediate can be avoided. A final ring closure and deprotonation result in **1**. This biosynthetic hypothesis was tested by conversion of all twenty isotopomers of (<sup>13</sup>C)GGPP, which were prepared by synthesis or enzymatically from the corresponding <sup>13</sup>C-labeled FPP and IPP isotopomers.<sup>[3c,6]</sup> For all substrates, the label ended up in the position expected according to our model (Figure S12).

The elementary steps involving hydrogen migrations or deprotonations were investigated by using (stereo)selectively deuterated probes. In several cases, an additional <sup>13</sup>C substitution was introduced to enhance the resonance of the carbon atom in <sup>13</sup>C NMR analyses and to render the resulting <sup>13</sup>C–<sup>2</sup>H bonds observable by triplet signals. The first 1,2-hydride shift from **A** to **B** was followed by conversion of (14-<sup>2</sup>H)GGPP with SaS, prepared from IPP and (2-<sup>2</sup>H)DMAPP<sup>[3c]</sup> with *Streptomyces coelicolor* FPP synthase (FPPS)<sup>[7]</sup> and GGPPS.<sup>[3c]</sup> GC-MS analysis of the product indicated the incorporation of one deuterium atom according to the increased weight of the molecular ion, while the fragment

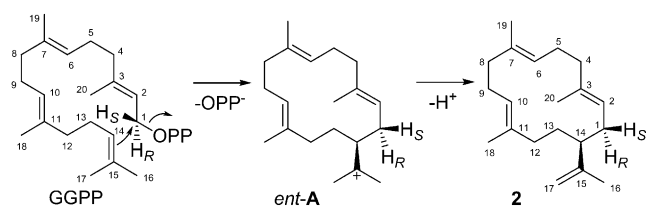
ion of **1** at  $m/z = 229$ , representing the loss of the *i*Pr group, did not change (Figure S13 A). Therefore, the deuterium atom had been incorporated in the *i*Pr group as expected. A 1,3-hydride migration from C1 into the *i*Pr group as an alternative to the two sequential 1,2-hydride migrations from **A** to **C** was ruled out by incubation of (*S*)- and (*R*)- (1-<sup>2</sup>H)GGPP<sup>[3c]</sup> with SaS, which yielded products with a fragment ion at  $m/z = 230$ , implying that the deuterium atom stayed within the tetracyclic core structure of **1** in both cases (Figure S13 B). The <sup>13</sup>C labeling from (16-<sup>13</sup>C)- and (17-<sup>13</sup>C)GGPP resulted in a scrambling (Figure S12) similar to what has previously been observed for other terpene cyclizations with 1,2-hydride migrations into an *i*Pr group,<sup>[3c,8]</sup> and reflects the similar distances for the migrating hydrogen atom to the two diastereotopic faces of the cation in **A**. In contrast, for 1,3-hydride migrations, a strict stereochemical course is always observed.<sup>[9]</sup> The stereochemical course for the second 1,2-hydride shift from **B** to **C** was investigated by conversion of (*S*)- and (*R*)- (1-<sup>13</sup>C,1-<sup>2</sup>H)GGPP<sup>[3c]</sup> with SaS. Whereas the *S* enantiomer yielded a product with a singlet for C1 in the <sup>13</sup>C NMR spectrum, the *R* enantiomer gave a product with a triplet resonance for C1, establishing the specific migration of the *pro-S* hydrogen atom from C1 of GGPP (Figure S14 A). The 1,2-hydride transfer from **D** to **E** was investigated with (3-<sup>13</sup>C,2-<sup>2</sup>H)GPP, synthesized according to a published procedure (Scheme S1),<sup>[3c]</sup> which was elongated with IPP and GGPPS to (11-<sup>13</sup>C,10-<sup>2</sup>H)GGPP followed by cyclization with SaS. The product showed the expected triplet in the <sup>13</sup>C NMR spectrum (Figure S14 B). The final deprotonation step to **1** proceeds from C4 of GGPP. Which of the two enantiotopic protons is lost can be addressed by stereoselective deuteration. For this purpose, (*E*)- and (*Z*)- (4-<sup>2</sup>H)IPP were synthesized (Scheme S2) and used for the GGPPS-catalyzed elongation of FPP to obtain (*S*)- and (*R*)- (4-<sup>2</sup>H)GGPP (Figure S15). The stereochemical course of this reaction includes attack of IPP at C4 from the *Si* face.<sup>[10]</sup> Further conversion with SaS revealed the specific loss of deuterium from (*E*)- (4-<sup>2</sup>H)IPP, whereas the deuterium from (*Z*)- (4-<sup>2</sup>H)IPP was retained, revealing that deprotonation of **G** proceeds as shown in Scheme 2.

We have recently developed a method that uses the stereoselectively deuterated precursors (*S*)- and (*R*)- (1-<sup>13</sup>C,1-<sup>2</sup>H)FPP and (*S*)- and (*R*)- (1-<sup>13</sup>C,1-<sup>2</sup>H)GPP to determine the absolute configurations of terpenes.<sup>[3c]</sup> The elongation of OPPs with IPP by OPP synthases proceeds with inversion of configuration at C1.<sup>[11]</sup> After conversion of the enantioselectively deuterated substrates with GGPPS and SaS, the defined stereochemical anchors at the deuterated carbon atoms were used to solve the absolute configuration of **1** by determining the relative configurations of the stereospecifically deuterated products. The additional <sup>13</sup>C substitution was introduced for highly sensitive product analysis by HSQC (Figures S16 and S17). The results with all four probes consistently pointed to the absolute configuration of **1** shown in Scheme 1.

The second enzyme from *A. albata* also did not accept GPP, FPP, and GFPP, but efficiently converted GGPP into one main and a few side products (Figure S18). The main product was purified, and its NMR data were identical to those of cembrene A (Table S3),<sup>[12]</sup> while the optical rotation



was  $[\alpha]_D^{20} = +12.0$  ( $c$  0.13,  $\text{CHCl}_3$ ). Based on the published optical rotations for the synthetic *S* ( $[\alpha]_D = +19.5$ )<sup>[13]</sup> and *R* enantiomers ( $[\alpha]_D = -12$ ,  $c$  0.85,  $\text{CHCl}_3$ )<sup>[12]</sup> these data pointed to the structure of (*S*)-(+)-cembrene A (**2**; Scheme 3) and identified the enzyme from *A. albata* as



**Scheme 3.** Cyclization mechanism from GGPP to **2**.

a cembrene A synthase (CAS). The cyclization mechanism from GGPP to **2** requires a 1,14-cyclization to the cembranyl cation (*ent-A*) and deprotonation of one of the geminal Me groups. SaS could potentially yield *ent-2* from intermediate **A**, reflecting the phylogenetic distance between the two enzymes, but *ent-A* is not a product of SaS. Incubation of ( $16\text{-}^{13}\text{C}$ )- and ( $17\text{-}^{13}\text{C}$ )-GGPP resulted in a distribution of labeling, and therefore indicated a relaxed stereochemical course for the deprotonation step (Figure S19). Incubation of (*S*)- and (*R*)-( $1\text{-}^{13}\text{C}, 1\text{-}^2\text{H}$ )-GGPP with CAS and product analysis by HSQC showed that the configuration at C1 is inverted during the 1,14-cyclization of GGPP (Figure S20).

Type I TSs generally exhibit the same  $\alpha$ -helical fold as first recognized for avian FPPS.<sup>[14]</sup> Bacterial enzymes, apart from geosmin synthase with two  $\alpha$ -domains,<sup>[15]</sup> adopt a single  $\alpha$ -domain architecture with several highly conserved motifs involved in the binding of the metal cofactor and substrate recognition.<sup>[16]</sup> This includes the aspartate-rich motif **DDXX**-(X)(D,E), the NSE triad **ND(L,I,V)XSXX(R,K)(E,D)**, the diphosphate (PP) sensor (**R** near the helix G break), and the **RY** dimer near the C-terminus. For SaS, the  $\text{Mg}^{2+}$  cofactor can be substituted by  $\text{Mn}^{2+}$ , resulting in a reduced activity of  $27 \pm 17\%$ , while for CAS, higher activity ( $172 \pm 12\%$ ) is observed with  $\text{Mn}^{2+}$  (Figure S21). No activity was observed with GGPP and SaS when no metal cofactor was added, demonstrating that residual  $\text{Mg}^{2+}$  in buffers or enzyme preparations does not account for the activity observed in experiments with  $\text{Mn}^{2+}$  (and vice versa).

The importance of several conserved residues in TSs for catalytic activity has been demonstrated by site-directed mutagenesis (SDM, critical residues identified in previous mutational studies are shown in bold above).<sup>[3f,15,17]</sup> SaS exhibits all of the conserved motifs as usual, with the exception of a Gly instead of the Ser in the NSE triad (Figures S22 and S23). Among all > 50 characterized bacterial TSs and their nearly 2500 close homologues from sequenced bacteria (Figure S1), a substitution of this Ser is observed in only four cases (Table S4). Installation of Ser by SDM (G229S) gave no soluble enzyme, suggesting that Gly with its conformational flexibility is of structural importance for enzyme folding of wild-type SaS. The crystal structure of selina-4(15),7(11)-diene synthase (SdS)<sup>[17d]</sup> shows hydrogen bonds between the PP sensor Arg178, a highly conserved

Tyr174 found in > 90% of bacterial TSs, and the first Asp225 of the NSE triad (Figure S23). In SaS and in approximately 5% of bacterial TSs, a Phe175 is found instead of Tyr. The F175Y variant gave a good enzyme yield, but the activity dropped to  $28 \pm 6\%$  with  $\text{Mg}^{2+}$ , and a similar loss of activity was observed with  $\text{Mn}^{2+}$ .

For spata-13,17-diene synthase (SpS) from *Streptomyces xinghaiensis*, the critical role of the highly conserved Pro and Leu residues located 21 and 14 positions upstream of the Asp-rich motif was recently demonstrated.<sup>[3f]</sup> The corresponding L72A variant of SaS gave no soluble protein, while P65A yielded wild-type levels of enzyme, but the activity dropped significantly with  $\text{Mg}^{2+}$  and  $\text{Mn}^{2+}$ . As can be seen in the crystal structure of SdS,<sup>[17d]</sup> these two residues are placed at the link between helices C and D (Figure S24) and are likely of structural relevance. In CAS, the position corresponding to Pro61 is naturally occupied by Ala. In this case, the A64P variant has lower activity than the wild type, but only with  $\text{Mg}^{2+}$ , while no effect was observed with  $\text{Mn}^{2+}$ .

A highly conserved Glu residue seen in > 93% of bacterial TSs is occupied by Gln160 in SaS. In SdS, this residue is involved in metal cofactor binding (Figure S25). Whereas gene expression of the SaS Q160E variant worked well, the enzyme showed no activity with either  $\text{Mg}^{2+}$  or  $\text{Mn}^{2+}$ . For CAS, the opposite exchange (E179Q) resulted in strongly reduced activity with both metal cations, and the E179K variant was inactive. An interesting structural feature of SdS is the salt bridge between a highly conserved Arg144 and a less conserved Glu192. We have recently shown for SpS that the D217E mutation within the salt bridge (Arg169 and Asp217) results in an inactive enzyme variant in combination with  $\text{Mn}^{2+}$ , but in increased activity with  $\text{Mg}^{2+}$ .<sup>[3f]</sup> The corresponding residues for SaS (Arg145 and Glu193) were mutated with shortening of the salt bridge by the R145K or E193D exchanges, which resulted in reduced activity (with  $\text{Mg}^{2+}$ ) or a complete loss thereof (with  $\text{Mn}^{2+}$ ). For the R145M variant, an only slight decrease in activity was observed for both metal cofactors. Of particular interest is the observation that both SpS<sup>[3f]</sup> and CAS have a naturally short salt bridge with participation of an Asp instead of the more regular Glu, and both enzymes are more efficient with  $\text{Mn}^{2+}$  than with  $\text{Mg}^{2+}$ . For CAS, the D212E mutation resulted in strongly decreased activity with  $\text{Mg}^{2+}$  and  $\text{Mn}^{2+}$ . These data suggest an influence of the length of this salt bridge, likely by alteration of the tilt angle between helices G and F on the active-site architecture, with consequences for metal binding. A short salt bridge with participation of Asp seems to favor catalysis with  $\text{Mn}^{2+}$  while a long salt bridge with Glu fosters  $\text{Mg}^{2+}$  binding; however, further experiments with other TSs are required to investigate whether this finding is generalizable.

A highly conserved Pro was identified 22 residues downstream of the PP sensor. In SdS, this residue is located at the bottom of helix H and seems to have an important structural function (Figure S26). In a few TSs, the corresponding position is occupied by Thr or Ser, but the P201T variant of SaS showed significantly reduced activity with both metal cofactors.

SaS was also investigated in terms of the result of changing the pH value from pH 7.4, which was used in the experiments

described above, to pH 8.2. Whereas no significant change in the product profile was observed with the wild-type enzyme in combination with  $Mg^{2+}$ , incubations with  $Mn^{2+}$  resulted in a new side product (Figure S3). This compound was isolated and identified by NMR spectroscopy (Table S5 and Figures S27–S33) as thunbergol (**3**). The absolute configuration of (1*R*,4*S*)-**3** was evident from the optical rotation ( $[\alpha]_D^{20} = -48$ ,  $c$  0.85,  $CHCl_3$ ) by comparison with (1*S*,4*R*)-**3** from *Pseudotsuga menziesii* ( $[\alpha]_D^{20} = +75.2$ ,  $c$  1.2,  $CHCl_3$ ),<sup>[18]</sup> establishing another example for a bacterial TS producing the opposite enantiomer as in plants.<sup>[1,9b,19]</sup> Compound **3** can be formed via the same intermediate **C** as **1** (Scheme 2), which was corroborated by the fact that the stereocenter at C14 has the same configuration in both products. The formation of **1** and **3** via **C** as a common intermediate is also mechanistically supported: Incubation of (2-<sup>2</sup>H)DMAPP with IPP, GGPPS, and SaS followed by GC-MS analysis of product **3** revealed the same 1,2-hydride shift from **A** to **B** found for **1** (Figure S34), again with a distribution of labeling from C16 and C17 (Figure S35). As for **1**, the enzymatic conversion of (*R*)- and (*S*)-(1-<sup>13</sup>C,1-<sup>2</sup>H)GGPP with SaS provided evidence for a stereoselective migration of the 1-*pro-S* hydrogen atom to **C** also for **3** (Figure S36).

None of the diterpenes identified from SaS or CAS were observed in headspace extracts from *A. albata*, whereas spiroviolene was reported in our previous study,<sup>[3c]</sup> suggesting that both enzymes are not expressed in laboratory cultures. Alternatively, **1** may be oxidized to an unknown product by a genetically clustered cytochrome P450 (Figure S37 and Table S6).

In summary, we have identified the products of two DTSSs from *A. albata*, one of them exhibiting the unprecedented structure of spiroalbatene. While the general principles of terpene biosynthesis are well understood, the recently accumulating data from isotope labeling experiments, enzyme crystallizations, enzyme mutagenesis, and variations of the incubation conditions provide more detailed insight, which may allow for predictive approaches on how to access new terpenes in the future. The phylogenetic tree of bacterial TSs (Figure S1) shows that the products of many enzymes are known today, but there are also many dark areas for continuing research on this interesting enzyme class.

## Acknowledgements

This work was funded by the DFG (DI1536/7-1) and the Fonds der Chemischen Industrie (PhD scholarship to J.R.). We thank Paolina Garbeva (Wageningen) for *Serratia plymuthica* PRI-2C.

## Conflict of interest

The authors declare no conflict of interest.

**Keywords:** biosynthesis · enzyme mechanisms · isotopes · soil microorganisms · terpenes

**How to cite:** *Angew. Chem. Int. Ed.* **2018**, *57*, 3238–3241  
*Angew. Chem.* **2018**, *130*, 3292–3296

- [1] J. S. Dickschat, *Nat. Prod. Rep.* **2016**, *33*, 87.
- [2] D. E. Cane, C. Pargellis, *Arch. Biochem. Biophys.* **1987**, *254*, 421.
- [3] a) A. Meguro, Y. Motoyoshi, K. Teramoto, S. Ueda, Y. Totsuka, Y. Ando, T. Tomita, S.-Y. Kim, T. Kimura, M. Igarashi, R. Sawa, T. Shinada, M. Nishiyama, T. Kuzuyama, *Angew. Chem. Int. Ed.* **2015**, *54*, 4353; *Angew. Chem.* **2015**, *127*, 4427; b) Y. Yamada, T. Kuzuyama, M. Komatsu, K. Shin-ya, S. Omura, D. E. Cane, H. Ikeda, *Proc. Natl. Acad. Sci. USA* **2015**, *112*, 857; c) P. Rabe, J. Rinkel, E. Dolja, T. Schmitz, B. Nubbemeyer, T. H. Luu, J. S. Dickschat, *Angew. Chem. Int. Ed.* **2017**, *56*, 2776; *Angew. Chem.* **2017**, *129*, 2820; d) J. S. Dickschat, J. Rinkel, P. Rabe, A. B. Kashkooli, H. J. Bouwmeester, *Beilstein J. Org. Chem.* **2017**, *13*, 1770; e) J. Rinkel, P. Rabe, X. Chen, T. G. Köllner, F. Chen, J. S. Dickschat, *Chem. Eur. J.* **2017**, *23*, 10501; f) J. Rinkel, L. Lauterbach, J. S. Dickschat, *Angew. Chem. Int. Ed.* **2017**, *56*, 16385; *Angew. Chem.* **2017**, *129*, 16603.
- [4] K. Tomita, Y. Hoshino, T. Miyaki, *Int. J. Syst. Bacteriol.* **1993**, *43*, 297.
- [5] J. S. Dickschat, K. A. K. Pahirulzaman, P. Rabe, T. A. Klapschinski, *ChemBioChem* **2014**, *15*, 810.
- [6] P. Rabe, L. Barra, J. Rinkel, R. Riclea, C. A. Citron, T. A. Klapschinski, A. Janusko, J. S. Dickschat, *Angew. Chem. Int. Ed.* **2015**, *54*, 13448; *Angew. Chem.* **2015**, *127*, 13649.
- [7] P. Rabe, J. Rinkel, B. Nubbemeyer, T. G. Köllner, F. Chen, J. S. Dickschat, *Angew. Chem. Int. Ed.* **2016**, *55*, 15420; *Angew. Chem.* **2016**, *128*, 15646.
- [8] a) I. Burkhardt, T. Siemon, M. Henrot, L. Studt, S. Rösler, B. Tudzynski, M. Christmann, J. S. Dickschat, *Angew. Chem. Int. Ed.* **2016**, *55*, 8748; *Angew. Chem.* **2016**, *128*, 8890.
- [9] a) J. Rinkel, P. Rabe, P. Garbeva, J. S. Dickschat, *Angew. Chem. Int. Ed.* **2016**, *55*, 13593; *Angew. Chem.* **2016**, *128*, 13791; b) P. Rabe, T. Schmitz, J. S. Dickschat, *Beilstein J. Org. Chem.* **2016**, *12*, 1839.
- [10] a) J. W. Cornforth, R. H. Cornforth, G. Popjak, L. Yengoyan, *J. Biol. Chem.* **1966**, *241*, 3970; b) H. V. Thulasiram, C. D. Poulter, *J. Am. Chem. Soc.* **2006**, *128*, 15819.
- [11] J. W. Cornforth, R. H. Cornforth, C. Donninger, G. Popjak, *Proc. R. Soc. London Ser. B* **1966**, *163*, 492.
- [12] R. Schwabe, I. Farkas, H. Pfander, *Helv. Chim. Acta* **1988**, *71*, 292.
- [13] T. Kato, M. Suzuki, T. Kobayashi, B. P. Moore, *J. Org. Chem.* **1980**, *45*, 1126.
- [14] L. C. Tarshis, M. Yan, C. D. Poulter, J. C. Sacchettini, *Biochemistry* **1994**, *33*, 10871.
- [15] J. Jiang, X. He, D. E. Cane, *Nat. Chem. Biol.* **2007**, *3*, 711.
- [16] D. W. Christianson, *Chem. Rev.* **2017**, *117*, 11570.
- [17] a) M. Seemann, G. Z. Zhai, J. W. de Kraker, C. M. Paschall, D. W. Christianson, D. E. Cane, *J. Am. Chem. Soc.* **2002**, *124*, 7681; b) M. Seemann, G. Zhai, K. Umezawa, D. Cane, *J. Am. Chem. Soc.* **1999**, *121*, 591; c) P. Baer, P. Rabe, C. A. Citron, C. C. D. O. Mann, N. Kaufmann, M. Groll, J. S. Dickschat, *ChemBioChem* **2014**, *15*, 213; d) P. Baer, P. Rabe, K. Fischer, C. A. Citron, T. A. Klapschinski, M. Groll, J. S. Dickschat, *Angew. Chem. Int. Ed.* **2014**, *53*, 7652; *Angew. Chem.* **2014**, *126*, 7783.
- [18] I. Wahlberg, I. Wallin, C. Narbonne, T. Nishida, C. R. Enzell, *Acta. Chem. Scand.* **1981**, *35b*, 65.
- [19] L. Ding, H. Goerls, K. Dornblut, W. Lin, A. Maier, H.-H. Fiebig, C. Hertweck, *J. Nat. Prod.* **2015**, *78*, 2963.

Manuscript received: January 10, 2018

Revised manuscript received: January 26, 2018

Accepted manuscript online: January 29, 2018

Version of record online: February 21, 2018

## Enzymmechanismen

Deutsche Ausgabe: DOI: 10.1002/ange.201800385  
Internationale Ausgabe: DOI: 10.1002/anie.201800385Zwei Diterpensynthesen für Spiroalbaten und Cembren A aus *Allokutzneria albata*

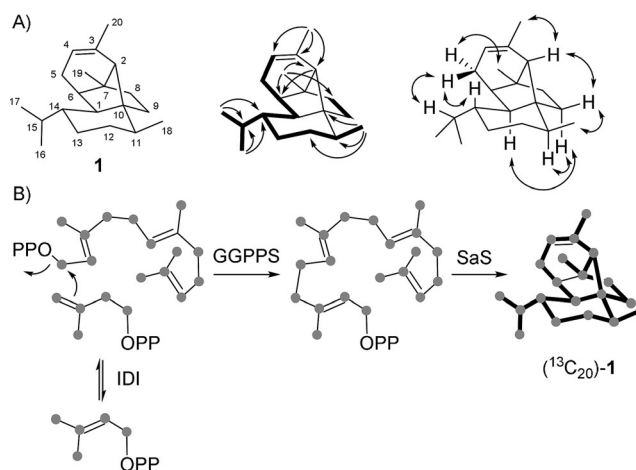
Jan Rinkel, Lukas Lauterbach, Patrick Rabe und Jeroen S. Dickschat\*

**Abstract:** Zwei bakterielle Diterpensynthesen aus dem Actinomyceten *Allokutzneria albata* wurden untersucht. Dies führte zur Identifizierung des strukturell neuartigen Produkts Spiroalbaten des ersten und Cembren A des zweiten Enzyms. Beide Enzyme wurden durch Isotopenmarkierungsexperimente, ortsgerichtete Mutagenese, Variation des Metallkofaktors und des pH-Wertes auf ihre Mechanismen untersucht. Für die Spiroalbaten-Synthese wurde eine pH- und  $Mn^{2+}$ -abhängige Bildung des Nebenproduktes Thunbergol beobachtet, das biosynthetisch mit Spiroalbaten verwandt ist.

Die erstaunliche strukturelle Komplexität von Terpenen wird durch hunderte bekannte polycyclische Kohlenstoffgerüste reflektiert. Diese werden alle durch Terpensynthesen (TS) in einem einzelnen enzymatischen Schritt aus wenigen linearen Oligoprenyldiphosphaten (OPP) gebildet, einschließlich Geranyldiphosphat (GPP) für Monoterpene ( $C_{10}$ ), Farnesyl-PP (FPP) für Sesquiterpene ( $C_{15}$ ), Geranylgeranyl-PP (GGPP) für Diterpene ( $C_{20}$ ) und Geranylarnesyl-PP (GFPP) für Sesterterpene ( $C_{25}$ ).<sup>[1]</sup> Beginnend mit der Pentalenensynthese aus *Streptomyces exfoliatus*,<sup>[2]</sup> haben vorausgehende Studien zur Entdeckung diverser bakterieller Mono- (MTS) und Sesquiterpensynthesen (STS) geführt.<sup>[1]</sup> Demgegenüber wurden nur wenige Typ-I-Diterpensynthesen (DTS) wie diejenigen für Cyclooctat-9-en-7-ol (CotB2), Spiroviolen, Tsukubadien, Hydropyren, 18-Hydroxydolabella-3,7-dien und Spata-13,17-dien charakterisiert,<sup>[3]</sup> wobei die Spata-13,17-dien-Synthese das erste bakterielle Enzym ist, das auch Sesterterpene bildet.<sup>[3d]</sup> Da GGPP im Vergleich mit GPP und FPP mehr Reaktionsmöglichkeiten hat, ist die Chance, neue Verbindungen zu entdecken, für Diterpene höher als für Mono- und Sesquiterpene. Es ist nicht möglich, aus der Aminosäuresequenz einer TS abzuleiten, welche Substratpräferenz das Enzym hat, aber eine Phylogenie von TS kann Kandidaten mit einer nahen Verwandtschaft zu charakterisierten DTS identifizieren, so dass DTS-Aktivität vermutet werden kann. Gleichzeitig sollte das zu studierende Enzym so entfernt verwandt von bekannten Enzymen sein, dass die Bildung desselben Produkts wie für das bekannte Enzym ausgeschlossen werden kann. Mit diesem Ansatz haben wir zwei TS aus dem tropischen Bodenbakterium *Allokutzneria*

*albata* DSM 44149<sup>[4]</sup> mit naher Verwandtschaft zu anderen bakteriellen DTS identifiziert, wie aus einem phylogenetischen Baum aus 2728 bakteriellen TS hervorgeht (Abbildung S1 in den Hintergrundinformationen).

Die Gene für beide Enzyme wurden durch homologe Rekombination in Hefe in den Expressionsvektor pYE-Express<sup>[5]</sup> kloniert, gefolgt von Genexpression in *Escherichia coli* und Reinigung des Proteins (Abbildung S2, für Accession Numbers siehe Hintergrundinformationen). GPP, FPP und GFPP wurden vom ersten Enzym nicht akzeptiert, aber GGPP wurde effizient in einen Diterpenkohlenwasserstoff umgesetzt (Abbildung S3). Die Verbindung wurde gereinigt und ihre Struktur per NMR-Spektroskopie aufgeklärt (Tabelle S2, Abbildungen S4–S10). Die wichtigsten  $^1H$ ,  $^1H$ -COSY-, HMBC- und NOESY-Korrelationen sind in Schema 1 A dargestellt, wodurch sich die Struktur eines spiro-



**Scheme 1.** Spiroalbaten (1). A) Die Kohlenstoffnummerierung für 1 zeigt durch identische Nummern an, welches Kohlenstoffatom aus welchem von GGPP hervorgeht (siehe Schema 2). Fette Bindungen:  $^1H$ ,  $^1H$ -COSY-Korrelationen, einfache Pfeile: HMBC-Korrelationen, Doppelpfeile: NOESY-Korrelationen. B) Enzymatische Synthese von  $(^{13}C_{20})$ -1. Graue Punkte repräsentieren  $^{13}C$ -Atome und fette Bindungen  $^{13}C$ ,  $^{13}C$ -COSY-Korrelationen.

tetracyclischen Diterpens mit neuem Molekülgerüst ergab, für das wir den Namen Spiroalbaten (1) vorschlagen. Somit wurde die DTS als Spiroalbaten-Synthese (SaS) identifiziert.

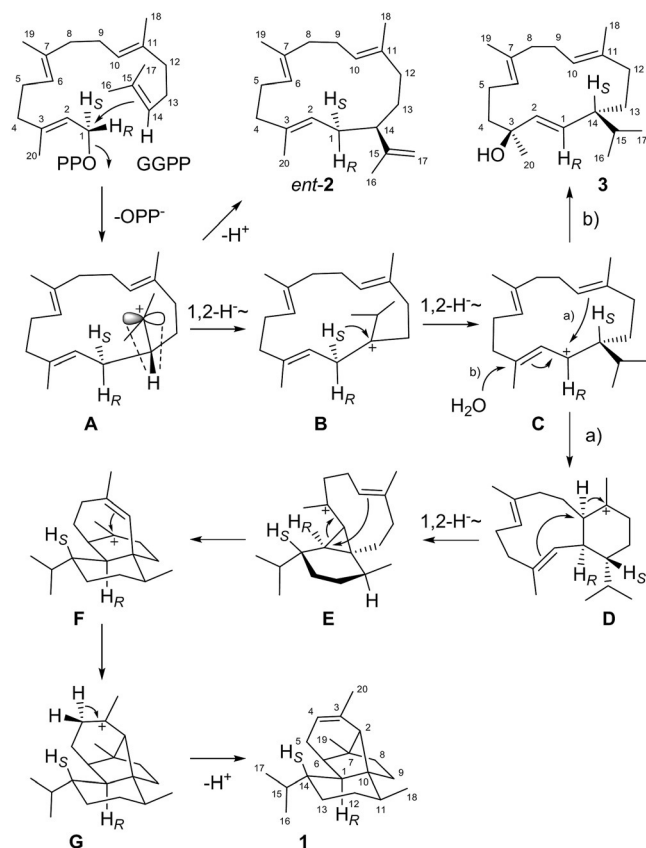
Die Struktur von 1 wurde durch  $^{13}C$ ,  $^{13}C$ -COSY-NMR-Messungen weiter gestützt. Zu diesem Zweck haben wir komplett isotopensubstituiertes  $(^{13}C_{20})$ GGPP aus  $(^{13}C_{15})$ FPP hergestellt.<sup>[6]</sup> In unserer früheren Synthese dieser Verbindung wurde auch  $(^{13}C_5)$ -3,3-Dimethylallylalkohol erhalten, der zu  $(^{13}C_5)$ DMAPP umgesetzt wurde. Eine Inkubation beider

[\*] J. Rinkel, L. Lauterbach, Dr. P. Rabe, Prof. Dr. J. S. Dickschat  
Kekulé-Institut für Organische Chemie und Biochemie  
Universität Bonn  
Gerhard-Domagk-Straße 1, 53121 Bonn (Deutschland)  
E-Mail: dickschat@uni-bonn.de

Hintergrundinformationen und die Identifikationsnummer (ORCID) eines Autors sind unter <https://doi.org/10.1002/ange.201800385> zu finden.

Verbindungen mit der Isopentenylidiphosphat-Isomerase (IDI) aus *Serratia plymuthica*, der GGPP-Synthase (GGPPS) aus *Streptomyces cyaneofuscatus*<sup>[3c]</sup> und SaS resultierte in der effizienten Produktion von (<sup>13</sup>C<sub>20</sub>)-**1** (Schema 1B). Produktanalyse per <sup>13</sup>C, <sup>13</sup>C-COSY-NMR-Spektroskopie (Abbildung S11) erlaubte die Beobachtung von Kreuzpeaks für alle bis auf eine der C-C-Konnektivitäten.

Ein biosynthetisches Modell für **1** ist in Schema 2 gezeigt. Ausgehend von GGPP führt eine 1,14-Cyclisierung über Kation **A** gefolgt von einer 1,2-Hydridverschiebung zu **B**.



**Schema 2.** Cyclisierungsmechanismus von GGPP zu **1** der SaS, hypothetische Bildung von *ent*-**2** aus **A** und Bildung von **3** aus **C**.

Eine zweite 1,2-Hydridwanderung zu **C** und Ringschluss ergeben **D**, das durch eine dritte 1,2-Hydridverschiebung und Cyclisierung das Cyclopropan-Intermediat **E** ergibt. Öffnung des dreigliedrigen Rings mit gleichzeitigem Ringschluss liefert **F**. Wenn die Umwandlung von **E** zu **F** konzertiert abläuft, kann ein sekundäres Kation als Intermediat vermieden werden. Ein letzter Ringschluss und Deprotonierung resultieren in **1**. Diese biosynthetische Hypothese wurde durch Umsetzung aller zwanzig Isotopomere von (<sup>13</sup>C)GGPP getestet, die synthetisch oder enzymatisch aus den korrespondierenden <sup>13</sup>C-markierten Isotopomeren von FPP und IPP erhalten wurden.<sup>[3c,6]</sup> Mit allen Substraten wurde die Markierung in den nach dem Modell zu erwartenden Positionen gefunden (Abbildung S12).

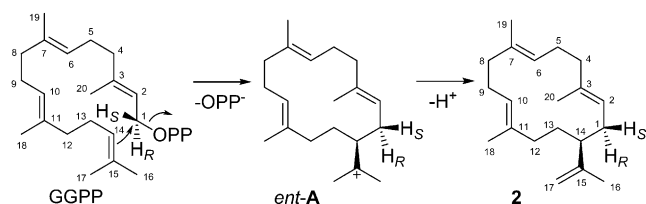
Die mit Hydridwanderungen oder Deprotonierung assoziierten Elementarschritte wurden unter Verwendung (ste-

reo)selektiv deuterierter Sonden untersucht. In vielen Fällen wurde zusätzlich eine <sup>13</sup>C-Substitution eingeführt, um die Signalstärke des Kohlenstoffatoms in einer <sup>13</sup>C-NMR-Analyse zu erhöhen und resultierende <sup>13</sup>C-<sup>2</sup>H-Bindungen durch Triplettensignale beobachtbar zu machen. Die erste 1,2-Hydridverschiebung von **A** zu **B** wurde durch Umsetzung von (14-<sup>2</sup>H)GGPP mit SaS verfolgt, das aus IPP und (2-<sup>2</sup>H)DMAPP<sup>[3e]</sup> mit der FPP-Synthase (FPPS) aus *Streptomyces coelicolor*<sup>[7]</sup> und der GGPPS<sup>[3c]</sup> erzeugt wurde. GC-MS-Analyse des Produktes zeigte den Einbau eines Deuteriumatoms durch ein erhöhtes Molekularion, während das Fragmentation von **1** bei  $m/z = 229$ , das den Verlust einer *iPr*-Gruppe repräsentiert, unverändert blieb (Abbildung S13A). Somit konnte der zu erwartende Deuteriumeinbau in die Isopropylgruppe gezeigt werden. Eine 1,3-Hydridwanderung von C1 in die *iPr*-Gruppe als Alternative zur Sequenz der zwei 1,2-Hydridwanderungen von **A** zu **C** wurde durch Inkubation von (*S*)- und (*R*)-(1-<sup>2</sup>H)GGPP<sup>[3c]</sup> mit SaS ausgeschlossen, was Produkte mit einem Fragmentation bei  $m/z = 230$  ergab, ergo verblieb das Deuterium in beiden Fällen im tetracyclischen Kern von **1** (Abbildung S13B). Die <sup>13</sup>C-Markierung aus (16-<sup>13</sup>C)- und (17-<sup>13</sup>C)GGPP führte zu einem Positionsaustausch im Produkt (Abbildung S12), der zuvor schon für andere Terpen cyclisierungen mit 1,2-Hydridwanderungen in eine *iPr*-Gruppe beschrieben worden war<sup>[3c,8]</sup> und die ähnlichen Abstände des wandernden Wasserstoffs zu den diastereotopen Flächen des Kations in **A** reflektiert. Im Gegensatz dazu wird für 1,3-Hydridverschiebungen immer ein strikter stereochemischer Verlauf beobachtet.<sup>[9]</sup> Der stereochemische Verlauf für die zweite 1,2-Hydridwanderung von **B** zu **C** wurde durch Umsetzung von (*S*)- und (*R*)-(1-<sup>13</sup>C,1-<sup>2</sup>H)GGPP<sup>[3e]</sup> mit SaS untersucht. Während das *S*-Enantiomer ein Produkt mit einem Singulett für C1 im <sup>13</sup>C-NMR-Spektrum lieferte, ergab das *R*-Enantiomer ein Produkt mit einem Triplett, wodurch die spezifische Wanderung des *pro-S*-Wasserstoffs von C1 des GGPPs etabliert wurde (Abbildung S14A). Der 1,2-Hydridtransfer von **D** zu **E** wurde mit (3-<sup>13</sup>C,2-<sup>2</sup>H)GPP verfolgt, das nach einer publizierten Route synthetisiert wurde (Schema S1)<sup>[3c]</sup> und mit IPP und GGPPS zu (11-<sup>13</sup>C,10-<sup>2</sup>H)GGPP verlängert wurde, gefolgt von Cyclisierung mit der SaS. Das Produkt zeigte das erwartete Triplett im <sup>13</sup>C-NMR-Spektrum (Abbildung S14B). Die abschließende Deprotonierung zu **1** erfolgt von C4 des GGPPs. Welches der enantiotopen Protonen verloren wird, kann durch stereoselektive Deuterierung adressiert werden. Dafür wurden (*E*)- und (*Z*)-(4-<sup>2</sup>H)IPP synthetisiert (Schema S2) und für die GGPPS-katalysierte Verlängerung von FPP zu (*S*)- und (*R*)-(4-<sup>2</sup>H)GGPP eingesetzt (Abbildung S15). Der stereochemische Verlauf dieser Verlängerung beinhaltet den Angriff von IPP an C4 von der *Si*-Seite.<sup>[10]</sup> Weitere Umsetzung mit SaS zeigte den spezifischen Verlust von Deuterium aus (*E*)-(4-<sup>2</sup>H)IPP, aber Einbau aus (*Z*)-(4-<sup>2</sup>H)IPP, woraus sich die in Schema 2 gezeigte Deprotonierung von **G** ergibt.

Wir haben jüngst eine Methode zur Aufklärung der absoluten Konfiguration von Terpenen entwickelt, die die stereoselektiv deuterierten Vorläufer (*S*)- und (*R*)-(1-<sup>13</sup>C,1-<sup>2</sup>H)FPP sowie (*S*)- und (*R*)-(1-<sup>13</sup>C,1-<sup>2</sup>H)GPP verwendet.<sup>[3c]</sup> Die Verlängerung dieser OPPs mit IPP durch OPP-Synthasen verläuft mit Inversion der Konfiguration an C1.<sup>[11]</sup> Nach

Umsetzung der enantioselektiv deuterierten Substrate mit GGPPs und SaS wurden die definierten stereochemischen Anker an den deuterierten Kohlenstoffatomen genutzt, um die absolute Konfiguration von **1** durch Bestimmung der relativen Konfigurationen der stereospezifisch deuterierten Produkte zu ermitteln. Die zusätzliche  $^{13}\text{C}$ -Substitution wurde für eine hochsensitive Produktanalyse per HSQC eingeführt (Abbildungen S16 und S17). Die Ergebnisse mit allen Proben ergaben konsistent die in Schema 1 gezeigte absolute Konfiguration für **1**.

Das zweite Enzym aus *A. albata* akzeptierte GPP, FPP und GFPP ebenfalls nicht, setzte GGPP aber effizient in ein Haupt- und einige Nebenprodukte um (Abbildung S18). Das Hauptprodukt wurde gereinigt und zeigte identische NMR-Spektren zu denen von Cembren A (Tabelle S3)<sup>[12]</sup> und einen Drehwert von  $[\alpha]_{\text{D}}^{20} = +12.0$  ( $c$  0.13,  $\text{CHCl}_3$ ). Mit den publizierten Drehwerten für die synthetischen *S*- ( $[\alpha]_{\text{D}} = +19.5$ )<sup>[13]</sup> und *R*-Enantiomere ( $[\alpha]_{\text{D}}^{20} = -12$ ,  $c$  0.85,  $\text{CHCl}_3$ )<sup>[12]</sup> ergab sich die Struktur von (*S*)-(+)-Cembren A (**2**, Schema 3), so



**Schema 3.** Cyclisierungsmechanismus von GGPP zu **2**.

dass das Enzym aus *A. albata* als Cembren-A-Synthase (CAS) identifiziert wurde. Der Cyclisierungsmechanismus von GGPP zu **2** erfordert eine 1,14-Cyclisierung zum Cembranyl-Kation (*ent*-**A**) und Deprotonierung von einer der geminalen Me-Gruppen. SaS könnte potentiell *ent*-**2** aus Intermediat **A** liefern, was die phylogenetische Distanz der beiden Enzyme unterstreicht, allerdings wird *ent*-**A** nicht als Produkt von SaS beobachtet. Die Umsetzung von (16- $^{13}\text{C}$ )- und (17- $^{13}\text{C}$ )GGPP ergab eine Verteilung der Markierung und damit einen relaxierten stereochemischen Verlauf für den Deprotonierungsschritt (Abbildung S19). Inkubation von (*S*)- und (*R*)-(1- $^{13}\text{C}$ ,1- $^2\text{H}$ )GGPP mit CAS und Produktanalyse per HSQC zeigte eine Inversion der Konfiguration an C1 für die 1,14-Cyclisierung von GGPP (Abbildung S20).

Typ-I-TS weisen generell dieselbe  $\alpha$ -helicale Faltung auf, die zuerst bei der FPPS des Huhns gefunden wurde.<sup>[14]</sup> Bakterielle Enzyme, mit Ausnahme der Geosmin-Synthase mit zwei  $\alpha$ -Domänen,<sup>[15]</sup> besitzen eine einzelne  $\alpha$ -Domäne mit mehreren hochkonservierten Motiven, die an der Bindung des Metallcofaktors und der Substraterkennung beteiligt sind.<sup>[16]</sup> Dazu gehören das Aspartat-reiche Motiv **DDXX(X)**-(**D,E**), die NSE-Triade **ND(L,I,V)XSXX(R,K)(E,D)**, der Diphosphat-Sensor (PP-Sensor, **R** in der Nähe des Bruchs der Helix G), und das **RY**-Dimer nah am C-Terminus. Für SaS kann der Cofaktor  $\text{Mg}^{2+}$  durch  $\text{Mn}^{2+}$  ersetzt werden, was zu einer reduzierten Aktivität von  $27 \pm 17\%$  führt, während für CAS mit  $\text{Mn}^{2+}$  eine höhere Aktivität mit  $\text{Mn}^{2+}$  beobachtet wird ( $172 \pm 12\%$ , Abbildung S21). Mit GGPP und SaS wird keine Aktivität beobachtet, wenn kein Metallcofaktor zuge-

geben wird, somit sind nicht Rückstände von  $\text{Mg}^{2+}$  in Puffern oder Enzympräparaten für die Aktivität in den Experimenten mit  $\text{Mn}^{2+}$  verantwortlich (und umgekehrt).

Die Bedeutung diverser konservierter Aminosäurereste für die katalytische Aktivität von TS ist durch ortsgerichtete Mutagenese (OGM) gezeigt worden (kritische Reste, die in früheren Mutationsstudien identifiziert wurden, sind oben fett dargestellt).<sup>[3,15,17]</sup> SaS weist alle üblichen konservierten Reste auf, mit Ausnahme eines Gly anstelle von Ser in der NSE-Triade (Abbildungen S22 und S23). Unter allen  $>50$  charakterisierten bakteriellen TS und ihren nahezu 2500 Homologen aus sequenzierten Bakterien (Abbildung S1) wird in nur vier Fällen eine Substitution dieses Ser gefunden (Tabelle S4). Einführung von Ser durch OGM (G229S) ergab kein lösliches Enzym, was nahelegt, dass Gly mit seiner Konformationsflexibilität von struktureller Bedeutung für die Enzymfaltung von Wildtyp-SaS ist. Die Kristallstruktur der Selina-4(15),7(11)-dien-Synthase (SdS)<sup>[17d]</sup> zeigt Wasserstoffbrücken zwischen dem PP-Sensor Arg178, einem hochkonservierten Tyr174, das in  $>90\%$  aller bakteriellen TS vorhanden ist, und dem ersten Asp225 der NSE-Triade (Abbildung S23). In SaS und ca. 5% der bakteriellen TS findet sich ein Phe175 anstelle des Tyr. Die F175Y-Variante ergab eine gute Enzymausbeute, aber die Aktivität fiel auf  $28 \pm 6\%$  mit  $\text{Mg}^{2+}$ , und mit  $\text{Mn}^{2+}$  wurde ein ähnlicher Aktivitätsverlust festgestellt.

Für die Spata-13,17-dien-Synthase (SpS) aus *Streptomyces xinghaiensis* wurde jüngst eine kritische Rolle der hochkonservierten Reste Pro und Leu gezeigt, die sich 21 bzw. 14 Positionen oberhalb des Asp-reichen Motives befinden.<sup>[3f]</sup> Die entsprechende L72A-Variante von SaS ergab kein lösliches Protein, während P65A eine Enzymausbeute ähnlich dem Wildtyp ergab, aber die Aktivität mit  $\text{Mg}^{2+}$  und  $\text{Mn}^{2+}$  signifikant abfiel. Wie in der Kristallstruktur von SdS zu sehen ist,<sup>[17d]</sup> sind diese beiden Reste an der Verbindung der Helices C und D lokalisiert (Abbildung S24) und haben vermutlich strukturelle Bedeutung. In CAS ist die zu Pro61 korrespondierende Position natürlicherweise mit Ala besetzt. In diesem Fall zeigt die A64P-Variante geringere Aktivität als der Wildtyp, allerdings nur mit  $\text{Mg}^{2+}$ , wohingegen kein Effekt mit  $\text{Mn}^{2+}$  festzustellen ist.

Ein hochkonserviertes Glu, das in  $>93\%$  der bakteriellen TS präsent ist, ist in SaS durch Gln160 besetzt. In SdS ist der entsprechende Rest an der Bindung des Metallcofaktors beteiligt (Abbildung S25). Während die Genexpression der Q160E-Variante von SaS gut funktionierte, zeigte das Enzym weder mit  $\text{Mg}^{2+}$  noch mit  $\text{Mn}^{2+}$  Aktivität. Für CAS ergab der umgekehrte Austausch (E179Q) eine stark reduzierte Aktivität mit beiden Metallkationen und die E179K-Variante war inaktiv. Ein interessantes Strukturmotiv der SdS ist eine Salzbrücke zwischen einem hochkonservierten Arg144 und einem weniger konservierten Glu192. Wir haben kürzlich für SpS gezeigt, dass die D217E-Mutation in der Salzbrücke (Arg169 und Asp217) in Kombination mit  $\text{Mn}^{2+}$  zu Inaktivität führt, während mit  $\text{Mg}^{2+}$  erhöhte Aktivität folgt.<sup>[3f]</sup> Die entsprechenden Reste in SaS (Arg145 und Glu193) wurden mit dem Ziel einer Verkürzung der Salzbrücke durch R145K- oder E193D-Austausch mutiert, wodurch sich eine reduzierte Aktivität (mit  $\text{Mg}^{2+}$ ) oder kompletter Aktivitätsverlust ergab

(mit  $\text{Mn}^{2+}$ ). Für die R145M-Variante wurde lediglich eine leicht erniedrigte Aktivität mit beiden Metallcofaktoren gefunden. Von besonderem Interesse ist die Beobachtung, dass sowohl SpS<sup>[3]</sup> als auch CAS natürlicherweise eine kurze Salzbrücke unter Beteiligung von Asp anstelle des üblichen Glu aufweisen und beide Enzyme mit  $\text{Mn}^{2+}$  effizienter als mit  $\text{Mg}^{2+}$  sind. Für CAS führt die D212E-Mutation zu einer stark reduzierten Aktivität mit  $\text{Mg}^{2+}$  und  $\text{Mn}^{2+}$ . Diese Daten lassen einen Einfluss der Länge der Salzbrücke, vermutlich durch Modulation des Neigungswinkels zwischen den Helices G und F, auf die Architektur des aktiven Zentrums vermuten, der Konsequenzen für die Metallbindung hat. Eine kurze Salzbrücke mit Beteiligung von Asp scheint die Katalyse durch  $\text{Mn}^{2+}$  zu fördern, während eine lange Salzbrücke  $\text{Mg}^{2+}$ -Bindung bevorzugt. Es sind aber weitere Experimente mit anderen TS erforderlich, um die Verallgemeinerbarkeit dieser Befunde zu belegen.

Ein hochkonserviertes Pro wurde 22 Positionen unterhalb des PP-Sensors identifiziert. In der SdS ist dieser Rest am Boden von Helix H lokalisiert und hat vermutlich eine wichtige strukturelle Funktion (Abbildung S26). In einigen TS ist die entsprechende Position mit Thr oder Ser besetzt, aber die P201T-Variante von SaS zeigte signifikant reduzierte Aktivität mit beiden Metallcofaktoren.

SaS wurde weiterhin bezüglich eines pH-Effekts durch eine Änderung von pH 7.4, wie in den oben beschriebenen Experimenten verwendet, nach pH 8.2 untersucht. Während sich keine signifikante Änderung des Produktspektrums für das Wildtypenzym in Kombination mit  $\text{Mg}^{2+}$  ergab, lieferten Inkubationen mit  $\text{Mn}^{2+}$  ein neues Nebenprodukt (Abbildung S3). Die Verbindung wurde isoliert und per NMR-Spektroskopie (Tabelle S5 und Abbildungen S27–S33) als Thunbergol (**3**) identifiziert. Die absolute Konfiguration von (1*R*,4*S*)-**3** wurde auf Basis des Drehwertes ( $[\alpha]_{\text{D}}^{20} = -48$ ,  $c$  0.85,  $\text{CHCl}_3$ ) durch Vergleich mit (1*S*,4*R*)-**3** aus *Pseudotsuga menziesii* ( $[\alpha]_{\text{D}}^{20} = +75.2$ ,  $c$  1.2,  $\text{CHCl}_3$ )<sup>[18]</sup> nachgewiesen, was ein weiteres Beispiel für eine bakterielle TS etabliert, die das andere Enantiomer als in Pflanzen produziert.<sup>[1,9b,19]</sup> Verbindung **3** kann über dasselbe Intermediat **C** wie **1** gebildet werden (Schema 2), was durch dieselbe Konfiguration des Stereozentrums an C14 für beide Produkte unterstützt wird. Auch mechanistisch zeigt sich die Bildung von **1** und **3** über **C** als gemeinsames Intermediat: Inkubation von (2-<sup>2</sup>H)DMAPP mit IPP, GGPPS und SaS gefolgt von GC-MS-Analyse des Produktes **3** deckte dieselbe 1,2-Hydridverschiebung von **A** nach **B** wie für **1** gefunden auf (Abbildung S34), wiederum mit einer Verteilung der Markierung aus C16 und C17 (Abbildung S35). Wie für **1** beobachtet zeigte die enzymatische Umsetzung von (*R*)- und (*S*)-(1-<sup>13</sup>C,1-<sup>2</sup>H)GGPP mit SaS auch für **3** eine stereoselektive Wanderung des 1-*pro-S*-Wasserstoffs im Schritt nach **C** (Abbildung S36).

Keines der von SaS und CAS identifizierten Diterpene konnte in Duftstoffextrakten von *A. albata* identifiziert werden, wohingegen von Spiroviolen in unserer früheren Studie berichtet wurde,<sup>[3c]</sup> was die Vermutung nahelegt, dass beide Enzyme in Laborkulturen nicht exprimiert werden. Alternativ könnte **1** durch ein genetisch geclustertes Cytochrom P450 zu einem unbekanntem Produkt oxidiert werden (Abbildung S37 und Tabelle S6).

Zusammenfassend haben wir die Produkte von zwei DTS aus *A. albata* identifiziert, von denen eines die ungewöhnliche Struktur von Spiroalbaten aufwies. Während die generellen Prinzipien der Terpenbiosynthese gut verstanden sind, geben die kürzlich erhaltenen Daten aus Isotopenmarkierungsexperimenten, Enzymkristallisationen und -mutagenesen sowie aus Variation der Inkubationsbedingungen detailliertere Einblicke, die in Zukunft Vorhersagen ermöglichen könnten, wie ein Zugang zu neuen Terpenen möglich ist. Die Phylogenie bakterieller TS (Abbildung S1) zeigt, dass die Produkte vieler Enzyme heute bekannt sind, es gibt aber auch viele dunkle Regionen für weitere Forschung an dieser interessanten Enzymklasse.

## Danksagung

Diese Arbeit wurde durch die DFG (DI1536/7-1) und den Fonds der Chemischen Industrie mit einem Promotionsstipendium an J.R. gefördert. Wir danken Paolina Garbeva (Wageningen) für *Serratia plymuthica* PRI-2C.

## Interessenkonflikt

Die Autoren erklären, dass keine Interessenkonflikte vorliegen.

**Stichwörter:** Biosynthese · Enzymmechanismen · Isotope · Terpene · Terrestrische Mikroorganismen

**Zitierweise:** *Angew. Chem. Int. Ed.* **2018**, *57*, 3238–3241  
*Angew. Chem.* **2018**, *130*, 3292–3296

- [1] J. S. Dickschat, *Nat. Prod. Rep.* **2016**, *33*, 87.
- [2] D. E. Cane, C. Pargellis, *Arch. Biochem. Biophys.* **1987**, *254*, 421.
- [3] a) A. Meguro, Y. Motoyoshi, K. Teramoto, S. Ueda, Y. Totsuka, Y. Ando, T. Tomita, S.-Y. Kim, T. Kimura, M. Igarashi, R. Sawa, T. Shinada, M. Nishiyama, T. Kuzuyama, *Angew. Chem. Int. Ed.* **2015**, *54*, 4353; *Angew. Chem.* **2015**, *127*, 4427; b) Y. Yamada, T. Kuzuyama, M. Komatsu, K. Shin-ya, S. Omura, D. E. Cane, H. Ikeda, *Proc. Natl. Acad. Sci. USA* **2015**, *112*, 857; c) P. Rabe, J. Rinkel, E. Dolja, T. Schmitz, B. Nubbemeyer, T. H. Luu, J. S. Dickschat, *Angew. Chem. Int. Ed.* **2017**, *56*, 2776; *Angew. Chem.* **2017**, *129*, 2820; d) J. S. Dickschat, J. Rinkel, P. Rabe, A. B. Kashkooli, H. J. Bouwmeester, *Beilstein J. Org. Chem.* **2017**, *13*, 1770; e) J. Rinkel, P. Rabe, X. Chen, T. G. Köllner, F. Chen, J. S. Dickschat, *Chem. Eur. J.* **2017**, *23*, 10501; f) J. Rinkel, L. Lauterbach, J. S. Dickschat, *Angew. Chem. Int. Ed.* **2017**, *56*, 16385; *Angew. Chem.* **2017**, *129*, 16603.
- [4] K. Tomita, Y. Hoshino, T. Miyaki, *Int. J. Syst. Bacteriol.* **1993**, *43*, 297.
- [5] J. S. Dickschat, K. A. K. Pahirulzaman, P. Rabe, T. A. Klapschinski, *ChemBioChem* **2014**, *15*, 810.
- [6] P. Rabe, L. Barra, J. Rinkel, R. Riclea, C. A. Citron, T. A. Klapschinski, A. Janusko, J. S. Dickschat, *Angew. Chem. Int. Ed.* **2015**, *54*, 13448; *Angew. Chem.* **2015**, *127*, 13649.
- [7] P. Rabe, J. Rinkel, B. Nubbemeyer, T. G. Köllner, F. Chen, J. S. Dickschat, *Angew. Chem. Int. Ed.* **2016**, *55*, 15420; *Angew. Chem.* **2016**, *128*, 15646.
- [8] a) I. Burkhardt, T. Siemon, M. Henrot, L. Studt, S. Rösler, B. Tudzynski, M. Christmann, J. S. Dickschat, *Angew. Chem. Int. Ed.* **2016**, *55*, 8748; *Angew. Chem.* **2016**, *128*, 8890.

- [9] a) J. Rinkel, P. Rabe, P. Garbeva, J. S. Dickschat, *Angew. Chem. Int. Ed.* **2016**, *55*, 13593; *Angew. Chem.* **2016**, *128*, 13791; b) P. Rabe, T. Schmitz, J. S. Dickschat, *Beilstein J. Org. Chem.* **2016**, *12*, 1839.
- [10] a) J. W. Cornforth, R. H. Cornforth, G. Popjak, L. Yengoyan, *J. Biol. Chem.* **1966**, *241*, 3970; b) H. V. Thulasiram, C. D. Poulter, *J. Am. Chem. Soc.* **2006**, *128*, 15819.
- [11] J. W. Cornforth, R. H. Cornforth, C. Donninger, G. Popjak, *Proc. R. Soc. London Ser. B* **1966**, *163*, 492.
- [12] R. Schwabe, I. Farkas, H. Pfander, *Helv. Chim. Acta* **1988**, *71*, 292.
- [13] T. Kato, M. Suzuki, T. Kobayashi, B. P. Moore, *J. Org. Chem.* **1980**, *45*, 1126.
- [14] L. C. Tarshis, M. Yan, C. D. Poulter, J. C. Sacchettini, *Biochemistry* **1994**, *33*, 10871.
- [15] J. Jiang, X. He, D. E. Cane, *Nat. Chem. Biol.* **2007**, *3*, 711.
- [16] D. W. Christianson, *Chem. Rev.* **2017**, *117*, 11570.
- [17] a) M. Seemann, G. Z. Zhai, J. W. de Kraker, C. M. Paschall, D. W. Christianson, D. E. Cane, *J. Am. Chem. Soc.* **2002**, *124*, 7681; b) M. Seemann, G. Zhai, K. Umezawa, D. Cane, *J. Am. Chem. Soc.* **1999**, *121*, 591; c) P. Baer, P. Rabe, C. A. Citron, C. C. D. O. Mann, N. Kaufmann, M. Groll, J. S. Dickschat, *ChemBioChem* **2014**, *15*, 213; d) P. Baer, P. Rabe, K. Fischer, C. A. Citron, T. A. Klapschinski, M. Groll, J. S. Dickschat, *Angew. Chem. Int. Ed.* **2014**, *53*, 7652; *Angew. Chem.* **2014**, *126*, 7783.
- [18] I. Wahlberg, I. Wallin, C. Narbonne, T. Nishida, C. R. Enzell, *Acta Chem. Scand.* **1981**, *35b*, 65.
- [19] L. Ding, H. Goerls, K. Dornblut, W. Lin, A. Maier, H.-H. Fiebig, C. Hertweck, *J. Nat. Prod.* **2015**, *78*, 2963.

Manuskript erhalten: 10. Januar 2018

Veränderte Fassung erhalten: 26. Januar 2018

Akzeptierte Fassung online: 29. Januar 2018

Endgültige Fassung online: 21. Februar 2018





## **Appendix K**

### **An Isotopic Labelling Strategy to Study Cytochrome P450 Oxidations of Terpenes**

*ChemBioChem* **2018**, *19*, 1498–1501.

DOI:10.1002/cbic.201800215



# An Isotopic Labelling Strategy to Study Cytochrome P450 Oxidations of Terpenes

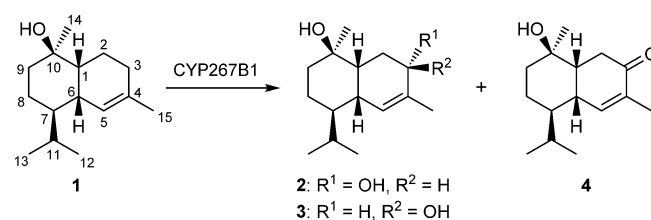
Jan Rinkel,<sup>[a]</sup> Martin Litzenburger,<sup>[b]</sup> Rita Bernhardt,<sup>[b]</sup> and Jeroen S. Dickschat<sup>\*[a]</sup>

The cytochrome P450 monooxygenase CYP267B1 from *Sorangium cellulosum* was applied for the enzymatic oxidation of the sesquiterpene alcohols T-muurolol and isodauc-8-en-11-ol. Various isotopically labelled geranyl and farnesyl diphosphates were used for product identification from micro-scale reactions, for the determination of the absolute configurations of unknown compounds, to follow the stereochemical course of a cytochrome P450-catalysed hydroxylation step, and to investigate kinetic isotope effects. Overall, this study demonstrates that isotopically labelled terpene precursors are highly useful to follow cytochrome P450 dependent oxidations of terpenes.

Biologically active terpenoids, such as the chemotherapeutic taxol; ingenol mebutate, which is applied in the treatment of actinic keratoses; or the antimalarial drug artemisinin, are usually polyoxygenated compounds.<sup>[1]</sup> Their biosynthesis proceeds from an oligoprenyl diphosphate (OPP) that is converted by a terpene synthase (TS) into a polycyclic terpene with multiple stereocentres. The TS product is subsequently functionalised by cytochrome P450 monooxygenases (P450s) or other classes of oxidases, and potentially further derivatised, for example, by acyl or methyl transferases. During the past two decades, many TSs have been characterised and are now available for the enantioselective preparation of their respective products.<sup>[2]</sup> The mechanisms of these astonishing enzymes can be investigated by quantum chemical calculations<sup>[3]</sup> or by feeding of isotopically labelled precursors.<sup>[4]</sup> A drawback of the feeding strategy is the intracellular dilution of labelling, which results in complex incorporation patterns that are sometimes difficult to interpret. Alternatively, in vitro experiments with advanced isotopically labelled precursors, such as OPPs, can be performed.<sup>[5]</sup> We have recently synthesised various labelled OPPs, including enantioselectively deuterated compounds, to study the mechanisms of TSs.<sup>[6]</sup> In many cases, the TS genes are clustered with genes coding for P450s; this suggests their common involvement in the biosynthesis of an oxidised terpene. P450s for terpene oxidations have been investigated in their biosynthetic context, that is, with their natural substrates,<sup>[4b,7]</sup> but biosynthetically unrelated TSs and P450s can also be used in different

combinations for selective oxidations that are chemically difficult to address.<sup>[8]</sup> Herein, we report on the development of a TS/P450 catalyst system for the enzymatic oxidation of sesquiterpenes and the application of isotopically labelled terpene precursors to study the P450-catalysed reactions.

In previous work, a total of 21 P450 genes were cloned and expressed from *Sorangium cellulosum* So ce56 and investigated for their activity towards fatty acids.<sup>[9]</sup> In this study, nine of these bacterial P450s (Table S1 in the Supporting Information) were tested in combination with a truncated bovine adrenodoxin (Adx<sub>4-108</sub>) and adrenodoxin reductase (AdR) as redox partners,<sup>[10]</sup> and the substrate (+)-T-muurolol (**1**), which was prepared by using T-muurolol synthase (TmS) from *Roseiflexus castenholzii* (Scheme 1).<sup>[11]</sup> CYP267B1 from *S. cellulosum* exhibit-



Scheme 1. Oxidation of **1** by CYP267B1 from *S. cellulosum* So ce56.

ed the highest efficiency of the tested enzymes with about 50% conversion of **1** into a mixture of one main and two side products (Figure S1 in the Supporting Information). EI-MS analysis of the main product showed an increase in the molecular ion of 16 Da, in comparison with **1**; this suggested the introduction of a second alcohol function or an epoxide. One of the minor products exhibited a very similar EI mass spectrum, which indicated a stereoisomer, whereas the mass spectrum of the second side product showed a molecular ion that was 14 Da larger, relative to that of **1**; this was in agreement, for example, with the corresponding ketone. P450s often catalyse allylic oxidations, so the products could be diastereomeric alcohols **2** and **3** and ketone **4** (Scheme 1). All three compounds are known,<sup>[12]</sup> so this system is ideal to use to demonstrate how a labelling strategy can be adopted for compound identification in a complex mixture of oxidation products. All 15 isotopomers of (<sup>13</sup>C)farnesyl diphosphate (FPP)<sup>[6a]</sup> were converted by TmS, followed by CYP267B1 oxidation, and <sup>13</sup>C NMR spectroscopic analysis (Figure S2). The most dramatic effect on the chemical shift for the labelled carbon was observed for all three products obtained from (4-<sup>13</sup>C)FPP (yellow dots in Figure S2); thus this key experiment unequivocally identified C4 of FPP, equal to C3 of **1**, as the site of oxidation for all three ox-

[a] J. Rinkel, Prof. Dr. J. S. Dickschat  
Kekulé-Institute of Organic Chemistry and Biochemistry, University of Bonn  
Gerhard-Domagk-Strasse 1, 53121 Bonn (Germany)  
E-mail: dickschat@uni-bonn.de

[b] Dr. M. Litzenburger, Prof. Dr. R. Bernhardt  
Institute of Biochemistry, Saarland University  
Campus, Building B2.2, 66123 Saarbrücken (Germany)

Supporting information and the ORCID identification numbers for the authors of this article can be found under: <https://doi.org/10.1002/cbic.201800215>.

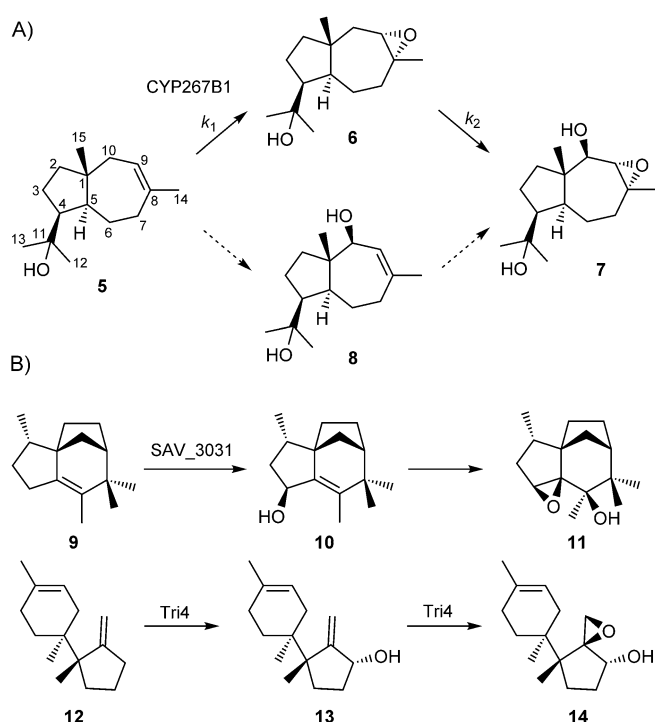
idation products. A comparison of the recorded spectrum with published NMR spectroscopic data<sup>[12]</sup> confirmed alcohol **2** as the main product and its epimer, **3**, and the corresponding ketone, **4**, as side products.

Based on the efficient conversion of **1**, which reflects the earlier observed broad spectrum of substrates from various compound classes,<sup>[13]</sup> CYP267B1 was also tested with the sesquiterpene alcohol (+)-isodauc-8-en-11-ol (**5**); a compound with unknown absolute configuration that is accessible with isodaucenol synthase (IdS) from *Streptomyces venezuelae*.<sup>[14]</sup> Compound **5** was efficiently converted into a main product, with HRMS data pointing to C<sub>15</sub>H<sub>26</sub>O<sub>3</sub>, and a minor compound, C<sub>15</sub>H<sub>26</sub>O<sub>2</sub> (Figure S3). The main product was isolated and its structure was elucidated by NMR spectroscopy as (1*S*\*,4*S*\*,5*S*\*,8*R*\*,9*S*\*,10*R*\*)-8,9-epoxyisodaucan-10,11-diol (**7**; Scheme 2A, Table S2, and Figures S4–S10). The minor product

enzyme binding for **5** ( $K_d = (11.6 \pm 1.0) \mu\text{M}$ ) and **6** ( $K_d = (45 \pm 10) \mu\text{M}$ ). A time course experiment gave the typical concentration curve for **6** as an intermediate (Figure S20), and allowed us to determine the rate constants for the reactions from **5** to **6** ( $k_1 = (0.24 \pm 0.05) \text{min}^{-1}$ ) and from **6** to **7** ( $k_2 = (0.048 \pm 0.005) \text{min}^{-1}$ ). Taken together, the significantly stronger binding and higher rate constant for **5** explain the rapid accumulation of **6** in the beginning of the reaction. Allyl alcohol **8** was not observed, although it cannot be excluded that this compound is also formed, but does not accumulate because of very fast oxidation to **7**.

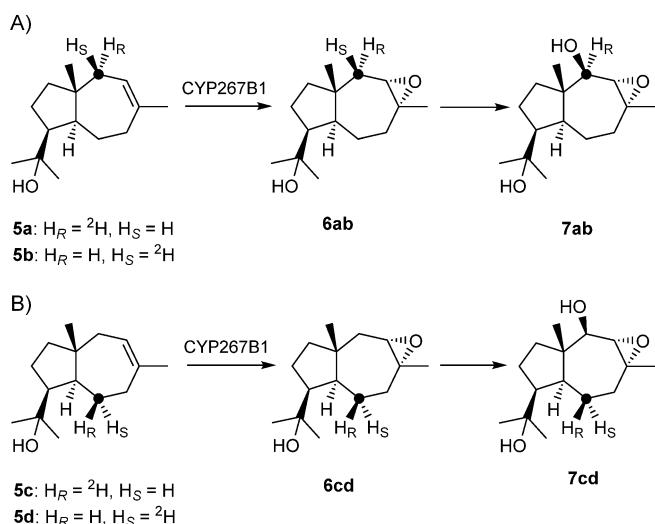
The observation that **5** is first epoxidised to **6** and then hydroxylated to **7** is rather surprising because P450-mediated oxidation at C10 should be easier for the allylic system in **5** than that next to the epoxide in **6**, and has implications for the biosynthesis of other multiply oxidised sesquiterpenoids. Arguably, the oxidation of an olefin first to an allyl alcohol and in a second step to an epoxy alcohol—this sequence also seems generally easier from a synthetic chemist's point of view—represents the usual case (notably, this argument does not address whether epoxidation or allylic hydroxylation is the preferred first step, but after epoxidation the introduction of the alcohol function can no longer make use of the reactive allylic position present in **5**). Corresponding biosynthetic transformations have been described for the conversion of *epi*-isozizaene (**9**) into 4,5-epoxy-2-*epi*-zizaan-6 $\beta$ -ol (**11**) with the participation of P450 SAV\_3031,<sup>[15]</sup> and trichodiene (**12**) into 12,13-epoxy-9,10-trichoan-2 $\alpha$ -ol (**14**) by P450 Tri4 along the biosynthetic pathway towards trichothecene mycotoxins (Scheme 2B),<sup>[16]</sup> whereas for PR toxin a similar question, with respect to the sequence of steps, is under debate.<sup>[17]</sup> The results obtained here demonstrate that predictions grounded on chemical logic are not always correct for P450s as a highly reactive class of enzymes, and multistep oxidations have to be addressed experimentally.

We have recently developed a method for the determination of the absolute configurations of terpenes that makes use of enantioselectively deuterated OPPs. After conversion with a TS, the stereochemical anchor of known absolute configuration in these substrates can be used to determine the relative orientation of other stereocentres in the product.<sup>[6c]</sup> For highly sensitive analysis by HSQC, the enantioselectively deuterated carbon was additionally <sup>13</sup>C-labelled. The absolute configuration of **5** was determined by conversion of (*R*)- and (*S*)-(1-<sup>13</sup>C,1-<sup>2</sup>H)FPP with IdS, followed by HSQC analysis of the products **5a** and **5b**, resulting in the structure of (1*R*,4*S*,5*S*)-**5** (Scheme 3A and Figure S21). Notably, terpene cyclisation requires FPP isomerisation into nerolidyl diphosphate (NPP) to establish the *Z*-configured double bond in **5** in the subsequent ring closure. This two-step cyclisation proceeds with net retention of configuration at C1 of FPP.<sup>[6b,18]</sup> In a second set of experiments, the substrates (*R*)- and (*S*)-(1-<sup>13</sup>C,1-<sup>2</sup>H)geranyl diphosphate (GPP) were elongated into the corresponding isotopomers of FPP in an enzymatic reaction with isopentenyl diphosphate (IPP) and FPP synthase (FPPS); a reaction known to proceed with inversion of configuration at C1 of GPP,<sup>[19]</sup> followed by cyclisation with IdS. HSQC analysis of the products **5c** and **5d** confirmed



**Scheme 2.** P450 oxidations of sesquiterpenes. A) Oxidation of **5** by CYP267B1. B) P450 oxidations in other characterised sesquiterpene biosynthetic pathways.

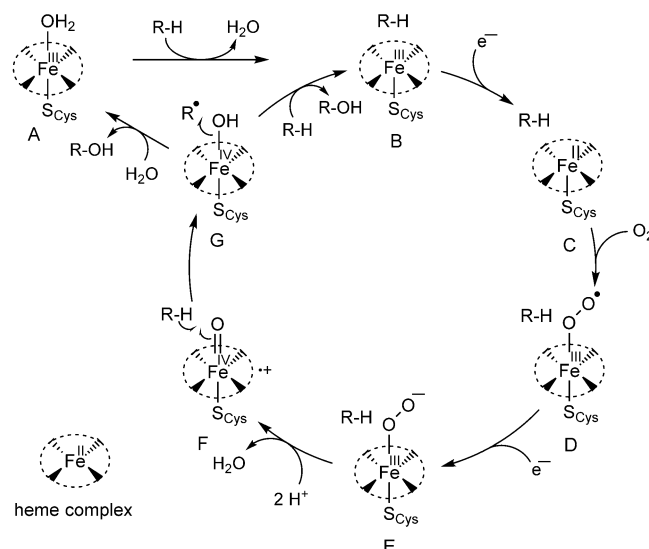
was obtained in too small amounts for isolation, but was assumed to be an intermediate or shunt product towards **7**, such as epoxide **6** or allyl alcohol **8**. The chemical oxidation of **5** with *meta*-chloroperoxybenzoic acid (*m*CPBA) was highly diastereoselective and yielded a compound with the same retention time and EI mass spectrum as those of **6**. Rigorous structure elucidation by NMR spectroscopy confirmed its identity as (1*R*\*,4*S*\*,5*S*\*,8*R*\*,9*S*\*)-8,9-epoxyisodaucan-11-ol (Table S3 and Figures S11–S17). Conversion of **6** with CYP267B1 resulted in the formation of **7**, and thus, identified **6** as an intermediate, rather than a shunt product (Figure S18); this was confirmed by binding studies with CYP267B1 (Figure S19), which revealed



**Scheme 3.** Absolute configuration of **5** and the stereochemical course for oxidation by CYP267B1 to **7**. A) Oxidation of **5a** and **5b** reveals the absolute configuration of **6** and the stereochemical course of the oxidation to **7**. B) Oxidation of **5c** and **5d** shows the absolute configurations of **6** and **7**. Black dots represent  $^{13}\text{C}$ -labelled carbon atoms.

the absolute configuration of **5** (Scheme 3B and Figure S22). Isotopomers **5c** and **5d** were subsequently oxidised by CYP267B1 and the obtained labelled oxidation products **7c** and **7d** were analysed by HSQC, which confirmed the corresponding absolute configuration of (1*S*,4*S*,5*S*,8*R*,9*S*,10*R*)-8,9-epoxyisodaucan-10,11-diol for **7** (Figures S23). Because of the small-scale reactions in these labelling experiments, only the double oxidation product **7** was visible in the HSQC analyses. For **6**, the corresponding absolute configuration of (1*R*,4*S*,5*S*,8*R*,9*S*)-8,9-epoxyisodaucan-11-ol can be assigned. Neither sesquiterpenoid has been reported previously.

The catalytic cycle of P450s<sup>[20]</sup> starts with resting state **A**, with  $\text{Fe}^{3+}$  bound to the protoporphyrin IX prosthetic group, a highly conserved cysteine of the protein, and a water molecule (Scheme 4). If a substrate  $\text{R-H}$  enters the active site, the weakly bound water is replaced (**B**). A one-electron reduction that is directed by a ferredoxin and a ferredoxin reductase (Adx/AdR in our system), with reduced nicotinamide adenine dinucleotide phosphate (NADPH) as an electron donor, results in **C** ( $\text{Fe}^{2+}$ ). Molecular oxygen binds to the free coordination site of  $\text{Fe}^{3+}$  in **D**, followed by another one-electron reduction to **E**. Protonation and elimination of water results in the catalytically active species **F** (compound I). This complex is characterised by a central  $\text{Fe}^{4+}$  with a bound oxo ligand and a delocalised electron in the porphyrin system.<sup>[21]</sup> A hydrogen atom is abstracted from the substrate to result in a radical intermediate (**G**). This radical recombines with the  $\text{Fe}^{4+}$ -bound hydroxy ligand (free radical oxygen rebound mechanism), and the resulting product,  $\text{R-OH}$ , is either replaced by water or another substrate molecule. This mechanism has been experimentally supported by unusually large intrinsic isotope effects for deuterated substrates,<sup>[22]</sup> demonstrating that the radical formation in **G** is usually rate limiting, as well as, in some cases, observed loss of stereochemical information at the oxidised



**Scheme 4.** Catalytic cycle of P450-catalysed oxidations.

carbon,<sup>[22a,b,23]</sup> and occasional allylic transposition of the site of oxidation.<sup>[24]</sup>

For CYP267B1, analysis of the products **7a** and **7b** obtained from (*R*)- and (*S*)-(1- $^{13}\text{C}$ ,1- $^2\text{H}$ )FPP via **5a** and **5b** by means of  $^{13}\text{C}$  NMR spectroscopy and GC-MS revealed a strict retention of configuration for the hydroxylation at C10 (Scheme 3A and Figures S24 and S25). CYP267B1 was also investigated for a kinetic isotope effect. For this purpose, racemic (1- $^2\text{H}$ )FPP was synthesised (Scheme S1) and converted by IdS into a 1:1 mixture of stereoisomers with either the 10-pro-*R* or 10-pro-*S* hydrogen substituted by deuterium (analogous to **5a** and **5b** in Scheme 3A, but without the  $^{13}\text{C}$  label). Subsequent oxidation with CYP267B1 gave about a 1:1 mixture of unlabelled **7** and ( $^2\text{H}$ )-**7** (Figure S26), thus demonstrating that, in contrast to the results from other investigated P450s,<sup>[22]</sup> no kinetic isotope effect was observed for CYP267B1.

In conclusion, CYP267B1 from *S. cellulosum* was investigated in sesquiterpene oxidations. T-Muurolol (**1**) was converted into three oxidation products. We have shown how  $^{13}\text{C}$ -labelling allows the rapid determination of the site of oxidation without product isolation; this offers an appealing strategy for the identification of minor products in complex mixtures. Isodauc-8-en-11-ol (**5**) was efficiently oxidised with a surprising order of steps, that is, first by epoxidation of the double bond and then by hydroxylation at the neighbouring carbon, which went against chemical intuition, but was supported by enzymatic conversion of the synthetic epoxide **6**, binding constants, and kinetic data. The use of stereoselectively deuterated substrates revealed the absolute configurations of **5** and its oxidation products, and gave insights into the stereochemical course of the hydroxylation at C10, which proceeded with strict retention of configuration. This may indicate very fast oxygen rebound after radical formation at the substrate, or even a concerted process without the generation of a radical intermediate. Finally, no deuterium isotope effect was observed; this demonstrates that, for CYP267B1, in contrast to the observa-

tions made with other P450s, hydrogen abstraction from the substrate is not the rate-limiting step. Future experiments in our laboratories with this remarkable enzyme, CYP267B1, will include its application in other terpene oxidations.

## Acknowledgements

This work was funded by grants from the Deutsche Forschungsgemeinschaft (DI1536/7-1 to J.S.D. and BE1343/23-2 to R.B.), and by a PhD fellowship from the Fonds der Chemischen Industrie to J.R.

## Conflict of Interest

The authors declare no conflict of interest.

**Keywords:** C–H activation · enzyme catalysis · isotope effects · reaction mechanisms · terpenoids

- [1] a) M. C. Wani, H. L. Taylor, M. E. Wall, P. Coggon, A. T. McPhail, *J. Am. Chem. Soc.* **1971**, *93*, 2325; b) S. M. Ogbourne, P. G. Parsons, *Fitoterapia* **2014**, *98*, 36; c) Y. Tu, *Nat. Med.* **2011**, *17*, 1217.
- [2] a) M. B. Quin, C. M. Flynn, C. Schmidt-Dannert, *Nat. Prod. Rep.* **2014**, *31*, 1449; b) J. Degenhardt, T. G. Köllner, J. Gershenzon, *Phytochemistry* **2009**, *70*, 1621; c) Q. Jia, T. G. Köllner, J. Gershenzon, F. Chen, *Trends Plant Sci.* **2018**, *23*, 121; d) J. S. Dickschat, *Nat. Prod. Rep.* **2016**, *33*, 87; e) X. Chen, T. G. Köllner, Q. Jia, A. Norris, B. Santhanam, P. Rabe, J. S. Dickschat, G. Shaulsky, J. Gershenzon, F. Chen, *Proc. Natl. Acad. Sci. USA* **2016**, *113*, 12132.
- [3] a) D. J. Tantillo, *Angew. Chem. Int. Ed.* **2017**, *56*, 10040; *Angew. Chem.* **2017**, *129*, 10172; b) D. T. Major, *ACS Catal.* **2017**, *7*, 5461; c) J.-Y. Chow, B.-X. Tian, G. Ramamoorthy, B. S. Hillerich, R. D. Seidel, S. C. Almo, M. P. Jacobson, C. D. Poulter, *Proc. Natl. Acad. Sci. USA* **2015**, *112*, 5661.
- [4] a) Y. Ye, A. Minami, A. Mandi, C. Liu, T. Taniguchi, T. Kuzuyama, K. Monde, K. Gomi, H. Oikawa, *J. Am. Chem. Soc.* **2015**, *137*, 11846; b) M. Okada, Y. Matsuda, T. Mitsunashi, S. Hoshino, T. Mori, K. Nakagawa, Z. Quan, B. Qin, H. Zhang, F. Hayashi, H. Kawaide, I. Abe, *J. Am. Chem. Soc.* **2016**, *138*, 10011; c) J. S. Dickschat, H. B. Bode, T. Mahmud, R. Müller, S. Schulz, *J. Org. Chem.* **2005**, *70*, 5174.
- [5] D. E. Cane, C. Abell, P. H. M. Harrison, B. R. Hubbard, C. T. Kane, R. Lattman, J. S. Oliver, S. W. Weiner, *Philos. Trans. R. Soc. Lond. B* **1991**, *332*, 123.
- [6] a) P. Rabe, L. Barra, J. Rinkel, R. Riclea, C. A. Citron, T. A. Klapschinski, A. Janusko, J. S. Dickschat, *Angew. Chem. Int. Ed.* **2015**, *54*, 13448; *Angew. Chem.* **2015**, *127*, 13649; b) J. Rinkel, P. Rabe, P. Garbeva, J. S. Dickschat, *Angew. Chem. Int. Ed.* **2016**, *55*, 13593; *Angew. Chem.* **2016**, *128*, 13791; c) P. Rabe, J. Rinkel, E. Dolja, T. Schmitz, B. Nubbemeyer, T. H. Luu, J. S. Dickschat, *Angew. Chem. Int. Ed.* **2017**, *56*, 2776; *Angew. Chem.* **2017**, *129*, 2820; d) T. Mitsunashi, J. Rinkel, M. Okada, I. Abe, J. S. Dickschat, *Chem. Eur. J.* **2017**, *23*, 10053; e) J. Rinkel, L. Lauterbach, P. Rabe, J. S. Dickschat, *Angew. Chem. Int. Ed.* **2018**, *57*, 3238; *Angew. Chem.* **2018**, *130*, 3292.
- [7] a) B. Zhao, X. Lin, L. Lei, D. C. Lamb, S. L. Kelly, M. R. Waterman, D. E. Cane, *J. Biol. Chem.* **2008**, *283*, 8183; b) R. Quaderer, S. Omura, H. Ikeda, D. E. Cane, *J. Am. Chem. Soc.* **2006**, *128*, 13036; c) A. Schiffrin, T. T. B. Ly, N. Günnewich, J. Zapp, V. Thiel, S. Schulz, F. Hannemann, Y. Khatri, R. Bernhardt, *ChemBioChem* **2015**, *16*, 337.
- [8] a) J. A. Dietrich, Y. Yoshikuni, K. J. Fisher, F. X. Woolard, D. Ockey, D. J. McPhee, N. S. Renninger, M. C. Y. Chang, D. Baker, J. D. Keasling, *ACS Chem. Biol.* **2009**, *4*, 261; b) A. Schiffrin, M. Litzenburger, M. Ringle, T. T. B. Ly, R. Bernhardt, *ChemBioChem* **2015**, *16*, 2624; c) T. T. B. Ly, A. Schiffrin, B. D. Nguyen, R. Bernhardt, *J. Agric. Food Chem.* **2017**, *65*, 3891; d) M. Putkaradze, M. Litzenburger, A. Abdulmughni, M. Milhim, E. Brill, F. Hannemann, R. Bernhardt, *Appl. Microbiol. Biotechnol.* **2017**, *101*, 8379.
- [9] Y. Khatri, F. Hannemann, K. M. Ewen, D. Pistorius, O. Perlova, N. Kagawa, A. O. Brachmann, R. Müller, R. Bernhardt, *Chem. Biol.* **2010**, *17*, 1295.
- [10] a) K. M. Ewen, M. Ringle, R. Bernhardt, *IUBMB Life* **2012**, *64*, 506; b) M. Litzenburger, F. Kern, Y. Khatri, R. Bernhardt, *Drug Metab. Dispos.* **2015**, *43*, 392.
- [11] a) P. Rabe, J. S. Dickschat, *Angew. Chem. Int. Ed.* **2013**, *52*, 1810; *Angew. Chem.* **2013**, *125*, 1855; b) P. Rabe, T. Schmitz, J. S. Dickschat, *Beilstein J. Org. Chem.* **2016**, *12*, 1839.
- [12] a) C.-L. Wu, S.-C. Chien, S.-Y. Wang, Y.-H. Kuo, S.-T. Chang, *Holzforchung* **2005**, *59*, 620; b) L. Ding, R. Pfoh, S. Rühl, S. Qin, H. Laatsch, *J. Nat. Prod.* **2009**, *72*, 99.
- [13] a) F. Kern, Y. Khatri, M. Litzenburger, R. Bernhardt, *Drug. Metabol. Dispos.* **2016**, *44*, 495; b) M. Litzenburger, R. Bernhardt, *Appl. Microbiol. Biotechnol.* **2016**, *100*, 4447.
- [14] P. Rabe, J. Rinkel, T. A. Klapschinski, L. Barra, J. S. Dickschat, *Org. Biomol. Chem.* **2016**, *14*, 158.
- [15] S. Takamatsu, X. Lin, A. Nara, M. Komatsu, D. E. Cane, H. Ikeda, *Microb. Biotechnol.* **2011**, *4*, 184.
- [16] T. Tokai, H. Koshino, N. Takahashi-Ando, M. Sato, M. Fujimura, M. Kimura, *Biochem. Biophys. Res. Commun.* **2007**, *353*, 412.
- [17] a) R. Riclea, J. S. Dickschat, *Angew. Chem. Int. Ed.* **2015**, *54*, 12167; *Angew. Chem.* **2015**, *127*, 12335; b) P. I. Hidalgo, E. Poirier, R. V. Ullan, J. Piqueras, L. Meslet-Cladiere, E. Coton, M. Coton, *Appl. Microbiol. Biotechnol.* **2017**, *101*, 2043.
- [18] D. Arigoni, *Pure Appl. Chem.* **1975**, *41*, 219.
- [19] J. W. Cornforth, R. H. Cornforth, G. Popjak, L. Yengoyan, *J. Biol. Chem.* **1966**, *241*, 3970.
- [20] B. Meunier, S. P. de Visser, S. Shaik, *Chem. Rev.* **2004**, *104*, 3947.
- [21] J. Rittle, M. T. Green, *Science* **2010**, *330*, 933.
- [22] a) J. T. Groves, G. A. McClusky, *Biochem. Biophys. Res. Commun.* **1978**, *81*, 154; b) R. E. White, J. P. Miller, L. V. Favreau, A. Bhattacharyya, *J. Am. Chem. Soc.* **1986**, *108*, 6024; c) R. H. McClanahan, A. C. Huitric, P. G. Pearson, J. C. Desper, S. D. Nelson, *J. Am. Chem. Soc.* **1988**, *110*, 1979.
- [23] M. H. Gelb, D. C. Heimbrook, P. Mätkönen, S. G. Sligar, *Biochemistry* **1982**, *21*, 370.
- [24] J. T. Groves, D. V. Subramanian, *J. Am. Chem. Soc.* **1984**, *106*, 2177.

Manuscript received: April 26, 2018

Accepted manuscript online: April 26, 2018

Version of record online: June 7, 2018

## Appendix L

### **Two Bacterial Diterpene Synthases from *Allokutzneria albata* Produce Bonnadiene, Phomopsene, and Allokutznerene**

Lukas Lauterbach, Jan Rinkel and Prof. Dr. Jeroen S. Dickschat\*

*Angew. Chem. Int. Ed.* **2018**, *57*, 8280–8283; *Angew. Chem.* **2018**, *130*, 8412–8415.

DOI:10.1002/anie.201803800 and DOI:10.1002/ange.201803800.

Reprinted from *Angew. Chem. Int. Ed.* **2018**, *57*, 8280–8283 and *Angew. Chem.* **2018**, *130*, 8412–8415 with kind permission from John Wiley and Sons.

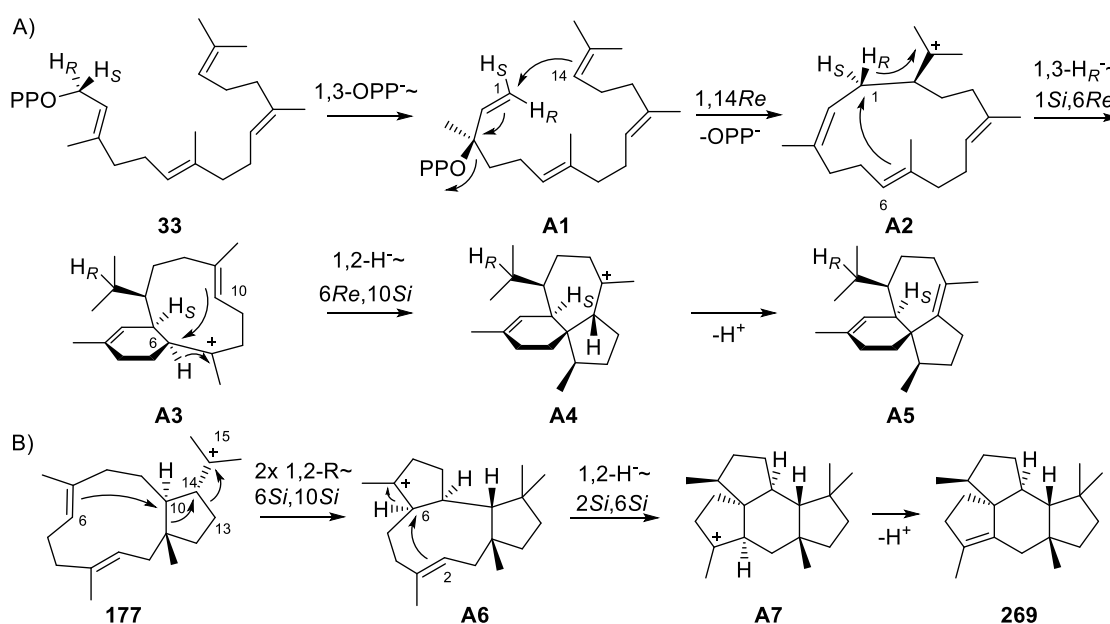
The synthesis of (*E*)- and (*Z*)-(4-<sup>13</sup>C,4-<sup>2</sup>H)IPP was performed by me. Additionally, the isolation and separation of products obtained from the bacterial phomopsene synthase was done by Lukas Lauterbach and me.

## Introduction

As discussed in Chapter 16, the product of the fungal phomopsene (**267**) synthase<sup>[270]</sup> from *Phomopsis amygdali* is mechanistically related to a family of di- and sesterterpenes, also including spiroviolene (**183**) and cattleyene (**274**). Therefore, the producing TSs might share a similar folding of their substrates to guide the cyclisation cascade into a defined direction. Since the CLSA headspace analysis of the actinomycete *Allokutzneria albata* resulted in the production of unknown diterpenes that could not be attributed to the already characterised DTSS for spiroalbatene (**228**) and cembrene A (**230**), this publication describes the characterisation of two other DTSS from the same organism, thereby exploring the rich diterpene metabolism of *A. albata*. One of these DTSS turned out to be the first bacterial phomopsene synthase, which demonstrates the widespread occurrence of **267** both in fungi and in bacteria.

## Summary

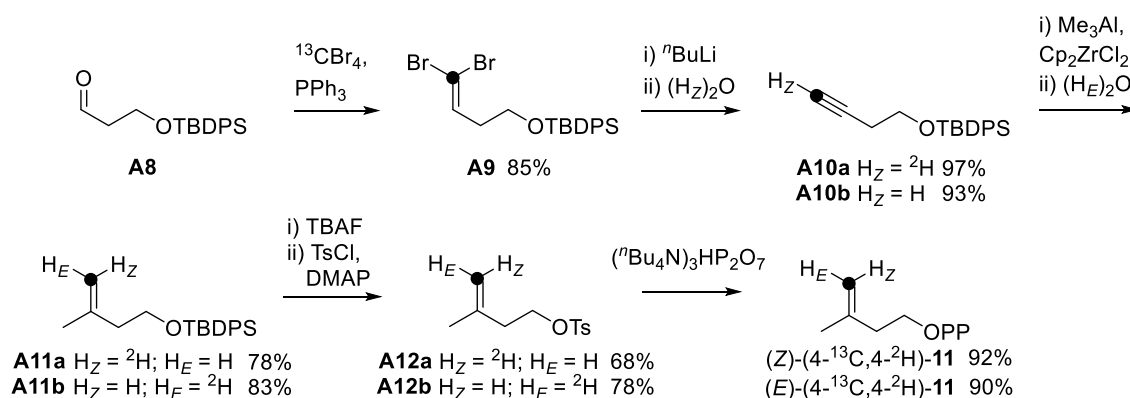
Two DTSS from *A. albata* were cloned, heterologously expressed in *E. coli* and characterised as a bonnadiene (**A5**, Scheme A1) synthase (BdS) and a phomopsene (**267**) synthase (PmS).<sup>[259]</sup> Their cyclisation mechanisms were studied in depth by isotopic labelling experiments. The proposed mechanism for BdS starts with isomerisation of GGPP to GLPP (**A1**), which undergoes 1,14-cyclisation to yield the macrocyclic cation **A2**. After a 1,3-hydride shift, a second ring is formed to give **A3**, followed by a 1,2-hydride migration and a 6,10-cyclisation yielding **A4**. Bonnadiene (**A5**), which contains an unprecedented carbon skeleton, is formed after deprotonation. This mechanism was challenged by conversion of all twenty (<sup>13</sup>C<sub>1</sub>)GGPP isotopomers to observe the incorporation of label into the expected positions. The two hydride migrations were followed by deuterium labelling.



**Scheme A1.** Proposed cyclisation mechanisms towards A) bonnadiene (**A5**) and B) allokutznerene (**269**).



The product identification from PmS proved more challenging, as a compound mixture of **267** and another related diterpene hydrocarbon was observed. The two products were separable on AgNO<sub>3</sub>-impregnated preparative silica TLC plates, establishing the structure of the second product as the new diterpene allokutznerene (**269**). Its formation is explainable from cation **177** by the known ring contraction- ring expansion sequence followed by an attack of C-6 to yield **A6**. This step deviates from the mechanism towards **267**, which was investigated in detail by in vitro conversion of deuterated IPP isotopologues<sup>[258c]</sup> and involves an attack of C-2. After a 1,2-hydride shift in **A6**, a 2,6-ring closure gives access to **A7** yielding **269** after deprotonation. Also with PmS, the mechanistic proposal was solidified by conversion of the singly labelled GGPP isotopomers and deuterated substrates to address the hydride shifts towards **267** and **269**. Conversion of both products with *m*CPBA yielded two oxidised epoxy-derivatives. Since because of signal overlay only one position in **A5** could be used to determine its absolute configuration by the existing library of enantioselectively deuterated substrates, (*E*)- and (*Z*)-(4-<sup>13</sup>C,4-<sup>2</sup>H)IPP were synthesised as shown in Scheme A2 based on the previously described route to non-<sup>13</sup>C labelled, selectively deuterated IPPs (Chapter 11). Starting from aldehyde **A8**, a Corey-Fuchs reaction<sup>[258b]</sup> using <sup>13</sup>CBr<sub>4</sub>, which was synthesised from relatively inexpensive (<sup>13</sup>C)methyl iodide,<sup>[258a]</sup> led to the dibromide **A9**, which was converted to the alkynes **A10** with the possibility to introduce deuterium in a D<sub>2</sub>O-based work-up. Negishi's carboalumination yielded methylated **A11** in a stereoselective way, in which the hydrogen from the work-up occupies the H<sub>E</sub> position at the olefin.<sup>[245]</sup> Deprotection and conversion to the tosylates **A12** without intermediary purification prevented a substantial loss of the volatile alcohol.<sup>[258c]</sup> The target substrates were then accessed by a substitution reaction with tris(tetrabutylammonium) hydrogen diphosphate.<sup>[198a]</sup>



**Scheme A2.** Synthesis of (*E*)- and (*Z*)-(4-<sup>13</sup>C,4-<sup>2</sup>H)IPP. TBAF: tetra-*n*-butylammonium fluoride; DMAP: 4-dimethylaminopyridine.

By using these substrates to elongate DMAPP in a known stereochemical course with FPPS and GGPPS, followed by conversion with BdS, three more stereochemical anchors of known absolute configurations could be assigned for **A5** with high sensitivity because of the additional <sup>13</sup>C label. Thereby, the synthesised IPPs not only proved useful in this case, but also extended the labelling toolbox for follow-up studies (Chapter 13+).



## Biosynthesis

International Edition: DOI: 10.1002/anie.201803800  
German Edition: DOI: 10.1002/ange.201803800Two Bacterial Diterpene Synthases from *Allokutzneria albata* Produce Bonnadiene, Phomopsene, and Allokutznerene

Lukas Lauterbach, Jan Rinkel, and Jeroen S. Dickschat\*

Dedicated to the Rheinische Friedrich-Wilhelms University of Bonn on the occasion of its 200<sup>th</sup> anniversary

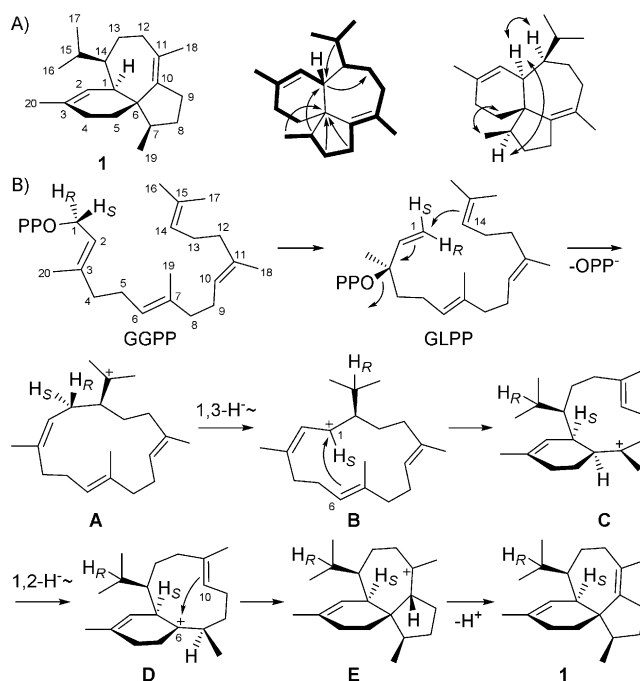
**Abstract:** Two diterpene synthases from *Allokutzneria albata* were studied for their products, resulting in the identification of the new compound bonnadiene from the first enzyme. Although phylogenetically unrelated to fungal phomopsene synthase, the second enzyme produced a mixture of phomopsene and a biosynthetically linked new compound, allokutznerene, as well as spiroviolene. Both enzymes were subjected to in-depth mechanistic studies involving isotopic labelling experiments, metal-cofactor variation, and site-directed mutagenesis. Oxidation products of phomopsene and allokutznerene are also discussed.

With well over 80,000 known compounds, terpenoids comprise the largest class of natural products. Nature uses a strikingly simple approach for their biosynthesis from dimethylallyl diphosphate (DMAPP) and isopentenyl PP (IPP), which are fused to form the oligomers geranyl PP (GPP), farnesyl PP (FPP), geranylgeranyl PP (GGPP), geranylgeranyl PP (GGPP), geranylgeranyl PP (GGPP), and longer oligoprenyl PPs, followed by cyclisation by terpene synthases (TSs).<sup>[1]</sup> The type I of these astonishing enzymes ionises the substrate by PP abstraction and provides a hydrophobic cavity in which a cationic cascade that is prompted by the inherent substrate reactivity results in a structurally complex, often polycyclic carbon skeleton with multiple stereocentres being formed in just one enzymatic step.<sup>[2]</sup> The products of the first characterised bacterial type I TSs were mono- and sesquiterpenes,<sup>[3]</sup> while recent research has resulted in the identification of structurally and biosynthetically more interesting diterpenes.<sup>[4]</sup> Herein, we describe two diterpene synthases (DTSs) from the soil actinomycete *Allokutzneria albata*, which led to the identification of two compounds with novel skeletons, as well as phomopsene, a diterpene previously reported from the fungus *Phomopsis amygdali*.<sup>[5]</sup>

GC/MS analysis of headspace extracts from *A. albata* showed the emission of diterpenes by this bacterium (Figure S1 in the Supporting Information). Two other recently identified DTSs from *A. albata* did not account for their production,<sup>[4g]</sup> which raises questions about their biosynthetic

origin. The genes for two uncharacterised TSs were cloned into the expression vector pYE-Express (for accession numbers, see the Supporting Information).<sup>[6]</sup> After gene expression in *Escherichia coli*, the recombinant proteins were purified (Figure S2) and incubated with GPP, FPP, GGPP, and GFPP. Both enzymes accepted GGPP but no other substrate. One of the enzymes formed the observed headspace constituents.

The first enzyme converted GGPP into a diterpene hydrocarbon (**1**, Scheme 1) with a new 6-7-5-membered spirotricyclic skeleton, the structure of which was elucidated by NMR spectroscopy (Table S2, Figures S3–S9). The structure was further supported by <sup>13</sup>C,<sup>13</sup>C-COSY that was recorded from (<sup>13</sup>C<sub>20</sub>)-**1** prepared from (<sup>13</sup>C<sub>15</sub>)FPP<sup>[7]</sup> and (<sup>13</sup>C<sub>5</sub>)DMAPP<sup>[4g]</sup> with isopentenyl diphosphate isomerase (IDI) from *Serratia plymuthica*<sup>[4g]</sup> and GGPP synthase (GGPPS) from *Streptomyces cyaneofuscatus*<sup>[4c]</sup> (Figure S10). Based on the ancient name of Bonn (Bonna, founded 12 BC during the regency of emperor Augustus), we propose the



**Scheme 1.** Bonnadiene (**1**). A) Structure elucidation (bold: <sup>1</sup>H,<sup>1</sup>H-COSY correlations, single-headed arrows: HMBC correlations, double-headed arrows: NOESY correlations) and carbon numbering (indicating the origin of each carbon from GGPP by same number). B) Cyclisation of GGPP to **1** by Bds.

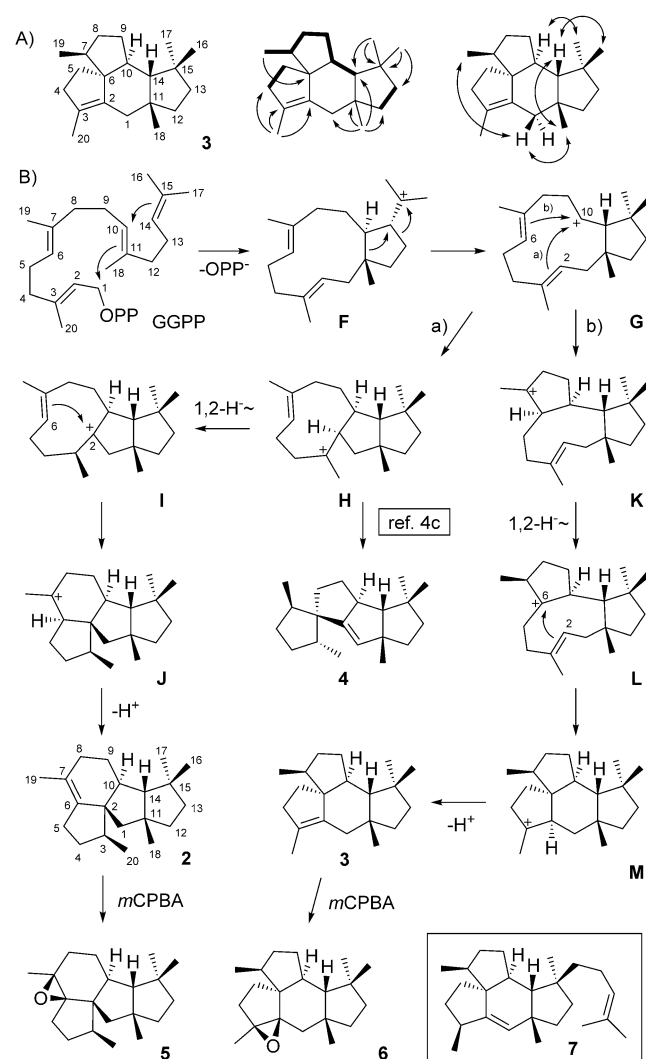
[\*] L. Lauterbach, J. Rinkel, Prof. Dr. J. S. Dickschat  
Kekulé-Institut für Organische Chemie und Biochemie, Rheinische  
Friedrich-Wilhelms-Universität Bonn  
Gerhard-Domagk-Straße 1, 53121 Bonn (Germany)  
E-mail: dickschat@uni-bonn.de

Supporting information and the ORCID identification number(s) for the author(s) of this article can be found under:  
<https://doi.org/10.1002/anie.201803800>.

name bonnadiene for **1** and bonnadiene synthase (BdS) for its corresponding DTS. A plausible cyclisation mechanism to **1** starts with the isomerisation of GGPP to (*R*)-geranylinalyl-PP (GLPP), a step that is required to explain the *Z*-configured double bond in the six-membered ring of **1**. As discussed for the corresponding isomerisation<sup>[8,9]</sup> of FPP and as reported for other diterpene cyclisations,<sup>[4d]</sup> GLPP is formed with *syn*-allylic transposition of PP with a distinct stereochemical fate for the 1-*pro-R* ( $H_R$ ) and 1-*pro-S* ( $H_S$ ) hydrogen atoms (note that a cyclisation via (*S*)-GLPP requires a positional exchange of  $H_R$  and  $H_S$  in this intermediate and would lead to the enantiomer of **1**). The first ring closure to **A** proceeds by *anti*- $S_N2'$  attack of C14 at C1 (GGPP numbering), and depending on the conformation of the macrocycle,  $H_R$  is closer to the cationic centre than  $H_S$  and will migrate in the 1,3-hydride shift to **B**. A subsequent ring closure to **C** is followed by a suprafacial 1,2-hydride shift to **D** and a third ring closure to **E** with attack of the cationic centre in **D** from the opposite face to the leaving hydride (the **C**-to-**E** transformation may be concerted). A final deprotonation step yields **1**. This mechanism was verified by incubation of all 20 isotopomers of ( $^{13}\text{C}$ )GGPP<sup>[4c,7]</sup> with BdS, resulting in the detection of the label by  $^{13}\text{C}$ -NMR in the expected positions in all cases (Figure S11), which excluded any surprising carbon backbone rearrangements as uncovered in other diterpene cyclisations.<sup>[4c,10]</sup> The incubation of (*R*)- and (*S*)-( $1\text{-}^2\text{H}$ )GGPP<sup>[4c]</sup> with BdS and product analysis by GC/MS confirmed the specific migration of  $H_R$  in the conversion of **A** into **B** through inspection of the fragment ion arising from loss of the *iPr* group (Figure S12). The 1,2-hydride shift from **C** to **D** was followed by using ( $3\text{-}^{13}\text{C}, 2\text{-}^2\text{H}$ )FPP,<sup>[11]</sup> which was elongated with IPP and GGPPs to ( $7\text{-}^{13}\text{C}, 6\text{-}^2\text{H}$ )GGPP and subsequently cyclised with BdS. With this substrate, the hydride shift resulted in a direct  $^{13}\text{C}$ - $^2\text{H}$  connection, as indicated by a triplet in the  $^{13}\text{C}$ -NMR (Figure S13). The absolute configuration of **1** was determined by using enantioselectively deuterated (*R*)- and (*S*)-( $1\text{-}^{13}\text{C}, 1\text{-}^2\text{H}$ )FPP,<sup>[4c]</sup> which were elongated with IPP and GGPPs under inversion of configuration at C1, followed by cyclisation with BdS (Figure S14). The known configurations at the deuterated carbons can be used to deduce the relative orientations of all the other stereocentres in **1**, which pointed to the absolute configuration as in Scheme 1. The diastereotopic hydrogen atoms at C9 of **1** showed identical chemical shifts, and therefore, previously synthesised (*R*)- and (*S*)-( $1\text{-}^{13}\text{C}, 1\text{-}^2\text{H}$ )GGPP<sup>[4c]</sup> could not be used to support the assigned absolute configuration of **1**. As an alternative, (*E*)- and (*Z*)-( $4\text{-}^{13}\text{C}, 4\text{-}^2\text{H}$ )IPP were synthesised (Scheme S1) and used to elongate DMAPP with FPP synthase (FPPS) from *Streptomyces coelicolor*<sup>[12]</sup> and GGPPs with known stereochemical course (*Si* attack at C4 of IPP),<sup>[13]</sup> followed by BdS cyclisation (Figure S15). This strategy gave access to three more stereochemical anchors in **1** for which the diastereotopic hydrogen atoms showed different chemical shifts, thus confirming the absolute configuration of **1**.

The second TS produced a mixture of two main diterpenes and a few trace compounds (Figure S1) that were not separable by column chromatography. Therefore, the product mixture was treated with *mCPBA*, which yielded two pairs of diastereomeric epoxides (Figure S16). Two of these com-

pounds were isolated and identified by NMR spectroscopy as phomopsene epoxide (**5**, Table S3, Figures S17–S23) and the epoxide **6** (Table S4, Figures S24–S30) of an unknown diterpene (Scheme 2). The terpene hydrocarbons were finally separated using silver nitrate impregnated silica gel.<sup>[14]</sup> The main compound was identical to phomopsene (**2**; Table S5), the product of a fungal DTS from *Phomopsis amygdali* (PaPS),<sup>[5]</sup> thus identifying the TS as a bacterial phomopsene synthase (PmS). The structure of the second product was elucidated by NMR (Table S6, Figures S31–S37) as a diterpene with a new skeleton, which was named allokutnerene (**3**) after the producing organism. Its structure was further supported by  $^{13}\text{C}, ^{13}\text{C}$ -COSY with the mixture of labelled **2** and **3** prepared with PmS from ( $^{13}\text{C}_{20}$ )GGPP (Figure S38). Traces of spiroviolene (**4**) were also identified by GC/MS and comparison to an authentic standard,<sup>[4c]</sup> which reflects the



**Scheme 2.** Products of bacterial phomopsene synthase (PmS).

A) Structure elucidation of **3** (bold:  $^1\text{H}, ^1\text{H}$ -COSY correlations, single-headed arrows: HMBC correlations, double-headed arrows: NOESY correlations) and carbon numbering (indicating the origin of each carbon from GGPP by same number). B) Cyclisation of GGPP to **2**, **3**, and **4** by PmS and chemical oxidation to **5** and **6** with *meta*-chloroperbenzoic acid (*mCPBA*). The box shows the known sesterterpene mangicdiene (**7**).<sup>[17]</sup>

close phylogeny between PmS and spiroviolene synthase (SvS) from *Streptomyces violens* (Figure S39).<sup>[4c]</sup>

The biosynthesis of all three compounds starts from GGPP by 1,11- and 10,14-cyclisation to **F**, followed by a ring expansion and ring contraction to the secondary cation **G**, which is also an intermediate towards the fungal compound variediene from *Emericella varicolor*.<sup>[15]</sup> **G** likely reacts in a concerted manner through attack of one of the two remaining double bonds to the cationic centre to give either **H** (path a) or **K** (path b). The mechanism for the formation of **4** from **H** was recently studied in detail,<sup>[4c]</sup> but **H** can also give access to **2** through a 1,2-hydride shift to **I**, ring closure to **J**, and deprotonation. A similar sequence explains the formation of **3** from **K** through 1,2-hydride migration to **L**, ring closure to **M**, and deprotonation. The mechanism for **2** was recently investigated by enzymatic synthesis of several deuterated GGPP isotopomers from deuterated IPPs, followed by cyclisation to **2** with PaPS and GC/MS analysis.<sup>[16]</sup> The data interpretation in this study proved to be difficult because assumptions about the EI-MS fragmentation mechanism of **2** had to be made to localise the incorporation sites of deuterium. The experiments for the cyclisation mechanism towards **3** described here simultaneously allowed a reinvestigation of the mechanism for **2**. Incubation of all 20 isotopomers of (<sup>13</sup>C)GGPP with PmS resulted in the incorporation of the label into the corresponding carbons of **2** and **3** in all cases, which provided evidence for the skeletal rearrangement from **F** to **G** (Figures S40 and S41). The conversion of (3-<sup>13</sup>C,2-<sup>2</sup>H)GGPP<sup>[4c]</sup> with PmS demonstrated the 1,2-hydride shift from **H** to **I** in the biosynthesis of **2** and the deprotonation from C2 towards **3** (Figure S42). Correspondingly, the incubation of (3-<sup>13</sup>C,2-<sup>2</sup>H)FPP<sup>[11]</sup> with IPP, GGPPS, and PmS indicated the 1,2-hydride shift from **K** to **L** in the cyclisation to **3** and the deprotonation from C6 in the cyclisation to **2** (Figure S43). In summary, these experiments confirmed the cyclisation mechanism for **2**<sup>[16]</sup> and gave detailed insight into a related mechanism for **3**.

The incubations of (*R*)- and (*S*)-(1-<sup>13</sup>C,1-<sup>2</sup>H)GGPP<sup>[4d]</sup> (Figure S44), (*R*)- and (*S*)-(1-<sup>13</sup>C,1-<sup>2</sup>H)FPP<sup>[4c]</sup> (Figure S45), (*R*)- and (*S*)-(1-<sup>13</sup>C,1-<sup>2</sup>H)GPP<sup>[4c]</sup> (Figure S46), and (*E*)- and (*Z*)-(4-<sup>13</sup>C,4-<sup>2</sup>H)IPP (Figures S47 and S48) with PmS all pointed to the absolute configurations for **2** and **3** shown in Scheme 2. Notably, the absolute configuration of **2** is the same as for the fungal compound, which is reflected by the same sign of optical rotation ( $[\alpha]_{\text{D}}^{25} = -27.2$ ,  $c$  0.42, CHCl<sub>3</sub>; lit.<sup>[5]</sup>  $[\alpha]_{\text{D}}^{25} = -97$ ,  $c$  0.27, CHCl<sub>3</sub>). The absolute configurations of **2** and **3** correspond to that of **4** from *S. violens*, in agreement with their common formation via **G** and the close relationship between PmS and SvS (Figure S39). Compound **3** is structurally related to the sesterterpene mangicdiene (**7**) from *Fusarium graminearum*, which was obtained in high yield from genetically engineered *E. coli*.<sup>[17]</sup>

Type I TSs exhibit a trinuclear (Mg<sup>2+</sup>)<sub>3</sub> cluster in the active site that is bound by highly conserved residues of the Asp-rich motif DDX(X)D and the NSE triad ND-(L,I,V)XSXXE.<sup>[18]</sup> The PP of the substrate coordinates to the Mg<sup>2+</sup> cations and forms hydrogen bonds to the PP sensor,<sup>[19]</sup> a highly conserved Arg that is usually found 46 positions upstream of the NSE triad. Mg<sup>2+</sup> can often be

substituted with Mn<sup>2+</sup>,<sup>[4fg,20]</sup> which is also the case for BdS and PmS with a loss of approximately half of the activity (Figures S49 and S50). Both enzymes were also studied by site-directed mutagenesis (SDM). We recently identified a salt bridge in the crystal structure of selinadiene synthase (SdS)<sup>[19]</sup> between Arg144 on helix F and Glu192 on helix G (Figure S51). These residues are conserved in most type I TSs, with the notable observation that for previously investigated enzymes, the usual Glu on helix G gave a higher activity with Mg<sup>2+</sup>, while enzymes with an Asp showed higher activity with Mn<sup>2+</sup>.<sup>[4fg]</sup> BdS (Glu202) and PmS (Glu182) contain a Glu in the corresponding position, in agreement with their higher activity with Mg<sup>2+</sup>. SDM of the salt bridge of BdS (R154K, R154M, E202D) and of PmS (R137K, R137M) produced inactive enzyme variants with both metal cofactors (Figures S49 and S50). An unusual residue of BdS is Lys169, a position that is often occupied by Glu (>93% of bacterial TS) or sometimes Asp (ca. 3%), but rarely ever by Lys.<sup>[4g]</sup> This residue coordinates to Mg<sup>2+</sup> in SdS (Glu159, Figure S51).<sup>[19]</sup> The BdS variant K169E showed only a slightly decreased activity with Mg<sup>2+</sup>, but was almost inactive with Mn<sup>2+</sup>. Although the application of Pearson's concept of hard and soft acids and bases<sup>[21]</sup> to explain ambident reactivity has recently been criticised,<sup>[22]</sup> it is still useful to assess the stability of metal complexes. The hard-hard interaction between Mg<sup>2+</sup> and the carboxylate function in the K169E variant may stabilise the trinuclear metal cluster to a similar extent as the wildtype enzyme, while the softer Mn<sup>2+</sup> is much better stabilised by the amino group of the original Lys than by the carboxylate in the K169E variant. The structure of SdS shows a Pro61 at the bottom of helix C and a Val68 at the start of helix D that serves as a spacer between helices D and G (Figure S52).<sup>[19]</sup> Both residues are highly conserved in type I TSs and are critical for the functionality of other DTSS.<sup>[4fg]</sup> SDM of these residues in BdS (P66A, V73A) and PmS (P58A, L65A) gave inactive enzyme variants in three cases (only the L65A variant of PmS showed around 10% residual activity), thus demonstrating that the critical role of these residues is generalisable.

In summary, we have identified the products of two DTSS from *A. albata* and studied their enzyme mechanisms through a combination of methods including the use of isotopically labelled substrates<sup>[23]</sup> and site-directed mutagenesis.<sup>[24]</sup> The first enzyme (BdS) produced bonnadiene (**1**), a diterpene with a new skeleton, and the second enzyme (PmS) generated a mixture of the fungal diterpene phomopsene (**2**),<sup>[5]</sup> the new compound allokutznerene (**3**), and the known diterpene spiroviolene (**4**).<sup>[4c]</sup> The mixture of **2–4** is emitted by agar plate cultures of *A. albata*, thus suggesting that PmS is expressed under laboratory culture conditions. The production of a fungal compound by PmS was rather surprising and represents the first case of a bacterial type I DTSS making the same product as a fungal enzyme.

## Acknowledgements

This work was funded by the DFG (DI1536/7-1) and by a PhD fellowship of the Fonds der Chemischen Industrie (to JR).

## Conflict of interest

The authors declare no conflict of interest.

**Keywords:** biosynthesis · enzyme mechanisms · isotopes · NMR spectroscopy · terpenes

**How to cite:** *Angew. Chem. Int. Ed.* **2018**, *57*, 8280–8283  
*Angew. Chem.* **2018**, *130*, 8412–8415

- 
- [1] J. S. Dickschat, *Nat. Prod. Rep.* **2016**, *33*, 87.  
[2] D. J. Tantillo, *Angew. Chem. Int. Ed.* **2017**, *56*, 10040; *Angew. Chem.* **2017**, *129*, 10172.  
[3] a) C. Nakano, H.-K. Kim, Y. Ohnishi, *ChemBioChem* **2011**, *12*, 1988; b) C. Nakano, H.-K. Kim, Y. Ohnishi, *ChemBioChem* **2011**, *12*, 2403; c) D. E. Cane, J. K. Sohng, C. R. Lamberson, S. M. Rudnicki, Z. Wu, M. D. Lloyd, J. S. Oliver, B. R. Hubbard, *Biochemistry* **1994**, *33*, 5846; d) X. Lin, R. Hopson, D. E. Cane, *J. Am. Chem. Soc.* **2006**, *128*, 6022.  
[4] a) S.-Y. Kim, P. Zhao, M. Igarashi, R. Sawa, T. Tomita, M. Nishiyama, T. Kuzuyama, *Chem. Biol.* **2009**, *16*, 736; b) Y. Yamada, T. Kuzuyama, M. Komatsu, K. Shin-ya, S. Omura, D. E. Cane, H. Ikeda, *Proc. Natl. Acad. Sci. USA* **2015**, *112*, 857; c) P. Rabe, J. Rinkel, E. Dolja, T. Schmitz, B. Nubbemeyer, T. H. Luu, J. S. Dickschat, *Angew. Chem. Int. Ed.* **2017**, *56*, 2776; *Angew. Chem.* **2017**, *129*, 2820; d) J. Rinkel, P. Rabe, X. Chen, T. G. Köllner, F. Chen, J. S. Dickschat, *Chem. Eur. J.* **2017**, *23*, 10501; e) J. S. Dickschat, J. Rinkel, P. Rabe, A. Beyraghdar Kashkooli, H. J. Bouwmeester, *Beilstein J. Org. Chem.* **2017**, *13*, 1770; f) J. Rinkel, L. Lauterbach, J. S. Dickschat, *Angew. Chem. Int. Ed.* **2017**, *56*, 16385; *Angew. Chem.* **2017**, *129*, 16603; g) J. Rinkel, L. Lauterbach, P. Rabe, J. S. Dickschat, *Angew. Chem. Int. Ed.* **2018**, *57*, 3238; *Angew. Chem.* **2018**, *130*, 3292.  
[5] T. Toyomasu, A. Kaneko, T. Tokiwano, Y. Kanno, Y. Kanno, R. Niida, S. Miura, T. Nishioka, C. Ikeda, W. Mitsuhashi, T. Dairi, T. Kawano, H. Oikawa, N. Kato, T. Sassa, *J. Org. Chem.* **2009**, *74*, 1541.  
[6] J. S. Dickschat, K. A. K. Pahirulzaman, P. Rabe, T. A. Klapschinski, *ChemBioChem* **2014**, *15*, 810.  
[7] P. Rabe, L. Barra, J. Rinkel, R. Riclea, C. A. Citron, T. A. Klapschinski, A. Janusko, J. S. Dickschat, *Angew. Chem. Int. Ed.* **2015**, *54*, 13448; *Angew. Chem.* **2015**, *127*, 13649.  
[8] D. Arigoni, *Pure Appl. Chem.* **1975**, *41*, 219.  
[9] J. Rinkel, P. Rabe, P. Garbeva, J. S. Dickschat, *Angew. Chem. Int. Ed.* **2016**, *55*, 13593; *Angew. Chem.* **2016**, *128*, 13791.  
[10] A. Meguro, Y. Motoyoshi, K. Teramoto, S. Ueda, Y. Totsuka, Y. Ando, T. Tomita, S.-Y. Kim, T. Kimura, M. Igarashi, R. Sawa, T. Shinada, M. Nishiyama, T. Kuzuyama, *Angew. Chem. Int. Ed.* **2015**, *54*, 4353; *Angew. Chem.* **2015**, *127*, 4427.  
[11] T. A. Klapschinski, P. Rabe, J. S. Dickschat, *Angew. Chem. Int. Ed.* **2016**, *55*, 10141; *Angew. Chem.* **2016**, *128*, 10296.  
[12] P. Rabe, J. Rinkel, B. Nubbemeyer, T. G. Köllner, F. Chen, J. S. Dickschat, *Angew. Chem. Int. Ed.* **2016**, *55*, 15420; *Angew. Chem.* **2016**, *128*, 15646.  
[13] J. W. Cornforth, R. H. Cornforth, G. Popjak, L. Yengoyan, *J. Biol. Chem.* **1966**, *241*, 3970.  
[14] a) A. S. Gupta, S. Dev, *J. Chromatogr.* **1963**, *12*, 189; b) M. v. Schantz, S. Juvonen, R. Hemming, *J. Chromatogr.* **1965**, *20*, 618.  
[15] B. Qin, Y. Matsuda, T. Mori, M. Okada, Z. Quan, T. Mitsuhashi, T. Wakimoto, I. Abe, *Angew. Chem. Int. Ed.* **2016**, *55*, 1658; *Angew. Chem.* **2016**, *128*, 1690.  
[16] S. S. Shinde, A. Minami, Z. Chen, T. Tokiwano, T. Toyomasu, N. Kato, T. Sassa, H. Oikawa, *J. Antibiot.* **2017**, *70*, 632.  
[17] G. Bian, Y. Han, A. Hou, Y. Yuan, X. Liu, Z. Deng, T. Liu, *Metab. Eng.* **2017**, *42*, 1.  
[18] D. W. Christianson, *Chem. Rev.* **2017**, *117*, 11570.  
[19] P. Baer, P. Rabe, K. Fischer, C. A. Citron, T. A. Klapschinski, M. Groll, J. S. Dickschat, *Angew. Chem. Int. Ed.* **2014**, *53*, 7652; *Angew. Chem.* **2014**, *126*, 7783.  
[20] a) A. J. Poulouse, R. Croteau, *Arch. Biochem. Biophys.* **1978**, *191*, 400; b) D. E. Cane, Q. Xue, B. Fitzsimons, *Biochemistry* **1996**, *35*, 12369.  
[21] R. G. Pearson, *J. Am. Chem. Soc.* **1963**, *85*, 3533.  
[22] H. Mayr, M. Breugst, A. R. Ofial, *Angew. Chem. Int. Ed.* **2011**, *50*, 6470; *Angew. Chem.* **2011**, *123*, 6598.  
[23] J. S. Dickschat, *Eur. J. Org. Chem.* **2017**, 4872.  
[24] M. Seemann, G. Z. Zhai, J. W. de Kraker, C. M. Paschall, D. W. Christianson, D. E. Cane, *J. Am. Chem. Soc.* **2002**, *124*, 7681.

Manuscript received: March 29, 2018

Accepted manuscript online: May 14, 2018

Version of record online: June 6, 2018

## Terpene

Deutsche Ausgabe: DOI: 10.1002/ange.201803800  
Internationale Ausgabe: DOI: 10.1002/anie.201803800Zwei bakterielle Diterpensynthesen aus *Allokutzneria albata* für Bonnadien sowie für Phomopsen und Allokutzneren

Lukas Lauterbach, Jan Rinkel und Jeroen S. Dickschat\*

Der Rheinischen Friedrich-Wilhelms-Universität Bonn zum 200. Jahrestag gewidmet

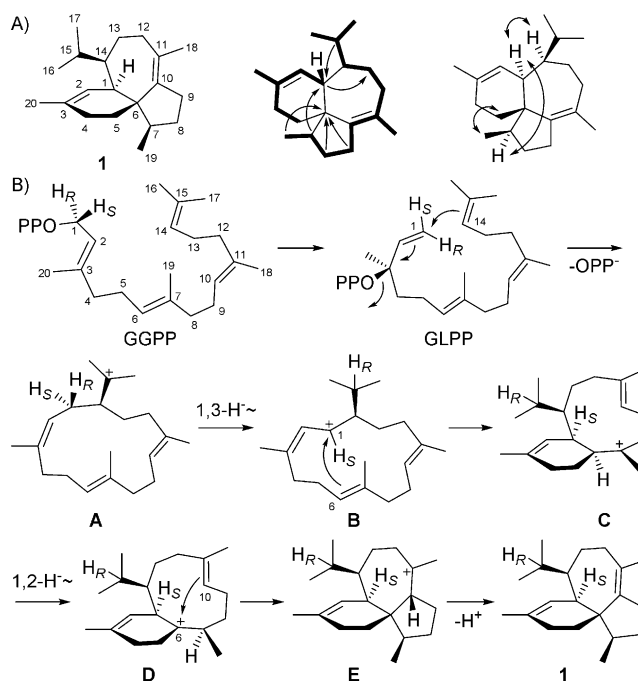
**Abstract:** Zwei Diterpensynthesen aus *Allokutzneria albata* wurden auf ihre Produkte untersucht. Das Produkt des ersten Enzyms wurde als die neue Verbindung Bonnadien identifiziert. Obwohl das zweite Enzym phylogenetisch nicht mit der pilzlichen Phomopsen-Synthese in Verbindung steht, produzierte es eine Mischung aus Phomopsen und einer biosynthetisch verwandten neuen Verbindung, Allokutzneren, sowie Spiroviolen. Beide Enzyme wurden im Detail durch Isotopenmarkierungsexperimente, Variation des Metallkofaktors und ortsgerichtete Mutagenese auf ihren Mechanismus untersucht. Oxidationsprodukte von Phomopsen und Allokutzneren werden ebenfalls diskutiert.

Mit gut 80000 bekannten Verbindungen stellen Terpene die größte Naturstoffklasse dar. Die Natur hat einen faszinierend einfachen Zugang für ihre Biosynthese aus Dimethylallyldiphosphat (DMAPP) und Isopentenyl-PP (IPP) entwickelt, die unter Bildung der Oligomere Geranyl-PP (GPP), Farnesyl-PP (FPP), Geranylgeranyl-PP (GGPP), Geranylarnesyl-PP (GFPP) und längerer Oligoprenyl-PPs verknüpft und anschließend durch Terpensynthasen (TSs) cyclisiert werden.<sup>[1]</sup> Der Typ I dieser erstaunlichen Enzyme ionisiert das Substrat durch PP-Abstraktion und stellt eine hydrophobe Kavität zur Verfügung, in der eine durch die inhärente Reaktivität getriebene kationische Kaskade durchlaufen wird, die in einem einzigen enzymatischen Schritt in einem strukturell komplexen, oft polycyclischen Kohlenstoffgerüst mit multiplen Stereozentren resultiert.<sup>[2]</sup> Die Produkte der ersten charakterisierten bakteriellen TS des Typs I waren Mono- und Sesquiterpene,<sup>[3]</sup> während die jüngste Forschung zur Identifizierung von strukturell und biosynthetisch interessanteren Diterpenen führte.<sup>[4]</sup> Wir berichten hier über zwei Diterpensynthesen (DTSS) aus dem Bodenbakterium *Allokutzneria albata* und die Identifizierung von zwei Produkten mit neuen Kohlenstoffgerüsten sowie von Phomopsen, einem bekannten Diterpen, das zuvor aus dem Pilz *Phomopsis amygdali* erhalten wurde.<sup>[5]</sup>

Die GC/MS-Analyse von Duftstoffextrakten von *A. albata* zeigte die Emission von Diterpenen durch dieses

Bakterium (Abbildung S1 der Hintergrundinformationen (SI)). Zwei andere jüngst identifizierte DTSS aus *A. albata* waren für ihre Produktion nicht verantwortlich,<sup>[4g]</sup> was die Frage nach ihrem biosynthetischen Ursprung aufwarf. Die Gene für zwei uncharakterisierte TSs wurden in den Expressionsvektor pYE-Express kloniert (für Zugangscodes siehe SI).<sup>[6]</sup> Nach Genexpression in *Escherichia coli* wurden die rekombinanten Enzyme gereinigt (Abbildung S2) und mit GPP, FPP, GGPP sowie GFPP inkubiert. Beide Enzyme akzeptierten GGPP, aber keines der anderen Substrate. Eines der Enzyme bildete die im Duftstoffextrakt beobachteten Verbindungen.

Das erste Enzym konvertierte GGPP in einen Diterpen-Kohlenwasserstoff (**1**; Schema 1) mit einem neuen 6-7-5-spirotricyclischen Gerüst, dessen Struktur durch NMR-Spektroskopie aufgeklärt wurde (Tabelle S2, Abbildungen S3–S9). Die Struktur wurde weiter durch <sup>13</sup>C,<sup>13</sup>C-COSY von (<sup>13</sup>C<sub>20</sub>)-**1** gestützt, das aus (<sup>13</sup>C<sub>15</sub>)FPP<sup>[7]</sup> und (<sup>13</sup>C<sub>5</sub>)DMAPP<sup>[4g]</sup> mit der Isopentenylidiphosphat-Isomerase (IDI) aus *Serratia plymu-*



**Scheme 1.** Bonnadien (**1**). A) Strukturaufklärung (fett: <sup>1</sup>H,<sup>1</sup>H-COSY-Korrelationen, einfache Pfeile: HMBC-Korrelationen, Doppelpfeile: NOESY-Korrelationen) und Kohlenstoffnummerierung (zeigt den Ursprung für jedes Kohlenstoffatom aus GGPP durch dieselbe Nummer). B) Cyclisierung von GGPP zu **1** durch Bds.

[\*] L. Lauterbach, J. Rinkel, Prof. Dr. J. S. Dickschat  
Kekulé-Institut für Organische Chemie und Biochemie  
Rheinische Friedrich-Wilhelms-Universität Bonn  
Gerhard-Domagk-Straße 1, 53121 Bonn (Deutschland)  
E-Mail: dickschat@uni-bonn.de

Hintergrundinformationen und die Identifikationsnummer (ORCID) eines Autors sind unter:  
<https://doi.org/10.1002/ange.201803800> zu finden.

*thica*<sup>[48]</sup> und der GGPP-Synthase (GGPPS) aus *Streptomyces cyaneofuscatus*<sup>[4c]</sup> erhalten wurde (Abbildung S10). In Anlehnung an den historischen Namen der Stadt Bonn (Bonna, gegründet 12 v. Chr. während der Regentschaft von Kaiser Augustus) schlagen wir den Namen Bonnadien für **1** und Bonnadien-Synthase (BdS) für die zugehörige DTS vor.

Ein plausibler Cyclisierungsmechanismus zu **1** startet mit der Isomerisierung von GGPP zu (*R*)-Geranylinalyl-PP (GLPP), einem Schritt, der notwendig ist, um die Bildung der *Z*-konfigurierten Doppelbindung im sechsgliedrigen Ring von **1** zu erklären. Wie für die entsprechende Isomerisierung von FPP diskutiert<sup>[8,9]</sup> und wie für andere Diterpencyclisierungen berichtet,<sup>[4d]</sup> wird GLPP mit *syn*-allylischer Transposition von PP mit definiertem stereochemischem Verlauf für die Wasserstoffatome 1-*pro-R* ( $H_R$ ) und 1-*pro-S* ( $H_S$ ) gebildet (man beachte, dass die Cyclisierung via (*S*)-GLPP einen Positionstausch von  $H_R$  und  $H_S$  in diesem Intermediat erfordert und zum Enantiomer von **1** führen würde). Der erste Ringschluss zu **A** verläuft mit *anti-S<sub>N</sub>2'*-Angriff von C14 an C1 (GGPP-Nummerierung), und abhängig von der Konformation des Makrocyclus ist  $H_R$  näher am kationischen Zentrum als  $H_S$  und wandert in einer 1,3-Hydridverschiebung unter Bildung von **B**. Auf einen anschließenden Ringschluss zu **C** folgen eine suprafaciale 1,2-Hydridverschiebung zu **D** und ein dritter Ringschluss zu **E** unter Angriff des kationischen Zentrums in **D** von der dem austretenden Hydrid gegenüberliegenden Seite (die Transformation von **C** zu **E** kann dann konzertiert ablaufen). Ein finaler Deprotonierungsschritt ergibt **1**.

Dieser Mechanismus wurde durch Inkubation von allen 20 Isotopomeren von (<sup>13</sup>C)GGPP<sup>[4c,7]</sup> mit BdS verifiziert, die in allen Fällen zur Detektion der Markierung durch <sup>13</sup>C-NMR-Spektroskopie in der erwarteten Position führte (Abbildung S11) und überraschende Gerüstumlagerungen ausschloss, die jüngst für andere Diterpencyclisierungen aufgedeckt wurden.<sup>[4c,10]</sup> Die Inkubation von (*R*)- und (*S*)-(1-<sup>2</sup>H)GGPP<sup>[4c]</sup> mit BdS und Produktanalyse per GC/MS bestätigten die spezifische Wanderung von  $H_R$  in der Reaktion von **A** zu **B** durch Inspektion des Fragmentions, das durch Abspaltung der *iPr*-Gruppe gebildet wird (Abbildung S12). Die 1,2-Hydridwanderung von **C** zu **D** wurde mit (3-<sup>13</sup>C,2-<sup>2</sup>H)FPP<sup>[11]</sup> verfolgt, das mit IPP und GGPPS zu (7-<sup>13</sup>C,6-<sup>2</sup>H)GGPP verlängert und danach mit BdS cyclisiert wurde. Mit diesem Substrat ergab die Hydridverschiebung ein Produkt mit direkter <sup>13</sup>C-<sup>2</sup>H-Bindung, die durch ein Triplett im <sup>13</sup>C-NMR-Spektrum manifestiert wurde (Abbildung S13).

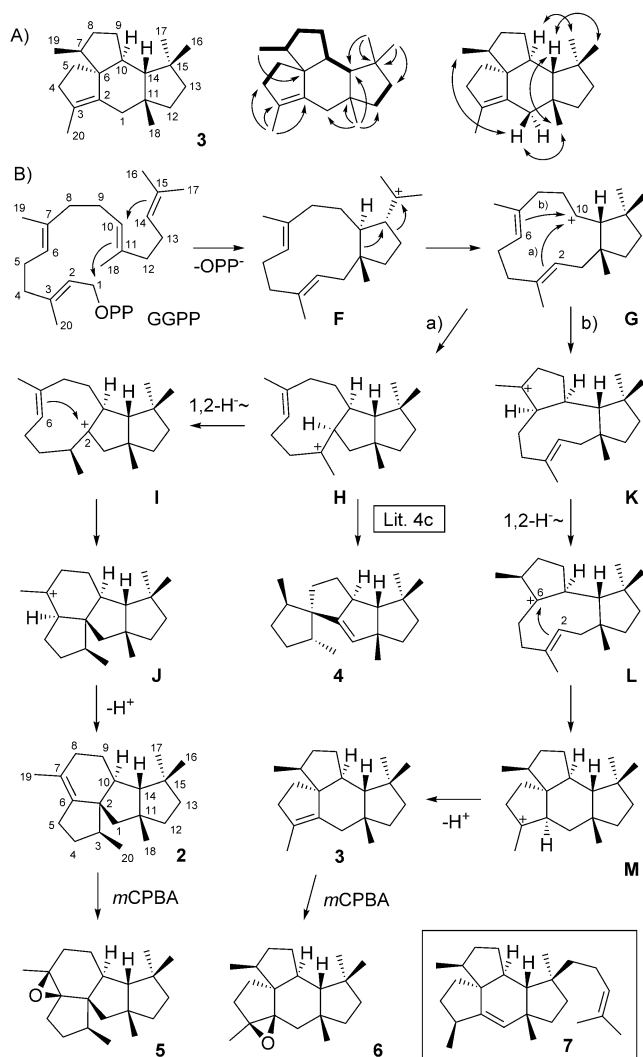
Die absolute Konfiguration von **1** wurde mit enantioselektiv deuteriertem (*R*)- und (*S*)-(1-<sup>13</sup>C,1-<sup>2</sup>H)FPP<sup>[4c]</sup> bestimmt, die mit IPP und GGPPS unter Inversion der Konfiguration an C1 verlängert und mit BdS cyclisiert wurden (Abbildung S14). Die bekannten Konfigurationen an den deuterierten Kohlenstoffatomen können dabei genutzt werden, um die relative Orientierung der anderen Stereozentren in **1** abzuleiten, was auf die absolute Konfiguration wie in Schema 1 verwies. Die diastereotopen Wasserstoffatome an C9 von **1** zeigten identische chemische Verschiebungen, sodass die zuvor synthetisierten Verbindungen (*R*)- und (*S*)-(1-<sup>13</sup>C,1-<sup>2</sup>H)GPP<sup>[4c]</sup> nicht herangezogen werden konnten, um die zugeordnete absolute Konfiguration von **1** zu

bestätigen. Daher wurden alternativ (*E*)- und (*Z*)-(4-<sup>13</sup>C,4-<sup>2</sup>H)IPP synthetisiert (Schema S1) und für die Verlängerung von DMAPP mit FPP-Synthase (FPPS) aus *Streptomyces coelicolor*<sup>[12]</sup> und GGPPS mit bekanntem stereochemischem Verlauf (*Si*-Angriff an C4 von IPP) verwendet,<sup>[13]</sup> gefolgt von einer Cyclisierung mit BdS (Abbildung S15). Diese Strategie ermöglichte einen Zugang zu drei weiteren stereochemischen Ankeren in **1**, für welche die diastereotopen Wasserstoffatome unterscheidbare chemische Verschiebungen zeigten und auf die absolute Konfiguration von **1** verwiesen.

Die zweite TS produzierte eine Mischung von Diterpenen mit zwei Haupt- und einigen Nebenprodukten (Abbildung S1), die nicht per Säulenchromatographie trennbar waren. Daher wurde das Produktgemisch mit *m*CPBA umgesetzt, wodurch zwei Paare diastereomerer Epoxide erhalten wurden (Abbildung S16). Zwei dieser Verbindungen wurden isoliert und per NMR-Spektroskopie als Phomopsen-Epoxid (**5**; Tabelle S3, Abbildungen S17–S23) und das Epoxid **6** (Tabelle S4, Abbildungen S24–S30) eines unbekanntes Diterpens identifiziert (Schema 2). Die Terpenkohlenwasserstoffe konnten letztlich unter Verwendung von mit Silbernitrat imprägniertem Kieselgel getrennt werden.<sup>[14]</sup> Das Hauptprodukt war identisch zu Phomopsen (**2**; Tabelle S5), dem Produkt einer pilzlichen DTS aus *Phomopsis amygdali* (PaPS),<sup>[5]</sup> sodass die TS als bakterielle Phomopsen-Synthase (PmS) identifiziert wurde. Die Struktur des zweiten Produktes wurde per NMR-Spektroskopie aufgeklärt (Tabelle S6, Abbildungen S31–S37) und erwies sich als Diterpen mit neuem Gerüst, das nach dem produzierenden Organismus Allokutzneren (**3**) genannt wurde. Die Struktur wurde durch <sup>13</sup>C,<sup>13</sup>C-COSY mit der Mischung von markiertem **2** und **3** bestätigt, die mit PmS aus (<sup>13</sup>C<sub>20</sub>)GGPP erhalten wurde (Abbildung S38). Weiterhin wurden Spuren von Spiroviolen (**4**) per GC/MS und Vergleich mit einem authentischen Standard identifiziert,<sup>[4c]</sup> was die nahe Phylogenie zwischen PmS und der Spiroviolen-Synthase (SvS) aus *Streptomyces violens* widerspiegelt (Abbildung S39).<sup>[4c]</sup>

Die Biosynthese von allen drei Verbindungen startet ausgehend von GGPP mit einer 1,11- und 10,14-Cyclisierung zu **F**, gefolgt von einer Ringerweiterung und Ringkontraktion zu dem sekundären Kation **G**, das auch als Intermediat zu der pilzlichen Verbindung Variedien aus *Emericella varicolor* beschrieben wurde.<sup>[15]</sup> **G** reagiert vermutlich in einer konzertierten Reaktion durch Angriff einer der verbleibenden Doppelbindungen am kationischen Zentrum entweder zu **H** (Weg a) oder zu **K** (Weg b). Der Mechanismus für die Bildung von **4** aus **H** wurde kürzlich im Detail studiert,<sup>[4c]</sup> aber **H** kann über eine 1,2-Hydridverschiebung zu **I**, Ringschluss zu **J** und Deprotonierung auch Zugang zu **2** geben. Eine ähnliche Sequenz erklärt die Bildung von **3** aus **K** durch 1,2-Hydridwanderung zu **L**, Ringschluss zu **M** und Deprotonierung. Der Mechanismus für **2** wurde jüngst per enzymatischer Synthese diverser deuterierter Isotopomere von GGPP aus deuterierten IPPs und nachfolgender Cyclisierung zu **2** mit PaPS und GC/MS-Analyse untersucht.<sup>[16]</sup> Die Interpretation der Daten in dieser Studie erwies sich als schwierig, weil Annahmen über den EI-MS-Fragmentierungsmechanismus von **2** getroffen werden mussten, um die eingebauten Deuteriumatome zu lokalisieren. Die hier beschriebenen Experimente zum





**Scheme 2.** Produkte der bakteriellen Phomopsen-Synthese (PmS). A) Strukturaufklärung von **3** (fett:  $^1\text{H},^1\text{H}$ -COSY-Korrelationen, einfache Pfeile: HMBC-Korrelationen, Doppelpfeile: NOESY-Korrelationen) und Kohlenstoffnummerierung (zeigt den Ursprung für jedes Kohlenstoffatom aus GGPP durch dieselbe Nummer). B) Cyclisierung von GGPP zu **2**, **3** und **4** durch PmS und chemische Oxidation zu **5** und **6** mit *meta*-Chlorperbenzoesäure (mCPBA). Der Kasten zeigt das bekannte Sesterterpen Mangicdien (**7**).<sup>[17]</sup>

Cyclisierungsmechanismus von **3** ermöglichten gleichzeitig eine erneute mechanistische Studie für **2**. Inkubation aller 20 Isotopomere von ( $^{13}\text{C}$ )GGPP mit PmS ergab den Einbau der Markierung in die entsprechenden Kohlenstoffatome von **2** und **3** in allen Fällen, sodass insbesondere die Gerüstumlagerung von **F** nach **G** nachgewiesen werden konnte (Abbildungen S40 und S41). Die Umsetzung von ( $3\text{-}^{13}\text{C}, 2\text{-}^2\text{H}$ )GGPP<sup>[4c]</sup> mit PmS demonstrierte die 1,2-Hydridverschiebung von **H** nach **I** in der Biosynthese von **2** und die Deprotonierung von C2 unter Bildung von **3** (Abbildung S42). Entsprechend zeigte die Inkubation von ( $3\text{-}^{13}\text{C}, 2\text{-}^2\text{H}$ )FPP<sup>[11]</sup> mit IPP, GGPPS und PmS die 1,2-Hydridwanderung von **K** nach **L** in der Cyclisierung zu **3** und die Deprotonierung von C6 in der Cyclisierung zu **2** (Abbildung S43). In Summe bestätigten diese Experimente den Cyclisierungsmechanismus

für **2**<sup>[16]</sup> und gaben detaillierte Einblicke in den verwandten Mechanismus für **3**.

Die Inkubationen von (*R*)- und (*S*)-( $1\text{-}^{13}\text{C}, 1\text{-}^2\text{H}$ )GGPP<sup>[4d]</sup> (Abbildung S44), (*R*)- und (*S*)-( $1\text{-}^{13}\text{C}, 1\text{-}^2\text{H}$ )FPP<sup>[4c]</sup> (Abbildung S45), (*R*)- und (*S*)-( $1\text{-}^{13}\text{C}, 1\text{-}^2\text{H}$ )GGPP<sup>[4c]</sup> (Abbildung S46) sowie (*E*)- und (*Z*)-( $4\text{-}^{13}\text{C}, 4\text{-}^2\text{H}$ )IPP (Abbildungen S47 und S48) mit PmS verwiesen übereinstimmend auf die absoluten Konfigurationen für **2** und **3**, wie in Schema 2 gezeigt. Die absolute Konfiguration von **2** ist dieselbe wie diejenige der pilzlichen Verbindung, was auch durch dasselbe Vorzeichen des Drehwertes gezeigt wird ( $[\alpha]_{\text{D}}^{25} = -27.2$ ,  $c$  0.42,  $\text{CHCl}_3$ ; Lit.<sup>[5]</sup>  $[\alpha]_{\text{D}}^{25} = -97$ ,  $c$  0.27,  $\text{CHCl}_3$ ). Die absoluten Konfigurationen von **2** und **3** entsprechen der von **4** aus *S. violens*, in Übereinstimmung mit der Bildung über das gemeinsame Intermediat **G** und der nahen Verwandtschaft zwischen PmS und SvS (Abbildung S39). Verbindung **3** ist strukturell ähnlich zum Sesterterpen Mangicdien (**7**) aus *Fusarium graminearum*, das in hoher Ausbeute mit einem gentechnisch modifizierten *E. coli*-Stamm zugänglich ist.<sup>[17]</sup>

Typ-I-TSs weisen einen dreikernigen ( $\text{Mg}^{2+}$ )<sub>3</sub>-Cluster in ihrem aktiven Zentrum auf, der durch hochkonservierte Reste des Asp-reichen Motivs DDXX(X)D und der NSE-Triade ND(L,I,V)XSXXXE gebunden wird.<sup>[18]</sup> Die PP-Einheit des Substrates koordiniert an die  $\text{Mg}^{2+}$ -Kationen und bildet Wasserstoffbrücken zum PP-Sensor,<sup>[19]</sup> einem hochkonservierten Arg, das sich üblicherweise 46 Positionen vor der NSE-Triade befindet.  $\text{Mg}^{2+}$  kann oft durch  $\text{Mn}^{2+}$  ersetzt werden,<sup>[4f,g,20]</sup> was auch für BdS und PmS mit einem Verlust von etwa der halben Aktivität der Fall ist (Abbildungen S49 und S50).

Beide Enzyme wurden auch durch ortsgerechte Mutagenese (OGM) studiert. Wir haben jüngst eine Salzbrücke in der Kristallstruktur der Selinadien-Synthese (SdS)<sup>[19]</sup> zwischen Arg 144 auf Helix F und Glu 192 auf Helix G identifiziert (Abbildung S51). Diese Reste sind in den meisten Typ-I-TSs konserviert, mit der erwähnenswerten Beobachtung, dass für zuvor untersuchte Enzyme mit dem üblichen Glu auf Helix G eine höhere Aktivität mit  $\text{Mg}^{2+}$  beobachtet wird, während Enzyme mit einem Asp höhere Aktivität mit  $\text{Mn}^{2+}$  zeigten.<sup>[4f,g]</sup> BdS (Glu202) und PmS (Glu182) enthalten ein Glu in der entsprechenden Position, in Übereinstimmung mit ihrer höheren Aktivität mit  $\text{Mg}^{2+}$ . OGM der Salzbrücke von BdS (R154K, R154M, E202D) und von PmS (R137K, R137M) ergab inaktive Enzymvarianten für beide Metallcofaktoren (Abbildungen S49 und S50). Ein ungewöhnlicher Rest von BdS ist Lys169, eine Position, die oft durch Glu (>93% der bakteriellen TS) oder manchmal Asp (ca. 3%), aber fast nie durch Lys besetzt wird.<sup>[4g]</sup> Dieser Rest koordiniert an  $\text{Mg}^{2+}$  in SdS (Glu159; Abbildung S51).<sup>[19]</sup> Die BdS-Variante K169E zeigte eine nur leicht verminderte Aktivität mit  $\text{Mg}^{2+}$ , war aber nahezu inaktiv mit  $\text{Mn}^{2+}$ .

Obwohl die Anwendung von Pearsons Konzept der harten und weichen Säuren und Basen<sup>[21]</sup> zur Erklärung ambiderer Reaktivität vor kurzem kritisch beleuchtet wurde,<sup>[22]</sup> ist es dennoch nützlich, die Stabilität von Metallkomplexen einzuschätzen. Die Hart-hart-Wechselwirkung zwischen  $\text{Mg}^{2+}$  und der Carboxylatgruppe in der K169E-Variante mag den dreikernigen Metallcluster ähnlich gut stabilisieren wie das Wildtyp-Enzym, aber das weichere  $\text{Mn}^{2+}$  wird viel besser

durch die Aminogruppe des ursprünglichen Lys als durch die Carboxylatgruppe der K169E-Variante stabilisiert.

Die Struktur von SdS zeigt ein Pro61 am Boden der Helix C und ein Val68 am Beginn der Helix D, das als Abstandhalter zwischen Helices D und G fungiert (Abbildung S52).<sup>[19]</sup> Beide Reste sind in Typ-I-TSs hochkonserviert und sind für die Funktion anderer DTSS entscheidend.<sup>[4f,g]</sup> OGM dieser Reste in BdS (P66A, V73A) und PmS (P58A, L65A) ergab inaktive Enzymvarianten in drei Fällen, lediglich die L65A-Variante wies ca. 10% Restaktivität auf, was die Verallgemeinerbarkeit der entscheidenden Rolle dieser Reste unterstreicht.

Zusammenfassend haben wir die Produkte von zwei DTSS aus *A. albata* identifiziert und die Enzymmechanismen durch eine Kombination leistungsfähiger Methoden wie der Umsetzung isopenmarkierter Substrate<sup>[23]</sup> und ortsgerichteter Mutagenese studiert.<sup>[24]</sup> Das erste Enzym (BdS) produzierte Bonnadien (**1**), ein Diterpen mit neuem Gerüst, während das zweite Enzym (PmS) eine Mischung aus dem pilzlichen Diterpen Phomopsen (**2**),<sup>[5]</sup> der neuen Verbindung Allokozneeren (**3**) und dem bekannten Spiroviolen (**4**) bildete.<sup>[4c]</sup> Die Mischung von **2–4** wird auch von Agarkulturen von *A. albata* abgegeben, was den Schluss nahelegt, dass PmS unter Laborbedingungen exprimiert wird. Die Produktion einer aus Pilzen bekannten Verbindung durch PmS war recht überraschend und ist das erste Beispiel einer bakteriellen Typ-I-DTS, die dasselbe Produkt bildet wie ein pilzliches Enzym.

## Danksagung

Diese Arbeit wurde von der DFG (DI1536/7-1) und durch ein Doktorandenstipendium des FCI (an JR) unterstützt.

## Interessenkonflikt

Die Autoren erklären, dass keine Interessenkonflikte vorliegen.

**Stichwörter:** Biosynthese · Enzymmechanismen · Isotope · NMR-Spektroskopie · Terpene

**Zitierweise:** *Angew. Chem. Int. Ed.* **2018**, *57*, 8280–8283  
*Angew. Chem.* **2018**, *130*, 8412–8415

- [1] J. S. Dickschat, *Nat. Prod. Rep.* **2016**, *33*, 87.  
[2] D. J. Tantillo, *Angew. Chem. Int. Ed.* **2017**, *56*, 10040; *Angew. Chem.* **2017**, *129*, 10172.  
[3] a) C. Nakano, H.-K. Kim, Y. Ohnishi, *ChemBioChem* **2011**, *12*, 1988; b) C. Nakano, H.-K. Kim, Y. Ohnishi, *ChemBioChem* **2011**, *12*, 2403; c) D. E. Cane, J. K. Sohng, C. R. Lamberson, S. M. Rudnicki, Z. Wu, M. D. Lloyd, J. S. Oliver, B. R. Hubbard, *Biochemistry* **1994**, *33*, 5846; d) X. Lin, R. Hopson, D. E. Cane, *J. Am. Chem. Soc.* **2006**, *128*, 6022.  
[4] a) S.-Y. Kim, P. Zhao, M. Igarashi, R. Sawa, T. Tomita, M. Nishiyama, T. Kuzuyama, *Chem. Biol.* **2009**, *16*, 736; b) Y.

- Yamada, T. Kuzuyama, M. Komatsu, K. Shin-ya, S. Omura, D. E. Cane, H. Ikeda, *Proc. Natl. Acad. Sci. USA* **2015**, *112*, 857; c) P. Rabe, J. Rinkel, E. Dolja, T. Schmitz, B. Nubbemeyer, T. H. Luu, J. S. Dickschat, *Angew. Chem. Int. Ed.* **2017**, *56*, 2776; *Angew. Chem.* **2017**, *129*, 2820; d) J. Rinkel, P. Rabe, X. Chen, T. G. Köllner, F. Chen, J. S. Dickschat, *Chem. Eur. J.* **2017**, *23*, 10501; e) J. S. Dickschat, J. Rinkel, P. Rabe, A. Beyraghdar Kashkooli, H. J. Bouwmeester, *Beilstein J. Org. Chem.* **2017**, *13*, 1770; f) J. Rinkel, L. Lauterbach, J. S. Dickschat, *Angew. Chem. Int. Ed.* **2017**, *56*, 16385; *Angew. Chem.* **2017**, *129*, 16603; g) J. Rinkel, L. Lauterbach, P. Rabe, J. S. Dickschat, *Angew. Chem. Int. Ed.* **2018**, *57*, 3238; *Angew. Chem.* **2018**, *130*, 3292.  
[5] T. Toyomasu, A. Kaneko, T. Tokiwano, Y. Kanno, Y. Kanno, R. Niida, S. Miura, T. Nishioka, C. Ikeda, W. Mitsunashi, T. Dairi, T. Kawano, H. Oikawa, N. Kato, T. Sassa, *J. Org. Chem.* **2009**, *74*, 1541.  
[6] J. S. Dickschat, K. A. K. Pahirulzaman, P. Rabe, T. A. Klapschinski, *ChemBioChem* **2014**, *15*, 810.  
[7] P. Rabe, L. Barra, J. Rinkel, R. Riclea, C. A. Citron, T. A. Klapschinski, A. Janusko, J. S. Dickschat, *Angew. Chem. Int. Ed.* **2015**, *54*, 13448; *Angew. Chem.* **2015**, *127*, 13649.  
[8] D. Arigoni, *Pure Appl. Chem.* **1975**, *41*, 219.  
[9] J. Rinkel, P. Rabe, P. Garbeva, J. S. Dickschat, *Angew. Chem. Int. Ed.* **2016**, *55*, 13593; *Angew. Chem.* **2016**, *128*, 13791.  
[10] A. Meguro, Y. Motoyoshi, K. Teramoto, S. Ueda, Y. Totsuka, Y. Ando, T. Tomita, S.-Y. Kim, T. Kimura, M. Igarashi, R. Sawa, T. Shinada, M. Nishiyama, T. Kuzuyama, *Angew. Chem. Int. Ed.* **2015**, *54*, 4353; *Angew. Chem.* **2015**, *127*, 4427.  
[11] T. A. Klapschinski, P. Rabe, J. S. Dickschat, *Angew. Chem. Int. Ed.* **2016**, *55*, 10141; *Angew. Chem.* **2016**, *128*, 10296.  
[12] P. Rabe, J. Rinkel, B. Nubbemeyer, T. G. Köllner, F. Chen, J. S. Dickschat, *Angew. Chem. Int. Ed.* **2016**, *55*, 15420; *Angew. Chem.* **2016**, *128*, 15646.  
[13] J. W. Cornforth, R. H. Cornforth, G. Popjak, L. Yengoyan, *J. Biol. Chem.* **1966**, *241*, 3970.  
[14] a) A. S. Gupta, S. Dev, *J. Chromatogr.* **1963**, *12*, 189; b) M. v. Schantz, S. Juvonen, R. Hemming, *J. Chromatogr.* **1965**, *20*, 618.  
[15] B. Qin, Y. Matsuda, T. Mori, M. Okada, Z. Quan, T. Mitsunashi, T. Wakimoto, I. Abe, *Angew. Chem. Int. Ed.* **2016**, *55*, 1658; *Angew. Chem.* **2016**, *128*, 1690.  
[16] S. S. Shinde, A. Minami, Z. Chen, T. Tokiwano, T. Toyomasu, N. Kato, T. Sassa, H. Oikawa, *J. Antibiot.* **2017**, *70*, 632.  
[17] G. Bian, Y. Han, A. Hou, Y. Yuan, X. Liu, Z. Deng, T. Liu, *Metab. Eng.* **2017**, *42*, 1.  
[18] D. W. Christianson, *Chem. Rev.* **2017**, *117*, 11570.  
[19] P. Baer, P. Rabe, K. Fischer, C. A. Citron, T. A. Klapschinski, M. Groll, J. S. Dickschat, *Angew. Chem. Int. Ed.* **2014**, *53*, 7652; *Angew. Chem.* **2014**, *126*, 7783.  
[20] a) A. J. Poulou, R. Croteau, *Arch. Biochem. Biophys.* **1978**, *191*, 400; b) D. E. Cane, Q. Xue, B. Fitzsimons, *Biochemistry* **1996**, *35*, 12369.  
[21] R. G. Pearson, *J. Am. Chem. Soc.* **1963**, *85*, 3533.  
[22] H. Mayr, M. Breugst, A. R. Ofial, *Angew. Chem. Int. Ed.* **2011**, *50*, 6470; *Angew. Chem.* **2011**, *123*, 6598.  
[23] J. S. Dickschat, *Eur. J. Org. Chem.* **2017**, 4872.  
[24] M. Seemann, G. Z. Zhai, J. W. de Kraker, C. M. Paschall, D. W. Christianson, D. E. Cane, *J. Am. Chem. Soc.* **2002**, *124*, 7681.

Manuskript erhalten: 29. März 2018

Akzeptierte Fassung online: 14. Mai 2018

Endgültige Fassung online: 6. Juni 2018

## Appendix M

### **A Clade II-D Fungal Chimeric Diterpene Synthase from *Colletotrichum gloeosporioides* Produces Dolasta- 1(15),8-diene**

*Angew. Chem. Int. Ed.* **2018**, *57*, 15887–15890.

DOI:10.1002/anie.201809954

&

*Angew. Chem.* **2018**, *130*, 16113–16117.

DOI:10.1002/ange.201809954



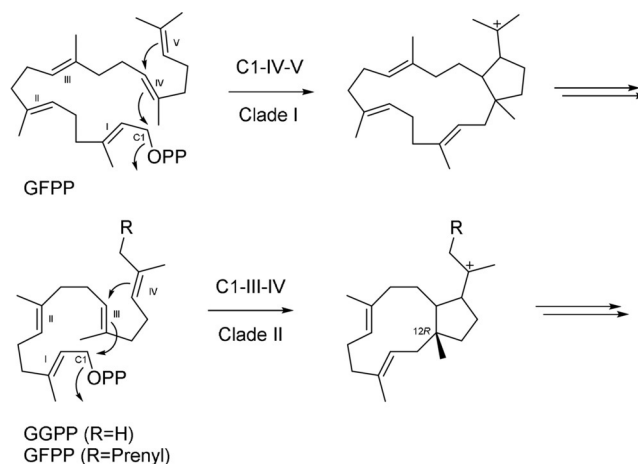
## Biosynthesis

International Edition: DOI: 10.1002/anie.201809954  
German Edition: DOI: 10.1002/ange.201809954A Clade II-D Fungal Chimeric Diterpene Synthase from *Colletotrichum gloeosporioides* Produces Dolasta-1(15),8-dieneGuangkai Bian<sup>+</sup>, Jan Rinkel<sup>+</sup>, Zhangqian Wang<sup>+</sup>, Lukas Lauterbach, Anwei Hou, Yujie Yuan, Zixin Deng, Tiangang Liu,<sup>\*</sup> and Jeroen S. Dickschat<sup>\*</sup>

**Abstract:** Based on a terpenoid overproduction platform in yeast for genome mining, a chimeric diterpene synthase from the endophytic fungus *Colletotrichum gloeosporioides* ES026 was characterized as the (5R,12R,14S)-dolasta-1(15),8-diene synthase. The absolute configuration was independently verified through the use of enantioselectively deuterated terpene precursors, which unequivocally established the predicted C1-III-IV cyclization mode for this first characterized clade II-D enzyme. Extensive isotopic labeling experiments and isolation of the intermediate (1R)- $\delta$ -araneosene supported the proposed cyclization mechanism.

**D**iterpenoids, which are produced from the universal precursor geranylgeranyl diphosphate (GGPP), represent a diverse class of structurally complex natural products with often highly potent bioactivities that are widely distributed in bacteria,<sup>[1]</sup> fungi,<sup>[2]</sup> plants,<sup>[3]</sup> marine invertebrates<sup>[4]</sup> and social amoebae.<sup>[5]</sup> GGPP is assembled from dimethylallyl diphosphate (DMAPP) and isopentenyl diphosphate (IPP) by a prenyltransferase (PT), or more specifically a GGPP synthase (GGPPS). The first committed step in the biosynthesis of diterpenes is the cyclization of the linear achiral GGPP into a usually polycyclic diterpene hydrocarbon or alcohol with multiple stereocenters. These remarkable transformations are performed by terpene synthases (TS) in just one enzymatic step involving a complex cascade reaction via cationic intermediates. Three classes of TSs are known, which can be distinguished by their amino acid sequences. Type I

TSs initiate the cationic cascade by elimination of diphosphate from the precursor, while type II enzymes act through protonation of an olefinic double bond. The recently discovered UbiA-related TSs also act through abstraction of diphosphate.<sup>[6]</sup> In fungi, bifunctional TSs with two domains are often found. These chimeric enzymes can combine type II and type I TS activities, or PT and any type of TS activity,<sup>[2]</sup> with the fusicocca-2,10(14)-diene synthase from *Phomopsis amygdali* as the first characterized example.<sup>[7]</sup> A phylogenetic analysis of the chimeric PT-type I TS combining enzymes revealed their division into two distinct clades (I and II), which further branch out into six subclades (A–F).<sup>[8]</sup> These clades reflect different initial cyclization modes, namely C1-IV-V cyclization for clade I and C1-III-IV cyclization for clade II (Scheme 1; herein the notation C1-III-IV indicates



**Scheme 1.** Initial cyclization steps in bifunctional terpene synthases from clade I (top) and clade II (bottom).

the attack on C-1 by the third double bond counting from the diphosphate terminus, followed by attack by the fourth double bond). Bifunctional TSs have been studied from five subclades, and for the three subclades of clade I, different stereochemical courses for the C1-IV-V cyclization have been observed. For clade II, only enzymes from subclades B and C are known,<sup>[2]</sup> while no clade II-D representative has been described. Here we report on the structures of the products obtained with a clade II-D TS from the endophytic fungus *Colletotrichum gloeosporioides* ES026, as well as in depth biochemical and mechanistic characterization.

During our screening program towards the identification of TSs from filamentous fungi with novel functionalities, the

[\*] Dr. G. Bian,<sup>[†]</sup> Dr. Z. Wang,<sup>[†]</sup> Dr. A. Hou, Y. Yuan, Prof. Z. Deng, Prof. T. Liu

Key Laboratory of Combinatorial Biosynthesis and Drug Discovery  
Ministry of Education and School of Pharmaceutical Sciences  
Wuhan University, Wuhan 430071 (China)

E-mail: liutg@whu.edu.cn

Homepage: <http://liugroup.whu.edu.cn/English/>

Prof. Z. Deng, Prof. T. Liu

Hubei Engineering Laboratory for Synthetic Microbiology  
Wuhan Institute of Biotechnology, Wuhan 430075 (China)

J. Rinkel,<sup>[†]</sup> L. Lauterbach, Prof. Dr. J. S. Dickschat

Kekulé-Institut für Organische Chemie und Biochemie

Rheinische Friedrich-Wilhelms-Universität Bonn

Gerhard-Domagk-Strasse 1, 53121 Bonn (Germany)

E-mail: dickschat@uni-bonn.de

Homepage: [https://www.chemie.uni-bonn.de/oc/forschung/arbeitsgruppen/ak\\_dickschat](https://www.chemie.uni-bonn.de/oc/forschung/arbeitsgruppen/ak_dickschat)

[†] These authors contributed equally to this work.

Supporting information and the ORCID identification number(s) for the author(s) of this article can be found under:

<https://doi.org/10.1002/anie.201809954>

endophyte *Colletotrichum gloeosporioides* ES026, which was isolated from the traditional Chinese medicinal plant *Huperzia serrata*,<sup>[9]</sup> was found to encode an unusually large number of putative TSs (Figure S1 in the Supporting Information). The chimeric enzyme Cg13742, which has an N-terminal TS and a C-terminal PT domain, grouped within clade II-D (Figure S2) and was selected for further study. Sequence alignment with other functionally characterized chimeric TSs from fungi (Figure S3) showed the presence of the highly conserved aspartate-rich motif <sup>108</sup>DDLTD, modified NSE triad <sup>242</sup>HDYCSWDKE,<sup>[10]</sup> the pyrophosphate sensor <sup>198</sup>R,<sup>[11]</sup> the <sup>336</sup>RY pair in the TS domain, and the two aspartate-rich motifs <sup>495</sup>DDVQD and <sup>620</sup>DDYQD in the PT domain.<sup>[12]</sup> As recently shown for mangicdiene synthase (FgMS) and fusariumdiene/fusagramineol synthase (FgFS) from *Fusarium graminearum*, a metabolic-engineering-based genome mining approach can provide high yielding heterologous expression strains that allow for the rapid characterization of TSs.<sup>[13]</sup> To determine the function of the silent *Cg13742* gene and its product, a mutant *C. gloeosporioides* ZW139 was constructed in which the genes for the key enzymes tHMG1 (3-hydroxy-3-methylglutaryl-CoA reductase), Idi (isopentenyl diphosphate isomerase), and Cg13742 were overexpressed. As a result, low-level production of the diterpene **1** was detected (Figure 1). To characterize the

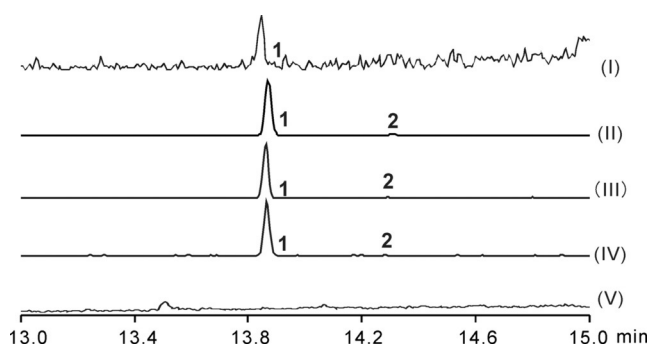


**Figure 1.** Diterpenes from CgDS. Total ion chromatograms of products obtained from (I) *C. gloeosporioides* ZW139, (II) CgDS with IPP and DMAPP, (III) CgDS with GGPP, (IV) *S. cerevisiae* ZW140, and (V) boiled CgDS with GGPP.

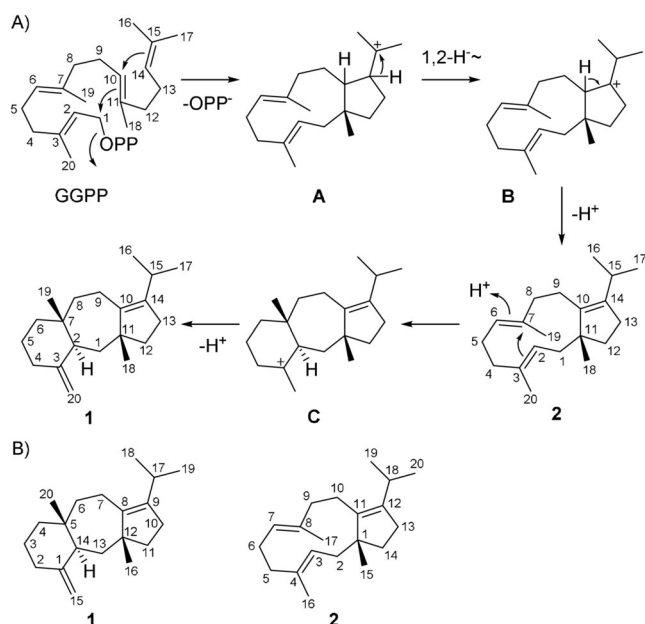
function of Cg13742 in vitro, the *Cg13742* gene was amplified by reverse transcriptase PCR and cloned into the expression vector pET28a. The gene was overexpressed in *Escherichia coli* and the resulting protein was purified (Figure S4). Incubation of Cg13742 with geranyl diphosphate (GPP) and farnesyl diphosphate (FPP) gave no products, while incubation with DMAPP and IPP or with GGPP resulted in the formation of **1**, along with traces of a second diterpene **2** (Figure 1 and Figure S5), thus indicating that the PT domain of Cg13742 can utilize DMAPP and IPP to generate GGPP for the TS domain to catalyze diterpene formation. A metal-ion dependency assay showed that Cg13742 required Mg<sup>2+</sup> (Figure S6), while a slightly reduced activity of 93 ± 6% was observed with Mn<sup>2+</sup> (normalized to Mg<sup>2+</sup>: 100 ± 12%), but other divalent cations (Ca<sup>2+</sup>, Fe<sup>2+</sup>, Co<sup>2+</sup>, Ni<sup>2+</sup>, Cu<sup>2+</sup> and Zn<sup>2+</sup>) gave no activity. To determine the

structure of **1**, a pZW140 plasmid harboring the *Cg13742* gene (Figure S7) was constructed and integrated into the engineered terpenoid precursor providing platform *Saccharomyces cerevisiae* YZL141 to generate the production strain *S. cerevisiae* ZW140.<sup>[13b]</sup> After 95 hours shaken-flask fermentation, the culture was extracted with hexane and **1** was purified with a yield of 7.3 mg L<sup>-1</sup>.

Compound **1**, [ $\alpha$ ]<sub>D</sub><sup>20</sup> = +122.1 (c 0.21, hexane), was identified by one- and two-dimensional NMR spectroscopy (Figures S8–S21), with full assignment of the NMR data for all carbons and hydrogens (Tables S3–S4), as the enantiomer of (5*S*,12*S*,14*R*)-dolasta-1(15),8-diene (lit.: [ $\alpha$ ]<sub>D</sub> = -115.2, c 2.40, hexane), a compound that was previously obtained from natural (-)- $\delta$ -araneosene through treatment with HCl in chloroform at -45 °C.<sup>[14]</sup> Thus, compound **1** is (5*R*,12*R*,14*S*)-dolasta-1(15),8-diene and Cg13742 is a *C. gloeosporioides* dolasta-1(15),8-diene synthase (CgDS). Neither **1** nor its enantiomer are known as natural products. Although the absolute configuration of **1** could be inferred from optical rotations, this finding was independently confirmed to make sure that the conclusions relating to the cyclization mechanism of clade II-D enzymes are correct. This was done through enzymatic conversion of several enantioselectively deuterated probes, including (*R*)- and (*S*)-(1-<sup>13</sup>C,1-<sup>2</sup>H)GGPP<sup>[5]</sup> and (*R*)- and (*S*)-(1-<sup>13</sup>C,1-<sup>2</sup>H)GPP (with additional IPP),<sup>[15]</sup> elongated by the PT domain into the corresponding GGPP isotopomers with inversion of configuration at C-1 of GPP.<sup>[16]</sup> The deuterium atoms were incorporated into the diastereotopic positions in line with the absolute configuration of (5*R*,12*R*,14*S*)-**1**. The <sup>13</sup>C labels in the used probes were introduced for sensitive detection by HSQC spectroscopy (Figures S22 and S23). Further confirmation was obtained using DMAPP and (*E*)- and (*Z*)-(4-<sup>13</sup>C,4-<sup>2</sup>H)IPP,<sup>[17]</sup> which were converted into the corresponding GGPP isotopomers by the PT domain of CgDS with known stereochemical course (*Si* face attack at C-4 of IPP).<sup>[18]</sup> Cyclization by the TS domain gave incorporation of deuterium into positions that were again indicative of an absolute configuration of (5*R*,12*R*,14*S*)-**1** (Figure S24).

Compound **2** was obtained from an in vitro incubation of recombinant CgDS with GGPP and identified by NMR as  $\delta$ -araneosene (Figures S25–S31, Table S5). Its optical rotation of [ $\alpha$ ]<sub>D</sub><sup>20</sup> = +161 (c 0.02, hexane) pointed to it being the enantiomer of the known natural product (-)-(1*S*)- $\delta$ -araneosene from *Sordaria araneosa* (lit.: [ $\alpha$ ]<sub>D</sub> = -127.6, c 3.04, hexane),<sup>[19]</sup> thus identifying the minor product of CgDS as (+)-(1*R*)- $\delta$ -araneosene (**2**).

The complex mechanisms of TSs, including fungal enzymes related to CgDS, can be efficiently studied through isotopic labelling experiments.<sup>[2b,20]</sup> The proposed cyclization mechanism for **1** proceeds through a typical clade II reaction, with initial C1-III-IV cyclization to **A**, followed by a 1,2-hydride shift to **B** and deprotonation to **2** (Scheme 2). Reprotonation at C-6 of GGPP initiates a second cyclization to **C**, followed by deprotonation to **1**. This mechanism was supported by an incubation experiment with (2-<sup>2</sup>H)DMAPP<sup>[5]</sup> and IPP, which were converted by the PT domain of CgDS into (14-<sup>2</sup>H)GGPP. The 1,2-hydride shift from **A** to **B** was evident from the EI mass spectrum of labeled **1**, showing the



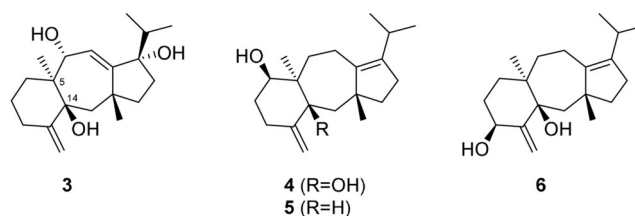
**Scheme 2.** A) Cyclization mechanism for CgDS. Carbon numbers of **1** and **2** show the origin of each carbon from GGPP by same number to allow easy following of labelling experiments. B) Carbon numbers for **1** and **2** as introduced in Ref. [14] that are used as locants to describe the absolute configurations by CIP nomenclature.

loss of deuterium by cleavage of the *i*Pr group (Figure S32 A). Deprotonation from C-10 of GGPP was demonstrated by an incubation of ( $2\text{-}^2\text{H}$ )GGPP (synthesized as shown in Scheme S1) and IPP with CgDS, resulting in a non-labeled product **1** via ( $10\text{-}^2\text{H}$ )GGPP (Figure S32 B). These experiments also clearly ruled out the hypothetical alternative of a 1,3-hydride shift from **A** and deprotonation from C-14 of GGPP to yield **2**. While terpene cyclizations usually follow a strict stereochemical course, a scrambling of the two diastereotopic geminal Me groups in GGPP is often observed for terpene cyclizations involving a 1,2-hydride shift into an *i*Pr group,<sup>[5,21]</sup> that is, the cationic center as in **A** is attacked by the migrating hydride from both diastereotopic faces. This was also the case for CgDS, as demonstrated by incubation experiments with ( $16\text{-}^{13}\text{C}$ )GGPP and ( $17\text{-}^{13}\text{C}$ )GGPP that gave a distribution of labeling over both corresponding Me groups in **1** (Figure S33). The reprotonation of **2** at C-6 of GGPP was followed by incubation of ( $6\text{-}^{13}\text{C}$ )GGPP in deuterium oxide buffer, resulting in a triplet in the  $^{13}\text{C}$  NMR due to  $^2\text{H}\text{-}^{13}\text{C}$  spin-coupling (Figure S34). The stereochemical course of the reprotonation<sup>[22]</sup> was evident from HSQC analysis of the product, revealing specific incorporation of deuterium into the 4-*pro-R* hydrogen of **1**. A feeding experiment with sodium ( $1\text{-}^{13}\text{C}$ )acetate gave results consistent with this mechanism (Table S6, Figure S35).

Neutral biosynthetic intermediates in terpene cyclisations have frequently been described, for example, recently for several plant sesterterpene synthases,<sup>[23]</sup> but do not always leak from the active site. They can sometimes be obtained from enzyme variants with exchange of a single amino acid residue involved in the reprotonation step.<sup>[24]</sup> Since it has been reported that **2** can be smoothly converted into **1** by mild acid

catalysis,<sup>[14]</sup> the question of whether **1** is truly an enzyme product, or just spontaneously formed from **2** under the culture and incubation conditions, was also addressed. Compound **2** was incubated with CgDS and without enzyme in incubation buffer. In both cases, similar amounts of **1** were detected (Figure S36), but the conversion was sluggish. These experiments demonstrated that the spontaneous conversion of **2** into **1** may participate to some extent, but a major role of the enzyme in the formation of **1** must be assumed, since the observed sluggish spontaneous conversion of **2** into **1** cannot explain the formation of **1** as main product. The reason why **2** is not converted faster into **1** in the presence of the enzyme in comparison to the experiment using only incubation buffer is not fully clear, but likely the protonation state of certain active-site residues involved in the reprotonation of **2** for its further cyclization is incorrect if the cyclisation cascade is not started with GGPP.

Previously reported dolastanes include dolatriol (**3**, Scheme 3), which was originally isolated from the poisonous sea hare *Dolabella auricularia*,<sup>[25]</sup> but is actually produced by brown algae and accumulates in the sea hare through its diet. Amijiol (**4**), 14-deoxyamijiol (**5**), and isoamijiol (**6**) are also



**Scheme 3.** Dolastane diterpenes from brown algae.

known from brown algae.<sup>[26]</sup> Notably, the algal compounds exhibit a 5,14-di-*epi* skeleton compared to fungal **1**. No TS for dolastane diterpenes has been reported so far, while the intermediate  $\delta$ -araneosene was observed as a side product of (+)-fusicocca-2,10(14)-diene synthase from *P. amygdali*.<sup>[7]</sup> Access to dolastanes is of high interest because several oxidized members of this class modulate the effects of other drugs in resistant *S. aureus* strains.<sup>[27]</sup> Functionalized dolastanes could be made accessible from **1** through the discovery of selective oxygenases or the development of chemical transformations.

In summary, we have identified a chimeric diterpene synthase from *C. gloeosporioides* as the (5*R*,12*R*,14*S*)-dolasta-1(15),8-diene synthase (CgDS) and were able to access this compound with a decent yield of  $7.3\text{ mg L}^{-1}$  from an engineered yeast strain. CgDS is the first described chimeric fungal clade II-D TS and catalyzes a C1-III-IV cyclization, which fits with the cyclization mode of other clade II enzymes. Unfortunately, as for several other clade II TSs, the precise stereochemical course of the initial C1-III-IV cyclization cannot be inferred from the structures of the final products **1** and **2**, but all so far characterized clade II enzymes uniformly introduce a 12*R* configuration.<sup>[2]</sup> Whether the subclades in clade II reflect different stereochemical courses with respect to the other stereogenic centers set in the initial

C1-III-IV cyclization, as is the case for the subclades of clade I, remains open. To answer this question, the characterization of further clade II enzymes with products showing the stereochemical course of the initial cyclization step will be required.

### Acknowledgements

This work was supported by the DFG (grant DI1536/7-1), by J1 Biotech Co., Ltd., grants from the Young Talents Program of National High-level Personnel of Special Support Program (The “Ten Thousand Talent Program”), the National Natural Science Foundation of China (31670090 and 31800032), and the China Postdoctoral Science Foundation (grant 2017M622507, 2018T110793).

### Conflict of interest

The authors declare no conflict of interest.

**Keywords:** biosynthesis · cyclases · diterpenes · dolastanes · isotopes

**How to cite:** *Angew. Chem. Int. Ed.* **2018**, *57*, 15887–15890  
*Angew. Chem.* **2018**, *130*, 16113–16117

- [1] a) J. S. Dickschat, *Nat. Prod. Rep.* **2016**, *33*, 87; b) Y. Yamada, T. Kuzuyama, M. Komatsu, K. Shin-ya, S. Omura, D. E. Cane, H. Ikeda, *Proc. Natl. Acad. Sci. USA* **2015**, *112*, 857.
- [2] a) T. Mitsuhashi, I. Abe, *ChemBioChem* **2018**, *19*, 1106; b) A. Minami, T. Ozaki, C. Liu, H. Oikawa, *Nat. Prod. Rep.* **2018**, <https://doi.org/10.1039/C8NP00026C>.
- [3] G. Appendino, in *Progress in the Chemistry of Organic Natural Products* (Eds.: A. D. Kinghorn, H. Falk, S. Gibbons, J. Kobayashi), Springer, Switzerland **2016**, pp. 1–90.
- [4] F. Berru , M. W. B. McCulloch, R. G. Kerr, *Bioorg. Med. Chem.* **2011**, *19*, 6702.
- [5] J. Rinkel, P. Rabe, X. Chen, T. G. K llner, F. Chen, J. S. Dickschat, *Chem. Eur. J.* **2017**, *23*, 10501.
- [6] a) M. J. Smanski, Z. Yu, J. Casper, S. Lin, R. M. Peterson, Y. Chen, E. Wendt-Pienkowski, S. R. Rajski, B. Shen, *Proc. Natl. Acad. Sci. USA* **2011**, *108*, 13498; b) Y.-I. Yang, S. Zhang, K. Ma, Y. Xu, Q. Tao, Y. Chen, J. Chen, S. Guo, J. Ren, W. Wang, Y. Tao, W.-B. Yin, H. Liu, *Angew. Chem. Int. Ed.* **2017**, *56*, 4749; *Angew. Chem.* **2017**, *129*, 4827.
- [7] T. Toyomasu, M. Tsukahara, A. Kaneko, R. Niida, W. Mitsuhashi, T. Dairi, N. Kato, T. Sassa, *Proc. Natl. Acad. Sci. USA* **2007**, *104*, 3084.
- [8] a) Y. Ye, A. Minami, A. Mandi, C. Liu, T. Taniguchi, T. Kuzuyama, K. Monde, K. Gomi, H. Oikawa, *J. Am. Chem. Soc.* **2015**, *137*, 11846; b) T. Mitsuhashi, J. Rinkel, M. Okada, I. Abe, J. S. Dickschat, *Chem. Eur. J.* **2017**, *23*, 10053.
- [9] X.-M. Zhao, Z.-Q. Wang, S.-H. Shu, W.-J. Wang, H.-J. Xu, Y.-J. Ahn, M. Wang, X. Hu, *PLoS One* **2013**, *8*, e61777.
- [10] a) C. M. Starks, K. Back, J. Chappell, J. P. Noel, *Science* **1997**, *277*, 1815; b) E. Y. Shishova, L. Di Costanzo, D. E. Cane, D. W. Christianson, *Biochemistry* **2007**, *46*, 1941.
- [11] P. Baer, P. Rabe, K. Fischer, C. A. Citron, T. A. Klapschinski, M. Groll, J. S. Dickschat, *Angew. Chem. Int. Ed.* **2014**, *53*, 7652; *Angew. Chem.* **2014**, *126*, 7783.
- [12] L. C. Tarshis, P. J. Proteau, B. A. Kellogg, J. C. Sacchettini, C. D. Poulter, *Proc. Natl. Acad. Sci. USA* **1996**, *93*, 15018.
- [13] a) G. Bian, Y. Han, A. Hou, Y. Yuan, X. Liu, Z. Deng, T. Liu, *Metab. Eng.* **2017**, *42*, 1; b) G. Bian, A. Hou, Y. Yuan, B. Hu, S. Cheng, Z. Ye, Y. Di, Z. Deng, T. Liu, *Org. Lett.* **2018**, *20*, 1626; c) G. Bian, Z. Deng, T. Liu, *Curr. Opin. Biotechnol.* **2017**, *48*, 234.
- [14] L. Jenny, H.-J. Borschberg, P. Acklin, *Tetrahedron* **1996**, *52*, 1549.
- [15] P. Rabe, J. Rinkel, E. Dolja, T. Schmitz, B. Nubbemeyer, T. H. Luu, J. S. Dickschat, *Angew. Chem. Int. Ed.* **2017**, *56*, 2776; *Angew. Chem.* **2017**, *129*, 2820.
- [16] H. V. Thulasiram, C. D. Poulter, *J. Am. Chem. Soc.* **2006**, *128*, 15819.
- [17] L. Lauterbach, J. Rinkel, J. S. Dickschat, *Angew. Chem. Int. Ed.* **2018**, *57*, 8280; *Angew. Chem.* **2018**, *130*, 8412.
- [18] J. W. Cornforth, R. H. Cornforth, G. Popjak, L. Yengoyan, *J. Biol. Chem.* **1966**, *241*, 3970.
- [19] L. Jenny, H.-J. Borschberg, *Helv. Chim. Acta* **1995**, *78*, 715.
- [20] a) J. S. Dickschat, *Eur. J. Org. Chem.* **2017**, 4872; b) T. Toyomasu, M. Tsukahara, H. Kenmoku, M. Anada, H. Nitta, J. Okanda, W. Mitsuhashi, T. Sassa, N. Kato, *Org. Lett.* **2009**, *11*, 3044.
- [21] a) I. Burkhardt, T. Siemon, M. Henrot, L. Studt, S. R sler, B. Tudzynski, M. Christmann, J. S. Dickschat, *Angew. Chem. Int. Ed.* **2016**, *55*, 8748; *Angew. Chem.* **2016**, *128*, 8890; b) J. Rinkel, L. Lauterbach, P. Rabe, J. S. Dickschat, *Angew. Chem. Int. Ed.* **2018**, *57*, 3238; *Angew. Chem.* **2018**, *130*, 3292.
- [22] P. Rabe, J. Rinkel, T. A. Klapschinski, L. Barra, J. S. Dickschat, *Org. Biomol. Chem.* **2016**, *14*, 158.
- [23] A. C. Huang, Y. J. Hong, A. D. Bond, D. J. Tantillo, A. Osbourn, *Angew. Chem. Int. Ed.* **2018**, *57*, 1291; *Angew. Chem.* **2018**, *130*, 1305.
- [24] K. A. Rising, C. M. Starks, J. P. Noel, J. Chappell, *J. Am. Chem. Soc.* **2000**, *122*, 1861.
- [25] G. R. Pettit, R. H. Ode, C. L. Herald, R. B. von Dreel, C. Michel, *J. Am. Chem. Soc.* **1976**, *98*, 4677.
- [26] M. Ochi, M. Watanabe, I. Miura, M. Taniguchi, T. Tokoroyama, *Chem. Lett.* **1980**, *9*, 1229.
- [27] C. S. de Figueiredo, S. M. Pinto de Menezes Silva, L. Silva Abreu, E. Ferreira da Silva, M. Sobral da Silva, G. E. Cavalcanti de Miranda, V. C. de O. Costa, M. Le Hyaric, J. Pinto de Sequeira, J. M. B. Filho, J. F. Tavares, *Nat. Prod. Res.* **2018**, <https://doi.org/10.1080/14786419.2018.1470512>.

Manuscript received: August 29, 2018

Accepted manuscript online: October 2, 2018

Version of record online: October 26, 2018



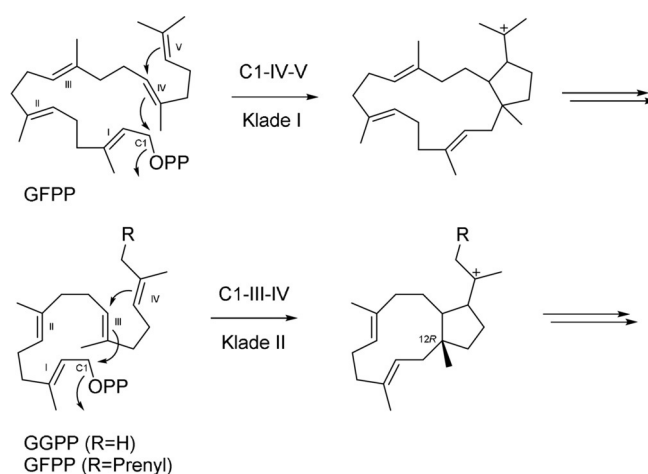
# Eine chimäre pilzliche Diterpensynthese der Klade II-D aus *Colletotrichum gloeosporioides* produziert Dolasta-1(15),8-dien

Guangkai Bian<sup>+</sup>, Jan Rinkel<sup>+</sup>, Zhangqian Wang<sup>+</sup>, Lukas Lauterbach, Anwei Hou, Yujie Yuan, Zixin Deng, Tiangang Liu\* und Jeroen S. Dickschat\*

**Abstract:** Basierend auf einer Plattform zur Überproduktion von Terpenoiden in Hefe für „Genome-Mining“ wurde eine chimäre Diterpensynthese aus dem endophytischen Pilz *Colletotrichum gloeosporioides* ES026 als (5*R*,12*R*,14*S*)-Dolasta-1(15),8-dien-Synthese charakterisiert. Die absolute Konfiguration wurde unabhängig durch die Verwendung enantioselektiv deuterierter Terpenvorstufen bestimmt, wodurch der vorhergesagte C1-III-IV-Cyclisierungsmodus dieses ersten charakterisierten Enzyms der Klade II-D bestätigt wurde. Isotopenmarkierungsexperimente und die Isolierung des Intermediates (1*R*)- $\delta$ -Araneosen stützen den vorgeschlagenen Cyclisierungsmechanismus.

**D**iterpenoide, die aus der universellen Vorstufe Geranylgeranyldiphosphat (GGPP) gebildet werden, repräsentieren eine diverse Klasse strukturell komplexer Naturstoffe mit oftmals hohen biologischen Aktivitäten, die in Bakterien,<sup>[1]</sup> Pilzen,<sup>[2]</sup> Pflanzen,<sup>[3]</sup> marinen Invertebraten<sup>[4]</sup> und sozialen Amöben weit verbreitet sind.<sup>[5]</sup> GGPP wird aus Dimethylallyldiphosphat (DMAPP) und Isopentenylidiphosphat (IPP) durch eine Prenyltransferase (PT), oder spezifischer eine GGPP-Synthase (GGPPS), gebildet. Der erste Schritt in der Biosynthese von Diterpenen ist die Cyclisierung des linearen, achiralen GGPP zu einem üblicherweise polycyclischen Diterpen-Kohlenwasserstoff oder -Alkohol mit multiplen Stereozentren. Diese erstaunlichen Transformationen werden durch Terpensynthasen (TS) in nur einem enzymatischen Schritt katalysiert, der eine komplexe Reaktionskas-

kade über kationische Intermediate beinhaltet. Drei Klassen von TS sind bekannt, die anhand ihrer Aminosäuresequenzen unterscheidbar sind. TS des Typs I initiieren die kationische Kaskade durch Eliminierung des Diphosphates aus der Vorstufe, während Enzyme des Typs II durch Protonierung einer olefinischen Doppelbindung agieren. Die jüngst entdeckten, mit UbiA verwandten TS agieren ebenfalls durch Abstraktion von Diphosphat.<sup>[6]</sup> In Pilzen werden oft bifunktionale TS mit zwei Domänen gefunden. Diese chimären Enzyme können Aktivitäten des Typs II und des Typs I oder einer PT und einer TS kombinieren,<sup>[2]</sup> wofür die Fusicocca-2,10(14)-dien-Synthase aus *Phomopsis amygdali* als das erste charakterisierte Beispiel gilt.<sup>[7]</sup> Eine phylogenetische Analyse der chimären TS mit der Kombination PT-Typ I TS zeigte deren Aufspaltung in zwei unterscheidbare Kladen I und II, mit einer weiteren Feinaufspaltung in sechs Unterklassen (A–F).<sup>[8]</sup> Diese Kladen reflektieren unterschiedliche initiale Cyclisierungsmodi, d. h. eine C1-IV-V-Cyclisierung für Klade I und eine C1-III-IV-Cyclisierung für Klade II (Schema 1; die Notation



**Scheme 1.** Initiale Cyclisierungsschritte in bifunktionalen TS der Klade I (oben) und der Klade II (unten).

C1-III-IV verweist darin auf den Angriff an C-1 durch die vom Diphosphat-Terminus ausgehende dritte Doppelbindung, gefolgt durch den Angriff der vierten Doppelbindung). Bifunktionale TS aus fünf dieser Unterklassen wurden bisher studiert, und für die drei Unterklassen der Klade I wurden unterschiedliche stereochemische Verläufe der C1-IV-V-Cyclisierung beobachtet. Aus Klade II sind nur Enzyme der Unterklassen B und C bekannt,<sup>[2]</sup> wohingegen kein Repräsentant der Klade II-D beschrieben wurde. Wir berichten hier

[\*] Dr. G. Bian,<sup>[†]</sup> Dr. Z. Wang,<sup>[†]</sup> Dr. A. Hou, Y. Yuan, Prof. Z. Deng, Prof. T. Liu  
Key Laboratory of Combinatorial Biosynthesis and Drug Discovery  
Ministry of Education and School of Pharmaceutical Sciences  
Wuhan University, Wuhan 430071 (China)  
E-Mail: liutg@whu.edu.cn  
Homepage: <http://liugroup.whu.edu.cn/English/>  
Prof. Z. Deng, Prof. T. Liu  
Hubei Engineering Laboratory for Synthetic Microbiology  
Wuhan Institute of Biotechnology  
Wuhan 430075 (China)

J. Rinkel,<sup>[†]</sup> L. Lauterbach, Prof. Dr. J. S. Dickschat  
Kekulé-Institut für Organische Chemie und Biochemie  
Rheinische Friedrich-Wilhelms-Universität Bonn  
Gerhard-Domagk-Straße 1, 53121 Bonn (Deutschland)  
E-Mail: dickschat@uni-bonn.de  
Homepage: [https://www.chemie.uni-bonn.de/oc/forschung/arbeitsgruppen/ak\\_dickschat](https://www.chemie.uni-bonn.de/oc/forschung/arbeitsgruppen/ak_dickschat)

[†] Diese Autoren haben zu gleichen Teilen zu der Arbeit beigetragen.  
 Hintergrundinformationen und die Identifikationsnummer (ORCID) eines Autors sind unter:  
<https://doi.org/10.1002/ange.201809954> zu finden.

über die Strukturen der Produkte, die mit einer TS der Klade II-D aus dem endophytischen Pilz *Colletotrichum gloeosporioides* ES026 erhalten wurden, und über eine umfassende biochemische und mechanistische Charakterisierung dieses Enzyms.

Während unseres Screening-Programms zur Identifizierung von TS aus filamentösen Pilzen mit neuen Funktionen wurde in dem Endophyten *Colletotrichum gloeosporioides* ES026, der aus der traditionellen chinesischen Heilpflanze *Huperzia serrata* isoliert wurde,<sup>[9]</sup> eine ungewöhnlich hohe Zahl an kodierten TS gefunden (Abbildung S1). Das chimäre Enzym Cgl13742 mit einer N-terminalen TS- und einer C-terminalen PT-Domäne wurde in Klade II-D eingruppiert (Abbildung S2) und wurde für weitere Studien ausgewählt. Ein Sequenz-Alignment mit anderen funktional charakterisierten chimären TS aus Pilzen (Abbildung S3) zeigte die Präsenz des hochkonservierten Aspartat-reichen Motivs <sup>108</sup>DDLTD, eine modifizierte NSE-Triade <sup>242</sup>HDYCSWDKE,<sup>[10]</sup> den Pyrophosphat-Sensor <sup>198</sup>R<sup>[11]</sup> und das <sup>336</sup>RY-Paar in der TS-Domäne sowie zwei Aspartat-reiche Motive <sup>495</sup>DDVQD und <sup>620</sup>DDYQD in der PT-Domäne.<sup>[12]</sup> Wie jüngst für die Mangicdien-Synthase (FgMS) und die Fusariumdien/Fusagramineol-Synthase (FgFS) aus *Fusarium graminearum* gezeigt, kann durch eine Kombination aus metabolischem Engineering und „Genome-Mining“ unter heterologer Expression ein Überproduktionsstamm erzeugt werden, der hohe Produktausbeuten liefert und eine schnelle Charakterisierung von TS ermöglicht.<sup>[13]</sup> Um die Funktion des stillen Gens *Cgl13742* und dessen Produkt zu klären, wurde die Mutante *C. gloeosporioides* ZW139 konstruiert, in der die Gene für die Schlüsselenzyme tHMG1 (3-Hydroxy-3-methylglutaryl-CoA-Reduktase), Idi (Isopentenylidiphosphat-Isomerase) und Cgl13742 überexprimiert wurden. Im Ergebnis wurde eine geringe Produktion des Diterpens **1** detektiert (Abbildung 1). Um die Funktion von *Cgl13742* in vitro zu charakterisieren, wurde das Gen *Cgl13742* durch PCR mit reverser Transkriptase amplifiziert und in den Expressionsvektor pET28a kloniert. Das Gen wurde in *Escherichia coli* exprimiert, und das resultierende Protein wurde gereinigt (Abbildung S4). Inkubation von Cgl13742 mit Geranyl- (GPP) und Farnesylidiphosphat (FPP) ergab kein Produkt, während die Inkubation mit DMAPP und IPP oder mit

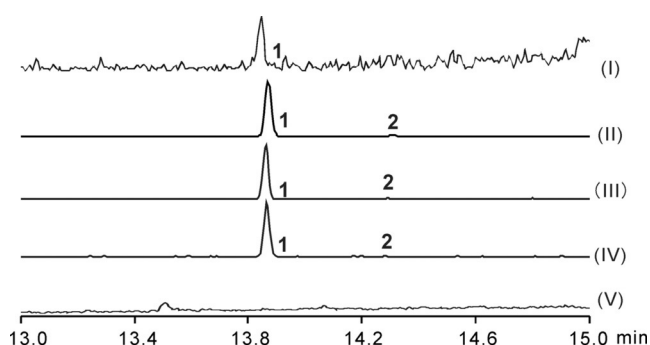


**Abbildung 1.** Diterpene erhalten mit CgDS. Totalionenstromchromatogramme der Produkte von (I) *C. gloeosporioides* ZW139, (II) CgDS mit IPP und DMAPP, (III) CgDS mit GGPP, (IV) *S. cerevisiae* ZW140 und (V) gekochtem CgDS mit GGPP.

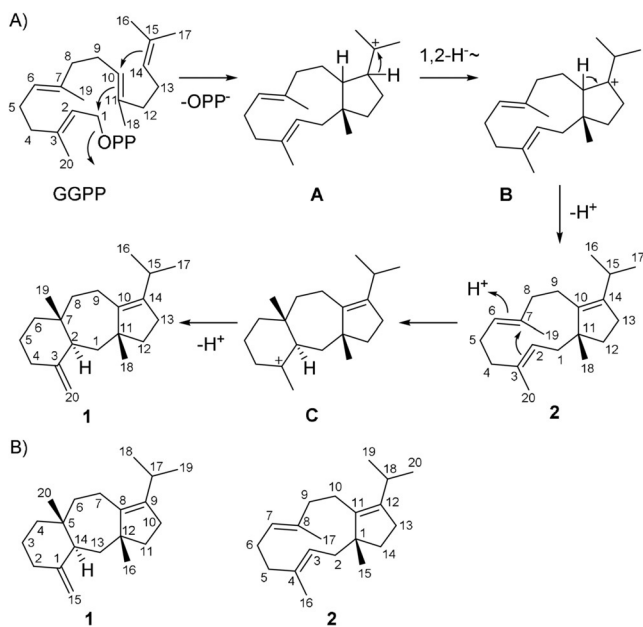
GGPP in der Bildung von **1** neben Spuren eines zweiten Diterpens **2** resultierte (Abbildungen 1 und S5). Dies zeigte, dass die PT-Domäne von Cgl13742 aus DMAPP und IPP das Oligomer GGPP bilden kann, das durch die TS-Domäne in Diterpene umgesetzt wird. Der Assay zur Metallionenabhängigkeit zeigte, dass Cgl13742  $Mg^{2+}$  benötigt (Abbildung S6), während eine leicht reduzierte Aktivität von  $93 \pm 6\%$  mit  $Mn^{2+}$  beobachtet wurde (bezogen auf  $Mg^{2+}$ :  $100 \pm 12\%$ ). Andere zweifach geladene Kationen ( $Ca^{2+}$ ,  $Fe^{2+}$ ,  $Co^{2+}$ ,  $Ni^{2+}$ ,  $Cu^{2+}$  und  $Zn^{2+}$ ) ergaben keine Aktivität. Um die Struktur von **1** zu bestimmen, wurde das Plasmid pZW140 mit dem Gen *Cgl13742* (Abbildung S7) konstruiert und in den Stamm *Saccharomyces cerevisiae* YZL141 mit optimiertem Biosyntheseweg zu den Terpenvorstufen integriert, wodurch der Produktionsstamm *S. cerevisiae* ZW140 erhalten wurde.<sup>[13b]</sup> Nach einer Fermentationszeit von 95 Stunden im Schüttelkolben wurde die Kultur mit Hexan extrahiert und **1** wurde mit einer Ausbeute von  $7.3 \text{ mg L}^{-1}$  isoliert.

Verbindung **1**,  $[\alpha]_D^{20} = +122.1$  ( $c$  0.21, Hexan), wurde durch ein- und zweidimensionale NMR-Spektroskopie (Abbildungen S8–S21) mit vollständiger Zuordnung der NMR-Daten zu allen Kohlenstoff- und Wasserstoffatomen (Tabellen S3–S4) als das Enantiomer von (5*S*,12*S*,14*R*)-Dolasta-1(15),8-dien (Lit.:  $[\alpha]_D = -115.2$ ,  $c$  2.40, Hexan) identifiziert. Diese Verbindung war zuvor als das Produkt einer Behandlung des Naturstoffes (–)- $\delta$ -Araneosen mit HCl in Chloroform bei  $-45^\circ\text{C}$  erhalten worden.<sup>[14]</sup> Verbindung **1** ist also (5*R*,12*R*,14*S*)-Dolasta-1(15),8-dien, und Cgl13742 ist eine *C. gloeosporioides*-Dolasta-1(15),8-dien-Synthase (CgDS). Weder **1** noch dessen Enantiomer sind als Naturstoff bekannt. Obwohl die absolute Konfiguration von **1** aus dessen optischer Aktivität abgeleitet werden konnte, wurde sie hier noch einmal unabhängig bestätigt, um sicherzustellen, dass die Schlussfolgerungen bezüglich des Cyclisierungsmechanismus von Enzymen der Klade II-D korrekt sind. Dies geschah durch enzymatische Umsetzungen diverser enantioselektiv deuterierter Proben, einschließlich (*R*)- und (*S*)-(1-<sup>13</sup>C,1-<sup>2</sup>H)GGPP<sup>[5]</sup> sowie (*R*)- und (*S*)-(1-<sup>13</sup>C,1-<sup>2</sup>H)GPP,<sup>[15]</sup> mit Zusatz von IPP, die enzymatisch durch die PT-Domäne in die entsprechenden Isotopomere des GGPP mit Inversion der Konfiguration an C-1 des GPP überführt wurden.<sup>[16]</sup> Die Deuteriumatome wurden in diastereotope Positionen eingebaut, die auf die absolute Konfiguration von (5*R*,12*R*,14*S*)-**1** verwiesen. Die <sup>13</sup>C-Markierungen in diesen Proben wurden zum Zweck einer empfindlichen Detektion durch HSQC-Spektroskopie eingeführt (Abbildungen S22 und S23). Die Ergebnisse wurden weiterhin mit DMAPP und (*E*)- bzw. (*Z*)-(4-<sup>13</sup>C,4-<sup>2</sup>H)IPP bestätigt,<sup>[17]</sup> die mit bekanntem stereochemischen Verlauf (Angriff an C-4 des IPP von der *Si*-Seite)<sup>[18]</sup> in die entsprechenden Isotopomere des GGPP überführt wurden. Cyclisierung durch die TS-Domäne führte erneut zum Einbau des Deuteriums in Positionen, die auf die absolute Konfiguration von (5*R*,12*R*,14*S*)-**1** hinwiesen (Abbildung S24).

Verbindung **2** wurde aus einer Inkubation der rekombinanten CgDS mit GGPP erhalten und per NMR als  $\delta$ -Araneosen identifiziert (Abbildungen S25–S31, Tabelle S5). Dessen optische Aktivität,  $[\alpha]_D^{20} = +161$  ( $c$  0.02, Hexan) verwies auf das Enantiomer des bekannten Naturstoffes (–)-

(1*S*)- $\delta$ -Araneosen aus *Sordaria araneosa* (Lit.:  $[\alpha]_D = -127.6$ ,  $c$  3.04, Hexan),<sup>[19]</sup> so dass das Nebenprodukt der CgDS als (+)-(1*R*)- $\delta$ -Araneosen (**2**) identifiziert wurde.

Die komplexen Mechanismen von TS, einschließlich mit CgDS verwandter pilzlicher Enzyme, können effizient in Isotopenmarkierungsstudien adressiert werden.<sup>[2b,20]</sup> Der vorgeschlagene Cyclisierungsmechanismus für **1** verläuft über eine typische Reaktion der Klade II mit initialer C1-III-IV-Cyclisierung zu **A**, gefolgt von einer 1,2-Hydridverschiebung zu **B** und Deprotonierung zu **2** (Schema 2). Reprotonierung



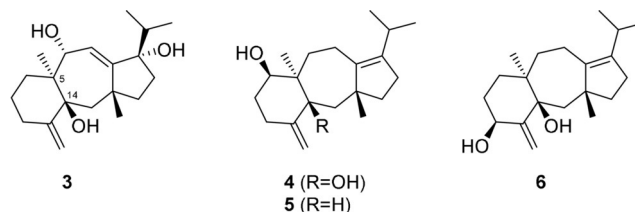
**Schema 2.** A) Cyclisierungsmechanismus für CgDS. Nummerierung der Kohlenstoffatome von **1** und **2** zeigt ihren Ursprung aus GGPP durch dieselbe Nummer an, sodass die beschriebenen Markierungsexperimente leicht zu verfolgen sind. B) Nummerierung der Kohlenstoffatome für **1** und **2** wie in Lit. [14] eingeführt. Diese Nummerierung wurde für die Lokanten zur Beschreibung der absoluten Konfigurationen nach CIP-Nomenklatur verwendet.

an C-6 von GGPP initiiert eine zweite Cyclisierung zu **C** mit abschließender Deprotonierung zu **1**. Dieser Mechanismus wurde durch ein Inkubationsexperiment mit (2-<sup>2</sup>H)DMAPP<sup>[5]</sup> und IPP gestützt, die durch die PT-Domäne von CgDS zu (14-<sup>2</sup>H)GGPP umgesetzt wurden. Die 1,2-Hydridverschiebung von **A** nach **B** zeigte sich im EI-Massenspektrum von markiertem **1**, das den Verlust des Deuteriums durch Abspaltung der *i*Pr-Gruppe anzeigte (Abbildung S32A). Die Deprotonierung von C-10 des GGPP wurde in einer Inkubation von (2-<sup>2</sup>H)GPP (Synthese wie in Schema S1 gezeigt) und IPP mit CgDS demonstriert, was in dem unmarkierten Produkt **1** über (10-<sup>2</sup>H)GGPP resultierte (Abbildung S32B). Weiterhin schlossen diese Experimente klar eine hypothetische Alternative über eine 1,3-Hydridverschiebung ausgehend von **A** und Deprotonierung von C-14 des GGPP zu **2** aus. Obwohl Terpencyclisierungen üblicherweise einem strikten stereochemischen Kurs folgen, wird für die diastereotopen geminalen Me-Gruppen in GGPP oft eine Verteilung beobachtet, wenn die Terpencyclisierungen eine 1,2-Hydridverschiebung

in eine *i*Pr-Gruppe beinhalten,<sup>[5,21]</sup> d. h. das kationische Zentrum in **A** wird von dem wandernden Hydrid von beiden diastereotopen Flächen angegriffen. Dies war auch für CgDS der Fall, wie Inkubationsexperimente mit (16-<sup>13</sup>C)GGPP und (17-<sup>13</sup>C)GGPP demonstrierten, die eine Verteilung der Markierungen über beide entsprechenden Me-Gruppen in **1** anzeigten (Abbildung S33). Die Reprotonierung von **2** an C-6 von GGPP wurde mithilfe von (6-<sup>13</sup>C)GGPP durch Inkubation in einem Deuteriumoxid-Puffer verfolgt, was in einem Triplett im <sup>13</sup>C-NMR infolge <sup>2</sup>H-<sup>13</sup>C-Spinkopplung resultierte (Abbildung S34). Der stereochemische Verlauf der Reprotonierung<sup>[22]</sup> wurde durch HSQC-Analyse des Produktes nachgewiesen, welche den spezifischen Einbau des Deuteriums in den 4-*pro-R*-Wasserstoff von **1** zeigte. Ein Fütterungsexperiment mit Natrium(1-<sup>13</sup>C)acetat lieferte mit diesem Mechanismus konsistente Ergebnisse (Tabelle S6, Abbildung S35).

Neutrale biosynthetische Intermediate wurden in Terpencyclisierungen oft beschrieben, wie z. B. kürzlich für mehrere pflanzliche Sesterterpensynthasen,<sup>[23]</sup> aber diese Intermediate entfallen nicht immer dem aktiven Zentrum. Sie können manchmal mit Enzymvarianten erhalten werden, in denen ein einzelner an der Reprotonierung beteiligter Aminosäurerest ausgetauscht wurde.<sup>[24]</sup> Da berichtet wurde, dass **2** durch milde Säurekatalyse leicht zu **1** reagiert,<sup>[14]</sup> sind wir auch der Frage nachgegangen, ob **1** ein echtes Enzymprodukt ist oder lediglich unter den Kultivierungs- bzw. Inkubationsbedingungen spontan aus **2** gebildet wird. Dazu wurde **2** sowohl mit als auch ohne CgDS in Inkubationspuffer umgesetzt. In beiden Fällen wurden ähnliche Mengen an **1** detektiert (Abbildung S36), diese Umsetzungen waren allerdings träge. Diese Experimente zeigten, dass die spontane Umsetzung von **2** zu **1** in geringem Umfang beteiligt ist, es muss aber eine wichtige Rolle des Enzyms für die Bildung von **1** angenommen werden, da die gefundene langsame spontane Umsetzung von **2** zu **1** die Bildung von **1** als Hauptprodukt nicht erklären kann. Der Grund, warum **2** in Gegenwart des Enzyms nicht schneller zu **1** umgesetzt wird als in dem Experiment ohne Enzym nur in Inkubationspuffer, ist nicht vollständig klar, aber vermutlich ist der Protonierungsstatus bestimmter Aminosäurereste des aktiven Zentrums, die an der Reprotonierung von **2** beteiligt sind, nicht korrekt, wenn die Reaktionskaskade nicht mit GGPP begonnen wird.

Zuvor beschriebene Dolastane umfassen Dolatriol (**3**, Schema 3), das zuerst aus dem giftigen Seehasen *Dolabella auricularia* isoliert wurde,<sup>[25]</sup> aber tatsächlich von Braunalgen produziert und im Seehasen aufgrund seiner Diät akkumuliert wird. Weiterhin sind Amijiol (**4**), 14-Deoxyamijiol (**5**) und Isoamijiol (**6**) aus Braunalgen bekannt.<sup>[26]</sup> Bemerkens-



**Schema 3.** Dolastan-Diterpene aus Braunalgen.

wertweise haben diese Verbindungen aus Algen ein 5,14-Di-*epi*-Gerüst im Vergleich zu pilzlichem **1**. Bisher ist keine TS für Dolastan-Diterpene bekannt, wohingegen das Intermediat  $\delta$ -Araneosen als Nebenprodukt der (+)-Fusicocca-2,10(14)-dien-Synthase aus *P. amygdali* beschrieben wurde.<sup>[7]</sup> Der Zugang zu Dolastanen ist von hohem Interesse, da mehrere oxidierte Vertreter dieser Verbindungsklasse die Wirkungen anderer Medikamente in resistenten Stämmen von *S. aureus* modulieren.<sup>[27]</sup> Funktionalisierte Dolastane könnten ausgehend von **1** zugänglich gemacht werden, wenn selektive Oxygenasen gefunden oder entsprechende chemische Transformationen entwickelt würden.

Zusammengefasst haben wir eine chimäre Diterpensynthase aus *C. gloeosporioides* als (5*R*,12*R*,14*S*)-Dolasta-1-(15),8-dien-Synthase (CgDS) identifiziert und konnten ihr Produkt mit einer akzeptablen Ausbeute von 7.3 mgL<sup>-1</sup> mithilfe eines genetisch manipulierten Hefestammes zugänglich machen. CgDS ist die erste beschriebene pilzliche TS der Klade II-D und katalysiert eine C1-III-IV-Cyclisierung, was mit den Cyclisierungsmodi der bekannten Enzyme der Klade II übereinstimmt. Unglücklicherweise kann wie für mehrere andere TS der Klade II der genaue stereochemische Verlauf der initialen C1-III-IV-Cyclisierung nicht aus den Produkten **1** und **2** abgeleitet werden, aber alle bisher charakterisierten Enzyme der Klade II führen auf einheitliche Weise eine 12*R*-Konfiguration ein.<sup>[2]</sup> Ob die Unterklassen der Klade II unterschiedliche stereochemische Verläufe im Hinblick auf die anderen in der initialen C1-III-IV-Cyclisierung gebildeten Stereozentren repräsentieren, wie es für die Unterklassen der Klade I der Fall ist, bleibt offen. Um diese Frage zu beantworten, wird es nötig sein, weitere Enzyme der Klade II mit Produkten, die den stereochemischen Verlauf der initialen Cyclisierung aufzeigen, zu charakterisieren.

## Danksagung

Diese Arbeit wurde gefördert durch die DFG (DI1536/7-1), durch J1 Biotech Co., Ltd., und durch Sachbeihilfen des Young Talents Program of National High-level Personnel of Special Support Program (The „Ten Thousand Talent Program“), der National Natural Science Foundation of China (31670090 und 31800032) sowie der China Postdoctoral Science Foundation (2017M622507, 2018T110793).

## Interessenkonflikt

Die Autoren erklären, dass keine Interessenkonflikte vorliegen.

**Stichwörter:** Biosynthese · Cyclasen · Diterpene · Dolastane · Isotope

**Zitierweise:** *Angew. Chem. Int. Ed.* **2018**, *57*, 15887–15890  
*Angew. Chem.* **2018**, *130*, 16113–16117

- [1] a) J. S. Dickschat, *Nat. Prod. Rep.* **2016**, *33*, 87; b) Y. Yamada, T. Kuzuyama, M. Komatsu, K. Shin-ya, S. Omura, D. E. Cane, H. Ikeda, *Proc. Natl. Acad. Sci. USA* **2015**, *112*, 857.
- [2] a) T. Mitsuhashi, I. Abe, *ChemBioChem* **2018**, *19*, 1106; b) A. Minami, T. Ozaki, C. Liu, H. Oikawa, *Nat. Prod. Rep.* **2018**, <https://doi.org/10.1039/C8NP00026C>.
- [3] G. Appendino in *Progress in the Chemistry of Organic Natural Products* (Hrsg.: A. D. Kinghorn, H. Falk, S. Gibbons, J. Kobayashi), Springer, Schweiz, **2016**, S. 1–90.
- [4] F. Berru , M. W. B. McCulloch, R. G. Kerr, *Bioorg. Med. Chem.* **2011**, *19*, 6702.
- [5] J. Rinkel, P. Rabe, X. Chen, T. G. K llner, F. Chen, J. S. Dickschat, *Chem. Eur. J.* **2017**, *23*, 10501.
- [6] a) M. J. Smanski, Z. Yu, J. Casper, S. Lin, R. M. Peterson, Y. Chen, E. Wendt-Pienkowski, S. R. Rajski, B. Shen, *Proc. Natl. Acad. Sci. USA* **2011**, *108*, 13498; b) Y.-I. Yang, S. Zhang, K. Ma, Y. Xu, Q. Tao, Y. Chen, J. Chen, S. Guo, J. Ren, W. Wang, Y. Tao, W.-B. Yin, H. Liu, *Angew. Chem. Int. Ed.* **2017**, *56*, 4749; *Angew. Chem.* **2017**, *129*, 4827.
- [7] T. Toyomasu, M. Tsukahara, A. Kaneko, R. Niida, W. Mitsuhashi, T. Dairi, N. Kato, T. Sassa, *Proc. Natl. Acad. Sci. USA* **2007**, *104*, 3084.
- [8] a) Y. Ye, A. Minami, A. Mandi, C. Liu, T. Taniguchi, T. Kuzuyama, K. Monde, K. Gomi, H. Oikawa, *J. Am. Chem. Soc.* **2015**, *137*, 11846; b) T. Mitsuhashi, J. Rinkel, M. Okada, I. Abe, J. S. Dickschat, *Chem. Eur. J.* **2017**, *23*, 10053.
- [9] X.-M. Zhao, Z.-Q. Wang, S.-H. Shu, W.-J. Wang, H.-J. Xu, Y.-J. Ahn, M. Wang, X. Hu, *PLoS One* **2013**, *8*, e61777.
- [10] a) C. M. Starks, K. Back, J. Chappell, J. P. Noel, *Science* **1997**, *277*, 1815; b) E. Y. Shishova, L. Di Costanzo, D. E. Cane, D. W. Christianson, *Biochemistry* **2007**, *46*, 1941.
- [11] P. Baer, P. Rabe, K. Fischer, C. A. Citron, T. A. Klapschinski, M. Groll, J. S. Dickschat, *Angew. Chem. Int. Ed.* **2014**, *53*, 7652; *Angew. Chem.* **2014**, *126*, 7783.
- [12] L. C. Tarshis, P. J. Proteau, B. A. Kellogg, J. C. Sacchettini, C. D. Poulter, *Proc. Natl. Acad. Sci. USA* **1996**, *93*, 15018.
- [13] a) G. Bian, Y. Han, A. Hou, Y. Yuan, X. Liu, Z. Deng, T. Liu, *Metab. Eng.* **2017**, *42*, 1; b) G. Bian, A. Hou, Y. Yuan, B. Hu, S. Cheng, Z. Ye, Y. Di, Z. Deng, T. Liu, *Org. Lett.* **2018**, *20*, 1626; c) G. Bian, Z. Deng, T. Liu, *Curr. Opin. Biotechnol.* **2017**, *48*, 234.
- [14] L. Jenny, H.-J. Borschberg, P. Acklin, *Tetrahedron* **1996**, *52*, 1549.
- [15] P. Rabe, J. Rinkel, E. Dolja, T. Schmitz, B. Nubbemeyer, T. H. Luu, J. S. Dickschat, *Angew. Chem. Int. Ed.* **2017**, *56*, 2776; *Angew. Chem.* **2017**, *129*, 2820.
- [16] H. V. Thulasiram, C. D. Poulter, *J. Am. Chem. Soc.* **2006**, *128*, 15819.
- [17] L. Lauterbach, J. Rinkel, J. S. Dickschat, *Angew. Chem. Int. Ed.* **2018**, *57*, 8280; *Angew. Chem.* **2018**, *130*, 8412.
- [18] J. W. Cornforth, R. H. Cornforth, G. Popjak, L. Yengoyan, *J. Biol. Chem.* **1966**, *241*, 3970.
- [19] L. Jenny, H.-J. Borschberg, *Helv. Chim. Acta* **1995**, *78*, 715.
- [20] a) J. S. Dickschat, *Eur. J. Org. Chem.* **2017**, 4872; b) T. Toyomasu, M. Tsukahara, H. Kenmoku, M. Anada, H. Nitta, J. Okanda, W. Mitsuhashi, T. Sassa, N. Kato, *Org. Lett.* **2009**, *11*, 3044.
- [21] a) I. Burkhardt, T. Siemon, M. Henrot, L. Studt, S. R sler, B. Tudzynski, M. Christmann, J. S. Dickschat, *Angew. Chem. Int. Ed.* **2016**, *55*, 8748; *Angew. Chem.* **2016**, *128*, 8890; b) J. Rinkel, L. Lauterbach, P. Rabe, J. S. Dickschat, *Angew. Chem. Int. Ed.* **2018**, *57*, 3238; *Angew. Chem.* **2018**, *130*, 3292.
- [22] P. Rabe, J. Rinkel, T. A. Klapschinski, L. Barra, J. S. Dickschat, *Org. Biomol. Chem.* **2016**, *14*, 158.
- [23] A. C. Huang, Y. J. Hong, A. D. Bond, D. J. Tantillo, A. Osbourn, *Angew. Chem. Int. Ed.* **2018**, *57*, 1291; *Angew. Chem.* **2018**, *130*, 1305.
- [24] K. A. Rising, C. M. Starks, J. P. Noel, J. Chappell, *J. Am. Chem. Soc.* **2000**, *122*, 1861.

- [25] G. R. Pettit, R. H. Ode, C. L. Herald, R. B. von Dreel, C. Michel, *J. Am. Chem. Soc.* **1976**, *98*, 4677.
- [26] M. Ochi, M. Watanabe, I. Miura, M. Taniguchi, T. Tokoroyama, *Chem. Lett.* **1980**, *9*, 1229.
- [27] C. S. de Figueiredo, S. M. Pinto de Menezes Silva, L. Silva Abreu, E. Ferreira da Silva, M. Sobral da Silva, G. E. Cavalcanti de Miranda, V. C. de O. Costa, M. Le Hyaric, J. Pinto de Sequeira, J. M. B. Filho, J. F. Tavares, *Nat. Prod. Res.* **2018**, <https://doi.org/10.1080/14786419.2018.1470512>.
- Manuskript erhalten: 29. August 2018  
Akzeptierte Fassung online: 2. Oktober 2018  
Endgültige Fassung online: 26. Oktober 2018
-



# Appendix N

## **A Branched Diterpene Cascade: The Mechanism of Spinodiene Synthase from *Saccharopolyspora spinosa***

*Angew. Chem. Int. Ed.* **2019**, *58*, 452–455.

DOI:10.1002/anie.201812216

&

*Angew. Chem.* **2019**, *131*, 461–465.

DOI:10.1002/ange.201812216





## Biosynthesis

International Edition: DOI: 10.1002/anie.201812216  
German Edition: DOI: 10.1002/ange.201812216A Branched Diterpene Cascade: The Mechanism of Spinodiene Synthase from *Saccharopolyspora spinosa*

Jan Rinkel, Lukas Lauterbach, and Jeroen S. Dickschat\*

**Abstract:** A diterpene synthase from *Saccharopolyspora spinosa* was found to convert geranylgeranyl diphosphate into the new natural products spinodiene A and B, accompanied by 2,7,18-dolabellatriene. The structures and the formation mechanism of the enzyme products were investigated by extensive isotopic labelling experiments, which revealed an unusual branched isomerisation mechanism towards the neutral intermediate 2,7,18-dolabellatriene. A Diels–Alder reaction was used to convert the main diterpene product with its rare conjugated diene moiety into formal sesterterpene alcohols.

Among nature's diverse ways to construct small molecules, terpene biosynthesis arguably provides the largest structural variety of natural products that are all made through astonishingly simple enzymatic concepts. Thus, the most important enzymes of this pathway, terpene synthases (TSs), can be seen as the combinatorial playground of evolution for generating small carbon skeletons for beneficial bioactive compounds. Type-I TSs convert a small variety of linear oligoprenyl diphosphates (OPPs), including geranyl- (GPP, C<sub>10</sub>), farnesyl- (FPP, C<sub>15</sub>), geranylgeranyl- (GGPP, C<sub>20</sub>), and geranylgeranyl diphosphate (GFPP, C<sub>25</sub>), into mostly polycyclic hydrocarbons or alcohols with multiple stereocentres.<sup>[1]</sup> These enzymes act on the substrate through diphosphate abstraction and provide a specific architecture of the active site for cation stabilisation, conformational discrimination, and selective termination of the reaction cascade.<sup>[2]</sup> The reaction mechanisms feature all kinds of cation chemistry, such as hydride migrations, proton shifts, and Wagner–Meerwein rearrangements, to yield structurally complex products in only one enzymatic step. Since a time-resolved experimental investigation of these cascades within the enzyme is not possible, structural studies,<sup>[1b]</sup> site-directed mutagenesis,<sup>[3]</sup> quantum chemical calculations,<sup>[4]</sup> and isotopic labelling studies<sup>[5]</sup> have led to a deeper understanding of the synthetic capabilities of TSs. In particular, labelling experiments in combination with in vitro techniques and modern NMR spectroscopy have proved to be an indispensable tool for experimentally testing proposed TS mechanisms. Although the incorporation of isotopes usually results in

clearly substituted product atoms that can be explained through one straightforwardly operating linear cascade, in the present study we addressed a challenging bacterial TS that deviates from this rule.

The soil actinomycete *Saccharopolyspora spinosa* NRRL 18395 is known for its production of spinosyns, a class of polyketide natural products that are used as potent insecticides.<sup>[6]</sup> Its genome harbours a TS, whose sequence features previously identified conserved motifs of TSs for diphosphate binding<sup>[7]</sup> and activation<sup>[8]</sup> together with structurally important residues (Figure S1).<sup>[5e,9]</sup> This TS was characterised as a hedycaryol synthase in our previous studies, but the reaction with FPP proved to be sluggish and its activity as a diterpene synthase (DTS) was not tested.<sup>[10]</sup> A phylogenetic analysis showed that the closest characterised relative was CotB2 for the diterpene cyclooct-9-en-7-ol (Figure S2).<sup>[11]</sup> A reinvestigation of the purified recombinant enzyme (Figure S3) has now demonstrated that GGPP is efficiently converted into a mixture of diterpenes (Figures 1 and S4). The compounds **1**, **2**, and **3** were isolated and their structures were assigned on the basis of one- and two-dimensional NMR experiments.

The obtained NMR data for the main product **1** (Table S1, Figures S5–S12) suggested the structure of a diterpene with a 6-7-5 ring system featuring a rare conjugated diene. NOE correlations fixed the relative configuration with an unusual *cis* stereochemistry at the fused five-membered ring. In terms of ring sizes, some similarity of **1** to the dolastane diterpenes<sup>[12]</sup> can be found, but the ring arrangement is different

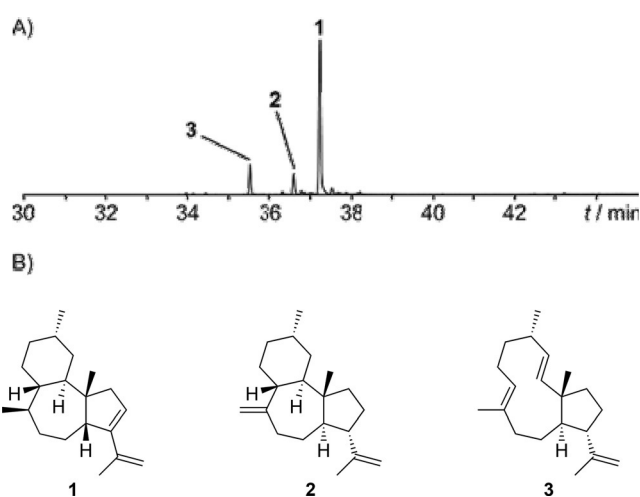


**Figure 1.** A) Total ion chromatogram of the products obtained from GGPP with SoS. B) Structures of the SoS main products spinodiene A (**1**), spinodiene B (**2**), and 2,7,18-dolabellatriene (**3**).

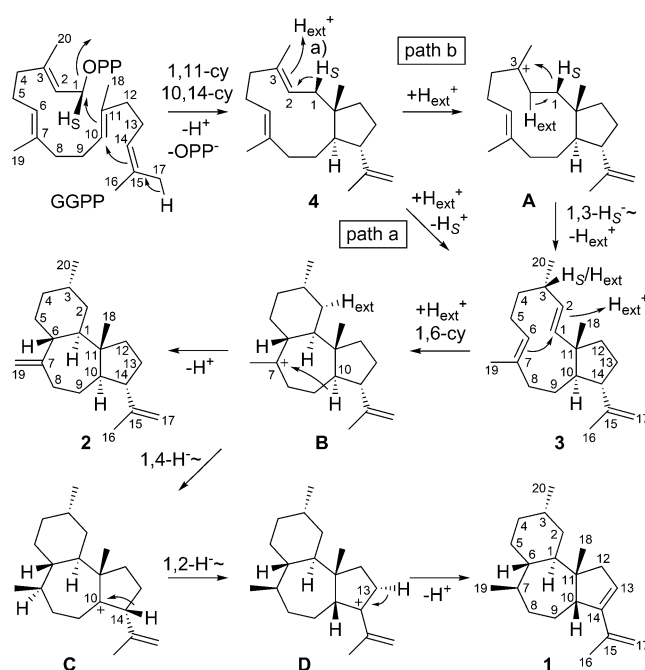
[\*] J. Rinkel, L. Lauterbach, Prof. Dr. J. S. Dickschat  
Kekulé-Institut für Organische Chemie und Biochemie  
Rheinische Friedrich-Wilhelms-Universität Bonn  
Gerhard-Domagk-Strasse 1, 53121 Bonn (Germany)  
E-mail: dickschat@uni-bonn.de

Supporting information and the ORCID identification number for one of the authors of this article can be found under:  
<https://doi.org/10.1002/anie.201812216>.

and **1** represents a new diterpene skeleton. With respect to the origin of its producing enzyme, **1** was named spinodiene A and the TS from *S. spinosa* characterised as a spinodiene synthase (SoS). Compound **2**, spinodiene B, (Table S2, Figures S13–S20) has a similar structure and the same skeleton as **1**, but a different stereochemistry at the five-membered ring and an exocyclic double bond. The third product **3** (Table S3, Figures S21–S27) was characterised as (+)-2,7,18-dolabellatriene with an optical rotation of  $[\alpha]_{\text{D}}^{20} = +23.0$  ( $c = 0.32$ ,  $\text{CHCl}_3$ ), which indicates it to be the enantiomer of *ent*-**3** ( $[\alpha]_{\text{D}}^{20} = -21$ ,  $c = 0.03$ ,  $\text{CHCl}_3$ ), known from the brown alga *Dilophus spiralis*.<sup>[13]</sup>

The biosynthesis of the three SoS products was investigated using all twenty ( $^{13}\text{C}$ )GGPP isotopomers that were obtained by synthesis<sup>[14]</sup> or prepared enzymatically from other synthetic  $^{13}\text{C}$ -labelled precursors such as GPP,<sup>[12c,15]</sup> FPP,<sup>[16]</sup> and isopentenyl diphosphate (IPP)<sup>[14]</sup> using a GGPP synthase (GGPPS) from *Streptomyces cyaneofuscatus*,<sup>[14]</sup> and converted by SoS to give a product mixture of singly  $^{13}\text{C}$ -labelled diterpenes **1–3**.  $^{13}\text{C}$ NMR analysis of these samples allowed for an unambiguous assignment of all the carbon atoms in these products to their originating positions in GGPP (Figures S28–S30). The absolute configurations of **1–3** were determined by conversion of enantioselectively deuterated and  $^{13}\text{C}$ -labelled probes. Sensitive HSQC experiments were used to delineate the incorporation of deuterium into diastereotopic positions in the products and thus simplifies the problem of solving the absolute configuration to the determination of the relative orientation of all the stereocentres with respect to the known absolute configuration of the labelled methylene groups in the target molecule. For this purpose, (*1R*)- and (*1S*)-(1- $^{13}\text{C}$ ,1- $^2\text{H}$ )GPP<sup>[14]</sup> were converted into (*9R*)- and (*9S*)-(9- $^{13}\text{C}$ ,9- $^2\text{H}$ )GGPP through elongation with IPP by using GGPPS. This reaction leads to an established inversion of configuration at C-1 of GPP.<sup>[17]</sup> The obtained HSQC data after conversion with SoS (Figures S31–S33) resulted in the absolute configurations shown in Figure 1, which is in line with the literature data for *ent*-**3**.<sup>[13]</sup> The same principle was extended for other positions by using (*1R*)- and (*1S*)-(1- $^{13}\text{C}$ ,1- $^2\text{H}$ )FPP,<sup>[14]</sup> which was only applicable to **2** (Figure S34), because of overlaying signals at C-5 in the case of **1** and **3**. Dimethylallyl diphosphate (DMAPP) was also elongated with (*E*)- and (*Z*)-(4- $^{13}\text{C}$ ,4- $^2\text{H}$ )IPP<sup>[15f]</sup> through a known stereochemical course<sup>[18]</sup> with FPP synthase (FPPS) from *S. coelicolor*<sup>[19]</sup> and GGPPS to target three more positions (C-4, C-8, and C-12) in a single experiment (Figures S35–S37). All the experiments resulted in the same conclusion on the absolute configurations of **1–3**.

The proposed cyclisation mechanism of SoS (Scheme 1) starts from GGPP with a combined 1,11- and 10,14-cyclisation driven by the abstraction of  $\text{OPP}^-$  and deprotonation to build up (*E,E*)-3,7,18-dolabellatriene (**4**),<sup>[13]</sup> which undergoes isomerisation to **3**, either by a direct reprotonation-deprotonation sequence (path a) or with a 1,3-hydride migration via cation **A** (path b). Protonation of **3** at C-2 induces further cyclisation to **B**, which provides access to **2** upon deprotonation of the Me group. A suprafacial 1,4-hydride shift in **B** yields cation **C**, which stabilises to the allylic tertiary cation **D** with another 1,2-hydride shift that proceeds with *anti*-attack,



**Scheme 1.** Cyclisation mechanism of SoS to its products **1–3**. The numbering of the carbon atoms indicates their origin from GGPP with the same number and deviates from the numbering used in Ref. [13].

and thus explains the *cis*-fused five-membered ring of **1**. A final deprotonation at C-13 builds the conjugated diene system.

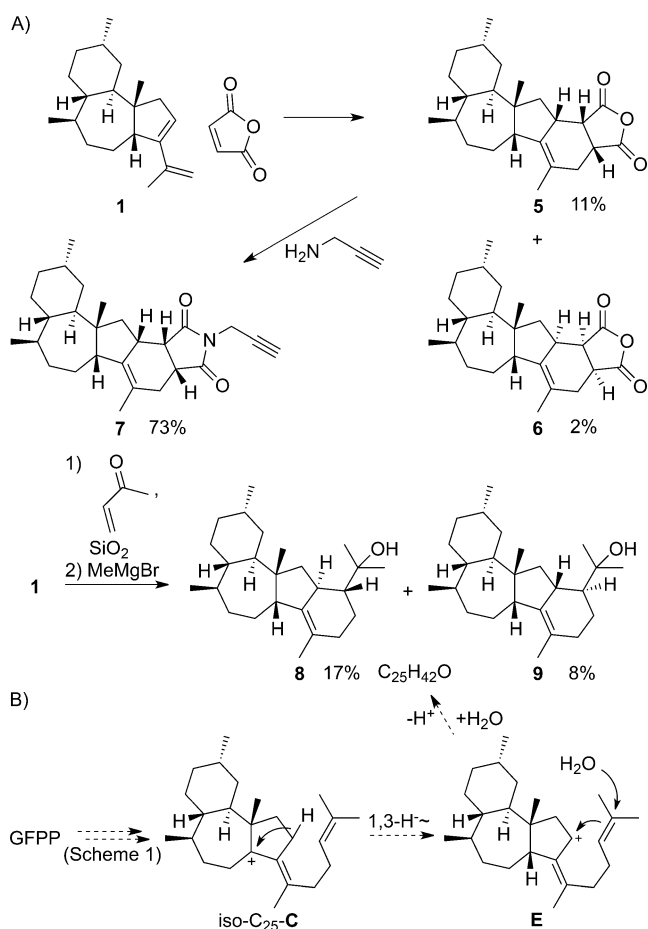
The incubations with (16- $^{13}\text{C}$ )GGPP and (17- $^{13}\text{C}$ )GGPP showed a flexible stereochemical course in the initial deprotonation towards **4**, as evident by the scrambled incorporation of the label into the Me and the methylene groups (Figures S28–S30), which hints to similar distances between the deprotonating base and the two positions. To address the isomerisation problem, (*1R*)- and (*1S*)-(1- $^{13}\text{C}$ ,1- $^2\text{H}$ )GGPP<sup>[20]</sup> were converted with SoS. This resulted in C-1 of **1–3** appearing in the  $^{13}\text{C}$ NMR spectra as singlets for the (*S*)-substrate and upfield shifted triplets arising from a direct  $^{13}\text{C}$ – $^2\text{H}$  bond for the (*R*)-substrate (Figure S38). This experiment demonstrates that  $\text{H}_R$  stays selectively at C-1 during the cyclisation, while  $\text{H}_S$  moves away. However, GC/MS analysis surprisingly demonstrated a partial loss of deuterium from the  $\text{H}_S$  position of **1–3**, but a full retainment of labelling from  $\text{H}_R$  (Figure S39). GC/MS analysis of the products obtained from an incubation experiment with enzymatically prepared (3- $^{13}\text{C}$ )GGPP in  $\text{D}_2\text{O}$  buffer showed the uptake of one or two deuterium atoms for **1** and **2**, but no incorporation or uptake of only one deuterium atom for **3** (Figure S40). These findings support a full incorporation of one deuterium downstream of **3**, in agreement with its protonation-induced cyclisation to **B** only being observed for **1** and **2**. An additional partial deuterium incorporation is found for the reactions leading to **3**. The  $^{13}\text{C}$ NMR spectrum of the product from (3- $^{13}\text{C}$ )GGPP in  $\text{D}_2\text{O}$  buffer revealed both a slightly upfield-shifted singlet and a more strongly upfield shifted triplet for C-3 of **1** and **3**. This finding demonstrates that the partial uptake of deuterium goes into position C-3, while the slight upfield shift of the singlet indicated additional deuterium incorporation at the

neighbouring carbon atom C-2 (Figure S41). Conclusively, C-3 of the enzyme products carries either a hydrogen atom from bulk water ( $H_{\text{ext}}$ ) or another hydrogen atom, for which we assumed the migrating  $H_S$  from C-1 would be a good candidate. Direct evidence for the partial  $H_S$  movement from C-1 to C-3 was obtained using the substrates ( $3\text{-}^{13}\text{C}, 1, 1\text{-}^2\text{H}_2$ )GGPP as well as ( $1R$ )- and ( $1S$ )-( $3\text{-}^{13}\text{C}, 1\text{-}^2\text{H}$ )GGPP, which were synthesised (Scheme S1, Figure S42). Conversion of these substrates with SoS indeed resulted in a singlet and a triplet for C-3 of **1** with ( $3\text{-}^{13}\text{C}, 1, 1\text{-}^2\text{H}_2$ )GGPP and also with the ( $1S$ )-deuterated sample, but only in a singlet with ( $1R$ )-( $3\text{-}^{13}\text{C}, 1\text{-}^2\text{H}$ )GGPP (Figure S43), which allowed for a direct tracking of the partial  $H_S$  location.

Combining these results, the challenging isomerisation of **4** to **3** can be rationalised by two pathways operating simultaneously (Scheme 1). Path a proceeds by a protonation (C-3) and deprotonation (C-1) sequence, which leads to a partial loss of  $H_S$ , and path b involves a protonation (C-2), 1,3-hydride migration, and deprotonation (C-2) sequence, which explains the observed partial movement of  $H_S$  to C-3.

The protonation at C-2 of **3**, for which hints were already obtained by the experiments described above (Figures S40 and S41), was followed by the incubation of ( $2\text{-}^{13}\text{C}$ )GGPP with SoS in  $D_2O$  buffer, which showed a complete incorporation of deuterium through the observation of triplets for C-2 of **1** and **2** (Figure S44). Reprotonation of **3** proceeds with a strict stereochemical course through addition to the *Si*-face, as followed by HSQC. The 1,4-hydride shift from **B** to **C** was confirmed by incubation of ( $2\text{-}^2\text{H}$ )GPP<sup>[12c]</sup> and ( $3\text{-}^{13}\text{C}$ )IPP with SoS and GGPPS (Figure S45, triplet for C-7), and the 1,2-hydride shift to **D** was demonstrated by the incubation of ( $2\text{-}^2\text{H}$ )DMAPP<sup>[20]</sup> and ( $2\text{-}^{13}\text{C}$ )IPP, synthesised from ( $2\text{-}^{13}\text{C}$ )acetic acid (Scheme S2), with SoS, FPPS, and GGPPS (Figure S46, triplet for C-10). For the stereochemical investigation of the final deprotonation step, ( $1R$ )- and ( $1S$ )-( $1\text{-}^2\text{H}$ )IPP were synthesised (Scheme S3, Figure S47) and incubated with isopentenyl diphosphate isomerase (IDI) from *Serratia plymuthica*,<sup>[5g]</sup> followed by its heat inactivation and elongation of the resulting ( $1R$ )- and ( $1S$ )-( $1\text{-}^2\text{H}$ )DMAPP with excess unlabelled IPP by FPPS and GGPPS to suppress the incorporation of additional labelled IPP units. This process yielded ( $13S$ )- and ( $13R$ )-( $13\text{-}^2\text{H}$ )GGPP, which were converted into **1** by SoS with selective deprotonation of  $H_S$  (Figure S48). The product profiles obtained from these samples indicated a significant shift in the product ratios depending on the isotopic nature of  $H_S$ , namely, a significant drop in the yield of **1** in the case of  $H_S = ^2\text{H}$ . In particular, the use of deuterium can sometimes lead to interesting effects, for example, a change in the product distribution for the H309A variant of pentalenene synthase helped to distinguish between alternative cyclisation mechanisms.<sup>[21]</sup> The nature of **3** as an intermediate was studied through the conversion of **3** into **1** by SoS. Although the enzymatic conversion of **3** failed, likely because the active site architecture is in a wrong state if the reaction is not started from GGPP, it was possible to intercept the cyclisation of ( $20\text{-}^{13}\text{C}$ )GGPP by the addition of unlabelled **3**. This product shows a moderate exchange with the active site bound intermediate  $^{13}\text{C}$ -labelled **3** and is further converted into **1** (Figure S49).

The conjugated diene moiety in **1** inspired us to explore the Diels–Alder (DA) chemistry of this new natural product. Challenged by the low availability of starting material from in vitro incubations, **1** was reacted with maleic anhydride (Scheme 2), which gave the main *endo* products **5** (Table S4,



**Scheme 2.** A) Diels–Alder reactions with **1**. B) Hypothetical terpene cyclisation mechanism from GFPP to **8** and **9**.

Figures S50–S57) and **6** (Table S5, Figures S58–S65). The main product **5** was further converted into the imido-alkyne **7** (Table S6, Figures S66–S73). We also aimed to exploit a DA reaction for the conversion of diterpene **1** into a formal sesterterpene. The DA reaction of **1** with methyl vinyl ketone on silica<sup>[22]</sup> produced a complex mixture of inseparable regio- and stereoisomers, but the sesterterpene alcohols **8** (Table S7, Figures S74–S81) and **9** (Table S8, Figures S82–S89) could be purified from the product mixture following a methyl-Grignard reaction. These compounds **8** and **9** represent formal sesterterpene alcohols with an isoprenoid-like carbon skeleton, for which a hypothetical biosynthesis can be rationalised through similar steps as determined for the SoS mechanism proceeding to *iso*- $\text{C}_{25}\text{-C}$  with a double bond at C-14 instead of C-15. A 1,3-hydride shift to **E**, cyclisations with different stereochemical courses, and attack of water can give rise to **8** and **9**.

In summary, we have characterised the function of a TS from *S. spinosa* as spinodiene synthase. This fascinating

enzyme converts GGPP into spinodienes A (**1**) and B (**2**), which feature a new diterpene skeleton, as well as 2,7,18-dolabellatriene (**3**). Extensive labelling studies were used to investigate the cyclisation mechanism of SoS, which harbours an interesting and challenging isomerisation step, for which two different coexisting mechanisms lead to the same products. In a combined synthesis-biosynthesis approach,<sup>[23]</sup> enzymatically prepared **1** was tested for DA reactions, which led to the synthesis of the artificial sesterterpene alcohols **8** and **9**. Their formation can be rationalised by a terpene cyclisation mechanism similar to the mechanism of SoS, but a sesterterpene synthase is unknown. The astonishing synthetic and mechanistic potential of TSs will also pave the way for future investigations into nature's enzymatic playground for small-molecule biosynthesis.

### Acknowledgements

This work was funded by the DFG (DI1536/7-1) and by a PhD fellowship of the Fonds der Chemischen Industrie (to J.R.). We thank Andreas Schneider for HPLC purifications.

### Conflict of interest

The authors declare no conflict of interest.

**Keywords:** biosynthesis · enzyme mechanisms · isotopes · NMR spectroscopy · terpenes

**How to cite:** *Angew. Chem. Int. Ed.* **2019**, *58*, 452–455  
*Angew. Chem.* **2019**, *131*, 461–465

- [1] a) J. S. Dickschat, *Nat. Prod. Rep.* **2016**, *33*, 87–110; b) D. W. Christianson, *Chem. Rev.* **2017**, *117*, 11570.
- [2] a) Y. Gao, R. B. Honzatko, R. J. Peters, *Nat. Prod. Rep.* **2012**, *29*, 1153; b) Y. J. Hong, D. J. Tantillo, *Chem. Sci.* **2013**, *4*, 2512.
- [3] a) M. Seemann, G. Zhai, J.-W. de Kraker, C. M. Paschall, D. W. Christianson, D. E. Cane, *J. Am. Chem. Soc.* **2002**, *124*, 7681; b) D. Morrone, M. Xu, D. B. Fulton, M. K. Determan, R. J. Peters, *J. Am. Chem. Soc.* **2008**, *130*, 5400; c) I. I. Abdallah, R. van Merkerk, E. Klumpenaar, W. J. Quax, *Sci. Rep.* **2018**, *8*, 9961; d) R. Driller, S. Janke, M. Fuchs, E. Warner, A. R. Mhashal, D. T. Major, M. Christmann, T. Brück, B. Loll, *Nat. Commun.* **2018**, *9*, 3971.
- [4] a) D. J. Tantillo, *Nat. Prod. Rep.* **2011**, *28*, 1035; b) T. Ansbacher, Y. Freud, D. T. Major, *Biochemistry* **2018**, *57*, 3773; c) M. Xu, M. Jia, Y. J. Hong, X. Yin, D. J. Tantillo, P. J. Proteau, R. J. Peters, *Org. Lett.* **2018**, *20*, 1200; d) D. J. Tantillo, *Angew. Chem. Int. Ed.* **2017**, *56*, 10040; *Angew. Chem.* **2017**, *129*, 10172.
- [5] a) D. E. Cane, *Chem. Rev.* **1990**, *90*, 1089; b) J. S. Dickschat, *Nat. Prod. Rep.* **2011**, *28*, 1917; c) A. Meguro, Y. Motoyoshi, K. Teramoto, S. Ueda, Y. Totsuka, Y. Ando, T. Tomita, S.-Y. Kim, T. Kimura, M. Igarashi, R. Sawa, T. Shinada, M. Nishiyama, T. Kuzuyama, *Angew. Chem. Int. Ed.* **2015**, *54*, 4353; *Angew. Chem.* **2015**, *127*, 4427; d) B. Qin, Y. Matsuda, T. Mori, M. Okada, Z. Quan, T. Mitsuhashi, T. Wakimoto, I. Abe, *Angew. Chem. Int. Ed.* **2016**, *55*, 1658; *Angew. Chem.* **2016**, *128*, 1690; e) J. S. Dickschat, *Eur. J. Org. Chem.* **2017**, 4872; f) L. Lauterbach, J. Rinkel, J. S. Dickschat, *Angew. Chem. Int. Ed.* **2018**, *57*, 8280; *Angew. Chem.* **2018**, *130*, 8412; g) J. Rinkel, L. Lauterbach, P. Rabe, J. S. Dickschat, *Angew. Chem. Int. Ed.* **2018**, *57*, 3238; *Angew. Chem.* **2018**, *130*, 3292; h) J. Takino, T. Kozaki, Y. Sato, C. Liu, T. Ozaki, A. Minami, H. Oikawa, *J. Am. Chem. Soc.* **2018**, *140*, 12392.
- [6] a) F. P. Mertz, R. C. Yao, *Int. J. Syst. Bacteriol.* **1990**, *40*, 34; b) H. J. Kim, M. W. Ruszczycky, S. Choi, Y. Liu, H. Liu, *Nature* **2011**, *473*, 109.
- [7] D. W. Christianson, *Chem. Rev.* **2006**, *106*, 3412.
- [8] P. Baer, P. Rabe, K. Fischer, C. A. Citron, T. A. Klapschinski, M. Groll, J. S. Dickschat, *Angew. Chem. Int. Ed.* **2014**, *53*, 7652; *Angew. Chem.* **2014**, *126*, 7783.
- [9] J. Rinkel, L. Lauterbach, J. S. Dickschat, *Angew. Chem. Int. Ed.* **2017**, *56*, 16385; *Angew. Chem.* **2017**, *129*, 16603.
- [10] J. S. Dickschat, K. A. K. Pahirulzaman, P. Rabe, T. A. Klapschinski, *ChemBioChem* **2014**, *15*, 810.
- [11] S.-Y. Kim, P. Zhao, M. Igarashi, R. Sawa, T. Tomita, M. Nishiyama, T. Kuzuyama, *Chem. Biol.* **2009**, *16*, 736.
- [12] a) G. R. Pettit, R. H. Ode, C. L. Herald, R. B. von Dreele, C. Michel, *J. Am. Chem. Soc.* **1976**, *98*, 4677; b) M. Ochi, M. Watanabe, I. Miura, M. Taniguchi, T. Tokoroyama, *Chem. Lett.* **1980**, *9*, 1229; c) G. Bian, J. Rinkel, Z. Wang, L. Lauterbach, A. Hou, Y. Yuan, Z. Deng, T. Liu, J. S. Dickschat, *Angew. Chem. Int. Ed.* **2018**, *57*, 15885; *Angew. Chem.* **2018**, *130*, 16113.
- [13] E. Ioannou, A. Quesada, M. M. Rahman, S. Gibbons, C. Vagias, V. Roussis, *J. Nat. Prod.* **2011**, *74*, 213.
- [14] P. Rabe, J. Rinkel, E. Dolja, T. Schmitz, B. Nubbemeyer, T. H. Luu, J. S. Dickschat, *Angew. Chem. Int. Ed.* **2017**, *56*, 2776; *Angew. Chem.* **2017**, *129*, 2820.
- [15] T. Mitsuhashi, J. Rinkel, M. Okada, I. Abe, J. S. Dickschat, *Chem. Eur. J.* **2017**, *23*, 10053.
- [16] P. Rabe, L. Barra, J. Rinkel, R. Riclea, C. A. Citron, T. A. Klapschinski, A. Janusko, J. S. Dickschat, *Angew. Chem. Int. Ed.* **2015**, *54*, 13448; *Angew. Chem.* **2015**, *127*, 13649.
- [17] H. V. Thulasiram, C. D. Poulter, *J. Am. Chem. Soc.* **2006**, *128*, 15819.
- [18] J. W. Cornforth, R. H. Cornforth, G. Popják, L. Yengoyan, *J. Biol. Chem.* **1966**, *241*, 3970.
- [19] P. Rabe, J. Rinkel, B. Nubbemeyer, T. G. Köllner, F. Chen, J. S. Dickschat, *Angew. Chem. Int. Ed.* **2016**, *55*, 15420; *Angew. Chem.* **2016**, *128*, 15646.
- [20] J. Rinkel, P. Rabe, X. Chen, T. G. Köllner, F. Chen, J. S. Dickschat, *Chem. Eur. J.* **2017**, *23*, 10501.
- [21] L. Zu, M. Xu, M. W. Lodewyk, D. E. Cane, R. J. Peters, D. J. Tantillo, *J. Am. Chem. Soc.* **2012**, *134*, 11369.
- [22] V. V. Veselovsky, A. S. Gybin, A. V. Lozanova, A. M. Moiseenkov, W. A. Smit, R. Caple, *Tetrahedron Lett.* **1988**, *29*, 175.
- [23] A. Kirschning, F. Hahn, *Angew. Chem. Int. Ed.* **2012**, *51*, 4012; *Angew. Chem.* **2012**, *124*, 4086.

Manuscript received: October 24, 2018

Accepted manuscript online: November 14, 2018

Version of record online: December 6, 2018

## Biosynthese

Deutsche Ausgabe: DOI: 10.1002/ange.201812216  
Internationale Ausgabe: DOI: 10.1002/anie.201812216Eine verzweigte Diterpenkaskade: der Mechanismus der Spinodien-Synthese aus *Saccharopolyspora spinosa*

Jan Rinkel, Lukas Lauterbach und Jeroen S. Dickschat\*

**Abstract:** Eine Diterpensynthese aus *Saccharopolyspora spinosa* konvertierte Geranylgeranyldiphosphat in die neuen Naturstoffe Spinodien A und B, begleitet von 2,7,18-Dolabellatrien. Die Strukturen und die Bildungsmechanismen der Enzymprodukte wurden mithilfe von Isotopenmarkierungsexperimenten studiert, wodurch ein ungewöhnlicher verzweigter Isomerisierungsmechanismus zu dem neutralen Intermediat 2,7,18-Dolabellatrien aufgedeckt wurde. Durch eine Diels-Alder-Reaktion wurde das Diterpen-Hauptprodukt mit seiner seltenen konjugierten Dien-Einheit in formale Sesterterpenalkohole überführt.

Unter den diversen Wegen der Natur, kleine Moleküle zu konstruieren, führt die Terpenbiosynthese zur wohl größten Strukturvielfalt unter den Naturstoffen, die alle durch erstaunlich einfache enzymatische Konzepte gemacht werden. Somit können die wichtigsten Enzyme dieses Biosyntheseweges, die Terpen-Synthasen (TS), als kombinatorische Spielwiese zum Aufbau kleiner Kohlenstoffgerüste für nützliche biologisch aktive Verbindungen gesehen werden. Typ-I-TS wandeln eine kleine Anzahl linearer Oligoprenyldiphosphate (OPPs), einschließlich Geranyl- (GPP, C<sub>10</sub>), Farnesyl- (FPP, C<sub>15</sub>), Geranylgeranyl- (GGPP, C<sub>20</sub>) und Geranylarnesyldiphosphat (GFPP, C<sub>25</sub>), in zumeist polycyclische Kohlenwasserstoffe oder Alkohole mit multiplen Stereozentren um.<sup>[1]</sup> Diese Enzyme wechselwirken mit dem Substrat durch Diphosphat-Abstraktion und stellen ein aktives Zentrum mit spezifischer Architektur für die Stabilisierung von Kationen und Substratkonformation sowie für die selektive Terminierung der Reaktionskaskade zur Verfügung.<sup>[2]</sup> Die Reaktionsmechanismen umfassen das gesamte Spektrum der typischen Kationenchemie wie Hydridwanderungen, Protonenverschiebungen und Wagner-Meerwein-Umlagerungen, um strukturell komplexe Produkte in nur einem enzymatischen Schritt zu erzeugen. Da zeitaufgelöste experimentelle Untersuchungen an diesen Reaktionskaskaden im Enzym nicht möglich sind, wurden Strukturstudien,<sup>[1b]</sup> ortsgerechte Mutagenesen,<sup>[3]</sup> quantenchemische Rechnungen<sup>[4]</sup> und Isotopenmarkierungsstudien<sup>[5]</sup> für ein vertieftes Verständnis der Möglichkeiten von TS für Synthesen durchgeführt. Insbesondere Markierungsexperimente in Kombination mit In-

vitro-Techniken und moderner NMR-Spektroskopie erwiesen sich als unverzichtbare Methode zur experimentellen Untersuchung von vorgeschlagenen TS-Mechanismen. Während der Einbau von Isotopen gewöhnlich in eindeutig substituierten Produktatomen resultiert, wofür zur Erklärung eine geradlinige Cyclisierungskaskade angeführt werden kann, präsentieren wir hier eine herausfordernde bakterielle TS, die von dieser Regel abweicht.

Der bodenbürtige Actinomycet *Saccharopolyspora spinosa* NRRL 18395 produziert die Spinosyne, eine Klasse von Polyketid-Naturstoffen, die als potente Insektizide verwendet werden.<sup>[6]</sup> Sein Genom beherbergt eine TS, deren Sequenz die gut bekannten konservierten Motive für Diphosphatanbindung<sup>[7]</sup> und -aktivierung<sup>[8]</sup> sowie strukturell wichtige Reste aufweist (Abbildung S1).<sup>[5g,9]</sup> Diese TS war in einer unserer früheren Arbeiten als Hedycaryol-Synthase charakterisiert worden, aber die Reaktion mit FPP erwies sich als träge und eine Aktivität als Diterpen-Synthase (DTS) war nicht geprüft worden.<sup>[10]</sup> Auf Basis einer phylogenetischen Analyse wurde CotB2 für das Diterpen Cyclooctat-9-en-7-ol als nächster Verwandter gefunden (Abbildung S2).<sup>[11]</sup> Die erneute Untersuchung des gereinigten rekombinanten Enzyms (Abbildung S3) zeigte nun, dass GGPP effizient in eine Mischung von Diterpenen umgesetzt wurde (Abbildungen 1 und S4). Die Verbindungen **1**, **2** und **3** wurden isoliert und ihre Strukturen wurden durch ein- und zweidimensionale NMR-Experimente aufgeklärt.

Die erhaltenen NMR-Daten für das Hauptprodukt **1** (Tabelle S1, Abbildungen S5–S12) verwiesen auf die Struktur

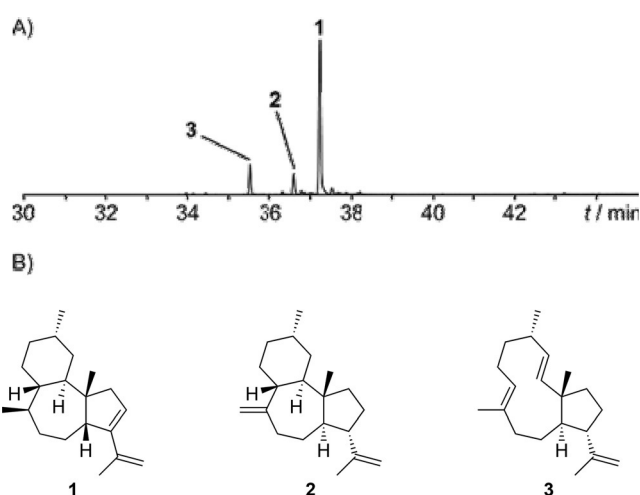


**Abbildung 1.** A) Gesamtionenstrom-Chromatogramm der mit SoS aus GGPP erhaltenen Produkte. B) Strukturen der Hauptprodukte von SoS: Spinodien A (**1**), Spinodien B (**2**) und 2,7,18-Dolabellatrien (**3**).

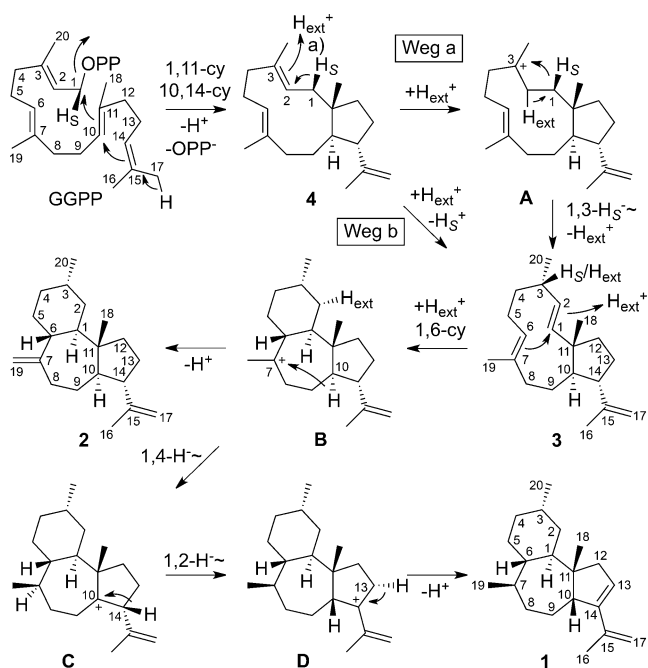
[\*] J. Rinkel, L. Lauterbach, Prof. Dr. J. S. Dickschat  
Kekulé-Institut für Organische Chemie und Biochemie  
Rheinische Friedrich-Wilhelms-Universität Bonn  
Gerhard-Domagk-Straße 1, 53121 Bonn (Deutschland)  
E-Mail: dickschat@uni-bonn.de

Hintergrundinformationen und die Identifikationsnummer (ORCID) eines Autors sind unter:  
<https://doi.org/10.1002/ange.201812216> zu finden.

eines Diterpens mit einem 6-7-5-Ringsystem und einer seltenen konjugierten Dien-Einheit. NOE-Korrelationen bestätigten eine relative Konfiguration mit ungewöhnlicher *cis*-Anordnung am anellierten Fünfring. Hinsichtlich der Ringgrößen hat **1** eine gewisse Ähnlichkeit mit Dolastan-Diterpenen,<sup>[12]</sup> aber die Ringanordnung ist unterschiedlich und **1** repräsentiert ein neues Diterpengerüst. Bezugnehmend auf den Ursprung des produzierenden Enzyms wurde **1** Spinodien A genannt, sodass die TS aus *S. spinosa* als Spinodien-Synthase (SoS) charakterisiert wurde. Verbindung **2**, Spinodien B (Tabelle S2, Abbildungen S13–S20), hat eine ähnliche Struktur und dasselbe Gerüst wie **1**, unterscheidet sich aber durch die Stereochemie am Fünfring und durch die exocyclische Doppelbindung. Das dritte Produkt **3** (Tabelle S3, Abbildungen S21–S27) wurde als (+)-2,7,18-Dolabellatrien mit einem Drehwert von  $[\alpha]_{\text{D}}^{20} = +23.0$  ( $c = 0.32$ ,  $\text{CHCl}_3$ ) identifiziert, ist also das Enantiomer von *ent*-**3** ( $[\alpha]_{\text{D}}^{20} = -21$ ,  $c = 0.03$ ,  $\text{CHCl}_3$ ), das aus der Braunalge *Dilophus spiralis* bekannt ist.<sup>[13]</sup>

Die Biosynthese der drei SoS-Produkte wurde mit allen zwanzig ( $^{13}\text{C}_1$ )GGPP-Isotopomeren untersucht, die durch Synthese<sup>[14]</sup> oder enzymatisch aus anderen synthetischen  $^{13}\text{C}$ -markierten Vorstufen wie GPP,<sup>[12c,15]</sup> FPP<sup>[16]</sup> und Isopentenylidiphosphat (IPP)<sup>[14]</sup> mit der GGPP-Synthase (GGPPS) aus *Streptomyces cyaneofuscatus* erhalten wurden.<sup>[14]</sup> Umsetzung mit der SoS lieferte eine Produktmischung einfach  $^{13}\text{C}$ -markierter Diterpene **1–3**. Eine  $^{13}\text{C}$ -NMR-Analyse dieser Proben erlaubte die unzweifelhafte Zuordnung aller Kohlenstoffatome in diesen Produkten bezüglich ihres Ursprungs aus GGPP (Abbildungen S28–S30). Die absoluten Konfigurationen von **1–3** wurden durch Konversion enantioselektiv deuterierter und  $^{13}\text{C}$ -markierter Proben bestimmt. Diese Methode nutzt empfindliche HSQC-Experimente, um den Einbau von Deuterium in diastereotop Positionen der Produkte zu verfolgen, und vereinfacht das Problem der Bestimmung der absoluten Konfiguration zu einer Bestimmung der relativen Orientierung aller Stereozentren zur bekannten absoluten Konfiguration der markierten Methylengruppen in den Zielmolekülen. Zu diesem Zweck wurden (1*R*)- und (1*S*)-(1- $^{13}\text{C}$ ,1- $^2\text{H}$ )GPP<sup>[14]</sup> durch die GGPPS mit IPP zu (9*R*)- und (9*S*)-(9- $^{13}\text{C}$ ,9- $^2\text{H}$ )GGPP verlängert. Für diese Reaktion ist die Inversion der Konfiguration an C-1 von GPP gut bekannt.<sup>[17]</sup> Die nach Umsetzung mit SoS erhaltenen HSQC-Daten (Abbildungen S31–S33) resultierten in den absoluten Konfigurationen wie in Abbildung 1 gezeigt, was mit den Literaturdaten für Verbindung *ent*-**3** im Einklang ist.<sup>[13]</sup> Dasselbe Prinzip wurde für andere Positionen unter Verwendung von (1*R*)- und (1*S*)-(1- $^{13}\text{C}$ ,1- $^2\text{H}$ )FPP<sup>[14]</sup> angewendet, was wegen überlappender Signale für C-5 von **1** und **3** nur für **2** eindeutige Ergebnisse lieferte (Abbildung S34). Dimethylallyldiphosphat (DMAPP) wurde ebenso mit (*E*)- und (*Z*)-(4- $^{13}\text{C}$ ,4- $^2\text{H}$ )IPP<sup>[5f]</sup> mit bekanntem stereochemischen Verlauf<sup>[18]</sup> durch die FPP-Synthase (FPPS) aus *S. coelicolor*<sup>[19]</sup> und GGPPS verlängert, um in einem einzigen Experiment drei weitere Positionen zu adressieren (C-4, C-8 und C-12, Abbildungen S35–S37). Alle Experimente verwiesen übereinstimmend auf dieselben absoluten Konfigurationen von **1–3**.

Der vorgeschlagene Cyclisierungsmechanismus der SoS (Schema 1) startet ausgehend von GGPP mit einer kombinierten 1,11- und 10,14-Cyclisierung, die durch die Abstraktion von  $\text{OPP}^-$  getrieben und durch Deprotonierung zu



**Schema 1.** Cyclisierungsmechanismus von SoS zu den Produkten **1–3**. Die Nummerierung der Kohlenstoffatome verweist durch identische Nummer auf den Ursprung aus GGPP und weicht von der in Lit. [13] eingeführten Nummerierung ab.

(*E,E*)-3,7,18-Dolabellatrien (**4**) abgeschlossen wird.<sup>[13]</sup> Verbindung **4** unterliegt einer Isomerisierung zu **3**, die entweder durch eine direkte Sequenz aus Reprotonierung und Deprotonierung (Weg a) oder mit einer 1,3-Hydridwanderung über Kation **A** (Weg b) ablaufen kann. Protonierung von **3** an C-2 induziert eine weitere Cyclisierung zu **B**, das durch Deprotonierung der Me-Gruppe Zugang zu **2** gibt. Eine suprafaciale 1,4-Hydridverschiebung in **B** liefert das Kation **C**, das sich mit einer weiteren 1,2-Hydridverschiebung mit *anti*-Angriff, der den *cis*-anellierten Fünfring in **1** erklärt, zum tertiären Allylkation **D** stabilisiert. Eine abschließende Deprotonierung an C-13 ergibt das konjugierte Dien-System.

Die Inkubationen mit (16- $^{13}\text{C}$ )GGPP und (17- $^{13}\text{C}$ )GGPP zeigten einen flexiblen stereochemischen Verlauf in der ersten Deprotonierung zu **4** durch einen auf die Me- und die Methylengruppe verteilten Einbau der Markierung (Abbildungen S28–S30), was auf ähnliche Distanzen der deprotonierenden Base zu beiden Positionen hinweist. Um das Problem der Isomerisierung zu adressieren, wurden (1*R*)- und (1*S*)-(1- $^{13}\text{C}$ ,1- $^2\text{H}$ )GGPP<sup>[20]</sup> mit der SoS umgesetzt, wodurch ein Singulett für das (*S*)-Substrat und ein hochfeldverschobenes Triplett wegen einer direkten  $^{13}\text{C}$ - $^2\text{H}$ -Bindung für das (*R*)-Substrat für C-1 von **1–3** im  $^{13}\text{C}$ -NMR-Spektrum resultierten (Abbildung S38). Dieses Experiment zeigt, dass  $\text{H}_R$  während der Cyclisierung selektiv an C-1 verbleibt, wohingegen  $\text{H}_S$  wandert. Eine GC/MS-Analyse zeigte allerdings

einen teilweisen Verlust des Deuteriums aus der  $H_S$ -Position für **1**–**3**, aber vollen Einbau der Markierung aus  $H_R$  (Abbildung S39). Ein Inkubationsexperiment mit enzymatisch hergestelltem ( $3\text{-}^{13}\text{C}$ )GGPP in einem  $\text{D}_2\text{O}$ -Puffer gefolgt von GC/MS-Analyse der Produkte demonstrierte die Aufnahme von einem oder zwei Deuteriumatomen für **1** und **2**, aber keinen Einbau oder Aufnahme nur eines Deuteriumatoms für **3** (Abbildung S40). Dieses Ergebnis unterstützt den vollen Einbau eines Deuteriums in den Cyclisierungsreaktionen nach **3**, was mit dessen durch Protonierung induzierter Cyclisierung zu **B** im Einklang ist und daher nur für **1** und **2** beobachtet wird. Ein zusätzlicher partieller Einbau von Deuterium wird für die vorangehenden Reaktionen zu **3** gefunden. Das  $^{13}\text{C}$ -NMR-Spektrum des Produktes von ( $3\text{-}^{13}\text{C}$ )GGPP in  $\text{D}_2\text{O}$ -Puffer zeigte sowohl ein leicht hochfeldverschobenes Singulett als auch ein stärker hochfeldverschobenes Triplet für C-3 von **1** und **3**, was den partiellen Einbau von Deuterium in Position C-3 demonstriert, während das leicht hochfeldverschobene Singulett einen zusätzlichen Deuteriumeinbau am benachbarten Kohlenstoff C-2 anzeigt (Abbildung S41). Also trägt C-3 der Enzymprodukte entweder ein Wasserstoff aus dem wässrigen Medium ( $H_{\text{ext}}$ ) oder ein anderes Wasserstoffatom, wofür das wandernde  $H_S$  von C-1 ein guter Kandidat ist. Ein direkter Nachweis für die partielle Bewegung von  $H_S$  von C-1 zu C-3 wurde mit den Substraten ( $3\text{-}^{13}\text{C}, 1, 1\text{-}^2\text{H}_2$ )GGPP sowie ( $1R$ )- und ( $1S$ )-( $3\text{-}^{13}\text{C}, 1\text{-}^2\text{H}$ )GGPP erhalten, die synthetisiert wurden (Schema S1, Abbildung S42). Konversion dieser Substrate mit der SoS resultierte tatsächlich in einem Singulett und einem Triplet für C-3 von **1** mit ( $3\text{-}^{13}\text{C}, 1, 1\text{-}^2\text{H}_2$ )GGPP und auch mit der ( $1S$ )-deuterierten Probe, aber mit ( $1R$ )-( $3\text{-}^{13}\text{C}, 1\text{-}^2\text{H}$ )GGPP wurde nur ein Singulett beobachtet (Abbildung S43), was die direkte Verfolgung der partiellen  $H_S$ -Positionen erlaubte.

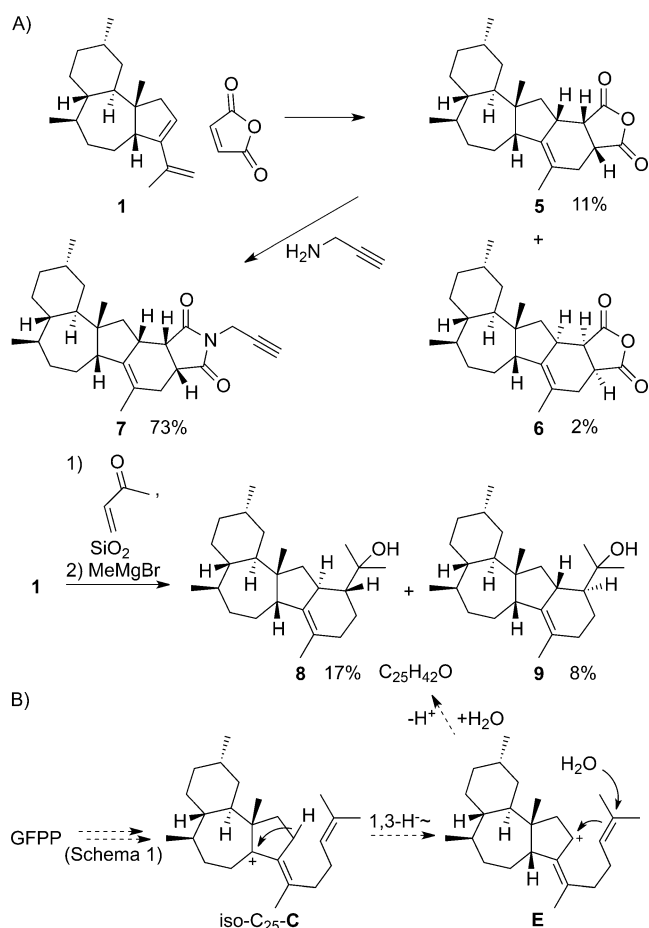
Zusammenfassend kann die herausfordernde Isomerisierung von **4** zu **3** durch zwei simultan ablaufende Reaktionspfade rationalisiert werden (Schema 1). Weg (a) verläuft über eine Sequenz aus Protonierung (C-3) und Deprotonierung (C-1), die zum teilweisen Verlust von  $H_S$  führt, und Weg (b) beinhaltet eine Sequenz aus Protonierung (C-2), einer 1,3-Hydridwanderung und einer Deprotonierung (C-2), was die beobachtete partielle Bewegung von  $H_S$  nach C-3 erklärt.

Die Protonierung an C-2 von **3**, für die bereits Hinweise durch die oben beschriebenen Experimente erhalten wurden (Abbildungen S40 und S41), wurde durch Inkubation von ( $2\text{-}^{13}\text{C}$ )GGPP mit SoS in  $\text{D}_2\text{O}$ -Puffer verfolgt, was durch Triplets den kompletten Einbau von Deuterium an C-2 von **1** und **2** anzeigte (Abbildung S44). Die Reprotonierung von **3** verläuft mit einem strikten stereochemischen Kurs durch Addition von der *Si*-Seite, wie durch HSQC verfolgt werden konnte. Die 1,4-Hydridverschiebung von **B** zu **C** wurde durch Inkubation von ( $2\text{-}^2\text{H}$ )GPP<sup>[12c]</sup> und ( $3\text{-}^{13}\text{C}$ )IPP mit SoS und GGPPS bestätigt (Abbildung S45, Triplet für C-7), und die 1,2-Hydridwanderung zu **D** wurde durch Inkubation von ( $2\text{-}^2\text{H}$ )DMAPP<sup>[20]</sup> und ( $2\text{-}^{13}\text{C}$ )IPP, letzteres synthetisiert aus ( $2\text{-}^{13}\text{C}$ )Essigsäure (Schema S2), mit SoS, FPPS und GGPPS bestätigt (Abbildung S46, Triplet für C-10). Für stereochemische Untersuchungen der finalen Deprotonierung wurden ( $1R$ )- und ( $1S$ )-( $1\text{-}^2\text{H}$ )IPP synthetisiert (Schema S3, Abbildung S47) und mit Isopentenylidiphosphat-Isomerase (IDI)

aus *Serratia plymuthica* inkubiert,<sup>[5a]</sup> gefolgt von deren Hitzeinaktivierung und Verlängerung des resultierenden ( $1R$ )- und ( $1S$ )-( $1\text{-}^2\text{H}$ )DMAPP mit einem Überschuss an unmarkiertem IPP durch FPPS und GGPPS, um den Einbau weiterer markierter IPP-Einheiten zu unterdrücken. Dieses Vorgehen ergab ( $13S$ )- und ( $13R$ )-( $13\text{-}^2\text{H}$ )GGPP, das mit SoS zu **1** mit selektiver Deprotonierung von  $H_S$  umgesetzt wurde (Abbildung S48). Die mit diesen Proben erhaltenen Produktzusammensetzungen zeigten eine signifikante Verschiebung der Produktverhältnisse in Abhängigkeit des verwendeten Isotops für  $H_S$ , d. h. einen signifikanten Rückgang der Bildung von **1** falls  $H_S = ^2\text{H}$ . Insbesondere die Verwendung von Deuterium kann manchmal interessante Effekte hervorrufen, z. B. konnte mit der H309A-Variante der Pentalenen-Synthase eine Veränderung in der Produktverteilung gefunden werden, die es erlaubte, zwischen zwei alternativen Cyclisierungsmechanismen zu unterscheiden.<sup>[21]</sup> Die Natur von **3** als Intermediat wurde durch den Versuch einer Umsetzung von **3** zu **1** mit der SoS studiert. Während diese enzymatische Umsetzung von **3** fehlschlug, vermutlich da das aktive Zentrum sich in einem falschen Zustand befindet, wenn die Reaktion nicht ausgehend von GGPP gestartet wird, war es möglich, die Cyclisierung von ( $20\text{-}^{13}\text{C}$ )GGPP durch Addition von unmarkiertem **3** abzufangen, was zu einem moderaten Austausch mit dem im aktiven Zentrum gebundenen intermediären  $^{13}\text{C}$ -markierten **3** führt, sodass auch unmarkiertes **3** weiter zu **1** umgesetzt wird (Abbildung S49).

Die konjugierte Dien-Einheit in **1** inspirierte uns, die Chemie dieses neuen Naturstoffs in Diels-Alder-Reaktionen (DA) zu untersuchen. Eine besondere Herausforderung lag in der geringen Verfügbarkeit von Startmaterial aus Enzyminkubationen, trotzdem konnte **1** mit Maleinsäureanhydrid zur Reaktion gebracht werden (Schema 2), was die *endo*-Produkte **5** (Tabelle S4, Abbildungen S50–S57) und **6** (Tabelle S5, Abbildungen S58–S65) lieferte. Das Hauptprodukt **5** wurde weiter in das Imido-Alkin **7** umgesetzt (Tabelle S6, Abbildungen S66–S73). Wir hatten weiterhin eine Umsetzung des Diterpens **1** durch DA-Reaktion in ein formales Sesterterpen zum Ziel. Dies gelang durch DA-Reaktion von **1** mit Methylvinylketon auf Silikagel,<sup>[22]</sup> was eine komplexe Mischung untrennbarer Regio- und Stereoisomere ergab, aber aus der Produktmischung einer nachfolgenden Me-Grignard-Reaktion konnten die Sesterterpenalkohole **8** (Tabelle S7, Abbildungen S74–S81) und **9** (Tabelle S8, Abbildungen S82–S89) isoliert werden. Die Verbindungen **8** und **9** repräsentieren formale Sesterterpenalkohole mit einem isoprenoiden Gerüst, für die eine hypothetische Biosynthese mit ähnlichen Schritten wie für den SoS-Mechanismus gefunden rationalisiert werden kann, nämlich mit Reaktionen zu *iso*- $\text{C}_{25}\text{-C}$  mit einer Doppelbindung an C-14 statt an C-15. Eine 1,3-Hydridverschiebung zu **E**, Cyclisierungen mit unterschiedlichem stereochemischem Verlauf und Angriff von Wasser liefern **8** und **9**.

Zusammengefasst haben wir die Funktion einer TS aus *S. spinosa* als Spinodien-Synthase aufgeklärt. Dieses faszinierende Enzym konvertiert GGPP in die Spinodiene A (**1**) und B (**2**) mit einem neuen Diterpengerüst sowie in 2,7,18-Dolabellatrien (**3**). Extensive Markierungsstudien wurden durchgeführt, um den Cyclisierungsmechanismus der SoS aufzu-



**Schema 2.** A) Diels-Alder-Reaktionen mit **1**. B) Hypothetischer Terpen-Cyclisierungsmechanismus von GFPP zu **8** und **9**.

decken, der eine interessante Isomerisierung umfasst, für die zwei unterschiedliche, coexistierende Mechanismen, die zum selben Produkt führen, gefunden wurden. In einer Kombination aus synthetischem und biosynthetischem Ansatz<sup>[23]</sup> wurde enzymatisch hergestelltes **1** in DA-Reaktionen eingesetzt, was einen Zugang zu den künstlichen Sesterterpenalkoholen **8** und **9** eröffnete. Deren Bildung kann durch einen Terpen-cyclisierungsmechanismus rationalisiert werden, der demjenigen der SoS ähnelt, aber eine entsprechende Sesterterpensynthese ist unbekannt. Das erstaunliche synthetische und mechanistische Potenzial von TS wird auch zukünftige Untersuchungen an den enzymatischen Reaktionen der Natur zu kleinen Molekülen ermöglichen.

### Danksagung

Diese Arbeit wurde durch die DFG (DI1536/7-1) und ein Doktorandenstipendium des Fonds der Chemischen Industrie (an J.R.) unterstützt. Wir danken Andreas Schneider für HPLC-Reinigungen.

### Interessenkonflikt

Die Autoren erklären, dass keine Interessenkonflikte vorliegen.

**Stichwörter:** Biosynthese · Enzymmechanismen · Isotope · NMR-Spektroskopie · Terpene

**Zitierweise:** *Angew. Chem. Int. Ed.* **2019**, *58*, 452–455  
*Angew. Chem.* **2019**, *131*, 461–465

- [1] a) J. S. Dickschat, *Nat. Prod. Rep.* **2016**, *33*, 87–110; b) D. W. Christianson, *Chem. Rev.* **2017**, *117*, 11570.  
[2] a) Y. Gao, R. B. Honzatko, R. J. Peters, *Nat. Prod. Rep.* **2012**, *29*, 1153; b) Y. J. Hong, D. J. Tantillo, *Chem. Sci.* **2013**, *4*, 2512.  
[3] a) M. Seemann, G. Zhai, J.-W. de Kraker, C. M. Paschall, D. W. Christianson, D. E. Cane, *J. Am. Chem. Soc.* **2002**, *124*, 7681; b) D. Morrone, M. Xu, D. B. Fulton, M. K. Determan, R. J. Peters, *J. Am. Chem. Soc.* **2008**, *130*, 5400; c) I. I. Abdallah, R. van Merkerk, E. Klumpenaar, W. J. Quax, *Sci. Rep.* **2018**, *8*, 9961; d) R. Driller, S. Janke, M. Fuchs, E. Warner, A. R. Mhasal, D. T. Major, M. Christmann, T. Brück, B. Loll, *Nat. Commun.* **2018**, *9*, 3971.  
[4] a) D. J. Tantillo, *Nat. Prod. Rep.* **2011**, *28*, 1035; b) T. Ansbacher, Y. Freud, D. T. Major, *Biochemistry* **2018**, *57*, 3773; c) M. Xu, M. Jia, Y. J. Hong, X. Yin, D. J. Tantillo, P. J. Proteau, R. J. Peters, *Org. Lett.* **2018**, *20*, 1200; d) D. J. Tantillo, *Angew. Chem. Int. Ed.* **2017**, *56*, 10040; *Angew. Chem.* **2017**, *129*, 10172.  
[5] a) D. E. Cane, *Chem. Rev.* **1990**, *90*, 1089; b) J. S. Dickschat, *Nat. Prod. Rep.* **2011**, *28*, 1917; c) A. Meguro, Y. Motoyoshi, K. Teramoto, S. Ueda, Y. Totsuka, Y. Ando, T. Tomita, S.-Y. Kim, T. Kimura, M. Igarashi, R. Sawa, T. Shinada, M. Nishiyama, T. Kuzuyama, *Angew. Chem. Int. Ed.* **2015**, *54*, 4353; *Angew. Chem.* **2015**, *127*, 4427; d) B. Qin, Y. Matsuda, T. Mori, M. Okada, Z. Quan, T. Mitsuhashi, T. Wakimoto, I. Abe, *Angew. Chem. Int. Ed.* **2016**, *55*, 1658; *Angew. Chem.* **2016**, *128*, 1690; e) J. S. Dickschat, *Eur. J. Org. Chem.* **2017**, 4872; f) L. Lauterbach, J. Rinkel, J. S. Dickschat, *Angew. Chem. Int. Ed.* **2018**, *57*, 8280; *Angew. Chem.* **2018**, *130*, 8412; g) J. Rinkel, L. Lauterbach, P. Rabe, J. S. Dickschat, *Angew. Chem. Int. Ed.* **2018**, *57*, 3238; *Angew. Chem.* **2018**, *130*, 3292; h) J. Takino, T. Kozaki, Y. Sato, C. Liu, T. Ozaki, A. Minami, H. Oikawa, *J. Am. Chem. Soc.* **2018**, *140*, 12392.  
[6] a) F. P. Mertz, R. C. Yao, *Int. J. Syst. Bacteriol.* **1990**, *40*, 34; b) H. J. Kim, M. W. Ruszczycky, S. Choi, Y. Liu, H. Liu, *Nature* **2011**, *473*, 109.  
[7] D. W. Christianson, *Chem. Rev.* **2006**, *106*, 3412.  
[8] P. Baer, P. Rabe, K. Fischer, C. A. Citron, T. A. Klapschinski, M. Groll, J. S. Dickschat, *Angew. Chem. Int. Ed.* **2014**, *53*, 7652; *Angew. Chem.* **2014**, *126*, 7783.  
[9] J. Rinkel, L. Lauterbach, J. S. Dickschat, *Angew. Chem. Int. Ed.* **2017**, *56*, 16385; *Angew. Chem.* **2017**, *129*, 16603.  
[10] J. S. Dickschat, K. A. K. Pahirulzaman, P. Rabe, T. A. Klapschinski, *ChemBioChem* **2014**, *15*, 810.  
[11] S.-Y. Kim, P. Zhao, M. Igarashi, R. Sawa, T. Tomita, M. Nishiyama, T. Kuzuyama, *Chem. Biol.* **2009**, *16*, 736.  
[12] a) G. R. Pettit, R. H. Ode, C. L. Herald, R. B. von Dreele, C. Michel, *J. Am. Chem. Soc.* **1976**, *98*, 4677; b) M. Ochi, M. Watanabe, I. Miura, M. Taniguchi, T. Tokoroyama, *Chem. Lett.* **1980**, *9*, 1229; c) G. Bian, J. Rinkel, Z. Wang, L. Lauterbach, A. Hou, Y. Yuan, Z. Deng, T. Liu, J. S. Dickschat, *Angew. Chem. Int. Ed.* **2018**, *57*, 15885; *Angew. Chem.* **2018**, *130*, 16113.  
[13] E. Ioannou, A. Quesada, M. M. Rahman, S. Gibbons, C. Vagias, V. Roussis, *J. Nat. Prod.* **2011**, *74*, 213.



- [14] P. Rabe, J. Rinkel, E. Dolja, T. Schmitz, B. Nubbemeyer, T. H. Luu, J. S. Dickschat, *Angew. Chem. Int. Ed.* **2017**, *56*, 2776; *Angew. Chem.* **2017**, *129*, 2820.
- [15] T. Mitsuhashi, J. Rinkel, M. Okada, I. Abe, J. S. Dickschat, *Chem. Eur. J.* **2017**, *23*, 10053.
- [16] P. Rabe, L. Barra, J. Rinkel, R. Riclea, C. A. Citron, T. A. Klapschinski, A. Janusko, J. S. Dickschat, *Angew. Chem. Int. Ed.* **2015**, *54*, 13448; *Angew. Chem.* **2015**, *127*, 13649.
- [17] H. V. Thulasiram, C. D. Poulter, *J. Am. Chem. Soc.* **2006**, *128*, 15819.
- [18] J. W. Cornforth, R. H. Cornforth, G. Popják, L. Yengoyan, *J. Biol. Chem.* **1966**, *241*, 3970.
- [19] P. Rabe, J. Rinkel, B. Nubbemeyer, T. G. Köllner, F. Chen, J. S. Dickschat, *Angew. Chem. Int. Ed.* **2016**, *55*, 15420; *Angew. Chem.* **2016**, *128*, 15646.
- [20] J. Rinkel, P. Rabe, X. Chen, T. G. Köllner, F. Chen, J. S. Dickschat, *Chem. Eur. J.* **2017**, *23*, 10501.
- [21] L. Zu, M. Xu, M. W. Lodewyk, D. E. Cane, R. J. Peters, D. J. Tantillo, *J. Am. Chem. Soc.* **2012**, *134*, 11369.
- [22] V. V. Veselovsky, A. S. Gybin, A. V. Lozanova, A. M. Moiseenkov, W. A. Smit, R. Caple, *Tetrahedron Lett.* **1988**, *29*, 175.
- [23] A. Kirschning, F. Hahn, *Angew. Chem. Int. Ed.* **2012**, *51*, 4012; *Angew. Chem.* **2012**, *124*, 4086.

Manuskript erhalten: 24. Oktober 2018

Akzeptierte Fassung online: 14. November 2018

Endgültige Fassung online: 6. Dezember 2018



## Appendix O

### **Addressing the Chemistry of Germacrene A by Isotope Labeling Experiments**

*Org. Lett.* **2019**, *21*, 2426–2429.

DOI:10.1021/acs.orglett.9b00725



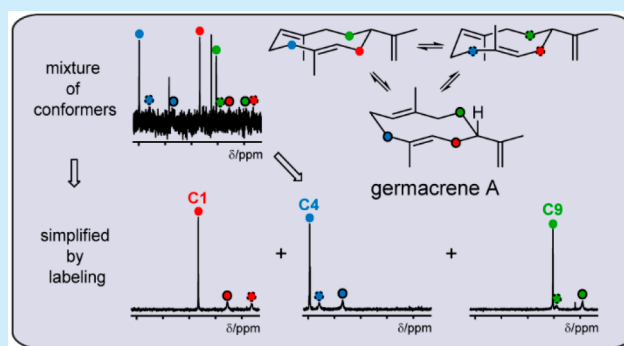
# Addressing the Chemistry of Germacrene A by Isotope Labeling Experiments

Jan Rinkel and Jeroen S. Dickschat\*<sup>✉</sup>

Kekulé-Institute for Organic Chemistry and Biochemistry, University of Bonn, Gerhard-Domagk-Str. 1, 53121 Bonn, Germany

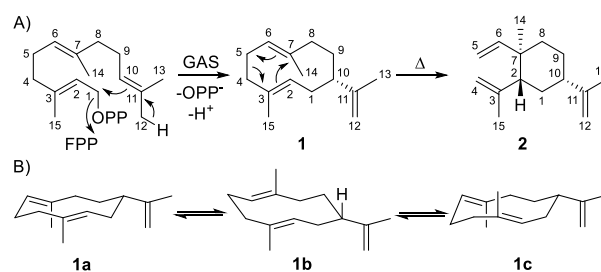
**S** Supporting Information

**ABSTRACT:** Despite the central role of germacrene A in sesquiterpene biosynthesis and its widespread occurrence in nature, its complete NMR characterization is still pending. This problem was solved through enzymatic preparation of germacrene A isotopomers that allowed for a full signal assignment to all three conformers. The obtained materials gave insights into the stereochemical course of the Cope rearrangement to  $\beta$ -elemene and uncovered the Cope rearrangement as a new EI-MS fragmentation reaction.



The sesquiterpene germacrene A (**1**) is probably the most abundant member of the germacrane class of natural products.<sup>1</sup> The molecule itself and the related germacradienyl cations are discussed as intermediates for numerous sesquiterpenoid biosynthesis pathways including those to eremophilanes, cadinanes, muurolanes, amorphanes, or eudesmanes,<sup>2</sup> via bicyclogermacrene to the maalianes, gorgonanones, and zieranes,<sup>3</sup> and to oxidation products such as germacrone<sup>4</sup> or costunolide.<sup>5</sup> Despite their comparably simple biosynthesis, germacranees are still challenging targets for synthetic chemistry.<sup>6</sup> First isolated in pure form in 1970 from the gorgonian *Eunicia mammosa*,<sup>7</sup> (–)-**1** was also found in aphids as an alarm pheromone,<sup>8</sup> in soft corals<sup>9</sup> and in termites,<sup>10</sup> whereas its enantiomer (+)-**1** is abundant in higher plants such as *Solidago canadensis*<sup>11</sup> and was recently also reported as a byproduct of a fungal intermedeol synthase from *Termitomyces*.<sup>12</sup> Also several germacrene A synthases covering both enantiomers have been investigated.<sup>13</sup> However, isolation, characterization, and handling of pure **1** is accompanied by severe experimental drawbacks that result from its reactivity. The double bonds of the ten-membered ring are known to undergo transannular cyclizations to the eudesmanes selin-11-en-4-ol, selina-4,11-diene,  $\alpha$ -selinene, and  $\beta$ -selinene under slightly acidic conditions such as silica based purifications.<sup>11</sup> A Cope rearrangement of **1** at elevated temperatures to  $\beta$ -elemene (**2**) is also frequently observed and characterizes its GC/MS behavior.<sup>7–14</sup> The reaction is reported to occur even at freezer storage of **1** over extended periods of time.<sup>7</sup> The ring system of **1** is represented by three conformers in solution, whose structures **1a–1c** (Scheme 1) have been assigned by NOE spectroscopy and coexist in a ratio of 5:3:2 in both CDCl<sub>3</sub> and C<sub>6</sub>D<sub>6</sub>. Although this ratio was reported to change to two NMR data sets (4:3) at 50 °C, no significant alteration compared to room temperature was found at –20 °C.<sup>15</sup>

**Scheme 1.** (A) Cyclization of FPP to (–)-Germacrene A (**1**) and Its Cope Rearrangement to (+)- $\beta$ -Elemene (**2**)<sup>a</sup>; (B) Structures of the Three Conformers of **1** Observed in Solution<sup>15</sup>



<sup>a</sup>The numbering of carbons reflect their origin from FPP.

Because of this complex mixture featuring broadened and overlapping signals, a complete NMR characterization of **1** has never been accomplished. The central role of **1** in terpene biosynthesis challenged us to address this task and other mechanistic aspects of the remarkable germacrene A chemistry with isotopically labeled terpene precursors.<sup>16</sup>

The marine actinomycete *Micromonospora marina* DSM 45555<sup>17</sup> harbors a terpene synthase (TS), whose overall amino acid sequence is phylogenetically clustered with an uncharacterized group of TSs from *Micromonospora* (Figure S1) and shows the typical conserved motifs (Figure S2). Its gene was cloned into the *E. coli* expression vector pYE-Express<sup>18</sup> (Table S1) and the resulting recombinant purified protein (Figure S3) possessed sesquiterpene cyclase activity, but no product was observed from geranyl- (C<sub>10</sub>), geranylgeranyl- (C<sub>20</sub>), or

Received: February 26, 2019

Published: March 12, 2019

geranylarnesyl diphosphate ( $C_{25}$ ). GC/MS analysis of the products obtained from farnesyl diphosphate (FPP,  $C_{15}$ ) showed a sharp peak corresponding to **2**, followed by a broad rising signal which ends with a sharp peak of **1** (Figure S4). This GC/MS behavior is typical for **1** and understandable by a Cope rearrangement taking place at the GC inlet and on the GC column promoted by rising temperatures. GC analysis on a chiral stationary phase and comparison to (+)-**2**, the Cope rearrangement product of (–)-**1** obtained with spata-13,17-diene synthase (SpS) from *Streptomyces xinghaiensis*,<sup>19</sup> and (–)-**2** obtained from a W335F variant of intermedeol synthase (STC4) from *Termitomyces*,<sup>12</sup> characterized the TS from *M. marina* as a (–)-germacrene A synthase (GAS) (Figure S5).

GAS was used to convert all 15 enzymatically or synthetically prepared isotopomers of ( $^{13}C_1$ )FPP<sup>16,20</sup> into the corresponding  $^{13}C$ -labeled samples of **1**. Their  $^{13}C$  NMR analysis allowed focus to be directed toward just one carbon position in the molecule for which strongly enhanced signals were obtained (Figures S6–S7). In all cases, one fairly sharp, yet still broadened signal was observed for conformer **1a** that is also found in the spectrum of unlabeled **1**, accompanied by two very broad signals for **1b** and **1c**, with peak integrals reflecting the reported ratio of 5:3:2.<sup>15</sup> Differentiation between **1b** and **1c** was also supported by the peak integrals of the corresponding HSQC spectra. With this information, it is well understandable why the NMR assignment of **1** is troublesome, because especially the broad signals of the two minor conformers are barely visible in the unlabeled case, but the  $^{13}C_1$ -labeling allowed for an assignment of all positions of **1a–1c** (Table 1). Only for the quaternary C-7 in **1b** and **1c** the assignment was obscured by low and overlaying signals. The incubations of ( $^{12-13}C$ )- and ( $^{13-13}C$ )FPP resulted in a scrambled incorporation of the labels into the corresponding

methyl and methylene groups, demonstrating a poor selectivity for the deprotonation step of GAS that is sometimes observed also for other TSs.<sup>12,21</sup>

The  $^1H$  NMR assignment of **1** was performed using enzymatically prepared enantiospecifically deuterated and at the same position  $^{13}C$ -labeled FPP isotopomers allowing for sensitive HSQC spectroscopy. Incubation experiments with GAS, FPP synthase (FPPS) from *S. coelicolor*,<sup>22</sup> dimethylallyl diphosphate (DMAPP), and (*Z*)- and (*E*)-(4- $^{13}C$ ,4- $^2H$ )-isopentenyl diphosphate (IPP)<sup>23</sup> followed by HSQC analysis of the product allowed for an unambiguous assignment of the hydrogen atoms of **1a–c** at C-4 and C-8 in a stereospecific manner (Figures S8–S9). In these experiments, the stereochemical information at C-4 of IPP is transferred with a known course to C-4 and C-8 of FPP (IPP attacks DMAPP and GPP in the FPPS-catalyzed formation of FPP from the Si face of C-4).<sup>24</sup> The other methylene groups C-1, C-5, and C-9 were addressed using (*1R*)- and (*1S*)-(1- $^{13}C$ ,1- $^2H$ )IPP, which were synthesized in analogy to the corresponding non- $^{13}C$ -labeled IPPs (Scheme S1, Figure S10).<sup>21</sup> Incubation with GAS, FPPS, and isopentenyl diphosphate isomerase (IDI)<sup>25</sup> from *E. coli* (Table S1, Figure S3) led to stereoselectively deuterated and  $^{13}C$ -labeled FPPs by elongation of IDI-produced (*1R*)- and (*1S*)-(1- $^{13}C$ ,1- $^2H$ )DMAPP with two units of labeled IPP with inversion of configuration at C-1,<sup>24b</sup> which were converted by GAS to **1**, labeled at C-1, C-5, and C-9. The resulting HSQC spectra allowed for an assignment of all hydrogens at these positions of **1a–1c** (Figures S11–S13). The remaining  $^1H$  chemical shifts of Me and olefinic CH groups were deduced from the HSQC spectra of the singly  $^{13}C$ -labeled samples (Figures S14–S20).

As pointed out by Woodward and Hoffmann, the strict stereochemical course of pericyclic reactions can be explained from the symmetry of the highest occupied molecular orbitals.<sup>26</sup> For unsubstituted systems the stereochemical course cannot be followed, but extensive deuterium labeling experiments demonstrated the validity of the Woodward–Hoffmann rules for the Diels–Alder stem system (butadiene + ethylene → cyclohexene).<sup>27</sup> For [3,3]-sigmatropic (e.g., Cope) rearrangements such deuterium labeling experiments at unsubstituted carbons have never been performed, likely because of the difficulties associated with the preparation of deuterium labeled materials in the required high stereochemical purity. In a textbook example the methylated substrates *meso*- and *rac*-3,4-dimethylhexa-1,5-diene were applied to study the stereochemical course of the Cope rearrangement.<sup>28</sup> In the course of this study, stereospecifically deuterated isotopomers of **1** were obtained enzymatically, carrying the labelings at the methylene positions C-4 and C-5 that are directly involved in the Cope rearrangement. The deuterated samples were thermally rearranged to **2**, which gave the unique opportunity to follow the stereochemical course of the Cope rearrangement for unsubstituted carbons by following the selective incorporation of each hydrogen atom at C-4 and C-5 of **1** into the positions of  $H_E$  and  $H_Z$  of **2** (Table S2, Figures S21–S22). The results demonstrated a strict stereochemical course for these hydrogens explainable by a chairlike transition state starting from the major conformer **1a**<sup>29</sup> (Scheme 2).

Further analysis of the rearrangement products by HSQC at the aliphatic positions C-1, C-8, and C-9 independently confirmed the absolute configuration of (+)-**2** (Figures S23–S24). Cope rearrangement of the 15 isotopomers of ( $^{13}C_1$ )-**1**

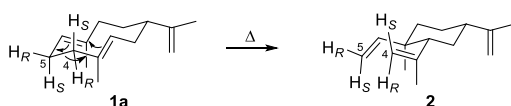
**Table 1.** NMR Data of **1** ( $C_6D_6$ , 298 K) Assigned to Its Conformers **1a–c**

$\delta$ /ppm	<b>1a</b>		<b>1b</b>		<b>1c</b>	
	no. <sup>a</sup>	$^{13}C$	$^1H$	$^{13}C$	$^1H$	$^{13}C$
C-1	35.3 <sup>b</sup>	$\alpha$ 2.10 $\beta$ 2.27	33.1	$\alpha$ 1.81 $\beta$ 2.29	31.3	$\alpha$ 1.82 $\beta$ 2.26
C-2	132.0 <sup>b</sup>	4.52 <sup>b</sup>	125.7	5.11	127.3	5.14
C-3	128.8 <sup>b</sup>	–	135.7	–	136.3	–
C-4	39.9	$\alpha$ 2.10 $\beta$ 1.87	37.4	$\alpha$ 2.15 $\beta$ 2.06	39.2	$\alpha$ 2.05 $\beta$ 2.06
C-5	27.1	$\alpha$ 2.19 $\beta$ 2.03	24.7	$\alpha$ 2.27 $\beta$ 1.98	24.7	$\alpha$ 2.01 $\beta$ 2.28
C-6	126.9 <sup>b</sup>	4.77 <sup>b</sup>	122.3	5.01	129.1	4.89
C-7	137.9 <sup>b</sup>	–	137.8 <sup>c</sup>	–	134.9 <sup>c</sup>	–
C-8	42.1 <sup>b</sup>	$\alpha$ 2.34 $\beta$ 2.02	41.9	$\alpha$ 2.06 $\beta$ 1.89	35.1	$\alpha$ 2.34 $\beta$ 1.67
C-9	34.1 <sup>b</sup>	$\alpha$ 1.51 $\beta$ 1.69	31.8	$\alpha$ 1.31 $\beta$ 1.52	33.8	$\alpha$ 1.68 $\beta$ 1.52
C-10	51.8 <sup>b</sup>	1.96	48.5	1.91	46.2	2.00
C-11	153.6 <sup>b</sup>	–	152.1	–	151.0	–
C-12	107.9 <sup>b</sup>	<i>Z</i> 4.79 <sup>b</sup> <i>E</i> 4.69 <sup>b</sup>	108.1	<i>Z</i> 4.82 <i>E</i> 4.72	108.8	<i>Z</i> 4.81 <i>E</i> 4.70
C-13	20.4 <sup>b</sup>	1.67 <sup>b</sup>	20.0	1.67	20.1	1.67
C-14	16.3 <sup>b</sup>	1.32 <sup>b</sup>	16.8	1.44	22.1	1.62
C-15	16.8 <sup>b</sup>	1.45 <sup>b</sup>	15.5	1.42 <sup>b</sup>	15.5	1.42

<sup>a</sup>Numbering as in Scheme 1. <sup>b</sup>Matching previous assignment.<sup>15</sup>

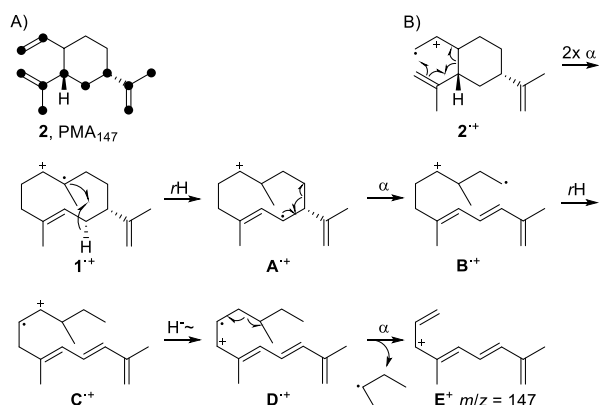
<sup>c</sup>Signals may be interchanged because of signal overlap.

**Scheme 2. Stereochemical Course of the Cope Rearrangement to 2**



resulted in the incorporation of labelings into the expected positions of **2** (Figure S25). The rearranged products allowed the EI-MS fragmentation of **2** to be studied by a position specific mass shift analysis (PMA) in which the contribution of each carbon to a fragment ion can be followed by the incorporation of labeling (Figure S26).<sup>30</sup> The formation of the fragment  $m/z = 147$  was particularly interesting, because it derives from two not directly connected carbon fragments of **2** (Scheme 3). Therefore, an unusual bond making event

**Scheme 3. (A) PMA<sub>147</sub> of  $\beta$ -Elemene (**2**);<sup>a</sup> (B) Proposed EI-MS Fragmentation Mechanism**



<sup>a</sup>Black dots represent carbon atoms that are part of this fragment.

between C-4 and C-5 during fragmentation has to be assumed. This is possible from **2**<sup>+</sup> by a radical-induced formal Cope rearrangement to **1**<sup>+</sup>, followed by a transannular hydrogen migration to **A**<sup>+</sup> and  $\alpha$ -cleavage to **B**<sup>+</sup>. Two more hydrogen movements via a six-membered transition state to **C**<sup>+</sup> and then to the fully conjugated octatetraenyl cation **D**<sup>+</sup> followed by  $\alpha$ -cleavage result in **E**<sup>+</sup> with  $m/z = 147$ . An alternative explanation for the formation of this fragment from a thermal back reaction of **2** to **1** in the ion source preceding ionization would require substantial conversion which has not been observed before for comparable systems, even at higher temperatures.<sup>31</sup>

The transformation from **1**<sup>+</sup> to **A**<sup>+</sup> along this fragmentation mechanism was further studied for its stereochemical course. Therefore, (1R)- and (1S)-(1-<sup>2</sup>H)FPP<sup>32</sup> were converted by GAS into the corresponding isotopomers of **1** that thermally rearranged into the **2** isotopomers during GC/MS analysis. Significantly more deuterium was lost during the formation of **E**<sup>+</sup> from the (*S*) sample as compared to the (*R*) sample (Figure S27), demonstrating the preferred movement of H<sub>S</sub> in the transformation from **1**<sup>+</sup> to **A**<sup>+</sup> likely as a result of a defined conformation of **1**<sup>+</sup> imprinted by the Cope-like transition state. In contrast, no stereochemical implications were found for the conversion of linear **B**<sup>+</sup> to **C**<sup>+</sup>, which was addressed with (*SR*)- and (*SS*)-(1-<sup>2</sup>H)FPP, enzymatically prepared from (1R)- and (1S)-(1-<sup>2</sup>H)GPP<sup>33</sup> and IPP with FPPS. Conversion with GAS and GC/MS analysis showed only a slight loss of

deuterium in both cases (Figure S28), which is explainable by the easier migration of hydrogen compared to deuterium due to the stronger C–D bond.

In conclusion, a sesquiterpene synthase from *M. marina* was identified as (–)-germacrene A synthase. Its product was not detected in headspace extracts of the actinomycete, suggesting that the gene was not expressed under laboratory culture conditions, but production of **1** was verified for the close relative *M. aurantiaca*, which harbors a TS from the same cluster (Figure S1, Figure S29). The TS from *M. marina* was used in vitro for isotopic labeling studies addressing the unique chemistry of **1**. With these experiments, a level of assignment for the NMR data of this conformationally difficult molecule has been reached that is beyond the possibilities of unlabeled material NMR, even at higher scales, by significantly simplifying the spectra using <sup>13</sup>C and <sup>2</sup>H. Stereoselectively deuterated samples of **1** allowed for experimentally tracing the stereochemical fate of the diastereotopic methylene hydrogen atoms during Cope rearrangement to  $\beta$ -elemene (**2**), affirming the **1a**-like transition state. Based on the mass spectra of all 15 isotopomers of (<sup>13</sup>C<sub>1</sub>)-**2**, a EI-MS fragmentation reaction was observed, in which a fragment ion was formed from two nonconnected parts of the carbon skeleton. This is explainable by a Cope fragmentation of **2**<sup>+</sup> to **1**<sup>+</sup>, which represents a new type of EI-MS fragmentation reaction. Taken together, this study underpins the crucial role of isotopically labeled compounds for reaching a deeper understanding in the characterization and reactions of complex compounds like the well-known but still surprising germacrene A.

## ■ ASSOCIATED CONTENT

### Supporting Information

The Supporting Information is available free of charge on the ACS Publications website at DOI: 10.1021/acs.orglett.9b00725.

Supplementary methods, figures, schemes, and NMR data of synthesized compounds (PDF)

## ■ AUTHOR INFORMATION

### Corresponding Author

\*E-mail: dickschat@uni-bonn.de.

### ORCID

Jeroen S. Dickschat: 0000-0002-0102-0631

### Notes

The authors declare no competing financial interest.

## ■ ACKNOWLEDGMENTS

This work was funded by the DFG (DI1536/7-1).

## ■ REFERENCES

- (1) (a) Adio, A. M. *Tetrahedron* **2009**, *65*, 1533. (b) Minnaard, A. J.; Wijnberg, J. B. P. A.; de Groot, A. *Tetrahedron* **1999**, *55*, 2115.
- (2) Cane, D. E. *Chem. Rev.* **1990**, *90*, 1089.
- (3) Hackl, T.; König, W. A.; Muhle, H. *Phytochemistry* **2004**, *65*, 2261.
- (4) Liao, Q.; Qian, Z.; Liu, R.; An, L.; Chen, X. *Antiviral Res.* **2013**, *100*, 578.
- (5) (a) de Kraker, J.-W.; Franssen, M. C. R.; de Groot, A.; König, W. A.; Bouwmeester, H. J. *Plant Physiol.* **1998**, *117*, 1381. (b) Liu, Q.; Majidi, M.; Cankar, K.; Goedbloed, M.; Charnikhova, T.; Verstappen,

- F. W.; de Vos, R. C.; Beekwilder, J.; van der Krol, S.; Bouwmeester, H. *J. PLoS One* **2011**, *6*, No. e23255.
- (6) Reddy, D. S.; Corey, E. J. *J. Am. Chem. Soc.* **2018**, *140*, 16909.
- (7) Weinheimer, A. J.; Youngblood, W. W.; Washecheck, P. H.; Karns, T. K. B.; Ciereszko, L. S. *Tetrahedron Lett.* **1970**, *11*, 497.
- (8) Bowers, W. S.; Nishino, C.; Montgomery, M. E.; Nault, L. R.; Nielson, M. W. *Science* **1977**, *196*, 680.
- (9) Dunlop, R. W.; Wells, R. J. *Aust. J. Chem.* **1979**, *32*, 1345.
- (10) Baker, R.; Parton, A. H.; Howse, P. E. *Experientia* **1982**, *38*, 297.
- (11) Adio, A. M.; Paul, C.; Tesso, H.; Kloth, P.; König, W. A. *Tetrahedron: Asymmetry* **2004**, *15*, 1631.
- (12) Burkhardt, I.; Kreuzenbeck, N.; Beemelmans, C.; Dickschat, J. S. *Org. Biomol. Chem.* **2019**, accepted, DOI: 10.1039/C8OB02744G.
- (13) (a) Pazouki, L.; Memari, H. R.; Kännaste, A.; Bichele, R.; Niinemets, Ü. *Front. Plant Sci.* **2015**, *6*, 111. (b) Bouwmeester, H. J.; Kodde, J.; Verstappen, F. W. A.; Altug, I. G.; de Kraker, J.-W.; Wallaart, T. E. *Plant Physiol.* **2002**, *129*, 134. (c) Bennett, M. H.; Mansfield, J. W.; Lewis, M. J.; Beale, M. H. *Phytochemistry* **2002**, *60*, 255. (d) Berteau, C. M.; Voster, A.; Verstappen, F. W.; Maffei, M.; Beekwilder, J.; Bouwmeester, H. *Arch. Biochem. Biophys.* **2006**, *448*, 3. (e) Prosser, I.; Phillips, A. L.; Gittings, S.; Lewis, M. J.; Hooper, A. M.; Pickett, J. A.; Beale, M. H. *Phytochemistry* **2002**, *60*, 691. (f) Agger, S. A.; Lopez-Gallego, F.; Hoye, T. R.; Schmidt-Dannert, C. *J. Bacteriol.* **2008**, *190*, 6084. (g) Yamada, Y.; Kuzuyama, T.; Komatsu, M.; Shin-ya, K.; Omura, S.; Cane, D. E.; Ikeda, H. *Proc. Natl. Acad. Sci. U. S. A.* **2015**, *112*, 857.
- (14) (a) Wilkins, K.; Schöller, C. *Actinomycetologica* **2009**, *23*, 27. (b) Citron, C. A.; Gleitzmann, J.; Laurenzano, G.; Pukall, R.; Dickschat, J. S. *ChemBioChem* **2012**, *13*, 202. (c) Rabe, P.; Citron, C. A.; Dickschat, J. S. *ChemBioChem* **2013**, *14*, 2345.
- (15) Faraldos, J. A.; Wu, S.; Chappell, J.; Coates, R. M. *Tetrahedron* **2007**, *63*, 7733.
- (16) Rabe, P.; Barra, L.; Rinkel, J.; Riclea, R.; Citron, C. A.; Klapschinski, T. A.; Janusko, A.; Dickschat, J. S. *Angew. Chem., Int. Ed.* **2015**, *54*, 13448.
- (17) Tanasupawat, S.; Jongrungruangchok, S.; Kudo, T. *Int. J. Syst. Evol. Microbiol.* **2010**, *60*, 648.
- (18) Dickschat, J. S.; Pahirulzaman, K. A. K.; Rabe, P.; Klapschinski, T. A. *ChemBioChem* **2014**, *15*, 810.
- (19) Rinkel, J.; Lauterbach, L.; Dickschat, J. S. *Angew. Chem., Int. Ed.* **2017**, *56*, 16385.
- (20) (a) Mitsuhashi, T.; Rinkel, J.; Okada, M.; Abe, I.; Dickschat, J. S. *Chem. - Eur. J.* **2017**, *23*, 10053. (b) Bian, G.; Rinkel, J.; Wang, Z.; Lauterbach, L.; Hou, A.; Yuan, Y.; Deng, Z.; Liu, T.; Dickschat, J. S. *Angew. Chem., Int. Ed.* **2018**, *57*, 15887.
- (21) Rinkel, J.; Lauterbach, L.; Dickschat, J. S. *Angew. Chem., Int. Ed.* **2019**, *58*, 452.
- (22) Rabe, P.; Rinkel, J.; Nubbemeyer, B.; Köllner, T. G.; Chen, F.; Dickschat, J. S. *Angew. Chem., Int. Ed.* **2016**, *55*, 15420.
- (23) Lauterbach, L.; Rinkel, J.; Dickschat, J. S. *Angew. Chem., Int. Ed.* **2018**, *57*, 8280; *Angew. Chem.* **2018**, *130*, 8412.
- (24) (a) Cornforth, J. W.; Cornforth, R. H.; Popjak, G.; Yengoyan, L. *J. Biol. Chem.* **1966**, *241*, 3970. (b) Thulasiram, H. V.; Poulter, C. D. *J. Am. Chem. Soc.* **2006**, *128*, 15819.
- (25) Hahn, F. M.; Hurlburt, A. P.; Poulter, C. D. *J. Bacteriol.* **1999**, *181*, 4499.
- (26) Woodward, R. B.; Hoffmann, R. *J. Am. Chem. Soc.* **1965**, *87*, 395.
- (27) (a) Houk, K. N.; Lin, Y.-T.; Brown, F. K. *J. Am. Chem. Soc.* **1986**, *108*, 554. (b) Lewis, D. K.; Brandt, B.; Crockford, L.; Glenar, D. A.; Rauscher, G.; Rodriguez, J.; Baldwin, J. E. *J. Am. Chem. Soc.* **1993**, *115*, 11728.
- (28) von E. Doering, W.; Roth, W. R. *Tetrahedron* **1962**, *18*, 67.
- (29) (a) de Kraker, J.-W.; Franssen, M. C. R.; de Groot, A.; Shibata, T.; Bouwmeester, H. J. *Phytochemistry* **2001**, *58*, 481. (b) Takeda, K. *Tetrahedron* **1974**, *30*, 1525.
- (30) Rabe, P.; Klapschinski, T. A.; Dickschat, J. S. *ChemBioChem* **2016**, *17*, 1333.
- (31) Kodama, M.; Yokoo, S.; Matsuki, Y.; Itô, S. *Tetrahedron Lett.* **1979**, *20*, 1687.
- (32) Rinkel, J.; Rabe, P.; Garbeva, P.; Dickschat, J. S. *Angew. Chem., Int. Ed.* **2016**, *55*, 13593.
- (33) Rinkel, J.; Rabe, P.; zur Horst, L.; Dickschat, J. S. *Beilstein J. Org. Chem.* **2016**, *12*, 2317.



## Appendix P

### **Diterpene Biosynthesis in Actinomycetes: Studies on Cattleyene Synthase and Phomopsene Synthase**

*Angew. Chem. Int. Ed.* **2019**, *58*, accepted.

DOI:10.1002/anie.201902950



## Accepted Article

**Title:** Diterpene Biosynthesis in Actinomycetes: Studies on Cattleylene Synthase and Phomopsene Synthase

**Authors:** Jan Rinkel, Simon Steiner, and Jeroen Sidney Dickschat

This manuscript has been accepted after peer review and appears as an Accepted Article online prior to editing, proofing, and formal publication of the final Version of Record (VoR). This work is currently citable by using the Digital Object Identifier (DOI) given below. The VoR will be published online in Early View as soon as possible and may be different to this Accepted Article as a result of editing. Readers should obtain the VoR from the journal website shown below when it is published to ensure accuracy of information. The authors are responsible for the content of this Accepted Article.

**To be cited as:** *Angew. Chem. Int. Ed.* 10.1002/anie.201902950  
*Angew. Chem.* 10.1002/ange.201902950

**Link to VoR:** <http://dx.doi.org/10.1002/anie.201902950>  
<http://dx.doi.org/10.1002/ange.201902950>

## COMMUNICATION

# Diterpene Biosynthesis in Actinomycetes: Studies on Cattleylene Synthase and Phomopsene Synthase

Jan Rinkel, Simon T. Steiner and Jeroen S. Dickschat\*

**Abstract:** Three diterpene synthases from actinomycetes were studied. The first enzyme from *Streptomyces cattleya* produced the novel compound cattleylene, and the other two enzymes from *Nocardia testacea* and *Nocardia rhamnosiphila* were identified as phomopsene synthases. The cyclisation mechanism of cattleylene synthase and the EI-MS fragmentation mechanism of its product were extensively studied by incubation experiments with isotopically labelled precursors. Oxidative transformations expanded the chemical space of these unique diterpenes.

The cationic cyclisation cascades towards terpenes belong to the most complex biosynthetic reactions in nature realised by a single enzyme.<sup>[1]</sup> Fascinatingly, only a few linear precursors, the oligoprenyl diphosphates, are sufficient to generate a large diversity of polycyclic skeletons with multiple stereogenic centres. For these transformations different types of enzymes have evolved, including type I terpene synthases (TSs) that ionise the substrate by diphosphate (PP) abstraction. There is a growing number of class II enzymes known, which catalyze formation of the intermediate for subsequent conversion by class I enzymes, sometimes combined in bifunctional enzymes such as the *ent*-kaurene synthase from *Fusarium fujikuroi* or the abietadiene synthase from *Abies grandis*.<sup>[2]</sup> A third class of enzymes with TS activity is related to the prenyltransferase UbiA involved in ubiquinone biosynthesis and also acts by PP abstraction.<sup>[3]</sup> Recently, in the fungus *Acremonium strictum* another type of TS (AsR6) for humulene was identified.<sup>[4]</sup> After discovery of the fusicoccadiene synthase from *Phomopsis amygdali*,<sup>[5]</sup> several other bifunctional diterpene synthases (DTS) with a geranylgeranyl PP synthase (GGPPS) and a TS domain were identified from fungi that catalyse an initial 1,11- and 10,14-cyclisation.<sup>[6]</sup> More recently, a series of bacterial monofunctional DTSs with the same initial cyclisation mode were reported,<sup>[7]</sup> with cyclooctat-9-en-7-ol synthase (CotB2) from *Streptomyces melanosporofaciens* as the first example.<sup>[8]</sup> Here we report on the characterisation of three bacterial type I TSs that were expected to be functional because of the presence of the highly conserved motifs involved in Mg<sup>2+</sup> cofactor and substrate binding and ionisation (Figure S1).<sup>[9]</sup> The enzymes were selected because they are closely related to known DTSs (Figure S2), as the complex mechanisms of DTSs are interesting to study by labelling

experiments. Derivatisations of their products by oxidation were performed to explore the chemistry of the obtained diterpenes.

Gene cloning and expression in *E. coli* followed by protein purification gave access to the recombinant enzymes (Figure S3).<sup>[10]</sup> Incubation of the first enzyme from *S. cattleya* with geranylgeranyl PP (GGPP) gave one major diterpene and a few minor products (Figure S4), but geranyl PP (GPP), farnesyl PP (FPP) and geranylarnesyl PP (GFPP) were not converted. The main product from GGPP was isolated and its structure was determined by NMR spectroscopy, including <sup>13</sup>C,<sup>13</sup>C-COSY with a sample of fully labelled (<sup>13</sup>C<sub>20</sub>)-**1** that was enzymatically prepared from (<sup>13</sup>C<sub>15</sub>)FPP<sup>[11]</sup> and (<sup>13</sup>C<sub>5</sub>)DMAPP<sup>[12]</sup> with isopentenyl PP isomerase (IDI) from *Serratia plymuthica*<sup>[12]</sup> and GGPPS from *Streptomyces cyaneofuscatus*<sup>[7a]</sup> (Table S3 and Figures S5–S13). These data resulted in the relative configuration of **1** (Scheme 1) for which we propose the name cattleylene. Thus, the enzyme was identified as cattleylene synthase (CyS).

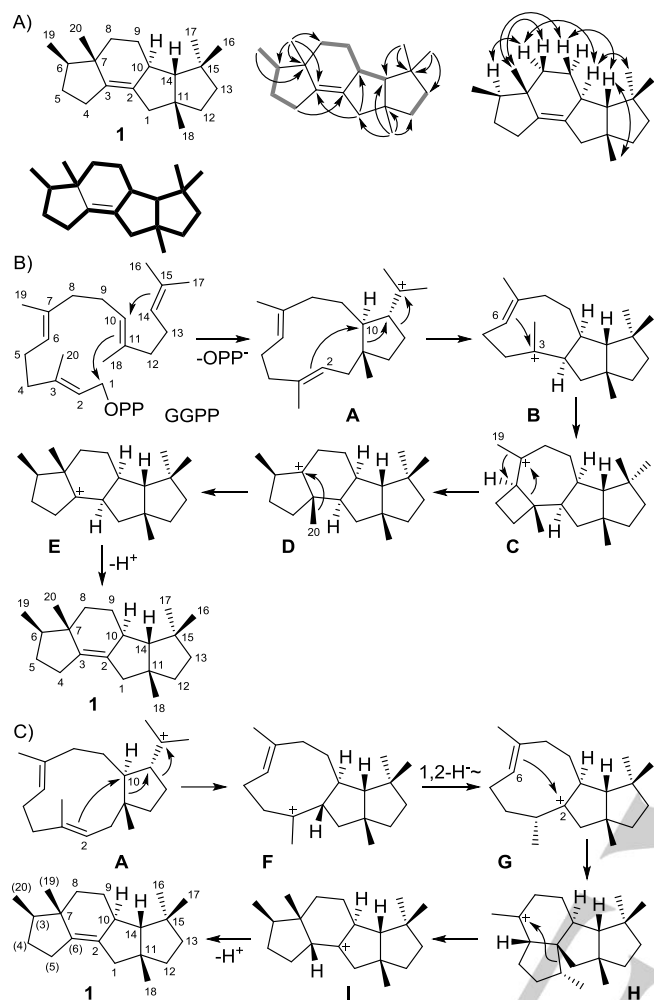
A proposed cyclisation mechanism for **1** starts by 1,11- and 10,14-cyclisation to **A**, followed by ring expansion, ring contraction and 2,10-cyclisation to **B**, likely concertedly to avoid secondary cation intermediates, and further 3,6-cyclisation to **C**. A subsequent dyotropic rearrangement with migration of Me-19 to **D**, Me-20 migration to **E** and final deprotonation of the antiperiplanar proton at C2 results in **1**. This mechanism is experimentally supported, because the labellings from all twenty (<sup>13</sup>C)GGPP isotopomers, prepared as reported previously,<sup>[7a,11,13]</sup> ended up in the expected positions (Figure S14, compare carbon numberings for **1** in Schemes 1A and 1B, carbons of GGPP and **1** with same number are biosynthetically linked). The deprotonation from C2 was evident from the product obtained from (3-<sup>13</sup>C,2-<sup>2</sup>H)GGPP<sup>[7a]</sup> (Figure S15A). The additional <sup>13</sup>C-label is not required to follow this deprotonation, but this substrate was used, because an initially proposed mechanism included a 1,2-hydride shift from C2 to C3 (Scheme 1C) that would have resulted in a triplet for C3 of **1** in the <sup>13</sup>C-NMR spectrum as a result of <sup>13</sup>C-<sup>2</sup>H spin coupling. Indeed, a singlet was observed (Figure S16), as expected for the mechanism of Scheme 1B.

The initially proposed mechanism proceeds from **A** by double skeletal rearrangement and 2,10-cyclisation to **F**. A subsequent 1,2-hydride migration to **G** and 2,6-cyclisation was suggested to lead to **H** that could undergo a Wagner-Meerwein rearrangement to **I** and a final deprotonation to **1**. This mechanism is also clearly ruled out by the results from the incubation experiments with all twenty isotopomers of (<sup>13</sup>C)GGPP with CyS that resulted in the incorporation of labelling into the wrong positions for C3, C4, C5, C6, C19 and C20 (compare carbon numbers in Schemes 1A and 1C). Furthermore, for this alternative mechanism deprotonation should occur from C6 of GGPP which is not the case as shown by incubation of (2-<sup>2</sup>H)FPP<sup>[7a]</sup> and isopentenyl PP (IPP) with GGPPS and CyS (Figure S15B).

[\*] Prof. Dr. Jeroen S. Dickschat, Jan Rinkel, Simon T. Steiner  
Kekulé-Institute for Organic Chemistry and Biochemistry  
University of Bonn  
Gerhard-Domagk-Straße 1, 53121 Bonn, Germany  
E-mail: dickschat@uni-bonn.de

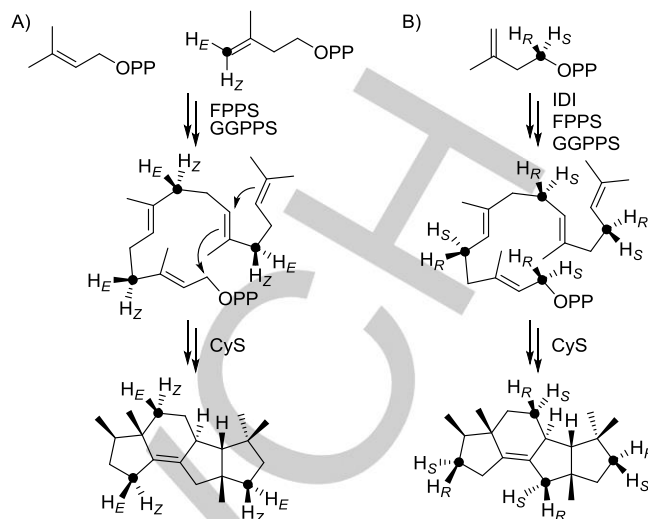
Supporting information for this article is given via a link at the end of the document.

## COMMUNICATION



**Scheme 1.** A) Structure of **1** (bold grey:  $^1\text{H},^1\text{H}$ -COSY, single-headed arrows: HMBC, double-headed arrows: NOESY, bold black:  $^{13}\text{C},^{13}\text{C}$ -COSY). B) Experimentally supported cyclisation mechanism from GGPP to **1**. C) Alternative mechanism that is disproven by labelling experiments (mismatching carbons are indicated by numbers in brackets).

The absolute configuration of **1** was determined using the stereoselectively deuterated probes (*E*- and *Z*)-(4- $^{13}\text{C},4\text{-}^2\text{H}$ )IPP<sup>[7c]</sup> that were enzymatically converted with DMAPP, FPP synthase (FPPS) from *S. coelicolor*<sup>[14]</sup> and GGPPS via a known stereochemical course<sup>[15]</sup> into the corresponding enantioselectively deuterated GGPP isotopomers, and then cyclised by CyS to yield labelled **1** (Scheme 2A). The deuterated carbons serve as stereochemical anchors of known absolute configuration that allow to conclude on the absolute configuration of **1**, by determination of the relative orientation of the incorporated deuterium atoms. This can be done with high sensitivity by HSQC spectroscopy in which the additional  $^{13}\text{C}$  labels strongly enhance the relevant signals (Figure S17). Similar experiments were performed with (*R*- and *S*)-(1- $^{13}\text{C},1\text{-}^2\text{H}$ )IPP<sup>[16]</sup> that were converted with IDI, FPPS, GGPPS and CyS into labelled **1** (Scheme 2B, Figure S18). Targeting every methylene group of **1**, all experiments pointed to the same absolute configuration as in Scheme 1.

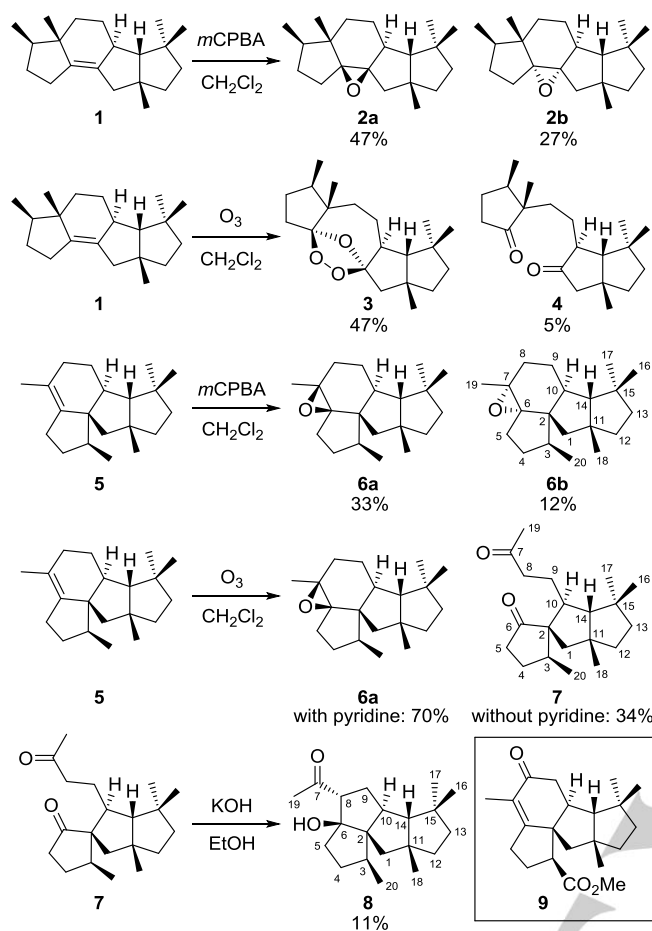


**Scheme 2.** Labelling experiments with stereoselectively deuterated IPPs to determine the absolute configuration of **1**. Black dots indicate  $^{13}\text{C}$ -labelled carbons.

To explore chemical transformations of the newly discovered diterpene to oxidised derivatives, **1** was subjected to epoxidation with *m*CPBA, yielding a separable mixture of the cattleyene epoxides **A** (**2a**) and **B** (**2b**, Scheme 3). Their structures were rigorously identified by NMR spectroscopy (Tables S4 and S5, Figures S19–S34). Ozonolysis of **1** resulted in the formation of cattleyene ozonide (**3**) as a single diastereoisomer, a compound that is thermally stable and can be observed by GC/MS (Figure S35), besides minor amounts of cattleyene dioxide (**4**). Both compounds were isolated and their structures determined by NMR spectroscopy (Tables S6 and S7, Figures S36–S51).

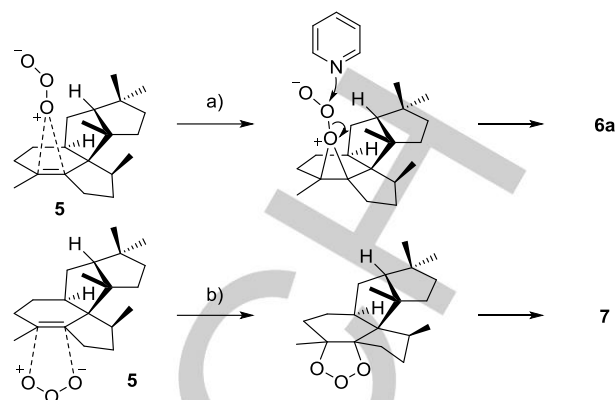
Two more enzymes from *Nocardia testacea* (gene locus ON38\_RS33295) and *N. rhamnosiphila* (NRH01S\_RS27945) only accepted GGPP, but not GPP, FPP and GFPP as substrate. GGPP was converted by both enzymes into phomopsene (**5**, Scheme 3 and Figure S52), identifying the enzymes as *N. testacea* (NtPS) and *N. rhamnosiphila* phomopsene synthases (NrPS). A fungal phomopsene synthase (PaPS) is known from *Phomopsis amygdali*,<sup>[17]</sup> and we have recently reported on a bacterial enzyme (PmS) from *Allokutzneria albata* producing a mixture of **5** and the related diterpene allokutznerene from GGPP.<sup>[7c]</sup> All four enzymes make the same enantiomer of **5** based on a comparison of optical rotations. Isolated **5** was treated with *m*CPBA to yield a separable mixture of epoxides **6a**<sup>[7c]</sup> and **6b**. The structure of the new compound **6b** was verified by NMR spectroscopy (Table S8, Figures S53–S60). The diterpene **5** was also subjected to ozonolysis. The reaction in  $\text{CH}_2\text{Cl}_2$  with pyridine as additive yielded a mixture of the epoxide **6a** and phomopsene dioxide (**7**, Figure S61), while without additive only **7** was obtained that was identified by NMR (Table S9, Figures S62–S69).

## COMMUNICATION



**Scheme 3.** Synthetic derivatisation of diterpenes and structure of the known natural derivative methyl phomopsenoate (**9**, boxed).

The formation of epoxides with ozone is sometimes observed for sterically demanding olefins<sup>[18]</sup> such as **5**. As we show here, the reaction can be promoted by the addition of pyridine. The selective formation of **6a** in the absence of **6b** is explainable by different accessibilities of the diastereotopic faces of the olefin in **5**. The top face is sterically more demanding, resulting in a formation of **6a** via the transition state shown in Scheme 4 (reaction a). Pyridine may act as an organocatalyst<sup>[19]</sup> that promotes decomposition of the ozone adduct. The bottom face of **5** is better accessible and ozone attacks only by 1,3-dipolar cycloaddition to **7** (reaction b), but not under formation of the epoxide **6b**. Also possible aldol reactions for the dioxides **4** and **7** were tested. Whereas **4** did not react under simple basic conditions, **7** was converted to a mixture of aldol products, from which the tetracyclic tertiary alcohol **8** could be isolated as the main product (Table S10, Figures S70–S77).



**Scheme 4.** Transition states for the ozonolysis of **5** explaining the formation of products **6a** and **7**.

The EI-MS fragmentation mechanisms of terpenes are difficult to address due to the limited accessibility of specifically labelled compounds. Early studies by Djerassi were based on synthetic labelled terpenes,<sup>[20]</sup> while feeding of labelled precursors to growing cultures usually results in only partial compound labelling.<sup>[21]</sup> Recently, deuterated isotopomers of IPP were used for the enzymatic synthesis of **5** to study its fragmentation mechanism.<sup>[22]</sup> Conversion of the twenty isotopomers of (<sup>13</sup>C)GGPP with CyS yielded specifically labelled isotopomers of **1** for which the EI mass spectra are shown in Figure S78. The information which carbon contributes to a fragment ion can be extracted from these mass spectra by “position specific mass shift analysis (PMA)” (Figure 1).<sup>[11a,23]</sup> Reaction mechanisms to the major fragment ions of **1** are discussed in Schemes S1–S3.

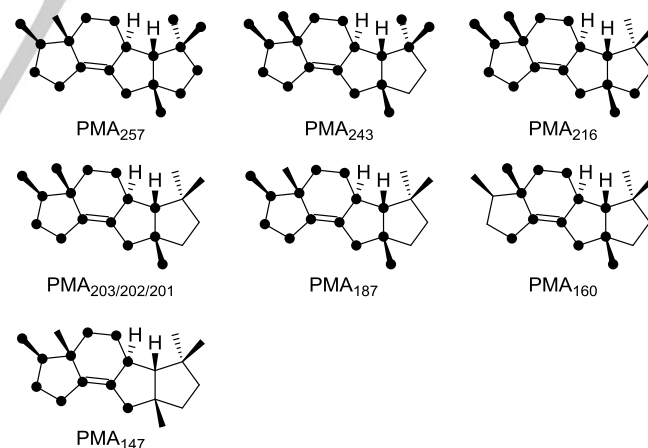


**Figure 1.** Position-specific mass shift analysis for **1**. Black dots indicate carbons that, if labelled, cause a shift of the indicated fragment ion PMA<sub>m/z</sub> and thus contribute to its formation.

In summary, we have characterised three new DTSS from actinomycetes. One enzyme from *Streptomyces cattleya* was found to produce the new natural product cattleyene with an unprecedented diterpene skeleton, while two enzymes from *Nocardia* were identified as phomopsene synthases. In all three

## COMMUNICATION

cases the corresponding diterpene product was found in headspace extracts of the encoding organisms (Figure S79), albeit in only low amounts from *S. cattleya* and *N. rhamnosiphila*, but clearly demonstrating gene expression and enzyme activity in vivo. In all three cases the TS gene is clustered with a gene for a cytochrome P450 (Figure S80), but no oxidation products of the diterpenes are currently known from the actinomycetes. In *P. amygdali*, **5** is oxidised and methylated to yield methyl phomopsenoate (**9**, Scheme 3) by the enzymes of a partially sequenced biosynthetic gene cluster,<sup>[17]</sup> but in *Nocardia* no methyltransferase gene is clustered with the DTS gene for **5**, suggesting that **9** is not a natural product in *Nocardia*. We will address the function of the cytochrome P450s in our future work and further investigate bacteria as an interesting and highly potent source of structurally and biosynthetically remarkable diterpenes.

## Acknowledgements

This work was supported by the DFG (DI1536/7-1). We thank Andreas J. Schneider for HPLC purifications.

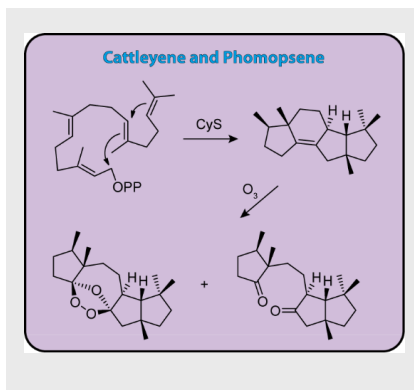
**Keywords:** enzyme mechanisms • isotopes • NMR spectroscopy • ozonolysis • terpenes

- [1] J. S. Dickschat, *Nat. Prod. Rep.* **2016**, *33*, 87.
- [2] a) H. Kawaide, R. Imai, T. Sassa, Y. Kamiya, *J. Biol. Chem.* **1997**, *272*, 21706; b) B. Stofer Vogel, M. R. Wildung, G. Vogel, R. Croteau, *J. Biol. Chem.* **1996**, *271*, 23262; c) R. Peters, *Nat. Prod. Rep.* **2010**, *27*, 1521.
- [3] a) M. J. Smanski, Z. Yu, J. Casper, S. Lin, R. M. Peterson, Y. Chen, E. Wendt-Pienkowski, S. R. Rajski, B. Shen, *Proc. Natl. Acad. Sci. USA* **2011**, *108*, 13498; b) Y. Yang, S. Zhang, K. Ma, Y. Xu, Q. Tao, Y. Chen, J. Chen, S. Guo, J. Ren, W. Wang, Y. Tao, W.-B. Yin, H. Liu, *Angew. Chem. Int. Ed.* **2017**, *56*, 4749.
- [4] R. Schor, C. Schotte, D. Wibberg, J. Kalinowski, R. J. Cox, *Nat. Commun.* **2018**, *9*, 1963.
- [5] T. Toyomasu, M. Tsukahara, A. Kaneko, R. Niida, W. Mitsuhashi, T. Dairi, N. Kato, T. Sassa, *Proc. Natl. Acad. Sci. USA* **2007**, *104*, 3084.
- [6] a) A. Minami, T. Ozaki, C. Liu, H. Oikawa, *Nat. Prod. Rep.* **2018**, *35*, 1330; b) T. Mitsuhashi, I. Abe, *ChemBioChem* **2018**, *19*, 1106.
- [7] a) P. Rabe, J. Rinkel, E. Dolja, T. Schmitz, B. Nubbemeyer, T. H. Luu, J. S. Dickschat, *Angew. Chem. Int. Ed.* **2017**, *56*, 2776; b) J. S. Dickschat, J. Rinkel, P. Rabe, A. Beyraghdar Kashkooli, H. J. Bouwmeester, *Beilstein J. Org. Chem.* **2017**, *13*, 1770; c) L. Lauterbach, J. Rinkel, J. S. Dickschat, *Angew. Chem. Int. Ed.* **2018**, *57*, 8280.
- [8] A. Meguro, Y. Motoyoshi, K. Teramoto, S. Ueda, Y. Totsuka, Y. Ando, T. Tomita, S.-Y. Kim, T. Kimura, M. Igarashi, R. Sawa, T. Shinada, M. Nishiyama, T. Kuzuyama, *Angew. Chem. Int. Ed.* **2015**, *54*, 4353.
- [9] a) C. M. Starks, K. Back, J. Chappell, J. P. Noel, *Science* **1997**, *277*, 1815; b) M. Seemann, G. Z. Zhai, J. W. de Kraker, C. M. Paschall, D. W. Christianson, D. E. Cane, *J. Am. Chem. Soc.* **2002**, *124*, 7681; c) P. Baer, P. Rabe, K. Fischer, C. A. Citron, T. A. Klapschinski, M. Groll, J. S. Dickschat, *Angew. Chem. Int. Ed.* **2014**, *53*, 7652.
- [10] J. S. Dickschat, K. A. K. Pahirulzaman, P. Rabe, T. A. Klapschinski, *ChemBioChem* **2014**, *15*, 810.
- [11] P. Rabe, L. Barra, J. Rinkel, R. Riclea, C. A. Citron, T. A. Klapschinski, A. Janusko, J. S. Dickschat, *Angew. Chem. Int. Ed.* **2015**, *54*, 13448.
- [12] J. Rinkel, L. Lauterbach, P. Rabe, J. S. Dickschat, *Angew. Chem. Int. Ed.* **2018**, *57*, 3238.
- [13] a) T. Mitsuhashi, J. Rinkel, M. Okada, I. Abe, J. S. Dickschat, *Chem. Eur. J.* **2017**, *23*, 10053; b) G. Bian, J. Rinkel, Z. Wang, L. Lauterbach, A. Hou, Y. Yuan, Z. Deng, T. Liu, J. S. Dickschat, *Angew. Chem. Int. Ed.* **2018**, *57*, 15887.
- [14] P. Rabe, J. Rinkel, B. Nubbemeyer, T. G. Köllner, F. Chen, J. S. Dickschat, *Angew. Chem. Int. Ed.* **2016**, *55*, 15420.
- [15] a) J. W. Cornforth, R. H. Cornforth, G. Popjak, L. Yengoyan, *J. Biol. Chem.* **1966**, *241*, 3970; b) H. V. Thulasiram, C. D. Poulter, *J. Am. Chem. Soc.* **2006**, *128*, 15819; c) J. W. Cornforth, R. H. Cornforth, C. Donninger, G. Popjak, *Proc. R. Soc. London, Ser. B*, **1966**, *163*, 492.
- [16] J. Rinkel, J. S. Dickschat, *Org. Lett.* **2019**, *21*, 2426.
- [17] T. Toyomasu, A. Kaneko, T. Tokiwano, Y. Kanno, R. Niida, S. Miura, T. Nishioka, C. Ikeda, W. Mitsuhashi, T. Dairi, T. Kawano, H. Oikawa, N. Kato, T. Sassa, *J. Org. Chem.* **2009**, *74*, 1541.
- [18] R. Criegee, *Chem. unserer Zeit* **1973**, *7*, 75.
- [19] R. Willand-Charnley, T. J. Fisher, B. M. Johnson, P. H. Dussault, *Org. Lett.* **2012**, *14*, 2242.
- [20] a) D. S. Weinberg, C. Djerassi, *J. Org. Chem.* **1966**, *31*, 115; b) J. Karliner, C. Djerassi, *J. Org. Chem.* **1966**, *31*, 1945; c) R. R. Muccino, C. Djerassi, *J. Am. Chem. Soc.* **1973**, *95*, 8726.
- [21] a) D. Spittler, A. Jux, J. Piel, W. Boland, *Phytochemistry* **2002**, *61*, 827; b) J. S. Dickschat, H. B. Bode, T. Mahmud, R. Müller, S. Schulz, *J. Org. Chem.* **2005**, *70*, 5174; c) C. A. Citron, R. Riclea, N. L. Brock, J. S. Dickschat, *RSC Advances* **2011**, *1*, 290.
- [22] S. S. Shinde, A. Minami, Z. Chen, T. Tokiwano, T. Toyomasu, N. Kato, T. Sassa, H. Oikawa, *J. Antibiot.* **2017**, *70*, 632.
- [23] a) P. Rabe, T. A. Klapschinski, J. S. Dickschat, *ChemBioChem* **2016**, *17*, 1333; b) J. Rinkel, P. Rabe, J. S. Dickschat, *Eur. J. Org. Chem.* **2019**, 351.

## COMMUNICATION

## COMMUNICATION

Three diterpene synthases from *Streptomyces cattleya* and *Nocardia* were characterised. The enzymes from *Nocardia* both yielded phomopsene, while the diterpene synthase from *S. cattleya* gave the new diterpene cattleyene. Its enzymatic formation was extensively studied by isotopic labelling experiments. Cattleyene and phomopsene were chemically converted by treatment with ozone, yielding surprising oxidation products.



Jan Rinkel, Simon T. Steiner and Jeroen S. Dickschat\*

Page No. – Page No.

**Diterpene Biosynthesis in Actinomycetes: Studies on Cattleyene Synthase and Phomopsene Synthase**



## Appendix Q

### **Stereochemical investigations on the biosynthesis of achiral (*Z*)- $\gamma$ -bisabolene in *Cryptosporangium arvum***

*Beilstein J. Org. Chem.* **2019**, *15*, 789–794.

DOI:10.3762/bjoc.15.75





# Stereochemical investigations on the biosynthesis of achiral (*Z*)- $\gamma$ -bisabolene in *Cryptosporangium arzum*

Jan Rinkel and Jeroen S. Dickschat\*

## Letter

Open Access

Address:  
Kekulé-Institute for Organic Chemistry and Biochemistry, University of  
Bonn, Gerhard-Domagk-Str. 1, 53121 Bonn, Germany

Email:  
Jeroen S. Dickschat\* - dickschat@uni-bonn.de

\* Corresponding author

Keywords:  
biosynthesis; carbocation chemistry; enzyme mechanisms; nerolidyl  
diphosphate; terpenes

*Beilstein J. Org. Chem.* **2019**, *15*, 789–794.  
doi:10.3762/bjoc.15.75

Received: 31 January 2019  
Accepted: 21 March 2019  
Published: 27 March 2019

This article is part of the thematic issue "Reactive intermediates –  
carbocations".

Guest Editor: S. R. Hare

© 2019 Rinkel and Dickschat; licensee Beilstein-Institut.  
License and terms: see end of document.

## Abstract

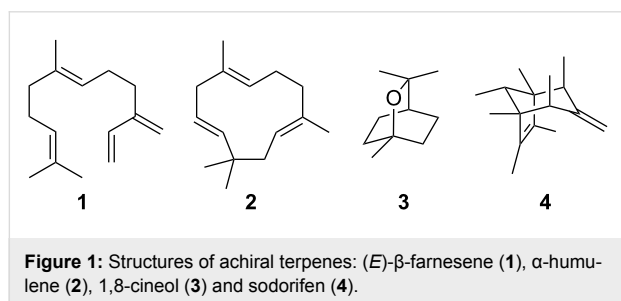
A newly identified bacterial (*Z*)- $\gamma$ -bisabolene synthase was used for investigating the cyclisation mechanism of the sesquiterpene. Since the stereoinformation of both chiral putative intermediates, nerolidyl diphosphate (NPP) and the bisabolylyl cation, is lost during formation of the achiral product, the intriguing question of their absolute configurations was addressed by incubating both enantiomers of NPP with the recombinant enzyme, which resolved in an exclusive cyclisation of (*R*)-NPP, while (*S*)-NPP that is non-natural to the (*Z*)- $\gamma$ -bisabolene synthase was specifically converted into (*E*)- $\beta$ -farnesene. A hypothetical enzyme mechanistic model that explains these observations is presented.

## Introduction

Given the enormous impact of chirality within biomolecules for all forms of life, it is fascinating to see how nature is able to maintain and reproduce stereochemical information. This concept largely involves the introduction of stereocentres to achiral starting materials by the action of enzymes. While reactions fulfilling this category are still challenging within synthetic chemistry, and methods managing to reach this goal are desperately desired, in the enzymatic world with its completely chiral environment these transformations are ubiquitous, which diminishes the hard border between achiral and chiral. One

intriguing example for this kind of reactivity is represented by terpene synthases (TSs), arguably building up the class of natural products with the highest density of stereochemical information, the terpenes. By providing a defined cavity including its molecular coating together with binding and activation of the diphosphate (OPP) moiety, these enzymes convert simple achiral oligoprenyl diphosphates into often complex, polycyclic hydrocarbons or alcohols with introduction of multiple stereocentres in just one enzymatic step [1-3]. With this approach, nature makes perfect use of the versatile chemistry of carboca-

tions with its hydride or proton shifts and Wagner–Meerwein rearrangements leading to a large variety of possible structures. Among terpenoid natural products, achiral compounds are rarely found, but still present. In this group, there are acyclic compounds like the linear sesquiterpene (*E*)- $\beta$ -farnesene (**1**, Figure 1), which is known as an alarm pheromone in aphids [4,5], but also monocyclic terpenes like  $\alpha$ -humulene (**2**), a widely occurring sesquiterpene in many essential oils [6,7]. Whereas the stereochemical imprint of a TS on achiral products is not directly visible, there still can be a chiral cyclisation cascade behind these terpenes. This is true as well for examples featuring a mirror plane like the monoterpene 1,8-cineol (eucalyptol, **3**), for which the absolute configuration of the intermediary terpinyl cation has been investigated using deuterium labelling, demonstrating different stereochemical courses in the plant *Salvia officinalis* [8,9] and in the bacterium *Streptomyces clavuligerus* [10]. Also the highly unusual methylated sesquiterpene sodorifen (**4**) possesses a mirror plane [11] making any labelling experiment hard to interpret and is nevertheless most likely biosynthesised through chiral intermediates [12]. For these cases, it is a particular challenge to uncover the stereochemical information hidden behind the achiral product structure. In this study, we addressed the chiral intermediates in the biosynthesis of the achiral sesquiterpene (*Z*)- $\gamma$ -bisabolene (**5**) by a TS from a soil bacterium.

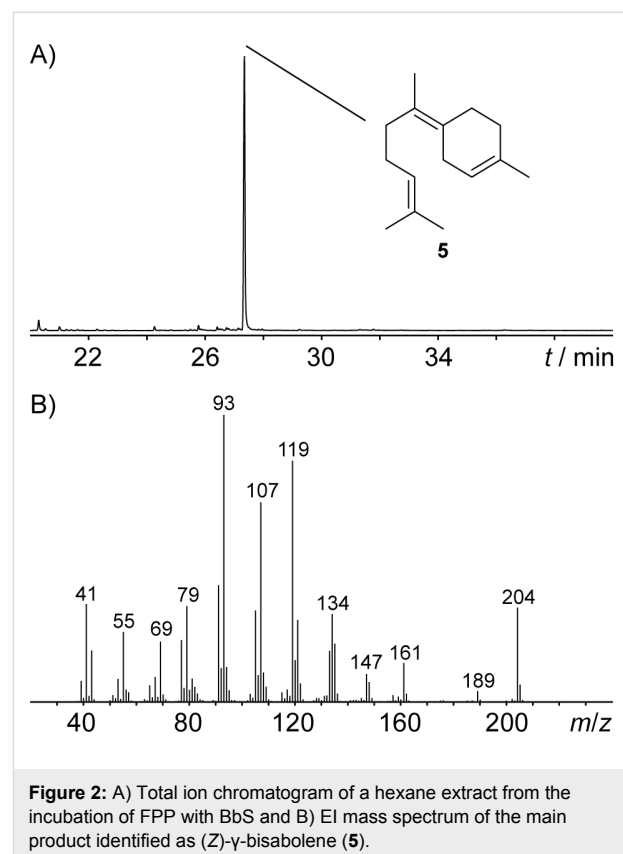


## Results and Discussion

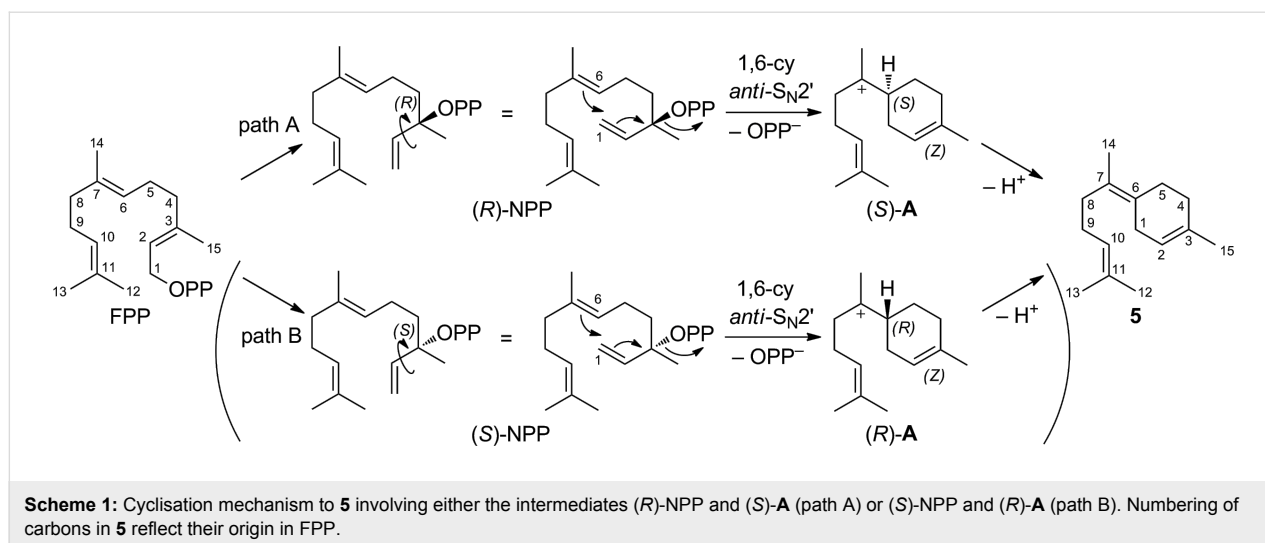
### Functional characterisation of a bacterial (*Z*)- $\gamma$ -bisabolene synthase

Within our efforts to characterise bacterial TSs with new functions and mechanisms, a TS (WP\_035857999) from the soil actinomycete *Cryptosporangium arzum* DSM 44712 was cloned into the *E. coli* expression vector pYE-express [13] (Table S1, Supporting Information File 1), because of its phylogenetic distance to characterised TSs (Figure S1, Supporting Information File 1). The amino acid sequence of the enzyme features known conserved motifs both for binding [14] and activation [15] of the diphosphate moiety together with structurally important residues [16,17] (Figure S2, Supporting Information File 1). For *in vitro* activity testing, the enzyme was expressed in *E. coli* BL21(DE3), purified (Figure S3, Supporting Informa-

tion File 1) and incubated with the common terpene precursors geranyl- (GPP, C<sub>10</sub>), farnesyl- (FPP, C<sub>15</sub>), geranylgeranyl- (GGPP, C<sub>20</sub>) and geranyl-farnesyl (GFPP, C<sub>25</sub>) diphosphate. With hexane extraction and GC–MS analysis, only the incubation with FPP yielded a terpene product (Figure 2) that was isolated and identified by one- and two dimensional NMR spectroscopy (Table S2, Supporting Information File 1), EIMS databases and GC retention index as the known sesquiterpene (*Z*)- $\gamma$ -bisabolene (**5**). Because the two olefinic carbon atoms of its quaternary double bond could not be unambiguously assigned from HMBC data, labelling experiments with (6-<sup>13</sup>C)- and (7-<sup>13</sup>C)FPP [18] were also conducted (Figure S4, Supporting Information File 1). These results characterise the TS from *C. arzum* as a (*Z*)- $\gamma$ -bisabolene synthase (BbS).



The achiral, monocyclic sesquiterpene **5** is abundant in many essential oils and was reported from different sources such as the liverwort *Dumortiera hirsuta* [19]. Its (*Z*)-configured exocyclic double bond has also attracted the attention of synthetic chemistry for a diastereoselective total synthesis [20–22]. The wide occurrence of **5** is likely connected to the simple biosynthesis from FPP featuring the common bisabolyll cation (**A**) as an intermediate after 1,6-cyclisation (Scheme 1). For this cyclisation, a formal isomerisation of the (*E*)-configured double bond in FPP to the (*Z*)-configured double bond in **A** is needed.



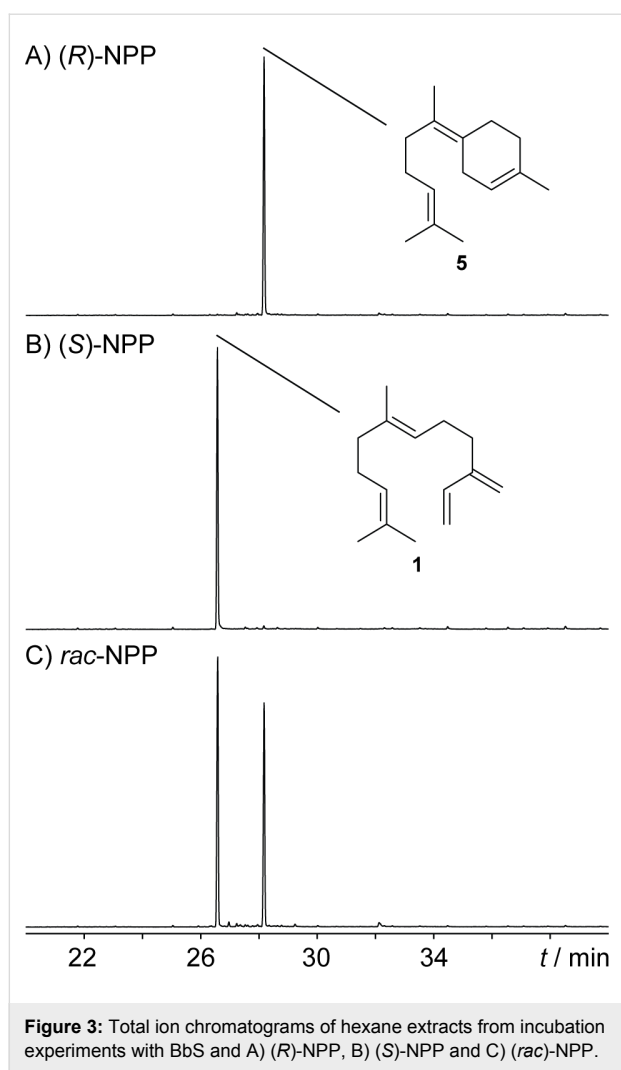
To address this problem, a 1,3-suprafacial transposition of OPP to nerolidyl diphosphate (NPP) is usually assumed [23]. This tertiary allylic diphosphate can undergo 1,6-cyclisation after a rotation around the C-2,C-3 single bond. Both NPP and **A** are chiral which raises the question of the active enantiomers in the BbS-catalysed reaction. This problem is challenging since the stereoinformation is destroyed in the final deprotonation step, which prevents any conclusion at the product stage, e.g., by use of enantioselectively labelled substrates [8–10]. If the nucleophilic attack of the C-6,C-7 double bond at the allylic system proceeds with an *anti* stereochemistry (*anti*-S<sub>N</sub>2' reaction), which is favoured for a concerted process and is also discussed for other cyclisation mechanisms [24–26], the four theoretically possible options for the BbS cyclisation mechanism are narrowed down to two possibilities: Either the reaction takes place via (*R*)-NPP resulting in (*S*)-**A** after ring closure (Scheme 1, path A) or via (*S*)-NPP, which would suggest involvement of (*R*)-**A** (Scheme 1, path B). This stereochemical link between NPP and **A** was also observed in a theoretical docking study with *epi*-isozizaene synthase suggesting (*S*)-NPP and (*R*)-**A** to be included in its cyclisation mechanism [27].

### The absolute configuration of the intermediates nerolidyl diphosphate and the bisabolylation

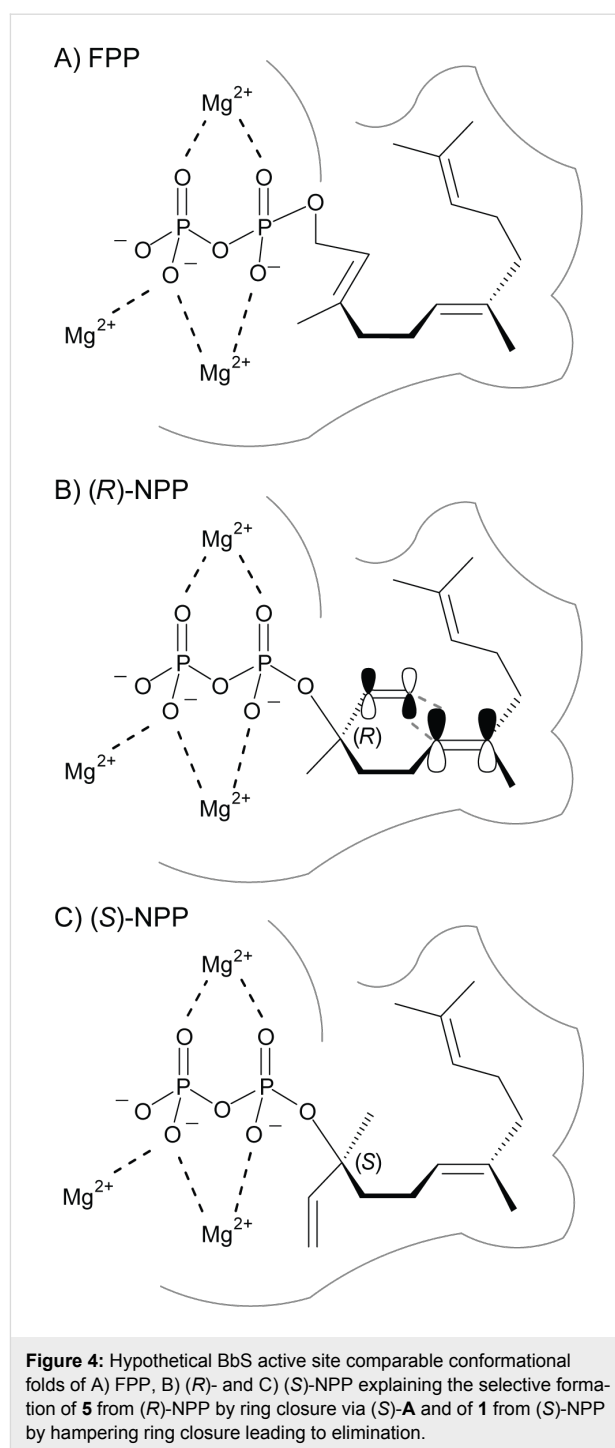
To address this question experimentally, (*R*)- and (*S*)-NPP were synthesised following a known route for enantioselective preparation of nerolidol [28] by Sharpless epoxidation of farnesol in analogy to the reported synthesis of geranylinaloyl diphosphates [29] (Scheme S1, Supporting Information File 1). Aiming for an easy and unambiguous interpretation of the incubation experiments, the synthesised nerolidol samples (showing moderate to good ee values as judged by Mosher ester analysis of the preceding epoxides, Figure S5, Supporting Information

File 1) were purified by preparative HPLC on a chiral stationary phase to >99% ee for both samples (Figure S6, Supporting Information File 1), before converting them into the NPPs. For comparison, also racemic NPP was synthesised by a Grignard reaction of geranylacetone with vinylmagnesium bromide. The two NPP samples featuring a well-defined stereocentre, and (*rac*)-NPP, were incubated with recombinant BbS, the experiments were extracted with hexane and analysed by GC–MS (Figure 3). A selective product formation was observed for the two enantiomers of NPP, which is surprising in the light of the fact that these reactive tertiary allylic diphosphates were often found to result in a complex mixture of terpene cyclase products and Mg<sup>2+</sup>-catalysed spontaneous hydrolysis products for other TSs [29,30]. While the reaction with (*R*)-NPP leads to BbS's native product **5**, for (*S*)-NPP formation of the acyclic elimination product (*E*)-β-farnesene (**1**) was observed, which was identified by EI mass spectral library and GC retention index (*I* = 1460 (HP-5MS), lit: *I* = 1459 (HP-5MS) [31]). Incubation with (*rac*)-NPP resulted in a nearly 1:1 mixture of both products, showing that both enantiomers of NPP were converted with similar efficiency.

These results clearly rule out (*S*)-NPP, but rationalise (*R*)-NPP as an intermediate in the cyclisation mechanism of BbS, and are in favour of the (*S*)-bisabolylation cation (**A**) to be deprotonated to **5** within the cascade reaction (Scheme 1, path A) [24–26], although the stereochemical link between NPP and **A** could not be demonstrated experimentally in this study. The formation of (*R*)-NPP from FPP as a 1,3-*syn*-allylic rearrangement can be rationalised in a binding mode of FPP, in which OPP is located on a defined face of the C-2,C-3-double bond by the enzyme's active site (e.g., on top of it, Figure 4A). This migration of OPP to C-3 results in a reorganisation of the resulting structure to a cisoid conformation for the follow up 1,6-ring closure. To



explain the astonishing selectivity between the two NPP enantiomers by BbS, different NPP conformations inside the chiral environment of the active site in BbS have to be assumed (Figure 4B + 4C). The architecture of the active site may stay the same in both cases, so a fixed OPP moiety with binding by the trinuclear  $\text{Mg}^{2+}$  cluster and a comparable folding of the isoprenoid chain in both cases is reasonable. Therefore, the two smallest substituents at the stereocentre formally change their places for the two enantiomers of NPP, representing a minor structural change of the substrate that can be tolerated in the active site. While the binding of (*R*)-NPP leads to a productive conformation that exhibits a close proximity between C-6 and C-1 for ring closure to (*S*)-**A** initiated by OPP abstraction, (*S*)-NPP cannot occupy this conformation for its different stereocentre. Instead, abstraction of the OPP moiety leads to an allylic cation with an unproductive conformation for further ring closure and is thus quenched by abstraction of a proton, presumably by participation of the diphosphate nearby, to give **1**.



## Conclusion

During the course of this work, a new TS from *C. aryum* was characterised as a (*Z*)- $\gamma$ -bisabolene (**5**) synthase (BbS). Despite its monocyclic achiral structure, the biosynthesis of **5** proceeds via two chiral intermediates, NPP and the bisabolyli cation (**A**), whereas the absolute configuration of the first was addressed experimentally by the synthesis and in vitro incubation of both enantiomers of NPP. These experiments clearly showed the

involvement of (*R*)-NPP in the BbS-catalysed reaction, whereas diphosphate was selectively eliminated from (*S*)-NPP by BbS to yield **1**. The selectivity is understandable by the fixed, chiral active site architecture of BbS promoting ring closure only for (*R*)-NPP. In future studies, this experimental approach will not only provide insights into the stereochemical identity of intermediates in cases of achiral terpenes inhibiting any conclusion from the product structure as shown here, but will also deepen our knowledge of general NPP utilisation by sesquiterpene synthases. The chirality of this tertiary diphosphate is currently largely underinvestigated in the characterisation of TSSs, even for cascades requiring its involvement.

## Supporting Information

Experimental details of culture conditions, gene cloning, protein purification, incubation experiments, isolation of **5** and HPLC purifications, the amino acid sequence of BbS, a phylogenetic tree with the location of BbS, SDS-PAGE analysis, listed NMR data of **5**, labelling experiments for NMR assignment, synthetic procedures for the NPPs, Mosher ester analysis of epoxides, and chiral GC analysis of nerolidols.

### Supporting Information File 1

Experimental part.

[<https://www.beilstein-journals.org/bjoc/content/supplementary/1860-5397-15-75-S1.pdf>]

## Acknowledgements

This work was funded by the Deutsche Forschungsgemeinschaft (DI1536/7-1). We thank Andreas J. Schneider for HPLC purifications.

## ORCID® iDs

Jeroen S. Dickschat - <https://orcid.org/0000-0002-0102-0631>

## References

- Christianson, D. W. *Chem. Rev.* **2017**, *117*, 11570–11648. doi:10.1021/acs.chemrev.7b00287
- Dickschat, J. S. *Nat. Prod. Rep.* **2016**, *33*, 87–110. doi:10.1039/c5np00102a
- Tantillo, D. J. *Angew. Chem., Int. Ed.* **2017**, *56*, 10040–10045. doi:10.1002/anie.201702363
- Bowers, W. S.; Nault, L. R.; Webb, R. E.; Dutky, S. R. *Science* **1972**, *177*, 1121–1122. doi:10.1126/science.177.4054.1121
- Gibson, R. W.; Pickett, J. A. *Nature* **1983**, *302*, 608–609. doi:10.1038/302608a0
- Katsiotis, S. T.; Langezaal, C. R.; Scheffer, J. J. C. *Planta Med.* **1989**, *55*, 634. doi:10.1055/s-2006-962205
- Bouajaj, S.; Benyamna, A.; Bouamama, H.; Romane, A.; Falconieri, D.; Piras, A.; Marongiu, B. *Nat. Prod. Res.* **2013**, *27*, 1673–1676. doi:10.1080/14786419.2012.751600
- Wise, M. L.; Savage, T. J.; Katahira, E.; Croteau, R. *J. Biol. Chem.* **1998**, *273*, 14891–14899. doi:10.1074/jbc.273.24.14891
- Wise, M. L.; Urbansky, M.; Helms, G. L.; Coates, R. M.; Croteau, R. *J. Am. Chem. Soc.* **2002**, *124*, 8546–8547. doi:10.1021/ja0265714
- Rinkel, J.; Rabe, P.; zur Horst, L.; Dickschat, J. S. *Beilstein J. Org. Chem.* **2016**, *12*, 2317–2324. doi:10.3762/bjoc.12.225
- von Reuß, S. H.; Kai, M.; Piechulla, B.; Francke, W. *Angew. Chem., Int. Ed.* **2010**, *49*, 2009–2010. doi:10.1002/anie.200905680
- von Reuss, S.; Domik, D.; Lemfack, M. C.; Magnus, N.; Kai, M.; Weise, T.; Piechulla, B. *J. Am. Chem. Soc.* **2018**, *140*, 11855–11862. doi:10.1021/jacs.8b08510
- Dickschat, J. S.; Pahirulzaman, K. A. K.; Rabe, P.; Klapschinski, T. A. *ChemBioChem* **2014**, *15*, 810–814. doi:10.1002/cbic.201300763
- Christianson, D. W. *Chem. Rev.* **2006**, *106*, 3412–3442. doi:10.1021/cr050286w
- Baer, P.; Rabe, P.; Fischer, K.; Citron, C. A.; Klapschinski, T. A.; Groll, M.; Dickschat, J. S. *Angew. Chem., Int. Ed.* **2014**, *53*, 7652–7656. doi:10.1002/anie.201403648
- Rinkel, J.; Lauterbach, L.; Dickschat, J. S. *Angew. Chem., Int. Ed.* **2017**, *56*, 16385–16389. doi:10.1002/anie.201711142
- Rinkel, J.; Lauterbach, L.; Rabe, P.; Dickschat, J. S. *Angew. Chem., Int. Ed.* **2018**, *57*, 3238–3241. doi:10.1002/anie.201800385
- Rabe, P.; Barra, L.; Rinkel, J.; Riclea, R.; Citron, C. A.; Klapschinski, T. A.; Janusko, A.; Dickschat, J. S. *Angew. Chem., Int. Ed.* **2015**, *54*, 13448–13451. doi:10.1002/anie.201507615
- Saritas, Y.; Bülow, N.; Fricke, C.; König, W. A.; Muhle, H. *Phytochemistry* **1998**, *48*, 1019–1023. doi:10.1016/s0031-9422(97)00484-6
- Anastasia, L.; Dumond, Y. R.; Negishi, E.-i. *Eur. J. Org. Chem.* **2001**, 3039–3043. doi:10.1002/1099-0690(200108)2001:16<3039::aid-ajoc3039>3.0.co;2-v
- Wolinsky, L. E.; Faulkner, D. J.; Finer, J.; Clardy, J. *J. Org. Chem.* **1976**, *41*, 697–699. doi:10.1021/jo00866a023
- Corey, E. J.; Seibel, W. L. *Tetrahedron Lett.* **1986**, *27*, 909–910. doi:10.1016/s0040-4039(00)84134-9
- Arigoni, D. *Pure Appl. Chem.* **1975**, *41*, 219–245. doi:10.1351/pac197541010219
- Rinkel, J.; Rabe, P.; Garbeva, P.; Dickschat, J. S. *Angew. Chem., Int. Ed.* **2016**, *55*, 13593–13596. doi:10.1002/anie.201608042
- Cane, D. E.; Tandon, M. *J. Am. Chem. Soc.* **1995**, *117*, 5602–5603. doi:10.1021/ja00125a029
- Hu, Y.; Chou, W. K. W.; Hopson, R.; Cane, D. E. *Chem. Biol.* **2011**, *18*, 32–37. doi:10.1016/j.chembiol.2010.11.008
- Pemberton, R. P.; Ho, K. C.; Tantillo, D. J. *Chem. Sci.* **2015**, *6*, 2347–2353. doi:10.1039/c4sc03782k
- Le, T. C.; Chauhan, K. R. *Nat. Prod. Commun.* **2014**, *9*, 297–298.
- Rinkel, J.; Rabe, P.; Chen, X.; Köllner, T. G.; Chen, F.; Dickschat, J. S. *Chem. – Eur. J.* **2017**, *23*, 10501–10505. doi:10.1002/chem.201702704
- Benedict, C. R.; Lu, J. L.; Pettigrew, D. W.; Liu, J.; Stipanovic, R. D.; Williams, H. J. *Plant Physiol.* **2001**, *125*, 1754–1765. doi:10.1104/pp.125.4.1754

31. Asuming, W. A.; Beauchamp, P. S.; Descalzo, J. T.; Dev, B. C.; Dev, V.; Frost, S.; Ma, C. W. *Biochem. Syst. Ecol.* **2005**, *33*, 17–26.  
doi:10.1016/j.bse.2004.06.005

## License and Terms

This is an Open Access article under the terms of the Creative Commons Attribution License (<http://creativecommons.org/licenses/by/4.0>). Please note that the reuse, redistribution and reproduction in particular requires that the authors and source are credited.

The license is subject to the *Beilstein Journal of Organic Chemistry* terms and conditions: (<https://www.beilstein-journals.org/bjoc>)

The definitive version of this article is the electronic one which can be found at:  
[doi:10.3762/bjoc.15.75](https://doi.org/10.3762/bjoc.15.75)



## Appendix R

### **Mechanistic investigations on multiproduct $\beta$ -himachalene synthase from *Cryptosporangium arvum***

*Beilstein J. Org. Chem.* **2019**, *15*, 1008–1019.

DOI:10.3762/bjoc.15.99





# Mechanistic investigations on multiproduct $\beta$ -himachalene synthase from *Cryptosporangium arvum*

Jan Rinkel and Jeroen S. Dickschat\*

## Full Research Paper

Open Access

Address:

Kekulé-Institute for Organic Chemistry and Biochemistry, University of Bonn, Gerhard-Domagk-Str. 1, 53121 Bonn, Germany

Email:

Jeroen S. Dickschat\* - dickschat@uni-bonn.de

\* Corresponding author

Keywords:

enzyme mechanisms; isotopes; mass spectrometry; promiscuity; terpenes

*Beilstein J. Org. Chem.* **2019**, *15*, 1008–1019.

doi:10.3762/bjoc.15.99

Received: 12 March 2019

Accepted: 26 April 2019

Published: 02 May 2019

This article is part of the thematic issue "Terpenes".

Associate Editor: D. Spring

© 2019 Rinkel and Dickschat; licensee Beilstein-Institut.

License and terms: see end of document.

## Abstract

A bacterial terpene synthase from *Cryptosporangium arvum* was characterised as a multiproduct  $\beta$ -himachalene synthase. In vitro studies showed not only a high promiscuity with respect to its numerous sesquiterpene products, including the structurally demanding terpenes longicyclene, longifolene and  $\alpha$ -longipinene, but also to its substrates, as additional activity was observed with geranyl- and geranylgeranyl diphosphate. In-depth mechanistic investigations using isotopically labelled precursors regarding the stereochemical course of both 1,1-cyclisation and 1,3-hydride shift furnished a detailed catalytic model suggesting the molecular basis of the observed low product selectivity. The enzyme's synthetic potential was also exploited in the preparation of sesquiterpene isotopomers, which provided insights into their EIMS fragmentation mechanisms.

## Introduction

The organic chemist usually prefers to work with pure compounds which lead to high requirements for the selectivity of reactions and often to tedious purification procedures, but encountering a pure compound in nature is quite rare. This does not result in reduced requirements for enzyme selectivity. The very opposite is mostly true, because proteins working in a compound mixture need to be precise [1]. However, in some cases, compound mixtures have proven to be superior to the properties of the single compounds by evolution. Examples demonstrating this principle can be found in pheromone chemistry, like the bark beetle aggregation blend of ipsdienol, ipsenol

and verbenol, for which synergistic effects were observed compared to the single compounds [2]. Also the sex pheromone of the cranberry white grub *Phyllophaga anxia* was identified as a compound mixture, consisting of L-valine methyl ester and L-isoleucine methyl ester at a 3:1 ratio [3]. Moreover, if there is a single enzyme that can produce a beneficial mixture, the advantage for the producing organism is even higher. Therefore, selectivity is not in every case the highest goal for evolution. An enzyme class, which is highly prone to a regulation of product selectivity for the production of either one or multiple compounds, are terpene synthases (TSs). These enzymes are able to

guide complex cascade reactions from structurally simple oligoprenyl diphosphates to often complex, polycyclic products [4–6] circumventing the low selectivity observed for carbocationic reactions by a defined active-site architecture. Although these enzymes are mostly highlighted for their great product selectivity, TSs producing only one compound are by far not the general case. Mostly, the main product is accompanied by several side products. Prominent examples are the TS identified from the plant *Medicago truncatula* with at least 27 products [7],  $\gamma$ -humulene synthase from *Abies grandis* with 52 products [8], and also the long known trichodiene synthase from *Fusarium sporotrichioides* produces at least 15 sesquiterpenes [9]. Some TSs can even accept multiple chain length substrates [10], a concept which seems to occur frequently in plants [11]. Whether the reduced selectivity of TSs both for substrates and for products can be attributed to imperfect catalysis, or if this function is even beneficial for the producing organism, remains elusive in most cases. Also the structural basis of promiscuous catalysis by TSs is largely unknown [12]. In this study, we present the characterisation of a bacterial TS with a reduced selectivity both for substrates and for products together with the challenging investigation of its cyclisation mechanism by labelling experiments.

## Results and Discussion

### A bacterial $\beta$ -himachalene synthase produces numerous side products

Apart from the recently assigned (*Z*)- $\gamma$ -bisabolene synthase (BbS) [13], the soil-dwelling actinomycete *Cryptosporangium arzum* DSM 44712 also possesses a second TS gene (accession no. WP\_035852539). Its encoded amino acid sequence (Figure S1, Supporting Information File 1) shares conserved motifs for TSs, but is phylogenetically distant to BbS and does not possess a close characterised relative among other bacterial TSs (Figure S2, Supporting Information File 1). Therefore, its gene was cloned into the *E. coli* expression vector pYE-Express [14] for functional characterisation (Table S1, Supporting Information File 1). The purified recombinant protein (Figure S3, Supporting Information File 1) was incubated with the common TS substrates geranyl- (GPP, C<sub>10</sub>), farnesyl- (FPP, C<sub>15</sub>), geranylgeranyl- (GGPP, C<sub>20</sub>) and geranyl-farnesyl (GFPP, C<sub>25</sub>) diphosphate. Whereas the latter diphosphate did not lead to any terpene product, the incubation with FPP showed a smooth conversion into several sesquiterpenes (Figure 1A) with compound **1** as the major peak after GC–MS analysis. However, also the incubations with GPP (Figure 1B) and GGPP (Figure 1C) led to several less complex terpene products, demonstrating a broadened substrate range for this enzyme. The annotated peaks were correlated by mass spectral libraries and retention indices (Table 1) to the known natural products **1–8** and **10–18** (Figure 2).

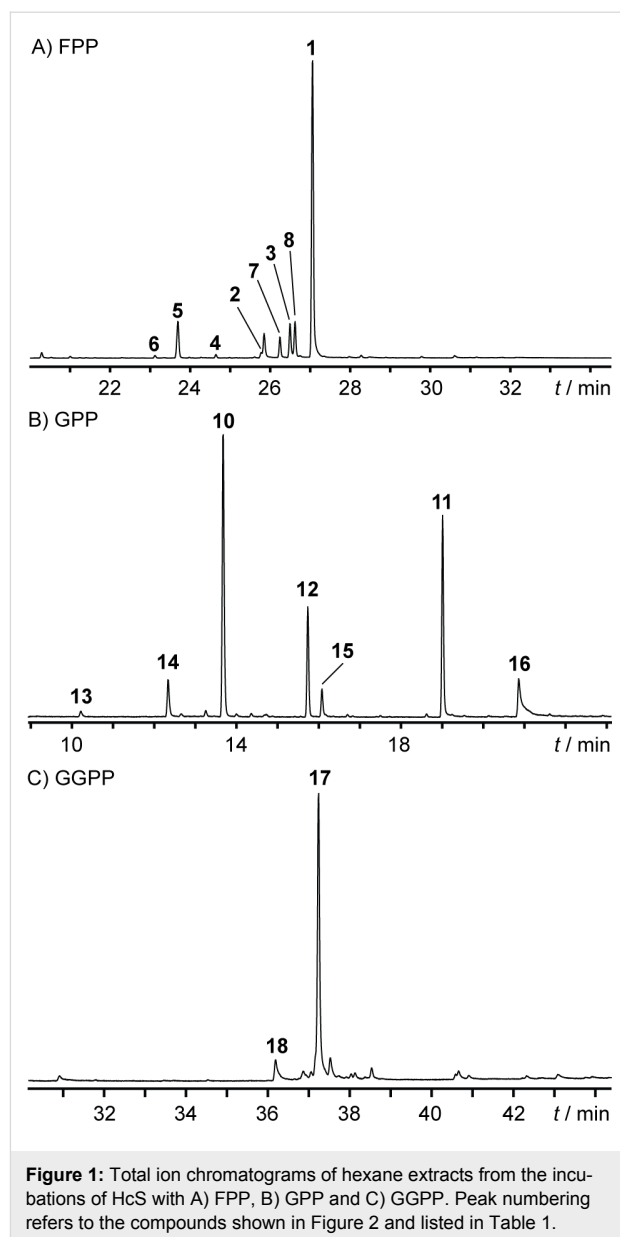


**Figure 1:** Total ion chromatograms of hexane extracts from the incubations of HcS with A) FPP, B) GPP and C) GGPP. Peak numbering refers to the compounds shown in Figure 2 and listed in Table 1.

In a large scale incubation,  $\beta$ -himachalene (**1**) was isolated, accompanied by smaller amounts of the double oxidation product  $\gamma$ -dehydro-*ar*-himachalene (**9**). Since **9** was only observed after prolonged incubation times, an auto-oxidation mechanism involving oxygen is assumed. Both compounds were analysed by one- and two-dimensional NMR spectroscopy (Tables S2 and S3, Supporting Information File 1). The absolute configuration of **1** was determined as the (+)-enantiomer, unanimously by optical rotary power measurement and an isotopic labelling strategy, which involved conversion of stereoselectively deuterated and at the same position <sup>13</sup>C-labelled FPPs by the TS to yield labelled **1** with incorporation of deuterium into diastereotopic hydrogen positions. Together with the relative configuration of the targeted methylene group as deduced by NOESY,

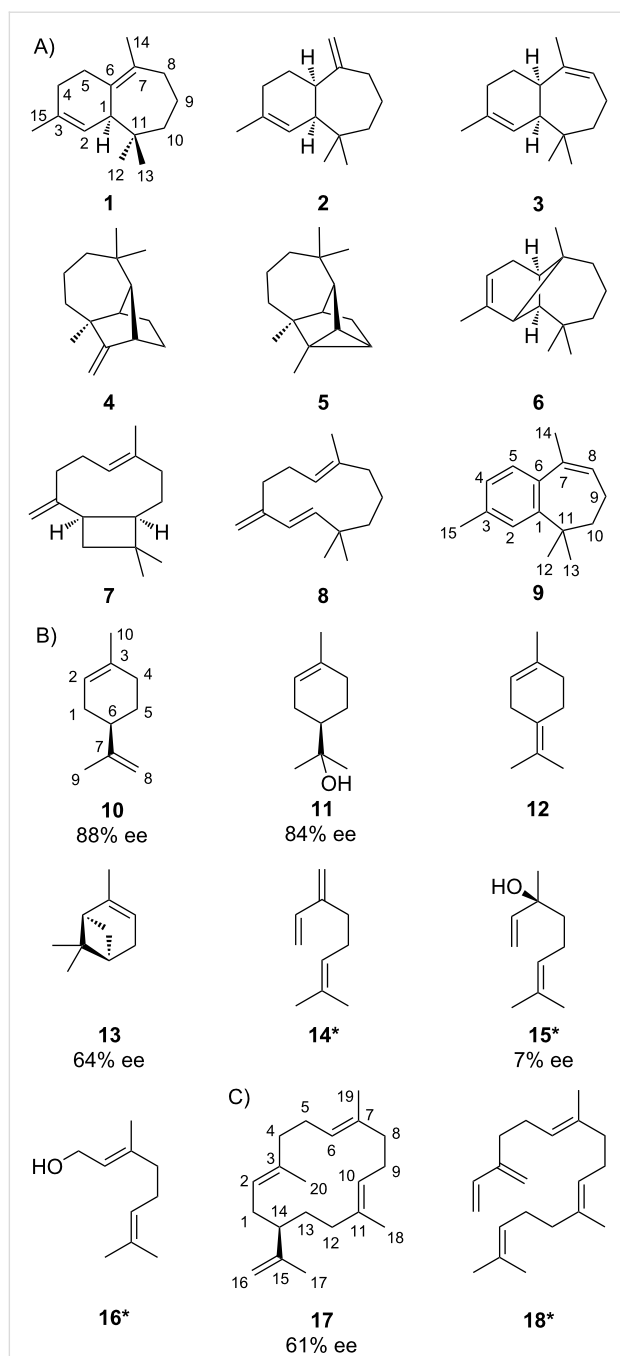


**Figure 2:** Structures of HcS products arising A) from FPP together with related oxidation product **9**, B) from GPP and C) from GGPP. The carbon numberings of **1** and **9** refer to the carbon positions of FPP as shown in Scheme 3, numberings of **10** and **17** are derived from that of GPP and GGPP, respectively. Compounds known to also originate from non-enzymatic hydrolysis are labelled with an asterisk. The enantiomeric excess values were determined based on GC analysis on a chiral phase.

the stereochemical outcome of these experiments, which can be easily monitored by sensitive HSQC, infers the absolute configuration of **1**. For **1**, C-5 was targeted by (1*R*)- and (1*S*)-(1-<sup>13</sup>C,1-<sup>2</sup>H)GPP [28], which were enzymatically elongated with

**Table 1:** HcS product identification by retention indices.

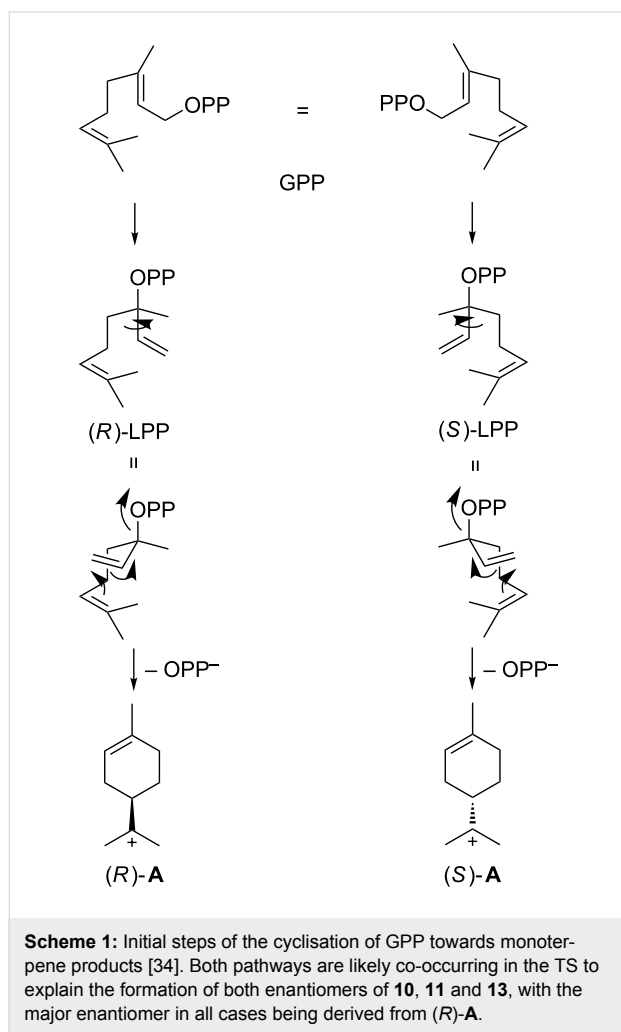
compound	$\beta^a$	$I$ (lit.)
from GPP		
$\alpha$ -pinene ( <b>13</b> )	934	934 [15]
$\beta$ -myrcene ( <b>14</b> )	992	992 [16]
limonene ( <b>10</b> )	1029	1031 [17]
$\alpha$ -terpinolene ( <b>12</b> )	1089	1088 [18]
linalool ( <b>15</b> )	1099	1098 [19]
$\alpha$ -terpineol ( <b>11</b> )	1191	1190 [19]
geraniol ( <b>16</b> )	1250	1253 [20]
from FPP		
$\alpha$ -longipinene ( <b>6</b> )	1355	1356 [21]
longicyclene ( <b>5</b> )	1376	1377 [21]
longifolene ( <b>4</b> )	1412	1413 [21]
$\alpha$ -himachalene ( <b>2</b> )	1461	1461 [22]
9- <i>epi</i> - $\beta$ -caryophyllene ( <b>7</b> )	1475	1471 [23]
$\gamma$ -humulene ( <b>8</b> )	1489	1487 [24]
$\gamma$ -himachalene ( <b>3</b> )	1490	1489 [22]
$\beta$ -himachalene ( <b>1</b> )	1507	1503 [25]
from GGPP		
$\beta$ -springene ( <b>18</b> )	1921	1918 [26]
cembrene A ( <b>17</b> )	1974	1979 [27]

<sup>a</sup>Retention index  $I$  on a HP-5MS column.

isopentenyl diphosphate (IPP) by farnesyl diphosphate synthase (FPPS) from *Streptomyces coelicolor* [29] with a known stereochemical course [30] (Figure S4, Supporting Information File 1). This principle was also applied to C-4 and C-8 utilising (*Z*)- and (*E*)-(4-<sup>13</sup>C,4-<sup>2</sup>H)IPP [31] for the elongation of dimethylallyl diphosphate (DMAPP) catalysed by FPPS in a known course [32]. Since both hydrogens at C-4 possess the same chemical shift, only C-8 could be used to solidify the absolute configuration (Figure S5, Supporting Information File 1).

GC analysis on a homochiral stationary phase was used to assign the absolute configurations of the observed chiral monoterpenes (*R*)-(+)-limonene (**10**), (*R*)-(+)- $\alpha$ -terpineol (**11**), (+)- $\alpha$ -pinene (**13**) and (*S*)-(+)-linalool (**15**) as shown in Figure 2 by comparison with commercially available standards (Figures S6–S9, Supporting Information File 1). The non-enzymatic degradation of GPP as a background reaction to **15** resulted in a substantial loss of stereoinformation for this compound (7% ee). Also the cyclised products **10**, **11** and **13** were not obtained in enantiomerically pure form (ee values were varying between 64% and 88%, as judged by integration), which may point to different possible binding and folding modes within the TS's

active site for GPP involving both enantiomers of linalyl diphosphate (LPP, Scheme 1) and the terpinyl cation (**A**). Other TSs producing an enantiomeric mixture of monoterpenes are also known, e.g., from *Pinus taeda* [33]. However, the major enantiomer of each cyclised monoterpene product described herein was found to be derived from (*R*)-**A**.



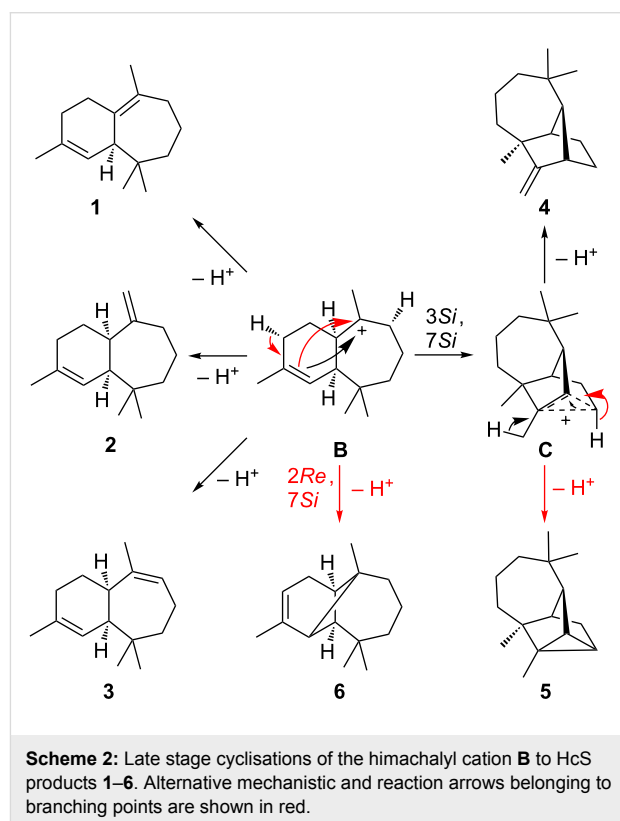
Compound **17** was isolated from a large scale incubation of the TS with GGPP and identified by NMR as cembrene A. Chiral phase GC analysis showed also in this case a mixture of enantiomers with the major one being (–)-cembrene A (61% ee), the enantiomer of the product obtained from a cembrene A synthase (CAS) from *Allokutzneria albata* [27], which was used for comparison (Figure S10, Supporting Information File 1).

Taken together, the overall more sluggish conversion of GPP and GGPP by the TS leading to enantiomeric mixtures, the higher biosynthetic complexity of the obtained sesquiterpenes and the absence of spontaneous hydrolysis products in the incubation with FPP compared to the appearance of **14** and **15** in the

incubation with GPP and **18** in the experiment with GGPP, this TS from *C. arvum* is characterised as a multiproduct (+)-β-himachalene synthase (HcS) possessing additional mono- and diterpene cyclase activity.

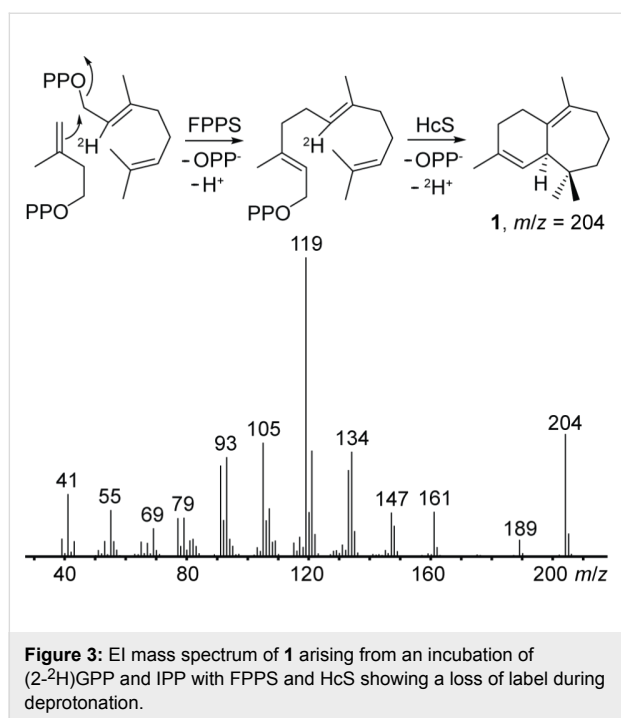
### The structures of its minor products reveal the cyclisation mechanism of HcS

Since **17** is a simple 1,14-cyclisation product, and all cyclised monoterpenes are derived from the extensively studied terpinyl cation [35,36], this work focusses on elucidating the more interesting sesquiterpene cyclase mechanism of HcS. Most sesquiterpene products **1–6** of HcS including the main product **1**, but also α-himachalene (**2**), γ-himachalene (**3**), longifolene (**4**), longicyclene (**5**), and α-longipinene (**6**) are traditionally considered to be derived from the himachalyl cation (**B**) [8,37] (Scheme 2).



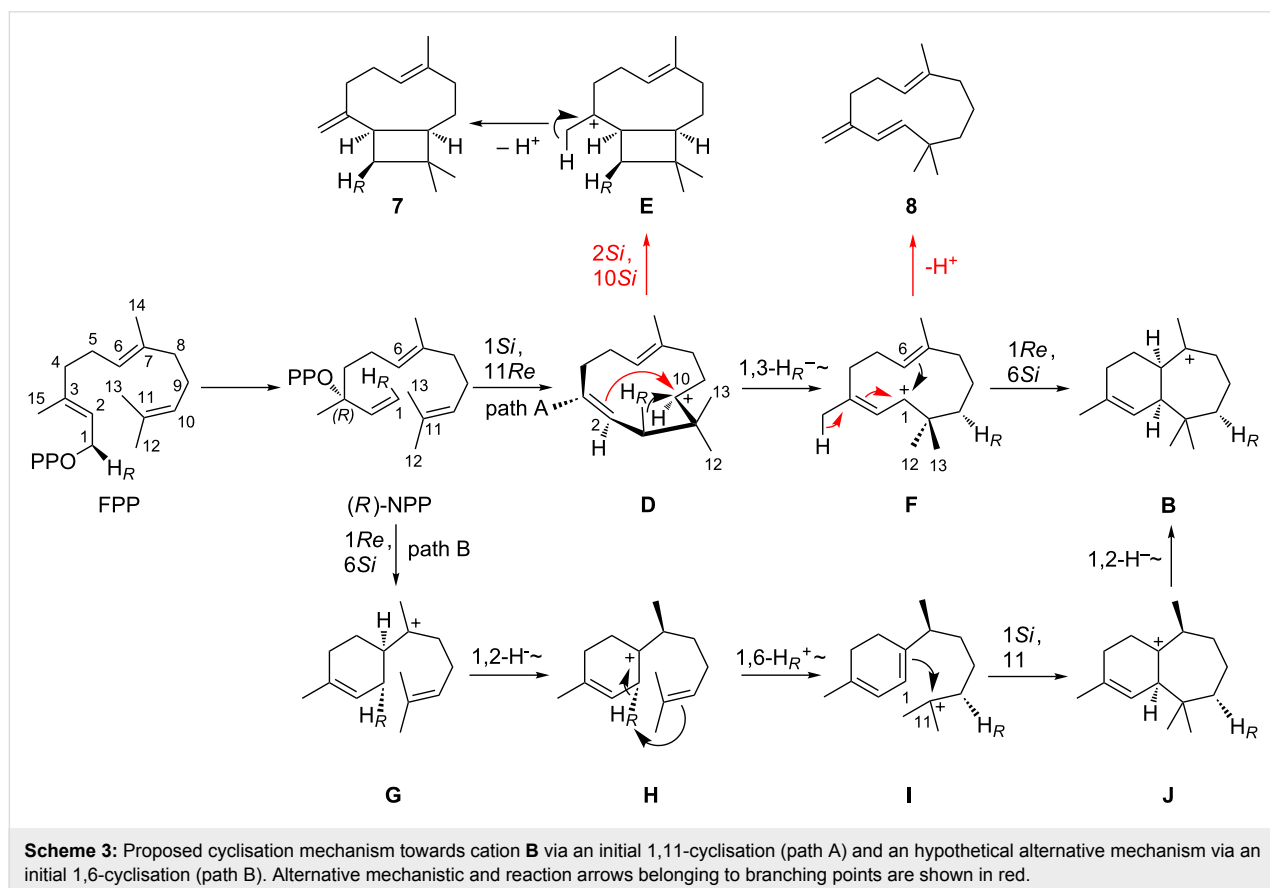
Whereas **1–3** are simple deprotonation products of **B**, **4** and **5** require a further 3,7-ring closure, leading to the non-classical cation **C**, which is a derivative of the 2-norbornyl cation [38]. This system either collapses by deprotonation at the methyl group to longifolene (**4**), or by deprotonation at C-4 with formation of a cyclopropane ring to longicyclene (**5**). Starting from **B**, a 2,7-ring closure and deprotonation at the same carbon atom gives α-longipinene (**6**). For the main product **1**, the deprotonation was followed by an incubation of HcS and FPPs with

(2-<sup>2</sup>H)GPP [39] and IPP, which resulted in unlabelled **1** as observed by GC–MS (Figure 3).



In case of a deprotonation at a methylene group, relevant for the formation of compounds **3**, **5** and **6**, the stereochemical course of these final steps could be followed by stereoselective deuterations. GC–MS analysis of the products obtained from the incubations with HcS, FPPS, DMAPP and (*Z*)- or (*E*)-(4-<sup>13</sup>C,4-<sup>2</sup>H)IPP showed a specific loss of H<sub>Z</sub> in all cases (Figure 4).

Intriguingly, all deprotonation steps leading to **1**, **3**, **5** and **6** proceed from the same face of **B**. Giving access to most products, cation **B** can be considered as the central branching point within the HcS catalysed cyclisation mechanism. To rationalise the formation of **B** starting from FPP, two different pathways were initially assumed (Scheme 3). Both start with a 1,3-*syn*-allylic rearrangement of OPP to (*R*)-nerolidyl diphosphate (NPP). This step is usually proposed to generate a (*Z*)-configured C-2,C-3 double bond after cyclisation [40]. Following the first mechanism (path A), a 1,11-cyclisation can yield secondary cation **D**, which either stabilises by 2,10-ring closure to give the caryophyllenyl cation **E** that can be deprotonated at the methyl group to yield 9-*epi*-(*E*)-β-caryophyllene (**7**), or **D** undergoes a 1,3-hydride shift to the allylic cation **F**. Deprotonation leads to γ-humulene (**8**), but a 1,6-ring closure gives access to **B**.



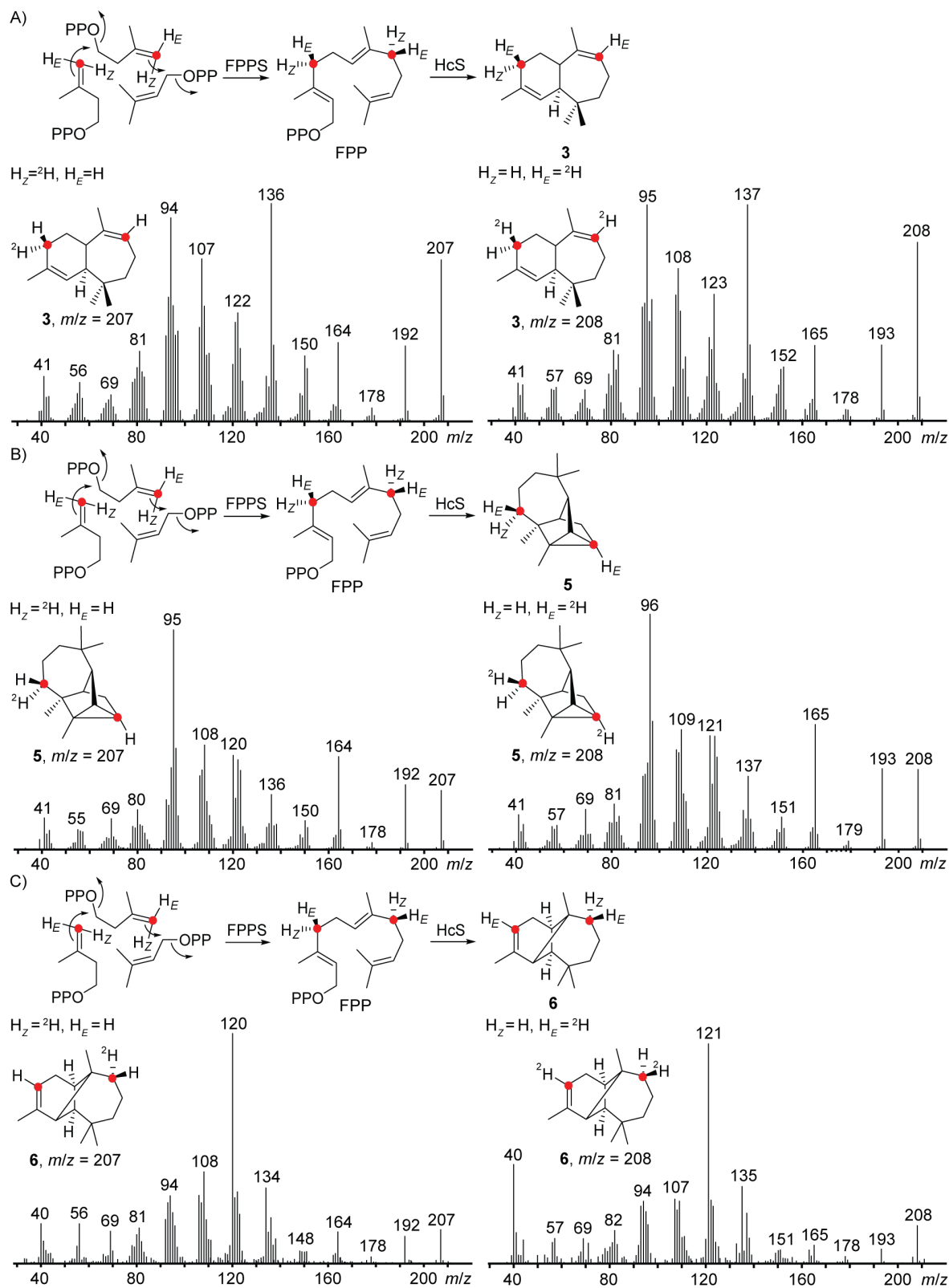


**Figure 4:** Stereochemical course of the final deprotonation step towards **3**, **5** and **6** investigated by GC-MS. EI mass spectra of labelled A) **3**, B) **5** and C) **6** obtained from the incubation of HcS and FPPS with DMAPP and (Z)-(4- ${}^{13}C, 4\text{-}{}^2H$ )IPP (left) or (E)-(4- ${}^{13}C, 4\text{-}{}^2H$ )IPP (right) indicating stereo-specific loss of one hydrogen atom.  ${}^{13}C$ -Labellings are indicated by red dots.



The second shown option, path B, assumes a 1,6-ring closure of (*R*)-NPP to the bisabolyl cation **G**. Proceeding with a 1,2-hydride shift to **H**, the key step is a 1,6-proton shift to give the tertiary cation **I**. This idea is derived from a very similar proton transfer starting from the bisabolyl cation, which occurs in the cyclisation mechanism to trichodiene [41]. A 1,11-cyclisation yields tertiary cation **J**, which can undergo a 1,2-hydride shift to **B**. While path B circumvents the secondary cation intermediate **D**, the HcS products **7** and **8** are hard to explain from path B. Together with the absence of any 1,6-cyclised bisabolene derived molecules in the product mixture their occurrence represent experimental evidence in favour of path A.

### Incubation experiments enlighten the stereochemical course of the 1,11-cyclisation and the 1,3-hydride shift

Although the general idea of path A appears to be straightforward at first sight, the details proved to be challenging as deeper insights for the stereochemistry of each step were obtained by incubation experiments. The question, whether (*R*)-NPP or its enantiomer (*S*)-NPP is involved in the HcS catalysed cyclisation cascade, was addressed by incubation of both enantiomerically pure substrates and (*rac*)-NPP [13] with HcS. The resulting chromatograms (Figure 5) clearly demonstrate (*R*)-NPP as an intermediate, which is a substrate for the production of **1–8** in approximately the same ratio as with FPP. In contrast, (*S*)-NPP is selectively converted into (*E*)- $\beta$ -farnesene (**19**, *I* = 1460 (HP-5MS), Lit. *I* = 1459 (HP-5MS) [42]). The same outcome regarding the formation of (*Z*)- $\gamma$ -bisabolene from (*R*)-NPP and FPP, but of **19** from (*S*)-NPP was recently also observed for BbS [13].

Targeting the stereochemical course of the 1,11-cyclisation of (*R*)-NPP to cation **D**, ( $12\text{-}^{13}\text{C}$ )- [43] and enzymatically prepared ( $13\text{-}^{13}\text{C}$ )FPP from ( $9\text{-}^{13}\text{C}$ )GPP [39] and IPP with FPPS were incubated with HcS to follow the fate of the geminal methyl groups for **1** (Figure 6). Combined with the relative orientation of each methyl group deduced by NOESY, these experiments showed an *11Re* attack preceding the formation of **D**. The observed absolute configurations of the monoterpenes **10**, **11** and **13** and of the diterpene **17** support this finding, because their formation requires involvement of the same face of the terminal isoprenoid double bond (*6Si* from GPP and *14Si* from GGPP). Therefore, a similar binding conformation for the terminal  $\text{C}_5$ -unit is reasonable for the three substrates.

To complete the mechanistic picture of the initial 1,11-cyclisation, also the stereochemical course at C-1 was investigated. Unfortunately, this position is disturbed by the follow-up 1,3-hydride shift in **1** and most products. However, in the side product **7** C-1 remains untouched after 1,11-cyclisation, which

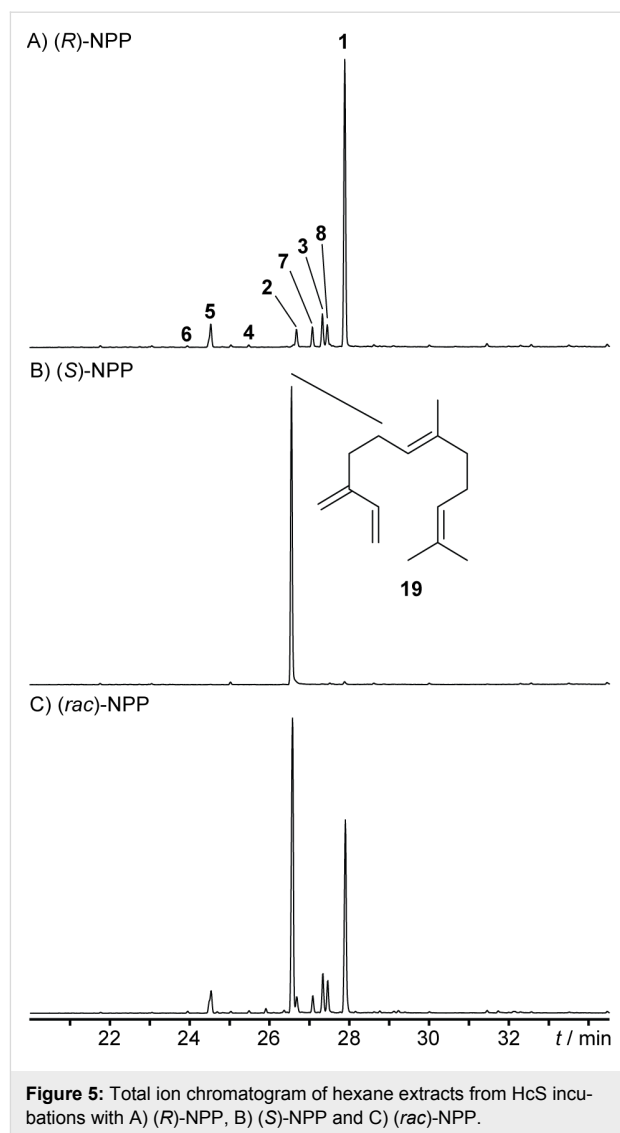
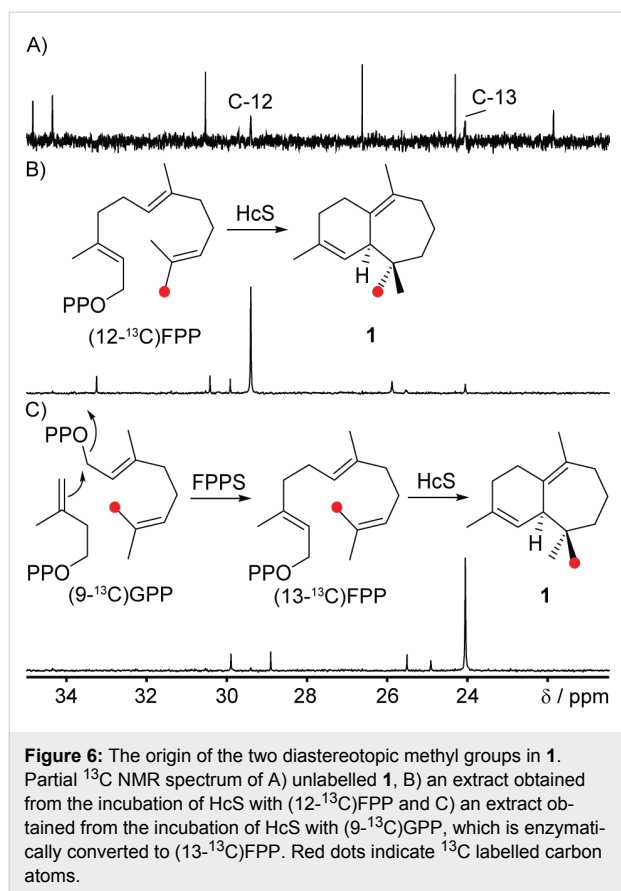


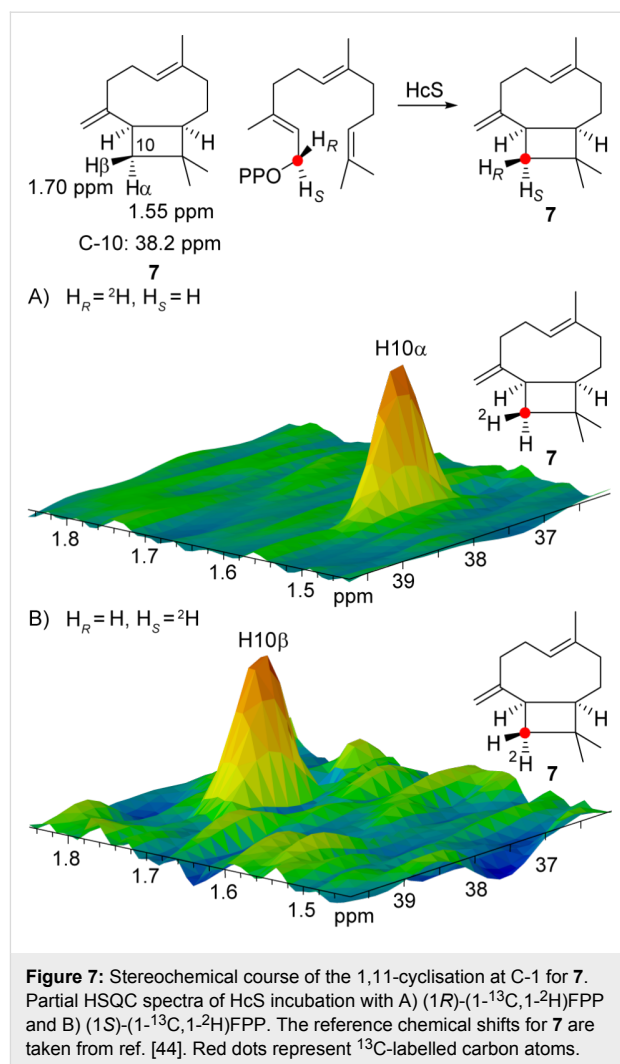
**Figure 5:** Total ion chromatogram of hexane extracts from HcS incubations with A) (*R*)-NPP, B) (*S*)-NPP and C) (*rac*)-NPP.

allows to investigate the stereochemical course of the first cyclisation step for this compound. First, the absolute configuration of **7** was assigned as shown in Figure 2 from the incubation experiments with (*E*)- and (*Z*)-( $4\text{-}^{13}\text{C}, 4\text{-}^2\text{H}$ )IPP, DMAPP, FPPS and HcS targeting the positions C-3 and C-7 (Figure S11, Supporting Information File 1), using published NMR data for **7** [44]. The stereochemical fate for the hydrogens at C-1 was then targeted by the incubation of (*1R*)- and (*1S*)-( $1\text{-}^{13}\text{C}, 1\text{-}^2\text{H}$ )FPP [28] with HcS (Figure 7).

The selective incorporation of deuterium into the diastereotopic positions of **7** is explainable by a *1S*,*11Re*-cyclisation of (*R*)-NPP. Given the absolute configuration of NPP and its formation via a 1,3-*syn*-allylic rearrangement from FPP, this ring closure represents an example of a formal *syn*- $\text{S}_{\text{N}}2'$  reaction. This is an intriguing observation, since for other TSs a NPP-cyclisation by *anti*- $\text{S}_{\text{N}}2'$  is usually described [40,45-47]. This

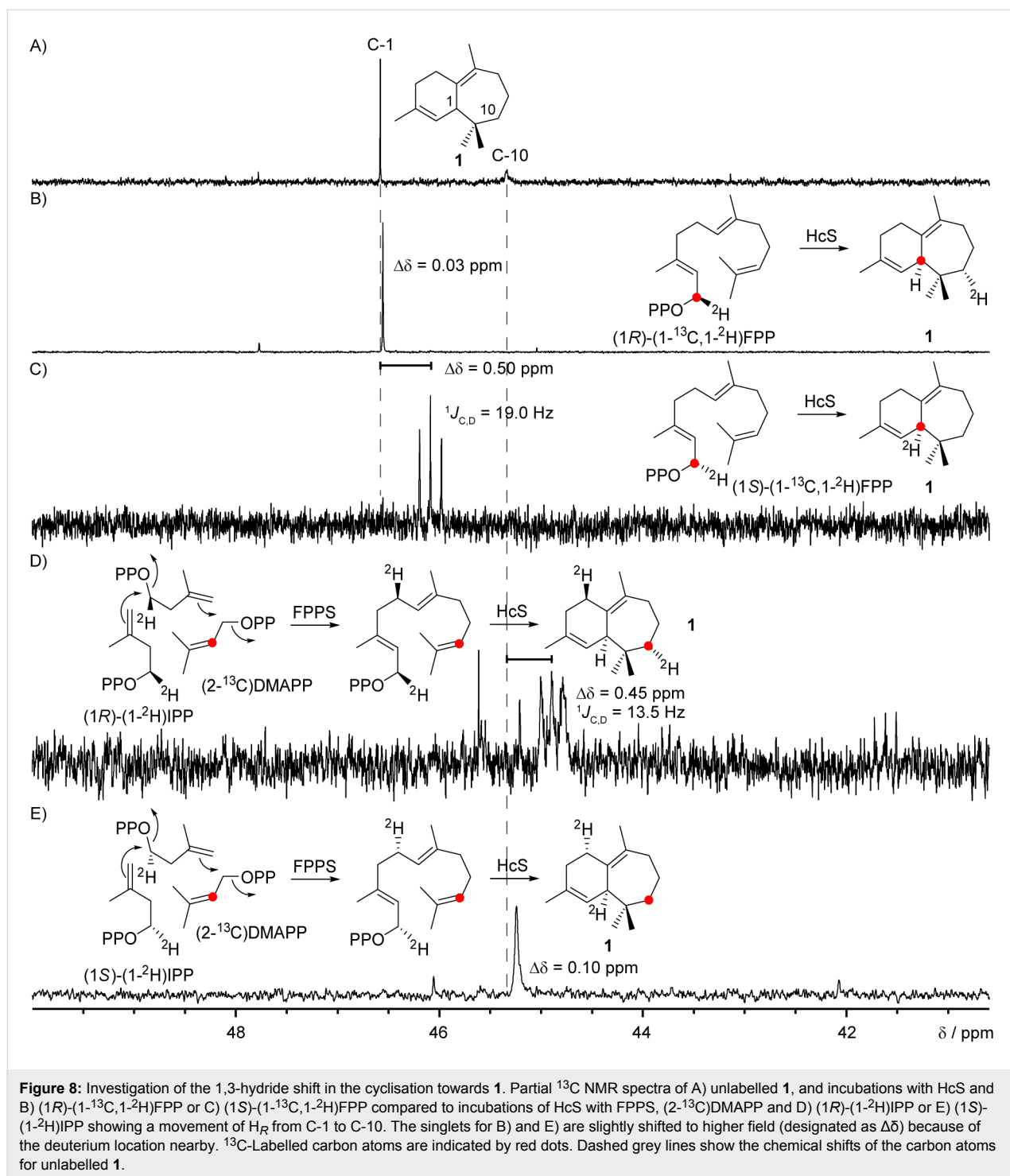


cyclisation mechanism is thought to be the predominant case, giving rise to a more energetically favoured transition state, but occasionally also the *syn*-stereochemistry was observed [48]. The rather unexpected stereochemical course of the HcS-catalysed cyclisation of NPP found herein therefore shows, that this step has to be investigated for *anti*- versus *syn*-attack experimentally for every single case, especially for a conformationally flexible situation like a 1,11-cyclisation. Intriguingly, the stereochemical course of the initial cyclisation step can even be substrate dependent. The 1,6-cyclisation towards the monoterpenes **10**, **11** and **13** as investigated by the incubation of  $(1\text{S})$ - and  $(1\text{R})$ - $(1\text{-}^{13}\text{C}, 1\text{-}^2\text{H})\text{GPP}$  with HcS and comparison to the NMR data of the commercial available products (Table S4–S8, Supporting Information File 1) clearly obeys the *anti*- $\text{S}_{\text{N}}2'$  case (Figures S12–S14, Supporting Information File 1). The observation that **15** was obtained as a nearly racemic mixture contrasts the far more selective incorporation of deuterium into the olefinic positions at C-1 of **15** (Figure S15, Supporting Information File 1). This result supports  $(\text{R})$ -LPP as an intermediate, formed by a 1,3-*syn*-allylic rearrangement to determine the observed stereochemical course at C-1, while the tertiary diphosphate might then undergo a non-enzymatic degradation to explain the high loss of stereoinformation in **15**. Also for the achiral  $\beta$ -myrcene (**14**), an imbalanced incorporation of



deuterium is found at C-1 (Figure S16, Supporting Information File 1). With the opposite stereochemical course than for **15**, **14** is likely derived from the minor enantiomer  $(\text{S})$ -LPP in analogy to **19** observed from  $(\text{S})$ -NPP. For the diterpene **17** (Table S9, Supporting Information File 1), similar investigations using  $(1\text{S})$ - and  $(1\text{R})$ - $(1\text{-}^{13}\text{C}, 1\text{-}^2\text{H})\text{GGPP}$  [49] with HcS resulted in the expected outcome for a direct 1,14-cyclisation of GGPP (Figure S17, Supporting Information File 1) in line with the results obtained with CAS from *A. albata* for *ent*-**17** [27]. Assuming similar chemical shifts at C-1 for **14** and **18**, the analogous signals for C-1 of **18** gave comparable results with the same stereochemical course as observed for **14**, although with lower preservation of stereoinformation (Figure S18, Supporting Information File 1).

To shed light on the stereochemical course of the 1,3-hydride shift connecting cations **D** and **F**, a series of labelling experiments were conducted to determine the origin of the shifting hydrogen (C-1) and its destination (C-10) for **1** (Figure 8). A

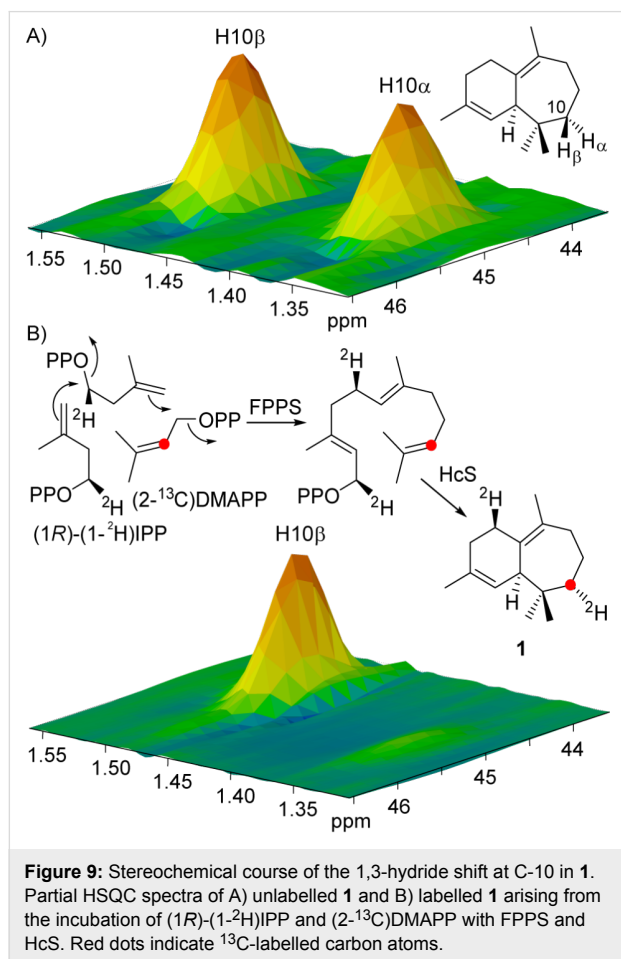


comparison of the  $^{13}\text{C}$  NMR spectra from the incubations of HcS with  $(1R)$ - and  $(1S)$ -( $1$ - $^{13}\text{C}$ , $1$ - $^2\text{H}$ )FPP, resulting in a singlet for the  $(R)$ -case and a triplet in the  $(S)$ -case indicating a direct C–D bond, clearly demonstrated the stereospecific migration of  $\text{H}_R$  from C-1. To complete the observations also for C-10,  $(2$ - $^{13}\text{C}$ )DMAPP was synthesised from  $(2$ - $^{13}\text{C}$ )-3-methylbut-2-en-1-ol [43] and incubated with  $(1R)$ - or  $(1S)$ -( $1$ - $^2\text{H}$ )IPP [50],

FPPS and HcS resulting in the expected opposite outcome than stated above, namely a triplet in the  $(R)$ -case and a singlet for the  $(S)$ -sample.

HSQC analysis of the material obtained from the incubation of  $(1R)$ -( $1$ - $^2\text{H}$ )IPP and  $(2$ - $^{13}\text{C}$ )DMAPP with FPPS and HcS also allowed for the assignment of the newly introduced diastereo-

topic position at C-10 (Figure 9). Together with the assignment of the hydrogens by NOESY in **1**, these data show a stereoselective incorporation of  $H_R-1$  into the  $H_\alpha$ -position at C-10 by a vanished crosspeak.

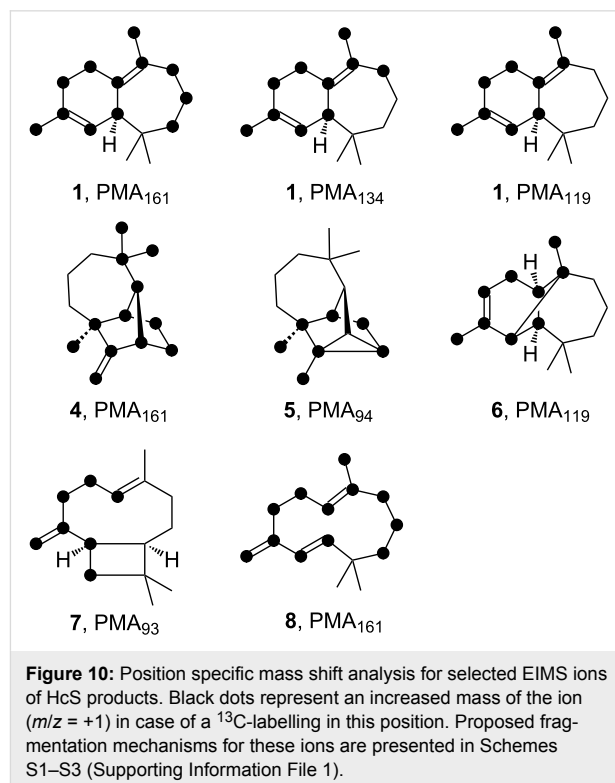


Combining the information deduced from the extensive incubation experiments stated above, a structural model for the reactive conformation of cation **D** is proposed (Figure S19, Supporting Information File 1). This intermediate, or structurally related transition states for the corresponding concerted reactions to avoid its secondary nature, are of central importance in understanding the initial HcS catalysed cyclisation towards cation **B**. The discussed conformation is imprinted by the structure of **7** with its relative conformation at the four-membered ring system allowing for a 2*Si*,10*Si*-cyclisation to **E** without major rotational changes and also reflects the short distance between  $H_R$  and C-10 for the 1,3-hydride shift towards the 10*Si* face leading to **F**. Intriguingly, the unusual *syn*- $S_N2'$  ring closure from (*R*)-NPP leads to the diphosphate moiety (OPP<sup>−</sup>) being located close to the “backside” of the cyclising molecule, which may give rise to an explanation of the multiproduct nature of HcS. At this location, OPP<sup>−</sup> can easily abstract “back-

wards” pointing hydrogen atoms from different positions which reflects the observation of the regio- and stereochemistry of the deprotonations.

### HcS provides access to labelled sesquiterpenes for EIMS fragmentation studies

Since HcS produces a mixture of structurally interesting sesquiterpenes, its synthetic abilities were also exploited to study EIMS fragmentation mechanisms. Therefore, all fifteen singly-<sup>13</sup>C labelled FPP isotopomers, either obtained by synthesis or enzymatically [39,43,51], were converted with HcS to result in mixtures of specifically labelled **1–8**. The incorporation of label into **1** was checked by <sup>13</sup>C NMR (Figure S20, Supporting Information File 1) and all samples were analysed by GC–MS. This allowed for the assignment of carbon positions to specific EI-fragments of the corresponding mass spectrum by observing an increase of +1 Da, if the labelled position is part of the fragment (position specific mass shift analysis, PMA [41,52,53]). Although for many fragments multiple overlaying fragmentation pathways were observed, some of them showed clear position dependent results, which are summarised in Figure 10. The EI mass spectra for each position and molecule laying the basis for the presented three fragments for **1** together with one fragment each for **4–8** are depicted in Figures S21–S26 (Supporting Information File 1). Possible EI-fragmentation mechanisms connected to them are discussed in Schemes S1–S3 (Supporting Information File 1).



## Conclusion

In summary, a new terpene synthase from *C. arvum* was characterised as a multiproduct (+)- $\beta$ -himachalene synthase. Accepting GPP, FPP and GGPP, HcS is a promiscuous enzyme, whose catalysis suffers from poor selectivity. Nevertheless, the formation of multiple sesquiterpene products demands for a challenging mechanistic model, which was refined by extensive labelling experiments. Several interesting details were disclosed including the stereochemical course of a 1,3-hydride migration from C-1 to C-10 and the 1,11-cyclisation featuring the unusual *syn*-S<sub>N</sub>2' attack. Combining various aspects of the initial cyclisation, the proposed conformer of cation **D** may also rationalise the reduced selectivity of HcS by its positioning of OPP<sup>-</sup>. Providing access to labelled isotopomers of its products, including structurally demanding polycyclic terpenes, HcS also served as a platform for investigating selected aspects of their EIMS fragmentation mechanisms. The labelling experiments performed with HcS described in this study therefore represent an encouragement to experimentally explore and elucidate every stereochemical detail of a terpene cyclisation mechanism for a comprehensive picture of the complex reactions, these amazing enzymes are able to catalyse.

## Supporting Information

Experimental details for gene cloning, gene expression, protein purification, incubation experiments with isotopically labelled precursors, preparative scale incubation and synthesis of (2-<sup>13</sup>C)DMAPP. The amino acid sequence of HcS, a phylogenetic tree of bacterial terpene synthases, SDS-PAGE analysis of the recombinant protein, listed NMR data for **1** and **9**, labelling experiments for the determination of the absolute configurations of **1** and **7**, chiral phase GC analysis of **10**, **11**, **13**, **15** and **17**, labelling experiments for the stereochemical course at C-1 of the monoterpenes and diterpenes, a graphical model for cation **D**, NMR spectra for the incubations of singly labelled FPPs with HcS, EIMS data for compounds **1** and **4-8** arising from these incubations and discussion of fragmentation mechanisms for selected ions.

### Supporting Information File 1

Additional material.

[<https://www.beilstein-journals.org/bjoc/content/supplementary/1860-5397-15-99-S1.pdf>]

## Acknowledgements

This work was funded by the Deutsche Forschungsgemeinschaft (DI1536/7-1).

## ORCID® IDs

Jeroen S. Dickschat - <https://orcid.org/0000-0002-0102-0631>

## References

- Hedstrom, L. *Enzyme Specificity and Selectivity*; eLS; John Wiley & Sons, Ltd.: Chichester, UK, 2010. doi:10.1002/9780470015902.a0000716.pub2
- Silverstein, R. M.; Rodin, J. O.; Wood, D. L. *Science* **1966**, *154*, 509–510.
- Zhang, A.; Robbins, P. S.; Leal, W. S.; Linn, C. E., Jr.; Villani, M. G.; Roelofs, W. L. *J. Chem. Ecol.* **1997**, *23*, 231–245. doi:10.1023/b:joec.0000006356.47959.ed
- Christianson, D. W. *Chem. Rev.* **2017**, *117*, 11570–11648. doi:10.1021/acs.chemrev.7b00287
- Dickschat, J. S. *Nat. Prod. Rep.* **2016**, *33*, 87–110. doi:10.1039/c5np00102a
- Tantillo, D. J. *Angew. Chem., Int. Ed.* **2017**, *56*, 10040–10045. doi:10.1002/anie.201702363
- Garms, S.; Köllner, T. G.; Boland, W. *J. Org. Chem.* **2010**, *75*, 5590–5600. doi:10.1021/jo100917c
- Steele, C. L.; Crock, J.; Bohlmann, J.; Croteau, R. *J. Biol. Chem.* **1998**, *273*, 2078–2089. doi:10.1074/jbc.273.4.2078
- Vedula, L. S.; Jiang, J.; Zakharian, T.; Cane, D. E.; Christianson, D. W. *Arch. Biochem. Biophys.* **2008**, *469*, 184–194. doi:10.1016/j.abb.2007.10.015
- Rinkel, J.; Lauterbach, L.; Dickschat, J. S. *Angew. Chem., Int. Ed.* **2017**, *56*, 16385–16389. doi:10.1002/anie.201711142
- Pazouki, L.; Niinemets, Ü. *Front. Plant Sci.* **2016**, *7*, No. 1019. doi:10.3389/fpls.2016.01019
- Dixit, M.; Weitman, M.; Gao, J.; Major, D. T. *ACS Catal.* **2017**, *7*, 812–818. doi:10.1021/acscatal.6b02584
- Rinkel, J.; Dickschat, J. S. *Beilstein J. Org. Chem.* **2019**, *15*, 789–794. doi:10.3762/bjoc.15.75
- Dickschat, J. S.; Pahirulzaman, K. A. K.; Rabe, P.; Klapschinski, T. A. *ChemBioChem* **2014**, *15*, 810–814. doi:10.1002/cbic.201300763
- Saroglou, V.; Dorizas, N.; Kyriotakis, Z.; Skaltsa, H. D. *J. Chromatogr. A* **2006**, *1104*, 313–322. doi:10.1016/j.chroma.2005.11.087
- Hazzit, M.; Baaliouamer, A.; Faleiro, M. L.; Miguel, M. G. *J. Agric. Food Chem.* **2006**, *54*, 6314–6321. doi:10.1021/jf0606104
- Karioti, A.; Hadjipavlou-Litina, D.; Mensah, M. L. K.; Fleischer, T. C.; Skaltsa, H. *J. Agric. Food Chem.* **2004**, *52*, 8094–8098. doi:10.1021/jf040150j
- Yáñez, X.; Pinzón, M. L.; Solano, F.; Sánchez, L. R. *Molecules* **2002**, *7*, 712–716. doi:10.3390/70900712
- Benkaci-Ali, F.; Baaliouamer, A.; Meklati, B. Y.; Chemat, F. *Flavour Fragrance J.* **2007**, *22*, 148–153. doi:10.1002/ffj.1773
- Yu, Y.; Huang, T.; Yang, B.; Liu, X.; Duan, G. *J. Pharm. Biomed. Anal.* **2007**, *43*, 24–31. doi:10.1016/j.jpba.2006.06.037
- Zeng, Y.-X.; Zhao, C.-X.; Liang, Y.-Z.; Yang, H.; Fang, H.-Z.; Yi, L.-Z.; Zeng, Z.-D. *Anal. Chim. Acta* **2007**, *595*, 328–339. doi:10.1016/j.aca.2006.12.022
- Andriamaharavo, N. R., Retention Data. *NIST Mass Spectrometry Data Center*, 2014.
- Mesa-Arango, A. C.; Betancur-Galvis, L.; Montiel, J.; Bueno, J. G.; Baena, A.; Durán, D. C.; Martínez, J. R.; Stashenko, E. E. *J. Essent. Oil Res.* **2010**, *22*, 568–574. doi:10.1080/10412905.2010.9700402

24. Bendiabdellah, A.; El Amine Dib, M.; Djabou, N.; Allali, H.; Tabti, B.; Muselli, A.; Costa, J. *Chem. Cent. J.* **2012**, *6*, No. 431. doi:10.1186/1752-153x-6-48
25. Quijano, C. E.; Salamanca, G.; Pino, J. A. *Flavour Fragrance J.* **2007**, *22*, 401–406. doi:10.1002/ffj.1812
26. Heinrich, G.; Pfeifhofer, H. W.; Stabentheiner, E.; Sawidis, T. *Ann. Bot. (Oxford, U. K.)* **2002**, *89*, 459–469. doi:10.1093/aob/mcf062
27. Rinkel, J.; Lauterbach, L.; Rabe, P.; Dickschat, J. S. *Angew. Chem., Int. Ed.* **2018**, *57*, 3238–3241. doi:10.1002/anie.201800385
28. Rabe, P.; Rinkel, J.; Dolja, E.; Schmitz, T.; Nubbemeyer, B.; Luu, T. H.; Dickschat, J. S. *Angew. Chem., Int. Ed.* **2017**, *56*, 2776–2779. doi:10.1002/anie.201612439
29. Rabe, P.; Rinkel, J.; Nubbemeyer, B.; Köllner, T. G.; Chen, F.; Dickschat, J. S. *Angew. Chem., Int. Ed.* **2016**, *55*, 15420–15423. doi:10.1002/anie.201608971
30. Thulasiram, H. V.; Poulter, C. D. *J. Am. Chem. Soc.* **2006**, *128*, 15819–15823. doi:10.1021/ja065573b
31. Lauterbach, L.; Rinkel, J.; Dickschat, J. S. *Angew. Chem., Int. Ed.* **2018**, *57*, 8280–8283. doi:10.1002/anie.201803800
32. Cornforth, J. W.; Cornforth, R. H.; Popják, G.; Yengoyan, L. *J. Biol. Chem.* **1966**, *241*, 3970–3987.
33. Phillips, M. A.; Wildung, M. R.; Williams, D. C.; Hyatt, D. C.; Croteau, R. *Arch. Biochem. Biophys.* **2003**, *411*, 267–276. doi:10.1016/s0003-9861(02)00746-4
34. Dickschat, J. S. *Nat. Prod. Rep.* **2011**, *28*, 1917–1936. doi:10.1039/c1np00063b
35. Sridivya, N.; Davis, E. M.; Croteau, R. B.; Lange, B. M. *Proc. Natl. Acad. Sci. U. S. A.* **2015**, *112*, 3332–3337. doi:10.1073/pnas.1501203112
36. Hong, Y. J.; Tantillo, D. J. *Org. Biomol. Chem.* **2010**, *8*, 4589–4600. doi:10.1039/c0ob00167h
37. Isegawa, M.; Maeda, S.; Tantillo, D. J.; Morokuma, K. *Chem. Sci.* **2014**, *5*, 1555–1560. doi:10.1039/c3sc53293c
38. Moss, R. A. *J. Phys. Org. Chem.* **2014**, *27*, 374–379. doi:10.1002/poc.3290
39. Bian, G.; Rinkel, J.; Wang, Z.; Lauterbach, L.; Hou, A.; Yuan, Y.; Deng, Z.; Liu, T.; Dickschat, J. S. *Angew. Chem., Int. Ed.* **2018**, *57*, 15887–15890. doi:10.1002/anie.201809954
40. Arigoni, D. *Pure Appl. Chem.* **1975**, *41*, 219–245. doi:10.1351/pac197541010219
41. Hong, Y. J.; Tantillo, D. J. *Org. Lett.* **2006**, *8*, 4601–4604. doi:10.1021/ol061884f
42. Asuming, W. A.; Beauchamp, P. S.; Descalzo, J. T.; Dev, B. C.; Dev, V.; Frost, S.; Ma, C. W. *Biochem. Syst. Ecol.* **2005**, *33*, 17–26. doi:10.1016/j.bse.2004.06.005
43. Rabe, P.; Barra, L.; Rinkel, J.; Riclea, R.; Citron, C. A.; Klapschinski, T. A.; Janusko, A.; Dickschat, J. S. *Angew. Chem., Int. Ed.* **2015**, *54*, 13448–13451. doi:10.1002/anie.201507615
44. Hinkley, S. F. R.; Perry, N. B.; Weavers, R. T. *Phytochemistry* **1994**, *35*, 1489–1494. doi:10.1016/s0031-9422(00)86882-x
45. Cane, D. E.; Tandon, M. *J. Am. Chem. Soc.* **1995**, *117*, 5602–5603. doi:10.1021/ja00125a029
46. Hu, Y.; Chou, W. K. W.; Hopson, R.; Cane, D. E. *Chem. Biol.* **2011**, *18*, 32–37. doi:10.1016/j.chembiol.2010.11.008
47. Rinkel, J.; Rabe, P.; Garbeva, P.; Dickschat, J. S. *Angew. Chem., Int. Ed.* **2016**, *55*, 13593–13596. doi:10.1002/anie.201608042
48. Benedict, C. R.; Lu, J. L.; Pettigrew, D. W.; Liu, J.; Stipanovic, R. D.; Williams, H. J. *Plant Physiol.* **2001**, *125*, 1754–1765. doi:10.1104/pp.125.4.1754
49. Rinkel, J.; Rabe, P.; Chen, X.; Köllner, T. G.; Chen, F.; Dickschat, J. S. *Chem. – Eur. J.* **2017**, *23*, 10501–10505. doi:10.1002/chem.201702704
50. Rinkel, J.; Lauterbach, L.; Dickschat, J. S. *Angew. Chem., Int. Ed.* **2019**, *58*, 452–455. doi:10.1002/anie.201812216
51. Mitsuhashi, T.; Rinkel, J.; Okada, M.; Abe, I.; Dickschat, J. S. *Chem. – Eur. J.* **2017**, *23*, 10053–10057. doi:10.1002/chem.201702766
52. Rabe, P.; Klapschinski, T. A.; Dickschat, J. S. *ChemBioChem* **2016**, *17*, 1333–1337. doi:10.1002/cbic.201600237
53. Rinkel, J.; Rabe, P.; Dickschat, J. S. *Eur. J. Org. Chem.* **2019**, 351–359. doi:10.1002/ejoc.201800217

## License and Terms

This is an Open Access article under the terms of the Creative Commons Attribution License (<http://creativecommons.org/licenses/by/4.0>). Please note that the reuse, redistribution and reproduction in particular requires that the authors and source are credited.

The license is subject to the *Beilstein Journal of Organic Chemistry* terms and conditions: (<https://www.beilstein-journals.org/bjoc>)

The definitive version of this article is the electronic one which can be found at: [doi:10.3762/bjoc.15.99](https://doi.org/10.3762/bjoc.15.99)

## Appendix S

### **The EI-MS Fragmentation Mechanisms of Bacterial Sesquiterpenes and Diterpenes**

*Eur. J. Org. Chem.* **2019**, 351–359.

DOI:10.1002/ejoc.201800217





## Terpene Fragmentation | Very Important Paper |



## VIP The EI-MS Fragmentation Mechanisms of Bacterial Sesquiterpenes and Diterpenes

Jan Rinkel,<sup>[a]</sup> Patrick Rabe,<sup>[a]</sup> and Jeroen S. Dickschat<sup>\*[a]</sup>

**Abstract:** The EI-MS fragmentation mechanisms of one bacterial sesquiterpene alcohol and four diterpene hydrocarbons have been investigated by using all 15 or 20 enzymatically synthesised <sup>13</sup>C<sub>1</sub>-labelled isotopomers of each molecule. A posi-

tion-specific mass shift analysis indicated the parts of the carbon backbone that form each fragment ion. Plausible fragmentation mechanisms have been developed and further strengthened by HR-MS/MS analyses.

## Introduction

During the past decades, gas chromatography coupled to electron-impact mass spectrometry (GC–EI-MS) has become a standard technology in the analysis and identification of volatile organic compounds (VOCs).<sup>[1]</sup> The technique is particularly useful for the identification of volatile natural products in complex compound mixtures. In the mass spectrometer the analyte is ionised by collision with an electron of sufficient energy, usually 70 eV, which creates a molecular ion [M]<sup>+</sup> that can be detected by a mass analyser. The ionisation process leaves the molecular ion in an excited state, which causes a series of fragmentation reactions to yield a variety of fragment ions. Together, the relative proportions of the molecular ion and the fragment ions create a signature motif that is characteristic for the analyte and can be used for its identification. For this purpose, the EI mass spectra of many natural and non-natural VOCs have been collected in large electronic libraries that allow for a rapid compound identification by a computer-assisted comparison of measured and library mass spectra. Several elementary reactions occur in the EI-MS fragmentations, including the cleavage of  $\sigma$  bonds ( $\sigma$ ), radical-induced or  $\alpha$  cleavage ( $\alpha$ ), charge-induced or inductive cleavage ( $i$ ) and radical rearrangements of hydrogen atoms ( $rH$ ) or the carbon skeleton ( $rC$ ), are known.<sup>[2]</sup> Some special reaction types represent combinations of these elementary reactions, for example, the retro-Diels–Alder fragmentation is a combination of two  $\alpha$  cleavages or of one  $\alpha$  and one inductive cleavage,<sup>[3]</sup> whereas the McLafferty rearrangement is a combined  $\gamma$ -H rearrangement and  $\alpha$  or inductive cleavage.<sup>[4]</sup> Important early contributions to the study of fragmentation mechanisms of volatile natural products by isotopic labelling experiments were made by Ryhage and Stenhagen,

who investigated methyl-branched fatty acid methyl esters,<sup>[5]</sup> and by Djerassi and co-workers, who studied mono- and triterpenoids by the introduction of specific labellings by semi-synthesis.<sup>[6]</sup>

Understanding of the formation of fragment ions in organic molecules is of interest, because it allows the structures of unknown compounds to be proposed, as we have recently shown based on the work of Ryhage and Stenhagen for fatty acid methyl esters derived from *Micromonospora aurantiaca*,<sup>[7]</sup> blastmycinones, a class of functionalised lactones from streptomycetes,<sup>[8]</sup> and several methylated monoterpenes associated with the bacterial biosynthesis of 2-methylisoborneol.<sup>[9]</sup> Although this approach requires the synthesis of reference material for unambiguous structure elucidation, it is still very useful for identifying trace compounds that are produced in too low amounts for isolation and NMR-based structure elucidation.

In particular, the complex cyclisation reactions catalysed by terpene synthases (TS) can be followed by using isotopically labelled precursors.<sup>[10]</sup> In some cases, feeding experiments with living cultures have been performed to study terpene cyclisations, and the incorporated labelling was localised by interpretation of the EI-MS fragmentation patterns.<sup>[11]</sup> Also, for such experiments, a detailed knowledge of the fragmentation mechanism is desirable. During the course of our recent work we prepared all 15 isotopomers of (<sup>13</sup>C)farnesyl diphosphate (FPP) and all 20 isotopomers of (<sup>13</sup>C)geranylgeranyl diphosphate (GGPP) by chemical and enzymatic synthesis.<sup>[12]</sup> These compounds can be converted by TSs into labelled terpenes and the isotopic labelling can be efficiently localised by <sup>13</sup>C NMR spectroscopy. Through this approach full sets of all 15 isotopomers of *epi*-isozizaene, the corvol ethers, *epi*-cubebol, isodauc-8-en-11-ol, protoillud-7-ene and asterisca-2(9),6-diene were prepared and their analysis by GC–EI-MS allowed us to investigate whether a carbon atom contributes to an observed fragment ion or not (position-specific mass shift analysis, PMA).<sup>[13]</sup> Here we present the EI-MS fragmentation mechanisms for the sesquiterpene alcohol T-muurolol (**1**) and the first study of diterpenes, represented by tsukubadiene (**2**), spata-13,17-diene (**3**), prenylkelsoene (**4**) and spiroalbatene (**5**, Figure 1).

[a] Kekulé-Institut für Organische Chemie und Biochemie, Rheinische Friedrich-Wilhelms-Universität Bonn, Gerhard-Domagk-Straße 1, 53121 Bonn, Germany  
E-mail: dickschat@uni-bonn.de  
[https://www.chemie.uni-bonn.de/oc/forschung/arbeitsgruppen/ak\\_dickschat](https://www.chemie.uni-bonn.de/oc/forschung/arbeitsgruppen/ak_dickschat)

Supporting information and ORCID(s) from the author(s) for this article are available on the WWW under <https://doi.org/10.1002/ejoc.201800217>.

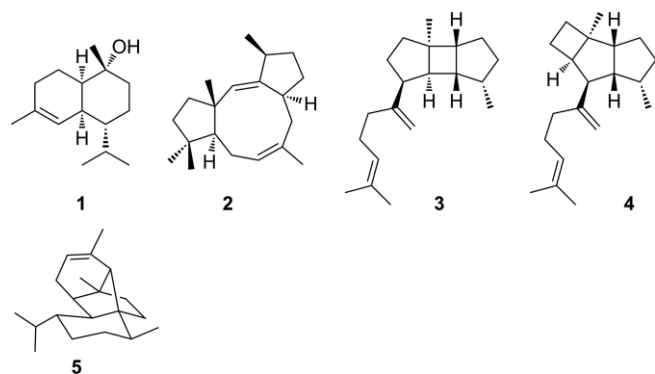


Figure 1. Structures of terpenes investigated in this study.

## Results and Discussion

The 15 isotopomers of ( $^{13}\text{C}$ )FPP were converted with T-murolol synthase from *Roseiflexus castenholzii*<sup>[14]</sup> and the products obtained were analysed by GC–MS (see Figure S1 in the Supporting Information). For comparison, unlabelled FPP was also enzymatically converted and the product analysed under the same conditions. For a particular isotopomer ( $^{13}\text{C}$ -**1**), a fragment ion  $m/z$  will either be increased by 1 Da in comparison with the same fragment ion of **1** or not, depending on whether the labelled carbon is part of the fragment ion or not. This information can be extracted from all 15 isotopomers of ( $^{13}\text{C}$ -**1**), a process for which we recently introduced the term position-specific mass shift analysis (PMA); the results of this analysis are summarised in Figure 2.

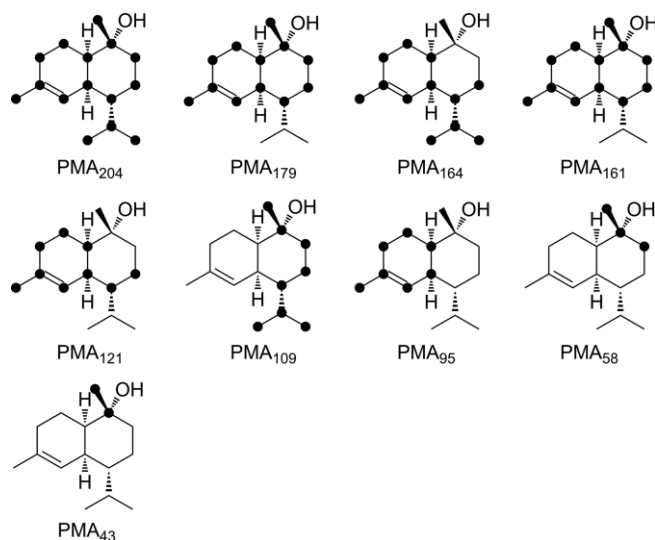
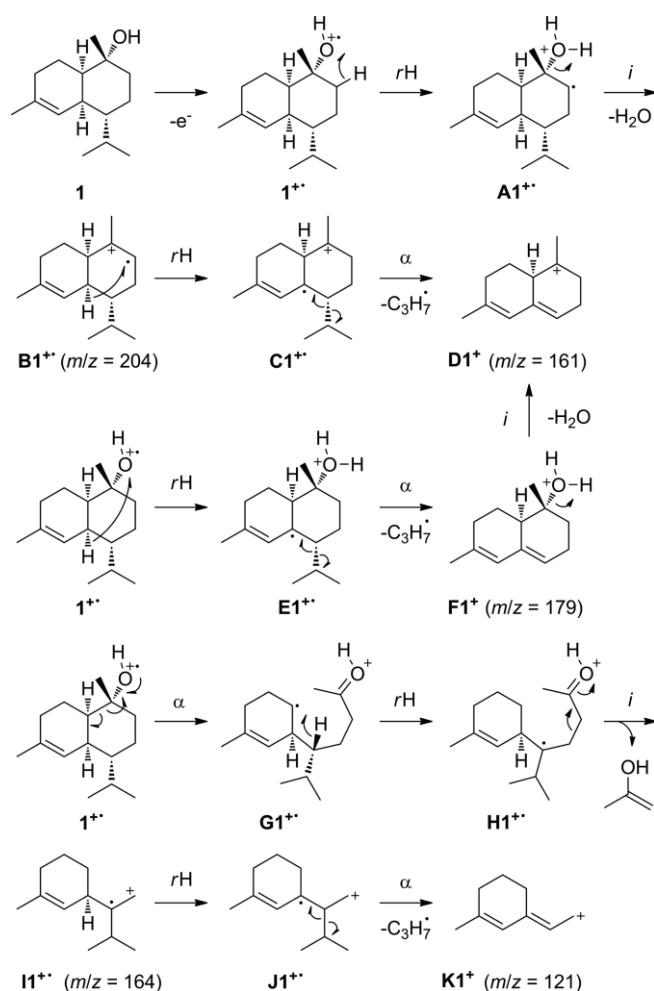


Figure 2. Position-specific mass shift analysis for **1**. Black dots represent carbon atoms contributing to the formation of the indicated fragment ion  $\text{PMA}_{m/z}$ .

The PMA for the fragment ion  $m/z = 204$  ( $\text{PMA}_{204}$ ) reveals that the formation of this fragment ion requires participation of the whole carbon backbone of **1** and thus proceeds by loss of water through ionisation at the hydroxy function to  $\mathbf{1}^+$ , rearrangement of one hydrogen likely from a neighbouring posi-

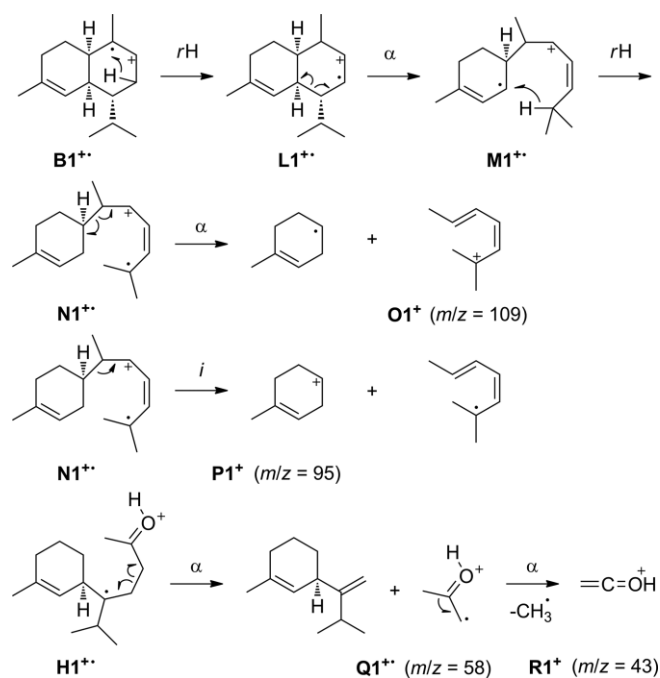
tion to  $\mathbf{A1}^+$  and inductive cleavage of water to  $\mathbf{B1}^+$  (Scheme 1). It should be emphasised that the investigation of  $^{13}\text{C}$ -labelled compounds does not allow hydrogen rearrangements to be followed, but all the reactions shown in this work lead to plausible intermediates that can explain the rupture of C–C bonds and usually involve reasonable three- to six-membered transition states. However, it cannot be excluded that multiple processes with hydrogen scrambling lead to the same or similar intermediates to those shown in the schemes presented here.  $\text{PMA}_{161}$  indicates loss of the isopropyl group, which is possible by hydrogen rearrangement from  $\mathbf{B1}^+$  to  $\mathbf{C1}^+$ , followed by  $\alpha$  cleavage to  $\mathbf{D1}^+$ . Similarly,  $\text{PMA}_{179}$  demonstrates loss of the isopropyl group, but fragment ion  $\mathbf{F1}^+$  still contains water and must arise from  $\mathbf{1}^+$  by hydrogen rearrangement to  $\mathbf{E1}^+$  and  $\alpha$  cleavage. Inductive cleavage of water opens another possible route towards  $\mathbf{D1}^+$ , and MS/MS analysis of both fragment ions  $m/z = 179$  and  $m/z = 204$  (see Figure S2 in the Supporting Information) gives evidence that indeed both mechanisms contribute to the formation of  $\mathbf{D1}^+$ .  $\text{PMA}_{164}$  gives rise to a mechanism involving  $\alpha$  cleavage of  $\mathbf{1}^+$  to  $\mathbf{G1}^+$ , hydrogen rearrangement to  $\mathbf{H1}^+$  and inductive cleavage of acetone to  $\mathbf{I1}^+$ . This fragment ion also proceeds to  $\mathbf{K1}^+$  by hydrogen rearrangement to  $\mathbf{J1}^+$  and  $\alpha$  cleavage, in agreement with  $\text{PMA}_{121}$  and as dem-



Scheme 1. Proposed mechanisms of EI-MS fragmentations of **1** (part I).

onstrated by MS/MS analysis of fragment ion  $m/z = 164$ . Although the formation of  $\mathbf{K1}^+$  is also possible from  $\mathbf{F1}^+$  (cf. MS/MS of  $m/z = 179$ ), this fragment ion does not arise from  $\mathbf{B1}^+$  or  $\mathbf{D1}^+$  after the elimination of water, which suggests that  $\mathbf{K1}^+$  is always generated by cleavage of acetone and the isopropyl group in a variable order of steps.

PMA<sub>109</sub> reveals fragment ion formation from the right half of **1**, which is possible from  $\mathbf{B1}^+$  by a sequence of hydrogen rearrangement to  $\mathbf{L1}^+$ ,  $\alpha$  cleavage to  $\mathbf{M1}^+$ , another hydrogen rearrangement to  $\mathbf{N1}^+$  and final homolytic cleavage to  $\mathbf{O1}^+$  (Scheme 2). Alternatively,  $\mathbf{N1}^+$  can fragment heterolytically to yield  $\mathbf{P1}^+$ . Starting from  $\mathbf{H1}^+$ , two sequential  $\alpha$  cleavages give rise to  $\mathbf{Q1}^+$  and then  $\mathbf{R1}^+$ , in agreement with the corresponding PMAs. Also, none of the fragment ions larger than  $m/z = 58$  analysed by MS/MS is a precursor of these two ions, which suggests their direct formation from the molecular ion, whereas MS/MS analysis of  $m/z = 58$  shows that  $\mathbf{Q1}^+$  is indeed a precursor of  $\mathbf{R1}^+$ .



Scheme 2. Proposed mechanisms of EI-MS fragmentations of **1** (part II).

The tsukubadiene synthase from *Streptomyces tsukubaensis*<sup>[12b,15]</sup> was used to convert all 20 (<sup>13</sup>C)GGPP isotopomers into the corresponding isotopomers of **2**. Their GC-MS analysis (see Figure S3 in the Supporting Information) allowed us to extract the PMA information for four pronounced fragment ions ( $m/z = 189$ , a pair at  $m/z = 148$  and  $149$ , and  $m/z = 133$ ) as shown in Figure 3. Note that the black circles in this figure indicate carbon atoms that fully contribute to the formation of a fragment ion, whereas the grey circles represent carbon atoms that contribute only partially, because of an alternative cleavage of one of two methyl groups in the formation of fragments  $m/z = 189$  and  $m/z = 133$ . These overlapping reaction pathways are evident from an only partially increased fragment ion by 1 Da, if the corresponding carbon atoms are labelled.

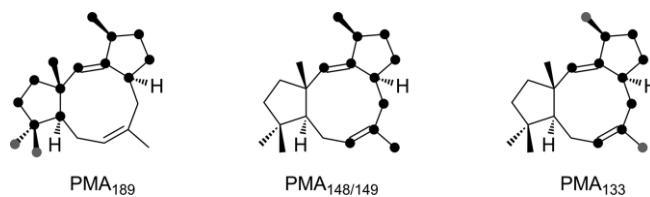
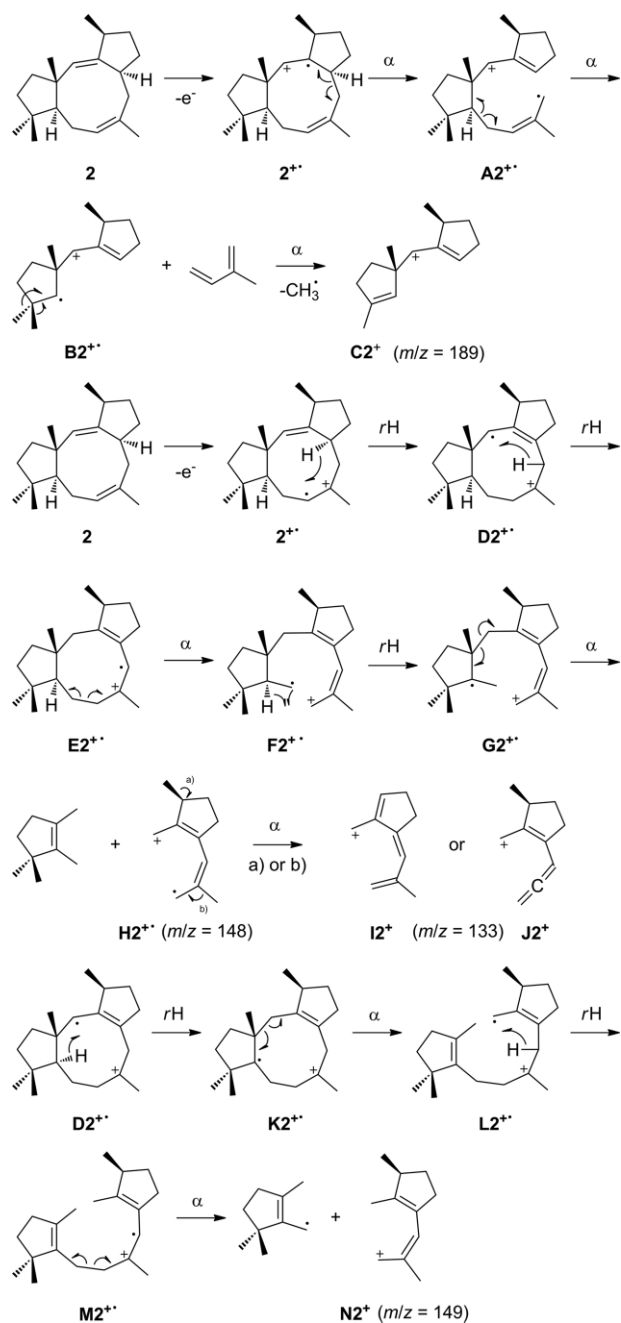


Figure 3. Position-specific mass shift analysis for **2**. Black dots represent carbon atoms contributing fully to the formation of the indicated fragment ion PMA <sub>$m/z$</sub> ; grey dots represent carbon atoms that contribute partially.

For **2**, the formation of the fragment ion  $m/z = 189$  can be explained by ionisation of an olefinic double bond to  $\mathbf{2}^+$ , followed by two  $\alpha$  fragmentations via  $\mathbf{A2}^+$  to  $\mathbf{B2}^+$  with loss of neutral isoprene (Scheme 3). A third  $\alpha$  fragmentation with loss of one of the two geminal methyl groups yields  $\mathbf{C2}^+$ . The fragment ions  $m/z = 148$  and  $149$  originate from the same part of the carbon backbone of **2** and the mechanisms for their formation are likely related. Ionisation of **2** at the other olefinic double bond to  $\mathbf{2}^+$  is followed by two hydrogen rearrangements via  $\mathbf{D2}^+$  to  $\mathbf{E2}^+$ . Subsequent  $\alpha$  cleavage to  $\mathbf{F2}^+$ , hydrogen rearrangement to  $\mathbf{G2}^+$  and another  $\alpha$  cleavage explain the formation of  $\mathbf{H2}^+$ . Cleavage of one of the two methyl groups yields  $\mathbf{I2}^+$  or  $\mathbf{J2}^+$ , in agreement with the PMA<sub>133</sub>. The formation of the fragment ion at  $m/z = 133$  from  $m/z = 148$  is also observed by MS/MS experiments (see Figure S4 in the Supporting Information). Starting from the common intermediate  $\mathbf{D2}^+$ ,  $m/z = 149$  can be formed by a hydrogen rearrangement to  $\mathbf{K2}^+$  and  $\alpha$  fragmentation to  $\mathbf{L2}^+$ , which can further react by another hydrogen rearrangement to  $\mathbf{M2}^+$  and  $\alpha$  cleavage to  $\mathbf{N2}^+$ . The important difference between the mechanisms for the formation of  $\mathbf{H2}^+$  and  $\mathbf{N2}^+$  is the transfer of one hydrogen atom from the left to the right half of the molecule in the reaction from  $\mathbf{D2}^+$  to  $\mathbf{K2}^+$ , which causes the mass difference of 1 Da between the two discussed fragment ions. This mass difference would also be explainable if  $\mathbf{N2}^+$  could further react by loss of one hydrogen atom, but MS/MS analysis of  $m/z = 149$  showed that this process is not relevant.

The spata-13,17-diene synthase from *Streptomyces xinghaiensis* was used to prepare the 20 isotopomers of (<sup>13</sup>C)-**3**.<sup>[15]</sup> Their EI mass spectra are shown in Figure S5 in the Supporting Information, and for six major fragment ions the PMA resulted in a clear picture of their origin (Figure 4). PMA<sub>229</sub> indicated the formation of the fragment ion  $m/z = 229$  by specific loss of the isopropylidene portion from the side-chain, which was rather surprising because this requires cleavage of a C=C double bond. Because the discussed fragment arises by loss of C<sub>3</sub>H<sub>7</sub>, the fragmentation mechanism likely includes a hydrogen transfer to the C<sub>3</sub> portion to be cleaved. A satisfactory explanation is given by the mechanism shown in Scheme 4, which starts with ionisation at the less substituted double bond to  $\mathbf{3}^+$ , followed by two hydrogen rearrangements via  $\mathbf{A3}^+$  to  $\mathbf{B3}^+$ . Through this process the double bond is shifted inwards so that another hydrogen transfer to  $\mathbf{C3}^+$  and  $\alpha$  fragmentation result in  $\mathbf{D3}^+$ . Generation of the fragment ion  $m/z = 203$  proceeds with loss of a prenyl group from the side-chain and is easily explained by  $\alpha$  cleavage in  $\mathbf{A3}^+$  to  $\mathbf{E3}^+$ .



Scheme 3. Proposed mechanisms of EI-MS fragmentations for **2**.

PMA<sub>190</sub> reveals the loss of the right five-membered ring of **3** as the relevant process for the formation of the corresponding fragment ion  $m/z = 190$ . Because of the ring strain of the cyclobutane the ionisation of **3** is also possible at one of its  $\sigma$  bonds. The most stable tertiary cation is formed if the charge of the resulting species **3<sup>+</sup>** remains in the left ring. Subsequent  $\alpha$  cleavage of the second bond of the original cyclobutane with loss of neutral methylcyclopentene leads to **F3<sup>+</sup>**. As is evident from PMA<sub>121</sub>, the fragment ion  $m/z = 121$  arises by further cleavage of a prenyl group from the side-chain. Two hydrogen rearrangements from **F3<sup>+</sup>** via **G3<sup>+</sup>** to **H3<sup>+</sup>** transfer the reactivity into the side-chain, allowing for an  $\alpha$  cleavage to **I3<sup>+</sup>** with loss of neutral isoprene. Instead of the two hydrogen transfers, a

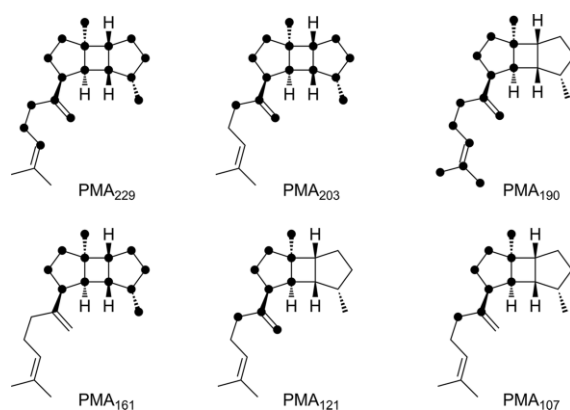
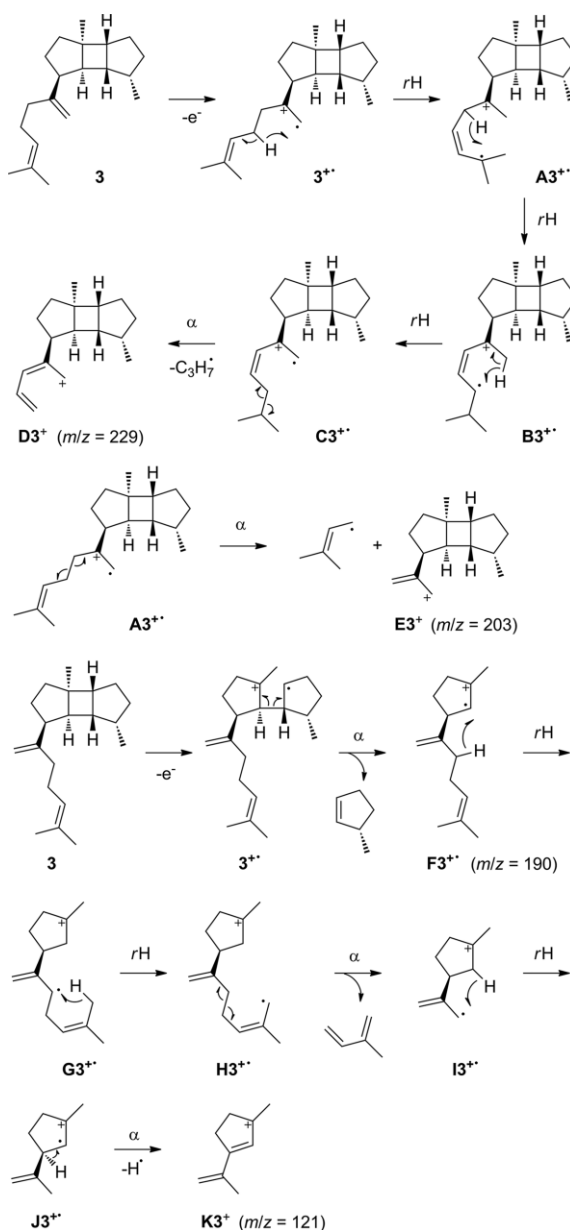


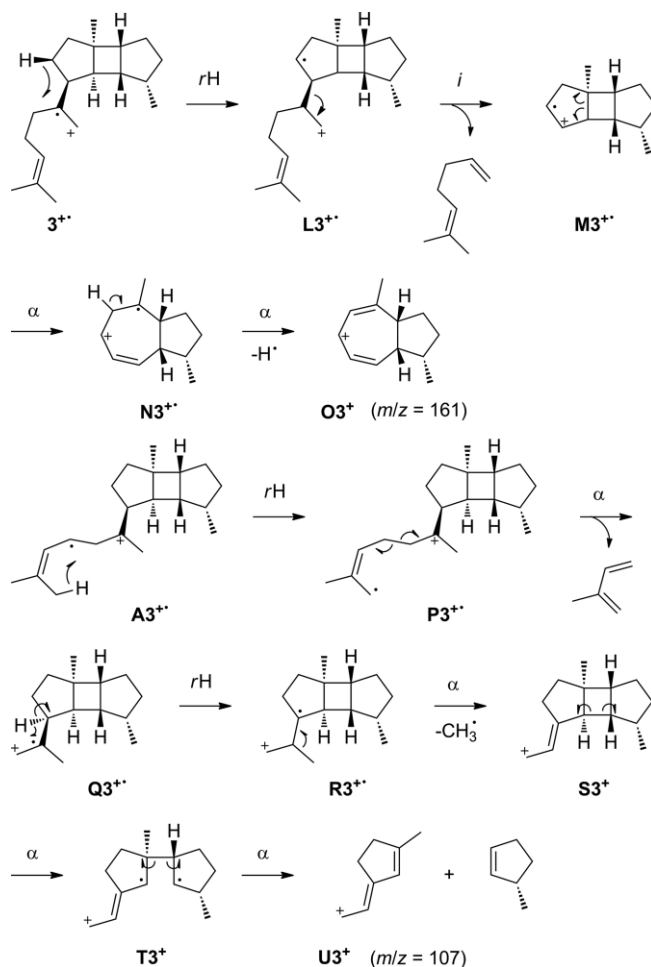
Figure 4. Position-specific mass shift analysis for **3**. Black dots represent carbon atoms contributing to the formation of the indicated fragment ion PMA <sub>$m/z$</sub> .



Scheme 4. Proposed mechanisms of EI-MS fragmentations of **3** (part I).

direct reaction from  $\mathbf{F3}^+$  to  $\mathbf{H3}^+$  is also possible, but only via a nine-membered transition state, which can be considered unlikely. Another hydrogen rearrangement to  $\mathbf{J3}^+$  and  $\alpha$  cleavage of a hydrogen explain the formation of  $\mathbf{K3}^+$ . The reaction from the fragment  $m/z = 190$  to  $m/z = 121$  is also confirmed by MS/MS analysis (see Figure S6 in the Supporting Information). MS/MS experiments on the fragment ion  $m/z = 203$ , represented by  $\mathbf{E3}^+$ , show that the reversed order of steps with loss of the prenyl group from the side-chain first and then loss of the right five-membered ring is less pronounced.

The fragment ion  $m/z = 161$  is formed from the bicyclic core structure of  $\mathbf{3}$  and includes the two directly connected methyl groups. After ionisation of  $\mathbf{3}$  to  $\mathbf{3}^+$ , a hydrogen transfer from a neighbouring ring carbon to  $\mathbf{L3}^+$  and inductive cleavage with loss of neutral 6-methylhepta-1,5-diene result in  $\mathbf{M3}^+$ , which reacts by ring-opening of the strained cyclobutane through  $\alpha$  fragmentation to  $\mathbf{N3}^+$  (Scheme 5). Another  $\alpha$  cleavage of a hydrogen establishes the pentadienyl cation in  $\mathbf{O3}^+$ . PMA<sub>107</sub> reveals the specific formation of the fragment ion  $m/z = 107$  from the left cyclopentane ring and includes the bound methyl group and a C<sub>2</sub> fragment from the side-chain. This is explainable from  $\mathbf{A3}^+$  by hydrogen rearrangement to  $\mathbf{P3}^+$  and  $\alpha$  fragmentation with loss of neutral isoprene to  $\mathbf{Q3}^+$ . A subsequent hydrogen shift to  $\mathbf{R3}^+$  induces methyl group cleavage to the



Scheme 5. Proposed mechanisms of EI-MS fragmentations of  $\mathbf{3}$  (part II).

allyl cation  $\mathbf{S3}^+$  that is followed by two more  $\alpha$  (or inductive) cleavages via  $\mathbf{T3}^+$  to  $\mathbf{U3}^+$ .

As a side-product, the spata-13,17-diene synthase from *S. xinghaiensis* also makes minor amounts of prenylkelsoene ( $\mathbf{4}$ ).<sup>[16]</sup> GC–EI–MS analysis of all 20 <sup>13</sup>C-labelled isotopomers (see Figure S7 in the Supporting Information) resulted in the identification of the origin of several fragment ions from the carbon skeleton of  $\mathbf{4}$ , as summarised by the PMAs presented in Figure 5. The formation of the base peak ion at  $m/z = 244$  requires cleavage of two carbon atoms from the cyclobutane portion. This is mechanistically understandable by the ionisation of  $\mathbf{4}$  to  $\mathbf{4}^+$  and two subsequent hydrogen rearrangements via  $\mathbf{A4}^+$  to  $\mathbf{B4}^+$  through five-membered transition states (Scheme 6). A direct reaction from  $\mathbf{4}^+$  to  $\mathbf{B4}^+$  is also reasonable. The intermediate  $\mathbf{B4}^+$  can further react by two  $\alpha$  cleavages to  $\mathbf{C4}^+$  with loss of neutral ethylene. A fragmentation with loss of 28 Da from the molecular ion has also been reported for the sesquiterpene kelsoene<sup>[17]</sup> and the tetraterpene poduran,<sup>[18]</sup> which exhibit the same tricyclic core structure as  $\mathbf{4}$ , but with a shorter and longer side-chain, respectively. The radical cation  $\mathbf{C4}^+$  can further react by  $\alpha$  cleavage to  $\mathbf{D4}^+$ , a fragment that explains the finding of PMA<sub>175</sub>. This secondary fragmentation is also supported by MS/MS analysis of the fragment ion  $m/z = 244$  (see Figure S8).

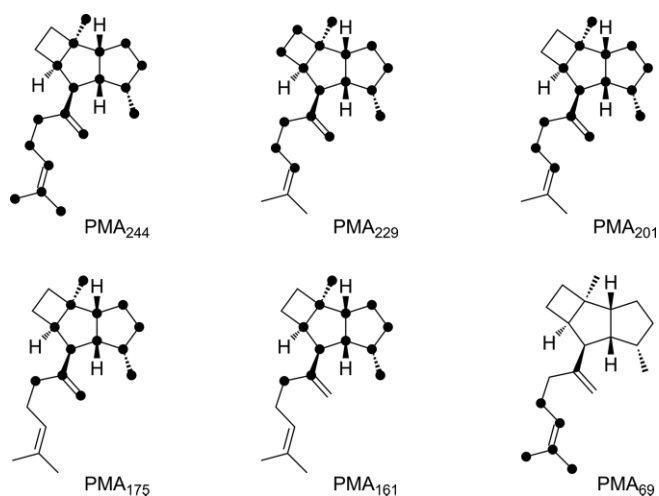
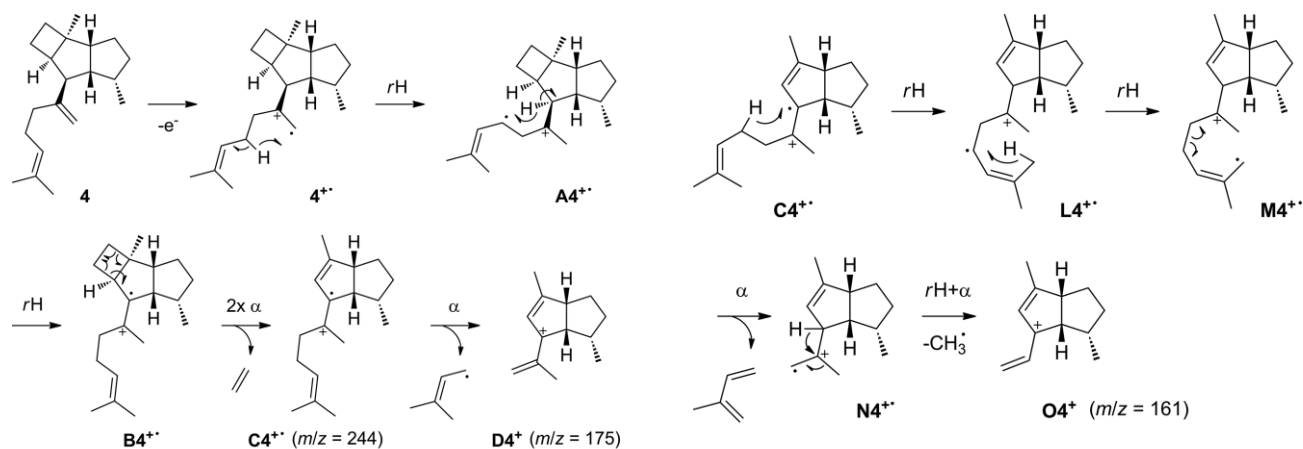
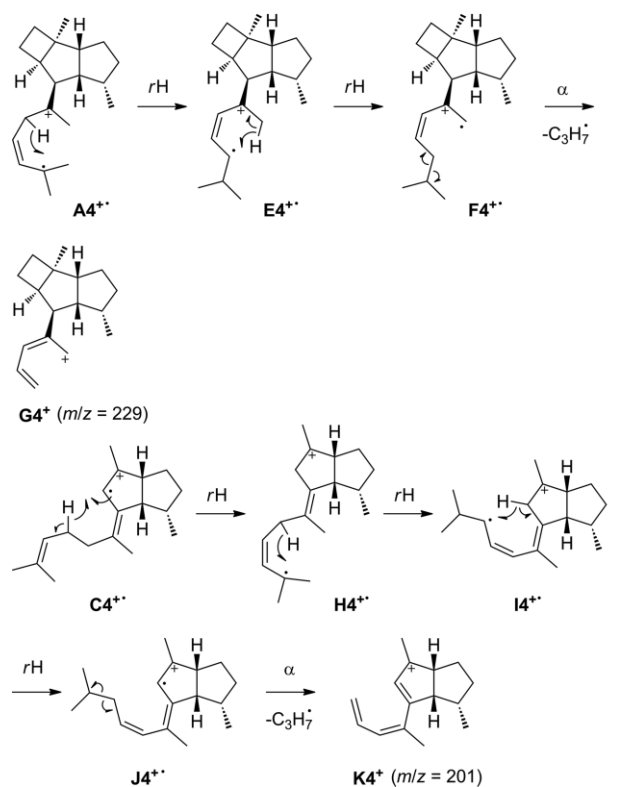


Figure 5. Position-specific mass shift analysis for  $\mathbf{4}$ . Black dots represent carbon atoms contributing to the formation of the indicated fragment ion PMA<sub>*m/z*</sub>.

As described above for  $\mathbf{3}$ , one of the main fragmentations of  $\mathbf{4}$  leads to the loss of the terminal isopropylidene group and a hydrogen from the side-chain. Essentially the same mechanism as for  $\mathbf{3}$ , that is, two hydrogen rearrangements from  $\mathbf{A4}^+$  to  $\mathbf{E4}^+$  and  $\mathbf{F4}^+$  followed by  $\alpha$  cleavage to  $\mathbf{G4}^+$  gives a satisfactory explanation. PMA<sub>201</sub> indicates a combination of both events, loss of neutral ethylene from the cyclobutane ring and of the isopropylidene group and a hydrogen from the side-chain. After the loss of ethylene in  $\mathbf{C4}^+$ , a series of hydrogen transfers results in  $\mathbf{H4}^+$ ,  $\mathbf{I4}^+$  and then  $\mathbf{J4}^+$ , which, upon  $\alpha$  cleavage, produces the conjugated heptatrienyl cation  $\mathbf{K4}^+$ . This secondary fragmentation is also indicated by MS/MS analysis of  $m/z = 244$ , whereas the reverse order of fragmentation events with first



Scheme 7. Proposed mechanisms of EI-MS fragmentations of **4** (part II).



Scheme 6. Proposed mechanisms of EI-MS fragmentations of **4** (part I).

the loss of the isopropylidene group and then the loss of ethylene is less important (note that MS/MS analysis of  $m/z = 229$  shows only a minor reaction to  $m/z = 201$ ).

PMA<sub>161</sub> reveals cleavage of ethylene from the cyclobutane ring and of the terminal C<sub>5</sub> unit and olefinic methylene group from the side-chain. This is possible from **C4<sup>•+</sup>** through two hydrogen rearrangements via **L4<sup>•+</sup>** to **M4<sup>•+</sup>** and a subsequent  $\alpha$  fragmentation with loss of neutral isoprene to **N4<sup>•+</sup>**. Another hydrogen rearrangement and  $\alpha$  fragmentation lead to the loss of the original methylene group as a methyl radical to produce **O4<sup>•+</sup>** (Scheme 7). The formation of the fragment ion  $m/z = 161$  from  $m/z = 244$  is also observed by an MS/MS experiment.

The recently described spiroalbatene synthase from *Allokutzneria albata* was used to convert the 20 (<sup>13</sup>C)GGPP isotopomers

into the corresponding singly <sup>13</sup>C-labelled spiroalbatenes (<sup>13</sup>C)-**5**.<sup>[19]</sup> Their analysis by GC-EI-MS (see Figure S9 in the Supporting Information) provided information on the origin of the fragment ions shown in Figure 6.

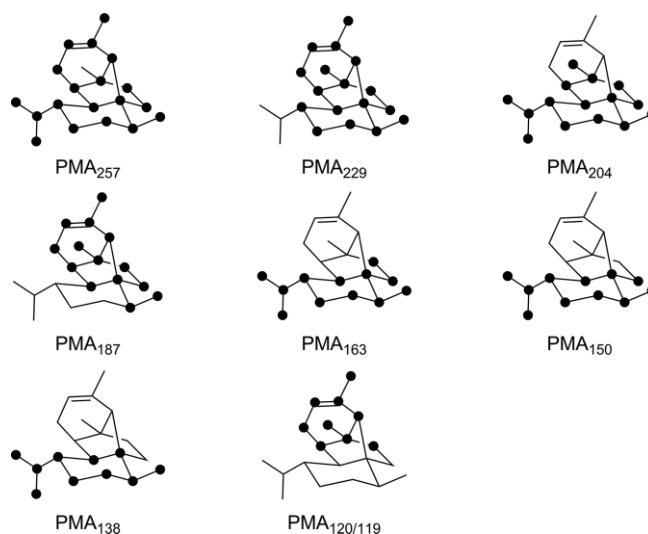
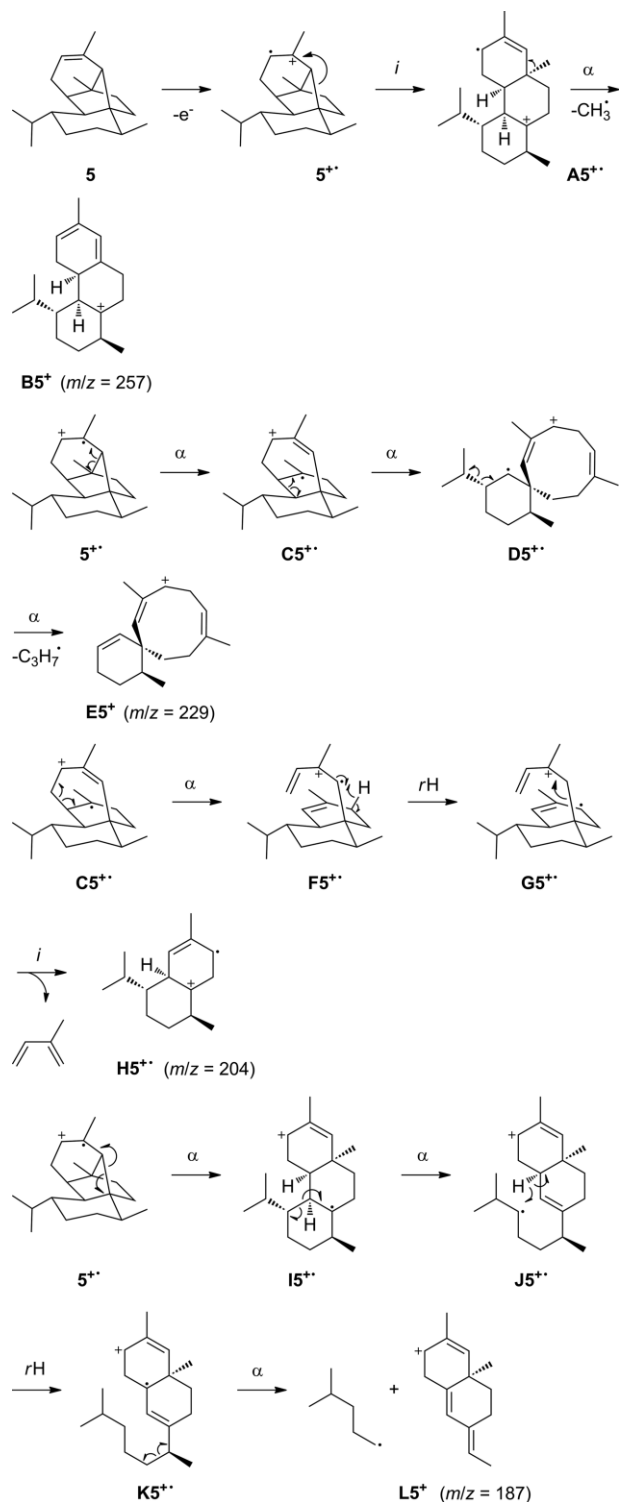


Figure 6. Position-specific mass shift analysis for **5**. Black dots represent carbon atoms contributing to the formation of the indicated fragment ion PMA <sub>$m/z$</sub> .

PMA<sub>257</sub> reveals the strongly preferred cleavage of one of the five methyl groups of **5** in the formation of the fragment ion  $m/z = 257$ . A plausible mechanism for this finding proceeds by the ionisation of **5** at the double bond to **5<sup>•+</sup>**, followed by inductive cleavage to the tricyclic radical cation **A5<sup>•+</sup>** (Scheme 8). An  $\alpha$  cleavage with loss of a methyl radical leads to **B5<sup>•+</sup>**. The fragment ion  $m/z = 229$  is formed by loss of the isopropyl group. This is explainable from **5<sup>•+</sup>** by two ring-opening reactions through  $\alpha$  fragmentations via **C5<sup>•+</sup>** to **D5<sup>•+</sup>** and a final  $\alpha$  cleavage of the isopropyl group to **E5<sup>•+</sup>**. The EI mass spectrum of **5** also shows a small fragment ion at  $m/z = 204$ , which requires the loss of neutral isoprene. PMA<sub>204</sub> demonstrates the specific extrusion of isoprene from the olefinic carbon atoms of **5** and the three neighbouring carbon atoms. A mechanistic hypothesis starts from **C5<sup>•+</sup>** and involves  $\alpha$  cleavage with ring-opening

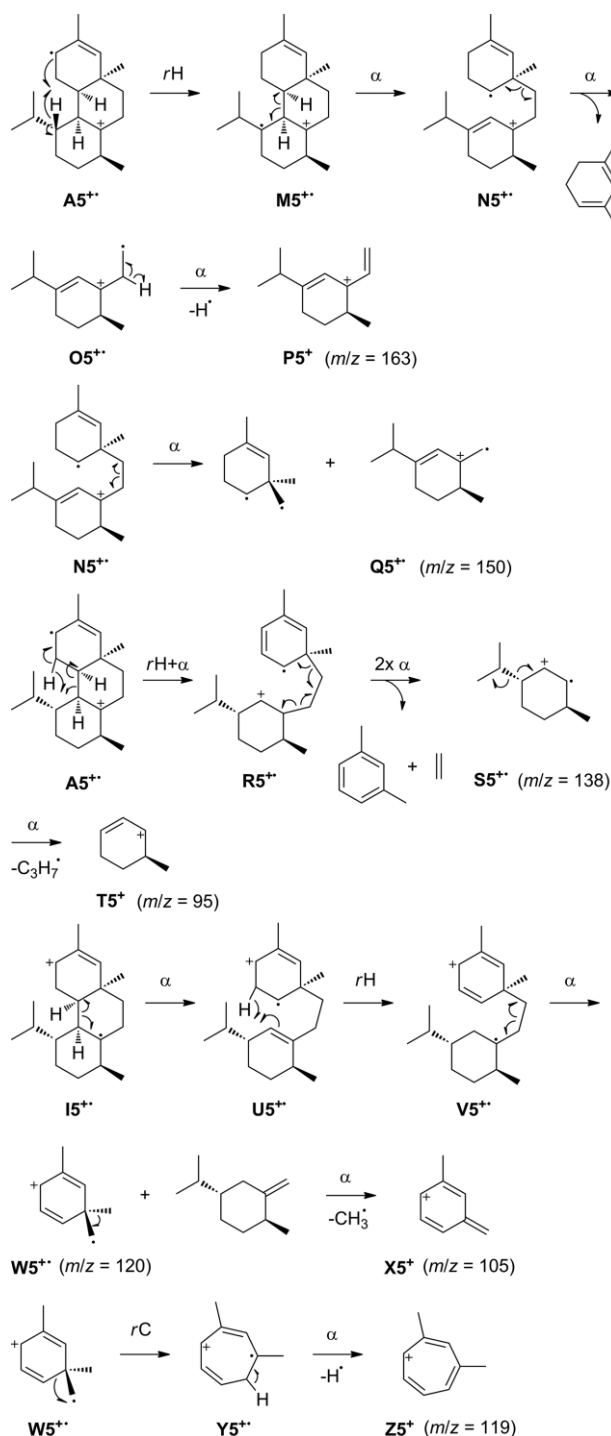
to  $F5^+$ . The loss of neutral isoprene is only possible after transfer of a hydrogen to the relevant carbon position, which can occur by hydrogen rearrangement to the allyl radical  $G5^+$ . Inductive cleavage of isoprene gives rise to  $H5^+$ . As indicated by PMA<sub>187</sub>, the fragment ion  $m/z = 187$  arises by cleavage of the isopropyl group together with a neighbouring  $C_3$  unit. This can be achieved from  $5^+$  by two sequential  $\alpha$  fragmentations via



Scheme 8. Proposed mechanisms of EI-MS fragmentations of **5** (part I).

$I5^+$  to  $J5^+$  and hydrogen rearrangement to the more stable allyl radical in  $K5^+$ . A final  $\alpha$  cleavage generates  $L5^+$ .

The fragment ion  $m/z = 163$  arises through cleavage of the six-membered ring containing the olefinic carbon atoms plus the two attached methyl groups. A plausible reaction path starts from  $A5^+$  by hydrogen transfer to  $M5^+$  (note that the participating carbons are close to each other because of the *syn* orientation of the hydrogen atoms and the methyl group at the bridgehead carbons) followed by two  $\alpha$  fragmentations



Scheme 9. Proposed mechanisms of EI-MS fragmentations of **5** (part II).

via  $\mathbf{N5}^+$  to  $\mathbf{O5}^+$  with loss of neutral 1,3-dimethylcyclohexa-1,3-diene (Scheme 9). A final loss of a hydrogen stabilises the primary radical in  $\mathbf{O5}^+$  with the formation of the conjugated pentadienyl cation in  $\mathbf{P5}^+$ . Alternatively,  $\mathbf{N5}^+$  can react by  $\alpha$  cleavage to  $\mathbf{Q5}^+$ , the structure of which is in agreement with the findings of PMA<sub>150</sub>.

The fragment ion  $m/z = 138$  represents the six-membered ring of **5** bearing the isopropyl and methyl groups. Its formation is explainable from  $\mathbf{A5}^+$  by  $\alpha$  fragmentation with concomitant hydrogen rearrangement to  $\mathbf{R5}^+$ , followed by double  $\alpha$  cleavage with the loss of neutral ethylene and *m*-xylene to  $\mathbf{S5}^+$ . This radical cation can also serve as direct precursor of  $\mathbf{T5}^+$  ( $m/z = 95$ ) by  $\alpha$  cleavage of the isopropyl group, which explains the observed efficient MS/MS fragmentation of  $m/z = 138$  to  $m/z = 95$  (see Figure S10 in the Supporting Information).

The base peak in the EI mass spectrum of **5** is observed at  $m/z = 120$  and is accompanied by the intense fragment ion  $m/z = 119$  generated from the same portion of **5**. A plausible mechanism in agreement with the findings of PMA<sub>120/119</sub> starts from  $\mathbf{I5}^+$  by  $\alpha$  fragmentation to  $\mathbf{U5}^+$  and hydrogen rearrangement to  $\mathbf{V5}^+$ . Another  $\alpha$  cleavage with loss of a neutral C<sub>11</sub> fragment to  $\mathbf{W5}^+$  and methyl group cleavage result in the *m*-xylyl cation  $\mathbf{X5}^+$ . Alternatively,  $\mathbf{W5}^+$  can react by rearrangement with ring expansion to  $\mathbf{Y5}^+$  and loss of a hydrogen to the 1,3-dimethyltropylium cation  $\mathbf{Z5}^+$ . MS/MS analysis of the fragment ion  $m/z = 120$  shows that secondary fragmentations indeed lead to both  $m/z = 119$  and 105, but methyl group cleavage is strongly preferred over the loss of hydrogen.

## Conclusions

This study has demonstrated that the introduction of single <sup>13</sup>C labels into terpenes can be used to unravel the complex mechanisms of EI-MS fragmentation reactions of these structurally often complex molecules. Ideally, for such investigations, the whole set of all possible <sup>13</sup>C<sub>1</sub> isotopomers should be made available. A total or semi-synthesis approach towards these compounds is impracticable, but if the labellings are introduced through the corresponding isotopomers of FPP and GGPP, terpene synthases can be used to provide the labelled terpenes through enzymatic synthesis. We will study further EI-MS fragmentation mechanisms of terpenes by using this approach in due course.

## Experimental Section

To record the GC-MS data, an Agilent (Santa Clara, CA, USA) 7890B GC instrument equipped with an HP5-MS fused silica capillary column (30 m, 0.25 mm i.d., 0.50  $\mu$ m film) connected to a 5977A mass detector was used. The GC parameters were 1) inlet pressure: 77.1 kPa, He at 23.3 mL min<sup>-1</sup>, 2) inlet temperature: 250 °C, 3) injection volume: 2  $\mu$ L, 4) temperature program: 5 min at 50 °C increasing at 5 °C min<sup>-1</sup> to 320 °C, 5) 60 s valve time, 6) carrier gas: He at 1.2 mL min<sup>-1</sup>. The MS parameters were 1) source: 230 °C, 2) transfer line: 250 °C, 3) quadrupole: 150 °C, 4) electron energy: 70 eV.

GC-MS/MS QToF analyses were performed with a 7890B GC instrument fitted with an HP5-MS fused silica capillary column (30 m,

0.25 mm i.d., 0.50  $\mu$ m film) connected to a 7200 accurate-mass QToF detector (Agilent). The GC parameters were 1) inlet pressure: 83.2 kPa, He at 24.6 mL min<sup>-1</sup>, 2) injection volume: 1  $\mu$ L, 3) split ratio: 50:1, 60 s valve time, 4) temperature program: 5 min at 50 °C increasing at 10 °C min<sup>-1</sup> to 320 °C, 5) carrier gas: He at 1 mL min<sup>-1</sup>. The MS parameters were 1) transfer line: 250 °C, 2) electron energy: 70 eV. The MS/MS parameters were 1) quadrupole temperature: 150 °C, 2) quadrupole mode: narrow ( $\pm 0.5$   $m/z$ ), 3) collision gas: N<sub>2</sub> at 1 mL min<sup>-1</sup>, 4) collision energy: 15 eV.

For the enzymatic preparation of all the T-muurolool <sup>13</sup>C isotopomers, the corresponding labelled diphosphates<sup>[12a]</sup> (0.5 mg) were dissolved in 25 mM NH<sub>4</sub>HCO<sub>3</sub> solution (1 mL). Binding buffer (1 mL, 20 mM Na<sub>2</sub>HPO<sub>4</sub>, 500 mM NaCl, 20 mM imidazole, 1 mM MgCl<sub>2</sub>, pH 7.4) and incubation buffer (4 mL, 50 mM Tris/HCl, 10 mM MgCl<sub>2</sub>, 20 % glycerol, pH 8.2) were added to these solutions. The reactions were started by addition of a purified (+)-T-muurolool synthase elution fraction (3 mL), prepared as described previously,<sup>[14b]</sup> and the mixtures were incubated for 4 h with shaking at 28 °C. The target terpene was extracted with C<sub>6</sub>D<sub>6</sub> (650 and 350  $\mu$ L) and the combined organic extracts were analysed by GC-MS. The preparation of labelled terpenes using tsukubadiene synthase (TdS),<sup>[12b]</sup> spatadiene synthase (SpS)<sup>[16]</sup> and spiroalbatene synthase (SaS)<sup>[19]</sup> have been described previously.

## Acknowledgments

This work was funded by the Deutsche Forschungsgemeinschaft (DFG) (DI1536/7-1) and the Fonds der Chemischen Industrie with a Ph. D. scholarship to J. R.

**Keywords:** Mass spectrometry · Reaction mechanisms · Isotopes · Terpenoids · Radical reactions

- [1] J. S. Dickschat, *Nat. Prod. Rep.* **2014**, *31*, 838–861.
- [2] F. W. McLafferty, F. Turecek, *Interpretation of Mass Spectra*, 4th ed., University Science Books, Mill Valley, CA, **1993**.
- [3] a) K. Biemann, *Angew. Chem. Int. Ed. Engl.* **1962**, *1*, 98–111; *Angew. Chem.* **1962**, *74*, 102; b) H. Budzikiewicz, J. I. Brauman, C. Djerassi, *Tetrahedron* **1965**, *21*, 1855–1879.
- [4] F. W. McLafferty, *Anal. Chem.* **1959**, *31*, 82–87.
- [5] a) R. Ryhage, E. Stenhagen, *Ark. Kemi* **1960**, *15*, 291–315; b) N. Dinh-Nguyen, R. Ryhage, S. Stallberg-Stenhagen, E. Stenhagen, *Ark. Kemi* **1961**, *18*, 393–399.
- [6] a) D. S. Weinberg, C. Djerassi, *J. Org. Chem.* **1966**, *31*, 115–119; b) J. Karliner, C. Djerassi, *J. Org. Chem.* **1966**, *31*, 1945–1956; c) R. R. Muccino, C. Djerassi, *J. Am. Chem. Soc.* **1973**, *95*, 8726–8733.
- [7] J. S. Dickschat, H. Bruns, R. Riclea, *Beilstein J. Org. Chem.* **2011**, *7*, 1697–1712.
- [8] R. Riclea, B. Aigle, P. Leblond, I. Schoenian, D. Spitteller, J. S. Dickschat, *ChemBioChem* **2012**, *13*, 1635–1644.
- [9] N. L. Brock, S. R. Ravella, S. Schulz, J. S. Dickschat, *Angew. Chem. Int. Ed.* **2013**, *52*, 2100–2104; *Angew. Chem.* **2013**, *125*, 2154.
- [10] J. S. Dickschat, *Eur. J. Org. Chem.* **2017**, 4872–4882.
- [11] a) D. Spitteller, A. Jux, J. Piel, W. Boland, *Phytochemistry* **2002**, *61*, 827–834; b) J. S. Dickschat, H. B. Bode, T. Mahmud, R. Müller, S. Schulz, *J. Org. Chem.* **2005**, *70*, 5174–5182; c) C. A. Citron, R. Riclea, N. L. Brock, J. S. Dickschat, *RSC Adv.* **2011**, *1*, 290–297; d) S. S. Shinde, A. Minami, Z. Chen, T. Tokiwano, T. Toyomasu, N. Kato, T. Sassa, H. Oikawa, *J. Antibiot.* **2017**, *70*, 632–638.
- [12] a) P. Rabe, L. Barra, J. Rinkel, R. Riclea, C. A. Citron, T. A. Klapschinski, A. Janusko, J. S. Dickschat, *Angew. Chem. Int. Ed.* **2015**, *54*, 13448–13451; *Angew. Chem.* **2015**, *127*, 13649; b) P. Rabe, J. Rinkel, E. Dolja, T. Schmitz, B. Nubbemeyer, T. H. Luu, J. S. Dickschat, *Angew. Chem. Int. Ed.* **2017**, *56*, 2776–2779; *Angew. Chem.* **2017**, *129*, 2820.



- [13] a) P. Rabe, T. A. Klapschinski, J. S. Dickschat, *ChemBioChem* **2016**, *17*, 1333–1337; b) P. Rabe, J. S. Dickschat, *Beilstein J. Org. Chem.* **2016**, *12*, 1380–1394; c) P. Rabe, J. Rinkel, B. Nubbemeyer, T. G. Köllner, F. Chen, J. S. Dickschat, *Angew. Chem. Int. Ed.* **2016**, *55*, 15420–15423; *Angew. Chem.* **2016**, *128*, 15646.
- [14] a) P. Rabe, J. S. Dickschat, *Angew. Chem. Int. Ed.* **2013**, *52*, 1810–1812; *Angew. Chem.* **2013**, *125*, 1855; b) P. Rabe, T. Schmitz, J. S. Dickschat, *Beilstein J. Org. Chem.* **2016**, *12*, 1839–1850.
- [15] a) Y. Yamada, T. Kuzuyama, M. Komatsu, K. Shin-ya, S. Omura, D. E. Cane, H. Ikeda, *Proc. Natl. Acad. Sci. USA* **2015**, *112*, 857–862; b) Y. Yamada, S. Arima, T. Nagamitsu, K. Johmoto, H. Uekusa, T. Eguchi, K. Shin-ya, D. E. Cane, H. Ikeda, *J. Antibiot.* **2015**, *68*, 385–394.
- [16] J. Rinkel, L. Lauterbach, J. S. Dickschat, *Angew. Chem. Int. Ed.* **2017**, *56*, 16385–16389; *Angew. Chem.* **2017**, *129*, 16603.
- [17] G. M. König, A. D. Wright, *J. Org. Chem.* **1997**, *62*, 3837–3840.
- [18] S. Schulz, C. Messer, K. Dettner, *Tetrahedron Lett.* **1997**, *38*, 2077–2080.
- [19] J. Rinkel, L. Lauterbach, P. Rabe, J. S. Dickschat, *Angew. Chem. Int. Ed.* **2018**, *57*, 3238–3241; *Angew. Chem.* **2018**, *130*, 3292.

---

Received: February 8, 2018



## Appendix T

### **Sesquiterpene cyclizations catalysed inside the resorcinarene capsule and application in the short synthesis of isolongifolene and isolongifolenone**

*Nat. Catal.* **2018**, *1*, 609–615.

DOI:10.1038/s41929-018-0115-4



# Sesquiterpene cyclizations catalysed inside the resorcinarene capsule and application in the short synthesis of isolongifolene and isolongifolenone

Qi Zhang<sup>1</sup>, Jan Rinkel<sup>2</sup>, Bernd Goldfuss<sup>3</sup>, Jeroen S. Dickschat<sup>2</sup> and Konrad Tiefenbacher<sup>1,4\*</sup>

Terpenes constitute the largest class of natural products and serve as an important source for medicinal treatments. Despite constant progress in chemical synthesis, the construction of complex polycyclic sesqui- and diterpene scaffolds remains challenging. However, natural cyclase enzymes are able to form the whole variety of terpene structures from just a handful of linear precursors. Man-made catalysts able to mimic such natural enzymes are lacking. Here, we describe examples of sesquiterpene cyclizations inside an enzyme-mimicking supramolecular catalyst. This strategy allowed the formation of the tricyclic sesquiterpene isolongifolene in only four steps. The mechanism of the catalysed cyclization reaction was elucidated using <sup>13</sup>C-labelling studies and density functional theory calculations.

For decades, terpene natural products have been popular target compounds for total synthesis due to their biological functions and medicinal applications<sup>1,2</sup>. The syntheses of complex polycyclic sesqui- and diterpene skeletons routinely involve long linear sequences. Although step count is only one way to evaluate a synthetic route, a long synthetic route generally suffers from two main disadvantages: (1) a large effort in manpower is required; and (2) the final yields of the natural products are usually low. For instance, in the shortest total synthesis of the sesquiterpene isolongifolene (A)<sup>3,4</sup>, six steps were required to assemble the intermediate 2 containing all necessary carbon atoms, which was converted to isolongifolene in another four steps. Similarly, in the shortest synthesis of longifolene (5)<sup>5</sup>, an initial four-step sequence smoothly introduced the majority of the required carbon atoms. However, another seven steps were required for the completion of the longifolene skeleton. In contrast, nature utilizes a fundamentally different approach to access cyclic terpenes like longifolene and isolongifolene. The simple linear substrate farnesyl pyrophosphate 6 is cyclized by an enzyme, termed terpene cyclase, to directly produce the framework of longifolene<sup>6</sup>. Longifolene is known to undergo facile acid-catalysed rearrangement to form isolongifolene<sup>7,8</sup>. A related mechanism could also be operational in natural enzymes. Isolongifolene has long been known to exist in some liverworts<sup>9</sup>, but its biosynthesis has not been elucidated yet (Fig. 1).

Fascinated by nature's elegance and high efficiency, synthetic organic chemists have strived to mimic the biosynthesis of terpene natural products. Generally, the biosynthesis of terpenes occurs via two reaction pathways, which differ in the mechanism of the substrate activation. The head-to-tail terpene<sup>10</sup> cyclization is initiated via electrophilic activation at the prenyl end (head) of the substrate, which subsequently cyclizes via a concerted mechanism. This class of cyclization has already been extensively reproduced in bulk solution and applied to total synthesis<sup>11</sup>. However, the head-to-tail terpene cyclization only produces very limited structural variety, which in the case of sesquiterpenes is limited to decalin frameworks. A much larger structural variety is produced by the

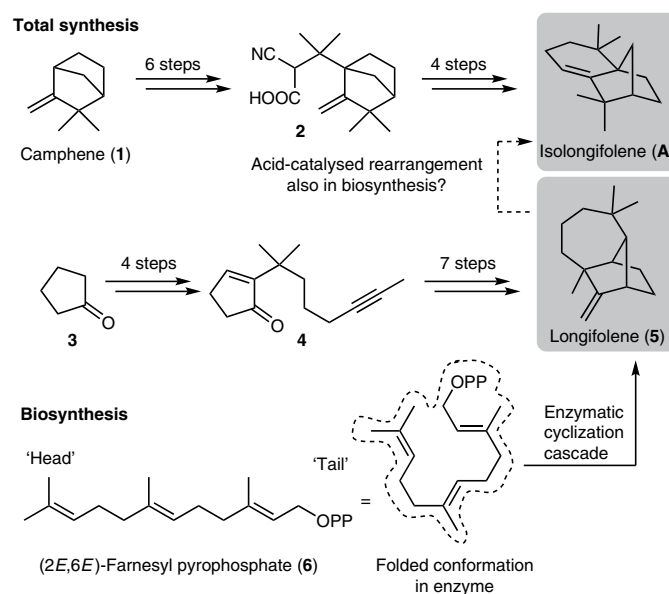


**Fig. 1 | Comparison of the total synthesis and biosynthesis<sup>6</sup> of isolongifolene<sup>3,4</sup> and longifolene<sup>5</sup>.** In the total syntheses, long synthetic sequences were required for the stepwise construction of the skeleton of isolongifolene and longifolene. In contrast, by utilizing linear farnesyl pyrophosphate as the substrate, the natural enzyme directly accessed longifolene via a cyclization–rearrangement cascade reaction. Acid-catalysed rearrangement reaction of longifolene is known to produce isolongifolene. However, the biosynthesis of isolongifolene is unknown.

so-called tail-to-head terpene<sup>10</sup> cyclization. In this cyclization type, the reaction is initiated by the formation of an allylic cation via the cleavage of the pyrophosphate group at the tail end of the acyclic terpene. Biomimetic tail-to-head terpene cyclizations employing

<sup>1</sup>Department of Chemistry, University of Basel, Basel, Switzerland. <sup>2</sup>Kekulé Institute of Organic Chemistry and Biochemistry, University of Bonn, Bonn, Germany. <sup>3</sup>Institut für Organische Chemie, Universität zu Köln, Cologne, Germany. <sup>4</sup>Department of Biosystems Science and Engineering, ETH Zürich, Basel, Switzerland. \*e-mail: [konrad.tiefenbacher@unibas.ch](mailto:konrad.tiefenbacher@unibas.ch)

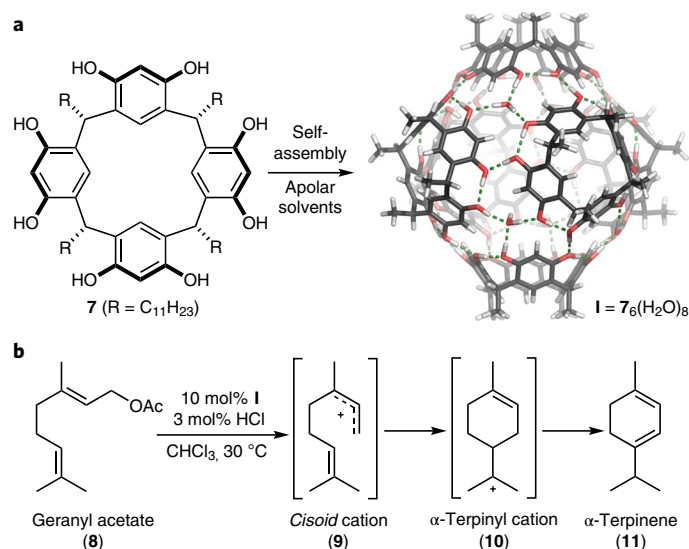


**Fig. 2 | Selective cyclization of the monoterpene geranyl acetate catalysed by the resorcinarene capsule.** **a**, The resorcinarene monomers **7** self-assemble in apolar solvents with eight water molecules to form the hexameric capsule **I** with an internal volume of 1.4 nm<sup>3</sup>. The capsule is capable of stabilizing cationic species via cation- $\pi$  interactions. **b**, The resorcinarene capsule was employed as an artificial terpene cyclase mimic for the cyclization of monoterpenes. The cyclization reactions were most likely facilitated by the stabilization of the cationic intermediates and transition states by the capsule.

man-made catalysts are challenging. There are a few literature examples describing the formation of polycyclic sesquiterpene structures in bulk solution by employing strong Brønsted or Lewis acids<sup>12–16</sup>. Such strategies rely mainly on the iterative protonation of the formed monocyclic intermediates, and are low yielding and unselective. One example of a selective sesquiterpene cyclization was reported by the Shenvi research group. Utilizing an unnaturally modified terpene precursor and stoichiometric amounts of aluminium Lewis acids, they were able to construct the highly strained funebrene skeleton<sup>10</sup>. One major obstacle in the reproduction of tail-to-head terpene cyclization using man-made catalysts is the instability of the highly reactive cationic intermediates involved in the reaction cascade, which are susceptible to exogenous nucleophiles or elimination reactions. Natural terpene cyclases circumvent this issue by enclosing the substrate within the enzymatic pocket and stabilizing key carbocations with precisely positioned aromatic residues<sup>17</sup>. Even more importantly, the uptake into the enzyme pocket facilitates the control over the substrate conformation. This conformation is then efficiently translated into the product and enables nature to produce the wide variety of structures with high fidelity. Regular Lewis or Brønsted acid catalysts inherently lack the ability to influence the flexible terpene precursor in a meaningful way. We reasoned that complex terpene cyclase enzymes may be mimicked by much simpler aromatic supramolecular capsules. Such systems were increasingly investigated as simple enzyme mimetics during the past decade<sup>18–28</sup>. The hexameric resorcinarene capsule **I**, originally disclosed by the Atwood group in 1997<sup>29</sup>, was identified by us<sup>30</sup> and the groups of Scarso and Strukul<sup>31</sup> as a supramolecular enzyme-like catalyst. Based on hydrogen bond interactions, capsule **I** self-assembles from six resorcinarene monomers **7** and eight water molecules in apolar solvents to enclose an internal volume of approximately 1.4 nm<sup>3</sup>. Importantly, capsule **I** is known to stabilize cationic guests inside its confinement via cation- $\pi$  interactions<sup>32,33</sup>. Recently, we reported that the resorcinarene capsule serves as an efficient catalyst for the tail-to-head cyclization of monoterpenes<sup>34,35</sup>. The relatively selective cyclization of geranyl acetate (**8**) to  $\alpha$ -terpinene (**11**) is noteworthy (Fig. 2). The preference for  $\alpha$ -terpinene as the sole major product relies on the full propagation of the positive charge along the reaction pathways, which is probably due to the stabilization of the cationic intermediates (for instance, **9** and **10**)

by the capsule. This preliminary result encouraged us to probe the cyclization of more complex substrates. Molecular modelling indicated that the precursor of cyclic sesquiterpenes, farnesol, easily fits the cavity of capsule **I**.

Here, we report the biomimetic tail-to-head cyclization of sesquiterpenes with **I** as the supramolecular catalyst. Using cyclization precursors related to those of natural enzymes, capsule-catalysed cyclizations enable direct access to several bicyclic and tricyclic sesquiterpene natural products. Stabilization of reaction intermediates was attributed to the encapsulation of the substrate into the cavity of the catalyst. Control on the substrate conformation was achieved by a combination of encapsulation and incorporating control elements into the substrate. In the case of the reaction of cyclofarnesyl acetate (**cycloFOAc**), the tricyclic sesquiterpene isolongifolene was formed as the single main cyclization product. This result raises new possibilities for the efficient synthesis of terpene natural products. Additionally, the mechanism of the formation of isolongifolene was elucidated by <sup>13</sup>C-labelling experiment and density functional theory (DFT) calculation.

## Results

**Cyclization of linear sesquiterpenes.** We started our investigation by testing the commercially available (*2E,6E*)-farnesol (**FOH**) under the optimized reaction conditions for monoterpene cyclizations (10 mol% **I** and 3 mol% HCl as catalysts, 33.3 mM in chloroform, 30 °C)<sup>35</sup>. According to gas chromatography analysis, complete conversion of the starting material was reached after 4 d. Subsequent analysis of the product mixture with <sup>1</sup>H and <sup>13</sup>C NMR spectroscopy (Supplementary Figs. 9 and 10) and comparison with literature data (Supplementary Tables 1 and 2) revealed the formation of polycyclic products (Fig. 3a), including 2-*epi*- $\alpha$ -cedrene (**B**),  $\alpha$ -cedrene (**C**),  $\epsilon$ -patchoulene (**D**),  $\delta$ -selinene (**E**) and 10-*epi*-zonarene (**F**).

The cyclization conditions rely on catalytic amounts of capsule **I** and HCl. To clarify whether HCl alone could activate the substrate and promote the cyclization reaction outside the capsule, a series of control experiments were performed. First, running the reaction without capsule **I** failed to effect any detectable formation of products under otherwise identical conditions. Second, the same was true when omitting the catalytic amounts of HCl. Formation of cyclic products was only detected in the presence of catalytic

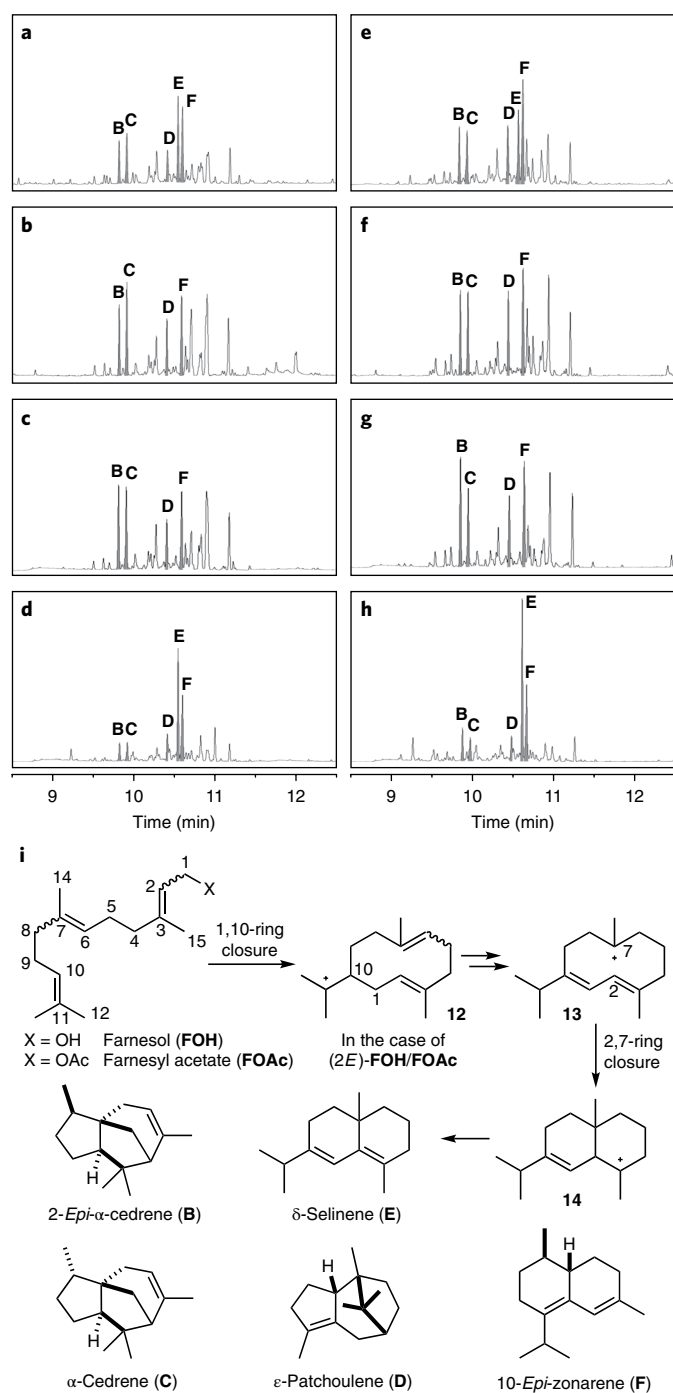


**Fig. 3 | Product analysis of the capsule-catalysed cyclization reactions of farnesyl substrates.** **a–h**, Gas chromatography traces of the cyclization reactions of (2*E*,6*E*)-FOH (**a**), (2*Z*,6*E*)-FOH (**b**), (2*Z*,6*Z*)-FOH (**c**), (2*E*,6*Z*)-FOH (**d**), (2*E*,6*E*)-FOAc (**e**), (2*Z*,6*E*)-FOAc (**f**), (2*Z*,6*Z*)-FOAc (**g**) and (2*E*,6*Z*)-FOAc (**h**) at full conversion of substrates. The intensities of the peaks in the gas chromatography traces are normalized to an internal standard (for full spectra, see Supplementary Figs. 1–8). **i**, Structures of the cyclization precursors, main cyclization products and proposed mechanism from (2*E*)-FOH/FOAc to  $\delta$ -selinene (**E**). The double bond geometry in the substrate accounts for the different product selectivities observed. The higher selectivity of the cyclization reaction of (2*E*,6*Z*)-FOAc is attributed to the conformational control of the substrate and the reaction intermediate. The farnesyl carbon framework is labelled with numbers (1–15).

amounts of capsule **I** (10 mol%) and HCl (3 mol%). Third, when the capsule was blocked with a strongly binding inhibitor (1.5 eq *n*Bu<sub>4</sub>NBr) in the presence of HCl, the cyclization products were formed only in trace amounts (<0.22%; compare Supplementary Tables 5 and 6). Additionally, <sup>1</sup>H NMR studies clearly indicated that the cyclization precursor is encapsulated to some extent, and is in slow exchange with the bulk solution (Supplementary Figs. 11 and 12). Taken together, these results provide strong evidence that the cyclization reactions indeed proceeded inside the confinement of the capsule. Furthermore, in line with our observations in the monoterpene cyclization, the reaction relies on synergistic interplay between the catalysts, capsule and HCl<sup>35</sup>.

It was demonstrated in the monoterpene cyclizations catalysed by capsule **I** that the double bond geometry of the substrate has a major influence on the product selectivity<sup>34,35</sup>. Therefore, the other double bond isomers of farnesol were synthesized according to literature procedures<sup>36</sup> and subjected to the cyclization conditions. The use of the 2*Z*-substrates did not improve product selectivity. More promiscuous product mixtures were formed in the reaction of (2*Z*,6*E*)- and (2*Z*,6*Z*)-farnesol (Fig. 3*b,c*). However, the (2*E*,6*Z*)-isomer displayed a markedly improved product selectivity (Fig. 3*d*). All four substrates were also tested with acetate as the leaving group (Fig. 3*e–h*)<sup>34,35</sup>. The most selective cyclization was achieved by employing (2*E*,6*Z*)-farnesyl acetate (FOAc) (Fig. 3*h*) as the substrate.  $\delta$ -Selinene (**E**) and 10-*epi*-zonarene (**F**) were formed as the main products in 18 and 10% yield, respectively (gas chromatography yields, corrected by internal standard and response factors; Supplementary Tables 3–5). Although the yield of  $\delta$ -selinene (18%) may appear modest at first, it is comparable to that of the natural  $\delta$ -selinene synthase (25%)<sup>37</sup>. In contrast with the monoterpene cyclization, where the variation of the leaving group dramatically changes the cyclization outcome<sup>35</sup>, the use of the acetate leaving group only slightly increased the product yields in the case of sesquiterpene cyclizations. This may indicate that the intramolecular attack of a  $\pi$ -bond on the transiently formed carbocation prevents the premature quenching of cationic intermediates by the cleaved leaving group.

The formation of  $\delta$ -selinene (**E**) is noteworthy. Mechanistically, it arises from an initial 1,10-cyclization followed by a reaction cascade<sup>37</sup> (Fig. 3*i* and Supplementary Fig. 13). The relatively useful yield (18%) of  $\delta$ -selinene in the reaction of (2*E*,6*Z*)-FOAc obviously indicates the preference for this reaction pathway (Fig. 3*h*). However, in the cyclization of (2*E*,6*E*)-FOAc (Fig. 3*e*), the selectivity for  $\delta$ -selinene is greatly attenuated. The preference for the 1,10-cyclization in the case of (2*E*,6*Z*)-FOAc probably stems from the suitable substrate conformation caused by the 6*Z* double bond. Intriguingly, the formation of  $\delta$ -selinene was not observed in the cyclization reactions of (2*Z*,6*E*)- and (2*Z*,6*Z*)-FOAc (Fig. 3*f,g*). This indicates that, with the substrates containing the 2*Z* double bond moiety, the alternative 1,6-ring closure mechanism is operational. When comparing the gas chromatography traces of all substrates, it is evident that the 1,10-cyclization path ((2*E*,6*Z*)-FOAc; Fig. 3*h*) displays higher product selectivity than the 1,6-pathway ((2*Z*,6*E*)-FOAc and (2*Z*,6*Z*)-FOAc; Fig. 3*f,g*). In the 1,10-cyclization path mechanism, a cyclodecadiene structure is formed as the first intermediate, whereas the 1,6-ring closure leads to the formation of a cyclohexene intermediate with a pendent octyl residue. It is likely that the higher strain in the cyclodecadiene intermediate limits its conformational freedom, which reduces the available reaction pathways and ultimately leads to higher selectivity.

These results demonstrate that conformational control of the substrate and intermediates is required for good selectivity in the cyclization reaction. As a long-term goal, we desire to effect this conformational control by utilizing less symmetrical supramolecular containers as the catalysts. However, for the time being, we explored an alternative way to limit the conformational

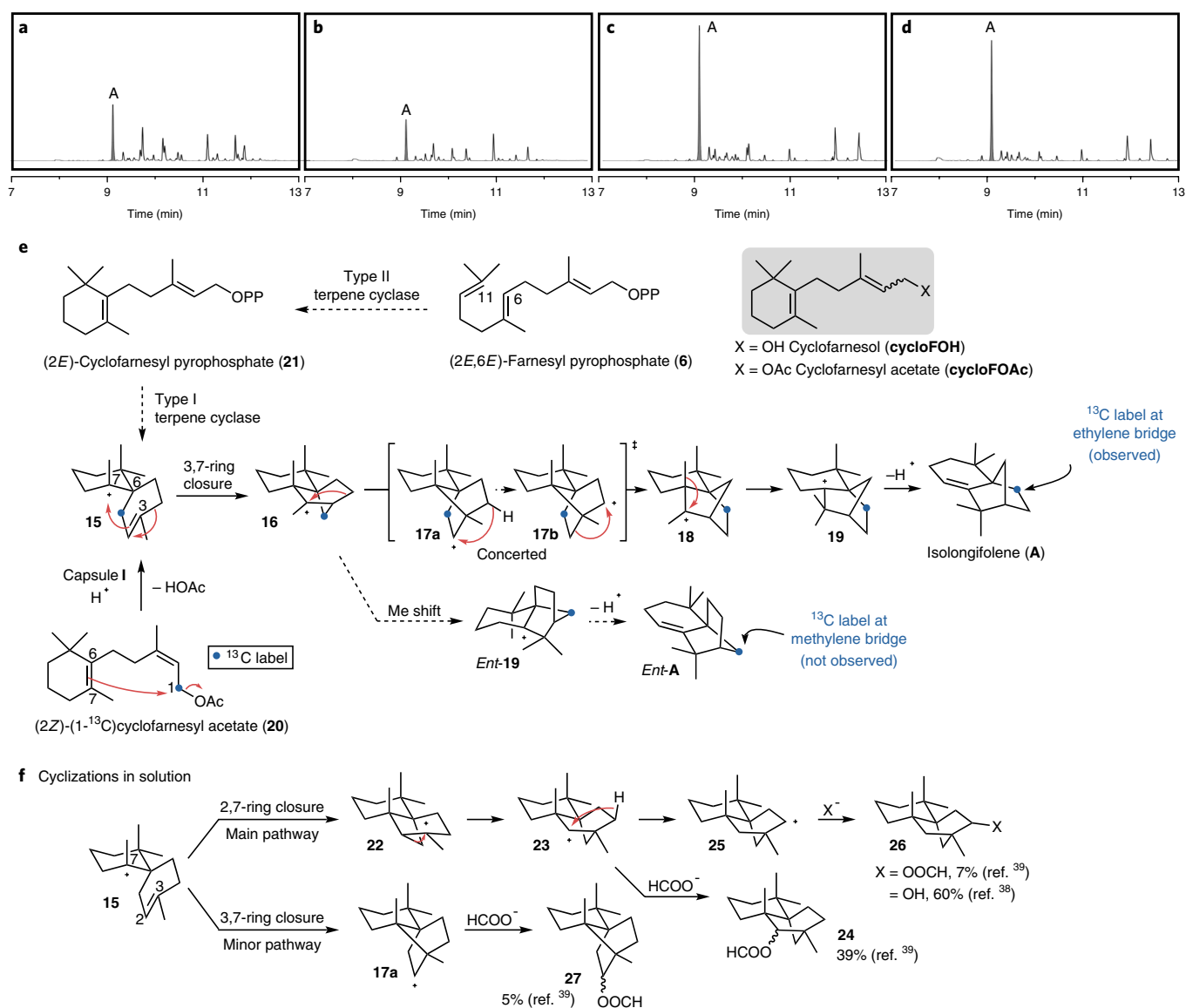


**Fig. 4 | Product analysis of the capsule-catalysed cyclization reactions of cyclofarnesyl substrates.** **a–d**, Gas chromatography traces of the cyclization reaction of (*Z*)-**cycloFOH** (**a**), (*E*)-**cycloFOH** (**b**), (*Z*)-**cycloFOAc** (**c**) and (*E*)-**cycloFOAc** (**d**) at full conversion of the substrates. The intensities of the peaks in the gas chromatography traces are normalized to an internal standard (for full spectra, see Supplementary Figs. 14–17). **e**, Proposed mechanism for the biosynthesis of isolongifolene. **f**, Literature results for the cyclization of cyclofarnesyl derivatives in solution utilizing chlorosulfonic acid or formic acid<sup>38,39</sup>.

flexibility of the substrate: incorporation of one ring into the cyclization precursor.

**Cyclization of monocyclic sesquiterpenes.** The cyclofarnesyl substrates (Fig. 4, grey box) were synthesized and investigated under the cyclization conditions. Indeed, the reactions of the cyclofarnesyl alcohols (**cycloFOH**; Fig. 4a,b) exhibited a higher degree of product selectivity than the corresponding acyclic farnesols. Moreover, the selectivity was further improved when the alcohol leaving group was replaced by an acetate moiety: a single major species was observed in the reactions of **cycloFOAc** (Fig. 4c,d). With the aid of gas chromatography-mass spectrometry analysis and NMR spectroscopy (Supplementary Figs. 18–20), the major product (gas chromatography yields of 29 and 23% starting from (*Z*)- and (*E*)-**cycloFOAc**, respectively; Supplementary Tables 7 and 8) was identified to be the tricyclic sesquiterpene isolongifolene (**A**)—a natural product that has been found in some liverworts<sup>9</sup>. Cyclizations of related

substrates have been reported in the literature using chlorosulfonic and formic acid<sup>38,39</sup>. Interestingly, the reactions in solution followed an alternative pathway (see discussion below).

**Mechanistic investigations.** The formation of isolongifolene potentially follows a mechanism related to the biosynthesis of the monoterpene camphene<sup>40</sup> (Fig. 4e). Initially, a 1,6-cyclization yields the spirocyclic intermediate **15**. In the case of (*Z*)-**cycloFOAc**, an isomerization of the allylic moiety has to occur before the cyclization. This also explains the convergence of the reactivity from the *E*- and *Z*-isomers. Intermediate **15** undergoes a 3,7-ring closure that according to DFT calculations (see below) is concerted with a Wagner–Meerwein 1,2-alkyl shift to form intermediate **16**. From cation **16**, two alternative pathways are conceivable. The first mechanism is more straightforward and involves a 1,2-methyl shift, followed by proton elimination to yield compound *ent*-**A**. Alternatively, a sequence consisting of a 1,2-alkyl shift, a



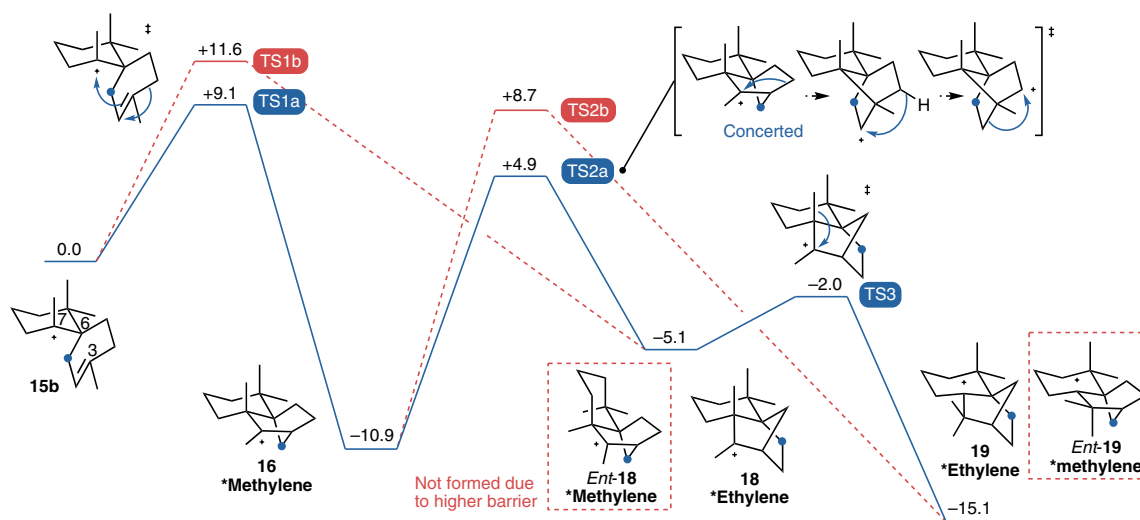


**Fig. 5 | Computed energy profile for the formation of protonated isolongifolene 19.** The reactions were calculated at the mPW1PW91/6-311 + G(d,p)//B3LYP/6-311 + G(d,p)-GD3BJ level of theory<sup>44,45,51</sup> (Supplementary Table 9 and the Supplementary Data). In accordance with the result obtained from the <sup>13</sup>C-labelling experiment, DFT calculation indicated that the reaction pathway involving the additional 1,3-hydride shift step (TS2a) is energetically favourable. Blue dots represent <sup>13</sup>C-labelled carbon atoms.

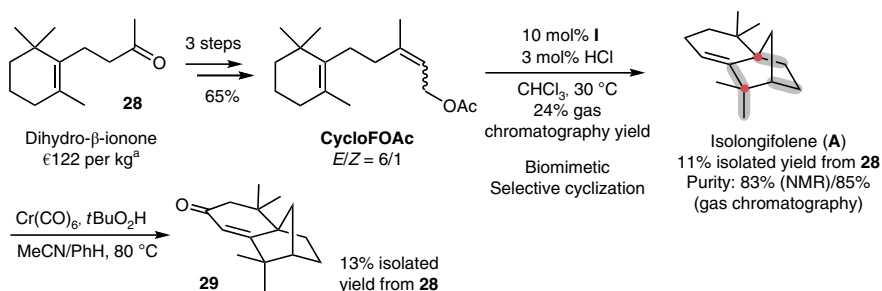


**Fig. 6 | Short synthesis of isolongifolene and isolongifolenone.** Starting from dihydro-β-ionone, isolongifolene was synthesized in a scalable four-step sequence involving capsule-catalysed tail-to-head terpene cyclization as the key step. The minor impurities contained in the isolated isolongifolene could be completely eliminated after an allylic oxidation reaction, yielding the natural product isolongifolenone as an analytically pure compound. Highlighted in grey are bonds formed/rearranged during the cascade reaction. Red dots represent quaternary carbon centers formed. <sup>a</sup>Online price quote from Sigma-Aldrich.

1,3-hydride shift and a second 1,2-alkyl shift (a concerted reaction according to DFT calculations; see below) would deliver cation **18**. Intermediate **18** would then deliver isolongifolene (**A**) via methyl shift and proton elimination. Although the second possibility initially seemed unlikely, recent experimental work on the cyclization mechanisms of the diterpenes cyclooctat-9-en-7-ol and tsukubadiene using isotopically labelled precursors resulted in the discovery of unexpected carbon backbone rearrangements<sup>41,42</sup>. This prompted us to experimentally differentiate between these two possibilities. For this purpose, the cyclization of (2*Z*)-(1-<sup>13</sup>C)cyclofarnesyl acetate (**20**), synthesized based on a known route to labelled farnesols (Supplementary Methods)<sup>13</sup>, was investigated. The more direct first mechanism would lead to the incorporation of the <sup>13</sup>C label at the methylene bridge. In contrast, the second mechanism would deliver the label at the ethylene bridge. Surprisingly, the isolongifolene formed contained the <sup>13</sup>C label exclusively on the ethylene bridge, ruling out the more direct route via *ent*-**19** (Supplementary Figs. 21–26). The reported cyclization studies of cyclofarnesyl derivatives in solution produced different products (Fig. 4f)<sup>38,39</sup>. An initial 2,7-ring closure and Wagner–Meerwein 1,2-alkyl shift produced intermediate **23**, which was either directly quenched by a nucleophile (product **24**) or underwent a 1,3-hydride

shift to form product **26**. The 3,7-ring closure pathway observed inside capsule **I** only occurred to a very small extent and, more importantly, the cation produced was immediately quenched by the nucleophile present to produce **27**. It is evident that in solution cationic intermediates are much more susceptible to quenching by the nucleophiles present. In addition, an alternative cyclization mechanism seems operational.

To learn more about the mechanism operational inside capsule **I**, DFT computations were performed (Supplementary Table 9 and Supplementary Data). The reactions depicted in Fig. 5 were calculated at the mPW1PW91/6-311 + G(d,p)//B3LYP/6-311 + G(d,p)-GD3BJ level of theory. The suitability of this computational method for carbocation rearrangements has been demonstrated before<sup>44,45</sup>. The energy barrier for the cyclization of **15** (that is, the most stable conformer **15b**) to **16** (TS1a, +9.1 kcal mol<sup>-1</sup>) is favoured by 2.5 kcal mol<sup>-1</sup> over an alternative cyclization leading to *ent*-**18** (TS1b, +11.6 kcal mol<sup>-1</sup>). Cation **16** rearranges via a concerted 1,2-alkyl/1,3-hydride/1,2-alkyl shift sequence (TS2a, +4.9 kcal mol<sup>-1</sup>) to **18**. A subsequent 1,2-Me shift (TS3, -2.0 kcal mol<sup>-1</sup>; shift of the *exo*-methyl group) rearranges **18** to the protonated isolongifolene **19**, which exhibits the <sup>13</sup>C label on its ethylene bridge. An alternative rearrangement of **16** (TS2b,

+8.7 kcal mol<sup>-1</sup>; shift of the *endo*-methyl group) yielding *ent*-**19** with a <sup>13</sup>C-labelled methylene group is prevented by a 3.8 kcal mol<sup>-1</sup> higher barrier. This 3.8 kcal mol<sup>-1</sup> higher barrier is due to the unfavourable *endo*-position of the 1,2-migrating methyl group in **16**. In contrast, **18** exhibits the 1,2-migrating methyl group in the *exo*-position, resulting in a smooth 1,2-Me rearrangement via **TS3** to produce **19** (Fig. 5).

The mechanism proposed may also be of relevance for the biosynthesis of isolongifolene. The acid-catalysed rearrangement of the sesquiterpene natural product longifolene is known to generate isolongifolene as the major product<sup>8</sup>. In principle, such a rearrangement could account for the biosynthetic origin of isolongifolene. The selective conversion of cyclofarnesyl acetate to isolongifolene catalysed by capsule **I** raises another mechanistic possibility, which involves cyclofarnesyl pyrophosphate **21** as the key intermediate (see Fig. 4e). Although **21** has not yet been described as naturally occurring, the cyclofarnesyl formate ester is a known natural product<sup>46</sup>. A type II terpene cyclase<sup>47</sup> may convert farnesyl pyrophosphate **6** to **21** via protonation on the distal double bond and nucleophilic attack of the internal double bond on the C11 position, followed by deprotonation at C6. Subsequently, the monocyclic intermediate **21** would be converted inside a type I terpene cyclase<sup>47</sup> in analogy to the reaction observed in capsule **I**. Such a synergistic operation of type I and type II terpene cyclase enzymes is known, for instance, in the biosynthesis of the diterpene natural product abietadiene and other labdane-related diterpenes<sup>17,48</sup>.

**Application in total synthesis.** The selective cyclization of cyclofarnesyl acetates also enables the shortest total synthesis of isolongifolene to date (Fig. 6). Starting from the inexpensive bulk chemical dihydro- $\beta$ -ionone (**28**), **cycloFOAc** was synthesized in a scalable three-step sequence. The capsule-catalysed cyclization of **cycloFOAc** serves as the key step, which allows the formation/rearrangement of four C–C bonds (highlighted in grey in Fig. 6) and the construction of two quaternary carbon centres (highlighted by red dots) in one step. In total, racemic isolongifolene was synthesized in 11% overall yield (83% NMR purity; 85% gas chromatography purity; Supplementary Figs. 27–30). This sequence provides isolongifolene (**A**) in only four steps and in preparatively useful yields (previously reported total syntheses: 10–19 steps)<sup>3,49</sup>. Although the isolongifolene obtained by separation using regular column chromatography is not analytically pure, it can serve as readily available material for further functionalization. Allylic oxidation of isolongifolene to the natural product isolongifolone (**29**)<sup>50</sup> facilitated the isolation as a pure compound. It was obtained in 13% isolated yield from **28** (Supplementary Fig. 31).

## Conclusion

We report examples of a selective tail-to-head sesquiterpene cyclization catalysed by an artificial enzyme mimic. In nature, the control over the conformation of farnesyl pyrophosphate is known to be a critical determinant for the ultimate product specificity<sup>17</sup>. In this study, this was achieved by a combination of encapsulating the substrate into the confined molecular capsule and incorporating control elements (*Z*-double bond and cyclohexene ring) into the substrate structure. The capsule-catalysed cyclization reactions may serve as a promising tool for the efficient construction of complex terpene natural products in the future. As a first proof of principle, a four-step synthesis of the complex tricyclic sesquiterpene natural product isolongifolene was achieved using biomimetic tail-to-head terpene cyclization as the key step. The mechanism of the cyclization and rearrangement cascade was elucidated through <sup>13</sup>C labelling experiments and DFT calculations. The proposed mechanism indicated that cyclofarnesyl pyrophosphate could potentially serve as a key intermediate in the biosynthesis of isolongifolene. In the future, we aim at achieving more efficient control of the substrate

conformation inside supramolecular capsules by tailoring the cavity shape. To this end, efforts will be devoted to modification of the present system or developing new catalysts, which are better suited to influencing the conformation of the bound substrate.

## Methods

**General procedure for the cyclization reaction.** Chloroform was filtered through basic aluminium oxide before use. To a solution of the resorcinarene capsule **I** (11.1 mg, 1.67  $\mu$ mol, 0.10 eq) in chloroform (200  $\mu$ l), we added, successively, HCl stock solution in chloroform (0.50  $\mu$ mol, 0.03 eq) and *n*-decane stock solution in chloroform (20  $\mu$ l, 167 mmol<sup>-1</sup>, 3.34  $\mu$ mol, 0.2 eq). Then, additional chloroform was added to reach a total volume of 500  $\mu$ l for the reaction mixture. After substrate (16.7  $\mu$ mol, 1.00 eq) was added, the reaction mixture was briefly agitated. An aliquot (approximately 10  $\mu$ l) of the reaction mixture was diluted with 0.2 ml *n*-hexane and subjected to gas chromatography analysis (initial sample). Meanwhile, the reaction was kept at 30 °C. After the indicated time, the reactions were sampled as described above and analysed by gas chromatography. Conversions and yields were calculated as described in our previous work<sup>34</sup>.

**Preparation and titration of HCl-concentrated chloroform solution.** HCl-concentrated chloroform solution was prepared by passing HCl gas (prepared by the dropwise addition of concentrated H<sub>2</sub>SO<sub>4</sub> to dry NaCl) through chloroform for around 30 min. The concentration of HCl in chloroform was determined as follows: to a solution of phenol red in EtOH (0.002 wt%, 2.5 ml), we added HCl-saturated chloroform (100  $\mu$ l) via a Microman M1 pipette equipped with plastic tips. Upon addition, the solution turned from yellow (neutral) to pink (acidic). The resulting solution was then titrated with 0.1 M ethanolic solution of triethylamine (NEt<sub>3</sub>). At the equivalence point, the solution turned from pink to yellow.

**Computational method.** Computed energies and cartesian coordinates of the optimized intermediates and transition states can be found in Supplementary Table 9 and the Supplementary Data, respectively. Localization of stationary points and their characterization as minima (no imaginary frequency) or transition structures (one imaginary frequency) was performed using Gaussian 16 (A.03)<sup>51</sup> with the B3LYP/6-311 + G(d,p)<sup>52</sup> method including Grimme's dispersion with Becke–Johnson damping<sup>53</sup>. For all localized species, mPW1PW91/6-311 + G(d,p)//B3LYP/6-311 + G(d,p)-GD3BJ<sup>54</sup> single-point computations provided electronic energies. The suitability of mPW1PW91//B3LYP computations for carbocation rearrangements was demonstrated recently<sup>44,45</sup>. Intrinsic reaction coordinate computations were performed for all transition structures to verify correct interconnections with their related reactants and products.

**Data availability.** The authors declare that the main data supporting the findings of this study are available within the article and its Supplementary Information files. The data that support the plots within the paper and other findings of this study are available from the corresponding author upon reasonable request.

Received: 6 February 2018; Accepted: 20 June 2018;  
Published online: 30 July 2018

## References

- Maimone, T. J. & Baran, P. S. Modern synthetic efforts toward biologically active terpenes. *Nat. Chem. Biol.* **3**, 396–407 (2007).
- Urabe, D., Asaba, T. & Inoue, M. Convergent strategies in total syntheses of complex terpenoids. *Chem. Rev.* **115**, 9207–9231 (2015).
- Sobti, R. R. & Dev, S. Synthesis of ( $\pm$ )-isolongifolene. *Tetrahedron Lett.* **8**, 2893–2895 (1967).
- Sobti, R. R. & Dev, S. Studies in sesquiterpenes—XLIII: isolongifolene (part 4): synthesis. *Tetrahedron* **26**, 649–655 (1970).
- Volkman, R. A., Andrews, G. C. & Johnson, W. S. Novel synthesis of longifolene. *J. Am. Chem. Soc.* **97**, 4777–4779 (1975).
- Arigoni, D. Stereochemical aspects of sesquiterpene biosynthesis. *Pure Appl. Chem.* **41**, 219–245 (1975).
- Berson, J. A. et al. Chemistry of methylbornyl cations. VI. The stereochemistry of vicinal hydride shift. Evidence for the nonclassical structure of 3-methyl-2-norbornyl cations. *J. Am. Chem. Soc.* **89**, 2590–2600 (1967).
- Yadav, J. S., Nayak, U. R. & Dev, S. Studies in sesquiterpenes—LV: isolongifolene(part 6): mechanism of rearrangement of longifolene to isolongifolene-I. *Tetrahedron* **36**, 309–315 (1980).
- Svensson, L. & Bendz, G. Essential oils from some liverworts. *Phytochemistry* **11**, 1172–1173 (1972).
- Pronin, S. V. & Shenvi, R. A. Synthesis of highly strained terpenes by non-stop tail-to-head polycyclization. *Nat. Chem.* **4**, 915–920 (2012).
- Yoder, R. A. & Johnston, J. N. A case study in biomimetic total synthesis: polyolefin carbocyclizations to terpenes and steroids. *Chem. Rev.* **105**, 4730–4756 (2005).

12. Ohta, Y. & Hirose, Y. Electrophile induced cyclization of farnesol. *Chem. Lett.* **1**, 263–266 (1972).
13. Andersen, N. H. & Syrdal, D. D. Chemical simulation of the biogenesis of cedrene. *Tetrahedron Lett.* **13**, 2455–2458 (1972).
14. Polovinka, M. P. et al. Cyclization and rearrangements of farnesol and nerolidol stereoisomers in superacids. *J. Org. Chem.* **59**, 1509–1517 (1994).
15. Gutsche, C. D., Maycock, J. R. & Chang, C. T. Acid-catalyzed cyclization of farnesol and nerolidol. *Tetrahedron* **24**, 859–876 (1968).
16. Susumu, K., Mikio, T. & Teruaki, M. Biogenetic-like cyclization of farnesol and nerolidol to bisabolene by the use of 2-fluorobenzothiazolium salt. *Chem. Lett.* **6**, 1169–1172 (1977).
17. Christianson, D. W. Structural biology and chemistry of the terpenoid cyclases. *Chem. Rev.* **106**, 3412–3442 (2006).
18. Pluth, M. D., Bergman, R. G. & Raymond, K. N. Proton-mediated chemistry and catalysis in a self-assembled supramolecular host. *Acc. Chem. Res.* **42**, 1650–1659 (2009).
19. Yoshizawa, M. & Fujita, M. Development of unique chemical phenomena within nanometer-sized, self-assembled coordination hosts. *Bull. Chem. Soc. Jpn.* **83**, 609–618 (2010).
20. Ronson, T. K., Zarra, S., Black, S. P. & Nitschke, J. R. Metal–organic container molecules through subcomponent self-assembly. *Chem. Commun.* **49**, 2476–2490 (2013).
21. Han, M., Engelhard, D. M. & Clever, G. H. Self-assembled coordination cages based on banana-shaped ligands. *Chem. Soc. Rev.* **43**, 1848–1860 (2014).
22. Zhang, G. & Mastalerz, M. Organic cage compounds—from shape-persistence to function. *Chem. Soc. Rev.* **43**, 1934–1947 (2014).
23. Leenders, S. H. A. M., Gramage-Doria, R., de Bruin, B. & Reek, J. N. H. Transition metal catalysis in confined spaces. *Chem. Soc. Rev.* **44**, 433–448 (2015).
24. Hof, F., Craig, S. L., Nuckolls, C. & Rebek, J. J. Molecular encapsulation. *Angew. Chem. Int. Ed.* **41**, 1488–1508 (2002).
25. Rebek, J. Molecular behavior in small spaces. *Acc. Chem. Res.* **42**, 1660–1668 (2009).
26. Ajami, D. & Rebek, J. More chemistry in small spaces. *Acc. Chem. Res.* **46**, 990–999 (2012).
27. Ajami, D., Liu, L. & Rebek, J. Jr Soft templates in encapsulation complexes. *Chem. Soc. Rev.* **44**, 490–499 (2015).
28. Jordan, J. H. & Gibb, B. C. Molecular containers assembled through the hydrophobic effect. *Chem. Soc. Rev.* **44**, 547–585 (2014).
29. MacGillivray, L. R. & Atwood, J. L. A chiral spherical molecular assembly held together by 60 hydrogen bonds. *Nature* **389**, 469–472 (1997).
30. Zhang, Q. & Tiefenbacher, K. Hexameric resorcinarene capsule is a Brønsted acid: investigation and application to synthesis and catalysis. *J. Am. Chem. Soc.* **135**, 16213–16219 (2013).
31. Bianchini, G., La Sorella, G., Canever, N., Scarso, A. & Strukul, G. Efficient isonitrile hydration through encapsulation within a hexameric self-assembled capsule and selective inhibition by a photo-controllable competitive guest. *Chem. Commun.* **49**, 5322–5324 (2013).
32. Shivanyuk, A. & Rebek, J. Reversible encapsulation by self-assembling resorcinarene subunits. *Proc. Natl Acad. Sci. USA* **98**, 7662–7665 (2001).
33. Avram, L. & Cohen, Y. Spontaneous formation of hexameric resorcinarene capsule in chloroform solution as detected by diffusion NMR. *J. Am. Chem. Soc.* **124**, 15148–15149 (2002).
34. Zhang, Q. & Tiefenbacher, K. Terpene cyclization catalysed inside a self-assembled cavity. *Nat. Chem.* **7**, 197–202 (2015).
35. Zhang, Q., Catti, L., Pleiss, J. & Tiefenbacher, K. Terpene cyclizations inside a supramolecular catalyst: leaving-group-controlled product selectivity and mechanistic studies. *J. Am. Chem. Soc.* **139**, 11482–11492 (2017).
36. Snyder, S. A., Treitler, D. S. & Brucks, A. P. Simple reagents for direct halonium-induced polyene cyclizations. *J. Am. Chem. Soc.* **132**, 14303–14314 (2010).
37. Steele, C. L., Crock, J., Bohlmann, J. & Croteau, R. Sesquiterpene syntheses from grand fir (*Abies grandis*): comparison of constitutive and wound-induced activities, and cDNA isolation, characterization, and bacterial expression of  $\delta$ -selinene synthase and  $\gamma$ -humulene synthase. *J. Biol. Chem.* **273**, 2078–2089 (1998).
38. Tanimoto, H., Kiyota, H., Oritani, T. & Matsumoto, K. Stereochemistry of a unique tricyclic compound prepared by superacid-catalyzed cyclization. *Synlett* **1**, 121–122 (1997).
39. Fräter, G., Müller, U. & Kraft, P. Synthesis of tricyclic ketones with sesquiterpene skeletons by acid-catalyzed rearrangement of  $\beta$ -monocyclofarnesol. *Helv. Chim. Acta* **82**, 522–530 (1999).
40. Croteau, R., Satterwhite, D. M., Cane, D. E. & Chang, C. C. Biosynthesis of monoterpenes. Enantioselectivity in the enzymatic cyclization of (+)- and (–)-linalyl pyrophosphate to (+)- and (–)-pinene and (+)- and (–)-camphene. *J. Biol. Chem.* **263**, 10063–10071 (1988).
41. Meguro, A. et al. An unusual terpene cyclization mechanism involving a carbon–carbon bond rearrangement. *Angew. Chem. Int. Ed.* **54**, 4353–4356 (2015).
42. Rabe, P. et al. Mechanistic investigations of two bacterial diterpene cyclases: spiroviolene synthase and tsukubadiene synthase. *Angew. Chem. Int. Ed.* **56**, 2776–2779 (2017).
43. Rabe, P. et al. Conformational analysis, thermal rearrangement, and EI-MS fragmentation mechanism of (1(10)*E*,4*E*,6*S*,7*R*)-germacradien-6-ol by <sup>13</sup>C-labeling experiments. *Angew. Chem. Int. Ed.* **54**, 13448–13451 (2015).
44. Matsuda, S. P. T., Wilson, W. K. & Xiong, Q. Mechanistic insights into triterpene synthesis from quantum mechanical calculations. Detection of systematic errors in B3LYP cyclization energies. *Org. Biomol. Chem.* **4**, 530–543 (2006).
45. Tantillo, D. J. Biosynthesis via carbocations: theoretical studies on terpene formation. *Nat. Prod. Rep.* **28**, 1035–1053 (2011).
46. Shimomura, O. & Johnson, F. H. The structure of *Latia* luciferin. *Biochemistry* **7**, 1734–1738 (1968).
47. Wendt, K. U. & Schulz, G. E. Isoprenoid biosynthesis: manifold chemistry catalyzed by similar enzymes. *Structure* **6**, 127–133 (1998).
48. Peters, R. J. Two rings in them all: the labdane-related diterpenoids. *Nat. Prod. Rep.* **27**, 1521–1530 (2010).
49. Ghosal, M., Kapha, T. K., Pal, S. K. & Mukherjee, D. Facile synthesis of ( $\pm$ )-isolongifolene and ( $\pm$ )-isolongifolenedione involving Ar<sub>1</sub>-5 cyclisations. *Tetrahedron Lett.* **36**, 2527–2528 (1995).
50. Zhang, A., Klun, J. A., Wang, S., Carroll, J. F. & Debboun, M. Isolongifolone: a novel sesquiterpene repellent of ticks and mosquitoes. *J. Med. Entomol.* **46**, 100–106 (2009).
51. Frisch, M. J. et al. *Gaussian 16*. Rev. A.03 (2016).
52. Becke, A. D. Density-functional thermochemistry. III. The role of exact exchange. *J. Chem. Phys.* **98**, 5648–5652 (1993).
53. Grimme, S., Ehrlich, S. & Goerigk, L. Effect of the damping function in dispersion corrected density functional theory. *J. Comput. Chem.* **32**, 1456–1465 (2011).
54. Adamo, C. & Barone, V. Exchange functionals with improved long-range behavior and adiabatic connection methods without adjustable parameters: the mPW and mPW1PW models. *J. Chem. Phys.* **108**, 664–675 (1998).

## Acknowledgements

This work was supported by funding from the European Research Council Horizon 2020 Programme (ERC Starting Grant 714620-TERPENECAT), Swiss National Science Foundation (as part of the NCCR Molecular Systems Engineering) and Bayerische Akademie der Wissenschaften (Junges Kolleg). We thank the computing center of the University of Cologne (RRZK) for providing CPU time on the DFG-funded supercomputer CHEOPS.

## Author contributions

K.T. conceived and supervised the project. K.T. and Q.Z. planned the project. Q.Z. carried out all the experiments except the synthesis of <sup>13</sup>C-labelled substrates, which were synthesized by J.R. J.S.D. conceived the investigations concerning the <sup>13</sup>C-labelled substrates. The <sup>13</sup>C-labelled products were analysed by J.S.D. and J.R., who elucidated the proposed mechanism for the formation of isolongifolene. B.G. performed the DFT calculations. Q.Z. and K.T. compiled the first draft of the manuscript. All authors contributed to the final version of the manuscript.

## Competing interests

The authors declare no competing interests.

## Additional information

Supplementary information is available for this paper at <https://doi.org/10.1038/s41929-018-0115-4>.

Reprints and permissions information is available at [www.nature.com/reprints](http://www.nature.com/reprints).

Correspondence and requests for materials should be addressed to K.T.

**Publisher's note:** Springer Nature remains neutral with regard to jurisdictional claims in published maps and institutional affiliations.



## Appendix U

### **Volatiles from the hypoxylaceous fungi *Hypoxylon griseobrunneum* and *Hypoxylon macrocarpum***

*Beilstein J. Org. Chem.* **2018**, *14*, 2974–2990.

DOI:10.3762/bjoc.14.277





# Volatiles from the hypoxylaceous fungi *Hypoxylon griseobrunneum* and *Hypoxylon macrocarpum*

Jan Rinkel<sup>1</sup>, Alexander Babczyk<sup>1</sup>, Tao Wang<sup>1</sup>, Marc Stadler<sup>2</sup> and Jeroen S. Dickschat<sup>\*1</sup>

## Full Research Paper

Open Access

### Address:

<sup>1</sup>Kekulé-Institut für Organische Chemie, Universität Bonn, Gerhard-Domagk-Straße 1, 53121 Bonn, Germany and <sup>2</sup>Abteilung Mikrobielle Wirkstoffe, Helmholtz-Zentrum für Infektionsforschung, Inhoffenstraße 7, 38124 Braunschweig, Germany

### Email:

Jeroen S. Dickschat\* - dickschat@uni-bonn.de

\* Corresponding author

### Keywords:

constitutional isomerism; gas chromatography; mass spectrometry; natural products; volatiles

*Beilstein J. Org. Chem.* **2018**, *14*, 2974–2990.  
doi:10.3762/bjoc.14.277

Received: 17 October 2018

Accepted: 22 November 2018

Published: 04 December 2018

Associate Editor: A. Kirschning

© 2018 Rinkel et al.; licensee Beilstein-Institut.  
License and terms: see end of document.

## Abstract

The volatiles emitted by the ascomycetes *Hypoxylon griseobrunneum* and *Hypoxylon macrocarpum* (Hypoxylaceae, Xylariales) were collected by use of a closed-loop stripping apparatus (CLSA) and analysed by GC–MS. The main compound class of both species were polysubstituted benzene derivatives. Their structures could only be unambiguously determined by comparison to all isomers with different substitution patterns. The substitution pattern of the main compound from *H. griseobrunneum*, the new natural product 2,4,5-trimethylanisole, was explainable by a polyketide biosynthesis mechanism that was supported by a feeding experiment with (*methyl*-<sup>2</sup>H<sub>3</sub>)methionine.

## Introduction

Fungi release a large number of different volatiles that belong to all kinds of natural product classes [1]. Many of these compounds are of interest, because they are markers for the production of fungal toxins and thus can help to distinguish between toxigenic and closely related non-toxigenic species. For example, the sesquiterpene trichodiene (**1**, Figure 1) is the precursor of the trichothecene family of mycotoxins [2], a class of highly bioactive secondary metabolites that belong to the strongest known inhibitors of protein biosynthesis in eukaryotes [3]. Similarly, the sesquiterpene aristolochene (**2**) is the parent hydrocarbon of PR toxin [4,5] and has been used as a marker to

differentiate between toxin producing and non-producing *Penicillium roqueforti* isolates [6]. On the other hand, fungal volatiles are interesting, because they contribute with their aroma to the flavour of many edible mushrooms. One of the first identified and certainly most widespread compounds is matsutake alcohol, (*R*)-oct-1-en-3-ol (**3**), that is produced inter alia by *Tricholoma matsutake* [7], a highly sought delicacy in the Japanese cuisine, the bottom mushroom *Agaricus bisporus*, and the penny bun *Boletus edulis* [8], as the name indicates a European equivalent to Matsutake in high-class cooking. Volatile organic compounds are also important in the interaction be-

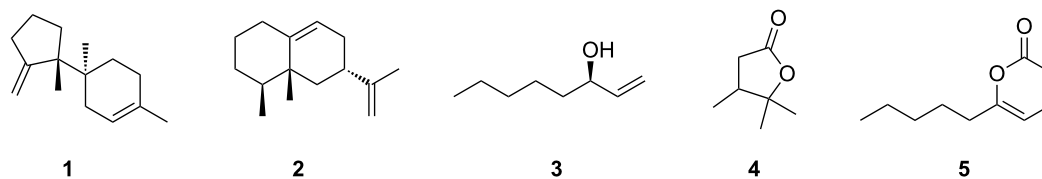


**Figure 1:** Structures of fungal volatiles. Trichodiene (1), aristolochene (2), (*R*)-oct-1-en-3-ol (3), 3,4-dimethylpentan-4-olide (4), and 6-pentyl-2H-pyran-2-one (5).

tween different species, e.g., between ophiostomatoid fungi and conifer bark beetles that show different behavioural responses to fungal volatiles [9]. Fungal volatiles can also be of importance in the interaction between plants and fungi. In some cases, fungal volatiles seem to be involved in the plant pathogenicity of fungi, as recently observed for 3,4-dimethylpentan-4-olide (4), a volatile from the ash pathogen *Hymenoscyphus fraxineus* that currently threatens the European ash population [10]. Both enantiomers of this lactone were found to inhibit ash seed germination and to cause necrotic lesions in the plant tissue. In other cases, fungal volatiles can have beneficial effects and may even be involved in the induction of systemic resistance in plants, as can be assumed for 6-pentyl-2H-pyran-2-one (5) that is produced by many fungi from the genus *Trichoderma* [11,12].

Fungal volatiles can be efficiently analysed by trapping, e.g., on charcoal filters with a closed-loop stripping apparatus (CLSA) that was developed by Grob and Zürcher [13], followed by filter extraction and GC–MS analysis of the obtained headspace extracts [14]. The unambiguous compound identification requires a good match of the recorded electron impact (EI) mass spectrum to a database spectrum and of the retention index, a standardised GC retention factor that is calculated from the retention times of the analytes and of *n*-alkanes [15], in comparison to an authentic standard or published data. A peculiar problem in the analysis of aromatic compounds with multiple substituents is that constitutional isomers with the same types of substituents, but different substitution patterns often have very similar mass spectra. Furthermore, some of the isomers may also have similar retention indices, and therefore it is mandatory for unambiguous structure elucidation to compare analytes that fall into this class to all the possible isomers. A similar problem can apply to the structural assignment of compounds with multiple stereocentres based on GC–MS data, because the various possible diastereomers usually also produce very similar mass spectra [16], a phenomenon that is also reported for *E* and *Z* stereoisomers and can lead to wrong structural assignments, if no authentic standards are used for comparison [17]. We have recently reported on two chlorinated aromatic compounds from an endophytic *Geniculosporium* sp. [18] and on a

series of structurally related phenols, benzaldehydes and anisole derivatives from *Hypoxylon invadens* [19] that could only be identified with certainty following this approach of extensive compound comparisons. Members of the family Hypoxylaceae are regarded to be extremely rich in secondary metabolites [20], but not much is known about volatiles from these fungi [21]. In continuation of this work, here we present the volatiles emitted by *Hypoxylon griseobrunneum* MUCL 53754 and *Hypoxylon macrocarpum* STMA 130423. These strains were selected, because both species released a characteristic and strong odour, as was already mentioned in the literature for *H. macrocarpum* [22,23], but the nature of the odoriferous compounds remained unknown. As will be shown, the bouquets of both species are composed mainly of highly substituted aromatic compounds whose structures were only securely identifiable by comparison to all the possible constitutional isomers with different ring substitution patterns.

## Results and Discussion

### Headspace analysis

The volatiles released by agar plate cultures of *H. griseobrunneum* and *H. macrocarpum* were collected using a CLSA [13]. After a collection time of one day the charcoal filter traps were removed and extracted with CH<sub>2</sub>Cl<sub>2</sub>, followed by GC–MS analysis of the obtained extracts. For both strains a large number of compounds from different compound classes including alcohols, ketones, esters, terpenes and pyrazines were identified. Besides the observed minor production of compounds from these classes aromatic compounds dominated, but the patterns were strain-specific.

### Identification of volatiles from *Hypoxylon griseobrunneum*

A representative total ion chromatogram for the volatiles released by *Hypoxylon griseobrunneum* is shown in Figure 2 and the results of the analysis are compiled in Table 1. Several compounds in the headspace extract were readily identified from their mass spectra and retention indices, including the widespread alcohol 2-methylbutan-1-ol (6) as one of the main compounds and traces of the corresponding acetate ester 7 (Table 1 and Figure 3). Small amounts of matsutake alcohol (3) were



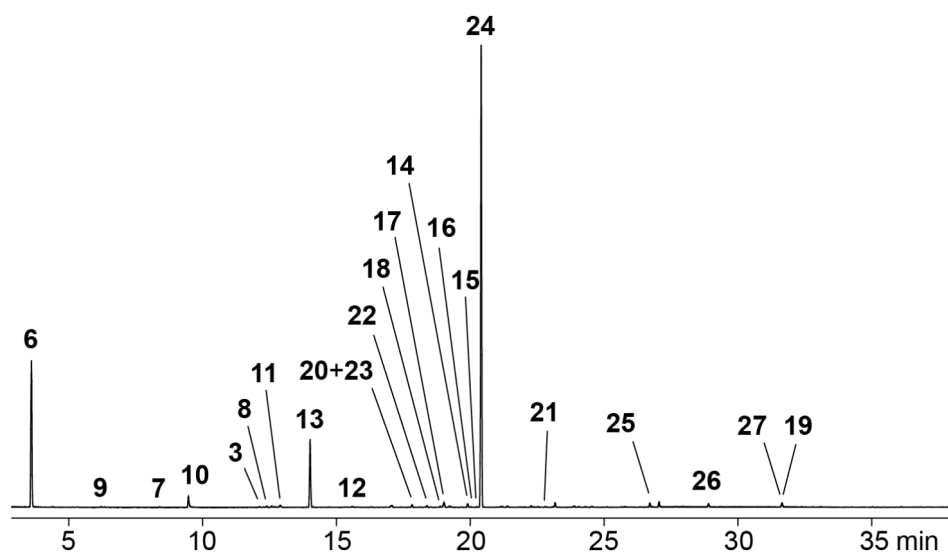
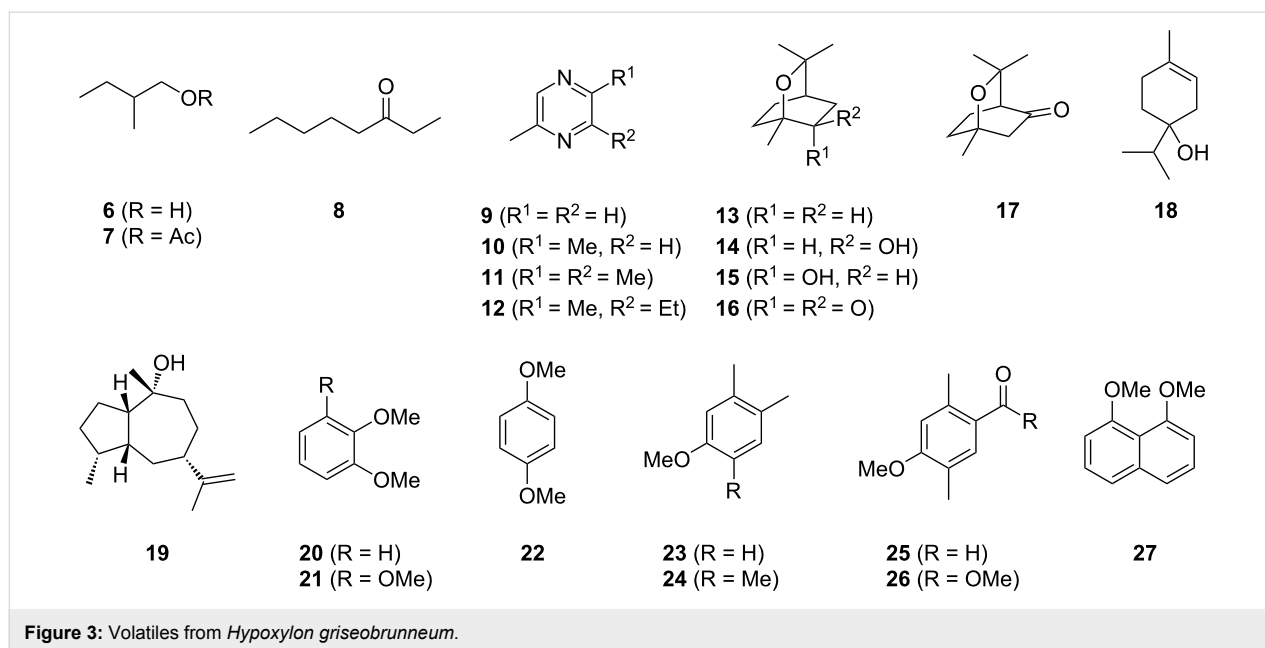


**Figure 2:** Total ion chromatogram of a CLSA headspace extract from *Hypoxylon griseobrunneum* MUCL 53754. Peak numbers refer to compound numbers in Table 1 and in Figure 3.

**Table 1:** Volatiles identified in the headspace extract from *Hypoxylon griseobrunneum* MUCL 53754.

compound	<i>I</i> <sup>a</sup>	<i>I</i> (lit.)	identification <sup>b</sup>	peak area <sup>c</sup>
2-methylbutan-1-ol ( <b>6</b> )	723	724 [25]	ms, ri, std	18.6%
methylpyrazine ( <b>9</b> )	817	819 [25]	ms, ri, std	<0.1%
2-methylbutyl acetate ( <b>7</b> )	874	875 [25]	ms, ri, std	<0.1%
2,5-dimethylpyrazine ( <b>10</b> )	903	908 [25]	ms, ri, std	1.5%
oct-1-en-3-ol ( <b>3</b> )	974	974 [25]	ms, ri, std	<0.1%
octan-3-one ( <b>8</b> )	982	979 [25]	ms, ri, std	<0.1%
trimethylpyrazine ( <b>11</b> )	995	1000 [25]	ms, ri, std	0.2%
1,8-cineole ( <b>13</b> )	1027	1026 [25]	ms, ri, std	8.5%
2-ethyl-3,6-dimethylpyrazine ( <b>12</b> )	1074	1077 [24]	ms, ri, syn	<0.1%
veratrole ( <b>20</b> )	1141	1141 [25]	ms, ri, std	0.2%
3,4-dimethylanisole ( <b>23</b> )	1141		ms, std	0.2%
1,4-dimethoxybenzene ( <b>22</b> )	1160	1161 [25]	ms, ri, std	0.2%
terpinen-4-ol ( <b>18</b> )	1174	1174 [25]	ms, ri	0.1%
3-oxo-1,8-cineole ( <b>17</b> )	1179	1186 [25]	ms, ri	0.7%
2 $\beta$ -hydroxy-1,8-cineole ( <b>14</b> )	1208	1217 [26]	ms, ri	0.4%
2-oxo-1,8-cineole ( <b>16</b> )	1213	1218 [27]	ms, ri	<0.1%
2 $\alpha$ -hydroxy-1,8-cineole ( <b>15</b> )	1220	1228 [26]	ms, ri	<0.1%
2,4,5-trimethylanisole ( <b>24</b> )	1225		ms, syn	54.5%
1,2,3-trimethoxybenzene ( <b>21</b> )	1308	1309 [28]	ms, ri, std	<0.1%
2,5-dimethyl- <i>p</i> -anisaldehyde ( <b>25</b> )	1456		ms, std	0.5%
methyl 2,5-dimethyl- <i>p</i> -anisate ( <b>26</b> )	1544		ms, syn	0.4%
1,8-dimethoxynaphthalene ( <b>27</b> )	1657	1657 [19]	ms, ri	0.3%
pogostol ( <b>19</b> )	1657	1651 [25]	ms, ri	0.3%

<sup>a</sup>Retention index *I* on a HP5-MS column. <sup>b</sup>Identification based on ms: identical mass spectrum, ri: identical retention index, std: comparison to a commercially available standard compound, syn: comparison to a synthetic standard. <sup>c</sup>Peak area in % of total peak area. The sum is less than 100%, because compounds originating from the medium, unidentified compounds and contaminants such as plasticisers are not mentioned.



also found. This volatile is frequently accompanied by other C<sub>8</sub> metabolites [1], which is reflected for *H. griseobrunneum* by the detection of octan-3-one (**8**). Trace amounts of a series of alkylated pyrazines including methylpyrazine (**9**), 2,5-dimethylpyrazine (**10**), trimethylpyrazine (**11**) and 2-ethyl-3,6-dimethylpyrazine (**12**) were also observed. These compounds were previously reported from the actinobacterium *Corynebacterium glutamicum* in which pyrazines are biosynthetically derived from acetoin and its higher homologs [24]. For unambiguous structure elucidation commercially available standards of **9–11** were used, while a synthesis of **12** was performed in our earlier study [24].

Furthermore, a group of monoterpenes and the sesquiterpene alcohol pogostol (**19**) that was previously reported from other fungi [29,30] were observed. Monoterpenes were comprised of terpinen-4-ol (**18**), 1,8-cineole (**13**) as one of the major compounds in the extracts, and small amounts of its oxidation products 2β-hydroxy-1,8-cineole (**14**), 2α-hydroxy-1,8-cineole (**15**), 2-oxo-1,8-cineole (**16**) and 3-oxo-1,8-cineole (**17**). The monoterpene ether **13** has previously been reported from other *Hypoxylon* spp. [31] and the responsible monoterpene synthase has been identified [32]. Its hydroxylated derivatives **14** and **15** were found in insects feeding on leaves of *Melaleuca alternifolia* that contain large amounts of **13** [26], and both alcohols **14** and **15** along with the ketones **16** and **17** were reported as metabolites of **13** in human milk [27].

The mass spectrum of the main compound **24** from *H. griseobrunneum* (Figure 4A) showed several fragment ions in the low *m/z* region typical for an aromatic compound, while the frag-

ment ion at *m/z* = 119 pointed to the loss of a methoxy group from the molecular ion ( $[M - 31]^+$ ), suggesting the structure of a trimethylanisole for **24**. Six constitutional isomers of this compound exist (Table 2). For four of these compounds the corresponding trimethylphenols were commercially available that were O-methylated with methyl iodide and K<sub>2</sub>CO<sub>3</sub> to yield compounds **24a**, **24b**, **24c** and **24e**. The other two isomers 2,3,4-trimethylanisole (**24d**) and 2,4,5-trimethylanisole (**24**) were obtained by *ortho*-methylation of 3,4-dimethylphenol (**28**) via a known procedure [33], followed by HPLC purification of the products 2,4,5-trimethylphenol (**29a**) and 2,3,4-trimethylphenol (**29b**) and subsequent O-methylation (Scheme 1). Comparison of the GC retention index of the natural product (*I* = 1225) to the retention indices of all six standards narrowed the possible structures down to those of 2,4,5-trimethylanisole (*I* = 1225) and 2,3,5-trimethylanisole (*I* = 1227), while all other isomers could be ruled out. The final structural assignment of 2,4,5-trimethylanisole for **24** was based on the better matching mass spectrum of this compound in comparison to the alternative of **24c**. Compound **24** has not been reported from other natural sources before.

The identification of **24** was further supported by a feeding experiment with (*methyl*-<sup>2</sup>H<sub>3</sub>)methionine. While the methylation pattern of the alternative structure **24c** is difficult to understand via a polyketide biosynthesis mechanism, the formation of the assigned structure of **24** by a polyketide synthase (PKS) can be easily rationalised (Scheme 2). The acetate starter unit, bound to the acyl carrier protein (ACP) of an iterative fungal PKS, can be elongated with malonyl-S-CoA (mal-S-CoA) followed by C-methylation with *S*-adenosyl-L-methionine (SAM). Two

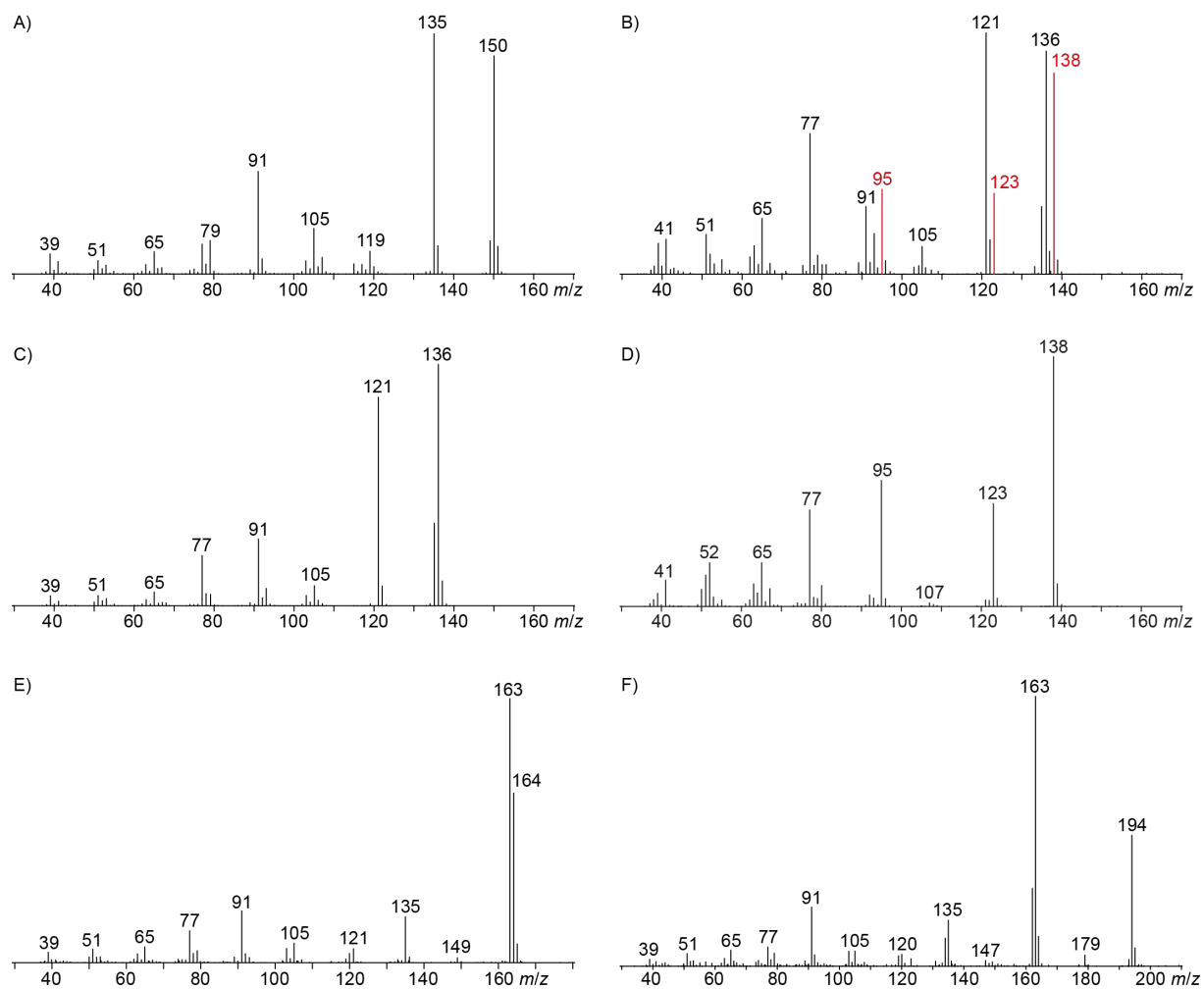


**Figure 4:** EI mass spectra of A) 2,4,5-trimethylanisole (**24**), B) the coeluting mixture of 3,4-dimethylanisole (**23**) and veratrole (**20**) with major peaks originating from **20** shown in red, C) the commercial standard of **23**, D) the commercial standard of **20**, E) 2,5-dimethyl-*p*-anisaldehyde (**25**), F) methyl 2,5-dimethyl-*p*-anisate (**26**).

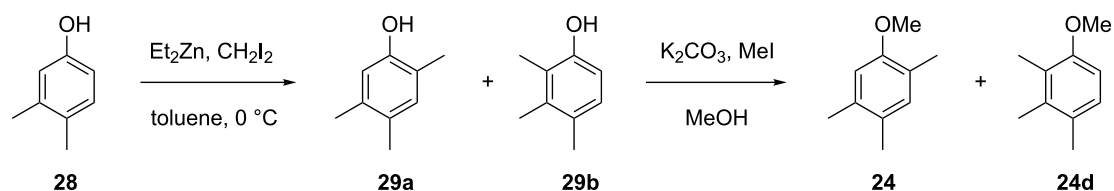
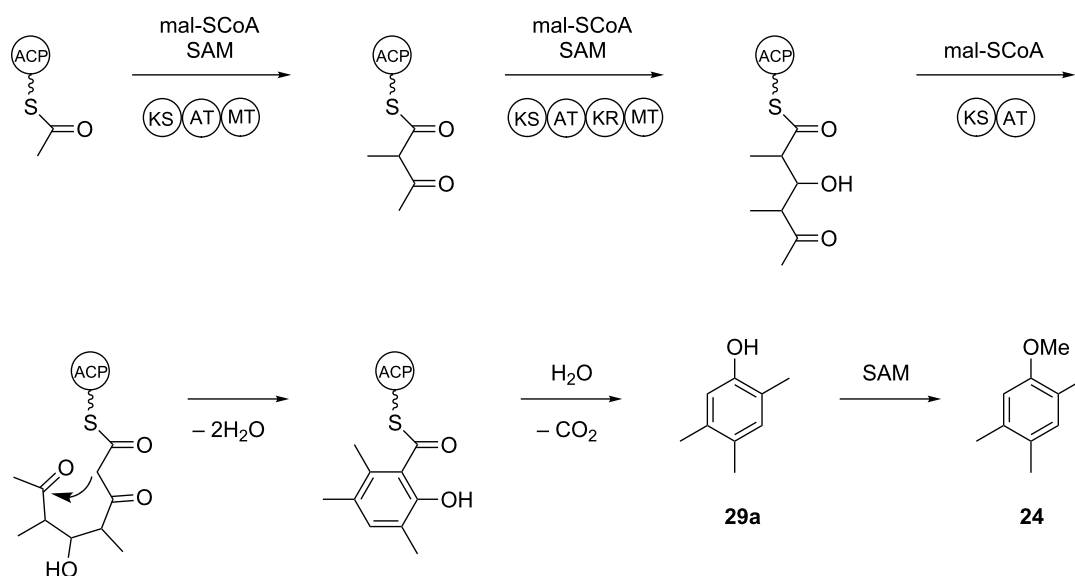
**Table 2:** Retention indices of all isomers of trimethylanisole.

structure	compound name <sup>a</sup>	<i>i</i> <sup>b</sup>
	2,4,6-trimethylanisole ( <b>24a</b> )	1157
	2,3,6-trimethylanisole ( <b>24b</b> )	1181
	2,4,5-trimethylanisole ( <b>24</b> )	1225

**Table 2:** Retention indices of all isomers of trimethylanisole. (continued)

	2,3,5-trimethylanisole ( <b>24c</b> )	1227
	2,3,4-trimethylanisole ( <b>24d</b> )	1257
	3,4,5-trimethylanisole ( <b>24e</b> )	1271

<sup>a</sup>The natural product from *H. griseobrunneum* is **24**, its isomers are designated **24a–e**. <sup>b</sup>Retention index *I* on a HP5-MS column.

**Scheme 1:** Synthesis of trimethylanisoles **24** and **24d**.**Scheme 2:** Hypothetical biosynthesis of **24**. ACP: acyl carrier protein, AT: acyl transferase, KR: ketoreductase, KS: ketosynthase, mal-SCoA: malonyl-SCoA, MT: methyl transferase, SAM: S-adenosyl-L-methionine.

more rounds of elongation with mal-SCoA, the first extension with C-methylation and action of a ketoreductase (KR), result in a tetraketide intermediate that can be cyclised by aldol conden-

sation, followed by elimination of water to result in the aromatic ring system. Thioester hydrolysis and decarboxylation produce **29a** that can be converted by SAM-dependent O-meth-

ylation into **24**. In summary, this hypothetical biosynthetic mechanism includes three SAM-dependent methylation steps. A feeding experiment with (*methyl*- $^2\text{H}_3$ )methionine, the biosynthetic precursor of SAM, resulted in the incorporation of labelling into up to three methyl groups of **24**, but not into the fourth methyl group (Figure 5), which is in line with the biosynthetic model of Scheme 2. Note that because of an isotope effect the isotopomers of **24** can be separated by gas chromatography depending on their deuterium content [34,35], which makes the usage of (*methyl*- $^2\text{H}_3$ )methionine superior to the usage of  $^{13}\text{C}$ -labelled methionine that would not have led to chromato-

graphic separation of the isotopomers. In conjunction with the low incorporation rates obtained here, the results would have been difficult to interpret.

Another trace compound emitted by *H. griseobrunneum* showed a molecular ion at  $m/z = 136$  and coeluted with exactly the same retention time as a second compound with a molecular ion at  $m/z = 138$ . In case of two coeluting compounds the individual compounds are often enriched in the right and left peak flanks, and their individual mass spectra can be extracted by careful background subtraction, but this was not the case here, so only

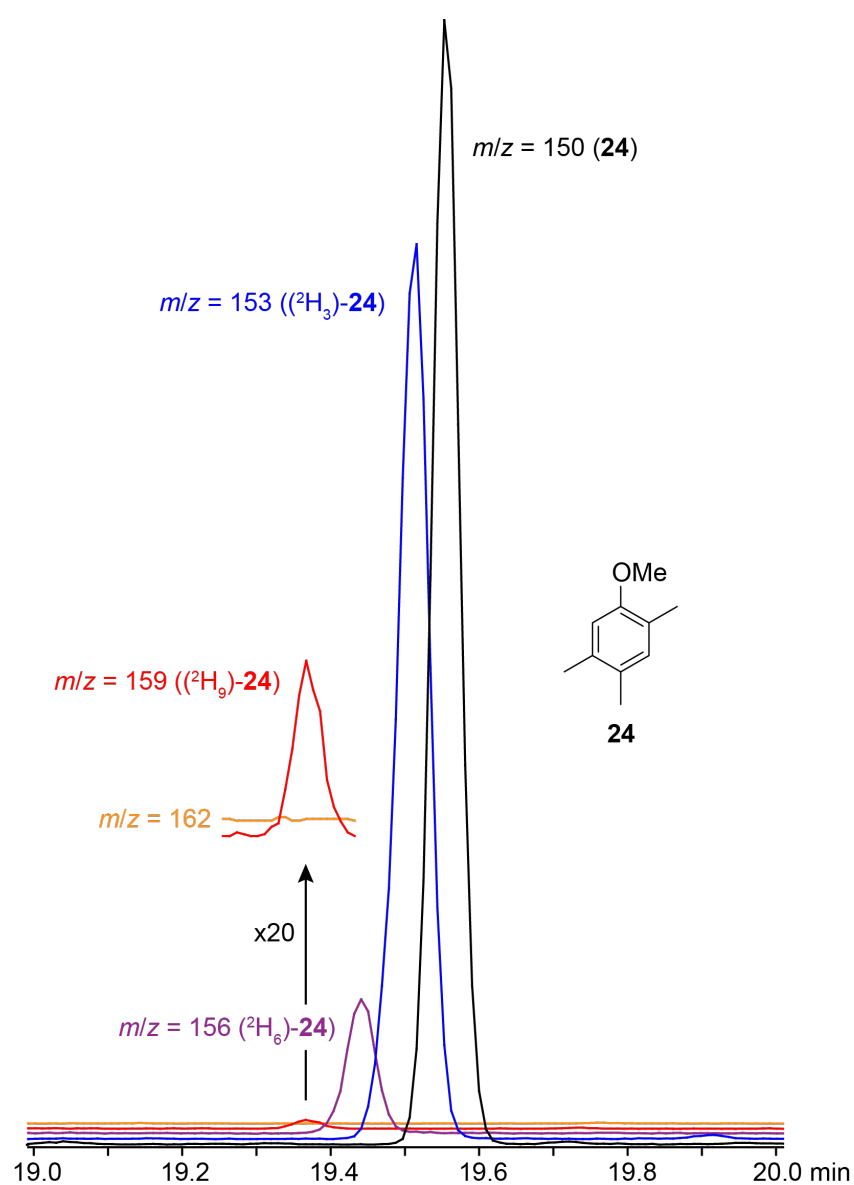


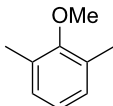
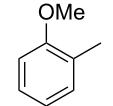
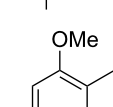
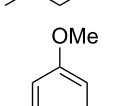
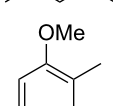
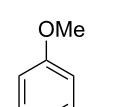
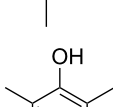
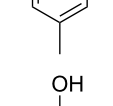
**Figure 5:** Biosynthesis of **24**. Feeding of (*methyl*- $^2\text{H}_3$ )methionine resulted in the incorporation of labelling into up to three methyl groups of **24**. The shown ion trace chromatograms represent unlabelled **24** (black,  $m/z = 150$ ), ( $^2\text{H}_3$ )-**24** (blue,  $m/z = 153$ ), ( $^2\text{H}_6$ )-**24** (purple,  $m/z = 156$ ), and ( $^2\text{H}_9$ )-**24** (red,  $m/z = 159$ ). No incorporation into the fourth methyl group was observed (no peak visible for  $m/z = 162$ ). For the ion trace chromatograms of  $m/z = 159$  and  $162$  also expansions ( $20\times$ ) are shown.

the mass spectrum of the compound mixture was obtained (Figure 4B). The analysis of the observed fragment ions suggested that the compound with the molecular ion at  $m/z = 136$  may be one of the isomers of dimethylanisole, explaining the fragment ion at  $m/z = 105$  by the loss of the methoxy group ( $[M - 31]^+$ ), and in agreement with the 14 Da lower molecular ion in comparison to **24**. All six isomers of dimethylanisole were commercially available and a comparison of retention indices together with a personal inspection of the mixed mass spectrum of Figure 4B and the mass spectrum of 3,4-dimethylanisole (Figure 4C) unequivocally identified the natural product as 3,4-dimethylanisole (**23**, Table 3). Furthermore, the alternative structure of a trimethylphenol was ruled out, because all the isomers eluted later than **23** (Table 3). Interestingly, the

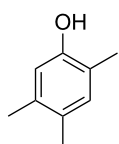
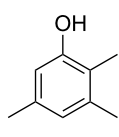
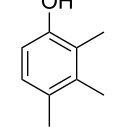
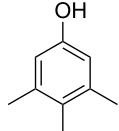
elution order of the trimethylphenols is the same as for the corresponding trimethylanisoles with respect to their substitution patterns, and each trimethylphenol consistently elutes slightly later with an increase of the retention index by ca. 30–50 points than the trimethylanisole analogue (Table 2 and Table 3), which is explainable by the significantly higher polarity of the phenols compared to the anisoles. Compound **23** was recently reported from *Euphorbia golondrina* [36], but was never observed as a fungal natural product so far.

Biosynthetically, the identified compound **23** can arise by a similar mechanism as discussed for **24**, potentially as a minor product of the same PKS, only the C-methylation step in the second round of chain extension needs to be skipped

**Table 3:** Retention indices of all isomers of dimethylanisole and trimethylphenol.

structure	compound name <sup>a</sup>	$i^b$
	2,6-dimethylanisole ( <b>23a</b> )	1056
	2,4-dimethylanisole ( <b>23b</b> )	1103
	2,5-dimethylanisole ( <b>23c</b> )	1104
	3,5-dimethylanisole ( <b>23d</b> )	1114
	2,3-dimethylanisole ( <b>23e</b> )	1128
	3,4-dimethylanisole ( <b>23</b> )	1141
	2,4,6-trimethylphenol ( <b>23f</b> )	1198
	2,3,6-trimethylphenol ( <b>23g</b> )	1227

**Table 3:** Retention indices of all isomers of dimethylanisole and trimethylphenol. (continued)

	2,4,5-trimethylphenol ( <b>23h</b> )	1262
	2,3,5-trimethylphenol ( <b>23i</b> )	1267
	2,3,4-trimethylphenol ( <b>23j</b> )	1296
	3,4,5-trimethylphenol ( <b>23k</b> )	1311

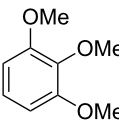
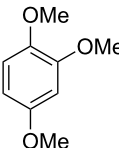
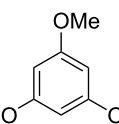
<sup>a</sup>The natural product from *H. griseobrunneum* is **23**, its isomers are designated **23a–k**. <sup>b</sup>Retention index *I* on a HP5-MS column.

(Scheme 2). However, during the feeding experiment with (*methyl*-<sup>2</sup>H<sub>3</sub>)methionine the formation of **23** was suppressed, possibly because the additional supply of methionine resulted in a higher efficiency of the programmed methylation steps towards **24**.

The additional signals in the mixed mass spectrum (Figure 4B) at *m/z* = 138, 123 and 95 that do not originate from **23** are present with similar relative proportions as in the mass spec-

trum of veratrole (**20**, Figure 4D), and indeed a commercial standard of **20** revealed the same retention index of *I* = 1141 as the natural product, thus confirming the structure of veratrole for the second of the coeluting compounds. Its isomer 1,4-dimethoxybenzene (**22**) and a trimethoxybenzene **21** were also detected. Comparison to all three commercially available isomers of trimethoxybenzene established the identity of **21** as 1,2,3-trimethoxybenzene (Table 4). 1,8-Dimethoxynaphthalene (**27**) was also found and has been reported previously from

**Table 4:** Retention indices of all isomers of trimethoxybenzene.

structure	compound name <sup>a</sup>	<i>I</i> <sup>b</sup>
	1,2,3-trimethoxybenzene ( <b>21</b> )	1308
	1,2,4-trimethoxybenzene ( <b>21a</b> )	1368
	1,3,5-trimethoxybenzene ( <b>21b</b> )	1409

<sup>a</sup>The natural product from *H. griseobrunneum* is **21**, its isomers are designated **21a** and **21b**. <sup>b</sup>Retention index *I* on a HP5-MS column.

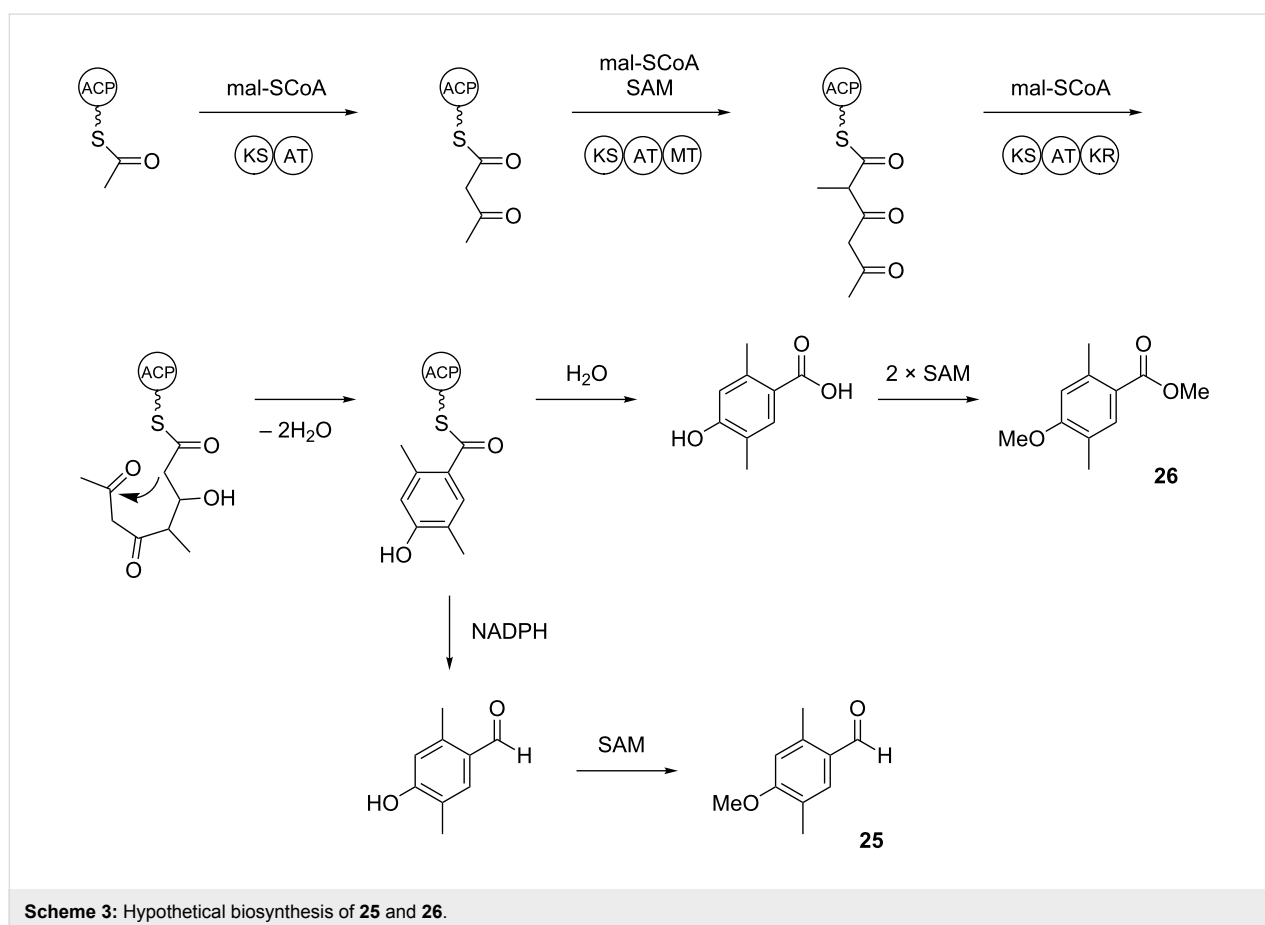
other *Hypoxylyon* spp. [19,37]. The corresponding compound 1,8-dihydroxynaphthalene is a known precursor of fungal melanin pigments [38].

Two trace compounds exhibited the mass spectra shown in Figure 4E and Figure 4F that were similar to database spectra of 2,5-dimethyl-*p*-anisaldehyde (**25**) and methyl 2,5-dimethyl-*p*-anisate (**26**). The substitution pattern of these compounds is well explained by polyketide biosynthesis logic (Scheme 3). Starting from ACP-bound acetate, two non-reducing elongations with malonyl-SCoA, the first without and the second with C-methylation, followed by another elongation with reduction of the 3-oxo group and cyclisation yields the aromatic system of **25** and **26**. Hydrolytic cleavage from the ACP and two methylations of the phenol and the carboxylic acid result in **26**, while reductive cleavage and methylation of the phenol give **25**. The aldehyde **25** was commercially available and matched the natural product in terms of mass spectrum and retention time. Compound **25** was transformed into the corresponding methyl ester by treatment with iodine and potassium hydroxide in methanol [39]. The obtained material also showed identical behaviour in the GC–MS analysis to natural **26**. Both compounds **25** and **26** are new natural products.

## Identification of volatiles from *Hypoxylyon macrocarpum*

The composition of the headspace extracts from *H. macrocarpum* (Figure 6 and Table 5) was completely different from the extracts of *H. griseobrunneum* with only the three compounds 2,5-dimethylpyrazine (**10**), trimethylpyrazine (**11**) and pogostol (**19**) being emitted by both species (Figure 7). The volatiles benzaldehyde (**32**) and 2-phenylethanol (**35**) as two of the main compounds, and the trace compounds 2-acetylfuran (**30**), 2-acetylthiazole (**31**), acetophenone (**33**), 1-phenylethanol (**34**), 1-phenylpropan-1,2-dione (**36**) and *m*-cresol (**37**) were readily identified from their mass spectra and retention indices and by comparison to authentic standards.

The main compounds released by *H. macrocarpum* were identified as 3,4-dimethoxytoluene (**43**) and 4-methylsalicylaldehyde (**39**), while 2,5-dimethylphenol (**38**) and 2-methoxy-4-methylbenzaldehyde (**40**) were detected in lower amounts. All four compounds were previously observed in the bouquet of *H. invadens* and unambiguously identified by comparison to all possible isomers with different ring substitution patterns [19]. Furthermore, comparison to all ten isomers of methoxy-methylbenzaldehydes described in this study allowed for the identifica-





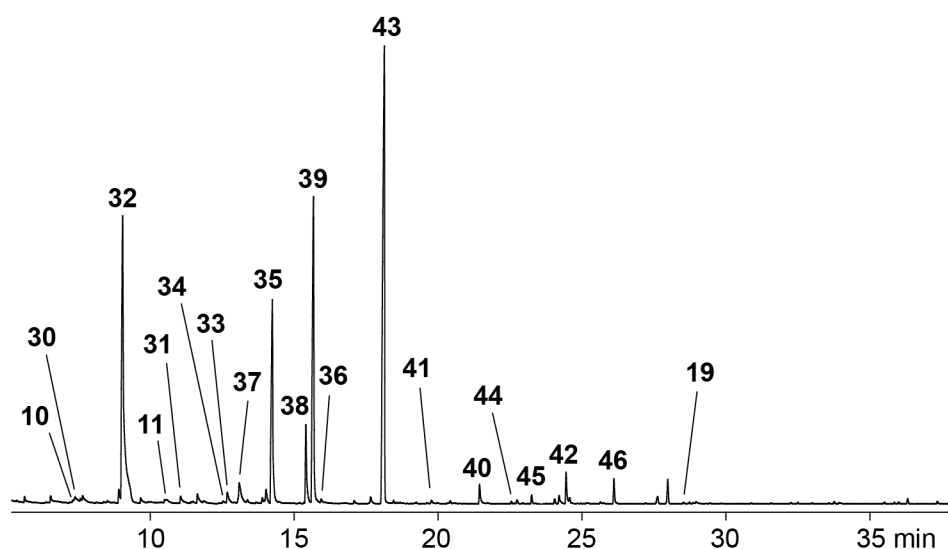


**Figure 6:** Total ion chromatogram of a CLSA headspace extract from *Hypoxylon macrocarpum* STMA 130423. Peak numbers refer to compound numbers in Table 5 and in Figure 7.

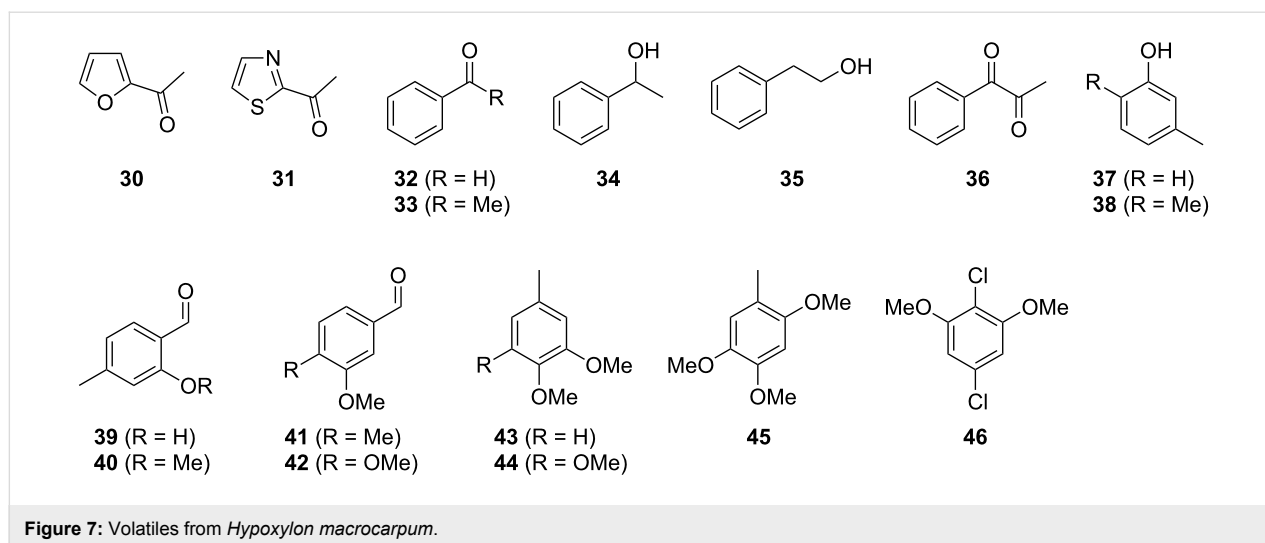
**Table 5:** Volatiles identified in headspace extract from *Hypoxylon macrocarpum* STMA 130423.

compound	$I^a$	$I$ (lit.)	identification <sup>b</sup>	peak area <sup>c</sup>
2,5-dimethylpyrazine ( <b>10</b> )	903	908 [25]	ms, ri, std	0.1%
2-acetylfuran ( <b>30</b> )	906	909 [25]	ms, ri, std	0.7%
benzaldehyde ( <b>32</b> )	952	952 [25]	ms, ri, std	22.8%
trimethylpyrazine ( <b>11</b> )	995	1000 [25]	ms, ri, std	0.5%
2-acetylthiazole ( <b>31</b> )	1012	1014 [25]	ms, ri, std	0.6%
1-phenylethanol ( <b>34</b> )	1054	1057 [25]	ms, ri, std	0.1%
acetophenone ( <b>33</b> )	1059	1059 [25]	ms, ri, std	0.8%
<i>m</i> -cresol ( <b>37</b> )	1071	1072 [25]	ms, ri	1.9%
2-phenylethanol ( <b>35</b> )	1105	1106 [25]	ms, ri, std	11.6%
2,5-dimethylphenol ( <b>38</b> )	1154	1152 [19]	ms, ri, std	3.6%
4-methylsalicylaldehyde ( <b>39</b> )	1162	1165 [19]	ms, ri, std	16.4%
1-phenylpropan-1,2-dione ( <b>36</b> )	1171	1175 [40]	ms, ri	0.1%
3,4-dimethoxytoluene ( <b>43</b> )	1243	1240 [19]	ms, ri, std	29.1%
3-methoxy-4-methylbenzaldehyde ( <b>41</b> )	1302	1307 [19]	ms, ri, std	0.2%
2-methoxy-4-methylbenzaldehyde ( <b>40</b> )	1365	1364 [19]	ms, ri, std	0.9%
3,4,5-trimethoxytoluene ( <b>44</b> )	1405		ms, std	0.1%
2,4,5-trimethoxytoluene ( <b>45</b> )	1436		ms, syn	0.3%
3,4-dimethoxybenzaldehyde ( <b>42</b> )	1483	1475 [25]	ms, ri, std	1.3%
2,5-dichloro-1,3-dimethoxybenzene ( <b>46</b> )	1552	1556 [18]	ms, ri, std	1.0%
pogostol ( <b>19</b> )	1657	1651 [25]	ms, ri	<0.1%

<sup>a</sup>Retention index  $I$  on a HP5-MS column. <sup>b</sup>Identification based on ms: identical mass spectrum, ri: identical retention index, std: comparison to a commercially available standard compound, syn: comparison to a synthetic standard. <sup>c</sup>Peak area in % of total peak area. The sum is less than 100%, because compounds originating from the medium, unidentified compounds and contaminants such as plasticisers are not mentioned.

tion of another trace compound from *H. macrocarpum* as 3-methoxy-4-methylbenzaldehyde (**41**). The chlorinated compound 2,5-dichloro-1,3-dimethoxybenzene (**46**) was also rigorously identified by comparison to all possible regioisomers that we had synthesised in a previous study [18]. Interestingly, the sub-

stitution pattern for the compound from *H. macrocarpum* is different to an isomer from the endophyte *Geniculosporium* sp. that was identified as 1,5-dichloro-2,3-dimethoxybenzene. Compound **46** has not been described as a natural product before. Another trace compound released by *H. macrocarpum*



exhibited a mass spectrum that pointed to the structure of a dimethoxybenzaldehyde (Figure 8A). Comparison to all six commercially available isomers (Table 6) showed the identity of the natural product and 3,4-dimethoxybenzaldehyde (**42**).

Finally, two trace compounds with almost identical mass spectra (Figure 8B and Figure 8C), but clear separation by gas chromatography, were suggested to be trimethoxytoluenes. Two isomers, 3,4,5-trimethoxytoluene (**44**) and 2,4,6-trimethoxy-

toluene (**44d**), were commercially available. 2,3,4-Trimethoxybenzaldehyde (**47**) was reduced to 2,3,4-trimethoxytoluene (**44a**) using PdCl<sub>2</sub> and Et<sub>3</sub>SiH [41] (Scheme 4), while the other three isomers were synthesised according to reported procedures [42–44]. Comparison of all six isomers to the two natural products (Table 7) resulted in their identification as 3,4,5-trimethoxytoluene (**44**) and 2,4,5-trimethoxytoluene (**45**). While **44** is a relatively widespread natural product, its isomer **45** has only once been tentatively identified by mass spectrometry in

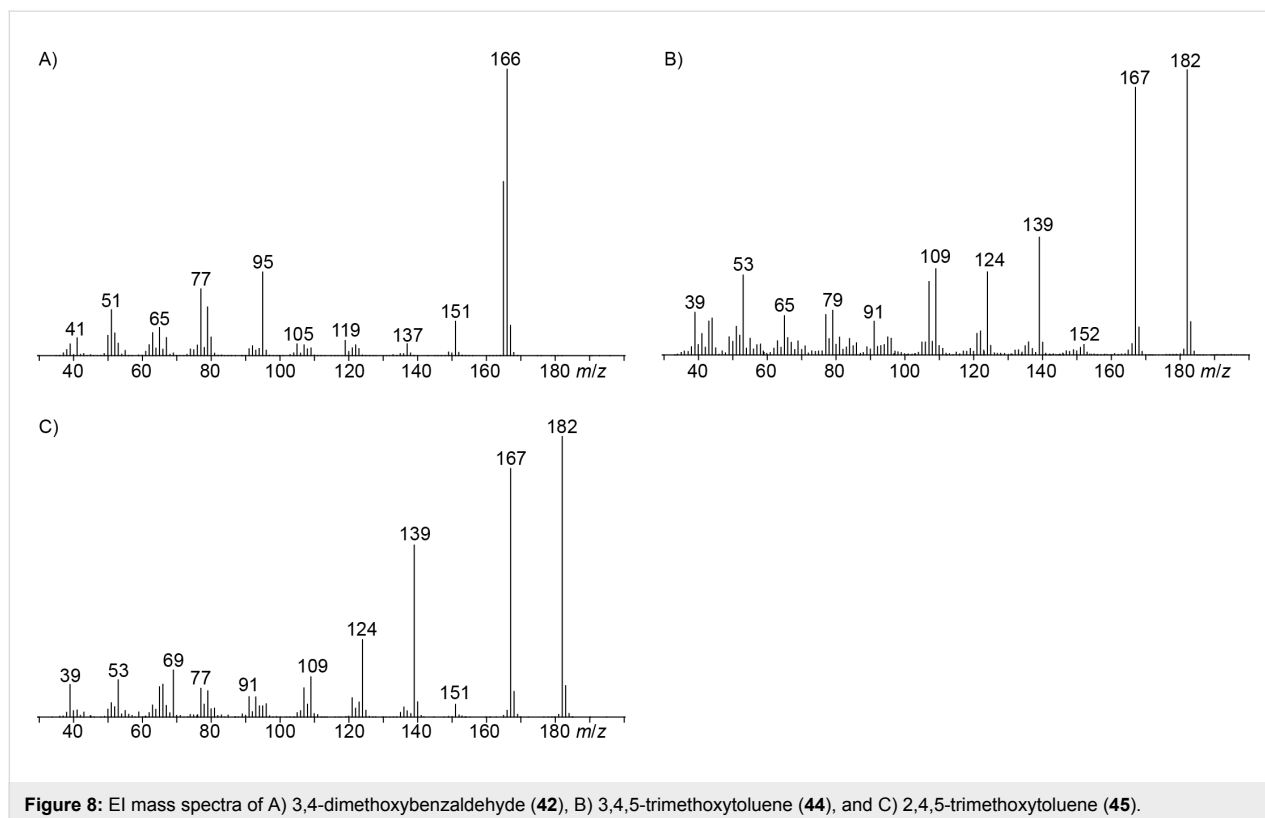
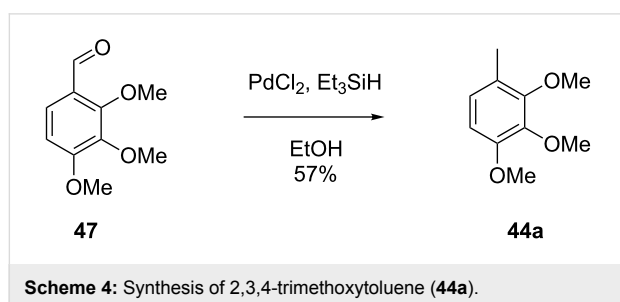


**Table 6:** Retention indices of all isomers of dimethoxybenzaldehyde.

structure	compound name <sup>a</sup>	<i>I</i> <sup>b</sup>
	2,3-dimethoxybenzaldehyde ( <b>42a</b> )	1391
	3,5-dimethoxybenzaldehyde ( <b>42b</b> )	1445
	2,5-dimethoxybenzaldehyde ( <b>42c</b> )	1468
	3,4-dimethoxybenzaldehyde ( <b>42</b> )	1483
	2,6-dimethoxybenzaldehyde ( <b>42d</b> )	1531
	2,4-dimethoxybenzaldehyde ( <b>42e</b> )	1543

<sup>a</sup>The natural product from *H. macrocarpum* is **42**, its isomers are designated **42a–e**. <sup>b</sup>Retention index *I* on a HP5-MS column.



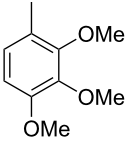
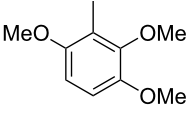
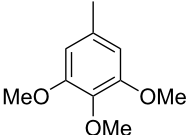
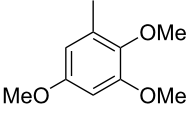
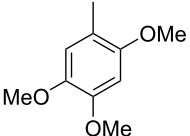
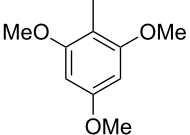
plants from the genus *Asarum* [45], but never from fungi before. However, it remains unclear how **45** was distinguished from **44** or other possible isomers in the earlier study.

## Conclusion

Both investigated ascomycetes, *Hypoxylon griseobrunneum* and *Hypoxylon macrocarpum*, were found to emit complex mixtures of volatiles, mainly composed of aromatic compounds. As we have demonstrated, for unequivocal structural assignments

based solely on GC–MS data it is important to compare the natural product to all possible constitutional isomers with different ring substitution patterns, because the mass spectra of these isomers are too similar to rely solely on MS data for compound identification. Therefore, also the retention index of the natural product must match the retention index of an authentic standard, and usually the retention indices of the isomeric aromatic compounds with different substitution patterns are sufficiently different for a confident structural assignment. Also biosynthetic considerations can help in the structure elucidation, because some aromatic substitution patterns are in line with a polyketide biosynthesis mechanism, while other substitution patterns may be difficult to understand. But such considerations should be made with care and should ideally be supported, e.g., by feeding experiments, as we have conducted in the present study. The main compounds of *H. griseobrunneum* were 2-methylbutan-1-ol, 1,8-cineol and 2,4,5-trimethylanisole, while *H. macrocarpum* released a completely different bouquet with the main compounds benzaldehyde, 2-phenylethanol,

**Table 7:** Retention indices of all isomers of trimethoxytoluene.

structure	compound name <sup>a</sup>	<i>i</i> <sup>b</sup>
	2,3,4-trimethoxytoluene ( <b>44a</b> )	1321
	2,3,6-trimethoxytoluene ( <b>44b</b> )	1397
	3,4,5-trimethoxytoluene ( <b>44</b> )	1405
	2,3,5-trimethoxytoluene ( <b>44c</b> )	1410
	2,4,5-trimethoxytoluene ( <b>45</b> )	1436
	2,4,6-trimethoxytoluene ( <b>44d</b> )	1488

<sup>a</sup>The natural products from *H. macrocarpum* are **44** and **45**, its isomers are designated **44a–d**. <sup>b</sup>Retention index *I* on a HP5-MS column.

4-methylsalicylaldehyde and 3,4-dimethoxytoluene. All these volatiles exhibit a characteristic smell and are likely main contributors to the odour produced by the fungi, but also some of the identified minor compounds may be important for the fungal fragrance. Notably, fungi of the genus *Hypoxylon* are interesting sources of new natural products, as exemplified by the identification of 2,4,5-trimethylanisole, 2,5-dimethyl-*p*-anisaldehyde and its corresponding methyl ester, and 2,5-dichloro-1,3-dimethoxybenzene. Therefore, it will be of high interest to investigate the volatiles from further *Hypoxylon* species in the near future.

## Experimental

### Strains and culture conditions

*Hypoxylon griseobrunneum* was obtained from a specimen collected in Martinique, Case Pilote, on a trail to Morne Venté on wood and bark of a dead dicotyledon branch in a mesophilic to xerophilic forest, on 25 August 2010 by Jacques Fournier [46]. A voucher specimen is deposited at the herbarium of the

University of Lille, France (LIP, No MJF10120) and the culture is deposited with MUCL (Louvain-la Neuve, Belgium) under the accession number MUCL 53754.

*Hypoxylon macrocarpum* was obtained from ascospores of a specimen collected in Germany, Rhineland-Palatinate Province in the vicinity of Forst, near the Pechsteinkopf from wood of *Fagus* on 20 October 2012 by Benno and Marc Stadler [21]. A voucher specimen is deposited in the fungarium of the Helmholtz Centre for Infection Research (HZI, Braunschweig, Germany) under the accession number STMA 130423.

### Analysis of volatiles

The volatiles emitted by agar plate cultures of *H. griseobrunneum* and *H. macrocarpum* were collected through a closed-loop stripping apparatus (CLSA) [13] for ca. 1 day at room temperature and under natural light-dark rhythm. The CLSA charcoal filter traps were extracted with CH<sub>2</sub>Cl<sub>2</sub> (50 μL, HPLC grade), followed by analysis of the extracts by GC–MS.

## GC–MS

GC–MS analyses were performed with a 7890A GC coupled to a 5975C inert mass detector (Agilent, Hewlett-Packard Company, Wilmington, USA). The GC was equipped with a HP5-MS fused silica capillary column (30 m, 0.25 mm i. d., 0.25  $\mu\text{m}$  film, Agilent). Conditions were inlet pressure: 77.1 kPa, He 23.3 mL  $\text{min}^{-1}$ ; injection volume: 1.5  $\mu\text{L}$ ; injector operation mode: splitless (60 s valve time); carrier gas: He at 1.2 mL  $\text{min}^{-1}$ ; GC program: 5 min at 50  $^{\circ}\text{C}$ , then increasing with 5  $^{\circ}\text{C min}^{-1}$  to 320  $^{\circ}\text{C}$ ; transfer line 300  $^{\circ}\text{C}$ ; electron energy 70 eV. Retention indices (*I*) were determined from a homologous series of *n*-alkanes ( $\text{C}_8\text{--C}_{38}$ ).

### Synthesis of 2,4,5-trimethylphenol (**29a**) and 2,3,4-trimethylphenol (**29b**)

Diiodomethane (2.14 g, 8.0 mmol, 2 equiv) was dissolved in dry toluene (3 mL) under an argon atmosphere and the solution was cooled to 0  $^{\circ}\text{C}$ . To the vigorously stirred solution,  $\text{Et}_2\text{Zn}$  in toluene (5.0 mL, 1.2 M, 6.0 mmol, 1.5 equiv) was added rapidly, followed immediately by the addition of 3,4-dimethylphenol (500 mg, 4.0 mmol) in toluene (3 mL). The reaction mixture was stirred at 0  $^{\circ}\text{C}$  for 5 min and then under reflux for 1.5 h. The reaction mixture was cooled to 0  $^{\circ}\text{C}$  and then quenched with an aqueous solution of  $\text{NaHCO}_3$  (10% w/w). The aqueous phase was extracted with diethyl ether for three times and the combined organic layers were dried over  $\text{MgSO}_4$ . The solvent was removed under reduced pressure and the crude product was purified by column chromatography on silica gel (cyclohexane/ethyl acetate 5:1). The obtained product contained **29a** and **29b** as a mixture which was separated by HPLC (KNAUER Wissenschaftliche Geräte GmbH, Berlin, Azura; DAICEL Chiralpak IA column, 5  $\mu\text{m}$ , 4.6  $\times$  250 mm; hexane/2-propanol 95:5; retention times: 9.66 min (**29b**) and 10.89 min (**29a**)). The pure products were obtained as colourless liquids.

**2,4,5-Trimethylphenol (29a)**. Yield: 14 mg (0.10 mmol, 3%).  $^1\text{H NMR}$  (500 MHz,  $\text{CDCl}_3$ , 298 K)  $\delta$  (ppm) 6.88 (s, 1H, CH), 6.59 (s, 1H, CH), 4.56 (br s, 1H, OH), 2.20 (s, 3H,  $\text{CH}_3$ ), 2.19 (s, 3H,  $\text{CH}_3$ ), 2.16 (s, 3H,  $\text{CH}_3$ );  $^{13}\text{C NMR}$  (125 MHz,  $\text{CDCl}_3$ , 298 K)  $\delta$  (ppm) 151.6 ( $\text{C}_q$ ), 135.2 ( $\text{C}_q$ ), 132.1 (CH), 128.4 ( $\text{C}_q$ ), 120.5 ( $\text{C}_q$ ), 116.3 (CH), 19.4 ( $\text{CH}_3$ ), 18.7 ( $\text{CH}_3$ ), 15.2 ( $\text{CH}_3$ ).

**2,3,4-Trimethylphenol (29b)**. Yield: 11 mg (0.08 mmol, 2%).  $^1\text{H NMR}$  (500 MHz,  $\text{CDCl}_3$ , 298 K)  $\delta$  (ppm) 6.87 (d,  $^3J = 8.1$  Hz, 1H, CH), 6.56 (d,  $^3J = 8.1$  Hz, 1H, CH), 4.54 (br s, 1H, OH), 2.22 (s, 3H,  $\text{CH}_3$ ), 2.20 (s, 3H,  $\text{CH}_3$ ), 2.19 (s, 3H,  $\text{CH}_3$ );  $^{13}\text{C NMR}$  (125 MHz,  $\text{CDCl}_3$ , 298 K)  $\delta$  (ppm) 151.7 ( $\text{C}_q$ ), 136.6 ( $\text{C}_q$ ), 128.8 ( $\text{C}_q$ ), 127.5 (CH), 122.6 ( $\text{C}_q$ ), 112.0 (CH), 20.3 ( $\text{CH}_3$ ), 16.0 ( $\text{CH}_3$ ), 12.1 ( $\text{CH}_3$ ).

### Synthesis of trimethylanisoles **24** and **24a–e**

To a solution of the respective phenol derivative (**23f–k**, 15.0 mg, 0.11 mmol, 1 equiv) in dry DMF (2.2 mL),  $\text{K}_2\text{CO}_3$  (15.2 mg, 0.11 mmol, 1 equiv) was added and the mixture was stirred at room temperature for 30 min. Methyl iodide (31 mg, 0.22 mmol, 2 equiv) was added and the reaction mixture was stirred at room temperature overnight. The reaction was quenched by addition of water and the aqueous phase was extracted three times with EtOAc. The combined organic layers were dried over  $\text{MgSO}_4$  and the solvent was removed under reduced pressure. The crude product was purified by column chromatography on silica gel (cyclohexane/ethyl acetate 20:1). The pure products were obtained as pale yellow liquids.

**2,4,5-Trimethylanisole (24)**. Yield: 5 mg (0.03 mmol, 32%). TLC (silica, cyclohexane/ethyl acetate 20:1):  $R_f = 0.48$ ;  $^1\text{H NMR}$  (500 MHz,  $\text{CDCl}_3$ , 298 K)  $\delta$  (ppm) 6.89 (s, 1H, CH), 6.63 (s, 1H, CH), 3.80 (s, 3H,  $\text{CH}_3$ ), 2.23 (s, 3H,  $\text{CH}_3$ ), 2.17 (s, 3H,  $\text{CH}_3$ ), 2.16 (s, 3H,  $\text{CH}_3$ );  $^{13}\text{C NMR}$  (125 MHz,  $\text{CDCl}_3$ , 298 K)  $\delta$  (ppm) 155.8 ( $\text{C}_q$ ), 134.6 ( $\text{C}_q$ ), 132.1 (CH), 128.0 ( $\text{C}_q$ ), 123.6 ( $\text{C}_q$ ), 112.1 (CH), 55.7 ( $\text{CH}_3$ ), 20.0 ( $\text{CH}_3$ ), 18.8 ( $\text{CH}_3$ ), 15.7 ( $\text{CH}_3$ ).

**2,4,6-Trimethylanisole (24a)**. Yield: 6 mg (0.04 mmol; 36%). TLC (silica, cyclohexane/ethyl acetate 20:1):  $R_f = 0.31$ ;  $^1\text{H NMR}$  (500 MHz,  $\text{CDCl}_3$ , 298 K)  $\delta$  (ppm) 6.82 (s, 2H, 2  $\times$  CH), 3.70 (s, 3H,  $\text{CH}_3$ ), 2.25 (s, 6H, 2  $\times$   $\text{CH}_3$ ), 2.24 (s, 3H,  $\text{CH}_3$ );  $^{13}\text{C NMR}$  (125 MHz,  $\text{CDCl}_3$ , 298 K)  $\delta$  (ppm) 154.9 ( $\text{C}_q$ ), 133.2 ( $\text{C}_q$ ), 130.6 (2  $\times$   $\text{C}_q$ ), 129.5 (2  $\times$  CH), 59.9 ( $\text{CH}_3$ ), 20.8 ( $\text{CH}_3$ ), 16.1 (2  $\times$   $\text{CH}_3$ ).

**2,3,6-Trimethylanisole (24b)**. Yield: 7 mg (0.05 mmol; 42%). TLC (silica, cyclohexane/ethyl acetate 20:1):  $R_f = 0.42$ ;  $^1\text{H NMR}$  (400 MHz,  $\text{CDCl}_3$ , 298 K)  $\delta$  (ppm) 6.92 (d,  $^3J = 7.6$  Hz, 1H, CH), 6.83 (d,  $^3J = 7.6$  Hz, 1H, CH), 3.70 (s, 3H,  $\text{CH}_3$ ), 2.27 (s, 3H,  $\text{CH}_3$ ), 2.24 (s, 3H,  $\text{CH}_3$ ), 2.20 (s, 3H,  $\text{CH}_3$ );  $^{13}\text{C NMR}$  (100 MHz,  $\text{CDCl}_3$ , 298 K)  $\delta$  (ppm) 156.9 ( $\text{C}_q$ ), 136.0 ( $\text{C}_q$ ), 129.6 ( $\text{C}_q$ ), 128.2 ( $\text{C}_q$ ), 128.0 (CH), 125.3 (CH), 60.0 ( $\text{CH}_3$ ), 20.0 ( $\text{CH}_3$ ), 16.2 ( $\text{CH}_3$ ), 12.4 ( $\text{CH}_3$ ).

**2,3,5-Trimethylanisole (24c)**. Yield: 8 mg (0.05 mmol; 48%). TLC (silica, cyclohexane/ethyl acetate 20:1):  $R_f = 0.47$ ;  $^1\text{H NMR}$  (400 MHz,  $\text{CDCl}_3$ , 298 K)  $\delta$  (ppm) 6.62 (s, 1H, CH), 6.55 (s, 1H, CH), 3.81 (s, 3H,  $\text{CH}_3$ ), 2.30 (s, 3H,  $\text{CH}_3$ ), 2.24 (s, 3H,  $\text{CH}_3$ ), 2.11 (s, 3H,  $\text{CH}_3$ );  $^{13}\text{C NMR}$  (100 MHz,  $\text{CDCl}_3$ , 298 K)  $\delta$  (ppm) 157.6 ( $\text{C}_q$ ), 137.7 ( $\text{C}_q$ ), 135.6 ( $\text{C}_q$ ), 123.1 (CH), 121.9 ( $\text{C}_q$ ), 109.0 (CH), 55.7 ( $\text{CH}_3$ ), 21.5 ( $\text{CH}_3$ ), 20.1 ( $\text{CH}_3$ ), 11.4 ( $\text{CH}_3$ ).

**2,3,4-Trimethylanisole (24d)**. Yield: 5 mg (0.03 mmol, 32%). TLC (silica, cyclohexane/ethyl acetate 20:1):  $R_f = 0.54$ ;

$^1\text{H}$  NMR (400 MHz,  $\text{CDCl}_3$ , 298 K)  $\delta$  (ppm) 6.96 (d,  $^3J = 8.3$  Hz, 1H, CH), 6.64 (d,  $^3J = 8.3$  Hz, 1H, CH), 3.79 (s, 3H,  $\text{CH}_3$ ), 2.23 (s, 3H,  $\text{CH}_3$ ), 2.18 (s, 3H,  $\text{CH}_3$ ), 2.17 (s, 3H,  $\text{CH}_3$ );  $^{13}\text{C}$  NMR (100 MHz,  $\text{CDCl}_3$ , 298 K)  $\delta$  (ppm) 156.0 ( $\text{C}_q$ ), 136.4 ( $\text{C}_q$ ), 128.6 ( $\text{C}_q$ ), 127.2 (CH), 125.1 ( $\text{C}_q$ ), 107.8 (CH), 55.8 ( $\text{CH}_3$ ), 20.3 ( $\text{CH}_3$ ), 16.0 ( $\text{CH}_3$ ), 12.1 ( $\text{CH}_3$ ).

**3,4,5-Trimethylanisole (24e).** Yield: 8 mg (0.05 mmol; 48%). TLC (silica, cyclohexane: ethyl acetate = 20:1):  $R_f = 0.37$ ;  $^1\text{H}$  NMR (400 MHz,  $\text{CDCl}_3$ , 298 K)  $\delta$  (ppm) 6.59 (s, 2H,  $2 \times \text{CH}$ ), 3.77 (s, 3H,  $\text{CH}_3$ ), 2.27 (s, 6H,  $2 \times \text{CH}_3$ ), 2.11 (s, 3H,  $\text{CH}_3$ );  $^{13}\text{C}$  NMR (100 MHz,  $\text{CDCl}_3$ , 298 K)  $\delta$  (ppm) 157.1 ( $\text{C}_q$ ), 137.7 ( $2 \times \text{C}_q$ ), 127.2 ( $\text{C}_q$ ), 113.2 (CH), 55.3 ( $\text{CH}_3$ ), 21.0 ( $2 \times \text{CH}_3$ ), 14.7 ( $\text{CH}_3$ ).

### Synthesis of methyl 2,5-dimethyl-*p*-anisate (26)

Similar to a reported procedure [39], 2,5-dimethyl-*p*-anisaldehyde (**25**, 1 g, 6.09 mmol, 1 equiv) was dissolved in MeOH (60 mL) and the solution was cooled to 0 °C. Solutions of KOH (1.045 g, 15.89 mmol, 2.6 equiv, in 20 mL MeOH) and  $\text{I}_2$  (2.01 g, 7.92 mmol, 1.3 equiv, in 10 mL MeOH) were added and the mixture was stirred for 90 min at 0 °C. The reaction was diluted with EtOAc, washed three times with saturated aqueous  $\text{Na}_2\text{S}_2\text{O}_3$  solution and subsequently with brine. The organic layer was dried over  $\text{MgSO}_4$  and the solvent was removed under reduced pressure. The crude product was purified via column chromatography (cyclohexane/ethyl acetate 10:1) on silica gel and the pure product was obtained as a colourless solid (277 mg, 1.43 mmol, 23%). TLC (silica, cyclohexane/ethyl acetate 3:1):  $R_f = 0.67$ .  $^1\text{H}$  NMR (500 MHz,  $\text{CDCl}_3$ , 298 K)  $\delta$  (ppm) 7.75 (s, 1H, CH), 6.64 (s, 1H, CH), 3.86 (s, 3H,  $\text{CH}_3$ ), 3.85 (s, 3H,  $\text{CH}_3$ ), 2.60 (s, 3H,  $\text{CH}_3$ ), 2.18 (s, 3H,  $\text{CH}_3$ );  $^{13}\text{C}$  NMR (125 MHz,  $\text{CDCl}_3$ , 298 K)  $\delta$  (ppm) 167.9 ( $\text{C}_q$ ), 160.6 ( $\text{C}_q$ ), 140.8 ( $\text{C}_q$ ), 133.4 (CH), 123.9 ( $\text{C}_q$ ), 120.9 ( $\text{C}_q$ ), 112.9 (CH), 55.5 ( $\text{CH}_3$ ), 51.6 ( $\text{CH}_3$ ), 22.1 ( $\text{CH}_3$ ), 15.8 ( $\text{CH}_3$ ).

### Synthesis of 2,3,4-trimethoxytoluene (44a)

According to a known procedure [41], to a solution of 2,3,4-trimethoxybenzaldehyde (**47**, 500 mg, 2.55 mmol, 1 equiv) in EtOH (13 mL),  $\text{SiEt}_3\text{H}$  (590 mg, 5.1 mmol, 2 equiv) was added under an argon atmosphere.  $\text{PdCl}_2$  (45.2 mg, 0.26 mmol, 10 mol %) was added and after stirring for 1 h, the reaction was quenched with  $\text{H}_2\text{O}$ . The mixture was extracted three times with  $\text{Et}_2\text{O}$  and the combined organic layers were dried over  $\text{MgSO}_4$ . The solvent was removed under reduced pressure and the crude product was purified via column chromatography on silica gel (cyclohexane/ethyl acetate 10:1). The pure product was obtained as a colourless liquid (267 mg, 1.47 mmol, 57%). TLC (silica, cyclohexane/ethyl acetate 3:1):  $R_f = 0.50$ ;  $^1\text{H}$  NMR (500 MHz,  $\text{C}_6\text{D}_6$ , 298 K)  $\delta$  (ppm) 6.73 (dq,  $^3J = 8.4$  Hz,

$^4J = 0.8$  Hz, 1H, CH), 6.38 (d,  $^3J = 8.4$  Hz, 1H, CH), 3.78 (s, 3H,  $\text{CH}_3$ ), 3.71 (s, 3H,  $\text{CH}_3$ ), 3.38 (s, 3H,  $\text{CH}_3$ ), 2.22 (d,  $^4J = 0.8$  Hz, 3H,  $\text{CH}_3$ );  $^{13}\text{C}$  NMR (125 MHz,  $\text{C}_6\text{D}_6$ , 298 K)  $\delta$  (ppm) 152.9 ( $\text{C}_q$ ), 152.8 ( $\text{C}_q$ ), 143.5 ( $\text{C}_q$ ), 124.7 (CH), 124.3 ( $\text{C}_q$ ), 108.0 (CH), 60.6 ( $\text{CH}_3$ ), 60.3 ( $\text{CH}_3$ ), 55.8 ( $\text{CH}_3$ ), 15.9 ( $\text{CH}_3$ ).

### Acknowledgements

This work was funded by the DFG (DI1536/9-1). We thank Andreas Schneider (Bonn) for compound purification by preparative HPLC and Jacques Fournier (Rimont, France) and Eric Kuhnert (Leibniz University Hannover) for their previous support in the characterisation of the *H. griseobrunneum* strain.

### ORCID® iDs

Marc Stadler - <https://orcid.org/0000-0002-7284-8671>

Jeroen S. Dickschat - <https://orcid.org/0000-0002-0102-0631>

### References

- Dickschat, J. S. *Nat. Prod. Rep.* **2017**, *34*, 310–328. doi:10.1039/c7np00003k
- Kimura, M.; Tokai, T.; Takahashi-Ando, N.; Ohsato, S.; Fujimura, M. *Biosci., Biotechnol., Biochem.* **2007**, *71*, 2105–2123. doi:10.1271/bbb.70183
- Wei, C.-M.; McLaughlin, C. S. *Biochem. Biophys. Res. Commun.* **1974**, *57*, 838–844. doi:10.1016/0006-291x(74)90622-6
- Riclea, R.; Dickschat, J. S. *Angew. Chem., Int. Ed.* **2015**, *54*, 12167–12170. doi:10.1002/anie.201506128
- García-Estrada, C.; Martín, J.-F. *Appl. Microbiol. Biotechnol.* **2016**, *100*, 8303–8313. doi:10.1007/s00253-016-7788-x
- Jeleń, H. H. *J. Agric. Food Chem.* **2002**, *50*, 6569–6574. doi:10.1021/jf020311o
- Murahashi, S. *Sci. Pap. Inst. Phys. Chem. Res. (Jpn.)* **1938**, *34*, 155–172.
- Zawirska-Wojtasiak, R. *Food Chem.* **2004**, *86*, 113–118. doi:10.1016/j.foodchem.2003.08.016
- Kandasamy, D.; Gershenzon, J.; Hammerbacher, A. *J. Chem. Ecol.* **2016**, *42*, 952–969. doi:10.1007/s10886-016-0768-x
- Citron, C. A.; Junker, C.; Schulz, B.; Dickschat, J. S. *Angew. Chem., Int. Ed.* **2014**, *53*, 4346–4349. doi:10.1002/anie.201402290
- Collins, R. P.; Halim, A. F. *J. Agric. Food Chem.* **1972**, *20*, 437–438. doi:10.1021/jf60180a010
- Wickel, S. M.; Citron, C. A.; Dickschat, J. S. *Eur. J. Org. Chem.* **2013**, 2906–2913. doi:10.1002/ejoc.201300049
- Grob, K.; Zürcher, F. *J. Chromatogr. A* **1976**, *117*, 285–294. doi:10.1016/0021-9673(76)80005-2
- Dickschat, J. S. *Nat. Prod. Rep.* **2014**, *31*, 838–861. doi:10.1039/c3np70080a
- Kováts, E. *Helv. Chim. Acta* **1958**, *41*, 1915–1932. doi:10.1002/hlca.19580410703
- Wang, T.; Mohr, K. I.; Stadler, M.; Dickschat, J. S. *Beilstein J. Org. Chem.* **2018**, *14*, 135–147. doi:10.3762/bjoc.14.9
- Dickschat, J. S.; Celik, E.; Brock, N. L. *Beilstein J. Org. Chem.* **2018**, *14*, 900–910. doi:10.3762/bjoc.14.77

18. Wang, T.; Rabe, P.; Citron, C. A.; Dickschat, J. S. *Beilstein J. Org. Chem.* **2013**, *9*, 2767–2777. doi:10.3762/bjoc.9.311
19. Dickschat, J. S.; Wang, T.; Stadler, M. *Beilstein J. Org. Chem.* **2018**, *14*, 734–746. doi:10.3762/bjoc.14.62
20. Helaly, S. E.; Thongbai, B.; Stadler, M. *Nat. Prod. Rep.* **2018**, *35*, 992–1014. doi:10.1039/c8np00010g
21. Pažoutová, S.; Follert, S.; Bitzer, J.; Keck, M.; Surup, F.; Šrůtka, P.; Holuša, J.; Stadler, M. *Fungal Diversity* **2013**, *60*, 107–123. doi:10.1007/s13225-013-0238-5
22. Pouzar, Z. *Czech Mycol.* **1978**, *32*, 19–21.
23. Mühlbauer, A.; Triebel, D.; Persoh, D.; Wollweber, H.; Seip, S.; Stadler, M. *Mycol. Progress* **2002**, *1*, 235–248. doi:10.1007/s11557-006-0021-z
24. Dickschat, J. S.; Wickel, S.; Boltzen, C. J.; Nawrath, T.; Schulz, S.; Wittmann, C. *Eur. J. Org. Chem.* **2010**, 2687–2695. doi:10.1002/ejoc.201000155
25. Adams, R. P. *Identification of Essential Oil Components by Gas Chromatography/Mass Spectrometry*; Allured: Carol Stream, 2009.
26. Southwell, I. A.; Russell, M. F.; Maddox, C. D. A.; Wheeler, G. S. *J. Chem. Ecol.* **2003**, *29*, 83–94. doi:10.1023/a:1021976513603
27. Kirsch, F.; Horst, K.; Röhrig, W.; Rychlik, M.; Buettner, A. *Metabolomics* **2013**, *9*, 483–496. doi:10.1007/s11306-012-0466-9
28. Wu, S.; Zorn, H.; Krings, U.; Berger, R. G. *Flavour Fragrance J.* **2007**, *22*, 53–60. doi:10.1002/ffj.1758
29. Amand, S.; Langenfeld, A.; Blond, A.; Dupont, J.; Nay, B.; Prado, S. *J. Nat. Prod.* **2012**, *75*, 798–801. doi:10.1021/np2009913
30. Barra, L.; Schulz, B.; Dickschat, J. S. *ChemBioChem* **2014**, *15*, 2379–2383. doi:10.1002/cbic.201402298
31. Tomsheck, A. R.; Strobel, G. A.; Booth, E.; Geary, B.; Spakowicz, D.; Knighton, B.; Floerchinger, C.; Sears, J.; Liarzi, O.; Ezra, D. *Microb. Ecol.* **2010**, *60*, 903–914. doi:10.1007/s00248-010-9759-6
32. Shaw, J. J.; Berbasova, T.; Sasaki, T.; Jefferson-George, K.; Spakowicz, D. J.; Dunican, B. F.; Portero, C. E.; Narváez-Trujillo, A.; Strobel, S. A. *J. Biol. Chem.* **2015**, *290*, 8511–8526. doi:10.1074/jbc.m114.636159
33. Lehnert, E. K.; Scott Sawyer, J.; Macdonald, T. L. *Tetrahedron Lett.* **1989**, *30*, 5215–5218. doi:10.1016/s0040-4039(01)93745-1
34. Dickschat, J. S.; Wenzel, S. C.; Bode, H. B.; Müller, R.; Schulz, S. *ChemBioChem* **2004**, *5*, 778–787. doi:10.1002/cbic.200300813
35. Dickschat, J. S.; Zell, C.; Brock, N. L. *ChemBioChem* **2010**, *11*, 417–425. doi:10.1002/cbic.200900668
36. Ndam, L. M.; Mih, A. M.; Tening, A. S.; Fongod, A. G. N.; Temenu, N. A.; Fujii, Y. *SpringerPlus* **2016**, *5*, 264. doi:10.1186/s40064-016-1928-8
37. Chang, C.-W.; Chang, H.-S.; Cheng, M.-J.; Liu, T.-W.; Hsieh, S.-Y.; Yuan, G.-F.; Chen, I.-S. *Chem. Biodiversity* **2014**, *11*, 949–961. doi:10.1002/cbdv.201300364
38. Bell, A. A.; Wheeler, M. H. *Annu. Rev. Phytopathol.* **1986**, *24*, 411–451. doi:10.1146/annurev.py.24.090186.002211
39. Citron, C. A.; Rabe, P.; Barra, L.; Nakano, C.; Hoshino, T.; Dickschat, J. S. *Eur. J. Org. Chem.* **2014**, 7684–7691. doi:10.1002/ejoc.201403002
40. Wang, Q.; Yang, Y.; Zhao, X.; Zhu, B.; Nan, P.; Zhao, J.; Wang, L.; Chen, F.; Liu, Z.; Zhong, Y. *Food Chem.* **2006**, *98*, 52–58. doi:10.1016/j.foodchem.2005.04.033
41. Mirza-Aghayan, M.; Boukherroub, R.; Rahimifard, M.; Zadmard, R. *J. Iran. Chem. Soc.* **2011**, *8*, 570–573. doi:10.1007/bf03249092
42. Buccini, M.; Punch, K. A.; Kaskow, B.; Flematti, G. R.; Skelton, B. W.; Abraham, L. J.; Piggott, M. J. *Org. Biomol. Chem.* **2014**, *12*, 1100–1113. doi:10.1039/c3ob42333f
43. O'Hara, P. S.; Incerti-Pradillos, C. A.; Kabeshov, M. A.; Shipilovskikh, S. A.; Rubtsov, A. E.; Elsegood, M. R. J.; Malkov, A. V. *Chem. – Eur. J.* **2015**, *21*, 4551–4555. doi:10.1002/chem.201500176
44. Takaya, Y.; Hotta, R.; Fujiwara, K.; Otani, R.; Uchiyama, Y.; Sakakibara, M.; Fukuda, E.; Niwa, M.; Inouye, K.; Oohata, A. A. *Org. Lett.* **2014**, *16*, 3660–3663. doi:10.1021/ol5014119
45. Hayashi, N.; Ding, J.; Ding, Z.; Chen, Z.; Yi, Y.; Komae, H. *Z. Naturforsch., C: J. Biosci.* **1990**, *45c*, 32–36. doi:10.1515/znc-1990-1-207
46. Kuhnert, E.; Fournier, J.; Peršoh, D.; Luangsa-ard, J. J. D.; Stadler, M. *Fungal Diversity* **2014**, *64*, 181–203. doi:10.1007/s13225-013-0264-3

## License and Terms

This is an Open Access article under the terms of the Creative Commons Attribution License (<http://creativecommons.org/licenses/by/4.0>). Please note that the reuse, redistribution and reproduction in particular requires that the authors and source are credited.

The license is subject to the *Beilstein Journal of Organic Chemistry* terms and conditions: (<https://www.beilstein-journals.org/bjoc>)

The definitive version of this article is the electronic one which can be found at: [doi:10.3762/bjoc.14.277](https://doi.org/10.3762/bjoc.14.277)





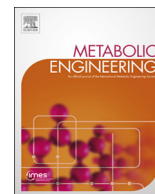
## Appendix V

### **From lignin to nylon: Cascaded chemical and biochemical conversion using metabolically engineered *Pseudomonas putida***

*Metab. Eng.* **2018**, *47*, 279–293.

DOI:10.1016/j.ymben.2018.03.003





# From lignin to nylon: Cascaded chemical and biochemical conversion using metabolically engineered *Pseudomonas putida*

Michael Kohlstedt<sup>a</sup>, Sören Starck<sup>a</sup>, Nadja Barton<sup>a</sup>, Jessica Stolzenberger<sup>a</sup>, Mirjam Selzer<sup>a</sup>, Kerstin Mehlmann<sup>c</sup>, Roland Schneider<sup>c</sup>, Daniel Pleissner<sup>c,d</sup>, Jan Rinkel<sup>b</sup>, Jeroen S. Dickschat<sup>b</sup>, Joachim Venus<sup>c</sup>, Jozef B.J.H. van Duuren<sup>a</sup>, Christoph Wittmann<sup>a,\*</sup>

<sup>a</sup> Institute of Systems Biotechnology, Saarland University, Germany

<sup>b</sup> Kekulé-Institute for Organic Chemistry and Biochemistry, University of Bonn, Germany

<sup>c</sup> Leibniz Institute for Agricultural Engineering and Bioeconomy, Potsdam, Germany

<sup>d</sup> Institute of Sustainable and Environmental Chemistry (ISEC), Leuphana University of Lüneburg, Germany

## ARTICLE INFO

### Keywords:

*Pseudomonas putida*  
 Funneling  
 Catechol dioxygenase  
 Phenol hydroxylase  
 Synthetic promoter library  
 Hydrothermal conversion  
 Lignin  
 Nylon 6,6  
 Catechol  
 Phenol  
 Cresol  
*Cis,cis*-muconic acid  
 Methyl muconic acid, adipic acid  
 Methyl adipic acid  
 Bionylon

## ABSTRACT

*Cis,cis*-muconic acid (MA) is a chemical that is recognized for its industrial value and is synthetically accessible from aromatic compounds. This feature provides the attractive possibility of producing MA from mixtures of aromatics found in depolymerized lignin, the most underutilized lignocellulosic biopolymer. Based on the metabolic pathway, the catechol (1,2-dihydroxybenzene) node is the central element of this type of production process: (i) all upper catabolic pathways of aromatics converge at catechol as the central intermediate, (ii) catechol itself is frequently generated during lignin pre-processing, and (iii) catechol is directly converted to the target product MA by catechol 1,2-dioxygenase. However, catechol is highly toxic, which poses a challenge for the bio-production of MA. In this study, the soil bacterium *Pseudomonas putida* KT2440 was upgraded to a fully genome-based host for the production of MA from catechol and upstream aromatics. At the core of the cell factories created was a designed synthetic pathway module, comprising both native catechol 1,2-dioxygenases, *catA* and *catA2*, under the control of the  $P_{cat}$  promoter. The pathway module increased catechol tolerance, catechol 1,2-dioxygenase levels, and catechol conversion rates. MA, the formed product, acted as an inducer of the module, triggering continuous expression. Cellular energy level and ATP yield were identified as critical parameters during catechol-based production. The engineered MA-6 strain achieved an MA titer of  $64.2 \text{ g L}^{-1}$  from catechol in a fed-batch process, which repeatedly regenerated the energy levels via specific feed pauses. The developed process was successfully transferred to the pilot scale to produce kilograms of MA at 97.9% purity. The MA-9 strain, equipped with a phenol hydroxylase, used phenol to produce MA and additionally converted *o*-cresol, *m*-cresol, and *p*-cresol to specific methylated variants of MA. This strain was used to demonstrate the entire value chain. Following hydrothermal depolymerization of softwood lignin to catechol, phenol and cresols, MA-9 accumulated  $13 \text{ g L}^{-1}$  MA and small amounts of 3-methyl MA, which were hydrolyzed to adipic acid and its methylated derivative to polymerize nylon from lignin for the first time.

## 1. Introduction

Found in terrestrial plants, lignin is the second most abundant biopolymer in the world. With the advent of biorefineries that use plant biomass, lignin has become a common by-product with potential to be used as raw material in the fuel and chemical industries. However, lignin remains the most underutilized lignocellulosic biopolymer (Rinaldi et al., 2016). Therefore, there is much interest in converting lignin to more diverse and valuable products (Ragauskas et al., 2014). Cascaded processes have shown promise in lignin valorization; these

processes first depolymerize lignin into mixtures of small aromatics and then biologically convert these aromatics to value-added chemicals (Linger et al., 2014).

The conversion of aromatics to *cis,cis*-muconic acid (MA) is a particularly attractive application (Xie et al., 2014). This dicarboxylic acid is a chemical that is recognized for its industrial value. MA provides synthetic access to terephthalic acid, 3-hexenedioic acid, 2-hexenedioic acid, 1,6-hexanediol, caprolactam, and caprolactone, which are important building blocks of commercial plastics (Matthiesen et al., 2016). MA is synthesized from aromatics by the upper catabolic pathways, all

\* Correspondence to: Campus A 1.5, 66123 Saarbrücken, Germany.  
 E-mail address: [christoph.wittmann@uni-saarland.de](mailto:christoph.wittmann@uni-saarland.de) (C. Wittmann).

of which converge at catechol as a central intermediate, which then undergoes ring *ortho*-cleavage to MA by the action of catechol 1,2-dioxygenase (Jiménez et al., 2014).

The gram-negative soil bacterium *Pseudomonas putida* KT2440 and related strains have emerged as candidates with the most potential for this type of production (Xie et al., 2014). For example, the inactivation of muconate cycloisomerase enables the production of MA via the catechol branch of the  $\beta$ -ketoadipate pathway from benzoate (van Duuren et al., 2011) and toluene (Chua and Hsieh, 1990). In addition, the expression of phenol-hydroxylating enzymes (Shingler et al., 1989) successfully mediates MA production from phenol in *P. putida* KT2440 (Vardon et al., 2015). More recently, the entire protocatechuate branch of the  $\beta$ -ketoadipate pathway was successfully connected to the catechol node, allowing MA formation from a greater number of substrates, including coniferyl alcohol, *p*-coumarate, vanillate, ferulate, and protocatechuate (Johnson et al., 2016). As a result, the upper pathways of the engineered aromatic catabolism act as a “biological funnel” to convert heterogeneous mixtures of aromatics to catechol as a central intermediate (Linger et al., 2014).

Catechol itself is very toxic (Park et al., 2004) via a diverse range of molecular mechanisms, ranging from the production of reactive oxygen species to direct protein damage (Schweigert et al., 2001). This toxicity poses a challenge for the application of this microbe in chemical production from lignin-based feedstocks. First, these raw materials can themselves contain significant fractions of catechol (Jeenpadiphat et al., 2016; Pandey and Kim, 2011; Schuler et al., 2017). Second, the conversion of crude mixtures of aromatics requires the engineering of heterologous catabolic pathways into the microbe, all of which additionally contribute to catechol accumulation, potentially leading to forced self-toxication. These factors could explain why the conversion of lignin liquor to MA by engineered *P. putida* KT2440 has so far resulted in the accumulation of upstream pathway intermediates and in production of MA at only the milligram scale (Vardon et al., 2014; Rodriguez et al., 2017).

Catechol tolerance and catechol removal are bottlenecks with significant impact. These bottlenecks occur at the so-far unaddressed “stem of the designed biological funnel”, potentially limiting the production efficiency of MA by *P. putida* KT2440 from lignin-based feedstocks and remaining key targets for strain engineering. Here, we address this issue. We describe a genealogy of metabolically engineered strains of *P. putida* KT2440 with enhanced catechol tolerance and conversion efficiency and an enhanced substrate spectrum. These engineered MA producers were then successfully applied to provide the first nylon from lignin in a cascaded chemical and biochemical process.

## 2. Materials and methods

### 2.1. Strains and plasmids

The wild-type *P. putida* KT2440 (DSM 6125) was obtained as the parent strain from the German Collection of Microorganisms and Cell Cultures (DSMZ, Braunschweig, Germany). The MA-producing strain *P. putida* JD1 was obtained from a previous study (van Duuren et al., 2011). *P. putida* CF600 and the plasmid pVI260, which carried the phenol hydroxylase genes *dmpKLMNOP* of the CF600 strain, were kindly donated by Victoria Shingler (University of Umeå, Sweden) (Shingler et al., 1989). *Escherichia coli* DH5 $\alpha$  (Invitrogen, Carlsbad, CA, USA) and *Escherichia coli* DH5 $\alpha$   $\lambda$ pir (Biomedal Lifescience, Cartuja, Spain) were obtained for cloning. The plasmids pEMG (Martinez-Garcia and de Lorenzo, 2011), pSEVA247M, pSEVA247C, and pSEVA247R (Silva-Rocha et al., 2013), kindly donated by Victor de Lorenzo (National Biotechnology Centre, Madrid, Spain), and the plasmid pCR 2.1 (Invitrogen) were used for cloning purposes. The strains were maintained as cryo-stocks in 15% (v/v) glycerol at  $-80^{\circ}\text{C}$ . Strains and plasmids are listed in Table 1.

**Table 1**  
Strains and plasmids used in this study.

Strain	Description	References
<i>E. coli</i> DH5 $\alpha$	<i>supE44</i> , $\Delta$ <i>lacU169</i> ( <i>q80 lacZ</i> $\Delta$ M15), <i>hsdR17</i> ( <i>rk-mk</i> +), <i>recA1</i> , <i>endA1</i> , <i>thi1</i> , <i>gyrA</i> , <i>relA</i>	Invitrogen
DH5 $\alpha$ $\lambda$ pir <i>P. putida</i> KT2440	$\lambda$ pir lysogen of DH5 $\alpha$ Wild type	Biomedal (Silva-Rocha et al., 2013)
CF600 JD1	Wild type catR-deficient mutant of KT2440	(Shingler et al., 1989) (van Duuren et al., 2011)
MA-1 MA-2 MA-3 MA-4 MA-5 MA-6 MA-7 MA-8 MA-9	KT2440 $\Delta$ <i>catBC</i> MA-1 $\Delta$ <i>endA-1</i> MA-1 $\Delta$ <i>endA-1</i> $\Delta$ <i>endA-2</i> MA-1 $P_{em7}$ <i>catA</i> $\Delta$ <i>pcaB</i> MA-1 $P_{em7-2}$ <i>catA</i> $\Delta$ <i>pcaB</i> MA-3 $P_{cat}$ <i>catA</i> <i>catA2</i> MA-1 $P_{cat}$ <i>catA</i> <i>catA2</i> MA-6 $P_{cat}$ <i>catA</i> <i>catA2</i> MA-6 $P_{GRO}$ <i>dmpKLMNOP</i>	This study This study This study This study This study This study This study This study This study
<i>Plasmids</i> pSEVA247C	Km <sup>R</sup> , <i>ori</i> pRO1600/ColE1, <i>cfp</i>	(Silva-Rocha et al., 2013)
pSEVA247M	Km <sup>R</sup> , <i>ori</i> pRO1600/ColE1, <i>msfgfp</i>	(Silva-Rocha et al., 2013)
pSEVA247R	Km <sup>R</sup> , <i>ori</i> pBBR1, <i>mCherry</i>	(Silva-Rocha et al., 2013)
pSEVA247C-Pgro pSEVA247M-Pgro	Km <sup>R</sup> , <i>ori</i> pRO1600/ColE1, $P_{gro}$ - <i>cfp</i> Km <sup>R</sup> , <i>ori</i> pRO1600/ColE1, $P_{gro}$ - <i>msfgfp</i>	This study This study
pSEVA247R-Pgro pSEVA247R-Ptuf pSEVA247R-Ptufk pSEVA247R-PEM7 pSEVA4413	Km <sup>R</sup> , <i>ori</i> pBBR1, $P_{gro}$ - <i>mCherry</i> Km <sup>R</sup> , <i>ori</i> pBBR1, $P_{tuf}$ - <i>mCherry</i> Km <sup>R</sup> , <i>ori</i> pBBR1, $P_{tuf}$ - <i>mCherry</i> Km <sup>R</sup> , <i>ori</i> pBBR1, $P_{em7}$ - <i>mCherry</i> Sm <sup>R</sup> , <i>ori</i> pRO1600/ColE1, $P_{em7}$	This study This study This study This study (Benedetti et al., 2016)
pEMG	Km <sup>R</sup> , <i>ori</i> R6K, <i>lacZ</i> $\alpha$ with two flanking I-SceI sites	(Martinez-Garcia and de Lorenzo, 2011)
pVI260	Cb <sup>R</sup> , <i>lacI</i> <sup>Q</sup> / $P_{tac}$ - <i>dmpKLMNOP</i>	(Bartilson et al., 1990)

### 2.2. Recombinant DNA procedures

Molecular cloning was performed according to standard protocols (Sambrook et al., 1989). All further details regarding the construction of synthetic promoters and genomic mutants are provided in the Supplementary information (Supplement S1, S2, S3).

### 2.3. Batch cultivation in shake flasks

*P. putida* KT2440 was grown in minimal medium, which contained the following components per liter: 7.5 g of glucose, 2 g of (NH<sub>4</sub>)<sub>2</sub>SO<sub>4</sub>, 7.75 g of K<sub>2</sub>HPO<sub>4</sub>, 4.25 g of NaH<sub>2</sub>PO<sub>4</sub>·2H<sub>2</sub>O, 0.1 g of MgCl<sub>2</sub>·6H<sub>2</sub>O, 10 mg of EDTA, 5 mg of FeSO<sub>4</sub>·7H<sub>2</sub>O, 1 mg of CaCl<sub>2</sub>·2H<sub>2</sub>O and 1 mL of a trace element stock solution. The trace element stock solution contained the following components per liter: 2 g of ZnSO<sub>4</sub>·7H<sub>2</sub>O, 1 g of MnCl<sub>2</sub>·2H<sub>2</sub>O, 0.4 g of CoCl<sub>2</sub>·6H<sub>2</sub>O, 0.3 g of Na<sub>2</sub>B<sub>4</sub>O<sub>7</sub>, 0.2 g of Na<sub>2</sub>MoO<sub>4</sub>·2H<sub>2</sub>O, 0.2 g of CuSO<sub>4</sub>·5H<sub>2</sub>O, and 0.2 g of NiCl<sub>2</sub>·6H<sub>2</sub>O. After mixing all the components, the pH value of the medium was adjusted to pH 7.0 using 2 M NaOH or 2 M HCl. Kanamycin (50 mg L<sup>-1</sup>) was added to the medium when growing plasmid-containing strains. Cells from a cryo-stock were first grown overnight on agar plates containing the minimal medium supplemented with 15 g L<sup>-1</sup> agar (Becton and Dickinson). Colonies were then inoculated into liquid pre-cultures in baffled shake flasks filled with 10% minimal medium, and the flasks were incubated on a rotary shaker (30 °C, 230 rpm; Multifors, Infors AG, Switzerland). During the exponential growth phase, cells were harvested by centrifugation (5 min, 4 °C, 8000  $\times$  g), washed once with fresh medium and then used

as inocula for the main culture, which was carried out as described above. During the degradation, production, and tolerance-testing experiments, the corresponding substrates were added from sterilized stocks either at the beginning of or during cultivation, as specified below. Unless otherwise stated, experiments comprised three biological replicates.

#### 2.4. Promoter screening in miniaturized bioreactors

Parallelized cultivation was carried out in 48-well FlowerPlates (m2p-labs GmbH, Baesweiler, Germany) in a parallelized bioreactor system, which was operated at 30 °C and 1300 rpm and in 85% humidity (BioLector, m2p-labs GmbH, Baesweiler, Germany). Each well was filled with 1 mL of minimal medium, which was prepared as described above, including the addition of kanamycin, but differed in the amount of glucose added (5 g L<sup>-1</sup>). Pre-cultures, grown as described above, served as inocula for the experiments. Cell concentration was measured on-line as the optical density at 620 nm (OD<sub>620</sub>). On-line fluorescence measurements of the reporter proteins used the following specific wavelengths for excitation/emission: 458/488 nm for CFP, 480/520 nm for msfGFP, and 580/610 nm for mCherry. In each case, the basal fluorescence of cells containing a vector without promoter was used to correct the data. For determination of the specific strength of a promoter, the corrected fluorescence signal, obtained in relative fluorescence units (RFU), was plotted against the measured cell concentration (Zobel et al., 2015). The slope derived from the correlation, expressed in specific fluorescence units (SFU), was assigned to the specific promoter activity (Alper et al., 2005). All experiments were conducted as three biological replicates.

#### 2.5. Catechol tolerance and degradation testing

To test catechol tolerance, cultivation was carried out in the parallelized bioreactor system as described above. The cell concentration was measured on-line as the optical density at 620 nm (OD<sub>620</sub>). With increasing catechol levels, the cells exhibited increasing length of the lag phase before starting to grow exponentially. In this case, the specific growth rate ( $\mu$ ) during the exponential growth phase was obtained by plotting the regression of  $\ln(\text{OD}_{620})$  over time. In addition, the duration of the lag phase was monitored. Cases in which the lag phase lasted for more than 72 h, i.e., the cell concentration did not increase during this time period, were considered to exhibit zero growth ( $\mu = 0$ ). Furthermore, the cells were analyzed for their capacity to convert catechol to MA. For this purpose, the conversion rate was determined by following the degradation of 2.5 mM catechol, which was added to cultures growing exponentially on glucose at a cell concentration of approximately 0.25 g (cell dry mass) L<sup>-1</sup>. The obtained rate was then corrected for the mean cell concentration during the incubation period, which yielded the specific catechol degradation rate (mmol g<sup>-1</sup> h<sup>-1</sup>). This measurement was additionally performed using cells that had been pre-induced with 5 mM benzoate at the beginning of culture growth. All experiments were conducted in three biological replicates.

#### 2.6. Hydrothermal depolymerization of lignin

Hydrothermal conversion was conducted in a 500-mL stirred, stainless steel pressure vessel (4575A, Parr Instruments, Moline, IL, USA). A suspension of 7.5 g of pine lignin (IndulinAT, S3Chemicals, Bad Oeynhausen, Germany) in 250 mL of demineralized water was added to the vessel, and then, the reactor was sealed. Subsequently, the stirrer speed was set to 400 rpm and nitrogen gas was used to purge the reactor five times. Hydrothermal conversion was conducted for 1 h at 395 °C. Then, the reactor was cooled down by using the internal cooling coil, flushing with cold water (8 °C) and using an external fan. Debris was separated from the obtained hydrolysate by centrifugation (10,000 × g, 5 min, room temperature). The process was repeated twelve times. The

supernatants from all the runs were combined and concentrated (RVC 2–33 IR vacuum concentrator, Christ Gefriertrocknungsanlagen, Osterode, Germany) to be used as raw material for MA production.

#### 2.7. Lab-scale production of MA from catechol

The production was conducted as a fed-batch process (30 °C, pH 7.0) in a 1-L bioreactor (DASGIP, Jülich, Germany). The pre-culture incubation and the preparation of the inoculum was performed as described above. The batch medium (500 mL) contained the following components per liter: 1.8 g of glucose, 15 g of (NH<sub>4</sub>)<sub>2</sub>SO<sub>4</sub>, 1.55 g of K<sub>2</sub>HPO<sub>4</sub>, 0.85 g of NaH<sub>2</sub>PO<sub>4</sub>·2H<sub>2</sub>O, 1.0 g of MgCl<sub>2</sub>·6H<sub>2</sub>O, 10 mg of EDTA, 10 mg of FeCl<sub>3</sub>·6H<sub>2</sub>O, 1 mg of CaCl<sub>2</sub>·2H<sub>2</sub>O, 1 mL of the above-mentioned trace element solution and 200 mg of Antifoam 204 (Sigma-Aldrich, Taufkirchen, Germany). The initial rate of aeration with pressurized air was set to 500 mL min<sup>-1</sup>. Throughout the culture period, the dissolved oxygen level was maintained above 50% saturation by adjusting stirrer speed and aeration rate. The reactor was operated as a pH-stat, coupling the addition of catechol as a substrate to automatic pH control (van Duuren et al., 2012; Wittmann et al., 1995). A decrease in pH value, indicating the conversion of catechol to MA, simultaneously triggered the addition of fresh catechol and the addition of alkali for pH correction. For this step, catechol (2.5 M) and NaOH (6 M) were connected to the reactor as separate solutions. The catechol feed was degassed using nitrogen to prevent oxidation. In addition, a nutrient feed was supplied to the cells with growth-promoting ingredients. The concentrated feed contained the following components per liter: 600 g of glucose, 50 g of (NH<sub>4</sub>)<sub>2</sub>SO<sub>4</sub>, 1.55 g of K<sub>2</sub>HPO<sub>4</sub>, 0.85 g of NaH<sub>2</sub>PO<sub>4</sub>·2H<sub>2</sub>O, 10 g of MgCl<sub>2</sub>·6H<sub>2</sub>O, 20 mg of EDTA, 20 mg of FeCl<sub>3</sub>·6H<sub>2</sub>O, 2 mg of CaCl<sub>2</sub>·2H<sub>2</sub>O, 10 mL of the above-mentioned trace element solution and 200 mg of Antifoam 204 (Sigma-Aldrich, Taufkirchen, Germany). The imposed rate of nutrient feed ( $F$ , mL h<sup>-1</sup>) was increased exponentially over time to allow the cells to grow at a specific low growth rate ( $\mu_{\text{set}} = 0.04 \text{ h}^{-1}$ ) (Eq. (1)).

$$F = \left( \frac{\mu_{\text{set}}}{Y_{X/S}} + m_s \cdot e^{0.02(t-t_0)} \right) \cdot \frac{V_L X_0 e^{\mu_{\text{set}}(t-t_0)}}{S_0} \quad (1)$$

In addition, the feed term considered the fact that the energy requirement for maintenance of the cells increased during the process. The biomass yield of *P. putida* grown on glucose ( $Y_{X/S} = 0.4 \text{ g g}^{-1}$ ) and the maintenance coefficient ( $m_s = 0.037 \text{ g g}^{-1} \text{ h}^{-1}$ ) were obtained from a previous study (van Duuren, 2013), whereas the current working volume ( $V_L$  in mL), cell dry mass (CDM) concentration at the beginning of the feed phase ( $X_0$ , g<sub>CDM</sub> L<sup>-1</sup>), and glucose concentration in the feed ( $S_0$ , g L<sup>-1</sup>) were all estimated from the corresponding experiment in this study. Advanced process configurations in the form of a regeneration fed-batch included phases lacking catechol dosing but involving pure nutrient feeding and pH control, as described below. The fed-batch processes were conducted as two biological replicates.

#### 2.8. Lab-scale production of MA from benzoate

The production of MA from benzoate was carried out in a 1-L bioreactor using the same settings that were used for catechol with one exception: benzoate (1.2 M) and NaOH (2.9 M) were added together as a single feed. The fed-batch process was conducted as two biological replicates.

#### 2.9. Lab-scale production of MA from a mixture of catechol and phenol

The production was conducted as miniaturized fed-batch process in shake flasks and included three biological replicates. The pre-culture scheme was as described above. The main culture was grown in 50 mL of minimal medium with 5 g L<sup>-1</sup> glucose. In addition, 40 feed beads (Kuhner, Birsfelden, Switzerland) were added, which continuously

released approximately  $0.13 \text{ g L}^{-1} \text{ h}^{-1}$  of glucose during the process. Starting two hours after inoculation, a mixture of catechol and phenol was added pulse wise. Every hour, 100- $\mu\text{L}$  shots were added from a concentrated stock (625 mM catechol, 125 mM phenol), each of which increased the level of catechol and phenol by 1.25 mM and 0.25 mM, respectively. The feed rates of the aromatics were chosen on the basis of the estimated specific conversion rates of the cells in batch culture (Fig. 8A). The pH value was kept constant at  $7.0 \pm 0.2$  by manual addition of 1.5 M NaOH.

#### 2.10. Lab-scale production of MA from lignin

The fed-batch production was carried out in a 100-mL bioreactor (DASGIP, Jülich, Germany). The pre-culture scheme, medium and different process parameters were essentially the same as those of the catechol-based fed-batch; however, the liquid volume was scaled down to 50 mL, and the concentrated lignin hydrolysate was added pulse-wise according to the actual catechol level in the broth, which was monitored using HPLC (see below).

#### 2.11. MA recovery and lab-scale purification

A straightforward purification process was used to recover MA from the culture broth (Vardon et al., 2015). For purification from the lignin-based fermentation, the decolorization step was conducted twice. After removal of the activated carbon by filtration, MA was precipitated by acidification to pH 1.5 with 37% HCl. In addition to the previously described protocol, the obtained crystals were washed once with deionized water and lyophilized (Christ Gefriertrocknungsanlagen, Osterode am Harz, Germany) to finally obtain a white crystalline powder.

#### 2.12. Pilot-scale production of MA from catechol

Pilot-scale fed-batch production of MA was carried out in a 72-L bioreactor (Biostat UD, B. Braun, Melsungen, Germany) using the optimal settings identified during lab-scale production (see above). The initial batch volume was 30 L. To avoid phases of catechol limitation and dosing interruption, the catechol feed was not only added in response to the pH trigger but was also supplied at a constant basal rate of  $20 \text{ mL h}^{-1}$ . When necessary, regeneration phases were integrated by deactivating the catechol feed and switching to pure NaOH titration until growth was recovered.

#### 2.13. MA recovery, purification and quality analysis at the pilot scale

Cells were separated from the broth using crossflow microfiltration (UFI-TEC, Oranienburg, Germany) with 0.2- $\mu\text{m}$  membranes (TAMI Industries, Nyons, France). Subsequently, 32% HCl was added to the filtrate until the pH value was less than 2. After the precipitation of white crystals, the depleted supernatant was discarded. The crystals were washed once in water to dissolve remaining impurities. A white and crystalline powder was obtained via spray drying of the suspension at  $50 \text{ }^\circ\text{C}$  (Mobile Minor, GEA, Soeborg, Denmark). Further details are provided in the Supplementary information (Supplement S4). In addition, the product was analyzed by HPLC, as described below, and by GC/MS (Barton et al., 2018). The analysis also included measurement of the elemental composition (CHNS, VARIO EL III, Elementar Analysensysteme, Langensfeld, Germany). In addition, the ion content was determined via cation and anion chromatography (Neu et al., 2016). Trace elements were monitored using inductively coupled plasma optical emission spectrometry (ICP-OES) (Wirth and Mumme, 2013).

#### 2.14. Hydrogenation of MA to adipic acid

Purified MA (426 mg, 3.00 mmol) was dissolved in dry

tetrahydrofuran (30 mL), and Pd on charcoal was added (300 mg, 5% Pd, 0.15 mmol). Catalytic hydrogenation was performed in a 170-mL hydrogenation reactor (Berghof, Eningen, Germany) in a hydrogen atmosphere (40 mbar) under stirring for 3 h at  $40 \text{ }^\circ\text{C}$ . The catalyst was removed by filtration through Celite (Sigma-Aldrich), which was followed by removal of the solvent under reduced pressure to yield adipic acid as a colorless solid (492 mg, 2.74 mmol, 91%). The purity of the product was verified by NMR spectroscopy and GC/MS analysis of the bis-*tert*-butyldimethylsilyl ester. This ester was obtained by reacting adipic acid (3 mg) with *tert*-butyldimethylsilyl chloride (TBSCl, 15 mg) and imidazole (7 mg) in DMSO (100  $\mu\text{L}$ ). The reaction mixture was heated for 1 h at  $60 \text{ }^\circ\text{C}$ . Water (400  $\mu\text{L}$ ) was added, and the aqueous phase was extracted with  $\text{Et}_2\text{O}$  (300  $\mu\text{L}$ ). The organic phase was dried with  $\text{MgSO}_4$  and analyzed by GC/MS using a 7890B GC connected to a 5977A mass detector (Agilent, Santa Clara, CA, USA) and separated on an HP5-MS fused silica capillary column (30 m, 0.25 mm i. d., 0.50- $\mu\text{m}$  film) with He as a carrier gas at a flow rate of  $1.2 \text{ mL min}^{-1}$ .

#### 2.15. Polymerization of bio-based adipic acid to nylon 6,6

Adipic acid was first reacted for 1 h with thionyl chloride at  $80 \text{ }^\circ\text{C}$  to obtain the corresponding salt. After cooling to room temperature, the di-acid chloride was dissolved in cyclohexane. Hexamethylene diamine (HMDA, 5% in  $\text{H}_2\text{O}$ ) was poured into a 20-mL glass vial, which was followed by careful addition of the solution of adipic acid in cyclohexane as a top layer. After cautious basification of the bottom layer, i.e., the HMDA solution, with 20% NaOH and waiting briefly for polycondensation to occur, the nylon thread formed was pulled out at the interface between the two immiscible phases.

#### 2.16. Quantification of cells, substrates and products

The cell concentrations of the shake flask and bioreactor cultures were monitored spectrophotometrically at 600 nm ( $\text{OD}_{600}$ ). To determine the CDM, cells were collected on pre-weighed and dried membrane filters (0.2  $\mu\text{m}$ , regenerated cellulose, 47 mm, Sartorius, Germany) using vacuum filtration. Then, the filters were washed with 0.9% NaCl and deionized water and then dried at  $80 \text{ }^\circ\text{C}$  until a constant weight was attained. A correlation factor of CDM [ $\text{g L}^{-1}$ ] =  $0.54 \times \text{OD}_{600}$  was determined. For experiments conducted in the parallelized bioreactor system, the cell concentrations were measured on-line (see above). Glucose was quantified using an enzyme kit (R-Biopharm, Darmstadt, Germany). Gluconate and 2-ketogluconate were quantified as described previously (Poblete-Castro et al., 2013). Aromatics and related metabolites were analyzed by HPLC as described previously (Barton et al., 2018). Further details are given in the Supplementary information (Supplement S5).

#### 2.17. Catechol 1,2-dioxygenase activity

Catechol 1,2-dioxygenase activity was measured as described previously (Jiménez et al., 2014). The specific enzyme activity was given in U (mg cell protein) $^{-1}$ .

#### 2.18. Quantification of energy parameters

Culture broth containing approximately 2.5 mg of CDM was harvested via vacuum filtration (0.45- $\mu\text{m}$  mixed cellulose esters membrane filters, 47 mm, Millipore). Filters were quickly cooled to  $-70 \text{ }^\circ\text{C}$  in pre-cooled tubes, which were filled with 60% (v/v) methanol in a dry ice/ethanol bath and incubated for extraction at the same temperature for 20 min with thorough mixing. After centrifugation (5 min,  $-20 \text{ }^\circ\text{C}$ , 8000  $\times g$ ), the supernatant was diluted with ice-cold water until the concentration of the residual methanol was less than 20% (v/v), and the sample was then frozen at  $-80 \text{ }^\circ\text{C}$  and lyophilized. The lyophilisate was resuspended in 0.5 mL of ATP assay buffer (ab83395, Abcam, UK),

which was followed by removal of the cellular proteins (10 kDa, Vivaspin 500, GE Healthcare, UK) for 30 min at 4 °C. The ATP content in the deproteinized extract was quantified using a colorimetric kit (ab83395, Abcam, UK). In addition, the sum of the ATP and ADP was determined by the colorimetric assay after pre-incubation of the deproteinized extract (100 µL) with 25 µL of a reaction buffer (75 mM potassium phosphate (pH 7.3), 15 mM MgCl<sub>2</sub>, 0.5 mM phosphoenolpyruvate and 20 µg of pyruvate kinase). This buffer converted all the ADP to ATP prior to the measurement. The sum of all three adenine nucleotides (ATP, ADP and AMP) was measured by the colorimetric assay after pre-incubation of the extract (100 µL) with 25 µL of a reaction buffer that now additionally contained 25 µg of myokinase to also convert AMP to ATP. In each case, pre-incubation was conducted for 15 min at 37 °C and then stopped by heating for 2 min to 100 °C. The concentrations of ATP, ADP and AMP were then obtained from the differences in the absorbance readings (Chapman et al., 1971). The adenylate energy charge (AEC), i.e., the energy level (Atkinson, 1968), was calculated according to the following formula (Eq. (2)):

$$AEC = \frac{[ATP] + \frac{1}{2}[ADP]}{[ATP] + [ADP] + [AMP]} \quad (2)$$

### 3. Results

#### 3.1. The basic producer *P. putida* MA-1 accumulates stoichiometric amounts of MA from catechol but suffers from weak tolerance

In a first step, the genome-based basic producer *P. putida* MA-1 was constructed by deletion of the *catBC* genes. As expected and as shown before (van Duuren et al., 2011), the elimination of *catBC* activity resulted in accumulation of MA from catechol and the model compound benzoate (Fig. 1AB). The MA yield from both substrates was 100%. When incubated with catechol from the beginning, the cells suffered from a prolonged lag phase and took approximately three times longer to complete the conversion of catechol to MA than when incubated with benzoate. *P. putida*. MA-1 was found to be sensitive to catechol. Catechol concentrations greater than 2 mM caused reduced growth rates (Fig. 2A), leading to a 50% growth reduction at an inhibitory catechol concentration (K<sub>i</sub>) of 7 mM. At 8 mM catechol, cell growth was completely inhibited. In addition, elevated levels of catechol caused substantial lengthening of the lag phase. Treatment of cells pre-incubated with glucose and already in the exponential growth phase with a low level of catechol exhibited greatly increased rates of degradation of the aromatic (Fig. 2B). The MA-1 strain utilized 2.5 mM catechol in less than an hour, corresponding to a specific conversion rate of 10 mmol g<sup>-1</sup> h<sup>-1</sup> (Fig. 3A). Cells that had been additionally pre-induced with benzoate, in fact, exhibited a 40% increase in activity (Fig. 2C, Fig. 3A). Under both conditions, the activity of the MA-1 strain was remarkably higher than that of the wild type. The MA-1 strain was also found to exhibit higher activity than the previously reported producer *P. putida* KT2440-JD1. The latter degraded catechol only when pre-induced with benzoate, and even then, degradation occurred at a much lower rate than that observed with the MA-1 strain. The differences in degradation rate were reflected by differences in catechol 1,2-dioxygenase activity, suggesting that the expression of this enzyme was a major factor that determined catechol conversion (Fig. 3B).

#### 3.2. *P. putida* MA-1 exhibits limited MA production in a catechol-based fed-batch process, but performs well on benzoate

When used in a catechol-based fed-batch process, the MA-1 strain attained a final MA titer of 19.5 g L<sup>-1</sup> within 50 h (Fig. 4AB). The catechol feed was started after 7 h. Initially, the chosen strategy worked well. As intended, the catechol was limiting, and MA was the only secreted product. After approximately 25 h, however, the performance

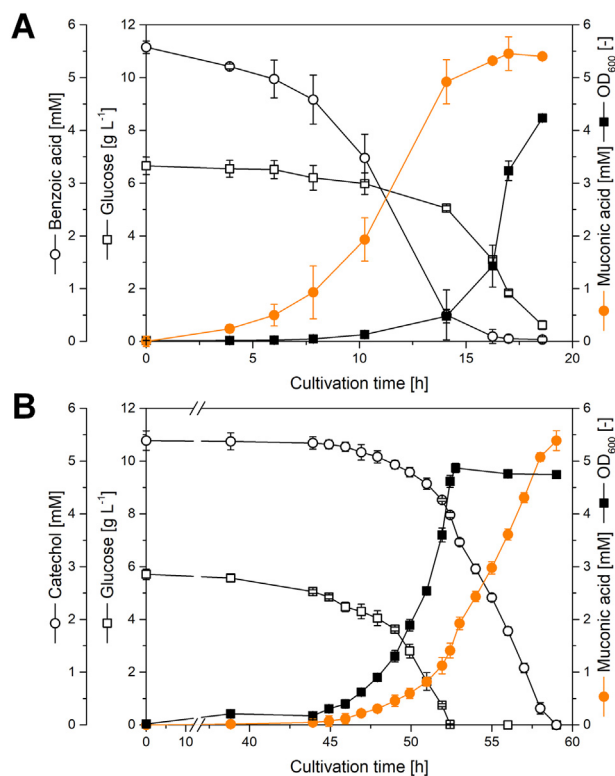


**Fig. 1.** Growth and *cis,cis*-muconic acid production by the engineered producer *Pseudomonas putida* KT2440 MA-1 in a mixture of benzoate plus glucose (A) and in a mixture of catechol plus glucose (B). The data reflect mean values and standard deviations of three replicates.

suddenly collapsed. The cells started to accumulate unmanageable levels of 2-ketogluconate and catechol. A catechol level of approximately 2.5 g L<sup>-1</sup> (45 mM) was rapidly attained, which stopped further growth and MA production. Toward the end of the process, the cells continued to convert glucose to 2-ketogluconate. The strain performed much better when benzoate was used instead of catechol. In an otherwise identical process setup, the product titer almost tripled to 48 g MA L<sup>-1</sup> (Fig. 4CD). Cell growth was maintained until the end, and benzoate did not accumulate in any phase of the process, as intended. Small amounts of gluconate were accumulated, corresponding to less than 1% of the glucose consumed.

#### 3.3. Regeneration during fed-batch production from catechol leads to recovery of the energy level in *P. putida* MA-1 and boosts the MA titer

To better understand the poor performance during the catechol fed-batch process and to eventually use the results to improve the setup, the fermentation was repeated with additional measurement of cellular energy parameters (Fig. 5ABCD). The process was initiated in a manner similar to the previous experiment. The catechol feed was added after 7 h, which initially resulted in the exclusive formation of MA. After approximately 15 h, the cells again started to accumulate 2-ketogluconate and catechol, halted growth, and slowed down production. The process conditions had a drastic impact on the energy levels of the cells in the bioreactor. The ATP content of the cells was highest, i.e., approximately 6 µmol g<sup>-1</sup>, during the initial batch phase of exponential growth in excess glucose (T1) (Fig. 5B). The value decreased slightly under glucose limiting conditions (T2) and decreased further upon switching to producing conditions and upon addition of catechol (T3). At all these initial time points, however, the energy level of *P. putida* MA-1, i.e., the AEC, remained above 0.7 (Fig. 5D) and thus within the range required for vital cells (Martínez-García et al., 2014). With

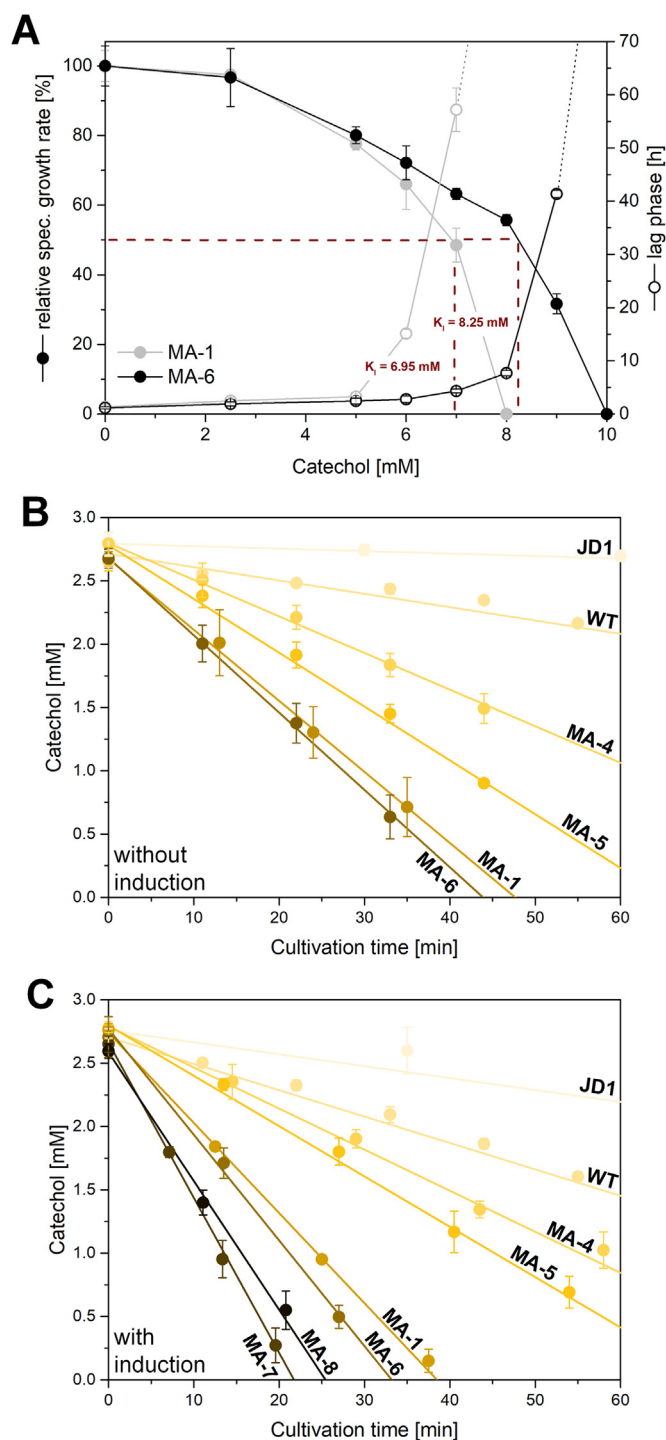


**Fig. 2.** Metabolic engineering of *Pseudomonas putida* KT2440 for enhanced tolerance to catechol (A) and enhanced utilization of catechol (B, C). The tolerance features include the lag phase and the exponential rate of growth on glucose in the presence of different levels of catechol. The latter is provided as relative value, normalized to the control without catechol (100%). The degradation of catechol was monitored for non-induced cells (B) and for cells pre-induced with 5 mM benzoate (C). In all strains except the wild type (WT), stoichiometric amounts of *cis,cis*-muconic acid were formed. The genetic background of the studied strains is given in Table 1. The data reflect mean values and standard deviations of three replicates.

further catechol feeding, however, the metabolism became perturbed: the AEC collapsed to a value below 0.4, which was associated with the lowest cellular ATP content observed during the process (T4). Notably,

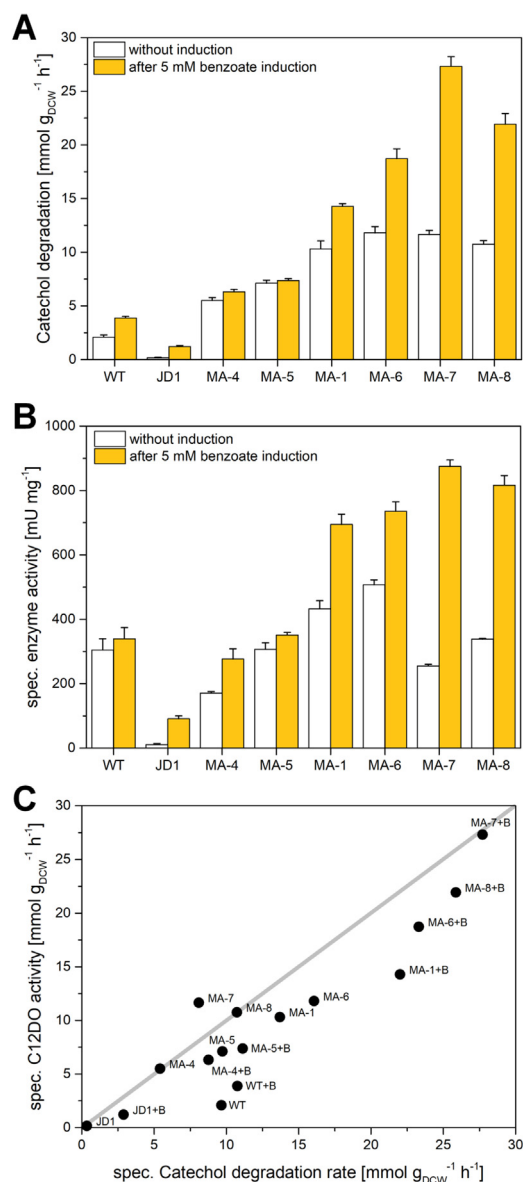


**Fig. 3.** Metabolic engineering of *Pseudomonas putida* KT2440 for enhanced catechol 1,2-dioxygenase activity. Specific catechol degradation rate of non-induced cells and cells pre-induced with 5 mM benzoate (A); enzymatic activity in crude cell extract of non-induced cells and cells pre-induced with 5 mM benzoate (B); and correlation between *in vivo* activity and *in vitro* enzyme capacity under all studied conditions (C). The genetic backgrounds of the studied strains are given in Table 1. The *in vivo* activity matched the specific degradation rate. The *in vitro* capacity (mmol g<sub>CDM</sub><sup>-1</sup> h<sup>-1</sup>) was deduced from the enzyme activity (U (mg cell protein)<sup>-1</sup>), considering 1 mg of CDM to contain 0.53 mg of cell protein. The data reflect mean values and standard deviations of three replicates.

the depleted energy level was accompanied by a change in the cell color from white to dark brown and even black (Fig. 5C). The affected energy metabolism coincided with the secretion of 2-ketogluconate and the loss of production performance. A phase of regeneration without further addition of catechol, but continued feeding of glucose, restored the growth of the cells completely, while the transiently accumulated amounts of 2-ketogluconate and catechol were completely degraded. The onset of catechol feeding after approximately 40 h then started a phase of extremely high productivity. Within only 15 h, the MA titer increased to a final value of 64.2 g L<sup>-1</sup>. The MA yield from catechol was 100%. The product yield, which was associated with the fed glucose, was 2.4 (mol MA) (mol glucose)<sup>-1</sup>. Cell vitality was fully restored



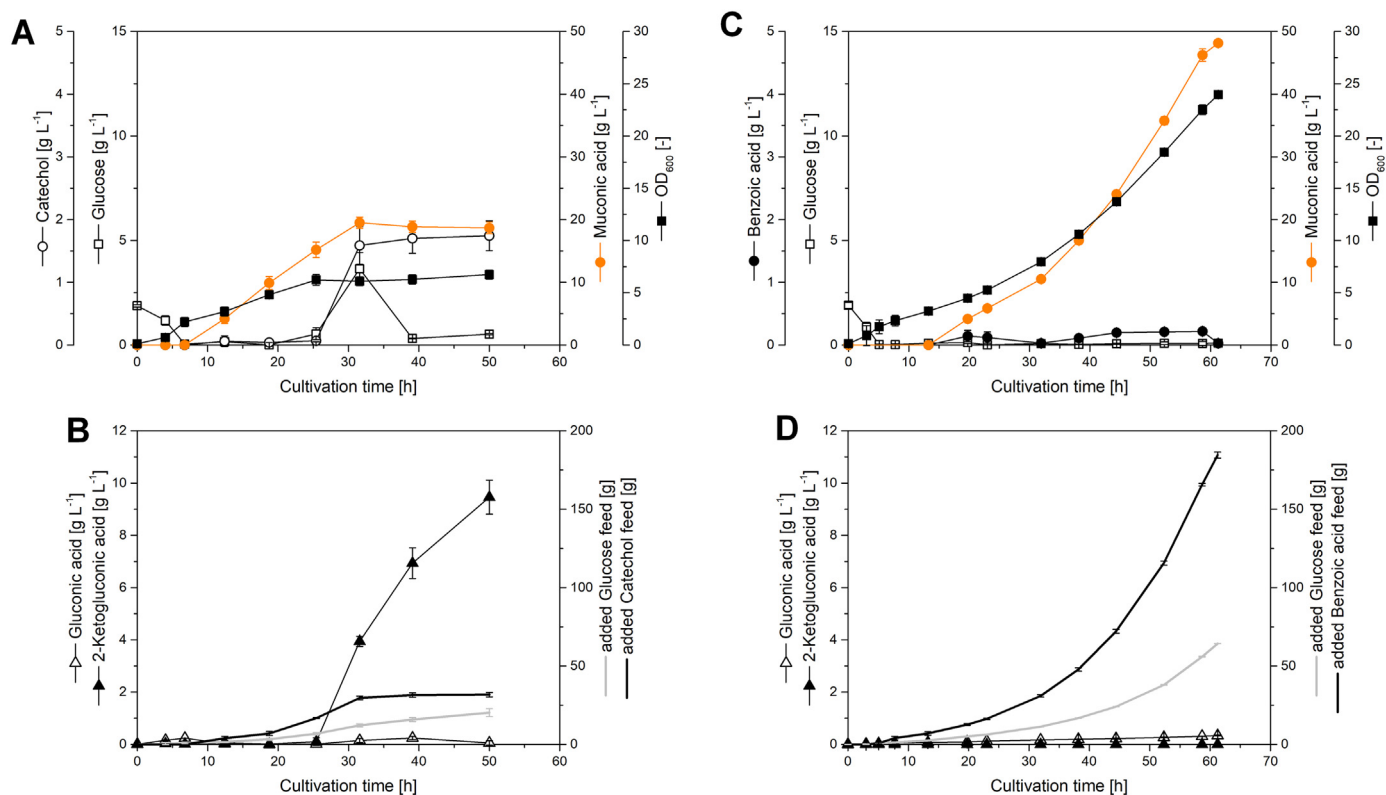


**Fig. 4.** Production performance of the engineered producer *Pseudomonas putida* KT2440 MA-1 on catechol and benzoate using a fed-batch bioreactor process. The automatic addition of catechol (A,B) or benzoate (C,D) as the substrate for *cis,cis*-muonic acid production, was coupled to the acidification of the medium (pH stat). For cell growth, an initial batch phase on glucose was followed by a feeding phase, adding further glucose to support growth at a reduced rate and during increased maintenance requirement. The data reflect mean values and standard deviations of two replicates.

during the regeneration phase, as demonstrated by the increased energy charge and ATP yield (T5, T6). Although the cells subsequently exhibited slight accumulation of 2-ketogluconate again, the high levels of MA production by the cells were retained until end of the process. MA was purified from the broth at 98.7% purity. To facilitate subsequent rounds of genomic engineering, the two endonucleases-coding genes *endA-1* and *endA-2* were deleted from the genome, yielding the strains MA-2 ( $\Delta endA-1$ ) and MA-3 ( $\Delta endA-1 \Delta endA-2$ ).

### 3.4. Modulation of *catA* expression by strong synthetic promoters does not outperform the native regulatory system

The distinctly weak tolerance of *P. putida* to catechol appeared to be unfavorable for high-level MA production. Boosting the expression of *CatA*, the major catechol-converting enzyme in this microbe (Jiménez et al., 2014), appeared to be a promising strategy to overcome this limitation. For this purpose, a library of synthetic promoters was generated to be coupled to the *catA* gene, using red fluorescent protein mCherry as a reporter system (see Supplement S6, S7). The homologous promoters  $P_{gro}$  (Martínez-García et al., 2014) and  $P_{tuf}$  (Becker et al., 2005) were chosen as starting points. In addition, the heterologous  $P_{em7}$  promoter, a synthetic promoter from the phage T7 (Zobel et al., 2015), was selected. This method yielded approximately 20 synthetic promoters that exhibited pronounced differences in color intensity (Fig. 6A) and expression strength (Fig. 6B). With respect to enhancement of the expression of *catA*, a subset of strong promoters appeared to be most promising. The achieved increase in promoter strength was substantial, i.e., 4-fold for  $P_{tufts-1}$ , 19-fold for  $P_{gro-4}$ , and 25-fold for  $P_{em7-2}$ . In addition, selected variants of  $P_{tuf}$  and  $P_{tufts}$  exhibited down-regulation of promoter activity by 2.5-fold ( $P_{tuf-1}$ ) and 1.3-fold ( $P_{tufts-2}$ ). All promoters were sequenced (see Supplement S6). The strains *P. putida* MA-4 and MA-5 expressed the genomic *catA* copy under the control

of the *em7* and *em7-2* promoters, respectively, instead of the native *cat* promoter. The mutated *em7-2* promoter enabled significantly higher catechol conversion than the original *em7* version (Fig. 3AB). Each strain exhibited a similar degradation rate with and without benzoate induction, as desired. Surprisingly, MA-5, which contained one of the strongest promoters of the synthesized library, did not outperform the MA-1 strain, which carried the native promoter region for *catA* expression. In fact, the catechol conversion rate of MA-5 was significantly lower than that of MA-1. The under-performance of the synthetic control was approximately 25% for non-induced cells and even 50% for cells pre-incubated with benzoate.

### 3.5. Additional *catA2* expression under the strong *cat* promoter significantly enhances catechol conversion and strain robustness

The positive effect of benzoate on catechol conversion (Fig. 3) and MA production (Fig. 4) indicated the beneficial contribution of the second catechol 1,2-dioxygenase, encoded by the *catA2* gene in *P. putida* (Jiménez et al., 2014). This gene is located downstream of the catabolic *ben* operon and is known to be induced by benzoate. Therefore, the next step of strain engineering was aimed at improving the use of this additional enzyme independently from the requirement for benzoate induction. The natural *cat* promoter, which enabled the high catechol conversion rate in the MA-1 strain, appeared most promisingly to also support *catA2* expression. Accordingly, a second genomic copy of the *catA2* gene was inserted downstream of the *catA* gene under the control of the native *cat* promoter. The generated mutant was designated *P. putida* MA-6. This mutant exhibited a significant increase in the catechol conversion rate, up to  $17 \text{ mmol g}^{-1} \text{ h}^{-1}$  (Fig. 2BC). In addition, MA-6 exhibited a 20% improvement in tolerance towards catechol ( $K_i = 8.3 \text{ mM}$ ) (Fig. 2A). In a fed-batch process, the fortified *P. putida* MA-6 strain accumulated  $36 \text{ g L}^{-1}$  MA within only 24 h at a yield of 1.0

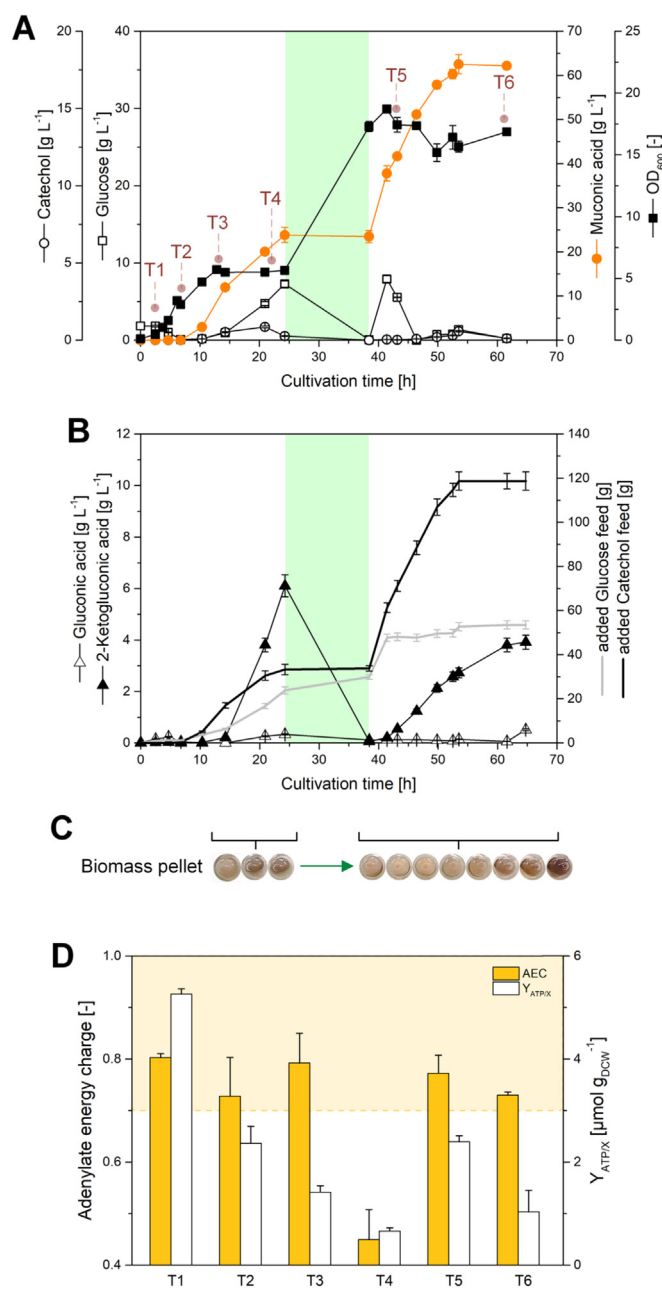


**Fig. 5. Advanced production of *cis,cis*-muonic acid from catechol by *Pseudomonas putida* KT2440 MA-1 using a fed-batch bioreactor process with transient cell regeneration.** During the initial phase, the automatic addition of catechol was coupled to acidification of the medium (pH stat). From 25–40 h of process time, the catechol feed was stopped but was then switched to the pH-coupled feeding again. The data comprise the cultivation profile (A, B), the color of the producing cells at different time points of cultivation (C), and the ATP yield and adenylate energy charge at time points T1 to T7 during fermentation. The data reflect mean values and standard deviations of two replicates.

(mol MA) (mol catechol)<sup>-1</sup> (Fig. 7). This yield surpassed that obtained with the MA-1 strain under comparable process settings. The achieved titer increased by almost 80%. The specific MA productivity and the volumetric productivity both exhibited 7.5-fold enhancement (Table 3).

### 3.6. Further enhancement of catechol 1,2-dioxygenase expression leads to faster conversion, but no further gain in strain robustness

Further rounds of metabolic engineering included additional copies

of catechol 1,2-dioxygenase-encoding genes into the genome of *P. putida*. The two producers MA-1 and MA-6 were each equipped with an additional complete catechol cluster in their genomes, i.e., P<sub>cat</sub> *catA catA2*. Accordingly, the strain MA-7 expressed the two clusters P<sub>cat</sub> *catA* and P<sub>cat</sub> *catA catA2* and revealed the highest conversion rate among the constructed strains. This strain also exhibited the highest levels of catechol 1,2-dioxygenase activity (870 mU mg<sup>-1</sup>). The strain MA-8, which contained a fully duplicated P<sub>cat</sub> *catA catA2* operon, did not exhibit further improvement in the catechol conversion rate. Neither of the two duplicate cluster strains, however, were more tolerant than the MA-6 strain or exhibited improved MA production (data not shown).

### 3.7. Genomic expression of phenol hydroxylase enables simultaneous conversion of catechol and phenol to MA and extends the substrate spectrum to cresols

The phenol hydroxylase genes *dmpKLMNOP* from *P. putida* CF600 were engineered into the genome of *P. putida* MA-6. The resulting fully genome-based mutant was designated MA-9. This mutant was capable of degrading phenol, as expected (data not shown). In a mixture with catechol, mimicking a lignin hydrolysate, phenol was co-consumed, although at a low rate (Fig. 8A). In this process, both aromatics were converted into MA to obtain a yield of 1 mol mol<sup>-1</sup>. The potential of the MA-9 strain for increased MA production from catechol and phenol was then investigated by a miniaturized fed-batch process in shake flasks (Fig. 8B). Upon pulse-wise feeding of catechol and phenol, the cells accumulated MA constantly without any loss in performance and attained a final MA titer of 6 g L<sup>-1</sup> after approximately 25 h. The levels of the two aromatics remained low throughout the process. The cells grew during the initial batch phase. Subsequently, with limited addition of glucose and by using feed beads, the cells were maintained in an active state without promoting further growth. Additional experiments revealed that MA-9 also used methylated phenols. GC/MS analysis indicated that the products formed were not MA but structurally related compounds (Fig. S3). Compared to MA, all prominent fragment ions were shifted by a mass-to-charge ratio (*m/z*) of 14 units. Given that cresols possess an additional methylene group not possessed by phenol, the products were determined to be methylated MA (Fig. 8C): 2-methyl muconic acid for *o*-cresol and *m*-cresol and 3-methyl muconic acid for *p*-cresol (Table 4). The position of the methyl group was specific for each cresol isomer and was a result the microbe using the *ortho*-pathway for cleavage of methylated variants of catechol (An et al., 2001). Transiently, small amounts of 3-methyl-catechol accumulated during the formation of 2-methyl-MA (data not shown). The conversion of the cresols was enabled by phenol hydroxylase. The parent strain MA-6, lacking this enzyme, did not have this capability.

### 3.8. The engineered producer *P. putida* MA-9 enables cascaded chemical and biological conversion of lignin to nylon 6,6

The cascaded process started with the depolymerization of lignin as a first step. For this purpose, softwood lignin was hydrolyzed to defined aromatic monomers by hydrothermal treatment in supercritical water. To provide sufficient material for the fermentation process, the hydrothermal lignin treatment was repeated twelve times. Incubation in a pressurized reactor provided a liquid phase with small aromatics, which was then concentrated (Table 2). The concentrates from all runs were combined, which yielded a mixture of catechol and phenol and small amounts of *p*-cresol, and *o*-cresol. The hydrolysate was fed as raw material to a fed-batch process that used *P. putida* MA-9. The engineered strain successfully converted the hydrolysate to MA within 54 h, attaining a final titer of 13 g L<sup>-1</sup> (Fig. 8C). At this time point, all the hydrolysate had been consumed. Catechol, phenol, and the cresols were completely consumed. The MA yield from the aromatics consumed was close to 100%. The molar ratio of the MA produced to the glucose consumed was approximately 20%. A small amount of 3-methyl MA

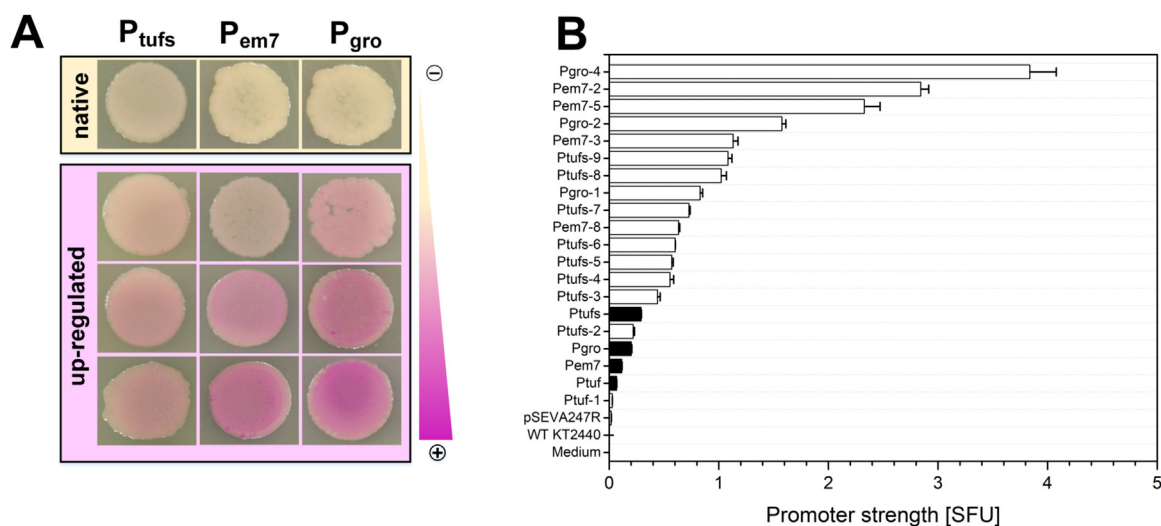


**Fig. 6.** Design and evaluation of synthetic promoters for fine-tuned gene expression in *Pseudomonas putida* KT2440 and corresponding mutants engineered for the production of *cis,cis*-muconic acid. Screening of cells expressing red fluorescent protein mCherry under the control of promoters of different strengths. The promoter library was created by mutagenesis of the native *P. putida* promoters  $P_{gro}$ ,  $P_{tufs}$  and  $P_{tufs}$  and the T7 phage promoter  $P_{em7}$  (A). Quantification of promoter strength by fluorescence-based measurement of mCherry expression. The specific strength of each promoter (RFU  $\text{mg}_{\text{CDM}}^{-1}$ ) was derived from the fluorescence intensity obtained after correcting for cell concentration (B). The data reflect mean values and standard deviations of three replicates.

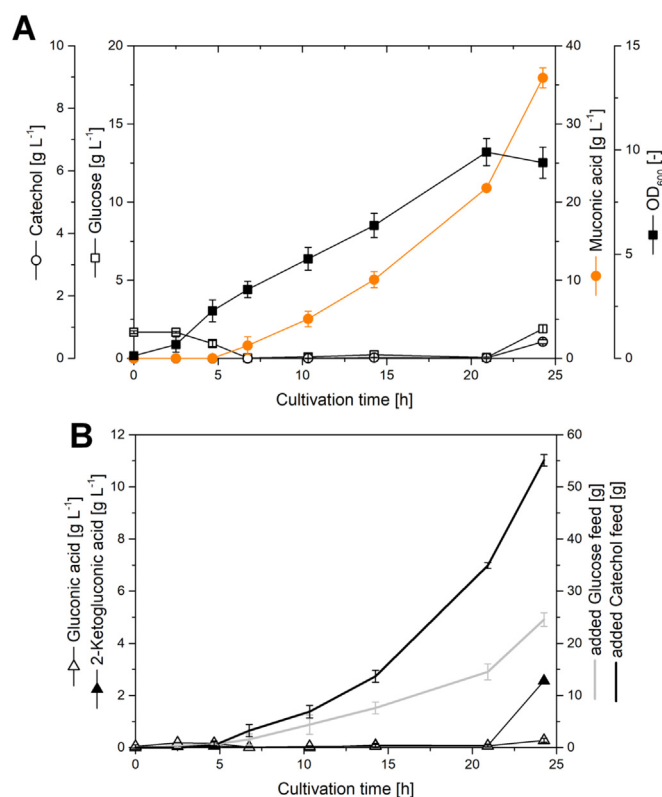


**Fig. 7.** Production performance of the engineered producer *Pseudomonas putida* KT2440 MA-6 on catechol using a fed-batch bioreactor process. The automatic addition of catechol as the substrate for *cis,cis*-muconic acid production was coupled to acidification of the medium (pH stat). For cell growth, an initial batch phase on glucose was followed by a feeding phase, adding further glucose to support growth at a reduced rate and during increased maintenance requirement. The data reflect mean values and standard deviations of two replicates.

was formed as a side product (Fig. S3). Throughout the process, the microbe exhibited robust production performance and even withstood an overdose of the hydrolysate, given by error, after 34 h. In fact, the

cells started to grow again once the excess aromatics had been degraded. The final broth volume was then taken further for product purification (Fig. 9). After cell separation and two treatments of the supernatant with active carbon, a clear solution was obtained, which was then acidified to crystallize the product. The crystals were washed and lyophilized to obtain a dry powder containing 96.3% MA as the final product. The purification protocol resulted in a certain degree of isomerization between MA and *cis,trans* muconic acid (Fig. S3); therefore, the MA finally obtained contained small amounts of *cis,trans* muconic acid and the 3-methylated counterpart of both MA and *cis,trans* muconic acid. The product was successfully hydrogenated to adipic acid and its methylated derivative, as validated by GC/MS analysis (Fig. S4). Finally, HMDA, the diamine counterpart for polymer synthesis, was condensed with the obtained bio-based adipic acids to form the first nylon originating from lignin (Fig. 10).

### 3.9. Scaled-up regeneration-based production provides pure MA at the kilogram scale from catechol

The lab-scale process was scaled up to a 50-L pilot-scale reactor to demonstrate the technical feasibility of the fermentation and devise an industrially applicable downstream-processing strategy. All process settings that proved to be successful at the lab-scale were now implemented on a larger scale. In particular, the concept of regeneration via reduced aromatics feeding (Fig. 5), which was shown to be successful, was integrated here to maintain culture viability. In total,  $25 \text{ g L}^{-1}$  MA was produced from catechol within 85 h (Fig. 10). In this process, the initial batch phase with glucose and the subsequent limited feeding supported the growth of the cells throughout the process. Catechol levels were maintained below 2 mM by the implemented feeding strategy. The number of living cells decreased during the pH-based phases of catechol feeding (Fig. 10B). Regeneration phases with reduced basal levels of catechol feeding initiated after 25, 50, and 75 h of process time re-established cellular vitality and provided long-term production performance. Purification of MA from the broth after fermentation involved cell separation, decolorization, precipitation of MA after acidification, sedimentation, washing of the crystals, and, finally, spray drying. Eventually a total of 1.5 kg of bio-based MA was recovered as a white powder from two individual runs. The purified MA was then further analyzed (see Supplement S8). NMR analysis of the MA revealed a purity of 97.9%. The elemental composition of the

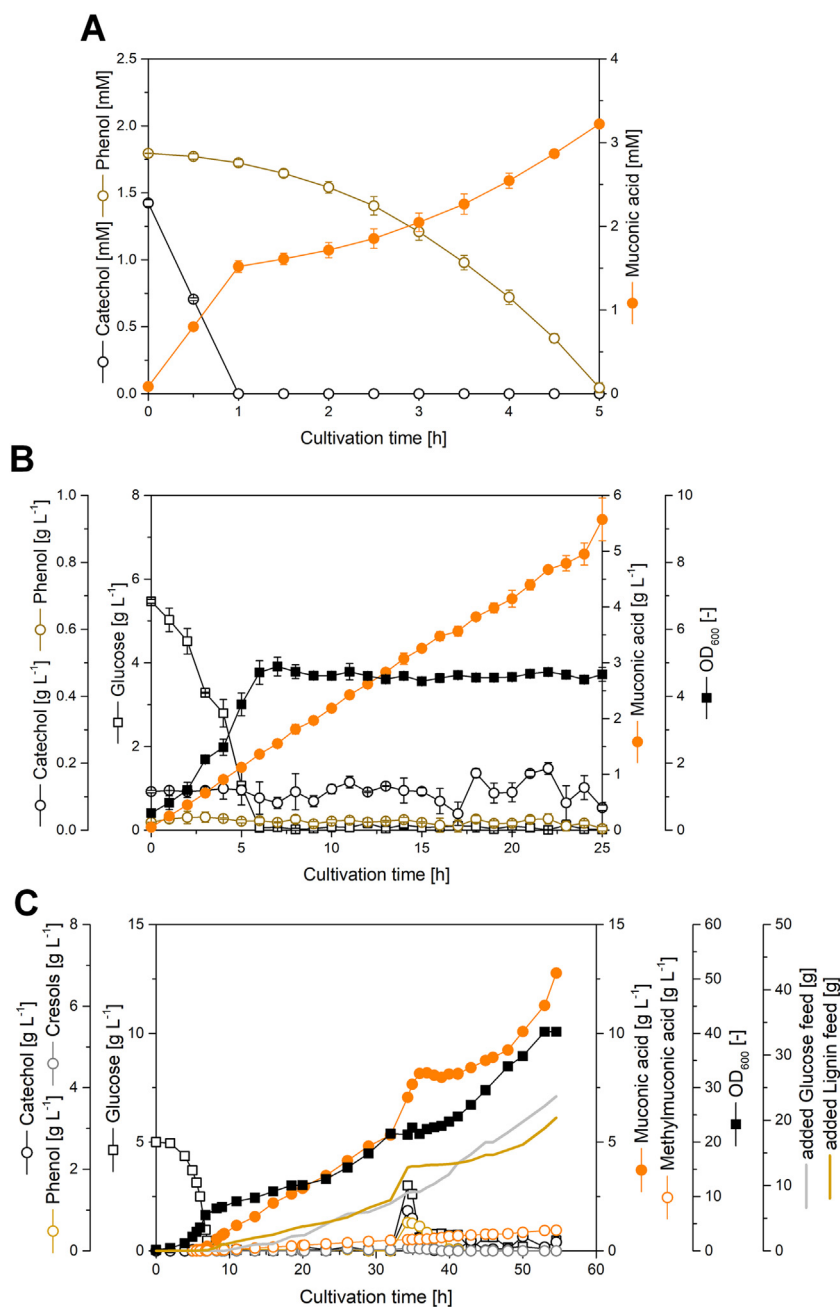


**Fig. 8.** Cascaded chemical and biochemical processes for the production of *cis,cis*-muconic from catechol and phenol (A, B) and from lignin (C). Production of *cis,cis*-muconic acid from catechol and phenol using the engineered producer *Pseudomonas putida* KT2440 MA-9 in shake flasks (A). Production of *cis,cis*-muconic acid from catechol and phenol using the engineered producer *Pseudomonas putida* KT2440 MA-9 in shake flasks with pulse-wise feeding of the aromatics and additional feeding of glucose as a growth substrate using feed beads (B). Production of *cis,cis*-muconic acid from softwood lignin hydrolysate using the engineered producer *Pseudomonas putida* KT2440 MA-9 in a fed-batch bioreactor process with pulse-wise feeding of the hydrolysate and additional feeding of glucose as a growth substrate (C). Data from the shake flask experiments (A, B) represent mean values and standard deviations of three replicates. The lignin process (C) was conducted as single experiment due to limited availability of the hydrolysate.

**Table 2**

Yield of aromatic monomers from hydrothermal treatment of softwood lignin (upper line) and composition of aromatic monomers after enrichment from the liquid phase (lower line).

Compound	Catechol	Phenol	<i>p</i> -Cresol	<i>o</i> -Cresol	Total
Yield [% w/w]	4.5 ± 0.0	2.4 ± 0.0	0.9 ± 0.0	0.1 ± 0.0	7.9 ± 0.1
Content (mM)	373 ± 5	222 ± 7	35 ± 1	2 ± 0	632 ± 13

product (50.6% C, 4.3% H) matched the theoretical value (50.6% C, 4.3% H) but revealed traces of S (0.05%) and N (0.03% N). Structurally, the product contained the *cis,cis* and *cis,trans* forms. Monitoring of the different fractions during purification revealed a continuous decrease in the residual ion content, with small fractions of NH<sub>4</sub><sup>+</sup>, Na<sup>+</sup>, SO<sub>4</sub><sup>2-</sup>, and Cl<sup>-</sup> remaining. Only minor amounts of trace elements were detected.

## 4. Discussion

### 4.1. The genomic producer *P. putida* MA-9 has set a benchmark in MA production from catechol and catechol-based lignin hydrolysates

MA is a chemical of recognized industrial value and is synthetically accessible from various aromatics via a highly attractive route (Beckham et al., 2016; Johnson et al., 2016; Linger et al., 2014; van Duuren et al., 2012). With respect to the metabolic pathways involved, catechol is the node for this type of production. On one hand, (i) catechol is a terminal pathway intermediate in MA biosynthesis regardless of the aromatic used and (ii) is a relevant medium ingredient that is generated during lignin pre-processing (Schuler et al., 2017; Wahyudiono and Goto, 2008). On the other hand, (iii) catechol is highly toxic (Schweigert et al., 2001). In this study, *P. putida* KT2440, a well-recognized industrial microbe (Kuepper et al., 2015; Nikel et al., 2015; Poblete-Castro et al., 2012, 2013; Tiso et al., 2016), was

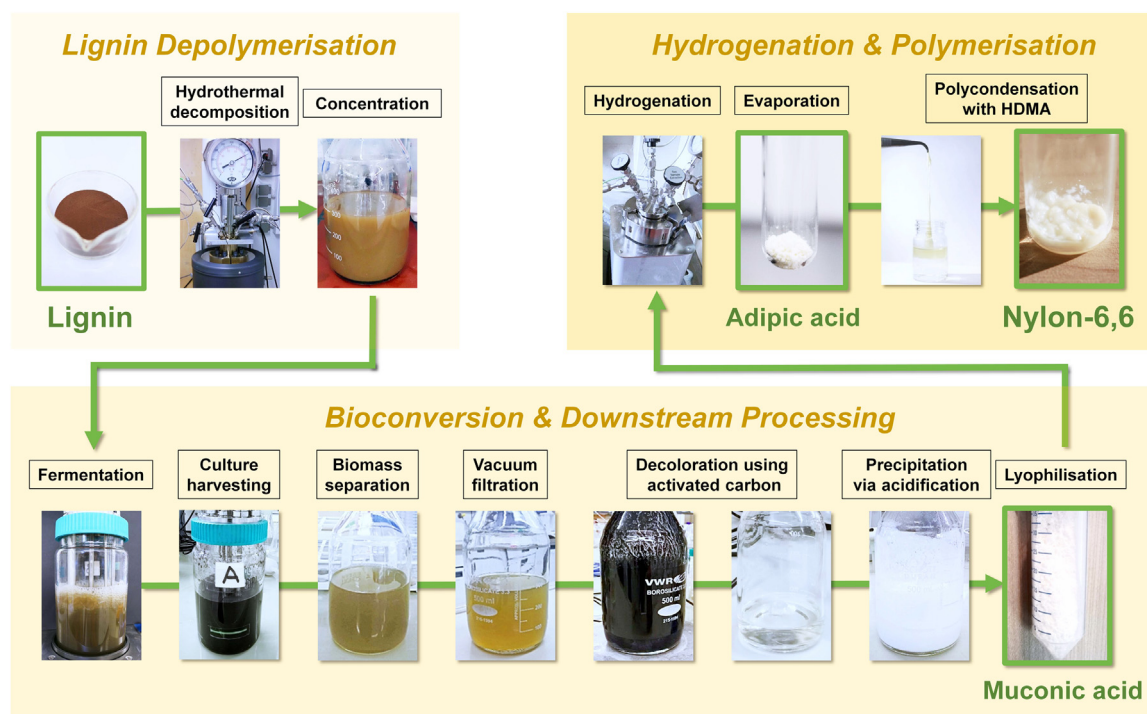


**Fig. 9.** Demonstration of the value chain from lignin to nylon. The cascaded process comprised hydrothermal depolymerization of lignin to a mixture of aromatics, containing mainly catechol, phenol and small amounts of cresols; biochemical conversion of the aromatics to *cis,cis*-muconic acid by the advanced producer *Pseudomonas putida* KT2440 MA-9; purification of *cis,cis*-muconic acid; hydrogenation to adipic acid; and final polymerization to nylon 6,6.

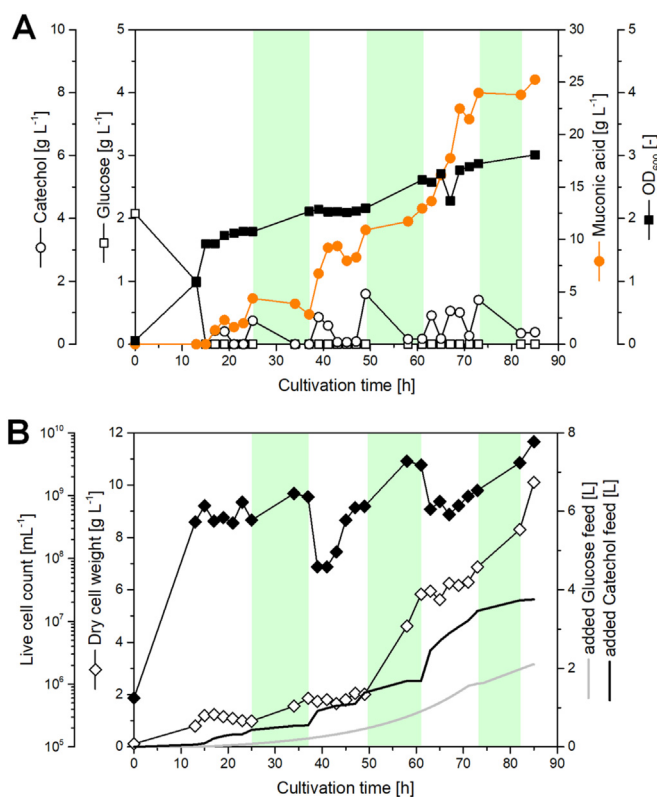


**Fig. 10.** Demonstration of technical feasibility by pilot-scale production of *cis,cis*-muconic acid from catechol using *Pseudomonas putida* KT2440 MA-6 in an advanced fed-batch process with transient regeneration phases. The process was conducted in a 50-L fermentation volume and included pilot-scale downstream purification of the product to 95% purity at the kilogram scale. The fermentation settings were derived from the optimized fed-batch process at the lab scale (Fig. 5).

upgraded to a fully genome-based host for the production of MA from catechol and upstream aromatics. To overcome previous limitations, targeted genomic modifications increased catechol tolerance (Fig. 2A), catechol 1,2-dioxygenase levels (Fig. 3), and catechol conversion rates (Fig. 2 BC). Subsequently, the engineered MA-1 strain achieved an MA titer of  $64.2 \text{ g L}^{-1}$  from catechol, which surpasses previously reported values by *P. putida* strains by more than tenfold (Table 3) and attains the maximum levels observed for MA production by microbes in general (Xie et al., 2014). The MA-9 strain, equipped with a phenol hydroxylase (Vardon et al., 2015), additionally used phenol as well as *o*-, *m*-, and *p*-cresol (Fig. 8AB) and accumulated  $13 \text{ g L}^{-1}$  MA from a lignin hydrolysate (Fig. 8C), which was 20-fold greater than recently obtained yields of MA (Johnson et al., 2017) (Table 3). The successful demonstration of the entire value chain with production of the first nylon from lignin (Fig. 9) and the transfer of the process to the pilot scale with production of kilograms of pure MA (Fig. 10) further underline the industrial impact of these developments.

#### 4.2. Synthetic promoters used to modulate *catA* expression do not outperform the ultra-strong native *cat* promoter

Although *P. putida* KT2440 is well-known for its ability to degrade small aromatics (Belda et al., 2016; Nelson et al., 2002) and is regarded one of the most efficient microbes for aromatic-based MA production (Xie et al., 2014), catechol production clearly poses a challenge (Fig. 1B, Fig. 4A) that deserves detailed inspection. *P. putida* KT2440 possesses a unique pathway architecture for benzoate catabolism. Two catechol 1,2-dioxygenases are central to this network: (i) CatA is expressed from the *cat* operon under positive regulation by MA and confers 95% of the total activity, while (ii) CatA2, expressed downstream of the *ben* operon upon induction by benzoate, is far less active but acts as a safety valve to address elevated levels of catechol inside the cell (Jiménez et al., 2014). CatA2 is also associated with the early regulation cascade. The enzyme is induced when benzoate becomes available and then mediates the activation of the *cat* operon via the

**Table 3**

Muonic acid (MA) production performance of engineered strains of *Pseudomonas putida* from catechol and lignin-based hydrolysates, derived by base catalysis and hydrothermal conversion (HTC). All processes were conducted as fed-batch with glucose as additional growth supporting carbon source. The data shown comprise the MA titer ( $C_{MA}$ ), the maximum specific productivity ( $q_{MA}$ ), and the volumetric productivity ( $P_V$ ).

Strain	Substrate	$C_{MA}$ [g L <sup>-1</sup> ]	$q_{MA}$ [g g <sub>DCW</sub> <sup>-1</sup> h <sup>-1</sup> ]	$P_V$ [g L <sup>-1</sup> h <sup>-1</sup> ]	Reference
ATCC 31916	Catechol	5.3	0.3 <sup>a</sup>	0.3 <sup>a</sup>	(Maxwell, 1988)
KT2440 MA-1	Catechol	19.5	0.2	0.6	This work
KT2440 MA-1 <sup>b</sup>	Catechol	64.2	0.8	4.5	This work
KT2440 MA-6	Catechol	36.1	1.5	4.4	This work
KT2440 CJ103	Base lignin	0.5	0.002 <sup>a</sup>	0.014 <sup>a</sup>	(Rodriguez et al., 2017)
KT2440 MA-9	HTC Lignin	13.0	0.08	1.0	This work

<sup>a</sup> Estimated from reference.

<sup>b</sup> Recuperation fed-batch with feeding pauses for cell regeneration.

formation of MA (Silva-Rocha and de Lorenzo, 2012). This strategy is well suited to handling the breakdown of benzoate (Fig. 1A) (Silva-Rocha and de Lorenzo, 2013). However, it is difficult for the cells to handle the catechol in the environment (Fig. 1B). The catechol-grown MA-1 strain suffered from prolonged lag phases (Fig. 3A) and low production performance (Fig. 4A). Previous studies have used overexpression of the canonical *catA* gene to support MA production in *P. putida* KT2440 (Vardon et al., 2015). CatA is the dominant catechol 1,2-dioxygenase (Jiménez et al., 2014), so the low production performance of the resulting mutant on catechol appeared to be due to insufficient amplification of the expression level by the chosen *tac* promoter. The replacement of the native control with a strong constitutive promoter appeared logical and intuitive given recent experience (Becker et al., 2011; Kind et al., 2014; Lange et al., 2017; Rohles et al., 2016). Surprisingly, the native *cat* promoter outperformed even the strongest synthetic sequences that were designed for constitutive overexpression (Fig. 3, Fig. 6). We concluded that unlike previous designs (Vardon et al., 2015), the native *cat* promoter should be maintained for optimal *catA* overexpression. This design, however, was the same as that of the basic MA-1 strain, which had already been proven to be suboptimal (Fig. 5).

#### 4.3. Co-expression of both catechol 1,2-dioxygenases under the control of the *cat* promoter provides a powerful engine for catechol conversion

The limited performance of the basic producer MA-1 on catechol led to further rounds of metabolic engineering. Observations made with benzoate-incubated cells indicated that the CatA2 enzyme was beneficial for MA production. These cells, in contrast to catechol-grown cells, expressed the *ben* operon and the downstream *catA2* gene in addition to the *cat* operon with the *catA* gene, leading to the presence of both catechol 1,2-dioxygenases in the cells. When grown in the presence of benzoate, the basic producer MA-1 accumulated MA up to a titer of 48 g L<sup>-1</sup>, which was more than threefold higher than that obtained in the presence of catechol (Fig. 5). In addition, MA-1 cells pre-induced with benzoate exhibited significantly increased catechol conversion rates and catechol 1,2-dioxygenase activity (Fig. 2, Fig. 3), which was obviously associated with the concerted action of both catechol 1,2-dioxygenases. CatA2 alone did not provide enough catalytic power, as shown with the previously developed mutant JD1 (van Duuren et al., 2011), which expresses CatA2 but not CatA (Jiménez et al., 2014) (Fig. 2). JD1 exhibited much lower MA accumulation from catechol than the MA-1 strain. To improve the production of MA from catechol, the co-expression of both *catA* and *catA2* appeared to be crucial. To eliminate the dependence of *catA2* expression on external benzoate, we designed a synthetic pathway module for catechol control and conversion (CCC): P<sub>cat</sub> *catA catA2*. MA, the formed product, acts as the inducer, efficiently triggering continuous expression of the module. This strategy proved to be highly successful. The advanced producer

MA-6, harboring the CCC module, revealed high catechol conversion, high tolerance to catechol, and high catechol 1,2-dioxygenase activity, surpassing the parent strain MA-1 under similar fed-batch conditions more than twofold with regard to product titer and maximum specific and volumetric productivity (Fig. 4A, Fig. 7A, Table 3). As shown, even higher conversion rates are feasible by introducing additional copies of the catechol 1,2-dioxygenase gene (Fig. 3), which could provide even faster production in the future. In all cases, the available enzyme activity amount almost matched the *in vivo* flux, indicating an almost 100% recruitment for the conversion.

#### 4.4. The synthetic catechol control and conversion (CCC) element enables high-efficiency MA production from mixtures of aromatics

The synthetic CCC element further enabled efficient MA production from a lignin hydrolysate with catechol as the main substrate (Fig. 8C). The producer MA-9 expressed phenol hydroxylase, which supplied additional catechol and two methyl catechols from the simultaneous conversion of phenol and different cresols. This additional challenge was well handled by the engineered producer, which tolerated even an accidental overdose during the process. It therefore appears promising to implement the CCC element as a core element in multi-substrate *P. putida* strains with additional catabolic pathways engineered into the genome (Fig. 11) in order to provide an “enhanced stem to the biological funnel”. This added capacity seems particularly relevant if the additional catabolic pathways are controlled by constitutive promoters (Fig. 8BC), which override the natural “less is more” strategies by which bacteria slow down upstream catabolism to prevent catechol accumulation (George and Hay, 2012).

#### 4.5. The developed recovery process highlights the impact of cellular energy charge and provides an efficient production mode at the technical scale

In addition, we provide a solution to minimize the impact of catechol on the bioprocess, allowing maintenance of the energy levels of the producer cells. It has long been known that intact metabolizing cells possess a large excess of energy rich adenylate phosphates over the energy poor forms (Chapman et al., 1971). With respect to the energy parameters of growing *P. putida* KT2440 cells, the ATP yield is approximately 5 μmol (g CDM)<sup>-1</sup> (Chavarría et al., 2013). The AEC, which describes the cellular energy status in a quantitative manner, is above 0.70 (Martínez-García et al., 2014). These values, which are indicative of physiologically healthy cells, were also observed during the initial phase of the standard fed-batch production process (Fig. 5). However, prolonged contact with the toxic substrate resulted in collapse of the cellular energy charge to 0.4, even though the catechol level in the medium was maintained at a low level (Fig. 5). It is well-known that catechol destroys the membrane potential and inhibits oxidative phosphorylation (Schweigert et al., 2001), which matches the

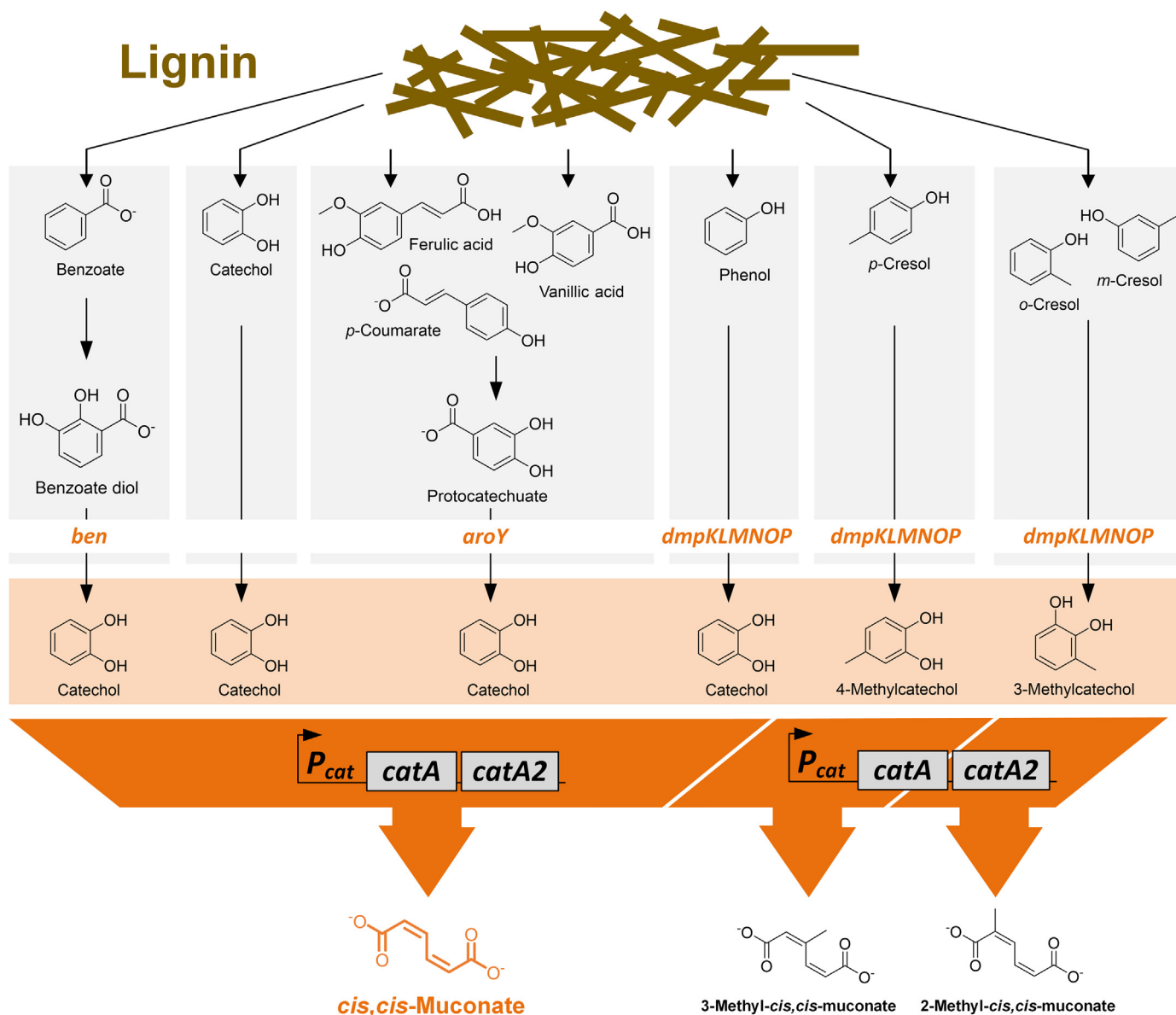


**Fig. 11.** From lignin to *cis,cis*-muconic acid and its methylated variants using engineered *Pseudomonas putida* strains in a cascaded chemical and biochemical process (A). Lignin is depolymerized into small aromatics. The generated mutant (depicted as gray squares) then produces *cis,cis*-muconic acid (MA) from the aromatic substrates by disrupting the  $\beta$ -ketoacid pathway at the level of muconate cycloisomerase, downstream of MA. *P. putida* naturally utilizes catechol and benzoate. Engineered strains additionally convert phenol (Vardon et al., 2015) and different cresols (this work) upon heterologous expression of phenol hydroxylase from *Pseudomonas* CF600 (Nordlund et al., 1990). The cresols lead to the formation of methylated products. The position of the methyl group is inferred from the fact that the microbe uses the *ortho*-pathway for cleavage of catechol (Park and Kim, 2003) and its methylated variants (An et al., 2001). The direction of aromatic compounds from the protocatechuate pathway to catechol requires the use of a protocatechuate decarboxylase (Sonoki et al., 2014).

observation. The energy shortage could also explain the sudden accumulation of 2-ketogluconate via oxidation. The oxidation of glucose to the keto acid is associated with the formation of 2 ATP (Ebert et al., 2011), so the activation of this pathway could theoretically represent an escape mechanism to generate ATP by other means. Interestingly, the energy limitation could be easily overcome by a feed pause, which enabled full recovery of the cellular energy charge and further growth and production. The process strategy was transferred to the pilot scale (Fig. 10). In our view, repeated recovery of cellular vitality, indicated by the increased live cell counts, was important for maintenance of a high production performance over almost 90 h. Coupled with downstream purification, the product could be obtained from this fermentation process at 97.9% purity. Given that the coupling to sophisticated purification strategies that included additional washing steps with

ethanol has proven valuable for the removal of traces of sulphur and nitrogen and final product polishing (Vardon et al., 2016), it appears feasible to deliver MA at the kilogram scale with sufficient purity for subsequent polymerization using the developed process. The acidic recovery step resulted in partial isomerization of the product to the *cis,trans* form (Fig. S3) (Carraher et al., 2017); however, this isomerization did not affect the subsequent hydrogenation to adipic acid. The clear impact of the cellular energy level highlights the importance of the co-substrate in the delivery of sufficient energy, suggesting that more detailed studies on glucose catabolism in *P. putida* KT2440 are required (Nikel et al., 2015). Novel energy-efficient strains could provide further improvement of performance (Lieder et al., 2015; Martínez-García et al., 2015, 2014).

Table 4

**Utilization of phenol and cresols by the engineered producer *Pseudomonas putida* KT2440 MA-9, expressing phenol hydroxylase from *Pseudomonas* CF600 (Shingler et al., 1989).** Each set-up contained 2 mM of the corresponding substrate in mineral salt medium together with glucose as a growth substrate. In addition, a control without added substrate was conducted. For comparison, the parent strain MA-6, lacking phenol hydroxylase activity, did not accumulate muconic acid or methylated muconic acid from any of the substrates.

Substrate	Muconic acid	2-Methyl muconic acid	3-Methyl muconic acid
Phenol	+	–	–
<i>o</i> -Cresol	–	+	–
<i>m</i> -Cresol	–	+	–
<i>p</i> -Cresol	–	–	+
Control	–	–	–

#### 4.6. The capability of *Pseudomonas putida* MA-9 to convert cresols expands the product spectrum to th methylated nylon

The producer MA-9 formed methylated MA from all cresol isomers (Fig. 8B). This capability was conferred by the introduced phenol hydroxylase complex *dmpKLMNOP* (Table 4). Although not specifically demonstrated for the enzyme from *P. putida* CF600, phenol hydroxylases are generally promiscuous and accept cresols almost as well as phenol (Kukor and Olsen, 1992). The results also indicated that at least one of the two catechol 1,2-dioxygenases in *P. putida* KT2440 can accept methylated catechols, a well-known property of this type of enzyme (An et al., 2001; Barton et al., 2018). This feature opens new possibilities and promising lines of research. First, MA with a single, stereochemically well-defined methyl group in the carbon backbone is hard to chemically synthesize, which likely explains the fact that such a chemical is not commercially available (Barton et al., 2018). Mixtures of MA and methylated MA variants from lignin feedstocks have promise in the development of plastics with new properties because methyl groups in MA affect the molecular architecture of polymers and subsequent properties of the composites derived from these polymers (Rorrer et al., 2016).

## 5. Conclusion

The engineered strains of *P. putida* KT2440 are valuable hosts for industrial MA production from aromatics. These strains are feasible producers of nylon from lignin via a cascaded chemical-biochemical process and are applicable in nylon production at the technical scale. At the core of these strains is a well-designed module, which confers catechol tolerance and conversion efficiency and exhibits a particularly attractive metabolic trait for industrial bio-production from aromatics and lignin-based feedstocks. Repeated recovery of the energy charge supports production performance of the bioprocess. The generated library of synthetic promoters opens various application-based possibilities for the fine-tuning of gene expression in *P. putida* KT2440 and related strains. For further rounds of promoter engineering, mCherry is a particularly useful reporter, as it offers straightforward visual screening, high signal intensity and low background interference. Future lines of research beyond this study could further elaborate the metabolism of aromatics in the producers to eventually develop a better understanding of these pathways for further optimization. Alternative catechol 1,2-dioxygenases might offer interesting properties to further strengthen the catechol module (Guzik et al., 2013). In addition, novel strategies toward glucose-free MA production from aromatics appear promising (Sonoki et al., 2018).

## Acknowledgments

We express deep thanks to Michel Fritz (Saarland University, Germany) for the excellent analytical support, Victor de Lorenzo

(National Centre for Biotechnology, Madrid, Spain) for the kind donation of different cloning plasmids for *Pseudomonas putida* KT2440, and Victoria Shingler (University of Umea, Sweden) for the kind donation of the plasmid containing the phenol hydroxylase of *P. putida* CF600. This work was financially supported by the German Ministry for Education and Research (BMBF) through the grants “BioNylon” (FKZ 03 V0757) and “LignoValue” (FKZ 031B0344A).

## Appendix A. Supplementary material

Supplementary data associated with this article can be found in the online version at <http://dx.doi.org/10.1016/j.ymben.2018.03.003>.

## References

- Alper, H., Fischer, C., Nevoigt, E., Stephanopoulos, G., 2005. Tuning genetic control through promoter engineering. *Proc. Natl. Acad. Sci. USA* 102, 12678–12683.
- An, H.R., Park, H.H., Kim, E.S., 2001. Cloning and expression of thermophilic catechol 1,2-dioxygenase gene (*catA*) from *Streptomyces setonii*. *FEMS Microbiol. Lett.* 195, 17–22.
- Atkinson, D.E., 1968. The energy charge of the adenylate pool as a regulatory parameter. Interaction with feedback modifiers. *Biochemistry* 7, 4030–4034.
- Bartilson, M., Nordlund, I., Shingler, V., 1990. Location and organization of the dimethylphenol catabolic genes of *Pseudomonas* CF600. *Mol. Gen. Genet.* 220, 294–300.
- Barton, N., Horbal, L., Starck, S., Kohlstedt, M., Luzhetskyy, A., Wittmann, C., 2018. Enabling the valorization of guaiacol-based lignin: integrated chemical and biochemical production of *cis,cis*-muconic acid using metabolically engineered *Amycolatopsis* sp. ATCC 39116. *Metab. Eng.* 45, 200–210.
- Becker, J., Klopprogge, C., Zelder, O., Heinzle, E., Wittmann, C., 2005. Amplified expression of fructose 1,6-bisphosphatase in *Corynebacterium glutamicum* increases *in vivo* flux through the pentose phosphate pathway and lysine production on different carbon sources. *Appl. Environ. Microbiol.* 71, 8587–8596.
- Becker, J., Zelder, O., Haefner, S., Schröder, H., Wittmann, C., 2011. From zero to hero—design-based systems metabolic engineering of *Corynebacterium glutamicum* for l-lysine production. *Metab. Eng.* 13, 159–168.
- Beckham, G.T., Johnson, C.W., Karp, E.M., Salvachua, D., Vardon, D.R., 2016. Opportunities and challenges in biological lignin valorization. *Curr. Opin. Biotechnol.* 42, 40–53.
- Belda, E., van Heck, R.G., Jose Lopez-Sanchez, M., Cruveiller, S., Barbe, V., Fraser, C., Klenk, H.P., Petersen, J., Morgat, A., Nikel, P.I., Vallenet, D., Rouy, Z., Sekowska, A., Martins Dos Santos, V.A., de Lorenzo, V., Danchin, A., Medigue, C., 2016. The revisited genome of *Pseudomonas putida* KT2440 enlightens its value as a robust metabolic chassis. *Environ. Microbiol.* 18, 3403–3424.
- Benedetti, I., de Lorenzo, V., Nikel, P.I., 2016. Genetic programming of catalytic *Pseudomonas putida* biofilms for boosting biodegradation of haloalkanes. *Metab. Eng.* 33, 109–118.
- Carraher, J.M., Pfennig, T., Rao, R.G., Shanks, B.H., Tessonnier, J.-P., 2017. *Cis,cis*-Muconic acid isomerization and catalytic conversion to biobased cyclic-C6-1,4-diacid monomers. *Green Chem.* 19, 3042–3050.
- Chapman, A.G., Fall, L., Atkinson, D.E., 1971. Adenylate energy charge in *Escherichia coli* during growth and starvation. *J. Bacteriol.* 108, 1072–1086.
- Chavarría, M., Nikel, P.I., Perez-Pantoja, D., de Lorenzo, V., 2013. The Entner-Doudoroff pathway empowers *Pseudomonas putida* KT2440 with a high tolerance to oxidative stress. *Environ. Microbiol.* 15, 1772–1785.
- Chua, J.W., Hsieh, J.H., 1990. Oxidative bioconversion of toluene to 1,3-butadiene-1,4-dicarboxylic acid (*cis,cis*-muconic acid). *World J. Microbiol. Biotechnol.* 6, 127–143.
- Ebert, B.E., Kurth, F., Grund, M., Blank, L.M., Schmid, A., 2011. Response of *Pseudomonas putida* KT2440 to increased NADH and ATP demand. *Appl. Environ. Microbiol.* 77, 6597–6605.
- George, K.W., Hay, A., 2012. Less is more: reduced catechol production permits *Pseudomonas putida* F1 to grow on styrene. *Microbiology* 158, 2781–2788.
- Guzik, U., Hupert-Kocurek, K., Sitnik, M., Wojcieszynska, D., 2013. High activity catechol 1,2-dioxygenase from *Stenotrophomonas maltophilia* strain KB2 as a useful tool in *cis,cis*-muconic acid production. *Antonie Van Leeuwenhoek* 103, 1297–1307.
- Jeenpadiphat, S., Mongkolpichayarak, I., Tungasmita, D.N., 2016. Catechol production from lignin by Al-doped mesoporous silica catalytic cracking. *J. Anal. Appl. Pyrolysis* 121, 318–328.
- Jiménez, J.I., Pérez-Pantoja, D., Chavarría, M., Díaz, E., de Lorenzo, V., 2014. A second chromosomal copy of the *catA* gene endows *Pseudomonas putida* mt-2 with an enzymatic safety valve for excess of catechol. *Environ. Microbiol.* 16, 1767–1778.
- Johnson, C.W., Abraham, P.E., Linger, J.G., Khanna, P., Hettich, R.L., Beckham, G.T., 2017. Eliminating a global regulator of carbon catabolite repression enhances the conversion of aromatic lignin monomers to muconate in *Pseudomonas putida* KT2440. *Metab. Eng. Commun.* 5, 19–25.
- Johnson, C.W., Salvachúa, D., Khanna, P., Smith, H., Peterson, D.J., Beckham, G.T., 2016. Enhancing muconic acid production from glucose and lignin-derived aromatic compounds via increased protocatechuate decarboxylase activity. *Metab. Eng. Commun.* 3, 111–119.
- Kind, S., Neubauer, S., Becker, J., Yamamoto, M., Völkert, M., Abendroth, G.V., Zelder, O., Wittmann, C., 2014. From zero to hero - production of bio-based nylon from



- renewable resources using engineered *Corynebacterium glutamicum*. *Metab. Eng.* 25, 113–123.
- Kuepper, J., Dickler, J., Biggel, M., Behnken, S., Jager, G., Wierckx, N., Blank, L.M., 2015. Metabolic engineering of *Pseudomonas putida* KT2440 to produce anthranilate from glucose. *Front. Microbiol.* 6, 1310.
- Kukor, J.J., Olsen, R.H., 1992. Complete nucleotide sequence of *tbuD*, the gene encoding phenol/cresol hydroxylase from *Pseudomonas pickettii* PKO1, and functional analysis of the encoded enzyme. *J. Bacteriol.* 174, 6518–6526.
- Lange, A., Becker, J., Schulze, D., Cahoreau, E., Portais, J.-C., Haefner, S., Schröder, H., Krawczyk, J., Zelder, O., Wittmann, C., 2017. Bio-based succinate from sucrose: high-resolution <sup>13</sup>C metabolic flux analysis and metabolic engineering of the rumen bacterium *Basfia succiniciproducens*. *Metab. Eng.* 44, 198–212.
- Lieder, S., Nikel, P.I., de Lorenzo, V., Takors, R., 2015. Genome reduction boosts heterologous gene expression in *Pseudomonas putida*. *Microb. Cell Fact.* 14, 23.
- Linger, J.G., Vardon, D.R., Guarneri, M.T., Karp, E.M., Hunsinger, G.B., Franden, M.A., Johnson, C.W., Chupka, G., Strathmann, T.J., Pienkos, P.T., Beckham, G.T., 2014. Lignin valorization through integrated biological funneling and chemical catalysis. *Proc. Natl. Acad. Sci. USA* 111, 12013–12018.
- Martínez-García, E., de Lorenzo, V., 2011. Engineering multiple genomic deletions in Gram-negative bacteria: analysis of the multi-resistant antibiotic profile of *Pseudomonas putida* KT2440. *Environ. Microbiol.* 13, 2702–2716.
- Martínez-García, E., Jatsenko, T., Kivisaar, M., de Lorenzo, V., 2015. Freeing *Pseudomonas putida* KT2440 of its proviral load strengthens endurance to environmental stresses. *Environ. Microbiol.* 17, 76–90.
- Martínez-García, E., Nikel, P.I., Aparicio, T., de Lorenzo, V., 2014. *Pseudomonas* 2.0: genetic upgrading of *P. putida* KT2440 as an enhanced host for heterologous gene expression. *Microb. Cell Fact.* 13, 159.
- Matthiesen, J.E., Carraher, J.M., Vasiliu, M., Dixon, D.A., Tessonnier, J.-P., 2016. Electrochemical conversion of muconic acid to biobased diacid monomers. *ACS Sustain. Chem. Eng.* 4, 3575–3585.
- Maxwell, P.C., 1988. Process for the Production of Muconic Acid, US4731328 A.
- Nelson, K.E., Weinel, C., Paulsen, I.T., Dodson, R.J., Hilbert, H., Martins dos Santos, V.A., Fouts, D.E., Gill, S.R., Pop, M., Holmes, M., Brinkac, L., Beanan, M., DeBoy, R.T., Daugherty, S., Kolonay, J., Madupu, R., Nelson, W., White, O., Peterson, J., Khouri, H., Hance, I., Chris Lee, P., Holtzapple, E., Scanlan, D., Tran, K., Moazzaz, A., Utterback, T., Rizzo, M., Lee, K., Kosack, D., Moestl, D., Wedler, H., Lauber, J., Stjepandic, D., Hoheisel, J., Straetz, M., Heim, S., Kiewitz, C., Eisen, J.A., Timmis, K.N., Dusterhoft, A., Tummler, B., Fraser, C.M., 2002. Complete genome sequence and comparative analysis of the metabolically versatile *Pseudomonas putida* KT2440. *Environ. Microbiol.* 4, 799–808.
- Neu, A.-K., Pleissner, D., Mehlmann, K., Schneider, R., Puerta-Quintero, G.I., Venus, J., 2016. Fermentative utilization of coffee mucilage using *Bacillus coagulans* and investigation of down-stream processing of fermentation broth for optically pure L (+)-lactic acid production. *Bioresour. Technol.* 211, 398–405.
- Nikel, P.I., Chavarría, M., Fuhrer, T., Sauer, U., de Lorenzo, V., 2015. *Pseudomonas putida* KT2440 strain metabolizes glucose through a cycle formed by enzymes of the Entner-Doudoroff, Embden-Meyerhof-Parnas, and pentose phosphate pathways. *J. Biol. Chem.* 290, 25920–25932.
- Nordlund, I., Powlowski, J., Shingler, V., 1990. Complete nucleotide sequence and polypeptide analysis of multicomponent phenol hydroxylase from *Pseudomonas* sp. strain CF600. *J. Bacteriol.* 172, 6826–6833.
- Pandey, M.P., Kim, C.S., 2011. Lignin depolymerization and conversion: a review of thermochemical methods. *Chem. Eng. Technol.* 34, 29–41.
- Park, H.J., Kim, E.S., 2003. An inducible *Streptomyces* gene cluster involved in aromatic compound metabolism. *FEMS Microbiol. Lett.* 226, 151–157.
- Park, W., Jeon, C.O., Cadillo, H., DeRito, C., Madsen, E.L., 2004. Survival of naphthalene-degrading *Pseudomonas putida* NCI 9816-4 in naphthalene-amended soils: toxicity of naphthalene and its metabolites. *Appl. Microbiol. Biotechnol.* 64, 429–435.
- Poblete-Castro, I., Becker, J., Dohnt, K., dos Santos, V.M., Wittmann, C., 2012. Industrial biotechnology of *Pseudomonas putida* and related species. *Appl. Microbiol. Biotechnol.* 93, 2279–2290.
- Poblete-Castro, I., Binger, D., Rodrigues, A., Becker, J., Martins Dos Santos, V.A., Wittmann, C., 2013. In-silico-driven metabolic engineering of *Pseudomonas putida* for enhanced production of poly-hydroxyalkanoates. *Metab. Eng.* 15, 113–123.
- Ragauskas, A.J., Beckham, G.T., Biddy, M.J., Chandra, R., Chen, F., Davis, M.F., Davison, B.H., Dixon, R.A., Gilna, P., Keller, M., Langan, P., Naskar, A.K., Saddler, J.N., Tschaplinski, T.J., Tuskan, G.A., Wyman, C.E., 2014. Lignin valorization: improving lignin processing in the biorefinery. *Science* 344, 1246843.
- Rinaldi, R., Jastrzebski, R., Clough, M.T., Ralph, J., Kennema, M., Bruijninx, P.C.A., Weckhuysen, B.M., 2016. Paving the way for lignin valorisation: recent advances in bioengineering, biorefining and catalysis. *Angew. Chem. Int. Ed.* 55, 8164–8215.
- Rodriguez, A., Salvachúa, D., Katahira, R., Black, B.A., Cleveland, N.S., Reed, M., Smith, H., Baidoo, E.E.K., Keasling, J.D., Simmons, B.A., Beckham, G.T., Gladden, J.M., 2017. Base-catalyzed depolymerization of solid lignin-rich streams enables microbial conversion. *ACS Sustain. Chem. Eng.* 5, 8171–8180.
- Rohles, C.M., Giesselmann, G., Kohlstedt, M., Wittmann, C., Becker, J., 2016. Systems metabolic engineering of *Corynebacterium glutamicum* for the production of the carbon-5 platform chemicals 5-aminovalerate and glutarate. *Microb. Cell Fact.* 15, 154.
- Rorrer, N.A., Dorgan, J.R., Vardon, D.R., Martinez, C.R., Yang, Y., Beckham, G.T., 2016. Renewable unsaturated polyesters from muconic acid. *ACS Sustain. Chem. Eng.* 4, 6867–6876.
- Sambrook, J., Fritsch, E.F., Maniatis, T., 1989. *Molecular cloning: A laboratory manual*, 2nd ed. Cold Spring Harbor Laboratory Press, New York.
- Schuler, J., Hornung, U., Kruse, A., Dahmen, N., Sauer, J., 2017. Hydrothermal liquefaction of lignin. *J. Biomater. Nanobiotechnol.* 8, 96–108.
- Schweigert, N., Zehnder, A.J.B., Eggen, R.I.L., 2001. Chemical properties of catechols and their molecular modes of toxic action in cells, from microorganisms to mammals. *Environ. Microbiol.* 3, 81–91.
- Shingler, V., Franklin, F.C., Tsuda, M., Holroyd, D., Bagdasarian, M., 1989. Molecular analysis of a plasmid-encoded phenol hydroxylase from *Pseudomonas* CF600. *J. Gen. Microbiol.* 135, 1083–1092.
- Silva-Rocha, R., de Lorenzo, V., 2012. A GFP-*lacZ* bicistronic reporter system for promoter analysis in environmental gram-negative bacteria. *PLoS One* 7, e34675.
- Silva-Rocha, R., de Lorenzo, V., 2013. The TOL network of *Pseudomonas putida* mt-2 processes multiple environmental inputs into a narrow response space. *Environ. Microbiol.* 15, 271–286.
- Silva-Rocha, R., Martínez-García, E., Calles, B., Chavarría, M., Arce-Rodriguez, A., de Las Heras, A., Paez-Espino, A.D., Durante-Rodriguez, G., Kim, J., Nikel, P.I., Platero, R., de Lorenzo, V., 2013. The Standard European Vector Architecture (SEVA): a coherent platform for the analysis and deployment of complex prokaryotic phenotypes. *Nucleic Acids Res.* 41, D666–D675.
- Sonoki, T., Morooka, M., Sakamoto, K., Otsuka, Y., Nakamura, M., Jellison, J., Goodell, B., 2014. Enhancement of protocatechuate decarboxylase activity for the effective production of muconate from lignin-related aromatic compounds. *J. Biotechnol.* 192 (Pt A), 71–77.
- Sonoki, T., Takahashi, K., Sugita, H., Hatamura, M., Azuma, Y., Sato, T., Suzuki, S., Kamimura, N., Masai, E., 2018. Glucose-free *cis,cis*-muconic acid production via new metabolic designs corresponding to the heterogeneity of lignin. *ACS Sustain. Chem. Eng.* 6, 1256–1264.
- Tiso, T., Sabelhaus, P., Behrens, B., Wittgens, A., Rosenau, F., Hayen, H., Blank, L.M., 2016. Creating metabolic demand as an engineering strategy in *Pseudomonas putida* - Rhamnolipid synthesis as an example. *Metab. Eng. Commun.* 3, 234–244.
- van Duuren, J.B.J.H., Wijte, D., Karge, B., dos Santos, V.A., Yang, Y., Mars, A.E., Eggink, G., 2012. pH-stat fed-batch process to enhance the production of *cis,cis*-muconate from benzoate by *Pseudomonas putida* KT2440-JD1. *Biotechnol. Prog.* 28, 85–92.
- van Duuren, J.B.J.H., Wijte, D., Leprince, A., Karge, B., Puchalka, J., Wery, J., Dos Santos, V.A., Eggink, G., Mars, A.E., 2011. Generation of a *catR* deficient mutant of *P. putida* KT2440 that produces *cis,cis*-muconate from benzoate at high rate and yield. *J. Biotechnol.* 156, 163–172.
- Vardon, D.R., Franden, M.A., Johnson, C.W., Karp, E.M., Guarneri, M.T., Linger, J.G., Salm, M.J., Strathmann, T.J., Beckham, G.T., 2015. Adipic acid production from lignin. *Energy Environ. Sci.* 8, 617–628.
- Vardon, D.R., Rorrer, N.A., Salvachua, D., Settle, A.E., Johnson, C.W., Menart, M.J., Cleveland, N.S., Ciesielski, P.N., Steirer, K.X., Dorgan, J.R., Beckham, G.T., 2016. *Cis,cis*-Muconic acid: separation and catalysis to bio-adipic acid for nylon-6,6 polymerization. *Green Chem.* 18, 3397–3413.
- Wirth, B., Mumme, J., 2013. Anaerobic digestion of waste water from hydrothermal carbonization of corn silage. *Appl. Bioenergy.* 1, 1–10.
- Wahyudiono, M.S., Goto, M., 2008. Recovery of phenolic compounds through the decomposition of lignin in near and supercritical water. *Chem. Eng. Process.* 47, 1609–1619.
- Wittmann, C., Zeng, A.P., Deckwer, W.D., 1995. Growth inhibition by ammonia and use of a pH-controlled feeding strategy for the effective cultivation of *Mycobacterium chlorophenolicum*. *Appl. Microbiol. Biotechnol.* 44, 519–525.
- Xie, N.Z., Liang, H., Huang, R.B., Xu, P., 2014. Biotechnological production of muconic acid: current status and future prospects. *Biotechnol. Adv.* 32, 615–622.
- Zobel, S., Benedetti, I., Eisenbach, L., de Lorenzo, V., Wierckx, N., Blank, L.M., 2015. Tn7-based device for calibrated heterologous gene expression in *Pseudomonas putida*. *ACS Synth. Biol.* 4, 1341–1351.



## Appendix W

### **Characterisation of the L-Cystine $\beta$ -Lyase PatB from *Phaeobacter inhibens*: An Enzyme Involved in the Biosynthesis of the Marine Antibiotic Tropodithietic Acid**

*ChemBioChem* **2017**, *18*, 2260–2267.

DOI:10.1002/cbic.201700358



# Characterisation of the L-Cystine $\beta$ -Lyase PatB from *Phaeobacter inhibens*: An Enzyme Involved in the Biosynthesis of the Marine Antibiotic Tropodithietic Acid

Jeroen S. Dickschat,<sup>\*[a]</sup> Jan Rinkel,<sup>[a]</sup> Tim Klapschinski,<sup>[a]</sup> and Jörn Petersen<sup>[b]</sup>

The L-cystine  $\beta$ -lyase from *Phaeobacter inhibens* is involved in the biosynthesis of the sulfur-containing antibiotic tropodithietic acid. The recombinant enzyme was obtained by heterologous expression in *Escherichia coli* and biochemically characterised by unambiguous chemical identification of the products formed from the substrate L-cystine, investigation of the substrate spectrum, determination of the enzyme kinetics, sequence alignment with closely related homologues and site-

directed mutagenesis to identify a highly conserved lysine residue that is critical for functionality. PatB from *P. inhibens* is a new member of the small group of characterised L-cystine  $\beta$ -lyases and the first example of an enzyme with such an activity that is required for the biosynthesis of an antibiotic. A comparison of PatB to previously reported enzymes with L-cystine  $\beta$ -lyase activity from bacteria and plants is given.

## Introduction

The antibiotic tropodithietic acid (TDA; Scheme 1), initially described as its tautomer thiotropocin, was first isolated from *Pseudomonas* sp. CB-104, and was shown to exhibit significant activity against various Gram-positive and -negative bacteria and ascomycete fungi at low micromolar concentrations.<sup>[1,2]</sup> The compound is also produced by marine alphaproteobacteria, including *Phaeobacter inhibens* DSM 17395<sup>[3,4]</sup> and various isolates of *Pseudovibrio*,<sup>[5,6]</sup> besides several other bacteria from the *Roseobacter* group.<sup>[7–9]</sup> Notably, all of these TDA-producing bacteria are associated with eukaryotes, such as sponges,<sup>[6]</sup> molluscs,<sup>[10]</sup> dinoflagellates<sup>[11]</sup> or marine green algae.<sup>[12]</sup> Because these symbionts may have beneficial effects for the host organisms by protecting them from infections with pathogens, such as *Vibrio anguillarum*,<sup>[13–15]</sup> the compound or its bacterial producers are potentially interesting, for example, for applications in fish aquaculture. A recent mode of action study revealed that TDA acted as an electroneutral H<sup>+</sup>/M<sup>+</sup> antiporter,<sup>[16]</sup> similar to polyether ionophores, such as monensin.<sup>[17]</sup>

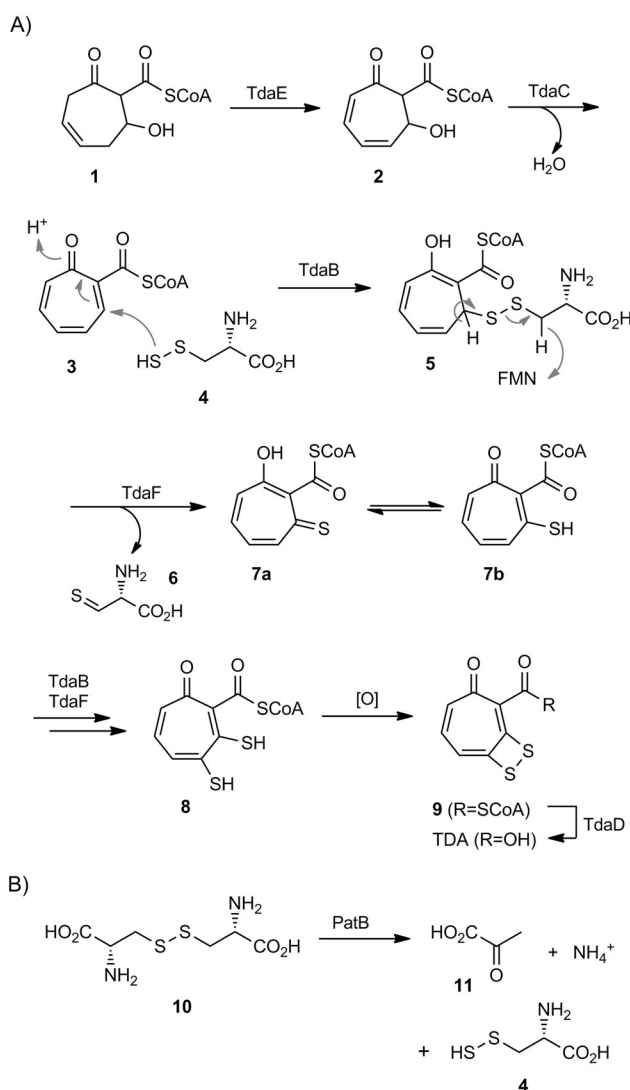
Feeding experiments with isotopically labelled precursors continue to be an effective method for studying biosynthetic pathways to secondary metabolites.<sup>[18]</sup> Through this approach, the biosynthesis of TDA was shown to proceed through degradation of L-phenylalanine to phenylacetic acid,<sup>[19,20]</sup> which was

further transformed by the phenylacetate catabolon.<sup>[21,22]</sup> Interestingly, a critical point mutation in the aldehyde dehydrogenase domain of the recombinant pathway enzyme PaaZ resulted in the spontaneous cyclisation of a reactive aldehyde intermediate to yield the seven-membered carbocycle **1**, which has been suggested as the starting point for further transformations to TDA (Scheme 1 A).<sup>[22]</sup> Similarly, deletion of the gene for the related aldehyde dehydrogenase Pacl resulted in the accumulation of tropone,<sup>[23]</sup> a compound that is also detected in headspace extracts of TDA-producing bacteria,<sup>[24]</sup> and is likely to be formed from **1** by spontaneous and/or enzymatic degradation by the enzymes encoded in the TDA biosynthetic gene cluster. Further steps of TDA biosynthesis depend on the TDA biosynthetic gene cluster,<sup>[8]</sup> the expression of which is under control of *N*-(3-hydroxydecanoyl)-L-homoserine lactone mediated quorum sensing in *P. inhibens*<sup>[25]</sup> and triggered in a positive feedback loop by its own metabolite in *Ruegeria* sp. TM1040.<sup>[26]</sup> Gene cluster regulation is different in *Pseudovibrio*.<sup>[6]</sup> A combination of bioinformatic analyses, gene knock-outs and feeding experiments with isotopically labelled precursors resulted in tentatively assigned functions of the enzymes encoded in the TDA biosynthetic gene cluster and suggested structures for the pathway intermediates.<sup>[27]</sup> Specifically, the direct sulfur precursor in TDA biosynthesis was suggested to be the notoriously unstable compound *S*-thio-L-cysteine (**4**) because deletion of a gene encoding PatB, an enzyme that exhibits high homology to L-cystathionine  $\beta$ -lyases, resulted in abolished TDA production that could neither be complemented by the addition of L-cysteine nor L-homocysteine (**18**). However, if PatB would act on the L-cysteine dimer, L-cystine (**10**; Scheme 1 B), the product **4** would be expected, which fits into the biosynthetic mechanism for TDA (Scheme 1 A).<sup>[27]</sup> Recently, Wang et al. showed the involvement of PatB in the biosynthesis of roseobactin,<sup>[28]</sup> an algicidal class of compounds struc-

[a] Prof. Dr. J. S. Dickschat, J. Rinkel, T. Klapschinski  
Kekulé-Institut für Organische Chemie und Biochemie  
Rheinische Friedrich-Wilhelms-Universität Bonn  
Gerhard-Domagk-Strasse 1, 53121 Bonn (Germany)  
E-mail: dickschat@uni-bonn.de

[b] Dr. J. Petersen  
Leibniz-Institut DSMZ  
Deutsche Sammlung von Mikroorganismen und Zellkulturen GmbH  
Inhoffenstrasse 7b, 38124 Braunschweig (Germany)

Supporting information and the ORCID identification numbers for the authors of this article can be found under <https://doi.org/10.1002/cbic.201700358>.



**Scheme 1.** TDA biosynthesis. A) Proposed biosynthetic pathway with suggested intermediates and bioinformatically assigned enzyme functions. CoA: coenzyme A, FMN: flavin mononucleotide. B) Cleavage of L-cysteine (**10**) by PatB to pyruvate (**11**); the suggested sulfur precursor of TDA biosynthesis, S-thio-L-cysteine (**4**); and ammonium.

turally and biosynthetically related to TDA and responsible for the switch from mutualistic to pathogenic behaviour of *P. inhibens* towards its algal symbionts.<sup>[29]</sup> Purified recombinant PatB, N-terminally fused to the solubility-enhancing domain NusA, was shown to convert **10** into a product with a free thiol group and with a mass corresponding to **4**, but L-cysteine or L-cystathionine (**17**) were not accepted by the fused enzyme.<sup>[28]</sup>

Herein, we present a detailed biochemical characterisation of recombinant PatB from *P. inhibens* that could be obtained as a His<sub>6</sub>-tagged soluble protein, including the unambiguous identification of the products generated from **10** by comparison to standards, its pH optimum and substrate tolerance, and a mechanistic investigation by site-directed mutagenesis.

## Results and Discussion

### Identification of PatB as cystine β-lyase

The *patB* gene from *P. inhibens* DSM 17395 (PGA1\_c00860; accession no. WP014878874) was amplified by PCR from genomic DNA and cloned into the expression vector pYE-Express by homologous recombination in yeast.<sup>[30]</sup> The gene was expressed in *Escherichia coli* BL21(DE3) and the recombinant His<sub>6</sub>-tagged protein was obtained in soluble form. Purification by Ni<sup>2+</sup>-NTA affinity chromatography yielded the pure protein eluate (Figure S1 in the Supporting Information) as a pale-yellow solution that indicated co-purification with the pyridoxal 5'-phosphate (PLP) cofactor (Figure S2). Also, MALDI-TOF MS measurements of the recombinant protein, in comparison to the apo-enzyme prepared by treatment with NaCNBH<sub>3</sub><sup>[31]</sup> and hydroxylamine,<sup>[32]</sup> showed a shift in the mass distribution that was approximately in line with the cofactor mass addition (Figure S3). The characterisation of the expected product **4** during incubation experiments of PatB with **10** was significantly hampered by the known instability of **4**, which led to rapid decomposition to L-cysteine (**10**) and elemental sulfur.<sup>[33]</sup> Therefore, substrate **10** was incubated with PatB, followed by trapping of the product by the addition of dimethyl sulfate. Analysis by HPLC-ESI-MS revealed the presence of a compound with the molecular mass of methylated **4** ( $m/z$  168.0147 [ $M+H$ ]<sup>+</sup>) and an isotope pattern in agreement with the presence of two sulfur atoms (Figure 1). A synthetic reference compound was obtained by nucleophilic substitution of cysteine (**13**) at the sulfane sulfur of S-methyl methanethiosulfonate (**12**) under slightly acidic conditions (Figure 1C). The product S-(methylthio)-L-cysteine (**14**) was obtained in 53% yield, characterised by NMR spectroscopy and proved to be identical to the compound formed by PatB-mediated lysis of **10** and subsequent methylation, in terms of both retention time and mass spectra.

The second product of the lysis of **10** by PatB was trapped by the addition of 4-fluorophenylhydrazine (**15**), which reacts with pyruvate (**11**) upon gentle warming to form a mixture of the *E* and *Z* hydrazones **16** that were detected by HPLC-MS (Figure 2). For comparison, an authentic sample of **11** was treated with **15** under the same conditions, yielding the hydrazones **16**, which had an identical elution time to that of the trapped products from enzyme incubation. Finally, the addition of Nessler reagent to the enzyme reaction produced an auburn precipitate, which indicated the detection of ammonium in the PatB reaction mixture. Taken together, these results established the conversion of **10** into **4**, **11** and ammonium by PatB; thus identifying this enzyme as an L-cystine β-lyase.

### Substrate tolerance of PatB

The substrate scope of PatB was investigated by incubation experiments with several compounds structurally related to **10** (Scheme 2A). L-Cystathionine (**17**) has a central function in the primary sulfur metabolism and is cleaved by L-cystathionine β-lyases into L-homocysteine (**18**), **11** and ammonium. In comparison to **10**, one sulfur atom is exchanged by a methylene

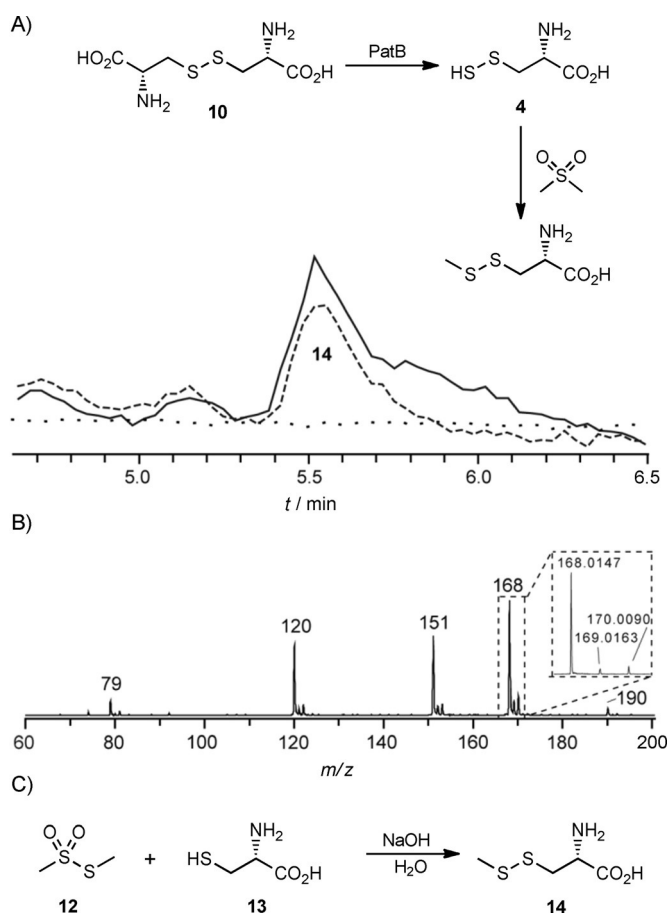


**Figure 1.** Identification of the product obtained by cleavage of **10** with PatB. A) HPLC-ESI-MS total ion chromatogram of the enzyme product obtained from **10** after methylation with dimethyl sulfate (-----), synthetic standard **14** (—) and a negative control without the enzyme (.....). B) ESI mass spectrum of the methylated enzyme product eluting at a retention time of 5.5 min ( $m/z$  calcd for  $C_4H_{10}NO_2S_2^+$ : 168.0147 [ $M+H$ ] $^+$ ; found: 168.0147); C) synthesis of reference compound **14**.

group in **17**. This compound was included to study the L-cystathionine  $\beta$ -lyase activity of PatB. In a recent study on three different dimethylsulfonylpropionate (DMSP) lyases (DddW, DddP and DddQ) from the marine bacterium *Ruegeria pomeroyi*, we showed that the selenium analogue of DMSP, dimethylselenio-propionate (DMSeP), was also accepted and efficiently converted into the lysis products dimethyl selenide and acrylate.<sup>[34]</sup> For a similar investigation into the tolerance of PatB towards an exchange of sulfur for selenium, L-selenocystine (**19**) was included in this study. Furthermore, the synthetic compound **14** and L-methionine (**22**) were tested as substrates.

The incubation of **17** with PatB resulted in efficient conversion into **18**, which was identified through HPLC-MS by comparison to a commercially available standard (Figure S4). The bis-selenium analogue of **10**, L-selenocystine (**19**), was also accepted as a substrate. As discussed above for the conversion of **10** into **4**, the initial product **20** proved to be unstable and was only detectable after its methylation by the addition of dimethyl sulfate to the enzyme reaction. A compound with the same chromatographic behaviour, tentatively identified from

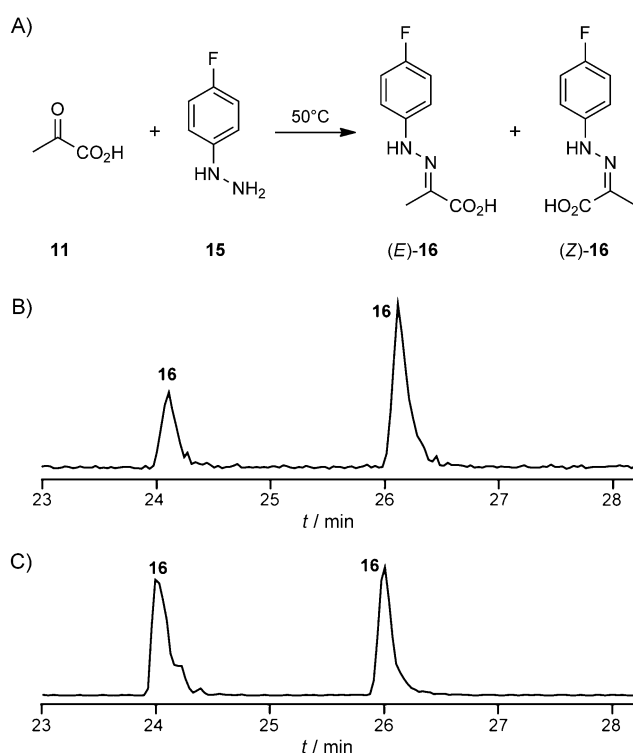
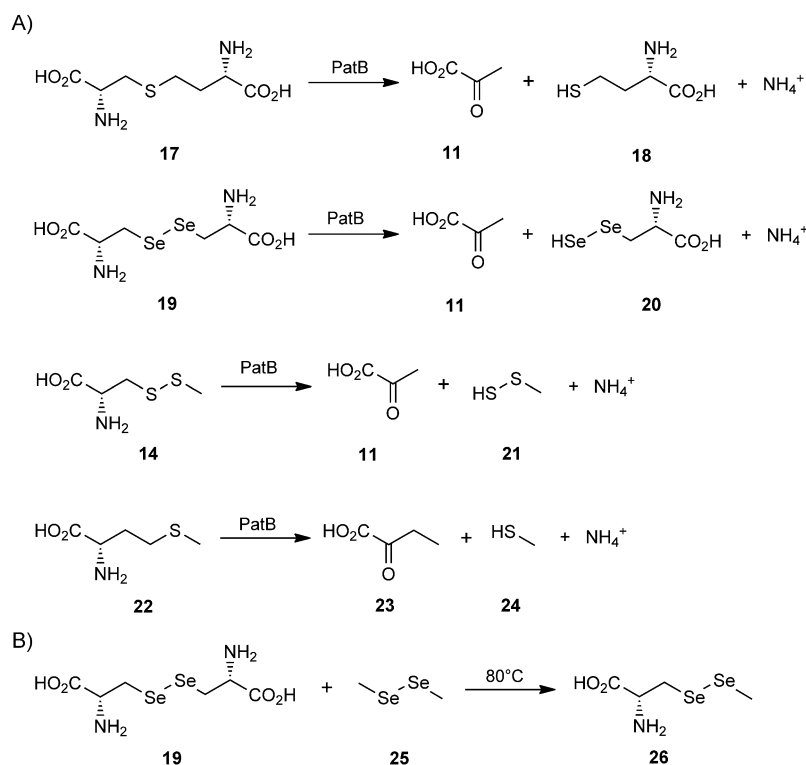


**Figure 2.** Identification of the product obtained by cleavage of **10** with PatB. A) Reaction of **11** and **15** to give the diastereomeric mixture of *E* and *Z* hydrazones **16**. B) HPLC-MS analysis (extracted ion chromatogram for  $m/z$  195) of the products obtained from the incubation of **10** with PatB and **15**. C) HPLC-MS analysis of the products obtained from **11** and **15** under the same conditions. The *E* and *Z* isomers of **16** could not be assigned to the individual signals in the HPLC-MS chromatograms.

its exact mass as compound **26**, was obtained in a metathesis reaction between **19** and dimethyl disulfide (**25**), which was achieved through gentle heating of the compound mixture (Figure 3).

The lysis of **14** by PatB resulted in the formation of volatile sulfur compounds that were captured by use of a solid-phase micro-extraction (SPME) fibre that allowed for the solvent-free analysis of volatile compounds by direct insertion of the fibre into the injection port of a GC/MS.<sup>[35,36]</sup> In addition to expected product **21**, which was found as a trace compound, several other sulfur volatile compounds, including methanethiol (**24**), dimethyl disulfide (**27**), dimethyl trisulfide (**28**) and dimethyl tetrasulfide (**29**), were detected (Figure 4A). All four compounds, **24** and **27–29**, are known as headspace constituents of many bacteria and fungi,<sup>[37,38]</sup> and their mass spectra were included in our mass spectral libraries to allow for their instantaneous and unambiguous identification. No mass spectrum was available for **21**, but the recorded mass spectrum showed a molecular ion, isotope and fragmentation pattern that were in accordance with the structure of **21** (Figure 4B). However, the isomeric structure to **21**, methanedithiol, cannot be completely ruled out based on the obtained MS data, although its formation would be difficult to understand. The formation of the other observed products can be understood by the oxidative dimerisation of **21** in the presence of air to give **29**, where-



Scheme 2. A) Substrate range of PatB. B) Metathesis reaction of **19** and **25**.

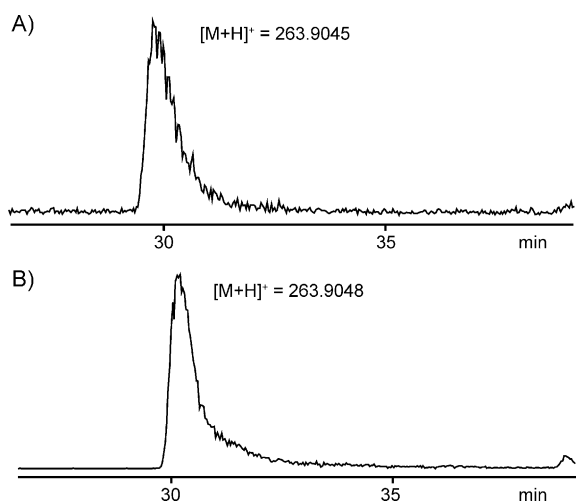


Figure 3. Identification of the lysis product obtained with PatB from **19** and by subsequent methylation with dimethyl sulfate. HPLC-MS analysis of A) the methylated enzyme product ( $m/z$  263.9045  $[M+H]^+$ ) and B) the synthetic reference compound **26** ( $m/z$  calcd for  $C_4H_{10}NO_2Se_2^+$ : 263.9036  $[M+H]^+$ ; found: 263.9048).

as subsequent metathesis reactions that occur under the thermal impact of GC analysis can explain the generation of **24**, **27** and **28** (Figure 4C). No cleavage of **22** into volatile sulfur compounds by PatB was observed, which showed that the enzyme had no  $\gamma$ -lyase activity.

### Enzyme kinetics of PatB

The enzyme kinetics of PatB were monitored by the addition of an excess of the Ellman reagent (5,5'-dithiobis-(2-nitrobenzoic acid))<sup>[39]</sup> to the enzyme incubations.<sup>[28]</sup> This reagent allows for the detection of free thiol groups, as formed during the lysis of **10** and its substrate analogues by PatB. Reaction of the Ellman reagent with free thiols results in the release of the 2-nitro-5-thiobenzoate dianion, which exhibits a yellow colour and can be quantified by the UV/Vis absorbance at  $\lambda = 412$  nm. The reagent also enables the recording of kinetic data for enzymes that produce free thiols, if the absorbance is measured in a time-resolved manner with different substrate concentrations. In the first set of experiments, the pH optimum for PatB was determined over a pH range that did not affect the molar absorption coefficient of the 2-nitro-5-thiobenzoate dianion ( $\epsilon = 14\,150$  L mol<sup>-1</sup> cm<sup>-1</sup>).<sup>[40]</sup> Therefore, the initial reaction rates for the conversion of **10** by PatB at a substrate concentration of 200  $\mu\text{mol L}^{-1}$  were determined, which revealed optimal conditions of pH 8.75 (Figure 5A; conditions above pH 9 resulted in the non-enzymatic decomposition of **10** and are not recommended for the Ellman reagent). The temperature optimum at pH 8.75 was found at 30 °C (Figure 5B).

The enzyme kinetics of PatB were determined for **10** and the other accepted substrates discussed above at pH 8.75 and 30 °C with different substrate concentrations, ranging from 200 to 3  $\mu\text{M}$ , through Lineweaver–Burk analysis. Substrate **10** exhibited a  $k_{\text{cat}}/K_M$  value of  $(3.6 \pm 0.3)$   $\mu\text{M}^{-1} \text{min}^{-1}$  (Table 1). The addition of PLP to the reaction did not result in any enhance-



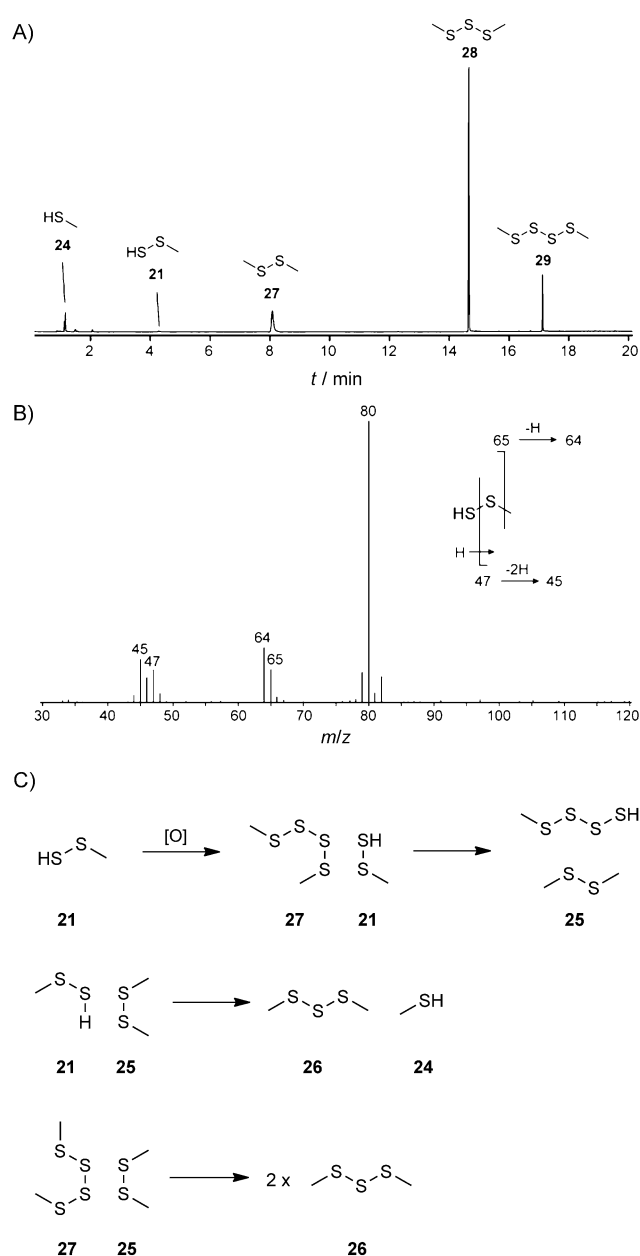


**Figure 4.** Products generated by the incubation of **14** with PatB. A) Total ion chromatogram of the volatile compounds released from the enzyme reaction and captured by SPME. B) EI mass spectrum of the putative initial product **21**. C) Reactions of **21** in the presence of air and under the thermal impact of GC/MS analysis to explain the observed product portfolio.

ment of this value. Synthetic compound **14** showed a slightly increased enzyme affinity (indicated by a moderately decreased  $K_M$ ) to that observed for **10**; this suggested that one fully established cysteinyl moiety in the substrate was sufficient for substrate binding; this is in agreement with the substrate binding determined from structural data of the L-cystine  $\beta$ -lyase from the cyanobacterium *Synechocystis*.<sup>[41]</sup> The significantly lower turnover number ( $k_{cat}$ ) for substrate analogue **14**, in comparison to that of **10**, resulted in an overall lower performance of PatB towards **14**. The  $k_{cat}/K_M$  indicated that **17** was

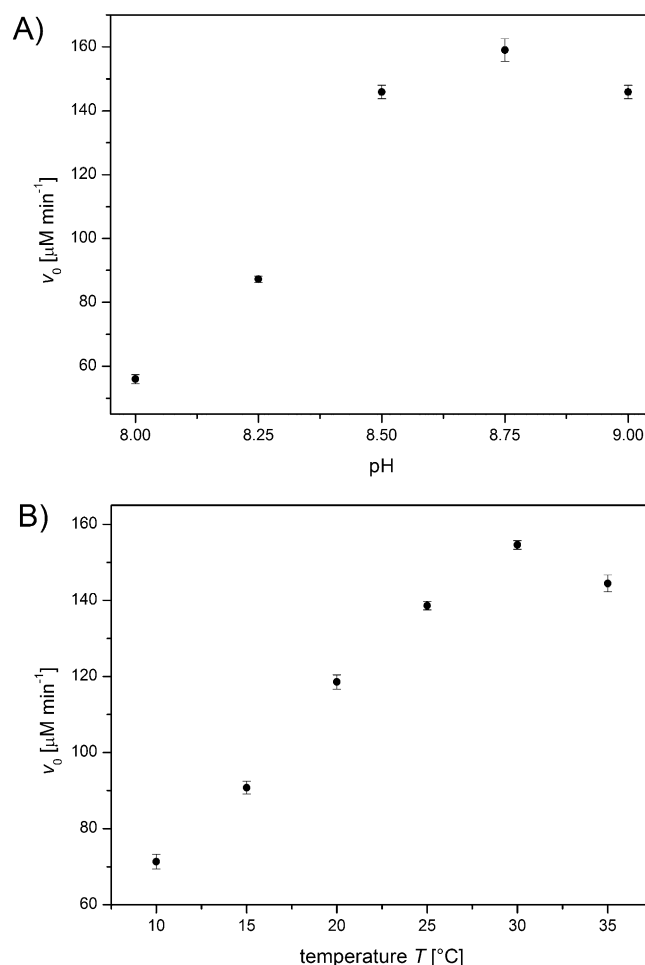


**Figure 5.** Optimum A) pH and B) temperature conditions for PatB determined from initial reaction rates with **10** ( $200 \mu\text{mol L}^{-1}$ ).

**Table 1.** Kinetic data for the enzymatic lysis of substrate analogues by PatB at pH 8.75 and  $30^\circ\text{C}$ .

Substrate	$k_{cat}$ [ $\text{min}^{-1}$ ] <sup>[a]</sup>	$K_M$ [ $\mu\text{M}$ ] <sup>[a]</sup>	$k_{cat}/K_M$ [ $\mu\text{M}^{-1} \text{min}^{-1}$ ]
<b>10</b>	$306 \pm 7$	$85 \pm 7$	$3.6 \pm 0.3$
<b>14</b>	$101 \pm 15$	$68 \pm 12$	$1.5 \pm 0.3$
<b>17</b>	$57 \pm 6$	$107 \pm 15$	$0.5 \pm 0.1$
<b>19</b>	$117 \pm 11$	$104 \pm 16$	$1.1 \pm 0.2$

[a] Determined from kinetic data summarised in Tables S5–S8.

converted with the lowest efficiency of the tested substrates. Selenium analogue **19** showed a decreased turnover number in comparison to that of **10**, although the enzyme affinity was almost the same, which reflected the similar electronic states and sizes of sulfur and selenium atoms (covalent radii of sulfur and selenium are 104 and 117 pm, respectively). The overall kinetics revealed that **19** was converted by PatB with lower catalytic efficiency than that of natural substrate **10** and substrate analogue **14**, but faster than that of **17**.

Interestingly, although the  $k_{cat}$  and  $K_M$  data determined for PatB from *P. inhibens* deviated from those reported for the

enzyme from *Synechocystis*, the overall kinetics in terms of  $k_{\text{cat}}/K_M$  matched very well (reported for the *Synechocystis* enzyme:  $k_{\text{cat}}/K_M = 36 \text{ Lmmol}^{-1} \text{ s}^{-1} = 2.16 \text{ L}\mu\text{mol}^{-1} \text{ min}^{-1}$ ). Similar to our findings, substrate analogue **17** was also converted by the enzyme from *Synechocystis* ( $k_{\text{cat}}/K_M = 0.36 \text{ L}\mu\text{mol}^{-1} \text{ min}^{-1}$ ) with much lower efficiency.<sup>[42]</sup>

### Site-directed mutagenesis

A BLAST search by using the sequence of PatB from *P. inhibens* revealed that closely related enzymes were widespread, particularly in bacteria of the *Roseobacter* group. The 500 closest hits showed a strongly conserved sequence length of between 370 and 418 amino acid residues. An amino acid sequence alignment of the 500 sequences returned 18 identical residues that occurred in all PatB homologues, as marked in the PatB sequence of *P. inhibens* in Figure S9. Among these residues, a highly conserved Lys is found (K235 in the enzyme from *P. inhibens*), which is assumed to be responsible for binding of the PLP cofactor, similar to the findings reported for the L-cystathionine  $\beta$ -lyase from *Arabidopsis thaliana*.<sup>[43]</sup> Site-directed mutagenesis of K235 yielded the two variants K235Q and K235M, which were both incubated with **10**. Both variants co-purified with PLP (Figure S2), probably due to non-covalent binding, but did not show any detectable conversion of this substrate, which established the critical role of K235 for enzyme functionality.

### Feeding experiments

The importance of PatB for TDA biosynthesis in *P. inhibens* DSM 17395 was shown previously in a combined knockout and feeding study with isotopically labelled ( $^{34}\text{S}$ )-L-cysteine.<sup>[27]</sup> Interestingly, labelling from ( $^{34}\text{S}$ )-L-cysteine is efficiently incorporated into TDA not only by *P. inhibens*, but also by *Phaeobacter gallaeciensis* DSM 26640, whereas labelling from the algal sulfur metabolite ( $^{34}\text{S}$ )DMSP<sup>[44]</sup> is not incorporated into TDA at all (Figure 6). *P. gallaeciensis* encodes a PatB homologue with 95% identical amino acid residues in its genome (WP\_024095761) that is also likely to function as a L-cystine  $\beta$ -lyase for the formation of the sulfur precursor (S)-thiocysteine for TDA biosynthesis. The finding that sulfur from DMSP is not incorporated into TDA is rather surprising, because it has been well documented that this compound is taken up and degraded into small, volatile sulfur compounds derived from **24** in *P. inhibens*.<sup>[45]</sup> However, this finding is in agreement with the reported incorporation of labelling from [ $^{35}\text{S}$ ]DMSP into proteins via [ $^{35}\text{S}$ ]MeSH by marine bacterioplankton. Specifically, these investigations demonstrated that the main portion of labelling in the proteins occurs in methionine, but not in cysteine.<sup>[46]</sup> These and our results indicate that the labelling from methionine is not quickly distributed to cysteine and TDA.

### Comparison to functionally related enzymes

A few previously described enzymes catalyse the same reaction as that described herein for PatB from *P. inhibens*. As

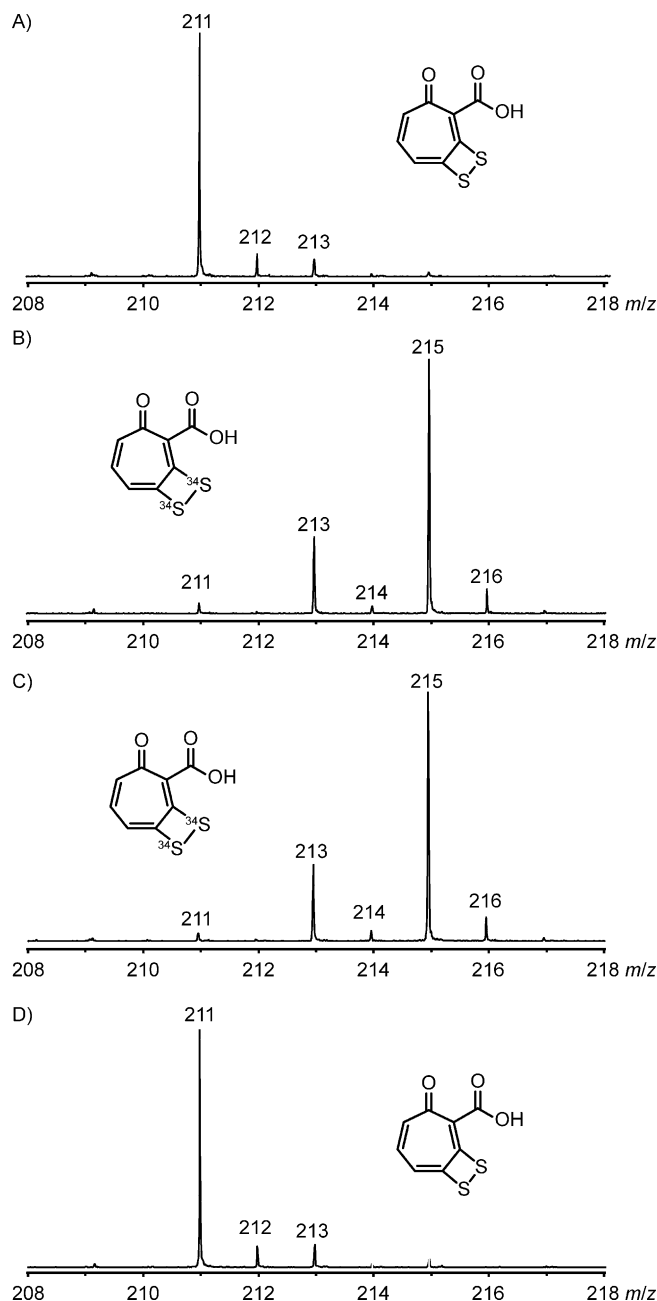


**Figure 6.** Feeding experiments with  $^{34}\text{S}$ -labelled precursors. Partial ESI mass spectrum showing the molecular ion  $[M+H]^+$  of A) unlabelled TDA, B)  $^{34}\text{S}$ -labelled TDA after feeding of [ $^{34}\text{S}$ ]-L-cysteine to *P. inhibens*, C)  $^{34}\text{S}$ -labelled TDA after feeding of [ $^{34}\text{S}$ ]-L-cysteine to *P. gallaeciensis*, and D) TDA with no incorporation of labelling after feeding of [ $^{34}\text{S}$ ]DMSP.

mentioned above, another L-cystine  $\beta$ -lyase has been reported from the cyanobacterium *Synechocystis*.<sup>[41,42]</sup> This enzyme shows only a weak sequence identity of 10% to the enzyme from *P. inhibens*, but its substrate tolerance is similarly broad. Furthermore, two L-cystine  $\beta$ -lyases from plants, one from *Brassica oleracea* and one from *A. thaliana*,<sup>[43,47]</sup> are known. The amino acid sequences of these two enzymes also strongly deviate from the sequence of PatB from *P. inhibens*. Notably, the L-cystine  $\beta$ -lyases from *Brassica* also accepts alternative substrates that are structurally related to **10**, although this has not

been investigated in detail for the *Arabidopsis* enzyme. Finally, the L-methionine  $\gamma$ -lyase from *Brevibacterium linens*, which also accepts **10** and catalyses its  $\beta$ -lysis, has been described.<sup>[48]</sup>

## Conclusion

The L-cystine  $\beta$ -lyase from *P. inhibens* was biochemically characterised. The enzyme cleaved **10** into **4**, **11** and ammonium, but also accepted structurally related substrate analogues with lower efficiency. Closely related homologues of this enzyme occur in many marine bacteria, particularly those of the *Roseobacter* group. An amino acid sequence alignment revealed a highly conserved lysine residue that was critical for enzyme functionality and most likely involved in binding of the PLP co-factor. A few enzymes with similar function have been characterised from other organisms, but none of these enzymes shows homology to PatB from *P. inhibens*. The previously reported involvement of PatB in the biosynthesis of TDA is further supported by the findings obtained during the course of this study. Notably, the unambiguous identification of the product **4** is in line with the suggested mechanism of sulfur incorporation into TDA, which is fundamentally different from that of other sulfur incorporation mechanisms reported for holomycin and thiomarinols (from cysteine),<sup>[49,50]</sup> gliotoxin (from glutathione)<sup>[51]</sup> or thiotetronate antibiotics (from cysteine).<sup>[52]</sup> Future experiments in our laboratory will address the further characterisation of intermediates and enzymes of the unique TDA biosynthetic pathway in *P. inhibens*.

## Acknowledgements

This work was funded by the DFG (SFB TR51 "Roseobacter") and by the Fonds der Chemischen Industrie.

## Conflict of Interest

The authors declare no conflict of interest.

**Keywords:** antibiotics • biosynthesis • enzymes • natural products • sulfur

- [1] K. Kintaka, H. Ono, S. Tsubotani, S. Harada, H. Okazaki, *J. Antibiot.* **1984**, *37*, 1294–1300.
- [2] E. M. Greer, D. Aebisher, A. Greer, R. Bentley, *J. Org. Chem.* **2008**, *73*, 280–283.
- [3] L. Liang, *Ph.D. Thesis*, University of Göttingen (Germany), **2003**.
- [4] T. Brinkhoff, G. Bach, T. Heidorn, L. Liang, A. Schlingloff, M. Simon, *Appl. Environ. Microbiol.* **2004**, *70*, 2560–2565.
- [5] A. Penesyan, J. Tebben, M. Lee, T. Thomas, S. Kjelleberg, T. Harder, S. Egan, *Mar. Drugs* **2011**, *9*, 1391–1402.
- [6] C. Harrington, F. J. Reen, M. J. Mooij, F. A. Stewart, J.-B. Chabot, A. F. Guerra, F. O. Glöckner, K. F. Nielsen, L. Gram, A. D. W. Dobson, C. Adams, F. O'Gara, *Mar. Drugs* **2014**, *12*, 5960–5978.
- [7] J. B. Bruhn, K. F. Nielsen, M. Hjelm, M. Hansen, J. Bresciani, S. Schulz, L. Gram, *Appl. Environ. Microbiol.* **2005**, *71*, 7263–7270.
- [8] H. Geng, J. B. Bruhn, K. F. Nielsen, L. Gram, L. Belas, *Appl. Environ. Microbiol.* **2008**, *74*, 1535–1545.

- [9] E. C. Sonnenschein, K. F. Nielsen, P. D'Alvise, C. H. Porsby, J. Melchiorson, J. Heilmann, P. G. Kalatzis, M. Lopez-Perez, B. Bunk, C. Spröer, M. Middelboe, L. Gram, *ISME J.* **2017**, *11*, 569–583.
- [10] C. Ruiz-Ponte, V. Cilia, C. Lambert, J. L. Nicolas, *Int. J. Syst. Bacteriol.* **1998**, *48*, 537–542.
- [11] T. R. Miller, R. Belas, *Appl. Environ. Microbiol.* **2004**, *70*, 3383–3391.
- [12] A. Penesyan, Z. Marshall-Jones, C. Holmstrom, S. Kjelleberg, S. Egan, *FEMS Microbiol. Ecol.* **2009**, *69*, 113–124.
- [13] C. Ruiz-Ponte, J. F. Samain, J. L. Sanchez, J. L. Nicholas, *Mar. Biotechnol.* **1999**, *1*, 52–59.
- [14] P. W. D'Alvise, S. Lillebo, M. J. Prol-Garcia, H. I. Wergeland, K. F. Nielsen, O. Bergh, L. Gram, *Plos One* **2012**, *7*, e43996.
- [15] W. Zhao, C. Dao, M. Karim, M. Gomez-Chiarri, D. Rowley, D. R. Nelson, *BMC Microbiol.* **2016**, *16*, 1.
- [16] M. Z. Wilson, R. Wang, Z. Gitai, M. R. Seyedsayamdost, *Proc. Natl. Acad. Sci. USA* **2016**, *113*, 1630–1635.
- [17] H. H. Mollenhauer, D. J. Morre, L. D. Rowe, *Biochim. Biophys. Acta Rev. Biomembr.* **1990**, *1031*, 225–246.
- [18] J. Rinkel, J. S. Dickschat, *Beilstein J. Org. Chem.* **2015**, *11*, 2493–2508.
- [19] D. E. Cane, Z. Wu, J. E. van Epp, *J. Am. Chem. Soc.* **1992**, *114*, 8479–8483.
- [20] M. Berger, N. L. Brock, H. Liesegang, M. Dogs, I. Preuth, M. Simon, J. S. Dickschat, T. Brinkhoff, *Appl. Environ. Microbiol.* **2012**, *78*, 3539–3551.
- [21] R. Teufel, V. Mascaraque, W. Ismail, M. Voss, J. Perera, W. Eisenreich, W. Haehnel, G. Fuchs, *Proc. Natl. Acad. Sci. USA* **2010**, *107*, 14390–14395.
- [22] R. Teufel, C. Gantert, M. Voss, W. Eisenreich, W. Haehnel, G. Fuchs, *J. Biol. Chem.* **2011**, *286*, 11021–11034.
- [23] R. Ross, S. Haas, E. Hammer, H. Herrmann, G. Burchhardt, *Mol. Genet. Genomics* **2002**, *267*, 656–663.
- [24] V. Thiel, T. Brinkhoff, J. S. Dickschat, S. Wickel, J. Grunenberg, I. Wagner-Döbler, M. Simon, S. Schulz, *Org. Biomol. Chem.* **2010**, *8*, 234–246.
- [25] M. Berger, A. Neumann, S. Schulz, M. Simon, T. Brinkhoff, *J. Bacteriol.* **2011**, *193*, 6576–6585.
- [26] H. Geng, R. Belas, *J. Bacteriol.* **2010**, *192*, 4377–4387.
- [27] N. L. Brock, A. Nikolay, J. S. Dickschat, *Chem. Commun.* **2014**, *50*, 5487–5489.
- [28] R. Wang, E. Gallant, M. R. Seyedsayamdost, *mBio* **2016**, *7*, e02118-15.
- [29] M. R. Seyedsayamdost, R. J. Case, R. Colter, J. Clardy, *Nat. Chem.* **2011**, *3*, 331–335.
- [30] J. S. Dickschat, K. A. K. Pahirulzaman, P. Rabe, T. A. Klapschinski, *ChemBioChem* **2014**, *15*, 810–814.
- [31] M. M. Whittaker, A. Penmatsa, J. W. Whittaker, *Arch. Biochem. Biophys.* **2015**, *568*, 64–70.
- [32] Q. Han, M. Xu, L. Tang, X. Tan, X. Tan, Y. Tan, R. M. Hoffman, *Clin. Chem.* **2002**, *48*, 1560–1564.
- [33] D. J. Smith, V. Venkatraghavan, *Synth. Commun.* **1985**, *15*, 945–950.
- [34] I. Burkhardt, L. Lauterbach, N. L. Brock, J. S. Dickschat, *Org. Biomol. Chem.* **2017**, *15*, 4432–4439.
- [35] C. L. Arthur, J. Pawliszyn, *Anal. Chem.* **1990**, *62*, 2145–2148.
- [36] J. S. Dickschat, *Nat. Prod. Rep.* **2014**, *31*, 838–861.
- [37] S. Schulz, J. S. Dickschat, *Nat. Prod. Rep.* **2007**, *24*, 814–842.
- [38] J. S. Dickschat, *Nat. Prod. Rep.* **2017**, *34*, 310–328.
- [39] G. L. Ellman, *Arch. Biochem. Biophys.* **1959**, *82*, 70–77.
- [40] P. W. Riddles, R. L. Blakeley, B. Zerner, *Anal. Biochem.* **1979**, *94*, 75–81.
- [41] T. Clausen, J. T. Kaiser, C. Steegborn, R. Huber, D. Kessler, *Proc. Natl. Acad. Sci. USA* **2000**, *97*, 3856–3861.
- [42] T. Lang, D. Kessler, *J. Biol. Chem.* **1999**, *274*, 189–195.
- [43] U. Breitingner, T. Clausen, S. Ehler, R. Huber, B. Laber, F. Schmidt, E. Pohl, A. Messerschmidt, *Plant Physiol.* **2001**, *126*, 631–642.
- [44] N. L. Brock, M. Menke, T. A. Klapschinski, J. S. Dickschat, *Org. Biomol. Chem.* **2014**, *12*, 4318–4323.
- [45] J. S. Dickschat, C. Zell, N. L. Brock, *ChemBioChem* **2010**, *11*, 417–425.
- [46] R. P. Kiene, L. J. Linn, J. González, M. A. Moran, J. A. Bruton, *Appl. Environ. Microbiol.* **1999**, *65*, 4549–4558.
- [47] K. Ukai, J. Sekiya, *Biosci. Biotechnol. Biochem.* **1997**, *61*, 1890–1895.
- [48] S. B. Hanniffy, M. Philo, C. Pelaez, M. J. Gasson, T. Requena, M. C. Martinez-Cuesta, *Appl. Environ. Microbiol.* **2009**, *75*, 2326–2332.
- [49] B. Li, C. Walsh, *Biochemistry* **2011**, *50*, 4615–4622.

- [50] A. C. Murphy, S.-S. Gao, L.-C. Han, S. Carobene, D. Fukuda, Z. Song, J. Hothersall, R. J. Cox, J. Crosby, M. P. Crump, C. M. Thomas, C. L. Willis, T. J. Simpson, *Chem. Sci.* **2014**, *5*, 397–402.
- [51] D. H. Scharf, P. Chankhamjon, K. Scherlach, T. Heinekamp, M. Roth, A. K. Brakhage, C. Hertweck, *Angew. Chem. Int. Ed.* **2012**, *51*, 10064–10068; *Angew. Chem.* **2012**, *124*, 10211–10215.
- [52] W. Tao, M. E. Yurkovich, S. Wen, K. E. Lebe, M. Samborskyy, Y. Liu, A. Yang, Y. Liu, Y. Ju, Z. Deng, M. Tosin, Y. Sun, P. F. Leadlay, *Chem. Sci.* **2016**, *7*, 376–385.

---

Manuscript received: July 4, 2017

Accepted manuscript online: September 12, 2017

Version of record online: October 20, 2017

---

## Appendix X

### **Acyl-group specificity of AHL synthases involved in quorum-sensing in *Roseobacter* group bacteria**

*Beilstein J. Org. Chem.* **2018**, *14*, 1309–1316.

DOI:10.3762/bjoc.14.112





# Acyl-group specificity of AHL synthases involved in quorum-sensing in *Roseobacter* group bacteria

Lisa Ziesche<sup>1</sup>, Jan Rinkel<sup>2</sup>, Jeroen S. Dickschat<sup>2</sup> and Stefan Schulz<sup>\*1</sup>

## Full Research Paper

Open Access

### Address:

<sup>1</sup>Institute of Organic Chemistry, Technische Universität Braunschweig, Hagenring 30, 38106 Braunschweig, Germany and  
<sup>2</sup>Kekulé-Institute of Organic Chemistry and Biochemistry, University of Bonn, Gerhard-Domagk-Str. 1, 53121 Bonn, Germany

### Email:

Stefan Schulz<sup>\*</sup> - stefan.schulz@tu-bs.de

\* Corresponding author

### Keywords:

*Dinoroseobacter shibae*; fatty acid composition; *N*-acylhomoserine lactones; quorum sensing; *Phaeobacter inhibens*

*Beilstein J. Org. Chem.* **2018**, *14*, 1309–1316.  
doi:10.3762/bjoc.14.112

Received: 12 February 2018

Accepted: 14 May 2018

Published: 05 June 2018

Associate Editor: K. N. Allen

© 2018 Ziesche et al.; licensee Beilstein-Institut.  
License and terms: see end of document.

## Abstract

*N*-Acylhomoserine lactones (AHLs) are important bacterial messengers, mediating different bacterial traits by quorum sensing in a cell-density dependent manner. AHLs are also produced by many bacteria of the marine *Roseobacter* group, which constitutes a large group within the marine microbiome. Often, specific mixtures of AHLs differing in chain length and oxidation status are produced by bacteria, but how the biosynthetic enzymes, LuxI homologs, are selecting the correct acyl precursors is largely unknown. We have analyzed the AHL production in *Dinoroseobacter shibae* and three *Phaeobacter inhibens* strains, revealing strain-specific mixtures. Although large differences were present between the species, the fatty acid profiles, the pool for the acyl precursors for AHL biosynthesis, were very similar. To test the acyl-chain selectivity, the three enzymes LuxI<sub>1</sub> and LuxI<sub>2</sub> from *D. shibae* DFL-12 as well as PgaI<sub>2</sub> from *P. inhibens* DSM 17395 were heterologously expressed in *E. coli* and the enzymes isolated for in vitro incubation experiments. The enzymes readily accepted shortened acyl coenzyme A analogs, *N*-pantothenoylcysteamine thioesters of fatty acids (PCEs). Fifteen PCEs were synthesized, varying in chain length from C<sub>4</sub> to C<sub>20</sub>, the degree of unsaturation and also including unusual acid esters, e.g., 2*E*,11*Z*-C18:2-PCE. The latter served as a precursor of the major AHL of *D. shibae* DFL-12 LuxI<sub>1</sub>, 2*E*,11*Z*-C18:2-homoserine lactone (HSL). Incubation experiments revealed that PgaI<sub>2</sub> accepts all substrates except C<sub>4</sub> and C<sub>20</sub>-PCE. Competition experiments demonstrated a preference of this enzyme for C<sub>10</sub> and C<sub>12</sub> PCEs. In contrast, the LuxI enzymes of *D. shibae* are more selective. While 2*E*,11*Z*-C18:2-PCE is preferentially accepted by LuxI<sub>1</sub>, all other PCEs were not, except for the shorter, saturated C<sub>10</sub>–C<sub>14</sub>-PCEs. The AHL synthase LuxI<sub>2</sub> accepted only C<sub>14</sub> PCE and 3-hydroxydecanoyl-PCE. In summary, chain-length selectivity in AHLs can vary between different AHL enzymes. Both, a broad substrate acceptance and tuned specificity occur in the investigated enzymes.

## Introduction

The *Roseobacter* group, a subgroup of the *Rhodobacteraceae* family, constitutes an important class of Gram-negative marine bacteria, occurring in many different habitats [1,2], in fresh water as well as on surfaces [3]. They can produce a variety of secondary metabolites, including antibiotics [4,5], volatile compounds [6,7], oligohydroxybutyrates [8] and a range of *N*-acyl-homoserine lactones (AHLs) [8–10]. AHLs are quorum-sensing signaling compounds that are used for cell–cell communication to regulate several physiological traits regulated by cell density, the ‘quorum’ [11–16], in roseobacters, e.g., in the production of the antibiotic tropodithietic acid in *Phaeobacter inhibens* [15] and cell differentiation in *Dinoroseobacter shibae* [14]. *Roseobacter* group AHLs are characterized by saturated, unsaturated and sometimes oxygenated acyl chains ranging in length between C<sub>8</sub> and C<sub>18</sub> [8] with the exception of the aromatic *p*-coumaroylhomoserine lactone produced by *Rugeria pomeroyi* DSS-3 [17].

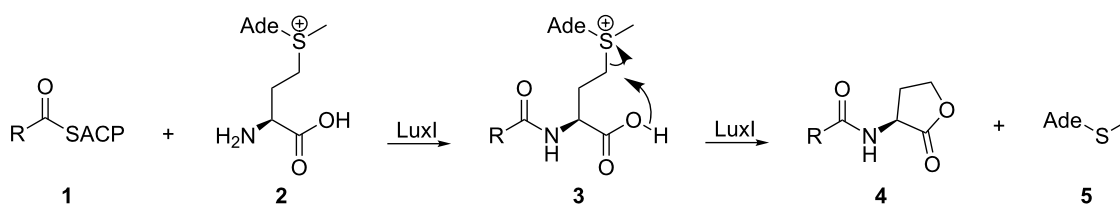
In a recent analysis we showed the AHL presence in 19 out of 24 *Roseobacter* group bacterial strains isolated from macroalgal surfaces [8]. The most widespread AHL was 7-tetradecenoyl-homoserine lactone (7-C14:1-HSL), present in seven strains. No clear correlation between phylogeny and AHL occurrence was observed. In some strains only one AHL was detected, while others such as *P. gallaeciensis* BS107 produced eight different AHLs [8].

The biosynthesis of AHLs is mediated by the enzyme LuxI or its homologs, and often accompanied by a regulator protein, LuxR [18,19]. An ACP-bound fatty acid acyl group **1** is transferred onto the amino group of *S*-adenosylmethionine (SAM, **2**) that is followed by substitution of the good leaving group 5'-deoxy-5'-thiomethyladenosine (**5**) of the thioester group, leading to homoserine lactone **4** formation (Scheme 1). Recently a LuxI-homolog, BjaI [20] preferring acyl-coenzyme A (CoA) substrates instead of the common ACP precursors, was characterized [21].

The LuxI-type enzymes are the most widespread and best understood AHL synthases. Four structures of LuxI-type en-

zymes have been published, covering both ACP and CoA-dependent structures with various chain lengths and different oxidation states of the acyl chain at C-3 [21–24]. A great diversity among AHL synthases is observed. The preference for unsubstituted, 3-oxo or 3-hydroxyacyl precursors is mediated by binding interactions inside the active site of AHL synthases [18,21]. Investigations on the chain-length selectivity of the AHL synthases are limited. BjaI can accept substrates ranging from isovaleryl-CoA, the native substrate, up to isononanoyl-CoA [21].

Three different LuxI homologs, LuxI<sub>1</sub>, LuxI<sub>2</sub>, and LuxI<sub>3</sub>, occur in *Dinoroseobacter shibae* DFL-12 [14]. Recently, we were surprised to find that the structures of AHLs synthesized by a LuxI homolog from *D. shibae* DFL-12 depended on the host in which the enzyme was expressed [10]. Expression of LuxI<sub>1</sub> in *E. coli* led to a predominant formation of a 2:1:0.3 mixture of 9-C18:1-homoserine lactone (HSL), C16:0-HSL and C14:0-HSL, while the overexpression in its parent strain furnished the native product, 2*E*,11*Z*-C18:2-HSL, accompanied by 4% each of 9-C18:1-HSL and 2,9-C16:2-HSL. While the native substrates of LuxI<sub>2</sub> and LuxI<sub>3</sub> were not detected because of their low concentration, their overexpression in *E. coli* led to the production of a 6:1 mixture of 7*Z*-C14:1-HSL and C14:0-HSL for LuxI<sub>2</sub> and no AHL formation for LuxI<sub>3</sub> [10]. The differences between the AHLs in terms of chain length and degree of unsaturation prompted us to investigate the acyl-chain selectivity of LuxI-type enzymes in roseobacters. Does the enzyme have an inherent selectivity for a specific acyl-chain precursor or does it react unselectively with every acyl-precursor available? In the latter case the presence of the acyl precursors would determine the structure of the final AHL. To answer this question, the fatty acid composition of the native roseobacters was determined and compared to the AHLs produced. In addition, LuxI-type enzymes were heterologously expressed in *E. coli* and the purified recombinant enzymes were tested with different precursors to probe their selectivity. Both model organisms of the *Roseobacter* group, *P. inhibens* (formerly *P. gallaeciensis* [25]) DSM17395 and *Dinoroseobacter shibae* DFL-12, were investigated, together with closely related *P. inhibens* strains T5 and



**Scheme 1:** Biosynthesis of AHLs by ACP-dependent LuxI type enzymes.



2.10 [26], to investigate strain variability. Previously, the LuxI homolog PgaI<sub>1</sub> from *P. inhibens* DSM 17395 has been characterized, producing *R*-3-OH-C10:0-HSL [15,27]. This strain produced additionally long chain AHLs such as C18:1-HSL [9] and contains a second AHL synthase, PgaI<sub>2</sub> [28], probably involved in the biosynthesis of the long chain AHLs. Here we report on the characterization of PgaI<sub>2</sub> from *P. inhibens* and of LuxI<sub>1</sub> and LuxI<sub>2</sub> from *D. shibae* by in vitro incubation experiments.

## Results and Discussion

The AHL production of four *Roseobacter* group strains was analyzed by a GC/MS-based method using XAD-16 as adsorbent in marine broth, developed by us [8]. The bacteria were isolated from different habitats: *D. shibae* DFL-12 was isolated from the dinoflagellate *Prorocentrum lima* [29], *P. inhibens* T5 was collected from a water sample of the German Wadden Sea [30], *P. inhibens* DSM17395 was isolated from seawater of larval cultures of the scallop *Pecten maximus* in Spain [25] and *P. inhibens* 2.10 stemmed from the surface of the green macroalga *Ulva australis* in Australia [31].

The results showed that *P. inhibens* 2.10 and *P. inhibens* DSM17395 produce the same four AHLs, 3-OH-C10:0-HSL as major components and known from previous analyses of *P. inhibens* [9,32], C16:0-HSL, C16:1-HSL, and C18:1-HSL (Table 1). *P. inhibens* T5 additionally produced 3-oxo-C10:0-HSL and C12:2-HSL with unknown location of the double bonds. *D. shibae* DFL-12 released C14:1-HSL, 3-oxo-C14-HSL, C18:1-HSL, and C18:2-HSL, similar to previous results [10,16].

In addition, the fatty acid profile of the four strains was determined. Therefore, bacterial colonies from agar plates were added to 20 µL of methanolic trimethylsulfonium hydroxide (TMSH) solution. This procedure lyses the bacteria and concomitantly transfers any bound or free fatty acid into its methyl ester (FAME) [33]. The extracts were analyzed by GC/MS (Figure 1). Short and long FAMES were detected, ranging from methyl octanoate to methyl icosanoate (Table 2). The three

*Phaeobacter* strains produced identical fatty acids. We identified FAMES with a C8:0, C12:0, C12:1, C16:0, C16:1, C17:0, C18:2, C18:0, C18:1, and C19:1 chain, the three last ones being the most abundant. *D. shibae* DFL-12 showed a similar fatty acid production, but no FAMES with C<sub>8</sub> or C<sub>12</sub> chains were detected. Instead, 3-OH-C10:0-HSL, C14:0, and C20:0 FAMES occurred in addition.

The location of the double bond of the major acids was determined by dimethyl disulfide (DMDS) derivatization [32,34]. The fragment ions at *m/z* 145 and 161 of the DMDS-derivative and the secondary fragments obtained by loss of the methyl ester group (*m/z* 129) located the position of the double bond in C12:1-FAME at C-5. Similarly, 9-C16:1 (*m/z* 145, 185, 217) and 11-C18:1-FAMES (*m/z* 145, 213, 245) were assigned. The three *Phaeobacter* strains showed also a small peak with identical mass spectrum compared to 11-C18:1-FAME eluting slightly earlier than the major compound, indicating minor amounts of 11*E*-C18:1-FAME next to the major 11*Z*-C18:1-FAME. DMDS adducts derived from *E*-configured double bonds elute slightly earlier than their *Z*-configured counterparts on apolar GC phases [34]. All four strains additionally contained 13-C18:1-FAME (*m/z* 61, 117, 241 and 273) in small amounts. The mass spectrum of C19:1-FAME differed from that of methyl nonadecenoate, but was identical to that of methyl 11-methyl-12-octadecenoate [29,35,36], as was that of its DMDS derivative (*m/z* 131, 241, 273, see Figures S1 and S2 in the Supporting Information File 1). Similarly, 13-C20:1 was identified in *D. shibae* DFL-12. Small amounts of a DMDS adduct of C18:2 were detected that added only one equivalent of DMDS. This reactivity is observed when a double bond is conjugated with a carbonyl group [37,38]. The ion at *m/z* 145 located one double bond at C-11, while the ions at *m/z* 211 and 243 revealed another unsaturation in the alkyl chain towards the carboxy terminus. These data indicate this FAME to be 2,11-C18:1, the parent acid of the major *D. shibae* AHL, 2*E*,11*Z*-C18:2-HSL [10]. The analysis performed with bacteria grown in liquid medium led to comparable results, indicating that the fatty acid composition does not depend on the culture method.

**Table 1:** Presence of different AHLs in four strains of *Roseobacter* group bacteria.<sup>a</sup>

strain	3-OH-C10:0-HSL	3-oxo-C10:0-HSL	C12:2-HSL	C14:1-HSL	3-oxo-C14:0-HSL	C16:0-HSL	C16:1-HSL	C18:1-HSL	C18:2-HSL
<i>P. inhibens</i> 2.10	40.5					15.9	12.9	30.6	
<i>P. inhibens</i> DSM17395	87.1					3.9	2.8	6.2	
<i>P. inhibens</i> T5	37.3	5.0	16.2			4.9	10.0	26.6	
<i>D. shibae</i> DFL-12				5.8	13.6			9.3	71.3

<sup>a</sup>Relative amounts of AHLs for each strain in %.

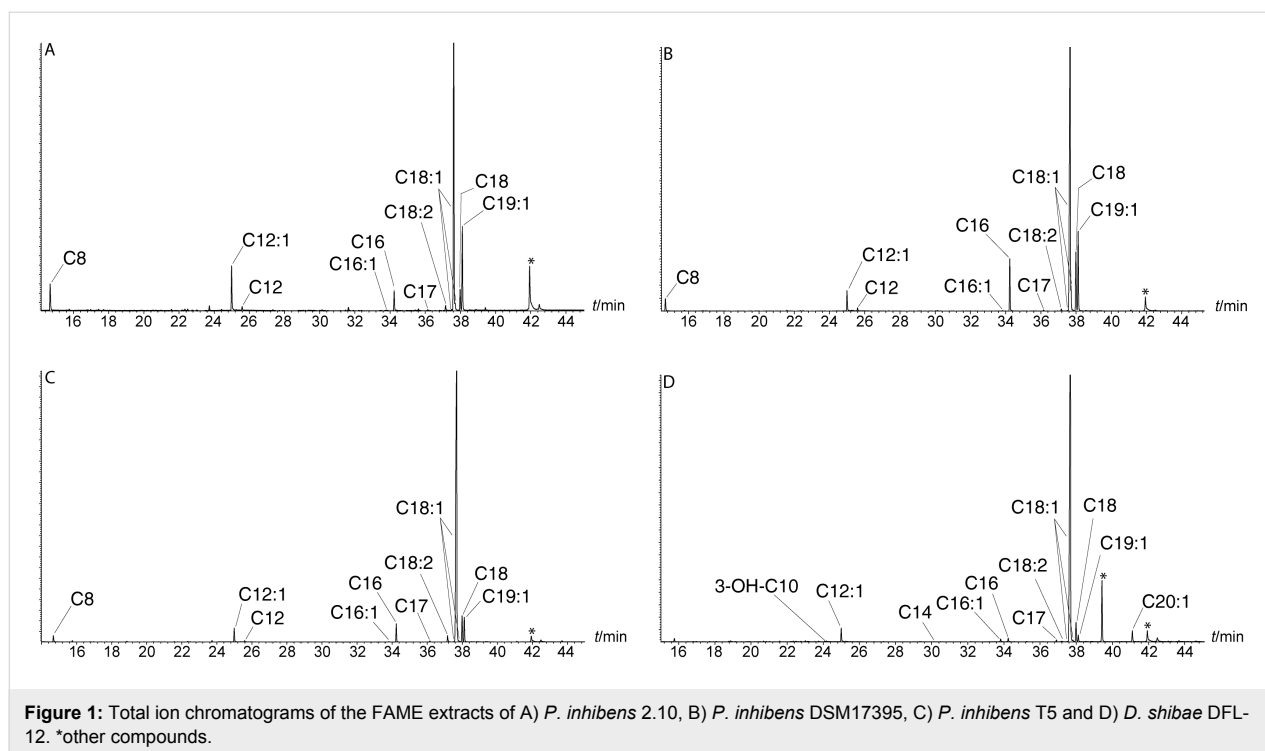


**Figure 1:** Total ion chromatograms of the FAME extracts of A) *P. inhibens* 2.10, B) *P. inhibens* DSM17395, C) *P. inhibens* T5 and D) *D. shibae* DFL-12. \*other compounds.

**Table 2:** Presence of bound or free fatty acids in four different *Roseobacter* group strains detected as methyl esters.<sup>a</sup>

	<i>P. inhibens</i>		<i>D. shibae</i>		<i>P. inhibens</i>		<i>D. shibae</i>	
	agar plate				liquid culture			
	2.10	DSM17395	T5	DFL-12	2.10	DSM17395	T5	DFL 12
C8:0	5.0	1.8	1.0		0.1	0.9	0.2	
3-OH-C10:0-HSL				0.1				0.5
C12:0	0.6	0.4	0.2		0.1	0.2	0.1	
5Z-C12:1	8.2	2.9	2.2	2.3	0.5	2.2	0.9	0.8
C14:0				<0.1				0.1
C16:0	3.8	7.5	3.0	0.6	4.3	2.6	2.2	0.3
9Z-C16:1	0.1	<0.1	<0.1	0.5	0.1	0.1	<0.1	0.2
C17:0	0.4	0.2	0.2	<0.1	0.1	0.1	0.1	<0.1
C18:0	3.9	8.6	4.6	2.6	2.1	1.8	1.8	3.4
11Z-C18:1	60.4	66.7	83.1	91.9	61.0	67.8	67.3	92.4
11E-C18:1	0.3	0.1	0.1	<0.1	0.1	0.1	0.1	0.1
13Z-C18:1	0.4	<0.1	<0.1	0.1	1.2	1.0	1.0	0.3
2E,11Z-C18:2	1.2	0.3	1.2	<0.1	3.2	1.8	2.9	<0.1
11Me-12E-C19:1	15.7	11.4	4.3	0.6	27.2	21.5	23.4	1.0
13Z-C20:1				1.2				0.9

<sup>a</sup>Relative peak areas of FAMES for each strain in %.

By comparing the fatty acid profiles and AHL production no direct correlation between fatty acids and AHLs can be observed. The major acid C18:1 is only reflected by a minor component in the AHL profile of the four strains. Small amounts of

2,11-C18:2 occur in all strains, only the *D. shibae* strain uses this acid as precursor for its major 2,11-C18:2-HSL. In contrast, the precursor acid 3-OH-C10:0-HSL is produced by *D. shibae*, but not present in the profiles of *P. inhibens*, which produces

large amounts of 3-OH-C10:0-HSL. Furthermore, the prominent acid 11Me-12-C18:1 is not used for AHL formation. Acids used for production of minor AHLs such as C14:1 or C12:2 were not detected.

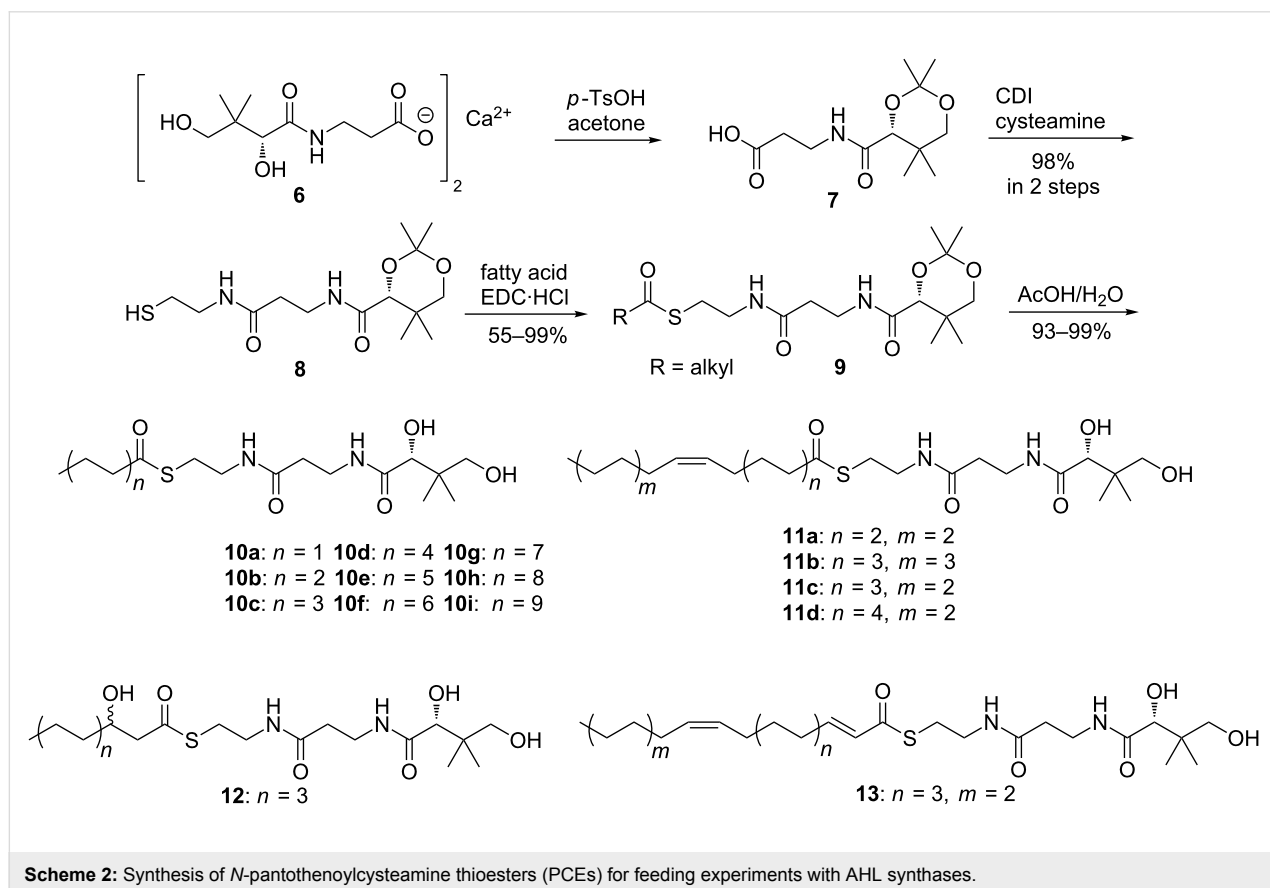
These results show that the fatty acid pool and AHL formation are indeed uncoupled. Although the fatty acid composition of the investigated strains is very similar, the AHL production differs largely. The complete absence or presence of only minor amounts of precursor acids of AHLs such as 2,11-C18:2 or 3-OH-C10:0-HSL might indicate that they are available only for AHL biosynthesis, but are not used for other physiological purposes. Such acids may be immediately transformed after their biosynthesis into an AHL, or are stored in a form not cleavable by the TMSH method used. These precursor acids may also originate from fatty acid degradation, a pathway that proceeds via free coenzyme A intermediates and not via acyl carrier protein-bound substrates like in the fatty acid biosynthesis.

These results led to the question whether the acyl-chain selectivity is an inherent property of the AHL synthase itself or whether this is determined by other factors, e.g., precursor availability. Therefore, LuxI-type synthases from *D. shibae*

(LuxI<sub>1</sub>, LuxI<sub>2</sub>) and from *P. inhibens* DSM17395 (PgaI<sub>2</sub>) were cloned and expressed in *E. coli* to allow in vitro experiments with suitable acyl precursors to probe AHL formation. After protein purification of the AHL synthases and incubation with the precursors *S*-adenosyl methionine (SAM) and different acyl derivatives (free fatty acids, SNAC esters, PCEs) the AHL production was determined using GC/MS [9,10,32]. Coenzyme A or abbreviated ACP analogs, *N*-pantothenoylcysteamine thioesters of fatty acids (PCEs) were synthesized (Scheme 2) to serve as substrate substitutes for the native precursors.

Calcium pantothenate (**6**) was protected with acetone forming acid **7** that was transformed with cysteamine into the protected thiol **8** [39]. Steglich esterification [40] with different free acids led to nine saturated PCEs **10a–i**, four monounsaturated acids (**11a–d**), 3-OH-C10:0-HSL PCE (**12**), and 2*E*,11*Z*-C18:2-PCE (**13**) after deprotection with acetic acid [41]. Although compounds **10–13** can be further purified by HPLC, the crude products proved to be pure enough for the next experiments.

The incubation experiments were performed with the three recombinant AHL synthases, SAM, and the different precursors **10–13**. The AHL-synthase PgaI<sub>2</sub> of *P. inhibens* showed a higher activity compared to the two *D. shibae* synthases. It



**Scheme 2:** Synthesis of *N*-pantothenoylcysteamine thioesters (PCEs) for feeding experiments with AHL synthases.

accepted all substrates, including unsaturated ones, with the exclusion of the very short C4:0 and very long C20:0-PCEs.

The AHL-synthase LuxI<sub>2</sub> was able to produce C14:0-HSL and 3-OH-C10-HSL in low concentration from the respective precursors. It is likely responsible for the formation of C14:0-HSL and 3-oxo-C14:0-HSL in *D. shibae* DFL-12. The AHL synthase LuxI<sub>1</sub> used five precursors to synthesize C8:0, C10:0, C12:0 and C14:0-HSL in low amounts, while 2*E*,11*Z*-C18:2-HSL, its native product, is formed in high concentration.

To further evaluate the selectivity of the promiscuous enzyme Pgal<sub>2</sub> from *P. inhibens*, competition experiments were performed. Targeting the optimal chain length of the fully saturated substrates first, a mixture with equal molar concentrations of the substrates **10a–h** was offered to the recombinant protein. GC/MS analysis of the resulting extract (Figure 2A) revealed a distribution of AHL products around the chain length of C<sub>10</sub> and C<sub>12</sub>, which were shown to be the most prominent products. In a second experiment with substrates **10a–i**, **11a–c**, and **12** also unsaturated substrates and the hydroxylated precursor were tested (Figure 2B). It turned out that the same distribution of the saturated AHLs as for the first experiment was observed with none of the additional substrates showing a significantly higher conversion. These results point to a very flexible active site of the investigated AHL synthase Pgal<sub>2</sub>, which converts a variety of substrates. The highest conversion efficiency in the competition experiments was found for the saturated substrates **10c** and **10d** with lower abundance of any AHL products deviating from

this chain length. It should be noted that the amount of added SAM was not sufficient to convert all substrates, so the product spectrum likely reflects different enzyme kinetics for the PCE substrates. In contrast, in the single-substrate incubation experiments (Table 3) an excess of SAM was used, and this may have led to the formation even of products that are disfavored in the competition experiments.

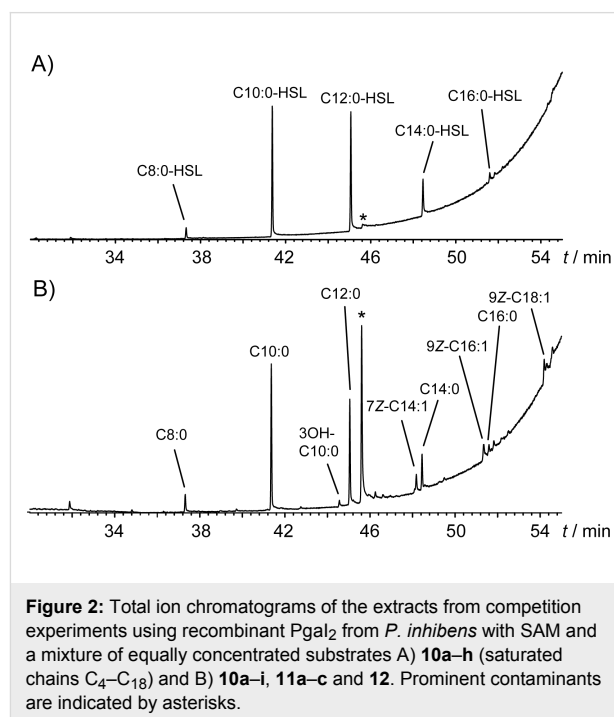


**Figure 2:** Total ion chromatograms of the extracts from competition experiments using recombinant Pgal<sub>2</sub> from *P. inhibens* with SAM and a mixture of equally concentrated substrates A) **10a–h** (saturated chains C<sub>4</sub>–C<sub>18</sub>) and B) **10a–i**, **11a–c** and **12**. Prominent contaminants are indicated by asterisks.

**Table 3:** Results of incubation experiments of single precursors **10–13** with *E. coli* constructs with recombinant AHL synthases Pgal<sub>2</sub>, LuxI<sub>1</sub> and LuxI<sub>2</sub> from different *Roseobacter* group bacteria.<sup>a</sup>

Precursor	AHL	<i>P. inhibens</i> Pgal <sub>2</sub>	<i>D. shibae</i> LuxI <sub>1</sub>	<i>D. shibae</i> LuxI <sub>2</sub>
<b>10a</b>	C4:0	–	–	–
<b>10b</b>	C6:0	x	–	–
<b>10c</b>	C8:0	xx	x	–
<b>10d</b>	C10:0	xx	x	–
<b>10e</b>	C12:0	xx	x	–
<b>10f</b>	C14:0	xx	x	x
<b>10g</b>	C16:0	x	–	–
<b>10h</b>	C18:0	x	–	–
<b>10i</b>	C20:0	–	–	–
<b>12</b>	3-OH-C10:0	xx	–	x
<b>11a</b>	7 <i>Z</i> -C14:1	xx	–	–
<b>11b</b>	9 <i>Z</i> -C16:1	xx	–	–
<b>11c</b>	9 <i>Z</i> -C18:1	xx	–	–
<b>11d</b>	11 <i>Z</i> -C18:1	xx	–	–
<b>13</b>	2 <i>E</i> ,11 <i>Z</i> -C18:2	xx	xx	–

<sup>a</sup>xx: high production, x: low production, –: no production.

## Conclusion

The results showed that the enzymes exhibit varying substrate plasticity. While the *P. inhibens* synthase Pgal<sub>2</sub> accepted most precursors, the best performance was observed with the saturated substrates harboring C<sub>10</sub> or C<sub>12</sub> chain lengths. In *P. inhibens* this enzyme is most likely responsible for the biosynthesis of long-chain AHLs. In contrast, *D. shibae* synthase LuxI<sub>1</sub> showed a high selectivity for 2*E*,11*Z*-C18:2-HSL and did not even accept similar substrates such as **11c** or **11d**. Interestingly, considerably shorter saturated substrates, e.g., **10e**, are accepted. The *D. shibae* synthase LuxI<sub>2</sub> synthase was even more selective. It seems likely that other factors than AHL synthase substrate specificity influence the observed formation of only certain AHLs by these wild-type enzymes. These factors might include selectivity found in enzymes activating or transporting acids to AHL synthases, or interact with the LuxI enzyme, either directly or indirectly. The combination of the different selectivity levels may eventually lead to the specific mixtures observed in the different AHL producing bacterial strains.

## Supporting Information

### Supporting Information File 1

Experimental, mass spectra, SDS page and NMR spectra.

[<https://www.beilstein-journals.org/bjoc/content/supplementary/1860-5397-14-112-S1.pdf>]

## Acknowledgements

We thank the Deutsche Forschungsgemeinschaft for supporting our work through the Transregional Collaborative Research Centre “Roseobacter” (SFB TRR 51/3) and the Fonds der Chemischen Industrie for a Ph.D. scholarship (to JR). Gene cloning by Seocho Kim is gratefully acknowledged.

## ORCID® iDs

Jeroen S. Dickschat - <http://orcid.org/0000-0002-0102-0631>

Stefan Schulz - <http://orcid.org/0000-0002-4810-324X>

## References

- Giebel, H.-A.; Kalhoefer, D.; Lemke, A.; Thole, S.; Gahl-Janssen, R.; Simon, M.; Brinkhoff, T. *ISME J.* **2011**, *5*, 8–19. doi:10.1038/ismej.2010.87
- Selje, N.; Simon, M.; Brinkhoff, T. *Nature* **2004**, *427*, 445–448. doi:10.1038/nature02272
- Freese, H. M.; Methner, A.; Overmann, J. *Front. Microbiol.* **2017**, *8*, No. 1659. doi:10.3389/fmicb.2017.01659
- Brock, N. L.; Nikolay, A.; Dickschat, J. S. *Chem. Commun.* **2014**, *50*, 5487–5489. doi:10.1039/c4cc01924e
- Seyedsayamdost, M. R.; Case, R. J.; Kolter, R.; Clardy, J. *Nat. Chem.* **2011**, *3*, 331–335. doi:10.1038/nchem.1002
- Thiel, V.; Brinkhoff, T.; Dickschat, J. S.; Wickel, S.; Grunenberg, J.; Wagner-Döbler, I.; Simon, M.; Schulz, S. *Org. Biomol. Chem.* **2010**, *8*, 234–246. doi:10.1039/B909133E
- Brock, N. L.; Menke, M.; Klapschinski, T. A.; Dickschat, J. S. *Org. Biomol. Chem.* **2014**, *12*, 4318–4323. doi:10.1039/c4ob00719k
- Ziesche, L.; Bruns, H.; Dogs, M.; Wolter, L.; Mann, F.; Wagner-Döbler, I.; Brinkhoff, T.; Schulz, S. *ChemBioChem* **2015**, *16*, 2094–2107. doi:10.1002/cbic.201500189
- Wagner-Döbler, I.; Thiel, V.; Eberl, L.; Allgaier, M.; Bodor, A.; Meyer, S.; Ebner, S.; Hennig, A.; Pukall, R.; Schulz, S. *ChemBioChem* **2005**, *6*, 2195–2206. doi:10.1002/cbic.200500189
- Neumann, A.; Patzelt, D.; Wagner-Döbler, I.; Schulz, S. *ChemBioChem* **2013**, *14*, 2355–2361. doi:10.1002/cbic.201300424
- Buchan, A.; Mitchell, A.; Cude, W. N.; Campagna, S. Acyl-Homoserine Lactone-Based Quorum Sensing in Members of the Marine Bacterial *Roseobacter* Clade: Complex Cell-to-Cell Communication Controls Multiple Physiologies. In *Stress and Environmental Regulation of Gene Expression and Adaptation in Bacteria*; de Bruijn, F. J., Ed.; Wiley Blackwell, 2016; pp 225–233. doi:10.1002/9781119004813.ch19
- Zan, J.; Liu, Y.; Fuqua, C.; Hill, R. T. *Int. J. Mol. Sci.* **2014**, *15*, 654–669. doi:10.3390/ijms15010654
- Schulz, S.; Höting, S. *Nat. Prod. Rep.* **2015**, *32*, 1042–1066. doi:10.1039/C5NP00006H
- Patzelt, D.; Wang, H.; Buchholz, I.; Rohde, M.; Gröbe, L.; Pradella, S.; Neumann, A.; Schulz, S.; Heyber, S.; Münch, K.; Münch, R.; Jahn, D.; Wagner-Döbler, I.; Tomasch, J. *ISME J.* **2013**, *7*, 2274–2286. doi:10.1038/ismej.2013.107
- Berger, M.; Neumann, A.; Schulz, S.; Simon, M.; Brinkhoff, T. *J. Bacteriol.* **2011**, *193*, 6576–6585. doi:10.1128/JB.05818-11
- Wang, H.; Ziesche, L.; Frank, O.; Michael, V.; Martin, M.; Petersen, J.; Schulz, S.; Wagner-Döbler, I.; Tomasch, J. *BMC Genomics* **2014**, *15*, No. 130. doi:10.1186/1471-2164-15-130
- Schaefer, A. L.; Greenberg, E. P.; Oliver, C. M.; Oda, Y.; Huang, J. J.; Bittan-Banin, G.; Peres, C. M.; Schmidt, S.; Juhaszova, K.; Sufirin, J. R.; Harwood, C. S. *Nature* **2008**, *454*, 595–599. doi:10.1038/nature07088
- Churchill, M. E. A.; Herman, J. P. Acyl-homoserine lactone biosynthesis: structure and mechanism. In *Chemical communication among bacteria*; Winans, S. C.; Bassler, B. L., Eds.; ASM Press: Washington, DC, 2008; pp 275–289. doi:10.1128/9781555815578.ch17
- Dickschat, J. S. *Nat. Prod. Rep.* **2010**, *27*, 343–369. doi:10.1039/b804469b
- Dong, S.-H.; Frane, N. D.; Christensen, Q. H.; Greenberg, E. P.; Nagarajan, R.; Nair, S. K. *Proc. Natl. Acad. Sci. U. S. A.* **2017**, *114*, 9092–9097. doi:10.1073/pnas.1705400114
- Lindemann, A.; Pessi, G.; Schaefer, A. L.; Mattmann, M. E.; Christensen, Q. H.; Kessler, A.; Hennecke, H.; Blackwell, H. E.; Greenberg, E. P.; Harwood, C. S. *Proc. Natl. Acad. Sci. U. S. A.* **2011**, *108*, 16765–16770. doi:10.1073/pnas.1114125108
- Chung, J.; Goo, E.; Yu, S.; Choi, O.; Lee, J.; Kim, J.; Kim, H.; Igarashi, J.; Suga, H.; Moon, J. S.; Hwang, I.; Rhee, S. *Proc. Natl. Acad. Sci. U. S. A.* **2011**, *108*, 12089–12094. doi:10.1073/pnas.1103165108
- Gould, T. A.; Schweizer, H. P.; Churchill, M. E. A. *Mol. Microbiol.* **2004**, *53*, 1135–1146. doi:10.1111/j.1365-2958.2004.04211.x
- Watson, W. T.; Minogue, T. D.; Val, D. V.; Beck von Bodman, S.; Churchill, M. E. A. *Mol. Cell* **2002**, *9*, 685–694. doi:10.1016/S1097-2765(02)00480-X

25. Buddruhs, N.; Pradella, S.; Göker, M.; Päufer, O.; Pukall, R.; Spröer, C.; Schumann, P.; Petersen, J.; Brinkhoff, T. *Int. J. Syst. Evol. Microbiol.* **2013**, *63*, 4340–4349. doi:10.1099/ijs.0.053900-0
26. Dogs, M.; Voget, S.; Teshima, H.; Petersen, J.; Davenport, K.; Dalingault, H.; Chen, A.; Pati, A.; Ivanova, N.; Goodwin, L. A.; Chain, P.; Detter, J. C.; Standfest, S.; Rohde, M.; Gronow, S.; Kyrpides, N. C.; Woyke, T.; Simon, M.; Klenk, H.-P.; Göker, M.; Brinkhoff, T. *Stand. Genomic Sci.* **2013**, *9*, 334–350. doi:10.4056/sigs.4448212
27. Bruhn, J. B.; Nielsen, K. F.; Hjelm, M.; Hansen, M.; Bresciani, J.; Schulz, S.; Gram, L. *Appl. Environ. Microbiol.* **2005**, *71*, 7263–7270. doi:10.1128/AEM.71.11.7263-7270.2005
28. Cude, W. N.; Buchan, A. *Front. Microbiol.* **2013**, *4*, No. 336. doi:10.3389/fmicb.2013.00336
29. Biebl, H.; Allgaier, M.; Tindall, B. J.; Koblizek, M.; Lünsdorf, H.; Pukall, R.; Wagner-Döbler, I. *Int. J. Syst. Evol. Microbiol.* **2005**, *55*, 1089–1096. doi:10.1099/ijs.0.63511-0
30. Martens, T.; Heidorn, T.; Pukall, R.; Simon, M.; Tindall, B. J.; Brinkhoff, T. *Int. J. Syst. Evol. Microbiol.* **2006**, *56*, 1293–1304. doi:10.1099/ijs.0.63724-0
31. Thole, S.; Kalhoefer, D.; Voget, S.; Berger, M.; Engelhardt, T.; Liesegang, H.; Wollherr, A.; Kjelleberg, S.; Daniel, R.; Simon, M.; Thomas, T.; Brinkhoff, T. *ISME J.* **2012**, *6*, 2229–2244. doi:10.1038/ismej.2012.62
32. Thiel, V.; Kunze, B.; Verma, P.; Wagner-Döbler, I.; Schulz, S. *ChemBioChem* **2009**, *10*, 1861–1868. doi:10.1002/cbic.200900126
33. Müller, K.-D.; Husmann, H.; Nalik, H. P.; Schomburg, G. *Chromatographia* **1990**, *30*, 245–248. doi:10.1007/BF02319701
34. Scribe, P.; Guezennec, J.; Dagaut, J.; Pepe, C.; Saliot, A. *Anal. Chem.* **1988**, *60*, 928–931. doi:10.1021/ac00160a019
35. Rontani, J.-F.; Christodoulou, S.; Koblizek, M. *Lipids* **2005**, *40*, 97–108. doi:10.1007/s11745-005-1364-6
36. Kerger, B. D.; Nichols, P. D.; Antworth, C. P.; Sand, W.; Bock, E.; Cox, J. C.; Langworthy, T. A.; White, D. C. *FEMS Microbiol. Ecol.* **1986**, *38*, 67–77. doi:10.1111/j.1574-6968.1986.tb01954.x
37. Vincenti, M.; Guglielmetti, G.; Cassani, G.; Tonini, C. *Anal. Chem.* **1987**, *59*, 694–699. doi:10.1021/ac00132a003
38. Bierl-Leonhardt, B. A.; DeVilbiss, E. D. *Anal. Chem.* **1981**, *53*, 936–938. doi:10.1021/ac00229a055
39. Gaudelli, N. M.; Townsend, C. A. *J. Org. Chem.* **2013**, *78*, 6412–6426. doi:10.1021/jo4007893
40. Neises, B.; Steglich, W. *Angew. Chem., Int. Ed. Engl.* **1978**, *17*, 522–524. doi:10.1002/anie.197805221
41. Agarwal, V.; Diethelm, S.; Ray, L.; Garg, N.; Awakawa, T.; Dorrestein, P. C.; Moore, B. S. *Org. Lett.* **2015**, *17*, 4452–4455. doi:10.1021/acs.orglett.5b02113

## License and Terms

This is an Open Access article under the terms of the Creative Commons Attribution License (<http://creativecommons.org/licenses/by/4.0>), which permits unrestricted use, distribution, and reproduction in any medium, provided the original work is properly cited.

The license is subject to the *Beilstein Journal of Organic Chemistry* terms and conditions:

(<https://www.beilstein-journals.org/bjoc>)

The definitive version of this article is the electronic one which can be found at:

doi:10.3762/bjoc.14.112

## Abstract

The cumulative doctoral thesis “Establishing a Comprehensive Toolbox for Isotopic Labelling Studies on Terpene Synthases” describes the synthesis and application of isotopically labelled compounds for the systematic *in vitro* investigation of recombinant terpene synthases to target both cyclisation mechanism and product structure. Methodically, the known approach of enantioselectively deuterated oligoprenyl diphosphate substrates was further developed by the addition of  $^{13}\text{C}$ -labelling, which led to a more sensitive detection of the labelled product by NMR. With a stereochemical anchor of known absolute configuration installed in the substrate and untouched by the enzymatic cyclisation mechanism, it is possible to infer the absolute configuration of the terpene product by following the incorporation of deuterium into the diastereotopic hydrogen positions. By combining chemical and enzymatic synthesis, it was finally possible to label every methylene group of the common terpene precursors by  $^{13}\text{C}$  and  $^2\text{H}$  in an enantioselective fashion. These extensions improve both feasibility and robustness of this method, which contributes to the challenging structure elucidation of terpene natural products, including their difficult to address absolute configurations. Depending on the cyclisation mechanism, also the stereochemical course of hydrogen movements can be delineated.

Connected to the expanding labelling possibilities, several newly identified terpene synthases from bacteria and fungi have been addressed covering various aspects of their catalysis such as substrate or product specificity, repetitive mechanistic motifs and stereochemical issues. The structural variety of the known and newly identified natural products thereby inspired further studies like tailored labelling experiments, site-directed mutagenesis, chemical modifications and the investigation of EI-MS fragmentation mechanisms. With few publications dealing with other aspects of natural product chemistry such as fungal aromatic volatiles, lignin degradation and selected aspects of the secondary metabolism of marine *Roseobacter* group bacteria also being included in this work, the main focus lays on a deepened understanding of terpene synthase reactions. The isotopically labelled substrates introduced in this study thereby represent a valuable experimental tool towards a comprehensive picture of these astonishing enzymes that create the largest group of natural products.